Thèse de doctorat de l'Université Bordeaux Montaigne

École Doctorale Montaigne Humanités (ED 480)

Spécialité : Sciences de la Terre et de l'Univers

Evolution sédimentaire, structurale et thermique d'un rift hyper-aminci : de l'héritage post-hercynien à l'inversion alpine
Exemple du bassin de Mauléon (Pyrénées)

présentée par Nicolas Saspiturry

Soutenue le 20 décembre 2019

devant le jury composé de :

Philippe **Razin (**Pr. ENSEGID – Bordeaux INP)	**Directeur de thèse**
Nicolas **Bellahsen (**MCF, HDR. iSTeP – Sorbonne Université)	**Rapporteur**
François **Guillocheau** (Pr. Géosciences-Rennes – Université Rennes 1)	**Rapporteur**
Yves **Lagabrielle** (CNRS. Géosciences-Rennes – Université Rennes 1)	**Examinateur**
Laurent **Jolivet (**Pr. iSTeP – Sorbonne Université)	**Examinateur**
Josep Anton **Muñoz** (Pr. – Universitat de Barcelona – España)	**Examinateur**
Olivier **Serrano** (Dr. – BRGM)	**Invité**
Thierry **Baudin** (Dr. – BRGM)	**Invité**
Philippe **Crumeyrolle** (Dr. – TOTAL)	**Invité**

« Montagnes Pyrénées, vous êtes mes amours
Cabanes fortunées, vous me plairez toujours.
Rien n'est si beau que ma patrie,
Rien ne plait tant à mon amie.
O montagnard, chantez en chœur
De mon pays, de mon pays,
La paix et le bonheur. »

André Dassary « Les Montagnards »



A mes montagnes,

A ma famille,

A mes amis, chers à mon cœur.

Avant-propos

Cette thèse a pour but de comprendre l'évolution tectono-sédimentaire et thermique d'un rift hyper-étiré en prenant en compte l'état initial de la croûte continentale post-hercynienne (Permien) et son implication dans l'orogenèse pyrénéenne, sur la base de l'exemple du bassin de Mauléon (Pyrénées nord-occidentales).

Cette thèse s'inscrit dans le cadre du programme international OROGEN, fondé par le BRGM, le département R&D de la compagnie pétrolière Total SA et le Centre National de la Recherche Scientifique (CNRS). La bourse et le fonctionnement de cette thèse ont été conjointement financés par la société Total SA et par le BRGM. Le projet Orogen est un consortium de recherche visant à améliorer la compréhension des processus orogéniques au cours d'un cycle complet de Wilson, sur la base de l'exemple de la chaîne des Pyrénées.

Cette thèse a été encadrée par Philippe Razin (Directeur de thèse), enseignant chercheur à l'ENSGID EA4592 Géoressources et environnement à Pessac, Olivier Serrano (BRGM ; co-encadrant) et Thierry Baudin (BRGM ; co-encadrant), tous trois membres du jury. Benoit Issautier (BRGM) et Cécile Allanic (BRGM) ont très largement contribué à l'encadrement de ces travaux de thèse. Sophie Leleu (ENSEGID) et Eric Lasseur (BRGM) ont également participé à l'encadrement de cette thèse.

Remerciements

Il y a de ça maintenant 7 ans que je suis arrivé dans le nord : à Bordeaux. Et oui, pour le basco-béarnais que je suis, la frontière se situe au niveau de l'Adour. Je suis monté au pôle avec la conviction de devenir hydrogéologue. Mais le destin en a décidé autrement... en effet, j'ai croisé **Philippe Razin** sur mon chemin. Je me rappelle maintenant ce que tu m'avais dit le jour de mon entretien pour rentrer à l'ENSEGID : « hydrogéologue ? on verra ». C'est sans aucun doute la rencontre qui a changé le cours de ma vie professionnelle. Tu es de ces personnes qui vivent la discipline qu'ils enseignent et qui ne transmettent pas uniquement leurs connaissances mais avant tout leur passion. Je tiens donc à te remercier, dans un premier temps, d'avoir été un enseignant exemplaire, à l'écoute, et d'avoir su me remettre sur le droit chemin de la Géologie. Mes prochains mots seront de plates excuses ! **Philippe**, je tiens à m'excuser car je t'ai fait déroger à une des promesses que tu t'étais faite à la fin de ta thèse. « Plus jamais je ne travaillerai sur le versant nord des Pyrénées, c'est complètement chiati… ! » Mais bon, il n'y a que les imbéciles qui ne changent pas d'avis… Je me rappelle le jour où tu m'as dit : « ça t'intéresse une thèse sur le bassin de Mauléon ? c'est chez toi, non ? ». Si on m'avait dit quand j'étais au lycée à Mauléon que je ferai une thèse pour comprendre la genèse de ce que j'ai sous les pieds, j'aurais sans doute répondu : « Quésaco ». Mais quand tu m'as présenté ce sujet de thèse il y a 4 ans, j'ai été flatté et honoré que tu me proposes d'être mon tuteur et donc en quelque sorte mon mentor. C'est donc maintenant le tuteur que je remercie. Merci d'avoir été présent au cours de ma thèse et de m'avoir fait grandir scientifiquement. Je sais maintenant que ma maison repose sur le chevauchement frontal des Pyrénées, ce n'est pas rien quand même, quoi que… Le destin ayant vraiment décidé de mon sort… on s'est retrouvé voisin… et la vie ne s'arrêtant pas au travail, je tiens enfin à remercier l'ami que je me suis fait. J'espère avoir la chance de transmettre, à mon tour, ma passion tout en essayant de devenir aussi pédagogue que toi. Merci pour les moments passés en ta compagnie. Je tiens également à te remercier **Monique**. Merci pour ton accueil chaleureux, pour l'organisation des soirées dégustations de vins et bien entendu pour tes délicieux desserts. On a eu de la chance, avec Florence, de vous avoir comme voisins !

Je tiens également à remercier le programme Orogen (BRGM, Total, CNRS) d'avoir financé ces travaux de recherche et de m'avoir donné l'opportunité de travailler dans la plus belle région du monde, le Béarn enfin le Pays Basque, enfin c'est plus moins pareil, on est tous épicuriens. Le bassin de Mauléon n'ayant pas de frontières, j'espère, de tout cœur, avoir réconcilié basques et béarnais à travers ces travaux de thèse.

Merci aux membres du jury pour avoir pris le temps de se déplacer et de relire mon manuscrit de thèse. Je tiens donc à remercier mes rapporteurs, **Nicolas Bellahsen** et **François Guillocheau**, mes examinateurs, **Yves Lagabrielle**, **Laurent Jolivet**, et **Josep Anton Muñoz**, et mon invité **Philippe Crumeyrolle**, c'est un honneur de vous avoir dans mon jury. Pour la petite anecdote, il se trouve que, depuis 4 ans, je dors dans l'ancien garage de ton grand père, **François**, donc qui de mieux que toi pour être rapporteur de ma thèse… je vais commencer à croire au destin à ce rythme…

Tous les chemins mènent à Rome paraît-il, en tout cas celui de ma thèse m'a mené encore plus au nord. C'est possible ça ? Il existe quelque chose après la Garonne ? Me voilà propulsé sur les terres, à première vue hostiles, de Jeanne d'Arc. Terres d'exil ou terres d'accueil ? En tout cas les exilés t'y accueillent le cœur ouvert. C'est pourquoi mes remerciements se portent maintenant vers **Olivier Serrano**, co-encadrant de ma thèse au BRGM. Merci de m'avoir fait confiance et d'avoir cru en moi pour mener à bien ces travaux de thèse. Merci pour ton soutien sans failles… oh le jeu de mot… dans cette épreuve semée d'embûches, tu as été présent dans tous les moments difficiles pour essuyer les pots cassés. Plus qu'un encadrant, comme bon nombre des gens avec qui j'ai pu travailler ces trois dernières années, tu es devenu un ami. Il est déjà loin le temps où on était à deux doigts de se prendre un cheval sur le capot de la voiture… Merci d'avoir été présent pour t'occuper de bon nombre de déboires administratifs et autres. Merci **Olivier** et **Anouk** de m'avoir accueilli chez vous. J'ai passé de très bon moments en votre compagnie et j'espère que l'on en passera de nombreux autres. Au fait, j'ai

appris qu'on allait former une équipe Anouk… j'espère que tu es prête à me supporter un peu plus longtemps ! Personnellement, je pense qu'il va falloir que l'on revoit très sérieusement l'éducation culinaire de **Fani**…

En effet, en acceptant de me lancer dans cette aventure je ne pensais pas devoir manger de la salade aux olives (des olives à la salade…) et de la tarte aux anchois par politesse. C'est vraiment de la cuisine ça ? Quèsaco, ça vient d'où ? Non je plaisante, je ne pensais surtout pas rencontrer, ce que je pourrais appeler une seconde famille. Il va m'être difficile de résumer en quelques phrases les deux ans de collocations passés ensemble. C'est un immense merci que je vous adresse et que je vous dois **Benoit Issautier** et **Juliette Stephan,** pour ne pas m'avoir fait payer de loyer... C'est vraiment gentlemen de votre part. J'ai même pu choisir ma chambre dans la nouvelle maison, c'est royal, même si je ne suis pas 100% satisfait de la couleur des murs, ça reste convenable. Je m'égare… C'est un immense remerciement que je vous dois, pour m'avoir si bien accueilli et fait une place dans votre famille. Merci **Benoit** pour ton implication dans ma thèse et merci pour ton soutien au jour le jour. Je n'ai pas appris que la géologie à vos côtés, j'ai également appris la vie en quelque sorte. C'est pourquoi je tiens à remercier vos deux adorables petits montres **Lily** et **Fani** qui ont le chic de vous redonner du baume au cœur et de vous faire comprendre les choses essentielles de la vie. Merci également de m'avoir inculqué l'art de la lèche… oh chef vous êtes beau, radieux et à la fois si charismatique en ce jour si terne d'automne… On notera que le padawan a très largement dépassé le jedi. Profite bien du canapé et de la table basse en mon absence, tu ne peux pas mieux travailler que dans ces conditions.

Le quartier à Saint Denis en Val étant relativement sympathique, il est temps de remercier les voisins. Merci à **Cécile Allanic** et **Nicolas Coppo** pour les barbecues, les parties de Pie Face et les moments passés au P'tit St Denis avec ma famille adoptive. Vous avez été des voisins très agréables et c'est pourquoi je déménage avec le cœur lourd. Je passe mon temps à m'égarer dans ces remerciements… je m'étais dit, faut pas que tu sois trop long… « sois précis et concis » … essaies de retenir les enseignements de Cécile parfois quand même… Je tiens à te remercier grandement, Cécile, de m'avoir co-encadré et supporté tout au long de cette thèse… Désolé d'avoir passé mon temps à envahir ton bureau et ta boîte mail… Je ne te remercierai jamais assez pour ton investissement et ton temps passé à essayer de remettre toutes mes idées dans un ordre logique et audible. Ça a été un plaisir de travailler avec toi, j'ai enfin compris les rouages et l'intérêt de la modélisation en géologie. Ton esprit synthétique et précis m'a permis de ne pas m'égarer à de nombreuses reprises.

J'ai passé pas mal de temps au cours de mon cursus à pratiquer le coup de marteau et c'est tout naturellement que j'ai essayé de me diversifier en faisant de la démolition chez les voisins. C'est fou comment les voisins sont sympathiques et accueillants dans le nord… Merci à **Justine Briais** et **Eric Lasseur** de m'avoir permis de me défouler sur vos murs, c'est vraiment thérapeutique. Je comprends mieux les gens qui paient pour démolir des trucs maintenant. Merci pour les bons moments passés dans votre nouveau chez vous, les travaux sont fédérateurs. Je tiens à te remercier, Eric, d'être à l'origine de ce sujet de thèse. Merci également pour ton implication dans ma thèse et pour les quelques jours passés avec moi sur le terrain. **Eric**, on a quand même passé de super soirées au Becs à Vin à refaire le monde… Merci **Ju** pour le week-end passé dans ta Bourgogne natale, on s'est éclaté et on a surtout éclaté l'Argentine… On attend votre crémaillère avec impatience avec **Florence**, les caves sont faites pour être vidées…

Ah non, nooooon, je n'ai jamais dit ça !!! Non, je ne suis toujours pas d'accord avec toi... Ces phrases vont me manquer et le personnage qui en est l'auteur me manquera tout autant. Je tiens à t'adresser un très grand merci **Thierry Baudin** pour ton implication dans ma thèse. Merci de m'avoir lancé sur le terrain et d'y avoir consacré deux semaines de ton temps au début de ma thèse. Ces deux semaines de terrain ont été très animés, à l'image de toutes nos discussions passionnantes. Je tiens donc à te remercier pour ces discussions endiablées et les tableaux recouverts de schémas à ne plus savoir ce qu'ils représentent. J'ai retrouvé ce que **Philippe** m'avait bien venté, à propos des récits, prouesses et qualités de son binôme de choc de l'époque. J'espère avoir l'opportunité de continuer à travailler avec toi par la suite.

Un grand merci à tous les autres membres de la grande famille du BRGM ayant bien voulu me supporter pour travailler : **Isabelle Thinon, Abdeltif Lahfid, Laurent Guillou-Frottier, Gaby Courrioux, Simon Andrieu et Benjamin Le Bayon**. Merci à **Isa** de m'avoir aiguillé sur la bibliographie relative aux marges hyper-étirés au début de ma thèse. Merci à **Abdel** pour la réalisation des mesures Raman et ton implication dans la relecture du papier. Merci **Laurent** d'avoir pris part à ce travail sur la thermicité et d'avoir réalisé le modèle numérique. Merci **Gaby** pour ton implication et le temps passé à travailler sur le modèle 3D sur le GeoModeller. Merci **Simon** pour les deux semaines passées avec toi sur le terrain sur les Calcaires des Cañons. Merci **Benjamin** pour ton implication sur la relecture des articles et tes données incorporées dedans. Je tiens également à remercier les personnes du BRGM avec qui je n'ai malheureusement pas travaillé mais avec qui j'ai passé de bons moments : **Adnand Bitri, Maxime Padel, Florence Cagnard, Renaud Coueffe et Guillaume Badinier**. Merci **Adnand**, je sais maintenant d'où vient l'expression favorite de **Philippe** : « c'est vraiment le merde ça » … enfin surtout l'accent et le jeu d'acteur… je crois qu'il y a plagia en y réfléchissant bien ! Je tiens également à te remercier **Maryline Mechin** pour ta bonne humeur et ton efficacité. Je ne sais pas comment la boutique tournerait sans toi…

Mes remerciements se tournent maintenant vers ma patrie bordelaise. Je tiens à te remercier grandement mon partenaire de bureau, **Aurélien Bordenave**, quoi de mieux qu'un béarnais pour partager son bureau… bien qu'exilés, on se croyait à la maison… Je ne pensais pas me faire un ami proche comme toi, mais nos esprits épicuriens se sont plutôt bien entendus. Je t'envie quelque part de m'abandonner pour repartir vers notre beau pays mais je sais que malgré la distance nous resterons soudés. La licorne va me manquer, au même titre que les kiwis… comment savoir maintenant quand une soirée sera réussie ? Il est maintenant temps de remercier mon second compère… amie sur les bancs de l'ENSEGID… colocataire… et collègue… **Constance Vinciguerra**, un grand merci pour les nombreux bons moments passés ensemble et ton soutien qui dure depuis maintenant 7 ans. Il temps que je m'excuse… désolé d'avoir essayé de t'empoisonner à plusieurs reprises ces dernières années… les carottes… les aubergines… les légumes quoi…On se suit de près dans ce dernier rush final, c'est pourquoi je te dis « merde » pour la suite.

Je tiens également à remercier les compères du 3ème étage, merci à **Carine Grélaud, Thibault Duteil, Mehdi Carmeille** et **Raphael Bourrillot**, et les partenaires de bureau : **Remi Joussiaume, Nicolas Grasseau** et **Coline Ariagno** pour la bonne ambiance et les bons moments passés ensemble. Merci monsieur le directeur, **Alain Dupuy**, d'avoir su perdre dans la dignité au babyfoot, promis je reviendrai pour te donner des conseils avisés… Je blague, merci de faire en sorte que l'ENSEGID soit un lieu convivial, où il fait bon venir travailler et où les gens se sentent bien. Je tiens donc à remercier tous les autres collègues de l'ENSEGID pour leur bonne humeur : **Sophie, Olivier, Marian, Michel, François, Alexandre, Grégory, Elicia, Anélia, Tamara, Myriam, Félix, Serge, Léa**, **Adrian, Corinne, Cristina, Ryma, Florian**. L'horoscope de **Michel** et les blagues de **François** vont me manquer… Il existe des gens sympas au rez-de-chaussée aussi… Merci à **Morgan Le Lous** pour les parties de squash endiablées, le week-end passé en ta compagnie au ski, ta gentillesse et ton humanité. Merci à **Alicia Corbeaux** et **Christine Ochoa** pour leur efficacité et leur bonne humeur quotidienne.

Je te dois également un grand merci **Sophie Leleu** pour m'avoir co-encadré sur des aspects spécifiques de ma thèse et pour avoir notamment grandement pris part au travail sur le Permien. Merci d'avoir pris le temps de venir sur le terrain et d'avoir participé à la relecture des articles de ma thèse. J'ai passé de très bons moments avec toi, j'espère que vous reviendrez avec ta petite famille faire la fête au mois d'août. Je garde un très bon souvenir de la prof, de la collègue et de l'amie. Encore merci.

C'est donc tout naturellement que mes remerciements se tournent vers **le team permien**. Je dois un très grand merci à **Bryan Cochelin** pour son implication dans l'écriture de l'article sur le Permien. Tu as très largement participé à la finalisation de cet article, qui est pour moi un des points les plus aboutis de mon travail, de notre travail. Merci pour ta bonne humeur, les parties de tennis et les soirées au Dix Fûts. Il est temps pour toi de t'envoler vers la Chine mais j'espère que l'on aura l'occasion, à nouveau, de faire parler déformation ductile et sédimentologie, car j'ai appris à tes côtés que l'intérêt de notre science réside dans l'intégration des données... ne nous mettons pas de barrières… Je tiens

également à remercier tout particulièrement **Chloé Bouscary** qui a récolté une partie des données qui ont permis la réalisation de cet article. Merci également à **Baptiste Lemire** pour les données qu'il a incorporé dans ce travail et à **Michel de Saint-Blanquat** pour les photos de lames minces. Merci également à **Romain Augier** de nous avoir permis, avec **Bryan**, de présenter nos résultats de recherche au laboratoire d'Orléans.

« Sage est celui qui recueille la sagesse des autres » (Juan Guerra Caceras). C'est avec beaucoup d'humilité et d'admiration pour le travail que tu as réalisé, au cours de ta vie, sur les Pyrénées que je tiens à te remercier, **Joseph Canérot**… C'est auprès des sachants que l'on apprend, c'est pourquoi je tiens à te remercier de t'être déplacé sur le terrain pendant près d'une semaine au lancement de ma thèse. Merci de m'avoir présenté ta vision de la géologie de mon beau pays. Merci de m'avoir accueilli à Toulouse pour discuter de mes résultats. Merci pour les nombreuses discussions fructueuses que nous avons eu. Nous n'avons malheureusement pas réussi à trouver le temps de repartir discuter sur le terrain, le nerf de la guerre, pour nous naturalistes, mais j'espère de tout cœur que nous aurons l'occasion de le faire.

Je tiens maintenant à remercier **la team rennaise**… Merci de m'avoir accueilli avec vous sur le terrain en 2016, au début de ma thèse, **Yves Lagabrielle**, **Serge Fourcade**, **Benjamin Corre**, et **Jessica Uzel**. Il est vrai qu'au début je me suis demandé… où suis-je tombé ? Moi sédimentologue… « Chez les frappadingues », vous me disiez… Mais à force de discuter et finalement de travailler avec vous, j'ai appris de nombreuses choses à vos côtés. Je tiens à te remercier **Yves** pour m'avoir permis de travailler avec vous. J'ai été honoré de travailler avec toi, et j'espère avoir l'occasion de remettre ça dans le futur. Je tiens également à te remercier **Riccardo Asti** pour les échanges fructueux que nous avons eu tout au long de ma thèse. L'union fait la force dans un domaine où la compétition prend parfois le dessus. Je tiens également à vous remercier **Alexandre** et **Jessica** pour les bons moments passés avec vous lors des rassemblements du projet. On sait maintenant qu'Aladin ne ment pas, les tapis volent… Je tiens également à remercier **Thibault Duretz** pour son implication dans la relecture de mon article. Merci également de m'avoir permis de venir présenter mes travaux de recherche au laboratoire de Rennes.

Il est maintenant temps de remercier les amis et proches qui sont tout aussi importants que les collègues et qui m'ont encadré tout au long de ce périple qu'est la thèse… Merci aux **Turbidites** : **Valentin**, **Tamara** et **ma moitié** (je ne vais pas te remercier tout de suite, il parait qu'on garde toujours le meilleur pour la fin) … Merci celui que j'aime appeler le batteur, j'espère qu'on aura l'occasion de poursuivre notre vacarme sonore. Merci à la chanteuse, tu vogues maintenant vers ta Bretagne natale, j'ai l'impression quand même que l'on a tous un peu de mal à se défaire de nos racines… Je te souhaite tout plein de bonnes choses… On n'aura fait qu'une seule représentation mais on se sera bien amusé… qui sait, il parait qu'il y aura des instruments le soir de la soutenance…

Merci à la **team pelote** du mardi midi, c'est un moment que j'attendais avec impatience ces dernières semaines car il m'a permis de m'aérer l'esprit en compagnie de gens sympathiques, des amis. Je tiens donc à vous remercier **Julien**, **Adrien**, **Gilles** et **Fred**. Un merci spécial à **Julien**, qui m'a soutenu pendant toutes ces années à Bordeaux, et avec qui j'ai passé et je passerai de très bons moments! Merci également à **Laurine** pour tous ces bons moments, un jour j'arriverai à t'amener dans les Pyrénées aussi !

Il est temps de remercier le noyau dur, les irréductibles Gaulois euh Palois… Bien que pas mal de kilomètres nous séparent et qu'à mon grand désespoir on ne s'est pas beaucoup vu au cours de ces trois dernières années, vous êtes de ces amis que l'on ne se fait qu'une fois dans une vie. Je tiens à vous remercier de m'avoir soutenu et d'être présent même à distance… C'est un grand merci que je vous dis **Carsu**, **Djedge** et **Pupuce** à vous et vos moitiés **Camille**, **Vivi** et **Lucie** ! Merci également à la dream team de Florence, **Méla** et **Pépéé**, de m'avoir accueilli dans votre groupe et d'être présentes et disponibles à chaque occasion. En espérant pouvoir peut-être, un jour, vous retrouver tous au pays… Le nord n'étant pas si loin, tout compte fait, retrouvons-nous dans un premier temps au banquet.

Il est maintenant temps de remercier ceux qui ont fait de moi ce que je suis. Merci **papa** et **maman** d'avoir soutenu mes choix professionnels. Le domaine de la géologie n'est pas conventionnel, ce n'est pas tous les parents qui auraient eu confiance en leur enfant. J'espère vous avoir prouvé que c'était le bon choix. Merci également d'avoir supporté mon retour à la maison lors de mes longues campagnes de terrain mais également le vas et viens, que dis-je, le défilé de mes encadrants qui ont, pour sûr, grandement appréciés votre hospitalité. J'en profite également pour vous remercier de l'accueil d'un bon nombre de mes amis au pays, chaque week-end d'août de mon anniversaire. Merci à mon petit frère **Florian** pour ton soutien au jour le jour, je sais que je peux toujours compter sur toi.

Sur les routes du Grand Nord, j'ai rencontré un professeur, un mentor puis un ami, des exilés, des collègues puis des amis mais avant tout la femme qui partage maintenant ma vie… Je suis monté dans le nord pour rencontrer une béarnaise c'est un comble… enfin de toute manière tout le monde sait bien qu'on ne se mélange pas, c'est pas un secret… Chaque jour qui passe à tes côtés est une source de joie. Je remercie le destin de t'avoir mis sur ma route. Je ne pense pas qu'il y ait de mots suffisamment forts pour te remercier. Tu es toujours là pour moi, dans n'importe quelle circonstance. Tu m'écoutes te raconter mes problèmes, tu me remontes le moral quand je suis triste, tu m'encourages quand je baisse les bras et tu me consoles quand je subis un échec. Les mots sont peu de choses pour te dire merci pour tout cela, c'est 4 000 mercis que je t'adresse ma **Floflo** pour m'avoir soutenu, supporté et écouté… Sans toi rien de tout ça n'aurait été possible, tu es le pilier de ce travail. On peut même dire que tu m'as inspiré un de mes articles... Merci et pardon à la fois pour les trois années de sacrifices que représentent la thèse. Il est temps pour nous de partir loin de nos chères Pyrénées pour prendre des vacances et un bon bol d'air frais qui nous sont amplement mérités…

Résumé

Localisé dans les Pyrénées occidentales, l'étude du bassin de Mauléon, permet d'appréhender l'évolution tectono-sédimentaire et thermique d'un rift hyper-aminci de son héritage pré-extensif à son inversion (cycle complet de Wilson). L'épisode permien reflète le passage de la convergence N-S enregistrée dans la Zone Axiale (310 à 290 Ma) à une phase d'extension E-W (290 et 275 Ma), conférant un héritage thermique, structural et rhéologique complexe à la lithosphère des Pyrénées occidentales. La préservation des traits paléogéographiques permo-triasiques rend impossible la réalisation d'un mouvement décrochant sénestre E-W au Mésozoïque entre l'Ibérie et l'Europe, dans cette partie des Pyrénées, questionnant les modalités d'ouverture des bassins nord-pyrénéens au Crétacé. Au cours de l'orogenèse alpine, le bassin hyper-étiré de Mauléon est inversé. La réactivation des structures crétacées conduit à la formation d'un pop-up lithosphérique dont les bordures présentent des styles de réactivation différents, localisé (Ibérie) vs distribué (Europe). La protubérance mantélique héritée de la phase de rifting crétacée empêche l'inversion complète du rift en jouant le rôle de buttoir. En 3D, les systèmes de chevauchement sont composés de plusieurs segments délimités par les zones de transferts N20° héritées du Permien conférant un caractère non-cylindrique au structures orogéniques pyrénéennes. L'héritage permien et crétacé contrôle à la fois l'évolution thermique synrift et post-collisionnelle du bassin de Mauléon. Les paléo-gradients géothermiques synrifts augmentent de manière graduelle des marges (~ 34°C/km) vers le bassin (~ 60°C/km). La température maximale est alors contrôlée par l'enfouissement et le flux thermique mantélique (100 mW.m-2). La différence de réponse thermique observées sur les bordures du bassin de Mauléon est liée au style de déformation compressive : diminution du gradient dans le domaine hyper-étiré et la marge européenne ~ 25.0 ± 2.7°C/km vs augmentation du gradient sur la marge ibérique < 30°C/km). L'étude tectono-sédimentaire des bassins mésozoïques adjacents d'Arzacq et de Tartas, couplée à un travail de synthèse sur les bassins péri-ibériques souligne les nombreuses différences existant entre ces bassins et ceux des marges hyper-étirées atlantiques. L'évolution de ces « bassins extensifs à pente douce » comprend trois grands stades de déformation : (1) un amincissement ductile de la croûte inférieure, sans déformation cassante significative dans la croûte supérieure, formant un rift symétrique (sag) ; (2) un glissement de la couverture prerift sur les évaporites du Trias; (3) une phase d'hyper-extension avec déformation fragile des marges proximales et amincissement ductile du domaine distal hyper-étiré (métamorphisme HT/BP).

Mots clés : (1) Pyrénées ; (2) bassin de Mauléon ; (3) Géodynamique (4) Héritage post-hercynien ; (5) Hyper-extension crétacée ; (6) Inversion alpine ; (7) Zones de transfert ; (8) Métamorphisme HT/BP ; (9) Evolution thermique.

Abstract

The western Pyrenean Mauléon basin allows to discuss the tectono-sedimentary and thermal evolution of a hyperextended rift through an entire Wilson cycle. During Permian time, the western Pyrenees record the shift between N-S convergence recorded in the Pyrenean Axial Zone (310 to 290 Ma) and dominant E-W extension (290 to 275 Ma). This latter stage is responsible for a complex thermal, structural and compositional inheritance of the Pyrenean lithosphere. The preservation of the original Permian-Triassic paleogeography and structure in the « Basque Massif » indicates that there was no major east-west Mesozoic strike-slip motion between the Iberian and European plates in this part of the Pyrenees, questioning the mechanisms responsible for the opening of the Early Cretaceous North-Pyrenean rift system. The Cretaceous Mauléon hyperextended rift basin was inverted during the Alpine orogeny. Reactivation of the former rift structures leads to the formation of a lithospheric scale pop-up whose edges are characterized by differing tectonic reactivation style, localized (Iberia) vs distributed (Europe). The previously exhumed mantle acts as a buttress inhibiting the complete closure of the basin. In 3D, the N120° thrusts systems edging the pop-up are composed of different thrust segments branching into the inherited Permian N20° transfer zones, highlighting the non-cylindrical geometry of the Pyrenean structures. Permian and Cretaceous structural inheritance both control the synrift and post-collisional thermal evolution of the Mauléon basin. Synrift paleogeothermal gradients gradually increased from the margins (~ 34°C/km) to the basin (~ 60°C/km). Maximum peak temperatures are both controlled by sedimentary burial and mantle heat flow (100 mW.m-2). The different post-collisional thermal responses of the Mauléon basin pop-up edges is linked to their tectonic reactivation style. On the European margin, the postrift isotherms were passively transported onto the proximal margin (« thin-skinned »). On the Iberian margin, peak temperatures were acquired after thrusting (« thick-skinned »). The review of the hyperextended Iberian-Eurasian plate boundary basins shows that they strongly differ from classical Atlantic-type passive margins. Three main stages of continental crust thinning can be inferred to describe the evolution of this smooth-slope type extensional basin : (1) a dominant ductile thinning of the lower crust, without significant brittle deformation of the upper crust, resulting in the formation of a symmetric sag basin; (2) basinward gliding of the prerift cover along the Late Triassic evaporites; (3) hyper-extension with brittle deformation on the proximal margins and dominant ductile thinning on the hyperextended rift domain (HT/LP metamorphism).

Key-words: (1) Pyrenees; (2) Mauléon basin; (3) Geodynamic; (4) Post-hercynian inheritance; (5) Cretaceous hyperextension; (6) Alpine inversion; (7) Transfer zones; (8) HT/LP metamorphism; (9) Thermal evolution.

Résumé étendu

La compréhension des processus relatifs à l'hyper-amincissement de la croûte continentale et à l'exhumation du manteau a connu un essor significatif dans les dernières décennies du fait de l'interprétation de données de sismique pétrolière le long des marges passives actuelles telles que les marges atlantiques. Cependant, leur faible accessibilité nécessite d'analyser ces processus au sein de systèmes fossiles tel que les Alpes ou les Pyrénées. Ces chaînes de montagnes résultent de l'inversion de systèmes de rift hyper-étirés dont les reliques ont été portées à l'affleurement au cours de l'orogenèse alpine. Bien que la géométrie de ces systèmes extensifs fossiles ait été récemment étudiée, de nombreuses questions subsistent : (1) Quel est le rôle de l'héritage prerift et synrift au cours de la formation et de l'inversion d'un système de rift hyper-étiré ? (2) En quoi les zones de transferts, obliques par rapport à la direction générale du système hyper-extensif, impactent-elles la géométrie du rift et de l'orogène ? (3) Comment évolue le gradient thermique d'un système de rift hyper-étiré en 3D, de la phase de rifting à celle post-compressive ? En ce sens, l'étude du bassin de Mauléon, dans les Pyrénées nord-occidentales, a permis d'appréhender l'évolution tectono-sédimentaire et thermique d'un rift hyper-aminci de son héritage pré-extensif à son inversion (cycle complet de Wilson). Pour répondre à ces questions, cette étude se base sur une approche pluridisciplinaire intégrant: (1) un travail de terrain le long de la marge ibérique inversée du bassin de Mauléon et sur les zones de transferts segmentant son domaine hyper-étiré (12 mois, ~ 2500 points d'observation), (2) l'interprétation de données de subsurface provenant de 64 puits et de 750 km de lignes sismiques, (3) 170 données de pic de température Raman sur 68 échantillons de terrain et 102 échantillons de forage, (4) un modèle thermique numérique simplifié visant à reproduire l'histoire thermique du bassin de Mauléon au cours des 120 derniers millions d'années et (5) un modèle 3D du bassin de Mauléon utilisant un algorithme de modélisation implicite implémenté dans le logiciel GeoModeller du BRGM.

Les résultats obtenus sur le bassin permien de Bidarray et le dôme granulitique de l'Ursuya, situés sur la bordure occidentale du bassin de Mauléon, reflètent le passage de la convergence N-S enregistrée dans la zone axiale pyrénéenne de 310 à 290 Ma à une phase d'extension E-W prenant place entre 290 et 275 Ma. Cette interprétation suggère que la croûte continentale de l'avant-pays de la chaîne varisque est restée chaude et partiellement fondue au cours de l'extension permienne dans les Pyrénées occidentales. Cet épisode confère un héritage thermique (gradient anormalement élevé), structural (déformation cassante N20° localisée dans la croûte supérieure et croûte continentale amincie) et rhéologique (granulites et migmatites exhumées en position de croûte supérieure) complexe à la lithosphère des Pyrénées occidentales.

La préservation des traits structuraux et paléogéographiques permo-triasiques, le long de la zone de transfert de Pamplona, rend impossible la réalisation d'un quelconque mouvement décrochant sénestre de direction E-W au cours du mésozoïque entre les plaques ibérique et européenne dans cette partie des Pyrénées occidentales. Ceci questionne donc la dynamique d'ouverture du système de rift nord-pyrénéen au Crétacé, dont la géométrie générale était interprétée comme le résultat de ce décrochement de grande ampleur. La structuration transverse de direction N20°, héritée du Permien, contrôle l'ouverture du système de rift crétacé. A petite échelle les zones de transfert crustales influencent l'émergence des systèmes diapiriques et contrôlent les dépôt-centres synrifts, à la fois dans le bassin de Mauléon et dans le bassin d'Aquitaine. A plus grande échelle, les zones de transferts lithosphériques de Pamplona et du Barlanès sont respectivement responsables du décalage vers le sud de l'axe du rifting mésozoïque entre le bassin de Mauléon et le bassin Basque-cantabre et de la dénudation locale du manteau sous-continental dans le secteur d'Urdach.

Au cours de la phase orogénique alpine, le bassin de Mauléon est inversé en un « pop-up » d'échelle lithosphérique dont la géométrie est contrôlée à la fois par l'héritage structural permien et crétacé. En nord-sud (2D), la réactivation des structures héritées du rifting crétacé entraine la formation d'un « pop-up » crustal dont les bordures accommodent la même quantité de raccourcissement, mais présentent des styles de réactivation tectonique différents, localisé (marge

ibérique : réactivation du détachement de Lakhoura) ou distribué (marge européenne : écaillage de la croûte et formation du système de chevauchement frontal nord pyrénéen). La convergence se poursuivant, les chevauchements de Gavarnie et de Guarga participent à l'empilement de nappes crustales formant l'antiforme de la Zone Axiale, au sein d'un pop-up d'échelle lithosphérique. La protubérance mantélique héritée de la phase de rifting crétacée est accentuée par ce style d'inversion et empêche l'inversion complète du rift de Mauléon. En 3D, les systèmes de chevauchement N120°de Lakhoura et du chevauchement frontal nord pyrénéen sont composés de plusieurs segments délimités par les zones de transferts N20° héritées du Permien. Ces segments de chevauchement antithétiques se branchent sur les zones de transferts, définissant un système en « tiroirs » permettant la fermeture progressive de l'ancien domaine de rift. La zone de transfert lithosphérique de Pampelune joue le rôle de buttoir bloquant la déformation à l'ouest et la propageant vers l'est. Ce mode de déformation compressif est responsable du caractère non cylindrique des structures de la zone-pyrénéenne résultant de l'inversion alpine du bassin de Mauléon.

Cet héritage complexe et polyphasé contrôle de manière significative l'évolution thermique synrift à post-collisionnelle du bassin de Mauléon. Les paléo-gradients géothermiques synrifts anormalement élevés coïncident avec le domaine hyper-étiré du bassin de Mauléon. Ils augmentent de manière centripète et graduelle depuis les marges proximales (~ 34°C/km) jusqu'au domaine hyper-étiré (~ 57-60°C/km). La température maximale atteinte par les séries prérifts à synrifts est contrôlée à la fois par l'enfouissement et par le flux thermique arrivant en base du domaine hyper-étiré. Ce dernier a été estimé, par modélisation thermique, à 100 mW.m-2 pour un gradient de 60°C/km.

Au cours de l'orogenèse alpine, les isothermes hérités de la phase de rifting crétacée ont été déformés et plissés au sein du « pop-up ». Le long de la marge européenne, les isothermes liés à la phase de rifting ont été préservés et transportés sur la marge proximale tandis que la marge ibérique enregistre une thermicité syn à post-collisionnelle. La différence de réponse thermique de part et d'autre du « pop-up » de Mauléon est directement liée au style de déformation au cours de l'inversion pyrénéenne, lui-même conditionné par l'héritage structural crétacé. La marge ibérique est affectée par une déformation pyrénéenne de type « thick-skin », induisant une augmentation du gradient géothermique. Au contraire, le domaine hyper-étiré du bassin de Mauléon et sa marge européenne sont caractérisés par une décroissance du gradient géothermique depuis l'amorce de la compression pyrénéenne jusqu'à nos jours, comme en témoigne le gradient actuel mesuré dans les puits ~ 25.0 ± 2.7°C/km. Ce faible gradient s'explique par une épaisseur crustale faible à moyenne (de 5 à 25 km), autrement dit par la présence d'un manteau sous-continental à faible profondeur hérité de la phase d'hyperextension crétacée. En 3D, les zones de transferts N20° héritées du permien segmentent à la fois la thermicité synrift dans le domaine hyper-étiré et la thermicité post-collisionnelle de la zone axiale des Pyrénées sous les unités chevauchantes de la marge sud du bassin de Mauléon.

L'étude tectono-sédimentaire des bassins mésozoïques de Mauléon, Arzacq et Tartas (cf. chapitre. 3), couplé à un travail de synthèse bibliographique sur les bassins mésozoïques de Parentis, du domaine Basque-cantabre, de Camèros, de Columbrets et de la zone nord pyrénéenne centrale et orientale a mis en évidence les nombreuses différences entre la structure et l'évolution de ces bassins et ceux des marges passives hyper-étirées de type atlantique. Ils ont récemment été définis comme des « smooth-slope type extensional basins », et diffèrent des marges passives hyper-étirées de type atlantique par l'absence de bloc basculés et un amincissement à dominante ductile de la croûte continentale dans le domaine hyper-étiré. Ces bassins présentent néanmoins des similitudes :

(1) ils résultent de l'hyper-extension au cours du Jurassique supérieur – Crétacé inférieur d'une croûte continentale préalablement amincie entre le Permien et le Jurassique;

(2) ils sont caractérisés par une importante épaisseur de série prérift à synrift, un paléo-gradient géothermique et/ou un flux de chaleur mantellique synrift élevé responsable d'un métamorphisme HT/BP des sédiments en base de bassin ;

(3) leur domaine hyper-aminci coïncide généralement, dans certains secteurs peu raccourcis, avec une anomalie gravimétrique positive illustrant la présence du manteau sous-continental à faible profondeur ;

(4) dans le domaine hyper-étiré, la croûte inférieure est très fine ou absente ;

(5) ils présentent une géométrie sensiblement symétrique ;

(6) la déformation extensive est découplée entre la croûte supérieure et la couverture prérift du fait de la présence d'un épais niveau évaporitique du Trias supérieur ;

(7) leur ouverture s'accompagne d'un glissement gravitaire de la couverture prerift sur ce niveau de décollement triasique ;

Ces bassins subissent une évolution extensive commune, polyphasée et synchrone. Ils peuvent être classés en fonction du taux d'amincissement de la croûte continentale, suivant un ordre de maturité du système extensif, du moins aminci au plus aminci : (1) bassin de Tartas, (2) bassins de Arzacq, Columbrets et Camèros, (3) bassin de Parentis, (4) bassins Basque-cantabre et de Mauléon, (5) bassins de la zone interne métamorphique des Pyrénées centrales et orientales. Trois grandes phases d'amincissement ont pu être interprétées de manière à rendre compte de la complexité géométrique et de l'amincissement crustal de ces bassins rift.

Dans les premiers stades d'amincissement de la croûte continentale, la déformation extensive est contrôlée par la présence de deux niveaux de découplage/décollement non connectés correspondant à la croûte moyenne et aux évaporites du Trias supérieur. Le premier permet un découplage de la déformation entre la croûte supérieure et inférieure, tandis que le second permet le découplage de la déformation entre la croûte supérieure et les séries sédimentaires mésozoïques. L'amincissement ductile de la croûte inférieure, sans déformation cassante significative dans la croûte supérieure, s'accompagne de la formation d'un bassin de rift symétrique de type sag. Au cours de cette étape, le profil de dépôt entre les marges et l'axe du bassin est relativement symétrique et peu profond comme en témoigne le développement de plateformes carbonatées et l'absence de dépôt turbiditique. Au fur et à mesure de l'extraction latérale de la croûte inférieure (amincissement), les bordures du rift s'inclinent en direction du bassin provoquant le glissement de la couverture prerift. Des plis et des diapirs accompagnent ce glissement de couverture. Ce décollement entraine une dénudation des marges proximales du rift. Après cette dénudation de la crôute supérieure et la soustraction tectonique de la croûte inférieure, les marges proximales subissent une déformation fragile tandis que le futur domaine hyper-étiré enregistre un amincissement ductile de la croûte supérieure engendrant la formation d'un rift sensiblement symétrique. Cette différence de style de déformation entre les marges et le domaine central est directement liée à l'augmentation de la température dans la partie axiale la plus profonde du bassin. Celle-ci est due à l'enfouissement de la croûte continentale du domaine hyper-étiré sous une série sédimentaire synrift épaisse, et à un flux thermique anormal au cœur du bassin. Au cours de cette phase ultime d'hyperextension, la subsidence au centre du bassin est accrue. Le profil de dépôt s'incline de manière significative. Les pentes sédimentaires deviennent plus abruptes et une importante sédimentation gravitaire se met en place dans le bassin profond. La sédimentation contrôle donc très clairement le style de déformation extensive le long de ce type de système hyper-étiré qui nécessitent à la fois un niveau de décollement évaporitique prérift et une importante épaisseur de séries sédimentaires synrifts pour se développer.

Extended abstract

The processes responsible for continental crust hyperextension and sub-continental mantle exhumation have been widely studied for last decades, particularly in Atlantic-type conjugate passive margins thanks to the interpretations of borehole data and petroleum seismic reflection profiles. However passive margins are difficult to access and this requires to analyze these opening processes on fossils systems as in the Alps or in the Pyrenees. The latter orogenic belts result from the inversion of former hyperextended systems whose relics have been brought to the outcrop during the alpine compression. Although the geometry of these fossil systems has been recently studied, many unresolved questions remain: (1) What is the role of inheritance during the formation and inversion of a hyperextended rift system? (2) What specific role is played by the oblique transfer zones during opening and closure of a rift? (3) How does evolve in 3D the thermal gradient of a hyperextended rift system from the rifting to the post-orogenic phase? In this sense, the Western Pyrenean Mauléon basin allows to discuss the tectono-sedimentary and thermal evolution of a hyperextended rift through an entire Wilson cycle. To answer these questions, a multidisciplinary approach was developed: (1) field work along the inverted Iberian margin of the Mauléon basin and across the transfer zones segmenting its hyperextended domain (12 months, ~ 2500 observed points), (2) interpretation of 64 wells and 750 km of seismic reflection profiles, (3) 170 RSCM peak temperatures on 68 field samples and 102 borehole samples, (4) a numerical modeling reproducing the thermal evolution of the Mauléon basin since 120 Ma and (5) a 3D model of the Mauléon basin using an implicit modeling algorithm (GeoModeller software).

The results obtained on the Permian Bidarray basin and the Ursuya granulitic dome, localized on the western edge of the Mauléon basin, evidenced that the western Pyrenees evidenced the shift between N-S convergence recorded in the Pyrenean Axial Zone (310 to 290 Ma) and dominant E-W extension (290 to 275 Ma). Our results suggest that the crust throughout the Pyrenees (the foreland of the Variscan belt) stayed hot and partially molten during early and middle Permian extension. In this scenario, strain was vertically partitioned within the crust, with a homogeneously and longitudinally flowing lower crust and an upper crust affected by widespread N20° normal faults and longitudinal strike-slip faults. This stage confers a complex thermal (abnormally high gradient), structural (N20° brittle deformation in the upper crust and thinned continental crust) and rheological (granulites and migmatites exhumed in upper crustal position) inheritance to the Western Pyrenees lithosphere.

The preservation of the original Permian-Triassic paleogeography and structure in the « Basque Massif » indicates that there was no major east-west Mesozoic strike-slip motion between the Iberian and European plates, in this part of the Pyrenees, questioning the mechanisms responsible for the opening of the Early Cretaceous North-Pyrenean rift system. N20° transverse structures inherited from the Permian extension clearly control the opening of the Cretaceous rift system. At first order, the N20° Pamplona and Barlanès lithospheric transfer zones are respectively responsible for the shift towards the south of the Cretaceous rifting axis between the Mauléon and the Basque-Cantabrian basins and the local denudation of the sub-continental mantle in the vicinity of Urdach. At second order, N20° crustal transfer zones favor the development of diapiric systems and control the location of synrift depocenters in the Mauléon, Arzacq and Tartas basins.

The Cretaceous Mauléon hyperextended rift basin was inverted during the Alpine orogeny. In 2D, reactivation of the former rift structures leads to the formation of a lithospheric scale pop-up whose edges accommodate the same amount of shortening but with differing tectonic reactivation style, localized (Iberia) vs distributed (Europe). To the south, the Lakhoura thrust accommodated almost all of the shortening of the Iberian rift margin because it was the only inherited existing structure available for reactivation. To the north, the antithetic Saint-Palais thrust butted up against the Lakhoura thrust and consequently could not accommodate major shortening. The Triassic salt layer acted as a weak detachment upon which a thin-skinned nappe stack developed by offscraping the sedimentary cover rocks. This stack includes the north-verging Bellevue and Sainte-Suzanne thrusts

rooted in the South verging Lakhoura thrust fault. In the basement beneath the Triassic décollement, the blunt-ended European acted as a backstop that induced southward underplating of the European proximal margin, initiating a blind in-sequence duplex-like crustal stack that propagated downward. This basal accretion has also steepened the European crust-mantle contact. Another consequence was the crosscutting of the Lakhoura thrust, inhibiting any displacement on its northern portion. This process has allowed to keep the cool and strong subcontinental mantle beneath the former rift at shallow depth. Thus, the latter one acted as a major rigid buttress in the succeeding compressional stages as no major accommodation of the compressive strain was then possible in this block of shallow mantle.

In the Iberian margin, too, convergence was accommodated independently in the cover and the basement owing to the presence of a salt detachment layer. In the cover strata, northward underthrusting of the Iberian margin formed the thin-skinned South Pyrenean piggyback structures. In the basement, the Gavarnie and Guarga thrusts were successively incorporated into the Axial Zone antiformal crustal nappe stack. This sequence of thick-skinned thrusts led to the progressive steepening of the crust-mantle contact in the Iberian margin, which accentuated the pre-existing mantle protrusion beneath the former rift. This dome of strong mantle buttressed the Mauléon hyperextended rift domain against convergence from both north and south and inhibited further inversion. In 3D, the N120° thrusts systems edging the pop-up are composed of different antithetic thrust segments branching into the inherited Permian N20° transfer zones, highlighting the non-cylindrical geometry of the Pyrenean structures. This overall structural pattern define drawers like structures allowing the closure, by stages, of the former rift domain. The lithospheric Pamplona transfer zone acted as a major buttress inhibiting the localization of the compressive strain to the west and inducing the eastward formation of the Mauléon basin pop-up.

The synrift and post-collisional history of the Mauléon basin can be approach through its thermal evolution as shown by the tight relationships between thermicity and structural framework. Indeed, the area of highest paleo-gradient corresponds with the positive gravity anomaly, interpreted as the presence at shallow depth (~10 km) of subcontinental mantle. Synrift paleogeothermal gradients gradually increased from the margins (~ 34°C/km) to the basin (~ 60°C/km). Maximum peak temperatures are both controlled by sedimentary burial and high mantle heat flow, estimated by numerical modeling of ~ 100 mW.m-2. During the alpine inversion, the previously acquired isotherms were folded or tilted inside the Mauléon pop-up whose edges present differing postcollisional thermal responses.

On the European margin the paleo-isotherms have been northward transported and deformed onto the proximal margin without temperature increase until now. As a result, the pre-collisional maximum paleothermal gradients of both the hyperextended domain and the European margin have been preserved.

On the Iberian margin, the geothermal gradient increased as the footwall of the Lakhoura thrust underwent heating after the collision, which reset its precollisional paleogeothermal record. This gradient increase can be linked to the thickening of the Iberian continental crust following the formation of the antiformal crustal stack in the Axial Zone. In 3D, N20° transfer zones inherited from Permian time are also responsible for the segmentation of the synrift thermicity such as well in the preserved hyperextended domain as in the post-collisional thermicity of the Lakhoura thrust footwall.

At the beginning of the collision, the northward motion of the Iberian slab beneath the Mauléon hyperextended domain must be held accountable for a steep decrease in the asthenospheric heat flow and explains both the preservation of the pre-collisional thermal gradients and even the currently low geothermal gradient (25.0 ± 2.7°C/km) in the Mauléon basin core and European margin. Unlike the Iberian margin, the European one never underwent significant thick-skin tectonics and retained its current Moho depth of 25-27 km. Its quite low geothermal gradient is the consequence of the presence at shallow depth of nonradiogenic subcontinental mantle.

A review of the hyperextended Iberian-Eurasian plate boundary basins shows that these basins present a lot of common pattern:

(1) They are characterized by a hyperextended continental crust fitting with the thick synrift depocenter showing an elevated synrift paleothermal gradient or mantle heat flow, responsible for a HT/LP metamorphism;

(2) They often coincide with positive Bouguer anomaly due to the asthenospheric upwelling. Lower crust is very thin, or locally absent beneath the hyperextended domain;

(3) They are affected by a strong partitioning of the extensional deformation between the Mesozoic cover and the upper continental crust due to the presence of a thick prerift salt décollement level;

(4) They all present a relative symmetric shape, and record a basinward gliding of the prerift cover, marked by prerift cover rafts in the basin edges and a stretched but continuous cover on the hyper-extended domain;

(5) All these basins are characterized by an inherited abnormally thin continental crust before the Late Jurassic to Early Cretaceous hyperextension;

(6) In the most mature stage of their evolution, these basins are characterized by depocenter migration in response to progressive development of asymmetric detachments controlling their late architecture.

All these basins share at least one common synrift thinning stage and can be classified following their continental crust thinning maturity. Hence, they can be ranked from least mature to most mature as follows: (1) Tartas, (2) Arzacq, Columbrets and Camèros, (3) Parentis, (4) Basco-cantabric and Mauléon (5) Internal Metamorphic Zone basin of central and eastern Pyrenees. They strongly differ from classical Atlantic-type passive margins and have thus been defined as smooth slope extensional basins. Their major discrepancies with Atlantic type hyperextended margins are the lack of tilted crustal blocks in their central part and the dominant ductile deformation of the hyperextend domain continental crust.

Three main stages of continental crust thinning can be inferred to describe the smooth-slope type basins evolution of the Iberian-Eurasian plates.

During the first sag basin stage, continental crust thinning is dominantly controlled by pure shear mechanism and ductile thinning of the lower crust due to the presence of two major decoupling shear levels. Firstly, the middle crust allows the decoupling of the deformation between the upper and lower crust which was laterally extruding. Secondly, prerift Triassic salt décollement decouples deformation between the upper crust and the sedimentary cover. This thinning stage is responsible for the formation of symmetric sag basin characterized by a smooth sedimentary slope as evidenced by the development shallow carbonate platforms.

As the lateral extraction of the lower crust pursues (thinning), the rift edges tilted towards the future hyperextend domain inducing the basinward gliding of the sedimentary cover along the prerift salt décollement level. This transitional stage marks the shift to a dominated simple shear regime responsible for the development of an asymmetric rift system evidenced by depocenters migration. Indeed, once the cover-gliding operated, deformation is no longer decoupled on the basin's edge and extensional detachment fault roots at depth between the thinned crust and the top of the mantle. At the surface, they connect to salt décollement level. In this final hyperextensional stage, the sedimentary profile is steep and the basin records the deposition of thick synrift turbidites. The proximal margins undergo brittle deformation, with normal faults occurring, while the hyperextended domain suffers a whole ductile thinning. This discrepancy of the extensional deformation style is directly linked to the basinward increase of mantle heat flow associated with significant thickness of synrift deposits. In such a way, prerift and synrift sedimentation clearly controls the deformation style of smooth-slope type extensional basins, that primarily need a thick prerift salt level accommodating the extensional deformation and then allowing the storage of a thick prerift to synrift sedimentary pile in the necking zone and hyperextended domain.

Sommaire

Avant-propos p. 5

Remerciements p. 7

Résumé p. 13

Abstract p. 15

Résumé étendu p. 17

Extended abstract p. 21

Chapitre. 1. Introduction p. 29

1. Introduction générale p. 33

2. Objet de l'étude : les Pyrénées occidentales, le bassin de Mauléon p. 36

3. Questions et objectifs scientifiques p. 40

4. Méthodologies appliquées p. 48

5. Organisation du manuscrit de thèse p. 50

Chapitre. 2. Héritage Permien p. 63

Chapitre. 2.1. Analyse sédimentaire des séries du Permien et du Trias du bassin de Bidarray p. 67

1. Introduction p. 71

2. Sedimentary analysis p. 71

Chapitre. 2.2. Evolution tectono-sédimentaire d'un système de rift contrôlé par une extension post-orogénique permienne et la formation d'un dôme métamorphique (bassin de Bidarray et dôme de l'Ursuya, Pyrénées occidentales) p. 77

Résumé étendu p. 81

Abstract p. 87

1. Introduction p. 87

2. Geological settings p. 88

3. Facies association and depositional models p. 91

4. Tectono-sedimentary analysis p. 95

5. Structural scheme of the Basque massifs p. 98

6. Structural analysis of the Ursuya granulitic unit p. 98

7. Discussion p. 103

8. Conclusion p. 106

Chapitre. 3. Hyperextension crétacée **p. 115**

Chapitre. 3.1. Symétrie vs asymétrie d'un rift hyper-étiré : exemple du bassin de Mauléon (Pyrénées occidentales, France) **p. 119**

Résumé étendu p. 123

Abstract p. 127

1. Introduction p. 127

2. Geological settings p. 128

3. The southern margin of the Mauléon basin from field observations p. 132

4. Seismic interpretation of the Mauléon basin and the southern part of the Aquitain basin p. 141

5. Top Jurassic to Cenomanian tectono sedimentary and geodynamic evolution of the Mauléon basin p. 145

6. Discussion and Conclusion p. 148

Chapitre. 3.2. Révision de l'enregistrement sédimentaire albo-cénomanien du bassin de Mauléon / Saint-Jean-de-Luz : polyphasage du glissement de la couverture le long du décollement salifère du Trias au cours de l'hyperextension crétacée (Pyrénées occidentales) **p. 163**

Résumé étendu p. 167

Abstract p. 169

1. Introduction p. 169

2. Geological settings p. 170

3. Methodology p. 173

4. Lithostratigraphic units p. 174

5. Boreholes observations p. 191

6. Tectono-sedimentary evolution of the Iberian rift margin p. 193

7. Discussion p. 199

8. Conclusions p. 201

Chapitre. 3.3. Rôle de l'héritage structural et de la tectonique salifère sur la formation des bassins de rift pseudo-symétriques d'Arzacq et de Tartas au cours de la phase d'hyperextension crétacée inférieure (sud-ouest de la France) **p. 207**

Résumé étendu p. 211

Abstract p. 213

1. Introduction p. 213

2. Geological settings p. 214

3. Methodology p. 216

4. Seismic profiles and well calibration p. 216
5. Seismic interpretation p. 222
6. Tectono-sedimentary evolution of the Aquitaine basin p. 226
7. Discussion p. 229
8. Conclusion p. 232

Chapitre.4. Orogenèse pyrénéenne **p. 243**

Chapitre. 4.1. Fermeture d'un système de rift hyper-étiré dans un pop-up orogénique lithosphérique : Rôle buttoir du manteau et impact de l'héritage structural du rifting crétacé **p. 247**

Résumé étendu p. 251
Abstract p. 253
1. Introduction p. 253
2. Rift inheritance in the Mauléon basin p. 253
3. Restauration of western Pyrenees cross section p. 254
4. Inversion modes during Pyrenean compression p. 257

Chapitre. 4.2. Zone de transfert lithosphériques contrôlant la non-cylindricité de l'orogenèse pyrénéenne (bassin hyper-étiré de Mauléon) **p. 263**

Abstract p. 267
1. Introduction p. 267
2. The North Pyrenean Zone: reactivation of a hyperextended rift p. 268
3. Methodology, data and results p. 270
4. Discussion p. 280
5. Conclusion p. 288

Chapitre. 5. Evolution thermique Mésozoïque à Cénozoïque **p. 295**

Chapitre. 5.1. Paléo-gradients géothermiques au sein d'un système rift hyper-étiré réactivé : exemple du rift fossile de Mauléon (Pyrénées occidentales) **p. 297**

Résumé étendu p. 303
Abstract p. 307
1. Introduction p. 307
2. The Mauléon basin Rift Domains and Sedimentary Infill p. 308
3. The Cretaceous Pyrenean Metasomatic Event p. 309
4. Methods p. 311
5. Results p. 312

6. Discussion p. 325

7. Conclusion p. 330

Chapitre. 6. Synthèse et Discussion **p. 345**

Chapitre. 6.1. Synthèse des principaux résultats **p. 349**

1. Le Permien, un héritage structural, thermique et rhéologique complexe de la lithosphère des Pyrénées occidentales p. 353

2. Implications de l'héritage permien sur la phase d'hyper-extension crétacée p. 354

3. Les bassins de Mauléon, Arzacq et Tartas : un nouveau type de rift hyper-étiré p. 354

4. Rôle de l'héritage crétacé au cours de l'orogenèse alpine p. 355

5. Les zones de transferts N20° à l'origine de la non-cylindricité des Pyrénées p. 356

6. Rôle de l'héritage permien et crétacé sur l'évolution thermique du rift nord-pyrénéen depuis sa création jusqu'à son inversion p. 357

Chapitre. 6.2. Discussion. « Smooth-slopes extensional basins » : En quoi l'enfouissement et le sel prérift contrôlent ils le style de déformation au cours de l'hyperextension ? **p. 359**

Résumé étendu p. 363

Abstract p. 365

1. Introduction p. 365

2. The Iberian-European plates Mesozoic basins p. 366

3. Tectono-sedimentary evolution of a smooth-slope type extensional basin p. 375

4. Atlantic-type vs smooth slope-type margins p. 378

5. Conclusion p. 381

Chapitre. 7. Conclusions **p. 393**

Annexe. 1 **p. 403**

Chapitre 1

Introduction

Chapitre 1. Introduction

Sommaire

1. Introduction générale p. 33

1.1. Du modèle de blocs basculés (1978) au modèle en cisaillement simple (1985) p. 33

1.2. L'exhumation du manteau sous-continental le long des marges passives p. 35

1.3. Le modèle d'amincissement polyphasé façonnant les marges hyper-étirées p. 35

2. Objet de l'étude : les Pyrénées occidentales, le bassin de Mauléon p. 36

3. Questions et objectifs scientifiques p. 40

3.1. Quel est l'héritage Permien dans les Pyrénées occidentales ? p. 40

3.2. Le rift nord pyrénéen est-il comparable aux marges hyper-étirées atlantique ? p. 41

3.3. L'héritage d'un système hyper-étiré contrôle-t-il la géométrie d'un orogène ? p. 42

3.4. Les zones de transferts impactent-elles la réactivation d'un rift hyper-étiré ? p. 44

3.5. Comment évolue le gradient thermique d'un système de rift hyper-étiré en 3D, du rifting à la phase post-compressive ? p. 45

4. Méthodologies appliquées p. 48

4.1. Approche terrain p. 48

4.2. Géo-référencement des données p. 48

4.3. Interprétation sismique, données de forages et transect diagraphique p. 48

4.4. Modélisation 3D du bassin de Mauléon p. 49

4.5. Spectroscopie Raman p. 49

4.6. Simulation numérique de l'évolution thermique du bassin de Mauléon p. 50

5. Organisation du manuscrit de thèse p. 50

Chapitre 1. Introduction

1. Introduction Générale

Depuis les années 1980, l''essor de l'exploration pétrolière et l'amélioration continue des techniques visant à imager la croûte continentale, ont permis d'améliorer de manière significative la compréhension de la morphologie des marges passives, et d'en explorer les différents types. Au premier ordre, le type de marge passive est essentiellement contrôlé par la cinématique des plaques, i.e. la direction d'extension.

Trois grandes familles sont alors distinguables **(Fig. 1)** : (1) les marges passives obliques à hyper-obliques dont l'ouverture est caractérisée par une extension oblique par rapport à la direction du rift et dont les exemples les plus étudiés correspondent aux systèmes du Golfe d'Aden (d'Acremont et al., 2005; Leroy et al., 2012; Autin et al., 2013; Bellahsen et al., 2013) et du Rift Est Africain (Morley et al., 1990; Chorowicz and Sorlien, 1992; Corti et al., 2007; Basile, 2015; Mortimer et al., 2016) (2) les marges transformantes, régies par une extension purement décrochante, et de fait parallèle à la direction du rift, induisant l'ouverture de bassin de type « pull-apart » (Aydin and Nur, 1982; Zhang et al., 1989; McClay and Dooley, 1995; Petrunin and Sobolev, 2006; Gürbüz, 2010) et (3) les marges passives divergentes caractérisées par une extension orthogonale à la direction du rift. Ces marges peuvent être faiblement magmatiques, exemple des marges Ibérie/Terre-Neuve (Manatschal et al., 2001; Whitmarsh et al., 2001; Wilson et al., 2001; Mohn et al., 2015) ou riches en magma, exemple de la marge brésilienne ou des Afar (Geoffroy, 2005; Geoffroy et al., 2014).

Le système de rift pyrénéen, objet de la présente étude, est considéré comme un système de rift divergent et faiblement magmatique. Les prochains paragraphes décrivent donc les processus régissant l'amincissement de la croûte continentale le long de ces systèmes.

1.1. Du modèle de blocs basculés (1978) au modèle en cisaillement simple (1985)

L'extension en cisaillement pur (McKenzie, 1978) conduit au développement de failles normales listriques, dont la déformation est accommodée par le basculement des blocs crustaux et le développement de structures syn-sédimentaires en éventails (**Fig. 2A** ; Faure et Chermette., 1989). Le taux d'extension crustale (facteur β) associé à ce style structural est en général inférieur à 2. La croûte continentale et le manteau-sous continental présentent un facteur β équivalent, conduisant au développement d'un système de rift symétrique. Le modèle en cisaillement pur ne peut cependant pas s'appliquer pour expliquer l'amincissement des domaines distaux des marges passives actuelles présentant des facteurs β très largement supérieurs à 2 (**Fig. 2B**; Manatschal et al., 2001; Whitmarsh et al., 2001; Wilson et al., 2001).

Le concept de faille de détachement est né de l'étude des « Metamorphic Core Complex » présent dans la zone des « basin and Range » aux Etats Unis. Ces domaines intracontinentaux ont subi une importante extension (**Fig. 3A**; Wernicke, 1981; Wernicke and Burchfiel, 1982; Davis, 1983; Fletcher and Hallet, 1983; Spencer, 1984; Hamilton, 1987; Wernicke and Axen, 1988). L'amincissement de ces domaines résulte d'une déformation extensive en cisaillement simple, provoquant le développement de failles normales listriques qui se branchent sur une faille plate. Cette dernière, dite faille de détachement, recoupe la lithosphère (Wernicke, 1985; Lister et al., 1986; Boillot et al., 1987; Lemoine et al., 1987). Le déplacement le long de ces structures lithosphériques engendre l'exhumation de roches granulitiques (croûte inférieure) et / ou de manteau sous-continental. Ces structures sont caractérisées par un facteur $\beta > 2$. Le décalage de la zone de remontée de l'asthénosphère par rapport à la zone de subsidence tectonique en surface induit une asymétrie prononcée des bordures conjuguées de ces systèmes extensifs. Ceci permet de différentier la « lower plate » de la « upper plate », correspondant respectivement au « footwall » et au « hanging-wall » du détachement (**Fig. 3B**; Lister et al., 1986). L'exhumation le long de ces failles conduit de manière générale à une inflexion de la faille par isostasie et à la formation de structures de type « rolling-hinge » (Spencer, 1984; Buck, 1988; Lavier et al., 1999).

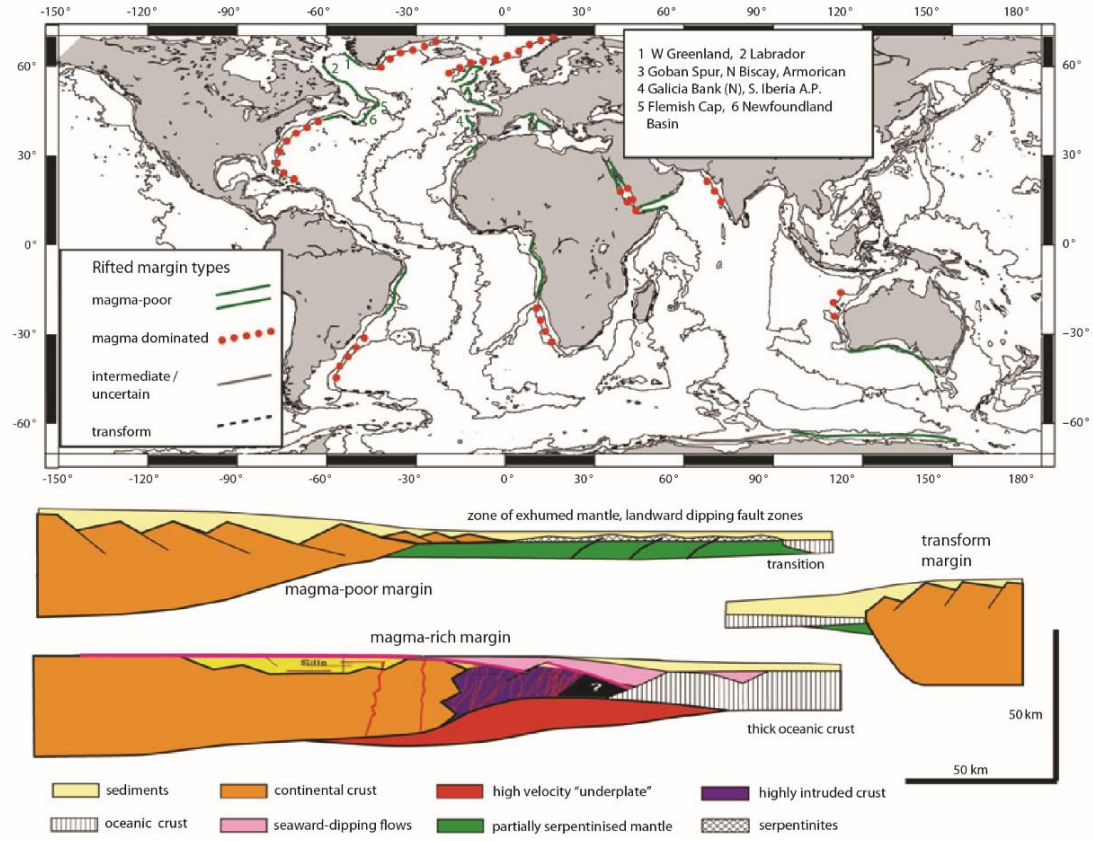


Fig. 1. Distribution mondiale des différents types de marges, i.e. marges faiblement magmatiques, marges magmatiques et marges transformantes (Reston and Manatschal, 2011).

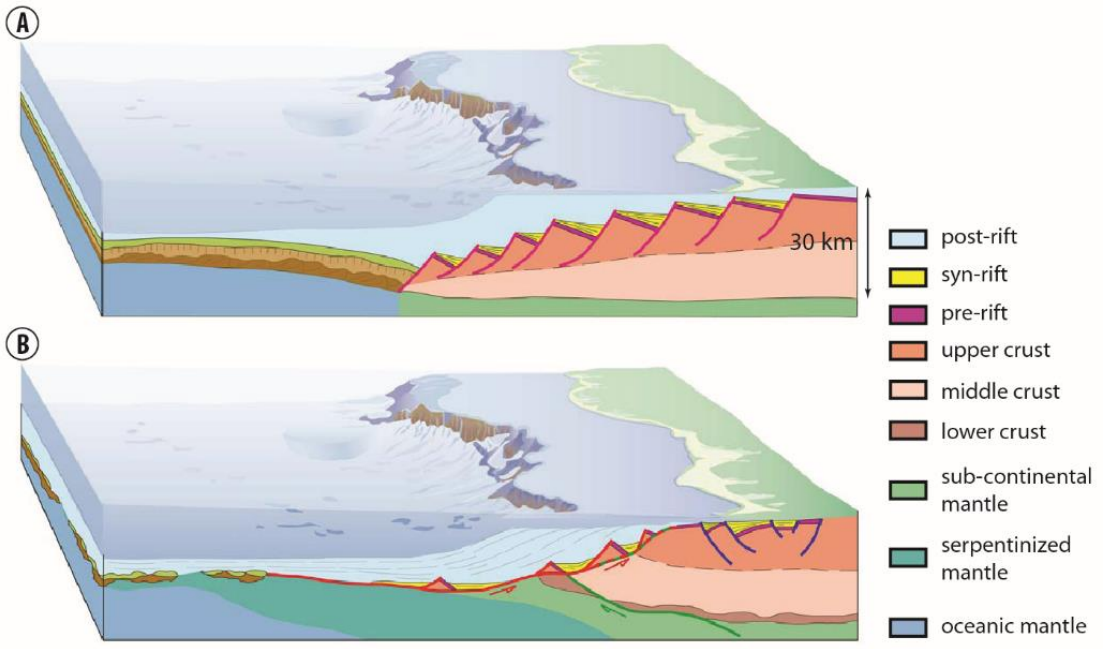


Fig. 2. Représentation schématique 3D de marges passives pauvres en magma **(A)** Représentation classique mettant en évidence des séries prérifts, synrifts et postrifts au-dessus d'une croûte continentale uniformément amincie. La croûte continentale supérieure est affectée par des failles normales listriques, tandis que la croûte inférieure est amincie de manière ductile ; **(B)** Représentation moderne de la géométrie complexe de la transition entre l'océan et le continent, résultant de l'exhumation du manteau sous-continental le long de failles de détachements transportant des blocs allochtones formés de croûte continentale. La croute océanique et le domaine continental sont alors séparés par une zone d'exhumation du manteau (Péron-Pinvidic and Manatschal, 2009).

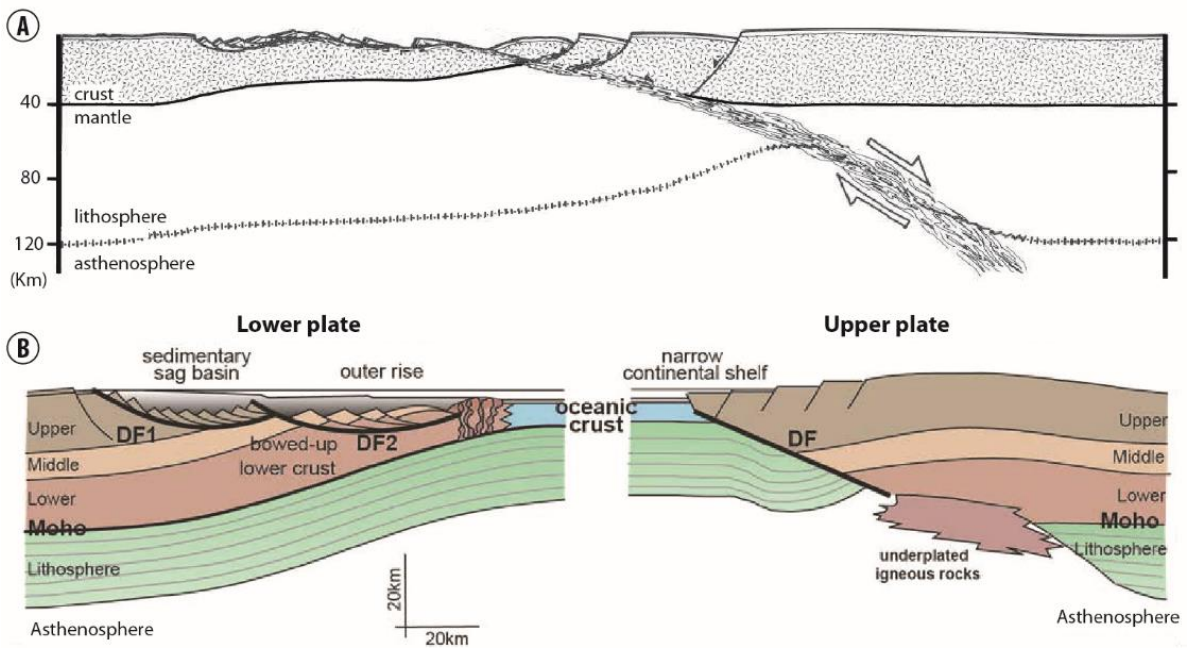


Fig. 3. (A) Amincissement de la lithosphère par cisaillement simple (Wernicke., 1985); **(B)** Représentation schématique de la géométrie d'une upper plate et d'une lower plate. DF, faille de détachement (Lister et al., 1986, modifié par Péron-Pinvidic et Manatschal., 2009).

Les zones de détachements sont le lieu d'une circulation préférentielle de fluides hydrothermaux, responsables, notamment, de la serpentinisation du manteau sous-continental (Manatschal et al., 2001; McCaig et al., 2007). Ce processus engendre la diminution du coefficient de friction le long de la faille et favorise l'exhumation du manteau sous-continental dans les stades ultimes de l'extension (Escartín et al., 1997, 2001; Lundin and Doré, 2011).

1.2. L'exhumation du manteau sous-continental le long des marges passives

Le concept de cisaillement simple développé par Wernicke.(1985) a ensuite été appliqué pour expliquer l'exhumation de manteau sous continental le long des domaines distaux des marges passives, dont les exemples les plus étudiés sont ceux de la plaine abyssale ibérique (Boillot et al., 1980) et des paléo-marges austro-alpines (Froitzheim and Manatschal, 1996; Manatschal and Nievergelt, 1997). La reconnaissance des détachements le long des marges passives a été rendu possible grâce à l'amélioration de l'imagerie sismique et l'identification du marqueur sismique S, qui a dans un premier temps été interprété comme une zone de cisaillement intra-crustale (de Charpal et al., 1978), et dans un second temps comme un détachement lithosphérique recoupant le Moho et favorisant l'exhumation du manteau sous-continental (Boillot et al., 1987, 1989). Au début des années 2000, plusieurs forages réalisés par le consortium de recherche « Ocean Drilling Program » dans la plaine abyssale ibérique ont permis de recouper ces discontinuités majeures et de montrer que l'exhumation du manteau était rendu possible grâce au développement de plusieurs détachements (Manatschal et al., 2001; Whitmarsh et al., 2001). Les coupes restaurées du système conjugué Ibérie/Terre-neuve, ont mis en évidence que les détachements se développent une fois que la croûte continentale présente une épaisseur inférieure à 10 km. L'amincissement de la croûte précédant l'initiation des détachements joue donc un rôle majeur et a été suggérée comme étant accommodée soit par le : (1) boudinage de la croûte inférieure (Reston, 1988), (2) fluage de la croûte inférieure vers la marge proximale (Brun and Beslier, 1996) ou vers le domaine distal (Driscoll and Karner, 1998) ou (3) le développement de plusieurs séquences de failles normales (Reston, 2005, 2007).

1.3. Le modèle d'amincissement polyphasé façonnant les marges hyper-étirées

La complexité structurale des marges passives atlantiques et alpines a conduit certains auteurs à proposer un modèle d'amincissement polyphasé (Whitmarsh et al., 2001; Manatschal, 2004; Lavier and Manatschal, 2006). Il se décompose en trois phases de rifting, aboutissant à la rupture

lithosphérique et l'exhumation du manteau sous-continental. Dans ce modèle d'amincissement crustal, le facteur β augmente de manière significative en direction du domaine distal du système de rift.

La phase d'étirement ou de « stretching » est assimilable à une phase de déformation cassante. Elle affecte la croûte supérieure et permet son amincissement par le biais de failles normales raides s'encrant dans la croûte moyenne et délimitant des bassins, en demi-grabens ou grabens. Ces derniers sont caractérisés par un remplissage sédimentaire en éventail (**Fig. 4A**; Manatschal, 2004). L'étape d'étirement de la croûte continentale s'opère selon un cisaillement pur de type McKenzie., 1978. Durant cette étape, la déformation est découplée à l'échelle de la croûte continentale, du fait d'un niveau ductile correspondant à la croûte moyenne (Buck, 1991). Cette première phase de rifting permet d'acquérir la morphologie des futures marges proximales **(Fig. 5)**. Le facteur β de ce domaine n'excède jamais 2 (Pérez-Gussinyé and Reston, 2001) et l'épaisseur crustale oscille entre 30±5 km (Péron-Pinvidic et al., 2013). Les marges proximales d'Ibérie et de Terre-Neuve sont respectivement caractérisées par le développement des bassins en graben et demi-graben de Jeanne d'Arc (Driscoll et al., 1995) et de Péniche (Alves et al., 2006).

La phase d'amincissement ou « thinning » enregistre l'amincissement de la croûte continentale de 30 à 10 km d'épaisseur, par boudinage et déformation ductile de la croûte moyenne (**Fig. 4B**; Lavier and Manatschal, 2006). Cette phase est responsable de l'édification de la zone de « necking » correspondant à un domaine d'amincissement brutal de la croûte continentale lié au développement de détachements ou failles listriques **(Fig. 5)**. Lorsque la croûte moyenne ductile a été soustraite, la déformation est alors couplée à l'échelle de toute la croûte qui se déforme de manière fragile. Cet amincissement brutal a été clairement mis en évidence par imagerie sismique le long des marges passives atlantiques, Angola/Brésil (Contrucci et al., 2004; Unternehr et al., 2010; Péron-Pinvidic et al., 2015), Ibérie/Terre-Neuve (Péron-Pinvidic et al., 2007; Péron-Pinvidic and Manatschal, 2009) et Groenland/Norvège (Osmundsen and Ebbing, 2008; Osmundsen and Péron-Pinvidic, 2018). Ce domaine est généralement formé de bassins synrifts présentant une épaisseur sédimentaire supérieure aux grabens composant la marge proximale (Péron-Pinvidic et al., 2013) et un facteur β supérieur à 2 (Pérez-Gussinyé and Reston, 2001).

La phase d'exhumation est responsable de l'amincissement de la croûte continentale d'une épaisseur de 10km à 0km (**Fig. 4C**; Whitmarsh et al., 2001; Lavier and Manatschal, 2006). Cette étape entraine la dénudation du manteau sous-continental le long de détachements affectant le Moho et étant caractérisés par un facteur β pouvant dépasser 10 (Pérez-Gussinyé and Reston, 2001). Elle permet l'édification d'une zone de transition océan-continent complexe présentant des blocs allochtones composés de croûte continentale et de séries prérifts basculées (**Fig. 5**; Péron-Pinvidic et al., 2007; Péron-Pinvidic and Manatschal, 2009; Masini et al., 2011, 2013). Il s'en suit une phase de rupture asthénosphérique qui engendre la formation d'un domaine de croûte océanique et l'individualisation des marges passives conjuguées (**Fig. 4D**).

L'identification de ces grands domaines structuraux jalonnant le système de rift hyper-étiré va représenter un enjeu majeur au cours de ces travaux de thèse. En effet, chacun de ces domaines présente des caractéristiques qui lui sont propres (Péron-Pinvidic et al., 2013), et attestent d'un héritage structural, rhéologique et thermique complexe.

2. Objet de l'étude : les Pyrénées occidentales, le bassin de Mauléon

Le développement du système de rift nord pyrénéen **(Fig. 6A)** est synchrone de l'ouverture du bassin hyper-étiré de Parentis (Pinet et al., 1987; Choukroune et al., 1990; Jammes, 2009; Jammes et al., 2010c; Ferrer et al., 2012) et des marges passives faiblement magmatiques du Golfe de Gascogne, caractérisées par un manteau sous-continental probablement exhumé à la transition océan-continent (Thinon, 1999; Thinon et al., 2003; Ferrer et al., 2008; Jammes et al., 2010a, 2010b; Roca et al., 2011; Tugend et al., 2014). Les modalités contrôlant l'ouverture du système de rift pyrénéen restent à ce jour controversées.

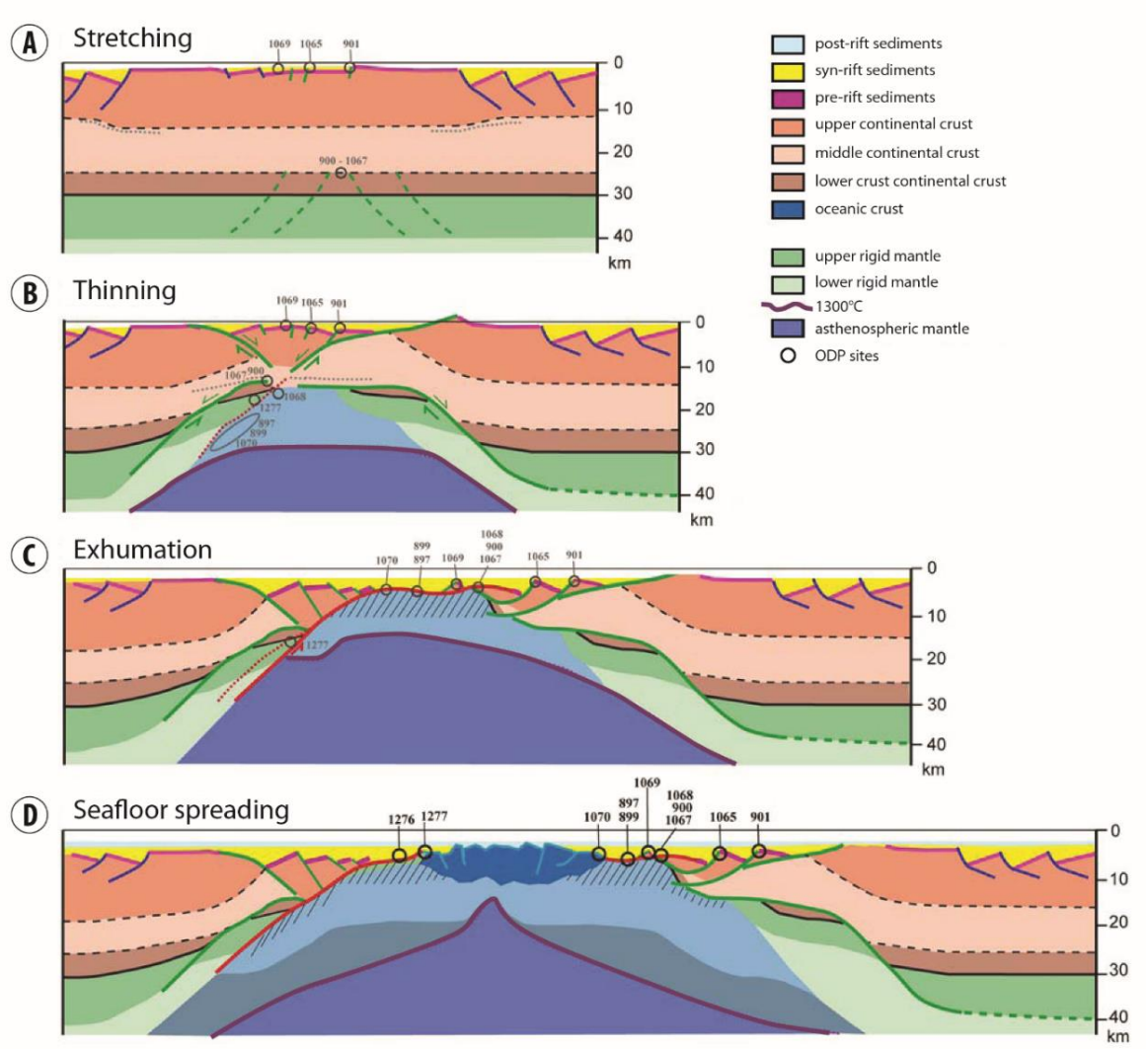


Fig. 4. Modèle conceptuel schématique montrant l'évolution d'une phase de rifting, sur la base des données récoltées le long des marges passives Ibérie/Terre-Neuve **(A)** La phase d'étirement est caractérisée par le développement de failles normales listriques affectant la croûte supérieure. Ces structures sont associées au développement de demi-grabens subsidents ; **(B)** La phase d'amincissement est caractérisée par le développement d'un système de détachements conjugués qui accommode l'exhumation de croûte moyenne à inférieure et/ou de manteau sous le block-H. Ce mode déformation est à la jonction entre un mode de déformation distribué et localisé ; **(C)** La phase d'exhumation est caractérisée par le développement de détachements qui recoupent la croûte continentale fragilisée et exhument le manteau sous-continental serpentinisé sur le fond du bassin rifté ; **(D)** La phase d'accrétion océanique responsable de l'individualisation des marges passives conjuguées et de l'individualisation d'une proto-croûte océanique (Péron-Pinvidic et Manatschal., 2009).

Les modèles cinématiques des plaques ibériques et européennes diffèrent en fonction des données qu'ils intègrent, i.e. données de terrains le long de la zone nord pyrénéenne, données offshore dans le Golfe de Gascogne et / ou reconstitution des anomalies magnétiques de la partie méridionale de l'Océan Atlantique Nord **(Fig. 6A)**. Deux grandes familles de modèles cinématiques s'opposent : (1) les modèles cinématiques proposant une ouverture en ciseaux du Golfe de Gascogne (Schoeffler, 1965; Souquet et al., 1977; Peybernès, 1978; Ducasse and Vélasque, 1988; Masson and Miles, 1984; Sibuet et al., 2004) (2) les modèles proposant une ouverture le long d'un grand décrochement Est-Ouest correspondant au tracé de la Faille Nord Pyrénéenne qui permet le coulissage vers l'est de la plaque ibérique par rapport à son homologue européenne (Le Pichon et al., 1971; Le Pichon and Sibuet, 1971; Choukroune et al., 1973a, 1973b; Choukroune and Mattauer, 1978; Olivet, 1996). Le dernier modèle d'ouverture engendre le développement de bassins de rifts syn-cinématiques de type pull-apart (Debroas, 1978, 1987, 1990; Canérot, 2017). Un modèle alternatif propose que le décrochement s'opère au cours du Jurassique supérieur à Aptien inférieur et que l'ouverture du système de rift nord pyrénéen soit orthogonale (Jammes, 2009; Jammes et al., 2009).

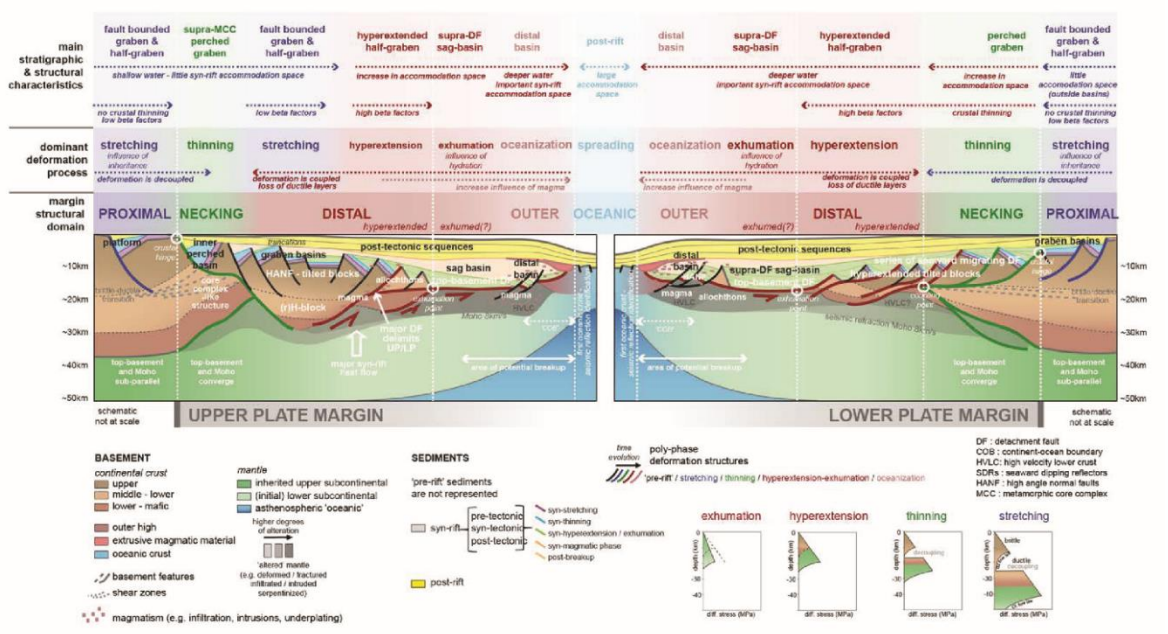


Fig. 5. Diagramme schématique résumant les principales caractéristiques structurales et stratigraphiques d'une upper plate d'une lower plate en fonction du domaine structural d'une marge passive (Péron-Pinvidic et al., 2015).

Le développement récent des concepts relatifs aux marges passives hyper-étirés a conduit certains auteurs à considérer le système de rift nord pyrénéen comme résultant de processus d'hyper-amincissement de la croûte continentale (Lagabrielle et al., 2010, 2016; Clerc et al., 2012, 2014, 2015, 2016; de Saint Blanquat et al., 2016; Teixell et al., 2016, 2018; Hart et al., 2017). A première vue, le bassin hyper-étiré de Mauléon **(Fig. 6B-E)**, présente des similitudes avec les marges passives atlantiques, à savoir :

(1) la présence d'une anomalie gravimétrique positive centrée sous le bassin (**Fig. 6B**; Grandjean, 1992, 1994; Casas et al., 1997), qui a récemment été interprétée comme la présence de manteau sous-continental à faible profondeur, (**Fig. 6D**; Wang et al., 2016; Wang, 2017),

(2) la présence de migmatites/granulites (Viennot and Kieh, 1928; Vielzeuf, 1984), dont l'exhumation a récemment été considérée comme prenant place au cours du rifting crétacé (**Fig. 6E**; Jammes et al., 2009; Masini et al., 2014; Hart et al., 2016, 2017),

(3) le remaniement de manteau sous-continental dans les séries synrifts albiennes (Roux, 1983; Duée et al., 1984; Fortané et al., 1986; Debroas et al., 2010), s'opérant le long d'un système de détachement actif au cours de la sédimentation (Lagabrielle and Bodinier, 2008; Jammes et al., 2009; Masini et al., 2014; Corre et al., 2016).

Bien que les Pyrénées résultent de l'inversion du système de rift mésozoïque nord pyrénéen (Souquet et al., 1977; Puigdefàbregas and Souquet, 1986; Vélasque and Ducasse, 1987; Ducasse and Vélasque, 1988; Puigdefàbregas et al., 1992), le bassin de Mauléon est exceptionnellement préservé **(Fig. 6C)** et permet de discuter :

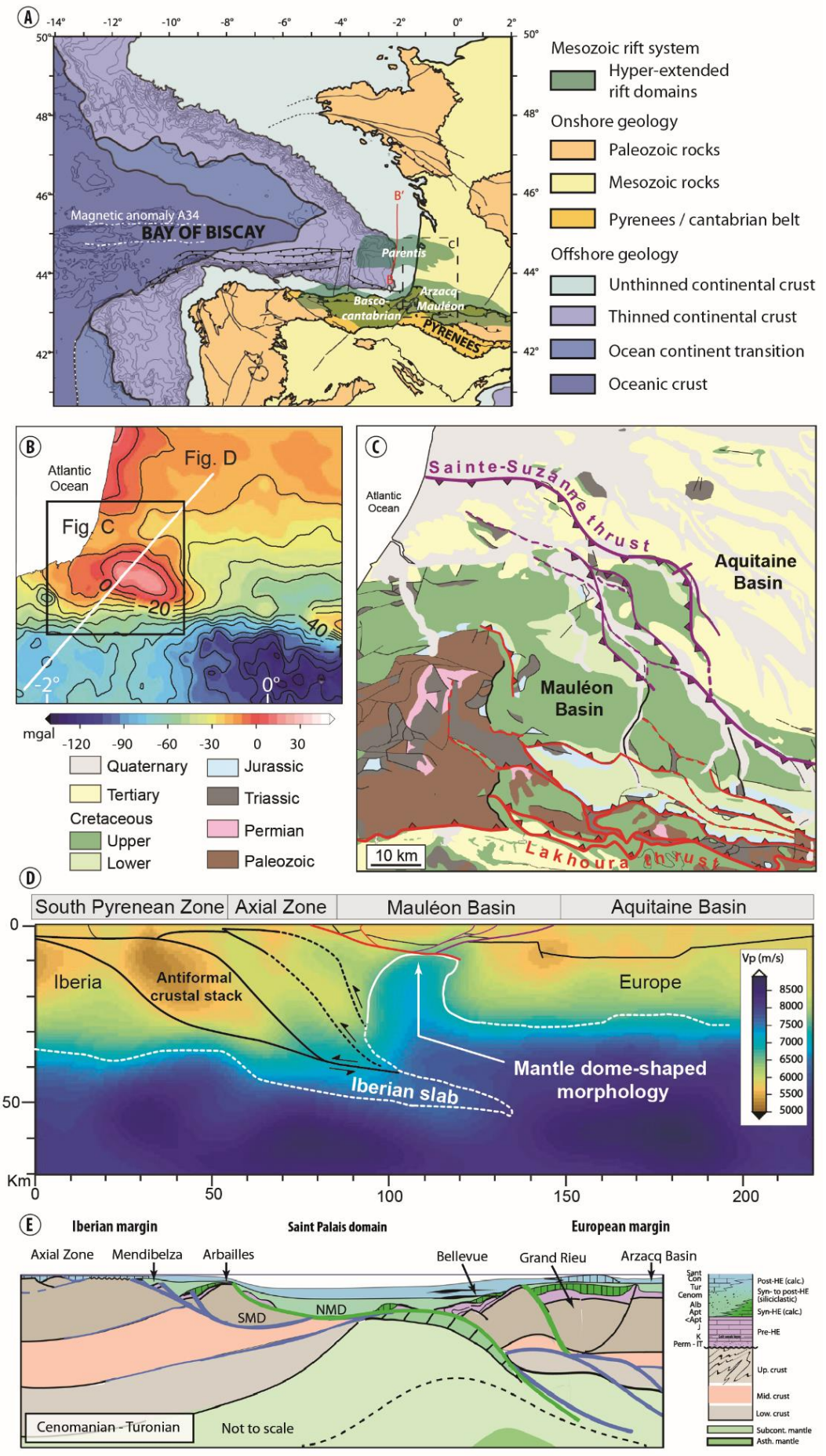
(1) de l'héritage complexe de la phase tardi-varisque et de son implication, portant à la fois sur la phase d'hyperextension crétacée et sur la phase de réactivation tertiaire,

(2) des modalités d'ouverture des bassins nord-pyrénéens et des processus responsables de l'hyperextension de la croûte continentale,

(3) de l'enregistrement tectono-sédimentaire d'un système de rift présentant une importante quantité de séries synrifts

(4) de l'impact de l'héritage lié à la phase d'hyperextension, sur l'inversion du bassin

(5) de l'évolution de la thermicité d'un système de rift, de sa création à sa réactivation.



Légende sur la page suivante

Fig. 6. (A) Carte du Golfe de Gascogne et des Pyrénées mettant en évidence les domaines orogéniques pyrénéens ainsi que le système de rift hyper-étiré crétacé (Manatschal et al., 2014); **(B)** Carte de l'anomalie gravimétrique de Bouguer des Pyrénées mettant en évidence l'anomalie positive centrée sur le bassin de Mauléon (modifiée d'après Chevrot et al., 2018); **(C)** Carte géologique du bassin de Mauléon, mettant en évidence la préservation du bassin au sein d'une structure en pop-up; **(D)** Modèle Vp résultant de l'inversion de données de sismique passive (modifié d'après Wang et al., 2016); **(E)** Modèle tectono-sédimentaire synthétique 2D de la section de rift Mauléon-Arzacq durant le stade post-tectonique du Cénomanien au Turonien (modifié d'après Masini et al., 2014). La croûte continentale est amincie au cours de l'Albien-Cénomanien par l'intermédiaire de détachements diachrones et à pendages vers le nord. SMD: le Détachement Sud Mauléon; NMD: le Détachement Nord Mauléon; HE: Hyperextension.

3. Questions et objectifs scientifiques

3.1. Quel est l'héritage permien dans les Pyrénées occidentales ?

La lithosphère continentale ne doit pas être considérée comme un simple empilement de couche (« layer cake ») thermiquement équilibrée **(Fig. 7A),** dans la mesure où ses propriétés sont complexes et modelées par les différentes étapes géodynamiques qui l'affectent. Une lithosphère continentale peut présenter un héritage complexe, i.e. structural, rhéologique et / ou thermique (Manatschal et al., 2015) **(Fig. 7B)**. Le développement des systèmes de rifts est impacté par de nombreux paramètres, tels que l'activité magmatique (Handy, 1989), l'épaisseur initiale de la croûte continentale (Bassi, 1991; Buck, 1991), ou encore l'épaisseur élastique de la lithosphère (McNutt et al., 1988; Lin and Watts, 2002). La présence de structures héritées dans la croûte supérieure, telles que des bassins de rift intracontinentaux post orogéniques, représentent un héritage majeur. Ils contrôlent, notamment, le développement des structures extensives dans les stades précoces de l'amincissement de la croûte supérieure, favorisant la localisation de la déformation (Mohn et al., 2010; Manatschal et al., 2015).

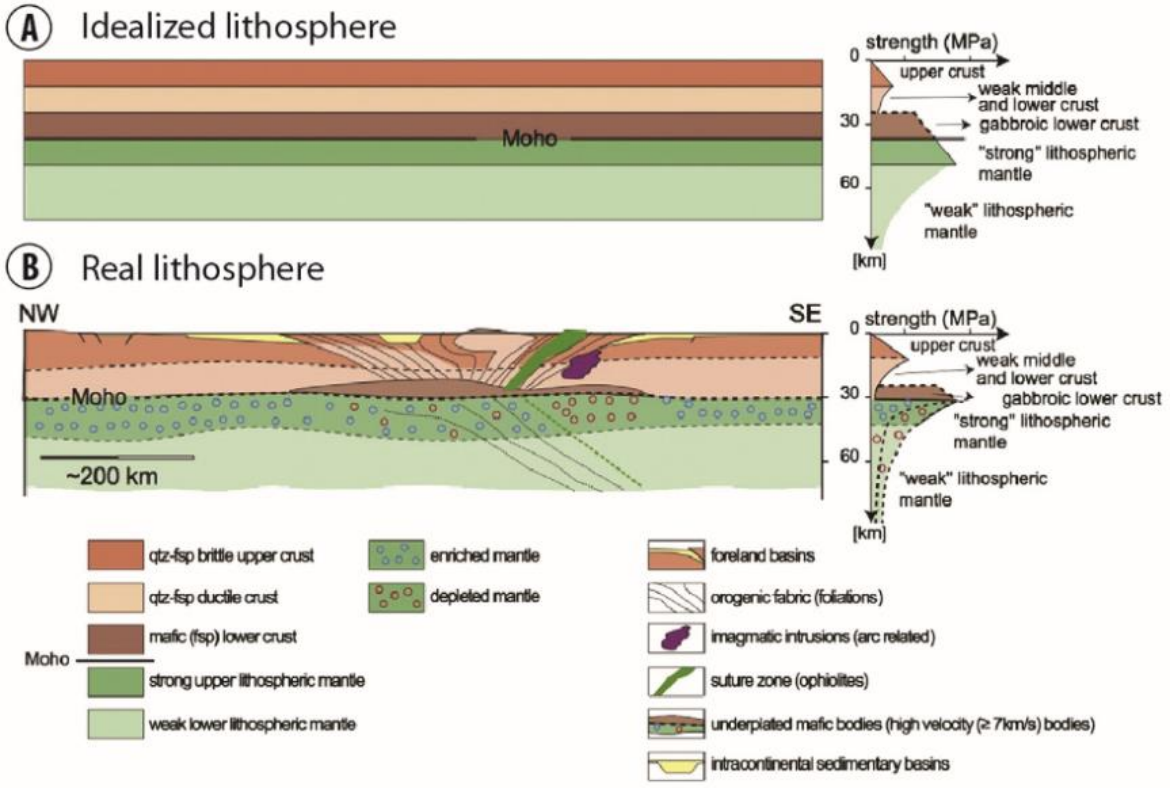


Fig. 7. Coupes d'échelle lithosphérique montrant **(A)** une lithosphère idéale et thermiquement équilibrée ; **(B)** une réelle lithosphère post-orogénique présentant une complexité liée à un héritage structural et rhéologique (Manatschal et al., 2015).

L'épisode varisque constitue un contexte favorable au développement des « Metamorphic Core Complex », qui exhument des unités migmatitiques et granulitiques en position relativement haute dans la croûte continentale, conférant un important héritage structural, rhéologique et thermique à la lithosphère européenne (Echtler and Malavieille, 1990; Malavieille et al., 1990; Van Den Driessche and Brun, 1992; Burg et al., 1994; Roger et al., 2015).

L'extension de la croûte continentale européenne au cours du Permien a été accommodée par la formation de nombreux bassins sédimentaires intracontinentaux post-orogéniquesdans les Pyrénées (Lucas, 1985; Bixel and Lucas, 1987) et le Massif Central (Echtler and Malavieille, 1990; Brun and van den Driessche, 1994; Pochat and Van Den Driessche, 2011), conférant un important héritage à la croûte continentale. La relation entre la formation de ces bassins sédimentaires et l'exhumation des granulites n'a jamais été étudiée dans les Pyrénées. En effet, les principales études portent sur les environnements de dépôts des séries permo-triasiques et le volcanisme alcalin associé (Lucas, 1968, 1977, 1985; Bixel and Lucas, 1983; Lago et al., 2004; Gretter et al., 2015; Mujal et al., 2016; Lloret et al., 2018).

Dans les Pyrénées occidentales, cet important héritage structural et thermique doit être défini avec précision, de manière à comprendre son impact potentiel sur les phases géodynamiques ultérieures, i.e. hyperextension crétacée et compression tertiaire. Le bassin Permien de Bidarray, localisé dans les Pyrénées occidentales, n'a été que très peu déformé au cours de la récente orogenèse pyrénéenne et constitue donc un lieu favorable pour appréhender l'héritage structural de ces bassins post-orogéniques. De plus, il est situé immédiatement au sud des granulites tardi-varisques du massif de l'Ursuya, ce qui en fait un lieu clé pour étudier la réponse structurale de la croûte supérieure et inférieure au cours de l'extension régionale post-orogénique varisque.

3.2. Le rift nord pyrénéen est-il comparable aux marges hyper-étirées atlantiques ?

Les modèles récents de marges hyper-étiré classiques ont été définis sur la base des marges de type atlantique, i.e. Angola/Brésil (Karner et al., 2003; Contrucci et al., 2004; Karner and Gambôa, 2007; Aslanian et al., 2009; Unternehr et al., 2010; Moulin et al., 2010; Aslanian and Moulin, 2013; Péron-Pinvidic et al., 2015), Ibérie/Terre-Neuve (**Fig. 8A**; Boillot et al., 1980, 1995; Reston et al., 1995; Whitmarsh et al., 2001; Manatschal et al., 2001, 2007; Reston, 2005, 2007; Péron-Pinvidic, 2006; Péron-Pinvidic et al., 2007; Reston and Pérez-Gussinyé, 2007; Sibuet et al., 2007; Péron-Pinvidic and Manatschal, 2009; Reston and McDermott, 2011; Mohn et al., 2015; Decarlis et al., 2015; Haupert et al., 2016), Norvège/Groenland (Osmundsen et al., 2002; Osmundsen and Ebbing, 2008; Peron-Pinvidic et al., 2012a, 2012b; Osmundsen and Péron-Pinvidic, 2018), et l'exemple fossile des Alpes (**Fig. 8B**; Masini, 2011; Masini et al., 2011, 2012, 2013). Toutes ces marges sont caractérisées par une très faible épaisseur de séries synrifts (« starved margin »), des taux d'extension très importants, une asymétrie prononcée des marges, et l'absence significative de sel prérift, favorisant le couplage de la déformation entre les séries prérifts et le socle lors de l'amincissement de la croûte continentale.

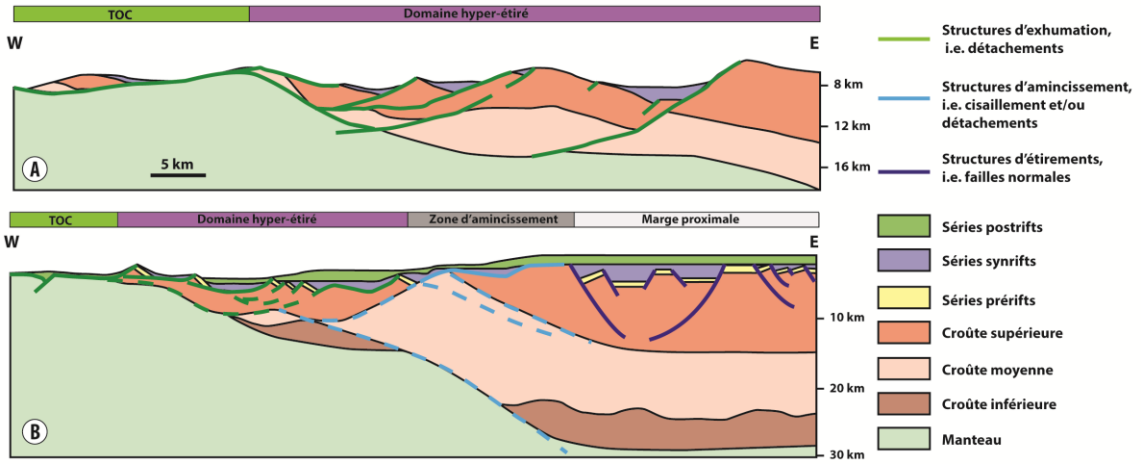


Fig. 8. (A) Interprétation d'une ligne sismique migrée en profondeur à la transition entre le domaine hyper-étiré et la transition océan contient (TOC) de la marge ibérique (Manatschal et al., 2001); **(B)** Coupe restaurée de la marge nord-ouest adriatique avant la phase de convergence alpine, prenant place au Crétacé supérieur (simplifié d'après Masini et al., 2011).

Du Jurassique supérieur au Crétacé, le système péri-ibérique est caractérisé par le développement de rift hyper-étirés qui différent des marges passives hyper-étirées classiques de par la présence d'une couverture évaporitique prérift notable, d'une géométrie essentiellement symétrique

des marges et d'une épaisse série synrift (~5km), tel que les bassins de Parentis (**Fig. 9A**; Pinet et al., 1987; Bois, 1992; Bois and Gariel, 1994; Ferrer et al., 2009, 2012; Jammes et al., 2010c), de Cameros (Guimerà et al., 1995; Casas-Sainz and Gil-Imaz, 1998; Casas et al., 2009; Omodeo Salè et al., 2014; Omodeo-Salé et al., 2017; Rat et al., 2019) et de Columbrets (**Fig. 9B**; Gallart et al., 1990; Ayala et al., 2015; Etheve, 2016; Etheve et al., 2018; Roma et al., 2018). Dans les Pyrénées occidentales, le système hyper-étiré de Mauléon semble s'apparenter à ces systèmes du fait de la présence d'une épaisse série évaporitique triasico-liasique (Curnelle, 1983), de dépôts synrifts (Boirie, 1981; Boirie and Souquet, 1982; Roux, 1983; Fixari, 1984; Souquet et al., 1985; Debroas et al., 2010) et postrifts (Casteras, 1971; Le Pochat et al., 1976; Henry et al., 1987) épais. L'étude tectono-sédimentaire du Crétacé du bassin de Mauléon permet de questionner : (1) les mécanismes responsables de l'hyperextension de la croûte continentale et (2) les similitudes et différences avec les marges hyper-étirées de type atlantique. Cette approche permet d'appréhender la question suivante : l'épaisseur de séries prérift à synrift contrôle-t-elle le style d'amincissement de la croûte continentale ?

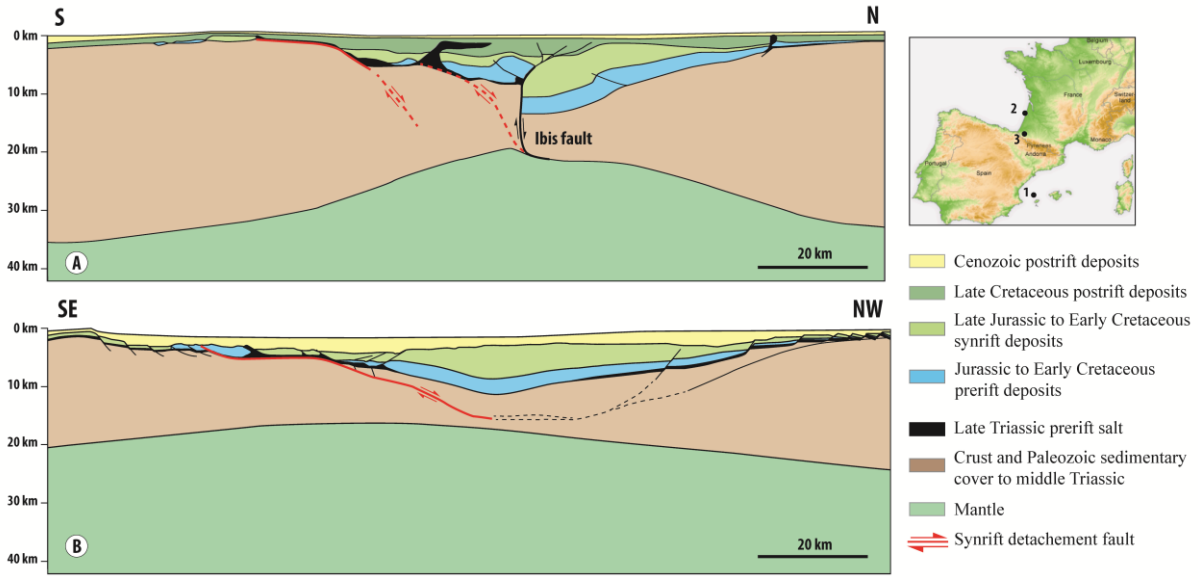


Fig. 9. Coupes actuelles d'échelle lithosphérique des bassins de **(A)** Parentis (e.g. Tugend et al., 2014), **(B)** Columbrets (Etheve et al., 2018) ; (1) le bassin de Columbrets, (2) le bassin de Parentis et (3) le bassin de Mauléon.

3.3. L'héritage d'un système hyper-étiré contrôle-t-il la géométrie d'un orogène ?

Les processus à l'origine de la rupture continentale sont responsables de l'individualisation et de la destruction de plaques tectoniques. Les domaines proximaux des rifts ou des marges passives hyper-étirés représentent les bordures des continents et peuvent potentiellement être le lieu d'ultérieures zones de collision continentale (Reston and Manatschal, 2011). Le système austro-alpin représente l'analogue fossile de systèmes de marges passives réactivées au cours d'une phase orogénique le plus étudié (Froitzheim and Manatschal, 1996; Manatschal and Nievergelt, 1997; Manatschal and Bernoulli, 1998; Wilson et al., 2001; Desmurs et al., 2001; Manatschal, 2004; Manatschal et al., 2006, 2007, 2011; Manatschal and Müntener, 2009; Beltrando et al., 2014; Decarlis et al., 2015). Les orogènes de type alpine sont interprétées comme résultant de la collision des précédentes marges, après la subduction du domaine océanique (Rubatto et al., 1998; Stampfli et al., 1998; Handy et al., 2010). Dans les Alpes, les travaux visant à comprendre l'impact de l'héritage lié à la phase d'hyper extension lors de la réactivation alpine ont montré que : (1) le manteau sous-continental serpentinisé le long de la transition océan/continent est fragilisé (Escartín et al., 1997, 2001; McCaig et al., 2007; Lundin and Doré, 2011) et joue le rôle de décollement lors de la phase de compression (Reston and Manatschal, 2011) (2) les détachements qui jalonnent le domaine hyper-étiré sont réactivés dans les prémisses de la phase de collision continentale (**Fig. 10A**; Mohn et al., 2011)et (3) les zones de necking qui séparent les marges proximales du domaine hyper-étiré jouent le rôle de buttoir au cours de la transition entre les phases de subduction et de collision continentale (**Fig. 10B**; Mohn et al., 2014).

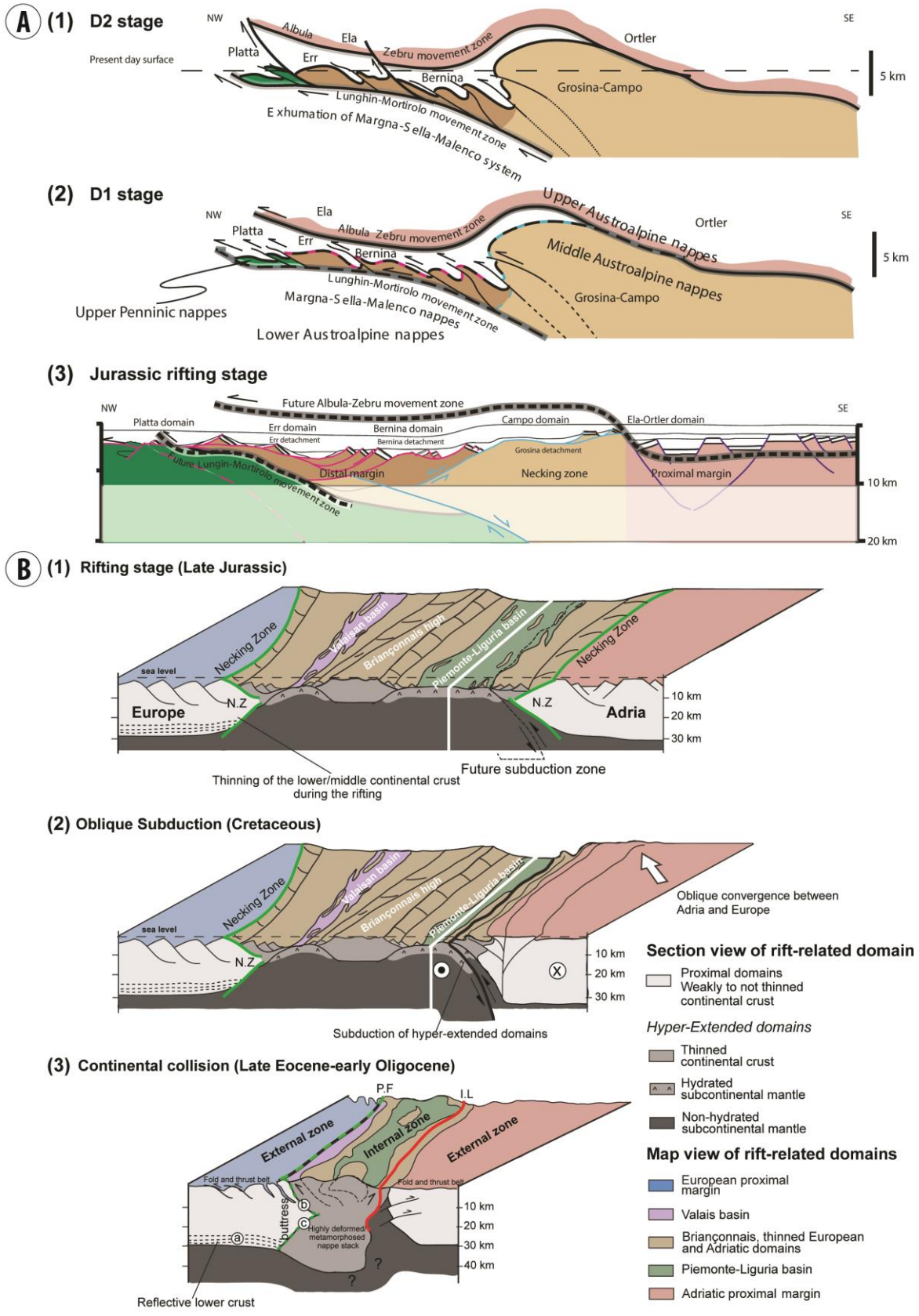


Fig. 10. (A) Restauration structurale à grande échelle, des nappes austroalpine et pénnique supérieures au sud-est de la Suisse et au nord de l'Italie, **(B1)** Phase alpine D2 ; **(B2)** Réactivation des structures de rift héritées au cours de la phase alpine D1; **(B3)** Structure jurassique de la marge Austroalpine (Mohn et al., 2011);**(B)** Modèle conceptuel illustrant le rôle de l'hyperextension jurassique sur l'architecture des Alpes. **(A1)** Stade du rifting jurassique ; **(A2)** Stade de subduction crétacée ; **(A3)** Stade de collision continentale prenant place entre l'Eocène supérieur et l'Oligocène (Mohn et al., 2014).

Les Pyrénées occidentales permettent de discuter du rôle de l'héritage d'un système de rift hyper-étiré n'ayant pas atteint la rupture asthénosphérique et ne présentant de fait pas d'étape de subduction océanique. En effet, les Pyrénées sont caractérisées par un sous-charriage de la plaque continentale ibérique sous le domaine hyper-étiré crétacé qui jalonne la zone nord-pyrénéenne (Mattauer, 1985; Engeser and Schwentke, 1986; McCaig, 1988; Choukroune and ECORS Team, 1989; Roure et al., 1989).

L'exemple du bassin de Mauléon nous permet :

(1) de discuter des mécanismes responsables de la préservation d'un système de rift dans un orogène,

(2) de proposer un modèle conceptuel de réactivation d'un système de rift hyper-étiré, dans lequel l'évolution structurale de l'orogenèse précoce est conditionnée par l'héritage de la phase d'hyperextension.

3.4. Les zones de transferts impactent-elles la réactivation d'un rift hyper-étiré ?

Les structures de transfert ou zones d'accommodation sont des traits structuraux classiques et bien connus des systèmes de rifts (Gibbs, 1984, 1990; Reynolds and Rosendahl, 1984; Chorowicz, 1989). Ces structures réactivent généralement des discontinuités crustales présentent dans la croûte supérieure, mais peuvent également être néoformées au cours de la phase de rifting. Les zones de déformations accommodent des changements de vergence de failles, de faciès sédimentaire et ou de subsidence le long d'un système de rift (**Fig. 11**; Lister et al., 1986; Gawthorpe and Hurst, 1993; Boillot et al., 1995; Young et al., 2001; Péron-Pinvidic et al., 2015). Ces structures ont été longuement étudiées et mises en évidence le long du rift est africain (Morley et al., 1990; Chorowicz and Sorlien, 1992; Corti et al., 2007; Basile, 2015; Mortimer et al., 2016), de la Mer Rouge (Moustafa, 1997; Mohriak and Leroy, 2013) ou encore du Golfe d'Aden (d'Acremont et al., 2005; Leroy et al., 2012; Autin et al., 2013; Bellahsen et al., 2013).

Elles sont également connues pour jouer un rôle majeur dans la localisation des zones transformantes océaniques qui réactivent des structures obliques aux systèmes de rift (Cochran and Martinez, 1988; Behn and Lin, 2000; d'Acremont et al., 2005; Bellahsen et al., 2013). Cependant, l'impact des structures de transfert lors de la réactivation d'un système de rift n'a que très peu été étudié (Etheridge, 1986; Calassou et al., 1993).

L'importance des structures obliques à la chaîne, de direction N20°, a été clairement mis en évidence dans les Pyrénées occidentales (Canérot, 1989, 2008; Canérot et al., 2005; Debroas et al., 2010) et orientales (Debroas and Souquet, 1976; Debroas, 1987). En effet, elles contrôlent la localisation des dépôcentres et l'halocinèse au cours de la phase de rifting crétacée.

L'étude du bassin de Mauléon permet :

(1) de comprendre le rôle des structures transverses à la direction de la chaîne, sur la géométrie de l'orogenèse pyrénéenne,

(2) d'extraire des concepts généraux sur la réactivation des zones de transfert affectant les rifts hyper-étirés.

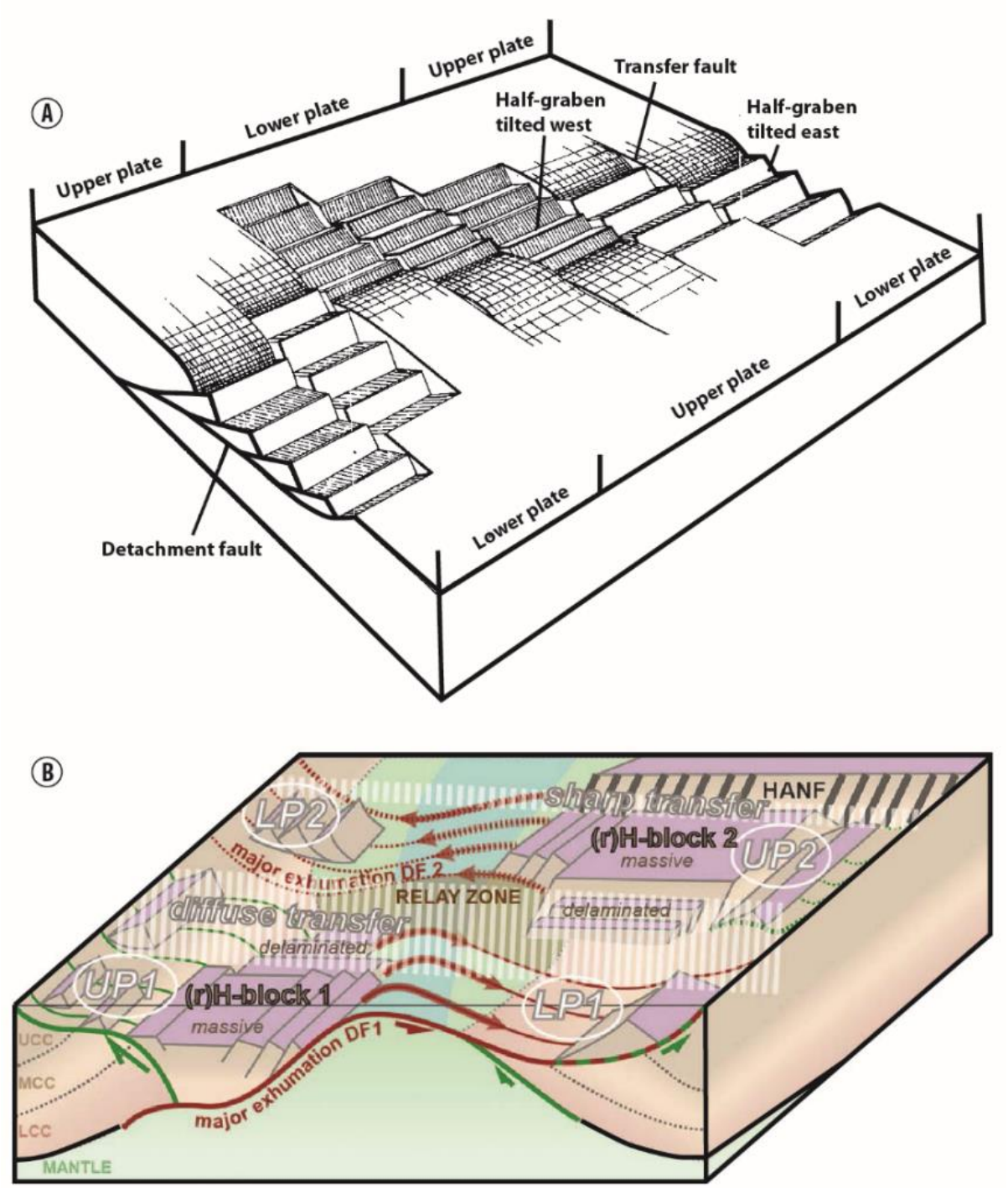


Fig. 11. (A) Changement de morphologie du système extensif, i.e. upper plate vs lower plate, de part et d'autre de structures de transfert obliques à la direction d'extension (Lister et al., 1986); **(B)** Schéma en 3D illustrant le changement de polarité du système extensif, i.e. upper plate vs lower plate, de part et d'autre d'une zone de transfert pouvant être diffuse ou nette. UCC, Croûte continentale supérieure ; MCC, Croûte continentale moyenne, LCC, Croûte continentale inférieure, DF, faille de détachement, HANF, faille normale de forte inclinaison ; UP, upper plate; LP, lower plate (Péron-Pinvidic et al., 2015).

3.5. Comment évolue le gradient thermique d'un système de rift hyper-étiré en 3D, du rifting à la phase post-compressive ?

Les exemples de marges passives actuelles, qui résultent de l'exhumation du manteau sous-continental le long de la transition océan-continent, semblent s'accompagner de conditions favorables au développement d'un gradient géothermique et d'un flux mantélique anormalement élevés (**Fig. 12A**; Davies, 2013; Pollack et al., 1993). Ceci a clairement été mis en évidence dans les modèles

numériques reproduisant la géométrie des marges hyper-étirées de l'Océan Atlantique, bien que ce ne soit pas le but premier de ces travaux (Huismans and Beaumont, 2003, 2008, 2011, 2014; Lavier and Manatschal, 2006; Brune et al., 2014, 2016). Le gradient thermique dans les modèles visant à reproduire les processus responsables de la déformation d'une lithosphère continentale ont montré qu'en période de rifting le gradient géothermique augmente puis diminue de manière conséquente lors de la réactivation en compression du système extensif (**Fig. 13**; Jammes et al., 2014; Jourdon et al., 2019).

Le gradient thermique estimé dans des systèmes de rift continental est généralement élevé, comme le montre l'exemple du rift antarctique, ~50 à 100°C/km (Berg et al., 1989). Des exemples français présentent également des gradients thermiques élevés aux alentours de 80-100°C/km, dans la région de Soultz et le Graben du Rhin (Genter et al., 2010). Cependant, la répartition du gradient géothermique synrift au sein des systèmes hyper-étiré, du domaine proximal au domaine distal, n'est pas facilement accessible. La compréhension de la répartition du gradient géothermique représente un paramètre clé et un enjeu majeur pour contraindre l'exploration pétrolière et géothermique de manière plus précise.

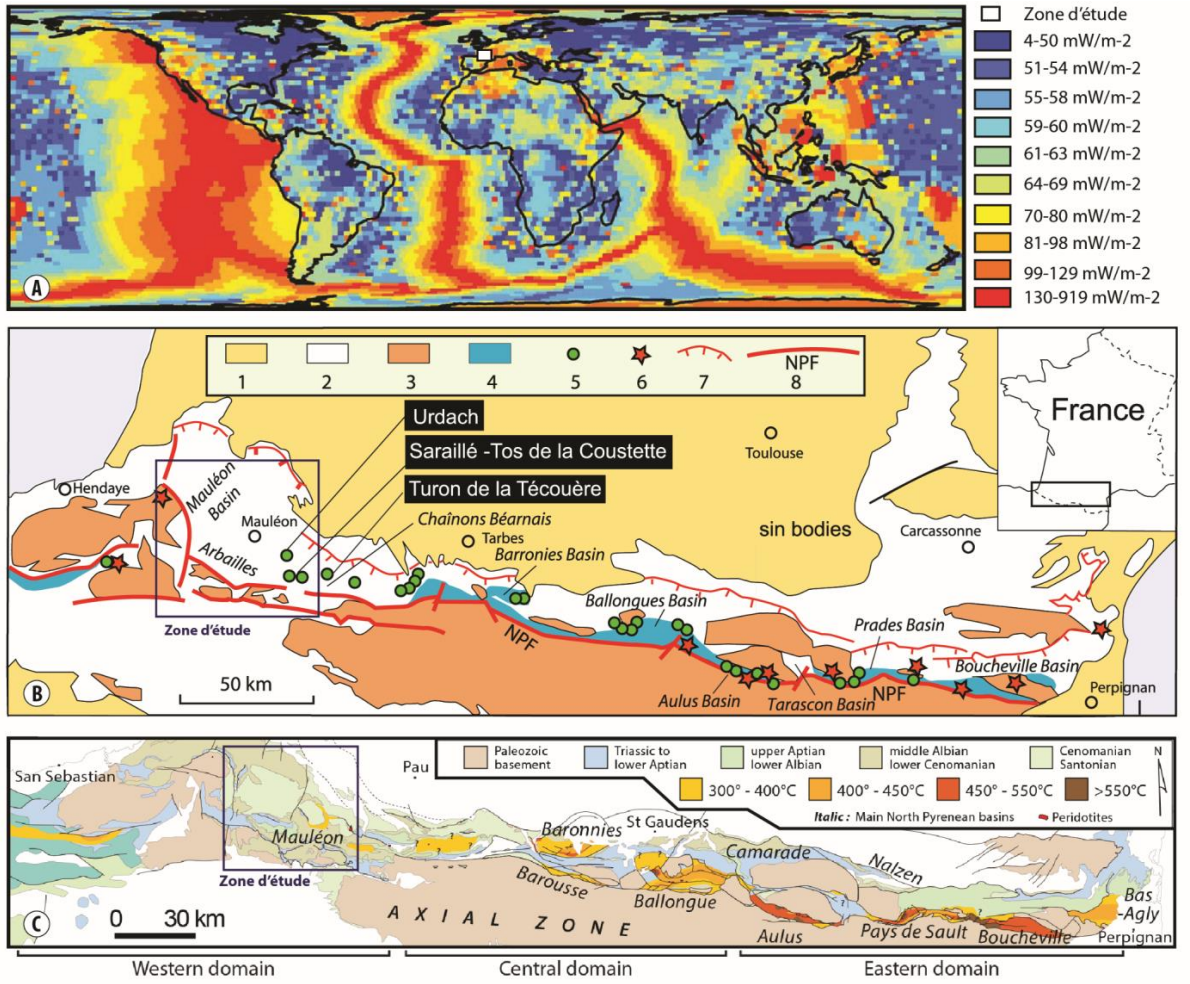


Fig. 12. (A) Carte globale représentant les valeurs de Heat Flow à la surface de Terre (mW/m^2) (Davies., 2013); **(B)** Cartes des Pyrénées représentant les principaux points d'affleurements de manteau sous-continental le long de la zone nord pyrénéenne (Lagabrielle et al., 2010) ; **(C)** Carte représentant les zones iso-métamorphiques le long de la zone nord pyrénéenne (Clerc et al., 2015).

Des travaux récents sur le système de rift des Pyrénées septentrionales ont mis en évidence que les affleurements de manteau sous-continental jalonnant la zone nord pyrénéenne (**Fig. 12B**; Fabriès et al., 1991, 1998) résultaient de processus d'hyperextension de la croûte continentale au cours de l'albo-cénomanien (Lagabrielle and Bodinier, 2008; Jammes, 2009; Jammes et al., 2009; Lagabrielle et al., 2010; Masini et al., 2014; Clerc et al., 2014; Clerc and Lagabrielle, 2014; Tugend et al., 2015; Corre et

al., 2016; Teixell et al., 2016). Contrairement aux marges fossiles alpines, dont les domaines océaniques et hyper-étirés ont subi une subduction au Crétacé (Rubatto et al., 1998; Stampfli et al., 1998 Handy et al., 2010), l'empreinte thermique synrift de la zone nord pyrénéenne n'a pas été effacée par un stade postérieur de subduction. La zone des Pyrénées septentrionales est donc un lieu privilégié pour évaluer l'évolution et la répartition en 3D du gradient géothermique d'un système hyper-étiré fossile. En effet, le métamorphisme haute température et basse pression mis en évidence tout au long du système de rift nord pyrénéen (**Fig. 12C**; Ravier, 1957; Albarède and Michard-Vitrac, 1978a, 1978b; Montigny et al., 1986; Golberg and Maluski, 1988; Golberg et al., 1986; Golberg and Leyreloup, 1990) est interprété comme la conséquence de l'amincissement de la croûte continentale au cours du Crétacé inférieur (Choukroune and Mattauer, 1978; Vielzeuf and Kornprobst, 1984; Debroas, 1990; Clerc et al., 2015). Cet aspect n'a que très peu été abordé dans la partie occidentale de la zone nord pyrénéenne. Le bassin hyper-étiré de Mauléon est relativement bien préservé de l'inversion pyrénéenne et présente plusieurs puits d'exploration pétrolière. La compréhension de ce système présente donc un intérêt majeur pour explorer l'organisation du gradient géothermique synrift en 3D et l'évolution du gradient au cours de la phase ultérieure de compression pyrénéenne.

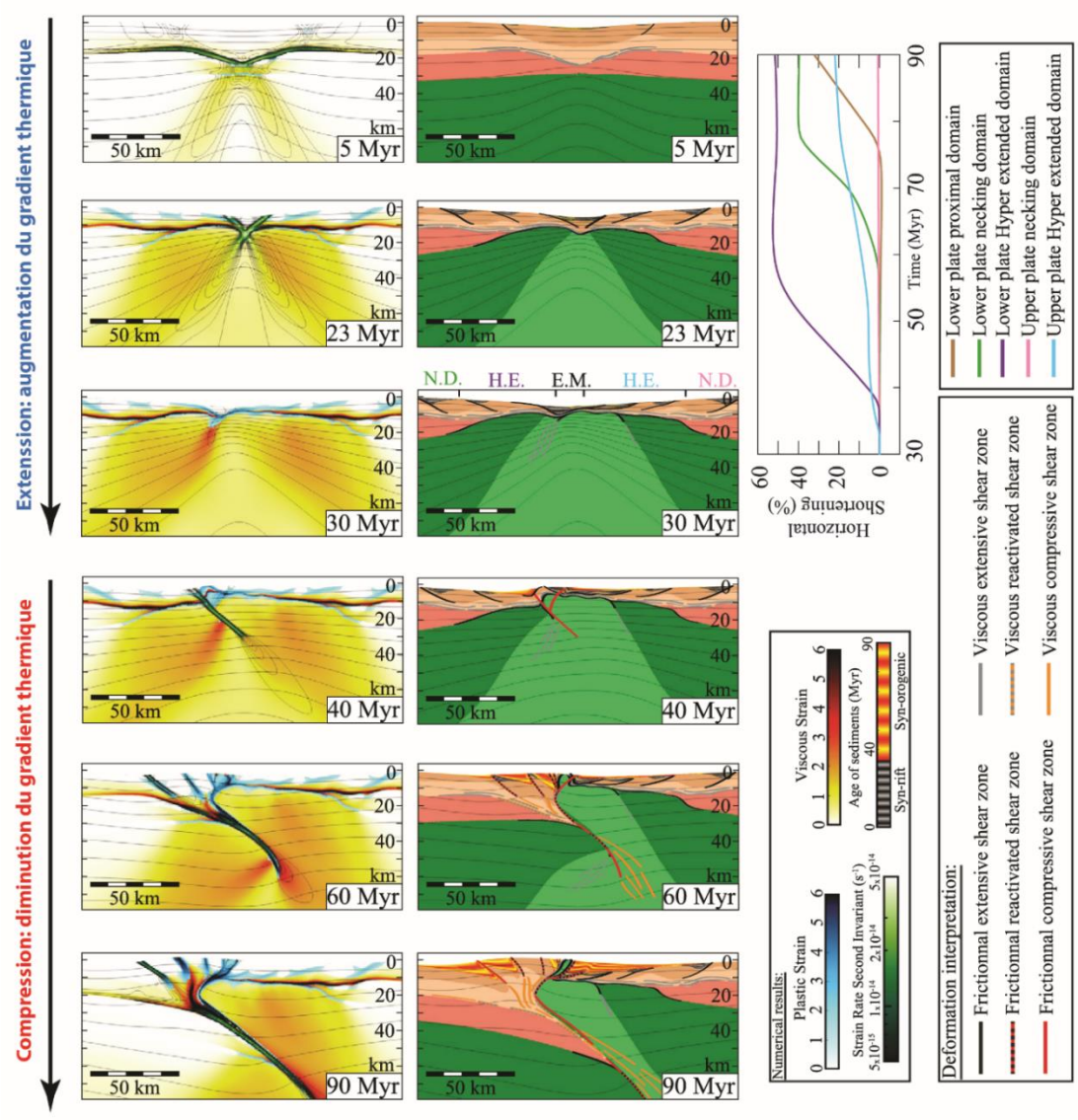


Fig. 13. Vitesse de phase d'extension de 5mm/an en 30Ma. La réactivation du système de rift hyper-étiré débute à 35Ma. Les couleurs de la colonne de gauche représentent la déformation plastique et visqueuse cumulative. Les couleurs du panneau de droite matérialisent les phases numériques de la modélisation. Les lignes noires représentent les zones de cisaillement étendues. Les lignes rouges matérialisent les zones de cisaillement en compression. Les lignes en pointillées correspondent aux zones de cisaillement réactivées. (Jourdon et al., 2019). N.D: domaine de necking ; H.E: domaine hyper-étiré ; E.M : zone d'exhumation du manteau sous-continental.

4. Méthodologies appliquées

4.1. Approche terrain

Dans le cadre de l'étude du bassin Permien de Bidarray, l'analyse de terrain a consisté à définir précisément les environnements de dépôts des séries continentales permo-triasiques et à lever des logs lithostratigraphiques de manière à identifier les principales variations d'épaisseurs et passages latéraux de faciès. Cette analyse sédimentaire a été couplée à une analyse structurale fine de la morphologie actuelle des Massifs Basques et du bassin de Bidarray. Le lien génétique de ce bassin intracontinental post-orogénique, avec les granulites/migmatites du dôme de l'Ursuya, a été appréhendé par le biais d'une analyse structurale et minéralogique terrain / microfaciès. Cette partie intègre des données provenant des thèses de B. Cochelin (2016) et B. Lemirre (2018). Ces thèses ont été financées par le programme de Recherche du Référentiel Géologique de la France, piloté par le BRGM (RGF, chantier Pyrénées).

Dans le cadre de l'évolution mésozoïque du bassin de Mauléon, l'approche de terrain a consisté à identifier l'évolution à la fois sédimentaire et structurale de la marge ibérique. La marge européenne et le domaine hyper-étiré du bassin de Mauléon ont essentiellement été calibrés par l'intermédiaire de données de sub-surfaces, i.e. sismique réflexion et puits d'exploration pétrolière. L'étude des relations entre le socle sédimentaire paléozoïques et les séries synrifts (Poudingues de Mendibelza), a permis de contraindre la géométrie du substratum paléozoïques au cours de l'Albien-Cénomanien le long de la marge ibérique. La réalisation de logs lithostratigraphiques, le long de la bordure ibérique, nous a permis de mettre en évidence le diachronisme du glissement de la couverture au cours de la phase d'hyperextension crétacée, par l'intermédiaire de l'analyse des éléments remaniés dans les brèches, olistolithes et olistostromes. L'importance des structures N20° sur l'évolution mésozoïques du bassin de Mauléon nous a conduit à réaliser une analyse micro à macrostructurale de terrain le long des zones de transfert N20° d'Iholdy et du Saison.

4.2. Géo-référencement des données

Les données récoltées sur le terrain ont été géoréférencées et stockées à l'aide du logiciel Geofield, développé par le BRGM dans le cadre du projet Référentiel Géologique de la France. Près de 2500 points d'observations structurales, cartographiques et/ou sédimentologiques ont été récoltés au cours de cette thèse. Les corrections cartographiques réalisées ont été intégrées dans la carte harmonisée du projet RGF Pyrénées, ainsi que dans la carte au 1/ 250 000 de la nouvelle Aquitaine, i.e. projet Aliénor. J'ai également participé de manière active à la rédaction de la notice de cette dernière en intégrant les données de la thèse dans la partie : évolution tectonique et géodynamique du cycle alpin des Pyrénées occidentales.

4.3. Interprétation sismique, données de forages et transect diagraphique

Les interprétations sismiques ont été réalisées à l'aide de Geographix® Discovery Suite. La conversion temps / profondeur a été réalisée à l'aide d'un champ de vitesse moyen, calculé sur la base de toutes les données temps / profondeur des puits de calibration.

Le chapitre 3.1. traite de la phase d'hyperextension crétacée affectant le bassin de Mauléon et intègre l'interprétation d'un profil sismique réflexion composite N-S, retraité par le BRGM en 2014 et 2017. La ligne sismique interprétée est une fusion des lignes MT104, MT112 (acquises par ESSO-Rep en 1969) et 83HBS02 (acquise par le SNEAP en 1981). La ligne composite présentée dans ce chapitre est calibrée par six puits d'exploration pétrolière, du sud au nord : Ainhice-1; Uhart-Mixe-1; Bellevue-1; Orthez-102; Amou-1; et Bastennes-Gaujacq-1.bis. Seul le puits Ainhice-1 atteint le socle paléozoïque du bassin de Mauléon.

Le chapitre 3.3 aborde l'évolution du bassin d'Aquitaine au cours de la phase d'hyperextension crétacée, sur la base de l'interprétation de six profils de sismique réflexion (d'une longueur totale de 300km), calibrés par trente-cinq puits pétroliers. Le profil N-S de Lacq-Pecorade est calibré par les puits de Lacq-131, Clèdes-201, Pecorade-18 et Pecorade-7. Le profil N-S de Rousse-Thèze est contraint par les puits Rousse-2, Rousse-1, Pau-4, Lons-1, Theze-301 et Theze-1. Le profil N-S de

Marsan à Lacq-Villeneuve de Larsan est calibré par les puits de Lacq-111, Lacq-115, Serres-Gaston-1, Coudures-201, Audignon-10 et Villeneuve de Marsan-1. Le profil N-S de Ger-Beaulieu est contraint par les puits de Ger-1, Ponton-Dessus-1, Lagrave-2, Moncaup-1, Beaulieu-1. Le profil E-W de Gamarde-Goudon est calibré par les puits de Gamarde les Bains-1, Amou-1, Boucoué-1, Lagrave-2 et Goudon-1. Pour finir, le profil E-W de Mont-de-Marsan / Lussagnet est contraint par les puits Mont-de-Marsan-1, Le Vignau 1 et Lussagnet-1.

Le chapitre 4.2 discute de l'importance des structures de transfert N20° dans le bassin de Mauléon et intègre deux profils de sismique réflexion de direction NW-SE recoupant ces structures. Ces lignes ont été retraitées par le BRGM en 2017 : la ligne MT116 (acquise par ESSO-Rep en 1969) et la ligne 82BAA12 (acquise par la SNEAP en 1981). Ce profil composite est calibré à l'aide du puits pétrolier Uhart-Mixe-1 et de la ligne sismique composite interprétée dans le chapitre 3.1, puisque cette dernière est sécante à la ligne MT116.

4.4. Modélisation 3D du bassin de Mauléon

Un modèle représentant la structure actuelle en 3D du bassin de Mauléon a été réalisé en collaboration avec C. Allanic (BRGM), dans le but de venir en appui à la campagne d'acquisition de sismique passive réalisée dans le cadre du projet OROGEN, i.e. projet MAUPASSACQ. Cette modélisation utilise un algorithme de modélisation implicite implémenté dans le logiciel GeoModeller (© BRGM-Intrepid-Geophysics, (Martelet et al., 2004; Calcagno et al., 2008). Ce logiciel reproduit des géométries géologiques 3D sur la base de l'interpolation d'un champ scalaire dans l'espace (Lajaunie et al., 1997), où un contact lithologique et le pendage des structures correspondent respectivement à une isovaleur et à la pente de ce champ. Les relations topologiques entre les différentes unités lithologiques et les relations géométriques, telles que les relations de superposition, d'intrusion ou de croisement, sont prises en compte par le biais d'une « pile lithologique », afin de reproduire de manière aussi réaliste que possible les systèmes géologiques complexes. À ce stade, la géométrie découle d'une extrapolation géostatistique des forages et des observations géologiques de surface.

Ce modèle tient compte des données suivantes : (1) cartes géologiques au 1/50 000 du BRGM rectifiées sur la base des nouvelles données acquises dans cette thèse, (2) les puits pétroliers (BEPH) et les puits de la banque de données du sous-sol (BSS), (3) les interprétations sismiques publiées dans la bibliographie et le présent manuscrit de thèse et (4) ~ 2 500 observations lithologiques et mesures structurelles nouvellement acquises dans le cadre de notre travail. Le modèle 3D présente douze enveloppes géologiques correspondant de la base au sommet au : (1) Manteau, (2) Socle, (3) Permien-Trias inférieur, (4) Trias salifère (5) Prérift, Jurassique, (6) Barrémien-Aptien (7) Albien-Cénomanien inférieur (8) Postrift, Cénomanien moyen à Maestrichtien (9) Eocène, (10) Oligocène, (11) Miocène et (12) Pliocène. Ce modèle a également permis de réaliser une carte d'interpolation des pendages avec superposition du schéma structural, dans le but de contraindre la déformation aux abords des structures de transfert N20° présentes dans le bassin de Mauléon et de discuter de leur cinématique (cf. chapitre 4.2).

4.5. Spectroscopie Raman

Les mesures Raman ont été réalisées au BRGM, par A. Lahfid, à l'aide d'un microspectromètre Renishaw inVia Reflex avec excitation à la source laser DPSS (Diode Pumped Solid State) de 514,5 nm. La puissance du laser qui atteint la surface de l'échantillon, à travers un objectif x 100 (ouverture numérique = 0,90) d'un microscope Leica DM2500, ne dépasse pas 0,1 mW. Avant chaque séance de mesure, le microspectromètre a été étalonné à l'aide de la ligne 520,5 cm^{-1} d'un silicium interne. Une fois la diffusion de Rayleigh éliminée par les filtres de bord, le signal Raman a d'abord été dispersé à l'aide d'un signal de 1 800 lignes / mm avant d'être analysé par un détecteur CCD à déplétion profonde (1024 x 256 pixels). Des spectres Raman d'au moins 10 particules ont été acquis, par échantillon, pour vérifier la cohérence des données. Renishaw Wire 4.1 a été utilisé pour l'étalonnage des instruments et les mesures Raman.

En laboratoire naturel, la structure du matériau carboné évolue en fonction de l'élévation de la température. Cette évolution irréversible est mesurable grâce à un nouveau géothermomètre, à savoir « Raman Spectroscopy of Carbonaceous Material » (RSCM) (Wopenka and Pasteris, 1993; Yui et al., 1996; Beyssac et al., 2002; Lahfid et al., 2010). Beyssac et al (2002) ont proposé le premier étalonnage de ce géothermomètre pour une plage de température maximale de 330 à 650°C. Lahfid et al. (2010) ont par la suite étendu leurs conditions d'applicabilité aux températures maximales atteintes par les roches au cours de la diagenèse et du métamorphisme de faible intensité. Toutes les températures maximales déterminées par la géothermométrie RSCM, ont été estimées qualitativement en comparant les spectres obtenus à ceux de la région de Glarus (Lahfid et al., 2010).

La méthodologie d'échantillonnage appliquée a consisté à sélectionner des échantillons dans les différents domaines structuraux du système de rift hyper-étiré de Mauléon, de manière à comprendre la répartition en 3D de l'anomalie thermique, liée à la phase de rifting et à son devenir au cours de l'inversion pyrénéenne du bassin. Cette étude est basée sur 102 échantillons prélevés sur des puits (Hasparren-101; Uhart-Mixe-1; Chéraute-1; Bellevue-1; Orthez-1; Les Cassières-2) et 68 échantillons de terrains.

4.6. Simulation numérique de l'évolution thermique du bassin de Mauléon

Pour appréhender l'évolution thermique du bassin de Mauléon au cours des cent vingt derniers millions d'années, un modèle thermique simplifié a été réalisé par L. Guillou-Frottier (BRGM). Dans ce travail, l'épaisseur des différentes unités ainsi que les taux de sédimentation et d'érosion sont estimés à partir des données recueillies dans le présent manuscrit de thèse ainsi que dans la bibliographie. La principale inconnue est la valeur du flux thermique du manteau et sa variation dans le temps. Trois contraintes majeures ont été prises en compte, à savoir : (1) un gradient synrift atteignant 60°C/km et perdurant au cours du Crétacé supérieur, (2) une température maximale de 600°C extrapolée à une profondeur de 10 km dans le domaine hyper-étiré et (3) un gradient actuel estimé à 25,0 ± 2,7 ° C / km.

Le modèle consiste à résoudre l'évolution thermique d'une partie de la croûte depuis le rifting crétacé inférieur jusqu'à l'actuel en suivant les étapes suivantes: (1) un flux de chaleur croissant dans le manteau de 120 à 80 Ma, à la base d'une croûte s'amincissant de 30km à 3km d'épaisseur de 120 à 90Ma, (ii) des événements de sédimentation (un de 120 à 80 Ma (stade synrift à postrift) et un autre plus lent, de 80 à 40 Ma (stade syn-compressif)) conduisant à une croûte épaisse de 21 km à 40 Ma, suivis (3) d'une érosion (de 40 à 15 Ma, stade post-compressif) aboutissant à une croûte de 14 km d'épaisseur (épaisseur actuelle) et (4) d'un stade de relaxation thermique se produisant au cours des quinze derniers millions d'années.

5. Organisation du manuscrit de thèse

Dans un premier temps, le chapitre 1 introduit et résume les principales avancées scientifiques relatives aux processus responsables de l'hyper-amincissement de la croûte continentale et de l'exhumation du manteau. Dans un second temps, le contexte géologique du bassin de Mauléon, faisant l'objet de cette étude, est brièvement détaillé. Pour finir, les grandes questions et objectifs scientifiques abordés dans ce manuscrit de thèse sont énoncées et les différentes méthodologies ayant été appliquées pour y répondre sont présentées.

Le chapitre 2 présente l'évolution tectono-sédimentaire de la bordure occidentale du bassin de Mauléon du Permien au Trias. Le chapitre 2.1 décrit précisément les faciès sédimentaires et les environnements de dépôt des séries permiennes et triasiques. Le chapitre 2.2 est composé d'un article scientifique publié dans le journal *Tectonophysics* et intitulé : « *Tectono-sedimentary evolution of a rift-system controlled by Permian post-orogenic extension and MCC formation (Bidarray basin and Ursuya dome, Western Pyrenees)* ». Cet article fait état de l'héritage structural, rhéologique et thermique de la lithosphère des Pyrénées occidentale, avant la phase d'extension crétacée.

Le chapitre 3 du manuscrit de thèse présente l'évolution tectono-sédimentaire des Pyrénées occidentales et du bassin d'Aquitaine au cours de la phase d'hyperextension crétacée. Le chapitre 3.1

est issu d'un article publié dans le journal *Marine and Petroleum Geology* et intitulé : « *Symmetry Vs. Asymmetry of a hyper-thinned rift: example of the Mauléon basin (Western Pyrenees, France) »*. Cet article décrit l'évolution sédimentaire et structurale du bassin de Mauléon de la fin du Jurassique au Cénomanien moyen. Le chapitre 3.2 se compose d'un article qui sera soumis dans le volume spécial du projet Orogen dans le *Bulletin de la Société Géologique de France*. Cet article s'applique à présenter la réponse sédimentaire du glissement de la couverture prérift le long de la marge ibérique du bassin de Mauléon / Saint Jean de Luz. Il s'intitule: *« Review of the Mauléon / Saint-Jean-de-Luz basin Albian - Cenomanian sedimentary record: salt-controlled polyphase cover gliding during hyperextension (Western Pyrenees) »*. Le chapitre 3.3 correspond à un article corédigé avec B. Issautier (BRGM), soumis dans un volume spécial du journal *Marine and Petroleum Geology*. Cet article présente l'évolution tectono-sédimentaire du bassin d'Aquitaine au cours de la phase d'hyperextension crétacée et s'intitule : *« Structural inheritance and salt tectonics controlling pseudosymmetric rift formation during Early Cretaceous hyperextension of the Arzacq and Tartas basins (southwest France) »*.

Le chapitre 4 présente le style structural et le timing de la réactivation du système de rift hyper-étiré de Mauléon au cours de la phase orogénique pyrénéenne. Le chapitre 4.1 traite de l'impact de l'héritage crétacé et comprend un article soumis dans le journal *Terra Nova, qui* s'intitule : « Closure of a hyperextended system in an orogenic lithospheric pop-up, Western Pyrenees: The role of mantle buttressing and rift structural inheritance ». Le chapitre 4.2 aborde, quant à lui, l'impact de l'héritage permien sur l'inversion tertiaire du bassin de Mauléon. Il correspond à un article en préparation qui sera soumis dans *Journal of structural Geology*. Il s'intitule: « Lithospheric transfer zones driving the non-cylindrical shape of the Pyrenean orogen (Mauléon hyperextended basin) ».

Le chapitre 5 présente l'évolution thermique en 3D d'un système de rift hyper-étiré, de sa création à sa réactivation. Il correspond à un article soumis dans le journal *Tectonics,* qui s'intitule : « Paleogeothermal Gradients across an Inverted Hyperextended Rift System: Example of the Mauléon Fossil Rift (Western Pyrenees) ».

Le chapitre 6.1 résume les principaux résultats des articles scientifiques présentés dans les chapitres précédents. Le chapitre 6.2 (Discussion de la thèse) discute du rôle fondamental du sel prerift et de l'enfouissement de la croûte continentale sous une épaisse série sédimentaire au cours de la phase d'hyperextension crétacée, affectant les bassins de rift à la limite de plaque Ibérie-Europe. Ce chapitre se compose d'un article de review qui sera soumis dans le journal *Basin Research.* Il s'intitule: « *Smooth-slopes extensional basins: How sedimentary burial and prerift salt control deformation style during hyperextension? »*. Le chapitre 7 présente les conclusions de ces travaux de thèse.

Références

Albarède, F., Michard-Vitrac, A., 1978. Datation du metamorphisme des terrains secondaires des Pyrenees par les methodes 39 Ar-40 Ar et 87 Rb-87 Sr; ses relations avec les peridotites associees. Bull. Société Géologique Fr. 7, 681–687.

Albarède, Francis, Michard-Vitrac, A., 1978. Age and Significance of the North Pyrenean Metamorphism. Earth Planet. Sci. Lett. 327–332.

Alves, T.M., Moita, C., Sandnes, F., Cunha, T., Monteiro, J.H., Pinheiro, L.M., 2006. Mesozoic–Cenozoic evolution of North Atlantic continental-slope basins: The Peniche basin, western Iberian margin. AAPG Bull. 90, 31–60.

Aslanian, D., Moulin, M., 2013. Palaeogeographic consequences of conservational models in the South Atlantic Ocean. Geol. Soc. Lond. Spec. Publ. 369, 75–90. https://doi.org/10.1144/SP369.5

Aslanian, D., Moulin, M., Olivet, J.-L., Unternehr, P., Matias, L., Bache, F., Rabineau, M., Nouzé, H., Klingelheofer, F., Contrucci, I., Labails, C., 2009. Brazilian and African passive margins of the Central Segment of the South Atlantic Ocean: Kinematic constraints. Tectonophysics 468, 98–112. https://doi.org/10.1016/j.tecto.2008.12.016

Autin, J., Bellahsen, N., Leroy, S., Husson, L., Beslier, M.-O., d'Acremont, E., 2013. The role of structural inheritance in oblique rifting: Insights from analogue models and application to the Gulf of Aden. Tectonophysics 607, 51–64. https://doi.org/10.1016/j.tecto.2013.05.041

Ayala, C., Torne, M., Roca, R., 2015. A review of the current knowledge of the crustal and lithospheric structure of the Valencia Trough basin. Bol. Geológico Min. 126, 533–552.

Aydin, A., Nur, A., 1982. Evolution of pull-apart basins and their scale independence. Tectonics 1, 91–105. https://doi.org/10.1029/TC001i001p00091

Basile, C., 2015. Transform continental margins — part 1: Concepts and models. Tectonophysics 661, 1–10. https://doi.org/10.1016/j.tecto.2015.08.034

Bassi, G., 1991. Factors controlling the style of continental rifting: insights from numerical modelling. Earth Planet. Sci. Lett. 105, 430–452.

Behn, M.D., Lin, J., 2000. Segmentation in gravity and magnetic anomalies along the US East Coast passive margin: Implications for incipient structure of the oceanic lithosphere. J. Geophys. Res. Solid Earth 105, 25769–25790.

Bellahsen, N., Leroy, S., Autin, J., Razin, P., d'Acremont, E., Sloan, H., Pik, R., Ahmed, A., Khanbari, K., 2013. Pre-existing oblique transfer zones and transfer/transform relationships in continental margins: New insights from the southeastern Gulf of Aden, Socotra Island, Yemen. Tectonophysics 607, 32–50. https://doi.org/10.1016/j.tecto.2013.07.036

Beltrando, M., Manatschal, G., Mohn, G., Dal Piaz, G.V., Brovarone, A.V., Masini, E., 2014. Recognizing remnants of magma-poor rifted margins in high-pressure orogenic belts: The Alpine case study. Earth-Sci. Rev. 131, 88–115.

Berg, J.H., Moscati, R.J., Herz, D.L., 1989. A petrologic geotherm from a continental rift in Antarctica. Earth Planet. Sci. Lett. 93, 98–108.

Beyssac, O., Goffé, B., Chopin, C., Rouzaud, J.N., 2002. Raman spectra of carbonaceous material in metasediments: a new geothermometer. J. Metamorph. Geol. 20, 859–871.

Bixel, F., Lucas, C., 1987. Approche Géodynamique du Permien et du Trias des Pyrénées dans le cadre du sud-ouest européen. Cuad. Geol. Ibérica 11, 57–81.

Bixel, F., Lucas, C.L., 1983. Magmatisme, tectonique et sédimentation dans les fossés stéphano-permiens des Pyrénées occidentales. Rev. Géologie Dyn. Géographie Phys. 24, 329–342.

Boillot, G., Beslier, M.O., Krawczyk, C.M., Rappin, D., Reston, T.J., 1995. The formation of passive margins: constraints from the crustal structure and segmentation of the deep Galicia margin, Spain. Geol. Soc. Lond. Spec. Publ. 90, 71–91.

Boillot, G., Féraud, G., Recq, M., Girardeau, J., 1989. Undercrusting by serpentinite beneath rifted margins: the example of the west Galicia margin (Spain). Nature 341, 523–525.

Boillot, G., Grimaud, S., Mauffret, A., Mougenot, D., Kornprobst, J., Mergoil-Daniel, J., Torrent, G., 1980. Ocean-continent boundary of the Iberian margin: a serpentinite diapir west of the Galicia Bank. Earth Planet. Sci. Lett. 48, 23–34.

Boillot, G., Recq, M., Winterer, E.L., Meyer, A.W., Applegate, J., Baltuck, M., Bergen, J.A., Comas, M.C., Davies, T.A., Dunham, K., others, 1987. Tectonic denudation of the upper mantle along passive margins: a model based on drilling results (ODP leg 103, western Galicia margin, Spain). Tectonophysics 132, 335–342.

Boirie, J.-M., 1981. Etude Sédimentologique des Poudingues de Mendibelza (Pyrénées Atlantiques). Université Paul Sabatier de Toulouse (Sciences), Toulouse.

Boirie, J.-M., Souquet, P., 1982. Les poudingues de Mendibelza: dépôts de cônes sous-marins du rift albien des Pyrénées. Bull. Cent. Rech. Explor.-Prod. Elf-Aquitaine 6, 405–435.

Bois, C., 1992. The evolution of the layered lower crust and the Moho through geological time in Western Europe: contribution of deep seismic reflection profiles. Terra Nova 4, 99–108.

Bois, C., Gariel, O., 1994. Deep Seismic Investigation in the Parentis basin (Southwestern France), in: Mascle, A. (Ed.), Hydrocarbon and Petroleum Geology of France. Springer Berlin Heidelberg, Berlin, Heidelberg, pp. 173–186. https://doi.org/10.1007/978-3-642-78849-9_13

Bouquet, B., 1986. La bordure mésozoïque orientale du Massif du Labourd (Pyrénées occidentales) : Stratigraphie-Sédimentologie-Structure-Implications Géodynamiques. Université de Pau et des Pays de l'Adour, Pau.

Brun, J.P., Beslier, M.O., 1996. Mantle exhumation at passive margins. Earth Planet. Sci. Lett. 142, 161–173.

Brun, J.-P., van den Driessche, J., 1994. Extensional gneiss domes and detachment fault systems; structure and kinematics. Bull. Société Géologique Fr. 165, 519–530.

Brune, S., Heine, C., Pérez-Gussinyé, M., Sobolev, S.V., 2014. Rift migration explains continental margin asymmetry and crustal hyper-extension. Nat. Commun. 5. https://doi.org/10.1038/ncomms5014

Brune, S., Williams, S.E., Butterworth, N.P., Müller, R.D., 2016. Abrupt plate accelerations shape rifted continental margins. Nature 536, 201–204. https://doi.org/10.1038/nature18319

Buck, W.R., 1991. Modes of continental lithospheric extension. J. Geophys. Res. 96, 20161–20178.

Buck, W.R., 1988. Flexural rotation of normal faults. Tectonics 7, 959–973.

Burg, J.-P., Van Den Driessche, J., Brun, J.-P., 1994. Syn- to post-thickening extension : mode and consequences. Comptes Rendus Académie Sci. Sér. 2 Sci. Terre Planètes 319, 1019–1032.

Calassou, S., Larroque, C., Malavieille, J., 1993. Transfer zones of deformation in thrust wedges: an experimental study. Tectonophysics 221, 325–344.

Calcagno, P., Chilès, J.-P., Courrioux, G., Guillen, A., 2008. Geological modelling from field data and geological knowledge: Part I. Modelling method coupling 3D potential-field interpolation and geological rules. Phys. Earth Planet. Inter. 171, 147–157.

Canérot, J., 2017. The pull apart-type Tardets-Mauléon basin, a key to understand the formation of the Pyrenees. Bull. Société Géologique Fr. 188, 35. https://doi.org/10.1051/bsgf/2017198

Canérot, J., 2008. Les Pyrénées: Histoire géologique. Atlantica.

Canérot, J., 1989. Rifting éocrétacé et halocinèse sur la marge ibérique des Pyrénées Occidentales (France). Conséquences structurales. Bull. Cent. Rech. Explor.-Prod. Elf-Aquitaine 13, 87–99.

Canérot, J., Hudec, M.R., Rockenbauch, K., 2005. Mesozoic diapirism in the Pyrenean orogen: Salt tectonics on a transform plate boundary. AAPG Bull. 89, 211–229. https://doi.org/10.1306/09170404007

Casas, A., Kearey, P., Rivero, L., Adam, C.R., 1997. Gravity anomaly map of the Pyrenean region and a comparison of the deep geological structure of the western and eastern Pyrenees. Earth Planet. Sci. Lett. 150, 65–78.

Casas, A.M., Villalaín, J.J., Soto, R., Gil-Imaz, A., del Río, P., Fernández, G., 2009. Multidisciplinary approach to an extensional syncline model for the Mesozoic Cameros basin (N Spain). Tectonophysics 470, 3–20. https://doi.org/10.1016/j.tecto.2008.04.020

Casas-Sainz, A.M., Gil-Imaz, A., 1998. Extensional subsidence, contractional folding and thrust inversion of the eastern Cameros basin, northern Spain. Geol. Rundsch. 86, 802–818. https://doi.org/10.1007/s005310050178

Casteras, M., 1971. Carte géologique de la France à 1/50 000: feuille de Tardets–Sorholus, Orléans, France.

Chorowicz, J., 1989. Transfer and transform fault zones in continental rifts: examples in the Afro-Arabian Rift System. Implications of crust breaking. J. Afr. Earth Sci. Middle East 8, 203–214. https://doi.org/10.1016/S0899-5362(89)80025-9

Chorowicz, J., Sorlien, C., 1992. Oblique extensional tectonics in the Malawi Rift, Africa. Geol. Soc. Am. Bull. 104, 1015–1023.

Choukroune, P., ECORS Team, 1989. The ECORS Pyrenean deep seismic profile reflection data and the overall structure of an orogenic belt. Tectonics 8, 23–39.

Choukroune, P., Le Pichon, X., Seguret, M., Sibuet, J.-C., 1973a. Bay of Biscay and Pyrenees. Earth Planet. Sci. Lett. 18, 109–118.

Choukroune, P., Mattauer, M., 1978. Tectonique des plaques et Pyrenees; sur le fonctionnement de la faille transformante nord-pyreneenne; comparaisons avec des modeles actuels. Bull. Société Géologique Fr. 7, 689–700.

Choukroune, P., Roure, F., Pinet, B., Team, E.P., 1990. Main results of the ECORS Pyrenees profile. Tectonophysics 173, 411–423.

Choukroune, P., Seguret, M., Galdeano, A., 1973b. Caracteristiques et evolution structurale des Pyrenees; un modèle de relations entre zone orogenique et mouvement des plaques. Bull. Société Géologique Fr. 7, 600–611.

Clerc, C., Boulvais, P., Lagabrielle, Y., de Saint Blanquat, M., 2014. Ophicalcites from the northern Pyrenean belt: a field, petrographic and stable isotope study. Int. J. Earth Sci. 103, 141–163. https://doi.org/10.1007/s00531-013-0927-z

Clerc, C., Lagabrielle, Y., 2014. Thermal control on the modes of crustal thinning leading to mantle exhumation: Insights from the Cretaceous Pyrenean hot paleomargins. Tectonics 33, 1340–1359. https://doi.org/10.1002/2013TC003471

Clerc, C., Lagabrielle, Y., Labaume, P., Ringenbach, J.-C., Vauchez, A., Nalpas, T., Bousquet, R., Ballard, J.-F., Lahfid, A., Fourcade, S., 2016. Basement – Cover decoupling and progressive exhumation of metamorphic sediments at hot rifted margin. Insights from the Northeastern Pyrenean analog. Tectonophysics 686, 82–97. https://doi.org/10.1016/j.tecto.2016.07.022

Clerc, C., Lagabrielle, Y., Neumaier, M., Reynaud, J.-Y., de Saint Blanquat, M., 2012. Exhumation of subcontinental mantle rocks: evidence from ultramafic-bearing clastic deposits nearby the Lherz peridotite body, French Pyrenees. Bull. Société Géologique Fr. 183, 443–459.

Clerc, C., Lahfid, A., Monié, P., Lagabrielle, Y., Chopin, C., Poujol, M., Boulvais, P., Ringenbach, J.C., Masini, E., de St Blanquat, M., 2015. High-temperature metamorphism during extreme thinning of the continental crust: a reappraisal of the North Pyrenean passive paleomargin. Solid Earth 6, 643–668.

Cochran, J.R., Martinez, F., 1988. Evidence from the northern Red Sea on the transition from continental to oceanic rifting. Tectonophysics 153, 25–53.

Contrucci, I., Matias, L., Moulin, M., Géli, L., Klingelhofer, F., Nouzé, H., Aslanian, D., Olivet, J.-L., Réhault, J.-P., Sibuet, J.-C., 2004. Deep structure of the West African continental margin (Congo, Zaïre, Angola), between 5 S and 8 S, from reflection/refraction seismics and gravity data. Geophys. J. Int. 158, 529–553.

Corre, B., Lagabrielle, Y., Labaume, P., Fourcade, S., Clerc, C., Ballèvre, M., 2016. Deformation associated with mantle exhumation in a distal, hot passive margin environment: New constraints from the Saraillé Massif (Chaînons Béarnais, North-Pyrenean Zone). Comptes Rendus Geosci. 348, 279–289. https://doi.org/10.1016/j.crte.2015.11.007

Corti, G., van Wijk, J., Cloetingh, S., Morley, C.K., 2007. Tectonic inheritance and continental rift architecture: Numerical and analogue models of the East African Rift system. Tectonics 26, n/a-n/a. https://doi.org/10.1029/2006TC002086

Curnelle, R., 1983. Evolution structuro-sédimentaire du Trias et de l'Infra-Lias d'Aquitaine. Bull Cent Rech Explor Prod Elf-Aquitaine 7, 69–99.

d'Acremont, E., Leroy, S., Beslier, M.-O., Bellahsen, N., Fournier, M., Robin, C., Maia, M., Gente, P., 2005. Structure and evolution of the eastern Gulf of Aden conjugate margins from seismic reflection data. Geophys. J. Int. 160, 869–890. https://doi.org/10.1111/j.1365-246X.2005.02524.x

Davies, J.H., 2013. Global map of solid Earth surface heat flow: Global Surface Heat Flow Map. Geochem. Geophys. Geosystems 14, 4608–4622. https://doi.org/10.1002/ggge.20271

Davis, G.H., 1983. Shear-zone model for the origin of metamorphic core complexes. Geology 11, 342–347. https://doi.org/10.1130/0091-7613(1983)11<342:SMFTOO>2.0.CO;2

de Charpal, O., Guennoc, P., Montadert, L., Roberts, D.G., 1978. Rifting, crustal attenuation and subsidence in the Bay of Biscay. Nature 275, 706–711. https://doi.org/10.1038/275706a0

de Saint Blanquat, M., Bajolet, F., Grand'Homme, A., Proietti, A., Zanti, M., Boutin, A., Clerc, C., Lagabrielle, Y., Labaume, P., 2016. Cretaceous mantle exhumation in the central Pyrenees: New constraints from the peridotites in eastern Ariège (North Pyrenean zone, France). Comptes Rendus Geosci. 348, 268–278. https://doi.org/10.1016/j.crte.2015.12.003

Debroas, E.J., 1990. Le flysch noir albo-cenomanien temoin de la structuration albienne a senonienne de la Zone nord-pyreneenne en Bigorre (Hautes-Pyrenees, France). Bull. Soc. Geol. Fr. VI, 273–285. https://doi.org/10.2113/gssgfbull.VI.2.273

Debroas, E.-J., 1987. Modèle de bassin triangulaire à l'intersection de décrochements divergents pour le fossé albo-cénomanien de la Ballongue (zone nord-pyrénéenne, France). Bull. Société Géologique Fr. 3, 887–898. https://doi.org/10.2113/gssgfbull.III.5.887

Debroas, E.J., 1978. Evolution de la fosse du flysch ardoisier de l'Albien superieur au Senonien inferieur (zone interne metamorphique des Pyrenees navarro-languedociennes). Bull. Société Géologique Fr. 7, 639–648.

Debroas, E.J., Canérot, J., Bilotte, M., 2010. Les brèches d'Urdach, témoins de l'exhumation du manteau pyrénéen dans un escarpement de faille vraconnien-cénomanien inférieur (Zone nord-pyrénéenne, Pyrénées-Atlantiques, France). Géologie Fr. 2, 53–63.

Debroas, E.J., Souquet, P., 1976. Sédimentogenèse et position structurale des flyschs crétacés du versant nord des Pyrénées centrales. Bull Bur Rech Géol Min I 305–320.

Decarlis, A., Manatschal, G., Haupert, I., Masini, E., 2015. The tectono-stratigraphic evolution of distal, hyper-extended magma-poor conjugate rifted margins: Examples from the Alpine Tethys and Newfoundland–Iberia. Mar. Pet. Geol. 68, 54–72. https://doi.org/10.1016/j.marpetgeo.2015.08.005

Desmurs, L., Manatschal, G., Bernoulli, D., 2001. The Steinmann Trinity revisited: mantle exhumation and magmatism along an ocean-continent transition: the Platta nappe, eastern Switzerland. Geol. Soc. Lond. Spec. Publ. 187, 235–266. https://doi.org/10.1144/GSL.SP.2001.187.01.12

Driscoll, N.W., Hogg, J.R., Christie-Blick, N., Karner, G.D., 1995. Extensional tectonics in the Jeanne d'Arc basin, offshore Newfoundland: implications for the timing of break-up between Grand Banks and Iberia. Geol. Soc. Lond. Spec. Publ. 90, 1–28. https://doi.org/10.1144/GSL.SP.1995.090.01.01

Driscoll, N.W., Karner, G.D., 1998. Lower crustal extension across the Northern Carnarvon basin, Australia: Evidence for an eastward dipping detachment. J. Geophys. Res. Solid Earth 103, 4975–4991. https://doi.org/10.1029/97JB03295

Ducasse, L., Velasque, P.-C., 1988. Géotraverse dans la partie occidentale des Pyrénées, de l'avant-pays aquitain au bassin de l'Ebre: effet d'une inversion structurale sur l'édification d'une chaîne intracontinentale. Université Paul Cézanne (Aix-Marseille). Faculté des sciences et techniques de Saint-Jérôme.

Ducasse, L., Velasque, P.-C., Muller, J., 1986. Glissement de couverture et panneaux basculés dans la région des Arbailles (Pyrénées occidentales): Un modèle évolutif crétacé de la marge nord-ibérique à l'Est de la transformante de Pamplona. Comptes Rendus Académie Sci. Sér. 2 Mécanique Phys. Chim. Sci. Univers Sci. Terre 303, 1477–1482.

Duée, G., Lagabrielle, Y., Coutelle, A., Fortané, A., 1984. Les lherzolites associées aux Chaînons Béarnais (Pyrénées Occidentales): Mise à l'affleurement anté-dogger et resédimentation albo-cénomanienne. Comptes-Rendus Séances Académie Sci. Sér. 2 Mécanique-Phys. Chim. Sci. Univers Sci. Terre 299, 1205–1210.

Echtler, H., Malavieille, J., 1990. Extensional tectonics, basement uplift and Stephano-Permian collapse basin in a late Variscan metamorphic core complex (Montagne Noire, Southern Massif Central). Tectonophysics 177, 125–138.

Engeser, T., Schwentke, W., 1986. Towards a new concept of the tectogenesis of the Pyrenees. Tectonophysics 129, 233–242. https://doi.org/10.1016/0040-1951(86)90253-2

Escartín, J., Hirth, G., Evans, B., 2001. Strength of slightly serpentinized peridotites: Implications for the tectonics of oceanic lithosphere. Geology 29, 1023. https://doi.org/10.1130/0091-7613(2001)029<1023:SOSSPI>2.0.CO;2

Escartín, J., Hirth, G., Evans, B., 1997. Effects of serpentinization on the lithospheric strength and the style of normal faulting at slow-spreading ridges. Earth Planet. Sci. Lett. 151, 181–189.

Etheridge, M.A., 1986. On the reactivation of extensional fault systems. Philos. Trans. R. Soc. Lond. Ser. Math. Phys. Sci. 317, 179–194.

Etheve, N., 2016. Le bassin de Valence à la frontière des domaines ibérique et méditerranéen: Evolution tectonique et sédimentaire du Mésozoïque au Cénozoïque. Université de Cergy Pontoise.

Etheve, N., Mohn, G., Frizon de Lamotte, D., Roca, E., Tugend, J., Gómez-Romeu, J., 2018. Extreme Mesozoic Crustal Thinning in the Eastern Iberia Margin: The Example of the Columbrets basin (Valencia Trough). Tectonics 37, 636–662.

Fabriès, J., Lorand, J.-P., Bodinier, J.-L., 1998. Petrogenetic evolution of orogenic lherzolite massifs in the central and western Pyrenees. Tectonophysics 292, 145–167.

Fabriès, J., Lorand, J.-P., Bodinier, J.-L., Dupuy, C., 1991. Evolution of the Upper Mantle beneath the Pyrenees: Evidence from Orogenic Spinel Lherzolite Massifs. J. Petrol. Special_Volume, 55–76. https://doi.org/10.1093/petrology/Special_Volume.2.55

Ferrer, O., Jackson, M.P.A., Roca, E., Rubinat, M., 2012. Evolution of salt structures during extension and inversion of the Offshore Parentis basin (Eastern Bay of Biscay). Geol. Soc. Lond. Spec. Publ. 363, 361–380. https://doi.org/10.1144/SP363.16

Ferrer, O., Roca, E., Benjumea, B., Muñoz, J.A., Ellouz, N., MARCONI Team, 2008. The deep seismic reflection MARCONI-3 profile: Role of extensional Mesozoic structure during the Pyrenean contractional deformation at the eastern part of the Bay of Biscay. Mar. Pet. Geol. 25, 714–730. https://doi.org/10.1016/j.marpetgeo.2008.06.002

Ferrer, O., Roca, E., Jackson, M.P.A., Muñoz, J.A., 2009. Effects of Pyrenean contraction on salt structures of the offshore Parentis basin (Bay of Biscay). Trab. Geol. 29.

Fixari, G., 1984. Stratigraphie, faciès et dynamique tecto-sédimentaire du flysch albien (flysch noir et poudingues de mendibelza) dans la région de Mauléon-Tardets (Pyrénées Atlantiques). Université Paul Sabatier de Toulouse (Sciences).

Fletcher, R.C., Hallet, B., 1983. Unstable extension of the lithosphere: A mechanical model for basin-and-range structure. J. Geophys. Res. Solid Earth 88, 7457–7466. https://doi.org/10.1029/JB088iB09p07457

Fortané, A., Duée, G., Lagabrielle, Y., Coutelle, A., 1986. Lherzolites and the western "Chaînons Béarnais" (French Pyrenees): Structural and paleogeographical pattern. Tectonophysics 129, 81–98. https://doi.org/10.1016/0040-1951(86)90247-7

Froitzheim, N., Manatschal, G., 1996. Kinematics of Jurassic rifting, mantle exhumation, and passive-margin formation in the Austroalpine and Penninic nappes (eastern Switzerland). Geol. Soc. Am. Bull. 108, 1120–1133. https://doi.org/10.1130/0016-7606(1996)108<1120:KOJRME>2.3.CO;2

Gallart, J., Rojas, H., Diaz, J., Dañobeitia, J.J., 1990. Features of deep crustal structure and the onshore-offshore transition at the Iberian flank of the Valencia Trough (Western Mediterranean). J. Geodyn. 12, 233–252.

Gawthorpe, R.L., Hurst, J.M., 1993. Transfer zones in extensional basins: their structural style and influence on drainage development and stratigraphy. J. Geol. Soc. 150, 1137–1152. https://doi.org/10.1144/gsjgs.150.6.1137

Genter, A., Evans, K., Cuenot, N., Fritsch, D., Sanjuan, B., 2010. Contribution of the exploration of deep crystalline fractured reservoir of Soultz to the knowledge of enhanced geothermal systems (EGS). Comptes Rendus Geosci. 342, 502–516.

Geoffroy, L., 2005. Volcanic passive margins. Comptes Rendus Geosci. 337, 1395–1408. https://doi.org/10.1016/j.crte.2005.10.006

Geoffroy, L., Le Gall, B., Daoud, M.A., Jalludin, M., 2014. Flip-flop detachment tectonics at nascent passive margins in SE Afar. J. Geol. Soc. 171, 689–694. https://doi.org/10.1144/jgs2013-135

Gibbs, A.D., 1990. Linked fault families in basin formation. J. Struct. Geol. 12, 795–803. https://doi.org/10.1016/0191-8141(90)90090-L

Gibbs, A.D., 1984. Structural evolution of extensional basin margins. J. Geol. Soc. 141, 609–620.

Golberg, J.M., Leyreloup, A.F., 1990. High temperature-low pressure Cretaceous metamorphism related to crustal thinning (Eastern North Pyrenean Zone, France). Contrib. Mineral. Petrol. 104, 194–207. https://doi.org/10.1007/BF00306443

Golberg, J.-M., Maluski, H., 1988. Données nouvelles et mise au point sur l'âge du métamorphisme pyrénéen. Comptes Rendus Académie Sci. Sér. 2 Mécanique Phys. Chim. Sci. Univers Sci. Terre 306, 429–435.

Golberg, J.M., Maluski, H., Leyreloup, A.F., 1986. Petrological and age relationship between emplacement of magmatic breccia, alkaline magmatism, and static metamorphism in the North Pyrenean Zone. Tectonophysics 129, 275–290. https://doi.org/10.1016/0040-1951(86)90256-8

Grandjean, G., 1994. Etude des structures crustales dans une portion de chaîne et de leur relation avec les bassins sédimentaires. Application aux Pyrénées occidentales. Bull Cent Rech Explor Prod Elf Aquitaine 18, 391–420.

Grandjean, G., 1992. Mise en évidence des structures crustales dans une portion de chaîne et de leur relation avec les bassins sédimentaires. Application aux Pyrénées occidentales au travers du Projet ECORS Arzacq-Pyrénées. Université des Sciences et Techniques du Languedoc.

Gretter, N., Ronchi, A., López-Gómez, J., Arche, A., De la Horra, R., Barrenechea, J., Lago, M., 2015. The Late Palaeozoic-Early Mesozoic from the Catalan Pyrenees (Spain): 60Myr of environmental evolution in the frame of the western peri-Tethyan palaeogeography. Earth-Sci. Rev. 150, 679–708. https://doi.org/10.1016/j.earscirev.2015.09.001

Guimerà, J., Alonso, Á., Mas, J.R., 1995. Inversion of an extensional-ramp basin by a newly formed thrust: the Cameros basin (N. Spain). Geol. Soc. Lond. Spec. Publ. 88, 433–453. https://doi.org/10.1144/GSL.SP.1995.088.01.23

Gürbüz, A., 2010. Geometric characteristics of pull-apart basins. Lithosphere 2, 199–206. https://doi.org/10.1130/L36.1

Hamilton, W., 1987. Crustal extension in the basin and Range Province, southwestern united States. Geol. Soc. Lond. Spec. Publ. 28, 155–176. https://doi.org/10.1144/GSL.SP.1987.028.01.12

Handy, M.R., 1989. Deformation regimes and the rheological evolution of fault zones in the lithosphere: the effects of pressure, temperature, grainsize and time. Tectonophysics 163, 119–152. https://doi.org/10.1016/0040-1951(89)90122-4

Handy, M.R., M. Schmid, S., Bousquet, R., Kissling, E., Bernoulli, D., 2010. Reconciling plate-tectonic reconstructions of Alpine Tethys with the geological–geophysical record of spreading and subduction in the Alps. Earth-Sci. Rev. 102, 121–158. https://doi.org/10.1016/j.earscirev.2010.06.002

Hart, N.R., Stockli, D.F., Hayman, N.W., 2016. Provenance evolution during progressive rifting and hyperextension using bedrock and detrital zircon U-Pb geochronology, Mauléon basin, western Pyrenees. Geosphere 12, 1166–1186. https://doi.org/10.1130/GES01273.1

Hart, N.R., Stockli, D.F., Lavier, L.L., Hayman, N.W., 2017. Thermal evolution of a hyperextended rift basin, Mauléon basin, western Pyrenees: Thermal evolution of hyperextended rift. Tectonics. https://doi.org/10.1002/2016TC004365

Haupert, I., Manatschal, G., Decarlis, A., Unternehr, P., 2016. Upper-plate magma-poor rifted margins: Stratigraphic architecture and structural evolution. Mar. Pet. Geol. 69, 241–261. https://doi.org/10.1016/j.marpetgeo.2015.10.020

Henry, J., Zolnaï, G., Le Pochat, G., Mondeilh, C., 1987. Carte géologique de la France au 1/50 000: feuille d'Orthez, Orléans, France.

Huismans, R.S., Beaumont, C., 2014. Rifted continental margins: The case for depth-dependent extension. Earth Planet. Sci. Lett. 407, 148–162. https://doi.org/10.1016/j.epsl.2014.09.032

Huismans, R.S., Beaumont, C., 2011. Depth-dependent extension, two-stage breakup and cratonic underplating at rifted margins. Nature 473, 74–78. https://doi.org/10.1038/nature09988

Huismans, R.S., Beaumont, C., 2008. Complex rifted continental margins explained by dynamical models of depth-dependent lithospheric extension. Geology 36, 163. https://doi.org/10.1130/G24231A.1

Huismans, R.S., Beaumont, C., 2003. Symmetric and asymmetric lithospheric extension: Relative effects of frictional-plastic and viscous strain softening. J. Geophys. Res. Solid Earth 108. https://doi.org/10.1029/2002JB002026

Jammes, S., 2009. Processus d'amincissement crustal en contexte transtensif: L'exemple du golfe de Gascogne et des Pyrénées basques. Strasbourg.

Jammes, S., Huismans, R.S., Muñoz, J.A., 2014. Lateral variation in structural style of mountain building: controls of rheological and rift inheritance. Terra Nova 26, 201–207. https://doi.org/10.1111/ter.12087

Jammes, S., Lavier, L., Manatschal, G., 2010b. Extreme crustal thinning in the Bay of Biscay and the Western Pyrenees: From observations to modeling. Geochem. Geophys. Geosystems 11. https://doi.org/10.1029/2010GC003218

Jammes, S., Manatschal, G., Lavier, L., 2010c. Interaction between prerift salt and detachment faulting in hyperextended rift systems: The example of the Parentis and Mauléon basins (Bay of Biscay and western Pyrenees). AAPG Bull. 94, 957–975. https://doi.org/10.1306/12090909116

Jammes, S., Manatschal, G., Lavier, L., Masini, E., 2009. Tectono-sedimentary evolution related to extreme crustal thinning ahead of a propagating ocean: Example of the western Pyrenees. Tectonics 28. https://doi.org/10.1029/2008TC002406

Jammes, S., Tiberi, C., Manatschal, G., 2010. 3D architecture of a complex transcurrent rift system: The example of the Bay of Biscay–Western Pyrenees. Tectonophysics 489, 210–226. https://doi.org/10.1016/j.tecto.2010.04.023

Jourdon, A., Le Pourhiet, L., Mouthereau, F., Masini, E., 2019. Role of rift maturity on the architecture and shortening distribution in mountain belts. Earth Planet. Sci. Lett. 512, 89–99. https://doi.org/10.1016/j.epsl.2019.01.057

Karner, G.D., Driscoll, N.W., Barker, D.H.N., 2003. Synrift regional subsidence across the West African continental margin: the role of lower plate ductile extension. Geol. Soc. Lond. Spec. Publ. 207, 105–129. https://doi.org/10.1144/GSL.SP.2003.207.6

Karner, G.D., Gambôa, L. a. P., 2007. Timing and origin of the South Atlantic pre-salt sag basins and their capping evaporites. Geol. Soc. Lond. Spec. Publ. 285, 15–35. https://doi.org/10.1144/SP285.2

Lagabrielle, Y., Bodinier, J.-L., 2008. Submarine reworking of exhumed sub-continental mantle rocks: field evidence from the Lherz peridotites, French Pyrenees: Cretaceous exhumation of pyrenean mantle. Terra Nova 20, 11–21. https://doi.org/10.1111/j.1365-3121.2007.00781.x

Lagabrielle, Y., Clerc, C., Vauchez, A., Lahfid, A., Labaume, P., Azambre, B., Fourcade, S., Dautria, J.-M., 2016. Very high geothermal gradient during mantle exhumation recorded in mylonitic marbles and carbonate breccias from a Mesozoic Pyrenean palaeomargin (Lherz area, North Pyrenean Zone, France). Comptes Rendus Geosci. 348, 290–300. https://doi.org/10.1016/j.crte.2015.11.004

Lagabrielle, Y., Labaume, P., de Saint Blanquat, M., 2010. Mantle exhumation, crustal denudation, and gravity tectonics during Cretaceous rifting in the Pyrenean realm (SW Europe): Insights from the geological setting of the lherzolite bodies. Tectonics 29. https://doi.org/10.1029/2009TC002588

Lago, M., Arranz, E., Pocovi, A., Galé, C., Gil-Imaz, A., 2004. Permian magmatism and basin dynamics in the southern Pyrenees: a record of the transition from late Variscan transtension to early Alpine extension. Geol. Soc. Lond. Spec. Publ. 223, 439–464.

Lahfid, A., Beyssac, O., Deville, E., Negro, F., Chopin, C., Goffé, B., 2010. Evolution of the Raman spectrum of carbonaceous material in low-grade metasediments of the Glarus Alps (Switzerland). Terra Nova 22, 354–360.

Lajaunie, C., Courrioux, G., Manuel, L., 1997. Foliation fields and 3D cartography in geology: principles of a method based on potential interpolation. Math. Geol. 29, 571–584.

Lavier, L.L., Buck, W.R., Poliakov, A.N.B., 1999. Self-consistent rolling-hinge model for the evolution of large-offset low-angle normal faults. Geology 27, 1127–1130. https://doi.org/10.1130/0091-7613(1999)027<1127:SCRHMF>2.3.CO;2

Lavier, L.L., Manatschal, G., 2006. A mechanism to thin the continental lithosphere at magma-poor margins. Nature 440, 324–328. https://doi.org/10.1038/nature04608

Le Pichon, X., Bonnin, J., Francheteau, J., Sibuet, J.C., 1971. Une hypothèse d'évolution tectonique du Golfe de Gascogne. Hist. Struct. Golfe Gasc. 2, 11–44.

Le Pichon, X., Sibuet, J.-C., 1971. Western extension of boundary between European and Iberian plates during the Pyrenean orogeny. Earth Planet. Sci. Lett. 12, 83–88. https://doi.org/10.1016/0012-821X(71)90058-6

Le Pochat, G., Bolthenhagen, C., Lenguin, M., Lorsignol, S., Thibault, C., 1976. Carte géologique de France au 1/50 000: Mauléon-licharre, Orléans, France.

Lemoine, M., Tricart, P., Boillot, G., 1987. Ultramafic and gabbroic ocean floor of the Ligurian Tethys (Alps, Corsica, Apennines): In search of a genetic imodel. Geology 15, 622–625. https://doi.org/10.1130/0091-7613(1987)15<622:UAGOFO>2.0.CO;2

Leroy, S., Razin, P., Autin, J., Bache, F., d'Acremont, E., Watremez, L., Robinet, J., Baurion, C., Denèle, Y., Bellahsen, N., Lucazeau, F., Rolandone, F., Rouzo, S., Kiel, J.S., Robin, C., Guillocheau, F., Tiberi, C., Basuyau, C., Beslier, M.-O., Ebinger, C., Stuart, G., Ahmed, A., Khanbari, K., Al Ganad, I., de Clarens, P., Unternehr, P., Al Toubi, K., Al Lazki, A., 2012. From rifting to oceanic spreading in the Gulf of Aden: a synthesis. Arab. J. Geosci. 5, 859–901. https://doi.org/10.1007/s12517-011-0475-4

Lin, A.T., Watts, A.B., 2002. Origin of the West Taiwan basin by orogenic loading and flexure of a rifted continental margin. J. Geophys. Res. Solid Earth 107, ETG–2.

Lister, G.S., Etheridge, M.A., Symonds, P.A., 1986. Detachment faulting and the evolution of passive continental margins. Geology 14, 246–250. https://doi.org/10.1130/0091-7613(1986)14<246:DFATEO>2.0.CO;2

Lloret, J., Ronchi, A., López-Gómez, J., Gretter, N., De la Horra, R., Barrenechea, J.F., Arche, A., 2018. Syn-tectonic sedimentary evolution of the continental late Palaeozoic-early Mesozoic Erill Castell-Estac basin and its significance in the development of the central Pyrenees basin. Sediment. Geol. 374, 134–157. https://doi.org/10.1016/j.sedgeo.2018.07.014

Lucas, C., 1985. Le grès rouge du versant nord des Pyrénées: essai sur la géodynamique de dépôts continentaux du permien et du trias.

Lucas, C., 1977. Le Trias des Pyrénées, corrélations stratigraphiques et paléogéographie. Bull. BRGM 2, 225–231.

Lucas, C., 1968. Le grès rouge du Comminges et de la Bigorre (Pyrénées centrales). Université Paul Sabatier de Toulouse (Sciences).

Lundin, E.R., Doré, A.G., 2011. Hyperextension, serpentinization, and weakening: A new paradigm for rifted margin compressional deformation. Geology 39, 347–350. https://doi.org/10.1130/G31499.1

Malavieille, J., Guihot, P., Costa, S., Lardeaux, J.M., Gardien, V., 1990. Collapse of the thickened Variscan crust in the French Massif Central: Mont Pilat extensional shear zone and St. Etienne Late Carboniferous basin. Tectonophysics 177, 139–149.

Manatschal, G., 2004. New models for evolution of magma-poor rifted margins based on a review of data and concepts from West Iberia and the Alps. Int. J. Earth Sci. 93. https://doi.org/10.1007/s00531-004-0394-7

Manatschal, G., Bernoulli, D., 1998. Rifting and early evolution of ancient ocean basins: the record of the Mesozoic Tethys and of the Galicia-Newfoundland margins. Mar. Geophys. Res. 20, 371–381. https://doi.org/10.1023/A:1004459106686

Manatschal, G., Engström, A., Desmurs, L., Schaltegger, U., Cosca, M., Müntener, O., Bernoulli, D., 2006. What is the tectono-metamorphic evolution of continental break-up: The example of the Tasna Ocean–Continent Transition. J. Struct. Geol. 28, 1849–1869. https://doi.org/10.1016/j.jsg.2006.07.014

Manatschal, G., Froitzheim, N., Rubenach, M., Turrin, B.D., 2001. The role of detachment faulting in the formation of an ocean-continent transition: insights from the Iberia Abyssal Plain. Geol. Soc. Lond. Spec. Publ. 187, 405–428. https://doi.org/10.1144/GSL.SP.2001.187.01.20

Manatschal, G., Lavier, L., Chenin, P., 2015. The role of inheritance in structuring hyperextended rift systems: Some considerations based on observations and numerical modeling. Gondwana Res. 27, 140–164. https://doi.org/10.1016/j.gr.2014.08.006

Manatschal, G., Müntener, O., 2009. A type sequence across an ancient magma-poor ocean–continent transition: the example of the western Alpine Tethys ophiolites. Tectonophysics, Tethyan tectonics of the Mediterranean region: some recent advances 473, 4–19. https://doi.org/10.1016/j.tecto.2008.07.021

Manatschal, G., Müntener, O., Lavier, L.L., Minshull, T.A., Péron-Pinvidic, G., 2007. Observations from the Alpine Tethys and Iberia–Newfoundland margins pertinent to the interpretation of continental breakup. Geol. Soc. Lond. Spec. Publ. 282, 291–324. https://doi.org/10.1144/SP282.14

Manatschal, G., Nievergelt, P., 1997. A continent-ocean transition recorded in the Err and Platta nappes (Eastern Switzerland). Eclogae Geol. Helvetiae 90, 3–28.

Manatschal, G., Sauter, D., Karpoff, A.M., Masini, E., Mohn, G., Lagabrielle, Y., 2011. The Chenaillet Ophiolite in the French/Italian Alps: An ancient analogue for an Oceanic Core Complex? Lithos, Alpine Ophiolites and Modern AnaloguesContinental Rifting to Oceanic LithosphereAlpine Ophiolites and Modern Analogues 124, 169–184. https://doi.org/10.1016/j.lithos.2010.10.017

Martelet, G., Calcagno, P., Gumiaux, C., Truffert, C., Bitri, A., Gapais, D., Brun, J.P., 2004. Integrated 3D geophysical and geological modelling of the Hercynian Suture Zone in the Champtoceaux area (south Brittany, France). Tectonophysics 382, 117–128.

Masini, E., 2011. L'évolution tectono-sédimentaire synrift des bassins de marge passive profonde: Exemples du bassin de Samedan (Alpes centrales, Suisse) et du bassin de Mauléon (Pyrénées basques françaises). Université de Strasbourg.

Masini, E., Manatschal, G., Mohn, G., 2013. The Alpine Tethys rifted margins: Reconciling old and new ideas to understand the stratigraphic architecture of magma-poor rifted margins. Sedimentology 60, 174–196. https://doi.org/10.1111/sed.12017

Masini, E., Manatschal, G., Mohn, G., Ghienne, J.-F., Lafont, F., 2011. The tectono-sedimentary evolution of a supra-detachment rift basin at a deep-water magma-poor rifted margin: the example of the Samedan basin preserved in the Err nappe in SE Switzerland: Tectono-sedimentary evolution of a supra-detachment rift basin. basin Res. 23, 652–677. https://doi.org/10.1111/j.1365-2117.2011.00509.x

Masini, E., Manatschal, G., Mohn, G., Unternehr, P., 2012. Anatomy and tectono-sedimentary evolution of a rift-related detachment system: The example of the Err detachment (central Alps, SE Switzerland). Geol. Soc. Am. Bull. 124, 1535–1551. https://doi.org/10.1130/B30557.1

Masini, E., Manatschal, G., Tugend, J., Mohn, G., Flament, J.-M., 2014. The tectono-sedimentary evolution of a hyper-extended rift basin: the example of the Arzacq–Mauléon rift system (Western Pyrenees, SW France). Int. J. Earth Sci. 103, 1569–1596. https://doi.org/10.1007/s00531-014-1023-8

Masson, D.G., Miles, P.R., 1984. Mesozoic seafloor spreading between Iberia, Europe and North America. Mar. Geol. 56, 279–287. https://doi.org/10.1016/0025-3227(84)90019-7

Mattauer, M., 1985. Présentation d'un modèle lithosphérique de la chaîne des Pyrénées. Comptes-Rendus Séances Académie Sci. Sér. 2 Mécanique-Phys. Chim. Sci. Univers Sci. Terre 300, 71–74.

McCaig, A.M., 1988. Deep geology of the Pyrenees. Nature 331, 480–481.

McCaig, A.M., Cliff, R.A., Escartin, J., Fallick, A.E., MacLeod, C.J., 2007. Oceanic detachment faults focus very large volumes of black smoker fluids. Geology 35, 935–938. https://doi.org/10.1130/G23657A.1

McClay, K., Dooley, T., 1995. Analogue models of pull-apart basins. Geology 23, 711–714.

McKenzie, D., 1978. Some remarks on the development of sedimentary basins. Earth Planet. Sci. Lett. 40, 25–32. https://doi.org/10.1016/0012-821X(78)90071-7

McNutt, M.K., Diament, M., Kogan, M.G., 1988. Variations of elastic plate thickness at continental thrust belts. J. Geophys. Res. Solid Earth 93, 8825–8838.

Mohn, G., Karner, G.D., Manatschal, G., Johnson, C.A., 2015. Structural and stratigraphic evolution of the Iberia–Newfoundland hyper-extended rifted margin: a quantitative modelling approach. Geol. Soc. Lond. Spec. Publ. 413, 53–89. https://doi.org/10.1144/SP413.9

Mohn, G., Manatschal, G., Beltrando, M., Haupert, I., 2014. The role of rift-inherited hyper-extension in Alpine-type orogens. Terra Nova 26, 347–353. https://doi.org/10.1111/ter.12104

Mohn, G., Manatschal, G., Masini, E., Müntener, O., 2011. Rift-related inheritance in orogens: a case study from the Austroalpine nappes in Central Alps (SE-Switzerland and N-Italy). Int. J. Earth Sci. 100, 937–961. https://doi.org/10.1007/s00531-010-0630-2

Mohn, G., Manatschal, G., Müntener, O., Beltrando, M., Masini, E., 2010. Unravelling the interaction between tectonic and sedimentary processes during lithospheric thinning in the Alpine Tethys margins. Int. J. Earth Sci. 99, 75–101. https://doi.org/10.1007/s00531-010-0566-6

Mohriak, W.U., Leroy, S., 2013. Architecture of rifted continental margins and break-up evolution: insights from the South Atlantic, North Atlantic and Red Sea–Gulf of Aden conjugate margins. Geol. Soc. Lond. Spec. Publ. 369, 497–535.

Montigny, R., Azambre, B., Rossy, M., Thuizat, R., 1986. K-Ar Study of cretaceous magmatism and metamorphism in the Pyrenees: Age and length of rotation of the Iberian Peninsula. Tectonophysics, The Geological Evolution of the Pyrenees 129, 257–273. https://doi.org/10.1016/0040-1951(86)90255-6

Morley, C.K., Nelson, R.A., Patton, T.L., Munn, S.G., 1990. Transfer zones in the East African rift system and their relevance to hydrocarbon exploration in rifts (1). AAPG Bull. 74, 1234–1253.

Mortimer, E.J., Paton, D.A., Scholz, C.A., Strecker, M.R., 2016. Implications of structural inheritance in oblique rift zones for basin compartmentalization: Nkhata basin, Malawi Rift (EARS). Mar. Pet. Geol. 72, 110–121. https://doi.org/10.1016/j.marpetgeo.2015.12.018

Moulin, M., Aslanian, D., Unternehr, P., 2010. A new starting point for the South and Equatorial Atlantic Ocean. Earth-Sci. Rev. 98, 1–37. https://doi.org/10.1016/j.earscirev.2009.08.001

Moustafa, A.R., 1997. Controls on the development and evolution of transfer zones: the influence of basement structure and sedimentary thickness in the Suez rift and Red Sea. J. Struct. Geol. 19, 755–768.

Mujal, E., Gretter, N., Ronchi, A., López-Gómez, J., Falconnet, J., Diez, J.B., De la Horra, R., Bolet, A., Oms, O., Arche, A., Barrenechea, J.F., Steyer, J.-S., Fortuny, J., 2016. Constraining the Permian/Triassic transition in continental environments: Stratigraphic and paleontological record from the Catalan Pyrenees (NE Iberian Peninsula). Palaeogeogr. Palaeoclimatol. Palaeoecol. 445, 18–37. https://doi.org/10.1016/j.palaeo.2015.12.008

Olivet, J.L., 1996. La cinématique de la plaque ibérique. Bull Cent Rech Explor Prod Elf Aquitaine 20, 131–195.

Omodeo Salè, S., Guimerà, J., Mas, R., Arribas, J., 2014. Tectono-stratigraphic evolution of an inverted extensional basin: the Cameros basin (north of Spain). Int. J. Earth Sci. 103, 1597–1620. https://doi.org/10.1007/s00531-014-1026-5

Omodeo-Salé, S., Salas, R., Guimerà, J., Ondrak, R., Mas, R., Arribas, J., Suárez-Ruiz, I., Martinez, L., 2017. Subsidence and thermal history of an inverted Late Jurassic-Early Cretaceous extensional basin (Cameros, North-central Spain) affected by very low- to low-grade metamorphism. basin Res. 29, 156–174. https://doi.org/10.1111/bre.12142

Osmundsen, P.T., Ebbing, J., 2008. Styles of extension offshore mid-Norway and implications for mechanisms of crustal thinning at passive margins: STYLES OF EXTENSION OFFSHORE NORWAY. Tectonics 27, n/a-n/a. https://doi.org/10.1029/2007TC002242

Osmundsen, P.T., Péron-Pinvidic, G., 2018. Crustal-Scale Fault Interaction at Rifted Margins and the Formation of Domain-Bounding Breakaway Complexes: Insights From Offshore Norway. Tectonics 37, 935–964. https://doi.org/10.1002/2017TC004792

Osmundsen, P.T., Sommaruga, A., Skilbrei, J.R., Olesen, O., 2002. Deep structure of the Mid Norway rifted margin. Nor. J. Geol. Geol. Foren. 82.

Pérez-Gussinyé, M., Reston, T., 2001. Rheological evolution during extension at nonvolcanic rifted margins: Onset of serpentinization and development of detachemnts leading to continental breakup. J. Geophys. Res.

Peron-Pinvidic, G., 2006. Morphotectonique et architecture sédimentaire de la transition océan-continent de la marge ibérique. Strasbourg 1.

Peron-Pinvidic, G., Gernigon, L., Gaina, C., Ball, P., 2012a. Insights from the Jan Mayen system in the Norwegian–Greenland sea—I. Mapping of a microcontinent. Geophys. J. Int. 191, 385–412. https://doi.org/10.1111/j.1365-246X.2012.05639.x

Peron-Pinvidic, G., Gernigon, L., Gaina, C., Ball, P., 2012b. Insights from the Jan Mayen system in the Norwegian–Greenland Sea—II. Architecture of a microcontinent. Geophys. J. Int. 191, 413–435. https://doi.org/10.1111/j.1365-246X.2012.05623.x

Péron-Pinvidic, G., Manatschal, G., 2009. The final rifting evolution at deep magma-poor passive margins from Iberia-Newfoundland: a new point of view. Int. J. Earth Sci. 98, 1581–1597. https://doi.org/10.1007/s00531-008-0337-9

Péron-Pinvidic, G., Manatschal, G., Masini, E., Sutra, E., Flament, J.M., Haupert, I., Unternehr, P., 2015. Unravelling the along-strike variability of the Angola–Gabon rifted margin: a mapping approach. Geol. Soc. Lond. Spec. Publ. 438, 49–76. https://doi.org/10.1144/SP438.1

Péron-Pinvidic, G., Manatschal, G., Minshull, T.A., Sawyer, D.S., 2007. Tectonosedimentary evolution of the deep Iberia-Newfoundland margins: Evidence for a complex breakup history. Tectonics 26, 1–19. https://doi.org/10.1029/2006TC001970

Peron-Pinvidic, G., Manatschal, G., Osmundsen, P.T., 2013. Structural comparison of archetypal Atlantic rifted margins: A review of observations and concepts. Mar. Pet. Geol. 43, 21–47. https://doi.org/10.1016/j.marpetgeo.2013.02.002

Petrunin, A., Sobolev, S.V., 2006. What controls thickness of sediments and lithospheric deformation at a pull-apart basin? Geology 34, 389. https://doi.org/10.1130/G22158.1

Peybernès, B., 1978. Dans les Pyrenees la paleogeographie antecenomanienne infirme la theorie d'un coulissement senestre de plusieurs centaines de kilometres le long de la "faille nord-pyreneenne" des auteurs. Bull. Société Géologique Fr. S7-XX, 701–709. https://doi.org/10.2113/gssgfbull.S7-XX.5.701

Pinet, B., Montadert, L., ECORS Scientific Party, 1987. Deep seismic reflection and refraction profiling along the Aquitaine shelf (Bay of Biscay). Geophys. J. Int. 89, 305–312. https://doi.org/10.1111/j.1365-246X.1987.tb04423.x

Pochat, S., Van Den Driessche, J., 2011. Filling sequence in Late Paleozoic continental basins: A chimera of climate change? A new light shed given by the Graissessac–Lodève basin (SE France). Palaeogeogr. Palaeoclimatol. Palaeoecol. 302, 170–186. https://doi.org/10.1016/j.palaeo.2011.01.006

Pollack, H.N., Hurter, S.J., Johnson, J.R., 1993. Heat flow from the Earth's interior: Analysis of the global data set. Rev. Geophys. 31, 267. https://doi.org/10.1029/93RG01249

Puigdefàbregas, C., Muñoz, J.A., Vergés, J., 1992. Thrusting and foreland basin evolution in the southern Pyrenees, in: Thrust Tectonics. Springer, pp. 247–254.

Puigdefàbregas, C., Souquet, P., 1986. Tecto-sedimentary cycles and depositional sequences of the Mesozoic and Tertiary from the Pyrenees. Tectonophysics 129, 173–203.

Rat, J., Mouthereau, F., Brichau, S., Crémades, A., Bernet, M., Balvay, M., Ganne, J., Lahfid, A., Gautheron, C., 2019. Tectonothermal Evolution of the Cameros basin: Implications for Tectonics of North Iberia. Tectonics 38, 440–469. https://doi.org/10.1029/2018TC005294

Ravier, J., 1957. Le métamorphisme des terrains secondaires des Pyrénées. Université, Faculté des Sciences.

Reston, T., Manatschal, G., 2011. Rifted Margins: Building Blocks of Later Collision, in: Arc-Continent Collision, Frontiers in Earth Sciences. Springer Berlin Heidelberg, pp. 3–21. https://doi.org/10.1007/978-3-540-88558-0_1

Reston, T.J., 2007. The formation of non-volcanic rifted margins by the progressive extension of the lithosphere: the example of the West Iberian margin. Geol. Soc. Lond. Spec. Publ. 282, 77–110. https://doi.org/10.1144/SP282.5

Reston, T.J., 2005. Polyphase faulting during the development of the west Galicia rifted margin. Earth Planet. Sci. Lett. 237, 561–576. https://doi.org/10.1016/j.epsl.2005.06.019

Reston, T.J., 1988. Evidence for shear zones in the lower crust offshore Britain. Tectonics 7, 929–945. https://doi.org/10.1029/TC007i005p00929

Reston, T.J., Krawczyk, C.M., Hoffmann, H.-J., 1995. Detachment tectonics during Atlantic rifting: analysis and interpretation of the S reflection, the west Galicia margin. Geol. Soc. Lond. Spec. Publ. 90, 93–109. https://doi.org/10.1144/GSL.SP.1995.090.01.05

Reston, T.J., McDermott, K.G., 2011. Successive detachment faults and mantle unroofing at magma-poor rifted margins. Geology 39, 1071–1074. https://doi.org/10.1130/G32428.1

Reston, T.J., Pérez-Gussinyé, M., 2007. Lithospheric extension from rifting to continental breakup at magma-poor margins: rheology, serpentinisation and symmetry. Int. J. Earth Sci. 96, 1033–1046. https://doi.org/10.1007/s00531-006-0161-z

Reynolds, D.J., Rosendahl, B.R., 1984. Tectonic expressions of continental rifting. EOS Trans Am Geophys Union 65, 1055.

Roca, E., Muñoz, J.A., Ferrer, O., Ellouz, N., 2011. The role of the Bay of Biscay Mesozoic extensional structure in the configuration of the Pyrenean orogen: Constraints from the MARCONI deep seismic reflection survey. Tectonics 30. https://doi.org/10.1029/2010TC002735

Roger, F., Teyssier, C., Respaut, J.-P., Rey, P.F., Jolivet, M., Whitney, D.L., Paquette, J.-L., Brunel, M., 2015. Timing of formation and exhumation of the Montagne Noire double dome, French Massif Central. Tectonophysics 640, 53–69.

Roma, M., Ferrer, O., Roca, E., Pla, O., Escosa, F.O., Butillé, M., 2018. Formation and inversion of salt-detached ramp-syncline basins. Results from analog modeling and application to the Columbrets basin (Western Mediterranean). Tectonophysics 745, 214–228. https://doi.org/10.1016/j.tecto.2018.08.012

Roure, F., Choukroune, P., Berastegui, X., Munoz, J.A., Villien, A., Matheron, P., Bareyt, M., Seguret, M., Camara, P., Deramond, J., 1989. Ecors deep seismic data and balanced cross sections: Geometric constraints on the evolution of the Pyrenees. Tectonics 8, 41–50. https://doi.org/10.1029/TC008i001p00041

Roux, J.-C., 1983. Recherches stratigraphiques et sédimentologiques sur les flyschs crétacés pyrénéens au sud d'Oloron (Pyrénées Atlantiques). Université Paul Sabatier de Toulouse (Sciences).

Rubatto, D., Gebauer, D., Fanning, M., 1998. Jurassic formation and Eocene subduction of the Zermatt-Saas-Fee ophiolites: implications for the geodynamic evolution of the Central and Western Alps. Contrib. Mineral. Petrol. 132, 269–287. https://doi.org/10.1007/s004100050421

Schoeffler, J., 1965. Une hypothèse sur la tectogénèse de la chaîne pyrénéenne et de ses abords. Bull Soc Géol Fr 7, 917–920.

Sibuet, J.-C., Srivastava, S., Manatschal, G., 2007. Exhumed mantle-forming transitional crust in the Newfoundland-Iberia rift and associated magnetic anomalies. J. Geophys. Res. Solid Earth 112. https://doi.org/10.1029/2005JB003856

Sibuet, J.-C., Srivastava, S.P., Spakman, W., 2004. Pyrenean orogeny and plate kinematics. J. Geophys. Res. Solid Earth 109, B08104. https://doi.org/10.1029/2003JB002514

Souquet, P., Debroas, E.-J., Boirie, J.-M., Pons, P., Fixari, G., Roux, J.-C., Dol, J., Thieuloy, J.-P., Bonnemaison, M., Manivit, H., others, 1985. Le groupe du Flysch noir (albo-cénomanien) dans les Pyrénées. Bull Cent Rech Exlpo-Prod Elf-Aquitaine Pau 9, 183–252.

Souquet, P., Peybènes, B., Bilotte, M., Debroas, E.-J., 1977. La chaîne alpine des Pyrénées. Géologie Alp. 53, 193–216.

Spencer, J.E., 1984. Role of tectonic denudation in warping and uplift of low-angle normal faults. Geology 12, 95–98. https://doi.org/10.1130/0091-7613(1984)12<95:ROTDIW>2.0.CO;2

Stampfli, G.., Mosar, J., Marquer, D., Marchant, R., Baudin, T., Borel, G., 1998. Subduction and obduction processes in the Swiss Alps. Tectonophysics 296, 159–204. https://doi.org/10.1016/S0040-1951(98)00142-5

Teixell, A., Labaume, P., Ayarza, P., Espurt, N., de Saint Blanquat, M., Lagabrielle, Y., 2018. Crustal structure and evolution of the Pyrenean-Cantabrian belt: A review and new interpretations from recent concepts and data. Tectonophysics 724, 146–170. https://doi.org/10.1016/j.tecto.2018.01.009

Teixell, A., Labaume, P., Lagabrielle, Y., 2016. The crustal evolution of the west-central Pyrenees revisited: Inferences from a new kinematic scenario. Comptes Rendus Geosci. 348, 257–267. https://doi.org/10.1016/j.crte.2015.10.010

Thinon, I., 1999. Structure profonde de la marge Nord Gascogne et du bassin armoricain. Université de Bretagne occidentale-Brest.

Thinon, I., Matias, L., RÉhault, J.P., Hirn, A., Fidalgo-GonzÁlez, L., Avedik, F., 2003. Deep structure of the Armorican basin (Bay of Biscay): a review of Norgasis seismic reflection and refraction data. J. Geol. Soc. 160, 99–116. https://doi.org/10.1144/0016-764901-103

Tugend, J., Manatschal, G., Kusznir, N.J., Masini, E., 2015. Characterizing and identifying structural domains at rifted continental margins: application to the Bay of Biscay margins and its Western Pyrenean fossil remnants. Geol. Soc. Lond. Spec. Publ. 413, 171–203. https://doi.org/10.1144/SP413.3

Tugend, J., Manatschal, G., Kusznir, N.J., Masini, E., Mohn, G., Thinon, I., 2014. Formation and deformation of hyperextended rift systems: Insights from rift domain mapping in the Bay of Biscay-Pyrenees. Tectonics 33, 1239–1276. https://doi.org/10.1002/2014TC003529

Unternehr, P., Peron-Pinvidic, G., Manatschal, G., Sutra, E., 2010. Hyper-extended crust in the South Atlantic: in search of a model. Pet. Geosci. 16, 207–215. https://doi.org/10.1144/1354-079309-904

Van Den Driessche, J., Brun, J.-P., 1992. Tectonic evolution of the Montagne Noire (French Massif Central): a model of extensional gneiss dome. Geodin. Acta 5, 85–97.

Velasque, P.-C., Ducasse, L., 1987. Géotraverse équilibrée dans les Pyrénées occidentales: argument en faveur d'un rift intraplaque pour expliquer l'amincissement crustal crétacé. Comptes Rendus Académie Sci. Sér. 2 Mécanique Phys. Chim. Sci. Univers Sci. Terre 304, 383–386.

Vielzeuf, D., 1984. Relations de phases dans le faciès granulite et implications géodynamiques: l'exemple des granulites des Pyrénées. Université Clermont-Ferrand II.

Vielzeuf, D., Kornprobst, J., 1984. Crustal splitting and the emplacement of Pyrenean lherzolites and granulites. Earth Planet. Sci. Lett. 67, 87–96. https://doi.org/10.1016/0012-821X(84)90041-4

Viennot, P., Kieh, Y., 1928. Observations pétrographiques dans le massif cristallin du Labourd (Basses Pyrénées). Bull Soc Géol Fr 28, 369–379.

Wang, Y., 2017. High resolution imaging of lithospheric structures by full waveform inversion of short period teleseismic P waves. Université Toulouse 3 Paul Sabatier (UT3 Paul Sabatier).

Wang, Y., Chevrot, S., Monteiller, V., Komatitsch, D., Mouthereau, F., Manatschal, G., Sylvander, M., Diaz, J., Ruiz, M., Grimaud, F., Benahmed, S., Pauchet, H., Martin, R., 2016. The deep roots of the western Pyrenees revealed by full waveform inversion of teleseismic P waves. Geology 44, 475–478. https://doi.org/10.1130/G37812.1

Wernicke, B., 1985. Uniform-sense normal simple shear of the continental lithosphere. Can. J. Earth Sci. 22, 108–125. https://doi.org/10.1139/e85-009

Wernicke, B., 1981. Low-angle normal faults in the basin and Range Province: nappe tectonics in an extending orogen. Nature 291, 645–648. https://doi.org/10.1038/291645a0

Wernicke, B., Axen, G.J., 1988. On the role of isostasy in the evolution of normal fault systems. Geology 16, 848–851. https://doi.org/10.1130/0091-7613(1988)016<0848:OTROII>2.3.CO;2

Wernicke, B., Burchfiel, B.C., 1982. Modes of extensional tectonics. J. Struct. Geol. 4, 105–115. https://doi.org/10.1016/0191-8141(82)90021-9

Whitmarsh, R.B., Manatschal, G., Minshull, T.A., 2001. Evolution of magma-poor continental margins from rifting to seafloor spreading. Nature 413, 150–154. https://doi.org/10.1038/35093085

Wilson, R.C.L., Manatschal, G., Wise, S., 2001. Rifting along non-volcanic passive margins: stratigraphic and seismic evidence from the Mesozoic successions of the Alps and western Iberia. Geol. Soc. Lond. Spec. Publ. 187, 429–452. https://doi.org/10.1144/GSL.SP.2001.187.01.21

Wopenka, B., Pasteris, J.D., 1993. Structural characterization of kerogens to granulite-facies graphite: applicability of Raman microprobe spectroscopy. Am. Mineral. 78, 533–557.

Young, M.J., Gawthorpe, R.L., Hardy, S., 2001. Growth and linkage of a segmented normal fault zone; the Late Jurassic Murchison–Statfjord North Fault, northern North Sea. J. Struct. Geol. 23, 1933–1952. https://doi.org/10.1016/S0191-8141(01)00038-4

Yui, T.-F., Huang, E., Xu, J., 1996. Raman spectrum of carbonaceous material: a possible metamorphic grade indicator for low-grade metamorphic rocks. J. Metamorph. Geol. 14, 115–124.

Zhang, P., Burchfiel, B.C., Chen, S., Deng, Q., 1989. Extinction of pull-apart basins. Geology 17, 814–817.

Chapitre 2

Héritage permien

Bref aperçu du chapitre 2 : Héritage permien

Le chapitre 2 de ce manuscrit de thèse s'attache à présenter l'évolution géodynamique du Carbonifère supérieur au Trias supérieur des Pyrénées occidentales, sur la base de l'évolution tectono-sédimentaire et structurale du bassin de Bidarray et du dôme granulitique à migmatitique de l'Ursuya. Le chapitre 2.1 décrit, en détail, les faciès sédimentaires du Permien et du Trias affleurant dans le bassin de Bidarray. Cette étude de terrain a permis de définir précisément les environnements de dépôts continentaux de ces systèmes sédimentaires.

Le chapitre 2.2 correspond à un article publié dans le journal *Tectonophysics*. Celui-ci décrit l'évolution géodynamique permienne des Pyrénées occidentales. Cette étude est basée sur une approche pluridisciplinaire intégrant l'évolution tectono-sédimentaire du bassin de Bidarray et son lien génétique avec l'exhumation du dôme métamorphique de l'Ursuya, au cours du Permien. Ce travail s'appuie sur : (1) des données sédimentologiques et structurales de terrains récoltées sur le bassin de Bidarray, (2) une mise à jour des précédentes cartes au 1/50 000 publiées par le BRGM et l'IGME et (3) une analyse structurale du dôme de l'Ursuya.

Chapitre 2.1

Analyse sédimentaire des séries du Permien et du Trias du bassin de Bidarray

Chapitre 2.1. Analyse sédimentaire des séries continentales du Permien et du Trias du bassin de Bidarray

Sommaire

1. Introduction **p. 71**

2. Sedimentary analysis **p. 71**

2.1. Lithofacies F1a: Chaotic breccias p. 71

2.2. Lithofacies F1b: Fine-grained breccias p. 71

2.3. Lithofacies F1c: Coarse-cemented breccias p. 71

2.4. Lithofaciès F2a: Matrix-supported breccias p. 74

2.5. Lithofacies F2b: Muddy breccias p. 74

2.6. Lithofacies F3a: Polygenic Conglomerates p. 75

2.7. Lithofacies F3b: Monogenic Conglomerates p. 75

2.8. Lithofacies F4: Lenticular stratified breccias p. 75

2.9. Lithofacies F5a: Coarse amalgamated sandstones p. 76

2.10. Lithofacies F5b: Tabular sandstones p. 76

2.11. Lithofacies F6: Siltstones p. 76

References p. 76

Chapitre 2.1. Analyse sédimentaire des séries continentales du Permien et du Trias du bassin de Bidarray

1. Introduction

This chapter describe the Permian-Triassic sedimentary facies of the Bidarray basin. These facies have been summarized in a table in the paper published in the Tectonophysics journal as only the facies association have been described in detail (chapter 2.2). This chapter permits to bring a precise point of view of the sedimentary work that have been done in this published study.

2. Sedimentary analysis

2.1. Lithofacies F1a: Chaotic breccias

This facies forms coarse clast-supported, silty-matrix breccias **(Fig. 1A)**. The matrix contains granules of quartz and Paleozoic elements ranging from 1 mm to 6 mm. F1a breccias form units ranging from 2 m up to 10 m thick. They consist of polygenic clasts with elements size ranging from 2 cm and up to 30 cm in diameter and an average size of 8 cm. The clasts are predominantly angular and include a large range of Devonian, Carboniferous and Silurian lithofacies (black shales, light gray micritic limestones, white and black quartzites, sandstones and quartz); their nature strongly varies laterally. F1a breccias form beds (15 cm to 50 cm in thickness), the base of which is not erosive. They mostly show chaotic fabric, or display clasts alignment following the stratification and more rarely cross-stratifications. These breccias are in tectonic contact with the basement as this latter is affected by cataclasites **(Fig. 1E)**.

Interpretation: This facies corresponds to hyper-concentrated flows developing in alluvial fan system. These hyper-concentrated flows have intermediate rheological characteristics between ordinary torrential flows and cohesive or no-cohesive debris flows (**Fig. 2**; Bull, 1977; Blair and McPherson, 1994). The hyper-concentrated current could be derived from the evolution of the rheological properties of debris-flow, which evolves towards a turbulent flow and a sedimentary dynamic dominated by traction mechanism flow (**Fig. 2**; Pierson and Scott, 1985; Benvenuti and Martini, 2002). The lithological heterogeneity of these breccias is related to the nature of the Paleozoic substratum with which they are in contact.

2.2. Lithofacies F1b: Fine-grained breccias

This facies consist of polygenic clast-supported breccias. Clasts are predominantly angular to sub-angular. These elements are very abundant (70 to 90%), and surrounded by a red silty matrix **(Fig. 1B)**. F1b breccias form units ranging from 2 m to 15 m in thickness. The clast average size is about 5 mm but can reach 5 to 30 cm. The clasts are mainly composed of quartz granules, sandstones, schists, gray micritic limestones and a small proportion of quartzites. These breccias are relatively well sorted and can display clast alignment following the bedding and some cross-stratifications.

Interpretation: The sedimentation mechanism of the F1b fine-grained breccias is quite similar to those of the F1a facies. The F1b facies corresponds to the distal part of hyper-concentrated alluvial fans (Pierson and Scott, 1985; Benvenuti and Martini, 2002). The decrease of the velocity flow allows to keep the coarse matrix of the F1a facies and to leave the biggest clasts upstream.

2.3. Lithofacies F1c: Coarse-cemented breccias

This facies consists of coarse clast-supported sedimentary breccias **(Fig. 1C)**. These breccias does only outcrop on top of the Cambrian meta-cover of the Ursuya granulites forming patches with an average area of 10 m^2 to 30 m^2. The matrix is cemented and predominantly made of red coarse-grained sandstone to siltstone. The breccias are poorly sorted with clast sizes ranging from granules to blocks up to 40 cm in diameter. Clasts are mainly angular, polygenic and include Cambrian quartz, quartzite and micaschists. These breccias are mostly chaotic and do not present any bedding.

Interpretation These deposits are characterized by a low transport and a relatively close source. These breccias corresponds to debris flow sedimentary mechanism (Coussot and Meunier, 1996; Iverson, 1997).


F1a. Chaotic breccias
A
B
F1b. Fine-grained breccias
C
F1c. Coarse-cemented breccias
D
F2a. Matrix-supported breccias
E
Cataclasites of Ordovician quartzites
F
F3a. Polygenic conglomerates
G
F3a. Polygenic conglomerates
Erosional surface
sandstones stratifications
H
F3a. Polygenic conglomerates

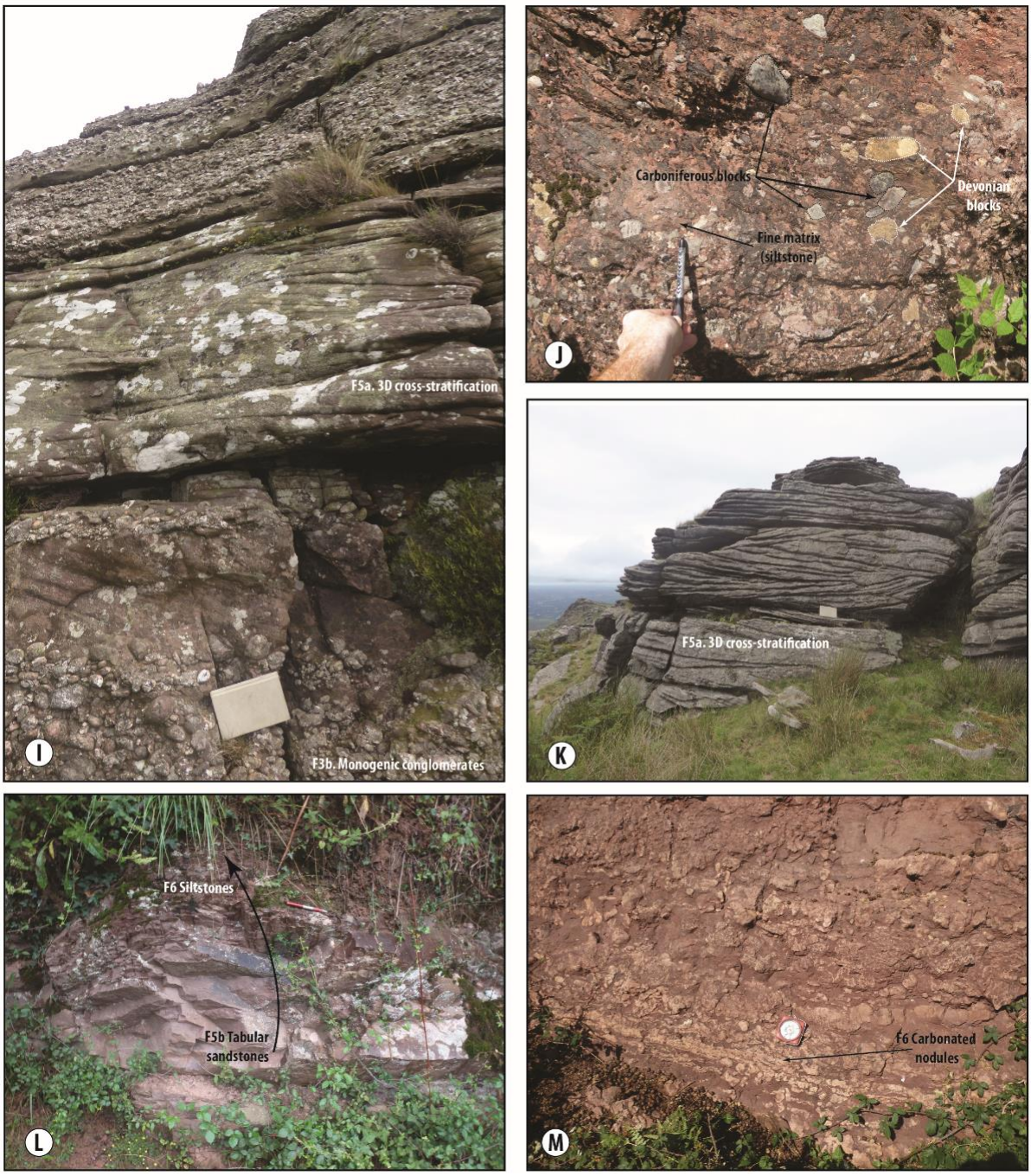


Fig. 1. Permian-Triassic continental facies of the Bidarray basin. **(A)** F1a facies: chaotic breccias made up of Paleozoic blocks aligned following the stratification; **(B)** F1b facies: fine-grained breccias corresponding to the matrix of the F1a breccias; **(C)** F1c facies: coarse-cemented breccias poorly sorted with Cambrian clasts; sizes range from granules to blocks (max 40 cm diameter); **(D)** F2a facies: matrix-supported breccias made of fine-grained matrix; these breccias are intercalated with clast rich breccias, the elements are made of Devonian to Carboniferous substratum; **(E)** Cataclasites affecting the meta-sedimentary basement along the western part of the Bidarray basin, corresponding to the paleo-normal fault controlling the destabilization of the Permian alluvial fans; **(F-H)** F3a facies: polygenic conglomerates made of sub-rounded pebbles with an average size of 2–3 cm; the conglomerates are made of planar oblique cross-stratification of 5–20 cm size and erosional gutter at their base. The F5a intercalations record the deposition of sandy bedforms within the conglomeratic fluvial channels or bars during flood falling stage; **(I)** F3b facies: monogenic conglomerates formed by quartzite pebbles with an average size of 8 cm intercalated with F5a amalgamated sandstones; **(J)** F4 facies: lenticular stratified breccias with angular polygenic Paleozoic clasts supported by a fine-grained matrix; **(K)** F5a facies: coarse amalgamated sandstones with 3D cross-stratifications. **(L)** F5b tabular sandstones passing on the top to F6 siltstones; **(M)** F6 facies: carbonated paleosols intercalated into siltstones.

2.4. Lithofaciès F2a: Matrix-supported breccias

This facies forms coarse polygenic breccias, with a silty-clay matrix **(Fig. 1D)**. The matrix is a siltstone to a fine-grained sandstone. These breccias consist of beds ranging from 10 cm to 60 cm in thickness. They are composed of « clast-rich-breccias » alternating with « matrix-supported breccias ». The base of the clast-rich beds can erode the matrix-supported beds. The elements size range from 2 cm up to 15 cm in diameter and an average size of 7 cm. The clasts are mainly composed of Devonian-Carboniferous light gray micritic limestones, meta-sandstones and quartzites. The clast-rich beds are relatively well sorted and the clasts can display alignment following the stratification. The « matrix-supported » beds are poorly sorted and chaotic.

Interpretation: This facies is interpreted to be related to debris flow alluvial fan deposits. A debris flow is a rapid gravity flow containing debris with an interstitial fluid composed of a small percentage of water plus argillaceous particles **(Fig. 2)**. The displacement of the sediments causes the interstitial fluid by the force of gravity (Coussot and Meunier, 1996; Iverson, 1997). The F2a matrix proportion lower than 40% tends to indicate that this type of debris-flow is non-cohesive (Blair & McPherson 1994; Levson & Rutter 2000). These deposits are characterized by a low transport and a relatively close source.

2.5. Lithofacies F2b: Muddy breccias

This facies consists of polygenic muddy breccias that is a matrix-supported breccia contening 30 to 40% of clast content. These breccias form beds ranging from 30 cm up to 2 m thick, with a non-erosive base. They comprise polygenic angular clasts, characterized by an average size of 6 cm with an upper limit of 30 cm. The clasts are mainly composed of black shales, quartzites, gray limestones and sandstones derived from Devonian and Carboniferous lithofacies. The elements are poorly sorted, but some beds are characterized by coarsening-up clasts, ranging from 2 cm to 10-30 cm.

Interpretation: The F2b facies can be interpreted as debris flow alluvial fans deposits **(Fig. 2)**. This type of deposit is comparable to a laminar flow of high viscosity, with a sediment load of more than 50% (Iverson, 1997). The proportion of more than 60% of matrix in this facies tends to indicate that this type of debris flow is cohesive (Blair and McPherson, 1994). These deposits are characterized by a short transport distance. Indeed, the lithological heterogeneity of these breccias is related to the nature of the Paleozoic substratum which they are in contact with.

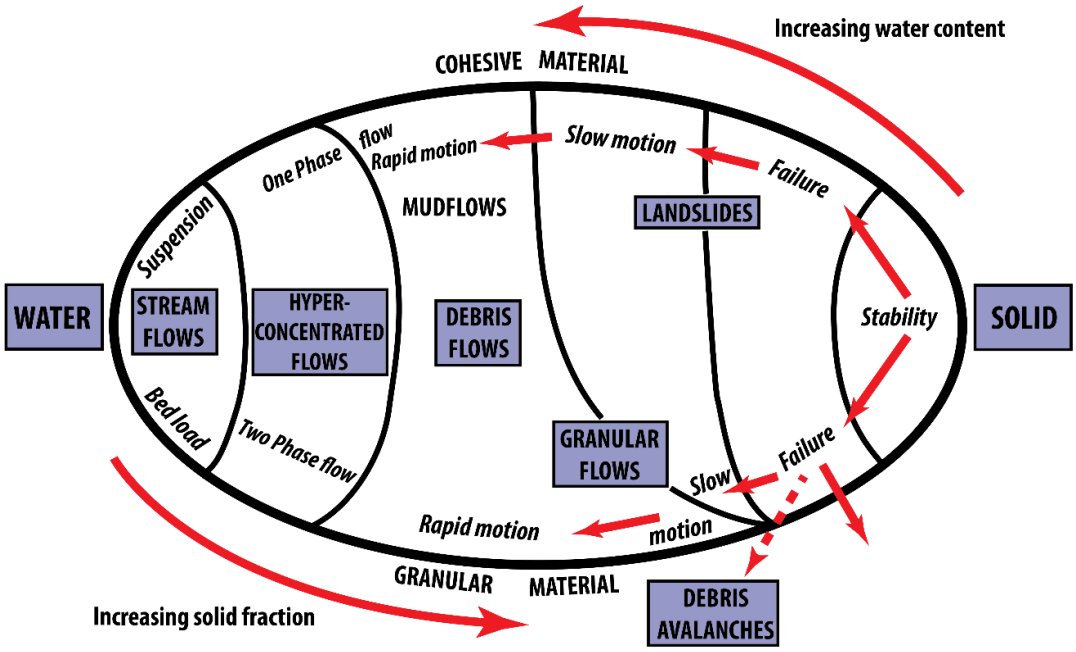


Fig. 2. Steep slope gravitational destabilization processes classification, according to the solid and liquid fraction proportion and the material type (modified from Coussot and Meunier, 1996).

2.6. Lithofacies F3a: Polygenic Conglomerates

This facies forms polygenic conglomerates with rounded to sub-rounded cobbles **(Fig. 1F-H)**. This facies forms fining up beds of 30 cm to 3 m in thickness. They form unit of 8 meters in which beds thickness decreases upward. These conglomerates are fairly well sorted and mainly composed of quartzites and quartz granules. The average size of the pebbles is 2-3 cm, with a maximum size of 8 cm. The rare sub-rounded elements correspond for the most part of Carboniferous gray micritic limestones. These conglomerates contain little or no matrix which is sandy when present. The conglomerates display mostly planar oblique cross-stratification forming bedsets of 5-20 cm. The base of the conglomeratic beds is erosive and can show erosional gutters. These conglomeratic beds are intercalated with sandstone facies. The stratified sandstones consist on relatively well-sorted medium to coarse sandstones **(Fig. 1H)**. They form fining-up beds ranging from 20 cm up to 70 cm in thickness and are composed of low-angle bedding, forming tabular bedforms. These bedforms stop laterally under the overlying erosive conglomerates, and can present a polygenic lag at their base. This latter is made of Paleozoic quartzites, quartz, sandstones and schists with an average size of 2-3 cm.

Interpretation: The F3a conglomerates represent the bedload deposits of longitudinal fluvial system (Bridge, 2009). The planar oblique stratifications are typical of 2D dunes located in the thalwegs of fluvial channels and within fluvial bars. The F5a intercalations record the deposition of sandy bedforms within the conglomeratic fluvial channels or bars during flood falling stage (Rust, 1978). The presence of quartzite and rounded quartz granules suggests the reshaping of an ancient sedimentary source, while the presence of sub-angular black shale elements demonstrates mixing with a nearby source. The stratified sandstones are interpreted to be related to high-flood deposits underlying the previous conglomerates that filled the fluvial channel. The top of this sandstone is eroded by the next channel, explaining their low lateral continuity.

2.7. Lithofacies F3b: Monogenic Conglomerates

This facies consits on monogenic conglomerates comprising well-sorted rounded elements **(Fig. 1I)**. These conglomerates form amalgamated fining-up erosive beds ranging from 1 m up to 5 m in thickness. It is clast-supported and the matrix is a coarse-grained sandstone. The pebbles are mainly quartzites or/and quartz granules, occasionally imbricated. The quartzites are very similar to the Cambrian clasts describe in F1c facies. The pebbles are characterized by an average size of 8-10 cm with an upper limit of 20 cm diameter. Low-angle to oblique cross-stratifications locally observed in some bed tops.

Interpretation: This facies is interpreted to be braided channel deposits. The bottom currents of channels are responsible of the pebbles imbrications (Bridge, 1993). The development of oblique cross-stratification could be interpreted as pebbly dune cross-beds formed during migration through the fluvial channel or it could correspond to large low-angle stratification within pebbly fluvial bar (Miall, 1977a).

2.8. Lithofacies F4: Lenticular stratified breccias

This facies forms a matrix to clast-supported polygenic lenticular breccias, for which the matrix is a red fine-grained siltstone. They are moderately well-sorted and made of Devonian to Carboniferous light gray micritic limestones, quartzites, shales, sandstones, and quartz granules **(Fig. 1J)**. The average size of the clasts is 2-5 cm, with a maximum of 8 cm. These breccias form beds ranging from 30 cm up to 2 m thick, with an erosional base within the F6a siltstones showing polygenic lag made of Paleozoic elements with an average size of 2-4 cm. This facies occasionally presents oblique cross-stratifications.

Interpretation: This facies is interpreted as channel deposits reworking the adjacent alluvial-fan pebbles (facies F1a-F1b). These breccias form classical sequences of channel fill-deposits, essentially preserving the base of the dune cross-strata (Bridge, 1993, 2009). Their small size and source suggest that the system is very localized at the foot of alluvial fans. These minor fluvial channels erode the

floodplain and are located into a longitudinal drainage system perpendicular to the alluvial fans alimentation.

2.9. Lithofacies F5a: Coarse amalgamated sandstones

This facies forms coarse amalgamated sandstones **(Figs. 1I and 1K)**. These sandstones consist of 1 m to 10 m thick units. They are characterized by trough cross-stratification ranging from 20 cm up to 1 m high and inclined from 15-30°. These 3D cross-stratification form fining-up and thinning-up beds ranging from 10 to 50 cm thick.

Interpretation: This facies is interpreted to be related to coarse fluvial braided channels. The 3D cross-stratification corresponds to dune migration and aggradation within channels (Miall, 1977b).

2.10. Lithofacies F5b: Tabular sandstones

This facies consists of very well-sorted fine to very fine sandstone **(Fig. 1L)**. These sandstones form tabular beds ranging from 2 cm up to 20 cm in thickness, with an non erosional base. They are intercalated with F6a siltstones and can present some planar laminations.

Interpretation: This facies is interpreted as overbank deposits within the floodplain during high flood period. From dynamic point of view, they are quite similar to sheetflood deposits (Bridge, 1993).

2.11. Lithofacies F6: Siltstones

This facies consits of fine-grained deposits ranging from siltstones to claystones **(Fig. 1L)**, intercalated with carbonaceous beds **(Fig. 1M)**. These siltstones are characterized by fine and regular horizontal laminations, visible due to small particle size variations. They are more or less indurated and mainly associated with F5b sandstones. This monotonous facies can remain homogeneous over 1 m to 10 m thick. The carbonate beds are characterized by a thickness lower than 10 cm and carbonate nodules of 1 cm to 5 cm diameter. This beds are not abundant and form units of 30 cm to 2m thick.

Interpretation: These siltstones are located laterally to the main channels of the longitudinal fluvial system. These deposits might be either floodplain deposits that are deposited by decantation during last stage of floods or deposited as distal fine-grained sediment on alluvial-fan lobes (Bridge, 2009). The carbonate beds correspond to paleosols that developed in floodplain deposits. This lithofacies is thought to record a rather long deposition time period.

References

Benvenuti, M., and I. P. Martini, 2002, Analysis of Terrestrial Hyperconcentrated Flows and their Deposit, in I. Peter Martini, V. R. Baker, and G. Garzn, eds., Flood and Megaflood Processes and Deposits: Oxford, UK, Blackwell Publishing Ltd., p. 167–193, doi:10.1002/9781444304299.ch10.

Blair, T. C., and J. G. McPherson, 1994, Alluvial fans and their natural distinction from rivers based on morphology, hydraulic processes, sedimentary processes, and facies assemblages: Journal of sedimentary research, v. 64, no. 3.

Bridge, J. S., 1993, Description and interpretation of fluvial deposits: a critical perspective: Sedimentology, v. 40, no. 4, p. 801–810.

Bridge, J. S., 2009, Rivers and floodplains: forms, processes, and sedimentary record: John Wiley & Sons.

Bull, W. B., 1977, The alluvial-fan environment: Progress in physical geography, v. 1, no. 2, p. 222–270.

Coussot, P and Meunier, M., 1996, Recognition, classification and mechanical description of debris flow, Earth Science Review, v. 40, p. 209–227.

Iverson, R. M., 1997, The physics of debris flows: Reviews of Geophysics, v. 35, no. 3, p. 245–296, doi:10.1029/97RG00426.

Levson, V. M., and N. W. Rutter, 2000, Influence of bedrock geology on sedimentation in Pre-Late Wisconsinan alluvial fans in the Canadian Rocky Mountains: Quaternary International, v. 68–71, p. 133–146, doi:10.1016/S1040-6182(00)00039-2.

Miall, A. D., 1977a, A review of the braided-river depositional environment: Earth-Science Reviews, v. 13, no. 1, p. 1–62.

Miall, A. D., 1977b, Lithofacies types and vertical profile models in braided river deposits: a summary: Geological Survey of Canada, p. 597–604.

Pierson, T. C., and K. M. Scott, 1985, Downstream Dilution of a Lahar: Transition From Debris Flow to Hyperconcentrated Streamflow: Water Resources Research, v. 21, no. 10, p. 1511–1524, doi:10.1029/WR021i010p01511.

Rust, B. R., 1978, Depositional models for braided alluvium, in Fluvial Sedimentology: Miall, Mem. Can. Soc. Pet. Geol, p. 605–625.

Chapitre 2.2

Evolution tectono-sédimentaire d'un système de rift contrôlé par une extension post-orogénique permienne et la formation d'un dôme métamorphique (bassin de Bidarray et dôme de l'Ursuya, Pyrénées occidentales)

Chapitre 2.2. Tectono-sedimentary evolution of a rift-system controlled by Permian post-orogenic extension and MCC formation (Bidarray basin and Ursuya dome, Western Pyrenees)

Sommaire

Résumé étendu p. 81

Abstract p. 87

1. Introduction **p. 87**

2. Geological settings **p. 88**

2.1. The Pyrenean Variscan belt p. 88

2.2. Post-Variscan Permian-Triassic extensional basins p. 89

2.3. Present day structure of the Western Pyrenees p. 89

3. Facies association and depositional models **p. 91**

3.1. FA1 facies association: Alluvial fan dominated by hyper-concentrated flows p. 92

3.2. FA2 facies association: Debris-flow alluvial fan p. 92

3.3. FA3a facies association: Coarse fluvial p. 92

3.4. FA3b facies association: Floodplain p. 92

3.5. FA4 facies association: Braided fluvial p. 95

4. Tectono-sedimentary analysis **p. 95**

4.1. Facies distribution of the Permian deposits (FA1-FA3) p. 95

4.2. Facies distribution of the Triassic deposits (FA4) p. 97

4.3. Permian to Triassic morpho-tectonics of the Western Basque Pyrenees p. 97

5. Structural scheme of the Basque massifs **p. 98**

6. Structural analysis of the Ursuya granulitic unit **p. 98**

7. Discussion **p. 103**

7.1. Permian age for the Louhossoa shear zone p. 103

7.2. Permian conceptual model of crustal thinning p. 103

7.3. Implications for the transition between the Variscan orogenic cycle and Pangea break-up p. 105

7.4. Tectonic implications for the structural scheme of the Western Pyrenees p. 106

8. Conclusion **p. 106**

Acknowledgements p. 107

References p. 107

Résumé étendu

Ce chapitre présente la réponse sédimentaire et structurale d'une croûte continentale affectée par une phase extensive dans un contexte de lithosphère anormalement chaude. Ces chapitres se focalisent sur le système de rift permien des Pyrénées occidentales, où l'étroit rift intra-continental post-orogénique de Bidarray est en contact direct avec les granulites varisques du massif de l'Ursuya. L'analyse sédimentaire des dépôts permiens et triasiques a permis de définir 11 faciès et 5 associations de faciès. Les dépôts permiens sont composés de cônes alluviaux dominés par des courants hyper-concentrés (FA1), des cônes alluviaux essentiellement composés de débris-flow (FA2), un système fluviatile grossier (FA3a) et des dépôts de plaine d'inondation (FA3b). Ces dépôts remanient le socle méta-sédimentaire paléozoïque (Ordovicien à Carbonifère), avec lequel elles sont en contact tectonique ou sédimentaire. La bordure occidentale du bassin permien de Bidarray est composée de cônes alluviaux (FA1), sédimentant au pied d'une faille normale de direction N0-20°. Ces dépôts proximaux sont remaniés en direction de l'est par un système fluviatile de drainage longitudinal, caractérisé par des directions de courants allant du nord vers le sud (FA3). Le bassin de Bidarray apparait comme un bassin de rift de direction N0-20°.

Les séries du Trias sont, quant à elles, caractérisées par un environnement de chenaux en tresses (FA4). Contrairement au Permien, le conglomérat basal du Trias est monogénique et remanie uniquement des quartzites. Ce changement majeur dans la sédimentation indique qu'au cours du Trias, les sources sédimentaires changent et / ou que la capacité de transport du système fluviatile est plus efficace, ne permettant la préservation que des éléments les plus compétents. Le système fluviatile triasique draine potentiellement une source nouvellement exhumée et disponible à l'érosion, qui pourrait s'apparenter aux quartzites cambriennes présentent au toit des granulites de l'Ursuya. La granulométrie plus grossières du Trias met en évidence l'agrandissement du système sédimentaire, dépassant largement la superficie des bassins confinés du Permien.

Les dépôts sédimentaires permiens se développent au sein d'un bassin extensif de direction N0-20° affectant la croûte supérieure. Ce bassin résulte d'une extension régionale WNW-ESE et est séparé de l'unité granulitique de l'Ursuya par l'intermédiaire de la zone de cisaillement E-W de Louhossoa à pendage vers le sud. Les séries permiennes atteignent leur puissance maximale dans la partie septentrionale du bassin de Bidarray (~ 500 m), à l'approche de l'accident de Louhossoa. L'étude structurale des granulites du massif de l'Ursuya montre que ces dernières furent exhumées dans la croûte supérieure via l'activation de la zone de cisaillement de Louhossoa présentant une cinématique extensive et située au toit du front de fusion. La structure de Louhossoa a été interprétée comme un détachement actif au cours du permien, pour les raisons suivantes : (1) La déformation au sein des granulites et des migmatites est rétrograde et débute à moyenne pression et haute température, avec une paragénèse dominante de haut grade tel que : sillimanite, feldspath potassique, andalousite, grenat et biotite. (2) Une seule et unique fabrique a été observée, sur le terrain et en lame mince, depuis les granulites jusqu'au faciès à chlorite affectant les méta-sédiments ordoviciens. L'exhumation rétrograde au sein de la zone de cisaillement de Louhossoa suggère que l'exhumation des granulites se fait de manière continue au cours d'une phase unique de déformation. (3) Les âges U-Pb sur les granulites de l'Ursuya, provenant de la bibliographie, indiquent que les granulites et les paragenèses cristallisent et sont déformées entre 295 Ma et 274 Ma. (4) Le pluton d'Itxassou intrude la partie méridionale de la zone de cisaillement de Louhossoa et ne montre pas d'évidence de déformation ductile en son sein. Il est donc postérieur à la déformation présente dans cette structure tectonique. Ce pluton post-cinématique permet donc de donner un âge minimum de 276.8 ± 1.9 Ma à la déformation le long de la zone de cisaillement de Louhossoa. (5) La partie orientale de la zone de cisaillement est recouverte en onlap par les turbidites santoniennes, soulignant la non réactivation de cette dernière après le Santonien.

Les résultats de cette étude ont permis d'aboutir à la proposition d'un modèle géodynamique conceptuel d'amincissement de la croûte continentale au Permien, dans lequel le développement du bassin intra-continental de Bidarray est synchrone de l'exhumation des granulites de l'Ursuya au cours d'une phase extensive prenant place entre 300 Ma et 275 Ma. Plusieurs arguments permettent de décrire le massif de l'Ursuya comme un « metamorphic core complex » extensif permien, résultant de

l'amincissement régional d'une lithosphère chaude et de la délamination du manteau lithosphérique suite à l'effondrement de la chaîne varisque : (1) Les granulites de l'Ursuya enregistrent une phase de décompression au cours de leur fluage latéral horizontal en profondeur, comme l'indique le développement de couronnes de cordiérite autour des grenats granulitiques. (2) L'aspect rétrograde de la déformation dans le détachement de Louhossoa, depuis les stades de fusion partielle jusqu'au faciès des schistes verts ; (3) La direction régionale E-W d'extension au sein des granulites et des migmatiques, compatible avec l'orientation du graben actif de Bidarray qui est bordé par des failles normales de direction N0-20°. (4) Le bassin de Bidarray se développe sur le « hanging wall » du détachement de Louhossoa. Le « footwall » est actuellement exposé et correspond au dôme granulitique de l'Ursuya. (5) Le remplissage sédimentaire continental du bassin de Bidarray semble synchrone du métamorphisme rétrograde affectant les granulites et du magmatisme alcalin d'âge Permien supérieur. Ce dernier pourrait correspondre à la signature, en surface, du fluage de la croûte inférieure à moyenne sous le bassin de Bidarray en contexte d'amincissement d'une lithosphère anormalement chaude.

Le développement du bassin de Bidarray et la formation du dôme métamorphique de l'Ursuya peut s'expliquer en deux étapes. Dans un premier temps, la lithosphère continentale est affectée par une phase d'amincissement en cisaillement pur, induisant de manière synchrone i) le développement de failles normales conjuguées au sein de la croûte supérieure et ii) le fluage longitudinal de la croûte inférieure partiellement fondue. Cette première étape d'amincissement crustal initie l'exhumation des granulites au sein d'un dôme métamorphique. Dans un second temps, l'instabilité induite par la flottabilité de la croûte inférieure ductile engendre son fluage vertical en direction de la zone de « necking » de la croûte supérieure, amorçant le développement d'un MCC. L'exhumation des granulites dans la croûte supérieure est alors rendue possible par la localisation de la déformation dans le détachement de Louhossoa, aujourd'hui observé dans la partie méridionale du massif de l'Ursuya. Dans le détail, le dôme de l'Ursuya peut être considéré comme un dôme permien de « type a ». En effet, les linéations d'étirement au sein des granulites sont parallèles à l'axe d'élongation du dôme gneissique de l'Ursuya et tendent à diverger vers l'extérieur du dôme (vers le sud) au niveau du détachement de Louhossoa. Le flanc nord du dôme et la potentielle continuité du détachement ne sont pas préservés en raison du charriage vers le sud de l'unité Mésozoïque d'Arberoue sur le massif de l'Ursuya. Dans ce modèle de MCC, le dôme de l'Ursuya reste cependant immature dans le sens ou seules les séries méta-sédimentaires paléozoïques (c'est-à-dire de bas grade métamorphique) sont remaniées dans les séries permo-triasiques. Le dôme a donc préservé une partie de sa couverture méta-sédimentaire au cours du Permien et du Trias, estimée à ~5 km. L'exhumation des granulites et migmatites, précédemment considérées dans la bibliographie comme résultant de la phase d'hyperextension prenant place au Crétacé, sont ici interprétées comme étant permiennes.

Ces nouveaux résultats suggèrent que la formation du graben de Bidarray et du dôme de l'Ursuya reflète le passage de la convergence N-S enregistrée dans la zone axiale pyrénéenne de 310 à 290 Ma à une phase d'extension E-W prenant place entre 290 et 275 Ma. L'extension E-W dans les massifs basques est compatible avec la formation des bassins pull apart d'âge Permien inférieur à moyen des Pyrénées orientales et de la péninsule ibérique. Cependant, les résultats de ce travail soutiennent l'interprétation selon laquelle la déformation permienne, dans les Pyrénées, était caractérisée par un amincissement homogène d'une croûte anormalement chaude plutôt que par la localisation de la déformation dans des décrochements dextres d'échelle lithosphérique. Nos résultats suggèrent que la croûte continentale de l'avant-pays de la chaîne varisque est restée chaude et partiellement fondue au cours de l'extension permienne, dans les Pyrénées. Dans ce scénario, la déformation est partitionnée verticalement dans la croûte. La croûte inférieure se déforme de manière ductile et homogène par fluage longitudinal contrairement à la croûte supérieure qui est dominée par une déformation cassante responsable de la formation de failles normales de direction N0-20°E et localement de décrochements longitudinaux. Un tel style de déformation induit le développement d'un gradient anormalement élevé, certainement supérieur à 60°C/km tel que le suggère l'analogie avec certains systèmes extensifs similaires. L'épisode permien confère donc un héritage thermique (gradient anormalement élevé), structural (déformation cassante localisée dans la croûte supérieure et

croûte continentale amincie) et compositionnel (granulites et migmatites exhumées en position de croûte supérieure) complexe à la lithosphère des Pyrénées occidentales.

Ces travaux mettent également en évidence que les directions structurales N0-20°E, connues pour jouer un rôle majeur au cours du rifting crétacé, pourraient être héritées du Permien. Le bassin de Bidarray et le dôme de l'Ursuya sont préservés et alignés avec la structure de transfert de Pamplona dont les bordures occidentale et orientale coïncident avec deux branches du rifting crétacé : le bassin de Mauléon et le bassin Basco-cantabrique. Cette structure de transfert de direction N20°E, apparait comme une structure lithosphérique héritée du Permien et réactivée au cours du rifting crétacé. La préservation des traits structuraux et paléogéographiques permo-triasiques rend impossible la réalisation d'un quelconque mouvement décrochant sénestre de direction E-W au cours du mésozoïque entre les plaques ibérique et européenne dans cette partie des Pyrénées. Ce mouvement décrochant déduit des reconstitutions cinématiques a donc pu affecter un domaine plus méridional ou a été distribué et donc délocalisé au sein des deux plaques impliquées durant le rifting crétacé.

Tectonophysics 768 (2019) 228180

Contents lists available at ScienceDirect

Tectonophysics

journal homepage: www.elsevier.com/locate/tecto

Tectono-sedimentary evolution of a rift system controlled by Permian post-orogenic extension and metamorphic core complex formation (Bidarray Basin and Ursuya dome, Western Pyrenees)

Nicolas Saspiturry[a,*], Bryan Cochelin[b], Philippe Razin[a], Sophie Leleu[a], Baptiste Lemirre[c], Chloé Bouscary[a], Benoit Issautier[d], Olivier Serrano[d], Eric Lasseur[d], Thierry Baudin[d], Cécile Allanic[d]

[a] Université Bordeaux Montaigne/EA 4592 Géoressources & Environnement, 1 allée Fernand Daguin, 33607 Pessac cedex, France
[b] Université d'Orléans, CNRS, BRGM, ISTO, UMR 7327, 1A Rue de la Ferollerie, 45071 Orléans, France
[c] Géosciences Environnement Toulouse, Université de Toulouse, CNRS, IRD, UPS, CNES, 31400 Toulouse, France
[d] Bureau de Recherche Géologique et Minière, 3 Avenue Claude Guillemin, 45100 Orléans, France

ARTICLE INFO

Keywords:
Post-orogenic rift
Permian
Metamorphic core complex
Detachment
Granulites
Continental deposits

ABSTRACT

This study documents the sedimentary and structural response of continental crust in relatively hot lithosphere that is subjected to extension. We focus on the Permian rift system in the Western Pyrenees, where the narrow, post-orogenic intracontinental extensional Bidarray Basin is in contact with late Variscan granulites of the Ursuya massif. The western margin of the N-S trending Bidarray Basin preserves alluvial fans dominated by hyperconcentrated flows and interdigitating eastward into a N-S trending fluvial system. Structural analysis of the Ursuya granulites shows that they underwent orogen-parallel mid-crustal flow and were exhumed owing to strain localization during retrogressive metamorphism within an extensional shear zone flanking an E-W elongated domal structure. We show that the Bidarray Basin formed during Permian time on the hanging wall of a south-vergent detachment system that developed in response to the formation of an immature "a-type" metamorphic core complex (the Ursuya massif) under regional E-W extension, resulting in homogeneous thinning of the hot crust. This core complex was later exposed by denudation during Cenomanian time. The preservation of the Permian and Triassic paleogeography and structure indicates that there has been no lateral motion between Iberia and Europe in the study area. The Cretaceous Pamplona transfer zone, responsible for the shift of the Mesozoic rift axis, reactivated a N-S trending Permian crustal heterogeneity.

1. Introduction

The structural architecture of crust subjected to extension depends strongly on the rheological structure of the lithosphere. The temperature at the Moho controls how deformation is accommodated in the crust (see the critical review of Brun et al., 2017). Whereas a cold lithosphere tends towards localized deformation, leading to necking of the whole crust, a hot lithosphere undergoes distributed deformation and necking confined to the upper crust, which leads to the formation of metamorphic core complexes (MCCs) (Brun, 1999; Tirel et al., 2004, 2008; Gueydan et al., 2008). Exhumation of the ductile crust within MCCs is favored by activation of extensional detachment faults (Coney, 1980). In response to increasing extension and uplift of the detachment footwall, half-grabens or graben basins are created and filled progressively by proximal sediments. This crustal configuration was first defined in the Basin and Range province (Davis and Coney, 1979; Wernicke, 1981; Wernicke and Burchfiel, 1982; Wernicke, 1985; Davis et al., 1986; Lister and Davis, 1989; Malavieille, 1993) and later in the Aegean domain (Lister et al., 1984; Avigad and Garkunkel, 1989). The two most common types of MCCs described in the Aegean domain are defined by the trend of the foliation dome with respect to the direction of regional crustal stretching: "a-type" MCCs are elongated parallel and "b-type" MCCs are elongated normal to the stretching direction (Jolivet et al., 2004; Le Pourhiet et al., 2012). Specifically, the main detachment faults flanking these two MCC types are either roughly parallel to or perpendicular to the direction of stretching. MCCs have been described in many tectonic settings, including areas of backarc extension, lateral escape into orogenic plateaus, late-orogenic collapse or anorogenic

* Corresponding author.
E-mail address: saspiturry.nicolas@gmail.com (N. Saspiturry).

https://doi.org/10.1016/j.tecto.2019.228180
Received 27 November 2018; Received in revised form 14 August 2019; Accepted 19 August 2019
Available online 21 August 2019
0040-1951/ © 2019 Elsevier B.V. All rights reserved.

Chapitre 2.2. Tectono-sedimentary evolution of a rift-system controlled by Permian post-orogenic extension and metamorphic core complex formation (Bidarray basin and Ursuya dome, Western Pyrenees)

Saspiturry, N., Cochelin, B., Razin, P., Leleu, S., Lemirre, B., Bouscary, C., Issautier, B., Serrano, O., Lasseur, E., Baudin, T., and Allanic, C., **2019**, Tectono-sedimentary evolution of a rift-system controlled by Permian post-orogenic extension and metamorphic core complex formation (Bidarray basin and Ursuya dome, Western Pyrenees): ***Tectonophysics*, doi: 10.1016/j.tecto.2019.228180**.

Abstract

This study documents the sedimentary and structural response of continental crust in relatively hot lithosphere that is subjected to extension. We focus on the Permian rift system in the Western Pyrenees, where the narrow, post-orogenic intracontinental extensional Bidarray basin is in contact with late Variscan granulites of the Ursuya massif. The western margin of the N-S trending Bidarray basin preserves alluvial fans dominated by hyperconcentrated flows and interdigitating eastward into a N-S trending fluvial system. Structural analysis of the Ursuya granulites shows that they underwent orogen-parallel mid-crustal flow and were exhumed owing to strain localization during retrogressive metamorphism within an extensional shear zone flanking an E-W elongated domal structure. We show that the Bidarray basin formed during Permian time on the hanging wall of a south-vergent detachment system that developed in response to the formation of an immature « a-type » metamorphic core complex (the Ursuya massif) under regional E-W extension, resulting in homogeneous thinning of the hot crust. This core complex was later exposed by denudation during Cenomanian time. The preservation of the Permian and Triassic paleogeography and structure indicates that there has been no lateral motion between Iberia and Europe in the study area. The Cretaceous Pamplona transfer zone, responsible for the shift of the Mesozoic rift axis, reactivated a N-S trending Permian crustal heterogeneity.

1. Introduction

The structural architecture of crust subjected to extension depends strongly on the rheological structure of the lithosphere. The temperature at the Moho controls how deformation is accommodated in the crust (see the critical review of Brun et al., 2017). Whereas a cold lithosphere tends toward localized deformation, leading to necking of the whole crust, a hot lithosphere undergoes distributed deformation and necking confined to the upper crust, which leads to the formation of metamorphic core complexes (MCCs) (Brun, 1999; Tirel et al., 2004, 2008; Gueydan et al., 2008). Exhumation of the ductile crust within MCCs is favored by activation of extensional detachment faults (Coney, 1980). In response to increasing extension and uplift of the detachment footwall, half-grabens or graben basins are created and filled progressively by proximal sediments. This crustal configuration was first defined in the basin and Range province (Davis and Coney, 1979; Wernicke, 1981; Wernicke and Burchfiel, 1982; Wernicke, 1985; Davis et al., 1986; Lister and Davis, 1989; Malavielle, 1993) and later in the Aegean domain (Lister et al., 1984; Avigad and Garfunkel, 1989). The two most common types of MCCs described in the Aegean domain are defined by the trend of the foliation dome with respect to the direction of regional crustal stretching: « a-type » MCCs are elongated parallel and « b-type » MCCs are elongated normal to the stretching direction (Jolivet et al., 2004, Le Pourhiet et al., 2012). Specifically, the main detachment faults flanking these two MCC types are either roughly parallel to or perpendicular to the direction of stretching. MCCs have been described in many tectonic settings, including areas of backarc extension, lateral escape into orogenic plateaus, late-orogenic collapse or anorogenic extension (see the review by Jolivet and Goffé, 2000). It has been demonstrated that the late evolution of the Variscan belt in Western Europe was a favorable context for the development of MCCs, as (1) the overthickened hinterland was affected by gravitational collapse (Echtler and Malavieille, 1990; Malavieille et al., 1990;

Burg et al., 1994; Roger et al., 2015) and (2) late- and post-orogenic delamination of the lithospheric mantle led to widespread magmatism and high temperature–low pressure (HT-LP) metamorphism (including production of granulites) in the foreland during the Carboniferous-Permian transition (e.g., Pin and Vielzeuf, 1983; Denèle et al., 2014; Martínez-Catalán et al., 2014; Laurent et al., 2017). Furthermore, crustal extension affected Western Europe during the Permian, leading to the formation of numerous sedimentary basins, as in the Pyrenees (Lucas, 1985; Bixel and Lucas, 1987). Unlike the Massif Central (e.g., Echtler and Malavieille, 1990; Brun and Van den Driessche, 1994; Pochat and Van den Driessche, 2011), the relationship between basin formation and exhumation of Early Permian migmatites or granulites has not been investigated in the Pyrenees; rather, the major studies have focused on the sedimentary environment of the Permian and Triassic deposits and the associated alkaline volcanism (Bixel and Lucas, 1983; Lucas, 1985; Lago et al., 2004; Rodriguez-Mendez et al., 2014; Gretter et al., 2015; Lloret et al., 2018). Furthermore, the Alpine overprint in these Permian basins due to nappe stacking during Pyrenean mountain building makes it difficult to reconstruct the tectonic context of basin formation (e.g., Saura and Teixell, 2006; Izquierdo-Llavall et al., 2013, 2014).

The Bidarray basin, a Permian basin in the Western Pyrenees **(Fig. 1)**, was only slightly deformed during the subsequent Pyrenean orogeny and is therefore a very favorable place to study the evolution of extensive post-orogenic basins. Moreover, it is located immediately south of the late-Variscan granulites forming the Ursuya massif **(Fig. 2)**, making it a key place to investigate the structural response of both upper and lower crust to regional post-orogenic extension. In this work, we present a sedimentary analysis of the Bidarray basin and a structural analysis of both the basin and the adjacent Ursuya granulitic dome. The geologic maps presented here derive from the harmonization and updating of the 1:50,000 maps published by the geological agencies of France and Spain (Casteras, 1971; Adler et al., 1972; Juch et al., 1972; Boissonnas et al., 1974; Le Pochat et al., 1976, 1978). We propose a tectonic model of crustal extension that accounts for both the development of the Bidarray basin and the exhumation of granulites within an MCC in Permian time. We also discuss the role of this Permian domain in the subsequent deformation phases, such as Cretaceous rifting and the Pyrenean orogeny.

2. Geologic setting

2.1. The Pyrenean Variscan belt

The Variscan belt of Western Europe records convergence and collisional mountain building between the Laurussia paleocontinent and the northern margin of Gondwana during the Devonian and Carboniferous (e.g., Matte and Hirn, 1988; Franke, 1989; Matte, 2001; Ballèvre et al., 2009; Paquette et al., 2017; Lotout et al., 2018). The Variscan belt was affected from 360 to 290 Ma by partial melting, post-orogenic extension (e.g., Faure et al., 2009) and the development of major transcurrent faults (Arthaud and Matte, 1975; Burg et al., 1994). In this orogenic context, the Pyrenees were located in the foreland of the Variscan belt and were mainly affected by late Variscan HT-LP metamorphism due to lithospheric mantle delamination (Denèle et al., 2014; Cochelin et al., 2017; Lemirre et al., 2019 and references therein). This metamorphism occurred between 310 and 290 Ma (see Denèle et al., 2014; Lemirre et al., 2019; Poitrenaud et al., 2019) and was responsible for partial melting of the middle and lower crust, which then intruded into the base of the upper crust of the Axial Zone as gneiss domes in compressional settings (**Fig. 1;** Denèle et al., 2007; 2009; Cochelin et al., 2017, 2018a, 2018b). Formed in an overall context of N-S horizontal shortening, these domes are elongated parallel to the regional direction of stretching in the middle and lower crust, like « a-type » MCCs (Cochelin et al., 2017, 2018b). Deposition of the earliest thin volcaniclastic sediments occurred in the Pyrenees synchronously with ductile flow within these gneiss domes (e.g., compare the ages obtained by Pereira et al., 2014, and Lemirre et al., 2019). While the partially exhumed middle crustal rocks correspond to migmatites in the Axial Zone, those exhumed in the North Pyrenean Zone and the Basque massifs in the westernmost Pyrenees **(Fig. 1)** reached the granulite facies and were mainly affected by intense crustal thinning during

extension at the Carboniferous-Permian transition (de Saint-Blanquat et al., 1990; de Saint-Blanquat, 1993; Olivier et al., 2004; Lemirre, 2018).

2.2. Post-Variscan Permian-Triassic extensional basins

It has long been accepted that the Permian extensional phase represents the transition between the Variscan orogenic cycle and the rifting that led to the breakup of Pangea and the opening of the Neo-Tethys ocean (e.g., Sengör et al., 1984; Stampfli, 2012). The Permian sediments were erosional products of the Paleozoic substratum, deposited mainly by different fluvial systems and alluvial fans in intracontinental basins (Lucas, 1968, 1977, 1985; Cassinis et al., 1995). The Pyrenees are characterized by a continuous record of Carboniferous to Permian sedimentation, like that in the Massif Central (e.g., Pellenard et al., 2017) but with far fewer lacustrine deposits (e.g., Pochat and Van den Driessche, 2011). The rocks are generally redbeds and do not record any flora or fauna. The Permian deposits are in unconformable or fault contact with the folded Variscan substratum. Despite the lack of geochronological constraints within the Bidarray basin, a middle to late Permian age can be advocated for these deposits because of (1) the alkaline magmatism interbedded with sediments and developing in the basin axis (Adler et al., 1972) that is known to be of latest Permian age elsewhere in the Pyrenees (Bixel and Lucas, 1983, 1987; Lucas, 1985; Orejana et al., 2008; Pereira et al., 2014), (2) the absence at the base of the sequence of the gray lacustrine deposits of latest Carboniferous (Stephanian) to early Permian age identified in the Ossau basin (Bixel, 1984; Lucas, 1985) and in the central Pyrenees (e.g., Gretter et al., 2015; Lloret et al., 2018) (although redbeds of that age are not ruled out in the Bidarray basin), and (3) the presence of the regional unconformity between uppermost Permian and overlying Triassic deposits that is known throughout the Pyrenees (Mey et al., 1968; Nagtegaal, 1969; Gisbert, 1981; Lucas, 1985; Gretter et al., 2015 and references therein).

Post-Variscan extensional basins are characterized in the Pyrenees by a half-graben morphology (Bixel and Lucas, 1987; Gretter et al., 2015; Lloret et al., 2018). The role of tectonic activity during sedimentation of breccia deposits in these basins has long been recognized (Lucas, 1977, 1985). The Alpine orogeny strongly affected the Permian basins bordering the Axial Zone of the Pyrenees and reactivated most of the Permian extensional and transtensional faults (e.g., Saura and Teixell, 2006; Izquierdo-Llavall et al., 2013, 2014). This Alpine overprint appears to decrease to the west, especially in the Basque massifs where the amount of shortening was less than in the Central and Eastern Pyrenees (Teixell, 1998). The Bidarray and Haut-Béarn basins are the most prominent preserved Permian depocenters of the Western Pyrenees (Bixel, 1984; Lucas, 1985). Two sets of structural features appear to have affected the development of the Permian-Triassic basins in this area, NNE-SSW trending faults that controlled the development of the Permian basins and ENE-WSW trending structures that were active during the Late Triassic (Lucas, 1985). These have been linked to a larger scale E-W sinistral fault system (Arthaud and Matte, 1975; Souquet et al., 1977; Lucas, 1985). Triassic deposits in these basins unconformably overlie both the Permian deposits and the Variscan sedimentary substratum (Lucas et al., 1980; Curnelle, 1983; Durand, 2006). Lucas (1968) and Curnelle (1983) defined the Permian-Triassic boundary in the Pyrenees as the base of the Upper Triassic (Carnian) monogenic conglomerates (Lucas et al., 1980). These coarse facies are therefore probably comparable to deposits related to the early (Triassic) phase of Atlantic rifting (Leleu et al., 2016). The Late Triassic extensional phase was then recorded by the development of thick evaporite deposits (Curnelle, 1983) and mantle-derived intrusions (ophites; see Rossi et al., 2003, and **Fig. 2**).

2.3. Present-day structure of the Western Pyrenees

The Pyrenean mountain range results from N-S shortening due to convergence and collision between Iberia and Europe from late Santonian to early Miocene time (Puigdefàbregas and Souquet, 1986; Olivet, 1996). The Pyrenees are classically divided into three structural zones: the Axial Zone consisting of a Variscan substratum, the South Pyrenean Zone, and the North Pyrenean Zone (**Fig. 1**; Choukroune, 1976).

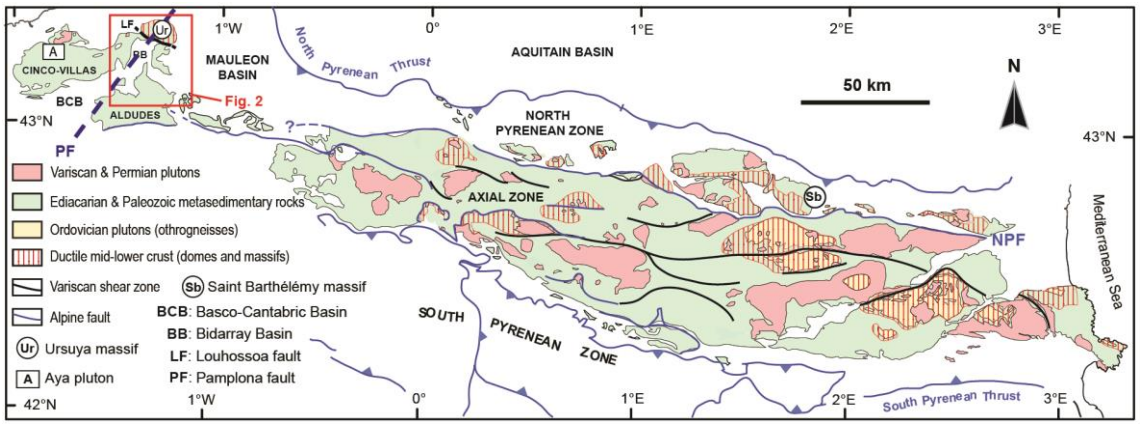
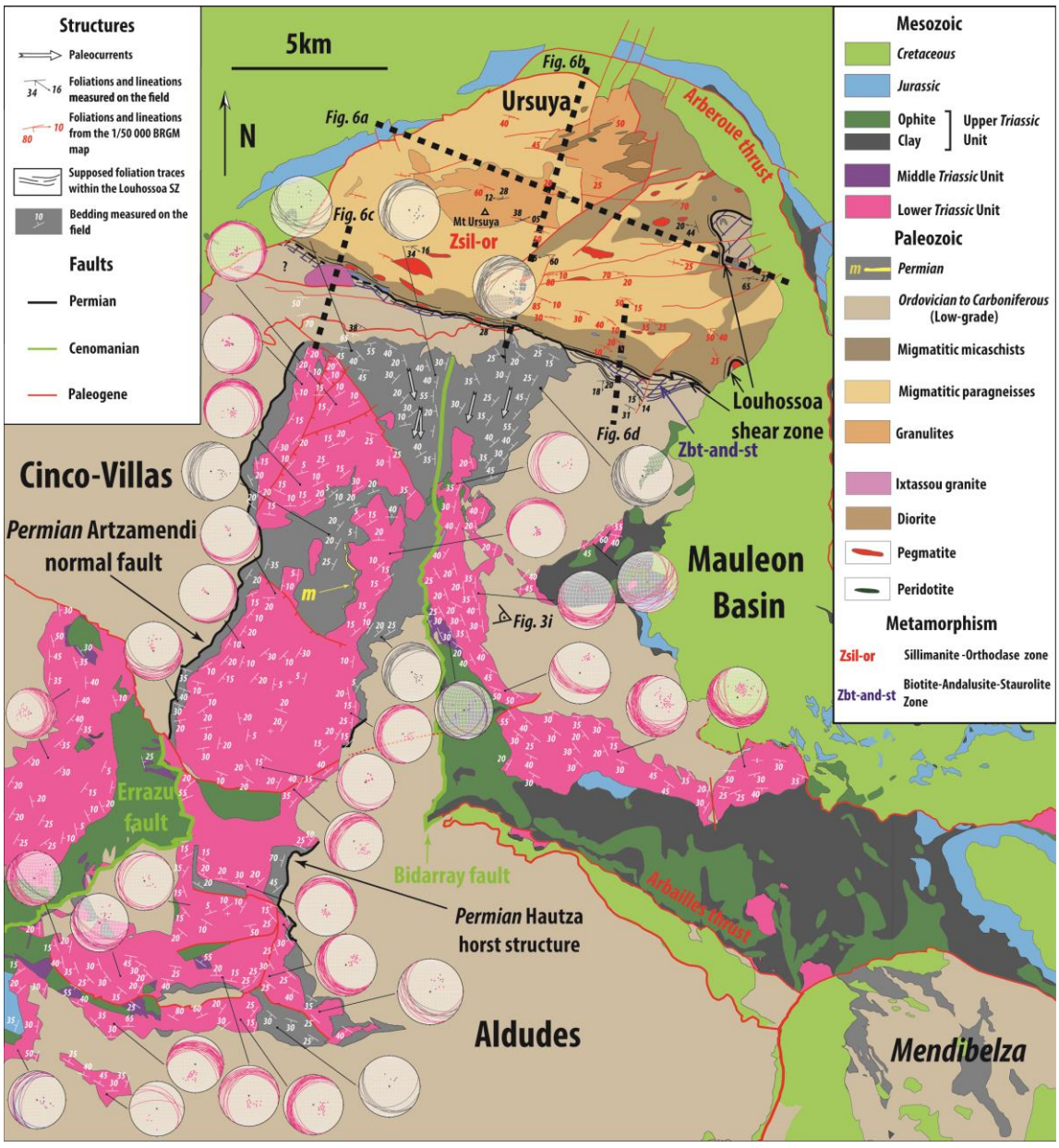


Fig. 1. Sketch map of the Pyrenees showing its major structural domains: North Pyrenean Zone, Axial Zone and South Pyrenean Zone. The Bidarray basin, in the western Pyrenees, is separated from the Ursuya granulitic dome by the Louhossoa fault and is bisected by the Pamplona fault, which separates the Mauléon and Basco-Cantabric basins of Early Cretaceous age (modified from Cochelin et al., 2017).



Caption on next page

Fig. 2. Simplified geologic map of the Bidarray basin. This Permian basin lies between the Aldudes, Cinco-Villas and Ursuya massifs of Paleozoic age. The Bidarray basin includes the Permian and Triassic rocks southwest of the Mauléon rift basin of Albian-Cenomanian age and south of the Louhossoa shear zone (modified from Casteras, 1971; Adler et al., 1972; Juch et al., 1972; Boissonnas et al., 1974; Le Pochat et al., 1976, 1978). Black lines: Permian Faults; green lines: Cenomanian Faults, red lines: Paleogene Faults. The white strike and dip symbols as well as the stereoplots represent new measurements of bedding planes. The gray, pink, purple and blue lines on the stereoplots represent bedding plane measurements respectively in Permian deposits, Late Triassic sandstones, Muschelkalk limestones and Jurassic limestones. The biotite-andalusite-staurolite metamorphic facies (Zbt-and-st) is indicated by blue hachures, and the bulk of the Ursuya unit consists of the sillimanite-orthoclase facies (Zsil-or). Late Permian alkaline magmatism is signified by a yellow field labeled « m ».

In the Western Pyrenees, the North Pyrenean Zone is represented by the Cretaceous Mauléon basin, thrusted to the north onto the Aquitaine domain and bordered to the south by the Axial Zone. The Mauléon basin is bounded to the west by Paleozoic crustal blocks known as the Basque massifs (Heddebaut, 1973; Muller and Roger, 1977) and is underlain by mantle rock at depths less than 10 km (Wang et al., 2016), making it a hyperextended Cretaceous rift basin (Jammes et al., 2009; Lagabrielle et al., 2010; Masini et al., 2014; Tugend et al., 2014; Teixell et al., 2016; Saspiturry et al., 2019). The Bidarray basin lies between the Mauléon basin and the Basque-Cantabrian basin, a similar hyperextended rift basin of Cretaceous age (Rat et al., 1983; Quintana et al., 2015; Ducoux, 2017) **(Fig. 1)**. Previous work has shown that segmentation of the Cretaceous rifting in this area was controlled by a N20° structural trend, and in particular by a putative structure called the Pamplona fault (**Fig. 1**; Schoeffler, 1982; Razin, 1989). The Pamplona fault is assumed to be a lithospheric structure without any expression at the outcrop scale, with the exception of N20° oriented diapirs south of the Aldudes massif (Richard, 1986).

The Bidarray basin corresponds to the upper part of a Paleozoic basement complex known as the Basque massifs, divided here into four units **(Fig. 2)**. The Aldudes and Cinco-Villas units are massifs composed of Ordovician to Carboniferous sedimentary rocks (Laverdière, 1930; Lamare, 1944; Heddebaut, 1967; Muller and Roger, 1977). The Ursuya unit (Viennot and Kieh, 1928; Lamare, 1939; Vielzeuf, 1984) is a massif mainly composed of Precambrian to Ordovician metasediments (Boissonnas et al., 1974) affected by HT-LP metamorphism that reached granulite facies during the early and middle Permian (Vielzeuf, 1984; Hart et al., 2016; Vacherat et al., 2017; Lemirre, 2018). The boundary between the Ursuya massif and Bidarray basin is defined by the Louhossoa fault (Lamare, 1931; Heddebaut, 1973; Lucas, 1985).

The metamorphic rocks of the highest grade granulites and surrounding migmatites are located in the center of the Ursuya massif, where they formed an anatectic dome (Boissonnas et al., 1974; Vielzeuf, 1984). The massif is interpreted as a part of the Variscan intermediate crust where metamorphism of the deepest facies took place at around 6 ± 0.5 kbar and 775 ± 50°C (Vielzeuf, 1984). The U-Pb age dataset obtained by Hart et al. (2016) and Vacherat et al. (2017) from gneisses of the Ursuya massif indicates that granulites and paragneisses crystallized and were deformed between 295 and 274 Ma. The Itxassou pluton intruded the southern part of the metamorphic series during this time, at 276.8 ± 1.9 Ma (Vacherat et al., 2017). Such late Permian plutonism is well known in the Basque massifs; for instance, the Aya pluton was emplaced within the Cinco-Villas massif at 267.1 ± 1.1 Ma (Denèle et al., 2012). The Ursuya granulitic unit was cooled below 300°C at the end of the Triassic, as evidenced by the 200 Ma cooling age obtained by $^{39}Ar/^{40}Ar$ dating of paragneisses of the Ursuya massif (Masini et al., 2014). Similar P/T paths indicating partial exhumation of granulites related to extension have been recorded across the Pyrenees (Vielzeuf, 1984; Guitard et al., 1996; de Saint-Blanquat et al., 1990; de Saint-Blanquat, 1993; Olivier et al., 2004). Nevertheless, the tectonic history that led to the exhumation of the Ursuya granulites remains unconstrained, as does its relationship with the coeval formation of the Bidarray basin.

3. Facies association and depositional models

This section presents results of our sedimentary analysis based on field work in the Bidarray basin. We characterized 11 Permian and Triassic sedimentary facies from which we defined 5 facies associations, described in detail below, that represent various depositional processes and environments in a continental realm **(Fig. 3 and Table 1)**. The facies

associations are named as follows: alluvial fans dominated by hyperconcentrated flows (FA1), debris-flow alluvial fans (FA2), coarse fluvial (FA3a), floodplain (FA3b), and braided fluvial (FA4). The first four associations represent the Permian deposits of the Bidarray basin, in which we defined two types of alluvial fans (FA1 and FA2). The alluvial fan facies are localized along the western basin margin, and the central part of the basin is dominated by deposits of a longitudinal fluvial system (FA3a) and floodplain deposits (FA3b). The last facies association (FA4) characterizes both the coarse fluvial Triassic deposits that overlie the Permian continental sequence and the surrounding Paleozoic substratum.

3.1. FA1 facies association: Alluvial fan dominated by hyperconcentrated flows

The FA1 facies association includes F1a chaotic breccia (60%; **Fig. 3A**) and F1b fine-grained breccia (40%) **(Table 1)** that form amalgamated bodies ranging in thickness from several to several tens of meters. These deposits are characterized by a short transport distance and a relatively close source. The FA1 facies association is interpreted as related to hyperconcentrated flows (Pierson and Scott, 1985; Benvenuti and Martini, 2002). This type of alluvial fan represents ~80% of those identified in the Bidarray basin. They are characterized by slopes of 1° to 12° and a length/width ratio greater than 1 (Blair and McPherson, 1994; Chamyal et al., 1997). The hyperconcentrated flows resulted from the evolution of debris flows towards a turbulent flow and a sedimentary dynamic dominated by traction flow (Pierson and Scott, 1985; Benvenuti and Martini, 2002). The F1b breccias also were deposited by hyperconcentrated flows and form the distal part of the alluvial fans. The down-fan decrease in flow velocity allowed preservation of the coarse matrix of the F1a facies and left the largest clasts upstream.

3.2. FA2 facies association: Debris-flow alluvial fan

The FA2 facies association consists of F2a matrix-supported breccia (65%; **Fig. 3C**), F2b muddy breccia (30%; **Fig. 3D**) and F1c cemented breccia (5%; **Fig. 3B**) **(Table 1)**. These breccias are organized in a succession of amalgamated layers many decimeters in thickness. They are characterized by a short transport distance and a relatively close source. The FA2 facies association corresponds to debris-flow alluvial fans (Blair and McPherson, 1994; Iverson, 1997). The relatively small proportion of matrix in the F2a facies (<40%) tends to indicate that this type of debris flow is noncohesive, whereas the larger proportion of matrix in the F2b facies (>60%) tends to indicate that this type of debris flow is cohesive (Blair and McPherson, 1994; Levson and Rutter, 2000). FA2 deposits represent 20% of the alluvial fans identified in the Bidarray basin. They are characterized by steeper average slopes than FA1 alluvial fans (4–25°) and a length/width ratio of 1 or less (Viseras et al., 2003). This type of alluvial fan has no middle part and transitions to a channelized system. Their watersheds (<10 km^2) are smaller than those of hyperconcentrated fans (>10 km^2) (e.g., Levson and Rutter, 2000; Leleu, 2005).

3.3. FA3a facies association: Coarse fluvial

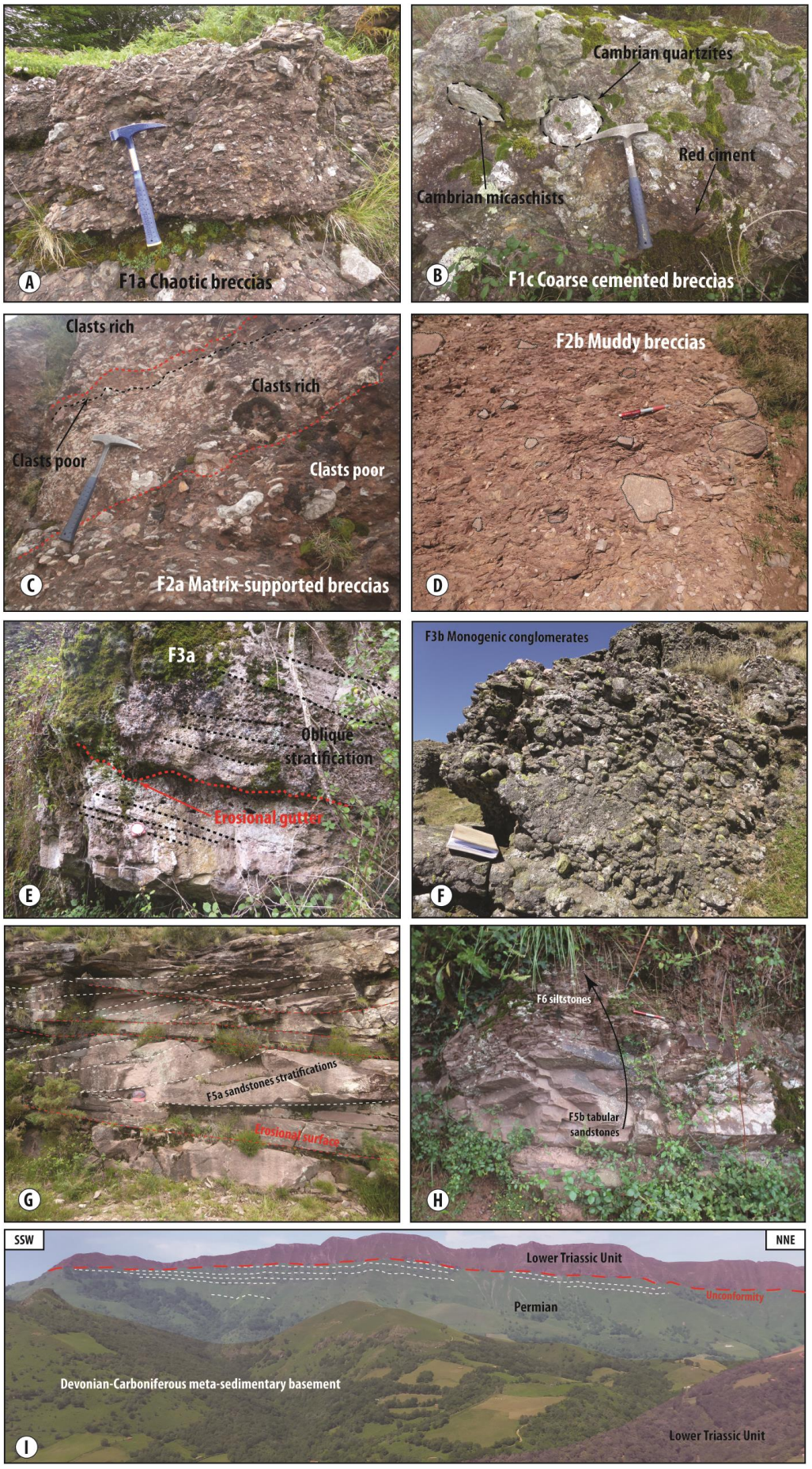
The FA3a facies association includes F3a polygenic conglomerate (80%; **Fig. 3E**) and F4 lenticular stratified breccia (20%) **(Table 1)**. These coarse deposits form units with thicknesses ranging from 2 m to 8 m. The conglomerate is interpreted as bedload deposits within braided fluvial channels (Miall, 1977a, 1977b; Rust, 1978; Bridge, 1993, 2009). The stratified sandstone in the conglomerate is interpreted as high-flood deposits underlying the previous conglomerates that filled the fluvial channel (Rust, 1978). This facies association is mostly composed of fluvial channels characterized by southward sediment transport, evidenced by five paleocurrent measurements in the F3a facies between N170° and N200° **(Fig. 2)**, consistent with paleocurrent directions reported by Boissonnas et al. (1974) and Lucas (1985). The F4 breccias commonly erode FA3b floodplain deposits, which correspond to fine-grained fluvial channelized deposits. The lateral extent of these channels is several tens of meters, and facies follow each other by forming thinning- and fining- upward sequences.

3.4. FA3b facies association: Floodplain

The FA3b facies association is characterized by a large proportion of F6 red siltstone and minor carbonate siltstone (70%), intercalated with F5b tabular sandstone with thicknesses ranging from 2 cm to 20 cm (30%)

Table 1. Lithofacies and depositional environments of Permian and Lower Triassic strata of the Bidarray basin.

Lithofacies	Description	Sedimentary structures	Depositional environment
F1a. Chaotic breccia	Matrix with polygenic granules (1–6 mm) units 2–10 m thick Angular polygenic clasts (2–30 cm; average size 8 cm)	Poorly sorted (chaotic fabric) Clasts aligned with stratification Rare cross-stratification Nonerosive base	Hyperconcentrated flows in alluvial fans (Pierson and Scott, 1985; Benvenuti and Martini, 2002)
F1b. Fine-grained breccia	Polygenic clast-supported breccia Angular to subangular clasts (average size 5 mm; max 30 cm) Red silty matrix units 2–15 m thick	Well sorted Clasts aligned with bedding Some cross-stratification	Distal hyperconcentrated flows in alluvial fans (Pierson and Scott, 1985; Benvenuti and Martini, 2002)
F1c. Cemented breccia	10 m^2 to 30 m^2 patches Cemented matrix of red coarse-grained sandstone Polygenic angular clasts ranging from granules to blocks (max 40 cm)	Poorly sorted (chaotic fabric) Absence of bedding	Debris flows in alluvial fans (Blair and McPherson, 1994; Iverson, 1997)
F2a. Matrix-supported breccia	Polygenic breccia Muddy matrix units 1–5 m thick	Clasts aligned with stratification Relatively well sorted clast-rich beds	Noncohesive debris flows in alluvial fans (Blair and McPherson, 1994; Iverson, 1997)
F2b. Muddy breccia	Matrix-supported breccias Beds 30 cm to 2 m thick Polygenic angular clasts (average size 6 cm; max 30 cm)	Poorly sorted Some beds with inverse coarse tail grading (2–30 cm thick) Nonerosive base	Cohesive debris flows in alluvial fans (Blair and McPherson, 1994; Iverson, 1997)
F3a. Polygenic conglomerate	Polygenic conglomerate Rounded to subrounded cobbles (average size 2–3 cm) Intercalations of tabular medium to coarse sandstone Fining-upward sandstone sequences (30 cm to 3 m thick)	Conglomerate: fairly well sorted; planar oblique cross-stratification; erosive base; erosional gutters Sandstone: low-angle bedding; polygenic lag	Bedload deposits of longitudinal fluvial system (Rust, 1978; Bridge, 2009)
F3b. Monogenic conglomerate	Monogenic conglomerate Amalgamated fining-upward erosive beds (1–5 m thick) Matrix of coarse-grained sandstone	Well sorted Low-angle to oblique cross-stratification in some bed tops Pebbles imbricated	Braided channel deposits (Miall, 1977a, 1977b; Bridge, 2009)
F4. Lenticular stratified breccia	Polygenic lenticular breccia Matrix of red fine-grained siltstone Angular clasts (average size of 2–5 cm) Beds 30 cm to 2 m thick	Moderately well sorted Some oblique cross-stratification	Channel-fill deposits preserving the base of dune cross-strata (Bridge, 1993, 2009)
F5a. Coarse amalgamated sandstone	Coarse amalgamated sandstone units 1–10 m thick Fining- and thinning-upward beds (10–50 cm thick)	Well sorted 3D cross-stratification (20 cm to 1 m thick)	Coarse fluvial braided channels (Miall, 1977a, 1977b; Bridge, 2009)
F5b. Tabular sandstone	Fine to very fine sandstone Tabular beds (2–20 cm thick)	Very well sorted Nonerosive base	Overbank deposits within the floodplain (Bridge, 1993, 2009)
F6. Siltstone	Siltstone to claystone Homogeneous units 1–10 m thick Intercalated carbonate beds with nodules 1–5 cm in diameter	Very well sorted Fine and regular horizontal laminations Small particle size variation	Floodplain or distal fine-grained sediment on alluvial-fan lobes (Bridge, 2009)



Caption on next page

Fig. 3. Outcrop photographs representing Permian-Triassic continental facies of the Bidarray basin. **(A)** F1a facies: chaotic breccia consisting of Paleozoic blocks aligned parallel with stratification; the matrix is microbreccia with Paleozoic clasts. **(B)** F1c facies: cemented poorly sorted breccia with Cambrian clasts ranging from granules to blocks (up to 40 cm in diameter). **(C)** F2a facies: matrix-supported breccia with fine-grained matrix and intercalated clast-rich breccia derived from Devonian to Carboniferous basement rocks. **(D)** F2b facies: muddy breccia consisting of polygenic angular Paleozoic clasts supported by a fine-grained matrix. **(E)** F3a facies: polygenic conglomerate made of subrounded pebbles (average size 2–3 cm); note planar oblique cross-stratification 5–20 cm thick (black dashed lines) and erosional gutter at its base (red dashed line). **(F)** F3b facies: monogenic conglomerate containing quartzite pebbles (average size 8 cm). **(G)** F5a facies: coarse amalgamated sandstone with 3D cross-stratification. **(H)** F5b tabular sandstone grading to F6 siltstone at top. **(I)** Annotated panoramic view of Iparla peak showing the unconformity between Triassic conglomerates and Permian deposits. The apparent erosional truncation of the Permian deposits toward the SSW is evidence of northward tilting of the Permian deposits before the Triassic conglomerates were laid down.

(Fig. 3H; Table 1). units of this facies association are 1 to 12 m thick and record the deposition of unconfined flows in a floodplain. The siltstone beds are deposited at the distal end of each flow by decantation mechanisms (Bridge, 1993, 2009). These are the most distal Permian deposits identified in the basin. The depositional environment of FA3b corresponds to a floodplain threaded with isolated low-energy channels.

3.5. FA4 facies association: Braided fluvial

The FA4 facies association is interpreted as braided fluvial channel deposits of Late Triassic age (Miall, 1977a, 1977b; Rust, 1978; Bridge, 1993, 2009). It is made up of equal parts F3b monogenic conglomerate **(Fig. 3F)** and F5a coarse amalgamated sandstone **(Fig. 3G)**. These deposits form units with thicknesses ranging from 5 m to 40 m in which basal monogenic conglomerate with quartzite pebbles gradually gives way upward to coarse amalgamated sandstone. Imbricated pebbles record strong paleocurrents (Bridge, 1993), and oblique cross-stratification corresponds to pebbly dune cross-beds formed during migration through the fluvial channel or to large-scale low-angle stratification within a fluvial bar (Miall, 1977b). The 3D cross-stratification in the F5a sandstone corresponds to dune migration and aggradation within fluvial channels (Miall, 1977a). The major differences from the Permian FA3a coarse fluvial facies association are its monogenic pebbles, greater pebble size, and greater bedform thickness. These observations indicate the development during Triassic time of a much larger basin than the Permian basin. This is reflected by the reworking of quartzite pebbles within a fluvial system with amalgamated braided channels, characterized by a gentler sedimentary slope than during Permian time. The Triassic depositional system may differ from the Permian one in having (1) a different sedimentary source that was limited to reworked Cambrian-Ordovician quartzite and (2) a greater transport distance and potentially climatic changes that may explain the preferential preservation of the most stable clasts (quartzite pebbles).

4. Tectono-sedimentary analysis

4.1. Facies distribution of Permian deposits (FA1 to FA3)

We made three correlation transects across the Bidarray basin, based on logged sections at 12 localities, in order to estimate the remnant thickness and facies variations of the Permian deposits, despite the paucity of stratigraphic markers inherent to continental deposits **(Fig. 4)**. The base of the Triassic conglomerate facies association (FA4) was taken as a datum for correlation as it forms a continuous surface at the top of the Permian deposits in all sections. It is a major erosive unconformity, and we therefore cannot exclude the possibility that parts of the uppermost Permian deposits were eroded. In any case, the early phase of basin fill is well preserved. Thickness variations are constrained by the basal Permian unconformity recognized at the base of most sedimentary sections. Log 12 is schematic and represents a composite section from the northern part of the basin.

The E-W transect provides a transverse section of the Bidarray basin at its north end **(Fig. 4B)**. In the western part (Log 1), the Permian deposits are composed of alluvial fans characterized by hyperconcentrated flows (FA1) that pass laterally to a coarse fluvial system (FA3a; Log 11). The easternmost part of this transect (Log 12) is characterized by finer-grained facies with a predominance of floodplain deposits (FA3b). This transect documents an eastward direction of sedimentary transport, an eastward increase of

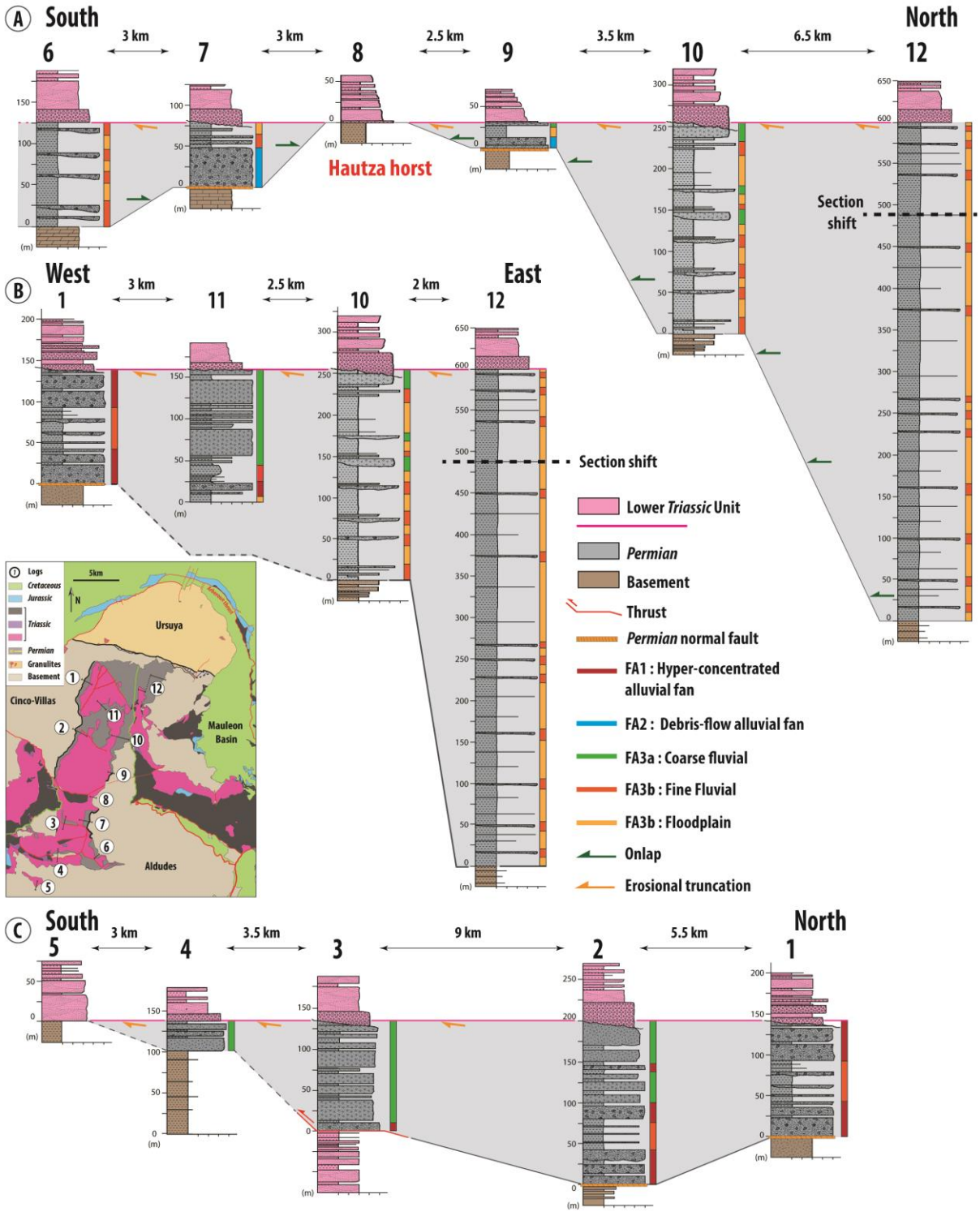


Fig. 4. Correlation transects showing the facies structure of the Permian Bidarray basin. Locations of logged sections are shown in the inset map. Facies associations are represented as colored columns to the right of each log. **(A)** Eastern transect: this part of the basin is characterized by distal facies, as shown by the dominance of the FA3 facies association (fluvial and floodplain deposits). The Permian deposits thin towards Log 8, where they disappear and the Triassic basal conglomerates are absent. The presence of alluvial fan deposits (FA2) on both sides of Log 8 is suggestive of a tectonic control (a Permian horst; see discussion in the text). **(B)** West-east transect: the Permian sedimentary system thickens to the east and is increasingly characterized by distal facies. **(C)** Western transect: the Permian facies are relatively proximal and thin towards the south. At the southern end, Permian strata are completely eroded and the basal Triassic conglomerates are absent.

subsidence and an unconformity between the Permian deposits and the Paleozoic substratum.

Two N-S trending transects extend along the eastern and western parts of the Bidarray basin, respectively **(Figs. 4A and 4C)**. In the

western transect **(Fig. 4C)**, the thickness of the Permian deposits varies between 0 and 200 m, decreasing towards the south. Breccias derived from hyperconcentrated flows within alluvial fans (FA1) are present in the northern part of the transect (Logs 1 and 2), along the contact with the Cinco-Villas Variscan substratum, and coarse-grained fluvial deposits (FA3a) dominate in the southern part (Logs 3 and 4).

The eastern transect is characterized by predominantly distal facies associations, specifically FA3b floodplain deposits **(Fig. 4A)**. However, thicknesses range widely, from 0 m to 600 m, along this transect. The Permian sequence is thickest in the northern part of the basin, around the location of composite Log 12. It thins towards Log 8, where no Permian deposits are preserved. Because Log 8 has debris-flow alluvial fans (FA2) on both adjacent logs, it is interpreted as a structural high during Permian time, the so-called Hautza horst.

Chaotic breccias (facies F1c, **Table 1**) are only present north of the Louhossoa fault, where they lie unconformably on the Cambrian-Ordovician metasedimentary cover of the Ursuya granulites. The F1c facies is analogous to the Permian-Triassic deposits, as evidenced by its position overlying the Paleozoic substratum, its red matrix and its continental sedimentary environment. We interpret these rocks as the most proximal and poorly sorted of the Permian breccias **(Fig. 3B)**. The angular shape of the clasts, derived from the Paleozoic substratum, indicates very short sediment transport distances and close sources **(Table 1)**.

4.2. Facies distribution of the Triassic deposits (FA4)

The Triassic conglomerates lie unconformably on the Permian sequence. Along the Iparla cuesta (Logs 9 and 10), the Permian strata appear to have been slightly tilted towards the NNE prior to the Triassic erosional truncation **(Fig. 3I)**. Indeed, part of the variations in thickness of the Permian deposits can be related to this pre-Triassic erosion. The erosional surface dips towards the SSW **(Fig. 3I)**. The Triassic conglomerates pinch out towards the Hautza horst (Log 8) whereas they can reach more than 40 m in thickness everywhere else. These variations in thickness of the Triassic conglomerates argue in favor of activity of the Hautza horst that continued from Permian into Triassic time.

4.3. Permian to Triassic morphotectonics of the Western Basque Pyrenees

The distribution and geometries of sedimentary facies show that the Permian Bidarray basin was a narrow continental basin, trending N10–20°, of which the main paleogeographical trends are still preserved. The tectonically controlled borders of this extensional basin are characterized by two types of alluvial fan systems (FA1 and FA2). The western margin is dominated by FA1 alluvial fans aligned in the N10–20° direction along the contact with the Devonian-Carboniferous rocks of the Aldudes massif. The N-S Artzamendi normal fault, dipping steeply towards the east, separates the area of high relief to the west and the Permian intracontinental basin to the east. The FA1 alluvial fans grade eastward to a coarse longitudinal fluvial system (FA3a) and floodplain (FA3b). Paleocurrent measurements show that the fluvial system is parallel to the axis of the basin and orthogonal to the eastward growth direction of the alluvial fans.

Debris-flow alluvial fans (FA2) are present in the southeastern part of the basin, close to Log 8 **(Fig. 4)**. The occurrence of these alluvial fans together with the thinning of the Permian sequence suggest that this area corresponds to a synsedimentary horst structure **(Fig. 4A)**. This horst seems to have been active until the Carnian, as shown by the hiatus in the basal Triassic conglomerates (Log 8). These alluvial fans are characterized by smaller drainage areas and steeper slopes than the FA1 alluvial fans on the western margin of the Permian basin. Further south, the Bidarray basin margin does not appear to be preserved. Permian deposits thin towards the SSW beneath the Triassic erosional unconformity, which is roughly horizontal, and the presence of a thrust contact between the Permian and Triassic deposits in the south **(Fig. 4C)** suggests that the original thickness of the Permian deposits cannot be fully constrained. The thickness variations of the Permian deposits may reflect both Permian differential subsidence and NNE tilting before deposition of the Carnian conglomerates.

The easternmost Permian deposits are characterized by distal fine-grained fluvial and

floodplain facies, which make up the greatest thickness of Permian deposits in the basin, and by their onlap over the Variscan substratum. Two hypotheses can be proposed to explain the geometry of the eastern part of the Permian Bidarray basin: (1) the basin is a half-graben controlled by the Artzamendi normal fault to the west and (2) the basin is a graben controlled by the Artzamendi fault and a conjugate eastern normal fault that is now concealed by Late Cretaceous calcareous turbidites lapping onto the Variscan substratum **(Fig. 2)**.

5. Structural scheme of the Basque massifs

The present-day structure of the Permian basin and its relationship with the adjoining Basque massifs are illustrated in **Figure 5** by 6 cross-sections that are based on the 12 logged sections. The Permian deposits of the Bidarray basin are preserved in the center of this present-day horst structure, where they are exposed along a syncline oriented N10–20° that is bordered to the west by a line of alluvial fans. Cross-sections 1 to 4 show the thickest Permian successions. Cross-section 5 displays the unconformity of the Triassic deposits particularly well, where the Permian deposits thin out to the east with steeper dips (20–25°) than the overlying Triassic rocks (10–15°). The N-S cross-section 6 shows that towards the south, the Permian deposits are thinner and the Triassic sequence lies directly on the Paleozoic rocks. In cross-sections 2 to 5, Triassic deposits lie directly upon Paleozoic rocks on the east side. The FA3a facies association, corresponding to the longitudinal fluvial drainage system of the Permian basin, is located in the center of the syncline and the floodplain deposits (FA3b) onlap the Devonian-Carboniferous substratum to the east (cross-sections 2 to 5). Cross-section 5 also shows the FA2 debris-flow alluvial fans near the Hautza horst. Southward propagating minor thick-skin tectonics, visible in N-S cross-section 6, is responsible for the formation of N90–110° folds, and related minor thrusts have tilted the Permian-Triassic deposits northward in the southern part of the basin.

The tilting of the Permian deposits and the subsequent Triassic erosive unconformity indicate that the tilt is pre-Triassic (pre-Carnian). The east-dipping Bidarray normal fault has a N0–10° orientation within the Bidarray basin and a N120–150° orientation along the Aldudes massif to the south **(Fig. 2)**. This normal fault is responsible for the southwestward tilting of the Lara-Jara massifs, clearly visible in the Triassic sequence **(Figs. 2 and 5)**. The Bidarray fault also affects the lower to middle Jurassic limestones in the area and the latest Albian to Cenomanian St.-Etienne de Baïgorry breccias (Merle, 1974). The offset of the Bidarray fault is interpreted as being of Cenomanian age (Saspiturry et al., 2019). Helium thermochronometric data from zircon reveal elevation-invariant ages of ca. 98 Ma in the Mauléon basin and a pronounced inversion point along the Bidarray fault (Hart et al., 2017). Thus, the proximal margin recorded rift-related exhumation and cooling at ca. 98 Ma. Offset on the fault increases southward from 300 m near cross-section 1 to 3000 m in cross-section 5 **(Fig. 5)**. The west-dipping Errazu normal fault is responsible for the eastward tilting of the Peñas de Betarte (cross-section 5, **Fig. 5**). Its estimated offset of about 2700 m is similar to that of the Bidarray fault, and it affects Late Triassic deposits, indicating that its offset postdates the Triassic. An analogy with the Bidarray fault suggests an Albian-Cenomanian age for offset on the Errazu fault. The Errazu and Bidarray normal faults are thus probably responsible for the formation of the Bidarray synform.

6. Structural analysis of the Ursuya granulitic unit

The outcropping part of the Ursuya massif corresponds to the southern half of a gneiss dome (Boissonnas et al., 1974), characterized by foliation planes oriented E-W and dipping roughly south **(Figs. 2 and 6)**. Outcrops expose a nearly continuous section of the dome, from the granulites and associated bodies of diorite and peridotite in its core to its metasedimentary envelope.

The foliation that defines the gneiss dome is highlighted by alternating leucosomes and paragneisses **(Fig. 7A)** made of garnet-sillimanite-biotite-feldspar-quartz aggregates. It corresponds to the most common granulitic paragenesis in the massif **(Figs. 7B and C)**. Biotite is uncommon in the granulites. As reported by Boissonnas et al. (1974), the surrounding migmatitic gneisses contain

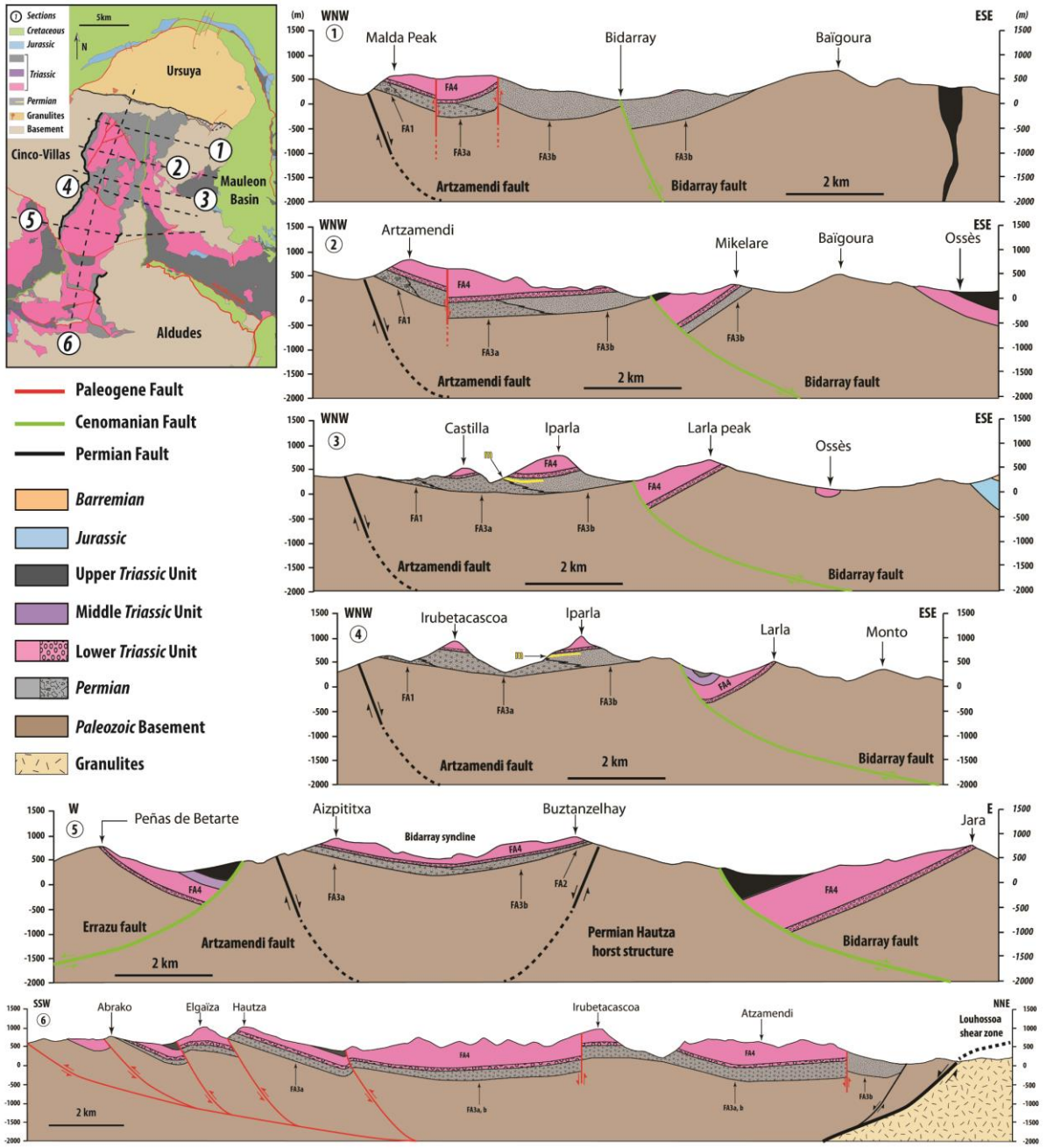


Fig. 5. (1–5) W-E cross-sections of the Bidarray basin, showing the current structural scheme of the Basque Pyrenees. The Basque massifs form a large horst structure with a central syncline holding Permian-Triassic deposits. Cenomanian offset on the Bidarray fault affects the eastern part of the basin, and its offset decreases northward towards the Ursuya granulites. Late Permian alkaline magmatism is signified by a yellow line labeled « m » in cross-sections 3 and 4. **(6)** N-S cross-section of the Bidarray basin, showing the tabular structure of the Upper Triassic sequence over a Permian sequence tilted towards the NNE. The Permian-Triassic deposits are monoclinal and are affected by a small amount of Tertiary deformation (southward thrusting). The Louhossoa shear zone separates the Permian basin from the Ursuya granulites. No vertical exaggeration.

cordierite that forms coronas around granulitic garnets **(Fig. 7D)**, which is typical of decompression during metamorphism. Sillimanite and biotite are more abundant in the migmatitic gneiss than in the granulitic gneiss. The foliation planes in both granulites and migmatites have mineral-stretching lineation manifested as quartz ribbons, elongated feldspar, fibrolitic sillimanite and biotite aggregates. This lineation has an E-W trend in the northern and central parts of the massif that changes gradually to a N120–130°E trend in the southern part of the massif **(Fig. 2)**. We observed predominantly symmetrical boudinage in the foliation **(Fig. 7A)** and locally double boudinage, suggesting a flattening component in the finite strain. The C′ shear bands bear striae-lineations parallel to those in the host.

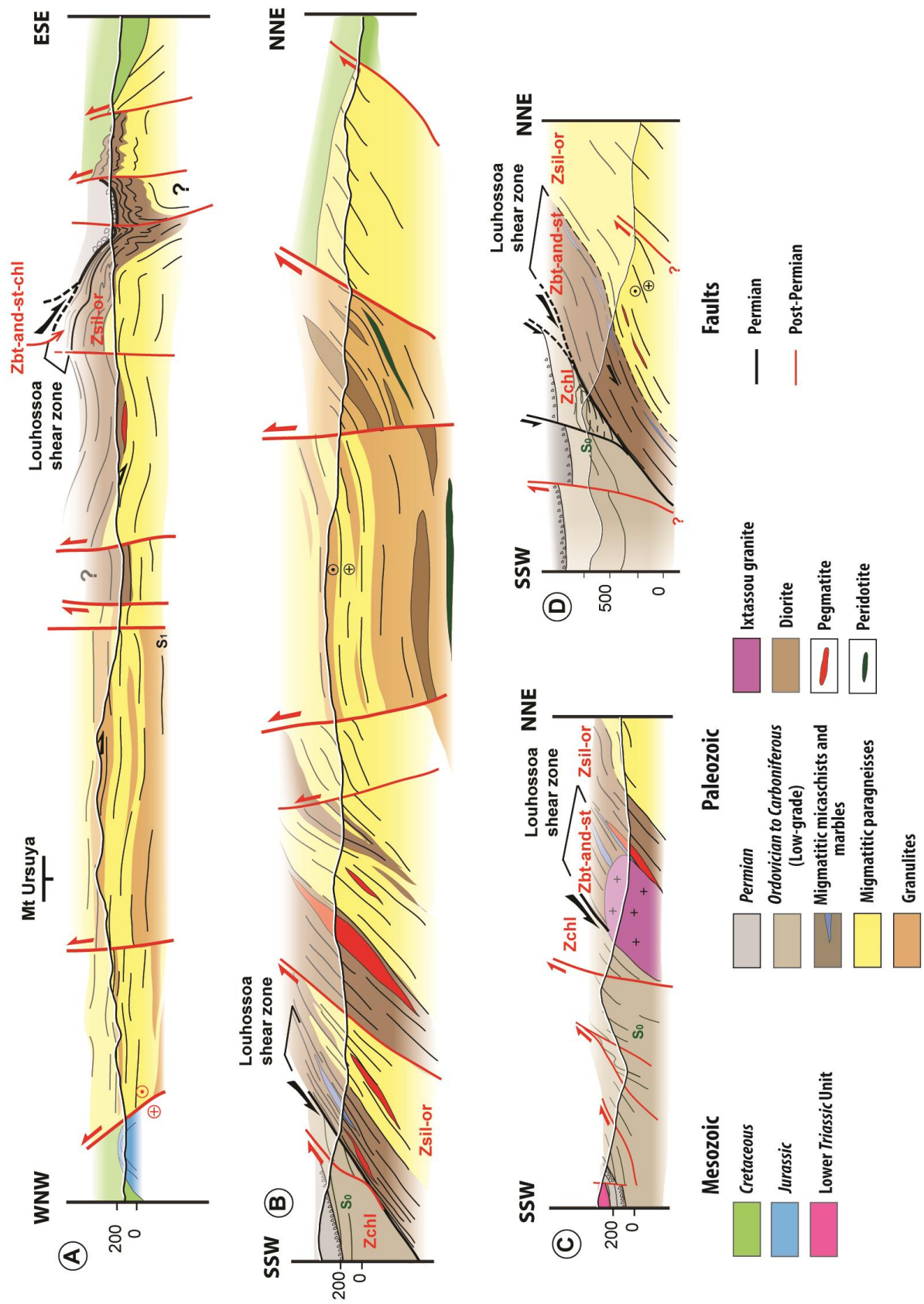


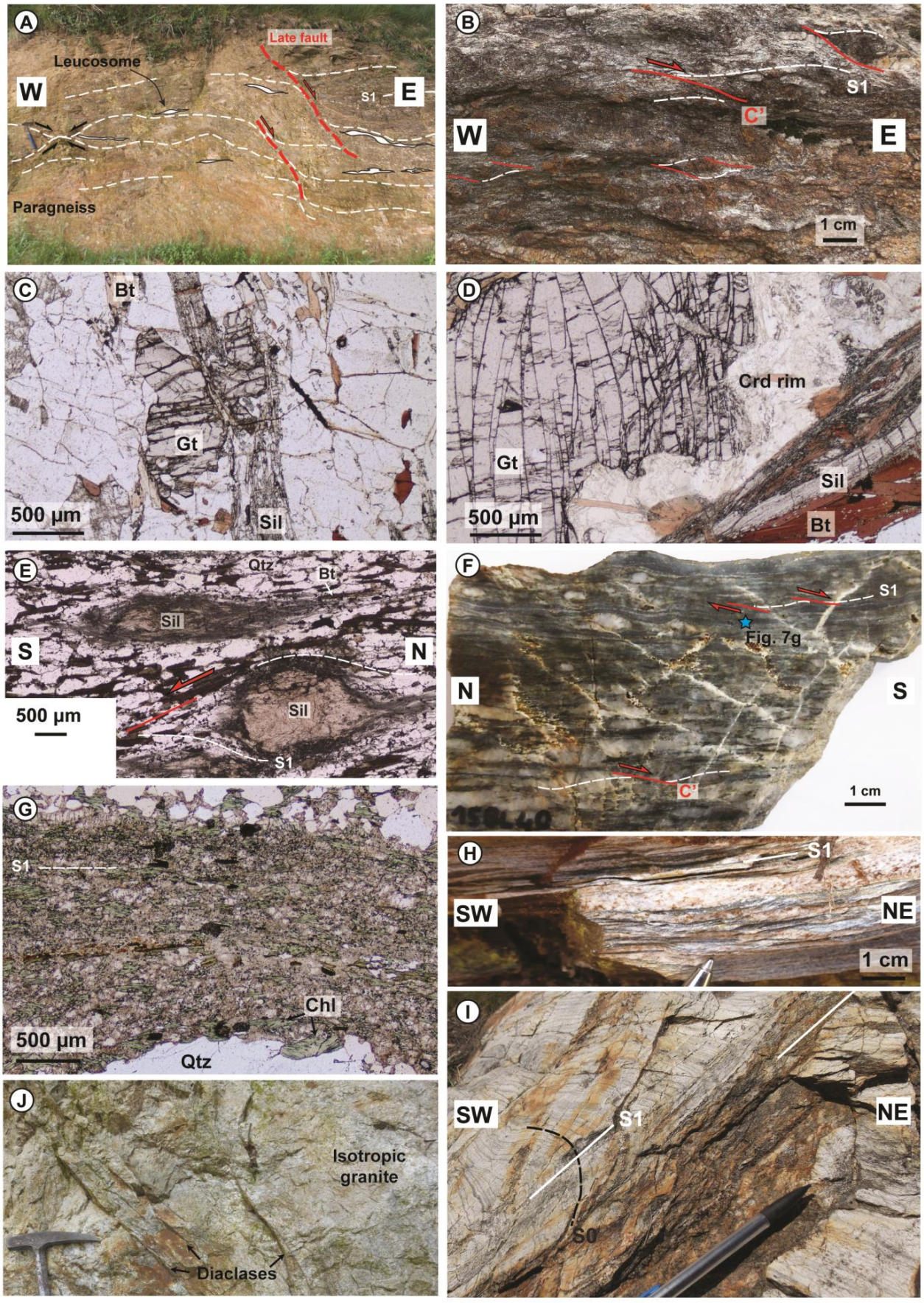
Fig. 6. Cross-sections of the Ursuya gneiss dome (locations in Fig. 2): **(A)** E-W cross-section of the whole massif, **(B)** N-S cross-section of the central part of the gneiss dome, **(C)** N-S cross-section of the southwestern limb, **(D)** N-S cross-section of the southern limb. Zbt-and-st, biotite-andalusite-staurolite zone; Zchl, chlorite zone; Zsil-or, silllimanite-orthoclase zone.

rocks, and garnet sigma-clasts attest to local noncoaxial top-to-the-east or southeast shear **(Figs. 6A, 6B and 7B)**.

The southernmost and easternmost parts of the gneiss dome display the transition between migmatites or paragneisses (sillimanite-orthoclase zone) and low-grade Ordovician sediments (chlorite zone) **(Fig. 2)**. This transition is characterized in the field by highly laminated paragneisses, mica schists, and metaquartzites **(Figs. 6, 7E and 7F)** hosting discontinuous marble layers and highly sheared pegmatites. The transition forms a regional-scale shear zone called the Louhossoa shear zone **(Figs. 2 and 6)**. This shear zone is mainly localized within the andalusite-biotite-staurolite zone and is ~500 m thick **(Figs. 2 and 6)**. The best descriptions of this shear zone can be made in the southeastern part of the massif, where all the structural levels are observed **(Fig. 6D)**. Elsewhere, outcrops are poor and observations are limited to scattered point exposures.

In the southern flank of the gneiss dome, mineral and stretching lineations within the shear zone take the form of quartz ribbons and biotite aggregates and turn progressively from a NW-SE to a N-S trend **(Fig. 2)**. As in the core of the gneiss dome, deformation is marked by flattening but is also associated with C′ shear bands showing a dominant non-coaxial top-to-the-south sense of shear **(Figs. 6 and 7E)**. The mylonitic foliation is parallel with the regional foliation, forming a single fabric mainly defined by high-grade parageneses (sillimanite, andalusite, biotite, K-feldspars; **Fig. 7E**). Within phyllonitic layers, chlorite is formed at the expense of biotite, which shows that deformation occurred under retrogressive conditions **(Figs. 7F and 7G)**. Upward within the chlorite zone, this mylonitic foliation, characterized by millimeter-scale alternating dark and light layers with no visible grains **(Fig. 7H)**, evolves into a pervasive crenulation cleavage, progressively preserving the original bedding of Ordovician sandstones **(Fig. 7I)**. The crenulation cleavage dips gently to the south or is subhorizontal, remaining roughly parallel to the foliation within the shear zone **(Fig. 6D)**. Over a distance of 200 m upward, in Paleozoic rocks, the cleavage disappears and only a poorly expressed crenulation lineation remains. In the southwestern part of the massif, the Itxassou microgranite intrudes the transitional zone between the migmatites and the low-grade Ordovician quartzite within the shear zone **(Figs 2 and 6C)**. The pluton displays no magmatic or gneissose fabric and is only affected by jointing **(Fig. 7J)**. The easternmost part of the Ursuya massif displays a similar sharp transition from migmatitic gneiss to chlorite-bearing mica schist and quartzite **(Figs. 2 and 6A)**. A few hundred meters below this transition, the foliations turn to NE-SW or N-S and dip moderately to the east **(Fig. 6A)**. Stretching lineations remain roughly E-W through the transition. In mica schist, meter-scale late folds showing mostly E-W and N-S axial planes and moderately plunging fold axes are superimposed on this first-order trend. As noted by Boissonnas et al. (1974), the transitional zone between high-grade and low-grade rocks corresponds to a shear zone containing highly laminated gneisses and mica schists. The apparent thickness of this transitional zone (the andalusite-staurolite zone) is highly variable (from ~200 to 0 m), and the shear zone appears to be a subtractive feature. Unfortunately, our observations here were limited to float rocks, and we were unable to make a detailed structural analysis of the shear zone in this area. Immediately above it, we observed Permian chaotic breccias of facies F1c (see **Figs. 3B and 6A**). This tectonic contact appears mostly eroded and is unconformably overlapped by Santonian deposits. This subtractive contact might be continuous as a part of it is preserved in the southeastern part of the massif **(Fig. 2)**.We thus interpret it as a single extensional low-angle shear zone (Louhossoa) across the whole gneiss dome.

The whole massif is affected by late brittle deformation in the form of faults with variable orientations and kinematics. The first set consists of N-S to N45°E trending normal faults **(Figs. 6 and 7A)**. A second set consists of E-W trending south-dipping normal faults, parallel to and merging into the Louhossoa shear zone **(Figs. 2 and 6D)**. A few of these latter faults also show reverse (top-to-the-north) kinematics, suggesting Alpine (re)activation of earlier normal faults **(Figs. 6B and D)** or reactivation of bedding planes in the low-grade basement **(Fig. 6C)**. The reverse faults are responsible for the folding or westward tilting of the eastern termination of the gneiss dome and the Louhossoa shear zone **(Fig. 6A)**.



Caption on next page

Fig. 7. Images of typical petrology and deformation in the Ursuya massif. **(A)** Subhorizontal foliation within migmatite, affected by symmetrical boudinage and late normal faults. **(B)** Top-to-the-east shearing in coarse-grained pelitic granulite (kinzigite) at Mt. Ursuya. **(C)** Photomicrograph of granulite facies paragneiss, showing scarce remnant biotite. **(D)** Photomicrograph of granulitic gneiss showing an altered cordierite corona around garnet, and abundant sillimanite and biotite. **(E)** Photomicrograph of sillimanite porphyroclasts within the Louhossoa shear zone showing top-to-the-south kinematics. **(F)** Top-to-the-south shearing in quartzite within the Louhossoa shear zone. **(G)** Photomicrograph of a phyllonitic layer in the quartzite of Fig. 7F, showing abundant chlorite formed at the expense of biotite. **(H)** Highly sheared metasediments at the top of the Louhossoa shear zone, within the chlorite zone. **(I)** Crenulation cleavage and bedding in Ordovician sandstone in the hanging wall of the Louhossoa shear zone belonging to the chlorite zone. **(J)** Itxassou granite showing isotropic fabric and jointing.

7. Discussion

7.1. Permian age of the Louhossoa shear zone

We propose that the Louhossoa shear zone is a detachment that was activated during the Permian development of the Bidarray basin, for the following reasons: (1) Deformation within the granulites and migmatites occurred at high temperature as indicated by high-grade parageneses such as sillimanite, K-feldspars, andalusite, garnet and biotite. The appearance of cordierite around granulitic garnets within the migmatitic gneisses implies decompression (see Vielzeuf, 1984) during syn-melt penetrative top-to-the-east shear. (2) We observed a single consistent fabric from the granulite to the chlorite-bearing Ordovician metasediments in the field and in thin sections. The retrogressive deformation within the Louhossoa shear zone suggests a continuous exhumation history during a single tectonic phase. (3) U-Pb ages from the Ursuya massif (Hart et al., 2016; Vacherat et al., 2017) indicate that granulites and paragneisses crystallized and were deformed between 295 and 274 Ma. (4) The Itxassou pluton intrudes the southern part of the metamorphic series, where deformation was localized, but remains isotropic. It is thus post-kinematic and its age of emplacement (276.8 ± 1.9 Ma; Vacherat et al., 2017) provides a minimum age for the deformation along the shear zone. (5) The eastern part of the Louhossoa shear zone is unconformably covered by Santonian calcareous turbidites, precluding a later activation or reactivation **(Fig. 2)**.

These observations do not support an activation of the Louhossoa shear zone in Albian to Cenomanian time during the last rifting phase before Pyrenean orogeny, as proposed by Jammes et al. (2009).

7.2. Conceptual model of Permian crustal thinning

A geodynamic conceptual model of continental crustal thinning is proposed to explain the development of the Bidarray basin as part of a Permian rift system **(Fig. 8)**. The development of this continental basin is of the same age as the exhumation of the Ursuya granulites (Hart et al., 2016). All of these structural and magmatic processes are interpreted as being related to a single extensional tectonic phase between ca. 300 and 275 Ma. Several arguments support the interpretation of the Ursuya massif as a Permian extensional MCC resulting from regional thinning of hot lithosphere following collapse of the Variscan belt and subsequent delamination of the lithospheric mantle: (1) Granulite recorded decompression during penetrative E-W horizontal ductile flow, as highlighted by cordierite coronas around granulitic garnets. (2) The exhumation of granulite and migmatite was then favored by strain localization within a retrogressive extensional shear zone such as the Louhossoa detachment, evolving from ductile shearing during partial melting to brittle normal faulting **(Figs. 6 and 8)**. (3) The E-W regional direction of stretching within granulites and migmatites **(Fig. 2)**, compatible with the orientation of the active Bidarray graben, was favored by the activation of N-S trending normal faults in the upper crust. (4) The Bidarray continental basin developed on the hanging wall of the Louhossoa detachment (cross-section 6 in **Fig. 5**), the footwall being currently exposed in the Ursuya granulites (**Fig. 6)**. (5) The structurally controlled deposition of Permian redbeds appears to be coeval with HT-LP granulite metamorphism, magmatism and HT deformation (Pereira et al., 2014; Hart et al., 2016; Vacherat et al., 2017). The alkaline volcanism in the center of the Bidarray basin in the latest Permian (Lucas, 1985; Bixel and Lucas, 1987) may be the surface signature of the middle and lower crustal flow below the

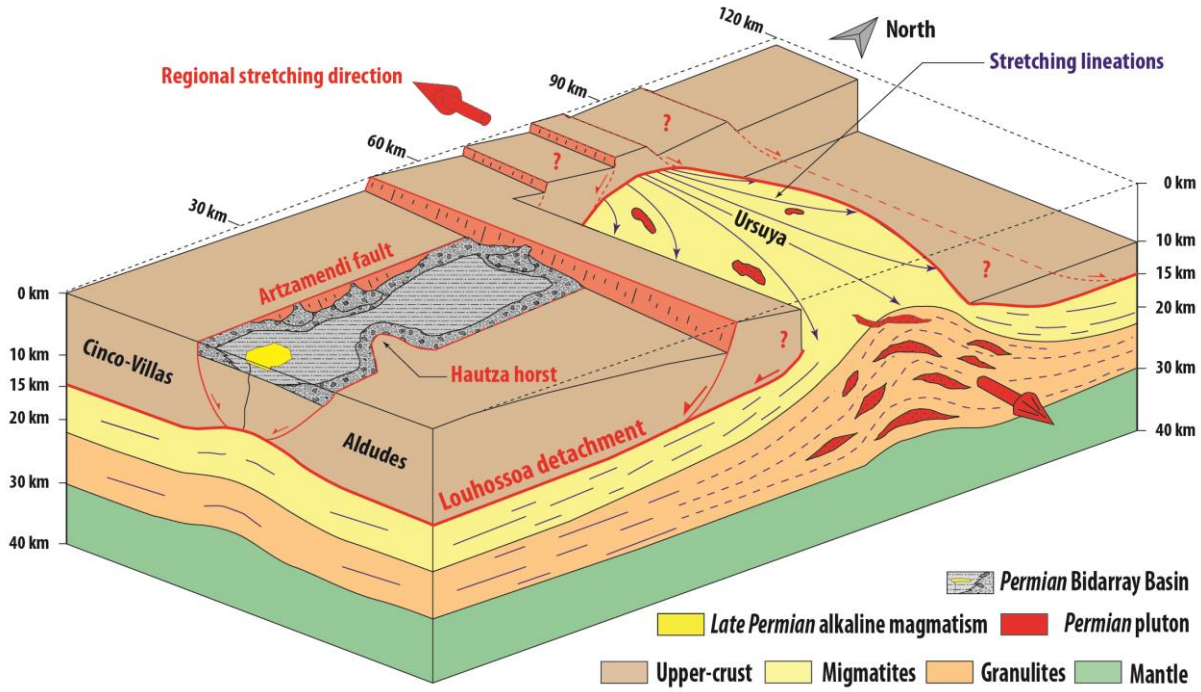


Fig. 8. Conceptual model of crustal thinning during Permian time. The N-S trending Bidarray basin develops on the hanging wall of an « a-type » MCC, tectonically controlled by the Artzamendi normal fault and the Hautza horst. The Ursuya MCC is characterized by an E-W major stretching direction, as shown by the E-W top-to-the-east stretching lineation within the granulites. Near the Louhossoa detachment the stretching lineations take a top-to-the-south direction, showing a southward normal displacement along this major shear zone.

basin and may reflect regional thinning of the lithosphere induced by continental rifting.

The development of the Permian basin and the genesis of the Ursuya MCC can be explained in two major phases. The first phase corresponds to pure shear thinning (sensu McKenzie, 1978) with the initiation of rifting by faulting in the upper crust while the partially molten lower crust is flowing longitudinally.

This first phase of crustal thinning initiated the exhumation of granulites under melt-present conditions, as exemplified in migmatites by destabilization of granulitic garnet into cordierite (**Fig. 7D**, see also Vielzeuf, 1984). Second, gravitational instability induced by the buoyancy of molten lower crust at depth implies a vertical flow of the ductile crust towards the necking zone of the upper crust, initiating the development of an extensional MCC (Tirel, 2004; Tirel et al., 2004; Jolivet et al., 2008; Le Pourhiet et al., 2012; Brun et al., 2017). The exhumation of deep molten rocks is favored by strain localization within major shear zones, here the Louhossoa detachment, developed at the top of the melting front (the gneiss dome envelope) and the flank of the MCC.

In detail, the stretching lineations are mainly parallel to the elongation axis of the gneiss dome and the orientation of the Louhossoa detachment, indicating the « a-type » morphology of the Ursuya MCC (see Jolivet et al., 2004). Divergence of stretching lineations from the core to the limbs **(Fig. 8)** is common in « a-type » MCCs and simply reflects gravitational instabilities within the buoyant and partially molten mid-lower crust, leading to its exhumation (Jolivet et al., 2004; Augier et al., 2005; Le Pourhiet et al., 2012). As strain localization occurs within the dome envelope, these MCCs tend to have a symmetrical shape (Jolivet et al., 2004). The northern flank of the Ursuya MCC has not been preserved because of the overprint of the Arberoue thrust during Paleogene time **(Fig. 2)**.

The Ursuya MCC appears to be immature, in that only low-grade Paleozoic rocks (Cambrian-Carboniferous metasediments) are reworked in the Permian and Triassic deposits. The Ursuya MCC retained a metasedimentary Paleozoic cover during

Permo-Triassic time. However, we interpret the facies F1c chaotic breccias as Permian-Triassic sedimentary breccias derived from the top of the Louhossoa detachment (the Cambrian-Ordovician metasedimentary cover of the MCC). During Permian time, the Bidarray basin was filled by continental deposits reworking the metasedimentary rocks of the MCC hanging wall (Devonian-Carboniferous metasediments). During Triassic time, the continental fluvial system changed sedimentary sources and reworked the thin remaining metasedimentary envelope of the Ursuya MCC (Cambrian-Ordovician quartzite). On the basis of our cross-sections **(Figs. 5 and 6)**, we suggest that the metasediments above the high-grade rocks from the Ursuya massif were approximately 5 km thick at the end of the Triassic. Taking into account that the Late Triassic corresponds to a major rifting phase in Western Europe (e.g., Frizon de Lamotte et al., 2015) and that most (>60%) of the rocks of the Upper Triassic unit in the study area are mantle-derived magmatic rocks (ophites, see **Fig. 2**; Rossi et al., 2003), we infer that the geotherm was probably much greater than 30°C/km at ca. 200 Ma. In magmatic rift systems, geotherms can easily exceed 100°C/km locally (e.g., Omenda, 1997; Chandrasekharam et al., 2018) and are about 40–60°C/km in many other rifts (e.g., Barnard et al., 1992; Ren et al., 2002; Ranalli and Rybach, 2005; Boone et al., 2018). We thus propose that a paleo-geotherm of about 50–60°C/km at the end of the Triassic is reasonable. The 200 Ma cooling age indicated by $^{39}Ar/^{40}Ar$ dates in the paragneisses of the Ursuya massif (Masini et al., 2014) suggest that the Ursuya high-grade rocks were probably exhumed up to 5–6 km depth during the Late Triassic **(Fig. 8)**. PT estimates for granulites from other north Pyrenean massifs support this interpretation; for example, in the Saint Barthélémy massif in the Central Pyrenees **(Fig. 1)**, deformation was mostly retrograde and led to the exhumation of granulite up to 2 kbar during the Late Carboniferous to Early Permian (de Saint Blanquat et al., 1990; de Saint Blanquat, 1993; Delaperrière et al., 1994; Lemirre, 2018). The Ursuya MCC recorded deformation patterns similar to those of transpressional gneiss domes elsewhere in the Pyrenees, such as (1) longitudinal horizontal flow of the partially molten middle and lower crust and (2) gradual strain localization at the top of the domes forming extensional shear zones with similar divergent lineation patterns (Cochelin et al., 2017, 2018b). But our study shows that the Basque massifs are the first documented example in the Pyrenees of Permian crustal thinning typical of an abnormally hot lithosphere permitting the formation of an MCC and its associated graben **(Fig. 8)**.

7.3. Implications for the transition between the Variscan orogenic cycle and Pangea breakup

The latest Carboniferous and earliest Permian (305–295 Ma) was a period of intensive reorganization of the collapsed Variscan belt in which mantle delamination led to the formation of several post-orogenic oroclines (e.g., Weil et al., 2010; Gutiérrez-Alonso et al., 2012). Our study suggests that the formation of the Ursuya MCC and Bidarray graben reflects the switch from dominant N-S convergence recorded in the Pyrenean Axial Zone from 310 to 290 Ma (during oroclinal bending; see Denèle et al., 2014; Cochelin et al., 2017; Lemirre et al., 2019) to overall E-W extension in the Pyrenean realm.

E-W extension in the Basque massifs is compatible with the interpretation of early and middle Permian basins in the eastern Pyrenees and Iberia as strike-slip basins (e.g., Gretter et al., 2015; Lloret et al., 2018). However, our study supports the interpretation that Permian deformation in the Pyrenees was characterized by homogeneous thinning of a hot crust rather than by strain localization into dextral mega-shear zones, as proposed by many authors (e.g., Muttoni et al., 2009; Domeier et al., 2012; Carreras and Druguet, 2014; Gretter et al., 2015). Our results suggest that the crust throughout the Pyrenees (the foreland of the Variscan belt) stayed hot and partially molten during early and middle Permian extension, as in other massifs in the previously collapsed hinterland of the Variscan belt, such as Corsica-Sardinia (e.g., Rossi et al., 2015; Gaggero et al., 2017), or in the Alps (e.g., Pohl et al., 2018). In this scenario, strain was vertically partitioned within the crust, with a homogeneously and longitudinally flowing lower crust and an upper crust affected by widespread N20°E normal faults and longitudinal strike-slip faults.

Homogeneous thinning of the hot continental crust in the Pyrenees and Iberia during the Permian may have had a first-order importance for later localization of the main rift system of the Central Atlantic during the Early Jurassic and the breakup of Pangea in the Triassic (Sengör et al., 1984; Ziegler, 1990; Stampfli, 1996, 2012; Vai, 2003; Ziegler and Stampfli, 2001; Leleu et al., 2016). Indeed, homogeneous thinning within a hot lithosphere implies formation of wide rather than narrow rifts (Brun, 1999). We propose that the Pyrenean realm was part of the wide rift system recognized in the rest of Iberia during the Permian (e.g., Leleu et al., 2016). Therefore, Late Triassic to Early Jurassic extension and drifting that affected the cooled lithosphere may have been localized farther west within a narrower Permian-Triassic rift zone (Leleu et al., 2016) or along crustal-scale inherited structures (e.g., Le Roy and Piqué, 2001). The previously homogeneously thinned crust of the Pyrenees was later affected by Early Cretaceous hyperextension and mantle exhumation (Jammes et al., 2009; Lagabrielle et al., 2010; Masini et al., 2014; Teixell et al., 2016; Saspiturry et al., 2019).

7.4. Tectonic implications for the structure of the Western Pyrenees

Our study addresses the Permian-Triassic tectonic evolution of the northwestern Pyrenees. The Permian Bidarray extensional basin is relatively well preserved **(Fig. 5)**, highlighting the small amount of deformation affecting this part of the Pyrenees during the Pyrenean orogeny. The basin is closely aligned with the putative transverse Pamplona fault, and its location coincides with the western and eastern edges of two branches of the Early Cretaceous Pyrenean rift system: the Mauléon and Basque-cantabrian basins, respectively **(Fig. 2)**. The Bidarray basin lies between two oppositely verging Cretaceous detachment faults (the Bidarray and Errazu faults) in a transfer zone corresponding to the Pamplona fault. Classically, the Pamplona fault is regarded not as a well-defined fault plane that can be observed at the outcrop scale, but as a broad crustal heterogeneity that controlled the opening of the Mauléon, Saint-Jean-de-Luz and Basque-Cantabrian rift basins during Cretaceous extension and their alpine reactivation during the Cenozoic basin inversion (Schoeffler, 1982; Rat et al., 1983; Richard, 1986; Razin, 1989; Claude, 1990). We demonstrate in this study that during Permian time this transfer zone was characterized by a succession of N0–20° grabens affecting the upper crust (including the Bidarray basin), separated by immature MCCs that exhumed middle and lower crust to shallow depths (including the Ursuya dome). Therefore, the Pamplona transfer zone appears to be a Permian inherited structure which was reactivated during Cretaceous rifting and was responsible for the shift towards the southwest of the Early Cretaceous Pyrenean rift axis.

Our crustal thinning model shows that, at the beginning of Cretaceous rifting, the Ursuya unit was characterized by a continental crust composed of granulitic mid-crustal rocks partially exhumed during Permian time. The Ursuya granulites were fully denudated and reworked during Cenomanian time in the Bonloc breccias, located under the Arberoue thrust (**Fig. 2**; Boissonnas et al. 1974; Claude, 1990). The perfect continuity of the Permian-Triassic paleogeographical and structural trends highlights the homogeneity of the Basque massifs, showing the absence of a major alpine discontinuity between the Cinco-Villas unit of European paleomagnetic affinity (Schott, 1985) and the Aldudes unit, part of the northern Iberian Cretaceous paleomargin (Schott, 1985). There is no physical continuity between the North Pyrenean fault as defined in the eastern and central Pyrenees (Choukroune, 1976) and interpreted as the tectono-magmatic axis of the Basque-Cantabrian basin (Rat et al., 1983). The preservation of the original paleogeography and structure of the Bidarray basin indicates that there was no major east-west Mesozoic strike-slip motion between the Iberian and European plates in this part of the Pyrenees (Schoeffler, 1965, 1982; Ducasse and Vélasque, 1988; Razin, 1989; Claude, 1990). Such strike-slip motion, deduced from plate kinematic reconstructions (Olivet, 1996; Rosenbaum et al., 2002; Sibuet et al., 2004), may have affected a more southerly area (Malod, 1982; Canérot, 2016) or may have been evenly distributed within the Cretaceous rift system.

8. Conclusion

This sedimentological and structural study indicates that the Western Pyrenees

record Permian E-W extension and a deformation pattern typical of a thinning hot lithosphere. We show that in the upper crust a N0–20° trending extensional basin (the Bidarray basin) is filled by interdigitating alluvial fans that advanced towards a longitudinal fluvial system in the center of the basin. Coevally with the development of this intracontinental rift basin, the middle and lower crust was affected by (1) LP granulitic metamorphism (in the Ursuya dome), (2) horizontal flow parallel to the direction of extension in the sedimentary basin, and (3) ductile exhumation within an E-W elongated « a-type » MCC. The granulites were exhumed thanks to strain localization at the fusion front within an extensional shear zone (detachment) under retrogressive conditions. Our work shows that the Ursuya granulites were exhumed in several phases, first to upper crustal level during Permian rifting related to the Pangea breakup, then completed by denudation at the end of Cretaceous rifting. Formation of the MCC during Permian rifting implies that the entire Pyrenean realm was characterized at the time by an abnormally hot lithosphere. In such a hot context, deformation was mainly homogeneous, and strain was partitioned between horizontal flow in the lower crust and diffuse strike-slip and normal faulting in the upper crust rather than giving rise to regional strike-slip megashear zones. The Mesozoic Pamplona transfer zone appears as an inherited major crustal heterogeneity of Permian age and oriented N0–20°, not visible at the outcrop scale as a single fault zone. Thus the main structures of Permian rifting appear to have controlled the development of Cretaceous rifting. The preservation of Permian-Triassic paleogeographic and structural patterns shows that a Mesozoic E-W strike-slip motion between the Iberian and European plates could not have taken place in this part of the Pyrenees.

Acknowledgments

This work is part of the Orogen project, cofunded by Total and BRGM, and the RGF project funded by the BRGM. BC acknowledges funding from Labex Voltaire (ANR-10-LABX-100-01), based at Orléans University and BRGM. We thank Orogen project managers Sylvain Calassou (Total), Emmanuel Masini (Total), Olivier Vidal (CNRS) and Isabelle Thinon (BRGM). Many thanks to Michel de Saint Blanquat for fruitful discussion about the geological background of the study area. The manuscript was greatly improved by reviews from Céline Ducassou and Jean Van den Driessche, whom we thank for their helpful comments.

References

Adler, R. E., H. U. Boer, H. Jordan, K. Klarr, H. F. Krausse, D. Muller, R. Muller, H. Requadt, H. Roth, and J. Thiele, 1972, Carte géologique de l'Espagne au 1/50000; feuille de Valcarlos, Madrid, Espagne: Instituto Geologico y Minero de España.

Arthaud, F., and P. Matte, 1975, Les Décrochements Tardi-hercyniens du sud-ouest de l'Europe. Géométrie et essai de reconstitution des conditions de la déformation: Tectonophysics, v. 25, p. 139–171.

Augier, R., Jolivet, L., Robin, C., 2005. Late Orogenic doming in the eastern Betic Cordilleras: Final exhumation of the Nevado-Filabride complex and its relation to basin genesis. Tectonics 24, TC4003, doi:10.1029/2004TC001687

Avigad, D., and Z., Garkunkel, 1989, Low-angle faults above and below a blueschist belt—Tinos Island, Cyclades, Greece. Terra Nova, v. 1, no. 2, p. 182–187, doi:10.1111/j.1365-3121.1989.tb00350.x

Ballèvre M., V., Bosse, C., Ducassou, P., Pitra, 2009, Palaeozoic history of the Armorican Massif: Models for the tectonic evolution of the suture zones. Comptes Rendus Geoscience, 341, 174-201, doi:10.1016/j.crte.2008.11.009.

Barnard P, C., Thompson, S., Bastow, M. A., Ducreux. C., and G. Marthurin, 1992, Thermal maturity development and source-rock occurrence in the red sea and gulf of Aden. Journal of Petroleum Geology, vol 15, p. 173–186, doi: 10.1111/j.1747-5457.1992.tb00961.x.

Benvenuti, M., and I. P. Martini, 2002, Analysis of Terrestrial Hyperconcentrated Flows and their Deposit, in I. Peter Martini, V. R. Baker, and G. Garzn, eds., Flood and Megaflood Processes and Deposits: Oxford, UK, Blackwell Publishing Ltd., p. 167–193, doi:10.1002/9781444304299.ch10.

Bixel, F., 1984, Le volcanisme stéphano-permien des Pyrénées. PhD thesis, University of Paul Sabatier, Toulouse, France, 638 p.

Bixel, F., and C. L. Lucas, 1983, Magmatisme, tectonique et sédimentation dans les fossés stéphano-permiens des Pyrénées occidentales: Revue de géologie dynamique et de géographie physique, v. 24, no. 4, p. 329–342.

Bixel, F., and C. Lucas, 1987, Approche Géodynamique du Permien et du Trias des Pyrénées dans le cadre du sud-ouest européen: Cuadernos Geología Ibérica, v. 11, p. 57–81.

Blair, T. C., and J. G. McPherson, 1994, Alluvial fans and their natural distinction from rivers based on morphology, hydraulic processes, sedimentary processes, and facies assemblages: Journal of sedimentary research, v. 64, no. 3.

Boissonnas, J., G. Le Pochat, C. Thibault, and M. Bernatzk, 1974, Carte géologique de la France au 1/50000; feuille d'Iholdy, Orléans, France: Bureau de Recherche Géologique et minière.

Boone, S.C., Kohn, B.P., Gleadow, A.J.W., Morley, C.K., Seiler, C., Foster, D.A., Chung, L., 2018, Tectono-thermal evolution of a long-lived segment of the East African Rift System: Thermochronological insights from the North Lokichar basin, Turkana, Kenya. Tectonophysics 744, p. 23–46, doi: 10.1016/j.tecto.2018.06.010.

Bridge, J. S., 1993, Description and interpretation of fluvial deposits: a critical perspective: Sedimentology, v. 40, no. 4, p. 801–810.

Bridge, J. S., 2009, Rivers and floodplains: forms, processes, and sedimentary record: John Wiley & Sons.

Brun, J.-P., 1999. Narrow rifts versus wide rifts: inferences for the mechanics of rifting from laboratory experiments. Philos. Trans. R. Soc. Lond. A 357, 695–710.

Brun, J. -P, and J., Van Den Driessche, 1994, Extensional gneiss domes and detachement fault systems: structure and kinematics, BSGF, 165, 6, p. 519–530.

Brun, J.-P., D., Sokoutis, C., Tirel, F., Gueydan, J., Van Den Driessche, M.-O., Beslier, 2017, Crustal versus mantle core comSplexes, Tectonophysics, available online 28 Sept 2017, doi : 10.1016/j.tecto.2017.09.017

Burg, J.-P., J. Van Den Driessche, and J.-P. Brun, 1994, Syn- to post-thickening extension : mode and consequences: Comptes rendus de l'Académie des sciences. Série 2. Sciences de la terre et des planètes, v. 319, no. 9, p. 1019–1032.

Canérot, J. C., 2016, The Iberian Plate: myth or reality?: Boletin Geologico y Minero, 127, p. 557-568.

Carreras J, Druguet E. 2014. Framing the tectonic regime of the NE Iberian Variscan segment. Geol. Soc. Spec. Publ. 405, 249–264. doi:10.1144/SP405.7

Cassinis, G., N. Toutin-Morin, and C. Virgili, 1995, A General Outline of the Permian Continental basins in Southwestern Europe. In: Scholle P.A., Peryt T.M., Ulmer-Scholle D.S. (eds) The Permian of Northern Pangea. Springer, Berlin, Heidelberg.

Casteras, M., 1971, Carte géologique de la France à 1/50 000: feuille de Tardets–Sorholus, Orléans, France: Bureau de Recherche Géologique et minière.

Chamyal, L. S., A. S. Khadkikar, J. N. Malik, and D. M. Maurya, 1997, Sedimentology of the Narmada alluvial fan, western India: Sedimentary Geology, v. 107, no. 3–4, p. 263–279.

Chandrasekharam, D., Lashin, A., Al Arifi, N., Al-Bassam, A.M., Varun, C., 2018, Geochemical evolution of geothermal fluids around the western Red Sea and East African Rift geothermal provinces. J. Asian Earth Sci, 164, p. 292–306, doi: 10.1016/j.jseaes.2018.06.013.

Choukroune, P., 1976, Strain patterns in the Pyrenean chain: Philosophical Transactions of the Royal Society of London A: Mathematical, Physical and Engineering Sciences, v. 283, no. 1312, p. 271–280.

Claude, D., 1990, Etude stratigraphique, sédimentologique et structurale des dépôts mésozoïques au nord du massif du Labourd: rôle de la faille de Pamplona (Pays Basque). PhD thesis, University of Bordeaux III, France, 437 p.

Cochelin, B., D. Chardon, Y. Denèle, C. Gumiaux, and B. Le Bayon, 2017, Vertical strain partitioning in hot Variscan crust: Syn-convergence escape of the Pyrenees in the Iberian-Armorican syntax: Bulletin de la Société Géologique de France, v. 188, no. 6, 39, doi:10.1051/bsgf/2017206

Cochelin, B., Lemirre, B., Denèle, Y., Blanquat, M. de S., Lahfid, A., Duchêne, S., 2018a, Structural inheritance in the central Pyrenees: the variscan to Alpine tectonometamorphic evolution of the axial zone. J. Geol. Soc., v. 175, 336–351, doi:10.1144/jgs2017-066.

Cochelin, B., Gumiaux, C., Chardon, D., Denèle, Y., Le Bayon, B., 2018b, Multi-scale strainfield analysis using geostatistics: Investigating the rheological behavior of the hot Variscan crust of the Pyrenees (Axial Zone). J. Struct. Geol., v. 116, 114–130, doi:10.1016/j.jsg.2018.07.024

Coney, P.J., 1980. Cordilleran metamorphic core complexes: an overview. In: Crittenden, M.D., Coney, P.J., Davis, G.H. (Eds.), Cordilleran Metamorphic Core Complexes. Geological Society of America Memoir, v. 153. pp. 7–34.

Curnelle, R., 1983, Evolution structuro-sédimentaire du Trias et de l'Infra-Lias d'Aquitaine: Bull. Cent. Rech. Explor. Prod. Elf-Aquitaine, v. 7, no. 1, p. 69–99.

Davis, G. A., G. S. Lister, and S. J. Reynolds, 1986, Structural evolution of the Whipple and South mountains shear zones, southwestern united States: Geology, v. 14, no. 1, p. 7–10, doi:10.1130/0091-7613(1986)14<7:SEOTWA>2.0.CO;2.

Davis, G. H., and P. J. Coney, 1979, Geologic development of the Cordilleran metamorphic core complexes: Geology, v. 7, no. 3, p. 120–124, doi:10.1130/0091-7613(1979)7<120:GDOTCM>2.0.CO;2.

Delaperrière E, de Saint Blanquat M, Brunel M, Lancelot J (1994) Géochronologie U Pb sur les zircons et monazites dans le massif du Saint Barthélémy. Bull Soc Géol Fr 2, 101–112

Denèle, Y., Olivier, P., Gleizes, G., Barbey, P., 2007. The Hospitalet gneiss dome (Pyrenees) revisited: lateral flow during Variscan transpression in the middle crust, Terra Nova, v. 19, 445–453, doi:10.1111/j.1365-3121.2007.00770.x.

Denèle, Y., Olivier, P., Gleizes, G., Barbey, P., 2009. Decoupling between the middle and upper crust during transpression-related lateral flow: variscan evolution of the Aston gneiss dome (Pyrenees, France), Tectonophysics, v. 477, 244–261, doi:10.1016/j.tecto.2009.04.033.

Denèle, Y., J.-L. Paquette, P. Olivier, and P. Barbey, 2012, Permian granites in the Pyrenees: the Aya pluton (Basque Country): Terra Nova, v. 24, no. 2, p. 105–113.

Denèle, Y., B. Laumonier, J.-L. Paquette, P. Olivier, G. Gleizes, and P. Barbey, 2014, Timing of granite emplacement, crustal flow and gneiss dome formation in the Variscan segment of the Pyrenees: Geological Society,

London, Special Publications, v. 405, no. 1, p. 265–287, doi:10.1144/SP405.5

Domeier, M., Van der Voo, R., Torsvik, T.H., 2012. Paleomagnetism and Pangea: The road to reconciliation. Tectonophysics 514–517, p.14–43, doi:10.1016/j.tecto.2011.10.021

Ducasse, L., and P.-C. Velasque, 1988, Géotraverse dans la partie occidentale des Pyrénées, de l'avant-pays aquitain au bassin de l'Ebre: effet d'une inversion structurale sur l'édification d'une chaîne intracontinentale: Université Paul Cézanne (Aix-Marseille). Faculté des sciences et techniques de Saint-Jérôme, 287 p.

Ducoux, M., 2017, Structure, thermicité et évolution géodynamique de la Zone Interne Métamorphique des Pyrénées. PhD thesis, University of Orléans, France, 646 p.

Durand, M., 2006, The problem of the transition from the Permian to the Triassic Series in southeastern France: comparison with other Peritethyan regions: Geological Society, London, Special Publications, v. 265, no. 1, p. 281–296.

Echtler, H., and J. Malavieille, 1990, Extensional tectonics, basement uplift and Stephano-Permian collapse basin in a late Variscan metamorphic core complex (Montagne Noire, Southern Massif Central): Tectonophysics, v. 177, no. 1–3, p. 125–138.

Faure, M., J.-M. Lardeaux, and P. Ledru, 2009, A review of the pre-Permian geology of the Variscan French Massif Central: Comptes Rendus Geoscience, v. 341, no. 2–3, p. 202–213.

Franke, W., 1989, Variscan plate tectonics in Central Europe—current ideas and open questions: Tectonophysics, v. 169, no. 4, p. 221–228, doi:10.1016/0040-1951(89)90088-7.

Frizon de Lamotte, D., B. Fourdan, S. Leleu, F. Leparmentier, and P. de Clarens (2015), Style of rifting and the stages of Pangea breakup, Tectonics, 34, 1009–1029, doi:10.1002/2014TC003760.

Gaggero, L., Gretter, N., Langone, A., Ronchi, A., 2017. U-Pb geochronology and geochemistry of late Paleozoic in Sardinia (southern Variscides). Geosci. Front. 8, 1263–1284, doi:10.1016/j.gsf.2016.11.015.

Gisbert, J., 1981, Estudio geologico-petrologico del Estefaniense-Permico de la Sierra del cadi (Pireneo de Lérida): Diagenesis y sedimentologia, Thesis, Universitu of Zaragosa, Spain.

Gretter, N., Ronchi, A., López-Gómez, J., Arche, A., De la Horra, R., Barrenechea, J., Lago, M., 2015, The Late Palaeozoic-Early Mesozoic from the Catalan Pyrenees (Spain): 60Myr of environmental evolution in the frame of the western peri-Tethyan palaeogeography. Earth-Science Reviews, v. 150, 679–708, doi: 10.1016/j.earscirev.2015.09.001

Gueydan, F., Morency, C., Brun, J.-P., 2008, Continental rifting as a function of lithosphere mantle strength, Tectonophysics, v. 460, 83–93, doi:10.1016/j.tecto.2008.08.012.

Guitard G, Vielzeuf D, Martinez F. 1996. Métamorphisme hercynien. In Synthèse Géologique et Géophysique Des Pyrénées vol. 1. Orléans (France) : BRGM-ITGE, pp. 501–584.

Gutiérrez-Alonso G, Johnston ST, Weil AB, Pastor-Galán D, Fernández-Suárez J. 2012. Buckling an orogen: The Cantabrian Orocline. GSA Today 22: 4–9, doi: 10.1130/GSATG141A.1.

Hart, N. R., D. F. Stockli, and N. W. Hayman, 2016, Provenance evolution during progressive rifting and hyperextension using bedrock and detrital zircon U-Pb geochronology, Mauléon basin, western Pyrenees: Geosphere, v. 12, no. 4, p. 1166–1186, doi:10.1130/GES01273.1.

Hart, N. R., D. F. Stockli, L. L. Lavier, and N. W. Hayman, 2017, Thermal evolution of a hyperextended rift basin, Mauléon basin, western Pyrenees: Thermal evolution of hyperextended rift: Tectonics, doi:10.1002/2016TC004365.

Heddebaut, C., 1967, Observations tectoniques sur le massif des Aldudes (Basses-Pyrénées): CR Som. Soc. Géol. de France, fasc, v. 7, p. 280–281.

Heddebaut, C., 1973, Etudes géologiques dans les massifs paléozoïques basques. PhD thesis, University of Lille, France, 263 p.

Iverson, R. M., 1997, The physics of debris flows: Reviews of Geophysics, v. 35, no. 3, p. 245–296, doi:10.1029/97RG00426.

Izquierdo-Llavall, E., Casas-Sainz, A., M., Oliva-Urcia, B., 2013, Heterogeneous deformation recorded by magnetic fabrics in the Pyrenean Axial Zone. Journal of Structural Geology, v. 57, 97–113, doi:10.1016/j.jsg.2013.10.005

Izquierdo-Llavall, E., Casas-Sainz, A., M., Oliva-Urcia, B., 2014, Heterogeneous deformation recorded by magnetic fabrics in the Palaeomagnetism and magnetic fabrics of the Late Palaeozoic volcanism in the Castejón-Laspaúles basin (Central Pyrenees). Implications for palaeoflow directions and basin configuration, Geological Magazine, v. 151, 777-797, doi: 10.1017/S0016756813000769

Jammes, S., G. Manatschal, L. Lavier, and E. Masini, 2009, Tectono-sedimentary evolution related to extreme crustal thinning ahead of a propagating ocean: Example of the western Pyrenees: Tectonics, v. 28, no. 4, doi:10.1029/2008TC002406.

Jolivet, L., and Goffé, B., 2000, Les dômes métamorphiques extensifs dans les chaînes de montagnes. Extension syn-orogénique et post-orogénique, Comptes Rendus Académie Sci. - Ser. IIA - Earth Planet. Sci, v. 330, p. 739–751, doi: 10.1016/S1251-8050(00)00220-2.

Jolivet, L., V. Famin, C. Mehl, T. Parra, C. Aubourg, R. Hébert, and P. Philippot, 2004, Strain localization during crustal-scale boudinage to form extensional metamorphic domes in the Aegean Sea: Special papers-Geological Society of America, p. 185–210.

Jolivet, L., R. Augier, C. Faccenna, F. Negro, G. Rimmele, P. Agard, C. Robin, F. Rossetti, and A. Crespo-Blanc, 2008, Subduction, convergence and the mode of backarc extension in the Mediterranean region: Bulletin de la Société Géologique de France, v. 179, no. 6, p. 525–550.

Juch, D., H. F. Krausse, D. Muller, H. Requadt, D. Schafer, J. Sole, and L. Villalobos, 1972, Carte géologique de l'Espagne au 1/50000; feuille de Maya del Baztan, Madrid, Espagne: Instituto Geologico y Minero de España.

Lagabrielle, Y., P. Labaume, and M. de Saint Blanquat, 2010, Mantle exhumation, crustal denudation, and gravity tectonics during Cretaceous rifting in the Pyrenean realm (SW Europe): Insights from the geological setting of the lherzolite bodies: Tectonics, v. 29, no. 4, doi:10.1029/2009TC002588.

Lago, M., Arranz Yagüe, E., Pocoví, A., Galé Bornao, C., Gil-Imaz, A., 2004, Lower Permian magmatism of the Iberian Chain and its relationship to extensional tectonics. In: Wilson, M., Neumann, E.R., Davies, G., Timmermann, M., Heeremans, M., Larsen, B.T. (Eds.), Permo-Carboniferous Magmatism and Rifting in Europe. Special Publication, Geological Society of London, v. 223, pp. 465–491.

Lamare, P., 1931, Sur l'existence du Permien dans les Pyrénées basques, entre la Vallée de Baztan (Navarre espagnole) et la Vallée de Baïgorry (Basse Navarre française): CR Somm. Soc. Geol. Fr, v. 16, p. 242–245.

Lamare, P., 1939, La série paléozoïque du massif du Baygoura et de la vallée de la Nive; ses relations avec les terrains secondaires environnants: Bulletin de la Société Géologique de France, v. 9, p. 163–184.

Lamare, P., 1944, La terminaison orientale du massif des Aldudes, aux environs d'Arnéguy, révision de la feuille de Saint-Jean-Pied-de-Port au 1/80 000: Bulletin de la Carte Géologique de France, v. 45, no. 216, p. 265–305.

Laurent O., Couzinié S., Zeh A., Vanderhaeghe O., Moyen J.,-F., Villaros A., et al. 2017, Protracted, coeval crust and mantle melting during Variscan late-orogenic evolution: U–Pb dating in the eastern French Massif Central. Int. J. Earth Sci., v. 106, 421–451. doi:10.1007/s00531-016-1434-9.

Laverdière, J.-W., 1930, Les formations paléozoïques de la vallée du Laurhibar: Mém. Soc. Géol. Nord. Lille, v. 55, p. 156–157.

Le Pochat, G., C. Bolthenhagen, M. Lenguin, S. Lorsignol, and C. Thibault, 1976, Carte géologique de France au 1/50 000: Mauléon-licharre, Orléans, France.

Le Pochat, G., C. Heddebaut, M. Lenguin, S. Lorsignol, P. Souquet, J. Muller, and P. Roger, 1978, Carte Géologique de France au 1/50 000: St Jean Pied de Port, Orléans, France.

Le Pourhiet, L., B. Huet, D. A. May, L. Labrousse, and L. Jolivet, 2012, Kinematic interpretation of the 3D shapes of metamorphic core complexes: Geochemistry, Geophysics, Geosystems, v. 13, no. 9.

Le Roy, P., & Piqué, A., 2001. Triassic–Liassic Western Moroccan synrift basins in relation to the Central Atlantic opening. Marine Geology 172, p. 359–381

Leleu, S., 2005, Les cônes alluviaux Crétacé supérieur/Paléocène en Provence: traceurs de l'évolution morpho-tectonique des stades précoces de collision. PhD thesis, University of Strasbourg 1, Strasbourg, France, 222 p.

Leleu, S., A. J. Hartley, C. van Oosterhout, L. Kennan, K. Ruckwied, and K. Gerdes, 2016, Structural, stratigraphic and sedimentological characterisation of a wide rift system: The Triassic rift system of the Central Atlantic Domain: Earth-Science Reviews, v. 158, p. 89–124.

Lemirre, B., 2018. Origine et développement de la thermicité dans les Pyrénées varisques. PhD thesis, Univ. Paul Sabatier, Toulouse, France, 299p.

Lemirre, B., Cochelin, B., Duchene, S., de Saint Blanquat, M., Poujol, M., 2019. Origin and duration of late orogenic magmatism in the foreland of the Variscan belt (Lesponne — Chiroulet — Neouvielle area, french Pyrenees). Lithos 336-337, p. 183-201, doi: 10.1016/j.lithos.2019.03.037

Levson, V. M., and N. W. Rutter, 2000, Influence of bedrock geology on sedimentation in Pre-Late Wisconsinan alluvial fans in the Canadian Rocky Mountains: Quaternary International, v. 68–71, p. 133–146, doi:10.1016/S1040-6182(00)00039-2.

Lister, G. S., and G. A. Davis, 1989, The origin of metamorphic core complexes and detachment faults formed during Tertiary continental extension in the northern Colorado River region, U.S.A.: Journal of Structural Geology, v. 11, no. 1, p. 65–94, doi:10.1016/0191-8141(89)90036-9.

Lister, G.S., Banga, G., and Feenstra, A., 1984, Metamorphic core complexes of cordilleran type in the Cyclades, Aegean Sea, Greece, Geology, v. 12, p. 221–225.

Lloret J., A., Ronchi, J., López-Gómez, N., Gretter, R., De la Horra, J., F., Barrenechea, A., Arche, 2018, Syn-tectonic sedimentary evolution of the continental late Palaeozoic-early Mesozoic Erill Castell-Estac basin and its significance in the development of the central Pyrenees basin, Sedimentary Geology, v. 374, 134-157, doi: 10.1016/j.sedgeo.2018.07.014

Lotout, C., Pitra, P., Poujol, M., Anczkiewick, R., Van Den Driessche, J., 2018, Timing and duration of Variscan high-pressure metamorphism in the French Massif Central: A multimethod geochronological study from the Najac Massif, Lithos, v. 308-309, 381-394, doi: 10.1016/j.lithos.2018.03.022

Lucas, C., 1968, Le grès rouge du Comminges et de la Bigorre (Pyrénées centrales). PhD thesis, University of Paul Sabatier, Toulouse, France, 132 p.

Lucas, C., 1977, Le Trias des Pyrénées, corrélations stratigraphiques et paléogéographie: Bulletin du BRGM, v. 2, p. 225–231.

Lucas, C., 1985, Le grès rouge du versant nord des Pyrénées: essai sur la géodynamique de dépôts continentaux du permien et du trias, PhD Thesis ('thèse d'état'), University of Paul Sabatier, Toulouse, France, 267 p.

Lucas, C., J. Doubinger, and J. Broutin, 1980, Premières datations palynologiques dans les grès triasiques des Pyrénées: CR Acad. Sci., Paris, v. 291, p. 517–520.

Malavieille, J., 1993, Late orogenic extension in mountain belts: insights from the basin and Range and the late Paleozoic Variscan belt: Tectonics, v. 12, no. 5, p. 1115–1130.

Malavieille, J., P. Guihot, S. Costa, J. M. Lardeaux, and V. Gardien, 1990, Collapse of the thickened Variscan crust in the French Massif Central: Mont Pilat extensional shear zone and St. Etienne Late Carboniferous basin: Tectonophysics, v. 177, no. 1–3, p. 139–149.

Malod, J., A, 1982, Comparaison de l'évolution des marges continentales au nord et au sud de la péninsule ibérique. PhD thesis ('Thèse d'état'), University of Paris, France, 235 p.

Martínez-Catalán J.,R., Pascual F.,J.,R, Montes A.,D., Fernández R.,D., Barreiro J.,G., Silva Í.,D.,D., et al. 2014, The late Variscan HT/LP metamorphic event in NW and Central Iberia: relationships to crustal thickening, extension, orocline development and crustal evolution, Geol Soc Spec Publ, v. 405, 225–247, doi: 10.1144/SP405.1.

Masini, E., G. Manatschal, J. Tugend, G. Mohn, and J.-M. Flament, 2014, The tectono-sedimentary evolution of a hyper-extended rift basin: the example of the Arzacq–Mauléon rift system (Western Pyrenees, SW France): International Journal of Earth Sciences, v. 103, no. 6, p. 1569–1596, doi:10.1007/s00531-014-1023-8.

Matte, P., 2001, The Variscan collage and orogeny (480–290 Ma) and the tectonic definition of the Armorica microplate: a review: Terra nova, v. 13, no. 2, p. 122–128.

Matte, P., and A. Hirn, 1988, Seismic signature and tectonic cross section of the Variscan crust in western France: Tectonics, v. 7, no. 2, p. 141–155.

McKenzie, D., 1978, Some remarks on the development of sedimentary basins: Earth and Planetary Science Letters, v. 40, no. 1, p. 25–32, doi:10.1016/0012-821X(78)90071-7.

Merle, J.-M., 1974, Recherches sur les relations paléogéographiques et structurales entre les massifs basques au sud de Saint-Jean-Pied-de-Port (Pyrénées occidentales). PhD thesis, University of Paul Sabatier, Toulouse, France, 142 p.

Mey, P. H. W., Nagtegaal, P. J. C., Roberti, K. J. and J. J. A. Hartevelt, 1968, Lithostratigraphic subdivision of post-Hercynian deposits in South-Central Pyrenees, Spain, Leidse. Geol. Meded, v. 41, p. 221–228.

Miall, A. D., 1977a, A review of the braided-river depositional environment: Earth-Science Reviews, v. 13, no. 1, p. 1–62.

Miall, A. D., 1977b, Lithofacies types and vertical profile models in braided river deposits: a summary: Geological Survey of Canada, p. 597–604.

Muller, J., and P. Roger, 1977, L'Evolution structurale des Pyrénées (Domaine central et occidental) Le segment hercynien, la chaîne de fond alpine: Géologie alpine, v. 53, no. 2, p. 149–191.

Muttoni, G., Gaetani, M., Kent, D.V., Sciunnach, D., Angiolini, L., Berra, F., Garzanti, E., Mattei, M., Zanchi, A., 2009. Opening of the Neo-Tethys Ocean and the Pangea B to Pangea A transformation during the Permian. GeoArabia 14 (4), p 17-48.

Nagtegaal, P, J, G, 1969, Sedimentology, paleoclimatology and diagenesis of post-Hercynian deposits in South-Central Pyrenees, Spain, Leidse. Geol. Meded, v. 42, p. 143–288.

Olivet, J. L., 1996, La cinématique de la plaque ibérique: Bull. Cent. Rech. Explor. Prod. Elf Aquitaine, v. 20, no. 1, p. 131–195.

Olivier, Ph., Gleizes, G., and Paquette, J.L., 2004, Gneiss domes and granite emplacement in an obliquely convergent regime: New interpretation of the Variscan Agly Massif (Eastern Pyrenees, France), in Whitney, D.L., Teyssier, C., and Siddoway, C.S., eds., Gneiss domes in orogeny: Geological Society of America Special Paper 380, p. 229–242.

Omenda, P.A., 1997. The geology and structural controls of the Olkaria goethermal system, Kenya. Geothermics 27, 1, pp 55-74

Orejana, D., Villaseca, C., Billström, K., Paterson, B. A., 2008, Petrogenesis of Permian alkaline lamprophyres and diabases from the Spanish Central System and their geodynamic context within western Europe, Contrib. Mineral. Petrol. 156, p. 477-500, doi:10.1007/s00410-008-0297-x

Paquette, J.-L., Ballèvre, M., Peucat, J.-J., Cornen, G., 2017, From opening to subduction of an oceanic domain constrained by LA-ICP-MS U-Pb zircon dating (Variscan belt, Southern Armorican Massif, France), Lithos, v. 294-295, 418-437, doi: 10.1016/j.lithos.2017.10.005

Pellenard, P., Gand, G., Schmitz, M., Galtier, J., Broutin, J., Stéyer, J-S., 2017, High-precision U-Pb zircon ages for explosive volcanism calibrating the NW European continental Autunian stratotype, Gondwana Research, v. 51, 118-136 doi: 10.1016/j.gr.2017.07.014

Pereira, M.F., Castro, A., Chichorro, M., Fernández, C., Díaz-Alvarado, J., Martí, J., Rodríguez, C., 2014, Chronological link between deep-seated processes in magma chambers and eruptions: Permo-Carboniferous magmatism in the core of Pangaea (Southern Pyrenees), Gondwana Res., v. 25, 290–308, doi: 10.1016/j.gr.2013.03.009

Pierson, T. C., and K. M. Scott, 1985, Downstream Dilution of a Lahar: Transition From Debris Flow to Hyperconcentrated Streamflow: Water Resources Research, v. 21, no. 10, p. 1511–1524, doi:10.1029/WR021i010p01511.

Pin, C., Vielzeuf, D., 1983. Granulites and related rocks in variscan median Europe: a dualistic interpretation. Tectonophysics 93, 47–74.

Pochat, S., and J., Van Den Driessche, 2011, Filling sequence in Late Paleozoic continental basins: A chimera of climate change? A new light shed given by the Graissessac–Lodève basin (SE France), Palaeogeogr. Palaeoclimatol. Palaeoecol, v. 302, p. 170–186, doi: 10.1016/j.palaeo.2011.01.006.

Pohl F., N., Froitzheim, G., Obermüller, F., Tomaschek, O., Schröder, T. J., Nagel, D., Sciunnach, and A., Heuser, 2018, Kinematics and Age of Syn-Intrusive Detachment Faulting in the Southern Alps: Evidence for Early Permian Crustal Extension and Implications for the Pangea A Versus B Controversy, Tectonics, first published 04 October 2018, doi: 10.1029/2018TC004974

Poitrenaud T, Poujol M, Augier R, Marcoux E (In Press) The polyphase evolution of a late-Variscan W/Au deposit (Salau, French Pyrenees): Insights from REE and U/Pb LA-ICP-MS analyses. Mineralium Deposita.

Puigdefàbregas, C., and P. Souquet, 1986, Tecto-sedimentary cycles and depositional sequences of the Mesozoic and Tertiary from the Pyrenees: Tectonophysics, v. 129, no. 1–4, p. 173–203.

Quintana, L., J. A. Pulgar, and J. L. Alonso, 2015, Displacement transfer from borders to interior of a plate: A crustal transect of Iberia: Tectonophysics, v. 663, p. 378–398, doi:10.1016/j.tecto.2015.08.046.

Ranalli, G., and L., Rybach, 2005, Heat flow, heat transfer and lithosphere rheology in geothermal areas: Features and examples, J. Volcanol. Geotherm. Res, v. 148, p. 3–19, doi: 10.1016/j.jvolgeores.2005.04.010.

Rat, P. et al., 1983, Vue sur le Cretacé basco-cantabrique et nord-ibérique: Une marge et son arriere-pays, ses environnements sedimentaires: Memoires geologiques Universite de Dijon, v. 9, p. 191.

Razin, P., 1989, Evolution tecto-sédimentaire alpine des Pyrénées basques à l'ouest de la transformante de Pamplona, Province du Labourd. PhD thesis, University of Bordeaux 3, France, 464 p.

Ren, J., Tamaki, K., Li, S., and Z., Junxia, 2002. Late Mesozoic and Cenozoic rifting and its dynamic setting in Eastern China and adjacent areas, Tectonophysics, v. 344, p. 175–205, doi: 10.1016/S0040-1951(01)00271-2.

Richard, P., 1986, Structure et évolution alpine des massifs paléozoïques du Labourd (Pays Basque français): Éditions du Bureau de recherches géologiques et minières, 374 p.

Rodríguez-Méndez L., J. Cuevas, J.J., Esteban, J. M., Tubía, S., Sergeev and A., Larionov, 2014, Age of the magmatism related to the inverted Stephanian–Permian basin of the Sallent area (Pyrenees), Geological Society, London, Special Publications 2014, v.394, doi: 10.1144/SP394.2

Roger, F., C. Teyssier, J.-P. Respaut, P. F. Rey, M. Jolivet, D. L. Whitney, J.-L. Paquette, and M. Brunel, 2015, Timing of formation and exhumation of the Montagne Noire double dome, French Massif Central: Tectonophysics, v. 640, p. 53–69.

Rosenbaum, G., G. S. Lister, and C. Duboz, 2002, Relative motions of Africa, Iberia and Europe during Alpine orogeny: Tectonophysics, v. 359, no. 1–2, p. 117–129, doi:10.1016/S0040-1951(02)00442-0.

Rossi, P., A. Cocherie, C. M. Fanning, and Y. Ternet, 2003, Datation U-Pb sur zircons des dolérites tholéiitiques pyrénéennes (ophites) à la limite Trias–Jurassique et relations avec les tufs volcaniques dits « infra-liasiques » nord-pyrénéens: Comptes Rendus Geoscience, v. 335, no. 15, p. 1071–1080, doi:10.1016/j.crte.2003.09.011.

Rossi, P., Cocherie, A., Fanning, C.M., 2015. Evidence in Variscan Corsica of a brief and voluminous Late Carboniferous to Early Permian volcanic-plutonic event contemporaneous with a high temperature/low-pressure metamorphic peak in the lower crust. Bull, Soc. géol. France, v. 186, p. 171–192.

Rust, B. R., 1978, Depositional models for braided alluvium, in Fluvial Sedimentology: Miall, Mem. Can. Soc. Pet. Geol, p. 605–625.

de Saint-Blanquat M., 1993. La faille normale du massif du Saint Barthélémy. Évolution hercynienne des massifs nord-pyrénéens catazonaux considérée du point de vue de leur histoire thermique. Geodin Acta 6: 59–77.

de Saint Blanquat, M., Lardeaux, J.M., Brunel, M., 1990, Petrological arguments for high temperature extensional deformation in the Pyrenean Variscan crust (Saint Barthélémy Massif, Ariège, France).Tectonophysics 177, 245–262.

Saspiturry, N., Razin, P., Baudin, T., Serrano, O., Issautier, B., Lasseur, E., Allanic, C., Thinon, I., and Leleu, S., 2019, Symmetry vs. Asymmetry of a hyper-thinned rift basin: example of the *Mauléon* basin (Western *Pyrenees*, *France*): Marine and Petroleum Geology, v. 104, p. 86–105, doi: 10.1016/j.marpetgeo.2019.03.031.

Saura, A., and A., Teixell, 2006, Inversion of small basins: effects on structural variations at the leading edge of the Axial Zone antiformal stack (Southern Pyrenees, Spain), Journal of Structural Geology, v. 28, 1909-1920, doi: 10.1016/j.jsg.2006.06.005

Schoeffler, J., 1965, Une hypothèse sur la tectonique de la chaîne pyrénéenne et de ses abords. Bull. Soc.Géol. Fr., 7, 6, p 917-920.

Schoeffler, J., 1982, Les transversales basco-landaises. Bull. Centre de Rech. Explor.-Prod. Elf-Aquitaine,6.1, 257-263.

Schott. J. J., 1985, Paléomagnétisme des séries rouges du Permien, du Trias et du Crétacé 919 inférieur dans les chaînes pyrénéo-cantabrique et nord-ouest ibérique, implications 920 géodynamiques. PhD thesis, University of Strasbourg, France.

Sengör, A.M.C., Yilmaz, Y., Songurlu, O., 1984. Tectonics of the Mediterranean Cimmerides: nature and evolution of the western termination of Palaeo-Tethys. In: Dixon, I.E., Robertson, A.F. (Eds.), The Geological Evolution of the Eastern Mediterranean. Special Publication, Geological Society of London 17, pp. 77-112.

Sibuet, J.-C., S. P. Srivastava, and W. Spakman, 2004, Pyrenean orogeny and plate kinematics: Journal of Geophysical Research: Solid Earth, v. 109, no. B8, p. B08104, doi:10.1029/2003JB002514.

Souquet, P., B. Peybènes, M. Bilotte, and E.-J. Debroas, 1977, La chaîne alpine des Pyrénées: Géologie alpine, v. 53, no. 2, p. 193–216.

Stampfli, G.M., 1996, Intra-Alpine terrane: a Palaeotethyan remnant in the Alpine Variscides, Eclogea Geol Helv, v. 89, p. 13–42.

Stampfli, G.M., 2012, The geodynamics of Pangea formation. Géologie de la France, 208–210.

Teixell, A., 1998, Crustal structure and orogenic material budget in the west central Pyrenees, Tectonics, v. 17, no. 3, 395-406, doi: 10.1029/98TC00561

Teixell, A., P. Labaume, and Y. Lagabrielle, 2016, The crustal evolution of the west-central Pyrenees revisited: Inferences from a new kinematic scenario: Comptes

Rendus Geoscience, v. 348, no. 3–4, p. 257–267, doi:10.1016/j.crte.2015.10.010.

Tirel, C., 2004, Dynamique de l'extension des domaines continentaux épaissis: dômes métamorphiques et écoulement de la croûte ductile. PhD thesis, University of Rennes 1, France.

Tirel, C., J.-P. Brun, and E. Burov, 2004, Thermomechanical modeling of extensional gneiss domes: Geological Society of America Special Papers, v. 380, p. 67–78, doi:10.1130/0-8137-2380-9.67.

Tirel, C., Brun, J.-P., Burov, E., 2008, Dynamics and structural development of metamorphic core complexes. J. Geophys. Res., v. 113, B04403, doi:10.1029/2005JB003694.

Tugend, J., G. Manatschal, N. J. Kusznir, E. Masini, G. Mohn, and I. Thinon, 2014, Formation and deformation of hyperextended rift systems: Insights from rift domain mapping in the Bay of Biscay-Pyrenees: Tectonics, v. 33, no. 7, p. 1239–1276, doi:10.1002/2014TC003529.

Vacherat, A., F. Mouthereau, R. Pik, D. Huyghe, J.-L. Paquette, F. Christophoul, N. Loget, and B. Tibari, 2017, Rift-to-collision sediment routing in the Pyrenees: A synthesis from sedimentological, geochronological and kinematic constraints: Earth-Science Reviews, v. 172, p. 43–74.

Vai, G, B., 2003, Development of the paleogeography of Pangea from Late Carboniferous to Early Permian, Palaeogeogr. Paleoclimatol. Palaeoecol, v. 196, p. 125–155.

Vielzeuf, D., 1984, Relations de phases dans le faciès granulite et implications géodynamiques: l'exemple des granulites des Pyrénées. PhD thesis, University of Clermont-Ferrand II, France.

Viennot, P., and Y. Kieh, 1928, Observations pétrographiques dans le massif cristallin du Labourd (Basses Pyrénées): Bull. Soc. Géol. Fr, v. 28, p. 369–379.

Viseras, C., M. L. Calvache, J. M. Soria, and J. Fernández, 2003, Differential features of alluvial fans controlled by tectonic or eustatic accommodation space. Examples from the Betic Cordillera, Spain: Geomorphology, v. 50, no. 1–3, p. 181–202.

Wang, Y. et al., 2016, The deep roots of the western Pyrenees revealed by full waveform inversion of teleseismic P waves: Geology, v. 44, no. 6, p. 475–478, doi:10.1130/G37812.1.

Weil A, Gutiérrez-alonso G, Conan J. 2010. New time constraints on lithospheric-scale oroclinal bending of the Ibero-Armorican Arc: a palaeomagnetic study of earliest Permian rocks from Iberia. J. Geol. Soc. 167: 127–143, doi: 10.1144/0016-76492009-002.

Wernicke, B., 1981, Low-angle normal faults in the basin and Range Province: nappe tectonics in an extending orogen: Nature, v. 291, no. 5817, p. 645–648, doi:10.1038/291645a0.

Wernicke, B., 1985, Uniform-sense normal simple shear of the continental lithosphere: Canadian Journal of Earth Sciences, v. 22, no. 1, p. 108–125, doi:10.1139/e85-009.

Wernicke, B., and B. C. Burchfiel, 1982, Modes of extensional tectonics: Journal of Structural Geology, v. 4, no. 2, p. 105–115, doi:10.1016/0191-8141(82)90021-9.

Ziegler, P.A., 1990, Permo-Triassic development of Pangaea. In: Ziegler, P.A. (Ed.)-Geological Atlas of Western and Central Europe. Shell International Petroleum Maatsschappij B.V. and Geological Society of London, p. 68–90.

Ziegler, P.A., Stampfli, G.M., 2001, Late Palaeozoic-Early Mesozoic plate boundary reorganization: collapse of the Variscan orogen and opening of Neotethys. Natura Bresciana. Annali del Museo Civico di Scienze Naturali di *Brescia* 25, p. 17–34.

Chapitre 3

Hyperextension crétacée

Bref aperçu du chapitre 3 : Hyperextension crétacée

Le chapitre 3 présente l'évolution tectono-sédimentaire des bassins de Mauléon, d'Arzacq et de Tartas au cours de la phase d'hyperextension crétacée. Le chapitre 3.1 est issue d'un article publié dans *Marine and Petroleum Geology*. Cet article décrit l'évolution sédimentaire et structurale du bassin de Mauléon de la fin du Jurassique au Cénomanien moyen. Il est basé sur une approche pluridisciplinaire intégrant : (1) des données sédimentologiques et structurales de terrain, (2) une mise à jour des précédentes cartes au 1/50 000 publiées par le BRGM et (3) l'analyse d'une ligne sismique pétrolière composite récemment retraitée par le BRGM et calibrée par six puits d'exploration pétrolière.

Le chapitre 3.2 est composé d'un article qui sera soumis dans le volume spécial du projet Orogen, dans le *Bulletin de la Société Géologique de France*. Ce chapitre détaille un évènement tectono-sédimentaire majeur prenant place à l'amorce de l'acquisition de l'asymétrie structurale du bassin de Mauléon. En effet, ce travail présente la réponse sédimentaire du glissement de la couverture prérift le long de la marge ibérique du bassin de Mauléon / Saint Jean de Luz.

Le chapitre 3.3 correspond à un article corédigé avec B. Issautier (BRGM), soumis en septembre 2019 dans un volume spécial du journal *Marine and Petroleum Geology*. Cet article présente l'évolution tectono-sédimentaire du Bassin d'Aquitaine au cours de la phase d'hyperextension crétacée. Le but de ce travail est de comprendre l'architecture à grande échelle du système de rift pyrénéen, partant d'un domaine ayant subi l'exhumation du manteau sous-continental (bassin de Mauléon) vers un domaine où l'amincissement crustal a été avorté dans une phase plus précoce (bassins d'Arzacq et de Tartas). Ce chapitre est basé sur l'analyse de données sismiques pétrolières et de puits d'exploration pétrolière.

Chapitre 3.1

Symétrie vs asymétrie d'un rift hyper-étiré : exemple du bassin de Mauléon (Pyrénées occidentales, France)

Chapitre 3.1. Symmetry Vs. Asymmetry of a hyper-thinned rift: example of the Mauléon basin (Western Pyrenees, France)

Sommaire

Résumé étendu p. 123

Abstract p. 127

1. Introduction p. 127

2. Geological settings p. 128

2.1. Present day structure of the western Pyrenees p. 128

2.2. The Mauléon basin p. 128

2.3. Tectono-sedimentary evolution of the Mauléon basin p. 129

2.4. Present day deep structure of the Mauléon basin p. 130

2.5. Available geodynamic models of the Mauléon rift basin p. 132

3. The southern margin of the Mauléon basin from field observations p. 132

3.1. The Axial Zone p. 132

3.2. The Saint-Engrâce – Bedous unit p. 133

3.3. The Mendibelza-Igountze unit: contacts between the Paleozoic basement and the synrift deposits p. 133

3.4. The Arbailles unit: tectonic and stratigraphic framework p. 139

3.5. The Saint-Palais unit p. 141

4. Seismic interpretation of the Mauléon basin and the southern part of the Aquitain basin p. 141

4.1. The Saint-Palais unit p. 143

4.2. The Bellevue unit p. 143

4.3. The Sainte-Suzanne unit p. 144

4.4. The Grand-Rieu/Arzacq unit p. 144

5. Top Jurassic to Cenomanian tectono sedimentary and geodynamic evolution of the Mauléon basin p. 145

5.1. Latest Jurassic to Neocomian uplift phase p. 145

5.2. Barremian to earliest Albian rifting stage 1: symmetric basin p. 145

5.3. Albian rifting stage 2: asymmetric basin p. 145

5.4. Late Cretaceous rifting stage 3: apparent symmetric basin p. 147

6. Discussion and Conclusion p. 148

References p. 151

Eléments supplémentaires p. 159

Résumé étendu

Les figures présentent dans la partie éléments supplémentaires, après l'article, sont nommées ES. et sont appelées dans le texte de l'article de manière à illustrer plus précisément certains propos. Les figures 10, 11, 13 et 14 du présent article, publié dans Marine and Petroleum Geology, ont été modifiées dans le manuscrit de thèse à partir de la restauration réalisée à postériori et publiée dans Terra Nova. Ces figures ne reflètent donc pas totalement celles publiées dans l'article de Marine and Petroleum Geology. Sur la base de l'exemple du bassin de Mauléon, cette étude s'attarde à comprendre l'évolution tectono-sédimentaire d'un rift hyper-étiré présentant une importante épaisseur de séries sédimentaires synrifts. Cette étude intégrée combine des données de terrain, des cartes géologiques de détail et des lignes sismiques. L'étude de terrain est essentiellement basée sur l'analyse de la marge ibérique du bassin de Mauléon. L'interprétation sismique couplée aux données de puits pétroliers ont permis la construction d'un transect N-S du bassin de Mauléon, permettant d'imager la transition avec la marge conjuguée septentrionale.

Le Jurassique est caractérisé par l'installation d'une plateforme carbonatée relativement continue se développant depuis la future marge ibérique du bassin de Mauléon jusqu'au bassin plus septentrional d'Arzacq. Cette plateforme est limitée à son sommet par une surface d'émersion et d'érosion datant du Jurassique terminal au Barrémien. Cet épisode se traduit par l'érosion de la plateforme jurassique, le développement de bauxites et une lacune des séries néocomiennes sensu stricto à l'échelle des Pyrénées. Cette phase d'émersion généralisée a, entre autre, été interprétée comme résultant d'un « doming » de l'asthénosphère précédant la phase de rifting du Crétacé inférieur.

L'évolution du bassin de Mauléon, au cours du Crétacé, apparait complexe et polyphasée. La transgression du Crétacé inférieur aboutit au développement d'une plateforme carbonatée restreinte, au cours du Barrémien. Du Barrémien à l'Aptien, la balance entre la production carbonatée et la création d'espace disponible permet l'aggradation de 1 600 m d'épaisseur de dépôts carbonatés peu profonds. Durant cette période, le taux de subsidence est donc relativement important et le profil de dépôt reste globalement plat. Cette subsidence homogène évolue entre l'Aptien supérieur et l'Albien inférieur basal. Les bordures du bassin sont caractérisées par un recul des plateformes carbonatées peu profondes, tandis que le centre des bassins d'Arzacq et de Mauléon enregistrent le développement d'une épaisse série de marnes plus profondes. Dans le centre de ces bassins, la création d'espace disponible dépasse largement la production carbonatée, induisant une inclinaison du profil de dépôt vers le centre des bassins. Par conséquent, au cours du Barrémien et de l'Albien inférieur, le bassin de Mauléon est symétrique et caractérisé par le développement de plateforme carbonatées peu profondes sur ces bordures. Yves Lagabrielle et co-auteurs (Annexe 1) ont mis en évidence que la déformation de la croûte continentale dans bassins péri-ibériques était découplée entre la couverture sédimentaire et la croûte. En effet, ces derniers ont montré que ce découplage était rendu possible du fait de la présence du sel triasique prérift. La subsidence entre le Barrémien et l'Albien inférieur a été interprétée comme résultant de l'amincissement ductile de la croûte inférieure sans déformation majeure dans la croûte supérieure. La réponse isostatique de cet amincissement se traduit par la formation d'un bassin « sag » symétrique caractérisé par un onlap des séries synchrones de l'amincissement en direction de ces bordures (« ductile crustal pure-shear thinning phase »).

De l'Albien au Cénomanien inférieur, la marge ibérique du bassin de Mauléon est affectée par des mouvements verticaux différentiels : (1) soulèvement de la patrie méridionale du bassin et (2) subsidence tectonique de la partie centrale. Ces mouvements sont responsables de la mise en place des conglomérats de Mendibelza (dépôts gravitaires grossiers profonds) passant en direction du bassin au Groupe du Flysch Noir (turbidites distales). Au même moment, le substratum de la marge ibérique enregistre un basculement de 15° à 30° vers le nord-ouest et la formation de faille normale syn-sédimentaires raides de direction N120°E, responsables de la déstabilisation des fan-deltas alimentant les conglomérats de Mendibelza. Ces derniers recouvrent le substratum Paléozoïque soulignant ainsi une lacune complète de la couverture jurassico-aptienne. Cette couverture doit être soustraite avant le dépôt des séries synrifts albiennes. Ce processus présenté en détail dans le chapitre 3.2 est interprété

comme le glissement de la couverture en direction du bassin, à l'Albien inférieur, le long du décollement matérialisé par le sel et les argilites du Trias supérieur. La marge européenne n'est pas affectée par le glissement de la couverture mésozoïque et enregistre moins de mouvements verticaux comme en atteste le développement d'une plateforme carbonaté albienne peu profonde. La légère inclinaison du profil de dépôt en direction de l'unité de Saint-Palais, est responsable d'un passage de faciès entre la plateforme carbonatée et le dépôt de marnes à spicules plus distales. Au sud du chevauchement de Saint-Palais, cette plateforme est remplacée par une épaisse série de flyschs noirs. Ceci suggère que le chevauchement de Saint-Palais correspond à la réactivation d'une paléo-faille normale à pendage vers le sud qui décale de manière significative la couverture jurassico-aptienne et qui permet une forte accumulation des séries synrifts albiens. La comparaison entre les marges européenne et ibérique met en évidence qu'au cours de l'Albien, le bassin acquiert sont asymétrie. En effet, l'enregistrement sédimentaire synrift est relativement différent de part et d'autre de ce bassin : la marge méridionale se compose de dépôts turbiditiques silicoclastiques grossiers, tandis que la marge septentrionale est caractérisée par le développement d'une plateforme carbonatée passant vers le sud à des marnes. De manière générale, l'asymétrie le long des systèmes de rifts fait suite à une phase d'amincissement en cisaillement simple. La faille normale de Saint-Palais est ici interprétée comme l'émergence d'un détachement à plongement vers le sud responsable du roll-over vers le nord de la marge ibérique. Ce dernier est accommodé par un tilt de 15° à 30°, en direction du nord-ouest, du socle ibérique lui-même décalé par des failles normales sub-verticales N120°E.

La période entre le Cénomanien moyen et le Santonien supérieur est marquée par une réorganisation de la distribution des faciès sédimentaires et un élargissement du bassin profond. A cette période, une plateforme carbonatée peu profonde se développe à la fois sur la marge européenne et ibérique du bassin de Mauléon (calcaires des cañons). Le long de la marge européenne, la limite plateforme / bassin est localisée au droit de la faille normale à pendage vers le sud bordant la partie méridionale du haut fond de Grand-Rieu séparant le bassin de Mauléon de celui d'Arzacq. Un nouveau détachement (Lakhoura) à pendage vers le nord cette fois, sépare la plateforme ibérique se développant sur la future Zone Axiale, des brèches de bas de pente (brèches d'Errozaté) recouvrant les conglomérats de Mendibelza. Ce détachement d'âge cénomanien moyen induit le basculement vers le sud du bloc des Arbailles, qui correspondait en partie à la structure en roll over albienne. L'unité des Arbailles matérialisant la bordure nord de la zone de « necking » ibérique représente un haut fond jusqu'au Santonien, comme en atteste l'âge des premières calci-turbidites du Crétacé supérieur, sédimentant au sud de cette unité. Au du Crétacé supérieur, les calci-turbidites remplissant le bassin de Mauléon sont essentiellement alimentées depuis la plateforme carbonatée européenne.

A la limite entre le Cénomanien inférieur et moyen, le bassin est donc affecté par un changement de style structural de ces marges conjuguées résultant d'un changement de vergence de la structure extensive principale. Ce processus est ici interprété comme un « flip-flop detachment tectonics » et confère une géométrie pseudo-symétrique finale au rift de Mauléon. Ce schéma structural pré-orogénique matérialise un héritage structural dans les Pyrénées occidentales qui jouera un rôle majeur lors de la compression. L'évolution tectono-sédimentaire du bassin de Mauléon présente de nombreuses similitudes avec ces homologues péri-ibériques : Arzacq, Basco-cantabrique, Parentis, Camèros, Colombrets et les bassins nord-pyrénéens plus orientaux. Le rôle majeur du sel prérift (Annexe 1) et l'impact de l'épaisseur des séries sédimentaires prérifts à synrifts sur le timing, la géométrie et les processus d'amincissement crustaux, affectant ces bassins, seront discutés dans le chapitre suivant de ce manuscrit.

Marine and Petroleum Geology 104 (2019) 86–105

Contents lists available at ScienceDirect

Marine and Petroleum Geology

journal homepage: www.elsevier.com/locate/marpetgeo

Research paper

Symmetry vs. asymmetry of a hyper-thinned rift: Example of the *Mauléon* Basin (*Western Pyrenees, France*)

Nicolas Saspiturry[a,*], Philippe Razin[a], Thierry Baudin[b], Olivier Serrano[b], Benoit Issautier[b], Eric Lasseur[b], Cécile Allanic[b], Isabelle Thinon[b], Sophie Leleu[a]

[a] Université Bordeaux Montaigne / EA 4592 Géoressources & Environnement, 1 Allée Fernand Daguin, 33607, Pessac Cedex, France
[b] BRGM-French Geological Survey, 3 Avenue Claude Guillemin, 45100, Orléans, France

ARTICLE INFO

Keywords:
Hyper-extended rift
Pyrenees
Detachment faulting
Mauléon basin
Early cretaceous

ABSTRACT

The aim of this study is to unravel the tectono-sedimentary evolution of a hyper-thinned rift, based on the example of the *Mauléon* Basin, a basin filled by thick synrift deposits. The integrated study combines field data, detailed geological mapping and seismic interpretation. The field study focuses on the Iberian margin of the *Mauléon* Basin. Seismic interpretation and well calibration along a N–S transect of the *Mauléon* Basin enable imaging the transition with the northern conjugate margin. The synrift records are very different on either side of the basin: the southern margin is composed of a proximal turbiditic s.l. siliciclastic system, whereas the northern margin is characterized by a carbonate system extending from the platform to the basin. We recognize the *Mauléon* rift as an apparent symmetric hyper-thinned rift, related to a southward dipping Albian detachment and a northward dipping Cenomanian one. Two stages of continental crustal thinning are inferred to explain the development of the *Mauléon* Basin. First, a Barremian to earliest Albian "ductile pure-shear thinning phase", responsible for the lower crustal thinning and the formation of a symmetric sag basin. Second, an Albian-Cenomanian simple-shear thinning phase, responsible for the onset of the southward dipping *Saint-Palais* detachment faulting and for evolution to an asymmetric basin. The Iberian margin appears as an upper plate and the European one as a lower plate during Albian time. At Early Cenomanian time, the basin was affected by structural changes of the margins resulting from shift in detachment direction, interpreted as "flip-flop detachment tectonics".

1. Introduction

Since the 1980's, conceptual rifting models have evolved from the pure-shear model (McKenzie, 1978), to the simple-shear model (Wernicke, 1981, 1985; Wernicke and Burchfiel, 1982; Davis, 1983; Spencer, 1984; Davis et al., 1986; Wernicke and Axen, 1988; Brun and van den Driessche, 1994) and, more recently, to numerical polyphasing models (Huismans and Beaumont, 2003, 2008; 2011, 2014; Tirel et al., 2004; Lavier and Manatschal, 2006; Brune et al., 2014, 2016; Svartman Dias et al., 2015). Much recent work describes the crustal thinning and modalities of mantle exhumation at actual hyper-thinned passive margins such as the Iberia-Newfoundland (Péron-Pinvidic et al., 2007; Haupert et al., 2016), Angola-Brazil (Unternehr et al., 2010; Péron-Pinvidic et al., 2015), and Australia-Antarctic (Gillard et al., 2015) margins. These have been modelled numerically in order to reproduce the geometry of the continental margins and to understand the development of crustal thinning detachment faults. Although the distal part of these extensional systems is well constrained offshore by seismic interpretation, few studies currently describe the proximal onshore domain. One of the most studied examples is the Jurassic Adriatic margin in the Alps (Masini et al., 2011, 2012, 2013). These authors describe the crustal detachment faults and sedimentary evolution of this starved system. Unlike the situation in the *Mauléon* rift basin, the hyper-thinning crustal models are based on real continental margins bordering oceanic domains. Where the *Pyrenees* are concerned, development of these conceptual models has led some authors to propose different models to explain the location of the Pyrenean mantle outcrops (Lagabrielle and Bodinier, 2008; Jammes et al., 2009, 2010a; 2010b; Lagabrielle et al., 2010, 2016; Clerc and Lagabrielle, 2014; Masini et al., 2014; Tugend et al., 2015a; Corre et al., 2016; Hart et al., 2016; Teixell et al., 2016). However, most of the hyper-thinning crustal models are based on mature passive continental margins characterized by mantle exhumation at the ocean-continent transition. The *Mauléon* Basin is an exceptional "laboratory" for the unravelling of the tectono-sedimentary

* Corresponding author.
E-mail address: saspiturry.nicolas@gmail.com (N. Saspiturry).

https://doi.org/10.1016/j.marpetgeo.2019.03.031
Received 4 September 2018; Received in revised form 15 January 2019; Accepted 23 March 2019
Available online 25 March 2019
0264-8172/ © 2019 Elsevier Ltd. All rights reserved.

Chapitre 3.1. Symmetry Vs. Asymmetry of a hyper-thinned rift: example of the Mauléon basin (Western Pyrenees, France)

Saspiturry, N., Razin, P., Baudin, T., Serrano, O., Issautier, B., Lasseur, E., Allanic, C., Thinon, I., and Leleu, S., **2019**, Symmetry vs. Asymmetry of a hyper-thinned rift basin: example of the Mauléon basin (Western Pyrenees, France): **Marine and Petroleum Geology**, v. 104, p. 86–105, **doi: 10.1016/j.marpetgeo.2019.03.031**.

Abstract

The aim of this study is to unravel the tectono-sedimentary evolution of a hyper-thinned rift, based on the example of the Mauléon basin, a basin filled by thick synrift deposits. The integrated study combines field data, detailed geological mapping and seismic interpretation. The field study focuses on the Iberian margin of the Mauléon basin. Seismic interpretation and well calibration along a N-S transect of the Mauléon basin enable imaging the transition with the northern conjugate margin. The synrift records are very different on either side of the basin: the southern margin is composed of a proximal turbiditic s.l. siliciclastic system, whereas the northern margin is characterized by a carbonate system extending from the platform to the basin. We recognize the Mauléon rift as an apparent symmetric hyper-thinned rift, related to a southward dipping Albian detachment and a northward dipping Cenomanian one. Two stages of continental crustal thinning are inferred to explain the development of the Mauléon basin. First, a Barremian to earliest Albian « ductile pure-shear thinning phase », responsible for the lower crustal thinning and the formation of a symmetric sag basin. Second, an Albian-Cenomanian simple-shear thinning phase, responsible for the onset of the southward dipping Saint-Palais detachment faulting and for evolution to an asymmetric basin. The Iberian margin appears as an upper plate and the European one as a lower plate during Albian time. At Early Cenomanian time, the basin was affected by structural changes of the margins resulting from shift in detachment direction, interpreted as « flip-flop detachment tectonics ».

1. Introduction

Since the 1980's, conceptual rifting models have evolved from the pure-shear model (McKenzie, 1978), to the simple-shear model (Wernicke 1981, 1985; Wernicke & Burchfiel 1982; Davis, 1983; Spencer 1984; Davis et al. 1986; Wernicke & Axen 1988; Brun & van den Driessche 1994) and, more recently, to numerical polyphasing models (Huismans and Beaumont, 2003, 2008, 2011, 2014; Tirel et al., 2004; Lavier and Manatschal, 2006; Brune et al., 2014, 2016; Svartman Dias et al., 2015). Much recent work describes the crustal thinning and modalities of mantle exhumation at actual hyper-thinned passive margins such as the Iberia-Newfoundland (Péron-Pinvidic et al., 2007; Haupert et al., 2016), Angola-Brazil (Unternehr et al., 2010; Péron-Pinvidic et al., 2015), and Australia-Antarctic (Gillard et al., 2015) margins. These have been modelled numerically in order to reproduce the geometry of the continental margins and to understand the development of crustal thinning detachment faults. Although the distal part of these extensional systems is well constrained offshore by seismic interpretation, few studies currently describe the proximal onshore domain. One of the most studied examples is the Jurassic Adriatic margin in the Alps (Masini et al., 2011, 2012, 2013). These authors describe the crustal detachment faults and sedimentary evolution of this starved system. Unlike the situation in the Mauléon rift basin, the hyper-thinning crustal models are based on real continental margins bordering oceanic domains. Where the Pyrenees are concerned, development of these conceptual models has led some authors to propose different models to explain the location of the Pyrenean mantle outcrops (Lagabrielle & Bodinier 2008, Jammes et al. 2009, 2010a, 2010b; Lagabrielle et al. 2010, 2016; Clerc & Lagabrielle, 2014; Masini et al. 2014; Tugend et al. 2015a; Corre et al. 2016; Hart et al. 2016; Teixell et al. 2016). However, most of the hyper-thinning crustal models are based on mature passive continental margins characterized by mantle exhumation at the ocean-continent transition. The Mauléon basin is an exceptional « laboratory » for the unravelling of the tectono-sedimentary evolution of a highly subsiding, thick, sedimentary, hyper-thinned rift. The evolution of this basin is synchronous to that of the hyper-

thinned Parentis rift basin (Pinet et al. 1987; Bois & ECORS Scientific team 1990; Jammes et al. 2010b, Ferrer et al. 2012; Masini et al. 2014) and to that of the Bay of Biscay continental margins, which are characterized by a hyper-thinned continental crust and a probably exhumed mantle at the ocean-continent transition (Ferrer et al., 2008; Roca et al., 2011; Tugend et al., 2014). Even though the Mauléon basin was inverted during the Pyrenean orogeny, it has retained the tectono-sedimentary record from its creation to its reactivation. Recently published geodynamical models of the Mauléon basin are mainly based on structural observations. The aim of this article is to analyze the stratigraphic and sedimentological characteristics of the syn-thinning deposits recording hyper-extension. This approach will make it possible to test the validity of the various models proposed and to bring new elements of interpretation. We propose a new model to explain the thinning of the continental crust beneath the Mauléon hyper-thinned rift basin, taking into account the sedimentary evolution of the basin through Cretaceous.

2. Geological setting

2.1. Present day structure of the western Pyrenees

The Pyrenean mountain belt results from a north-south convergence and collision between Iberian and European continental blocks from the Late Santonian to the Early Miocene (Puigdefàbregas and Souquet, 1986; Olivet, 1996; Rosenbaum et al., 2002; Sibuet et al., 2004; Gong et al., 2008). The deformation of this intracontinental domain is linked to the northward migration of the Iberian plate and to inversion of the previous Cretaceous north-Pyrenean basin (Ducasse and Vélasque, 1988). The central and eastern parts of the Pyrenees can be divided into three structural zones: the North-Pyrenean Zone (NPZ), the Axial Zone, and the South-Pyrenean Zone (SPZ) (**Fig. 1A**; Choukroune, 1976). The NPZ – located between two major faults, the North Pyrenean Fault (NPF) to the south, and the North Pyrenean Frontal Thrust (NPFT) to the north (**Fig. 1B**; Choukroune and ECORS Team, 1989; Daignières et al., 1994) – is composed of folded Mesozoic cover and Paleozoic units. The commonly named Metamorphic Internal Zone (MIZ), along the southern part of the NPZ, corresponds to a narrow, east-west, vertically metamorphosed and severely deformed zone (Ravier, 1957). The MIZ is characterized by high-temperature and low-pressure metamorphism related to Albian-Cenomanian rifting (Albarède and Michard-Vitrac, 1978; Montigny et al., 1986; Golberg and Maluski, 1988; Golberg and Leyreloup, 1990; Boulvais et al., 2006; Clerc et al., 2015).

In the western Pyrenees, the NPZ is represented by the Cretaceous Mauléon basin, thrusted to the north onto the Aquitaine basin and bordered to the south by the Axial Zone, where Paleozoic rocks are unconformably overlain by Late Cretaceous shallow marine carbonates (Souquet, 1967). The Mauléon basin is bounded to the west by Paleozoic blocks commonly known as the « Massifs Basques » (Heddebaut, 1973; Muller and Roger, 1977). The MIZ and the NPF disappear in the western part of the Pyrenees (Choukroune, 1976; Hall and Johnson, 1986; Canérot et al., 2004). The compressive phase is responsible for a greater shortening rate in the central and eastern Pyrenees (Muñoz, 1992; Vergés et al., 1995; Beaumont et al., 2000; Mouthereau et al., 2014) than in the western Pyrenees (Teixell, 1996, 1998), inducing better preservation of the Mauléon basin. The minor deformation of the western NPZ is linked to diachronism at onset of the thrusting of the Pyrenean compressive phase, older to the east (Santonian) and younger to the west (Middle Eocene), due to Iberian plate kinematics (Souquet et al., 1977; Séguret and Daignières, 1986; Olivet, 1996). This diachronism is the result of the configuration of the plates before convergence, with a more stretched domain in the western Pyrenees. The MIZ re-appears in the commonly named « Nappes des Marbres » corresponding to the center of the Albian Basque-cantabrian basin (Rat et al., 1983).

2.2. The Mauléon basin

The Mauléon basin corresponds to a Cretaceous subsiding domain, filled by thick Albian to Upper Cretaceous deep basin deposits. The Mendibelza-Igountze southern unit correspond to the inverted elements of the paleo-southern Mauléon basin margin (Muller and Roger, 1977; Canérot et al., 1978; Puigdefàbregas and Souquet, 1986). This unit is

composed of a Devonian-Carboniferous sedimentary substratum (Laverdière, 1930; Paris, 1964; Casteras et al., 1967; Mirouse, 1967), and a thick Albian synrift Mendibelza Formation (Lamare, 1946). The Mendibelza-Igountze unit is thrusted towards the south onto the Larrau-Saint Engrâce Triassic window (Galharague, 1966) and the Late Cretaceous carbonate cover of the Axial Zone, along the Lakhoura Thrust (Lamare 1941; Casteras 1943; Ducasse et al. 1986; Teixell 1993). The Arbailles unit is separated from the Mendibelza unit by the steeply dipping Arbailles Thrust (Lamare, 1948), also called the « Licq Fault » (Teixell et al., 2016). The Arbailles unit is characterized by a preserved Jurassic-Lower Cretaceous carbonate sequence folded in a N110° trending syncline. This syncline is bounded to the north by a major normal fault separating it from the Saint-Palais unit. This latter is represented by a thick (~ 6,000 m) Albian to Late Cretaceous flysch sequence deformed in N110° trending folds of various wave lengths. The north-eastern part of this unit is affected by the Saint-Palais, Bellevue and Sainte-Suzanne (NPFT) northward Pyrenean thrusts (Daignières et al., 1994; Teixell, 1998). During Cretaceous time, the Mauléon basin is separated from the Aquitaine basin by the « Grand-Rieu » Ridge (Serrano et al., 2006). The Labourd and Aldudes units are composed of an Ordovician to Carboniferous sedimentary basement (Laverdière, 1930; Lamare, 1944; Heddebaut, 1967, 1973), overlain respectively by Permian-Triassic continental deposits (Lucas, 1985) and an Upper Cretaceous carbonate platform (Souquet, 1967). The Labourd-Aldudes N20° units, forming the western margin of the Mauléon rift basin **(Fig. 2)**, coincide with the commonly named Pamplona Fault identified by the authors Richard, 1986; Razin, 1989; Claude, 1990; Larrasoaña et al., 2003; Pedreira et al., 2007. The northern part of the Labourd unit is composed of the Ursuya granulites (Viennot and Kieh, 1928; Lamare, 1939; Boissonnas et al., 1974; Hart et al., 2016).

The eastern part of the Mauléon basin is materialized by the « Chaînons Béarnais », corresponding to a N110° anticline and syncline system, affecting a Jurassic to Early Cretaceous carbonate cover (Canérot, 1988). This sedimentary cover is associated with lherzolite outcrops: « Urdach, Tos de la Coustette, Saraillé, Turon de la Técouère » (Fabriès et al., 1991, 1998). The Urdach mantle body is reworked into Late Albian to Cenomanian synrift breccias, composed of Paleozoic basement and mantle clasts (Roux, 1983; Fortané et al., 1986; Jammes et al., 2009; Debroas et al., 2010; Lagabrielle et al., 2010).

2.3. Tectono-sedimentary evolution of the Mauléon basin

The Permian-Triassic post-Hercynian continental deposits filled extensional basins, such as the Bidarray basin **(Fig. 2)**, located in the Labourd-Aldudes units (Bixel and Lucas, 1983, 1987). The Late Triassic deposits are characterized by a Lower Triassic Sandstone unit, a Middle Triassic Carbonate unit and an Upper Triassic shale, evaporite and ophite complex (Curnelle, 1983; Lucas, 1985; Rossi et al., 2003). During the Jurassic, a carbonate platform developed in a relatively stable tectonic context (Delfaud and Henry, 1967; Lenoble, 1992; James, 1998). The end of the Jurassic is characterized by large scale exposure of the Aquitain-Pyrenean domain. The Neocomian is lacking on this part of Pyrenees and is recorded by the development of the bauxites (Combes et al., 1998; James, 1998; Canérot., 2008). During Early Barremian, localized subsidence of the previously emerged domain favored the transgression of carbonate platform deposits that continued until the earliest Albian (Delfaud and Villanova, 1967; Arnaud-Vanneau et al., 1979). The end of this period is marked locally by extensive halokinetic deformation, associated with the first normal faults and the development of distal spicules marls (Canérot, 1988, 1989; Canérot and Lenoble, 1993; James and Canérot, 1999; Canérot et al., 2005).

The deposition of a thick, deep-marine conglomeratic sequence on the southern margin (Mendibelza-Igountze unit) of the newly formed Mauléon basin is considered as marking the onset of the Albian rifting basin, with a strong differentiation between an uplifted southern domain being the source of the conglomerates and a strongly subsiding deep-marine basin to the north (Souquet et al., 1985; **Fig. 2**). In the basin axis, more distal turbidites of the Black Flysch group, time-equivalent to the Mendibelza Conglomerates on the southern margin, constitute the first

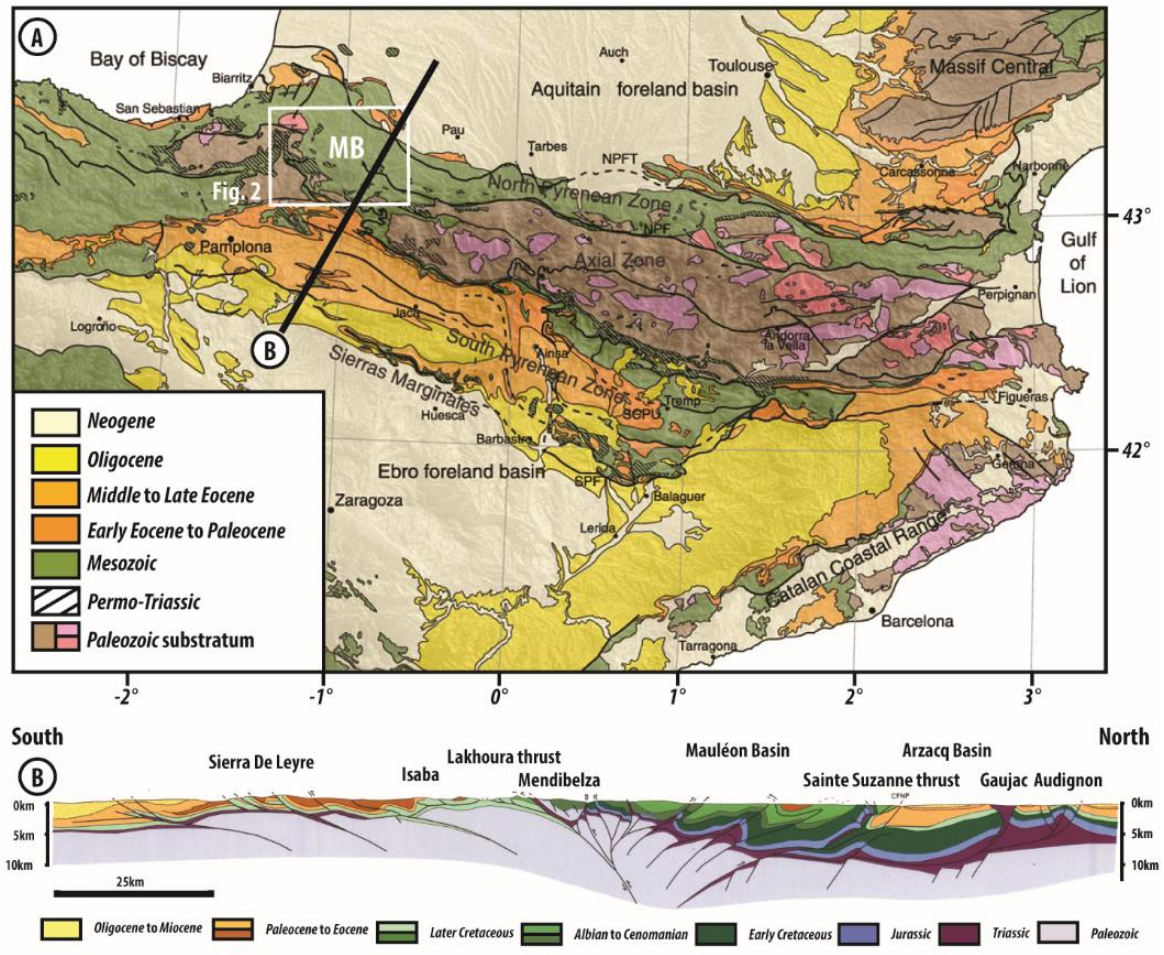


Fig. 1. **(A)** Geological map of the Pyrenees showing the structural domains of the belt: North Pyrenean Zone, Axial Zone and South Pyrenean Zone (Mouthereau et al., 2014). NPFT: North Pyrenean Frontal Thrust; MB: Mauléon basin; **(B)** Geological cross-section across the Western Pyrenees showing from north to south, the: Audignon ridge, Arzacq basin, Mauléon basin, Mendibelza unit, Lakhoura Thrust, Isaba unit and Sierra de Leyre unit (AGSO and BRGM., 2018).

stratigraphic unit of the North-Pyrenean rift. At the same time, along the more gently-dipping northern margin, the albian shallow-marine carbonate deposits grade southwards to more distal marl-dominated sedimentation (Biteau et al., 2006).

The Mauléon basin widened during the Cenomanian to Santonian (Canérot, 2017). Active carbonate turbiditic systems supplied by the Aquitain platform to the north are responsible for the deposition of a thick carbonate flysch sequence at the basin axis (Razin, 1989). At the southern margin, the transgressive « Calcaires des Cañons » carbonate platform onlaps the previously emerged Paleozoic basement, currently exposed in the Axial Zone (Casteras and Souquet, 1964; Souquet, 1967; Alhamawi, 1992). Chaotic gravity-flow sedimentation characterized the southern tectonically-controlled erosional slope (Durand-Wackenheim et al., 1981). From Late Santonian to Eocene times, a thick deep-water sequence deriving from eastern syn-tectonic siliciclastic systems accumulated in the Mauléon basin. Finally, the basin was deformed and inverted by the Pyrenean compression from the Middle Eocene to the Miocene (Puigdefàbregas and Souquet, 1986; Bosch et al., 2016; Labaume et al., 2016).

2.4. Present day deep structure of the Mauléon basin

Gravimetric studies highlight a strong positive gravity anomaly under the Mauléon basin (Grandjean, 1992, 1994; Casas et al., 1997). This was previously considered as a dense intra-crustal anomaly (Grandjean, 1994) but is now interpreted, by some authors, as being induced by the proximity of the lithospheric mantle below a thinned crust (Wang et al., 2016; Wang, 2017). Recent research efforts focusing on mantle exhumation have linked denudation of the « Chaînons Béarnais » mantle

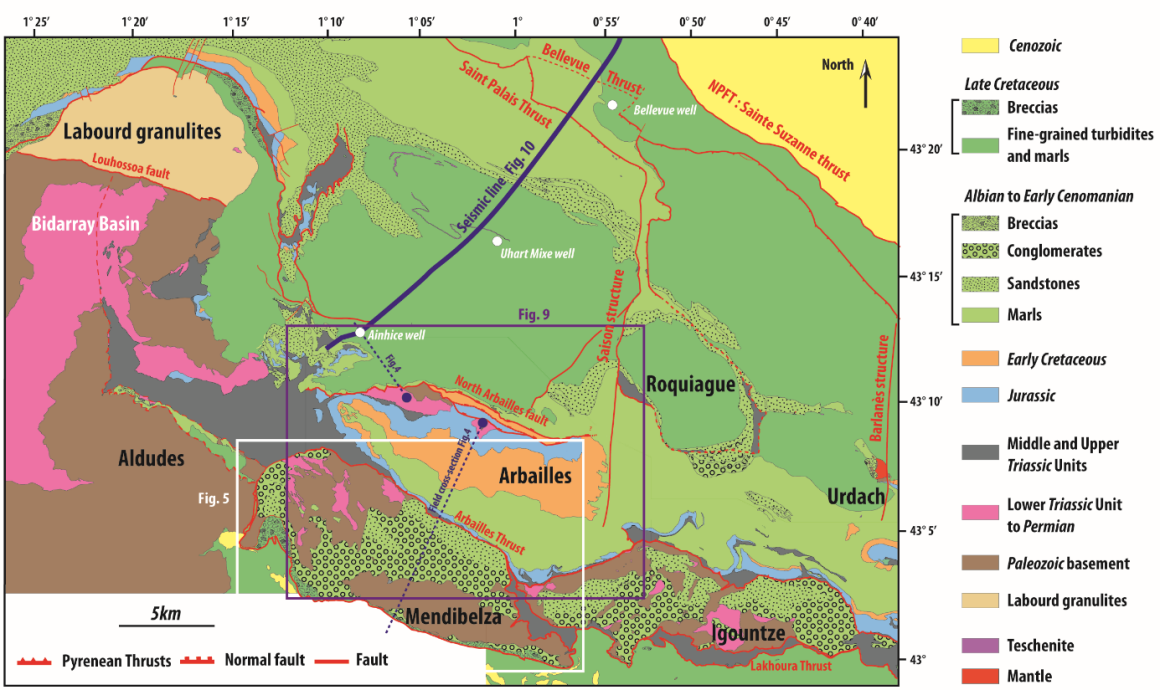


Fig. 2. Geological map showing the main structural units of the Iberian Mauléon margin, from west to south: Labourd granulites, Bidarray basin, Aldudes unit, Mendibelza-Igountze unit. The Mauléon basin geological map presented in this paper derive from an update of the published 1/50 000 geological maps (Casteras et al., 1970, 1971; Boissonnas et al., 1974; Le Pochat et al., 1976, 1978; Henry et al., 1987).

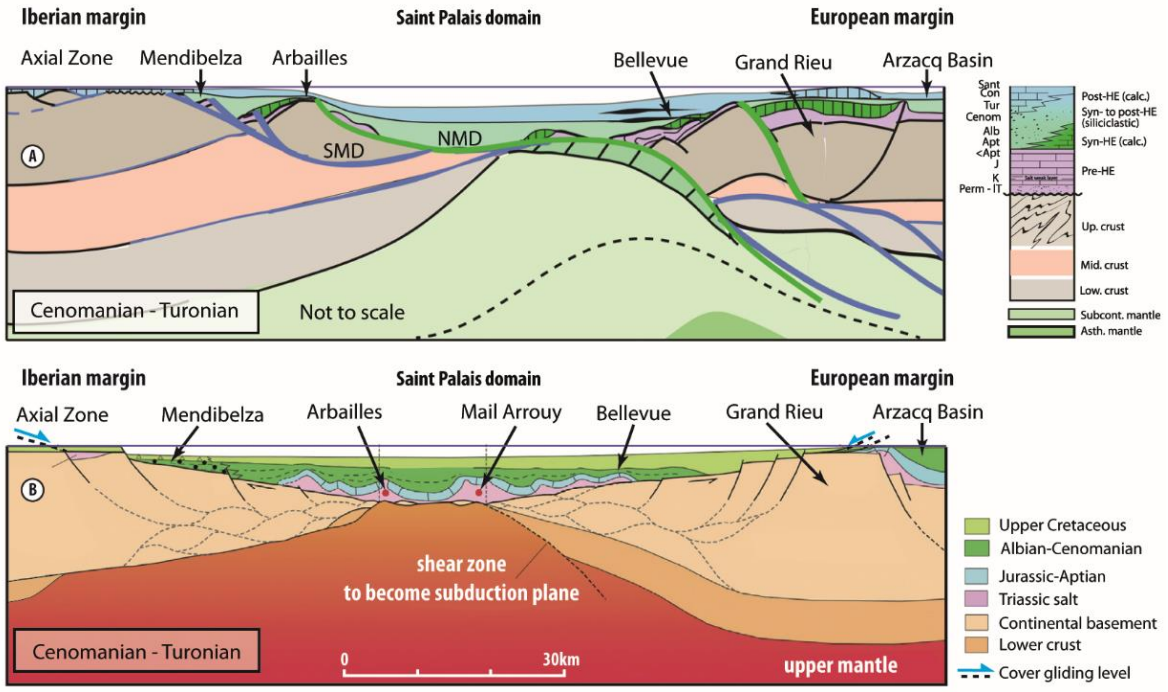


Fig. 3. (A) 2D synthetic tectono-sedimentary model of the Mauléon-Arzacq rift section during the Cenomanian to Turonian post-tectonic stage (modified from Masini et al., 2014). The continental crust is thinned during Albian time as the result of the development of two diachronous northward dipping detachments. SMD: South Mauléon Detachment; NMD: North Mauléon Detachment; HE: Hyper-extension; **(B)** Late Cretaceous restoration of the Mauléon basin. The dashed lines correspond to supposed anastomosed shear zones contributing to continental crust thinning (modified from Teixell et al., 2016). This model proposes a boudinage-like geometry of the crust, with narrow continental margins (<40 km wide).

outcrops to Albian hyper-thinning crustal mechanisms along a low angle detachment fault (Jammes et al. 2009; Lagabrielle et al. 2010; Masini et al. 2014; Tugend et al. 2014; Corre et al. 2016; Teixell et al. 2016). The inversion of this rift basin is responsible for the Iberian

northward underplating (Mattauer, 1985; Engeser and Schwentke, 1986; McCaig, 1988; Choukroune et al., 1990).

2.5. Available geodynamic models of the Mauléon rift basin

The crustal thinning process of the Mauléon rift basin during Albian times has been debated recently (Jammes et al., 2009; Masini et al., 2014; Tugend et al., 2014, 2015a; Corre et al., 2016; Teixell et al., 2016; **Fig. 3**). Rifting reconstructions differ from crustal thinning models, salt tectonics and synrift filling geometries. The first models describe this basin as a classical rift, thinned by basinward-dipping, crustal, normal faults, responsible for the development of tilted blocks on the southern margin of the rift (Boirie., 1981; Boirie and Souquet, 1982; Fixari, 1984; Souquet et al., 1985; Canérot and Delavaux, 1986; Canérot, 1988; Ducasse and Vélasque, 1988; Souquet, 1988). In recent models of crustal hyper-thinning processes, sub-continental mantle exhumation is interpreted as being related to northward-dipping detachment faults in the distal part of the basin (Jammes et al. 2009; Tugend et al. 2014, 2015a; Masini et al. 2014; **Fig 3A**). According to these models, the southern margin of the Mauléon basin corresponds to the « lower plate » and the northern Grand-Rieu ridge to the « upper plate » (sensu Wernicke, 1985; Lister et al., 1986). The Ursuya granulites are also considered as lower to middle crust exhumed during this Albian extensional stage. Two extensional fault systems, the north and south Mauléon detachments, could be responsible for the southward tilting of the Mendibelza and Arbailles units (Masini et al., 2014). An alternative model suggests that the Albian thinning of the continental crust was caused by a process of crustal boudinage and led to the creation of a symmetric basin and sliding of the Mesozoic cover from the margins towards the basin axis on each margin (Lagabrielle et al., 2010; Corre et al., 2016; Teixell et al., 2016; **Fig. 3B**).

Our working approach was to reconstruct a N-S cross-section of the present-day Mauléon basin, using a field approach on the southern margin and seismic data to illustrate the northern one. The Albian reconstitution of this cross-section allows to consider the tectono-sedimentary evolution of the basin, focusing on the Albian-Cenomanian rifting phase. The first part of this paper focuses on a description of the southern margin of the Mauléon rift basin based on outcrop data. The second part focuses on the deep geometry of the Mauléon basin, using the interpretation of a N-S reprocessed composite seismic reflection profile. This line shows the deep geometry of the conjugate rift margins. The third part of the paper presents a new N-S composite crustal section of the entire Mauléon basin, and a reconstitution at Cenomanian time. We propose a new model of crustal thinning highlighting the individualization of the Iberian and European conjugate rift margins.

3. The southern margin of the Mauléon basin from field observations

Field work has enabled updating of the 1/ 50 000 BRGM geological maps. The latter image the Iberian margin of the Mauléon basin: (1) Mendibelza unit; and (2) Arbailles unit **(Fig. 4A)**. The southern margin of the Mauléon basin was deformed during the Eocene alpine compression along several southward-verging thrusts. The most significant of these, known as the Lakhoura Thrust, is responsible for the under-thrusting of the Axial Zone beneath the North-Pyrenean units **(Fig. 4)**. Five structural units bounded by tectonic contacts have been defined from south to north on this inverted margin **(Fig. 4B)**: (1) The Axial Zone, formed by the Paleozoic basement and its Late Cretaceous cover (over-thrust by the northern units along the Lakhoura Thrust); (2) The Saint-Engrâce/Bedous unit, composed of a complex assemblage of Triassic rocks thrusted onto the Axial Zone to the south; (3) The Mendibelza-Igountze unit, including Albian deep-marine synrift deposits onlapping the Paleozoic sedimentary basement **(Fig. 5)**; (4) The Arbailles unit, represented by carboniferous rocks overlain by a continental to shallow marine Triassic to earliest Albian sequence; and (5) the Saint-Palais unit formed, essentially, of a thick Albian to Late Cretaceous turbiditic sequence overlying a deformed Jurassic to Early Cretaceous Carbonate unit.

3.1. The Axial Zone

The Palaeozoic basement of the Axial Zone is stratigraphically covered by a shallow marine carbonate sequence, Cenomanian to

Santonian in age, known as the « Calcaires des Cañons » (Souquet, 1967; **Fig. 6A**). This carbonate platform succession is overlain by deeper Late Santonian to Maastrichtian marine sediments composed of argillaceous mudstone (« calcshists ») containing planktonic foraminifera, grading upward and laterally to siliciclastic deposits. This deep marine depositional setting continues at least until the Early Lutetian in this domain. The Paleozoic rocks are not greatly deformed near the contact with the Late Cretaceous carbonates.

3.2. The Saint-Engrâce – Bedous unit

This unit has extensive eastward continuity (Aspe Valley), justifying its name Bedous. The Saint-Engrâce-Bedous unit observed in the Larrau tectonic window is a discontinuous thin band of Triassic rocks delimited by two thrusts and squeezed between the Axial Zone to the south and the Mendibelza – Igountze unit to the north (Ducasse and Vélasque, 1988; Teixell, 1993). The Saint-Engrâce-Bedous unit is composed of the Middle Triassic Carbonate unit and the Upper Triassic shale, evaporite and ophite complex. These Triassic rocks are affected by EW-trending folds indicating a southward displacement of the Lakhoura Thrust system.

3.3. The Mendibelza-Igountze unit: contacts between the Paleozoic basement and the synrift deposits

The Mendibelza-Igountze unit is composed of Albian deep-marine synrift deposits onlapping the Paleozoic sedimentary basement. The Mendibelza synrift conglomeratic gravity flow deposits have already been studied, by the following authors: Fournier 1905, 1908; Lamare 1939, 1946, 1948; Gubler et al. 1947; Magné 1948; Viers 1956; Paris 1964; Poignant 1965; Galharague 1966; Merle 1974, Boirie 1981; Fixari 1984; Souquet et al. 1985. The Palaeozoic substratum of the Mendibelza Formation (Fm.) is composed of Late Devonian to Carboniferous sedimentary rocks **(Fig. 5)**. This substratum is exposed at two highs: the Esterençuby high to the north and the Occabe high to the south. The Albian conglomeratic Mendibelza Fm. is very thick (2,000 m; **Fig. 6A, ES. 1A**) at the northern block, much thinner at the southern one. The pebbles in this conglomerates are made up of Paleozoic sedimentary basement and Early Albian carbonate platform in the Igountze area (« Floridées limestones »). In this area, the base of this conglomeratic sequence is composed of discontinuous calci-turbidites reworking the Early Albian carbonate platform and the Paleozoic basement. In the Mendibelza area, the base of this formation is characterized by discontinuous base-of-slope sedimentary breccias reworking the Lower Triassic Sandstone unit **(Figs. 7A and B, ES. 1B-D)**. These discontinuous Igountze calci-turbidites and Mendibelza breccias materialized the base of the Mendibelza Formation, that is overlied by three southward back-stepping mega-sequences defined by Souquet et al., 1985. The Mendibelza conglomerates are overlain by Cenomanian to Santonian polymictic chaotic breccias reworking the « Calcaires des Cañons » carbonate platform of the Axial Zone and angular blocks of the Paleozoic sedimentary basement. These deposits attest a base-of-slope palaeogeographic boundary between the Axial Zone and the Mendibelza-Igountze unit during the Late Cretaceous. Along the N-S geological cross-section **(Fig. 4)**, the Mendibelza-Igountze unit is overthrust southward by the Lakhoura Thrust, onto the Axial Zone and the Saint-Engrâce unit. The Mendibelza-Igountze unit is also thrusted towards the west, onto the Aldudes unit. The Cretaceous to Paleocene synrift and postrift strata are affected by the Lakhoura Thrust, as shown by their vertical to overturned position along the front of the Lakhoura Thrust on the southern limit of the Mendibelza unit, indicating that this thrust is post Cretaceous. First rift models described the Mendibelza-Igountze unit as turbiditic proximal cones installed on the southward tilted blocks affecting the Iberian margin of the Mauléon Albian basin (Boirie and Souquet, 1982; Fixari, 1984; Souquet et al., 1985; Canérot and Delavaux, 1986; Canérot, 1988; Ducasse and Vélasque, 1988; Souquet, 1988). However, in the light of recent understanding of crustal hyper-thinning processes, Masini et al. (2014) have interpreted the southward tilting of the Mendibelza-Arbailles unit as resulting from the development of a northward detachment fault. To evaluate these different hypotheses, a

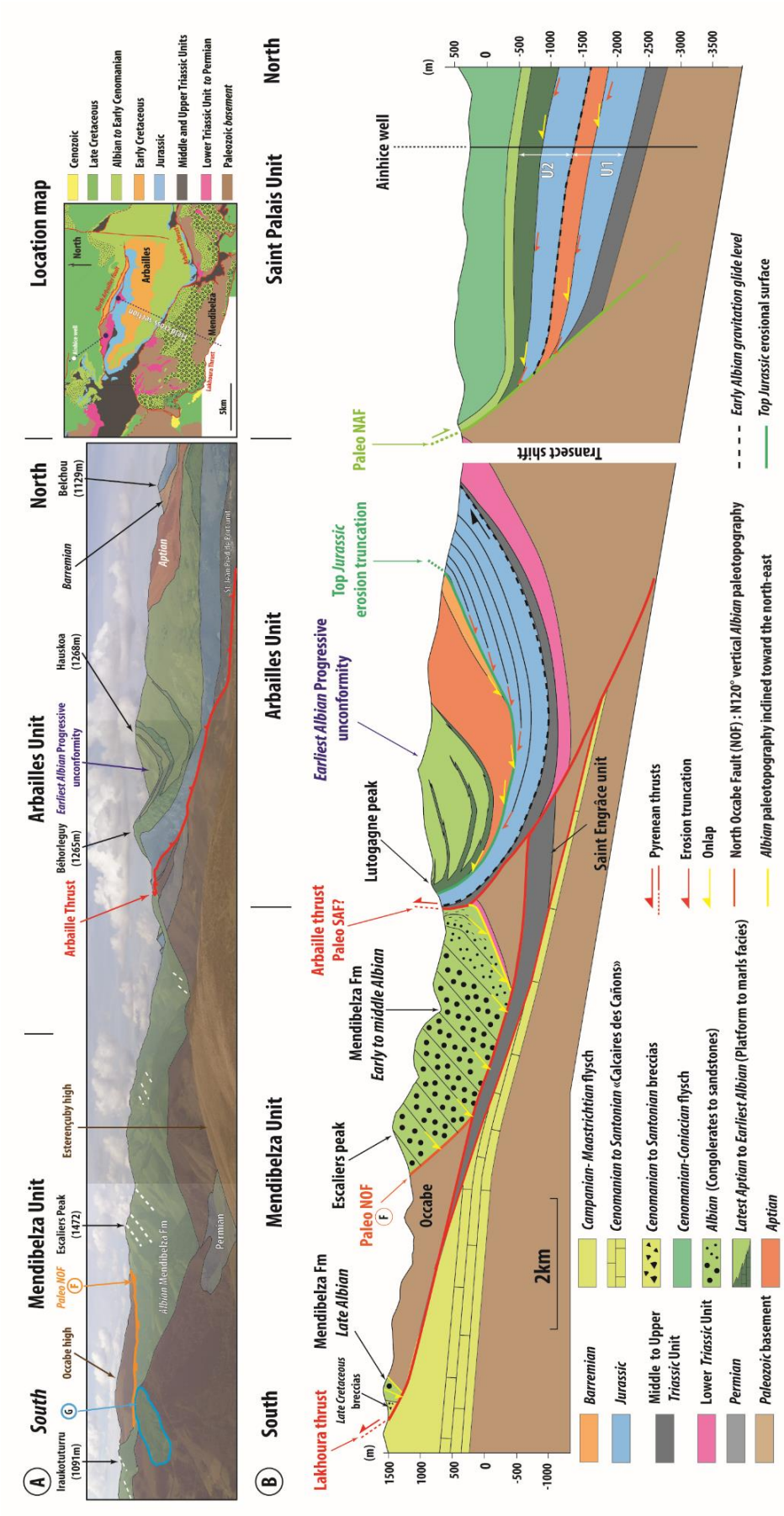


Fig. 4. (A) Panoramic view of the Mendibelza and Arbailles units. The Mendibelza Formation is characterized by the absence of wedge-shaped syn-tectonic growth strata in the Albian synrift sequence and a N120°-30°SW orientation. These conglomerates stop on the Albian North Occabe paleo-normal fault (NOF) whose current orientation is N110°-45°N. The Arbailles unit is characterized by a progressive unconformity affecting the Aptian to earliest Albian deposits, showing a northward inclination of the sedimentary profile at this time; **(B)** Current-day geological cross-section showing from north to south the: Saint-Palais, Arbailles, Mendibelza, Saint-Engrâce/Bedous and Axial Zone units. The Arbailles unit is characterized by Jurassic cover eroded to the south, overlain by a southward back-stepping Early Cretaceous carbonate platform. The Arbailles unit is separated from the Mendibelza unit by the steep Arbailles Thrust. The Mendibelza unit overthrust the Axial Zone and the Larrau/Saint-Engrâce units due to the Lakhoura Thrust.

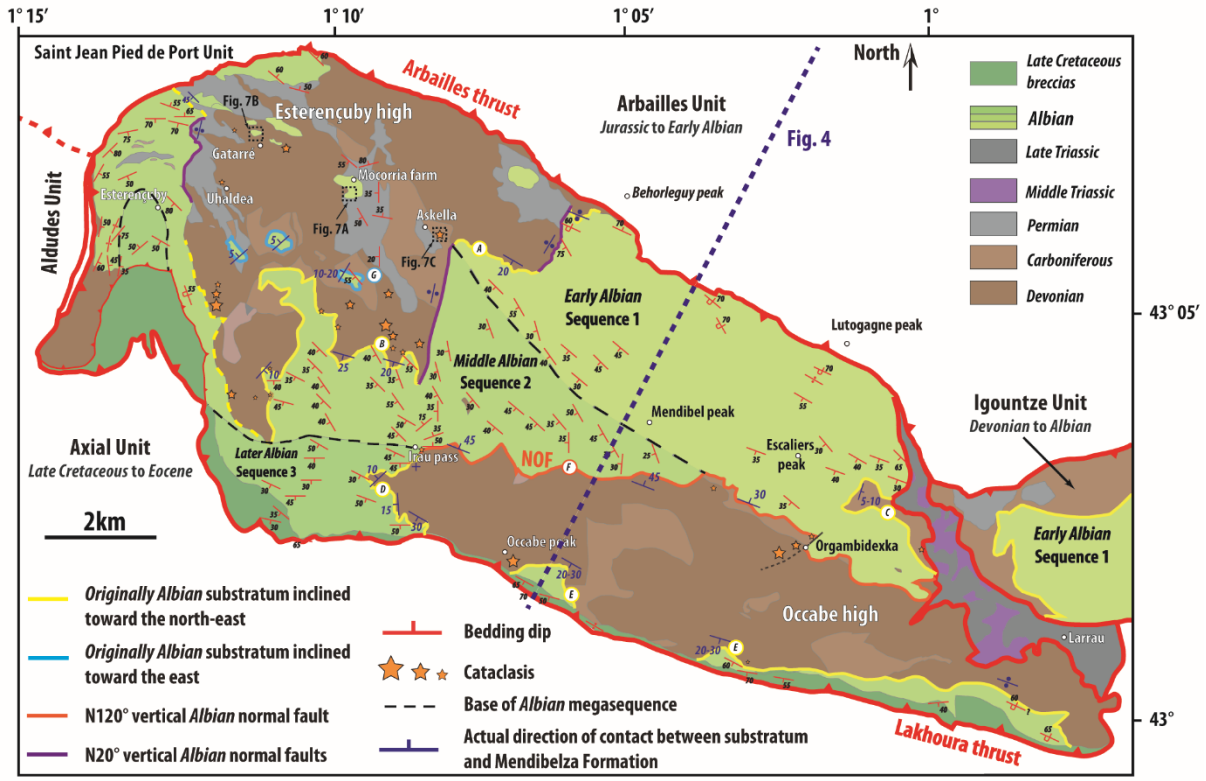


Fig. 5. Geological map of the Mendibelza unit, modified from the 1/50 000 BRGM geological maps (Casteras et al., 1970, 1971; Le Pochat et al., 1978). The Mendibelza Formation is composed of three main synrift mega-sequences, younger and younger towards the south, defined by Souquet et al. (1985). The stereographic representations show the Albian orientation of the contact between the Mendibelza conglomerates strata and the sedimentary basement. The Mendibelza unit is separated from the Arbailles unit by the steep Arbailles fault and is overthrust towards the south by the Lakhoura Thrust. The North Occabe Fault (NOF) is fossilized by the Albian Megasequences 1 and 2, indicating an Early to Middle Albian age for this fault.

detailed field analysis was conducted to determine the nature of the substratum / cover contacts and the synrift deposit geometry. All the contacts observed in the field between the substratum and the synrift deposits are primary contacts that were not reactivated during the Pyrenean orogeny. Two kinds of contacts have been distinguished: (1) depositional surfaces; and (2) syn-sedimentary faults. All these surfaces have been corrected for post-depositional tilting in order to reconstruct their geometries at the time of the synrift deposition **(Fig. 8)**.

3.3.1. Albian depositional surfaces

The depositional surfaces (yellow and blue lines in **Fig. 5**) are in all cases characterized by an angular unconformity with the Albian synrift strata. This unconformity is between 15–40° **(Fig. 8)**. Our facies analysis of the Mendibelza Fm. confirms that this unit consists of conglomeratic gravity-flow deposits (Boirie, 1981; Boirie and Souquet, 1982; Fixari, 1984; Souquet et al., 1985). The composition, the very coarse granulometry and the roundness of the clasts suggest that this base-of-slope gravity system was fed by non-preserved shelf-edge fan-deltas, reworking the Paleozoic meta-sedimentary units in an uplifted southern area located in the present day Axial Zone. In this context, these deep marine conglomerates are considered to have been deposited in a close to horizontal position. In addition, the Mendibelza Fm. is currently stacked with an average regional dip of N120°–30 to 40°SW, without any wedge-shaped syn-tectonic growth strata. These characteristics make it possible to reconstruct the inclination of the depositional surfaces of the synrift albian deposits on the Palaeozoic substratum **(Fig. 8)**. The surfaces are generally tilted from 15° to 40° towards the NE to NNE, with an average value of 30°, once the Mendibelza Fm. strata have been reseated in the original horizontal position **(ES. 2)**. This shows that the Albian substratum of the proximal part of the Mauléon basin was inclined towards the basin axis at the time of the synrift Mendibelza Fm. deposition. Locally, the Esterençuby high

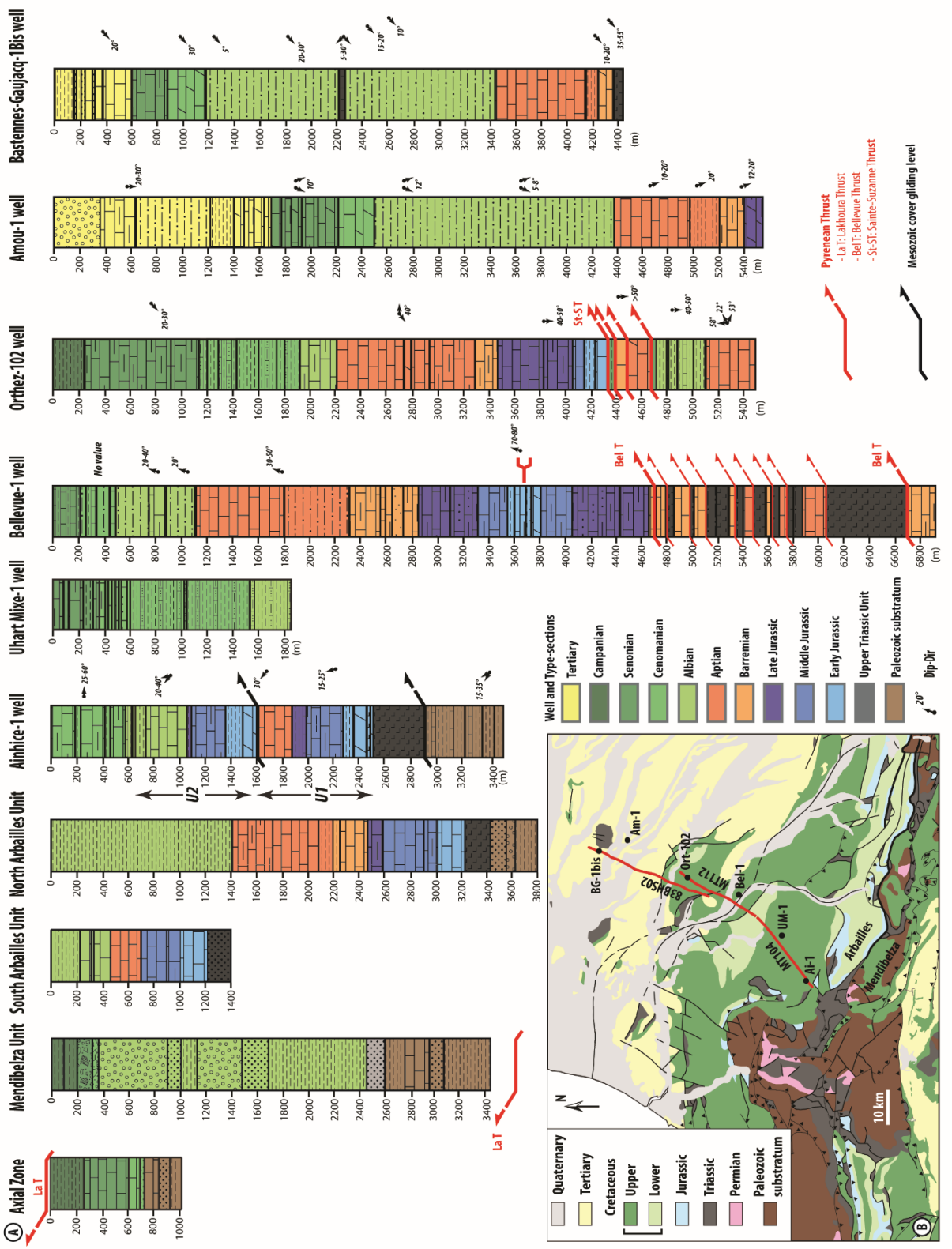


Fig. 6. (A) To the south: synthetic sedimentary succession of the Axial Zone, Mendibelza unit, South Arbailles unit and North Arbailles unit; To the north: sedimentary facies of the six wells calibrating the interpreted N-S composite seismic reflection profile (Fig. 10). **(B)** Location of the N-S composite seismic reflection profile (Fig. 10) on the 1 / 400 000 BRGM geological map of Pyrenees (Baudin and Barnolas, 2008). From south to north the MT104, MT112 and 83HBS02 seismic lines. Ai-1: Ainhice-1 well, UM-1: Uhart Mixe-1 well, Bel-1: Bellevue-1 well, Ort-102: Orthez-102 well, Am-1: Amou-1 well and BG-1bis: Bastennes Gaujacq-1bis well.

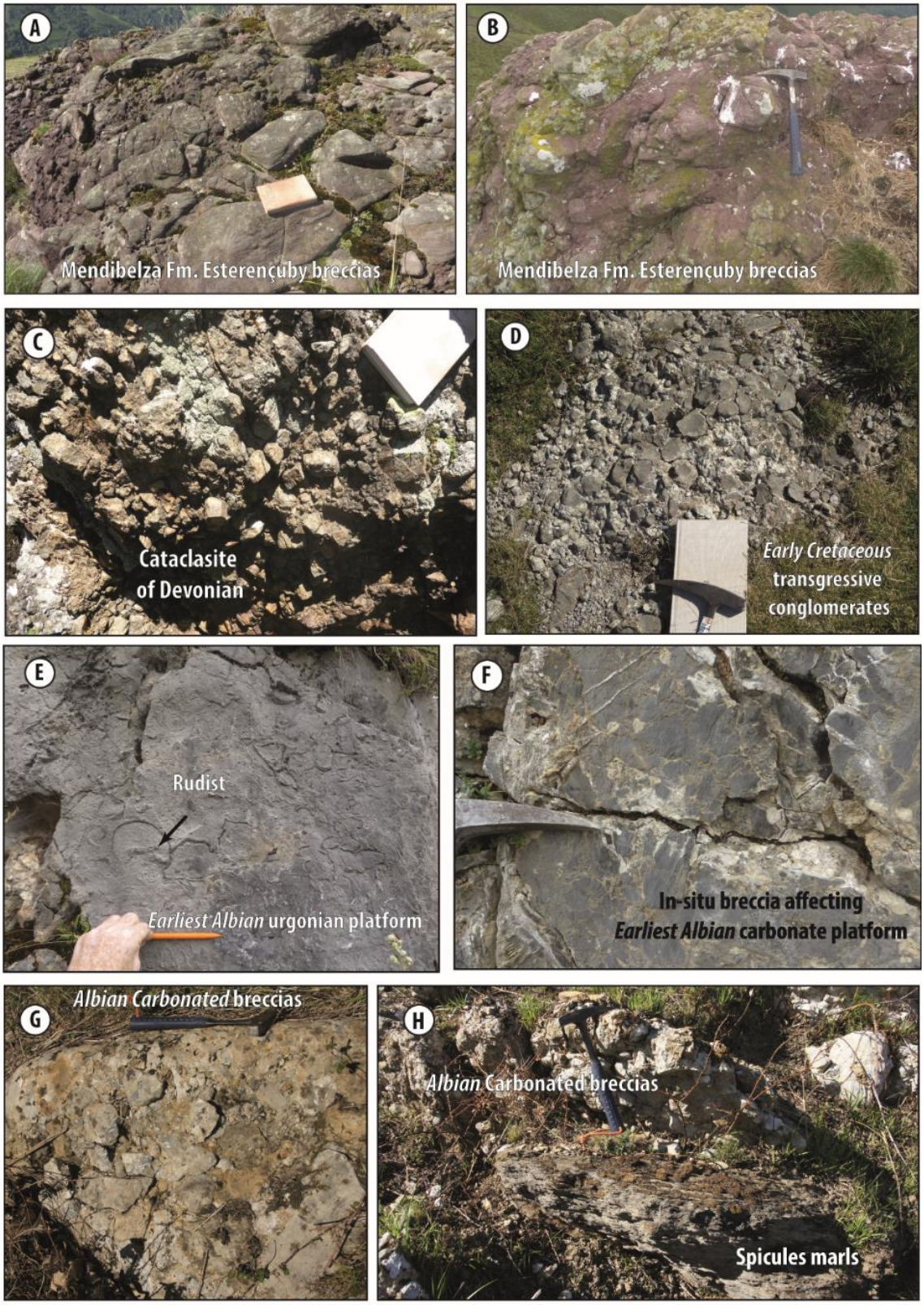


Fig. 7. See Figs. 5 and 9 for location. **(A-B)** Early Albian Esterençuby breccias reworking the Lower Triassic Sandstone unit. These discontinuous breccias are located at the base of the Megasequence one of the Mendibelza Formation defined by Souquet et al. (1985); **(C)** Cataclasites affecting the sedimentary Paleozoic basement of the Esterençuby high; **(D)** Early Cretaceous transgressive conglomerates reworking the Kimmeridgian carbonate deposits; **(E)** latest Aptian-earliest Albian « Mélobésiées » carbonate platform on the southern part of the Arbailles Syncline; **(F)** In-situ breccias of the Late Aptian-earliest Albian carbonate platform deposits, due to the northward inclination of the sedimentary profile; **(G-H)** Carbonate breccias intercalated with spicule marls on the northern corner of the Arbailles unit. These breccias correspond to the northward reworking of the Late Aptian-earliest Albian carbonate platform.

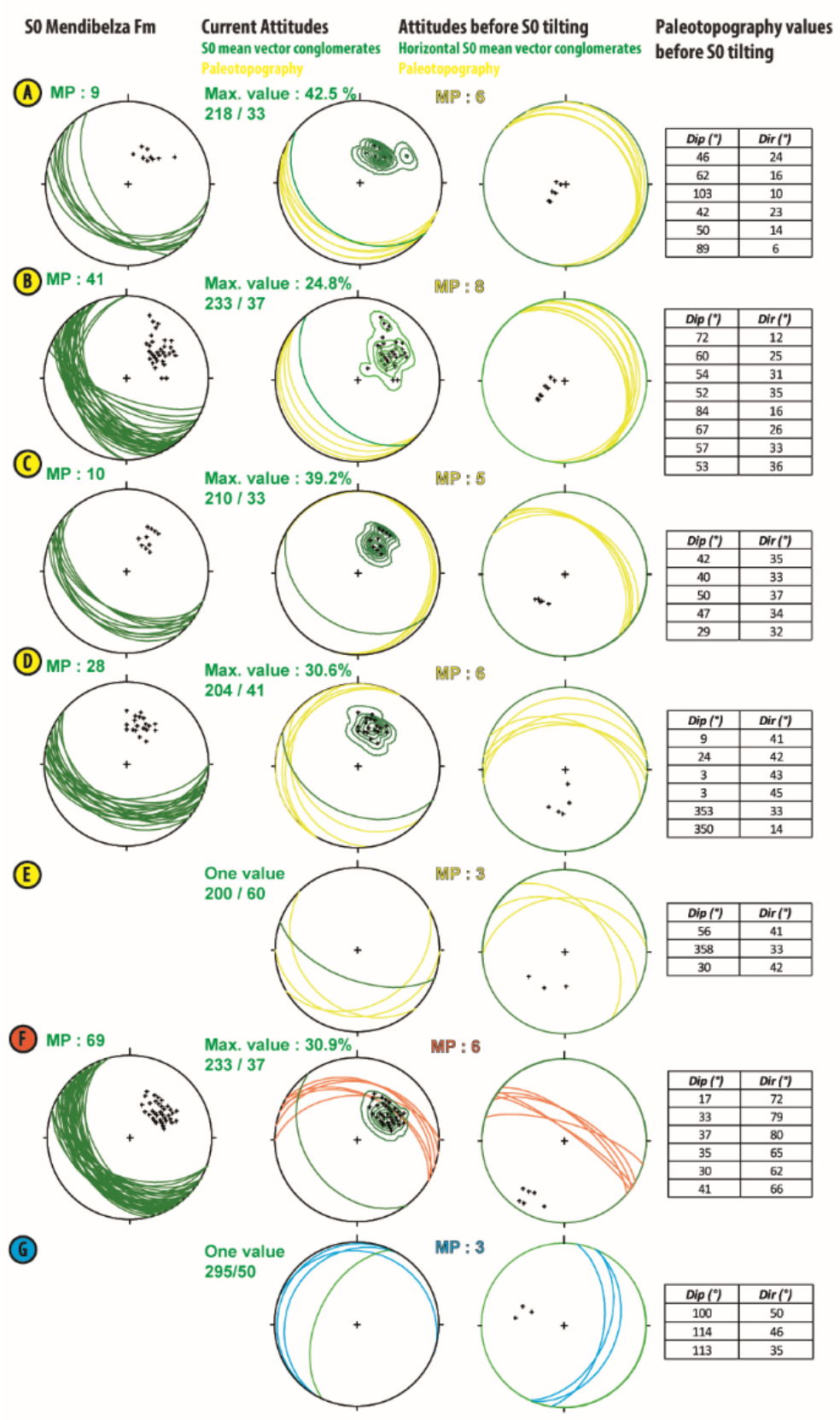


Fig. 8. Stereographic representation of the structural data showing the current and the Albian orientation of the contacts between the Mendibelza conglomerates strata and the Paleozoic sedimentary basement of the Mendibelza unit. The sites are localized on the map Fig 5. The first column represents the current Mendibelza Formation strata. Second column shows the current orientation of the contacts between Mendibelza Formation strata and the Paleozoic basement. The third column shows the Albian orientation of the contacts. The average value of the Albian yellow surface is N131-35°NE. The NOF represented by the site F is characterized by a sub-vertical Albian orientation. MP: Measurements planes.

is characterized by an albian surface inclined at 30° to 50° towards the east **(ES. 3)**.

3.3.2. Albian synsedimentary vertical normal faults

Two fault systems have been identified: (1) the N110°–45°NNE North Occabe Fault (NOF, in orange in **Figs. 5 and 8**); and (2) the N20° vertical normal Esterençuby faults (in purple in **Fig. 5**). These faults have an angular relationship of between 75° and 90° with the strata of Mendibelza conglomerates. Reconstruction of these faults indicates an original orientation and dip of N120°–75 to 85° NE for the NOF and an unchanged N20° vertical for the Esterençuby faults. The Early-Middle Albian megasequences 1 and 2 of the Black Flysch (Souquet et al., 1985) were deposited during the activity of the NOF which is sealed by the upper part of megasequence 2 **(Fig. 5)**. The stratal geometries and geological mapping show that the activity of the N20° Esterençuby fault system was contemporary with the NOF, i.e. during the Early-Middle Albian.

Megasequence 3 onlapped the Occabe high during the Late Albian. The occurrence of chaotic gravity flow deposits from the Late Albian to Santonian, on the Occabe domain implies the presence of a tectonically controlled scarp in between the emerged to shallow marine Axial Zone and the deep marine Mendibelza domain. However, this fault scarp is now overprinted by the Lakhoura Thrust. Therefore, these faults are diachronous and increasingly younger towards the southern margin of the Mauléon basin, since the North Occabe Fault is sealed by Middle Albian deposits. These observations are in agreement with the southward back-stepping of the Albian deposits (Souquet et al., 1985).

The Palaeozoic rocks are affected locally by low temperature weak deformations **(Fig. 7C, ES. 1E)**. But several of these cataclasites are sealed by Permian sediments indicating a Late-Hercynian age for this deformation **(Fig. 5, ES. 1F-H)**. These observations do not therefore confirm the occurrence of cataclasites punctuating a detachment fault between the Hercynian basement and the Albian synrift deposits, as proposed by Jammes et al. (2009), Masini et al. (2014).

3.3.3. The Mendibelza unit: preliminary interpretations

Most previous publications describe the Mendibelza unit as an Early Albian southward tilted block, characterized by a stratigraphic or tectonic contact between the substratum and the Albian Mendibelza conglomerates (Ducasse et al. 1986; Souquet et al. 1985; Ducasse & Vélasque 1988; Souquet 1988; Masini et al. 2014). However, the present study, based on field analysis and structural reconstruction, does not support these interpretations. Quite the opposite in fact: it shows an absence of wedge-shaped syn-tectonic growth strata in the Albian synrift sequence and depositional surface on the hercynian substratum inclined from 15 to 40° towards the NE. The hercynian substratum of the Mendibelza unit dips towards the Mauléon basin axis. The tilt of this unit towards the NE is marked by the development of diachronous N120° normal faults that are increasingly younger towards the south. The present day tilting of the Albian sequence, about 45° towards the south, postdates the Mendibelza Formation.

3.4. The Arbailles unit: tectonic and stratigraphic framework

The contact between the Arbailles and the Mendibelza units corresponds currently to a vertical fault. Due to the overturned and northward-dipping position of the Albian sequence of the Mendibelza unit to the south, this fault is interpreted as a verticalized southward-directed thrust fault called the Arbailles Thrust (Ducasse and Vélasque, 1988, **Fig. 4**). This thrust is locally retro-thrusting towards the north, indicating a later northward displacement of the Mendibelza unit responsible for the verticalization of the previous Arbailles Thrust (Dumont et al., 2015). The Arbailles unit is bounded northward by a set of northward-dipping to sub-vertical normal faults, known as the North Arbailles Fault (NAF, **Fig. 9**). These N120° faults result in a juxtaposition of Barremian - Aptian shallow-marine carbonate deposits to the south, and deeper marine marl-dominated Albian deposits to the north. This set of faults disappears eastward. In fact, the Arbailles unit is overlapped eastward by the Albian-Cenomanian Tardets Black Flysch group deposits (Souquet et al., 1985). Westward, the

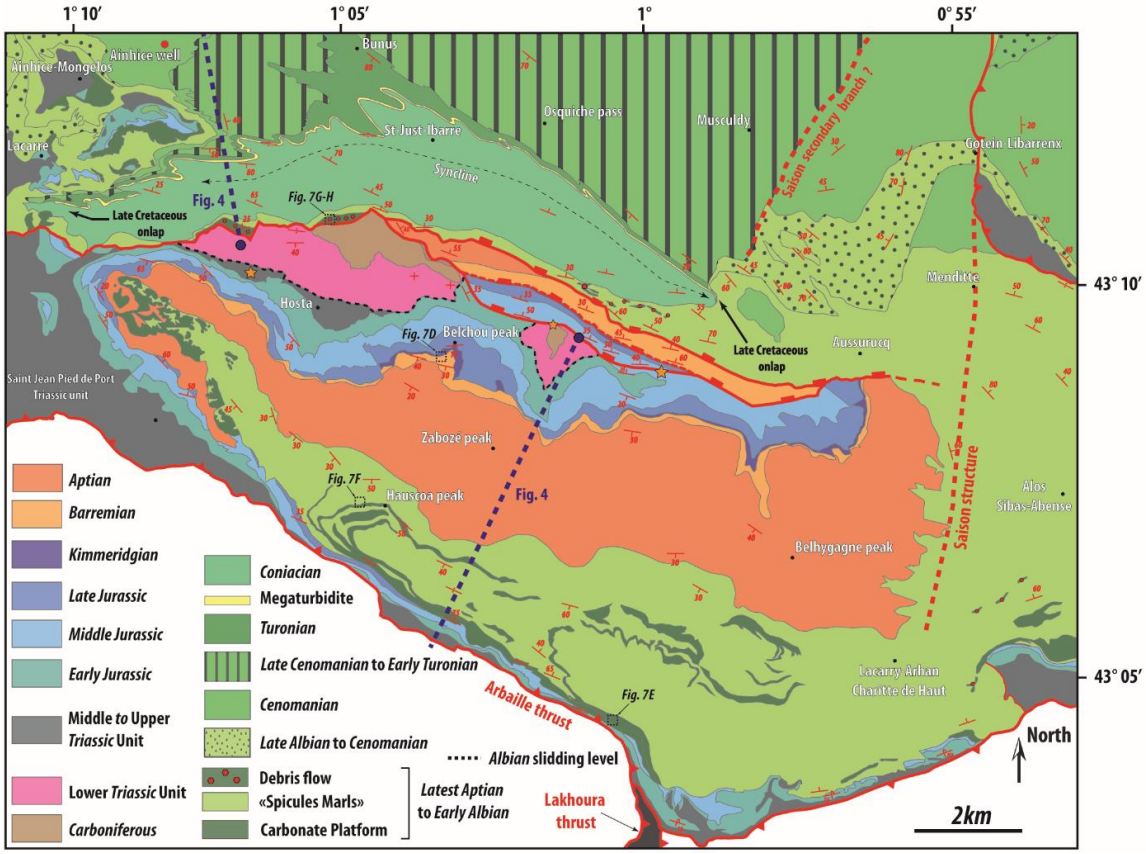


Fig. 9. Geological map of the Arbailles unit and the southern part of the Saint-Palais unit, using updated BRGM 1/50 000 maps (Casteras et al., 1971; Boissonnas et al., 1974; Le Pochat et al., 1976, 1978). The Arbailles unit is separated from the Saint-Palais unit by N120° normal faults known as the North Arbailles Fault (NAF). These maps highlight the southward erosion of the Jurassic cover and the southward back stepping of the Barremian to Aptian carbonate platform, onlapping the previous eroded Jurassic deposits. In the North of the Arbailles unit, the Late Cretaceous deposits onlapped the Albian rift sequence towards the south from Cenomanian to Santonian time.

Arbailles unit is bounded by the Saint-Jean-Pied-de-Port Upper Triassic unit.

The Arbailles unit consists of a carboniferous basement, a Late Triassic sequence and a Mesozoic cover **(Figs. 4 and 9)**. In this sector, the Late Triassic shales and evaporites overlie the Lower Triassic sandstone unit, without any Middle Triassic carbonate unit. The Upper Triassic unit is widely exposed on the south-west and consists of ophites and numerous cargneules indicating a wide zone of deformation. There is a classical Jurassic sequence above the Upper Triassic unit (Lenoble, 1992). This Jurassic sequence is limited at the top by an erosional surface marked by greater and greater truncation towards the south-west, explaining the lack of most of the Late Jurassic in the southern part of the Arbailles unit **(Fig. 6A)**. This unconformity is linked to the Late Jurassic - Early Cretaceous emersion phase, associated regionally with the development of bauxites (Combes et al., 1998; James, 1998; Canérot et al., 1999). The geometry of this surface reflects the tilt of the Jurassic deposits towards the north during this period. This emersion extends as far as the base of the Barremian, as evidenced by the lack of Neocomian deposits in the Arbailles unit **(Fig. 6A)**.

The Barremian to earliest Albian carbonate platform deposits onlap the Jurassic carbonate platform towards the south-west **(Fig. 6A)**. This onlapping is highlighted by the southward thinning of the Barremian deposits and the interbedding of transgressive conglomerates including pebbles reworked from the pre-existing Kimmeridgian carbonates **(Fig. 7D)**. The Aptian carbonates (Urgonian facies) overlying the Barremian to the north backstep towards the south and onlap the eroded Jurassic sequence directly in this direction. The thickness of the Aptian deposits increases northward without significant facies change, indicating a northward increase in subsidence (towards basin axis, **Figs. 4, 6A and 9, ES.4A**).

From Late Aptian to earliest Albian, algal carbonates (« Mélobésiées » limestone) onlap the eroded Jurassic sequence in the southern part of the Arbailles unit **(Fig. 7E)**. Intraformational breccias **(Fig. 7F)** attest to the presence at that time of an unstable depositional setting and probably a slight inclination of the depositional profile. This is confirmed by the northward change in facies from shallow marine carbonates to deeper marine spicule marls with intercalations of some carbonate debrites towards the north **(Fig. 7G and H)**. This Late Aptian-Early Albian sequence is affected by two kinds of progressive unconformity: (1) a generalized and progressive northward thickening of this sequence at the scale of the Arbailles unit, linked to a northward increase in the subsidence rate; and (2) a growth strata unconformity of shorter wavelength that result from diapiric movements on the southern edge of the Arbailles unit (Canérot, 1988, 1989, 2008; Canérot and Lenoble, 1993; **ES. 4B**).

3.5. The Saint-Palais unit

The Saint-Palais unit is located between the Arbailles unit and the Saint-Palais Thrust. The Saint-Palais unit formed the Albian - Late Cretaceous depocenter of the Mauléon basin. At outcrop scale, this unit is folded into N120° synclines / anticlines of pluri-kilometric wavelength, composed of Early Albian spicule marls and Middle Cenomanian - Turonian carbonate distal turbidites. The northern part of this unit is affected by the N110-120° overturned Saint-Palais anticline. Field work confirms that the distal Late Cretaceous carbonate turbidites are sourced from the north by the European carbonate platform, as shown by the N150–200° directed paleocurents measured in the field. These Late Cretaceous carbonate deposits overlaid the Albian sequence unconformably. This is shown by the southward distal onlap of the Late Cretaceous deposits on the Albian synrift sequence, on the southern edge of the Saint-Palais unit.

4. Seismic interpretation of the Mauléon basin and the southern part of the Aquitain basin

Unlike the southern margin that has been observed directly in the field (Mendibelza and Arbailles units), the architecture of the central part and the northern conjugate margin of the Mauléon basin have been explored from seismic data and well calibration **(Figs. 6 and 10)**. This section focuses on the deep geometry of the Mauléon basin from the interpretation of a N-S composite seismic reflection profile, reprocessed by the BRGM in 2017 (MT104 and MT112 acquired by ESSO-Rep in 1969 on the Mauléon-Tardets exploration permit, **cf 4.2**). The seismic line interpreted is a merger of lines MT104, MT112 and 83HBS02 (acquired by SNEAP in 1981 and reprocessed by BRGM in 2014; **Fig. 10**). The seismic interpretation was carried out using the Geographix® Discovery Suite that allows for each CDP of the seismic profile to export its X, Y, time, amplitude and depth values. Seismic/well tie is obtained by using the time / depth curves acquired in the boreholes and derived from the recording of checkshots. The time / depth conversion was performed using a mean velocity field calculated on the basis of all the time / depth data of the calibration wells, integrating their deviations **(Fig. 11)**. The top basement has been calibrated taking into account the ECORS seismic reflection profile (Daignières et al., 1994). The composite line presented in this paper is calibrated with six wells **(Fig. 6)**, from south to north: Ainhice-1 (3,540.85 m depth); Uhart-Mixe-1 (1,868.8 m depth); Bellevue-1 (6,909 m depth); Orthez-102 (5,489.10 m depth); Amou-1 (5,543 m depth); and Bastennes-Gaujacq-1.bis (4,442.10 m depth). Only the Ainhice-1 well reaches the Paleozoic basement of the Mauléon basin. The studied SSW-NNE seismic line through the Mauléon basin cuts across four distinct structural units, separated from one another by thrust faults **(Fig. 10)**. From south to north, the units are as follows: (1) Saint-Palais; (2) Bellevue; (3) Sainte-Suzanne; and (4) Grand-Rieu/Arzacq **(Figs. 6 and 10)**. The Saint-Palais unit corresponds to the central and deepest part of Mauléon basin, while the Bellevue and Sainte Suzanne units belong to its northern margin. The Bellevue and Sainte Suzanne thrusts involved the European basement. Using the field cross-section **(Fig. 4B)** and well-velocity models calibrating the interpreted composite seismic reflection profile **(Fig. 10)**, we propose a depth migrated section of the entire Mauléon basin **(Fig. 11)**.

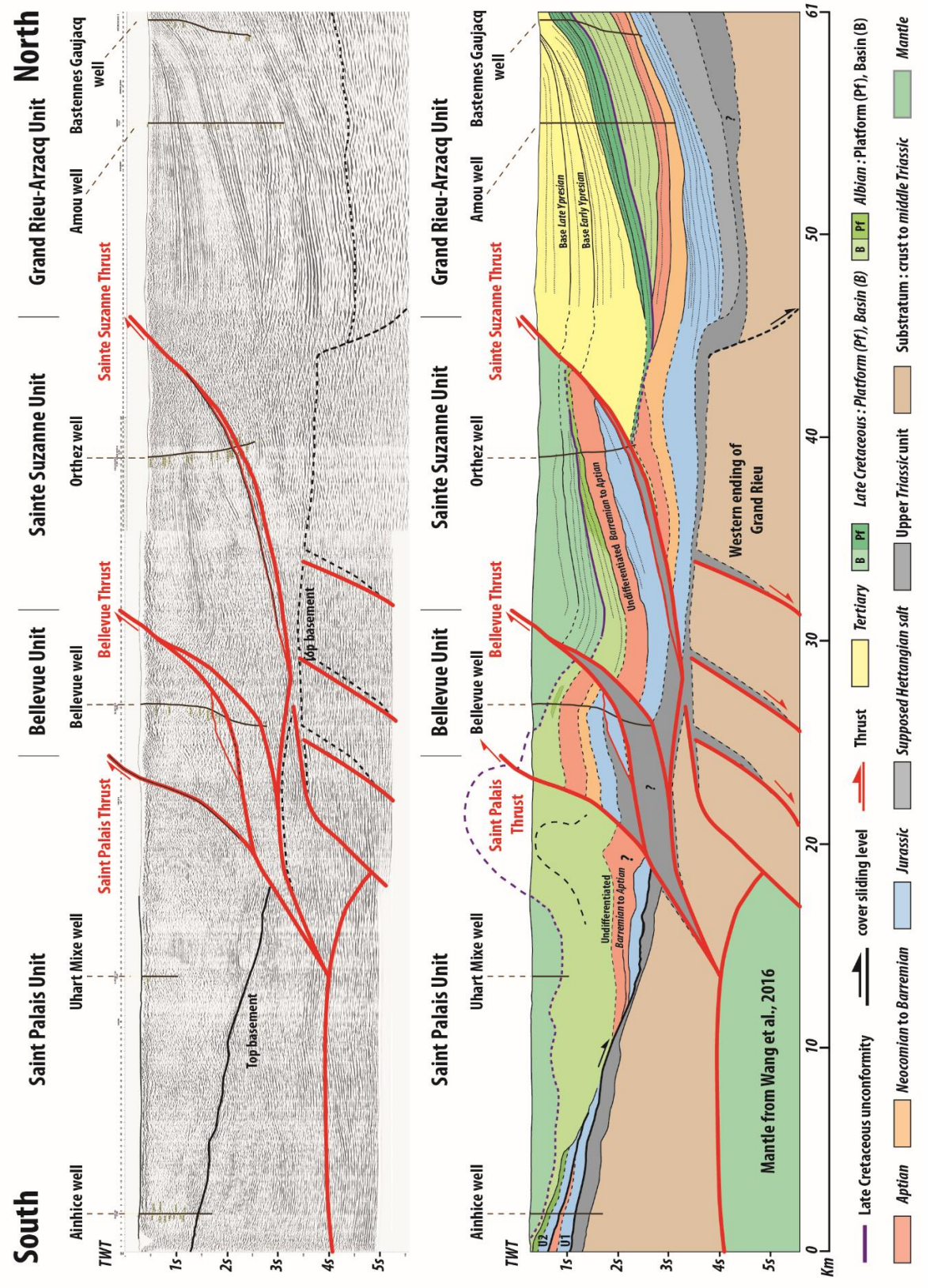


Fig. 10. Modified from original article. Interpretation of a N-S petroleum reflection composite seismic line, reprocessed by the BRGM in 2017 (MT104, MT112 and 83HBS02). This composite seismic line shows the deep geometry of the Mauléon basin and its European margin. This seismic line through the Mauléon basin cuts across four distinct structural units, separated from one another by thrusting overlaps. From south to north, the units are as follows: (1) Saint-Palais, (2) Bellevue, (3) Sainte Suzanne, and (4) Grand-Rieu/Arzacq. The Saint-Palais unit corresponds to the Albian rift depocenter. The Bellevue and Sainte Suzanne units materialized the northern conjugate margin of the Albian Cretaceous Mauléon rift basin, and the Barremian-Aptian depocenter.

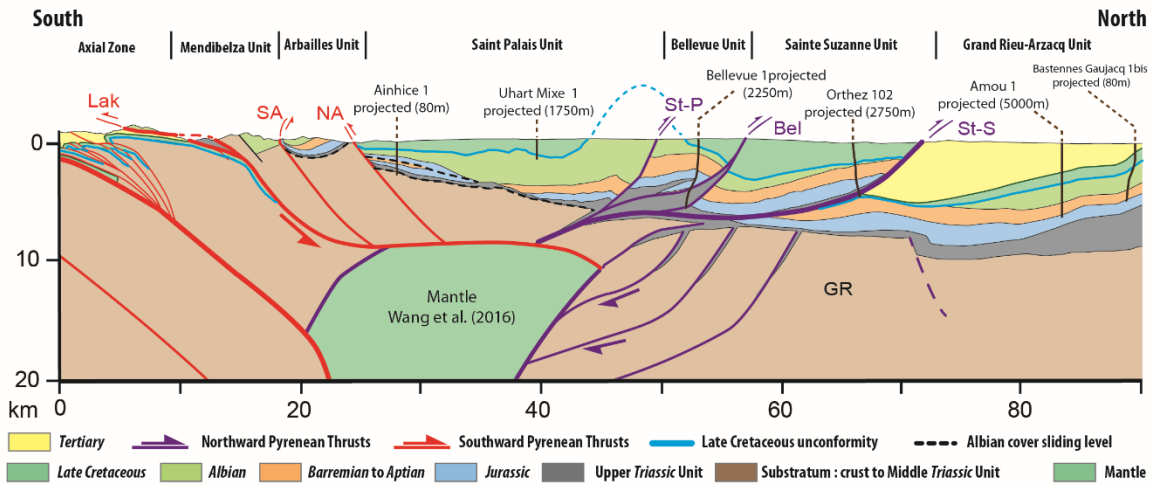


Fig. 11. Modified from original article. N-S Composite cross-section of the Mauléon basin. The southern part corresponds to the field cross-section Fig. 4 and the northern part of the section is calibrated by the seismic line. The Mendibelza and Arbailles units correspond to the southern margin of the Mauléon basin. The Saint-Palais unit represents the Albian rift depocenter. The Bellevue and Sainte Suzanne units materialized the northern rift margin. Lak: Lakhoura, SA: South Arbailles, NA: North Arbailles, St-P: Saint-Palais, Bel: Bellevue, St-S: Sainte-Suzanne, GR: Grand-Rieu.

4.1. The Saint-Palais unit

The Palaeozoic substratum below the Saint-Palais unit is tilted towards the north, being at a depth of around 2,900 m in the Ainhice-1 well **(Fig. 6)** and of 7,000 m in the central part of the basin. The base of this well is characterized by Paleozoic basement, overlain by the thick Upper Triassic salt unit materializing a major decoupling level between the basement and the sedimentary cover. This Triassic salt unit is grading upward to two Mesozoic cover units characterized by a normal polarity and separated by a tectonic contact. The Lower unit, U1, consists of a complete Jurassic sequence, up to the Kimmeridgian, covered by Late Aptian Urgonian limestones. unit U1 is characterized by a hiatus of the Neocomian to the Early Aptian. The Upper unit, U2, is composed of the same Jurassic but the Kimmeridgian marls are thinner than in U1, grading upward to Earliest Albian carbonate platform deposits **(Fig. 6A)**. These cover units are overlain by Middle to Late Albian spicule marls and siliciclastic turbidites. The Albian basinal deposits thicken towards the north and reach their maximum thickness in the Saint-Palais Anticline, clearly identified in the field. The Saint-Palais domain corresponds to the depocenter of the Albian basin, with an estimated thickness of up to 4,000–5,000 m (Roux, 1983; Fixari, 1984; Souquet et al., 1985). The upper part of the Saint-Palais unit is formed by the Upper Cretaceous carbonate-dominated flysch, which reaches a thickness of more than 1,500 m in the Uhart Mixe well.

4.2. The Bellevue unit

The Bellevue unit is located between the Saint-Palais and the Bellevue Thrusts. The Bellevue Thrust is responsible for the offset of the Jurassic-Cretaceous cover and the displacement of the Bellevue unit onto the Sainte Suzanne unit. The Paleozoic basement is located at a depth of around 8,000 m under the Bellevue unit. This unit is composed of a complex structure whose most obvious feature is the Bellevue Anticline affecting the Mesozoic cover intersected in the Bellevue well. The northward Bellevue Thrust is marked by a 1,800 m thick tectonized zone composed of Late Triassic salt and Barremian carbonate slices. These Barremian units could be tectonically incorporated to the Triassic salt forming the overturned flank of the overlying anticline evidenced in the Bellevue well **(Fig. 6)**. In fact, this tectonized interval is overlain by an overturned Jurassic carbonate unit composed of Dogger to Kimmeridgian deposits. Above, the Bellevue unit is made up of a complete Jurassic to Late Cretaceous sequence in a normal position. The Early cretaceous sequence is characterized by a lack of Neocomian. The Barremian to Aptian carbonate platform unit lying unconformably on the Portlandian is more than 1,500 m thick. The Barremian deposits are composed of limestones with annelids and 500 m thick of more distal Sainte-Suzanne marls. The Aptian is mainly composed of

Urgonian limestones. The Albian thins towards the North and is represented by spicule marls including intercalations of carbonate mudstone indicating the proximity of the northern Aquitanian carbonate platform. The Late Cretaceous sequence is made up of Cenomanian to Coniacian carbonate turbidites.

4.3. The Sainte-Suzanne unit

The Sainte-Suzanne Thrust corresponds to the major north verging thrust responsible for a displacement of more than 17 km of the Mauléon basin deposits onto the south Aquitain Grand Rieu unit **(Fig. 10)**. It can be considered as the North-Pyrenean Frontal Thrust in this part of the Pyrenees. The Sainte Suzanne unit is made up of a very thick Jurassic to Campanian sequence, slightly inclined and thickening towards the south. It has been crosscut by the Orthez-102 well where the Sainte Suzanne Thrust has been identified at a depth of 4,320 m **(Fig. 6)**. The Jurassic is made up of a complete sequence of marine carbonate platform deposits from Hettangian to Kimmeridgian, truncated under the Early Cretaceous deposits, as evidenced by the north-directed erosional truncations. The 1 000m thick Early Cretaceous sequence is characterized by a lack of Neocomian. The Barremian is characterized by shallow marine carbonate deposits with annelids showing that this unit is more proximal than the Bellevue unit. The Aptian is sub-isopachous and is composed of shallow marine carbonate platform deposits (Urgonian facies). The Albian deposits are also made up of carbonate platform deposits thickening towards the south. These facies are therefore more proximal than the Albian deposits of the Bellevue unit. A clear truncation of the Albian reflections is seen towards the north, below the Late Cretaceous calcareous flysch. This latter calci-turbidite sequence is thinning and onlapping to the north on top of the eroded Albian sequence.

4.4. The Grand-Rieu/Arzacq unit

The Grand-Rieu – Arzacq unit is the footwall of the Sainte Suzanne Thrust and corresponds to the southern part of the Aquitain basin. From the seismic data, the Paleozoic basement below the Sainte Suzanne Thrust can be estimated to be at a depth of 8,500 m. It is assumed to be overlain by a more or less continuous Triassic unit. The inferred Liassic unit present in the Aquitain basin to the north appears to pinch-out southwards against a diapiric structure associated with a normal fault. This Mesozoic tectonic structure marks the boundary between the Grand-Rieu Ridge to the South and the commonly named Arzacq basin corresponding to a highly subsiding domain during Albian times. The overlying Middle to Late Jurassic carbonates are more continuous and isopachous. The top of the Jurassic sequence corresponds to a major exposure surface marked by north-directed erosional truncations under the Barremian transgressive carbonate deposits, as indicated in the Amou well. This unconformity is time-equivalent to the one describe in the Arbailles unit on the southern margin of the Mauléon basin. During the latest Jurassic and the Neocomian period, the northern margin of the Mauléon basin was tilted towards the south, unlike the southern margin that was tilted towards the north. The Barremian to Aptian sequence of the Grand-Rieu unit is relatively isopachous and consists mainly of shallow marine carbonate platform deposits. The Albian deposits form a thick unit of fairly deep marine spicule marls indicating a strong subsidence rate of the Arzacq basin, as indicated in the Amou and Bastennes-Gaujacq **(Fig. 6)**. A large wave-length anticline affects the Jurassic - Albian sequence at the transition between the Grand-Rieu Ridge and the Arzacq basin (Grand-Rieu Anticline). A major truncation of the folded strata below the Cenomanian carbonate platform deposits attests to the Late-Albian to Early Cenomanian age of this deformation. In the Grand-Rieu – Arzacq unit the Late Cretaceous is represented by sub-isopachous carbonate platform deposits. During the Tertiary, this domain was characterized by a very high subsidence rate, increasing towards the South, as attested by the very thick Tertiary sequence at the front of the Sainte Suzanne Thrust. Local southward dipping clinoforms can be observed south of the Bastennes-Gaujacq well, probably related to the growth of this diapiric structure. The very great thickness of the Tertiary sequence attests to the strong flexural subsidence of the Grand-Rieu – Arzacq unit but also to the large displacement and uplift of the Mauléon basin along the Sainte-Suzanne Thrust, since no Tertiary deposits have been preserved in the Mauléon basin (even if they were deposited over this entire flexure domain). Most of the Tertiary flexural

subsidence occurs before the Late Lutetian, as shown by the thickening of the Danian to Lower Ypresian deposits towards the south.

5. Top Jurassic to Cenomanian tectono sedimentary and geodynamic evolution of the Mauléon basin

5.1. Latest Jurassic to Neocomian uplift phase

The Jurassic is characterized by an extensive and relatively continuous carbonate platform spreading between the southern Mauléon basin margin (Arbailles unit) and the Arzacq basin **(Fig. 12A)**. At its top, the platform is limited by a major unconformity resulting from an emersive and erosional phase dated from the latest Jurassic to Barremian **(Fig. 12B)**. This event is evidenced by the development of bauxites and the lack of Neocomian deposits both in the Pyrenees and the Arzacq basin (Combes et al., 1998; James, 1998; Canérot et al., 1999). Before the Early Cretaceous transgression, the Jurassic platform is characterized by a synform morphology extending from the southern margin of the Mauléon basin to the Arzacq basin. It is revealed respectively by the south-directed and north-directed erosional truncations affecting the Jurassic in the Arbailles and the Arzacq units **(Fig. 11)**. This deformation stage implies the uplift of these domains, corresponding partly to the Early Cretaceous Mauléon basin edges; while in the meantime, subsidence stops in the synform axis. Mechanism responsible for the uplift of the entire Pyrenean-Aquitaine domain might be related to an asthenosphere upwelling preceding the Early Cretaceous rifting.

5.2. Barremian to earliest Albian rifting stage 1: symmetric basin

After the Late Jurassic – Early Cretaceous exposure/weathering stage, onset of transgression leads to the development of an extensive restricted carbonate platform during the Barremian. From Barremian to Aptian time, the balance between carbonate production and creation of available space favors the aggradation of 1 600m thick shallow marine carbonate facies, witnessing a highly subsiding stage controlling a relative-flat depositional profile **(Figs. 6 and 12C)**. This homogeneous subsidence stage evolves during Late Aptian to the earliest Albian. The basin's edges were characterized by the back-stepping of the shallow carbonate platform, while the Mauléon and Arzacq basins center are composed of deeper spicule marls. In this domain, creation of available space exceeded the carbonate production, resulting in the relocating of the carbonate factory on the basin's edges. Paleogeography reorganization was thus controlled by the differential subsidence regime responsible for a steeper depositional profile.

As a consequence, during the Barremian - earliest Albian time the Mauléon basin was a symmetric basin, characterized by shallow marine carbonate platforms on each basin edges. The absence of brittle deformation within the upper-crust excludes the application of the pure-shear model developed by McKenzie (1978) to explain the subsidence regime of this basin. A symmetric synrift sag basin with no brittle deformation in the upper crust has been proposed from numerical modeling (Karner et al., 2003). In this model, the subsidence of the basin results from lower crustal ductile thinning favored by decoupling between the upper and lower crusts. We propose that the initiation of the Mauléon sag basin results from thinning of the lower crust, without any major deformation of the upper crust. The isostatic response to the lower crustal thinning induces regional sagging and onlapping of the syn-thinning deposits on each side of the basin. The rifting stage 1 can be interpreted as a « ductile crustal pure-shear thinning phase ».

5.3. Albian rifting stage 2: asymmetric basin

At Albian time, the southern margin of the Mauléon basin was affected by differential vertical movements: (1) uplift of the southern part of the basin; and (2) tectonic subsidence towards the north **(Fig. 12E)**. They are responsible for the onset of the Mendibelza deep gravity flow deposits passing distally to the Black Flysch group towards the Saint-Palais depocenter **(Fig. 12E)**. At this time, the Iberian margin substratum was characterized by a northward dipping surface with an average slope angle of 15–30° **(Fig. 8)**. This surface was affected by syn-sedimentary albian N120° southward-propagating high-angle normal faults, controlling the destabilization of the fan-delta system into the deep basin **(Fig. 12E)**.

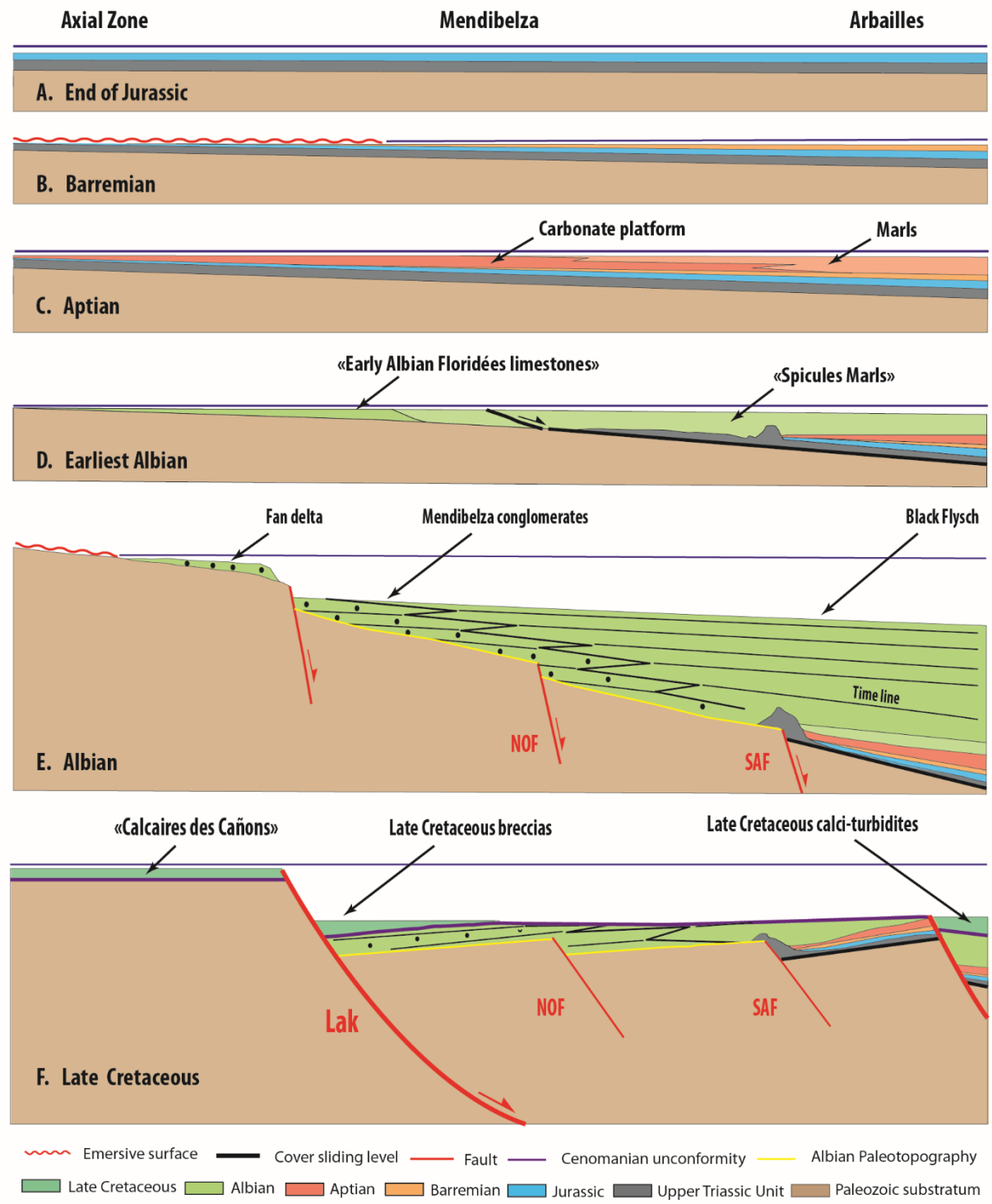


Fig. 12. Schematic tectono-sedimentary evolution of the southern margin of the Mauléon basin from the end of Jurassic to Late Cretaceous time. **(A)** During the Jurassic, this domain is characterized by the development of a carbonate platform. **(B)** The Jurassic platform underwent an emersion phase from the end of Jurassic to the base of Barremian time. This emersive phase was responsible for erosion of the previous carbonate platform, as shown by the southward erosional truncations affecting the Jurassic under the Early Cretaceous deposits. **(C)** The Early Cretaceous is characterized by a lack of Neocomian and the development of a flat carbonate platform during Barremian-Early Aptian time. During Late Aptian time, the previous carbonate platform distalized towards the north into more distal spicule marls, showing a slight tilt of the depositional profile. **(D)** At Early Albian time, the southern Mauléon margin was affected by the gravitational sliding of the Mesozoic cover towards the north leading to local diapirism. **(E)** The Albian time was characterized by differential vertical movements responsible for the uplift of the southern margin and tectonic subsidence towards the north. This stage is materialized by the sedimentation of the Mendibelza Fm. proximal turbiditic s.l. siliciclastic system, onlapping towards the south a Paleozoic basement inclined towards the north. The northward tilt of the Iberian margin is affected by southward propagating N120° normal faults. **(F)** At Cenomanian time, the Mendibelza-Arbailles unit was affected by a tilt towards the south

These faults were sealed by younger synrift back-stepping deposits of the Mendibelza Fm. towards the south.

The conglomerates directly overlain the Paleozoic substratum of the Mendibelza unit, indicating the entire Mesozoic lacks **(Fig. 5)**, while it was continuous throughout the Pyrenean-Aquitaine domain. Thus, the Mesozoic cover of this unit need to be subtracted prior to the sedimentation of the Albian synrift Mendibelza sequence. It leads to the development of an emerged Axial Zone during the rifting stage 2. The sliding level consists of the thick Upper Triassic shale, evaporite and ophite complex systematically brecciated and / or deformed under the prerift cover of the Iberian margin. This mass-sliding is recorded within the Ainhice-1 well Mesozoic cover unit overlap (units U1 and U2, **Fig. 6**). The stratigraphic differences between these two Mesozoic cover units, suggest an origin of the upper one from a southern marginal part of the basin where the Jurassic-Cretaceous hiatus is greatest. Thus, the Early Albian Axial Zone denudation is linked to the northward mass sliding of the Mesozoic cover towards the Mauléon basin axis in response to the Iberian margin northward tilting **(Fig. 12D)**.

At the same period, the European margin of the Mauléon basin recorded less vertical movements and tectonic activity than the southern margin. Unlike the Iberian conjugate margin, this northern domain is not subject to gravitational sliding of the Mesozoic cover. Indeed, no regional uplift and associated coarse-grained alluvial-derived gravity-flow deposits are evidenced in the Arzacq, Sainte-Suzanne and Bellevue units. The Albian period is mainly represented by a shallow marine carbonate platform recognized in the Arzacq and Sainte-Suzanne units **(Figs. 6 and 13)**. The slightly southward-dipping depositional profile is responsible for a facies transition between shallow-marine algae limestones and deeper spicule marls in the Sainte Suzanne unit. In Saint Palais and Bellevue units, the Jurassic-Aptian sedimentary cover is significantly normally offset, which allows the accumulation of thick deep Albian facies to the south of the Saint-Palais Thrust, suggesting that this latter corresponds to a southward dipping Albian normal fault **(Figs. 11 and 13)**. This fault is part of the northern Mauléon Albian basin's margin. The thick interval with very deformed Triassic material intersected at the base of the Bellevue well is interpreted as an Albian diapiric ridge developing on the northern edge of the Albian Mauléon basin **(Fig. 6)**.

Comparison between the southern and northern margins shows that the Mauléon basin acquired asymmetry during the Early Albian time: (1) deep basin turbiditic deposits on the Iberian margin and (2) carbonate platform on the European one. According to most of the models that consider a simple-shear deformation process to explain the asymmetry of a rift (Wernicke, 1985; Lister et al., 1986), the Mauléon basin's asymmetry is interpreted as resulting from the activation of the southward dipping Saint-Palais Detachment during the Early Albian **(Fig. 13)**. Following Lister et al. (1986) the Albian Iberian margin corresponds to the upper plate and the European one to the lower plate. The Saint-Palais Detachment might be responsible for the northward Iberian margin tilting, this former being part of a major crustal scale roll-over. The roll-over structure is accommodated by N120° oriented and steeply dipping normal faults that propagate towards the south (i.e. NAF, NOF). They are antithetic to the Saint-Palais structure. During Albian time, the width of the Mauléon deep basin, measured from platform to platform, was around 50 km.

5.4. Late Cretaceous rifting stage 3: apparent symmetric basin

During the Late Cretaceous period, a carbonate platform developed on both edges of the Mauléon basin, and the deep basin became wider **(Figs. 6 and 13)**. Indeed, the width of the Mauléon deep basin, measured from platform to platform, was around 100 km wide. The Grand-Rieu Ridge represents a major palaeogeographic boundary between the carbonate platform of the European margin and the center of the Mauléon basin (Razin, 1989; Serrano et al., 2006). The transition between the carbonate platform and the basinal carbonate turbidites is governed by a southward dipping normal fault between the Sainte Suzanne unit and the Arzacq basin. The calcareous flysch deposited in the Mauléon basin was derived mainly by gravity flows coming from the northern Aquitain carbonate platform. These calcareous turbidites onlap the previous Albian

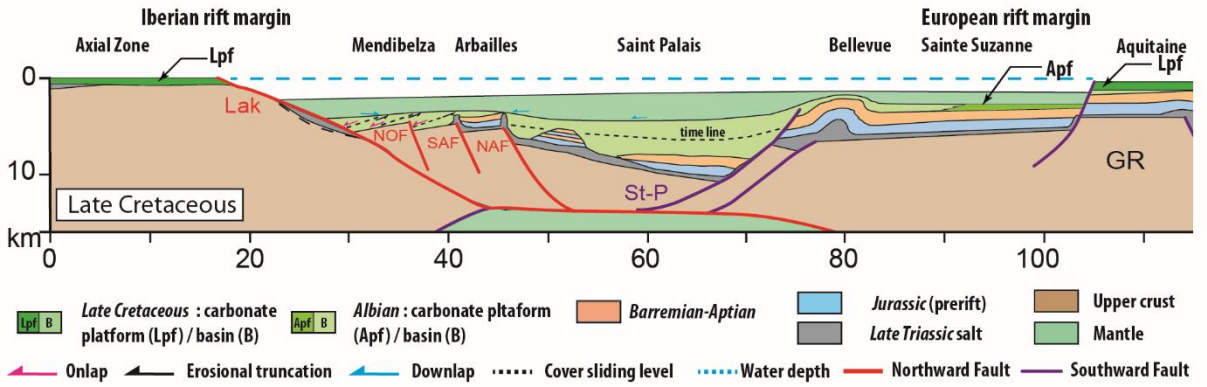


Fig. 13. Modified from original article. Schematic cross-section of the Mauléon basin during Late Cretaceous showing the asymmetry of the rift basin margins and the geometry of the Cretaceous deposits. Lak: Lakhoura detachment, NOF: North Occabe fault, SAF: South Arbailles fault, NAF: North Arbailles fault, St-P: Saint-Palais detachement, GR : Grand Rieu.

deposits towards the Sainte-Suzanne unit to the north and the Saint-Palais to Mendibelza units to the south **(Fig. 13)**. The development of the Grand-Rieu Anticline attests of salt movement at Early Cenomanian time.

On the southern margin the commonly named Late Cretaceous « Calcaires des Cañons » carbonate platform deposits lie unconformably over the previously exposed Palaeozoic basement of the Axial Zone **(Fig. 13)**. Towards the north, in the Mendibelza unit, base-of-slope chaotic breccias attest of a normal fault-controlled platform-basin transition between the southern carbonate platform developing on the Axial Zone and the Mauléon basin **(Fig. 13)**. Several arguments indicate that a second and opposite detachment occurred at Early Cenomanian time: the northward verging Lakhoura Detachment **(Fig. 13)**. This syn-sedimentary fault, currently inverted as the Lakhoura Thrust **(Fig. 5)**, is interpreted as being responsible for the southward tilting of the Mendibelza/Arbailles units. The Early Cenomanian age of this tilting is attested by: (1) the absence of wedge-shaped syn-tectonic growth strata in the Albian synrift sequence of the Mendibelza unit; (2) the 98 Ma cooling age obtained on the (Hart et al., 2017), responsible for the southward tilt of the Lower Triassic Sandstone unit in the Saint-Jean-Pied-de-Port area (Masini et al., 2014); and (3) the onlap of the Late Cretaceous deposits on the tilted and eroded Albian sequence in the north of the Arbailles unit (Casteras et al., 1971; Ducasse and Vélasque, 1988; **Fig. 9**). This observation implies that the northern edge of the Arbailles unit becomes a structural high in the basin during Early Cenomanian. This structural high is fossilized at Santonian time as highlighted by the age of the first deposits passing over it.

6. Discussion and Conclusion

The northwestern Pyrenees present a strong positive gravity anomaly under the Mauléon rift basin (Grandjean, 1994; Casas et al., 1997) resulting from the presence at low depth (~10 km) of lithospheric mantle (Wang et al., 2016). This high mantle body position implies the existence of a very thin continental crust arguing for a hyper-thinning Cretaceous rifting stage. In this work, we assume that the Saint-Palais and Lakhoura structures affect the lithospheric mantle. They are responsible for the hyper-thinning of the Mauléon basin continental crust. However, this rift basin have not underwent oceanic spreading as classical basins along the Atlantic Ocean (Manatschal., 2004; Péron-Pinvidic et al., 2007; Haupert et al., 2016), or in the Alps fossil margins (Manatschal et al., 2006, Masini et al., 2011, Mohn et al., 2014 et Decarlis et al., 2015). Another significant difference with these classical hyper-extended magma poor margins is the thickness of the syn-thinning deposits in the hyper-extended domain (~ 8 km thick in Mauléon basin vs. less than 1 km thick on the Atlantic and Alps margins). The thick synrift deposits record a complex polyphasic thinning history from Barremian to Early Cenomanian time.

During stage 1, the Mauléon basin is symmetric as evidenced by the development of a carbonate platform on each basin edges. The carbonate production counterbalances the high accommodation, resulting in a near flat sedimentary profile. We interpret the creation

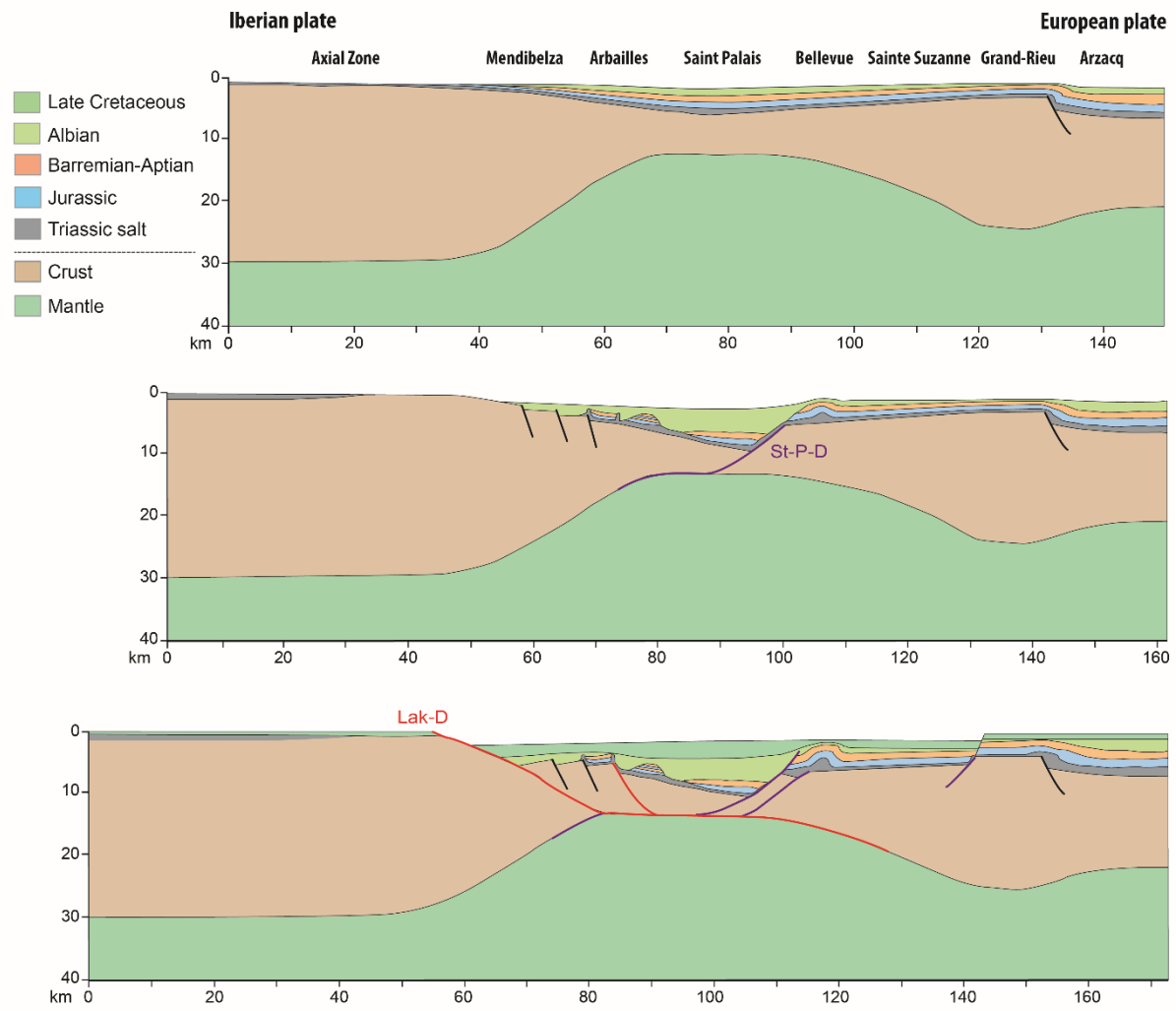


Fig.14. Modified from original article. Geodynamical model of crustal thinning of the Mauléon hyper-thinned rift basin. The genesis of the Mauléon basin comprises two lithospheric thinning stages. **(A)** Barremian to Aptian rifting stage 1: « ductile pure-shear thinning phase » affecting mainly the lower crust, inducing the formation of a symmetric synrift sag basin. **(B)** Albian rifting stage 2: simple-shear thinning phase inducing the development of an asymmetric synrift basin, characterized by proximal turbiditic system on the southern margin and carbonate platform deposits on the northern one. The Saint-Palais southward detachment fault is responsible for the hyper-thinning of the sub-continental crust during Albian time. **(C)** Middle Cenomanian rifting stage 3: the southern margin was tilted towards the south along a northward dipping detachment fault responsible for local sub-continental mantle denudation, resulting in the formation of an apparent symmetric rift basin. St-P-D: Saint-Palais detachement, Lak-D: Lakhoura detachment.

of accommodation as a result of ductile thinning of the lower crust, without affecting the upper-crust **(Fig. 14A)**. This thinning stage shares similarity with the crustal scale boudinage process, previously proposed at Albian time (Lagabrielle et al, 2010; Corre et al, 2016; Teixell et al, 2016; **Fig. 3B**). However, only the lower crust is affected by ductile thinning, favored by the presence of a decoupling level in between the lower and upper crusts. The resulting synrift sag basin morphology is quite similar to the Mesozoic Columbrets sag basin, which does not present any evidence of deep basin gravitary sedimentary infill (Etheve, 2016 and Etheve et al, 2018).

At Albian time (stage 2), the rift fabric totally changed. The basin was affected by « simple-shear thinning » due to the development of the southward dipping Saint-Palais Detachment **(Fig. 14B)**. This crustal thinning phase affected the entire lithosphere, forming an asymmetric rift basin, as previously proposed in the simple-shear models (Jammes et al, 2009; Tugend et al, 2014, 2015a; Masini et al. 2014, **Fig. 3A**). However, unlike the previous models, the Albian rifting stage initiates with simple shear thinning, without distributed extension in the upper crust (pure shear thinning sensus McKenzie., 1978). Lavier and Manatschal., 2006 have evidenced using numerical modeling that the continental crust

was already thin (~20km) when simple shear thinning starts. In the case of the Mauléon basin we propose that the Early Cretaceous stage favors the ductile thinning of the lower crust before beginning the Albian-Cenomanian simple shear thinning stage.

The Saint-Palais detachment is responsible for the northward Iberian margin roll-over. This interpretation strongly contrasts with previous models arguing for an Albian southward tilt of the Iberian margin along a northward dipping normal fault (Boirie., 1981; Fixari., 1984; Souquet et al., 1985; Ducasse and Vélasque., 1988) or crustal scale detachments (Jammes et al., 2009; Masini et al., 2014). In this scheme, we propose that rift asymmetry controls the asymmetric sedimentary profile. Actually, the Iberian margin (roll-over) is composed of a proximal turbiditic s.l. system whereas the European one (southward gently-dipping) is characterized by a carbonate platform. Similarly, to the Columbrets basin (Etheve., 2016 and Etheve et al., 2018), the onset of simple shear thinning is synchronous with the basinward prerift cover-sliding along the Late Triassic salt décollement. Such Early Albian gravity tectonics have already been reported all along the Iberian rift margin (Bouquet, 1986; Ducasse et al., 1986; Ducasse and Vélasque, 1988; Lagabrielle et al., 2010; Corre et al., 2016; Teixell et al., 2016; **Fig. 3B**). However, one of the major discrepancies with the previous models is the absence of gravitational cover sliding along the European rift margin **(Fig. 3B)**. The sliding of the Mesozoic cover led to local diapirism along the Iberian margin, as shown by the lateral facies variations from shallow carbonate platform to spicule marls around the diapiric structures (Canérot, 1988, 1989; Canérot and Lenoble, 1993; James and Canérot, 1999; Canérot et al., 2005).

The paleogeography of the Early Cretaceous Mauléon basin, derived from the sedimentary record is not compatible with a major strike-slip drift of the Iberian plate as proposed in kinematic reconstructions (Le Pichon et al., 1971; Roest and Srivastava, 1991; Olivet, 1996; Rosenbaum et al., 2002; Sibuet et al., 2004; Gong et al., 2008). We assume that the Iberia sinistral strike-slip motion did occur on a more southward structure (Malod., 1982; Canérot., 2016) developed earlier during Late Jurassic (Tugend et al., 2015b) and / or may have been evenly distributed within the Cretaceous rift system.

At Early Cenomanian time (final stage 3), the southward tilting of the Mendibelza-Arbailles units, – formerly considered as Early Albian (Boirie, 1981; Boirie and Souquet, 1982; Fixari, 1984; Souquet et al., 1985; Ducasse and Vélasque, 1988; Masini et al., 2014) – is induced by the change of detachment vergence and the development of the Lakhoura northward dipping Detachment. The Arbailles unit thus becomes a structural high bordering the southern hyper-thinned Mauléon basin domain. Consequently, we assume that the Arbailles unit becomes a tilted block at Early Cenomanian time.

Therefore, the tectono-sedimentary evolution of the Mauléon rift basin during the stages 2 and 3 is defined by the development of two antithetic and diachronous detachments, i.e. the Albian southward dipping Saint-Palais detachment during Stage 2 and the Early Cenomanian northward dipping Lakhoura one during Stage 3. The change in detachment vergence between Albian and Cenomanian time can be interpreted as « flip-flop detachment tectonic » (Sauter et al., 2013; Geoffroy et al., 2014; Gillard et al., 2015), highlighting the diachronous shift from upper-plate to lower-plate morphology along a same margin section. This double successive asymmetry is responsible for the apparent final symmetry of this hyper-thinned rift. This work reconciliates the previous rift models, i.e. symmetric (Souquet, 1988; Ducasse and Vélasque, 1988), asymmetric (Jammes et al., 2009; Masini et al., 2014; Tugend et al., 2015a, **Fig. 3A**) or mixed (Lagabrielle et al., 2010; Corre et al., 2016; Teixell et al., 2016, **Fig. 3B**). The polyphase thinning history is responsible for the hyper-thinning of the continental crust and the development of a relatively narrow hyper-thinned rift domain **(Fig. 14C)**.

In three dimensions, the Mauléon basin appears relatively complex and not cylindrical. On our synthetic 2D transect **(Fig. 14C)**, the mantle is systematically overlain by a hyper-thinned crust whereas eastward (Urdach), it has been denuded and partly reworked into synrift deposits (Roux, 1983; Duée et al., 1984; Fortané et al., 1986; Debroas et al., 2010;

Lagabrielle et al., 2010; Teixell et al., 2016). We consider the Saint-Palais Detachment as responsible for the hyper-thinning of the continental crust, while the Lakhoura one might be responsible for partial mantle denudation. This is consistent with the Urdach mantle/crust contact that display top north-east shear direction (Corre., 2017). Thus, it appears that the basin morphology changes along strike, due to N0°-20° transverse structures such as the Pamplona (Richard, 1986; Razin, 1989; Claude, 1990; Larrasoaña et al., 2003; Pedreira et al., 2007; Díaz et al., 2012), the Saint-Jean-Pied-de-Port, Saison, Barlanès and Ossau structures (Canérot, 2008, 2017; Debroas et al., 2010). This N0°-20° structuration seems to clearly control the 3D geometry of the Saint-Palais hyper-extended rift domain, and will be the purposed of future investigations.

Acknowledgements

This study was conducted within the framework of the integrated geological Orogen research project (TOTAL, BRGM, and INSU). We are very grateful to the reviewers and to the editor, who contributed to the improvement of this manuscript. We would like to thank the Orogen project managers Sylvain Calassou (Total), Emmanuel Masini (Total), Olivier Vidal (CNRS) and French geological survey - BRGM. We also thank Joseph Canérot for the numerous scientific discussions on the tectono-sedimentary evolution of the Mendibelza and Arbailles units. The authors thank Geoffrey Bird for the English review.

References

AGSO and BRGM, 2018, Synthèse géophysique et géologique des Pyrénées - Volume 3 : Cycle alpin : Phénomènes alpins – 2015, Edition AGSO and BRGM, scientific committee : A. AUTRAN, M. DURAND-DELGA and J.M. FONBOTÉ, 480 p., 286 figs.

Albarède, F., and A. Michard-Vitrac, 1978, Age and Significance of the North Pyrenean Metamorphism: Earth and Planetary Science Letters, no. 40, p. 327–332.

Alhamawi, M., 1992, Sédimentologie, Pétrographie Sédimentaire et Diagenèse des Calcaires du Crétacé supérieur de la Marge Ibérique: Bordeaux 1, 356 p.

Arnaud-Vanneau, A., H. Arnaud, J. Charollais, M.-A. Conrad, P. Cotillon, S. Ferry, J.-P. Masse, and B. Peybernès, 1979, Paléogéographie des calcaires urgoniens du sud de la France: Géobios, v. 3, p. 363–383.

Baudin, T., and A. Barnolas, 2008, Carte Géologique des Pyrénées au 1/400000, Orléans, France: Bureau de Recherche Géologique et minière.

Beaumont, C., J. A. Muñoz, J. Hamilton, and P. Fullsack, 2000, Factors controlling the Alpine evolution of the central Pyrenees inferred from a comparison of observations and geodynamical models: Journal of Geophysical Research, v. 105, no. B4, p. 8121–8145.

Biteau, J.-J., A. Le Marrec, M. Le Vot, and J.-M. Masset, 2006, The Aquitaine basin: Petroleum Geoscience, v. 12, p. 247–273.

Bixel, F., and C. Lucas, 1987, Approche Géodynamique du Permien et du Trias des Pyrénées dans le cadre du sud-ouest européen: Cuadernos Geología Ibérica, v. 11, p. 57–81.

Bixel, F., and C. L. Lucas, 1983, Magmatisme, tectonique et sédimentation dans les fossés stéphano-permiens des Pyrénées occidentales: Revue de géologie dynamique et de géographie physique, v. 24, no. 4, p. 329–342.

Boirie, J.-M., 1981, Etude Sédimentologique des Poudingues de Mendibelza (Pyrénées Atlantiques): Toulouse, Université Paul Sabatier (Sciences), 114 p.

Boirie, J.-M., and P. Souquet, 1982, Les poudingues de Mendibelza: dépôts de cônes sous-marins du rift albien des Pyrénées: Bulletin Centres Recherches Exploration-Production Elf-Aquitaine, v. 6, no. 2, p. 405–435.

Bois, C., and ECORS Scientific team, 1990, Major geodynamic processes studied from the ECORS deep seismic profiles in France and adjacent areas: Tectonophysics, v. 173, no. 1–4, p. 397–410.

Boissonnas, J., G. Le Pochat, C. Thibault, and M. Bernatzk, 1974, Carte géologique de la France au 1/50000; feuille d'Iholdy, Orléans, France: Bureau de Recherche Géologique et minière.

Bosch, G. V., A. Teixell, M. Jolivet, P. Labaume, D. Stockli, M. Domènech, and P. Monié, 2016, Timing of Eocene–Miocene thrust activity in the Western Axial Zone and Chaînons Béarnais (west-central Pyrenees) revealed by multi-method thermochronology: Comptes Rendus Geoscience, v. 348, no. 3–4, p. 246–256, doi:10.1016/j.crte.2016.01.001.

Boulvais, P., P. de Parseval, A. D'Hulst, and P. Paris, 2006, Carbonate alteration associated with talc-chlorite mineralization in the eastern Pyrenees, with emphasis on the St. Barthelemy Massif: Mineralogy and Petrology, v. 88, no. 3–4, p. 499–526, doi:10.1007/s00710-006-0124-x.

Bouquet, B., 1986, La bordure mésozoïque orientale du Massif du Labourd (Pyrénées occidentales) : Stratigraphie-Sédimentologie-Structure-Implications Géodynamiques: Pau, Université de Pau et des Pays de l'Adour, 219 p.

Brun, J.-P., and J. van den Driessche, 1994, Extensional gneiss domes and detachment fault systems; structure and kinematics: Bulletin de la Société Géologique de France, v. 165, no. 6, p. 519–530.

Brune, S., C. Heine, M. Pérez-Gussinyé, and S. V. Sobolev, 2014, Rift migration explains continental margin asymmetry and crustal hyper-extension: Nature Communications, v. 5, doi:10.1038/ncomms5014.

Brune, S., S. E. Williams, N. P. Butterworth, and R. D. Müller, 2016, Abrupt plate accelerations shape rifted continental margins: Nature, v. 536, no. 7615, p. 201–204, doi:10.1038/nature18319.

Canérot, J., 1988, Manifestations de l'halocinèse dans les chaînons béarnais (zone Nord-Pyrénéenne) au Crétacé inférieur: Comptes rendus de l'Académie des sciences Série 2, v. 306, no. 15, p. 1099–1102.

Canérot, J., 1989, Rifting éocrétacé et halocinèse sur la marge ibérique des Pyrénées Occidentales (France). Conséquences structurales: Bulletin Centres Recherches Exploration-Production Elf-Aquitaine, v. 13, p. 87–99.

Canérot, J., 2008, Les Pyrénées: Histoire géologique: Atlantica.

Canérot, J., C, 2016, The Iberian Plate: myth or reality?: Boletin Geologico y Minero, 127, p. 557-568.

Canérot, J., 2017, The pull apart-type Tardets-Mauléon basin, a key to understand the formation of the Pyrenees: Bulletin de la Société géologique de France, v. 188, no. 6, p. 35, doi:10.1051/bsgf/2017198.

Canérot, J., B. Peybernes, and R. Ciszak, 1978, Présence d'une marge méridionale à l'emplacement de la zone des chainons béarnais (Pyrénées basco-béarnaises): Bulletin de la Société Géologique de France, v. S7-XX, no. 5, p. 673–676, doi:10.2113/gssgfbull.S7-XX.5.673.

Canérot, J., and F. Delavaux, 1986, Tectonique et sédimentation sur la marge nord-ibérique des chaînons béarnais (Pyrénées-béarnaises). Remise en question de la signification des lherzolites du sommet de Saraillé: Comptes rendus de l'Académie des sciences. Série 2, v. 302, no. 15, p. 951–956.

Canérot, J., and J.-L. Lenoble, 1993, Diapirisme crétacé sur la marge ibérique des Pyrénées occidentales; exemple du pic de Lauriolle; comparaisons avec l'Aquitaine, les Pyrénées centrales et orientales: Bulletin de la Société Géologique de France, v. 164, no. 5, p. 719–726.

Canérot, J., C. Majesté-Menjoulas, and Y. Ternet, 1999, Le cadre stratigraphique et géodynamique des altérites et des bauxites sur la marge ibérique des Pyrénées occidentales (France): Comptes Rendus de l'Académie des Sciences-Series II. Earth and Planetary Science, v. 328, no. 7, p. 451–456.

Canérot, J., C. Majesté-Menjoulas, and Y. Ternet, 2004, Nouvelle interprétation structurale de la « faille Nord-Pyrénéenne » en vallée d'Aspe (Pyrénées-Atlantiques). Remise en question d'un plutonisme ophitique danien dans le secteur de Bedous: Comptes Rendus Geoscience, v. 336, no. 2, p. 135–142, doi:10.1016/j.crte.2003.11.004.

Canérot, J., M. R. Hudec, and K. Rockenbauch, 2005, Mesozoic diapirism in the Pyrenean orogen: Salt tectonics on a transform plate boundary: AAPG Bulletin, v. 89, no. 2, p. 211–229, doi:10.1306/09170404007.

Casas, A., P. Kearey, L. Rivero, and C. R. Adam, 1997, Gravity anomaly map of the Pyrenean region and a comparison of the deep geological structure of the western and eastern Pyrenees: Earth and Planetary Science Letters, v. 150, no. 1–2, p. 65–78.

Casteras, M., 1943, Sur la structure de la partie orientale des Pyrénées basques: Comptes rendus de l'Académie des sciences, v. 216, p. 572–574.

Casteras, M., M. Frey, and J. Galharague, 1967, Sur les terrains paléozoïques et sur la structure du massif de Mendibelza (Basses-Pyrénées): Comptes Rendus de l'Académie des Sciences-Série D, v. 264, no. 13, p. 1677–1682.

Casteras, M., M. Gottis, M. Clin, J. Guignard, J. Paris, and J. Galharague, 1971, Carte géologique de la France au 1/ 50 000, feuille de Tardets–Sorholus, Orléans, France.

Casteras, M., and P. Souquet, 1964, Sur la constitution et sur la structure de la couverture crétacée de la zone primaire axiale pyrénéenne à l'ouest du Pic d'Anie: Comptes rendus de l'Académie des sciences, v. 259, p. 2881–2886.

Casteras, M., P. Souquet, G. Culot, and J. Galharague, 1970, Carte géologique de la France au 1/50 000: feuille de Larrau, Orléans, France.

Chelalou, R., T. Nalpas, R. Bousquet, M. Prevost, A. Lahfid, J. C. Ringenbach, and J. F. Ballard, 2016, New sedimentological, structural and paleo-thermicity data on the Boucheville basin (eastern north Pyrenean zone, France): Compte Rendu Géoscience, doi:10.1016/j.crte.2015.11.008

Choukroune, P., 1976, Strain patterns in the Pyrenean chain: Philosophical Transactions of the Royal Society of London A: Mathematical, Physical and Engineering Sciences, v. 283, no. 1312, p. 271–280.

Choukroune, P., and ECORS Team, 1989, The ECORS Pyrenean deep seismic profile reflection data and the overall structure of an orogenic belt: Tectonics, v. 8, no. 1, p. 23–39.

Choukroune, P., F. Roure, B. Pinet, and E. P. Team, 1990, Main results of the ECORS Pyrenees profile: Tectonophysics, v. 173, no. 1–4, p. 411–423.

Claude, D., 1990, Etude stratigraphique, sédimentologique et structurale des dépôts mésozoïques au nord du massif du Labourd: rôle de la faille de Pamplona (Pays Basque): Université de Bordeaux III, 437 p.

Clerc, C., and Y. Lagabrielle, 2014, Thermal control on the modes of crustal thinning leading to mantle exhumation: Insights from the Cretaceous Pyrenean hot paleomargins: Tectonics, v. 33, no. 7, p. 1340–1359, doi:10.1002/2013TC003471.

Clerc, C., A. Lahfid, P. Monié, Y. Lagabrielle, C. Chopin, M. Poujol, P. Boulvais, J. C. Ringenbach, E. Masini, and M. de St Blanquat, 2015, High-temperature metamorphism during extreme thinning of the continental crust: a reappraisal of the North Pyrenean passive paleomargin: Solid Earth, v. 6, no. 2, p. 643–668.

Combes, P.-J., B. Peybernès, and A. F. Leyreloup, 1998, Altérites et bauxites, témoins des marges européenne et ibérique des Pyrénées occidentales au Jurassique supérieur—Crétacé inférieur, à l'ouest de la vallée d'Ossau (Pyrénées-Atlantiques, France): Comptes Rendus de l'Académie des Sciences-Series II, Earth and Planetary Science, v. 327, no. 4, p. 271–278.

Corre, B., Y. Lagabrielle, P. Labaume, S. Fourcade, C. Clerc, and M. Ballèvre, 2016, Deformation associated with mantle exhumation in a distal, hot passive margin environment: New constraints from the Saraillé Massif (Chaînons Béarnais, North-Pyrenean Zone): Comptes Rendus Geoscience, v. 348, no. 3–4, p. 279–289, doi:10.1016/j.crte.2015.11.007.

Corre, B., 2017, La bordure nord de la plaque ibérique à l'Albo-Cénomanien. Architecture d'une marge passive de type ductile (Chaînons Béarnais, Pyrénées Occidentales): Université de Rennes 1, 320p.

Curnelle, R., 1983, Evolution structuro-sédimentaire du Trias et de l'Infra-Lias d'Aquitaine: Bull. Cent. Rech. Explor. Prod. Elf-Aquitaine, v. 7, no. 1, p. 69–99.

Daignières, M., M. Séguret, M. Specht, and E. Team, 1994, The Arzacq-western Pyrenees ECORS deep seismic profile, in Hydrocarbon and petroleum geology of France: Springer, p. 199–208.

Davis, G. H., 1983, Shear-zone model for the origin of metamorphic core complexes: Geology, v. 11, no. 6, p. 342–347, doi:10.1130/0091-7613(1983)11<342:SMFTOO>2.0.CO;2.

Davis, G. A., G. S. Lister, and S. J. Reynolds, 1986, Structural evolution of the Whipple and South mountains shear zones, southwestern united States: Geology, v. 14, no. 1, p. 7–10, doi:10.1130/0091-7613(1986)14<7:SEOTWA>2.0.CO;2.

Debroas, E. J., J. Canérot, and M. Bilotte, 2010, Les brèches d'Urdach, témoins de l'exhumation du manteau pyrénéen dans un escarpement de faille vraconnien-cénomanien inférieur (Zone nord-pyrénéenne, Pyrénées-Atlantiques, France): Géologie de la France, v. 2, p. 53–63.

Decarlis, A., G. Manatschal, I. Haupert, and E. Masini, 2015, The tectono-stratigraphic evolution of distal, hyper-extended magma-poor conjugate rifted margins: Examples from the Alpine Tethys and Newfoundland–Iberia: Marine and Petroleum Geology, v. 68, p. 54–72, doi:10.1016/j.marpetgeo.2015.08.005.

Delfaud, J., and J. Henry, 1967, Evolution des bassins jurassiques dans la zone nord-pyrénéenne occidentale: 64ème congrès AFAS Bordeaux, p. 75–80.

Delfaud, J., and M. Villanova, 1967, Evolution des bassins pendant le Crétacé inférieur dans les Pyrénees occidentales et la bordure de l'Aquitaine: 64ème congrès AFAS Bordeaux, p. 87–92.

Díaz, J., D. Pedreira, M. Ruiz, J. A. Pulgar, and J. Gallart, 2012, Mapping the indentation between the Iberian and Eurasian plates beneath the Western Pyrenees/Eastern Cantabrian Mountains from receiver function analysis: Tectonophysics, v. 570–571, p. 114–122, doi:10.1016/j.tecto.2012.07.005.

Ducasse, L., and P.-C. Vélasque, 1988, Géotraverse dans la partie occidentale des Pyrénées, de l'avant-pays aquitain au bassin de l'Ebre: effet d'une inversion structurale sur l'édification d'une chaîne intracontinentale: Université Paul Cézanne (Aix-Marseille). Faculté des sciences et techniques de Saint-Jérôme, 287 p.

Ducasse, L., P.-C. Vélasque, and J. Muller, 1986, Glissement de couverture et panneaux basculés dans la région des Arbailles (Pyrénées occidentales): Un modèle évolutif crétacé de la marge nord-ibérique à l'Est de la transformante de Pamplona: Comptes rendus de l'Académie des sciences. Série 2, Mécanique, Physique, Chimie, Sciences de l'univers, Sciences de la Terre, v. 303, no. 16, p. 1477–1482.

Ducoux, M., 2017, Structure, thermicité et évolution géodynamique de la Zone Interne Métamorphique des Pyrénées. PhD thesis, University of Orléans, France, 646 p.

Duée, G., Y. Lagabrielle, A. Coutelle, and A. Fortané, 1984, Les lherzolites associées aux Chaînons Béarnais (Pyrénées Occidentales): Mise à l'affleurement anté-dogger et resédimentation albo-cénomanienne: Comptes-rendus des séances de l'Académie des sciences. Série 2, Mécanique-physique, chimie, sciences de l'univers, sciences de la terre, v. 299, no. 17, p. 1205–1210.

Dumont, T., Replumaz, A., Rouméjon, S., Briais, A., Rigo, A., Bouillin, J.-P., 2015. Microseismicity of the Béarn range: Reactivation of inversion and collision structures at the northern edge of the Iberian plate: SEISMICITY AND STRUCTURES IN W. PYRENEES. Tectonics 34, 934–950. https://doi.org/10.1002/2014TC003816

Durand-Wackenheim, C., P. Souquet, and G. Thiébaut, 1981, La brèche d'Errozaté (Pyrénées-Atlantiques): faciès de résedimentation en milieu profond de matériaux d'une plateforme carbonatée crétacée à substratum hercynien: Bulletin de la Société d'Histoire Naturelle de Toulouse, v. 117, p. 87–94.

Engeser, T., and W. Schwentke, 1986, Towards a new concept of the tectogenesis of the Pyrenees: Tectonophysics, v. 129, no. 1–4, p. 233–242, doi:10.1016/0040-1951(86)90253-2.

Etheve, N., 2016, Le bassin de Valence à la frontière des domaines ibérique et méditerranéen: Evolution tectonique et sédimentaire du Mésozoïque au Cénozoïque: Université de Cergy Pontoise, 291 p.

Etheve, N., G. Mohn, D. Frizon de Lamotte, E. Roca, J. Tugend and J. Gomez-Romeu, 2018, Extreme Mesozoic Crustal Thinning in the Eastern Iberia Margin: The Example of the Columbrets basin (Valencia Trough): Tectonics, n° 37, doi: 10.1002/2017TC004613.

Fabriès, J., J.-P. Lorand, and J.-L. Bodinier, 1998, Petrogenetic evolution of orogenic lherzolite massifs in the central and western Pyrenees: Tectonophysics, v. 292, no. 1–2, p. 145–167.

Fabriès, J., J.-P. Lorand, J.-L. Bodinier, and C. Dupuy, 1991, Evolution of the Upper Mantle beneath the Pyrenees: Evidence from Orogenic Spinel Lherzolite Massifs: Journal of Petrology, v. Special_Volume, no. 2, p. 55–76, doi:10.1093/petrology/Special_Volume.2.55.

Ferrer, O., M. P. A. Jackson, E. Roca, and M. Rubinat, 2012, Evolution of salt structures during extension and inversion of the Offshore Parentis basin (Eastern Bay of Biscay): Geological Society, London, Special Publications, v. 363, no. 1, p. 361–380, doi:10.1144/SP363.16.

Ferrer, O., E. Roca, B. Benjumea, J. A. Muñoz, N. Ellouz, and MARCONI Team, 2008, The deep seismic reflection MARCONI-3 profile: Role of extensional Mesozoic structure during the Pyrenean contractional deformation at the eastern part of the Bay of Biscay: Marine and Petroleum Geology, v. 25, no. 8, p. 714–730, doi:10.1016/j.marpetgeo.2008.06.002.

Fixari, G., 1984, Stratigraphie, faciès et dynamique tecto-sédimentaire du flysch albien (flysch noir et poudingues de mendibelza) dans la région de Mauléon-Tardets (Pyrénées Atlantiques): Université Paul Sabatier de Toulouse (Sciences), 197 p.

Fortané, A., G. Duée, Y. Lagabrielle, and A. Coutelle, 1986, Lherzolites and the western "Chaînons Béarnais" (French Pyrenees): Structural and paleogeographical pattern: Tectonophysics, v. 129, no. 1–4, p. 81–98, doi:10.1016/0040-1951(86)90247-7.

Fournier, E., 1905, Études géologiques sur la partie occidentale de la chaîne des Pyrénées entre la vallée d'Aspe et celle de la Nive: Bulletin de la Société Géologique de France, v. 5, p. 699–723.

Fournier, E., 1908, Etudes sur les Pyrénées Basques:(Basses-Pyrénées, Navarre et Guipuzcoa): Bulletin des services de la carte géologique de la France et des topographies souterraines, v. 18, no. 121, p. 491–548.

Galharague, J., 1966, Étude géologique de la zone de relais des massifs d'Igounce et de Mendibelza (Basses-Pyrénées).

Geoffroy, L., B. Le Gall, M. A. Daoud, and M. Jalludin, 2014, Flip-flop detachment tectonics at nascent passive margins in SE Afar: Journal of the Geological Society, v. 171, no. 5, p. 689–694, doi:10.1144/jgs2013-135.

Gillard, M., J. Autin, G. Manatschal, D. Sauter, M. Munschy, and M. Schaming, 2015, Tectonomagmatic evolution of the final stages of rifting along the deep conjugate Australian-Antarctic magma-poor rifted margins: Constraints from seismic observations: Australian-Antarctic margins evolution: Tectonics, v. 34, no. 4, p. 753–783, doi:10.1002/2015TC003850.

Golberg, J. M., and A. F. Leyreloup, 1990, High temperature-low pressure Cretaceous metamorphism related to crustal thinning (Eastern North Pyrenean Zone, France): Contributions to Mineralogy and Petrology, v. 104, no. 2, p. 194–207, doi:10.1007/BF00306443.

Golberg, J.-M., and H. Maluski, 1988, Données nouvelles et mise au point sur l'âge du métamorphisme pyrénéen: Comptes rendus de l'Académie des sciences. Série 2, v. 306, no. 6, p. 429–435.

Gong, Z., C. G. Langereis, and T. A. T. Mullender, 2008, The rotation of Iberia during the Aptian and the opening of the Bay of Biscay: Earth and Planetary Science Letters, v. 273, no. 1–2, p. 80–93, doi:10.1016/j.epsl.2008.06.016.

Grandjean, G., 1992, Mise en évidence des structures crustales dans une portion de chaîne et de leur relation avec les bassins sédimentaires. Application aux Pyrénées occidentales au travers du Projet ECORS Arzacq-Pyrénées: Université des Sciences et Techniques du Languedoc, 291 p.

Grandjean, G., 1994, Etude des structures crustales dans une portion de chaîne et de leur relation avec les bassins sédimentaires. Application aux Pyrénées occidentales: Bull. Cent. Rech. Explor. Prod. Elf Aquitaine, v. 18, no. 2, p. 391–420.

Gubler, Y., M. Casteras, R. Ciry, and P. Lamare, 1947, Sur l'âge des poudingues dits de Mendibelza dans le bassin du Laurhibar, au SE de Mendive (Basse Pyrénées: Compte Rendu de la Société Géologique de France, v. 17, p. 329–330.

Hall, C. A., and J. A. Johnson, 1986, Apparent western termination of the North Pyrenean fault and tectonostratigraphic units of the western north Pyrenees, France and Spain: Tectonics, v. 5, no. 4, p. 607–627.

Hart, N. R., D. F. Stockli, and N. W. Hayman, 2016, Provenance evolution during progressive rifting and hyperextension using bedrock and detrital zircon U-Pb geochronology, Mauléon basin, western Pyrenees: Geosphere, v. 12, no. 4, p. 1166–1186, doi:10.1130/GES01273.1.

Hart, N. R., D. F. Stockli, L. L. Lavier, and N. W. Hayman, 2017, Thermal evolution of a hyperextended rift basin, Mauléon basin, western Pyrenees: Thermal evolution of hyperextended rift: Tectonics, doi:10.1002/2016TC004365.

Haupert, I., G. Manatschal, A. Decarlis, and P. Unternehr, 2016, Upper-plate magma-poor rifted margins: Stratigraphic architecture and structural evolution: Marine and Petroleum Geology, v. 69, p. 241–261, doi:10.1016/j.marpetgeo.2015.10.020.

Heddebaut, C., 1973, Etudes géologiques dans les massifs paléozoïques basques: Université des Sciences et Techniques de Lille, 263 p.

Heddebaut, C., 1967, Observations tectoniques sur le massif des Aldudes (Basses-Pyrénées): CR Som. Soc. Géol. de France, fasc, v. 7, p. 280–281.

Henry, J., G. Zolnaï, G. Le Pochat, and C. Mondeilh, 1987, Carte géologique de la France au 1/50 000: feuille d'Orthez, Orléans, France.

Huismans, R. S., and C. Beaumont, 2003, Symmetric and asymmetric lithospheric extension: Relative effects of frictional-plastic and viscous strain softening: Journal of Geophysical Research: Solid Earth, v. 108, no. B10, doi:10.1029/2002JB002026.

Huismans, R. S., and C. Beaumont, 2008, Complex rifted continental margins explained by dynamical models of depth-dependent lithospheric extension: Geology, v. 36, no. 2, p. 163, doi:10.1130/G24231A.1.

Huismans, R. S., and C. Beaumont, 2011, Depth-dependent extension, two-stage breakup and cratonic underplating at rifted margins: Nature, v. 473, no. 7345, p. 74–78, doi:10.1038/nature09988.

Huismans, R. S., and C. Beaumont, 2014, Rifted continental margins: The case for depth-dependent extension: Earth and Planetary Science Letters, v. 407, p. 148–162, doi:10.1016/j.epsl.2014.09.032.

James, V., 1998, La plate-forme carbonatée ouest-pyrénéenne au jurassique moyen et supérieur stratigraphie séquentielle, stades d'évolution, relations avec la subsurface en aquitaine méridionale: Toulouse, Université Paul Sabatier (Sciences), 351 p.

James, V., and J. Canérot, 1999, Diapirisme et structuration post-triasique des Pyrénées occidentales et de l'Aquitaine méridionale (France): Eclogae Geologicae Helvetiae, v. 92, p. 63–72.

Jammes, S., G. Manatschal, L. Lavier, and E. Masini, 2009, Tectono-sedimentary evolution related to extreme crustal thinning ahead of a propagating ocean: Example of the western Pyrenees: Tectonics, v. 28, no. 4, doi:10.1029/2008TC002406.

Jammes, S., G. Manatschal, and L. Lavier, 2010a, Interaction between prerift salt and detachment faulting in hyperextended rift systems: The example of the Parentis and Mauléon basins (Bay of Biscay and western Pyrenees): AAPG Bulletin, v. 94, no. 7, p. 957–975, doi:10.1306/12090909116.

Jammes, S., C. Tiberi, and G. Manatschal, 2010b, 3D architecture of a complex transcurrent rift system: The example of the Bay of Biscay–Western Pyrenees: Tectonophysics, v. 489, no. 1–4, p. 210–226, doi:10.1016/j.tecto.2010.04.023.

Johnson, J. A., and C. A. Hall, 1989, Tectono-stratigraphic model for the Massif D'Igountze-Mendibelza, western Pyrenees: Journal of the Geological Society, v. 146, no. 6, p. 925–932, doi:10.1144/gsjgs.146.6.0925.

Karner, G. D., N. W. Driscoll, and D. H. N. Barker, 2003, Synrift regional subsidence across the West African continental margin: the role of lower plate ductile extension: Geological Society, London, Special Publications, v. 207, no. 1, p. 105–129, doi:10.1144/GSL.SP.2003.207.6.

Labaume, P., F. Meresse, M. Jolivet, and A. Teixell, 2016, Exhumation sequence of the basement thrust units in the west-central Pyrenees. Constraints from apatite fission track analysis: Geogaceta, v. 60, p. 11–14.

Lagabrielle, Y., and J.-L. Bodinier, 2008, Submarine reworking of exhumed sub-continental mantle rocks: field evidence from the Lherz peridotites, French Pyrenees: Cretaceous exhumation of pyrenean mantle: Terra Nova, v. 20, no. 1, p. 11–21, doi:10.1111/j.1365-3121.2007.00781.x.

Lagabrielle, Y., C. Clerc, A. Vauchez, A. Lahfid, P. Labaume, B. Azambre, S. Fourcade, and J.-M. Dautria, 2016, Very high geothermal gradient during mantle exhumation recorded in mylonitic marbles and carbonate breccias from a Mesozoic Pyrenean palaeomargin (Lherz area, North Pyrenean Zone, France): Comptes Rendus Geoscience, v. 348, no. 3–4, p. 290–300, doi:10.1016/j.crte.2015.11.004.

Lagabrielle, Y., P. Labaume, and M. de Saint Blanquat, 2010, Mantle exhumation, crustal denudation, and gravity tectonics during Cretaceous rifting in the Pyrenean realm (SW Europe): Insights from the geological setting of the lherzolite bodies: Tectonics, v. 29, no. 4, doi:10.1029/2009TC002588.

Lamare, P., 1939, La série paléozoïque du massif du Baygoura et de la vallée de la Nive; ses relations avec les terrains secondaires environnants: Bulletin de la Société Géologique de France, v. 9, p. 163–184.

Lamare, P., 1944, La terminaison orientale du massif des Aldudes, aux environs d'Arnéguy, révision de la feuille de Saint-Jean-Pied-de-Port au 1/80 000: Bulletin de la Carte Géologique de France, v. 45, no. 216, p. 265–305.

Lamare, P., 1946, Les formations détritiques crétacées du massif de Mendibelza: Bulletin de la Socète Géologique de France, v. 16, no. 5, p. 265–312.

Lamare, P., 1941, Remarques sur la structure du Pays Basques: Bulletin de la Societe Geologique de France, v. 11, p. 97–112.

Lamare, P., 1948, Sur le passage latéral des faciès détritiques grossiers du Crétacé du massif de Mendibelza aux faciès schisto-gréseux classiques de l'Albien des Pyrénées: Comptes rendus de l'Académie des sciences, v. 226, no. 8, p. 683–685.

Larrasoaña, J. C., J. M. Parés, H. Millán, J. del Valle, and E. L. Pueyo, 2003, Paleomagnetic, structural, and stratigraphic constraints on transverse fault kinematics during basin inversion: The Pamplona Fault (Pyrenees, north Spain): Tectonics, v. 22, no. 6, doi:10.1029/2002TC001446.

Laverdière, J.-W., 1930, Les formations paléozoïques de la vallée du Laurhibar: Mém. Soc. Géol. Nord. Lille, v. 55, p. 156–157.

Lavier, L. L., and G. Manatschal, 2006, A mechanism to thin the continental lithosphere at magma-poor margins: Nature, v. 440, no. 7082, p. 324–328, doi:10.1038/nature04608.

Le Pichon, X., J. Bonnin, U. J. Francheteau and J. C. Sibuet, 1971, Une hypothèse d'évolution tectonique du golfe de Gascogne. In : Histoire structurale du golfe de Gascogne, ed Technip., IV, 11, p. 1-44.

Le Pochat, G., C. Bolthenhagen, M. Lenguin, S. Lorsignol, and C. Thibault, 1976, Carte géologique de France au 1/50 000: Mauléon-licharre, Orléans, France.

Le Pochat, G., C. Heddebaut, M. Lenguin, S. Lorsignol, P. Souquet, J. Muller, and P. Roger, 1978, Carte Géologique de France au 1/50 000: St Jean Pied de Port, Orléans, France.

Lenoble, J.-L., 1992, Les plates-formes carbonatées ouest-pyrénéennes du dogger à l'Albien, stratigraphie séquentielle et évolution géodynamique: Université Paul Sabatier de Toulouse (Sciences), 395 p.

Lister, G. S., M. A. Etheridge, and P. A. Symonds, 1986, Detachment faulting and the evolution of passive continental margins: Geology, v. 14, no. 3, p. 246–250, doi:10.1130/0091-7613(1986)14<246:DFATEO>2.0.CO;2.

Lucas, C., 1985, Le grès rouge du versant nord des Pyrénées: essai sur la géodynamique de dépôts continentaux du permien et du trias: 267 p.

Magné, 1948, Nouvelles observations relatives à l'âge des poudingues du pic Errozaté (massif de Mendibelza): Compte Rendu de la Société Géologique de France, p. 163–165.

Malod, J., A, 1982, Comparaison de l'évolution des marges continentales au nord et au sud de la péninsule ibérique. PhD thesis ('Thèse d'état'), University of Paris, France, 235 p.

Manatschal, G., 2004, New models for evolution of magma-poor rifted margins based on a review of data and concepts from West Iberia and the Alps: International

Journal of Earth Sciences, v. 93, no. 3, doi:10.1007/s00531-004-0394-7.

Manatschal, G., A. Engström, L. Desmurs, U. Schaltegger, M. Cosca, O. Müntener, and D. Bernoulli, 2006, What is the tectono-metamorphic evolution of continental break-up: The example of the Tasna Ocean–Continent Transition: Journal of Structural Geology, v. 28, no. 10, p. 1849–1869, doi:10.1016/j.jsg.2006.07.014.

Masini, E., G. Manatschal, G. Mohn, J.-F. Ghienne, and F. Lafont, 2011, The tectono-sedimentary evolution of a supra-detachment rift basin at a deep-water magma-poor rifted margin: the example of the Samedan basin preserved in the Err nappe in SE Switzerland: Tectono-sedimentary evolution of a supra-detachment rift basin: basin Research, v. 23, no. 6, p. 652–677, doi:10.1111/j.1365-2117.2011.00509.x.

Masini, E., G. Manatschal, G. Mohn, and P. Unternehr, 2012, Anatomy and tectono-sedimentary evolution of a rift-related detachment system: The example of the Err detachment (central Alps, SE Switzerland): Geological Society of America Bulletin, v. 124, no. 9–10, p. 1535–1551, doi:10.1130/B30557.1.

Masini, E., G. Manatschal, and G. Mohn, 2013, The Alpine Tethys rifted margins: Reconciling old and new ideas to understand the stratigraphic architecture of magma-poor rifted margins: Sedimentology, v. 60, no. 1, p. 174–196, doi:10.1111/sed.12017.

Masini, E., G. Manatschal, J. Tugend, G. Mohn, and J.-M. Flament, 2014, The tectono-sedimentary evolution of a hyper-extended rift basin: the example of the Arzacq–Mauléon rift system (Western Pyrenees, SW France): International Journal of Earth Sciences, v. 103, no. 6, p. 1569–1596, doi:10.1007/s00531-014-1023-8.

Mattauer, M., 1985, Présentation d'un modèle lithosphérique de la chaîne des Pyrénées: Comptes-rendus des séances de l'Académie des sciences. Série 2, Mécanique-physique, chimie, sciences de l'univers, sciences de la terre, v. 300, no. 2, p. 71–74.

McCaig, A. M., 1988, Deep geology of the Pyrenees: Nature, v. 331, p. 480–481.

McKenzie, D., 1978, Some remarks on the development of sedimentary basins: Earth and Planetary Science Letters, v. 40, no. 1, p. 25–32, doi:10.1016/0012-821X(78)90071-7.

Merle, J.-M., 1974, Recherches sur les relations paléogéographiques et structurales entre les massifs basques au sud de Saint-Jean-Pied-de-Port (Pyrénées occidentales): Université Paul Sabatier de Toulouse (Sciences), 142 p.

Mirouse, R., 1967, Le Dévonien des Pyrénées occidentales et centrales (France): International Symposium on the Devonian System, v. I, p. 153–170.

Mohn, G., Manatschal, G., Beltrando, and M., Haupert, I., 2014, The role of rift-inherited hyper-extension in Alpine-type orogens: Terra Nova, v. 26, p. 347–353, doi: 10.1111/ter.12104.

Montigny, R., B. Azambre, M. Rossy, and R. Thuizat, 1986, K-Ar Study of cretaceous magmatism and metamorphism in the Pyrenees: Age and length of rotation of the Iberian Peninsula: Tectonophysics, v. 129, no. 1, p. 257–273, doi:10.1016/0040-1951(86)90255-6.

Mouthereau, F., P.-Y. Filleaudeau, A. Vacherat, R. Pik, O. Lacombe, M. G. Fellin, S. Castelltort, F. Christophoul, and E. Masini, 2014, Placing limits to shortening evolution in the Pyrenees: Role of margin architecture and implications for the Iberia/Europe convergence: Tectonics, v. 33, no. 12, p. 2014TC003663, doi:10.1002/2014TC003663.

Muller, J., and P. Roger, 1977, L'Evolution structurale des Pyrénées (Domaine central et occidental) Le segment hercynien, la chaîne de fond alpine: Géologie alpine, v. 53, no. 2, p. 149–191.

Muñoz, J. A., 1992, Evolution of a continental collision belt: ECORS-Pyrenees crustal balanced cross-section, in K. R. McClay, ed., Thrust Tectonics: Springer Netherlands, p. 235–246, doi:10.1007/978-94-011-3066-0_21.

Olivet, J. L., 1996, La cinématique de la plaque ibérique: Bull. Cent. Rech. Explor. Prod. Elf Aquitaine, v. 20, no. 1, p. 131–195.

Paris, J.-P., 1964, Étude d'une partie du massif d'Igounce et de ses abords septentrionaux en Barétous et Basse-Soule: Faculté des Sciences de l'Université de Toulouse, 121 p.

Pedreira, D., J. A. Pulgar, J. Gallart, and M. Torné, 2007, Three-dimensional gravity and magnetic modeling of crustal indentation and wedging in the western Pyrenees-Cantabrian Mountains: Journal of Geophysical Research, v. 112, no. B12, doi:10.1029/2007JB005021.

Péron-Pinvidic, G., G. Manatschal, T. A. Minshull, and D. S. Sawyer, 2007, Tectono-sedimentary evolution of the deep Iberia-Newfoundland margins: Evidence for a complex breakup history: Tectonics, v. 26, no. 2, p. 1–19, doi:10.1029/2006TC001970.

Péron-Pinvidic, G., G. Manatschal, E. Masini, E. Sutra, J. M. Flament, I. Haupert, and P. Unternehr, 2015, Unravelling the along-strike variability of the Angola–Gabon rifted margin: a mapping approach: Geological Society, London, Special Publications, v. 438, no. 1, p. 49–76, doi:10.1144/SP438.1.

Pinet, B., L. Montadert, and ECORS Scientific Party, 1987, Deep seismic reflection and refraction profiling along the Aquitaine shelf (Bay of Biscay): Geophysical Journal International, v. 89, no. 1, p. 305–312, doi:10.1111/j.1365-246X.1987.tb04423.x.

Poignant, A., 1965, Révision du Crétacé inférieur en Aquitaine occidentale et méridionale: Université Paris, 317 p.

Puigdefàbregas, C., and P. Souquet, 1986, Tecto-sedimentary cycles and depositional sequences of the Mesozoic and Tertiary from the Pyrenees: Tectonophysics, v. 129, no. 1–4, p. 173–203.

Rat, P. et al., 1983, Vue sur le Cretacé basco-cantabrique et nord-ibérique: Une marge et son arriere-pays, ses environnements sedimentaires: Memoires geologiques Universite de Dijon, v. 9, p. 191.

Ravier, J., 1957, Le métamorphisme des terrains secondaires des Pyrénées: Université, Faculté des Sciences.

Razin, P., 1989, Evolution tecto-sédimentaire alpine des Pyrénées basques à l'ouest de la transformante de Pamplona, Province du Labourd: Université Bordeaux 3, 464 p.

Richard, P., 1986, Structure et évolution alpine des massifs paléozoïques du Labourd (Pays Basque français): Éditions du Bureau de recherches géologiques et minières, 374 p.

Roca, E., J. A. Muñoz, O. Ferrer, and N. Ellouz, 2011, The role of the Bay of Biscay Mesozoic extensional structure in the configuration of the Pyrenean orogen: Constraints from the MARCONI deep seismic reflection survey: Tectonics, v. 30, no. 2, doi:10.1029/2010TC002735.

Roest, W. R and S. P. Srivastava., 1991, Kinematics of the plate boundaries between Eurasia, Iberia ,and Africa in the North Atlantic from the Late Cretaceous to the present: Geology, v. 19, p. 613–616.

Rosenbaum, G., G. S. Lister, and C. Duboz, 2002, Relative motions of Africa, Iberia and Europe during Alpine orogeny: Tectonophysics, v. 359, no. 1–2, p. 117–129, doi:10.1016/S0040-1951(02)00442-0.

Rossi, P., A. Cocherie, C. M. Fanning, and Y. Ternet, 2003, Datation U-Pb sur zircons des dolérites tholéiitiques pyrénéennes (ophites) à la limite Trias–Jurassique et relations avec les tufs volcaniques dits « infra-liasiques » nord-pyrénéens: Comptes Rendus Geoscience, v. 335, no. 15, p. 1071–1080, doi:10.1016/j.crte.2003.09.011.

Roux, J.-C., 1983, Recherches stratigraphiques et sédimentologiques sur les flyschs crétacés pyrénéens au sud d'Oloron (Pyrénées Atlantiques): Université Paul Sabatier de Toulouse (Sciences), 224 p.

Sauter, D., M. Cannat, S. Rouméjon, M. Andreani, D. Birot, A. Bronner, D. Brunelli, J. Carlut, A. Delacour, and V. Guyader, 2013, Continuous exhumation of mantle-derived rocks at the Southwest Indian Ridge for 11 million years: Nature Geoscience, v. 6, no. 4, p. 314.

Séguret, M., and M. Daignières, 1986, Crustal scale balanced cross-sections of the Pyrenees; discussion: Tectonophysics, v. 129, no. 1, p. 303–318, doi:10.1016/0040-1951(86)90258-1.

Serrano, O., J. Delmas, F. Hanot, R. Vially, J.-P. Herbin, P. Houel, and B. Tourlière, 2006, Le bassin d'Aquitaine: valorisation des données sismiques, cartographie structurale et potentiel pétrolier: Bureau de Recherche Géologique et minière, 245 p.

Sibuet, J.-C., S. P. Srivastava, and W. Spakman, 2004, Pyrenean orogeny and plate kinematics: Journal of Geophysical Research: Solid Earth, v. 109, no. B8, p. B08104, doi:10.1029/2003JB002514.

Souquet, P., 1988, Evolución del margen noribérico en los Pyreneos durante el Mesozoico: Rev. Soc. Geol. España, v. 1, p. 349–356.

Souquet, P., 1967, Le Crétacé supérieur Sud-Pyrénéen, en Catalogne, Aragon et Navarre: E. Privat.

Souquet, P., B. Peybernes, M. Bilotte, and E.-J. Debroas, 1977, La chaîne alpine des Pyrénées: Géologie alpine, v. 53, no. 2, p. 193–216.

Souquet, P. et al., 1985, Le groupe du Flysch noir (albo-cénomanien) dans les Pyrénées: Bull Cent. Rech Exlpo-Prod Elf-Aquitaine Pau, v. 9, p. 183–252.

Spencer, J. E., 1984, Role of tectonic denudation in warping and uplift of low-angle normal faults: Geology, v. 12, no. 2, p. 95–98, doi:10.1130/0091-7613(1984)12<95:ROTDIW>2.0.CO;2.

Svartman Dias, A. E., L. L. Lavier, and N. W. Hayman, 2015, Conjugate rifted margins width and asymmetry: The interplay between lithospheric strength and thermomechanical processes: Journal of Geophysical Research: Solid Earth, v. 120, no. 12, p. 2015JB012074, doi:10.1002/2015JB012074.

Teixell, A., 1993, Coupe géologique du massif d'Igountze: implications sur l'évolution structurale de la bordure sud de la zone nord-pyrénéenne occidentale: Comptes rendus de l'Académie des sciences. Série 2, Mécanique, Physique, Chimie, Sciences de l'univers, Sciences de la Terre, v. 316, no. 12, p. 1789–1796.

Teixell, A., 1996, The Anso transect of the southern Pyrenees: basement and cover thrust geometries: Journal of the Geological Society, v. 153, no. 2, p. 301–310, doi:10.1144/gsjgs.153.2.0301.

Teixell, A., 1998, Crustal structure and orogenic material budget in the west central Pyrenees: Tectonics, v. 17, no. 3, p. 395–406, doi:10.1029/98TC00561.

Teixell, A., P. Labaume, and Y. Lagabrielle, 2016, The crustal evolution of the west-central Pyrenees revisited: Inferences from a new kinematic scenario: Comptes Rendus Geoscience, v. 348, no. 3–4, p. 257–267, doi:10.1016/j.crte.2015.10.010.

Tirel, C., J.-P. Brun, and E. Burov, 2004, Thermomechanical modeling of extensional gneiss domes: Geological Society of America Special Papers, v. 380, p. 67–78, doi:10.1130/0-8137-2380-9.67.

Tugend, J., G. Manatschal, N. J. Kusznir, E. Masini, G. Mohn, and I. Thinon, 2014, Formation and deformation of hyperextended rift systems: Insights from rift domain mapping in the Bay of Biscay-Pyrenees: Tectonics, v. 33, no. 7, p. 1239–1276, doi:10.1002/2014TC003529.

Tugend, J., G. Manatschal, N. J. Kusznir, and E. Masini, 2015a, Characterizing and identifying structural domains at rifted continental margins: application to the Bay of Biscay margins and its Western Pyrenean fossil remnants: Geological Society, London, Special Publications, v. 413, no. 1, p. 171–203, doi:10.1144/SP413.3.

Tugend, J., G. Manatschal, and N. J. Kusznir, 2015b, Spatial and temporal evolution of hyperextended rift systems: Implication for the nature, kinematics, and timing of the Iberian-European plate boundary: Geology, v. 43, p. 15–18, doi: 10.1130/G36072.1.

Unternehr, P., G. Peron-Pinvidic, G. Manatschal, and E. Sutra, 2010, Hyper-extended crust in the South Atlantic: in search of a model: Petroleum Geoscience, v. 16, no. 3, p. 207–215, doi:10.1144/1354-079309-904.

Vacherat, A., F. Mouthereau, R. Pik, M. Bernet, C. Gautheron, E. Masini, L. Le Pourhiet, B. Tibari, and A. Lahfid, 2014, Thermal imprint of rift-related processes in orogens as recorded in the Pyrenees: Earth Planet. Sci. Lett.,408, 296–306, doi:10.1016/j.epsl.2014.10.014.

Vergés, J., H. Millán, E. Roca, J. A. Muñoz, M. Marzo, J. Cirés, T. D. Bezemer, R. Zoetemeijer, and S. Cloetingh, 1995, Eastern Pyrenees and related foreland basins: pre-, syn- and post-collisional crustal-scale cross-sections: Marine and Petroleum Geology, v. 12, no. 8, p. 903–915, doi:10.1016/0264-8172(95)98854-X.

Viennot, P., and Y. Kieh, 1928, Observations pétrographiques dans le massif cristallin du Labourd (Basses Pyrénées): Bull. Soc. Géol. Fr, v. 28, p. 369–379.

Viers, G., 1956, Observations structurales sur les Pyrénées occidentales: Bull. Soc. géol. France, v. 6, no. 6, p. 713–726.

Wang, Y., 2017, High resolution imaging of lithospheric structures by full waveform inversion of short period teleseismic P waves: Université Toulouse 3 Paul Sabatier (UT3 Paul Sabatier), 244 p.

Wang, Y. et al., 2016, The deep roots of the western Pyrenees revealed by full waveform inversion of teleseismic P waves: Geology, v. 44, no. 6, p. 475–478, doi:10.1130/G37812.1.

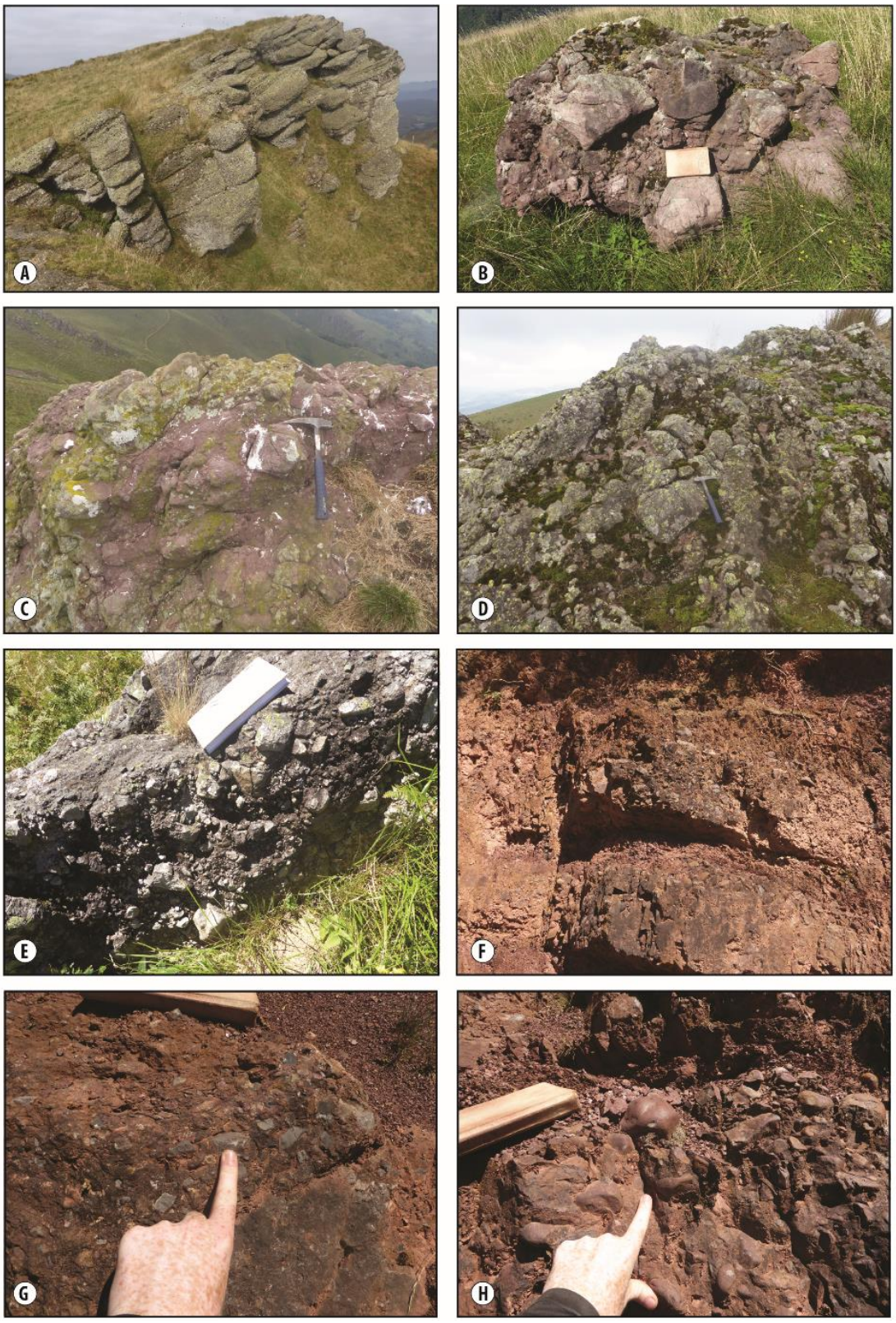
Wernicke, B., 1981, Low-angle normal faults in the basin and Range Province: nappe tectonics in an extending orogen: Nature, v. 291, no. 5817, p. 645–648, doi:10.1038/291645a0.

Wernicke, B., 1985, Uniform-sense normal simple shear of the continental lithosphere: Canadian Journal of Earth Sciences, v. 22, no. 1, p. 108–125, doi:10.1139/e85-009.

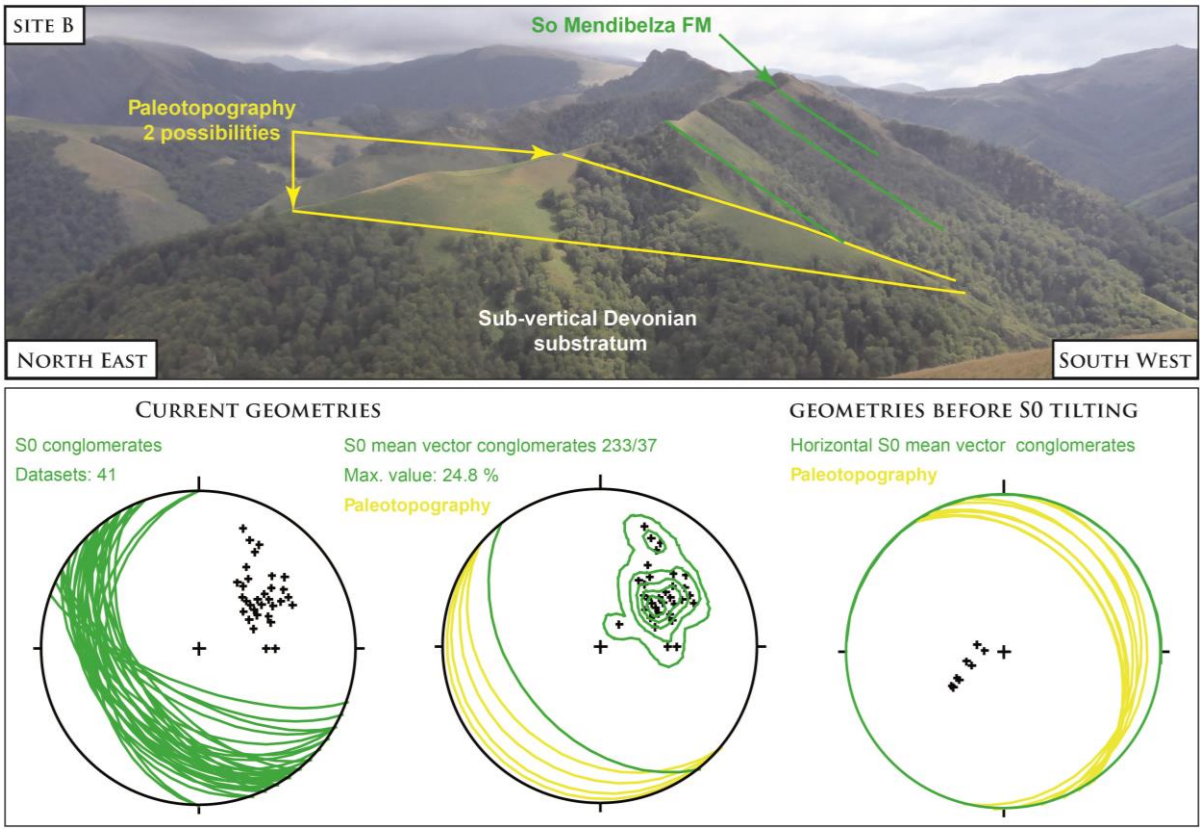
Wernicke, B., and B. C. Burchfiel, 1982, Modes of extensional tectonics: Journal of Structural Geology, v. 4, no. 2, p. 105–115, doi:10.1016/0191-8141(82)90021-9.

Wernicke, B., and G. J. Axen, 1988, On the role of isostasy in the evolution of normal fault systems: Geology, v. 16, no. 9, p. 848–851, doi:10.1130/0091-7613(1988)016<0848:OTROII>2.3.CO;2.

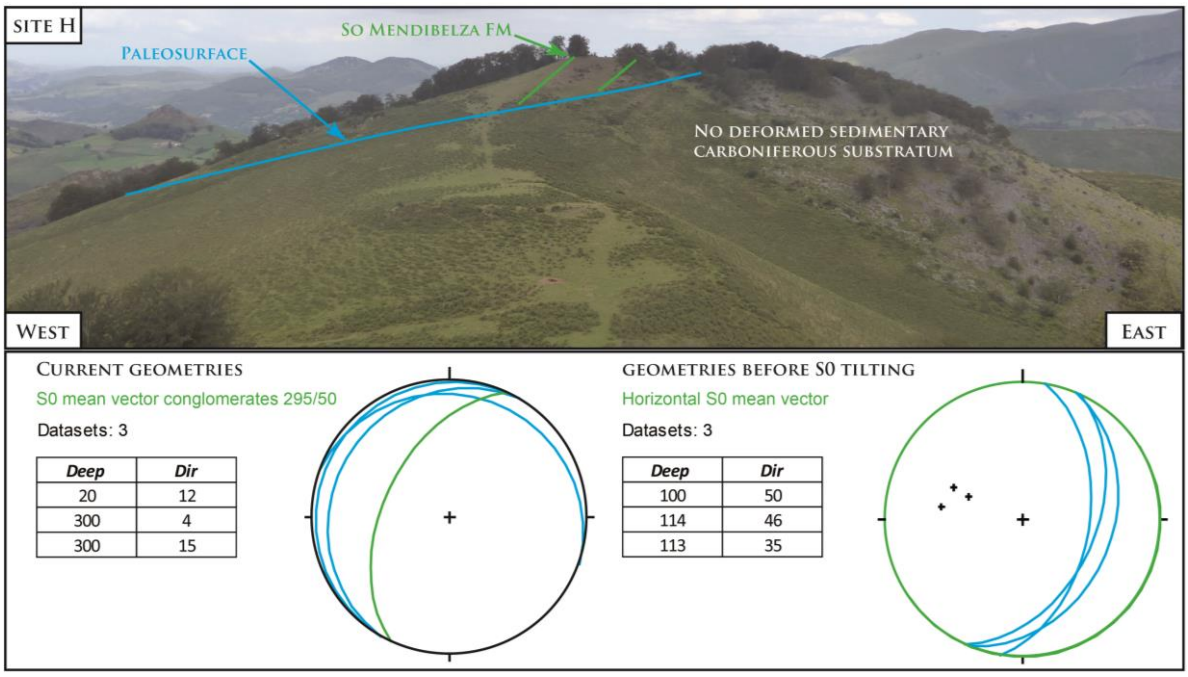
Eléments supplémentaires



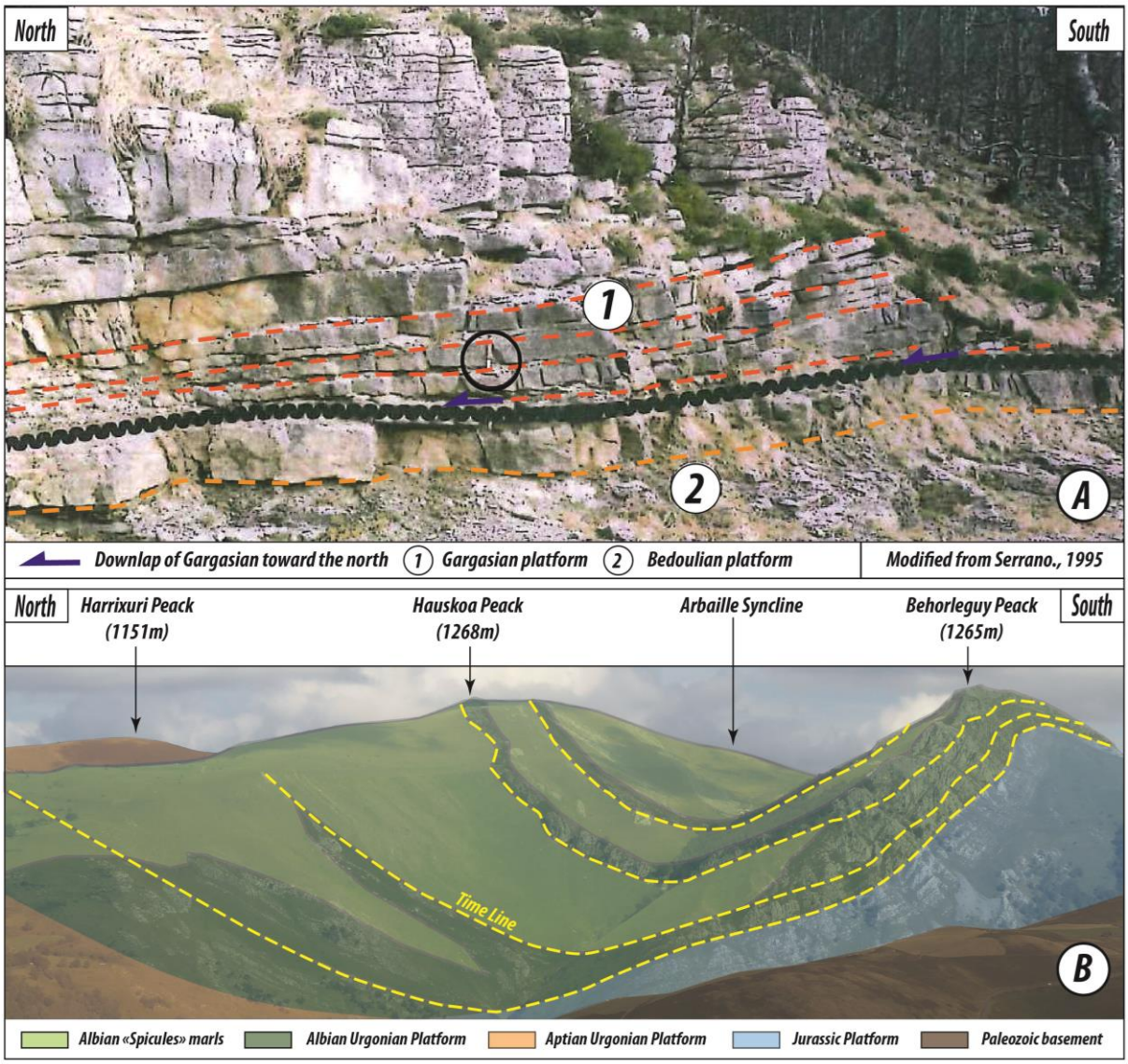
ES. 1. (A) Poudingues de Mendibelza ; **(B-D)** Brèches d'Esterençuby, d'âge Albien inférieur, remaniant les grès rouges continentaux de la base du Trias. Ces brèches discontinues sont localisées à la base de la Mégaséquence 1 de la Formation de Mendibelza définie par Souquet et al. (1985) ; **(E)** Cataclasites affectant le socle méta-sédimentaire paléozoïque du massif d'Esterençuby ; **(F-H)** Séries continentales permiennes du centre du massif d'Esterençuby, précédemment cartées comme albiennes et scellant la déformation cassante affectant le socle méta-sédimentaires (ES. 1E).



ES. 2. Vue panoramique NE-SW de la paléo-surface B. Les poudingues de Mendibelza reposent en onlap vers le sud sur le socle paléozoïque méta-sédimentaire et présentent un pendage moyen de l'ordre de N155°E, 45°SW (traits verts). La surface d'onlap matérialisée en jaune plonge, avec un angle plus faible que les poudingues de Mendibelza, en direction du sud-ouest. Une fois les Poudingues de Mendibelza remis à l'horizontale, la paléosurface jaune est caractérisée par un plongement de 10-30° vers le NE, au cours de l'Albien.



ES. 3. Vue panoramique de la paléo-surface H. Les poudingues de Mendibelza reposent en onlap vers le sud sur le socle paléozoïque méta-sédimentaire et présentent un pendage moyen de l'ordre de N205°E, 50°ENE (traits verts). La surface d'onlap matérialisée en bleu plonge, avec un angle plus faible que les poudingues de Mendibelza, en direction de l'ENE. Une fois les Poudingues de Mendibelza remis à l'horizontale, la paléosurface bleu est caractérisée par un plongement de 35-50° vers l'est, au cours de l'Albien.



ES. 4. (A) Point bars dans les séries carbonatées du Gargasien montrant des terminaisons en downlap vers le nord sur les séries bédouliennes sous-jacentes, dans la partie nord occidentale du massif des Arbailles. **(B)** Discordance progressive des séries de l'Albien inférieur basal, mettant en évidence un taux de subsidence différentiel plus important en direction du nord, se traduisant par une rétrogradation de la plateforme carbonatée à Mélobésiées en direction du sud et le développement de marnes à spicules au nord. Cette discordance progressive de faible angle résulte de l'activation d'une ride diapirique au cours de la sédimentation.

Chapitre 3.2

Synthèse de l'enregistrement sédimentaire Albien-Cénomanien du bassin de Mauléon / Saint-Jean-de-Luz : glissement gravitaire polyphasé de la couverture sur le sel du Trias (Pyrénées occidentales)

Chapitre 3.2. Review of the Mauléon / Saint-Jean-de-Luz basin Albian - Cenomanian sedimentary record: salt-controlled polyphase cover gliding during hyperextension (Western Pyrenees)

Sommaire

Résumé étendu p. 167

Abstract p. 169

1. Introduction p. 169

2. Geological settings p. 170

2.1. Structural units of the western Pyrenees Iberian rift margin p. 170

2.2. The Mesozoic Mauléon / Saint-Jean-de-Luz sedimentary evolution p. 171

3. Methodology p. 173

4. Lithostratigraphic units p. 174

4.1. Mendibelza Formation p. 174

4.2. Saint Palais Formation p. 175

4.3. Bustince Formation (New) p. 175

4.4. Zugarramurdi Formation p. 181

4.5. Flysch de Mixe Formation p. 182

4.6. Amotz Formation p. 183

4.7. Saint-Etienne-de-Baïgorry Formation p. 184

4.8. Errozaté Formation p. 184

4.9. Flysch à Silex Formation p. 186

4.10. Calcaires des Cañons Formation p. 189

4.11. Calcaires de Sare Formation p. 191

5. Boreholes observations p. 191

5.1. Ainhice-1 borehole p. 191

5.2. Ustaritz-1 borehole p. 191

6. Tectono-sedimentary evolution of the Iberian rift margin p. 193

6.1. Aldudes-Ainhice transect p. 193

6.2. Cinco-Villas /Espelette transect p. 195

6.3. Ursuya-Arberoue transect p. 195

6.4. Bidarray-Hiruraitzeta transect p. 197

7. Discussion p. 199

7.1. basinward gravity-driven cover gliding along salt décollement level: a synrift polyphasic process p. 199

7.2. Impact of inherited transfer zone on the 3D distribution of gravity-driven cover gliding p. 200

7.3. basin's morphology evolution throughout the rift period p. 200

8. Conclusions p. 201

Acknowledgements p. 201

References p. 201

Résumé étendu

Les Pyrénées sont caractérisées par la présence d'un niveau de décollement majeur correspondant aux évaporites et argiles du Trias, ainsi qu'aux marnes sus-jacentes du Lias. Le bassin hyper-étiré de Mauléon / Saint-Jean-de-Luz (Pyrénées occidentales) est connu pour avoir subi une phase de glissement gravitaire de la couverture prérift au cours du rifting crétacé, résultant de l'activation de ce décollement. Cependant, l'initiation de ce processus et sa réponse sédimentaire sont peu contraints et font donc l'objet de cette étude.

Ce travail se base sur une importante synthèse bibliographique des formations et des membres des séries albo-cénomaniennes le long de la marge ibérique du bassin de Mauléon / Saint-Jean-de-Luz, couplée à de nouvelles données complémentaires. Dix-huit unités lithostratigraphiques ont été considérées parmi lesquelles trois sont ici décrites pour la première fois : Formation de Bustince ; Membre d'Aguerréborda et Membre d'Hiruraitzeta. Des études complémentaires sur quatre unités ont été réalisées pour affiner leurs géométries, âges et faciès sédimentaires : Membre de Bonloc, Formation des Calcaires des Cañons, Membre d'Irey et Membre d'Honto.

Le long de la marge ibérique du bassin de Mauléon, l'enregistrement sédimentaire et l'analyse des faciès mettent en évidence une morphologie complexe de la transition plateforme / bassin de l'Albien au Cénomanien. A l'Albien inférieur, l'amorce de la tectonique cassante dans le bassin de Mauléon se traduit par le développement d'une transition très rapide entre les dépôts gravitaires grossiers de bas de pente de Mendibelza déposés au pied de la marge ibérique et les turbidites de faible densité sédimentant plus au nord dans le bassin. En effet, les Poudingues de Mendibelza sont globalement dominés par des processus d'avalanche, passant vers le nord à des turbidites relativement distales (Formation de Saint-Palais). L'absence de courants turbiditiques hyper-concentrés entre ces deux formations suggère une efficacité médiocre du transport. Cette dernière est directement liée à l'importante rupture de pente le long de la marge ibérique, empêchant le transport des sédiments sur une distance significative.

A la transition entre le domaine occidental de Saint-Jean-de-Luz et celui plus oriental de Mauléon, le système de transport évolue à la fin de l'Albien supérieur, comme en témoigne le dépôt de turbidites hyper-concentrées préservées au sein de la formation du Flysch de Mixe. Ces dernières attestent d'un système de transport plus efficace que celui des Poudingues de Mendibelza. Les brèches de pied de pente d'Amotz passent à des faciès marneux, hémipélagiques à courant de turbidité faiblement dilué, dans lesquels sont intercalés des faciès granulaires de haute densité.

Le Cénomanien enregistre le développement de deux systèmes turbiditiques radicalement différents. La plus grande partie des dépôts est dominée par les turbidites carbonatées formant le Flysch à Silex. Cette formation est caractérisée par le développement de turbidites de faible densité alimentées depuis la plateforme carbonatée européenne. A la base de cette série turbiditique, s'intercalent, des turbidites silicoclastiques plus matures, dominées par des courants de haute densité et des courants hyper-concentrés (Membres d'Aguerréborda et d'Hiruraitzeta). Ces membres attestent d'un système de transport efficace le long d'une pente sous-marine relativement peu inclinée.

L'enregistrement sédimentaire Albien à Cénomanien de la marge ibérique de ce bassin souligne le caractère diachrone du glissement de la couverture qui semble se produire tout au long de la phase d'hyperextension crétacée. Chaque phase de glissement de la couverture peut être rattachée à un épisode de structuration majeur du bassin. Le premier stade de glissement de la couverture prend place à l'Albien inférieur et est synchrone de l'amorce de la phase d'amincissement en cisaillement simple, affectant la croûte continentale du bassin de Mauléon (détachement de Saint-Palais). Le développement du détachement de Saint-Palais est tenu responsable du « roll-over » de la marge ibérique du bassin de Mauléon en direction du NE. Cet épisode majeur dans la structuration du bassin engendre le glissement de la couverture mésozoïque des unités de la marge ibérique en direction du domaine hyper-étiré, le long des domaines des Aldudes, de Mendibelza et d'Igountze.

La seconde phase de glissement est datée de l'Albien supérieur et coïncide avec l'ouverture du bassin de Mauléon / Saint-Jean-de-Luz, en direction de l'ouest. Cet épisode est responsable de la

dénudation du socle de l'unité du Cinco-Villas. Ceci pourrait s'expliquer par le développement d'une structure tectonique responsable du basculement du domaine du Cinco-Villas en direction du nord, engendrant le glissement de sa couverture prérift dans cette même direction. Cependant, la qualité médiocre des affleurements et la déformation pyrénéenne rendent difficile la définition de la géométrie précise de cet éventuel système de détachement.

Pour finir, le développement du détachement à vergence nord de Lakhoura, au Cénomanien moyen, est synchrone du glissement de la couverture prerift des domaines de l'Ursuya et de Bidarray, matérialisant la bordure occidentale du bassin de Mauléon. Cet épisode de glissement est responsable de la dénudation sous-marine des granulites de l'Ursuya dont l'exhumation est, quant à elle, permienne.

L'enregistrement sédimentaire du glissement de la couverture a mis en évidence que ce processus est suivi de la formation de dépôts gravitaires grossiers (brèches, conglomérats, olistostromes et klippes sédimentaires) remaniant, dans un premier temps, la couverture prérift du toit du décollement puis le socle dénudé de la marge ibérique (mur du décollement). Les turbidites intercalées avec ces dépôts grossiers permettent de dater de manière relative le glissement de la couverture et donc les phases de structuration du bassin.

Chapitre 3.2. Review of the Mauléon / Saint-Jean-de-Luz basin Albian - Cenomanian sedimentary record: salt-controlled polyphase cover gliding during hyperextension (Western Pyrenees)

Saspiturry, N., Razin, P., Issautier, B., Lasseur, E., Andrieu, S., and Serrano, O., **in prep**, Review of the Mauléon / Saint-Jean-de-Luz basin Albian - Cenomanian sedimentary record: salt-controlled polyphase cover gliding during hyperextension (Western Pyrenees): It will be submitted **to Orogen special publication in *Bulletin de la Société Géologique de France***.

Abstract

Hyperextended rifts often record massive gravity-driven processes inducing the basinward gliding of the prerift sedimentary cover along salt décollement level. In this work, we propose to precise and to refine the schedule of detachment faulting and rift margin tilting by studying the sedimentary record associated to those gravity-driven cover gliding. Observations were realized on the Mauléon / Saint-Jean-de-Luz rift basin, which develop in response to continental crust thinning during the Albian-Cenomanian hyperextension affecting the North Pyrenean Zone. In the meantime, its southern Iberian rift margin suffers gravity-driven gliding of the sedimentary cover. Stratigraphical and sedimentological analysis evidence that this process is polyphasic and takes place during the Early Cretaceous hyperextension. In fact, three main stages of basinward cover gliding have been identified: (1) Early Albian, (2) Late Albian and (3) Middle Cenomanian. This process initiates, in Early Albian time, during the onset of simple shear thinning affecting the continental lithosphere in the Mauléon basin. Each sliding phase is followed by the deposition of deep marine olistostrome. They firstly rework the glided Mesozoic cover and in a second time the newly denudated Paleozoic to Triassic substratum of the Iberian margin. Successive gliding corresponds to the Early Albian Saint Palais and Middle Cenomanian Lakhoura detachments and the Late Albian westward widening of the rift basin. This study brings new piece of work to better characterize and assess the tectono-sedimentary record of hyperextended rift system.

1. Introduction

Knowledge on passive margins have significantly increased during the last decades, partly due to oil & gas exploration and International Ocean Drilling Programs on the Atlantic hyperextended margins such as Angola and Brazil (Karner et al., 2003; Contrucci et al., 2004; Moulin et al., 2005, 2010; Karner and Gambôa, 2007; Aslanian et al., 2009; Unternehr et al., 2010) Iberia and Newfoundland (Boillot et al., 1987, 1989; Driscoll et al., 1995; Manatschal et al., 2001; Péron-Pinvidic et al., 2007; Péron-Pinvidic and Manatschal, 2009; Reston, 2009; Pérez-Gussinyé, 2013; Haupert et al., 2016) or central Norway and East Groenland (Weigel et al., 1995; Kodaira et al., 1998; Mjelde et al., 2001, 2008; Reston, 2007; Péron-Pinvidic et al., 2012). Similarly, the description of fossil margins in the Alps (Lemoine et al., 1987; Froitzheim and Manatschal, 1996; Manatschal and Nievergelt, 1997; Manatschal et al., 2006, 2011; Beltrando et al., 2014; Mohn et al., 2014; Decarlis et al., 2015) conducted researchers to propose new models detailing the mechanisms responsible for sub-continental mantle denudation and exhumation, thanks to detachement faults characterization. Consequently, hyperextended rifts are well described from a structural and geometry point of view (see Péron-Pinvidic et al., 2013 for a review), but the associated sedimentary record is still poorly addressed, although some studies describe the sedimentary infill of distal supra-detachment basins (Masini et al., 2011, 2012; Ribes et al., 2019). Gravity-driven processes are commonly known in hyperextended rifts and are characterized by the formation of raft tectonics and basinward gliding of the prerift-postrift sedimentary cover along salt décollement level (Duval et al., 1992; Brun and Fort, 2011). The initiation of this gravity-driven process is controlled by the thickness variation of the sedimentary pile, the presence of salt décollement (Lundin, 1992; Liro and Coen, 1995; Rouby et al., 2002) and the basinward tilting of the proximal margin (Fort et al., 2004b, 2004a; Cobbold and Szatmari, 1991; Demercian et al., 1993; Gaullier et al., 1993). One major area of improvement remains the sequential

evolution of hyperextended rift system through time, since most of the models detailing the geometry of these basins only consider the final evolutional stages. Consequently, the onset and duration of a detachement fault is rarely known. In this work, through the analysis of the sedimentary record resulting from the basinward cover gliding, we try to better assess the timing of rift margin tilting and synrift detachement faults onset.

In this perspective, the North Pyrenean rift system is a key analog for the analysis of such processes as it suffered hyperextension during Early Cretaceous (Lagabrielle and Bodinier, 2008; Jammes et al., 2009; Lagabrielle et al., 2010, 2016; Clerc et al., 2012, 2015; Clerc and Lagabrielle, 2014; Masini et al., 2014; Tugend et al., 2015; Teixell et al., 2016, 2018; Espurt et al., 2019). More specifically, the Mauléon / Saint-Jean-de-Luz hyperextended basin (Western Pyrenees) spanned gravity-driven cover sliding during the Cretaceous rifting stage (Bouquet, 1986; Ducasse et al., 1986; Lagabrielle et al., 2010, 2019; Corre et al., 2016; Teixell et al., 2016; Asti et al., 2019; Saspiturry et al., 2019). However, the timing and causes of this process is steal unclear. In this scope, we analyze and restore the tectono-sedimentary evolution of four proximal rift margin - hyperextended deep basin transects across the Iberian rift margin. We thus discuss the significance, geometry and timing of the gravity cover gliding through the following interrogations: (i) Is this process polyphase? (ii) Is there a link between cover gliding and extensional tectonic stages?

2. Geological setting

2.1. Structural units of the western Pyrenees Iberian rift margin

The Pyrenees result from the inversion of the Early Cretaceous rift basins, during the Santonian to Oligocene (Puigdefàbregas and Souquet, 1986; Olivet, 1996). These basins developed along a roughly N110° direction, which is in part responsible for the current trend of the Pyrenean realm (Souquet et al., 1977). The western Pyrenees are composed of three major structural domains corresponding to the South-Pyrenean Zone, the Axial Zone and the North-Pyrenean Zone **(Fig. 1)** (Souquet et al., 1975). In its western part, the North Pyrenean Zone corresponds to the closure of the Early Cretaceous Mauléon / Saint-Jean-de-Luz rift basin (Ducasse and Vélasque, 1988). The eastern Mauléon domain is separated from the western Saint-Jean-de-Luz one by the so-called N20° Pamplona crustal discontinuity (Richard, 1986; Razin, 1989; Claude, 1990; Larrasoaña et al., 2003; Pedreira et al., 2007). This basin is currently bordered to the north by the North Pyrenean Frontal Thrust and to the south by the Lakhoura Thrust system responsible for a lithosphere pop-up structure (**Fig. 1**; Daignières et al., 1994; Teixell et al., 2016; Saspiturry et al., 2019c).

The Massif Basques are composed of four structural units: Labourd, Cinco-Villas, Aldudes and Mendibelza-Igountze Units (Lamare., 1936) being part of the inverted southern margin of the Mauléon Saint-Jean-de-Luz basin. The Labourd unit is composed of the Ursuya, Baigoura and Artzamendi sub-units (Lamare., 1936). In this work we redefine some of this structural units in order to better describe the Early Cretaceous tectono-sedimentary evolution of this inverted margin.

Both Cinco-Villas and Aldudes Units consists of Ordovician to Carboniferous sedimentary rocks (Laverdière 1930; Lamare 1944; Heddebaut 1967; Muller & Roger 1977; **Figs. 2 & 3**). They respectively correspond to the inverted southern margin of the Saint-Jean-de-Luz and Mauléon rift domains.

The Bidarray and Ursuya Units are located (in-) between the Cinco-Villas and Aldudes Units and were previously considered as part of the Labourd Unit by Lamare., 1936. The Bidarray Unit is a singular domain of the Massif Basques as it is a Permian rift basin developed along a metamorphic core complex corresponding to the Ursuya Unit, which upwelled lower crust granulites facies (Saspiturry et al., 2019b). The boundary between the Bidarray and Ursuya Units is defined by the east-west trending Louhossoa shear zone (**Fig 2**, Lamare, 1931; Heddebaut, 1973; Le Pochat et al., 1978; Saspiturry et al., 2019b). The Permian continental facies of the Bidarray basin (Lucas., 1985) unconformably overlain the Paleozoic basement while the lower Triassic (Bundtsandstien facies) rests unconformably upon the Permian deposits. The Bidarray Unit lacks the post-Triassic sedimentary cover **(Fig. 2)**. The Ursuya Unit (Viennot and Kieh, 1928; Lamare, 1939; Vielzeuf, 1984) is mainly

composed of Precambrian to Ordovician metasediments (Boissonnas et al. 1974) affected by HT-LP metamorphism that reached granulite facies during Early-Mid Permian times (Vielzeuf 1984, Hart et al., 2016, Vacherat et al., 2017, Lemirre, 2018). The Bidarray and Ursuya Units are aligned along the N-S Pamplona Fault and materialized the southwestern edge of the Mauléon rift domain.

The Saint-Etienne-de-Baïgorry Unit is made up of Late Albian to Early Cenomanian marls and breccias (Merle. 1974). This narrow unit is pinched (in-)between two southward-directed thrusts, separating it from the Aldudes unit to the south and the Saint-Jean-Pied-de-Port unit to the north **(Fig. 2)**. The Saint-Jean-Pied-de-Port Unit integrates the previous Baigoura subunit being part of the Labourd Unit (Lamare., 1936). It is characterized by a Paleozoic sedimentary basement, overlain by southward dipping Late Triassic continental deposits **(Fig. 2)**. Highly deformed bodies of diabase with ophitic structure (ophites), shales and micritic limestones (Lucas., 1985), and more rarely Early-Mid Jurassic deposits end this succession (Le Pochat et al., 1978). Saint-Jean-Pied-de-Port Unit have been interpreted as an Early to Mid-Cenomanian southward tilted block resulting from the development of the synrift Lakhoura detachment (Hart et al., 2017; Saspiturry et al., 2019a). The northern edge of this unit is bounded by the North Arbailles Fault, an Early Albian - Mid Cenomanian synrift normal fault (Saspiturry et al., 2019a), which delimitates it from the Saint Palais unit **(Fig. 2)**.

Eastward, the Mendibelza-Igountze Unit is slightly thrusted onto the Aldudes, Saint-Jean-Pied-de-Port and Saint-Etienne-de-Baïgorry western Units **(Fig. 2)**. It corresponds to Devonian-Carboniferous meta-sediments (Paris, 1964; Mirouse, 1967) unconformably overlain by Albian to Late Cretaceous very coarse-grained gravity flow deposits conglomerates (Souquet et al., 1985) and Late Cretaceous breccias (Durand-Wackenheim et al., 1981). To the north of the Mendibelza Unit, the Arbailles Unit is composed of a Jurassic to Early Cretaceous carbonate sequence folded as a syncline **(Fig. 2)**. It is bounded to the North and the South in its northern and southern edges respectively by the North Arbailles and South Arbailles thrusts (e.g. Saspiturry et al., 2019a).

To the North of the Basques massifs, the North-Pyrenean Cretaceous flysch domain is characterized by the development of the Albian to Early Cenomanian Black flysch group (e.g. Souquet et al., 1985). To the west of the N20° Iholdy transfer zone, only the Late Albian to Early Cenomanian mega-sequence III of the Black Flysch group is present (Souquet et al. 1985; Razin. 1989; Claude. 1990). This pattern implies a diachronous westward opening of the basin. In the Saint-Jean-de-Luz domain, these deposits are southward thrusted over the Cinco-Villas Unit **(Figs. 2 & 3)** along the Amotz thrust corresponding to the reactivation of a Late Albian normal fault (Razin. 1989; **Fig. 3**). The synrift deposits are overlain with a thick succession of Late Cretaceous calcareous-turbidites. In two localities, the Jurassic to Aptian prerift carbonate sequence is exposed below the synrift sequence. To the north-west of the Saint-Jean-Pied-de-Port Unit, the Osses Late Triassic shale and evaporites are overlain by the Aguerreborda Jurassic to Barremian limestones, while to the north of the Ursuya Unit, this prerift sequence is exposed along the Arberoue back-thrust **(Fig. 2)**.

2.2. The Mesozoic Mauléon / Saint-Jean-de-Luz sedimentary evolution

The Mesozoic sedimentary record of this basin initiates on Late Triassic times with the development of continental clastics deposits (Buntsandstein) grading to marine carbonate (Muschelkalk) and finally to marine shales and evaporates, (Keuper) (Curnelle, 1983; Rossi et al., 2003). The Keuper evaporates sharply influences the Early Cretaceous rift basins geometry (Duretz et al., 2019) and serves as a decollement layer for Cretaceous detachments and Tertiary thrusts (e.g. Teixell., 1998, 2016, 2018). During the Jurassic, the Pyrenean domain is characterized by the development of a widespread stable carbonate platform (Peybernès., 1976; Lenoble, 1992; James, 1998; Canérot. 2008). The top of the platform is affected by a major exposure stage testified by the development of bauxites lying unconformably on Middle to Late Jurassic formations and onlapped by Barremian to Late Aptian deposits (Canérot et al., 1999). This Jurassic – Cretaceous unconformity is much pronounced southward and westward as Barremian to Albian carbonate deposits onlap towards the south-west a more and more

truncated Jurassic sequence. From Barremian to Early Albian time, the future Mauléon basin records the development of a shallow restricted carbonate platform (Cassou, 1968; Arnaud-Vanneau et al., 1979; Martin-Closas and Peybernès, 1987; Serrano, 1995; Canérot, 2008) while the future Saint-Jean-de-Luz basin is emerged (Razin., 1989).

The Mauléon / Saint-Jean-de-Luz trough forms during the Albian to Cenomanian times in response to simple shear thinning (Claude, 1990; Johnson & Hall, 1989; Jammes et al., 2009, Lagabrielle et al., 2010, Masini et al., 2014). During Early Albian time, the Mauléon domain spans the development of the south- dipping Saint Palais detachment (Saspiturry et al., 2019a). At that time, the Iberian margin is characterized by the deposition of the Mendibelza conglomerates (**Fig. 4**; Boirie., 1981) corresponding to syn-rift base-of-slope coarse-grained gravity-flow deposits. They grade northward to distal siliciclastic turbidites (Marnes de St Palais and Flysch de Mixe Formations, **Fig. 4**; Souquet et al., 1985). In Late Albian time, the rift system propagates westward in the Saint-Jean-de-Luz domain, forming the Mauléon / Saint-Jean-de-Luz rift basin. This western basin extension is characterized by the development of the Zugarramurdi deltaic system, the Amotz deep basin gravity breccias and the Flysch de Mixe deposits (Souquet et al., 1985; Razin., 1989).

On the conjugated European margin, a shallow carbonate platform passing in a distal position to the Saint Palais spicules marls develops throughout the Albian (e.g. Saspiturry et al., 2019a and references therein). Following the Late Albian individualization of Mauléon / Saint-Jean-de-Luz rift basin, the Mauléon domain records the onset of the Middle Cenomanian north- dipping Lakhoura detachment (Saspiturry et al., 2019a). This structure will represent the Iberian margin platform / basin transition during all the Late Cretaceous. From Cenomanian to Santonian time, the Mauléon / Saint-Jean-de-Luz basin is characterized by postrift subsidence and the development of a carbonate platform on the conjugate margins. Along the Iberian margin, the Calcaires des Canyons (Souquet., 1967; Merle.,1974) and the Calcaires de Sarre Formations (Razin, 1989) unconformably rest upon the folded Paleozoic meta-sediments. These proximal deposits mainly grade towards the deep basin to calcareous turbidites whose first sequence corresponds to the Flysch à Silex Formation (Boissonnas et al., 1974; Le Pochat et al., 1978).

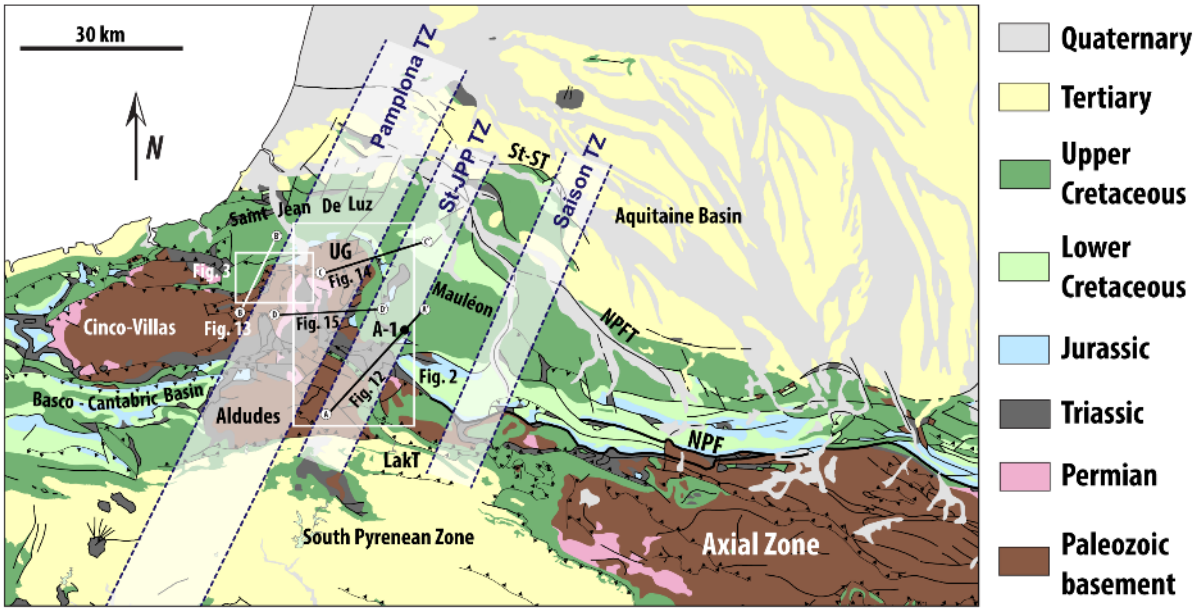


Fig. 1. Geological maps of the western Pyrenees modified from the 1 / 400 000 BRGM geological map of Pyrenees (Baudin and Barnolas, 2008). A-1: Ainhice-1 well; NPF: North Pyrenean Fault; NPFT: North Pyrenean Frontal Thrust; UG: Ursuya granulites; LakT: Lakhoura thrusts; St-ST: Sainte-Suzanne thrust; AA': Aldudes-Ainhice transect (Fig. 12); BB': Cinco-Villas/Espelette transect (Fig. 13); CC': Ursuya-Arberoue transect (Fig. 14) and DD': Bidarray-Hiruraitzeta transect (Fig. 15); TZ: transfer zone; St-JPP TZ: Saint-Jean-Pied-de-Port transfer zone.

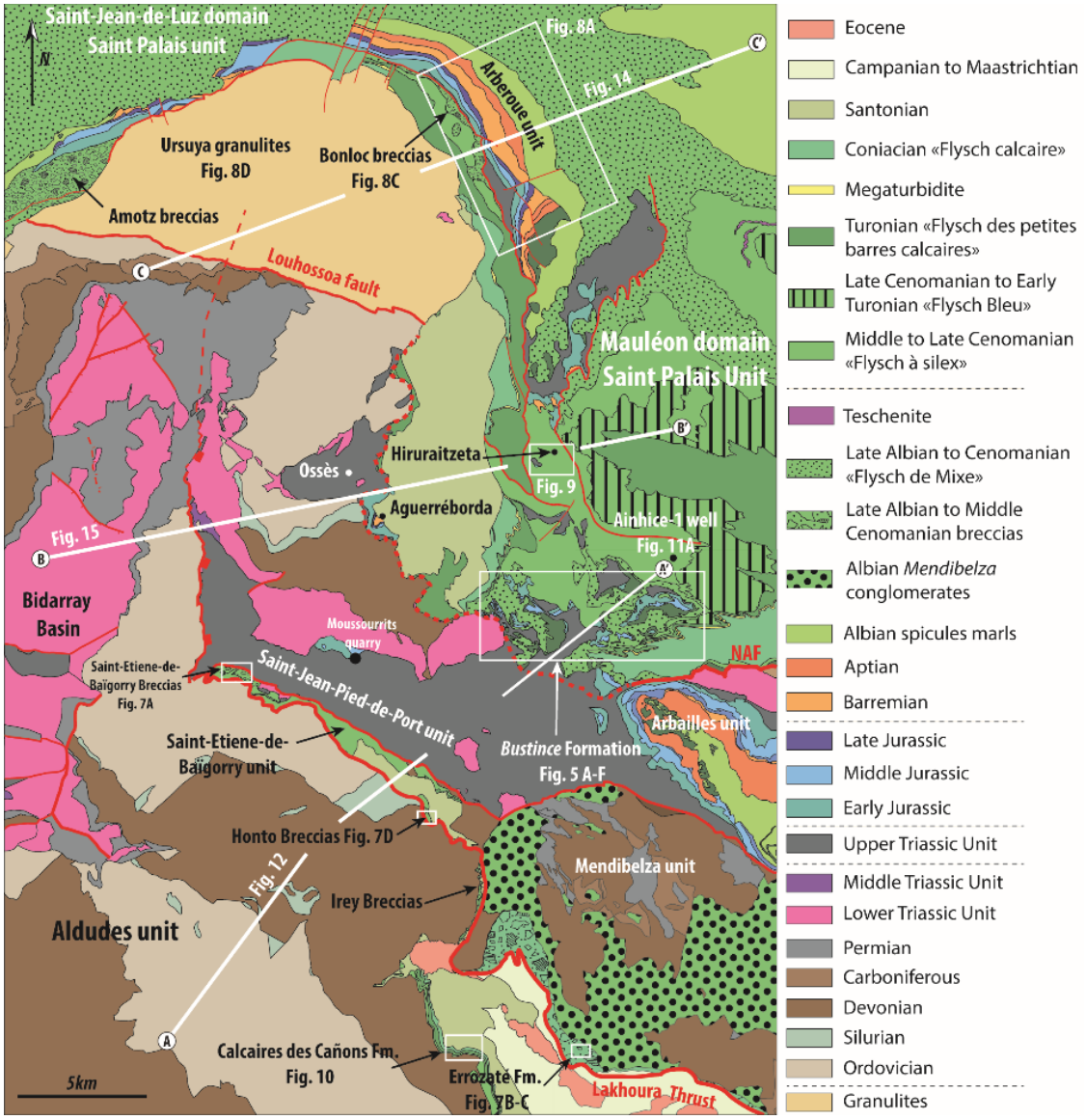


Fig. 2. Geological map showing the main units of the Mauléon Iberian rift margin: Mendibelza, Arbailles, Aldudes, Saint-Etienne-de-Baïgorry, Saint-Jean-Pied-de-Port, Bidarray, Saint-Palais, Ursuya and Arberoue (modified from Casteras et al., 1971; Kieken and Thibault, 1972; Boissonnas et al., 1974; Le Pochat et al., 1976, 1978; Henry et al., 1987).

3. Methodology

This study is based on the detailed analysis of the Early Albian to Cenomanian sedimentary sequence in the Mauléon / Saint-Jean-de-Luz basin. 18 lithostratigraphic units are described below, 3 of them for the first time. A detailed facies analysis was performed for these 3 new units on the field. Supplementary studies were realized on the Bonloc Member, Calcaires des Canyons Formation, Irey member and Honto breccias to refine their geometry, age and facies association. Two boreholes were analyzed and interpreted (Ainhice-1 in Mauléon Basin and Ustaritz-1 wells in Saint-Jean de Luz Basin). 9 lithostratigraphy units have been described using bibliography: (1) Razin. (1989) for the Saint-Jean-de-Luz area, (2) Souquet. (1967), Merle. (1974), Boirie. (1981), Fixari. (1984), Souquet et al. (1985), Bouquet. (1986), and Claude. (1990) for the Mauléon area and (3) geological maps (Casteras et al., 1971; Kieken and Thibault, 1972; Boissonnas et al., 1974; Le Pochat et al., 1976, 1978; Henry et al., 1987). Stratigraphic correlation of the different units studied is based mainly on biostratigraphic markers and facies similarity. These formations have been correlated in order to reconstruct the successive depositional profiles along the southern margin of the Mauléon / Saint-Jean-de-Luz basin from Albian to Cenomanian. It allows to discuss the timing and the causes of the syn-sedimentary deformation such as extensional tectonic, gravitary tectonic or diapirism.

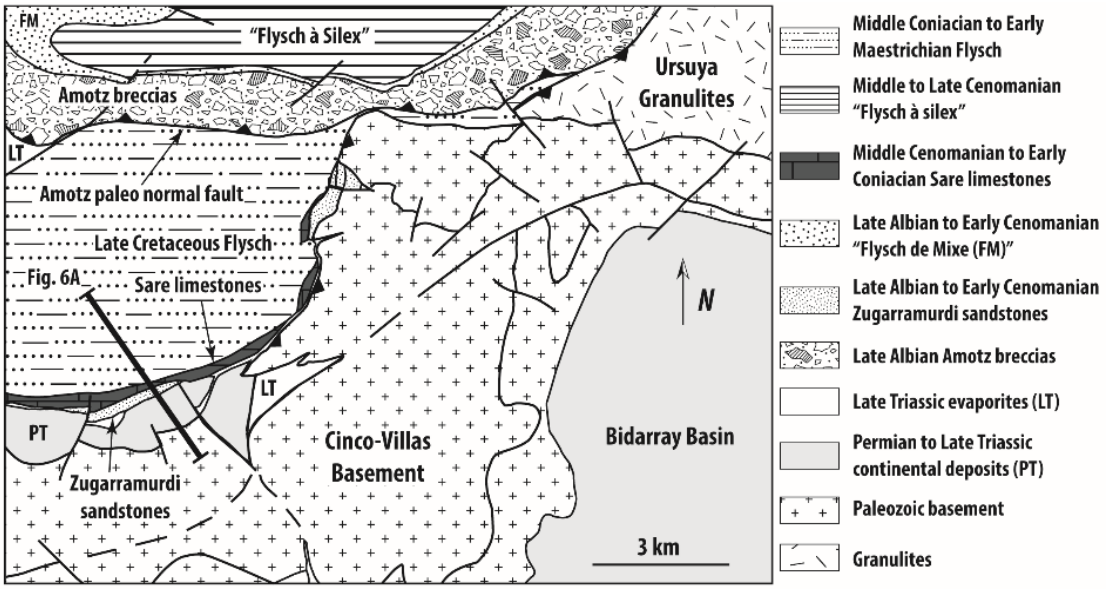


Fig. 3. Geological maps of the Cinco-Villas unit showing its Cretaceous sedimentary cover (modified from Razin, 1989).

4. Lithostratigraphic units

The following part gives a "sedimentary description", the age and the stratigraphical boundaries of each lithostratigraphical unit **Table 1** and a chronostratigraphic chart **(Fig. 4)** summarize all these characteristics.

4.1. Mendibelza Formation

Lithostratigraphy description. Defined by Souquet (1985), Fixari. (1984) and Boirie (1981), the Mendibelza Formation consist of a thick conglomeratic succession which clasts are essentially of Paleozoic (Devonian-Carboniferous) and Triassic age (sandstone and ophites). In very rare case, Albian limestone are reworked (Calcaires à Mélobésiées) **(Tab. 1)**.

Regional aspect. The Mendibelza formation crops out within the Mendibelza and Igountze units materializing the inverted Iberian necking zone of the former Mauléon hyperextended rift basin (Saspiturry et al., 2019). This formation is characterized by a thickness that can locally reach more than 2 000 m thick (Boirie et Souquet., 1982; Souquet et al., 1985).

Boundaries. The base of the Mendibelza Formation corresponds to a stratigraphic contact in onlap on the Paleozoic meta-sediments of the Mendibelza unit. Upward, this formation is onlap by the Cenomanian to Santonian Errozaté Formation (c.f. 4.8.).

Age. The stratigraphic correlation of the Mendibelza Formation evidenced an Albian age for this formation (Boirie, 1981; Fixari, 1984; Frey, 1968; Gubler et al., 1947; Johnson and Hall, 1989; Lamare, 1948, 1946; Magné, 1948; Souquet et al., 1985; **Tab. 1**).

Former facies sedimentology analysis Boirie & Souquet. (1982) defined eight sedimentary facies on the Mendibelza Formation the: (F1) chaotic Breccias, (F2) unorganized conglomerates, (F3) stratified and imbricated conglomerates, (F4) fining-up conglomerates interbedded with medium to coarse-grained sandstones with planar laminations at the base and current ripples on top, (F5) massive or laminated sandstone with dune and mega-ripples, (F6) silty sandstones, (F7) dark pelites, (F8) olistolithes. Most of the clasts range between 10cm to 1m, and can in very rare case reach gigantic size. The F1, F2 and F8 facies materialize immature sedimentary accumulation and correspond to gravity sedimentation influenced by a steep underwater slope evidencing the basinward collapse of the Albian Iberian rift margin. These mass-transport deposits generally followed by highly concentrated turbidity currents corresponding to the conglomeratic proximal channelized flows forming the facies F3 and F4. The channels overflows are responsible for the development of more distal deposits controlled by tractive mechanisms at the end of the channeled systems (F5 and F6 facies). The F7 facies results from decantation mechanism. These coarse deposits have been interpreted as base-of-slope turbiditic sequences fed by not preserved fan deltaic systems, reworking the Paleozoic meta-sedimentary basement (Saspiturry et al., 2019a).

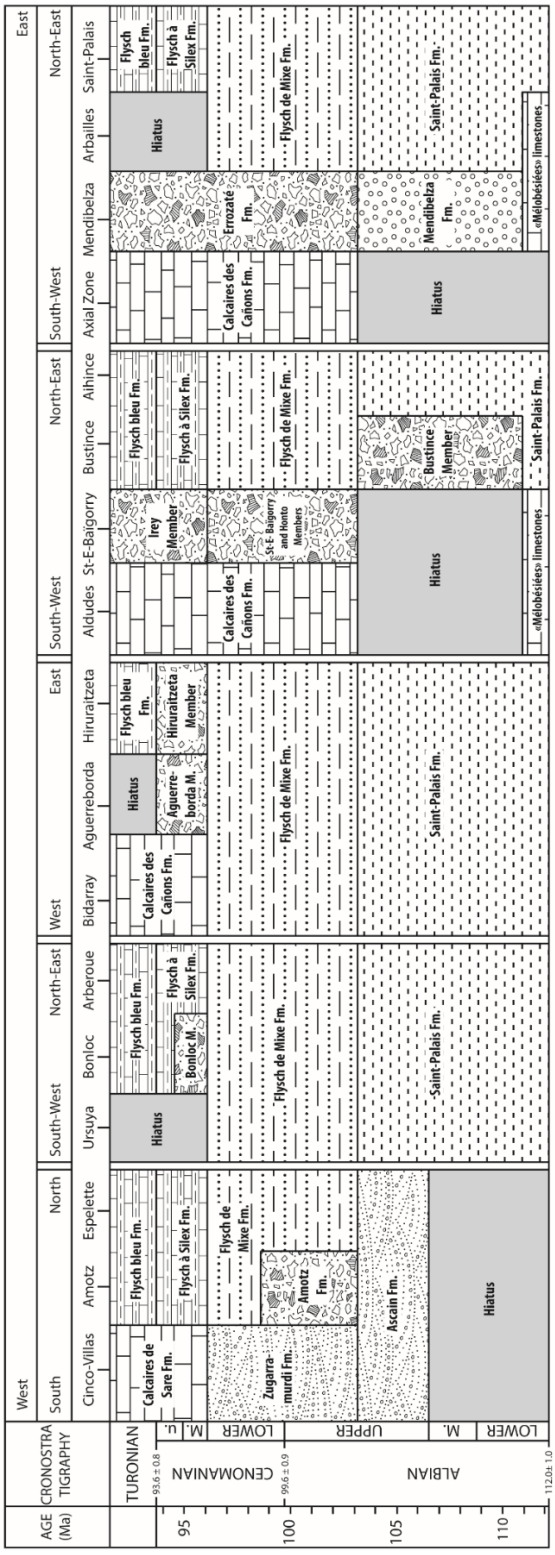


Fig. 4. Albian to Turonian chronostratigraphic chart of the Mauléon /Saint-Jean-de-Luz Iberian margin and deep basin, with indications of the formations and member proposed in this work. Chronostratigraphic scale is based on Gradstein et al. (2004).

4.2. Saint Palais Formation

Lithostratigraphy description. The Saint-Palais Formation is composed of black marls (Boltenhagen. 1966, Souquet et al., 1985). These marls represent more than 90% of this formation and contain many spicules, Globigerina, Rotalidae, ostracode, as well as Bryozoans, Mélobésiées and Dasycladaceae Algae (Castéras et al., 1970b; Casteras et al., 1971; Le Pochat et al., 1976). They were considered by the authors as deep basin facies.

Regional aspect. This formation fills the entire Mauléon area and is absent from the Saint-Jean-de-Luz domain. These marls can locally reach more than 1 500 m thick (Souquet et al., 1985).

Boundaries. The Saint Palais marls unconformably lie over the Jurassic to Albian classical prerift carbonate platform and is overlied by the Flysch de Mixe or the Flysch à Silex Formations.

Age. The stratigraphic markers argue in favor of an Albian age for this formation (Casteras et al., 1970b; Casteras et al., 1971; Boissonnas et al., 1974; Le Pochat et al., 1976; Souquet et al., 1985; **Tab. 1**).

New facies sedimentology analysis: the marls show a well-laminated structure similar to the G facies of Ricci & Lucchi. (1975) and they correspond to pelagic-hemiplegic to dilute turbidite current deposits. Several fining upward normal graded sandstone beds are interlayered within the marls, and they display complete Bouma sequences (Bouma, 1962) or partly complete sequences (Tb-d and Tc-d). They represent low-density turbidites. Clasts at the base of the beds can present a gravel lag with millimetric to centimetric polygenic clasts, containing Paleozoic meta-sediments and Late Triassic ophites.

4.3. Bustince Formation (New)

Lithostratigraphy description. Bustince Formation is composed of clast-supported breccias characterized by angular to sub-angular clasts, ranging from 1 cm to 10 cm. Clasts correspond to Jurassic to Early Albian limestone, Late Triassic ophites **(Figs. 5A & 5B)**. In rare cases, the facies corresponds to monogenic breccias of Late Triassic ophites or Earliest Albian Saint-Palais spicules marls **(Fig. 5C)**. The rare matrix is composed of micrometric clasts of the same lithology than the clasts reworked into the breccias. Massive Early-Mid Jurassic to Early Albian olistolithes and sedimentary klippes which represents up to

15km2 outcrops seem to be embedded within these breccias **(Fig. 5D)**. The contact between these "blocks" and the breccias is not visible which first conducted the geologists to interpret them as outcrops of pre-rift substratum (Le Pochat et al., 1978). On the contrary, Bouquet (1986) proposed that these outcrops might be olistostrome embedded within distal turbidites facies. A striking feature of these olistostromes is the different inner stratigraphy between the southern and northern olistostromes. The southern olistostrome shows a lack of Late Jurassic, Barremian and Aptian sequences. On the opposite, the northern olistostrome displays a more complete Mesozoic cover in which Late Jurassic, Barremian to Aptian sequence exist. Laminated pelites **(Fig. 5E)** and fine-grained sand beds are both intercalated within this breccias and olistolithes.

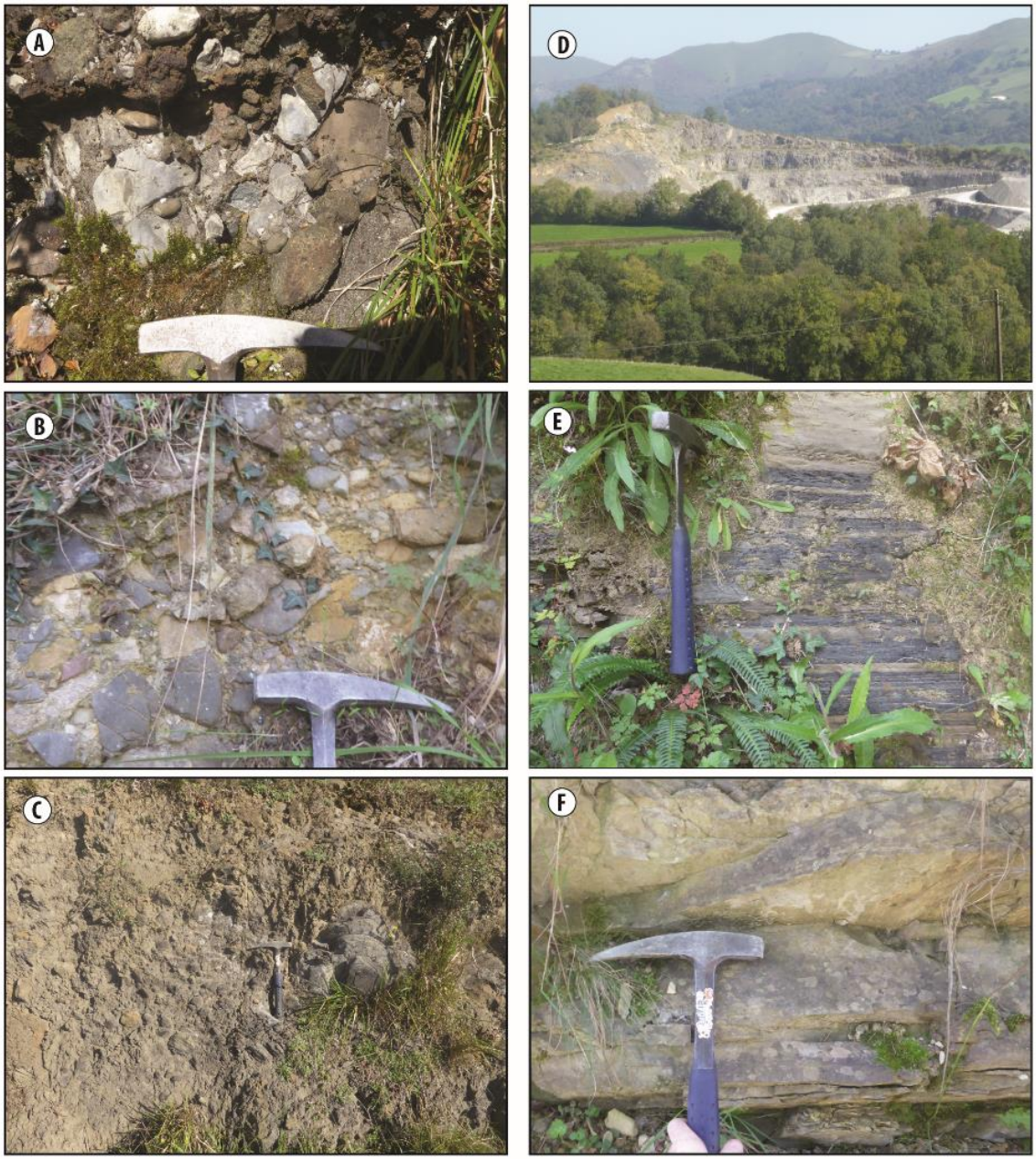


Fig. 5. (A) Polygenic clast-supported breccias reworking the Late Triassic ophites, the Early Jurassic limestones and the Early Albian "Mélobésiées limestones"; **(B)** Polygenic clast-supported breccias with Early Jurassic and Early Albian limestones clasts, ranging from 0.5 cm up to 5 cm in diameter; **(C)** Monogenic breccias made up of centimetric to decimetric clasts of the Saint-Palais Early Albian spicules marls; **(D)** Bustince-Iriberry career of Early Albian "Mélobésiées" limestones, olistolithes representing up to 15km2; **(E)** interbedded laminated pelites; **(F)** interbedded silico-clastic turbidites composed of incomplete Bouma sequence.

Table.1. Inventory of the lithostratigraphic formations and members with reference to previous works. The table contain a lithological description of the sedimentary facies, the interpretation of the depositional environment, the fossil content and the estimated age.

Antecedents	Lithology	Depositional environment	Fossils	Age
Mendibelza Formation (Boirie, 1981; Boirie and Souquet, 1982; Fixari, 1984; Frey, 1968; Gubler et al., 1947; Johnson and Hall, 1989; Lamare, 1948, 1946; Magné, 1948; Souquet et al., 1985)	Alternating chaotic breccias, unorganized conglomerates, stratified and imbricated conglomerates, fining-up conglomerates interbedded with medium to coarse-grained sandstones with planar laminations at the base and current ripples on top, massive or laminated sandstone with dune and mega-ripples, silty sandstones, dark pelites and olistolithes. Conglomerates pebbles imbrications indicate northwestward paleo-currents. The elements are mostly composed of Paleozoic to Triassic meta-sediments, and more rarely to Albian limestones.	Deep basin conglomeratic gravity-flow deposits and turbidites	*Douvilleiceras mammillatum*, *Puzosia* sp., *Kossmatella* cf. *demolyi*, *Beudanticeras*, *Inoceramus concentricus*, *Phylloceras velledae*, *Kossmatella* cf. *muehlenbecki*, *Hamites* sp., *Anisoceras* cf. *armatum*,	Early to Late Albian
Saint Palais Formation (Boltenhagen. 1966; Casteras et al., 1970b; Casteras et al., 1971; Boissonnas et al., 1974; Le Pochat et al., 1976; Henry et al., 1989; Souquet et al., 1985)	The laminated black marls with spicules represents 90% of this formation. Interbedded fine-grained and fining-upward sandstone corresponds to Bouma b-c. These beds can present a gravel lag with millimetric to centimetric polygenic clasts of Paleozoic to Late Triassic meta-sediments.	Hemipelagic deposits interbedded with turbidites of low density	*Kosmatella* sp. aff. *chabandi*, *Puzozia* cf. *quenstedti*, *Desmoceras latidorsatum*, *Ptychoceras* sp., *Beudanticeras* sp., *Hoplites* sp., *Inoceramus* cf. *concentricus*, *Variamussium* cf. *squamulum*, *Thalmanninella*, *Globigerina waschitensis*, *Aghardiellopsis cretaca*,	Latest Aptian to Early Cenomanian
Bustince Formation (Bouquet. 1986 ***and present work***)	Clast-supported breccias with angular to sub-angular clasts, ranging from 1 cm to 10 cm made up of Jurassic to Early Albian limestone, Late Triassic ophites. Massive Early-Mid Jurassic to Early Albian olistolithes and sedimentary (up to 15km2) embedded within the clast-supported breccias, laminated pelites and fine-grained siliciclastic Bouma turbidites.	Deep basin clast-supported breccias, olistolithes and sedimentary klippes	No discriminant fauna	Early to Middle Albian
Zugarramurdi Formation (Razin, 1989)	The conglomerates are composed of gravels of white quartz (80%), Carboniferous black shales, and fine to medium grained sandstones with organic debris. The conglomeratic levels appear in the form of channelized bodies of plurimetric dimension in which the elements are rounded, fairly well sorted and clast supported. The matrix is sandy or sometimes carbonated. They frequently exhibit fining-up clasts and oblique stratifications indicating a unidirectional transport from WSW towards the ENE.	Deltaic system	No discriminant fauna	Late Albian to Early Cenomanian

Flysch de Mixe Formation (Boissonnas et al., 1974; Bouquet, 1986; Claude, 1990; Kieken and Thibault, 1972; Le Pochat et al., 1976; Razin, 1989; Souquet et al., 1985)	Alternating laminated, sandy turbidites and conglomerates. The laminated pelites represents 70 - 90% of the deposits. The coarse sandy turbidites consist of 1 cm up to 20 cm thick beds with organic clasts and a carbonate cement. The base is composed of a lag with rounded and poorly sorted Paleozoic-Triassic elements. The conglomerates are characterized by a decimetric to rarely metric thickness. Their coarse and sub-rounded elements are made up of Paleozoic meta-sediments.	Hemipelagic deposit with turbidites of low density (sandstones) and and high density (conglomerates)	*Thalmanninella brotzeni*, *Globigerina waschitensis*, *Rotalipora appenninica*,	Late Albian to Early Cenomanian
Amotz Formation (Debourle and Deloffre, 1976; Heddebaut, 1973; Razin, 1989; Richard, 1986)	Alternating clast-supported polygenic breccias composed of (i) Mesozoic cover elements and (ii) Paleozoic and Triassic clasts. The basal breccias are mainly composed of Late Triassic ophites, Hettangian dolomites, Pliensbachian and Late Albian limestones. Upward, the breccias reworked Devonian-Carboniferous meta-sediments, Late Triassic sandstones and ophites, and blocks of the Zugarramurdi Formation. The blocks are mainly decimetric to metric, but can be decametric to hectometric.	Deep basin clast supported debris flow and sedimentary klippes	No discriminant fauna	Late Albian to Early Cenomanian
Saint Etienne de Baïgorry Formation (Le Pochat et al., 1978; Merle, 1974)	Polygenic clast-supported breccias with clasts size ranging from 5 cm up to 1.5 m. The clasts correspond to Late Triassic ophites and limestones, Carboniferous limestones, Devonian schists and Late Albian limestones. Some siliciclastic-limestones are interbedded with the breccias.	Deep basin clast supported debris-flow	Breccias clasts *Hensonina lenticularis*, *Agardhiellopsis cretacea*, *Paraphyllum primaevum*, Siliciclastic-limestones *Hensonina lenticularis*, *Paraphyllum primaevum*, *Orbitolines*, *Charentia* sp.,	Middle to Late Albian
Errozaté breccias Formation (Durand-Wackenheim et al., 1981; Le Pochat et al., 1978; Merle, 1974)	Clast-supported breccias composed of Paleozoic meta-sedimentary basement, Late Triassic ophites and Late Albian to Santonian Calcaires des Canyons limestones. The elements size vary from 1 cm up to 3 m.	Deep basin clast supported calcareous debris flow	*Hensonia lenticularis*, *Charentia*. sp. , *Charentia cuvillieri*, *Favusella waschitensis*, *Orbitolina conica*, *Orbitolina cuvillieri*, *Trocholina* gr. T *Arabica*, *Praeglobotruncana delrioensis*, *Rotalipora cushmani*, *Praealveolina cushmani*, *Praealveolina cretacea*, *Orbitolina conica*, *Orbitolina paeneconica*, *Orbitolina concava*,	Latest Albian to Santonian
Honto Member (Le Pochat et al., 1978; Merle, 1974)	Pink calcareous breccias with numerous angular to sub-angular clasts of Paleozoic meta-sediments and Late Albian limestones. Late Albian limestone clasts range from 4 cm gravels to 1 m block. Paleozoic clasts consist of quartzites, schists and micrite limestones as well as rare Late Triassic ophites. The calcareous to sandy matrix contains Orbitolines, Polyps and Algae.	Deep basin debris-flow ***(New)***	*Hensonia lenticularis* *Favusella waschitensis*	Middle to Late Albian

Irey Member (Le Pochat et al., 1978; Merle, 1974)	The lower unit is characterized by micrometer scale sandy limestones with Late Albian pinkish micro brecciated limestones with primary pebbles. The carbonate matrix is composed of Orbitolines, Polypis and Bryozoans. On the upper unit, the carbonate breccias with Paleozoic meta-sediments are interbedded with small beds of 5 to 10 cm thick calcareous cement breccias, reworking exclusively Paleozoic small elements, black shales and quartzites.	Deep basin matrix supported calcareous debris flow ***(New)***	*Trocholina gr. T arabica* *Orbitolina conica* *Praealveolina cretacea* *Charentia cuvillieri*	Early Cenomanian to Turonian
Flysch à silex Formation (Boissonnas et al., 1974; Le Pochat et al., 1976; Mathey, 1986; Richard, 1986)	Alternating grey marls, partly complete Bouma sequences and rare breccias. The compact grey are organized in metric to decametric thick units. Calcareous turbidites facies are 5 cm to 1 m, rarely 2 m thick beds of grey cherts-riched calcarenites. The coarse fraction is composed of Paleozoic angular clasts mainly made up of shale, quartz, quartzite and sandstone, numerous Triassic clasts and reworked benthic microorganisms. The fine fraction presents peloids, small benthic foraminiferas, calcispheres, and spicules. These calcarenites beds are tabular, and their basal stratification surface is sharp and plane. These calcareous-turbidites are characterized by southward directed paleo-currents varying from N160° to N210°.	Deep basin distal calcareous turbidites	*Thalmanninella* *Rotalipora cushmani* *Globotruncana stephani* *Gumbelina* *Stomiosphera spherical*	Middle to Late Cenomanian
Bonloc Member (Boissonnas et al., 1974; Claude, 1990)	Polygenic breccias containing clasts of granulites, gneiss with garnet, quartzite gneiss, pegmatites, Devonian-Carboniferous micaschists and quartzites. Few clasts of Late Triassic reddish sandstones and Albian “Mélobésiées” limestones were identified. The matrix is almost absent and the clasts are very angular. The clast size ranges from 5 cm up to 1.5 m. These breccias are interbedded with strongly weathered calcareous turbidites of the Flysch à Silex Formation.	Deep basin clast supported debris flow and calcareous turbidites	No discriminant fauna	Middle to Late Cenomanian
Aguerréborda Member ***(New)***	Fining-upward breccias with angular clasts, ranging from 1 cm up to 20 cm and a clast-supported texture. Clasts are polygenic but only composed of Jurassic, Barremian and Aptian limestones. Bed tops corresponds to fine-grained calcareous turbidites with planar laminations at the base, passing to undulated to oblique laminations on top.	Deep basin clast supported debris flow	No discriminant fauna	Middle to Late Cenomanian

Hiruraitzeta-Member ***(New)***	Breccias interbedded within Tc to Te Bouma calcareous turbidites of the Flysch à Silex Formation. Clasts are polygenic. The clasts are essentially angular and include a large range of Late Triassic ophites, Devonian meta-sandstones and Carboniferous marbles. Their size is ranging from 1 cm to 8 cm. They are mainly organized in 5 cm to 15 cm thick beds.. Upward, these breccias are followed by a 10-15 m thick ophite olistolithe, grading vertically to a 15 m thick breccias unit composed of monogenic clasts of Late Triassic ophites. whose bed thickness varies from 2 m up to 4 m and the clasts size ranges from 2 cm up to 40 cm.	Deep basin clast supported debris flow and calcareous turbidites	No discriminant fauna	Middle to Late Cenomanian
Calcaires des Canyons Formation (Alhamawi, 1992; Le Pochat et al., 1978; Merle, 1974; Souquet, 1967 ***and present work***)	At the base, the formation is characterized by 15 m thick silico-clastic siltstones, sandstones and micro-conglomerates. Clasts nature only corresponds to Devonian dolomites, quartzites and schists. This unit grades vertically to Cenomanian-Turonian carbonate facies characterized by grainstones with bivals and peloids, packstone with praealveolina, orbitolines, rudists and bivals, floatstone with rudists and finally, mudstone to wackstone with praealveolina and miliols.	Inner platform	*Trocholina arabica* *Trocholina* gr. T. *Arabica* *Praealveolina cretacea* *Praealveolina* simplex *Orbitolina conica* *Ovalveolina ovum* *Pseudocyclammina rugosa* *Chrysalidina gradata* *Charentia cuvillieri* *Nezzata* simplex	Early Cenomanian to Santonian
Calcaires de Sare Formation (Feuillée. 1964; Mathey, 1986; Prave, 1986; Razin, 1989; Richard, 1986)	The basal terrigenous limestones corresponds to siliciclastic limestones containing millimetric to centimetric clasts of white quartz (80%), Carboniferous shale, sandstone, argillites, Triassic ophite, rudist fragments, algae and gastropods. Upward, reef limestones are made up of decametric bioherms with a low lateral continuity. They grade laterally to biodetritic limestones (calcarudites and calcarenites) that represent the major part of the formation. The coarser facies are mainly composed of rudist fragments, algae debris, gastropods, polyps, bryozoans, echinoderms, Cuneolins, Miliolidae, as well as intraclastics biomicrite or biosparite.	Inner platform	*Caprina adversa* *Sphaerulites foliaceus* *Duraria pyrenaica* *Dicarinella concavata* Globotruncana	Middle Cenomanian to Early Coniacian

Regional aspect. The Bustince chaotic complex outcrops in the southern-western part of the Saint-Palais unit **(Fig. 2)**. The thickness of this unit is quite difficult to assess due to the poor outcropping conditions.

Boundaries. This formation is overlain with a 15 m to 30 m thick mixed carbonated and detrital turbidite sequence attributed to the Late Albian to Early Cenomanian third synrift mega-sequence (**Fig. 4**; Souquet et al., 1985) corresponding to the Flysch de Mixe Formation.

Age. The Bustince Formation developed during the Early to Mid Albian as: (1) the older pebbles reworked are earliest Albian in age and (2) the formation grade upward to the Flysch de Mixe Fm. **(Tab. 1)**.

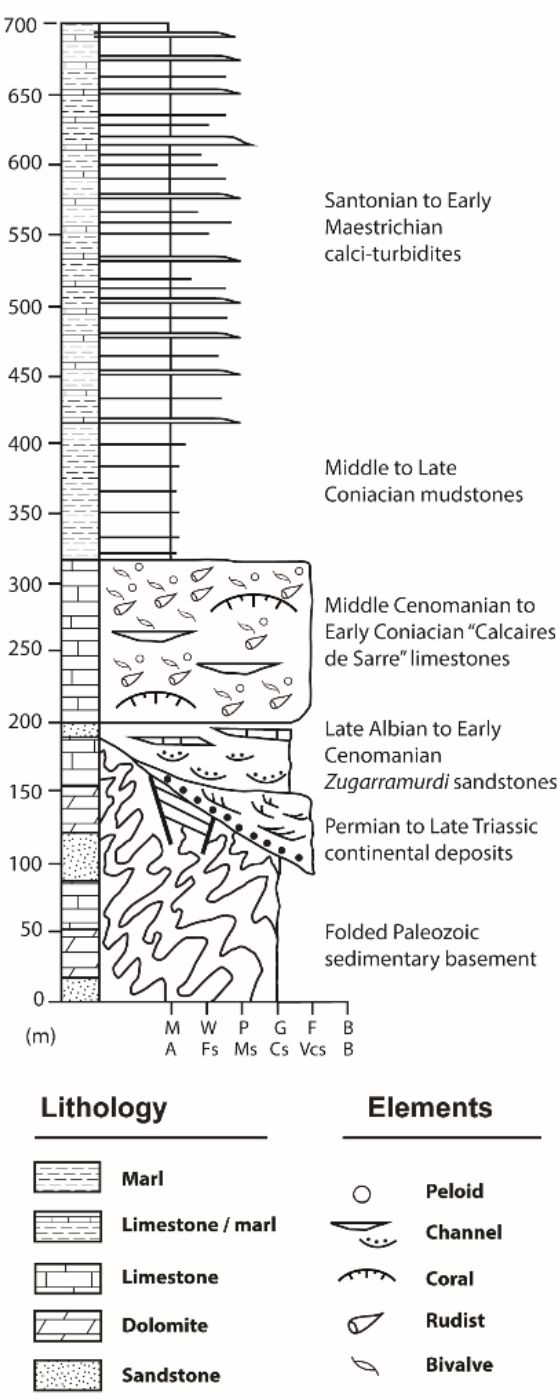


Fig. 6. Synthetic lithostratigraphic succession of the Cinco-Villas unit (modified from Razin, 1989).

New facies sedimentology analysis. The sand beds intercalated within the breccias display incomplete Bouma sequences, suggesting low-density turbidites deposits. On the contrary, the breccias are dominated by clasts-supported (F3 of Mutti, 1977 and 1992) and more rarely coarse-matrix supported textures (hyperconcentrate F2 of Mutti, 1977 and 1992), with poor to null sorting and organization. No pebbles imbrications are visible suggesting poor bedload current, and we interpret these deposits are base of slope turbidites deposits essentially produced by avalanching. This assumption is strengthen by the existence of huge blocks which we might attribute to massive slope-failure collapse attesting for the existence of an unstable very steep scarp enabling efficient transportation of the sedimentary load.

4.4. Zugarramurdi Formation

Lithostratigraphy description. The Zugarramurdi Formation (Leaf. 1964; Prave. 1986) correspond to conglomerate, which clasts of gravel size are white quartz (80%), Carboniferous black shales, and fine to medium grained sandstones with organic debris (Razin. 1989). The basal transgressive surface over the Cinco-Villas unit basement is underlined by a clayey and detritic level of 50 cm thick very rich in organic matter. The transition with the overlying Calcaires de Sare Formation is materialized by some interbedded carbonate platform limestones within the Zugarramurdi sandstones (Razin. 1989).

Regional aspect. This formation crops out on the northern domain of the Cinco-Villas unit and presents a thickness varying from 10 m to 100 m thick. Northward of the Saint Palais unit, the Zugarramurdi sandstones are absent and the Late Albian to Early Cenomanian sequence is characterized by the development of Late Albian -Early Cenomanian Amotz Formation (c.f. 4.6).

Boundaries. The Zugarramurdi Formation rests upon the Cinco-Villas unit characterized by a folded Paleozoic meta-sedimentary basement as well as Permian to Late Triassic fluvial deposits **(Figs. 6 and 7D)**. This observation highlights the lack of Jurassic to Early Albian sequence on the Cinco-Villas unit. The Zugarramurdi sandstones progressively grade upward to the Mid Cenomanian- Early Coniacian Calcaires de Sarre Formation (**Figs. 4, 6 & 7D**; c.f. 4.11).

Age. No elements have been found allowing to bio-stratigraphically date the Zugarramurdi Formation **(Tab. 1)**. However, the affinities with the terrigenous supra-urgonian complex (Rat, 1959) and its position at the base of Calcaires de Sarre Formation (Feuillée, 1964, 1967), make it possible to propose a Late Albian to Early Cenomanian age for this formation (Razin. 1989).



Fig. 7. (A) Late Albian Saint Etienne de Baïgorry clast-supported polygenic breccias essentially composed of ophites and Paleozoic meta-sediments and more rarely of Late Albian carbonate platform; **(B-C)** Respectively the red and grey member of the Late Cretaceous Errozaté polygenic breccias made up of metric Late Albian, Cenomanian and Turonian platform blocks, Late Triassic ophites and Paleozoic sedimentary basement; **(D)** Late Albian Honto matrix-supported polygenic breccias made up of Paleozoic clasts and Late Albian carbonate platform elements of 2 cm up to 1 m in diameter; LT: Late Triassic; P: Paleozoic; Oph: Ophite.

Former facies sedimentology analysis (Razin, 1989): the conglomerates are organized in channels, and display a fairly good sorting, clasts-supported texture and rounded clasts The matrix is sandy and eventually carbonated and they show fining upward trend as well as 3D megaripples. The sandier channels, often exibits a basal conglomerates lag, grading to 3D megaripples and fining upward trend. The paleocurrent analysis indicates a unidirectional transport from WSW towards the ENE (Prave. 1986).The sedimentological characteristics of the Zugarramurdi sandstones, i.e bedload conglomerates contain within channel bodies ; and their interdigitating within carbonate platform facies argue for fluvio-deltaic deposits (Razin, 1989).

4.5. Flysch de Mixe Formation

Lithostratigraphy description. The Flysch de Mixe Formation is composed of a very monotonous and unorganized alternation of different classical facies of the Black Flysch turbiditic group, already described in the Tardets (Boirie. 1981; Roux. 1983; Fixari. 1984) and Deva (Garcia Mondejar. 1982; Garcia Mondejar et al, 1985) areas. The Formation is dominated by black micaceous silty marls with interbedded fine-grained to coarse sandstones. The sand intervals consist of 1cm to 20cm thick beds marked by a sharp planar base and a wavier uppermost surface. Thickness of the pelitie layers is decimetric to plurimetric, and they represent 70 to 90% of the Flysch de Mixe Formation. The last 10%/ correspond to sandy deposits. The formation is considered to be supplied in sediments from west to east (Razin, 1989).

Regional aspect. The Flysch de Mixe Formation crops on a large area as it is located both on the Mauléon and Saint-Jean-de-Luz area. The thickness of this formation can reach

1 200 m to 1 500 m thick in the basin center and thin towards the south passing laterally in the Saint-Jean-de-Luz area to the Amotz Formation.

Boundaries. The lower limit of the Flysch de Mixe Formation corresponds to a gradual transition with the Amotz Formation (c.f. 4.6.; **Fig. 4**) towards the south and on the Ustaritz borehole (c.f. 5.2.). The upper limb of this formation is materialized by the onlap of the Mid - Late Cenomanian Flysch à Silex Formation (c.f. 4.9.; **Fig. 4**).

Age. This formation is dated from the Late Albian to Early Cenomanian by Ammonites and stratigraphic relationship with the overlaying Flysch à Silex Formation (Souquet et al., 1985; Razin. 1989; Claude. 1990; **Tab. 1**).

Former facies sedimentology analysis (Razin, 1989): The laminated pelites correspond to pelagic to hemiplegic deposits, similar to the G facies of Ricci & Lucchi. (1975). They are interbedded with very thin planar to oblic laminated fine-coarse sandstone. These later correspond to small turbidites event, and they sometimes present a lenticular bedding respectively typical of D3 and E facies of Ricci & Lucchi., 1975.

The thicker sandy interval is generally marked at the base micro-conglomerate, with rounded, poorly sorted Paleozoic-Triassic elements (Razin. 1989). Bioturbations (horizontal worm burrows) are frequently observed below this basal surface. The micro-conglomerates grade upward to sandstones with parallel to oblique laminations, suggesting bedload current. These facies are typical of the Bouma sequence. These facies represents 80% of the non pelitic deposits of the Flysch de Mixe Formation (Razin. 1989).

Conglomerates facies are marginal in the Flysch de Mixe Formation, and they are characterized by few centimeters to exceptionally 1m thick beds. Clasts are sub-rounded Paleozoic meta-sediments. Razin. (1989) identified three facies: (1) disorganized sandy matrix-supported (F2 of Mutti, 1977, 1992); (2) clasts-supported conglomerates with reverse and normal grading (F3 of Mutti, 1977, 1992), (3) fining-upward stratified conglomerates, where the coarse interval grades without transition to oblique or parallel lamination sandy bed with (transition between the R and S facies of Lowe, 1982). These three facies are typical of proximal turbidites ranging from hyperconcentrate (Facies F) to high-density turbidity current deposits (Facies R and S). The co-existing proximal turbidites deposits embedded in marls question the geometry of the system. No channels or lobes were described which suggests a poorly channelized system.

4.6. Amotz Formation

Lithostratigraphy description. The Amotz breccias have been firstly described by Lamare. (1954a; 1957) and then attributed to the third sequence of the Black Flysch Group by Razin. (1989). These breccias crops out to the north of the Amotz thrust and have been sampled on 1 000 m thick in the Ustaritz-1 well (c.f. 5.2; Teyssonnières. 1983). Two types of breccias can be distinguished according to the nature of the clasts: (i) the breccias composed of Mesozoic cover elements and (ii) breccias derived from the Paleozoic and Triassic substratum (Razin. 1989). The basal breccias are polygenic and mainly composed of Late Triassic ophites, Hettangian dolomites, Pliensbachian limestones with belemnites and Late Albian "Mélobésiées" limestones (Heddebaut, 1973; Debourle and Deloffre, 1976; Richard, 1986; Razin, 1989). Upward, the breccias are composed of Devonian-Carboniferous meta-sediments, Late Triassic sandstones and ophites, and blocks of the Zugarramurdi sandstones (Razin. 1989). The blocks are mainly decimetric to metric, but can be locally decametric to hectometric (sedimentary klippes). The uppermost part of the Amotz Formation is more stratified and composed of breccias interbedded with pelites and sandy levels. These matrix-supported debris flow are metric to decametric and evolve upward to immature turbidites corresponding to the A2 facies of Ricci &Lucchi. (1975).

Boundaries. The base of the Amotz breccias corresponds locally to (i) a tectonic contact (Amotz south-verging thrust), and elsewhere to (ii) a stratigraphic contact with the Zugarramurdi Formation (**Fig. 6**; Razin. 1989). The uppermost limit of the Amotz Formation is materialized by the onlap of the Late Albian to Early Cenomanian Flysch de Mixe or the Mid to Late Cenomanian Flysch à Silex Formations (Razin, 1989; **Fig. 4**).

Regional aspect. This Amotz Formation crops out on the Saint-Jean-de-Luz domain, to the north of the Amotz thrust. The thickness of this serie is difficult to evaluate as it is rarely complete, still it varies between 100 m and 1 000 m thick.

Age. The relationship with the Flysch de Mixe and Flysch à Silex Formations allows to propose a Late Albian to Early Cenomanian age for this formation (Razin. 1989; **Tab. 1**). Thus, the Amotz formation materialize part of the third mega-sequence of the Black flysch Group (Souquet et al., 1985).

Former facies sedimentology analysis (Razin, 1989). Facies might be divided in two types: breccias and olistolithes. Breccias show both clast and sandy-matrix supported texture suggesting F2 and F3 facies according to Mutti, 1977 and 1992; which implies hyperconcentrate flow. The olistolithes of huge size (100m or more) suggests, alike in Bustince Formation significant slope failure and the collapse of a large talus volume. The uppermost Amotz Formation shows metric to plurimetric-scale, generally clasts-supported conglomerates. They present a chaotic organization with rare reverse and normal grading, and very rare pebbles imbrications (south to north paleocurrent direction). They grade vertically to gravelly sandstone and pelites, attesting for a flow transformation from hyperconcentrate to high density turbidites. No mature turbidites facies were observed, probably due to the proximal position in the system, as well as the shaly material reworked enabling the production of fine-grained deposits.

4.7. Saint-Etienne-de-Baïgorry Formation

Description. The Saint-Etienne-de-Baïgorry Formation consists of polygenic blocks from 5 cm up to 1.5 m in diameter, with an average block size of 50 cm **(Fig. 7A)**. Clasts essentially correspond to Late Triassic ophites and limestones (Muschelkalk), Carboniferous limestones, Devonian schists and Late Albian limestones (Merle, 1974). These latter contain numerous Polyps, Orbitolins, Algae, and *Hensonia lenticularis*. The Saint-Etienne-de-Baïgorry breccias grade upward to black marls corresponding to the Saint-Palais Formation.

Regional aspect. This formation is marked by abrupt thickness variations from null to 75 m, over short distances and outcrop in the western corner of the Saint-Etienne-de-Baïgorry unit.

Boundaries. The Saint-Etienne-de-Baïgorry Formation is delimited both to the north and to the south by thrusts, separating it from the Aldudes domain to the south and the Saint Jean Pied de Port domain to the north **(Fig. 2)**.

Age. Its stratigraphic position within the Saint Palais Formation and the stratigraphic correlation suggest to a Late Albian age (**Tab. 1**; Merle, 1974; Le Pochat et al., 1978).

New facies sedimentology analysis. These breccias present a clast-supported texture, a lack of sorting and they grade in a distal position to deep-sea Saint-Palais Formation. The combination of the clast size, clast-supported texture and the transition with deep-sea gravity facies argue for a turbidites origin. In this scope, these breccias might correspond to the Mutti F3 facies corresponding to clast-supported debris flow (Mutti, 1977 and 1992). The relative sharp lateral transition between these breccias and the low-density turbidite facies of Saint-Palais Formation argue for a very poor efficient transportation system, since very rare hyperconcentrate deposits were observed. Consequently, the transport is dominated by avalanching rather than channelized flow) and Saint Palais Formation.

4.8. Errozaté Formation

Description. The Errozaté breccias are composed of clasts of Late Cretaceous Calcaires des Canyons (c.f. 4.10.), Paleozoic meta-sedimentary basement and the Upper Triassic deposits. This formation is made up, from base to top, of pink, red, grey and reddish clast-supported breccias. The 20 m thick pink breccia is composed, at the base, of Paleozoic clasts, similarly to the underlying Mendibelza Formation (c.f. 4.1.). The rare cement is carbonated and slightly sandy. The elements size is of the order of dm^3. The clasts are angular and consist of: (1) Paleozoic meta-sediments, (2) Late Triassic ophites, (3) Late Albian pink limestones with *Hensonia lenticularis* and Mélobésiées and (4) Late Albian red detrital limestones with Polyps, Orbitolins, *Favusella waschitensis*, Caprinesa and Algae (Merle. 1974). The following 20 m thick red breccia reworks large blocks of (Fig. 7B): (1) Late Albian red limestones with

Caprinidae and Polyps (2) Late Albian pink limestones with Mélobésiées (3) Early to Mid-Cenomanian dark grey limestones of the Calcaires des Canyons Formation (c.f. 4.10.) and (4) Late Triassic ophites and more rarely Paleozoic meta-sediments (Le Pochat et al., 1978). The red breccia passes vertically to the 50 m thick grey breccia (Fig. 7C). It is characterized by a carbonate matrix. The clasts of this breccia are essentially composed of: (1) Late Albian red limestones and Late Cenomanian - Turonian grey limestones both corresponding to the Calcaires des Canyons limestones, (2) Paleozoic meta-sediments and (3) Late Triassic ophites (Merle. 1974). The upper part of this formation is composed of 50 m thick reddish breccias reworking the Coniacian Calcaires des Canyons Formation, Paleozoic meta-sediments and late Triassic ophites. The elements size vary from 1 cm up to 3 m.

Boundaries. This Formation overlaps the Late Albian third mega-sequence of the Mendibelza Formation (Souquet et al., 1985) and it is bounded on top by the Mid to Late Coniacian Flysch à fucoïdes (**Fig. 4**; Merle, 1974; Le Pochat et al., 1978).

Regional aspect. These breccias crops out to the south of the Mendibelza unit. Their thickness varies from 50 m to 150 m thick.

Age. The stratigraphic correlation of the Errozaté Formation evidenced a late Albian to late Santonian age (Souquet, 1967; Merle, 1974; Le Pochat et al., 1978).

New facies sedimentology analysis. The breccias present a slightly sandy carbonate matrix-supported texture. This feature indicates debris-flow type transportation, probably due to a non-stable carbonate platform partly collapsing basinward (Durand-Wackenheim et al., 1981). Limy nature of the matrix indicates carbonate debris-flow probably derived from non-consolidated mudstone export of the platform-which allows lithified blocks transportation. The presence of Paleozoic clasts suggests an erosion of the basement by the debris flow wrenching rocks on the slope. The presence of Late Albian carbonate clasts within the basal Errozaté breccias is enigmatic since no outcrops of this carbonate platform are described in the area. In fact, the Calcaires des Canyons carbonate platform is attributed to the Early Cenomanian to Santonian (c.f. 4.10). Moreover, the relative rare and geography constrained observation of these Late Albian limestone clasts witness a probable isolated patch reefs carbonate platform, completely eroded before the Late Cretaceous transgression and reworked into the previously described basal breccias.

4.8.1. Honto member (new)

Lithostratigraphy description. Defined in the Honto region, this member of the Errozaté Formation is made up of pink calcareous breccias with numerous angular to sub-angular clasts of Paleozoic meta-sediments and Late Albian limestones. The Late Albian limestone clasts range from 4 cm gravels to 1 m block **(Fig. 7D)**. Paleozoic clasts consist of quartzites, schists and micrite limestones as well as rare Late Triassic ophites **(Fig. 7D)**. The calcareous to sandy matrix contains *Favusella waschitensis*, flat Orbitolines, Polyps and Algae (Merle. 1974). These breccias are quite similar to the basal pink breccias of the Errozaté Formation, although they do not significantly rework Late Triassic ophites.

Boundaries. The basal limit of this member corresponds to a tectonic contact with the Aldudes unit Paleozoic meta-sediments, while the upper one is stratigraphic as these breccias progressively grade to the Saint Palais Formation (c.f. 4.2.; **Fig. 4**).

Regional aspect. The Honto member crops on the eastern domain of the Saint-Etienne-de-Baïgorry unit **(Fig. 2)**. This member shows variable thickness up to ~20-40 m, and it laterally passes to the Saint-Palais spicules marls Formation (c.f. 4.2.).

Age. The fauna content, the stratigraphic correlation of the Honto member and the stratigraphic relationship with the Saint-Palais Formation evidenced a Late Albian age for this member (Merle. 1974; **Tab. 1**).

New facies sedimentology analysis: The Honto member is very similar to the Errozaté breccias, i.e carbonate matrix supported texture. For these reasons, this member is interpreted as base of slope breccias, while it was previously considered as carbonate platform sequence stratigraphically equivalent to the base of the

Calcaires des Canyons Formation (Merle. 1974).

4.8.2. Irey member (new)

Lithostratigraphy description. Around the Irey pass, this member is composed of ~20 - 40 m thick breccias formed by the superposition of two levels. The lower one is characterized by micrometer scale sandy limestones with Late Albian pinkish micro brecciated limestones with primary pebbles. The carbonate matrix is composed of Trocholina gr. *Trocholina arabica*, Orbitolines, Polypis, Bryozoans, greenish schistose sandy marls (Merle. 1974). The upper level is quite similar of the first one, but the matrix mainly contains *Praeglobotruncana delrioensis*, *Rotalipora appennica*, microbregnate limestones with Globotruncana sp., Praealveolina sp., Cuneolins, Rotalidae, Textularids (Merle. 1974). The carbonate breccias with Paleozoic meta-sediments are interbedded with small beds of 5 to 10 cm thick calcareous cement breccias, reworking exclusively Paleozoic small elements, black shales and quartzites.

Boundaries. Generally, the lower and upper contacts of this member are bounded with thrusts. Locally, these breccias are overlain by Santonian calcareous turbidites.

Regional aspect. The Irey member is caught in-between two westward thrusts, separating it from the Aldudes unit to the west and the Mendibelza one to the east **(Fig. 2)**.

Age. The presence of *Praeglobotruncana delrioensis* and *Rotalipora appennica* provides a large range of Cenomanian to Turonian age (Merle. 1974; **Tab. 1**).

New facies sedimentology analysis: Alike the Honto member, this sedimentary unit was considered as carbonate platform deposits, time equivalent to the Calcaires des Canyons Formation (Merle. 1974). However, the presence of polygenic clasts reworking both the Calcaires des Canyons carbonate platform (c.f. 4.10.) and the Paleozoic basement of the Aldudes domain evidenced that these deposits corresponds to deep basin carbonated debris flow.

4.9. Flysch à Silex Formation

Lithostratigraphy description. The Flysch à Silex Formation corresponds calcareous turbidites made up of grey marls interbedded with thin sand and breccias beds **(Figs. 8A & 8B)**. The grey marls facies corresponds to compact grey silty marls, in metric to decametric thick layers (Razin. 1989). In the upper part of the formation, the terrigenous fraction decreases forming centimetric to decimetric beds. The coarse fraction (medium-grained carbonated sand) is composed of: (1) Paleozoic angular clasts mainly made up of shale, quartz, quartzite and sandstone, (2) numerous Triassic clasts in the upper part of the formation (red sandstone and argillite, bipyramid quartz) and (3) reworked benthic microorganisms, increasing in abundance in the series: Orbitolines, Miliolidae, Textularidés, Lituoïdés (Daxia), Cuneolines, rare Praealveolina, echinoderms clasts, molluscs, Algae (Razin. 1989). The fine fraction (fine-carbonated sand and silt) presents peloids, small benthic foraminiferas, calcispheres, and spicules. These levels show sharp and flat basal surface. At the base of the formation, the upper limit of the beds is progressive, while towards the top of the formation, this same limit is sharp (Razin. 1989). The base of the Flysch à Silex Formation is intruded by Middle Cenomanian alkaline magmatism (Teschenyte) forming pluri-kilometric sills (Rossy et al., 1992).

Boundaries. At the base, the Flysch à Silex Formation rests on onlap above the Late Albian to Early Cenomanian Flysch de Mixe or the Amotz Formations. On top, this formation grades progressively to the Turonian calcareous turbidites (Razin. 1989).

Regional aspect. The Flysch à Silex Formation crops out in all the Mauléon / Saint-Jean-de-Luz basin and is characterized by a thickness varying from 100 m to more than 1 000 m (Razin. 1989).

Age. Biostratigraphic markers (Boissonnas et al., 1974; Le Pochat et al., 1976; Mathey, 1986; Richard, 1986; **Tab. 1**) as well as the stratigraphic relationship with the older Flysch de Mixe and Amotz Formations, the overlaying Turonian turbidites (Bouquet, 1986; Razin, 1989) and the intrusive alkaline magmatism (Rossy et al., 1992) allows to propose a Mid to Late Cenomanian age for this formation.

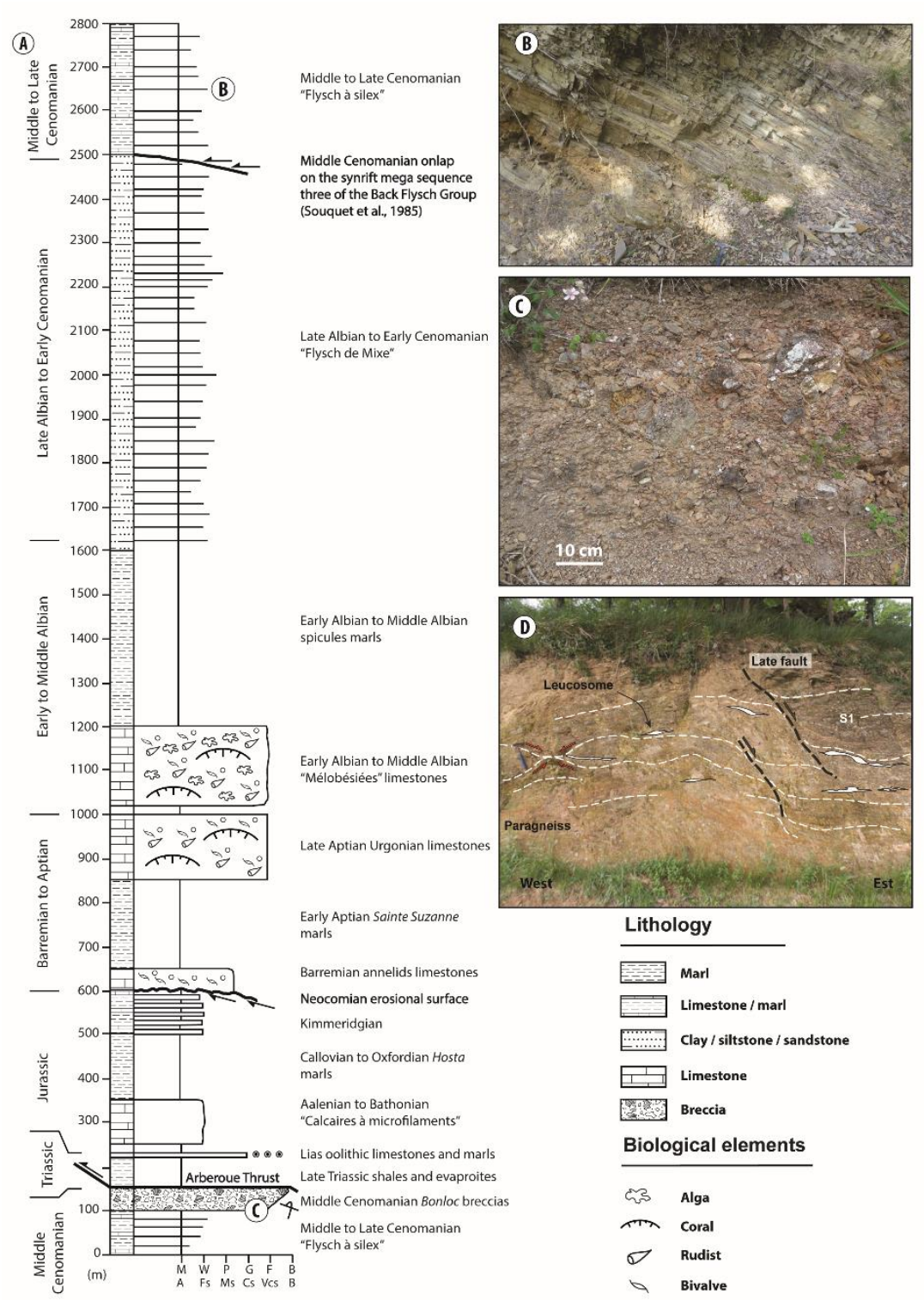


Fig. 8. (A) Schematic lithostratigraphic succession of the Arberoue domain; **(B)** Middle to Late Cenomanian Flysch à Silex Formation made up of fine grained calcareous turbidites composed of incomplete Bouma sequence; **(C)** Middle Cenomanian polygenic clast-supported Bonloc breccias composed of granulites, gneiss, pegmatites, micaschists and quartzites; **(D)** Ursuya granulites.

Former facies sedimentology analysis: The grey marls correspond to pelagic-hemipelagic facies with carbonate and clastic turbidites influxes. These coarser beds are characterized by partly complete Bouma sequences (Bouma, 1962), grading from fining upward, parallel lamination, undulating lamination, and uniform pelitic interval at the top. They thus correspond to low-density turbidity currents. A large amount of cherts are visible, and paleocurrent shows south

to south-east direction (Boissonnas et al., 1974; Le Pochat et al., 1976; Roux, 1983; Razin, 1989; Claude, 1990).

4.9.1. Bonloc breccias member

Lithostratigraphy description. The Bonloc member consists of polygenic breccias containing clasts of granulites, gneiss with garnet, quartzite gneiss, pegmatites, Devonian-Carboniferous micaschists and quartzites **(Fig. 8C)**. The lower crustal material reworked in these breccias is derived from the Ursuya granulitic unit **(Fig. 8D)**. Few clasts of Late Triassic reddish sandstones and Albian "Mélobésiées" limestones were identified (Claude 1990). The matrix is almost absent and the clasts are very angular (Boissonnas et al., 1974). The clast size ranges from 5 cm up to 1.5 m. These breccias are interbedded with strongly weathered fine to medium grained calcareous turbidites comparable to the one describe in the Flysch à Silex Formation (c.f. 4.9).

Boundaries. The Bonloc breccias are southward thrusted along the Arberoue thrust. On top, this member grades to the upper part of the Flysch à Silex Formation.

Regional aspect. The Bonloc breccias are located to the northeast of the Ursuya granulites and to the south of the Arberoue Thrust **(Fig. 2)**. These breccias can reach a thickness of nearly 300 m (Claude, 1990).

Age. The Bonloc breccias was previously considered as Late Albian to Early Cenomanian breccias (Boissonnas et al., 1974; Claude, 1990). However, these breccias inter-fingers with the Flysch à Silex Formation, which implicates a Mid-Late Cenomanian age to the Bonloc Breccias. The biostratigraphical analysis performed for our study do not permit to attribute a precise age for these turbidites. However, they are at least Late Cretaceous in age differing strongly with the Late Albian age previously proposed by Boissonnas et al. (1974) and Claude. (1990). Weathering of the Flysch à Silex often hardly allows to distinguish it from the Flysch de Mixe Formation (c.f. 4.5.), which explains why it has never been mapped in the Saint-Jean-de-Luz domain before 1980 (Raoul. 1957; Lamare. 1962, 1964) and why some authors have considered the Bonloc breccias as a member of the Flysch de Mixe Formation (Boissonnas et al., 1974; Claude, 1990).

Former facies sedimentology analysis They were interpreted as deep basin gravity deposits (Claude, 1990). The clast-supported matrix and the interfingering with the Flysch à Silex Formation argue for turbidite facies typical of the Mutti F3 facies (Mutti, 1977, 1992).

4.9.2. The Hiruraitzeta Member (New)

Lithostratigraphy description: The Hiruraitzeta domain records a complete Cenomanian succession **(Fig. 9A)**. The Hiruraitzeta Member is stratigraphically located at the transition between the Flysch de Mixe Formation and the Flysch à Silex Formation. This member can be divided into three units: (i) 65 m of alternating limestone and breccia beds at the base, followed by (ii) 15 m thick olistolithe and breccias unit and (iii) 15 m thick breccias unit.

The lower mixed detrital-carbonate unit mainly consists of alternating breccias and carbonate. Detrital influx corresponds to breccias interbedded within the calcareous turbidites **(Fig. 9B)**. They consist of polygenic clasts whose size is ranging from 1 cm to 8 cm, organized in 5 cm to 15 cm thick beds. More occasionally, these breccias form unit of 1 m up to 2 m thick with block size ranging from 5 cm up to 30 cm **(Fig. 9C)**. The clasts are essentially angular and include a large range of Late Triassic ophites, Devonian meta-sandstones and Carboniferous marbles. The first unit is then followed by a 10-15 m thick olistolithes of ophites **(Fig. 9A)**, grading vertically to a 15 m thick breccias unit **(Fig. 9D)**. It is composed of monogenic Late Triassic ophites breccias organized in fining upward sequences. The bed thickness varies from 2 m up to 4 m and the clasts size ranges from 2 cm up to 40 cm **(Fig. 9D)**.

Regional aspect. This new member crops out on the Hiruraitzeta area localized to the south-west of the Saint-Palais unit. This member is characterized by a thickness of around 100 m.

Boundaries. The base of the Hiruraitzeta member corresponds to the upper part of the Late Albian Early Cenomanian Flysch de Mixe Formation **(Fig. 4)**. The upper limit of this new member grades upward to the upper part of the Flysch à Silex Formation passing to the Flysch Bleu Formation of Turonian age (**Fig. 4**; Castéras et al., 1970b; Boissonnas et al., 1974; Le Pochat et al., 1976).

Age. The stratigraphic position in between the Flysch de Mixe and Flysch à Silex formations suggests a Mid-Late Cenomanian age for the Hiruraitzeta Member **(Tab. 1)**.

New sedimentology facies analysis: The carbonate beds correspond to fine-grained facies with wavy laminae grading to parallel laminated and finally massive mudstone. These facies correspond to the Tb-Tc-Td(e) facies of the low-density turbidites Bouma sequence (Bouma, 1962). At the base of the formation siliclastic and carbonate-clasts breccias with frequent reverse-grading beds and poor matrix content argue for hyperconcentrated to gravelly high density turbidity current. This facies passes vertically to normal graded coarse sandstone and current ripples to wavy laminated coarse sandstone. This transition is typical of the gravelly high density to sandy high-density turbidity current change. On top of these clastic influxes, are deposited fine-grained calcareous turbidites with planar laminations at the base, passing to undulated to oblique laminations on top, characteristics of the low density turbidity currents. The interlayered siliclastic facies shows a clast-supported texture, close to the Mutti F3 facies (Mutti, 1977, 1992). The presence of olistolithes in the uppermost member demonstrates the proximity of a relative steep slope providing this coarse influx and suggest steep slope-controlled gravitary deposits. The Hiruraitzeta member corresponds to calcareous turbidites interbedded with deep basin tractive gravity flow deposits and olistolithes (Razin, 1989). The calcareous turbidites show typical low-density turbidites facies (Tc-Te; Bouma 1962).

4.9.3. Aguerréborda breccias member (New)

Lithostratigraphy description. The Aguerréborda member is composed of fining-upward breccias characterized by angular clasts, ranging from 1 cm up to 20 cm **(Fig. 9E)**. The breccias are characterized by a clast-supported texture. The clasts are polygenic but only composed of prerift sedimentary cover, i.e. Jurassic, Barremian and Aptian limestones.

Boundaries. The Aguerréborda member unconformably rests on the prerift Barremian limestones and it is overlain with the Coniacian to Santonian calcareous turbidites.

Regional aspect. This member is only outcropping on the Aguerreborda domain localized to the north the Saint-Jean-Pied-de-Port unit.

Age. These breccias are attributed to the Mid to Late Cenomanian for the following reasons: (1) their stratigraphic relationship with the Barremian limestones and the Coniacian to Santonian calcareous turbidites, (2) these clast-supported breccias are overlain with calcareous turbidites which regionally develop only from Mid Cenomanian time and (3) the facies analogy of this upper fine-sandy level with the Flysch à Silex Formation.

New sedimentology facies analysis: Clasts-supported texture suggest a bedload transport within a calcareous turbidity current; while the laminated facies on top correspond to low-density turbidites (Bouma, 1962).

4.10. Calcaires des Canyons Formation

Lithostratigraphy description. The Calcaires des Canyons Formation is composed of carbonate and more rarely siliciclatic rocks, especially in the lower part of the Cenomanian deposits (Ternet, 1965; Souquet, 1967; Alhamawi, 1992; Ternet et al., 2004). The new lithostratigraphic section measured on the Aldudes unit illustrates the base of the Calcaires des Canyons Formation. This section begins with 15 m of silico-clastic siltstones, sandstones and micro-conglomerates. Clasts nature only corresponds to Devonian dolomites, quartzites and schists **(Fig. 10A)**. This unit grades vertically to Cenomanian-Turonian carbonate facies characterized by the development of grainstones with bivals and peloids, packstone with praealveolina, orbitolines, rudists and bivals **(Fig. 10D)**, floatstone with rudists and finally, mudstone to wackstone with praealveolina and miliols **(Fig. 10A-C)**. These facies correspond to the typical miliols and rudists-rich Calcaires des Canyons facies.

Boundaries. The Calcaires des Canyons Formation unconformably rests upon the Paleozoic sedimentary basement of the Aldudes unit and is overlain with the Campanian calcareous flysch.

Regional aspect. This formation is present all along the inverted Iberian rift margin of the North-Pyrenean rift system. The formation thickness varies from 100 m to 600 m thick.

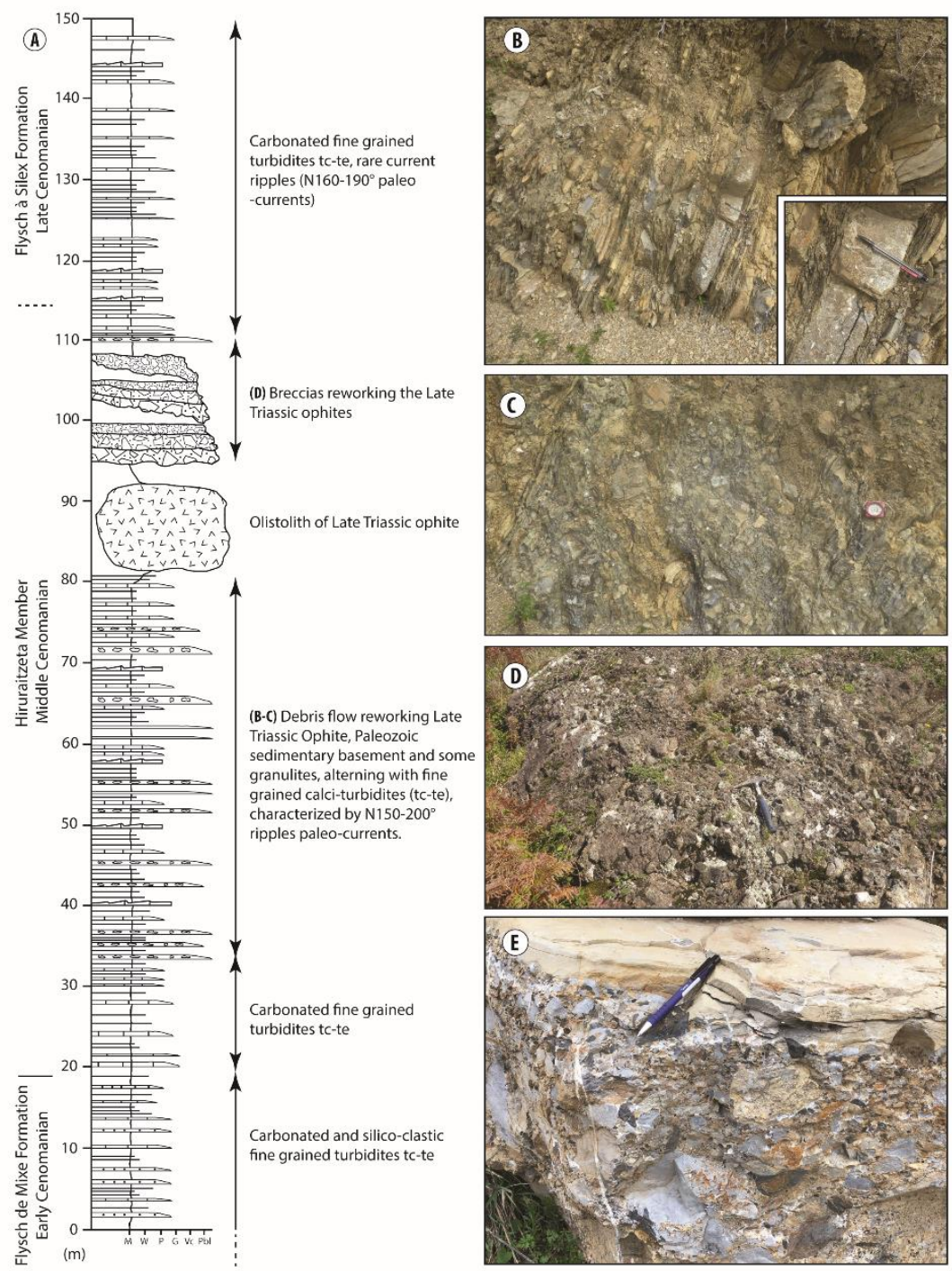


Fig. 9. (A) Hiruraitzeta lithostratigraphic succession showing the Cenomanian deep basin record of the Mauléon basin Saint Palais unit; **(B)** Middle Cenomanian fine-grained calci-turbidite made up of incomplete Bouma sequence, interdigitating with out of sequence clast-supported polygenic breccias reworking clasts of Paleozoic meta-sediments and Late Triassic ophites; **(C)** Middle Cenomanian metric unit of polygenic breccias reworking clasts of Paleozoic meta-sediments and Late Triassic ophites; **(D)** Monogenic class-supported breccias reworking the Late Triassic ophites; **(E)** Aguerreborda member, polygenic clast-supported breccias made up of Jurassic and Early Cretaceous limestones.

Age. The Calcaires des Canyons Formation is Cenomanian to late Santonian in age based on benthic and planktonic foraminifera and green algae (Ternet, 1965; Souquet, 1967; Merle, 1974; Le Pochat et al., 1978; Alhamawi, 1992; Ternet et al., 2004; **Tab. 1**). The Cenomanian is dated by the foraminifer association *Praealveolina cretacea*, *Ovalveolina ovum* and *Chysalidina gradata* in the Aldudes section (Merle, 1974; Le Pochat *et al*., 1978).

New sedimentology facies analysis: The basal 15 m thick silico-clastic units corresponds to a

transgressive sequence marked in its lowermost part by an erosive conglomerate which rework the underlying substratum. Based on the limestone texture and fauna assemblages, the Calcaires des Canyons carbonate platform facies are interpreted as deposited in lagoon to shoreface environments. In such a case, the Aldudes Unit is characterized by the development of a carbonate platform from the Cenomanian to Turonian, a drowning during Coniacian that accelerates at Santonian time.

4.11. Calcaires de Sare Formation

Lithostratigraphy description. The Calcaires de Sare Formation (Lamare, 1954b, 1964, Feuillée, 1962, 1964, 1967, 1971; Mathey, 1986; Prave, 1986) presents several types of lithofacies: (1) terrigenous limestones, (2) reef limestones, (3) biodetritic limestones and (4) fine limestones with calcispheres (Razin. 1989). The terrigenous limestones contain millimetric to centimetric clasts of white quartz (80%), Carboniferous shale, sandstone, Triassic ophite, rudist fragments and algae (Razin. 1989). This facies appears at the base of the formation, where it marks the transition with the Zugarramurdi Formation. Reef limestones are made up of decametric bioherms passing to biodetritic limestones representing the major part of the formation. The coarser facies are mainly composed of rudist fragments, algae debris, gastropods, polyps, bryozoans, echinoderms, Cuneolins, Miliolidae, as well as intraclastics biomicrite or biosparite (Razin. 1989). Fine calcarenites are made up of biomicrites with pellets, echinoderm spicules, small benthic foraminifers and rudist debris. Finally, the fine limestones with calcispheres mark the uppermost part of the formation and the transition with the Flysch à fucoïdes Fm (Feuillée. 1964). The synsedimentary fluids extrusions on calcareous beds and the intercalation of thin bioclastic layers with erosive base (storm deposits), testify of a relatively deep and unstable environment for these uppermost deposits (Razin. 1989).

Boundaries. This formation rests unconformably over the Paleozoic sedimentary basement or the Zugarramurdi Fm. A sharp contact marks the transition between Calcaires de Sare Fm and the overlying deep basin argillaceous Mid to Late Coniacian Flysch à fucoïdes (**Fig. 7D**).

Regional aspect. This formation only crops out on the Cinco-Villas unit. The formation's thickness ranges between 100 m and 200 m.

Age. The base of these limestones is attributed to the Mid Cenomanian to Turonian thanks to stratigraphic correlation (**Tab. 1**; Feuillée. 1964; Mathey, 1986). The top of this formation is attributed to the Early Coniacian as it grades progressively to the Middle to late Coniacian Flysch à fucoïdes Formation (Razin, 1989).

Genesis. This formation is classically interpreted as deposited in an inner platform bordered by build ups (Prave, 1986; Richard, 1986; Razin, 1989). At the base, this platform is shallow, strongly agitated and locally temporarily interrupted by terrigenous inputs. The uppermost deposits are characteristics of a relatively deep and unstable environment.

5. Boreholes observations

5.1. Ainhice-1 borehole

The base of the succession in this well corresponds to Paleozoic rocks, overlain by a thick Upper Triassic sequence, essentially composed of salt **(Fig. 11A)**. This Triassic salt is overlain a duplicate Mesozoic sedimentary cover (Lower unit: U1; Upper Unit: U2) separated by a fault. The Lower Unit, U1, consists of a complete Jurassic sequence (except the uppermost Late Jurassic), directly covered by Late Aptian Urgonian limestones. Unit U1 is thus characterized by a Neocomian to Early Aptian gap. The Upper Unit, (U2) displays the exact same stratigraphy, yet the Kimmeridgian marls are thinner than in U1 and unconformably overlain with Earliest Albian carbonate platform deposits (characterized by numerous Mélobésiées), implying a larger gap than U1. **(Fig. 11A)**. Both U1 and U2 are overlain with Late Albian to Early Cenomanian turbidites of the Flysch de Mixe Fm. The top of the borehole is characterized by the development of the Mid to Late Cenomanian Flysch à Silex Formation.

5.2. Ustaritz-1 borehole

The base of the Ustaritz-1 borehole reaches a thick Upper Triassic sequence, composed of salt, clay and ophites **(Fig. 11B)**. This sequence is overlain with around 50 m thick Upper Hettangian breccias and dolomitic limestone (Teyssonnières. 1983).

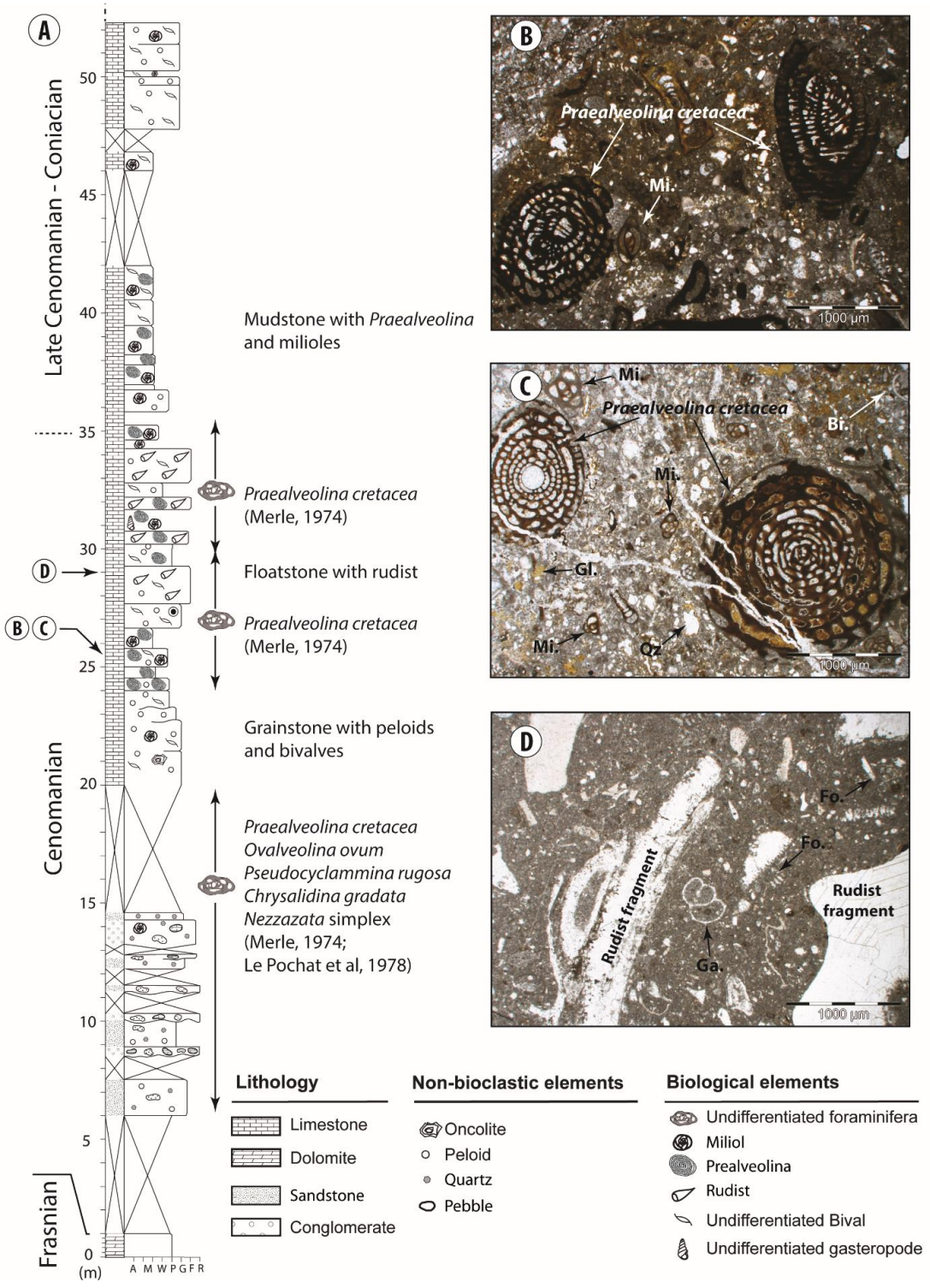


Fig. 10. (A). Sedimentary log of the Alludes Cenomanian to Early Coniacian carbonate platform; **(B-C).** Wackestone to packstone with *alveolina*, miliolids (Mi.), bivalves (Bi.), quartz (Qz) and glauconite (Gl.); **(D).** Rudist fragments rich wackestone with well –preserved gastropods (Ga.) and foraminifera (Fo.).

This Upper Hettangian unit is directly overlain by a 1200 m thick Late Albian chaotic and polymictic breccia corresponding to the Amotz Formation (c.f. 4.6.). This breccia is made up of blocks deriving from Late Triassic (ophite, clay and salt), (2) Hettangian to Sinemurian (dolomitic limestone) and (3) Latest Albian (mélobésiées Limestone). These breccias are interbedded with finer-grained gravity flow deposits containing the same elements than the breccias. This Amotz breccia is gradually overlain by the Flysch de Mixe Formation which is about 850 m thick.

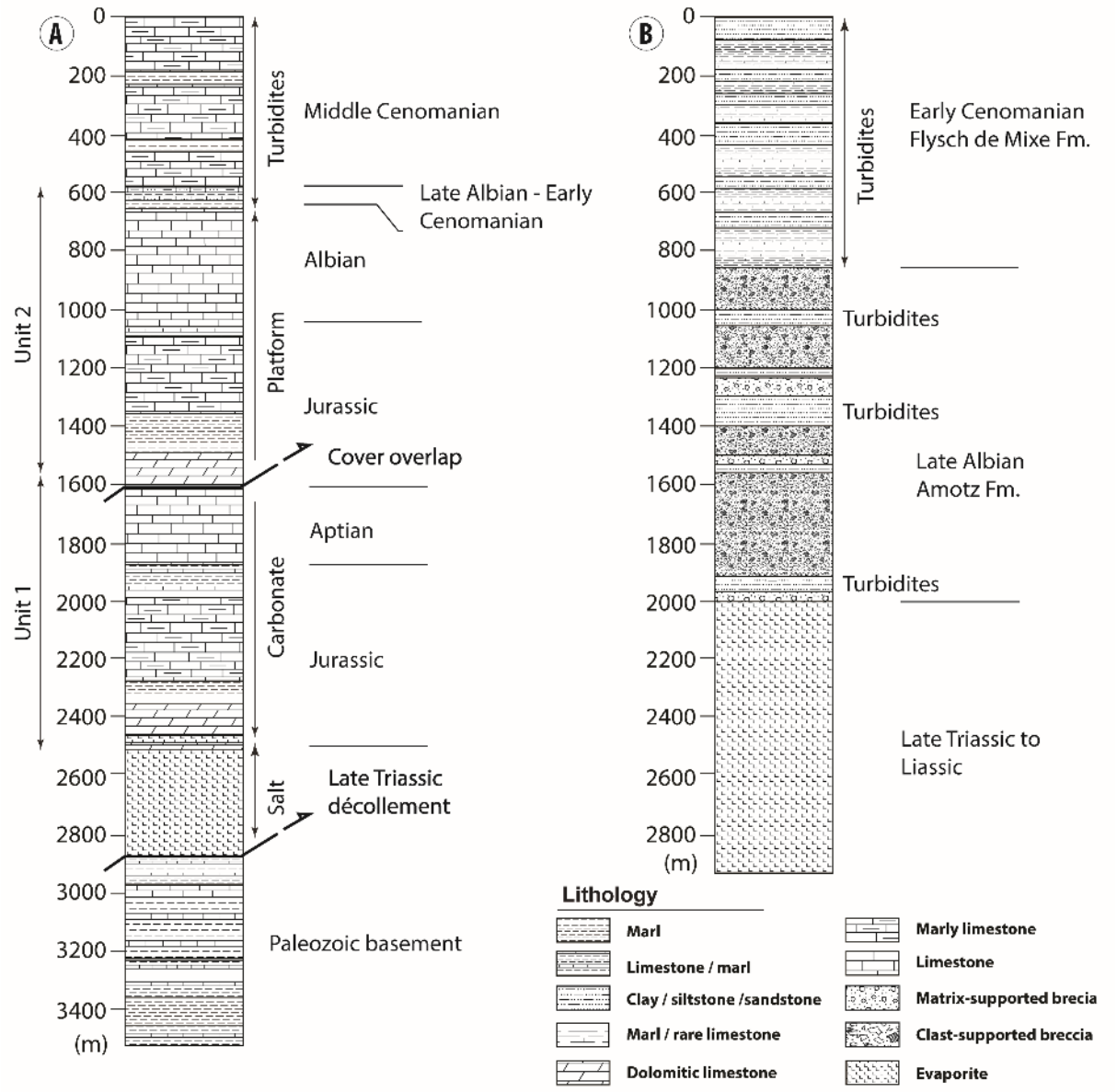


Fig. 11. Stratigraphic succession and sedimentary facies of the **(A)** Ainhice-1 borehole; **(B)** Ustaritz-1 borehole.

6. Tectono-sedimentary evolution of the Iberian rift margin

In the following chapter, we propose to describe the sedimentary geometry and discuss the tectono-sedimentary evolution of the Mauléon / Saint-Jean-de-Luz basin southern margin between the Aldudes and the Cinco-Villas domains **(Fig. 1)**. The distance between the easternmost and the westernmost transects is about 40 km. The first (eastern) section illustrates the Early Albian evolution of the southern margin of the Mauléon basin between Aldudes and Ainhice areas **(Fig. 2)**. The second (western) one focuses on the Late Albian evolution of the southern margin of the Saint-Jean-de-Luz basin between Cinco Villas and Espelette areas **(Fig. 3)**. The two last ones concern the evolution of the south-western margin of the Mauléon basin during Cenomanian times along the Pamplona transfer zone (Ursuya-Arberoue and Bidarray-Hiruraitzeta transects, **Fig. 2**).

6.1. Aldudes-Ainhice transect

6.1.1. Late Jurassic to Early Albian

The ante-rift sedimentary record corresponds to Jurassic to Early Albian carbonate facies. They are encountered only in the northern Saint-Palais unit (Bustince Formation) and in subsurface (Ainhice-1 well, **Figs. 2 and 11**). The Iberian Margin itself is deprived of any Jurassic and pre-rift sediments,

as a consequence of the Latest Jurassic - Early Cretaceous exposure stage **(Figs. 12A-12B & 12C)**.

6.1.2. Early to Middle Albian

Sedimentary record in this-area truly starts during the Early Albian: the olistolithes and sedimentary klippes of the Bustince Formation (c.f. 4.3.) and the tectonic overlap of the two Mesozoic units in the Ainhice-1 well (c.f. 5.1.) are Early-Mid Albian in age. Olistostromes display different content from north to south (cf 4.3). The southern one contains a much more truncated Jurassic-Early Cretaceous series. This pattern is identical to the Arbailles unit stratigraphy in which: (i) erosion of the Jurassic is much pronounced southward and (ii) Early Cretaceous transgression is more complete to the north (Canérot, 2008; Saspiturry et al., 2019a). Thus the northern olistostromes is probably derived from a much distal northern position than the southern one, probably wrenched from the more proximal margin. Westward, the Albian synrift sequence is marked by the development of the base of slope turbidites gravity flow deposits corresponding to the Mendibelza Formation (c.f. 4.1.). The gigantic blocks observed in Bustince are much rarer here. Paleocurrents indicate that they are derived from southwestern fan delta systems (Aldudes domain), reworking the Paleozoic sedimentary basement and the Late Triassic of the Iberian proximal rift margin. A key feature within Mendibelza conglomerates is the lack of Mesozoic clasts, suggesting that these fan deltas eroded a proximal margin domain where the prerift Mesozoic cover was lacking. This is very consistent with the Aldudes domain where Paleozoic basement is directly capped by a Late Cretaceous Carbonate platform (c.f. 4.10; Calcaires des Canyons), meaning that pre-rift cover was removed from it. Since no pre-rift sediments were reworked, this stratigraphy pile had to be substracted prior to the Late Cretaceous onlap. We thus propose that the ante-rift Aldudes sedimentary cover glided towards the north, at Earliest Albian time, along the Late Triassic salt décollement level **(Fig. 12D)**. This assumption is strengthen by the cataclastic texture of this surface displays in the Saint-Jean-Pied-de-Port area (Boissonnas et al. 1974), suggesting strong shear processes. Eastward, this major cover-gliding episode explains the lack of Mesozoic clasts within the Mendibelza conglomerates which reworked the new denudated Paleozoic basement of the Aldudes proximal rift margin domain. This cover gliding led to the dislocation of the Mesozoic cover, and had a significant consequence on the margin morphology: it created a steep sub-marine scarp of dislocated Mesozoic cover to the south of the Bustince area **(Fig. 12D)**. Gigantic portion of this slope then collapsed due to syn-rift tectonic activity, and reworked as olistolithes and sedimentary klippes within the Bustince Formation (c.f. 4.3.). The monogenic clast-supported debris flow made up of the Late Triassic ophites at the base of the Bustince Formation might be the erosion product of the basal cataclastic surface developed along the Late Triassic cover décollement level. In subsurface and in a most distal position, the ante-rift sedimentary cover is duplicated in the Ainhice well without any reverse offset (c.f. 5.1.), suggesting tectonic normal offset or gravitary sliding.

6.1.3. Late Albian to Early Cenomanian.

During Late Albian time, a discontinuous carbonate platform starts to develop onto the denudated Aldudes Paleozoic substratum as evidenced by the occurrence of Late Albian carbonate platform clasts reworked into the base of slope Honto and Saint-Etienne-de-Baïgorry breccias **(Fig. 9E)**. Synrift tectonic instabilities disrupts the platform development and induces its collapse into basinward propagating debris flow. Downslope turbidity currents incorporates Paleozoic clasts on the Aldudes domain slope, which explain the polygenic character of the Honto and Baïgorry gravity deposits **(Fig. 12E)**.

6.1.4. Middle to Late Cenomanian

During the Late Cretaceous, the Aldudes proximal rift margin spans the development of the transgressive "Calcaires des Canyons" carbonate platform (c.f. 4.10.) overlaying the Paleozoic meta-sedimentary substratum **(Fig. 12F)**. In between Early and Middle Cenomanian time, the Saint-Jean-Pied-de-Port Triassic Unit tilts towards the south due to the development of the north dipping Lakhoura detachment system (Saspiturry et al., 2019a; **Fig. 12F**). This fault separates the Aldudes proximal margin from the northern domain.

They are respectively characterized by inner-ramp to shoreface carbonate–ramp facies (Calcaires des Canons Formation), and deep basin gravity deposits (Errozaté (c.f. 4.8.) and Irey (c.f. 4.8.2.) breccias) reworking both the "Calcaires des Canyons" carbonate platform and the Paleozoic sedimentary basement (Fig. 12F). In the meantime, the North Arbailles Fault separates the Saint-Jean-Pied-de-Port southward tilted block from the Saint-Palais domain (Saspiturry et al., 2019a). During the Late Cretaceous, this deep basin domain is supplied by northern-derived low-density calcareous turbidites of the Flysch à Silex Formation (c.f. 4.9.). These turbidites are onlapping on the previous synrift sequence and are supplied from the European platform developing on the northern Mauléon proximal rift margin **(Fig. 12F)**.

6.2. Cinco-Villas /Espelette transect

6.2.1. Late Jurassic to Middle Albian

The only prerift Mesozoic carbonates identified on this transect are clasts reworked within the syn-rift Late Albian to Early Cenomanian Amotz Formation (c.f. 4.6.). These breccias are characterized by the lack of Middle to Late Jurassic and Barremian-Aptian clasts, arguing for a more pronounced exposure and erosion during Neocomian than in the Aldudes domain. This is responsible for (1) the erosion of the Jurassic sequence down to the Early Jurassic **(Fig. 13A)** and (2) the no-deposition of the Barremian-Aptian limestones **(Fig. 13B)**. The presence of the Albian "Mélobésiées" limestones clasts in the Amotz breccias suggests that these limestones were deposited directly over the partly eroded Early Jurassic sequence. These shallow Mélobésiées limestones are time-equivalent to the Saint-Palais Formation (cf. 4.2 ; **Fig. 13C**).

6.2.2. Late Albian to Early Cenomanian.

The Amotz breccias, evidencing the syn-rift sedimentary record within the basin are synchronous with the Late Albian to Early Cenomanian Zugarramurdi Formation (c.f. 4.4.). This latter corresponds to a deltaic system developing over the Cinco-Villas Paleozoic and Late Triassic sedimentary basement **(Fig. 13D)** supplied basinward the Amotz Breccias (c.f. 5.2. Ustaritz-1 borehole recording 1 000m thick of Amotz breccias) and the Flysch de Mixe Formation (c.f. 4.5.; **Fig. 13D**). The development of the Zugarramurdi Formation implies the substraction of the Mesozoic cover from the Cinco-Villas basement prior to its sedimentation. This process is interpreted as Late Albian northward large-scale cover gliding favored by the Late Triassic salt décollement **(Fig. 13D)**. In a first time, the dislocated carbonate cover supplied the base of the Amotz breccias with mainly prerift cover elements forming debris flow sequences, while the giant sedimentary klippes of Paleozoic and Triassic meta-sediments (c.f. 4.6.) attest of a Paleozoic basement source, coming from a basin scarp, corresponding to the Amotz normal fault **(Fig. 13E)**.

6.2.3. Middle to Late Cenomanian

During the Late Cretaceous, the Cinco-Villas proximal margin spans the development of a shallow carbonate platform materialized by the Calcaires de Sare Formation (c.f. 4.11.), time equivalent to the Calcaires des Canyons Formation (Aldudes domain, c.f. 4.10.) **(Fig. 10E)**. In the basin, the siliciclastic Flysch de Mixe Formation (c.f. 4.5.) is unconformably capped by fine grained calcareous turbidites coming from the European carbonate platform and corresponding during Middle to Late Cenomanian time to the Flysch à Silex Formation (c.f. 4.9.; **Fig. 13E**).

6.3. Ursuya-Arberoue transect

6.3.1. Late Jurassic to Early Cenomanian

The Jurassic-Aptian carbonate cover identified in the Arberoue unit is one of the most complete sequence outcropping on the western part of the Mauléon basin **(Fig. 14A)**. In fact, only the Tithonian and the Neocomian deposits lack, highlighting a relative slight Early Cretaceous exposure and weathering stage **(Figs. 14A-14D)** compared to other proximal margin section. This is directly linked to the more distal position of this unit during the Latest Jurassic – Earliest Cretaceous uplift stage. This residual prerift carbonate sequence is overlain during the Late Albian to Early Cenomanian times by the Flysch de Mixe Fm.

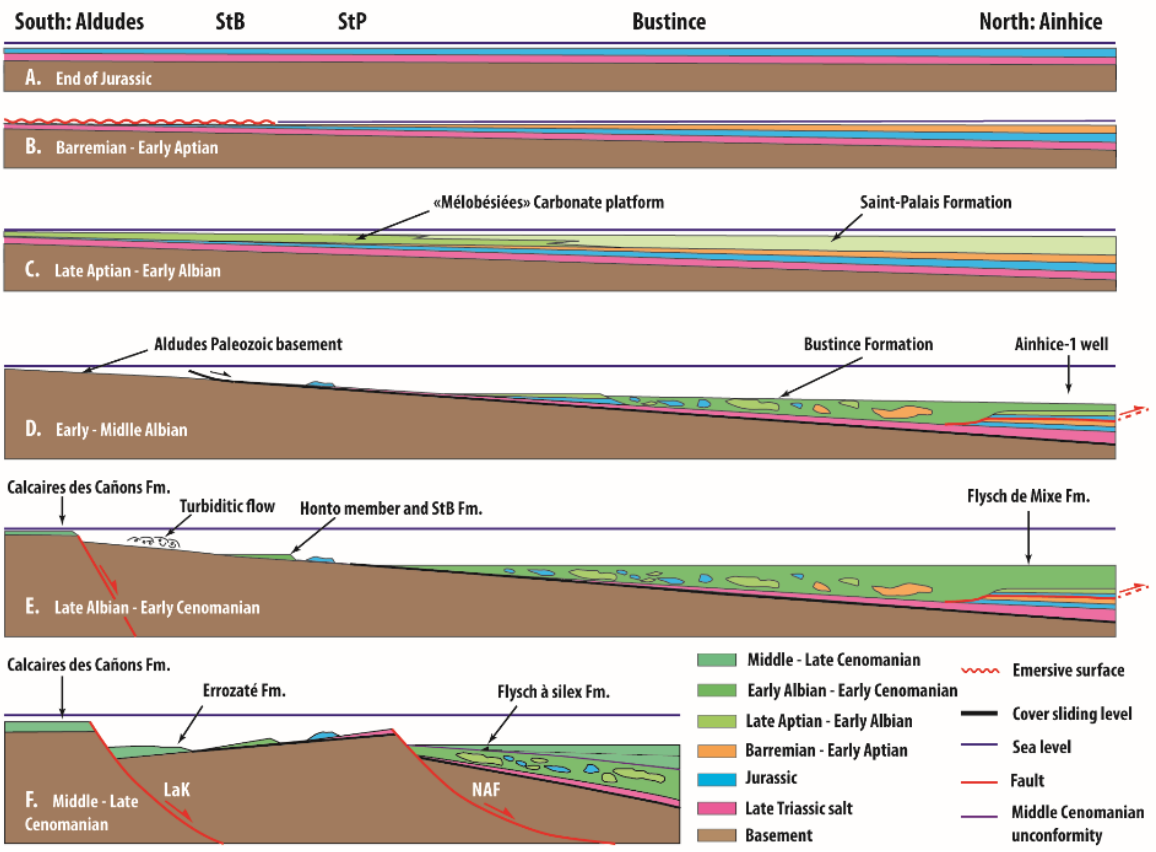


Fig. 12. Jurassic to Late Cenomanian schematic tectono-sedimentary evolution of the Iberian rift margin along the Aldudes-Ainhice transect. **(A)** End of Jurassic; **(B)** Barremian to Early Aptian; **(C)** Late Aptian to Early Albian; **(D)** Early to Middle Albian; **(E)** Late Albian to Early Cenomanian; **(F)** Middle to Late Cenomanian; StB: Saint-Etienne-de-Baïgorry unit; StP: Saint-Jean-Pied-de-Port unit; Lak: Lakhoura detachment; NAF: North Arbailles Fault; Fm.: Formation.

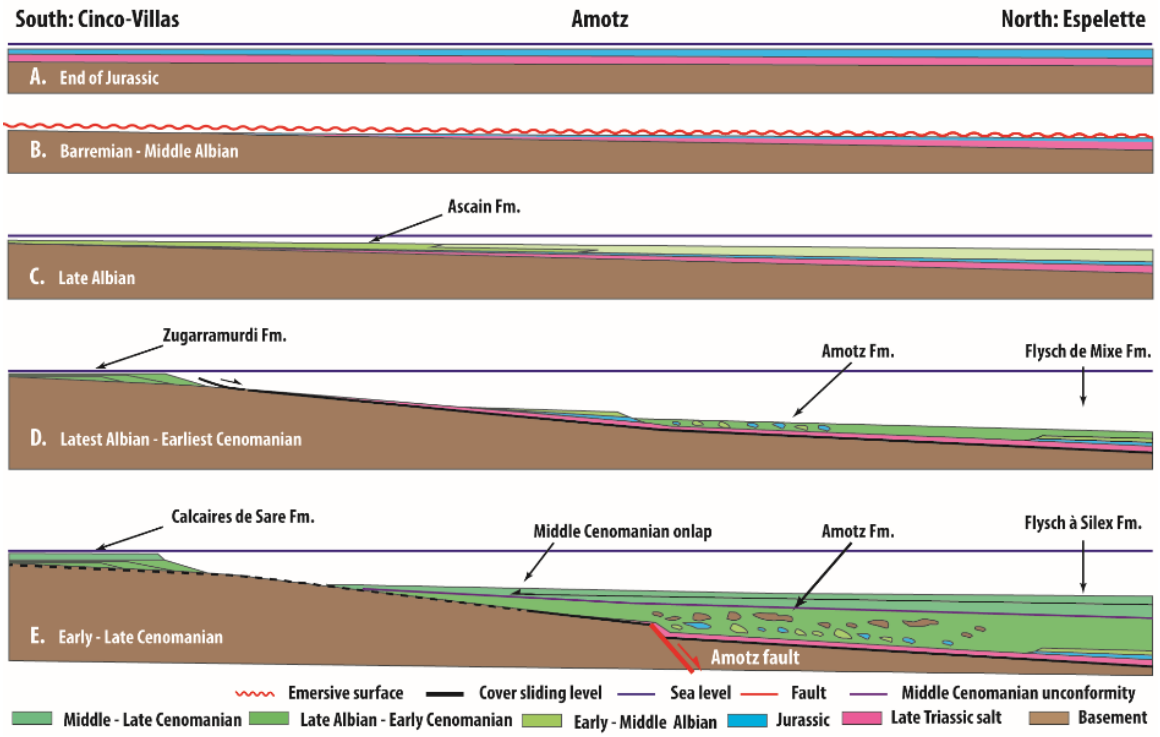


Fig. 13. Jurassic to Late Cenomanian schematic tectono-sedimentary evolution of the Iberian rift margin along the Cinco-Villas / Espelette transect. **(A)** End of Jurassic; **(B)** Barremian to Middle Albian; **(C)** Late Albian; **(D)** Latest Albian to Earliest Cenomanian; **(E)** Early to Late Cenomanian; Fm.: Formation.

6.3.2. Middle to Late Cenomanian

A very local, yet significant information of the sedimentary record of this transect is the presence of granulites clasts within the Mid-Late Cenomanian deep basin gravity deposits of the Bonloc member (c.f. 4.9.1.). For the first time, lower crustal material is reworked within the Mesozoic deposits. This observation suggests that the Ursuya granulites were denudated on a submarine scarp during the Mid-Late Cenomanian time. We interpret the denudation of the Ursuya granulitic unit as the immediate consequence of the northward cover gliding of the Jurassic to Early Cretaceous prerift carbonate cover and synrift Flysch de Mixe Formation turbidites along the Late Triassic décollement level **(Fig. 14E)**. The glided sedimentary cover previously capping the Ursuya granulites corresponds to the Arberoue cover unit currently thrusted towards the south **(Fig. 2)**. This thrust reuse the previous cover décollement level as evidenced by the presence of Late Triassic deposits along the Arberoue thrust. Again, the genesis of the cover-gliding creates a trough responsible for a rapid platform-basin transition **(Fig. 14E)**.

The Bonloc Breccias grades laterally to calcareous turbidites of the Flysch à Silex Formation, onlapping towards the south, the newly denudated Ursuya granulites. Thus, during Mid to Late Cenomanian times this transect was characterized by two interdigitating turbiditic system: (i) the Flysch à Silex low density turbidites corresponding to the export of the European platform and (ii) the Bonloc proximal and coarse grained gravity deposits reworking the newly denudated Ursuya granulites. The absence of Jurassic to Early Cenomanian clasts within the Bonloc Formation highlights the fact that the sedimentary cover glided towards the basin axis in one single piece and have not suffered dislocation compared to the Aldudes transect (Bonloc Formation and Ainhice-1 borehole) and the Cinco-Villas / Espelette transect (Amotz Formation). Similarly, to the base of the Bustince Formation, the Late Triassic clasts of ophites within the Bonloc breccias, could correspond to cataclasites of the décollement level reworked into the Bonloc breccias.

6.4. Bidarray-Hiruraitzeta transect

6.4.1. Late Jurassic to Early Cenomanian

Along the Bidarray-Hiruraitzeta transect, the Jurassic and Early Cretaceous carbonate platform deposits outcrop on the Aguerréborda domain **(Fig. 2)**. The prerift cover is also present in the overlaying Aguerréborda member. The Jurassic to Early Albian stratigraphic succession is heavily truncated compared to the one of the Arberoue transect attesting of a more important Early Cretaceous exposure and weathering stage than in the Arberoue domain **(Figs. 15A to 15D)**. These carbonate deposits are overlain by the synrift Late Albian to Early Cenomanian Flysch de Mixe Formation (c.f. 4.5.; **Fig. 15E**).

6.4.2. Middle to Late Cenomanian

Similarly, to the Ursuya-Arberoue transect, the Bidarray-Hiruraitzeta one undergoes the denudation of the Bidarray and Ossès proximal margin domain during Middle Cenomanian time in response to the eastward gliding of its Jurassic to Early Cenomanian sedimentary cover **(Fig. 15F)**. The Late Triassic décollement level is widely outcropping on the Ossès domain and the dismantled sedimentary cover partly outcrop on the Aguerréborda domain **(Figs. 2 and 15F)**. This tectonic event is followed by the deposition, over the Aguerréborda glided cover, of gravity flow deposits reworking both the glided cover and the Late Triassic décollement level (Aguerréborda member, c.f. 4.9.3.). Eastward, the Middle to Late Cenomanian Hiruraitzeta member records the gravity driven cover gliding thought the development of two interdigitating turbiditic system: (i) Bouma-type calcareous turbidites derived from the southward export of the European carbonate platform along important distance (Flysch à Silex turbiditic facies, c.f. 4.9.) and (ii) turbiditic currents resulting in the formation of clast-supported debris flow interbedded with olistolithes of Late Triassic ophites supplied from the west and reworking the newly denudated Ossès basement.

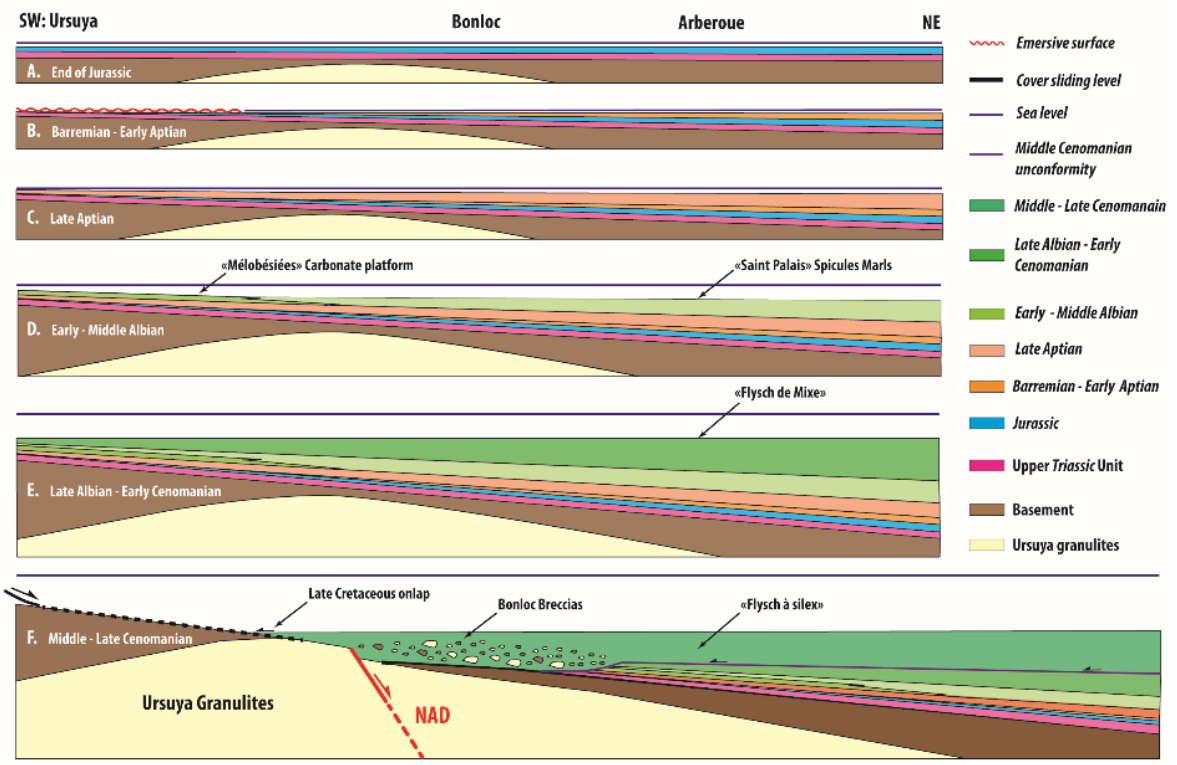


Fig. 14. Jurassic to Late Cenomanian tectono-sedimentary evolution of the Iberian rift margin along the Ursuya / Arberoue transect. **(A)** End of Jurassic; **(B)** Barremian to Early Aptian; **(C)** Late Aptian; **(D)** Early to Middle Albian; **(E)** Late Albian to Early Cenomanian **(F)** Middle to Late Cenomanian. NAD: North Arbailles detachment; Fm.: Formation.

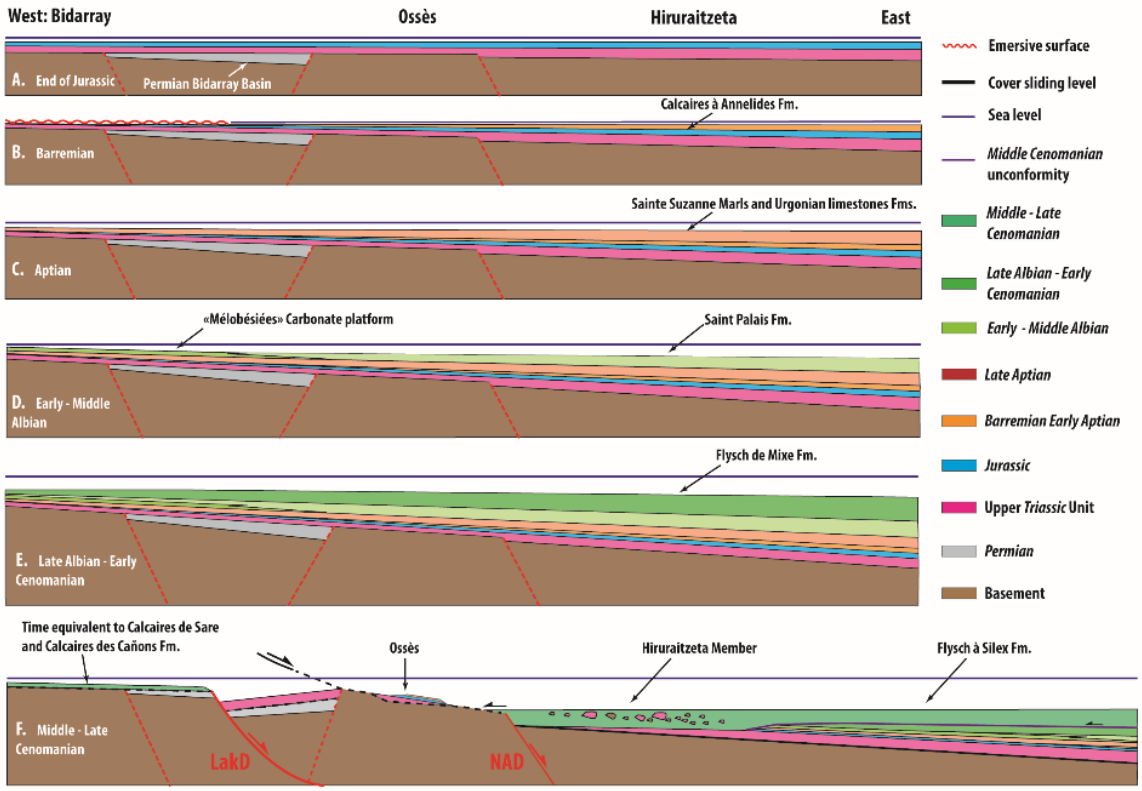


Fig. 15. Jurassic to Late Cenomanian tectono-sedimentary evolution of the Iberian rift margin along the Bidarray/ Hiruraitzeta transect. **(A)** End of Jurassic; **(B)** Barremian; **(C)** Aptian; **(D)** Early to Middle Albian; **(E)** Late Albian to Early Cenomanian **(F)** Middle to Late Cenomanian. LakD: Lakhoura detachment; NAD: North Arbailles detachment; Fm.: Formation.

7. Discussion

7.1. Basinward gravity-driven cover gliding along salt décollement level: a synrift polyphasic process

The importance of extensional tectonics implies motions along décollement levels and detachment faults. In the Pyrenees, the most important décollement level corresponds to the Late Triassic evaporites and clays, and the overlying Liassic marls (Durand-Delga, 1964; Bessière, 1987; Berger et al., 1993; Fonteilles et al., 1993; Jammes et al., 2009; Lagabrielle et al., 2010; Jammes et al., 2010; Clerc et al., 2015). The Mauléon / Saint-Jean-de-Luz hyperextended basin (Western Pyrenees) is known to span gravity-driven cover gliding during the Cretaceous rifting stage due to the activation of this major décollement level (Bouquet, 1986; Ducasse et al., 1986; Lagabrielle et al., 2010, 2019; Corre et al., 2016; Teixell et al., 2016; Asti et al., 2019; Saspiturry et al., 2019a). However, the timing of this process was not precisely addressed and remained unclear. The restoration of the tectono-sedimentary evolution of the four proximal rift margin - hyperextended deep basin transect across the Iberian rift margin, presented in the previous chapter, have shown that this process can be polyphase. Each cover-gliding phase seems to correspond to different and diachronous tectonic stages being part of the Cretaceous hyperextension. These correlations will be discussed in the next section.

7.1.1. Early Albian cover gliding: a consequence of the onset of synrift brittle deformation on the Mauléon basin

Our work shown that cover gliding affecting the Iberian margin starts at Early Albian time **(Fig. 12)**, contemporary of the onset of simple shear thinning affecting the Mauléon basin (Jammes et al., 2009; Masini et al., 2014; Gómez-Romeu et al., 2019). The development of the Saint-Palais detachment is responsible for the roll-over of the Mauléon domain Iberian margin and is interpreted to induce the gliding of the Mesozoic cover from the Aldudes (c.f. 6.1.), Mendibelza and Igountze margin units (Saspiturry et al., 2019a). The onset of basinward gravity-driven cover gliding seems to be time equivalent to local diapirism along the Iberian margin of the Mauléon basin, as evidenced by lateral facies variations from shallow carbonate platform (Calcaires à Mélobésiées Fm.) to spicule marls (Saint-Palais Fm.) around the diapiric structures during early Albian (Canérot, 1988, 1989; Canérot and Lenoble, 1993; James and Canérot, 1999; Canérot et al., 2005). In the same way, to the east of the Saison transfer zone **(Fig. 1)**, a crustal-scale balanced cross-section showed an Early Albian system of salt anticlines (salt walls), separated by synformal mini-basins with continuity of the Jurassic–Cretaceous prerift cover resulting from the basinward gliding of this latter (Labaume and Teixell, 2014).

7.1.2. Late Albian cover gliding: a response to the westward Mauléon rift opening

The Late Albian cover gliding affecting the Cinco-Villas unit (c.f. 6.2.), corresponding to the southern Iberian margin of the Saint-Jean-de-Luz domain is time equivalent to the westward opening of the Mauléon rift basin during Late Albian time (Razin. 1989). This stage is probably related to the development of an extensive tectonic structure, on the Saint-Jean-de- Luz domain responsible for the tilt towards the north of the Cinco-Villas domain, inducing the northward gliding of the Mesozoic cover into the deep basin **(Fig. 13)**. However, the poor outcrops quality and the Pyrenean thrusting overprint being difficult to define the geometry of this possible detachment system.

7.1.3. Middle Cenomanian cover gliding: a control of the Lakhoura and North Arbailles detachment system

Finally, the Middle Cenomanian development of the Lakhoura and North Arbailles northward dipping detachment system (Saspiturry et al., 2019a) is synchronous to the basinward gliding of the prerift and the synrift cover of the Ursuya (c.f. 6.3.1.) and Bidarray (c.f. 6.3.2.) margin domains **(Figs. 14 and 15)**. This cover gliding stage is responsible for the denudation of the Ursuya granulites at the end of the hyperextension affecting the Mauléon / Saint-Jean-de-Luz basin. Thus, the Ursuya granulites undergo a polyphasic history since their Permian exhumation (Vielzeuf 1984, Hart et al., 2016, Vacherat et al., 2017, Lemirre, 2018; Saspiturry et al., 2019b) to their Middle Cenomanian denudation. Gravity driven cover

gliding tectonic seems to also match the repartition of N20° inherited transfer zones. Their role in controlling this process is presented in the next paragraph.

7.2. Impact of inherited transfer zone on the 3D distribution of gravity-driven cover gliding

For many authors, the disorganization of the structural elements of the western Pyrenees could be linked to the existence of the N20° Pamplona transfer zone (Muller et Roger 1977; Schoeffler 1982; Richard 1986; Razin 1989; Claude 1990), inherited from Permian age (Saspiturry et al., 2019b) and responsible for the shift of the Pyrenean rift axis between the Mauléon and Basco-cantabric basins **(Fig. 1)**. Eastward, some transfer zone, as the Saint-Jean-Pied-de-Port, Saison, Barlanès and Ossau ones are known to control the subsidence, the sedimentary profile and the halokinesis during the Albian-Cenomanian continental rifting (Canérot, 1989, 2008, 2017; Canérot et al., 2005; Debroas et al., 2010). The diachronous cover gliding seems to match with the position of the inherited N20° Permian transfer zones affecting the Mauléon Saint-Jean-de-Luz hyperextended basin. In fact, it appears that the cover gliding is Early Albian in age to the east of the Saint-Jean-Pied-de-Port and Saison transfer zones while it is Late Albian and Middle Cenomanian in age respectively to the west and to the east of the Pamplona transfer zone **(Fig. 1)**. These N20° transfer zones seem to clearly condition the 3D diachronism and repartition of the Iberian margin basinward cover gliding during hyperextension. The large timing difference of cover gliding along the Iberian rift margin over such short distances calls into question the east-west continuity of tectonic structures and thus bears upon the origin of the non-cylindrical geometry of the Mauléon / Saint-Jean-de-Luz hyperextended rift system that seems to be controlled by previous inherited Permian crustal heterogeneities. The impact of such inherited N20° structuration on subsequent rifting and compression will be the purposed of future investigations.

7.3. Basin's morphology evolution throughout the rift period

Sedimentary record and facies analysis reveal a complex platform-basin morphology evolution across the Iberian Mauléon basin margin during Albian-Cenomanian. Onset of the Early Albian brittle rift sequence (Saspiturry et al., 2019a) is characterized by very rapid transition from coarse-grained base of slope conglomerates and low-density turbidites. This is illustrated by the Mendibelza / Saint-Palais formation transition. The first one corresponds to base of slopes conglomerates, probably dominated by avalanching process, while the second one mainly shows distal turbidites. Poor existence of hyperconcentrate turbidity currents in between both formation suggests a poor transportation efficiency directly related to a high angle slope-basin break annihilating the sediment transport, and a sudden spreading of the sediments.

This low-maturity transportation system evolves in Late Albian time to more preserved hyperconcentrate deposits within the Flysch de Mixe formation attesting of a more efficient system. Amotz base of slope breccias thus grade to marls dominated facies (hemipelagic to low-diluted turbidity current) in which high-density sandy facies suggest strong bedload processes. This feature suggests a basinal "smoother" slope on which turbidity currents might evolve from avalanching-hyperconcentrate proximal facies (Amotz breccias) to sandy high-density facies and low-density to diluted facies (Flysch de Mixe).

The Latest Albian –Cenomanian period is an interesting syn-rift sequence since it spans the development of two radically different system. Most of the sedimentation is dominated by calcareous turbidites (Flysch à Silex), characterized by northern derived low-density turbidites, in which are interlayered siliciclastic turbidites in its lowermost portion (Hiruraitzeta and Aguerréborda members). The base of Hiruraitzeta member contain quite mature hyperconcentrate to high-density facies, and they attest of an efficient transportation (relative low angle-slope) derived from the erosion of a southwestern source (Ossès domain). This pattern shows that western branch of Lakhoura detachement fault has a minor activity since it does not control such a steep long-lasting slope compared to the Early and Late Albian rift sequences. We demonstrated previously that this scarp is rapidly fossilized by Bonloc Breccias, and Lakhoura play is necessary very brief.

8. Conclusions

Our work highlights that the Mauléon / Saint-Jean-de-Luz smooth-slope-type rift basin undergoes polyphasic gravity-driven basinward cover gliding along the Late Triassic salt décollement. Three stages of gravity-driven cover gliding have been evidenced: (1) Early Albian, (2) Late Albian and (2) Middle Cenomanian. In the case of the Mauléon / Saint-Jean-de-Luz basin, the cover gliding stages and the related olistostrome are time equivalent to the onset of the main detachment systems responsible for the continental crust thinning and / or the widening of the hyperextended rift basin. In such a way, the sedimentary record of gravity-driven cover gliding along the proximal margins of smooth slope-type basins, should be take into account to better assess the complex synrift record and the timing of detachment faulting. In fact, the resulting gravity deposits can be used to date the onset of the synrift detachment faults responsible for the continental crust thinning and the sub-continental mantle exhumation. Sedimentary record of cover gliding has evidenced that this process is followed, first, by the deposition of gravity deposits reworking mainly the glided and fragmented prerift to synrift sedimentary cover of the décollement footwall and then the newly denudated proximal margin basement of the décollement hanging-wall. The turbiditic deposits interbedded with the olistolithes and sedimentary klippes resulting from the basinward gliding of the sedimentary cover allow to date relatively this gravity deposits and thus the deformation stage affecting the basin.

Acknowledgements

This study was conducted within the framework of the integrated geological Orogen research project (TOTAL, BRGM, and INSU).

References

Alhamawi, M., 1992, Sédimentologie, pétrographie sédimentaire et diagenèse des calcaires Crétacé supérieur de la marge ibérique, Vallées d'Ossau - Vallée d'Aspe, Haute Chaîne, Pyrénées Atlantiques: Université Bordeaux 1, 356 p.

Arnaud-Vanneau, A., H. Arnaud, J. Charollais, M.-A. Conrad, P. Cotillon, S. Ferry, J.-P. Masse, and B. Peybernès, 1979, Paléogéographie des calcaires urgoniens du sud de la France: Géobios, v. 3, p. 363–383.

Aslanian, D. et al., 2009, Brazilian and African passive margins of the Central Segment of the South Atlantic Ocean: Kinematic constraints: Tectonophysics, v. 468, no. 1–4, p. 98–112, doi:10.1016/j.tecto.2008.12.016.

Asti, R., Y. Lagabrielle, S. Fourcade, B. Corre, and P. Monié, 2019, How Do Continents Deform During Mantle Exhumation? Insights From the Northern Iberia Inverted Paleopassive Margin, Western Pyrenees (France): Tectonics, p. 2018TC005428, doi:10.1029/2018TC005428.

Beltrando, M., G. Manatschal, G. Mohn, G. V. Dal Piaz, A. V. Brovarone, and E. Masini, 2014, Recognizing remnants of magma-poor rifted margins in high-pressure orogenic belts: The Alpine case study: Earth-Science Reviews, v. 131, p. 88–115.

Bilotte, M., 1985, Le Crétacé Supérieur des plate-fromes Est Pyrenéennes: Université Paul Sabatier de Toulouse (Sciences), 442 p.

Bilotte, M., 1984, Les grands Foraminiféres benthiques du Crétacé supérieur pyrénéen. Biostratigraphie. Refléxions sur les correlations mésogéennes: Benthos, v. 83, p. 61–67.

Boillot, G. et al., 1987, Tectonic denudation of the upper mantle along passive margins: a model based on drilling results (ODP leg 103, western Galicia margin, Spain): Tectonophysics, v. 132, no. 4, p. 335–342.

Boillot, G., G. Féraud, M. Recq, and J. Girardeau, 1989, Undercrusting by serpentinite beneath rifted margins: the example of the west Galicia margin (Spain): Nature, v. 341, no. 6242, p. 523–525.

Boirie, J.-M., 1981, Etude Sédimentologique des Poudingues de Mendibelza (Pyrénées Atlantiques): Toulouse, Université Paul Sabatier de Toulouse (Sciences), 114 p.

Boirie, J.-M., and P. Souquet, 1982, Les poudingues de Mendibelza: dépôts de cônes sous-marins du rift albien des Pyrénées: Bulletin Centres Recherches Exploration-Production Elf-Aquitaine, v. 6, no. 2, p. 405–435.

Boissonnas, J., G. Le Pochat, C. Thibault, and M. Bernatzk, 1974, Carte géologique de la France au 1/50000; feuille d'Iholdy, Orléans, France: Bureau de Recherche Géologique et minière.

Bouquet, B., 1986, La bordure mésozoïque orientale du Massif du Labourd (Pyrénées occidentales) : Stratigraphie-Sédimentologie-Structure-Implications Géodynamiques: Pau, Université de Pau et des Pays de l'Adour, 219 p.

Brun, J.-P., and X. Fort, 2011, Salt tectonics at passive margins: Geology versus models: Marine and Petroleum Geology, v. 28, no. 6, p. 1123–1145, doi:10.1016/j.marpetgeo.2011.03.004.

Canérot, J., 2008, Les Pyrénées: Histoire géologique: Atlantica.

Cassou, A. M., 1968, La formation des 'Marnes de Sainte-Suzanne'et ses faciès latéraux en Aquitaine occidentale (essai de zonation et de datation): Bulletin du Centre de recherches de Pau-SNPA, v. 2, p. 263–281.

Castéras, M., J. Canérot, J. Paris, D. Tisin, M. Azambre, and H. Alimen, 1970b, Carte géologique de la France au 1/50000; feuille d'Oloron Sainte Marie, Orléans, France.

Casteras, M., M. Gottis, M. Clin, J. . Guignard, J. Paris, and J. Galharague, 1971, Carte géologique de la France au 1/ 50 000, feuille deTardets–Sorholus, Orléans, France.

Claude, D., 1990, Etude stratigraphique, sédimentologique et structurale des dépôts mésozoïques au nord du massif du Labourd: rôle de la faille de Pamplona (Pays Basque): Université de Bordeaux III, 437 p.

Clerc, C., and Y. Lagabrielle, 2014, Thermal control on the modes of crustal thinning leading to mantle exhumation: Insights from the Cretaceous Pyrenean hot paleomargins: Tectonics, v. 33, no. 7, p. 1340–1359, doi:10.1002/2013TC003471.

Clerc, C., Y. Lagabrielle, M. Neumaier, J.-Y. Reynaud, and M. de Saint Blanquat, 2012, Exhumation of subcontinental mantle rocks: evidence from ultramafic-bearing clastic deposits nearby the Lherz peridotite body, French Pyrenees: Bulletin de la Société géologique de France, v. 183, no. 5, p. 443–459.

Clerc, C., A. Lahfid, P. Monié, Y. Lagabrielle, C. Chopin, M. Poujol, P. Boulvais, J. C. Ringenbach, E. Masini, and M. de St Blanquat, 2015, High-temperature metamorphism during extreme thinning of the continental crust: a reappraisal of the North Pyrenean passive paleomargin: Solid Earth, v. 6, no. 2, p. 643–668.

Cobbold, P. R., and P. Szatmari, 1991, Radial gravitational gliding on passive margins: Tectonophysics, v. 188, no. 3–4, p. 249–289.

Contrucci, I., L. Matias, M. Moulin, L. Géli, F. Klingelhofer, H. Nouzé, D. Aslanian, J.-L. Olivet, J.-P. Réhault, and J.-C. Sibuet, 2004, Deep structure of the West African continental margin (Congo, Zaïre, Angola), between 5 S and 8 S, from reflection/refraction seismics and gravity data: Geophysical Journal International, v. 158, no. 2, p. 529–553.

Corre, B., Y. Lagabrielle, P. Labaume, S. Fourcade, C. Clerc, and M. Ballèvre, 2016, Deformation associated with mantle exhumation in a distal, hot passive margin environment: New constraints from the Saraillé Massif (Chaînons Béarnais, North-Pyrenean Zone): Comptes Rendus Geoscience, v. 348, no. 3–4, p. 279–289, doi:10.1016/j.crte.2015.11.007.

Daignières, M., M. Séguret, M. Specht, and E. Team, 1994, The Arzacq-western Pyrenees ECORS deep seismic profile, *in* Hydrocarbon and petroleum geology of France: Springer, p. 199–208.

Debourle, A., and R. Deloffre, 1976, Pyrénées occidentales, Béarn, Pays Basque: Masson, 175 p.

Debroas, E.-J., 1987, Modèle de bassin triangulaire à l'intersection de décrochements divergents pour le fossé albo-cénomanien de la Ballongue (zone nord-pyrénéenne, France): Bulletin de la Société géologique de France, v. 3, no. 5, p. 887–898, doi:10.2113/gssgfbull.III.5.887.

Debroas, E. J., and P. Souquet, 1976, Sédimentogenèse et position structurale des flyschs crétacés du versant nord des Pyrénées centrales: Bull. Bur. Rech. Géol. Min., I, p. 305–320.

Decarlis, A., G. Manatschal, I. Haupert, and E. Masini, 2015, The tectono-stratigraphic evolution of distal, hyper-extended magma-poor conjugate rifted margins: Examples from the Alpine Tethys and Newfoundland–Iberia: Marine and Petroleum Geology, v. 68, p. 54–72, doi:10.1016/j.marpetgeo.2015.08.005.

Demercian, S., P. Szatmari, and P. R. Cobbold, 1993, Style and pattern of salt diapirs due to thin-skinned gravitational gliding, Campos and Santos basins, offshore Brazil: Tectonophysics, v. 228, no. 3–4, p. 393–433.

Driscoll, N. W., J. R. Hogg, N. Christie-Blick, and G. D. Karner, 1995, Extensional tectonics in the Jeanne d'Arc Basin, offshore Newfoundland: implications for the timing of break-up between Grand Banks and Iberia: Geological Society, London, Special Publications, v. 90, no. 1, p. 1–28, doi:10.1144/GSL.SP.1995.090.01.01.

Ducasse, L., and P.-C. Velasque, 1988, Géotraverse dans la partie occidentale des Pyrénées, de l'avant-pays aquitain au bassin de l'Ebre: effet d'une inversion structurale sur l'édification d'une chaîne intracontinentale: Université Paul Cézanne (Aix-Marseille). Faculté des sciences et techniques de Saint-Jérôme, 287 p.

Ducasse, L., P.-C. Velasque, and J. Muller, 1986, Glissement de couverture et panneaux basculés dans la région des Arbailles (Pyrénées occidentales): Un modèle évolutif crétacé de la marge nord-ibérique à l'Est de la transformante de Pamplona: Comptes rendus de l'Académie des sciences. Série 2, Mécanique, Physique, Chimie, Sciences de l'univers, Sciences de la Terre, v. 303, no. 16, p. 1477–1482.

Durand-Wackenheim, C., P. Souquet, and G. Thiébaut, 1981, La brèche d'Errozaté (Pyrénées-Atlantiques): faciès de résedimentation en milieu profond de matériaux d'une plateforme carbonatée crétacée à substratum hercynien: Bulletin de la Société d'Histoire Naturelle de Toulouse, v. 117, p. 87–94.

Duval, B., C. Cramez, and M. P. A. Jackson, 1992, Raft tectonics in the Kwanza basin, Angola: Marine and Petroleum Geology, v. 9, no. 4, p. 389–404.

Espurt, N., P. Angrand, A. Teixell, P. Labaume, M. Ford, M. de Saint Blanquat, and S. Chevrot, 2019, Crustal-scale balanced cross-section and restorations of the Central Pyrenean belt (Nestes-Cinca transect): Highlighting the structural control of Variscan belt and Permian-Mesozoic rift systems on mountain building: Tectonophysics, v. 764, p. 25–45.

Fort, X., J. P. Brun, and F. Chauvel, 2004b, Contraction induced by block rotation above salt (Angolan margin): Marine and Petroleum Geology, v. 21, no. 10, p. 1281–1294.

Fort, X., J.-P. Brun, and F. Chauvel, 2004a, Salt tectonics on the Angolan margin, synsedimentary deformation processes: AAPG bulletin, v. 88, no. 11, p. 1523–1544.

Froitzheim, N., and G. Manatschal, 1996, Kinematics of Jurassic rifting, mantle exhumation, and passive-margin formation in the Austroalpine and Penninic nappes (eastern Switzerland): Geological Society of America Bulletin, v. 108, no. 9, p. 1120–1133, doi:10.1130/0016-7606(1996)108<1120:KOJRME>2.3.CO;2.

Gaullier, V., J. P. Brun, G. Gueīrin, and H. Lecanu, 1993, Raft tectonics: the effects of residual topography below a salt deīcollement: Tectonophysics, v. 228, no. 3–4, p. 363–381.

Hart, N. R., D. F. Stockli, and N. W. Hayman, 2016, Provenance evolution during progressive rifting and hyperextension using bedrock and detrital zircon U-Pb geochronology, Mauléon Basin, western Pyrenees: Geosphere, v. 12, no. 4, p. 1166–1186, doi:10.1130/GES01273.1.

Hart, N. R., D. F. Stockli, L. L. Lavier, and N. W. Hayman, 2017, Thermal evolution of a hyperextended rift basin, Mauléon Basin, western Pyrenees: Thermal evolution of hyperextended rift: Tectonics, doi:10.1002/2016TC004365.

Haupert, I., G. Manatschal, A. Decarlis, and P. Unternehr, 2016, Upper-plate magma-poor rifted margins: Stratigraphic architecture and structural evolution: Marine and Petroleum Geology, v. 69, p. 241–261, doi:10.1016/j.marpetgeo.2015.10.020.

Heddebaut, C., 1973, Etudes géologiques dans les massifs paléozoïques basques: Université des Sciences et Techniques de Lille, 263 p.

Heddebaut, C., 1967, Observations tectoniques sur le massif des Aldudes (Basses-Pyrénées): CR Som. Soc. Géol. de France, fasc, v. 7, p. 280–281.

Henry, J., G. Zolnaï, G. Le Pochat, and C. Mondeilh, 1987, Carte géologique de la France au 1/50 000: feuille d'Orthez, Orléans, France.

Jammes, S., G. Manatschal, L. Lavier, and E. Masini, 2009, Tectono-sedimentary evolution related to extreme crustal thinning ahead of a propagating ocean: Example of the western Pyrenees: Tectonics, v. 28, no. 4, doi:10.1029/2008TC002406.

Johnson, J. A., and C. A. Hall, 1989, Tectono-stratigraphic model for the Massif D'Igountze-Mendibelza, western Pyrenees: Journal of the Geological Society, v. 146, no. 6, p. 925–932, doi:10.1144/gsjgs.146.6.0925.

Karner, G. D., N. W. Driscoll, and D. H. N. Barker, 2003, Syn-rift regional subsidence across the West African continental margin: the role of lower plate ductile extension: Geological Society, London, Special Publications, v. 207, no. 1, p. 105–129, doi:10.1144/GSL.SP.2003.207.6.

Karner, G. D., and L. a. P. Gambôa, 2007, Timing and origin of the South Atlantic pre-salt sag basins and their capping evaporites: Geological Society, London, Special Publications, v. 285, no. 1, p. 15–35, doi:10.1144/SP285.2.

Kieken, M., and C. Thibault, 1972, Carte géologique de la France au 1/50 000: feuille d'Hasparren, Orléans, France.

Kodaira, S., R. Mjelde, K. Gunnarsson, H. Shiobara, and H. Shimamura, 1998, Structure of the Jan Mayen microcontinent and implications for its evolution: Geophysical Journal International, v. 132, no. 2, p. 383–400.

Lagabrielle, Y. et al., 2019, Mantle exhumation at magma-poor passive continental margins. Part I. 3D architecture and metasomatic evolution of a fossil exhumed mantle domain (Urdach lherzolite, north-western Pyrenees, France): BSGF - Earth Sciences Bulletin, v. 190, p. 8, doi:10.1051/bsgf/2019007.

Lagabrielle, Y., and J.-L. Bodinier, 2008, Submarine reworking of exhumed sub-continental mantle rocks: field evidence from the Lherz peridotites, French Pyrenees: Cretaceous exhumation of pyrenean mantle: Terra Nova, v. 20, no. 1, p. 11–21, doi:10.1111/j.1365-3121.2007.00781.x.

Lagabrielle, Y., C. Clerc, A. Vauchez, A. Lahfid, P. Labaume, B. Azambre, S. Fourcade, and J.-M. Dautria, 2016, Very high geothermal gradient during mantle exhumation recorded in mylonitic marbles and carbonate breccias from a Mesozoic Pyrenean palaeomargin (Lherz area, North Pyrenean Zone, France): Comptes Rendus Geoscience, v. 348, no. 3–4, p. 290–300, doi:10.1016/j.crte.2015.11.004.

Lagabrielle, Y., P. Labaume, and M. de Saint Blanquat, 2010, Mantle exhumation, crustal denudation, and gravity tectonics during Cretaceous rifting in the Pyrenean realm (SW Europe): Insights from the geological setting of the lherzolite bodies: Tectonics, v. 29, no. 4, doi:10.1029/2009TC002588.

Lamare, P., 1939, La série paléozoïque du massif du Baygoura et de la vallée de la Nive; ses relations avec les terrains secondaires environnants: Bulletin de la Société Géologique de France, v. 9, p. 163–184.

Lamare, P., 1944, La terminaison orientale du massif des Aldudes, aux environs d'Arnéguy, révision de la feuille de Saint-Jean-Pied-de-Port au 1/80 000: Bulletin de la Carte Géologique de France, v. 45, no. 216, p. 265–305.

Lamare, P., 1931, Sur l'existence du Permien dans les Pyrénées basques, entre la Vallée de Baztan (Navarre espagnole) et la Vallée de Baïgorry (Basse Navarre française): CR Somm. Soc. Geol. Fr, v. 16, p. 242–245.

Laverdière, J.-W., 1930, Les formations paléozoïques de la vallée du Laurhibar: Mém. Soc. Géol. Nord. Lille, v. 55, p. 156–157.

Le Pochat, G., C. Bolthenhagen, M. Lenguin, S. Lorsignol, and C. Thibault, 1976, Carte géologique de France au 1/50 000: Mauléon-licharre, Orléans, France.

Le Pochat, G., C. Heddebaut, M. Lenguin, S. Lorsignol, P. Souquet, J. Muller, and P. Roger, 1978, Carte Géologique de France au 1/50 000: St Jean Pied de Port, Orléans, France.

Lemoine, M., P. Tricart, and G. Boillot, 1987, Ultramafic and gabbroic ocean floor of the Ligurian Tethys (Alps, Corsica, Apennines): In search of a genetic imodel: Geology, v. 15, no. 7, p. 622–625, doi:10.1130/0091-7613(1987)15<622:UAGOFO>2.0.CO;2.

Liro, L. M., and R. Coen, 1995, Salt deformation history and postsalt structural trends, offshore southern Gabon, West Africa.

Lundin, E. R., 1992, Thin-skinned extensional tectonics on a salt detachment, northern Kwanza Basin, Angola: Marine and Petroleum Geology, v. 9, no. 4, p. 405–411.

Manatschal, G., A. Engström, L. Desmurs, U. Schaltegger, M. Cosca, O. Müntener, and D. Bernoulli, 2006, What is the tectono-metamorphic evolution of continental break-

up: The example of the Tasna Ocean–Continent Transition: Journal of Structural Geology, v. 28, no. 10, p. 1849–1869, doi:10.1016/j.jsg.2006.07.014.

Manatschal, G., N. Froitzheim, M. Rubenach, and B. D. Turrin, 2001, The role of detachment faulting in the formation of an ocean-continent transition: insights from the Iberia Abyssal Plain: Geological Society, London, Special Publications, v. 187, no. 1, p. 405–428, doi:10.1144/GSL.SP.2001.187.01.20.

Manatschal, G., and P. Nievergelt, 1997, A continent-ocean transition recorded in the Err and Platta nappes (Eastern Switzerland): Eclogae Geologicae Helvetiae, v. 90, no. 1, p. 3–28.

Manatschal, G., D. Sauter, A. M. Karpoff, E. Masini, G. Mohn, and Y. Lagabrielle, 2011, The Chenaillet Ophiolite in the French/Italian Alps: An ancient analogue for an Oceanic Core Complex? Lithos, v. 124, no. 3–4, p. 169–184, doi:10.1016/j.lithos.2010.10.017.

Martin-Closas, C., and B. Peybernès, 1987, Datation de la transgression éocrétacée dans les Pyrénéesbasco-béarnaises à l'aide des Charophytes: Geobios, v. 20, no. 5, p. 695–700, doi:10.1016/S0016-6995(87)80024-4.

Masini, E., G. Manatschal, G. Mohn, J.-F. Ghienne, and F. Lafont, 2011, The tectono-sedimentary evolution of a supra-detachment rift basin at a deep-water magma-poor rifted margin: the example of the Samedan Basin preserved in the Err nappe in SE Switzerland: Tectono-sedimentary evolution of a supra-detachment rift basin: Basin Research, v. 23, no. 6, p. 652–677, doi:10.1111/j.1365-2117.2011.00509.x.

Masini, E., G. Manatschal, G. Mohn, and P. Unternehr, 2012, Anatomy and tectono-sedimentary evolution of a rift-related detachment system: The example of the Err detachment (central Alps, SE Switzerland): Geological Society of America Bulletin, v. 124, no. 9–10, p. 1535–1551, doi:10.1130/B30557.1.

Masini, E., G. Manatschal, J. Tugend, G. Mohn, and J.-M. Flament, 2014, The tectono-sedimentary evolution of a hyper-extended rift basin: the example of the Arzacq–Mauléon rift system (Western Pyrenees, SW France): International Journal of Earth Sciences, v. 103, no. 6, p. 1569–1596, doi:10.1007/s00531-014-1023-8.

Mathey, B., 1986, Les flyschs Crétacé supérieur des Pyrénées basques: age, anatomie, origine du matériel, milieu du dépôt et relations avec l'ouverture du Golfe de Gascogne: Dijon, Université de Bourgogne, 403 p.

Merle, J.-M., 1974, Recherches sur les relations paléogéographiques et structurales entre les massifs basques au sud de Saint-Jean-Pied-de-Port (Pyrénées occidentales): Université Paul Sabatier de Toulouse (Sciences), 142 p.

Mjelde, R., P. Digranes, M. Van Schaack, H. Shimamura, H. Shiobara, S. Kodaira, O. Naess, N. Sørenes, and E. Vågnes, 2001, Crustal structure of the outer Vøring Plateau, offshore Norway, from ocean bottom seismic and gravity data: Journal of Geophysical Research: Solid Earth, v. 106, no. B4, p. 6769–6791, doi:10.1029/2000JB900415.

Mjelde, R., T. Raum, A. J. Breivik, and J. I. Faleide, 2008, Crustal transect across the North Atlantic: Marine Geophysical Researches, v. 29, no. 2, p. 73.

Mohn, G., G. Manatschal, M. Beltrando, and I. Haupert, 2014, The role of rift-inherited hyper-extension in Alpine-type orogens: Terra Nova, v. 26, no. 5, p. 347–353, doi:10.1111/ter.12104.

Moulin, M., D. Aslanian, J.-L. Olivet, I. Contrucci, L. Matias, L. Géli, F. Klingelhoefer, H. Nouzé, J.-P. Réhault, and P. Unternehr, 2005, Geological constraints on the evolution of the Angolan margin based on reflection and refraction seismic data (ZaïAngo project): Geophysical Journal International, v. 162, no. 3, p. 793–810, doi:10.1111/j.1365-246X.2005.02668.x.

Moulin, M., D. Aslanian, and P. Unternehr, 2010, A new starting point for the South and Equatorial Atlantic Ocean: Earth-Science Reviews, v. 98, no. 1–2, p. 1–37, doi:10.1016/j.earscirev.2009.08.001.

Olivet, J. L., 1996, La cinématique de la plaque ibérique: Bull. Cent. Rech. Explor. Prod. Elf Aquitaine, v. 20, no. 1, p. 131–195.

Pérez-Gussinyé, M., 2013, A tectonic model for hyperextension at magma-poor rifted margins: an example from the West Iberia–Newfoundland conjugate margins: Geological Society, London, Special Publications, v. 369, no. 1, p. 403–427, doi:10.1144/SP369.19.

Peron-Pinvidic, G., L. Gernigon, C. Gaina, and P. Ball, 2012, Insights from the Jan Mayen system in the Norwegian–Greenland sea—I. Mapping of a microcontinent: Geophysical Journal International, v. 191, no. 2, p. 385–412, doi:10.1111/j.1365-246X.2012.05639.x.

Péron-Pinvidic, G., and G. Manatschal, 2009, The final rifting evolution at deep magma-poor passive margins from Iberia-Newfoundland: a new point of view: International Journal of Earth Sciences, v. 98, no. 7, p. 1581–1597, doi:10.1007/s00531-008-0337-9.

Péron-Pinvidic, G., G. Manatschal, T. A. Minshull, and D. S. Sawyer, 2007, Tectonosedimentary evolution of the deep Iberia-Newfoundland margins: Evidence for a complex breakup history: Tectonics, v. 26, no. 2, p. 1–19, doi:10.1029/2006TC001970.

Péron-Pinvidic, G., G. Manatschal, and P. T. Osmundsen, 2013, Structural comparison of archetypal Atlantic rifted margins: A review of observations and concepts: Marine and Petroleum Geology, v. 43, p. 21–47, doi:10.1016/j.marpetgeo.2013.02.002.

Prave, A. R., 1986, An Interpretation of Late Cretaceous Sedimentation and Tectonics and the Nature of Pyrenean Deformation in the Northwestern Basque Pyrenees: A Thesis in Geology: Pennsylvania State University.

Puigdefàbregas, C., and P. Souquet, 1986, Tecto-sedimentary cycles and depositional sequences of the Mesozoic and Tertiary from the Pyrenees: Tectonophysics, v. 129, no. 1–4, p. 173–203.

Razin, P., 1989, Evolution tecto-sédimentaire alpine des Pyrénées basques à l'ouest de la transformante de Pamplona, Province du Labourd: Bordeaux 3, 464 p.

Reston, T., 2007, Extension discrepancy at North Atlantic nonvolcanic rifted margins: Depth-dependent stretching or unrecognized faulting? Geology, v. 35, no. 4, p. 367–370, doi:10.1130/G23213A.1.

Reston, T. J., 2009, The structure, evolution and symmetry of the magma-poor rifted margins of the North and Central Atlantic: A synthesis: Tectonophysics, v. 468, no. 1–4, p. 6–27, doi:10.1016/j.tecto.2008.09.002.

Ribes, C., J.-F. Ghienne, G. Manatschal, A. Decarlis, G. D. Karner, P. H. Figueredo, and C. A. Johnson, 2019, Long-lived mega fault-scarps and related breccias at distal rifted margins: Insights from present-day and fossil analogues: Journal of the Geological Society, p. jgs2018-181, doi:10.1144/jgs2018-181.

Richard, P., 1986, Structure et évolution alpine des massifs paléozoïques du Labourd (Pays Basque français): Éditions du Bureau de recherches géologiques et minières, 374 p.

Rossy, M., B. Azambre, and F. Albarède, 1992, REE and Sr/1bNd isotope geochemistry of the alkaline magmatism from the Cretaceous North Pyrenean Rift Zone (France-Spain): Chemical Geology, v. 97, no. 1, p. 33–46, doi:10.1016/0009-2541(92)90134-Q.

Rouby, D., S. Raillard, F. Guillocheau, R. Bouroullec, and T. Nalpas, 2002, Kinematics of a growth fault/raft system on the West African margin using 3-D restoration: Journal of Structural Geology, v. 24, no. 4, p. 783–796.

Roux, J.-C., 1983, Recherches stratigraphiques et sédimentologiques sur les flyschs crétacés pyrénéens au sud d'Oloron (Pyrénées Atlantiques): Université Paul Sabatier de Toulouse (Sciences), 224 p.

Saspiturry, N., P. Razin, T. Baudin, O. Serrano, B. Issautier, E. Lasseur, C. Allanic, I. Thinon, and S. Leleu, 2019, Symmetry vs. asymmetry of a hyper-thinned rift: Example of the Mauléon Basin (Western Pyrenees, France): Marine and Petroleum Geology, v. 104, p. 86–105, doi:10.1016/j.marpetgeo.2019.03.031.

Serrano, O., 1995, Stratigraphie séquentielle du barremo-bédoulien du massif des Arbailles (Pyrénées occidentales-Pays Basques), DEA: Université Paul Sabatier Toulouse III, 46 p.

Souquet, P., 1967, Le Crétacé supérieur Sud-Pyrénéen, en Catalogne, Aragon et Navarre: E. Privat.

Souquet, P. et al., 1985, Le groupe du Flysch noir (albo-cénomanien) dans les Pyrénées: Bull Cent. Rech Exlpo-Prod Elf-Aquitaine Pau, v. 9, p. 183–252.

Souquet, P., M. Bilotte, J. Canerot, E. Debroas, B. Peybernés, and J. Rey, 1975, Nouvelle interprétation de la structure des Pyrénées: CR Acad Sci Paris, v. 281, p. 609–612.

Souquet, P., B. Peybènes, M. Bilotte, and E.-J. Debroas, 1977, La chaîne alpine des Pyrénées: Géologie alpine, v. 53, no. 2, p. 193–216.

Teixell, A., P. Labaume, P. Ayarza, N. Espurt, M. de Saint Blanquat, and Y. Lagabrielle, 2018, Crustal structure and evolution of the Pyrenean-Cantabrian belt: A review and new interpretations from recent concepts and data: Tectonophysics, v. 724, p. 146–170, doi:10.1016/j.tecto.2018.01.009.

Teixell, A., P. Labaume, and Y. Lagabrielle, 2016, The crustal evolution of the west-central Pyrenees revisited: Inferences from a new kinematic scenario: Comptes Rendus Geoscience, v. 348, no. 3–4, p. 257–267, doi:10.1016/j.crte.2015.10.010.

Tugend, J., G. Manatschal, and N. J. Kusznir, 2015, Spatial and temporal evolution of hyperextended rift systems: Implication for the nature, kinematics, and timing of the Iberian-European plate boundary: Geology, v. 43, no. 1, p. 15–18, doi:10.1130/G36072.1.

Unternehr, P., G. Peron-Pinvidic, G. Manatschal, and E. Sutra, 2010, Hyper-extended crust in the South Atlantic: in search of a model: Petroleum Geoscience, v. 16, no. 3, p. 207–215, doi:10.1144/1354-079309-904.

Vielzeuf, D., 1984, Relations de phases dans le faciès granulite et implications géodynamiques: l'exemple des granulites des Pyrénées: Université Clermont-Ferrand II.

Viennot, P., and Y. Kieh, 1928, Observations pétrographiques dans le massif cristallin du Labourd (Basses Pyrénées): Bull. Soc. Géol. Fr, v. 28, p. 369–379.

Weigel, W., E. R. Flüh, H. Miller, A. Butzke, G. A. Dehghani, V. Gebhardt, I. Harder, J. Hepper, W. Jokat, and D. Kläschen, 1995, Investigations of the East Greenland continental margin between 70 and 72 N by deep seismic sounding and gravity studies: Marine Geophysical Researches, v. 17, no. 2, p. 167–199.

Chapitre 3.3

Rôle de l'héritage structural et de la tectonique salifère sur la formation des bassins de rift pseudo-symétriques d'Arzacq et de Tartas au cours de la phase d'hyperextension crétacée inférieure (sud-ouest de la France)

Chapitre 3.3. Structural inheritance and salt tectonics controlling pseudosymmetric rift formation during Early Cretaceous hyperextension of the Arzacq and Tartas basins (southwest France)

Sommaire

Résumé étendu p. 211

Abstract p. 213

1. Introduction p. 213

2. Geological settings p. 214

2.1. Structural framework of the Arzacq and Tartas basins p. 214

2.2. Tectono-sedimentary evolution of the Aquitaine basin p. 214

2.3. Deep structure of the Arzacq and Tartas basins p. 216

3. Methodology p. 216

4. Seismic profiles and well calibration p. 216

4.1. Lacq-Pécorade profile p. 216

4.2. Rousse-Thèse profile p. 217

4.3. Lacq-Villeneuve de Marsan profile p. 218

4.4. Ger-Beaulieu profile p. 221

4.5. Gamarde-Gourdon profile p. 221

4.6. Mont de Marsan-Lussagnet profile p. 222

5. Seismic interpretation p. 222

5.1. Arzacq basin p. 222

5.2. Tartas basin p. 225

6. Tectono-sedimentary evolution of the Aquitaine basin p. 226

6.1. Early Jurassic aborted rift and pull-apart basins p. 226

6.2. Latest Jurassic to Neocomian uplift phase p. 226

6.3. Barremian to early Aptian rifting stage 1: symmetric rift basins p. 227

6.4. Late Aptian to Albian stage 2: Widespread rifting and onset of asymmetry p. 228

6.5. Cenomanian postrift cooling phase p. 229

7. Discussion p. 229

7.1. Crustal thinning: the role of prerift salt p. 229

7.2. Transfer faults of the Arzacq basin p. 230

7.3. The Arzacq and Tartas basins within the Pyrenean rift system p. 230

8. Conclusion p. 232

References p. 232

Supplementary material p. 232

Résumé étendu

Les sous-bassins d'Arzacq et de Tartas correspondent à la partie la plus méridionale du Bassin Aquitain. Ils prennent naissance au Crétacé inférieur au cours de la phase de rifting aboutissant à l'océanisation du Golfe de Gascogne. Les sous-bassins d'Arzacq et de Tartas sont peu déformés, ce qui permet de discuter précisément l'évolution tectono-sédimentaire de ces bassins au cours du rifting crétacé.

La présente étude repose sur l'interprétation de 5 profils sismiques N-S répartis depuis le domaine de Grand Rieu, au sud, jusque sur la Plateforme Nord-Aquitaine, au nord. Un sixième profil est-ouest transverse aux précédents permet d'appréhender la géométrie des bassins d'Arzacq et de Tartas en 3D. Au travers de puits de calage, des séquences tectono-sédimentaires ont été identifiées, permettant de mieux définir les phases de structuration de ces bassins. Outre l'histoire crétacée, un important détail a été apporté aux séries prérifts afin d'évaluer l'héritage structural et son impact sur l'ouverture crétacée.

A la fin du Trias, les bassins d'Arzacq et de Tartas sont individualisés par l'actuelle ride E-W d'Audignon. Ils présentent une géométrie asymétrique, et leur bordure méridionale est faillée et raide (Faisceau Nord-Grand Rieu et Faisceau Nord-Audignon). Ces failles accommodent le dépôt de puissantes séries évaporitiques. Ce dispositif perdure une partie du Jurassique, comme en témoignent les séries réduites mais complètes sur le domaine de Grand Rieu. Néanmoins, la plateforme carbonatée jurassique montre une grande continuité et homogénéité de faciès.

Au Jurassique terminal-Crétacé basal, les « seuils » de Grand Rieu et d'Audignon se soulèvent, comme en témoignent les nombreuses troncatures infra-barrémiennes sur leurs bordures. Arzacq et Tartas se différencient à nouveau par la mise en place de séries laguno-saumâtres néocomiennes en leur centre, s'amincissant vers les marges des bassins. Il faut attendre le Bédoulien pour voir Arzacq et Tartas ne former qu'un seul et unique bassin dans lequel se développent les faciès urgoniens.

A l'Albien, ces deux sous-bassins s'individualisent à nouveau, et se singularisent par leur géométrie. Le dépôcentre du bassin de Tartas présente une géométrie symétrique. Au contraire, le bassin d'Arzacq acquiert une asymétrie légère, à partir de l'Albien, comme en témoigne la migration de son dépôcentre. En effet, dans la partie occidentale du bassin d'Arzacq, le dépôcentre migre vers le nord le long d'un décollement à pendage sud. Dans la partie orientale du bassin d'Arzacq, le dépôcentre Albien se déplace en direction du sud en réponse au glissement gravitaire vers le nord de la couverture prérift. Ce changement de géométrie, de part et d'autre du bassin d'Arzacq, s'opère au droit de la zone de transfert N20° du Barlanès. C'est par ailleurs le long de cette même zone de transfert que se développe le diapir N20° de Lussagnet. L'activité synrift Albienne est scellée par les dépôts peu profonds carbonatés de la formation de Pilo qui repose en légère discordance sur les séries synrifts.

Chapitre 3.3. Structural inheritance and salt tectonics controlling pseudosymmetric rift formation during Early Cretaceous hyperextension of the Arzacq and Tartas basins (southwest France)

Issautier, B., Saspiturry, N., and Serrano, O., **submitted**, Structural inheritance and salt tectonics controlling pseudosymmetric rift formation during Early Cretaceous hyperextension of the Arzacq and Tartas basins (southwest France): submitted to ***Marine and Petroleum Geology Special Publication***.

Abstract

Arzacq and Tartas are two Cretaceous basins developing in the Bay of Biscay neighborhood. They thus belong to the Albian hyperthinned rift system, and recent studies stresses the role of simple shear thinning on the genesis of regional asymmetric hyperthinned basins. However, these two basins differ from them in having a pseudosymmetric morphology. We address the Early Cretaceous tectono-sedimentary evolution of the Arzacq and Tartas rift basins, two subsidiary basins in the Aquitaine basin, and the lithospheric processes implied in their genesis. These basins did not suffer major brittle deformation during rifting stage. Our results stress a change between Aptian and Albian. : Arzacq basin shifted from a symmetric to a slightly asymmetric (pseudosymmetric) configuration. This change was controlled by gravity sliding of the prerift sedimentary cover in the eastern Arzacq basin, moving its depocenter south, and salt diapirism in the western Arzacq basin, moving its depocenter north. Several inherited Paleozoic structures reactivated as transfer faults appear to be responsible for this depocenter shift, the emplacement of salt diapirs, and defining the lateral extent of gravity sliding. The Tartas basin maintained a symmetric regime throughout the Early Cretaceous, except along the Barlanès transfer fault where the Lussagnet salt diapir originated. Two drivers of subsidence are thus envisaged in the Arzacq basin: a Neocomian-Aptian crustal thinning stage, followed by reactivation of Paleozoic faults in Albian time accompanied by salt diapirism and gravity cover sliding. Thus, this basins formed part of a series of rift basins that progressed in maturity southward, from a simple sag basin (Tartas) to a slightly asymmetric basin (aborted detachment, Arzacq) to a hyperthinned basin (Mauléon). Our results offer new insights on the role of: (1) structural inheritance in partitioning extensional strain, (2) transfer faults on the sedimentary record during crustal thinning, and (3) prerift salt décollement level.

1. Introduction

Models of continental crust thinning have grown in complexity and detail from their origins in the pure-shear model, resulting in the development of a symmetric rift (McKenzie, 1978), and the simple-shear models, producing asymmetric margins (Wernicke, 1981; Lister et al., 1986). Recent work on the magma-poor Atlantic margins and fossil margins of the Alps have led to a better understanding of the geodynamic evolution of asymmetric margins that lead to a hyperthinned continental crust (Manatschal et al., 2004; Lavier et Manatschal, 2006; Péron-Pinvidic et al., 2009, 2015; Unternehr et al., 2010; Masini et al., 2011, 2012; Haupert et al., 2016). Similarly, it is well established that the Early Cretaceous reorganization of the Iberia and Europe plates (Roest and Srivastava, 1991; Olivet, 1996; Rosenbaum et al., 2002; Sibuet et al., 2004; Gong et al., 2008) led to the development of the Pyrenean hyperextended rift system. In the pre-existing Aquitaine basin of southwestern France, this process involved the opening of the V-shaped Bay of Biscay margin and proposed exhumation of sub-continental mantle at the ocean-continent transition (Thinon, 1999; Ferrer et al., 2008; Roca et al., 2011; Tugend et al., 2014), the formation of the North Pyrenean basins (Jammes et al., 2009; Lagabrielle et al., 2010; Masini et al., 2014; Clerc and Lagabrielle, 2014; Corre et al., 2016; Teixell et al., 2016; Hart et al., 2016, 2017), and the formation of the Parentis basin along the Atlantic margin (Pinet et al. 1987; Bois and ECORS Scientific team, 1990; Bois, 1992; Ferrer et al., 2008, 2012; Tugend et al., 2014). Whereas the development of these domains is well constrained, the sedimentary record of this hyperthinned rift is poorly addressed in the symmetric rift system of the Arzacq and Tartas basins, a closely associated pair of small basins in the southern Aquitaine basin (Daignières et al., 1994; Bourrouilh et al., 1995; Serrano et al., 2006). Consequently, the geometry of these two

basins and the mechanisms responsible for their opening are still uncertain, and few studies have addressed the geodynamic evolution and sedimentary record of hyperthinned rift basins with a symmetric geometry (Etheve et al., 2018).

Numerical models (Karner et al., 2003) have highlighted the role of lower crustal thinning processes in the development of synrift sag basins. These rifted basins are not affected by distributed extension in the upper crust, as a result of decoupling beneath the upper crust along a layer in the middle crust. The resulting rift is characterized by the absence of brittle deformation and by the development of a symmetric trough-shaped basin. This thinning mechanism has been proposed to explain the symmetric geometry of the Mauléon rift basin located to the south of the Aquitaine basin (Saspiturry et al., 2019a).

As a consequence, the Tartas and Arzacq basins are a promising site for studying the evolution of synrift sag basins located on the periphery of hyperthinned rifted basins in a warm thermal regime. In this paper we combine interpretation of seismic reflection profiles and borehole data to reconstruct the tectono-sedimentary evolution of these basins and their crustal thinning mechanisms.

2. Geological setting

2.1. Structural framework of the Arzacq and Tartas basins

The Aquitaine basin lies between the North Pyrenean Frontal Thrust, the Massif Central and the Bay of Biscay **(Fig. 1A)**. The basin developed during Mesozoic and Cenozoic time over inherited Hercynian structural trends; among these is the N110° Celtaquitaine Flexure (BRGM et al., 1974), which separates the Arzacq and Tartas basins from the North Aquitaine platform (Serrano et al., 2006). These two basins, the Arzacq to the south and the Tartas to the north, are separated by the Audignon, Pécorade, Antin-Maubourguet structures (Mauriaud, 1987; Serrano et al., 2006). They first developed as rift basins during Latest Jurassic to Albian time in an extensional context and then were reactivated by convergence during the Pyrenean orogenesis (Mauriaud, 1987; Mediavilla, 1987; Serrano et al., 2006).

The Grand Rieu domain **(Fig. 1A)** accommodated major relative displacement between the Early Cretaceous hyperthinned Mauléon basin to the south (Souquet et al., 1985; Canérot, 2008; Masini et al., 2014) and the rifted Arzacq basin to the north (Daignières et al., 1994; Bourrouilh et al., 1995). The north flank of the Grand Rieu is bounded by a normal fault with significant offset in the Triassic and earliest Jurassic (Hettangian), accommodating rapid subsidence and anhydrite deposition to its north (Curnelle, 1983). The Grand Rieu thus is an inherited structural high that accumulated carbonate deposits throughout the Jurassic (Serrano et al., 2006).

2.2. Tectono-sedimentary evolution of the Aquitaine basin

The Aquitaine basin first formed in the Late Permian with extension related to the dislocation of Pangea (Burg et al., 1994). Extension continued throughout the Triassic and into the Hettangian, leading to an aborted rift basin characterized by clastic rocks, carbonates, thick evaporites and bodies of diabase with ophitic structure (ophites) (Curnelle, 1983; Curnelle et Dubois, 1986; Rossi et al., 2003). The Jurassic was a tectonically stable period marked by the development of a widespread carbonate platform (Delfaud and Henry, 1967; Delfaud, 1969; Peybernès, 1976). At the end of the Jurassic, the entire platform was confined, as suggested by the deposition of restricted dolomite and anhydrite facies (BRGM et al., 1974) that correspond to the Dolomie de Mano Formation (Serrano et al., 2006). In the meantime, the Pyrenean carbonate platform was uplifted, weathered (creating bauxite deposits) and partly eroded (Combes et al., 1998; James, 1998; Canérot et al., 1999). The Cretaceous sedimentary sequence rests unconformably upon these Jurassic deposits (Serrano et al., 2006).

The Early Cretaceous was a structurally active time in which the Aquitaine basin evolved into different sub-basins characterized by very rapid subsidence (up to 130 m/My, Désaglaux and Brunet, 1990), including the Arzacq and Tartas basins. The onset of transgression after the Late Jurassic gave rise to poorly preserved sedimentary breccias (the Breche Limite Formation) that reworked the underlying Jurassic deposits (Peybernès, 1976).

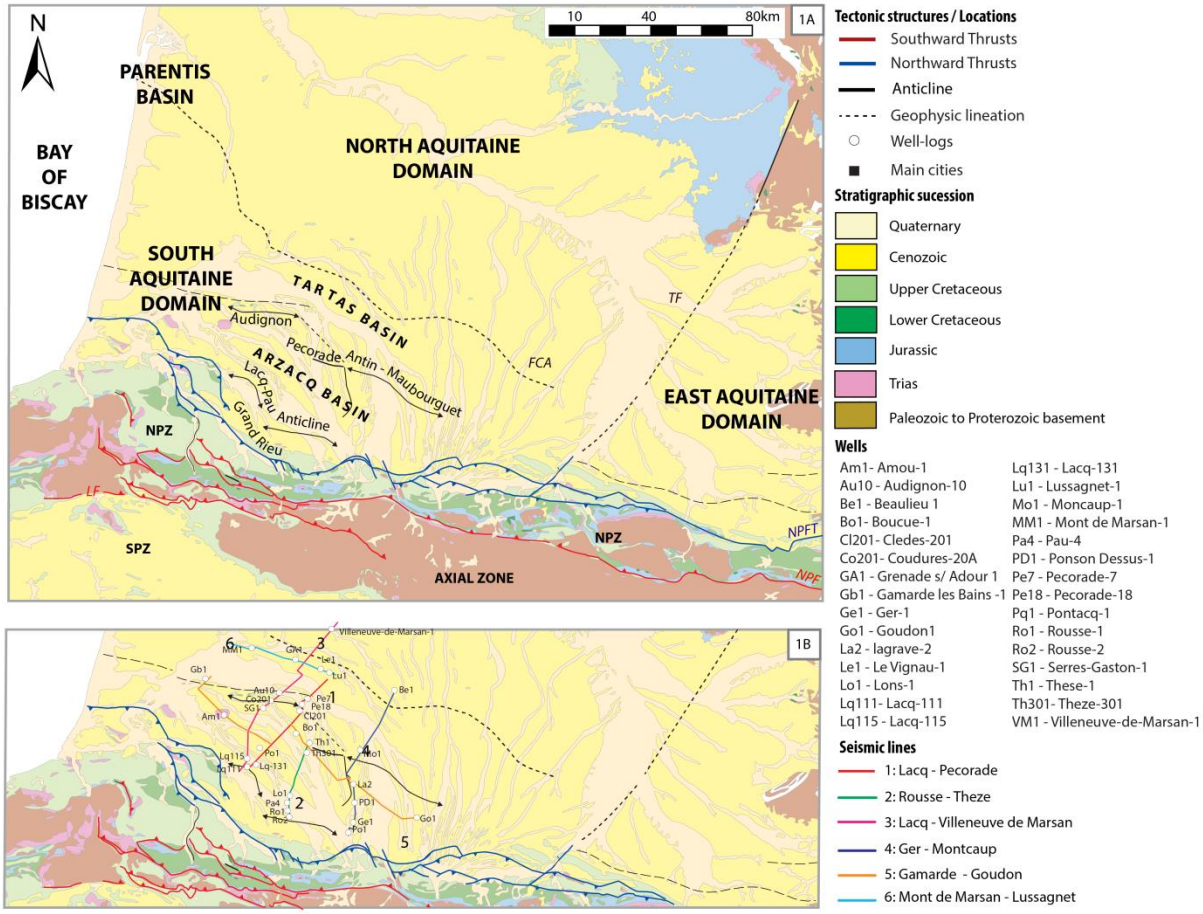


Fig. 1. Geologic maps of the Aquitaine-Pyrenees area. **(A)** Major structures and domains; **(B)** Locations of seismic reflection profiles.

These grade upward into shallow marine to continental carbonate and clastic deposits (Bouroullec and Deloffre, 1970). They correspond to brackish facies characterized by units of limestone (with ostracods and algae), dolomite and reddish sandstone (Calcaires de Ger Formation, Argiles du Gamma Ray Formation). These facies give way upward to black sandy shale with characea, ostracods and coprolites. The transgression continued in the Barremian with the development of limestone with oolites, annelids, chofatellas and coprolites (Calcaire à Annélides Formation, Delfaut, 1969; Peybèrnes and Combe, 1987)

In detail, the upper Neocomian and Barremian lagoonal deposits are subdivided from base to top into the Calcaires à Algues Formation, Lower Calcaires à Annélides Formation, Argiles du Latéolog Formation, and Upper Calcaires à Annélides Formation (Biteau and Canérot, 2008). For the sake of brevity they are all referred to here as the Calcaires à Annélides Formation.

A major inundation resulted in the deposition of the Sainte Suzanne Marls Formation (Delfaud, 1969), which represents a relatively deep open marine facies rich in cephalopods, and marls continued to spread across the entire area of the Pyrenees. A subsequent regression starting in the middle to late Aptian led to the development of the Pyrenean Urgonian facies (e.g. Bouroullec et al., 1979; Peybernès, 1979, 1982). It is characterized by limestone rich in algae, rudists and Iraqia (Mailh-Arrouy–Brassempouy Formation, Serrano et al., 2006). These rocks reflect the development of widespread inner-ramp depositional environments, and they grade locally to argillaceous limestone (Lower Clèdes Formation, Serrano et al., 2006). In the late Aptian and early Albian, the edges of the Arzacq and Tartas basins saw the development of shallow carbonate facies (Gaujacq Formation and Brassempouy Formation) while the central basin significantly subsided, as evidenced by the deposition of argillaceous limestone (Geaune and Upper Clèdes Formations). In a

distal position is the marl facies of the Marnes d'Assat Formation (Serrano et al., 2006), known in the North Pyrenean Zone as the Marnes de Saint Palais Formation or Spicules Marls Formation (Delfaud and Henry, 1967; Souquet et al., 1985). The Aquitaine basin also hosted halokinetic activity beginning in the latest Jurassic (Mauriaud, 1987; Mediavilla, 1987) and culminating during the Albian. An unconformity separates the Cenomanian and Albian sequences, the origin of which is uncertain although previous authors have interpreted it as representing a stage of compressive deformation (Biteau al., 2006). This question is addressed in the present study.

2.3. Deep structure of the Arzacq and Tartas basins

Gravimetric studies have mapped a strong positive gravity anomaly associated with the hyperthinned Mauléon basin (Grandjean, 1992, 1994; Casas et al., 1997). Formerly interpreted as a dense intracrustal body (Grandjean, 1994), it is now thought to represent the presence of lithospheric mantle at shallow depths (Masini et al., 2014). This interpretation is supported by a recent seismic velocity model that places the current mantle-crust contact at around 10 km depth (Wang et al., 2016; Wang, 2017). The absence of similar gravity anomalies in the Arzacq and Tartas basins suggests that their history involves less significant Early Cretaceous thinning. Moreover, these basins became a wider flexural basin related to the Pyrenean exhumation during Campanian to late Eocene time. Still, the 22 km depth of the current subcontinental mantle (Wang et al., 2016) remains as a sign of crustal thinning during the Albian rifting stage.

3. Methodology

This paper relies on the interpretation of seismic reflection profiles within the Arzacq and Tartas basins to analyze two topics in detail: the origin and evolution of Early Cretaceous depocenters and the depositional environments implied by the geometry of the sedimentary sections. A database of 35 wells was established to constrain correlations among these profiles **(Supplementary materials 1 to 6)**. They were harmonized on the basis of lithostratigraphy, and they were short-distance (500 m) projected to ensure the best possible calibration. In this paper we discuss six profiles, representing more than 300 km of interpreted data **(Fig. 1B)**.

Our interpretation relies on the seismic stratigraphy method of Mitchum et al. (1977) and is based on correlating onlaps, toplaps and downlaps. We recognized five Cretaceous tectono-sedimentary sequences in the wells that were used to interpret the composite seismic reflection profiles: Neocomian-Barremian, lower Aptian, upper Aptian, Albian, and Cenomanian-Turonian. Three Jurassic and Triassic lithostratigraphic sequences were also considered: Triassic-Hettangian evaporites, Hettangian carbonates- Oxfordian, and Kimmeridgian.

The Neocomian-Barremian sequence condenses a great deal of geologic history in a small stratigraphic thickness. The Neocomian (Berriasian to Hauterivian) was a long and complex period that encompassed bauxite development in the Pyrenees and the onset of shallow and narrow basins characterized by the Calcaire de Ger and Argiles du Gamma Ray Formations. Yet, the thickness of these formations rarely exceeds 20 m, and they cannot be distinguished in seismic reflection profiles. Consequently, the Neocomian sequence was combined with the Barremian sequence in our seismic interpretation, but we differentiated the two sequences in the well lithostratigraphy for greater insight into the basin's sedimentary dynamics.

4. Seismic profiles and well calibration

The following section aims at detailing the seismic reflection profiles and the wells used to calibrate them. For each of these profile, a short description of the major structural unit is provided, as well as thicknesses of the formation further constraining the seismic interpretation. Depth of the stratigraphy markers and formation thicknesses were directly measured on the boreholes, while the tectono-sedimentary sequence thicknesses are measured in two-way travel time (TWT) on the seismic reflection profiles.

4.1. Lacq-Pécorade profile

The Lacq-Pécorade seismic reflection profile is 35 km long and oriented north-south **(Figs. 1B and 2)**. It is calibrated by the Lacq-131, Clèdes-201, Pécorade-18 and Pécorade-7

wells **(Supplementary Material 1)**. The northern part of the profile corresponds to the southern edge of the Pécorade ridge **(Fig. 1B)** as evidenced by the progradations visible within the Campanian-Maastrichtian sequence (Issautier et al., in prep.). The Lacq-131 well reaches a depth of 4300 m within Tithonian dolomite (Dolomie de Mano Formation). This is overlain by the Neocomian-Barremian sequence, beginning with 60 m of Berriasian-Valanginian black shale (Argiles du Gamma Ray Formation) that grades into a relatively thick shallow carbonate sequence of Barremian age (Calcaires à Annélides Formation). The Lower Aptian sequence appears relatively thick with 500 m of marl (Sainte Suzanne Marls Formation) passing upward into nearly 2000 m of undifferentiated Albian-Aptian limestone (no well cuttings). The Clèdes-201 well penetrated Tithonian dolomite (Dolomie de Mano Formation) down to a depth of 3543 m. This facies is overlain with 50 m of restricted-marine deposits of the Berriasian-Hauterivian and nearly 200 m of Barremian shallow limestone (Calcaires à Annélides Formation). The lower Aptian sequence measures 275 m and consists of marl (Sainte Suzanne Marls Formation). The upper Aptian corresponds to 400 m of alternating shale and shallow limestone (Brassempouy–Mail d'Arrouy Formation) grading upward into 1000 m of Albian marl (Assat Formation). Both the Pécorade-18 and Pécorade-7 wells penetrate shallow Barremian deposits resting on Kimmeridgian-Tithonian dolomite (Dolomie de Mano Formation). The rest of the Lower Cretaceous section consists of lower Aptian marl (Saint Suzanne Marls Formation), upper Aptian argillaceous limestone (Clèdes Formation) and Albian argillaceous limestone (Geaune Formation) and marl (Assat Formation).

4.2. Rousse-Theze profile

The Rousse-Theze seismic reflection profile is oriented north-south and is located 20 km east of the Lacq-Pécorade profile **(Figs. 1B and 3)**. It is calibrated by the Rousse-2, Rousse-1, Pau-4, Lons-1, Theze-301 and Theze-1 wells **(Supplementary Material 2)**. The major structure on this seismic section is the Lacq-Pau Anticline **(Fig. 1A)**, characterized by steeply dipping reverse faults that favored the pop-up of this anticline during Eocene compression (**Fig. 3** ; Serrano et al., 2006). The Rousse-2 well reaches Liassic-Triassic deposits directly overlain by an Aptian sequence, no more than 50 m in total thickness, consisting of very thin lower Aptian marl (Saint Suzanne Marls Formation) and upper Aptian shallow carbonate rocks (Brassempouy–Mail d'Arrouy Formation). Subsequently, the entire Middle and Upper Jurassic and much of the Lower Cretaceous are unrepresented in this well. The upper Aptian sequence is capped by a thin Albian sequence of shallow carbonates (Gaujacq Formation). The Upper Cretaceous sequence is represented by nearly 3000 m of turbidites and base-of-slope breccias at the Lower-Upper Cretaceous transition. The Rousse-1 well penetrates Oxfordian dolomite (Dolomie de Meillon Formation) capped by Kimmeridgian-Tithonian dolomite (Dolomie de Mano Formation). These Upper Jurassic rocks are unconformably overlain by 2500 m of Upper Cretaceous turbidites; thus, this well lacks the entire Lower Cretaceous. The Pau-4 well penetrates 300 m into marly limestone of Albian age (Upper Clèdes Formation) overlain by a 1700 m Upper Cretaceous sequence. The Lons-1 well, roughly 6000 m deep, reaches lower Kimmeridgian dolomitic limestone (Dolomie de Belair Formation). The uppermost Jurassic is represented by dolomite and breccia of Tithonian age (Dolomie de Mano Formation). It is directly overlain by 250 m of Barremian restricted-marine limestone (Calcaire à Annélides Formation), thus Neocomian rocks are absent. This grades upward to 500 m of lower Aptian marl (Saint Suzanne Marls Formation) and 800 m of argillaceous limestone (Lower Clèdes Formation). The uppermost Lower Cretaceous rocks are a 1500-m-thick Albian marly sequence (Assat Formation), and Campanian to Maastrichtian turbidites rest upon them. The Theze-301 and Theze-1 wells both penetrate Oxfordian marl (Marnes à Ammonites Formation) that grades upward to Kimmeridgian-Tithonian dolomite (Dolomie de Mano Formation). The Lower Cretaceous sequence is characterized by marginal to continental facies (Calcaire de Ger Formation and Gamma Ray Formation) in the Theze-1 well, whereas these facies are absent in the

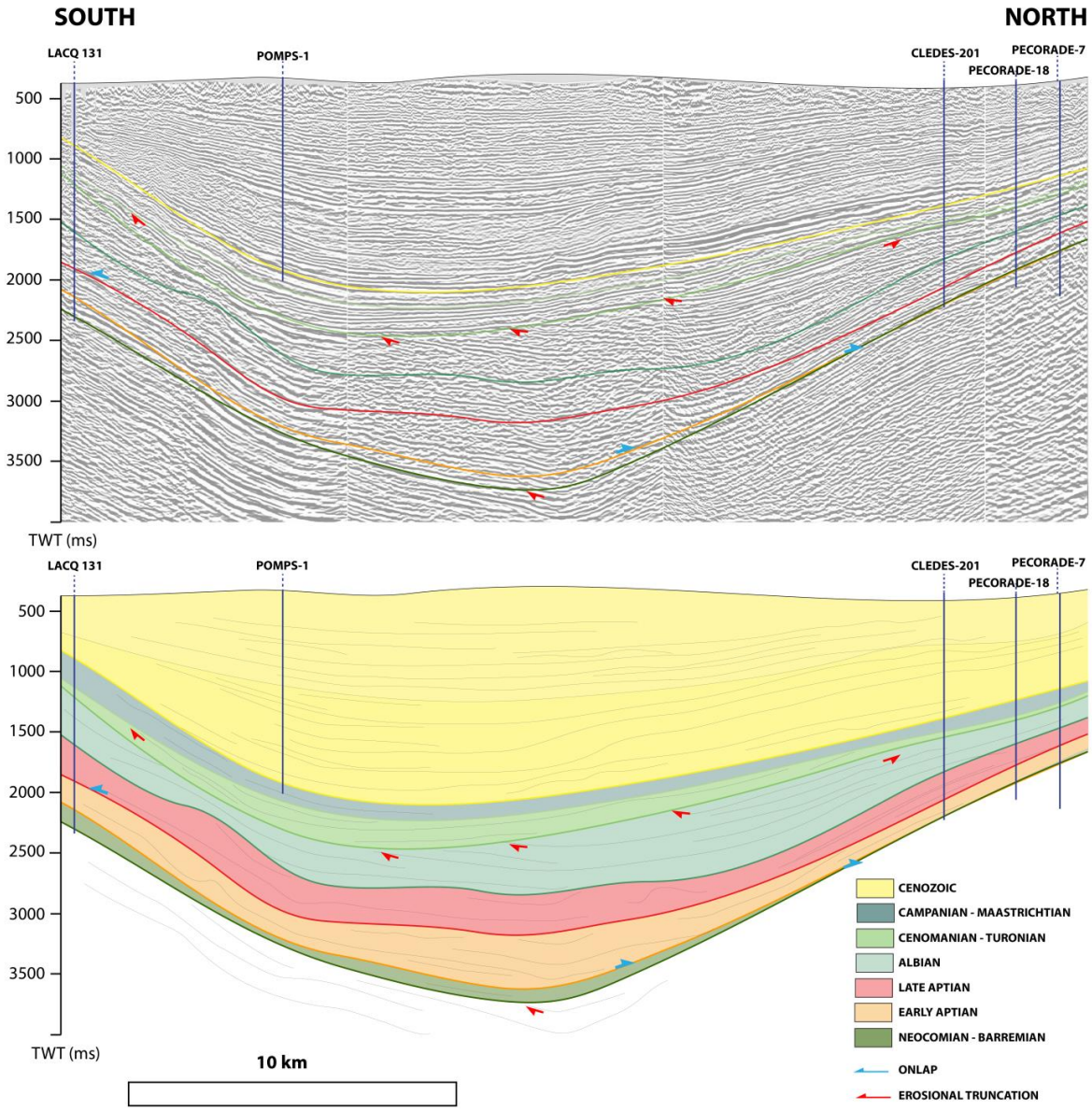


Fig. 2. Lacq-Pécorade seismic reflection profile. All Lower Cretaceous sequences define a symmetric basin. Onlaps are clearly visible within the early infill (Neocomian to Aptian). Subsidence increases during Albian time, and the Cenomanian sequence partly erodes the Albian deposits.

Theze-301 well, where Barremian restricted-marine shallow limestone (Calcaires à Annélides Formation) rests directly upon Tithonian dolomite. The overlying sequences are common to both wells and consist of lower Aptian marl (Sainte Suzanne Marls Formation), upper Aptian shallow to argillaceous limestone (Mailh Arrouy - Brassempouy Formation and Lower Clèdes Formation), and 1300 m of Albian limestone (Gaujacq Formation) and marl (Assat Formation).

4.3. Lacq–Villeneuve de Marsan profile

The Lacq–Villeneuve de Marsan seismic reflection profile is parallel to and west of the Lacq-Pécorade profile and extends farther north, covering both the Arzacq and Tartas basins, along a section more than 60 km long **(Figs. 1B and 4)**. Six wells constrain the interpretation: Lacq-129129, Lacq-115, Serres-Gaston-1, Coudures-201, Audignon-10 and Villeneuve de Marsan-1 **(Supplementary Material 3)**. The main structures along this profile are the Lacq-Pau Anticline and the Audignon ridge **(Fig. 1B)**. The Lacq-129 well reaches Tithonian dolomite (Dolomie de Mano Formation), which is overlain by a Lower Cretaceous sequence that begins with 100 m of limestone of Berriasian-Valanginian age (Calcaire de Ger Formation). This grades into

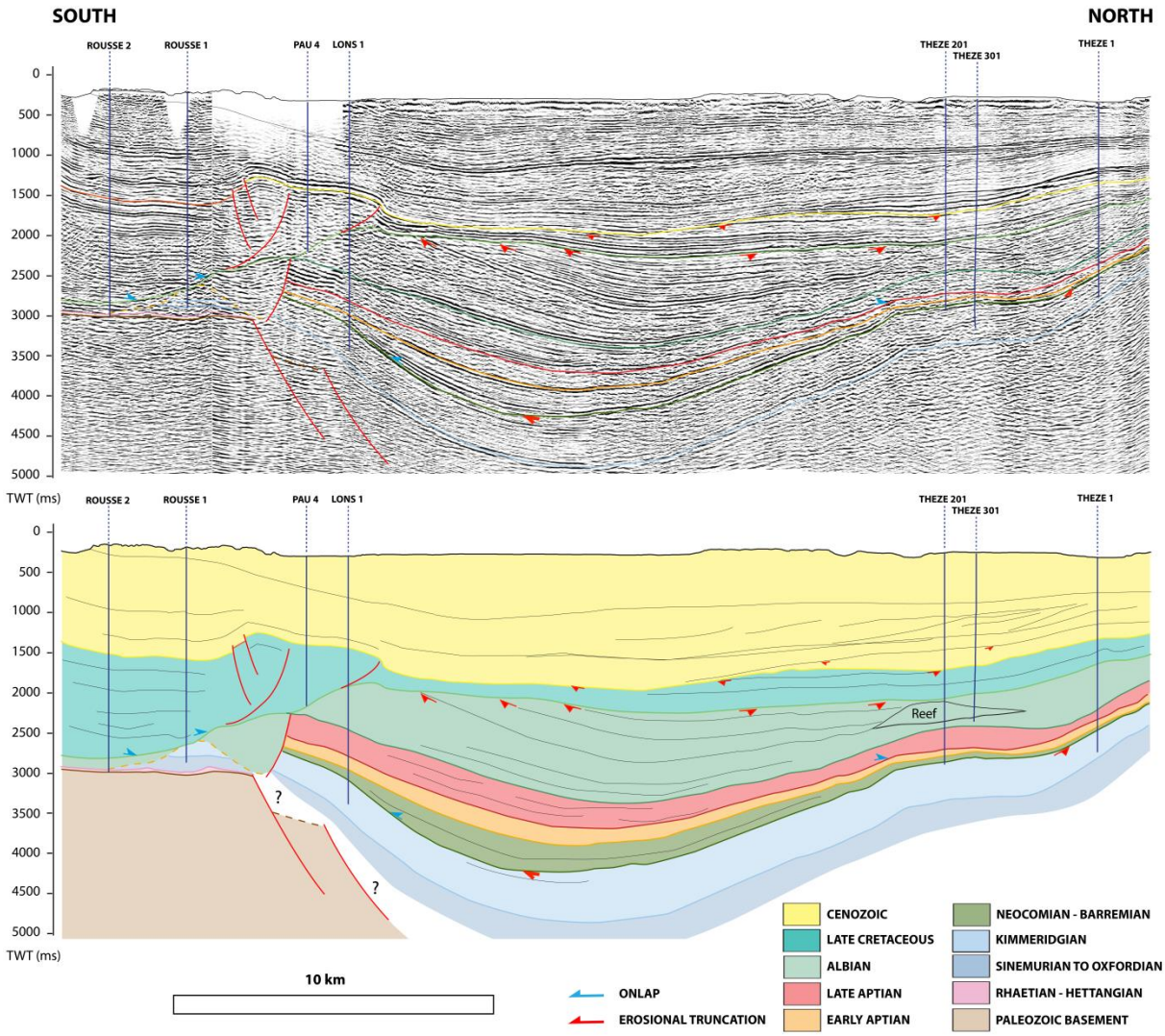


Fig. 3. Rousse-Theze seismic reflection profile, showing the Grand Rieu domain between the Mauléon and Arzacq basins. The depocenter of the Albian sequence in the Arzacq basin migrates south from its position in underlying Lower Cretaceous sequences.

300 m of Barremian shallow carbonates (Calcaire à Annélides Formation), 550 m of lower Aptian marl (Sainte Suzanne Marls Formation) and 1000 m of upper Aptian shallow carbonates (Mailh Arrouy–Brassempouy Formation). The Lower Cretaceous sequence ends with 500 m of Albian marl (Assat Formation). The Lacq-115 well shows the same succession). The Serres Gaston-1 well, on the south side of the Audignon ridge, reaches Tithonian rocks at 5300 m depth that are directly overlain by 200 m of Barremian shallow marine carbonates (Calcaire à Annélides Formation), suggesting that Berriasian to Hauterivian rocks are absent. Overlying these is 200 m of lower Aptian marl (Sainte Suzanne Marls Formation) and roughly 600 m of upper Aptian argillaceous limestone (Lower Clèdes Formation). The well is topped by nearly 2500 m of Albian marly rocks (Assat Formation).

The Coudures-201 well reaches Oxfordian dark marl (Ammonite Marls Formation), partly injected with salt, overlain by 20 m of Barremian shallow carbonates (Calcaires à Annélides Formation); the intervening interval of the Upper Jurassic and most of the Neocomian is absent. The rest of the Lower Cretaceous sequence consists of 60 m of lower Aptian marl (Sainte Suzanne Marls Formation), 500 m of upper Aptian shallow carbonates (Mailh Arrouy–Brassempouy Formation) and 2700 m of Albian marl (Assat Formation).

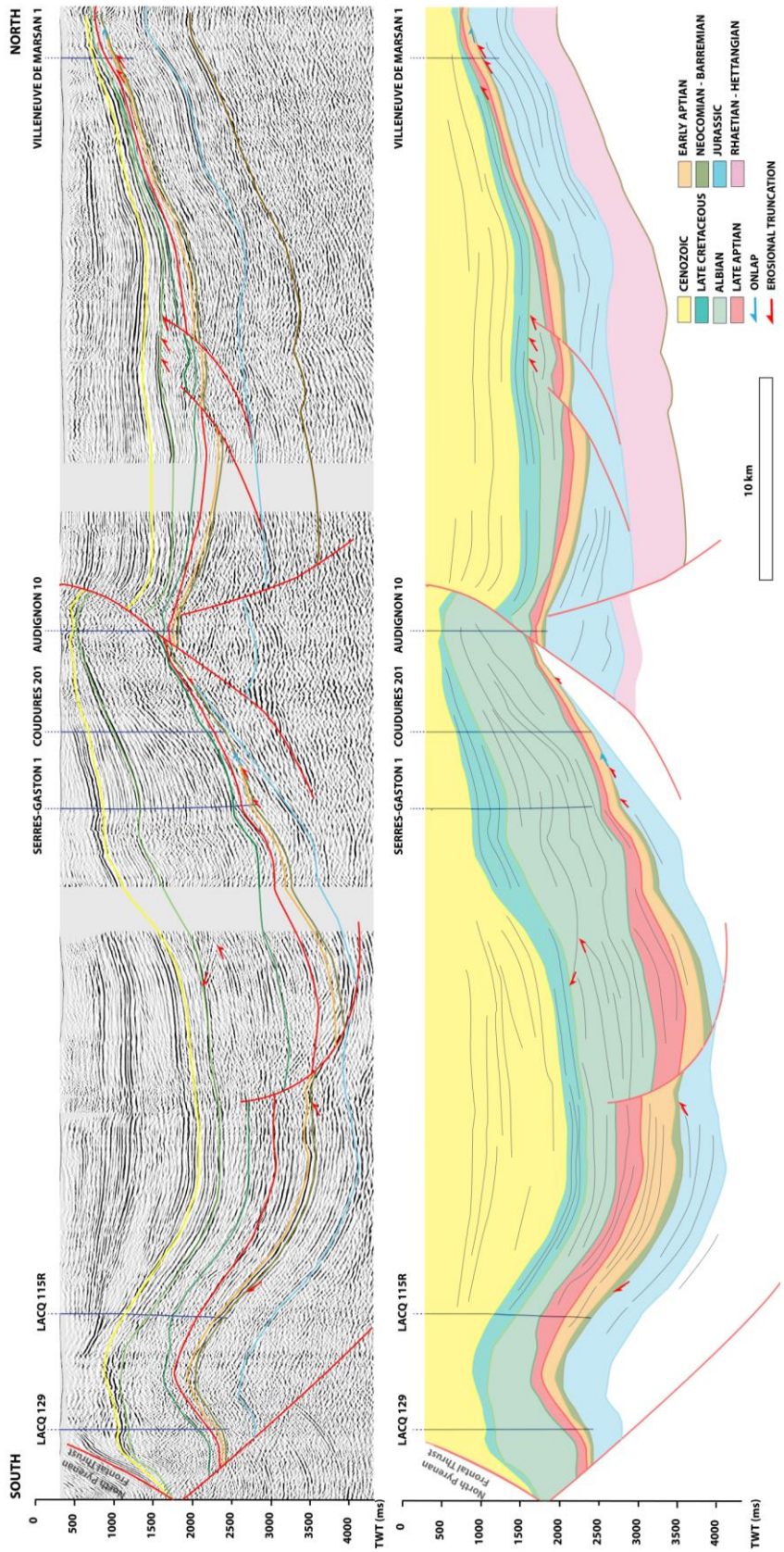


Fig. 4. Lacq–Villeneuve de Marsan seismic reflection profile. The Neocomian to Barremian sequence shows both the Arzacq and Tartas basins, which are connected during the early Aptian (Marnes de Sainte Suzanne transgression). The Albian sequence shows clearly differentiated basins: the Tartas basin remains symmetric and the Arzacq basin acquires a slight asymmetry as the depocenter migrates north.

The Audignon-10 well is emplaced on a diapir structure and crosses both an allochthonous unit that was transported northward and the underlying autochthonous unit. The base of the well lies in Kimmeridgian and Tithonian dolomite (Dolomie de Mano Formation) that is overlain by 10 m of Barremian restricted-marine facies (Calcaire à Annélides Formation) and 30 m of lower Aptian open-marine marl (Sainte Suzanne Marls Formation). This is succeeded by a 300 m sequence of shallow limestone and dolomite (Mailh Arrouy–Brassempouy Formation) that grades upward to Albian spicule-bearing marls picular marl (Assat Formation). The allochthonous unit, above a decollement at 2500 m depth, consists mainly of Triassic salt and slabs of Lower Cretaceous and Jurassic rocks, not described here, that are overlain by 2000 m of Albian spicular marl (Assat Formation). The Villeneuve de Marsan-1 well constrains the sedimentary record of the Tartas basin and North Aquitaine platform. It penetrates a condensed Cretaceous sequence, resting conformably upon Tithonian dolomite (Dolomie de Mano Fm), in which the Albian is absent. The Lower Cretaceous sequence consists of 150 m of Berriasian to Hauterivian shallow carbonates (Calcaire de Ger Formation) grading upward to a similar facies 120 m thick with Barremian fauna (Calcaires à Annélides Formation). Lower Aptian marly limestone (Sainte Suzanne Marls Formation) ends this succession, which is unconformably overlain by Cenomanian deposits.

4.4. Ger-Beaulieu profile

The Ger-Beaulieu seismic reflection profile is oriented north-south and covers the Grand Rieu domain and the Arzacq basin **(Figs. 1B and 5)**. It is constrained by 5 wells: the Ger-1, Ponton-Dessus-1, Lagrave-2, Moncaup-1, and Beaulieu-1 wells **(Supplementary Material 4)**. The base of the Ger-1 well is in the Oxfordian dolomite of the Meillon Formation, which is overlain by 700 m of Kimmeridgian-Tithonian dolomite and limestone (Dolomie de Mano Fm). The basal Lower Cretaceous deposits consist of 60 m of Berriasian-Valanginian restricted marine carbonates to continental shale (Calcaire de Ger Fm and Argiles du Gamma Ray Fm). They grade upward into 250 m of Barremian shallow carbonates (Calcaires à Annélides Fm) followed by 600 m of lower Aptian marl (Sainte Suzanne Marls Formation) and 500 m of upper Aptian rocks, the shallow Urgonian facies and the deeper argillaceous limestone facies (Gaujac, Brassempouy and Lower Clèdes Formations). The Lower Cretaceous sequence ends with 500 m of Albian marl (Assat Formation). The Ponton-Dessus-1 and Lagrave-2 wells display the same succession, although the Berriasian-Valanginian sequence is thinner (<20 m in Ponton-Dessus-1, 10 m in Lagrave-2), and the Albian sequence is absent in the Lagrave-2 well. In both wells, Lower Cretaceous deposits rest conformably upon Tithonian rocks. The Moncaup-1 well, located at the northern edge of the Arzacq basin, reaches Triassic-Hettangian evaporites overlain by a lower Aptian reduced marly sequence (50 m of Sainte Suzanne Marls Fm). The upper Aptian sequence is condensed as well (50 m) and consists of a shallow carbonate facies (Mailh-Arrouy--Brassempouy Formation). It is overlain by 500 m of Albian argillaceous carbonates (Geaune Formation and Upper Clèdes Fm). The Beaulieu-1 well contains Cenomanian rocks onlapping Kimmeridgian carbonate deposits, evidence that the entire Lower Cretaceous is absent here.

4.5. Gamarde-Goudon profile

The Gamarde-Goudon seismic reflection profile is oriented west-east across the Arzacq basin **(Figs. 1B and 6)**. It extends from the Landes salt diapirs zone (Gamarde-les-Bains-1 well) to the Tarbes area (Goudon-1 well). It is calibrated by the Gamarde-les-Bains-1, Amou-1, Boucoue-1, Lagrave-2 and Goudon-1 wells **(Supplementary Material 5)**. The Gamardes-les-Bains-1 well exhibits a reduced Lower Cretaceous sequence that consists of 500 m of upper Aptian shallow carbonates (Mailh-Arrouy/Brassempouy Fm.) overlain by 1500 m of Albian marl and argillaceous limestone (Assat Fm.). The lowermost Cretaceous and the entire Jurassic are absent in this well, which bottoms out in Triassic-Hettangian anhydrites. The base of the Amou-1 well is in Kimmeridgian and Tithonian dolomite (Dolomie de Mano Formation and Lons Fm.) overlain by 200 m of shallow Barremian facies (Calcaire à Annelides Fm.), and the Neocomian is absent. Above these is 200 m of Aptian marly facies (Saint Suzanne Marls), 600 m of upper Aptian shallow limestone (Mailh-Arrouy/Brassempouy Formation), and nearly

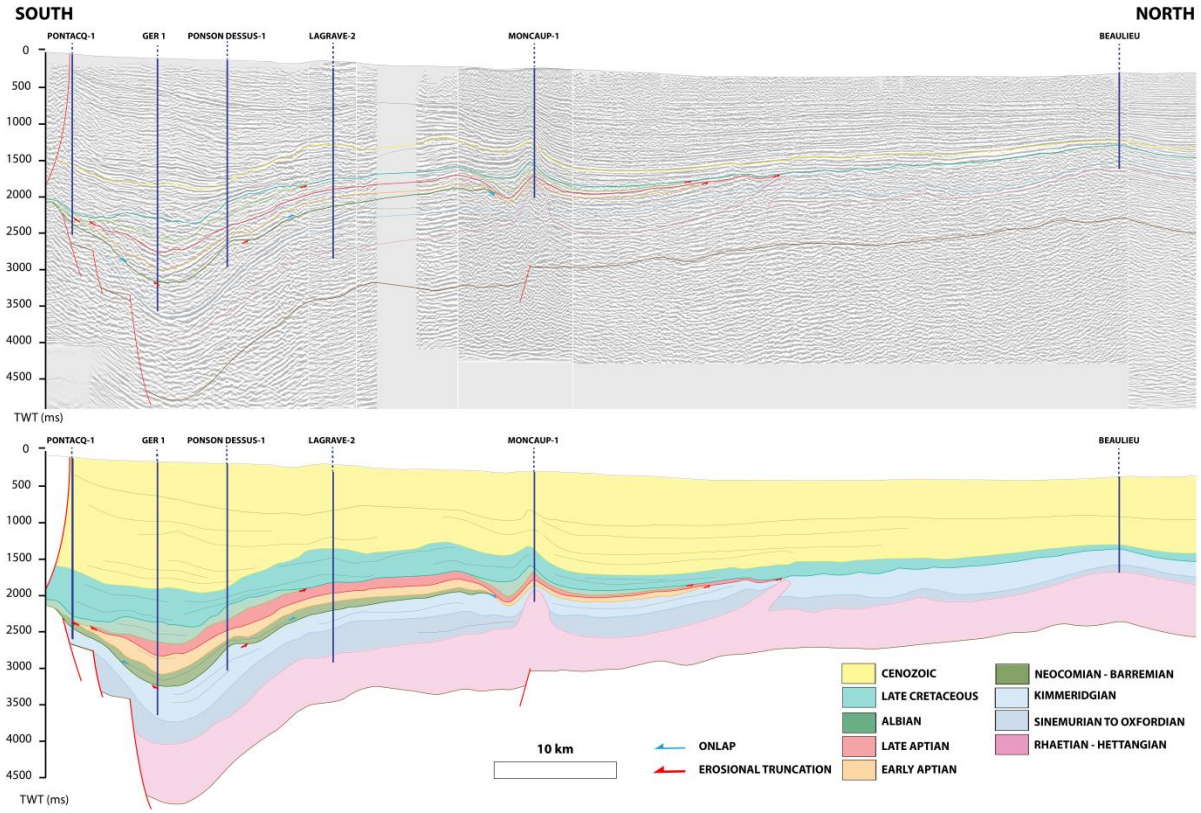


Fig. 5. Ger-Beaulieu seismic reflection profile. Prerift sedimentary cover is absent in the Grand Rieu domain, which is onlapped by the Albian sequence. The Albian depocenter migrates south, in contrast with the aligned Jurassic and Early Cretaceous depocenters.

2000 m of Albian marl (Assat Formation). The Boucue-1 well does not extend beyond an Albian sequence. The Lagrave-2 well is described as part of the Ger-Beaulieu profile. The Goudon-1 well lacks the entire Lower Cretaceous, as Cenomanian deposits directly overlie Kimmeridgian strata.

4.6. Mont de Marsan–Lussagnet profile

The Mont de Marsan–Lussagnet seismic reflection profile is oriented east-west within the Tartas basin **(Figs. 1B and 7)**. The major structure in this profile is the Lussagnet salt diapir. The profile is calibrated by the Mont-de-Marsan-1, Grenade-sur-Adour-1 and Lussagnet-1 wells **(Supplementary Material 6)**. The base of the Mont-de-Marsan-1 well is in Oxfordian black shale (Ammonite Marls Formation) and Kimmeridgian dolomite (Dolomie de Mano Formation). A 200 m sequence of upper Aptian shallow carbonates (Mailh-Arrouy--Brassempouy Formation) rests directly upon the Kimmeridgian, evidence of a significant gap between Tithonian and Lower Cretaceous (Berriasian to lower Aptian) rocks. The Aptian sequence is overlain by 800 m of Albian shallow dolomite (Gaujacq Formation). The base of the grenade-sur-Adour-1 well is in Tihonian-Kimmeridgian dolomites at 3600 m (Lons and Mano formations). These are directly overlain by 700 m of Barremian shallow facies (Calcaire à Annélides Formation), 60 m of lower Aptian marly deposits (Sainte Suzanne Marls Formation), 160 m of upper Aptian rocks , and a 250 m succession of Albian shallow carbonates (Gaujacq Formation). The Lussagnet-1 well penetrates a 1300 m thick sequence of undifferentiated Albian and upper Aptian carbonates resting upon a Dogger-Liassic sequence, implying a gap that includes most of the Upper Jurassic and much of the Lower Cretaceous.

5. Seismic Interpretation

5.1. Arzacq basin

In the Lacq–Villeneuve de Marsan seismic reflection profile **(Fig. 4)**, the key observation is the existence of two steep normal faults bounding the Audignon Ridge—the northern

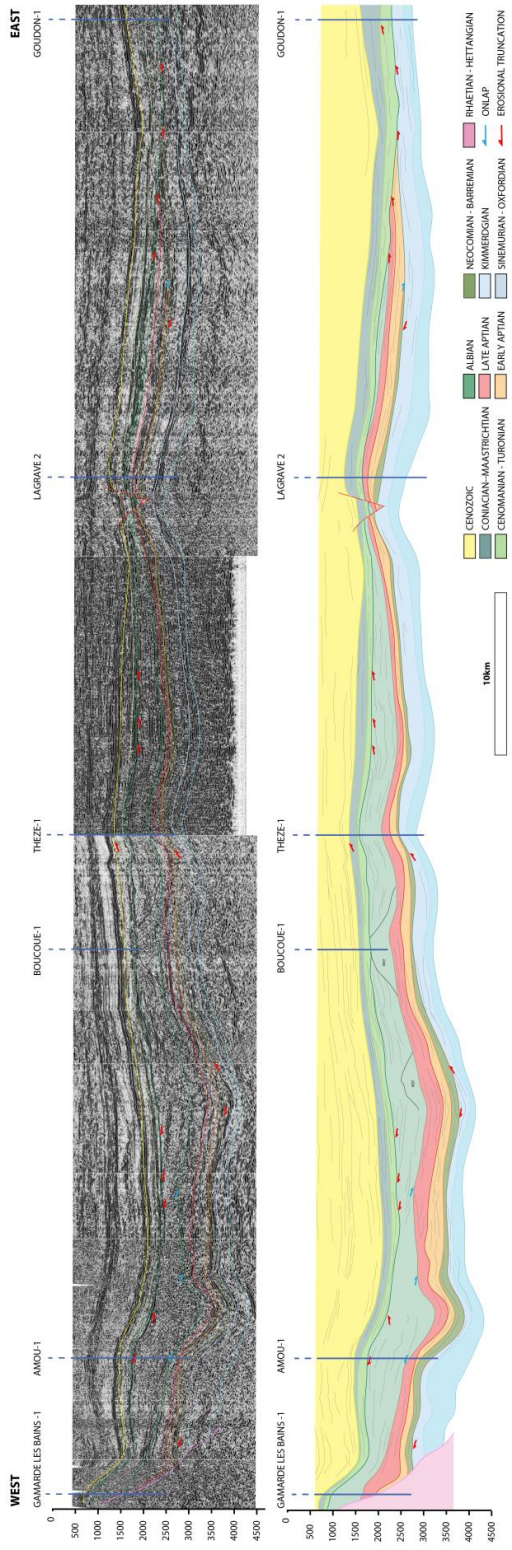


Fig. 6. Gamarde-Goudon seismic reflection profile. This long west-to-east transect displays no visible tectonic activity, as the Albian sequence is relatively isopachous except at the ends of the transect where it is affected by salt diapirism (Gamarde les Bains) and Late Cretaceous erosion (Goudon). Note that a narrow syncline develops within the Albian sequence in the Amou area.

one dipping north, the southern one dipping south—that define it as a horst. Its northern flank exposes a massive accumulation of Upper Triassic to Lower Jurassic evaporites, which decreases in thickness toward the northern Tartas basin. Similarly, the Ger-Beaulieu seismic profile **(Fig. 5)** is characterized by steep north-dipping normal faults that accommodate the offset of the basement south of the Arzacq basin. These faults too expose thick sections of evaporites that decrease in thickness to the north toward the Arzacq basin's northern edge. The Middle and Upper Jurassic sequences are relatively isopachous, and their depocenters do not migrate, thus these sequences have their greatest thickness in the central axis of the Arzacq basin.

The base of the Lower Cretaceous is the Neocomian-Barremian sequence, which rests unconformably upon a partly eroded Jurassic surface evident as toplap markers below the Lower Cretaceous basal surface. In the Audignon-10 well on the Lacq–Villeneuve de Marsan profile **(Fig. 4)**, pre-Cretaceous erosion removed the entire Kimmeridgian sequence. On the Rousse-Theze seismic reflection profile **(Fig. 3)**, several basal Cretaceous onlap markers are clearly visible that document onlap in both northward and southward directions. These markers migrate towards the basin's edges, Grand Rieu to the south and Pécorade to the north **(Figs. 2 and 4)**, and the Ger-Beaulieu seismic reflection profile shows the same features in the eastern Arzacq basin **(Fig. 5)**. To sum up, the Neocomian-Barremian sequence is thickest in the central trough of the Arzacq basin and thins toward its north and south edges. This thickness variation corresponds to the onlap of the Neocomian brackish to coastal facies and its replacement by Barremian inner-platform deposits, which barely transgressed the Audignon and Grand-Rieu domains where their thickness is negligible.

Unlike the sequence just described, the Aptian deposits show only a slight reduction in thickness on the basin edges **(Fig. 2)**. The base of the Aptian sequence is a widespread lower offshore marly facies (Sainte Suzanne Marls Formation) that indicates a sudden and general deepening of the depositional profile. The marl onlaps a reduced Neocomian-Barremian sequence on the Pécorade ridge at the north edge of the Arzacq basin **(Fig. 2)** and a partly to completely eroded Jurassic sequence on the

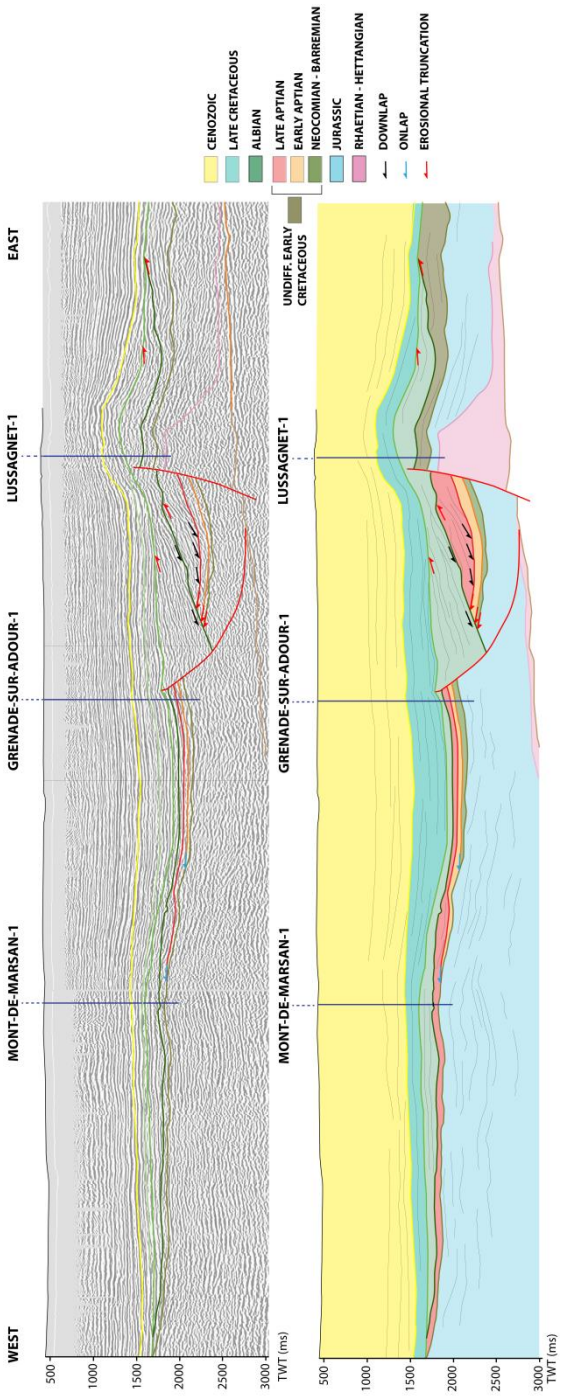


Fig. 7. Mont de Marsan–Lussagnet seismic reflection profile. Salt tectonism affects the Albian sequence, as attested by clear growth strata controlled by growth of the Lussagnet salt diapir.

Audignon ridge **(Fig. 4)**. This unconformable relationship is also clear in the Rousse-Theze seismic reflection profile **(Fig. 3)** where lower Aptian rocks rest directly on basement (south of the Pau-4 well). Several onlap markers are visible within the Marnes de Sainte Suzanne Formation in the Lacq-Pécorade seismic reflection profile **(Fig. 2)**. These onlaps demonstrate the expansion of the area of sedimentation toward the basin's edges. The upper Aptian sequence consists mainly of a shallow carbonate facies (Urgonian facies, representing an inner ramp with rudist bioherms) that passes locally into marl deposits. This sequence is thicker in the central trough and thinner at the northern and southern edges of the Arzacq basin **(Figs. 2–4)**. This thinning is most visible close to the Audignon ridge (Fig. 4) and towards the Grand Rieu domain, where onlap is visible in the Lacq-131 well **(Fig. 3)**. In the west-east Gamarde-Goudon profile **(Fig. 6)**, a striking point is the absence of Lower Cretaceous deposits in the eastern part of the profile (Goudon-1 well). There the Cenomanian sequence rests unconformably on partly eroded Kimmeridgian deposits, as shown by several toplap markers below the basal Cretaceous surface. Between the Boucue-1 and Theze-1 wells, several toplaps are similarly visible below the Neocomian basal surface. Notably, the Neocomian to upper Aptian sequences east of the Amou-1 well give way to a synform consisting of a large, sharply defined increase in thickness of overlying Albian deposits.

The significant thickness variations of the Albian sequence mark a change in the basin's regime. Several carbonate build-ups appear in the Gamarde-Goudon profile **(Fig. 6)**, and a sharp thickness increase east of the Amou-1 well has numerous onlaps from either side of this synform. A gradual eastward decrease in thickness decrease, associated with toplap markers, includes a pinchout in the Lagrave-2 well. Consequently, preservation of the sequence is poor in the eastern part of the profile, probably related to a latest Albian to pre-Cenomanian erosional stage.

North-south cross sections show that the Arzacq basin entered a more asymmetric and strongly subsiding stage during Albian time. The Albian sequence (1s TWT) is twice as thick as the underlying upper Aptian and Neocomian-Barremian sequences (0.5s TWT) in the Rousse-Theze profile **(Fig. 3)** and three times as thick as the Neocomian-to-upper Aptian sequence in the Lacq–Villeneuve de Marsan profile (1.5s TWT ; **Fig. 4**). Both profiles also show radically different depocenter locations and depositional profiles. The greatest thickness increase is at the southern edge of the Arzacq basin on the Rousse-Theze profile **(Fig. 3)** and at the northern edge of the Arzacq basin on the

Lacq–Villeneuve de Marsan section **(Fig. 4)**. Regarding the depositional profile, the platform-basin transition shifts north with time on the Lacq–Villeneuve de Marsan seismic reflection profile **(Fig. 4)** and south on the Rousse-Theze seismic reflection profile **(Fig. 3)**. A slight southward migration of the Albian depocenter (3–5 km) is visible in the Ger-Beaulieu profile **(Fig. 5)** over the Grand Rieu paleo-Jurassic fault(s).

In the Grand Rieu domain, the Jurassic to Triassic sedimentary cover is absent in the Rousse-2, Ger-1 and Pau-2 wells, where Cretaceous rocks directly overlie the Paleozoic substratum **(Figs. 3 and 4)**. Here the Albian basin displays a very complex shape, with a thick sequence to the north of Grand Rieu that is partly disconnected from a small and narrow basin to the south (**Fig. 2;** between the Pau-4 and Rousse-1 wells). Both sequences consist of marly facies of the Assat Formation except in the Rousse-2 well, where a bioclastic carbonate facies (Gaujacq Formation) occupies the southern edge of the Arzacq basin. This more proximal facies on the southern edge is consistent with the southward thickness reduction of the Albian sequence **(Fig. 2)**.

On the north side of the Arzacq basin, the Lacq–Villeneuve de Marsan profile shows a massive thickness increase on the southern flank of the Audignon structure, where the Albian facies consists of marl **(Fig. 2)**. The Albian depocenter migrates 5 km north, while the southern edge of the Arzacq basin displays a gently north-dipping margin. The depositional profile of the basin reflects this asymmetry, with proximal facies on the gently dipping south margin and more distal marl on the steep north margin.

The Cenomanian sequence overlies the Albian deposits unconformably, as illustrated by the toplap markers. This unconformity is considerable on the south flank of the Audignon structure, where shallow carbonate deposits sharply contrast with the underlying deep Albian facies. On Grand Rieu, this erosive surface lies between the shallow platform deposits in the Arzacq basin and deep-water turbidites in the northern Mauléon basin.

To summarize, the Arzacq basin had two different stages of structural evolution during the Early Cretaceous. Stage 1 (Neocomian to middle Aptian) was characterized by a symmetric basin in which subsidence was greater in the central trough. This difference in subsidence was not accommodated by faults, as witnessed by the absence of synsedimentary wedges. The Barremian to Aptian carbonate facies indicates a uniform, nearly flat depositional profile, yet the maximum thickness of the Barremian-Aptian sequence at the center of the basin (1100m) attests to a relative high subsidence rate at this time, approximately -60 m/My. Stage 2 (late Aptian to Albian) featured the development of slightly asymmetric basins in which the geometry and depositional profile were differently organized in the western and northern parts of the South Aquitaine domain. This stage was also marked by an increase in the subsidence rate.(>80m/My)

5.2. Tartas basin

The Lacq–Villeneuve de Marsan seismic reflection profile provides a north-south transect of the Tartas basin, the southern edge of which is delimited by the normal fault at the north edge of the Audignon horst **(Fig. 4)**. As in the Arzacq basin, a Neocomian-Aptian sequence of shallow carbonates unconformably overlies the Upper Jurassic sequence, including onlap markers that progress towards the basin's edges **(Fig. 4)**. These onlaps document the confinement of brackish inner ramp Neocomian (Berriasian–Hauterivian) facies within a trough. The Tartas and Arzacq basins were not connected at this stage, because Neocomian facies are absent in the northern Arzacq basin; rather, the Neocomian facies shift sharply northward as shown in the Villeneuve de Marsan well. There, the lower Aptian sequence is significantly reduced and upper Aptian to Albian strata are absent owing to erosion below the Late Cretaceous basal surface (toplap markers). Nevertheless, these rocks reach their maximum thickness in the central trough, like the Neocomian-Barremian sequence. The Albian sequence is marked by the development of salt tectonics in the heart of the basin, illustrated by wedge growth strata controlled by gently south-dipping structures along which salt might have migrated.

In the western part of the west-east Mont de Marsan–Lussagnet seismic reflection profile **(Fig. 7)**, the Neocomian-Barremian and lower Aptian sequences appear relatively isopachous. They clearly onlap towards the Mont-de-

Marsan-1 well, where the upper Aptian sequence directly overlies Jurassic deposits and spreads far to the west. The Albian sequence consists of shallow carbonate facies throughout the profile. It is consistently about 1000 m thick between the Mont-de-Marsan-1 well and a fault just east of the Grenade-sur-Adour well, but on the other side of this fault it thickens in a wedge-shaped basin between the fault and the Lussagnet-1 well. The growth of this basin began in the late Aptian (and probably earliest Albian) as witnessed by the large-scale westward downlaps in response to uplift of the Lussagnet salt diapir. This first sequence, which measures roughly 0.5 in TWT thickness, was partly truncated during a late Albian stage showing a westward tilt and remarkable stratal growth (0.75 TWT thickness). The Cenomanian sequence regionally overlies the previous sequences, and numerous toplaps appear below its basal surface.

6. Tectono-sedimentary evolution of the Aquitaine basin

6.1. Early Jurassic aborted rift and pull-apart basins

During the latest Triassic and earliest Jurassic, incipient rifting between the modern-day Europe and Iberia plates led to the initiation (or reactivation) of major north-dipping normal faults in the Aquitaine basin region, along which thick bodies of evaporites accumulated **(Fig. 8)**. At that time, sedimentation was condensed over the relatively high Grand Rieu and Audignon-Pécorade-Antin-Maubourguet domains, and sediment thicknesses decreased away from the normal faults **(Fig. 8)**. In the Late Triassic and Hettangian, the Aquitaine basin region thus consisted of shallow carbonate platforms (Grand Rieu and Audignon domains) bounded by steep normal faults that accommodated rapid deepening of the intervening basins. This horst-basin pattern persisted throughout the Jurassic, during which time the depositional sequence was relatively isopachous.

Previous authors (BRGM et al., 1974; Curnelle, 1983; Brunet, 1984, 1991) have attributed these high subsidence rates (100 m/Myr) and initiation of Grand Rieu normal faulting to the accelerated disruption of Pangea in the Late Triassic and Early Jurassic during the initial opening of the Tethys. Nevertheless, the Audignon, Pécorade and Antin-Maubourguet ridges have been previously interpreted as structures of latest Jurassic to Albian-Aptian age (Bouroullec et al., 1979; Mauriaud, 1997; Serrano, 2001; Serrano et al., 2006); however, we demonstrate here that their origin was part of the earlier opening of the Tethys.

The aborted rift in the Aquitaine region led to the development of an asymmetric substratum, which hosted stable depocenters throughout the Early and Middle Jurassic **(Fig. 8)**. The steep southern margins and gently dipping northern margins of the initial Arzacq and Tartas basins suggest that they originated as pull-apart basins opened during a transtensive stage (Zak and Freund, 1981; Ben-Avraham and Zoback, 1992; Wu et al., 2009).

6.2 Latest Jurassic to Neocomian uplift phase

The latest Jurassic and earliest Cretaceous were marked by the emersion and weathering of the Jurassic carbonate platform in the Pyrenean realm. Our interpreted seismic reflection profiles show that the Arzacq basin was affected as well by this major episode. Its response to this event included both uplifting domains and subsiding domains. Evidence of uplifting domains includes thickness reduction and erosion of the Tithonian sequence over the major structural highs of the Arzacq basin: the Grand Rieu, Audignon, Pécorade and Antin-Maubourguet ridges. In these areas, the Neocomian (Berriasian to Hauterivian) interval is always absent, meaning that the Barremian are the first deposits postdating the event. However, where Tithonian facies are preserved, significant thicknesses of Neocomian facies also remain (Calcaire de Ger Formation and Argiles du Gamma Ray Formation), indicating that these areas underwent subsidence. Consequently, the Late Jurassic to Neocomian period corresponds to a vast, heterogeneous doming stage that extended far beyond the Pyrenean domain (Canérot, 2008). This general uplift was characterized in the Aquitaine basin by subemersive to eroded structural highs bounding subsiding domains that held shallow, poorly connected brackish seas **(Fig. 8)**. This setting suggests that asthenospheric upwelling uplifted domains bounded by inherited Tethyan faults and localized subsiding basins between them.

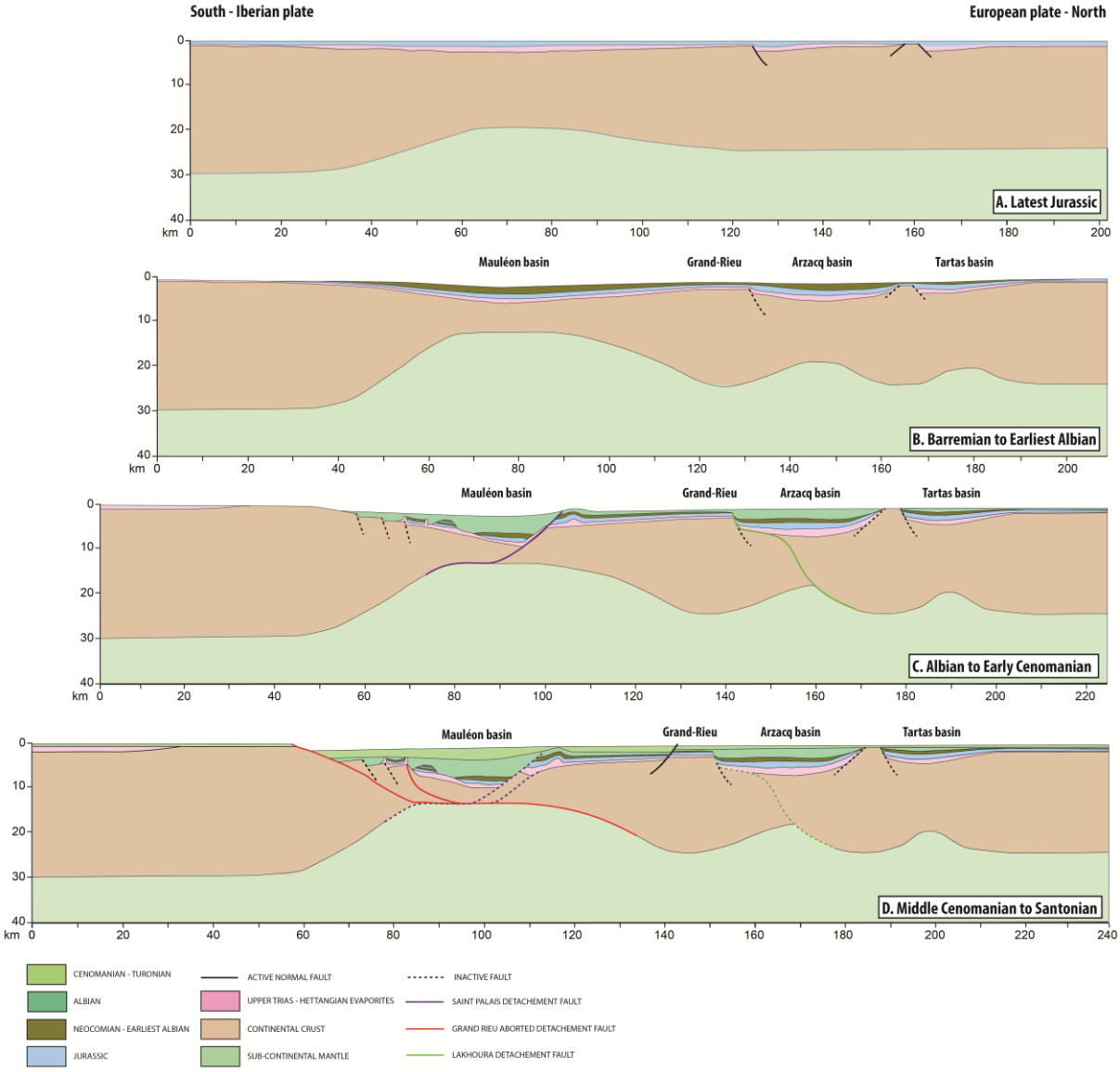


Fig. 8. North-south restored sections (no vertical exaggeration) showing the evolution of the Aquitaine basin and North Pyrenean Zone (modified after Saspiturry et al., 2019a), including the Arzacq and Tartas basins. A half-graben developing in Late Triassic to Hettangian time accumulated a thick evaporite sequence, which in turn controlled the emplacement of the Arzacq and Tartas basins in Berriasian-Barremian time. The two basins differentiated during the Albian, the Arzacq basin acquiring an asymmetric cross section following gravity sliding of the sedimentary cover on the northern Grand Rieu flank and the Tartas basin remaining a simple sag basin.

6.3. Barremian to early Aptian rifting stage 1: Symmetric rift basins

The thickness of the Barremian sequence indicates that the Early Cretaceous transgression only slightly overspilled the Grand Rieu and Audignon-Pécorade-Antin-Maubourguet domains **(Fig. 8)**. The transgression did not extend over the Arbailles domain (Mauléon basin) until the Aptian, as the Barremian is absent there (Canérot et al., 1978; Martin-Closas and Peybernès, 1987; Combes et al., 1998; Canérot, 2008; Saspiturry et al., 2019a). The fact that the basin's depocenter was the same in Neocomian and Barremian time implies that the subsidence regime was continuous **(Fig. 8)**. As a result, this period saw the development of a shallow sea flooding small, disconnected structural lows located between the structural domains inherited from the Late Jurassic doming stage: the Arbailles, Grand Rieu, and Audignon highs and the Celtaquitaine Flexure. The transgression accelerated in the early Aptian, as suggested by the regional extent of the Saint Suzanne Marls Formation and by the regional paleogeographic reorganization. Indeed, widespread marginal-marine deposits of the Calcaire à Annélides

Formation grade vertically to these marls, tracing a direct transition to relatively deep open marine conditions. Their extent suggests that the Tartas, Arzacq and Mauléon basins became connected for the first time in the Cretaceous, and they remained connected into the late Aptian with the development of the shallow Urgonian platform.

In this first stage, we interpret the relative lack of brittle deformation affecting the upper crust, the deep subsidence in the basin center and the unchanging depocenter as a response to thinning of the lower crust during Neocomian uplift that did not affect the upper crust. The lower crustal thinning was responsible for the basin subsidence and the progressive onlap of deposits towards the basin margins. This process favors the development of rift basins with a sag geometry. Subsidence of 0.8 s TWT over a 20 My period signifies a subsidence rate of roughly 60 m/My. The constant position of the Barremian and Neocomian depocenters suggests that the Late Jurassic to Neocomian doming was the driver of this crustal thinning stage. It is quite similar to the Barremian-Aptian history of the Mauléon basin, where a synrift sag basin morphology preceded the development of an asymmetric basin in the Albian and Cenomanian (Saspiturry et al., 2019a).

6.4. Late Aptian to Albian stage 2: Widespread rifting and onset of asymmetry

The Tartas and Arzacq basins became separated again during the Albian **(Fig. 8)**, and they show different geometries. The Tartas basin remained symmetric throughout the Albian except in the Lussagnet area, where the rise of a salt diapir controlled the development of a mini-basin. In the meantime, The Arzacq basin became slightly non-symmetric (pseudosymmetric). Pseudosymmetry of Arzacq is attested on the Rousse-Theze and Ger-Beaulieu profiles which show Albian sequence thickening southward, depocenter shifting a few kilometers southward and deep marly facies to the south, whereas the Lacq–Villeneuve de Marsan profile shows a northward thickening together with a northward shift of the the dépocentre, and deep marly facies to the north

The Rousse-Theze profile shows remnant of Jurassic deposits below the Rousse-1 well, in the Grand Rieu domain, that is disconnected from the continuous Jurassic cover in the Arzacq basin **(Fig.3)**. The intervening space is filled with Albian deposits, which we interpret as the result of early Albian gravity sliding: northward movement of the sedimentary cover on a detachment over a Triassic-Jurassic salt layer that created accommodation space for Albian sediment. Similar gravity sliding is documented in the adjacent Mauléon basin (Ducasse et al., 1986; Teixell et al., 2016; Saspiturry et al., 2019a). The erosion of the Albian sequence in the neighborhood of Pau anticline suggests that local minor halokinetic movements responded to the uplift of the northern Grand Rieu domain. This inference is supported by recent results (Saspiturry et al., 2019a) that document the generation of an anticline by late Albian and early Cenomanian salt diapirism in the Grand Rieu domain.

The Lacq–Villeneuve de Marsan profile documents the development of significant Albian asymmetry in the Audignon area, where a thick marly basin developed on the current Audignon anticline in which the depocenter migration and depositional profile orientation are northward rather than southward. No gravity sliding is evident here, and it is possible that salt diapirism (with internal truncations) was responsible for the development of a salt-controlled basin on the southern flank of the Audignon anticline. The increase in thickness overlies normal faults of Early Jurassic age, suggesting that this major structure was reactivated throughout the Mesozoic..

In this rifting stage, subsidence was more localized and more strongly controlled by brittle deformation than in the previous stage. The depocenters were offset in different directions, and subsidence rates were approximately 1 s TWT over a 13 My time period, or roughly 115 m/My, double the rate during the previous stage. Two subsiding domains can be distinguished: a western one as shown in the Lacq–Villeneuve de Marsan profile and an eastern one around the Pau area. In the western domain, depocenters migrated northward in response to massive salt diapirism on the Audignon-Pécorade ridge. In the eastern domain, depocenters migrated southward consequent to northward gravity sliding upon thick underlying evaporites, which was probably a response to the initiation and

abortion of a detachment similar to what is described in the North Pyrenean basins. In both cases, the deformation controlling the subsidence was accommodated by salt tectonics localized along major structures.

6.5. Cenomanian postrift cooling phase

Numerous toplap markers are visible below the Cenomanian base in every seismic reflection profile in the Arzacq and Tartas basins, marking a significant unconformity between the Lower and Upper Cretaceous sequences. This pattern is especially visible in the Arzacq basin, where north- and south-oriented toplaps are visible on the southern and northern margins, respectively. These record vertical displacement of the Grand Rieu and Audignon, Pécorade, Antin-Maubourguet domains between latest Albian and early or mid-Cenomanian time. This uplift is likely related to flexural rebound of the rift edges at the beginning of the postrift regime (e.g. Weissel and Karner, 1989; Petit et al., 2007; Nemcok. 2016). The unconformity thus is a break-up unconformity that formed during the transition between the tectonically active rift stage and the quieter and more stable postrift stage **(Fig. 8)**.

7. Discussion

7.1. Crustal thinning: The role of prerift salt

The Aquitaine basin is an immature rift basin in the sense that it did not evolve into a truly brittle and asymmetric rifted basin. Whereas the Tartas basin remained a sag basin throughout the Early Cretaceous, the Arzacq basin went through an intermediate stage between a sag basin and a hyperthinned basin like the Mauléon rift (Jammes et al., 2009; Lagabrielle et al., 2010; Masini et al., 2014; Saspiturry et al., 2019a), the Parentis rift (Jammes et al., 2010; Ferrer et al., 2012; Tugend et al., 2014) and the Bay of Biscay continental margin (Ferrer et al., 2008; Roca et al., 2011; Tugend et al., 2014). In detail, the slightly asymmetric Arzacq basin was not affected by the significant detachment faults that led to the pronounced asymmetry seen in adjacent hyperthinned basins. Accommodation was instead controlled by salt tectonic, including large-scale salt diapirism and gravity sliding of the prerift sedimentary cover on a décollement within a salt layer. Such tectonic setting has been recently reproduce by numerically modeling based on the example of the North-Pyrenean synrift sag basin geometries (Duretz et al., 2019). In the adjacent Mauléon basin, salt-lubricated sliding on its Iberian margin (Ducasse et al., 1986; Bouquet, 1986; Lagabrielle et al., 2010; Teixell et al., 2016) has been interpreted as the stage preceding the early Albian initiation of the south-dipping Saint-Palais detachment (Saspiturry et al., 2019a).

However, the Arzacq basin differs from its neighboring basins in the magnitude of crustal thinning. For instance, several areas in the North Pyrenean Zone are characterized by a denudated subcontinental mantle, the origin of which is strongly debated but is generally considered to have included a rifting stage that caused the hyperthinned crust to delaminate and lead to the presence of mantle rocks at very shallow depths (Vissers et al., 1997; Jammes et al., 2009; Lagabrielle et al., 2010; Masini et al., 2014; Saspiturry et al., 2019a). However, the present-day Moho in the Arzacq basin is interpreted at 22 km depth (Wang et al., 2016), which is not compatible with extreme crustal thinning. For these reasons, we suggest that an aborted detachment fault controlled the slight asymmetry of the Arzacq basin, and that decoupling focused within thick evaporites insulated the sedimentary cover, with its lack of visible brittle structures, from crustal thinning below the salt layers

The unconformity below the Cenomanian sequence is highly pronounced near the Grand Rieu and Audignon-Pécorade-Antin-Maubourguer domains. In some areas, it is associated with the growth of small salt anticlines. Such deformation on the basin borders implies that these domains underwent late uplift, probably related to thermal reequilibration at the end of the rift stage **(Fig. 8)**. This interpretation strongly contrasts with previous studies that have linked this unconformity to a poorly constrained compressive stage (Biteau et al., 2006). In the Mauléon basin, postrift deposits do not predate the mid to late Cenomanian, after a flip-flop detachment directed extension onto the Iberian margin on the Lakhoura detachment fault and beheaded the previous detachment (Saint-Palais detachment fault) on the European margin. Consequently, the postrift stage is diachronous between the Arzacq and Mauléon basins.

7.2. Transfer faults of the Arzacq basin

In the North Pyrenean Zone, few studies have addressed the effect of transfer faults on the opening of the Cretaceous basins. Nevertheless, a major structure, the Pamplona fault, is believed to offset the axis of the Early Cretaceous rift (Razin, 1989; Claude, 1990; Larrasoaña et al., 2003; Vergès, 2003). This offset the Mauléon basin to the north and the basque-cantabrian basin to the south. The Mauléon basin was also affected by three N20° transfer faults within the North Pyrenean Zone (Peybernès and Souquet, 1984; Canérot, 2008, 2017). From east to west these are the Ossau, Barlanès and Saison transfer faults (Canérot, 2017). Recent work interprets this network of faults as inherited from the late Paleozoic Hercynian collapse stage (Saspiturry et al., 2018, 2019b).

These three major transfer faults also appear to account for the east-west segmentation within the Arzacq and Tartas basins **(Fig. 9)**. The Ossau transfer fault controls the N110° southward offset of the Antin-Maubourguet Ridges with respect to the Pécorade anticline. The Barlanès transfer fault controls the eastern termination of the Pécorade anticline, and in the Tartas basin, it appears to control the position and elongation of the Lussagnet salt diapir. The most striking impact of the Barlanès transfer fault is in the Audignon area, where it governs the position of the massive Audignon salt diapir along the Audignon structural high. This major structure is also responsible for a proximal and distal margin inversion across the fault **(Fig. 9)**. The Saison transfer fault may appear in the Gamarde-Goudon seismic reflection profile **(Fig. 5)** where an abrupt increase in the thickness of the Albian sequence east of the Amou-1 well may correspond to Albian activity on the transfer fault. In our interpretation, then, inherited late Hercynian structures (Saspiturry et al., 2018, 2019b) control, through the N110 faults, the emplacement of gravity slides and salt diapirs while N20 faults act as transfer zones segmenting the Arzacq and Tartas basins from east to west **(Fig. 10)**. The concept of transfer faults inverting the orientation of proximal and distal domains in adjacent basin segments has been invoked elsewhere on Atlantic margins (Lister et al., 1986; Péron-Pinvidic et al., 2015; Péron-Pinvidic and Osmundsen, 2018).

7.3. The Arzacq and Tartas basins within the Pyrenean rift system

Many studies describe the development of sedimentary basins associated with the opening of the Bay of Biscay, marked by significant hyperthinning structures. Most of them highlight the existence of detachment faults that accommodate this crustal thinning. We suggest here that similar structures formed but were curtailed early in the rifting history of the Arzacq basin, while the Tartas basin never underwent hyperthinning. In a north-south section that restores spreading between the Mauléon basin and the North Aquitaine Platform, we propose that the maturity of rifting decreases away from the main rift axis in the North Pyrenean basins **(Fig. 8)**. The Mauléon and Parentis basins, in the heart of the Albian-Cenomanian rift zone, underwent the greatest crustal thinning. The Arzacq basin was only moderately thinned, as shown by the relatively deep Moho there (22 km); nevertheless, its rifting stage included intense tectonic activity marked by salt diapirism and gravity sliding. We propose, on the basis of the basin's depositional asymmetry, that these events were related to an aborted detachment. On the Iberia plate, the Columbrets and Cameros basins show features of a similar history (Casas et al., 2009; Omodéo Salè et al., 2014; Etheve et al., 2018; Roma et al., 2018; Omodeo Salè et al., 2019; Rat et al., 2019), referred to as salt-detached ramp-synclines (Roma et al., 2018) or extensional synclines (Casas et al., 2009). In these basins, crustal thinning was controlled by detachment faults, by which an upper-crust ramp generated large-scale salt-migration synclines controlled by roll-over structures that we might interpret as the result of gravity sliding followed by diapir development. Like the Arzacq basin, the Columbrets and Cameros basins are located on the periphery of the Cretaceous rifting and did not evolve in a mature rift system. The Tartas basin represents the common initial state of all these basins.

To sum up, the Pyrenean-Biscay rift can be described as a four-part combination consisting of an oceanic domain where complete loss of continental crust led to development of oceanic crust (Bay of Biscay), a mature rift system in

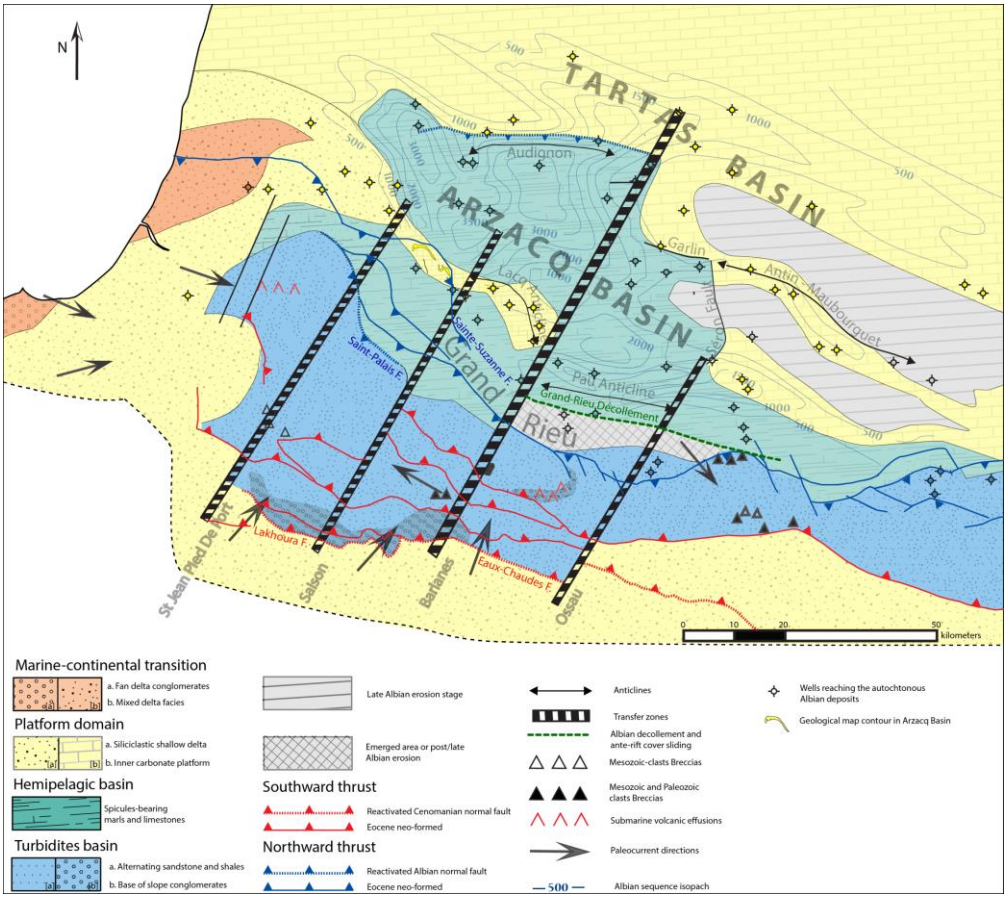


Fig. 9. Albian paleogeography in the Pyrenees-Aquitaine domain (modified after ; Canérot et al., 2017; GSO, and BRGM, 2019; Saspiturry et al., 2019a). The N110 and N20 structural trends largely govern facies transitions. These inherited structures account for salt tectonics in the Audignon area (northward deepening) and the eastern Arzacq basin (southward deepening). Transfer faults control the lateral inversion of the proximal-distal orientation within the Arzacq basin as well as the emplacement of the Lussagnet diapir in the Tartas basin.

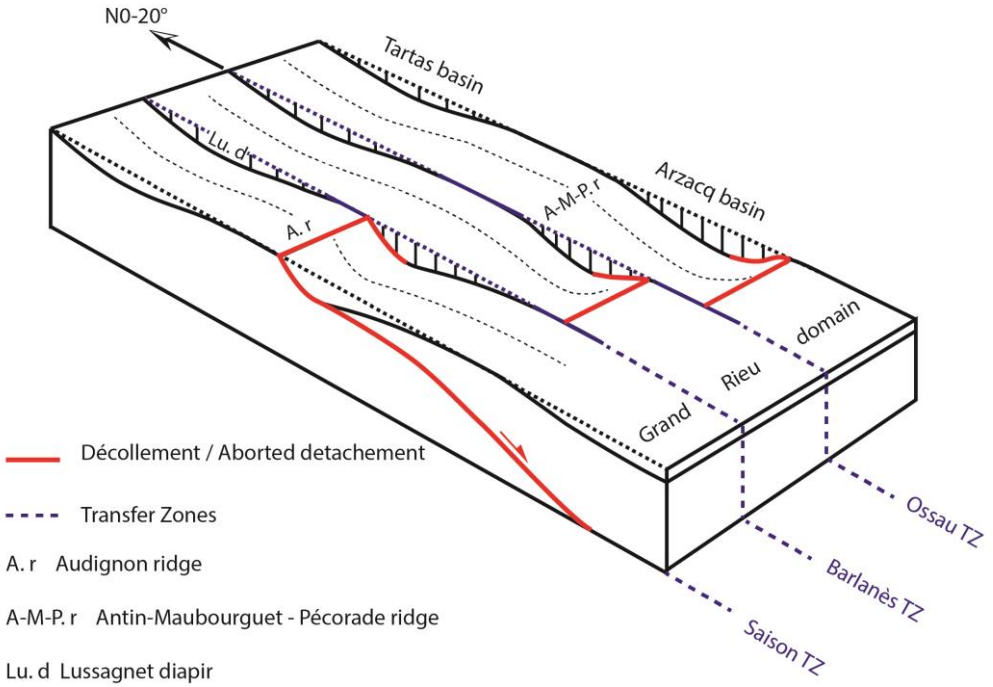


Fig. 10. 3D block diagram of the northern Mauléon basin, Arzacq basin, and Tartas basin showing the effects of the décollement and detachment faulting on the synrift basin morphology.

which detachments favored crustal thinning and development of non-symmetric basins (North Pyrenean basins, Parentis basin), an immature rift system affected by salt tectonics and controlled by a décollement representing an aborted detachment (Arzacq basin, Columbrets basin, Caméros basin), and a symmetric sag basin without brittle structures where crustal thinning was accommodated by ductile crustal flow (Tartas basin).

8. Conclusion

The Arzacq and Tartas basins, part of the broader Pyrenean-Atlantic rift system, display different records of the Early Cretaceous rifting stage. Whereas the Tartas basin remained a symmetric sag basin throughout the Early Cretaceous, the Arzacq basin experienced a first sag stage (Berriasian–Aptian) followed by a rapidly subsiding, slightly asymmetric stage (Albian).

We interpret the sag morphology as linked to thinning of the European lower crust in which normal faulting did not affect the upper crust. The subsidence of the Early Cretaceous basins appears to have been controlled by their inherited Jurassic framework, as the edges of the Early Cretaceous depocenters coincide with major early Mesozoic horsts (Grand Rieu and Audignon). In the Arzacq basin, Albian salt tectonics was responsible for the basin's asymmetry, which varies along strike with the influence of transfer faults (the Saint Jean Pied de Port, Saison, Barlanès and Ossau transfer zones). The intersection of these transfer faults and inherited N110 faults led to the development of a giant salt diapir in the Audignon region (in which the asymmetry developed on the north side) and to massive gravity sliding and creation of accommodation space in the Grand Rieu domain (in which the asymmetry developed on the south side).

From a larger regional perspective, the Arzacq and Tartas basins are in the periphery of the main area of major extension, and they decrease in their degree of crustal thinning with increasing distance from the rifting axis. We propose a multistage scheme for the evolution of basins in this large-scale setting. The first rifting stage is typified by the sag geometry of the Tartas basin, in which crustal thinning is accommodated by subtractive processes in the ductile crust that are decoupled from the sedimentary cover by the presence of significant evaporite layers. This initial stage might evolve with further crustal thinning into a stage typified by slightly asymmetric basins (such as the Arzacq, Columbrets and Caméros basins) in which large-scale salt tectonics causes brittle deformation accompanying the onset and abortion of a detachment fault. These basins evolve with further thinning into mature rift systems in which well-developed detachment faults lead to efficient crustal thinning (North Pyrenean basins, Parentis basin) and finally give birth to domains of oceanic crust (Bay of Biscay).

Acknowledgments

This study was conducted within the framework of the Orogen integrated geologic research project funded by TOTAL, BRGM, and INSU. We are very grateful to the reviewers and to the editor, who contributed to the improvement of this manuscript. We would like to thank the Orogen project managers Sylvain Calassou (Total), Emmanuel Masini (Total), Olivier Vidal (CNRS) and the French geological survey (BRGM). We also warmly thank Andrew Alden for the English review.

References

AGSO and BRGM, 2018, Synthèse géophysique et géologique des Pyrénées - Volume 3 : Cycle alpin : Phénomènes alpins – 2015, Edition AGSO and BRGM, coordinated by A. BARNOLAS (1982-2001), B. GUÉRANGÉ (1982-90) J.C. CHIRON (1991-95) and S. COURBOULEIX (1996-2001), scientific committee : A. AUTRAN, M. DURAND-DELGA and J.M. FONBOTÉ, 480 p., 286 figs.

Ben-Avraham, Z., and M. D. Zoback (1992), Transform-normal extension and asymmetric basins; an alternative to pull-apart models, Geology, 20, 423–426, doi:10.1130/00917613(1992)020<0423:TNEAAB>2.3.CO;2

Biteau J.J., and Canérot, J. 2008. La chaîne des Pyrénées et ses avants-pays d'Aquitaine et de l'Ebre, structure, évolution géodynamique et systèmes pétroliers. Revue de l'Union Française des géologuges, n°155.

Bois, C., and ECORS Scientific Party, 1990, Major geodynamic processes studied from the ECORS deep seismic profiles in France and adjacent areas: Tectonophysics, v. 173, p. 397–410.

Bouquet, B., 1986, La bordure mésozoïque orientale du Massif du Labourd (Pyrénées occidentales) : Stratigraphie-Sédimentologie-Structure-Implications Géodynamiques: Pau, Université de Pau et des Pays de l'Adour, 219 p.

Bouroullec, J., Deloffre, R. 1970. Interprétation sédimentologique et paléogéographique par microfaciès du Crétacé inférieur basal d'Aquitaine Sud-Ouest. 1970, Bull. Centre Rech. Pau-SNPA, vol 4, n°2, pp. 381-429

Bouroullec, J., J. Delfaud, and R. Deloffre, 1979, Organisations sédimentaire et paléocologique de l'Aptien supérieur à faciès urgonien dans les Pyrénées occidentales et l'Aquitaine méridionale: Géobios, no. 3, p. 25–43.

Bourrouilh, R., J.-P. Richert, and G. Zolnaï, 1995, The North Pyrenean Aquitaine basin, France: Evolution and Hydrocarbons: AAPG Bulletin, v. 79, no. 6, p. 831–853.

BRGM, Elf, Esso, & SNPA, 1974, Géologie du bassin d'aquitaine (BRGM Ed). Paris: BRGM Editions.

Brunet, M.F., 1984. Subsidence history of the Aquitaine basin determined from subsidence curves, Geological Magazine 121(05):421 - 428

Brunet, M. F., 1991, Subsidence et Géodynamique du bassin d'Aquitaine. Relations avec l'ouverture de l'Atlantique. Thèse Sci. Univ. Paris VI, 288p.

Burg, J.-P., J. Van Den Driessche, and J.-P. Brun, 1994, Syn- to post-thickening extension : mode and consequences: Comptes rendus de l'Académie des sciences. Série 2. Sciences de la terre et des planètes, v. 319, no. 9, p. 1019–1032.

Canérot, J., 2008, Les Pyrénées: Histoire géologique: Atlantica.

Canérot, J., 2017, The pull apart-type Tardets-Mauléon basin, a key to understand the formation of the Pyrenees, Bull. Soc. géol. Fr. BSGF - Earth Sciences Bulletin 188, 35.

Canérot, J., Peybernes, B., Ciszak, R., 1979, Presence d'une marge meridionale a l'emplacement de la zone des chainons bearnais (Pyrenees basco-bearnaises). Bulletin de la Société Géologique de France; S7-XX (5): 673–676. doi: https://doi.org/10.2113/gssgfbull.S7-XX.5.673

Canérot, J., C. Majesté-Menjoulas, and Y. Ternet, 1999, Le cadre stratigraphique et géodynamique des altérites et des bauxites sur la marge ibérique des Pyrénées occidentales (France): Comptes Rendus de l'Académie des Sciences-Series IIA-Earth and Planetary Science, v. 328, no. 7, p. 451–456.

Casas, A., P. Kearey, L. Rivero, and C. R. Adam, 1997, Gravity anomaly map of the Pyrenean region and a comparison of the deep geological structure of the western and eastern Pyrenees: Earth and Planetary Science Letters, v. 150, no. 1–2, p. 65–78.

Casas, A., Villalaín, J.J., Soto, R., Gil-Imaz, A., Del Río, P., Fernández, G., 2009, Multidisciplinary approach to an extensional syncline model for the Mesozoic Cameros basin (N Spain), Tectonophysics, Volume 470, Issues 1–2, Pages 3-20, ISSN 0040-1951, https://doi.org/10.1016/j.tecto.2008.04.020.

Claude, D., 1990, Etude stratigraphique, sédimentologique et structural des dépôts Mésozoïques au Nord du Massif du Labourd. Role de la Faille de Pamplona (Pays Basque). Thèse de doctorat, Université de Bordeaux.

Clerc, C., and Y. Lagabrielle, 2014, Thermal control on the modes of crustal thinning leading to mantle exhumation: Insights from the Cretaceous Pyrenean hot paleomargins: Tectonics, v. 33, no. 7, p. 1340–1359, doi:10.1002/2013TC003471.

Combes, P.-J., B. Peybernès, and A. F. Leyreloup, 1998, Altérites et bauxites, témoins des marges européenne et ibérique des Pyrénées occidentales au Jurassique supérieur—Crétacé inférieur, à l'ouest de la vallée d'Ossau (Pyrénées-Atlantiques, France): Comptes Rendus de l'Académie des Sciences-Series IIA-Earth and Planetary Science, v. 327, no. 4, p. 271–278

Corre, B., Y. Lagabrielle, P. Labaume, S. Fourcade, C. Clerc, and M. Ballèvre, 2016, Deformation associated with mantle exhumation in a distal, hot passive margin environment: New constraints from the Saraillé Massif (Chaînons Béarnais, North-Pyrenean Zone): Comptes Rendus Geoscience, v. 348, no. 3–4, p. 279–289, doi:10.1016/j.crte.2015.11.007.

Curnelle, R., 1983, Evolution structuro-sédimentaire du Trias et de l'Infra-Lias d'Aquitaine: Bull. Cent. Rech. Explor. Prod. Elf-Aquitaine, v. 7, no. 1, p. 69–99.

Curnelle R., Dubois P., 1986. Evolution des grands bassins sédimentaires français: bassins de Paris, d'Aquitaine et du Sud-Est. Bull. Soc. géol. Fr., 8, 526-546

Daignières, M., M. Séguret, M. Specht, and E. Team, 1994, The Arzacq-western Pyrenees ECORS deep seismic profile, in Hydrocarbon and petroleum geology of France: Springer, p. 199–208.

Delfaud J. 1969. Essai sur la géologie dynamique du domaine Aquitano-pyrénéen durant le Jurassique et le Crétacé inférieur. Thèse doctorat de l'Université de Bordeaux.

Delfaud, J., and J. Henry, 1967, Evolution des bassins jurassiques dans la zone nord-pyrénéenne occidentale: 64ème congrès AFAS Bordeaux, p. 75–80.

Desegaulx, P. and Brunet, M.-F., 1990. Tectonic subsidence of the Aquitaine basin since Cretaceous times, Bull. Soc. géol. France 8 (VI), pp. 29–306.

Ducasse, L., P.-C. Velasque, and J. Muller, 1986, Glissement de couverture et panneaux basculés dans la région des Arbailles (Pyrénées occidentales): Un modèle évolutif crétacé de la marge nord-ibérique à l'Est de la transformante de Pamplona: Comptes rendus de l'Académie des sciences. Série 2, Mécanique, Physique, Chimie, Sciences de l'univers, Sciences de la Terre, v. 303, no. 16, p. 1477–1482.

Duretz, T., Asti, R., Lagabrielle, Y., Brun, J-P., Jourdon, A., Clerc, C., and Corre, B, 2019, Numerical modelling of Cretaceous Pyrenean Rifting: The interaction between mantle exhumation and syn-rift salt tectonics. basin Research, doi: 10.1111/bre.12389.

Etheve, N., Mohn, G., Frizon de Lamotte, D., Roca, E., Tugend, J., & Gómez-Romeu, J. (2018). Extreme Mesozoic crustal thinning in the eastern Iberia margin: The example of the Columbrets basin (Valencia Trough). Tectonics, 37, 636–662, doi: 10.1002/2017TC004613

Ferrer, O., E. Roca, B. Benjumea, J. A. Muñoz, N. Ellouz, and MARCONI Team, 2008, The deep seismic reflection MARCONI-3 profile: Role of extensional Mesozoic

structure during the Pyrenean contractional deformation at the eastern part of the Bay of Biscay: Marine and Petroleum Geology, v. 25, no. 8, p. 714–730, doi:10.1016/j.marpetgeo.2008.06.002.

Ferrer, O., M. P. A. Jackson, E. Roca, and M. Rubinat, 2012, Evolution of salt structures during extension and inversion of the Offshore Parentis basin (Eastern Bay of Biscay): Geological Society, London, Special Publications, v. 363, no. 1, p. 361–380, doi:10.1144/SP363.16.

Gong, Z., C. G. Langereis, and T. A. T. Mullender, 2008, The rotation of Iberia during the Aptian and the opening of the Bay of Biscay: Earth and Planetary Science Letters, v. 273, no. 1–2, p. 80–93, doi:10.1016/j.epsl.2008.06.016.

Grandjean, G., 1992, Mise en évidence des structures crustales dans une portion de chaîne et de leur relation avec les bassins sédimentaires. Application aux Pyrénées occidentales au travers du Projet ECORS Arzacq-Pyrénées: Université des Sciences et Techniques du Languedoc, 291 p.

Grandjean, G., 1994, Etude des structures crustales dans une portion de chaîne et de leur relation avec les bassins sédimentaires. Application aux Pyrénées occidentales: Bull. Cent. Rech. Explor. Prod. Elf Aquitaine, v. 18, no. 2, p. 391–420

Hart, N. R., D. F. Stockli, and N. W. Hayman, 2016, Provenance evolution during progressive rifting and hyperextension using bedrock and detrital zircon U-Pb geochronology, Mauléon basin, western Pyrenees: Geosphere, v. 12, no. 4, p. 1166–1186, doi:10.1130/GES01273.1.

Hart, N. R., D. F. Stockli, L. L. Lavier, and N. W. Hayman, 2017, Thermal evolution of a hyperextended rift basin, Mauléon basin, western Pyrenees: Thermal evolution of hyperextended rift: Tectonics, doi:10.1002/2016TC004365.

Haupert, I., G. Manatschal, A. Decarlis, and P. Unternehr, 2016, Upper-plate magma-poor rifted margins: Stratigraphic architecture and structural evolution: Marine and Petroleum Geology, v. 69, p. 241–261, doi:10.1016/j.marpetgeo.2015.10.020.

James, V., 1998, La plate-forme carbonatée ouest-pyrénéenne au jurassique moyen et supérieur stratigraphie séquentielle, stades d'évolution, relations avec la subsurface en aquitaine méridionale: 351 p.

Jammes, S., G. Manatschal, L. Lavier, and E. Masini, 2009, Tectono-sedimentary evolution related to extreme crustal thinning ahead of a propagating ocean: Example of the western Pyrenees: Tectonics, v. 28, no. 4, doi:10.1029/2008TC002406.

Karner, G. D., N. W. Driscoll, and D. H. N. Barker, 2003, Synrift regional subsidence across the West African continental margin: the role of lower plate ductile extension: Geological Society, London, Special Publications, v. 207, no. 1, p. 105–129, doi:10.1144/GSL.SP.2003.207.6.

Lagabrielle, Y., P. Labaume, and M. de Saint Blanquat, 2010, Mantle exhumation, crustal denudation, and gravity tectonics during Cretaceous rifting in the Pyrenean realm (SW Europe): Insights from the geological setting of the lherzolite bodies: Tectonics, v. 29, no. 4, doi:10.1029/2009TC002588.

Larrasoaña, J. C., J. M. Parés, H. Millán, J. del Valle, and E. L. Pueyo, 2003, Paleomagnetic, structural, and stratigraphic constraints on transverse fault kinematics during basin inversion: The Pamplona Fault (Pyrenees, north Spain): Tectonics, v. 22, no. 6, doi:10.1029/2002TC001446.

Lavier, L. L., and G. Manatschal, 2006, A mechanism to thin the continental lithosphere at magma-poor margins: Nature, v. 440, no. 7082, p. 324–328, doi:10.1038/nature04608.

Lenoble, J.-L., 1992, Les plates-formes carbonatées ouest-pyrénéennes du dogger à l'Albien, stratigraphie séquentielle et évolution géodynamique: Université Paul Sabatier de Toulouse (Sciences), 395 p.

Lister, G. S., M. A. Etheridge, and P. A. Symonds, 1986, Detachment faulting and the evolution of passive continental margins: Geology, v. 14, no. 3, p. 246–250, doi:10.1130/0091-7613(1986)14<246:DFATEO>2.0.CO;2.

Manatschal, G., 2004, New models for evolution of magma-poor rifted margins based on a review of data and concepts from West Iberia and the Alps: International Journal of Earth Sciences, v. 93, no. 3, doi:10.1007/s00531-004-0394-7.

Martin-Closas, C., Pebernès, B., 1987, Datation de la transgression éocrétacée dans les Pyrénées basco-béarnaises à l'aide des Charophytes, Geobios, Volume 20, Issue 5, Pages 695-700, ISSN 0016-6995, https://doi.org/10.1016/S0016-6995(87)80024-4.

Masini, E., G. Manatschal, G. Mohn, J.-F. Ghienne, and F. Lafont, 2011, The tectono-sedimentary evolution of a supra-detachment rift basin at a deep-water magma-poor rifted margin: the example of the Samedan basin preserved in the Err nappe in SE Switzerland: Tectono-sedimentary evolution of a supra-detachment rift basin: basin Research, v. 23, no. 6, p. 652–677, doi:10.1111/j.1365-2117.2011.00509.x.

Masini, E., G. Manatschal, G. Mohn, and P. Unternehr, 2012, Anatomy and tectono-sedimentary evolution of a rift-related detachment system: The example of the Err detachment (central Alps, SE Switzerland): Geological Society of America Bulletin, v. 124, no. 9–10, p. 1535–1551, doi:10.1130/B30557.1.

Masini, E., G. Manatschal, J. Tugend, G. Mohn, and J.-M. Flament, 2014, The tectono-sedimentary evolution of a hyper-extended rift basin: the example of the Arzacq–Mauléon rift system (Western Pyrenees, SW France): International Journal of Earth Sciences, v. 103, no. 6, p. 1569–1596, doi:10.1007/s00531-014-1023-8.

Mauriaud, P. 1987. Le bassin d'Aquitaine. Pétrole et Techniques, 335, 38–41.

McKenzie, D., 1978, Some remarks on the development of sedimentary basins: Earth and Planetary Science Letters, v. 40, no. 1, p. 25–32, doi:10.1016/0012-821X(78)90071-7

Mediavilla, F. 1987. La tectonique salifère d'Aquitaine. Le bassin de Parentis. Pe´trole et Techniques, 335, 35–37.

Mitchum R.M., Vail, P.R., Thompson, S., 1977. Seismic stratigraphy and global changes of sea level, part 2: The depositional sequence as a basic unit for stratigraphic analysis C.E Payton (Ed.), Seismic Stratigraphy, Am. Assoc. Pet. Geol. Mem., 26, pp. 53-62

Nemčok, M. (2016). Mechanics of rifting and transition to drift phases. In Rifts and Passive Margins: Structural Architecture, Thermal Regimes, and Petroleum Systems (pp. 31-75). Cambridge: Cambridge University Press. doi:10.1017/CBO9781139198844.003

Olivet, J. L., 1996, La cinématique de la plaque ibérique: Bull. Cent. Rech. Explor. Prod. Elf Aquitaine, v. 20, no. 1, p. 131–195.

Omodeo Salè, S., Guimerà, J., Mas, R., 2014, Tectono-stratigraphic evolution of an inverted extensional basin: the Cameros basin (north of Spain), Int J Earth Sci (Geol Rundsch) 103:1597–1620 DOI 10.1007/s00531-014-1026-5

Omodeo-Salé, S., Ondrak, R., Arribas, J., Mas, R., Guimerà, J. and Martínez, L. (2019), Petroleum systems modelling in a fold-and-thrust belt setting: the inverted cameros basin, north-central spain. Journal of Petroleum Geology, 42: 145-171. doi:10.1111/jpg.12728

Péron-Pinvidic, G., and G. Manatschal, 2009, The final rifting evolution at deep magma-poor passive margins from Iberia-Newfoundland: a new point of view: International Journal of Earth Sciences, v. 98, no. 7, p. 1581–1597, doi:10.1007/s00531-008-0337-9.

Péron-Pinvidic, G., Osmundsen, P., 2018, The Mid Norwegian - NE Greenland conjugate margins: Rifting evolution, margin segmentation, and breakup, Marine and Petroleum Geology, Volume 98, Pages 162-184, ISSN 0264-8172, doi.org/10.1016/j.marpetgeo.2018.08.011.

Péron-Pinvidic, G., G. Manatschal, E. Masini, E. Sutra, J. M. Flament, I. Haupert, and P. Unternehr, 2015, Unravelling the along-strike variability of the Angola–Gabon rifted margin: a mapping approach: Geological Society, London, Special Publications, v. 438, no. 1, p. 49–76, doi:10.1144/SP438.1.

Petit, C., Fournier, M., Gunnell, Y., 2007, Tectonic and climatic controls on rift escarpments: Erosion and flexural rebound of the Dhofar passive margin (Gulf of Aden, Oman), Journal of geophysical research, vol. 112, B03406, doi:10.1029/2006JB004554, 2007

Peybernès, B. 1976. Le Jurassique et le Crétacé inférieur des Pyrénées franco-espagnoles. Thèse État de l' Université de Toulouse, 459 p

Peybernès, B., 1979, L'Urgonien des Pyrénées, Essai de synthèse: Geobios, v. 12, p. 79–87.

Peybernès, B., 1982, Création puis évolution de la marge nord-ibérique des Pyrénées au Crétacé inférieur: Cuadernos de Geología Ibérica, v. 8, p. 987–1004.

Peybernès, B., Combes, J.P, 1987. Le problème de la limite Jurassique-Crétacé dans les Pyrénées occidentales entre Lourdes et Saint-Jean-Pied-de-Port; cadre stratigraphique et géodynamique des Bauxites Basco-béarnaises, Strata, Série 1, vol°3.

Peybernès, B., Souquet, P., 1984, Basement blocks and tecto-sedimentary evolution in the Pyrenees during Mesozoic times, Geological Magazine, Vol. 121, no. 4, September, pp. 397-539

Pinet, B., L. Montadert, and ECORS Scientific Party, 1987, Deep seismic reflection and refraction profiling along the Aquitaine shelf (Bay of Biscay): Geophysical Journal International, v. 89, no. 1, p. 305–312, doi:10.1111/j.1365-246X.1987.tb04423.x.

Rat, J., Mouthereau, F., Brichau, S., Crémades, A., Bernet, M., Balvay, M., et al. (2019). Tectonothermal evolution of the Cameros basin: Implications for tectonics of North Iberia. Tectonics, 38, 440–
469. https://doi.org/10.1029/2018TC005294

Roca, E., J. A. Muñoz, O. Ferrer, and N. Ellouz, 2011, The role of the Bay of Biscay Mesozoic extensional structure in the configuration of the Pyrenean orogen: Constraints from the MARCONI deep seismic reflection survey: Tectonics, v. 30, no. 2, doi:10.1029/2010TC002735.

Roest, W. R., S. P. Srivastava, 1991, Kinematics of the plate boundaries between Eurasia, Iberia, and Africa in the North Atlantic from the Late Cretaceous to the present: Geology, v.19, p. 613–616.

Roma, M., Ferrer, O., Roca, E., Pla, O., Escosa, F., Butillé, M., 2018, Formation and inversion of salt-detached ramp-syncline basins. Results from analog modeling and application to the Columbrets basin (Western Mediterranean), Tectonophysics, Volume 745, Pages 214-228, ISSN 0040-1951, https://doi.org/10.1016/j.tecto.2018.08.012.

Rosenbaum, G., G. S. Lister, and C. Duboz, 2002, Relative motions of Africa, Iberia and Europe during Alpine orogeny: Tectonophysics, v. 359, no. 1–2, p. 117–129, doi:10.1016/S0040-1951(02)00442-0.

Rossi, P., A. Cocherie, C. M. Fanning, and Y. Ternet, 2003, Datation U-Pb sur zircons des dolérites tholéiitiques pyrénéennes (ophites) à la limite Trias–Jurassique et relations avec les tufs volcaniques dits « infra-liasiques » nord-pyrénéens: Comptes Rendus Geoscience, v. 335, no. 15, p. 1071–1080, doi:10.1016/j.crte.2003.09.011.

Saspiturry, N., Cochelin, B., Razin, P., Leleu, S., Lemirre, B., Issautier, B., Serrano, O., Lasseur, E., Baudin, T., 2018, Post-Hercynian tectono-sedimentary evolution of an extensive intra-continental rift basin controlled by the upwelling of a metamorphic core complex (Bidarray basin, Western Pyrenees, Réunion des Sciences de la Terre, 26eme edition, Lille.

Saspiturry, S., Razin, P., Baudin, T., Serrano, O., Issautier, B., Lasseur, E., Allanic, C., Thinon, T., Leleu, S. 2019a. Symmetry vs. asymmetry of a hyper-thinned rift: Example of the Mauléon basin (Western Pyrenees, France), Marine and Petroleum Geology, Volume 104, 2019, pp. 86-105, ISSN 0264-8172, doi: 10.1016/j.marpetgeo.2019.03.031.

Saspiturry, N., Cochelin, B., Razin, P., Leleu, S., Lemirre, B., Bouscary, C., Issautier, B., Serrano, O., Lasseur, E., Baudin, T., and Allanic, C., 2019b. Tectono-sedimentary evolution of a rift-system controlled by Permian post-orogenic extension and metamorphic core complex formation (Bidarray basin and Ursuya dome, Western Pyrenees) : Tectonophysics, doi: 10.1016/j.tecto.2019.228180.

Serrano, O., 2001, Le Crétacé supérieur- Paléogène du bassin compressif Nord-pyrénéen (bassin de l'Adour) Sédimentologie, Stratigraphie, Géodynamique: Université Rennes 1, 342 p.

Serrano, O., J. Delmas, F. Hanot, R. Vially, J.-P. Herbin, P. Houel, and B. Tourlière, 2006, Le bassin d'Aquitaine: valorisation des données sismiques, cartographie structurale et potentiel pétrolier: Bureau de Recherche Géologique et minière, 245 p.

Sibuet, J.-C., S. P. Srivastava, and W. Spakman, 2004, Pyrenean orogeny and plate kinematics: Journal of Geophysical Research: Solid Earth, v. 109, no. B8, p. B08104, doi:10.1029/2003JB002514.

Souquet, P. et al., 1985, Le groupe du Flysch noir (albo-cénomanien) dans les Pyrénées: Bull Cent. Rech Exlpo-Prod Elf-Aquitaine Pau, v. 9, p. 183–252.

Teixell, A., P. Labaume, and Y. Lagabrielle, 2016, The crustal evolution of the west-central Pyrenees revisited: Inferences from a new kinematic scenario: Comptes Rendus Geoscience, v. 348, no. 3–4, p. 257–267, doi:10.1016/j.crte.2015.10.010.

Thinon, I., 1999,. Structure profonde de la Marge Nord Gascogne et du bassin Armoricain: PhD thesis, Ifremer-IUEM, Brest, France.

Tugend, J., G. Manatschal, N. J. Kusznir, E. Masini, G. Mohn, and I. Thinon, 2014, Formation and deformation of hyperextended rift systems: Insights from rift domain mapping in the Bay of Biscay-Pyrenees: Tectonics, v. 33, no. 7, p. 1239–1276, doi:10.1002/2014TC003529.

Unternehr, P., G. Peron-Pinvidic, G. Manatschal, and E. Sutra, 2010, Hyper-extended crust in the South Atlantic: in search of a model: Petroleum Geoscience, v. 16, no. 3, p. 207–215, doi:10.1144/1354-079309-904.

Vergés, J., 2003, Evolución de los sistemas de rampas oblicuas de los Pirineos meridionales: fallas del Segre y Pamplona. Boletín Geológico y Minero, 114 (1): 87-101 ISSN: 0366-0176

Vissers, R.L.M., Drury, M.R., Newman, J.,Fliervoet, T.F., 1997, Mylonitic deformation in upper mantle peridotites of the North Pyrenean Zone (France): implications for strength and strain localization in the lithosphere, Tectonophysics, Volume 279, Issues 1–4, ISSN 0040-1951, https://doi.org/10.1016/S0040-1951(97)00128-5.

Wang, Y., 2017, High resolution imaging of lithospheric structures by full waveform inversion of short period teleseismic P waves: Université Toulouse 3 Paul Sabatier (UT3 Paul Sabatier), 244 p.

Wang, Y. et al., 2016, The deep roots of the western Pyrenees revealed by full waveform inversion of teleseismic P waves: Geology, v. 44, no. 6, p. 475–478, doi:10.1130/G37812.1.

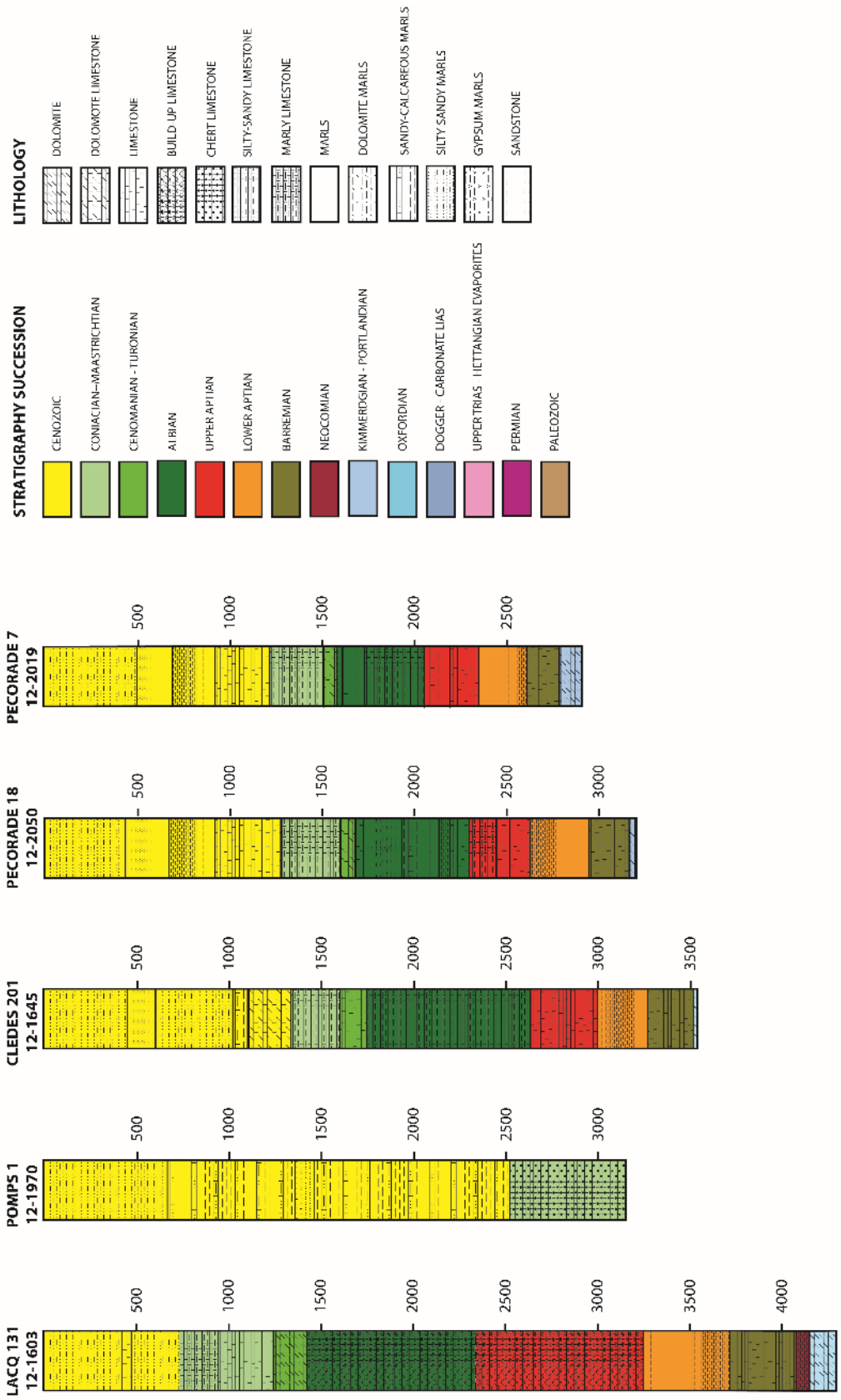
Weissel, J. K., and G. D. Karner (1989), Flexural uplift of rift flanks due to mechanical unloading of the lithosphere during extension, J. Geophys. Res., 94(B10), 13919–13950, doi:10.1029/JB094iB10p13919.

Wernicke, B., 1985, Uniform-sense normal simple shear of the continental lithosphere: Canadian Journal of Earth Sciences, v. 22, no. 1, p. 108–125, doi:10.1139/e85-009.

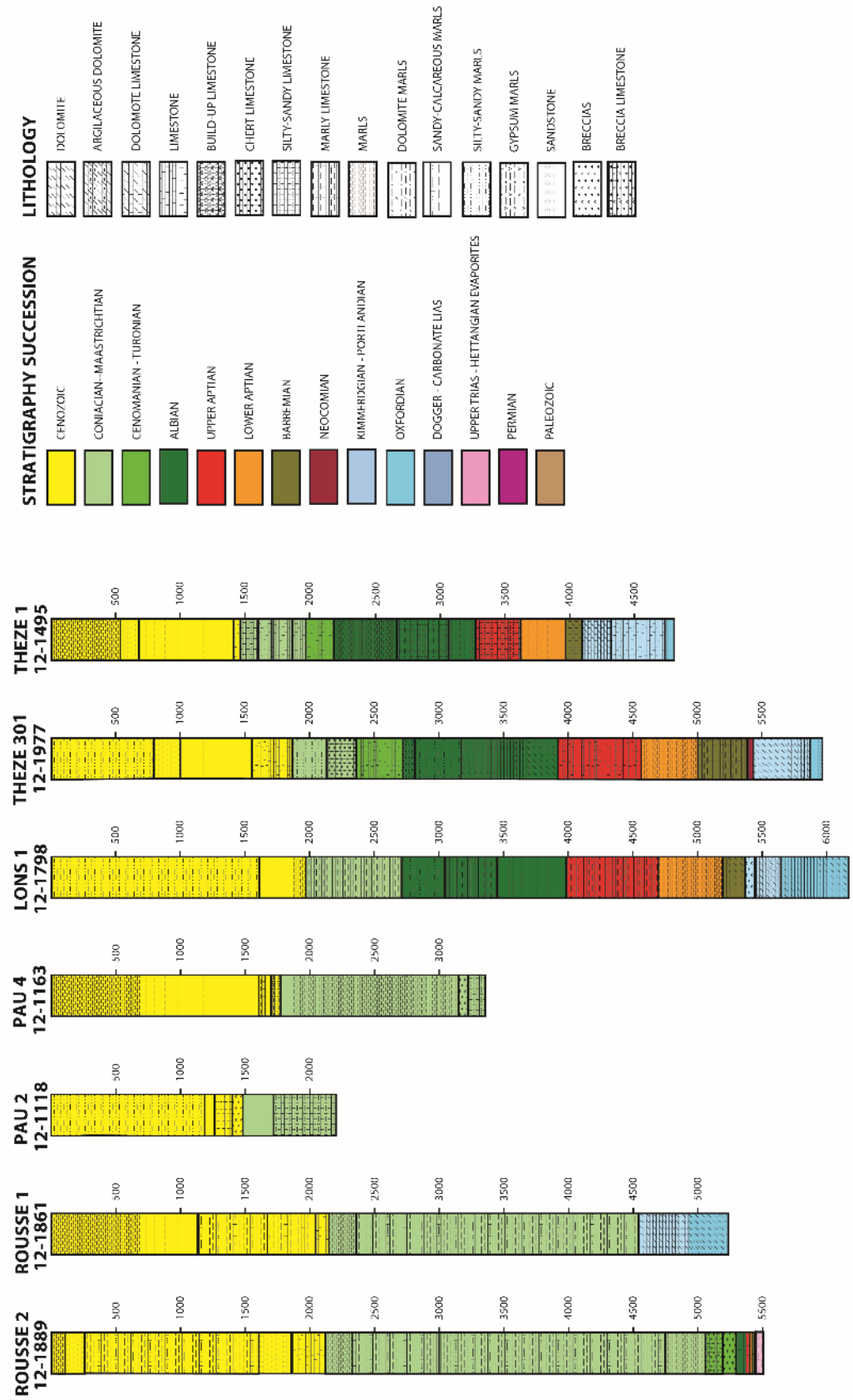
Wu, J., McClay, K., Whitehouse, P., Dooley, T., 2009. 4D Analogue modeling of transtensional pull-apart basins, Marine and Petroleum Geology, vol 26, n°8. DOI: 10.1016/j.marpetgeo.2008.06.007

Zak, I., Freund, R., 1981, Asymmetry and basin migration in the Dead Sea rift R. Freund, Z. Garfunkel (Eds.), The Dead Sea Rift, Tectonophysics, 80 (1981), pp. 27-38

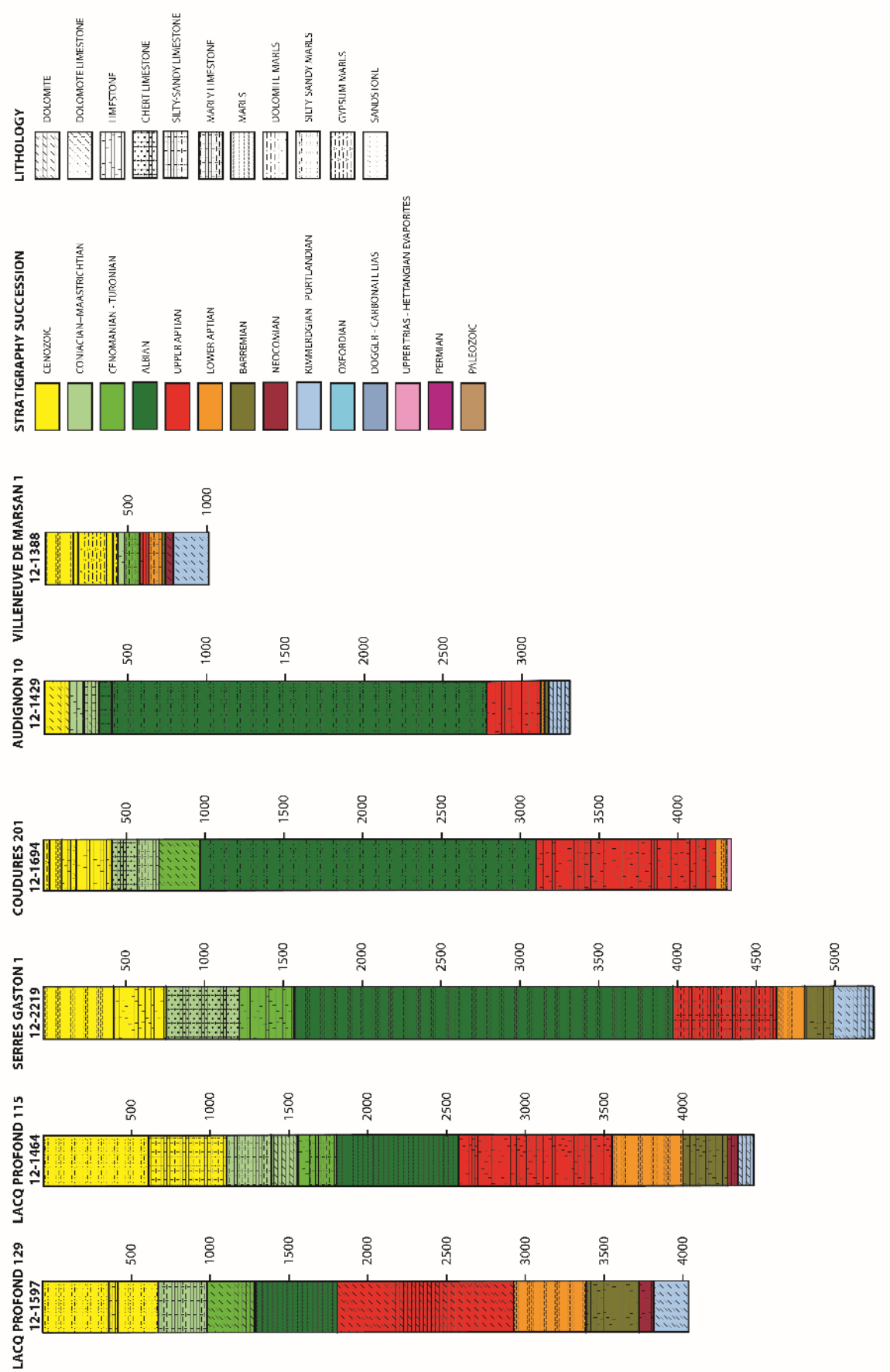
Supplementary Material



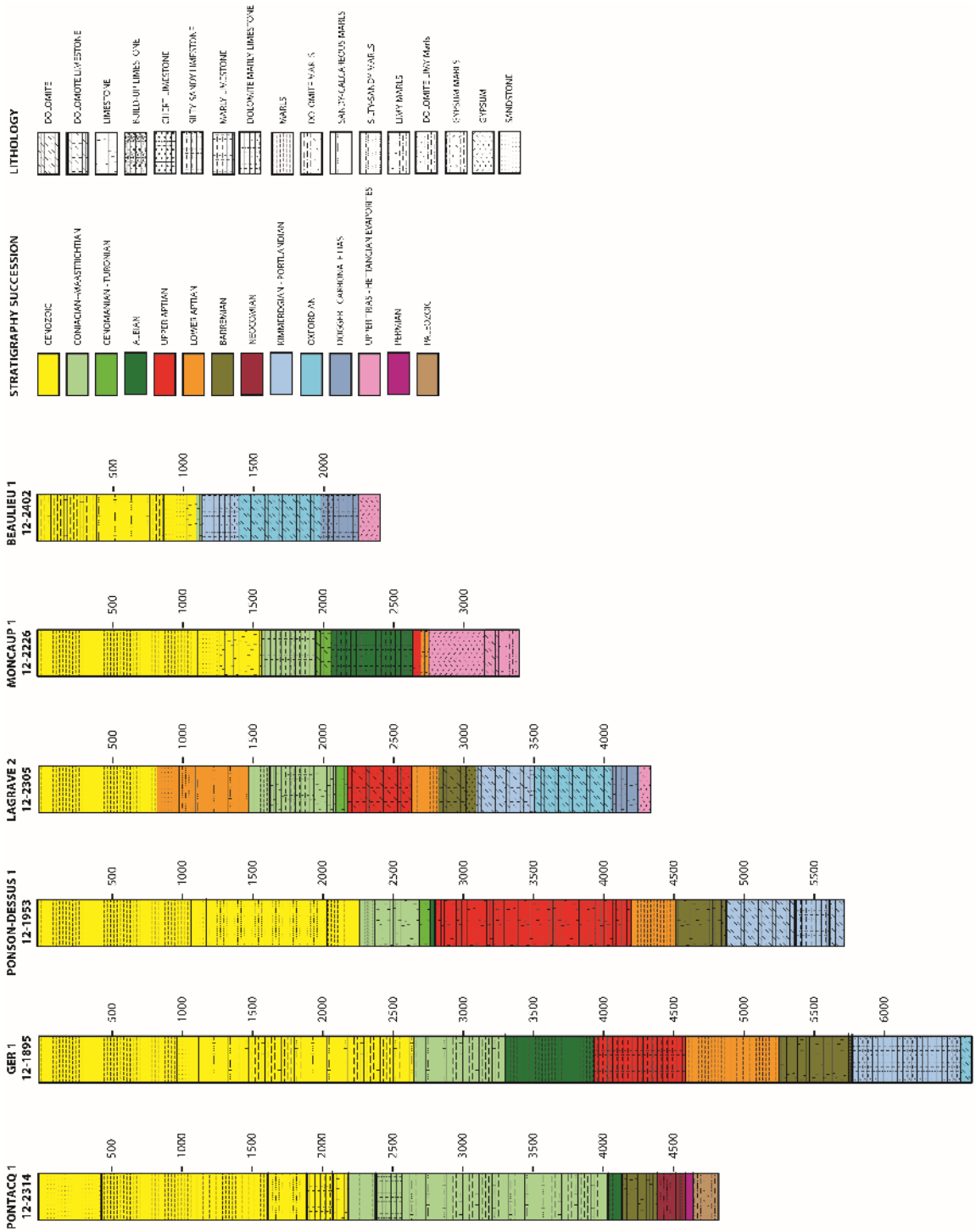
Supplementary Material. 1. Wells calibration of the Lacq-Pécorade profile.



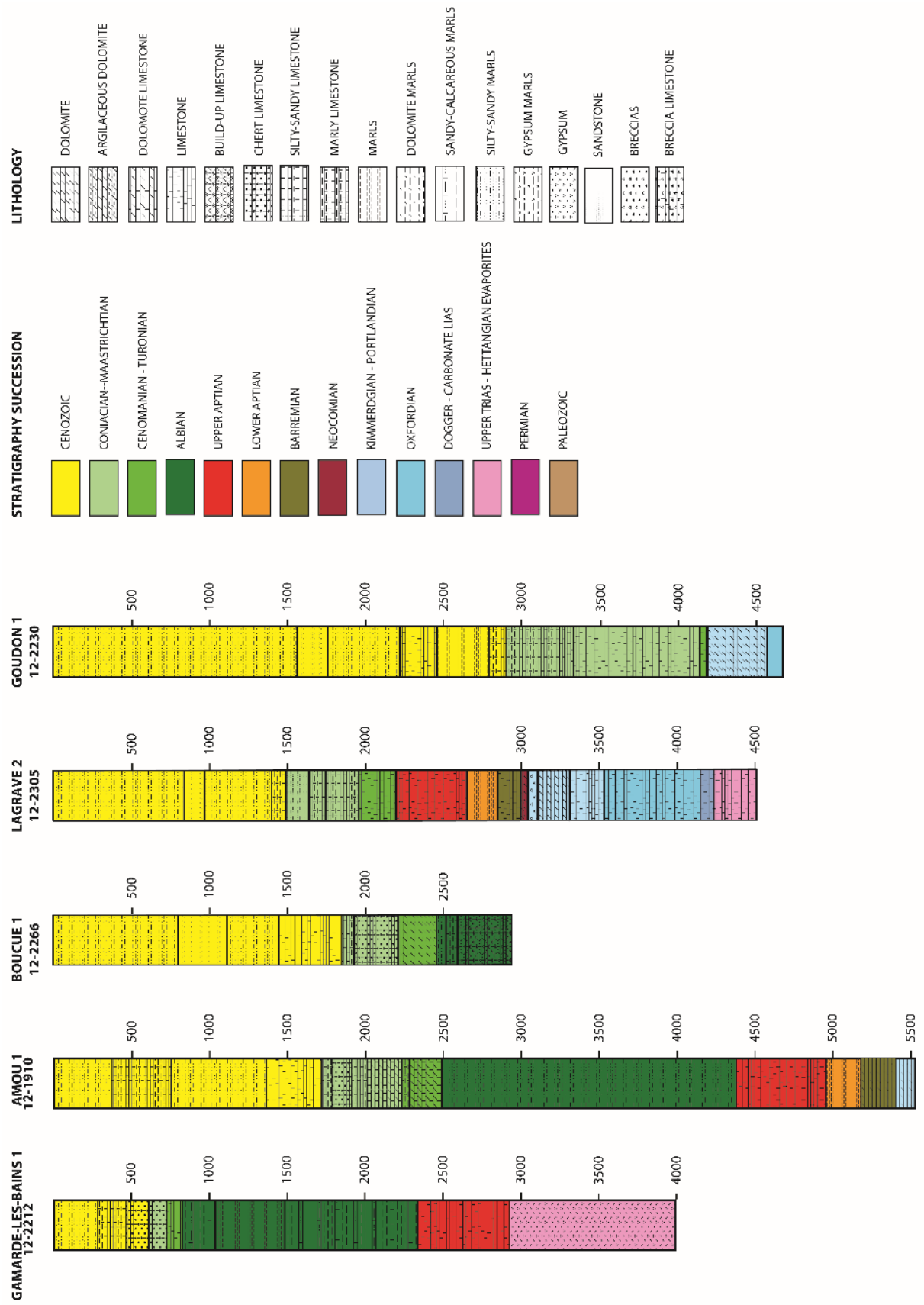
Supplementary Material. 2. Wells calibration of the Rousse-Thèse profile.



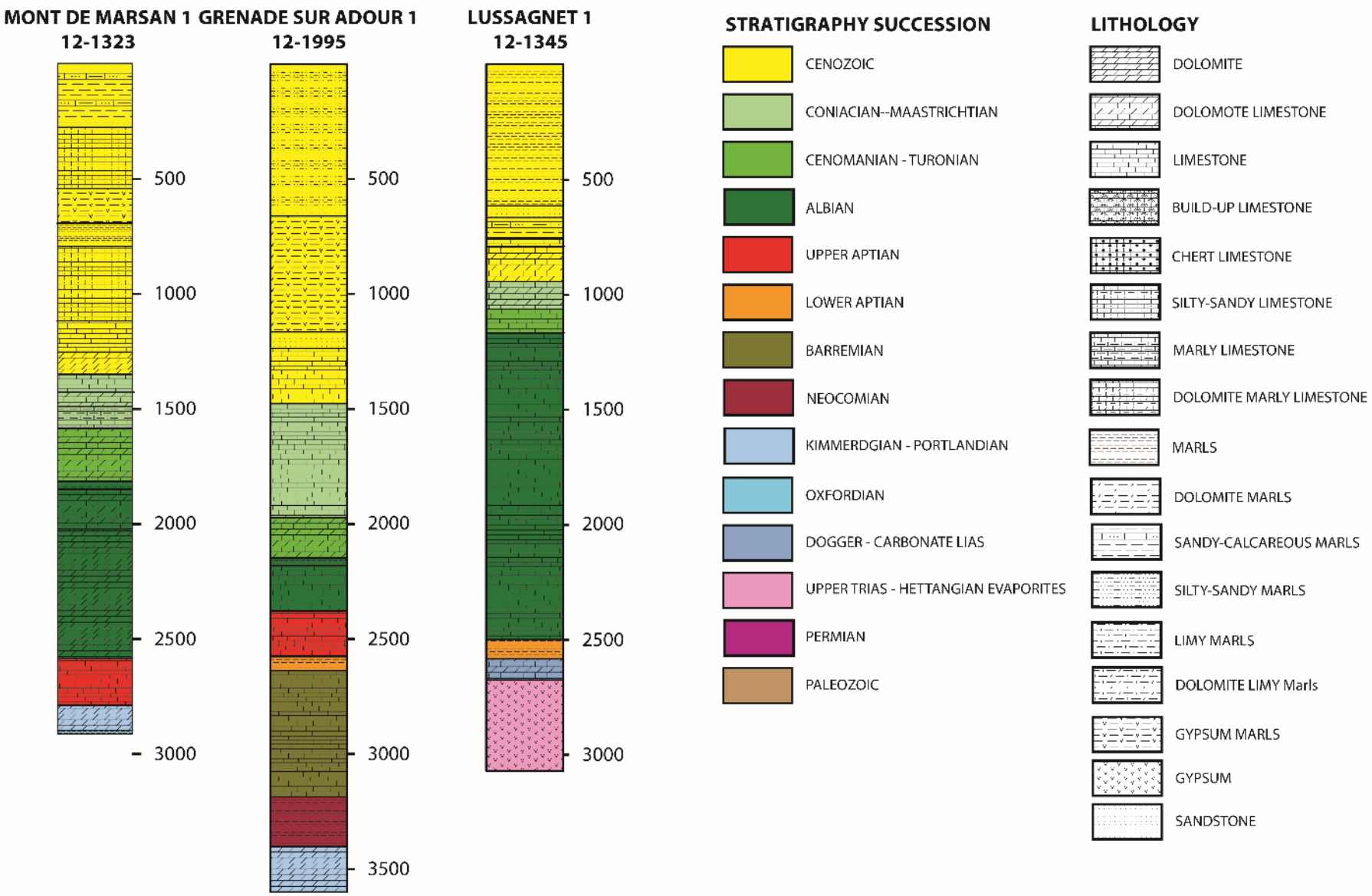
Supplementary Material. 3. Wells calibration of the Lacq-Villeneuve de Marsan profile.



Supplementary Material. 4. Wells calibration of the Ger-Beaulieu profile.



Supplementary Material. 5. Wells calibration of the Gamarde-Gourdon profile.



Supplementary Material. 6. Wells calibration of the Mont de Marsan - Lussagnet profile.

Chapitre 4

Orogenèse pyrénéenne

Bref aperçu du chapitre 4 : Orogenèse pyrénéenne

Le chapitre 4 du manuscrit de thèse présente le style structural de la réactivation du système de rift hyper-étiré de Mauléon au cours de la phase orogénique pyrénéenne. Le chapitre 4.1 est constitué d'un article soumis dans le journal *Terra Nova* en avril 2019. Cet article est basé sur la restauration d'une coupe crustale balancée N-S recoupant les Pyrénées occidentales. Cette restauration permet d'estimer un taux de raccourcissement du bassin de Mauléon et de discuter de l'impact de la phase d'hyperextension crétacée sur les processus responsables de la réactivation du bassin de Mauléon au sein d'un pop-up d'échelle lithosphérique.

Le chapitre 4.2 correspond à un article en préparation pour soumission dans *Journal of structural Geology*. Ce travail pluridisciplinaire intègre : (1) des données de spectroscopie Raman, (2) une approche terrain couplant analyses structurales et microstructurales, (3) des données sismiques pétrolières retraitées par le BRGM et (4) de la modélisation implicite 3D. Cet article permet de discuter de l'impact des structures de transferts N20°E, sur la géométrie en 3D des systèmes de chevauchements, bordant le pop-up lithosphérique de Mauléon.

Chapitre 4.1

Fermeture d’un système de rift hyper-étiré dans un pop-up orogénique lithosphérique : Rôle buttoir du manteau et impact de l’héritage structural du rifting crétacé

Chapitre 4.1. Closure of a hyperextended system in an orogenic lithospheric pop-up, Western Pyrenees: The role of mantle buttressing and rift structural inheritance

Sommaire

Résumé étendu p. 251

Abstract p. 253

1. Introduction **p. 253**

2. Rift inheritance in the Mauléon basin **p. 253**

3. Restauration of western Pyrenees cross section **p. 254**

4. Inversion modes during Pyrenean compression **p. 257**

Acknowledgements p. 260

References p. 260

Résumé étendu

Le rift hyper-étiré de Mauléon, d'âge Crétacé inférieur, est parfaitement préservé au sein de la partie nord-occidentale de l'orogenèse pyrénéenne. Dans le chapitre 4 du présent manuscrit de thèse nous discutons de l'évolution et de la préservation du bassin de Mauléon, au cours du tertiaire, à partir de la restauration d'une coupe balancée N-S d'échelle crustale recoupant la chaîne pyrénéenne sur une distance de 153-km. Cette restauration met en évidence un taux de raccourcissement minimum de 67 km (31%) dans les Pyrénées occidentales. Ce raccourcissement est distribué sur cinq chevauchements dans le « prowedge » (43 km) et trois chevauchements dans le « retrowedge » (24 km). Cette restauration met en évidence que le raccourcissement est accommodé de manière distincte dans le socle et la couverture.

Le « prowedge » ibérique se matérialise par un empilement de nappes de 50 km d'épaisseur formant une structure antiforme correspondant à la Zone Axiale, dont le chevauchement de Lakhoura correspond à l'unité supérieure. Cette structure crustale s'apparentant à un duplex et résulte de l'activation successive des chevauchements de Lakhoura, Gavarnie et Guarga. Le chevauchement de Lakhoura est d'âge Eocène supérieur et accommode près de 20 km de raccourcissement. Les chevauchements mineurs Sud et Nord Arbailles réactivent d'anciennes failles normales et accommodent une faible partie du raccourcissement. Ils correspondent à des ramifications se branchant sur le chevauchement de Lakhoura. Le chevauchement de Gavarnie accommode environ 15 km de raccourcissement entre l'Eocène supérieur et l'Oligocène inférieur. La structure de Guarga, quant à elle, est active entre l'Oligocène supérieur et le Miocène inférieur basal et porte environ 8 km de raccourcissement. La couverture sédimentaire du « prowedge » ibérique enregistre un raccourcissement similaire à celui de la Zone Axiale. Ce dernier est distribué sur différent chevauchements en séquence formant le bassin piggy-back sud pyrénéen décollé sur les évaporites du Trias supérieur.

Au sein du « retrowedge », les chevauchements de Saint-Palais, Bellevue et Sainte-Suzanne affectent la couverture sédimentaire mésozoïque européenne. La plupart de l'inversion du domaine hyper-étiré du bassin de Mauléon est accommodée par le plissement de la couverture mésozoïque contre l'escarpement de la faille normale de Saint-Palais, héritée de la phase d'hyperextension crétacée. Les chevauchements « thin-skin » de Bellevue et de Sainte-Suzanne se propagent vers le nord par l'intermédiaire du décollement correspondant au sel du Trias supérieur. Les chevauchements de Bellevue et de Sainte Suzanne émergent respectivement au droit d'un ancien diapir synrift albien et de l'escarpement de la faille normale bordant la partie méridionale de Grand Rieu. Le chevauchement de Bellevue accommode 4 km de raccourcissement alors que celui de Sainte Suzanne supporte quasiment la totalité du raccourcissement de la couverture du « retrowedge » européen (18 km). La déformation interne de la couverture mésozoïque représente 2 km de raccourcissement. Du fait du découplage de la déformation entre le socle et la couverture, le socle européen accommode également 24 km de raccourcissement formant une structure s'apparentant à un duplex crustal responsable de l'épaississement de la croûte continentale européenne (unités E.1 à E.4).

Dans les premiers stades d'inversion du bassin de Mauléon, la structure pseudo-symétrique du système de rift influence de manière significative la localisation de la contrainte compressive. Le bassin hyper-étiré de Mauléon est inversé en une structure de type pop-up dans laquelle les deux bordures accommodent la même quantité de raccourcissement (~ 20 km). Ce pop-up est bordé au sud et au nord par les chevauchements de Lakhoura et de Sainte Suzanne, d'âge Eocène supérieur. Cependant, les deux bordures de ce pop-up présentent des styles de réactivation différents. Au sud, le chevauchement de Lakhoura accommode la quasi totalité du raccourcissement de la marge ibérique. Ce chevauchement réactive le détachement cénomanien de Lakhoura, représentant la dernière structure extensive active du système de rift, induisant le sous charriage d'une partie de la marge proximale ibérique sous la zone de « necking » ibérique. Au nord, la structure de Saint-Palais est tronquée par celle de Lakhoura. Elle ne peut donc pas accommoder une quantité significative de raccourcissement bien que sa portion supérieure soit légèrement réactivée. Le niveau de sel du Trias joue le rôle de niveau de détachement au dessus duquel se développe un empilement de nappes

n'impliquant pas ou peu de socle et raccourcissant de manière significative la couverture sédimentaire européenne. Cet empilement inclus les chevauchements à vergence nord de Bellevue et de Saint-Suzanne qui s'enracinent vers le sud sur le chevauchement de Lakhoura. Dans le socle, sous le détachement du Trias supérieur, la zone de « necking » abrupte européenne joue le rôle de buttoir induisant le sous charriage vers le sud de la marge proximale européenne. Il en résulte la formation d'un empilement aveugle de nappes crustales (units E.1 à E.4). Cette accrétion basale induit la verticalisation du contact entre la croûte continentale et le manteau européen. Une autre conséquence du sous charriage de la marge européenne est le recoupement du chevauchement de Lakhoura par les unités crustale E.1 à E.4, empêchant tout déplacement majeur dans sur sa portion la plus septentrionale. Ce processus empêche également l'enfouissement en profondeur du manteau sous-continental exhumé au Crétacé. Au cours des phases de déformations ultérieures, aucune accommodation de la déformation compressive n'a été possible dans cette unité mantélique peu profonde qui joue le rôle majeur de buttoir rigide. Ce buttoir, en étant soulevé tout au long de l'édification du système orogénique, a permis de préserver le système de rift hyper-étiré de Mauléon de l'érosion affectant le pop-up.

De même que sur la marge européenne, le long de la marge ibérique, la convergence a été accommodée de manière indépendante entre la couverture et le socle du fait de la présence du niveau de détachement du sel du Trias supérieur. A la fois les structures « thin-skin » et « thick-skin » se propagent vers l'extérieur du pop-up. Dans la couverture, le sous-charriage vers le nord de la marge ibérique induit le développement du bassin d'avant pays piggy-back sud pyrénéen (déformation « thin-skin »). Dans le socle, les chevauchements de Gavarnie et de Guarga ont été successivement incorporés dans l'empilement de nappes crustales formant l'antiforme de la Zone Axiale. Ces chevauchements « thick-skin » en séquence ont conduit à la verticalisation du contact entre la croûte continentale et le manteau le long de la paléo-marge ibérique. Ce processus accentue la protubérance mantélique existante sous le rift antérieur. Ce dôme rigide de manteau empêche l'inversion complète du bassin de Mauléon.

L'héritage structural lié à l'épisode antérieur de rifting et l'effet buttoir du manteaux sous-continental rigide ont également été présentés, dans le cas du bassin de Bilbao, par Antonio Pedrera, comme étant des paramètres majeurs contrôlant la réactivation de ce système de rift. Cependant, la réactivation de ce système plus occidental a été avortée dans un stade d'inversion plus précoce que le bassin de Mauléon. Bien que le bassin de Mauléon ait été affecté par un raccourcissement plus important, ce dernier n'a pas atteint le stade de collision continentale. Les modélisations numériques disponibles dans la bibliographie, visant à reproduire la géométrie des orogènes, suggèrent que si l'inversion avait atteint des stades plus avancés, l'unité mantélique présente sous le bassin aurait été complétement incorporée au prisme orogénique, du fait de la poursuite de l'accrétion basale de la croûte continentale. Dans ce cas, cette unité mantélique aurait été soulevée et déconnectée du manteau lithosphérique. Dans ce scénario, l'érosion aurait retiré le remplissage sédimentaire du Mauléon, portant le manteau à l'érosion.

40 km plus à l'Est, Antonio Teixell propose que la croûte inférieure ibérique du bassin de Mauléon est découplée de la croûte supérieure et subductée vers le nord. De manière synchrone, la croûte européenne est indentée dans son homologue ibérique induisant la formation d'une structure en crocodile. Ce style d'inversion permet de repousser le manteau sous-continental et d'aboutir à un moho actuel à 30 km de profondeur. Cette interprétation implique la fermeture totale du précédant système de rift et un raccourcissement de l'ordre de 120 km. Cette importante différence de style structural sur une si courte distance questionne la continuité est-ouest des structures tectoniques et met en évidence le caractère non-cylindrique de la chaine pyrénéenne. En effet, les restaurations publiées dans les Pyrénées centrales et orientales attestent de raccourcissement bien supérieur à ceux évalués dans les Pyrénées occidentales (125 km et 165 km).

Chapitre 4.1. Closure of a hyperextended system in an orogenic lithospheric pop-up, Western Pyrenees: The role of mantle buttressing and rift structural inheritance

Saspiturry, N., Razin, P., Allanic, C., Issautier, B., Baudin, T., Lasseur, E., Serrano, O., and Leleu, S., **submitted**, Closure of a hyperextended system in an orogenic lithospheric pop-up, Western Pyrenees: The role of mantle buttressing and rift structural inheritance: ***Terra Nova***.

Abstract

The Early Cretaceous hyperextended Mauléon rift is localized in the northwestern Pyrenean orogen. We infer the Tertiary evolution of the Mauléon basin through the restoration of a 153-km-long crustal-scale balanced cross section of the Pyrenean belt. Our restoration documents at least 67 km (31%) of orogenic shortening in the Western Pyrenees. Initial shortening was accommodated in the rift domain through inversion of inherited crustal structures. This stage resulted in the formation of a pop-up structure, in which the opposite edges underwent the same amount of shortening but with different tectonic reactivation styles, localized vs distributed. Further convergence was accommodated through underthrusting of the Iberian margin, which formed the Axial Zone antiformal stack of crustal nappes within a lithospheric pop-up. Thin-skinned and thick-skinned structures propagated outward from the heart of this pop-up, a block of strong mantle that acted as a buttress inhibiting complete inversion of the Mauléon rift basin.

1. Introduction

Inherited structures in the hyperextended rift are commonly thought to strongly control deformation styles when these rifts undergo compression (Mohn et al., 2011, 2014; Jammes et al., 2014; Jourdon et al., 2019). Crustal thinning mechanisms that lead to hyperextended continental crust and exhumation of subcontinental mantle have been intensively studied in Atlantic magma-poor margins (e.g., Péron-Pinvidic et al., 2007; Unternehr et al., 2010; Decarlis et al., 2015). That research has renewed interest in the geodynamic processes responsible for mantle exhumation in the Mauléon basin in the northwestern Pyrenees (Lagabrielle & Bodinier, 2008; Jammes et al., 2009; Lagabrielle et al., 2010; Masini et al., 2014; Tugend et al., 2015; Teixell et al., 2016). The Austro-Alpine system is a well-studied fossil analogue of inverted hyperextended magma-poor margins (Froitzheim & Manatschal, 1996; Manatschal & Bernoulli, 1998; Desmurs et al., 2001; Manatschal, 2004; Manatschal et al., 2006, 2007, 2011; Beltrando et al., 2014). Recent studies have elucidated the role of inherited hyperextension features during mountain building in the Alps: (1) the subcontinental mantle is weakened by serpentinization (Escartín et al., 1997, 2001; McCaig et al., 2007; Lundin & Doré, 2011) and acts as a décollement during compression (Reston & Manatschal, 2011); (2) the detachments responsible for continental crust thinning and mantle exhumation are inverted early during orogenesis (Mohn et al., 2011); and (3) the necking zones between the proximal margins and the hyperextended domain act as buttresses at the transition between subduction and continental collision (Mohn et al., 2014). This paper describes the role of inherited hyperextended structures on strain localization during compression in the Pyrenean orogen. The Mauléon basin, partly formed by imbrication of the margins of the earlier Mauléon rift (Ducasse et al., 1986), is an exceptional place to address the mechanisms that allow closure of hyperextended rift domains in an orogen. In this paper, we address the Tertiary inversion of the Mauléon basin through the restoration of a crustal-scale balanced cross section of the Western Pyrenees.

2. Rift inheritance in the Mauléon basin

A strong positive gravity anomaly centred upon the Mauléon basin (Grandjean, 1992, 1994; Casas et al., 1997) **(Fig. 1A)** is interpreted as the presence at shallow depth (~10 km) of continental lithospheric mantle (Wang et al., 2016). This feature represents partial denudation of the mantle (Chevrot et al., 2018) during Cretaceous hyperextension of the continental crust (Jammes et al., 2009;

Lagabrielle et al., 2010; Masini et al., 2014; Clerc & Lagabrielle, 2014; Corre et al., 2016; Teixell et al., 2016). This former rift domain is bordered today by antithetic thrusts forming a pop-up structure (**Fig. 1B**; Ducasse & Vélasque, 1988; Daignières et al., 1994). The Early Cretaceous evolution of the Mauléon rift basin was defined by diachronous activity on two antithetic extensional structures (Saspiturry et al., 2019). The south-vergent Saint-Palais normal fault accommodated thinning of the European margin in Albian time. During Cenomanian time, it was crosscut by the Lakhoura detachment system, which shaped the Iberian necking zone. As a result, the European necking zone had an abrupt termination, as it was not bounded by two major detachments, whereas the Iberian necking zone was smooth, bounded by the Lakhoura and North Arbailles detachments (Saspiturry et al., 2019). These asymmetric rifting processes thus gave rise to a pseudosymmetric hyperextended rift. This interpretation may reconcile previous characterizations of the Mauléon basin as a symmetric (Ducasse et al., 1986; Souquet, 1988), asymmetric (Jammes et al., 2009; Masini et al., 2014), or mixed rift (Lagabrielle et al., 2010; Teixell et al., 2016). In this paper, we address the Tertiary inversion of the Mauléon basin through the restoration of a crustal-scale balanced cross section of the Western Pyrenees.

3. Restoration of western Pyrenees cross section

Recent Mauléon basin observations in the North Pyrenean Zone (Saspiturry et al., 2019), a revised section of the South Pyrenean Zone (Ducasse & Vélasque, 1988), and a P-wave velocity (Vp) lithospheric model constructed by full-waveform inversion (Wang et al., 2016) **(Fig. 2)** have been integrated to compile a NNE-SSW crustal-scale balanced cross section 153 km in length across the Mauléon basin **(Fig. 3)**. This balanced cross-section, respecting thrust tectonic concepts (Dahlstrom, 1969; Boyer & Elliott, 1982; Elliott, 1983), was used as a construction model incorporating the surface and subsurface observations available to date. Balancing and restoration were based on conservation of bed lengths and thicknesses. An area-balance approach was applied to all structural units. The Late Triassic salt formation was not completely balanced because its extreme mobility required it to be balanced in three dimensions and because its initial thickness was unknown. Shortening values were estimated at the level of the Late Cretaceous « Calcaires des Cañons » in the southern part of the profile and the Jurassic prerift cover limestones in the northern part. The overall shortening rate represents a minimum estimated value owing to the uncertainties in displacements of the thrust systems and internal deformations.

The surficial thrust system of the Western Pyrenean belt consists of bi-vergent thrust sheets that inverted the Cretaceous rift margins during Eocene time (McCaig, 1988; Teixell, 1998). The western part of this belt exhibits an important asymmetry. Its north-verging retrowedge is narrow (53 km) and includes the inverted northern part of the Mauléon hyperextended domain, the European rift margin and the Aquitaine foreland basin **(Fig. 2A)**. Its south-verging prowedge is wide (100 km) and includes the Axial Zone, the South Pyrenean piggyback basin and the northern edge of the Ebro basin **(Fig. 2B)**. The Vp model images deeper structures of the Pyrenean orogen, notably (1) the Iberian slab reaching 50 km depth under the Mauléon basin, (2) a dome of lithospheric mantle at shallow depth (~10 km) under the Mauléon basin, and (3) the relatively flat European Moho at depths between 25 and 28 km **(Fig. 2C)**.

Our palinspastic restoration of the cross section to Santonian time indicates a minimum shortening of 67 km (31%) **(Fig. 3)**. This shortening is distributed on five thrusts in the southern prowedge (43 km) and three thrusts in the northern retrowedge (24 km). The restoration also shows that the shortening in the basement has a separate counterpart in the overlying sedimentary cover.

The Iberian prowedge is a 50-km-thick antiformal stack of crustal nappes in the Axial Zone of which the uppermost structure is the Lakhoura thrust. This duplex-like crustal stack resulted from the successive activation of the Lakhoura, Gavarnie, and Guarga thrusts (Labaume et al., 1985, 2016; Teixell, 1996, 1998; Soler et al., 1998). The Lakhoura thrust reactivated the Lakhoura detachment in late Eocene time, underplating parts of the Iberian proximal rift margin onto the Iberian necking zone **(Fig. 3)**. This thrust accommodated a total

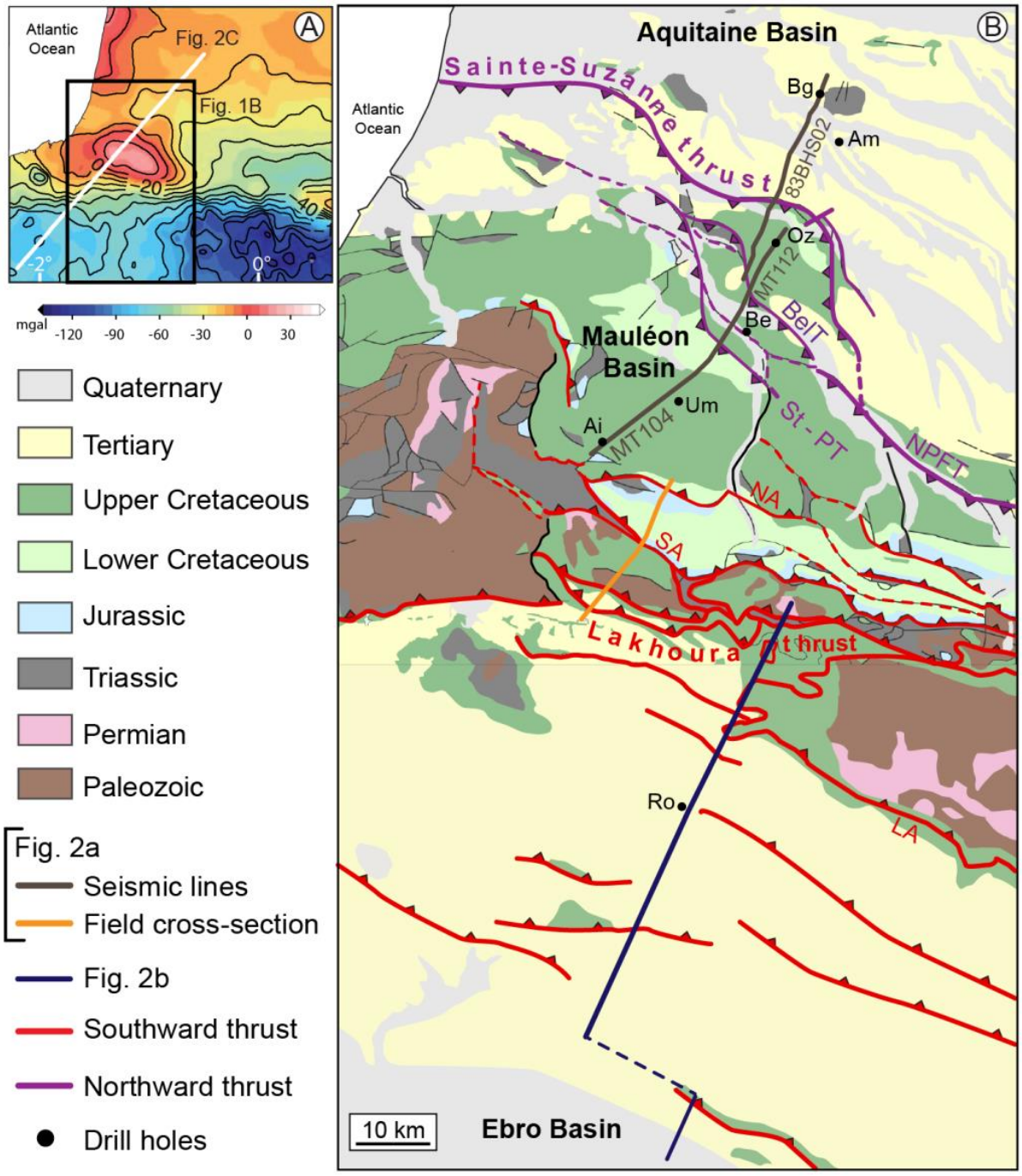


Fig. 1. (A) Bouguer gravity map of the western Pyrenees showing a strong positive anomaly centred upon the Mauléon basin (modified from Chevrot et al., 2018). Contour interval, 10 mgal. **(B)** Bedrock and structural map highlighting the pop-up structure of the Mauléon basin with its flanking thrust faults. Main north-vergent thrust faults (purple) are, from north to south, the Sainte-Suzanne thrust, North Pyrenean frontal thrust (NPFT), Bellevue thrust (BelT), and Saint-Palais thrust (St-PT). Main south-vergent thrust faults (red) are, from south to north, the Lakhoura thrust, South Arbailles thrust (SA), and North Arbailles thrust (NA). Seismic reflection lines (dark grey) and a field traverse (gold) define the crustal profile shown in Figure 2a (modified from Saspiturry et al., 2019). Field traverse (blue) defines the crustal profile of the South Pyrenean piggyback basin shown in Figure 2b (modified from Ducasse & Vélasque, 1988). Drill holes: Ai—Ainhice; Am—Amou; Be—Bellevue; Bg—Bastennes-Gaujacq; Oz—Orthez; Ro—Roncal; Um—Uhart-Mixe.

shortening of nearly 20 km. Also participating were the minor South and North Arbailles thrusts, which reactivated normal faults soling into the Lakhoura detachment as splay faults of the Lakhoura thrust. The Gavarnie thrust accommodated nearly 15 km of shortening during late Eocene to early Oligocene time, and shortening on the Guarga thrust during the late Oligocene to earliest Miocene was nearly 8 km. These quantities are consistent with previous

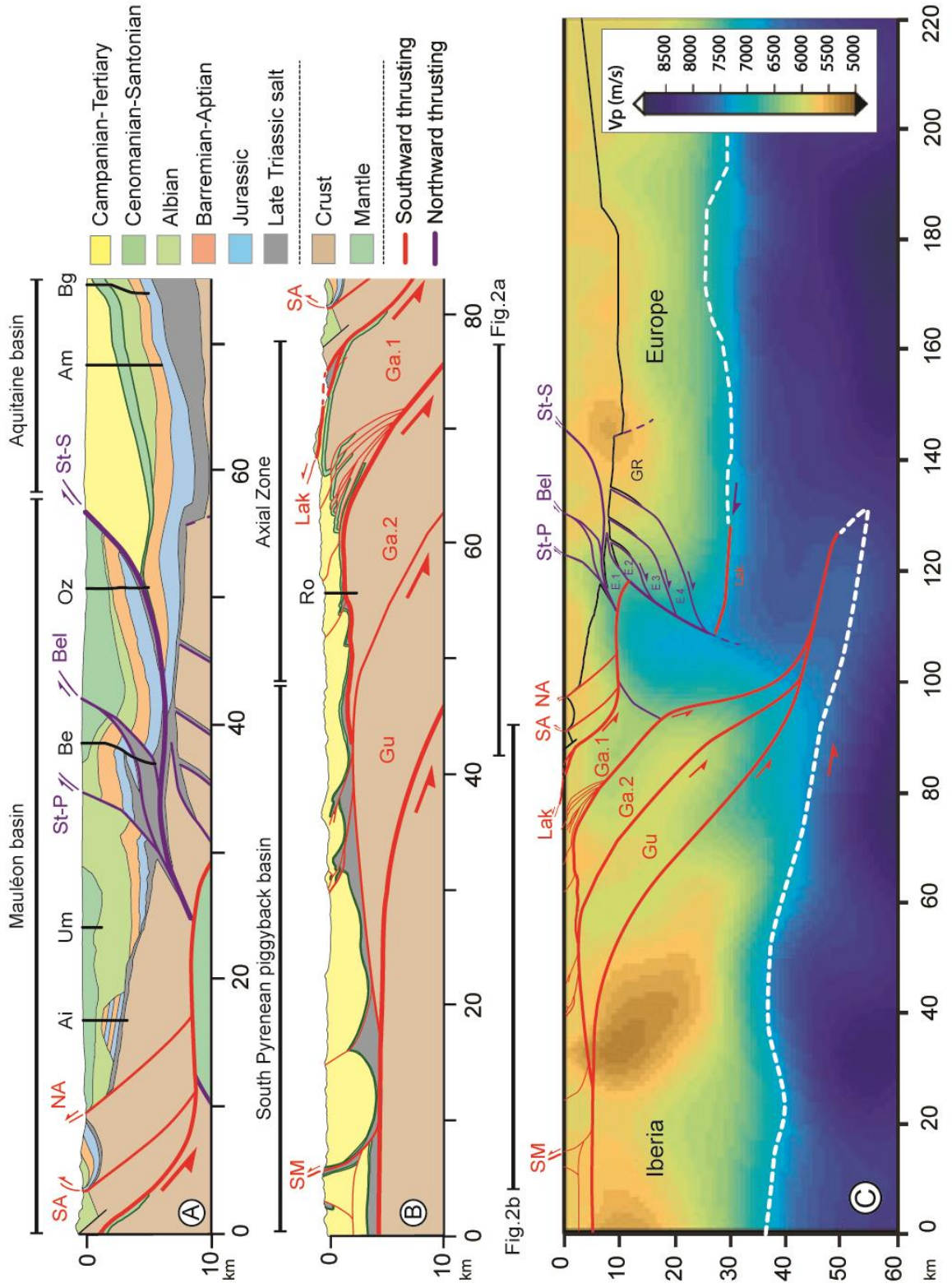


Fig. 2. (A) Geological section through the present-day Mauléon basin based on interpreted seismic lines and field data (location in Figure 1b; modified from Saspiturry et al., 2019). The Mauléon basin is preserved within a pop-up structure formed during N-S Pyrenean compression. **(B)** Field traverse defining the crustal profile of the South Pyrenean piggyback basin and the upper part of the Axial Zone antiformal crustal nappe stack (location in Figure 1b; modified from Ducasse & Vélasque, 1988). **(C)** Vp model showing the presence at shallow depth of continental lithospheric mantle (location in Figure 1a; modified from Wang et al., 2016). Dashed white line = mantle-crust interface. Thrust faults: SM—Sierras Marginalès; Gu—Guarga; Ga.2—Gavarnie.2; Ga.1—Gavarnie.1; Lak—Lakhoura; SA—South Arbailles; NA—North Arbailles; St-P—Saint-Palais; Bel—Bellevue; St-S—Sainte-Suzanne. Structural units: E.1—European crustal unit 1; E.2—European crustal unit 2; E.3—European crustal unit 3; E.4—European crustal unit 4; GR—Grand Rieu. Drill holes are identified in Figure 1

studies documenting shortening of 15 km on both the Gavarnie and Guarga thrusts (Teixell, 1998; Teixell et al., 2016). The different shortening values for the Guarga thrust reflect the fact that ours is a minimum value. In the sedimentary cover of the Iberian prowedge above the Lakhoura thrust, a commensurate amount of shortening is distributed in a sequence of thrusts in the South Pyrenean piggyback basin.

In the retrowedge, the Saint-Palais, Bellevue, and Sainte-Suzanne thrusts affected the European sedimentary cover **(Fig. 3)**. Most of the inversion in the hyperextended domain was accommodated by folding of the Mesozoic cover against the backstop of the inherited Saint-Palais normal fault. The Bellevue and Sainte-Suzanne thin-skinned thrusts propagated northward on a décollement through Triassic salt deposits. The Bellevue thrust emerged as a splay fault as it impinged on an Albian synrift diapir, and the Sainte-Suzanne thrust left the décollement and reached the surface when butting up against the South Grand Rieu fault scarp. The 24 km of shortening in the retrowedge sedimentary cover is distributed on the Bellevue thrust (4 km), Sainte-Suzanne thrust (18 km), and internal deformation in the Mesozoic cover (2 km). As a result of decoupling between the basement and the cover, 24 km of shortening in the European basement led to the formation of a duplex-like crustal stack that thickened the European continental crust (units E.1-E.4, **Figs. 2C & 3**).

4. Inversion modes during Pyrenean compression

In the first stages of compression, the pseudosymmetric structure of the rift influenced strain localization. Indeed, the Mauléon hyperextended rift was inverted in a pop-up structure in which both sides were shortened by nearly the same amount (~20 km). This pop-up is bounded to the south and north by the Lakhoura and Sainte-Suzanne thrusts, respectively, of late Eocene age. However, the two edges of the pop-up had different tectonic reactivation styles. To the south, the Lakhoura thrust accommodated nearly all of the shortening of the Iberian rift margin because it was the only existing structure available for reactivation. To the north, the Saint-Palais thrust was truncated by the Lakhoura detachment and consequently could not accommodate major shortening (although its head portion did reactivate). The Triassic salt layer acted as a weak detachment upon which a thin-skinned nappe stack developed by offscraping the sedimentary cover rocks. This stack includes the north-verging Bellevue and Sainte-Suzanne thrusts rooted in the Lakhoura thrust fault. In the basement beneath the detachment, the blunt-ended European necking zone acted as a backstop that induced southward underplating of the European proximal margin, initiating a blind in-sequence duplex-like crustal stack that propagated downward (crustal units E.1 to E.4, **Fig. 3**). This basal accretion resulted in steepening the European crust-mantle contact. Another consequence was the crosscutting of the Lakhoura thrust, inhibiting any displacement on its severed northern portion. This process prevented the cool, strong subcontinental mantle beneath the former rift from being displaced at depth. In succeeding compressional stages, no major accommodation of the compressive strain was possible in the block of shallow mantle, which thus acted as a major rigid buttress. This buttress, by being uplifted en bloc throughout the evolution of the orogen, protected the hyperextended rift against further erosion within the pop-up.

In the Iberian margin, too, convergence was accommodated independently in the cover and the basement owing to the presence of a salt detachment layer. In that case, however, both thin-skinned and thick-skinned structures propagated outward. In the cover strata, northward underthrusting of the Iberian margin formed the thin-skinned South Pyrenean piggyback basin. In the basement, the Gavarnie and Guarga thrusts were successively incorporated into the Axial Zone antiformal crustal nappe stack. This sequence of thick-skinned thrusts led to the progressive steepening of the crust-mantle contact in the Iberian margin, which accentuated the preexisting mantle protrusion beneath the former rift. This dome of strong mantle buttressed the Mauléon hyperextended rift domain against convergence from both north and south and inhibited its complete inversion.

Structural rift inheritance and buttressing by strong subcontinental mantle have also been proposed as the controlling factors during rift

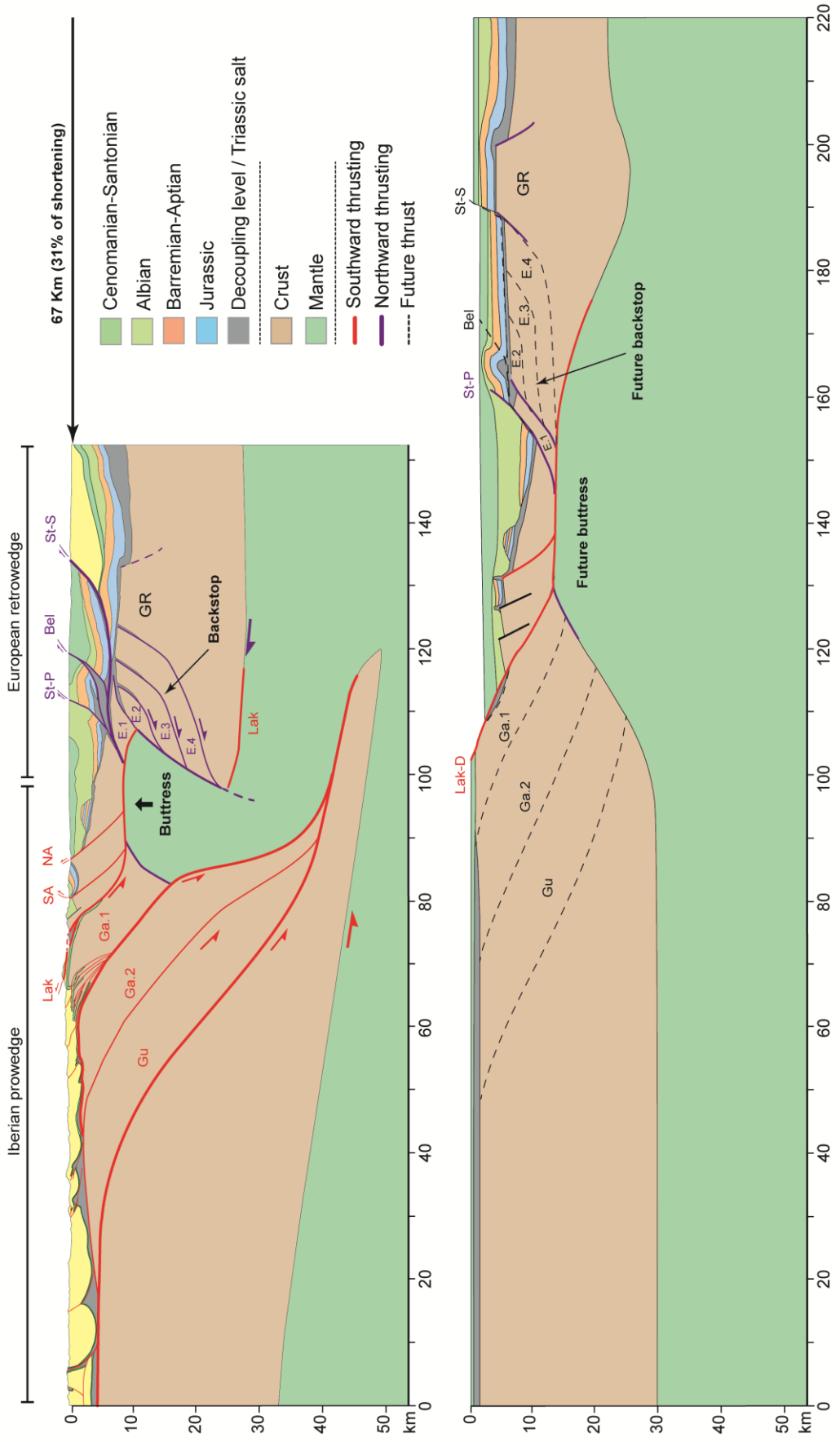


Fig. 3. Crustal-scale balanced cross section (top) and its palinspastic restoration to Santonian time (bottom), integrating the sections shown in Figure 2. Location in Figure 1a. Abbreviations as in Figure 2.

reactivation in the Bilbao area 130 km west of our study area (**Fig. 4**; Pedrera et al., 2017). Compression ceased to affect the Bilbao system at an earlier stage of reactivation than in the Mauléon basin, as evidenced by (1) the smaller estimated shortening (34 km) in the Bilbao system (**Figs. 4C & D**; Pedrera et al., 2017) than in the Mauléon basin (67 km; **Figs. 4A & B**), (2) a positive Bouguer anomaly in the Bilbao system, interpreted as the presence at shallow depth of lithospheric mantle, that is 50 km wide as contrasted to the 25-km-wide anomaly in the Mauléon basin (Grandjean, 1994), and (3) the absence of an antiformal crustal nappe stack in the Bilbao area corresponding to the Axial Zone (**Fig. 4**). Even though the Mauléon basin underwent more shortening than the Bilbao system, it did not reach the continent-continent collisional stage. Numerical modelling shows that, had reactivation continued to advance, the mantle block would have been fully incorporated in the orogenic prism as basal accretion of the continental crust continued, and it would have been uplifted and separated from the rest of the lithospheric mantle (Selzer et al., 2008; Pfiffner, 2017). In this scenario, erosion would have removed the sedimentary infill of the hyperextended Mauléon basin.

On the basis of a NNE-SSW balanced cross section 40 km east of our cross section, Teixell et al. (2016) proposed that the lower crust on the Iberian side of the Mauléon basin was decoupled from the upper crust and subducted northward. Synchronously, the European continental crust was indented into the Iberian continental crust, leading to a wedge or crocodile structure and depressing the Moho to its current depth of 30 km under the basin. This interpretation implies the complete closure of the rift, the downward displacement of the previously exhumed subcontinental mantle, and a total shortening of 120 km at this locality (Teixell et al., 2016).

The large difference in structural templates along the Pyrenean belt over such short distances calls into question the east-west continuity of tectonic structures and thus bears upon the origin of the non-cylindrical folding geometry of the Pyrenean belt. Indeed, published restorations of balanced cross sections across the Central and Eastern Pyrenees feature total shortening values ranging

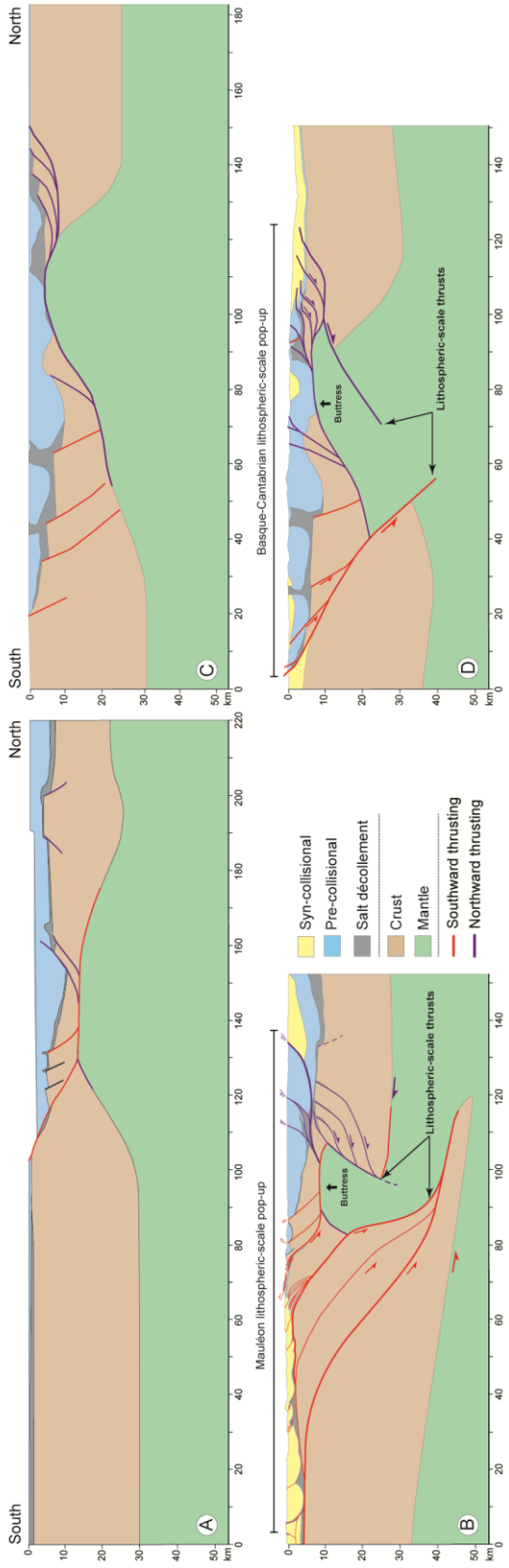


Fig. 4. Palinspastic restoration to Late Cretaceous time (top) and its Crustal-scale balanced cross section (bottom), **(A-B)** Mauléon basin, simplified Figure 3 sections; **(C-D)** Bascque-cantabrian basin (modified from Pedrera et al., 2017).

from 120 to 165 km (Roure et al., 1989; Muñoz, 1992; Vergés et al., 1995; Beaumont et al., 2000; Mouthereau et al., 2014; Teixell et al., 2018; Grool et al., 2018; Espurt et al., 2019). The discrepancy between these shortening values depends on both the width of the exhumed subcontinental mantle domain considered by various authors and the non-cylindricity of the Pyrenees. Several factors could be invoked to explain this non-cylindricity: (1) the polarity change of the Early Cretaceous rift system across the north-south-trending Toulouse fault (Chevrot et al., 2018), (2) the diachronicity of thick-skinned deformation along the Pyrenean belt resulting from inherited segmentation, older to the east (Santonian) and younger to the west (late Eocene), and (3) the presence or absence of a strong mantle buttress beneath the hyperextended rift system.

Acknowledgements

This work is part of Saspiturry's Ph.D. research conducted as part of the OROGEN project, cofunded by Total S.A., BRGM, and Institut national de sciences de l'Univers (INSU). We thank OROGEN project managers Sylvain Calassou (Total), Emmanuel Masini (Total), Olivier Vidal (Centre National de Recherche Scientifique) and Isabelle Thinon (BRGM).

References

Beaumont, C., Muñoz, J.A., Hamilton, J., and Fullsack, P., 2000. Factors controlling the Alpine evolution of the central Pyrenees inferred from a comparison of observations and geodynamical models. *Journal of Geophysics Research*, **105**, 8121-8145.

Beltrando, M., Manatschal, G., Mohn, G., Dal Piaz, G.V., Brovarone, A.V., and Masini, E., 2014. Recognizing remnants of magma-poor rifted margins in high-pressure orogenic belts: The Alpine case study. *Earth Science Review*, **131**, 88-115.

Boyer, S.E., Elliott, D., 1982. The geometry of thrust systems. AAPG Bull. 66, 1196–1230.

Casas, A., Kearey, P., Rivero, L., and Adam, C.R., 1997. Gravity anomaly map of the Pyrenean region and a comparison of the deep geological structure of the western and eastern Pyrenees. *Earth and Planetary Science Letters*, **150**, 65-78.

Chevrot, S., Sylvander, M., Diaz, J., Martin, R., Mouthereau, F., Manatschal, G., Masini, E., Calassou, S., Grimaud, F., Pauchet, H., and Ruiz, M., 2018. The non-cylindrical crustal architecture of the Pyrenees. *Scientific Reports*, **8**.

Clerc, C., Lagabrielle, Y., 2014. Thermal control on the modes of crustal thinning leading to mantle exhumation: Insights from the Cretaceous Pyrenean hot paleomargins. *Tectonics*, **33**, 1340-1359.

Corre, B., Lagabrielle, Y., Labaume, P., Fourcade, S., Clerc, C., and Ballèvre, M., 2016. Deformation associated with mantle exhumation in a distal, hot passive margin environment: New constraints from the Saraillé Massif (Chaînons Béarnais, North-Pyrenean Zone). *Comptes Rendus Géosciences*, **348**, 279-289.

Dahlstrom, C.D.A., 1969. Balanced cross sections. Canadian Journal of Earth Sciences, **6**, 743-757.

Daignières, M., Séguret, M., Specht, M., and Team, E., 1994. The Arzacq-western Pyrenees ECORS deep seismic profile, in: *Hydrocarbon and Petroleum Geology of France. Springer*, 199-208.

Decarlis, A., Manatschal, G., Haupert, I., and Masini, E., 2015. The tectono-stratigraphic evolution of distal, hyper-extended magma-poor conjugate rifted margins: Examples from the Alpine Tethys and Newfoundland–Iberia. *Marine and Petroleum Geology*, **68**, 54-72.

Desmurs, L., Manatschal, G., and Bernoulli, D., 2001. The Steinmann Trinity revisited: mantle exhumation and magmatism along an ocean-continent transition: the Platta nappe, eastern Switzerland. *Geological Society of London Special Publication*, **187**, 235-266.

Ducasse, L., Vélasque, P.-C., 1988. Géotraverse dans la partie occidentale des Pyrénées, de l'avant-pays aquitain au bassin de l'Ebre: effet d'une inversion structurale sur l'édification d'une chaîne intracontinentale. Unpubl. doctoral dissertation, Université Paul Cézanne (Aix-Marseille).

Ducasse, L., Vélasque, P.-C., and Muller, J., 1986. Glissement de couverture et panneaux basculés dans la région des Arbailles (Pyrénées occidentales): Un modèle évolutif crétacé de la marge nord-ibérique à l'Est de la transformante de Pamplona. *Comptes Rendus de l'Académie des Sciences Série 2 Mécanique Physique Chimie Science de l'Univers Science de la Terre*, **303**, 1477-1482.

Elliott, D., 1983. The construction of balanced cross-sections. *Journal of Structural Geology*, 101-101.

Escartín, J., Hirth, G., Evans, B., 1997. Effects of serpentinization on the lithospheric strength and the style of normal faulting at slow-spreading ridges. *Earth and Planetary Science Letters*, **151**, 181-189.

Escartín, J., Hirth, G., Evans, B., 2001. Strength of slightly serpentinized peridotites: Implications for the tectonics of oceanic lithosphere. *Geology*, **29**, 1023.

Espurt, N., Angrand, P., Teixell, A., Labaume, P., Ford, M., de Saint Blanquat, M., and Chevrot, S., 2019. Crustal-scale balanced cross-section and restorations of the Central Pyrenean belt (Nestes-Cinca transect): Highlighting the structural control of Variscan belt and Permian-Mesozoic rift systems on mountain building. *Tectonophysics*, **764**, 25-45.

Froitzheim, N., Manatschal, G., 1996. Kinematics of Jurassic rifting, mantle exhumation, and passive-margin formation in the Austroalpine and Penninic nappes

(eastern Switzerland). *Geological Society of American Bulletin*, **108**, 1120-1133.

Grandjean, G., 1992. Mise en évidence des structures crustales dans une portion de chaîne et de leur relation avec les bassins sédimentaires. Application aux Pyrénées occidentales au travers du Projet ECORS Arzacq-Pyrénées. Unpubl. doctoral dissertation, Université des Sciences et Techniques du Languedoc.

Grandjean, G., 1994. Etude des structures crustales dans une portion de chaîne et de leur relation avec les bassins sédimentaires. Application aux Pyrénées occidentales. *Bulletin Centre Recherche Exploration Production Elf Aquitaine*, **18**, 391-420.

Grool, A.R., Ford, M., Vergés, J., Huismans, R.S., Christophoul, F., and Dielforder, A., 2018. Insights into the crustal-scale dynamics of a doubly vergent orogen from a quantitative analysis of its forelands: A case study of the eastern Pyrenees. *Tectonics*, **37**, 450-476.

Jammes, S., Manatschal, G., Lavier, L., and Masini, E., 2009. Tectono-sedimentary evolution related to extreme crustal thinning ahead of a propagating ocean: Example of the western Pyrenees. *Tectonics*, **28**.

Jammes, S., Huismans, R.S., and Muñoz, J.A., 2014. Lateral variation in structural style of mountain building: controls of rheological and rift inheritance. *Terra Nova*, **26**, 201-207.

Jourdon, A., Le Pourhiet, L., Mouthereau, F., and Masini, E., 2019. Role of rift maturity on the architecture and shortening distribution in mountain belts. *Earth and Planetary Science Letters*, **512**, 89-99.

Labaume, P., Séguret, M., and Seyve, C., 1985. Evolution of a turbiditic foreland basin and analogy with an accretionary prism: Example of the Eocene South-Pyrenean basin. *Tectonics*, **4**, 661-685.

Labaume, P., Meresse, F., Jolivet, M., and Teixell, A., 2016. Exhumation sequence of the basement thrust units in the west-central Pyrenees. Constraints from apatite fission track analysis. *Geogaceta*, **60**, 11-14.

Lagabrielle, Y., Bodinier, J.-L., 2008. Submarine reworking of exhumed sub-continental mantle rocks: field evidence from the Lherz peridotites, French Pyrenees: Cretaceous exhumation of Pyrenean mantle. *Terra Nova*, **20**, 11-21.

Lagabrielle, Y., Labaume, P., and de Saint Blanquat, M., 2010. Mantle exhumation, crustal denudation, and gravity tectonics during Cretaceous rifting in the Pyrenean realm (SW Europe): Insights from the geological setting of the lherzolite bodies. *Tectonics*, **29**.

Lundin, E.R., Doré, A.G., 2011. Hyperextension, serpentinization, and weakening: A new paradigm for rifted margin compressional deformation. *Geology*, **39**, 347-350.

Manatschal, G., 2004. New models for evolution of magma-poor rifted margins based on a review of data and concepts from West Iberia and the Alps. *International Journal of Earth Sciences*, **93**.

Manatschal, G., Bernoulli, D., 1998. Rifting and early evolution of ancient ocean basins: the record of the Mesozoic Tethys and of the Galicia-Newfoundland margins. *Marine Geophysical Researches*, **20**, 371-381.

Manatschal, G., Engström, A., Desmurs, L., Schaltegger, U., Cosca, M., Müntener, O., and Bernoulli, D., 2006. What is the tectono-metamorphic evolution of continental break-up: The example of the Tasna Ocean–Continent Transition. *Journal of Structural Geology*, **28**, 1849-1869.

Manatschal, G., Müntener, O., Lavier, L.L., Minshull, T.A., and Péron-Pinvidic, G., 2007. Observations from the Alpine Tethys and Iberia–Newfoundland margins pertinent to the interpretation of continental breakup. *Geological Society of London Special Publication*, **282**, 291-324.

Manatschal, G., Sauter, D., Karpoff, A.M., Masini, E., Mohn, G., and Lagabrielle, Y., 2011. The Chenaillet Ophiolite in the French/Italian Alps: An ancient analogue for an Oceanic Core Complex? *Lithos*, **124**, 169-184.

Masini, E., Manatschal, G., Tugend, J., Mohn, G., and Flament, J.-M., 2014. The tectono-sedimentary evolution of a hyper-extended rift basin: the example of the Arzacq–Mauléon rift system (Western Pyrenees, SW France). *International Journal of Earth Sciences*, **103**, 1569-1596.

McCaig, A.M., 1988. Deep geology of the Pyrenees. *Nature*, **331**, 480-481.

McCaig, A.M., Cliff, R.A., Escartin, J., Fallick, A.E., and MacLeod, C.J., 2007. Oceanic detachment faults focus very large volumes of black smoker fluids. *Geology*, **35**, 935-938.

Mohn, G., Manatschal, G., Masini, E., and Müntener, O., 2011. Rift-related inheritance in orogens: a case study from the Austroalpine nappes in Central Alps (SE-Switzerland and N-Italy). *International Journal of Earth Sciences*, **100**, 937-961.

Mohn, G., Manatschal, G., Beltrando, and M., Haupert, I., 2014. The role of rift-inherited hyper-extension in Alpine-type orogens. *Terra Nova*, **26**, 347-353.

Mouthereau, F., Filleaudeau, P.-Y., Vacherat, A., Pik, R., Lacombe, O., Fellin, M.G., Castelltort, S., Christophoul, F., and Masini, E., 2014. Placing limits to shortening evolution in the Pyrenees: Role of margin architecture and implications for the Iberia/Europe convergence. *Tectonics*, **33**.

Muñoz, J.A., 1992. Evolution of a continental collision belt: ECORS-Pyrenees crustal balanced cross-section, in: *McClay, K.R. (Ed.), Thrust Tectonics. Springer Netherlands*, 235-246.

Pedrera, A., García-Senz, J., Ayala, C., Ruiz-Constán, A., Rodríguez-Fernández, L.R., Robador, A., and González Menéndez, L., 2017. Reconstruction of the exhumed mantle across the North Iberian Margin by crustal-scale 3-D gravity inversion and geological cross section. *Tectonics*, **36**, 3155-3177.

Péron-Pinvidic, G., Manatschal, G., Minshull, T.A., and Sawyer, D.S., 2007. Tectono-sedimentary evolution of the deep Iberia-Newfoundland margins: Evidence for a complex breakup history. *Tectonics*, **26**, 1-19.

Pfiffner, O.A., 2017. Thick-skinned and thin-skinned tectonics: a global perspective. *Geosciences*, **7**.

Reston, T., Manatschal, G., 2011. Rifted Margins: Building Blocks of Later Collision, in: *Arc-Continent Collision, Frontiers in Earth Sciences. Springer Berlin Heidelberg*, 3-21.

Roure, F., Choukroune, P., Berastegui, X., Munoz, J.A., Villien, A., Matheron, P., Bareyt, M., Seguret, M., Camara, P., and Deramond, J., 1989. ECORS deep seismic data and balanced cross sections: Geometric constraints on the evolution of the Pyrenees. *Tectonics*, **8**, 41-50.

Saspiturry, N., Razin, P., Baudin, T., Serrano, O., Issautier, B., Lasseur, E., Allanic, C., Thinon, I., and Leleu, S., 2019. Symmetry vs. asymmetry of a hyper-thinned rift: Example of the Mauléon basin (Western Pyrenees, France). *Marine and Petroleum Geology*, **104**, 86-105.

Selzer, C., Buiter, S.J., and Pfiffner, O.A., 2008. Numerical modeling of frontal and basal accretion at collisional margins. *Tectonics* ,**27**.

Soler, D., Teixell, A., and García-Sansegundo, J., 1998. Amortissement latéral du chevauchement de Gavarnie et sa relation avec les unités sud-pyrénéennes. *Comptes Rendus Académie des Sciences Série 2A*, **327**, 699-704.

Souquet, P., 1988. Evolución del margen noribérico en los Pyreneos durante el Mesozoico. *Rev Soc Geol Esp*, **1**, 349-356.

Teixell, A., 1996. The Anso transect of the southern Pyrenees: basement and cover thrust geometries. *Journal of Geological Society*, **153**, 301-310.

Teixell, A., 1998. Crustal structure and orogenic material budget in the west central Pyrenees. *Tectonics*, **17**, 395-406.

Teixell, A., Labaume, P., and Lagabrielle, Y., 2016. The crustal evolution of the west-central Pyrenees revisited: Inferences from a new kinematic scenario. *Comptes Rendus Géosciences*, **348**, 257-267.

Teixell, A., Labaume, P., Ayarza, P., Espurt, N., de Saint Blanquat, M., and Lagabrielle, Y., 2018. Crustal structure and evolution of the Pyrenean-Cantabrian belt: A review and new interpretations from recent concepts and data. *Tectonophysics*, **724**, 146-170.

Tugend, J., Manatschal, G., Kusznir, N.J., and Masini, E., 2015. Characterizing and identifying structural domains at rifted continental margins: application to the Bay of Biscay margins and its Western Pyrenean fossil remnants. *Geological Society of London Special Publication*, **413**, 171-203.

Unternehr, P., Peron-Pinvidic, G., Manatschal, G., and Sutra, E., 2010. Hyper-extended crust in the South Atlantic: in search of a model. *Petroleum Geoscience*, **16**, 207-215.

Vergés, J., Millán, H., Roca, E., Muñoz, J.A., Marzo, M., Cirés, J., Bezemer, T.D., Zoetemeijer, R., and Cloetingh, S., 1995. Eastern Pyrenees and related foreland basins: pre-, syn- and post-collisional crustal-scale cross-sections. *Marine and. Petroleum Geology*., **12**, 903-915.

Wang, Y., Chevrot, S., Monteiller, V., Komatitsch, D., Mouthereau, F., Manatschal, G., Sylvander, M., Diaz, J., Ruiz, M., Grimaud, F., Benahmed, S., Pauchet, H., and Martin, R., 2016. The deep roots of the western Pyrenees revealed by full waveform inversion of teleseismic P waves. *Geology*, **44**, 475-478.

Chapitre 4.2

Zones de transfert lithosphériques contrôlant la non-cylindricité de l'orogenèse pyrénéenne (Bassin hyper-étiré de Mauléon)

Chapitre 4.2. Lithospheric transfer zones driving the non-cylindrical shape of the Pyrenean orogen (Mauléon hyperextended basin)

Sommaire

Abstract p. 267

1. Introduction p. 267

2. The North Pyrenean Zone: reactivation of a hyperextended rift p. 268

3. Methodology, data and results p. 270

3.1. RSCM Raman spectroscopy of carbonaceous material p. 270

3.1.1. Analytical method and thermometry p. 270

3.1.2. The Lakhoura thrust system thermicity p. 270

3.2. Field observations and paleostress reconstruction p. 271

3.2.1. Data and methodology p. 271

3.2.2. Lakhoura thrust segments kinematic p. 271

3.2.3. The Iholdy transverse structure p. 272

3.2.4. The Saint-Palais microstructures p. 272

3.2.5. The Saison transverse structure p. 273

3.3. Seismic interpretation p. 273

3.3.1. Data and methodology p. 273

3.3.2. The Iholdy transverse structure p. 277

3.3.3. The Saison transverse structure p. 277

3.4. 3D implicit geological modelling of the Mauléon basin p. 280

3.4.1. Methodology and data p. 280

3.4.2. 2D isovalues map from 3D interpolation p. 280

3.4.3. 3D structural framework of the Mauléon basin p. 280

4. Discussion p. 280

4.1. Characterization of the Mauléon basin syn-collisional transfer zones p. 280

4.1.1. Variable deformation patterns along a transfer zone p. 280

4.1.2. Segmentation of the Mauléon basin pop-up in several corridors p. 283

4.2. Role of transfer zones during hyperextended Mauléon rift reactivation p. 284

4.2.1. Definition of the drawer system p. 284

4.2.2. Scissor closure of the rift domain vs Labourd buttress impacting the evolution of the Mauléon basin drawer model p. 285

4.3. The non-cylindrical shape of the Pyrenean belt: result of inherited lithospheric segmentation p. 285

4.3.1. Pamplona and Barlanès inherited lithospheric transfer zones p. 285

4.3.2. Tertiary structural discrepancies from both sides of the Barlanès lithospheric transfer zone p. 286

4.3.3. From crustal to lithospheric scale drawer system model p. 287

5. Conclusion p. 288

References p. 289

Chapitre 4.2. Lithospheric transfer zones driving the non-cylindrical shape of the Pyrenean orogen (Mauléon hyperextended basin)

Saspiturry, N., Allanic, C., Courrioux, G., Serrano, O., Lahfid, A., Le Bayon, B., Baudin, T., Razin, P., and Issautier, B., **in prep**, Lithospheric transfer zones driving the non-cylindrical shape of the Pyrenean orogen (Mauléon hyperextended basin): It will be submitted to ***Journal of structural Geology***.

Abstract

Despite tertiary Pyrenean orogenesis, the Mauléon Early Cretaceous hyperextended basin remains preserved in the heart of a lithospheric pop-up structure. RSCM Raman Spectroscopy of Carbonaceous Material, paleostress reconstructions, seismic interpretations and 3D implicit geological modeling of the Mauléon basin bring out the presence of N20° transfer zones. The thrust segments of the N120° Lakhoura and North Pyrenean Frontal thrust systems edging the Mauléon basin pop-up branch into these transfer zones defining corridors with differing shortening rate. This overall structural pattern defines drawers like structures allowing the closure, by stages, of the former rift domain. This concept can be both applied to the crustal and to the lithospheric scale. This study enhances the role of lithospheric inherited autochthonous transfer zones on the reactivation of a hyperextended rift basin and bears upon the origin of the non-cylindrical shape of the Pyrenean belt.

1. Introduction

Transfer fault, accommodation zone or relay structure have been the terms introduced respectively by Gibbs, 1984; Reynolds and Rosendahl, 1984, to define the cross fault that allow linkage between extension faults with differing slip rates. Transfer zones are classical features of continental rift system and correspond to major relay zones that involve a number of faults minor relay structures (see Fossen and Rotevatn, 2016 for a review). They materialize cross faults inside a rift segment accommodating part of the extension (Chorowicz, 1989). The transfer faults correspond to high angle and short fault compare to transform faults and are parallel to the transport direction (Gibbs, 1990). These structures are known to control differential subsidence rates, sedimentary facies variations or detachment fault dip orientations, across rift and passive margin (Etheridge, 1986; Boillot et al., 1995; Young et al., 2001). In fact, the structural asymmetry of passive margins frequently reverses on opposite sides of transfer zones (Lister et al., 1986; Etheridge et al., 1987; Chorowicz, 1989; Gibbs, 1990; Péron-Pinvidic et al., 2015).

Transfer zones initiate at early rifting stage as evidenced by the analogical (Acocella et al., 1999, 2000, 2005; Bellahsen and Daniel, 2005; Zwaan et al., 2018) and numerical models (Corti et al., 2007). They have been widely studied along, the North Sea Viking Graben (Gibbs, 1984; Fossen et al., 2010), the Gulf of Suez (Angelier, 1985; Milani and Davison, 1988; Bosworth, 1994; Moustafa, 1996, 1997; McClay and Khalil, 1998), the East African rift (Morley et al., 1990; Chorowicz and Sorlien, 1992; Corti et al., 2007; Basile, 2015; Mortimer et al., 2016), the Red Sea (Moustafa, 1997; Mohriak and Leroy, 2013), the Aegean Sea (Gawthorpe and Hurst, 1993) or the Gulf of Aden (d'Acremont et al., 2005; Leroy et al., 2012; Autin et al., 2013; Bellahsen et al., 2013). During lithospheric break-up and oceanic crustal spreading, the location of future oceanic transform zones are known to be controlled by the reactivation of pre-existing oblique transfer faults (Cochran and Martinez, 1988; Behn and Lin, 2000; d'Acremont et al., 2005; Bellahsen et al., 2013). However, the impact of such inherited structures during rift or passive margin reactivation has been poorly investigated. Analogical model shows that vertical basement offsets or horizontal offsets of a backstop induced deformation in transfer zones in sandbox thrust wedges (Calassou et al., 1993).

The development of the E-W North Pyrenean hyperextended rift system (Jammes et al., 2009; Lagabrielle et al., 2010; Masini et al., 2014; Teixell et al., 2016; Saspiturry et al., 2019a) is synchronous with the opening of the Bay of Biscay passive margins (Thinon, 1999; Thinon et al., 2003; Ferrer et al., 2008; Roca et

al., 2011) **(Fig. 1)**. The modalities controlling the opening of the Pyrenean rift system are still controversial. However, the role of oblique N20°transfer zones during the Cretaceous rifting stage, has been clearly demonstrated on central/eastern Pyrenees (Debroas and Souquet, 1976; Debroas, 1987).

For many authors, the disorganization of the structural elements of the western Pyrenees could be linked to the existence of the N20° Pamplona transfer zone (Muller and Roger, 1977; Schoeffler, 1982; Richard, 1986; Razin, 1989; Claude, 1990), inherited from Permian age (Saspiturry et al., 2019b) and responsible for the shift of the Pyrenean rift axis between the Mauléon and basco-cantabric basins **(Fig. 1)**. At smaller scale, the Mauléon cretaceous rift basin is affected by N20° transfer zones controlling the subsidence, the sedimentary profile and the halokinesis (Canérot, 1989, 2008; Canérot et al., 2005; Debroas et al., 2010). Compressive displacements between the different tectonic segments defined by these transfer zones seem to be favored by a system of N20° dextral lateral ramps (Zolnaï, 1975; Schoeffler, 1982). Our study illustrates and discuss the role of the Mauléon basin N20° transfer zones during subsequent rift reactivation. We use a pluri-disciplinary approach based on field structural analyses, seismic interpretations, Raman spectroscopy and 3D geomodeling, to discuss the role of inherited transfer zones (1) on the partitioning of the compressive strain, (2) on the post-collisional thermicity and (3) on the resulting non-cylindrical shape of the Pyrenees.

2. The North Pyrenean Zone: reactivation of a hyperextended rift

The Pyrenean mountain belt is the consequence of the collision between the Iberian and European plates during the Late Santonian / Early Miocene (Puigdefàbregas and Souquet, 1986; Olivet, 1996; Rosenbaum et al., 2002; Sibuet et al., 2004; Gong et al., 2008). The deformation of this intracontinental domain is induced by the northward displacement of the Iberian plate. It implies the reactivation of the Early Cretaceous rift system localized all along the North-Pyrenean Zone (**Fig. 1A**; Choukroune, 1976; Ducasse and Vélasque, 1988). This North Pyrenean rift system is described by recent works as the result of the hyper-thinning of the continental crust, resulting in the exhumation of the sub-continental mantle (Lagabrielle and Bodinier, 2008; Lagabrielle et al., 2010, 2016; Masini et al., 2014; Teixell et al., 2016; Clerc et al., 2016; de Saint Blanquat et al., 2016). Indeed, the current strong positive gravity anomalies evidenced in the western Pyrenees (**Fig. 1B**; Grandjean, 1992, 1994; Casas et al., 1997) are interpreted as the presence of lithospheric mantle still close to the surface (~ 10 km depth) (Wang et al., 2016).

Nevertheless, the opening modes of the Early Cretaceous rift system is still questioned. Among the proposed kinematic models, two of which stand out.: (1) a scissor opening of the Bay of Biscay margins (Schoeffler, 1965; Souquet et al., 1977; Peybernès, 1978; Masson and Miles, 1984; Sibuet et al., 2004) and / or (2) a large E-W strike-slip fault system allowing the eastward displacement of the Iberian plate along the North Pyrenean Fault (Le Pichon et al., 1971; Le Pichon and Sibuet, 1971; Choukroune et al., 1973a, 1973b; Choukroune and Mattauer, 1978; Olivet, 1996). The second model implies the opening of pull-apart type rift basins associated to major NE-SW structures transverse to the E-W trending Pyrenean rift system (Debroas, 1978, 1987, 1990; Canérot, 2017). The most significant Pyrenean transverse structure corresponds to the Pamplona fault **(Fig. 1A)**. Classically, the Pamplona fault is not considered as a well-defined fault plane that can be observed at the outcrop scale but as a major N20° paleogeographic crustal scale limb (Schoeffler, 1982; Rat et al., 1983; Richard, 1986; Razin, 1989; Claude, 1990; Larrasoaña et al., 2003; Pedreira et al., 2007) inherited from Permian time (Saspiturry et al., 2019b). This major transverse structure is aligned with Labourd domain composed of the Aldudes unit made up of Paleozoic metasediments (Heddebaut, 1967, 1973; Muller and Roger, 1977), overlain by the N20° Permian-Triassic Bidarray basin (Lucas, 1985; Saspiturry et al., 2019b), limited northward by the Ursuya granulites (**Fig. 1C**; Vielzeuf, 1984). The Pamplona transverse structure forms a zone limiting western part of the Mauléon basin and eastern part of the Basque-cantabrian basin **(Fig. 1A)**. This structure also segments the Parentis and Mauléon positive Bouguer anomalies **(Fig. 1B)**.

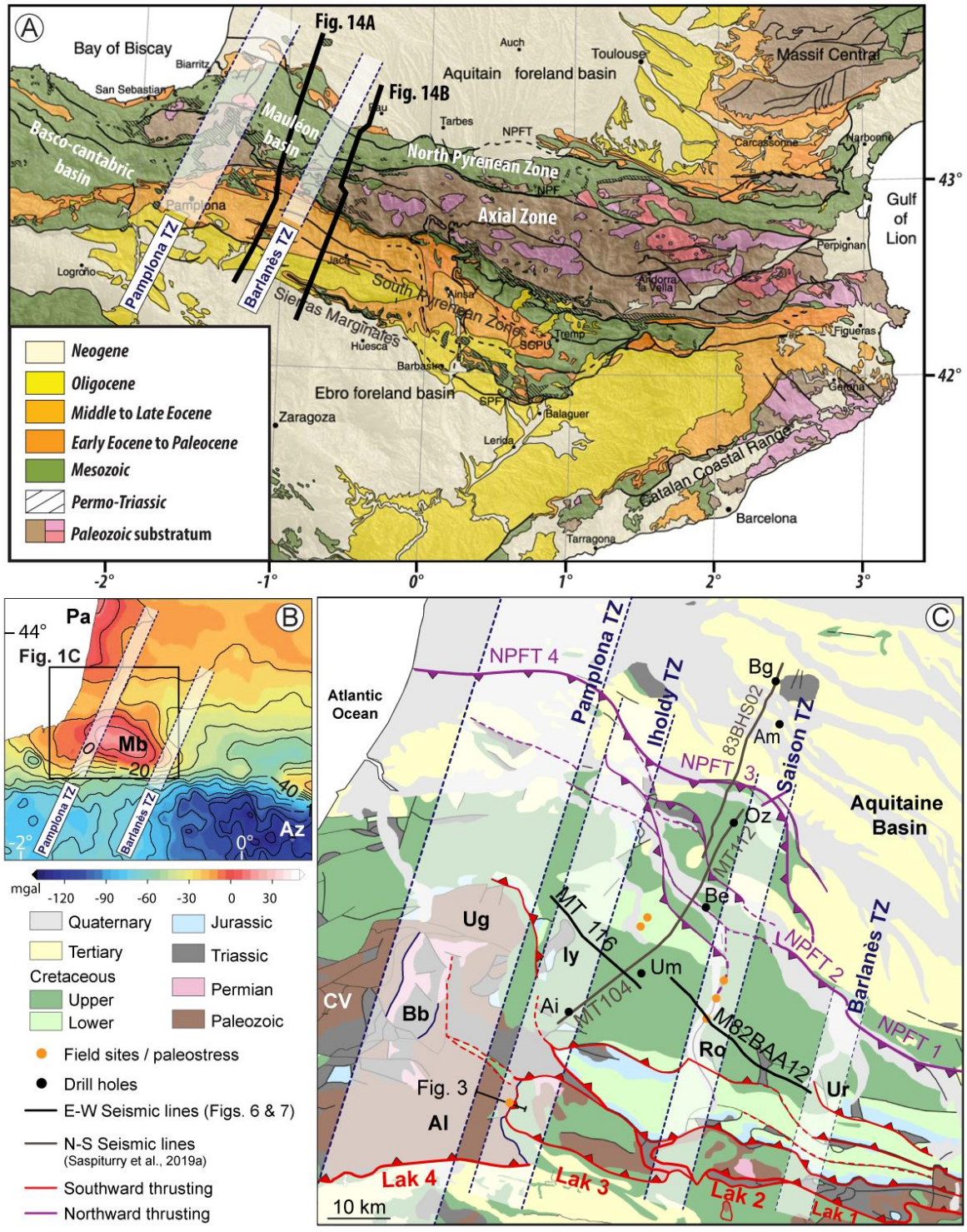


Fig. 1. (A) Geological map of the Pyrenees showing (1) the structural domains of the belt: North Pyrenean Zone, Axial Zone and South Pyrenean Zone and (2) the major Pamplona and Barlanès N20° transfer zones (modified from Mouthereau et al., 2014). TZ: Transfer Zone. **(B)** Bouguer gravity map of the western Pyrenees showing a strong positive anomaly centered upon the Mauléon and the Parentis basins (modified from Chevrot et al., 2018). These anomalies are separated by the Pamplona transfer zone to the west and the Barlanès transfer zone to the east. Contour interval, 10 mgal. Mb: Mauléon basin; Az: Axial Zone. **(C)** Bedrock and structural map highlighting the pop-up structure of the Mauléon basin with its flanking thrust faults. Main north-vergent and south-vergent thrust faults are respectively represented in purple and red. Seismic reflection lines are represented in dark gray (Saspiturry et al., 2019a) and in black (present study). Drill holes constraining the seismic interpretation: Bg: Bastennes-Gaujacq; Am: Amou; Oz: Orthez; Be: Bellevue; Um: Uhart-Mixe; Ai: Ainhice. Structural domains: Ug: Ursuya granulites; CV: Cinco-Villas; Bb: Bidarray basin; Al: Aldudes; Ur: Urdach; Ro: Roquiague diapir; Iy: Iholdy diapir. NPFT 1 / NPFT 4: segments of the North Pyrenean frontal thrust system; Lak 1 / Lak 4: segments of the Lakhoura thrust system; TZ: Transfer Zone. Location on figure 1B.

In the western Pyrenees, the North-Pyrenean Zone corresponds to the Mauléon basin, Cretaceous subsiding domain, filled by thick Albian to Upper Cretaceous deep basin deposits **(Fig. 1C)** (Souquet et al., 1985). It is currently preserved in a pop-up structure edged to the north by the northward North-Pyrenean Frontal thrust system (Choukroune and ECORS Team, 1989; Daignières et al., 1994) and to the south by the southward Lakhoura thrust system (**Fig. 1**; Teixell, 1993). The western edge of this cretaceous rift basin coincides with the eastern edge of Pamplona structure which thus plays necessarily as a transfer fault. The Albian-Cenomanian Mauléon rift system displays other N20° structures respectively corresponding from west to east to Iholdy, Saison and Barlanès structures (**Fig. 1C**, Canérot, 1989, 2008). They are mainly deduced from the repartition of the synrift depocenters and of the salt diapirs that lie on them (Canérot et al., 2005; Debroas et al., 2010). Some of them are supposed to play a significant role in the whole structural framework. For instance, the N20° Barlanès structure is punctuated by the Urdach sub-continental mantle outcrops (Fabriès et al., 1991, 1998) reworked into the Albian-Cenomanian Urdach synrift breccias (Roux, 1983; Fortané et al., 1986; Jammes et al., 2009; Lagabrielle et al., 2010; Debroas et al., 2010). This spatial correlation suggests that the Barlanès N20° structure is prominently implied during sub-continental mantle synrift denudation. Despite these key observations, the Mauléon basin transverses structures are not thoroughly structurally constrained, although authors agree to give them syn-collisional strike-slip components during tertiary reactivation (Richert, 1967, 1968; Henry et al., 1968; Zolnaï, 1975; Schoeffler, 1982). This study addresses in more details the structural characteristics of these transverse structures and discuss their impact on the partitioning of the tertiary compressive strain.

3. METHODOLOGY, DATA AND RESULTS

3.1. RSCM Raman Spectroscopy of Carbonaceous Material

3.1.1. Analytical method and thermometry

The Raman analysis were performed at BRGM using a Renishaw inVia Reflex microspectrometer with Diode Pumped Solid State (DPSS) laser source excitation of 514.5 nm. The laser power attaining the surface of the sample, using a Leica DM2500 microscope and a ×100 objective (numerical aperture = 0.90), never surpass 0.1 mW. The 520.5 cm−1 line of an internal silicon have been used to calibrate the microspectrometer. Rayleigh diffusion was eliminated by edge filters, the Raman signal was firstly dispersed using 1800 lines/mm signal before analyzing by a deep depletion CCD detector (1024 × 256 pixels). Raman spectra of at least 10 particles were acquired on each sample to check data consistency. Renishaw Wire 4.1 was used for instrument calibration and Raman measurements.

The carbonaceous material structure changes irreversibly according to the increase of the temperature. Raman microspectroscopy permits to measure this major structural deformation of carbonaceous material (e.g. Wopenka and Pasteris, 1993; Yui et al., 1996; Beyssac et al., 2002a, 2002b; Lahfid et al., 2010). The calibration developed for the Raman Spectroscopy of Carbonaceous Material (RSCM) method have been performed for maximum temperatures ranging from 330-650°C (Beyssac et al., 2002) and enlarged to ranges of temperatures corresponding to low-grade metamorphism and diagenesis (Lahfid et al., 2010). In the present work, the measured temperatures are named RSCM peak temperatures and have been evaluated qualitatively comparing the acquire spectra with Glarus area (Lahfid et al., 2010).

3.1.2. The Lakhoura thrust system thermicity

Raman spectroscopy of carbonaceous material has been performed in order to evaluate the west-east RSCM peak temperature repartition on the footwall of the Lakhoura thrust system, between the Barlanès transfer zone to the east and the Iholdy transfer zone to the west **(Fig. 2)**. Twenty-height field samples of Campanian-Maastrichtian to Danian deposits have been collected and analyzed (**Tab.1**; Saspiturry et al., 2019d and present work). They illustrate the maximum temperature reached by the footwall of the Lakhoura 1, Lakhoura 2 and Lakhoura 3 thrust segments. These samples underwent RSCM peak temperature ranging from 300°C to

160°C **(Fig. 2)**. To the east of the Barlanès transfer zone, the footwall of the Lakhoura 1 thrust segment reaches RSCM peak temperatures of 280-300°C. Between, the Barlanès and the Saison transfer zones, the footwall of the Lakhoura 2 thrust segment records RSCM peak temperatures varying from 220°C to 250°C.

Westward, the footwall of the Lakhoura 3 thrust segment, localized between the Iholdy transfer zone to the east and the Saison transfer zone to the west, underwent RSCM peak temperatures varying from 160°C to 180°C. Consequently, the RSCM peak temperatures decrease toward the east by stages each time a transfer zone is crossed.

3.2. Field observations and paleostress reconstruction

3.2.1. Data and methodology

Fieldwork was conducted mainly on the southern Lakhoura thrust system and inside the transfer zones to investigate associated deformations at various scales and at the junction between each other. The deformations observed in the field are mainly reliable to transcurrent and reverse kinematics. Our fieldwork is based on microstructural measurements (fault and striation measurements, schistosity and sense of shear, veins, fold geometries…). When dataset was appropriate (sufficient number of striated faults), we performed paleostress computations.

Resolved shear stress orientation on each fault surface is assumed to be parallel to the measured striation with the correct shear sense (Wallace, 1951; Bott, 1959). We used a systematic collection of minor faults to determine paleostress axis direction using the "direct inversion method" of Angelier (1990). Results include the orientation of major, intermediate and minor stress axes (σ1, σ2 and σ3, respectively), the ellipsoid form parameter $R = (\sigma 1 - \sigma 3)/(\sigma 1 - \sigma 3)$ and the average misfit angle (the angle between the computed optimum slikenline and the measured one). We used the "TectonicsFP" software (Sperner et al., 1993) for calculations and graphical outputs.

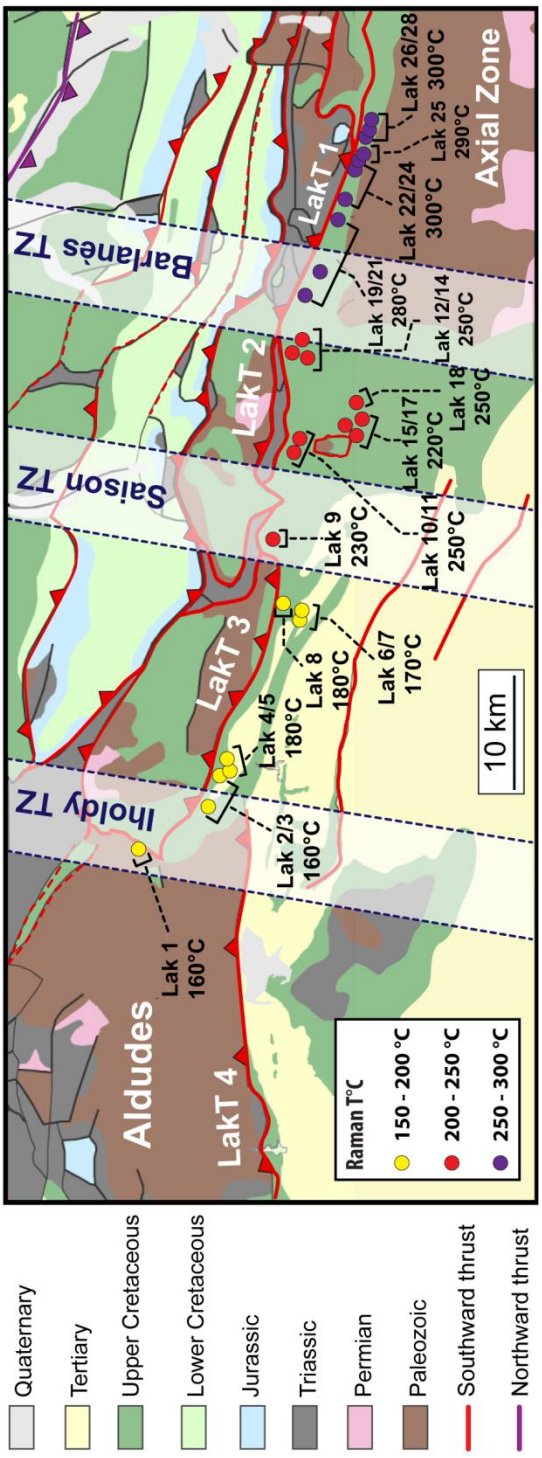


Fig. 2. Map showing the distribution of the RSCM peak temperatures on the Lakhoura thrust system footwall. The RSCM peak temperatures increases eastward from 160°C to 300°C, by stages, each time a transfer zones is crossed. LakT 1 / LakT 4: segments of the Lakhoura thrust system; TZ: transfer zone.

3.2.2. Lakhoura thrust segments kinematic

All along the Lakhoura thrust, schistosity (S1 and S0-1) is trending around NW-SE **(Fig. 3A)**. This schistosity is

associated to several shear zones. In the western part of the Iholdy transverse structure, schistosity (S1) measured into the Santonian flysch is mainly oriented NW-SE and associated to stretching lineations with a top to the south-southwest sense of shear **(Fig. 3C)**, thus with an inverse sinistral associated kinematic. Eastward, in the Lakhoura 3 thrust segment, the Mendibelza unit is thrusted onto the Campanian to Early Eocene sediments, the shear zone affecting the Paleozoic basement in the hanging wall of the Lakhoura thrust indicates a top to the SW (N230°) sense of shear **(Fig. 3B)**. At the eastern side of the Barlanès transverse structure (LakT 1 segment), shear zone affects the Campanian flysch into the footwall of the Lakhoura thrust **(Fig. 3D)**. The flysch is deformed with recumbent folds (fold axis: N140, 10°, and axial plane: N140-15°) compatible with west-southwest sense of shear (top to N230°). Moreover, shear planes (C: 35°/35°) bearing stretching lineation with a top to the west-southwest sense of shear has been measured. All the measurements and observations on the different segments of the Lakhoura thrust are consistent and compatible with an inverse, slightly sinistral kinematic.

3.2.3. The Iholdy transverse structure

This section presents the geometry of the Lakhoura 3 thrust segment in the vicinity of the Iholdy N20° transverse structure **(Fig. 4A)**. Eastward, the Mendibelza unit is thrusted towards the south-west onto the Campanian to Early Eocene sediments by the N120° Lakhoura 3 thrust segment. Approaching the Aldudes domain, the Lakhoura 3 thrust segment turns into a N20° direction and branches into the Iholdy transverse structure **(Fig. 4A)**. At this junction, the Albian conglomerates of the Mendibelza unit are affected by a kilometric and symmetric N-S syncline with average orientations of N167°-64° fold axis and N236°-80° axial plane and **(Figs. 4B and 4C)**. Towards the south, the average syncline axis turns into N185°, 64° **(Fig. 4A)**. To the north, along the N20° Iholdy transverse structure, the Paleozoic basement of the Lakhoura nappe is affected by several shear zones oriented with shear-planes in average C82°, 50° and schistosity in average S182°, 70°, evidencing a displacement top to the west (N262°) **(Fig. 4D)**.

Figure 4E synthetize the whole structures observed in the field at the junction between the damages zones of the N20° Iholdy transverse structure and the N120° Lakhoura 3 thrust segment. All the measurements and observations are compatible with an inverse dextral kinematic on the N20° Iholdy transverse structure and an inverse sinistral kinematic on the N120° Lakhoura 3 thrust segment **(Fig. 4E)**. Both of these two major structures are thus kinematically coherent with a top to the west-southwest sense of displacement and thus formed synchronously. Thus, the compressive strain is partitioned between N20° transverse structures and N120° thrust segments.

3.2.4. The Saint-Palais microstructures

Microstructures were observed and measured within the corridor located between the Iholdy transfer zone to the west and the Saison transfer zone to the east **(Fig. 1A)**. At this site, the Cretaceous marls are tilted to the SSE by nearly 70° **(Fig. 5A and 5E)**. Brittle deformations are mainly inverse and transcurrent. Systematic measurements allow to pool the data in two families with a coherent kinematic to each **(Fig. 5E and 5F)**. Within the strike-slip phase **(Fig. 5E)**, the fault planes are mainly trending NNW-SSE with a pure dextral strike-slip kinematic. These fault planes could be observed at centimetric scale and at decametric scale as well, offsetting the previously tilted stratifications **(Fig.5A)**. To a lesser extent, stratifications planes could be reused as fault planes with a sinistral kinematic compatible with the previous fault family **(Fig. 5B and 5E)**. Paleostress calculations provide a pure strike-slip paleostress tensor with subhorizontal $\sigma 1$ oriented N36° **(Fig. 5E)**. It should be noted as well that a set of vertical veins have been measured in similar directions (roughly N40°) thus corresponding to the opening of tensile fractures. The inverse phase is characterized by WNW-ESE inverse fault planes, from centimeters to decametric scales, with a dip ranging from 20° to 70°, thus respectively crosscutting the stratifications or reusing it **(Fig. 5F)**. Associated inverse stria is mainly dip-slip **(Fig. 5D)**. A set of veins creeps in the stratifications, probably during the compressive state of stress **(Fig.5F)**. These veins are subsequently striated horizontally with transcurrent movements.

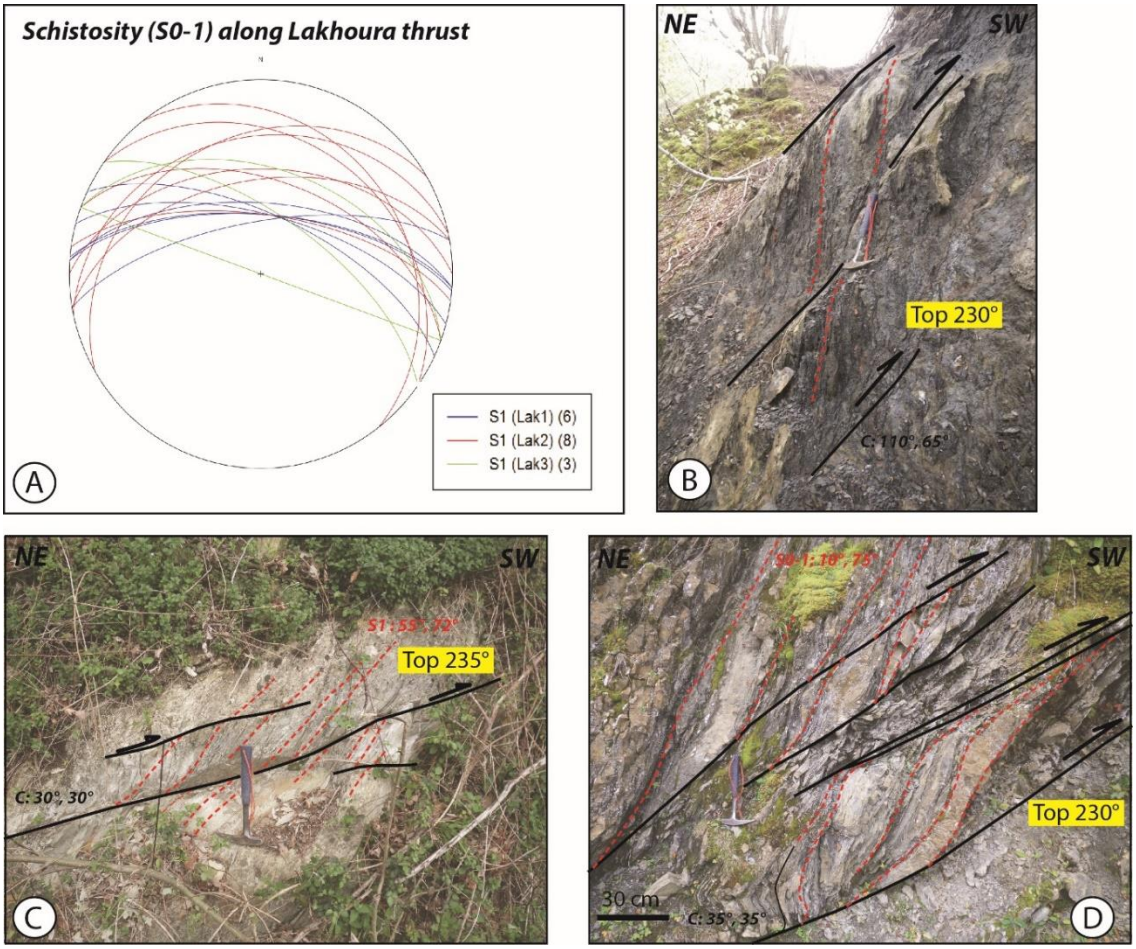


Fig. 3. Lakhoura thrust kinematics (all structural values are indicated in dip direction). **(A)** Lower hemisphere stereographic projection of regional S0-1 measurements along the Lakhoura thrust (a color for each segment); **(B)** Shear zones affecting the Paleozoic basement on the Lak3 thrust segment, giving a top to the N230° sense of shear; **(C)** Shear zone affecting Santonian flysch on the Lak4 thrust segment, giving a top to the 235° sense of shear; **(D)** Shear zones affecting the Campanian Flysch on the Lak1 thrust segment with a top to the N230° sense of shear.

Paleostress calculations provide a compressive paleostress tensor with a subhorizontal σ1 oriented N194°. For the two phases (strike-slip and inverse), the determined main stress axis σ1 is oriented roughly NE-SW, leading to the conclusion that all these deformations are kinematically coherent and thus could have occur synchronously.

3.2.5. The Saison transverse structure

Along the N20° Saison transverse structure **(Fig. 1A)**, microstructural observations and data have been collected along the Saison river which offers fresh large outcrops allowing high-quality observations. A panel of deformations attests for pure dextral transcurrent kinematic along N30° directions. Within the middle Cenomanian calcareous turbidites, stratification is verticalized along the N30° direction, while the regional trend is generally roughly N110°. The centimetric most competent layers within the stratigraphic pile could be folded asymmetrically along N30° direction **(Fig.6A)**. Asymmetries indicate systematically vertical dextral simple shear. Fold axes are reported on the stereographic projection, showing a recurrent dip to the south of roughly 50° **(Fig. 6D)**. Most competent layers could be stretched to form boudins aligned within the schistosity N30° associated to metric shear zones within the finest layers, all indicating dextral shear sense **(Fig. 6B)**. Fault stria data allow to reconstruct the strike-slip paleostress tensor **(Fig. 6C and 6D)**.

3.3. Seismic interpretation

3.3.1. Data and Methodology

This part of the study focuses on the deep geometry of the Mauléon basin N20° Iholdy and Saison transverse structures from the interpretation of two NW-SE seismic

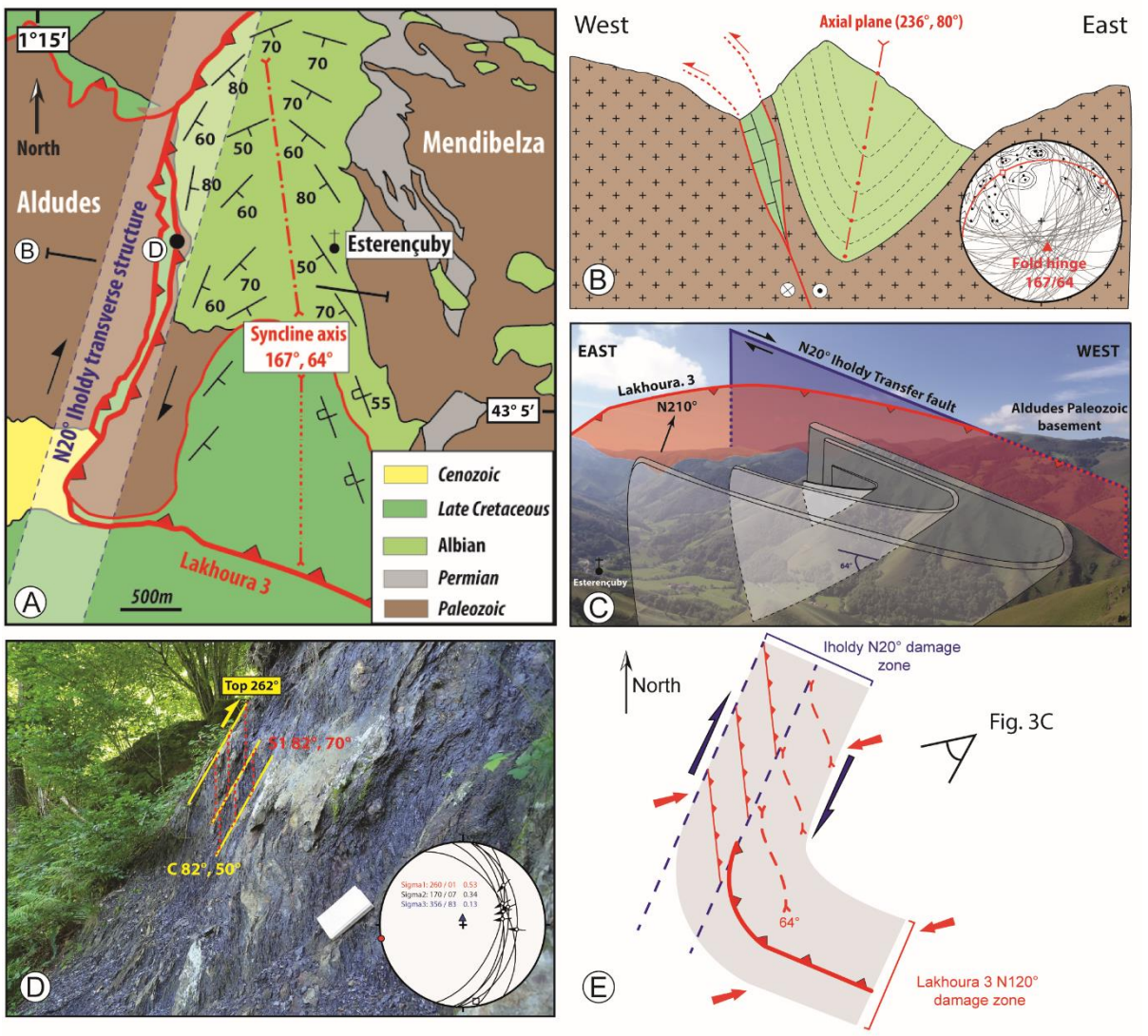


Fig. 4. Junction between the Lakhoura 3 thrust segment and the Iholdy N20° transverse structure **(A)** Geological map of the Lakhoura 3 thrust segment at the vicinity of the Iholdy N20° transverse structure; **(B)** West-east cross-section located on Fig. 4A of the kilometric syncline within the Albian cover. At the right bottom, lower hemisphere stereographic projection of regional stratification measurements evidencing the geometry of the syncline; **(C)** View towards the southwest of the Albian cover syncline at the junction between the Iholdy N20° transverse structure and the Lakhoura 3 thrust segment. The point of view is located on Fig. 4E; **(D)** Shear zones affecting the Aldudes Paleozoic basement on the footwall of the Iholdy transverse structure giving a top N262° displacement; (E) Synthetic representation of the whole structural framework linking the structures kinematically coherent within the damage zones of the inverse dextral N20° Iholdy transverse structure and the inverse sinistral N120° Lakhoura 3 thrust segment.

reflection profiles, reprocessed by the BRGM in 2017 (MT116 acquired by ESSO-Rep in 1969 (Mauléon-Tardets exploration permit) and 82BAA12 (Buzy-Asson exploration permit) acquired by SNEA(P) **(Figs. 7 and 8)**. The reprocessing performed consists of PSTM (Post Stack Time Migration) sequence. The results are of good quality concerning the MT line, despite the year of acquisition of this survey. The 82BAA12 line is much noisier in depth which makes its interpretation less reliable. The quality of this seismic line only allows to interpret its western ending. On the other hand, it illustrates Roquiagues structure and geometric relations with the surrounding sedimentary series. The seismic interpretation was carried out using the Geographix® Discovery Suite. Seismic/well tie is obtained by using the time / depth curves acquired in the boreholes and derived from the recording of checkshots.

The MT116 and the 82BAA12 seismic reflection profiles show respectively the Iholdy and Saison transfer zones on the hyper-extended domain of the Mauléon basin. Four markers have been distinguish on these lines

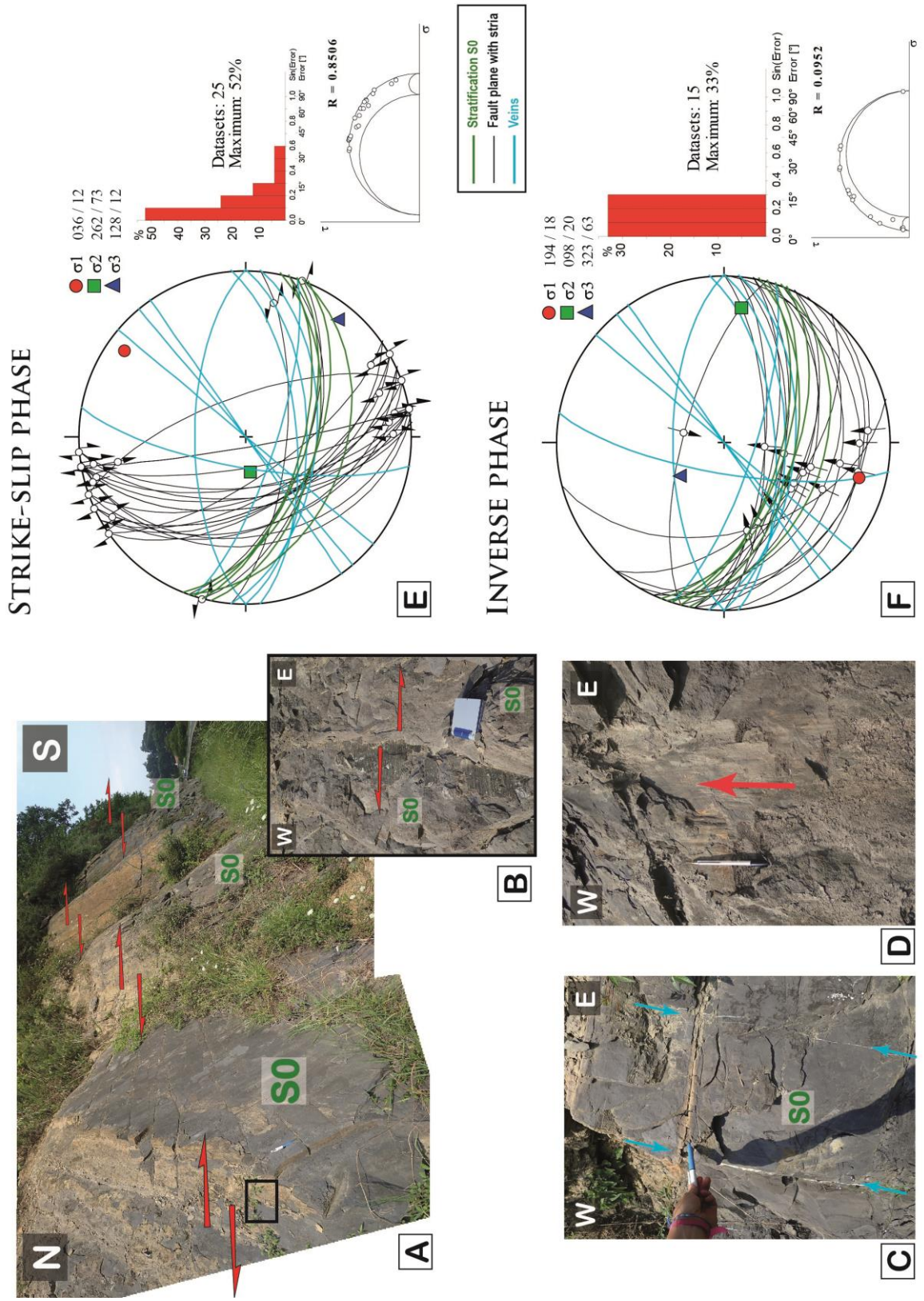


Fig. 5. The Saint-Palais microstructures **(A)** N160° trending dextral strike-slip offsetting the tilted stratification S0 ; **(B)** N100° trending sinistral strike-slip re-using stratification planes; **(C)** N45° trending millimetric veins; **(D)** E-W inverse fault plane with dip-slip striae; **(E and F)** Schmidt stereographic projection (lower hemisphere) of fault/stria measurements for the strike-slip **(E)** and inverse **(F)** phases, associated to stratifications and veins measurements. For each deformation phase, calculated paleostress tensor is represented in addition with the misfit histogram between the calculated and the measured stria and the ellipsoid form parameter R.

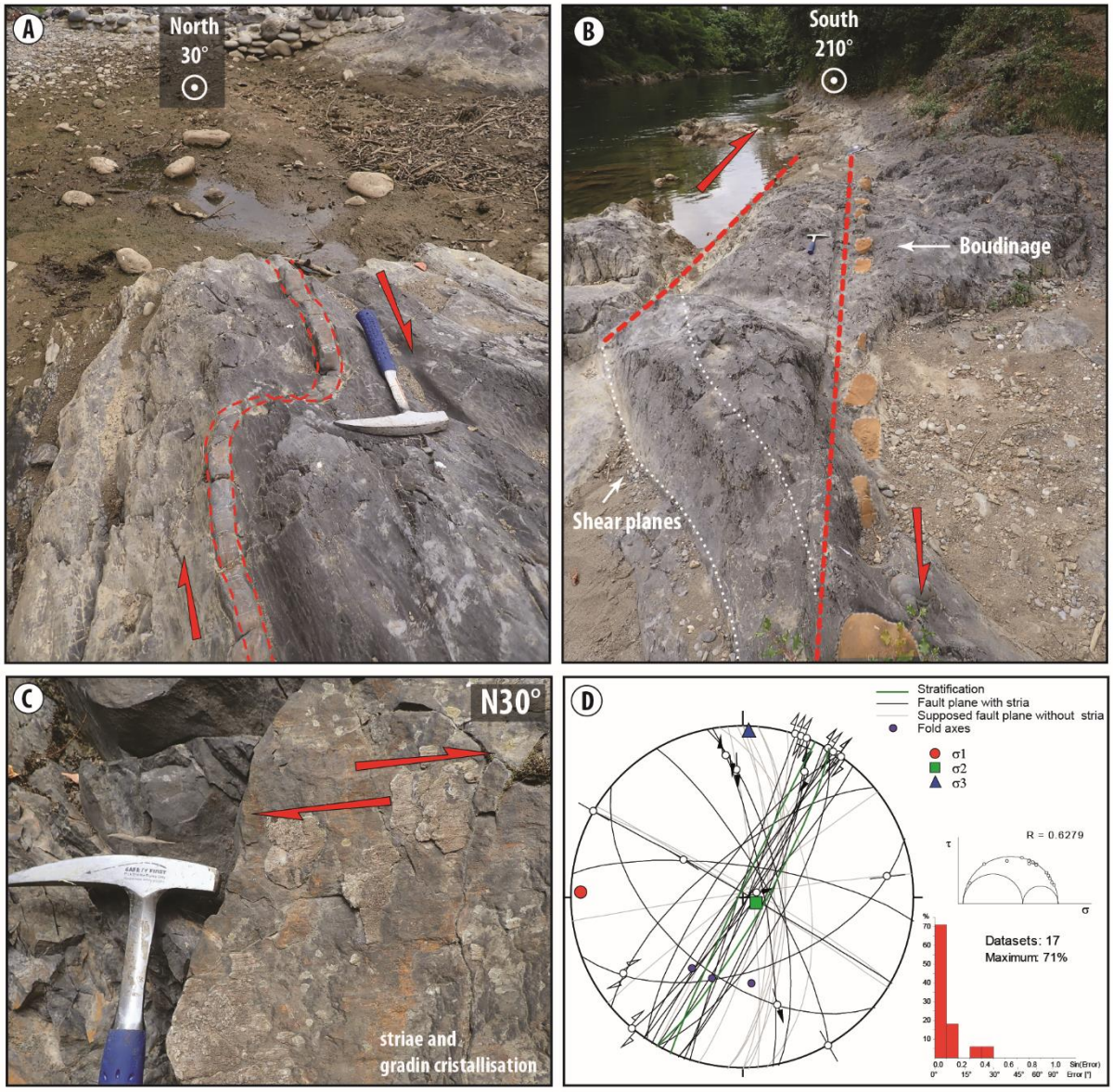


Fig. 6: Microstructures associated to the Saison transverse structure **(A)** Asymmetric folding attesting for dextral kinematic along N30° direction, **(B)** Dextral vertical shear zone along N30° direction associated with boudinage of the most competent layers in the middle Cenomanian calcareous turbidites. **(C)** Kinematic indicator of the dextral movements along the vertical fault planes, **(D)** Stereographic projection (lower hemisphere) of the fault-stria data collected along the Saison transfer zone, misfit histogram and ellipsoid form parameter R.

(1) Basement top, (2) Late Triassic salt top, (3) Aptian limestones and marls top and (4) Albian marls top. The MT116 line is calibrated using the markers identified in the published N-S composite seismic reflection profiles recently published by Saspiturry et al., 2019a. This line cross-cut the MT116 seismic reflection profile on its easternmost part and is a merger of lines MT104, MT112 and 83HBS02 reprocessed by BRGM in 2014 **(Fig, 1C)**. The hyper-extended domain of this crossing composite line is calibrated using two boreholes: Ainhice-1 (3,540.85 m depth) and Uhart-Mixe-1 (1,868.8 m depth). The Ainhice-1 well calibrates the four makers evidenced on the MT116 line as it reach the Palaeozoic substratum at a depth of around 2,900 m. The Uhart-Mixe-1 borehole and the 1/50 000 geological maps (Boissonnas et al., 1974; Le Pochat et al., 1976) allow to constrain the top Albian sequence. The 82BAA12 seismic reflection profile is not crosscuted by any seismic reflection profile with a borehole calibration **(Fig. 1)**. This profile has been calibrated in merging it with the MT104 (Saspiturry et a., 2019a) and MT116 (present study) seismic reflection profiles located

respectively at 4200m westward and 5000m north-westward.

The top Albian and the top Late Triassic salt are partly calibrated using the 1/50 000 geological maps (Casteras et al., 1971; Le Pochat et al., 1976).

3.3.2. The Iholdy transverse structure

The MT116 seismic reflection profile **(Fig. 7)** illustrates the Iholdy transverse structure. In this section, the Paleozoic basement and the Mesozoic cover draw an asymmetric syncline. To the NW, the Paleozoic basement is steeply dipping towards the SE from 1500 ms to 2600 ms, whereas to the SE, the basement is slightly tilted towards the NW. It reaches a time-depth of 2100 ms in the easternmost part of the seismic reflection profile. To the West, the Paleozoic basement is affected by N20° high angle westward deeping faults with a normal offset of around 300 ms each (blue lines). To the west, the Mesozoic cover is affected by the thin-skin Arberoue southward thrust. The Jurassic to Aptian prerift sequence is isopach (tabular seismic facies) but not continuous and follow the same trend than the Paleozoic basement with a western unit that is more tilted than the eastern one. This sequence is interpreted to slide towards the Mauléon rift axis during Albian time (Bouquet, 1986; Ducasse et al., 1986; Ducasse and Vélasque, 1988; Lagabrielle et al., 2010; Corre et al., 2016; Teixell et al., 2016; Saspiturry et al., 2019a), explaining its no continuous character.

On the south-eastern flank of the syncline, the Albian synrift sequence is thicker towards the Iholdy transfer zone. It displays divergent seismic facies and reach a maximum thickness of around of 2000ms. The Albian deposits are thinner on the Iholdy transfer zone (around 500-1000ms thick). Thus, the transfer zone seems to be responsible for differential accomodation rate during the Albian rifting stage.

The Albian sequence is affected by a weld diapir outcropping southward and corresponding to the N20° Iholdy diapir **(Fig. 1)**. This diapir grows up along one of the high angle normal fault affecting the Paleozoic basement and delimitating the eastern edge of the Iholdy transverse structure. The Late Cretaceous only outcrop to the east. The Iholdy transverse structure appears as a complex differential accomodation zone controlling a major Albian depocenter and do not corresponds to a single fault plane that propagate both on the cover and the Paleozoic basement. In this part of the basin, the Iholdy structure have been slightly inverted during the Tertiary but preserved its inherited Albian normal offset.

3.3.3. The Saison transverse structure

The 82BAA12 seismic reflection profile illustrates the deep structure of the Saison transverse structure **(Fig. 8)**. The Paleozoic basement seems to deep towards the SE and is affected by a westward steeply dipping fault with a normal offset of around 500 ms. The Jurassic to Aptian prerift sequence is not well identified on this seismic line. The Albian synrift sequence is characterized by three depocenter, that seems to be controlled by the upwelling of the Roquiague diapiric structure. This diapir growth up along the normal fault affecting the basement.

Two main Albian depocenter are localized on both sides of this diapir. They are characterized by a thickness that increase towards the diapiric structure, reaching a time thickness of around 1 300 ms. On top of the diapir, the Albian sequence is very thin, i.e. 100-300 ms and is localized on a syncline. This significant variation of the accomodation rate during the Albian time, argue in favor of the activity of the Roquiague diapir at that time. As the Albian sequence, the Late Cretaceous draws three synclines. The more significant is localized on top of the Roquiague diapir, as shown by the 1 000 ms time thickness of the Cenomanian deposits on its axis. This observation highlights the development of a more important subsidence on this syncline than during Albian time.

During the Late Cretaceous, the Roquiague diapir seems to collapse, increasing the subsidence of the mini-basin located right above it and leading to the expulsion of the salt on the mini-basin edges.

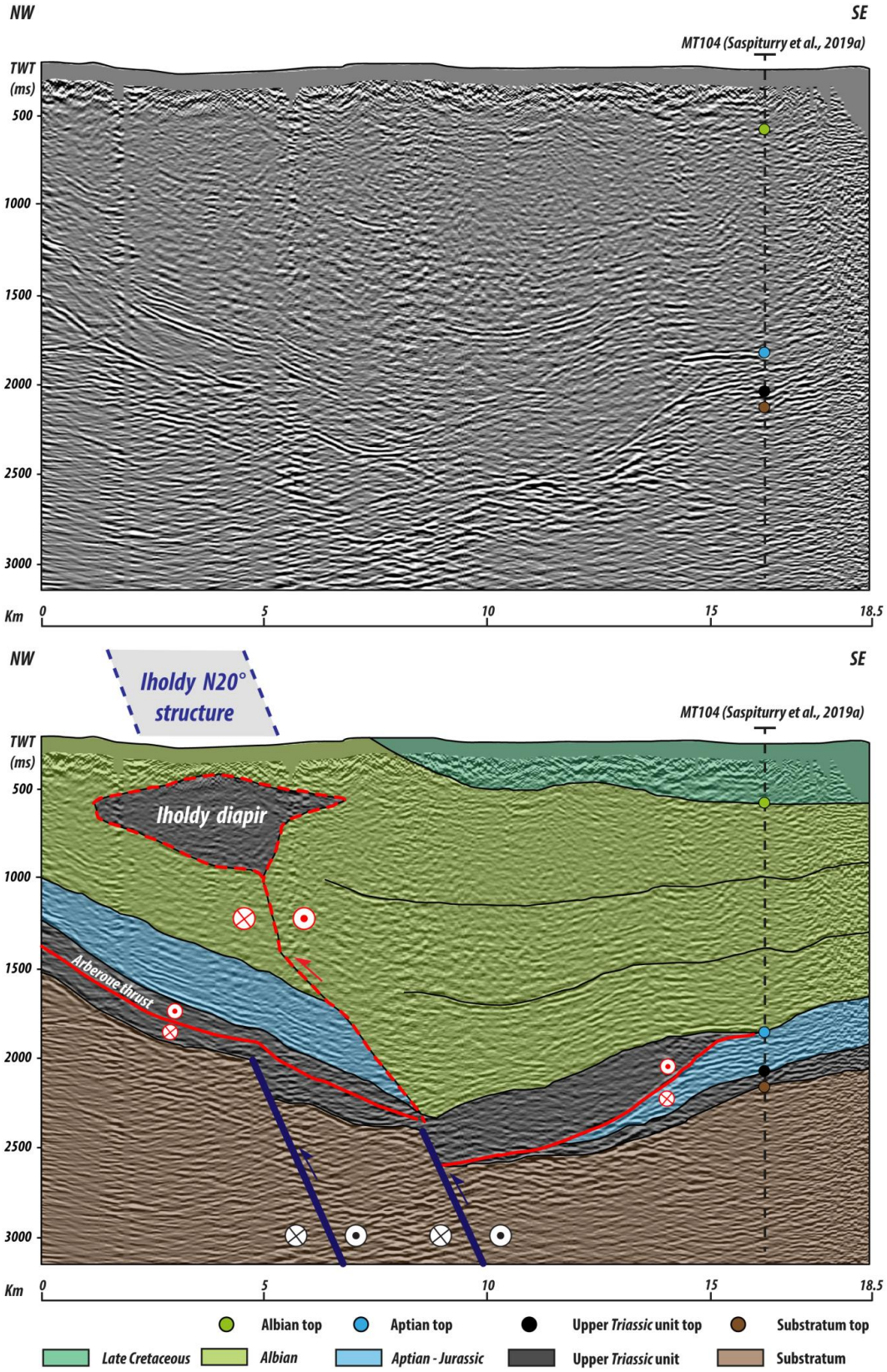


Fig 7. Interpretation of the NW-SE MT116 petroleum seismic reflection profile, reprocessed by the BRGM in 2017. This seismic line shows the deep geometry of the Iholdy transverse structure. This seismic line through the Mauléon basin hyper-extended domain cuts across an asymmetric syncline in which Paleozoic basement is affected by steeply dipping normal fault. The Albian sequence significantly thicken towards the Iholdy transverse structure highlighting its synrift major normal offset. The Iholdy weld diapir seems to grow up on the Albian sequence right above one of the high angle normal fault affecting the Paleozoic basement.

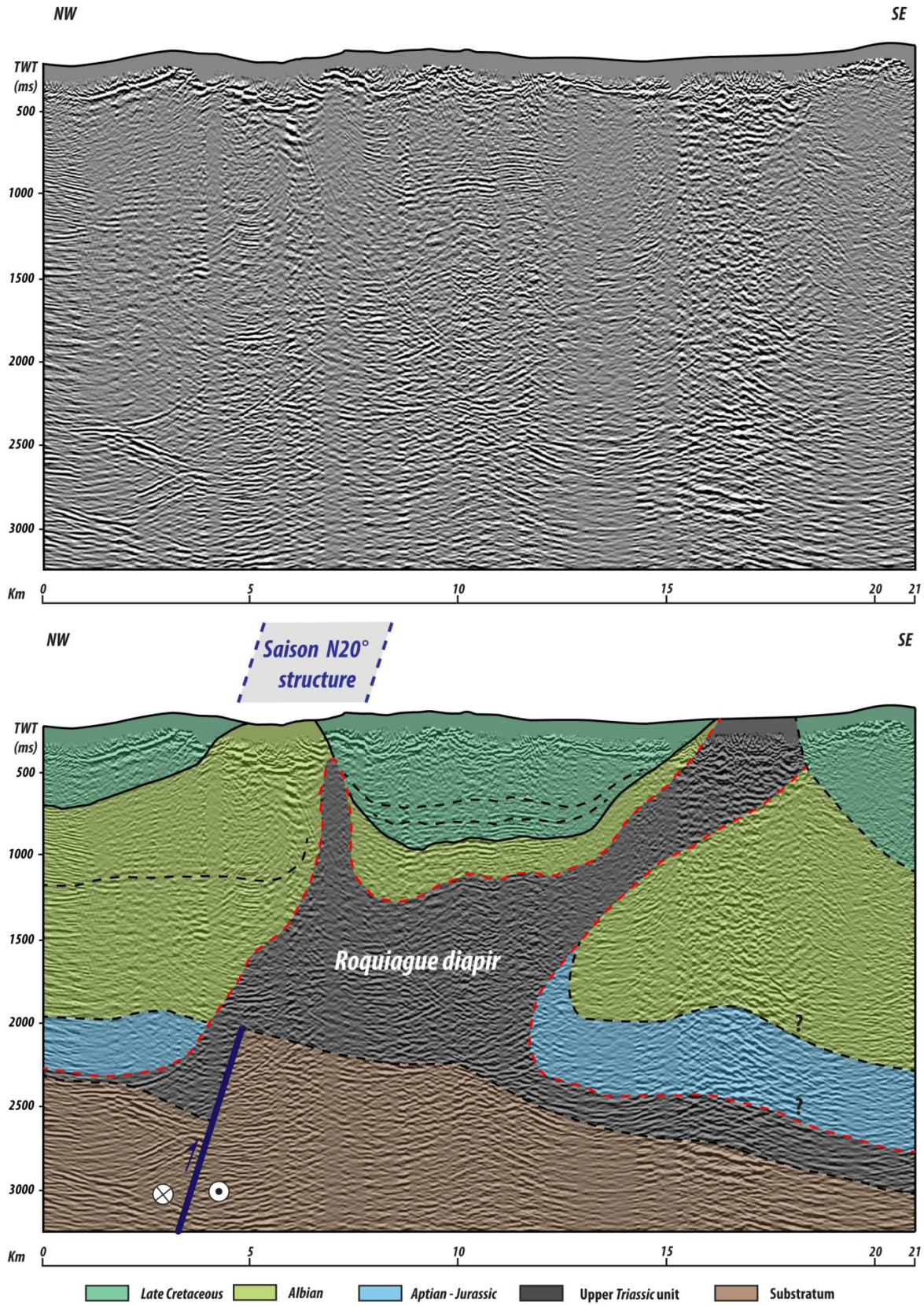


Fig. 8. Interpretation of the NW-SE 82BAA12 petroleum reflection seismic line, reprocessed by the BRGM in 2017. This seismic line through the Mauléon basin hyper-extended domain shows the deep geometry of the Saison transverse structure. The Paleozoic basement is dipping towards the east and is affected by a high angle westward dipping normal fault. The Albian sequence significantly thinner towards the Saison transverse structure. The Roquiague diapir seems to grow up along the high angle normal fault affecting the Paleozoic basement. This diapiric activity is responsible for the development of two main Albian depocenter and the formation of a late Cretaceous mini-basin.

3.4. 3D implicit geological modelling of the Mauléon basin

3.4.1. Methodology and Data

Reconstructing the current 3D geometry of the basin offers the most up to date view of the Mauléon basin structures and allows to propose geometries of the basin in accordance with the whole available dataset. We used the ‘‘3D Geomodeller’’ software (© BRGM - Intrepid Geophysics; http://www.geomodeller.com) which reproduces 3D geological geometries based on interpolation of a scalar field in space (Aug 2004; Chilès et al. 2006, Lajaunie et al. 1997), where a lithological contact corresponds to an isovalue of this field and the dip of the structures corresponds to the gradient of this field.

The topological relationships between the different lithological units and the geometrical relationships, like superposition, intrusion or cross-cutting relations, are taken into account through a ‘‘lithological pile’’, in order to reproduce complex geological systems as realistically as possible (Calcagno et al, 2008). At this stage, the geometry derives from a geostatistical extrapolation of surface geological observations of contacts and dips.

The following dataset have been included in the structural model of the Mauléon basin: (1) 1/50 000 BRGM geological maps (Cartes à citer), (2) 556 wells from BEPH (Bureau des ressources énergétiques du sous-sol) http://www.minergies.fr and from BSS (Banque du sous-sol) http://infoterre.brgm.fr/page/banque-sol-bss, (3) seismic interpretations (Saspiturry et al., 2019a) (4) around 2 500 structural measurements half from geological maps and half newly acquired.

The geological pile of the model contains 12 geological formations, from base to top: (1) mantle, (2) basement, (3) Permian to Lower Triassic, (4) Upper Triassic fault (5) Jurassic, (6) Barremian to Aptian (7) Albian to lower Cenomanian (8) Middle Cenomanian to Maastrichtian (9) Eocene, (10) Oligocene, (11) Miocene and (12) Pliocene.

3.4.2. 2D Isovalues map from 3D interpolation

As the cokriging method consider the strike and the dip of a formation as respectively, the orientation and the gradient of the potential field for this formation, it is thus possible to constrain precisely spatial change of geometries if structural measurements are sufficient and homogeneously distributed, as it is the case for the Mauléon basin in our study (**Fig. 9**, top). The 3D scalar fields of the synrift and postrift formations are represented in maps with the position of the Iholdy and Saison transfer zones (**Fig. 9**, bottom).

We can observe that the regional trend of stratifications is nearly N120°. Although, approaching the transfer zones, strike of stratifications turn into N-S to N20° directions, either with clockwise or anticlockwise rotations of S0, even along the same transfer zone (as for example to the north of Iholdy transfer zone in the synrift formation). Most of the disruptions of the continuity of the N120° stratifications are aligned more or less effectively along two N30° direction corresponding to the Iholdy and the Saison transfer zones. Between the Iholdy and the Saison transfer zones, a corridor containing few disruptions of S0 is evidenced with postrift sediments folded symmetrically of which axes are confined between the two zones and do not pass through.

3.4.3. 3D structural framework of the Mauléon Basin

Geological modelling process conducts to include faults to reproduce the coherency of the structures. The **figure 10** presents 3D views of the structural framework. N120° antithetic thrusts provide to the Mauléon basin its general pop-up shape. Nevertheless, this form is not cylindrical but evolves laterally, by stages, each time crossing a transfer zone. Such observations imply that thrusting might be branching into transcurrent fault zones acting thus as transfer zones.

4. DISCUSSION

4.1 Characterization of the Mauléon basin syn-collisional transfer zones

4.1.1. Variable deformation patterns along a transfer zone

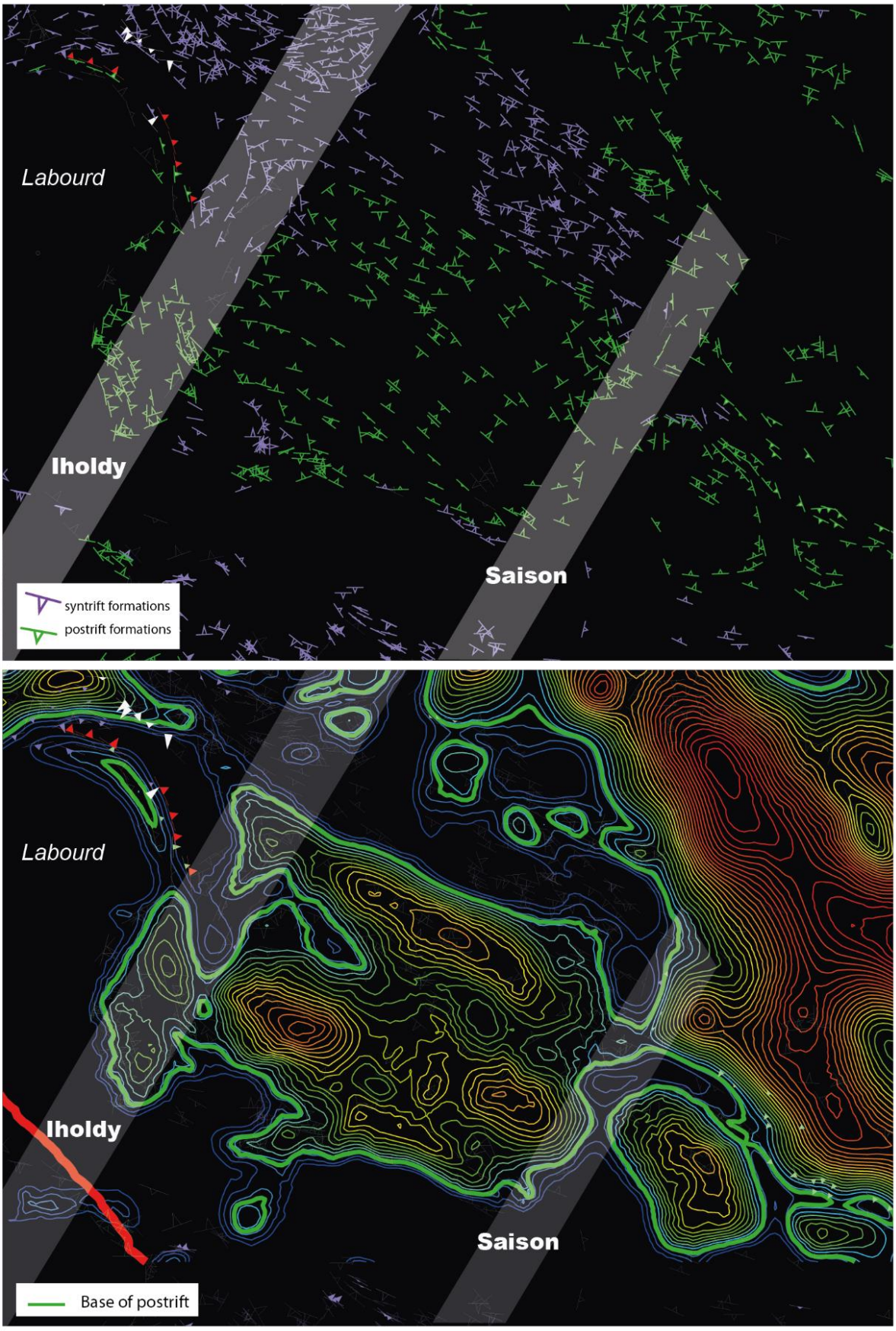


Fig. 9. Maps of the structural measurements for synrift and postrift formations (top) and corresponding calculated isopotential lines resulting from the cokriging method (bottom).

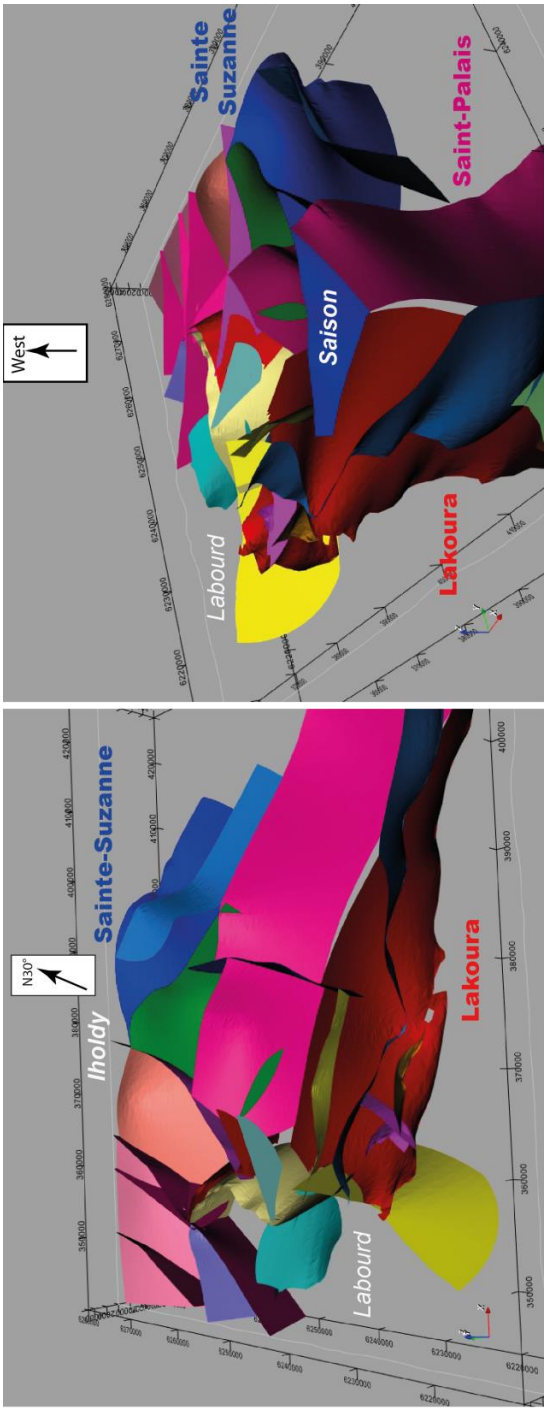


Fig. 10. 3D model of the structural framework of the geological model illustrating the Mauléon pop-up with associated transfer zones. View to the N30° direction to the left and to the west to the right.

Seismic interpretation, RSMC thermometry, paleostress reconstruction and 3D implicit modeling bring out the presence of N20° crustal transfer zones. They are especially essential in the 3D model to be able to reproduce coherent current 3D geometries of the inverted hyperextended Mauléon basin (cf. 3.4.). The presence of these transfer zones have been firstly deduced from the correlated repartition of the Albian-Cenomanian synrift depocenters localized between the Iholdy, Saison and Barlanès transfer zones (Canérot et al., 2005; Canérot. 2008; Debroas et al., 2010). These authors interpreted as well the spatial distribution of salt diapirs (e.g. Iholdy and Roquiague diapirs) as the presence of early Cretaceous synrift normal faults rooting in the Paleozoic basement **(Fig. 11)**. We present in this study the first images of basement apparent normal offset on the newly reprocessed and reinterpreted MT116 and 82BAA12 seismic reflection profiles **(Fig. 11)**. Note that a sketchy interpretation of the MT116 profile has been proposed by Zolnaï (1975). However, at that time, the poor quality of the seismic reflection profile annoys to detail geometries, neither in the Mesozoic cover nor in the basement, around the Iholdy transfer zone. Likewise, the Iholdy and Saison transfer zones were scarcely structurally constrained from field observations. The few authors proposed for these features various definitions: « accidents de coulissage à déplacements obliques » (Richert., 1967, 1968); « zones tectoniques du Béarn et du Pays Basque » (Henry et al., 1968); « failles de décrochements » (Zolnaï., 1975); « Transversales basco-landaises » (Schoeffler., 1977). All agree that these structures are characterized mostly by syncollisional strike-slip kinematics, nevertheless without integrating them in a coherent regional structural pattern. Our observations allow to propose for these features the definition of transfer zones according to more recent literature (Gibbs, 1984; Reynolds and Rosendahl, 1984; Chorowicz, 1989; Gibbs, 1990). In the following paragraph, we will expose the arguments supporting this interpretation.

Along the same transfer zone, the structural expressions vary. They do not correspond to single continuous fault planes but rather to diffuse deformation zones, more or less intense. This diffuse deformation explains partly why these transfer zones were not precisely represented on 1/50000 BRGM geological maps (Castéras et al., 1970, 1971; Boissonnas et al., 1974; Le Pochat et al., 1976, 1978; Henry et al., 1987). They are mostly deduced from the juxtaposition of different lithological facies lying on both side of a

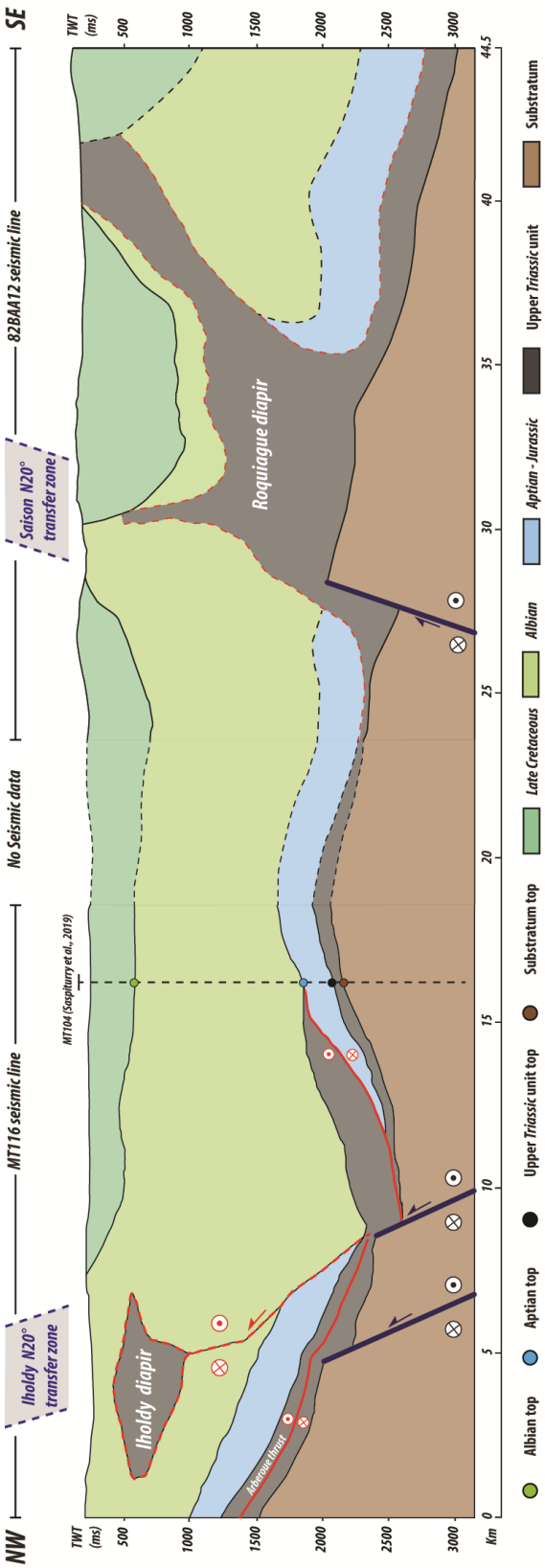


Fig. 11. SW-SE TWT composite cross-section corresponding to a merged of the MT116 and 82BAA12 seismic reflection profiles showing the deep crustal geometry of the Iholdy and Saison transfer zones.

narrow zone but without being able to precisely locate a major fault structure. Nevertheless, the entire set of deformations is aligned along N20° zones. They are mostly constituted of several faults in relay, creating wide deformation zones where structural measurements of stratification are often deflected or verticalized (cf. 3.4.2.). Paleostress reconstructions for the south of the Iholdy and the north of the Saison transfer zones confirm that locally, they are characterized by dextral strike-slip kinematic (cf. 3.2.). However, isovalues map from the Mauléon 3D model shows different geometries of stratification virgations along a same transfer zone (cf. 3.4.2.). It attests for spatial kinematic variabilities along the latter, ruling out the previous interpretation of a single strike-slip fault. These spatial kinematic variabilities require the presence of others oblique structures accommodating the differential movements. Indeed, 3D model construction necessitates that each segments of both the North Pyrenean and Lakhoura N120° thrust systems branch into the N20° transfer zones (cf. 3.4.3.). It implies the synchronicity of the N120° thrust systems and the N20° transfer zones. This geometrical relationship is locally confirmed by field observations on the Lakhoura 3 thrust segment that branch into the southern portion of the Iholdy transfer zone (cf. 3.2.2.). Paleostress directions and orientation of microstructures confirm that the Iholdy transfer zone and this thrust segment are kinematically coherent at this branching site. Thus, the compressive strain is partitioned between transfer zones and thrust systems.

4.1.2. Segmentation of the Mauléon basin pop-up in several corridors

This segmentation is visible at the scale of the entire Mauléon basin pop-up **(Fig. 12)**. It comes down to the stronger shortening of the pop-up structure towards the east, in stages, each time a N20° transfer zone is crossed (cf. 3.4.3.). It attests for different shortening rates on both sides of a transfer zone. The pop-up is thus segmented in corridors, each with its own shortening rate, in-between two N20° transfer zones in a hand, and external antithetic thrust segments being parts of the N120° North Pyrenean Frontal and Lakhoura thrust systems on the other hand. The westward decrease of the shortening rate is also evidenced by the

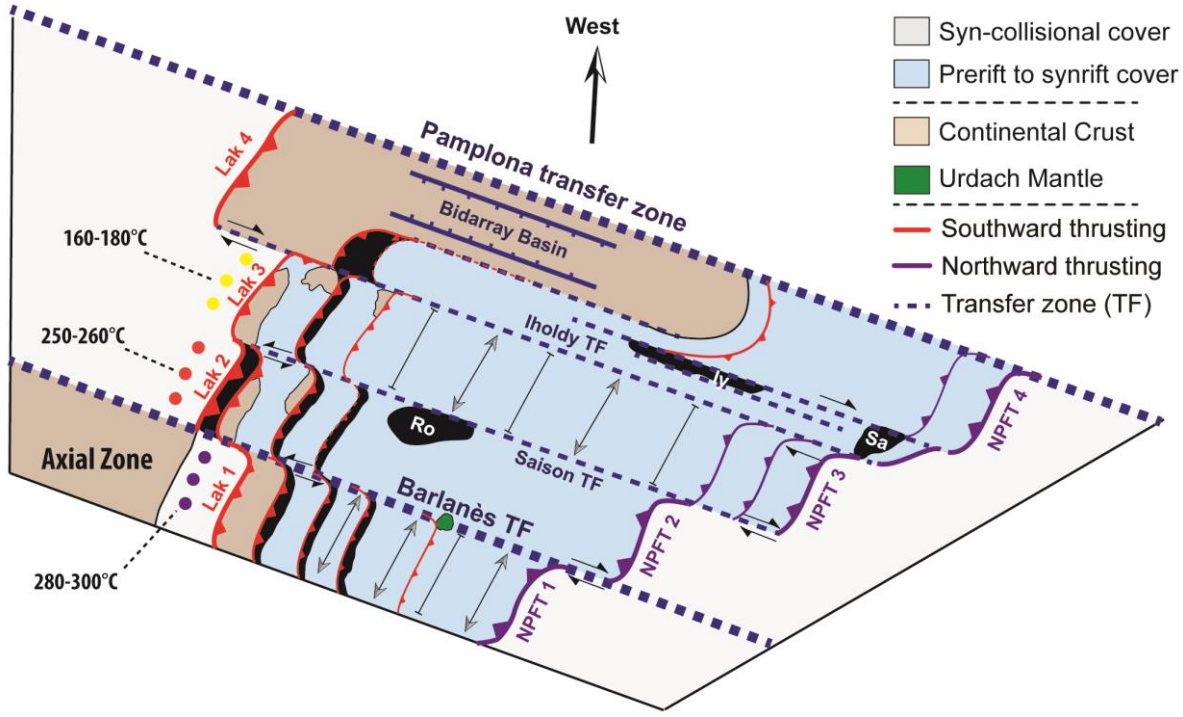


Fig. 12. Perspective map of the pop-up structure of the Mauléon basin showing its segmentation with N20° transfer zones. Double arrows represent fold axes associated with the shortening. TF: transfer zone; Ro: Roquiague diapir; Iy: Iholdy diapir; Sa: Salies diapir; Lak 1, Lak 2, Lak 3, Lak 4 correspond respectively to the Lakhoura thrust segments 1, 2, 3 and 4; NPFT 1, NPFT 2, NPFT 3, NPFT 4 correspond respectively to the North Pyrenean Frontal thrust segments 1, 2, 3 and 4.

spatial distribution of the RSCM peak temperatures values obtained on the footwall of the Lakhoura thrust system (c.f. 3.1.2., **Fig. 12**). These RSCM peak temperatures result of a post-collisional heating of the footwall of the Lakhoura thrust in response to tertiary continental crust thickening (Saspiturry et al., 2019d). Indeed, RSCM peak temperatures values decrease towards the west, from 300°C to 160°C, by stages, in each corridor. In average, when crossing westward the Barlanès and the Saison transfer zones, RSCM peak temperatures decrease suddenly of, respectively 50°C and 70°C **(Fig. 12)**. The evolution by successive stages of the RSCM peak temperature evidences a homogeneous shortening, therefore a homogeneous thickening rate, specific to each corridor. Thus, these corridors, between N20° transfer zones, deform independently, strain being accommodated by different structures such as N120° fold axes (with nearly vertical axial planes) and N120° thrust segments (cf. 3.4.2; **Fig. 12**). This compartmentalization is clear in the core of the pop-up. Going to the external edges of the pop-up, it becomes diffuse and is expressed by folds axes and thrust segments virgations crossing the transfer zones. Thus inside a corridor, intensity of deformation gradually decreases from the core to the edges of the pop-up.

4.2. Role of transfer zones during hyperextended Mauleon rift reactivation: a drawer system

4.2.1. Definition of the drawer system

2D numerical modeling (Gómez-Romeu et al., 2019) and crustal cross-sections restorations (Teixell et al., 2016; Saspiturry et al., 2019c) demonstrate that the tertiary inversion of the Mauléon basin is possible through the underthrustings of the former rift margins, reactivating synrift detachments. Rift closure results in the formation of a N120° trending pop-up structure edged by antithetic thrust systems (i.e. North Pyrenean Frontal and Lakhoura thrust systems). However, we evidence in this study the lack of east-west continuity of the N120° compressive structures inside the Mauléon pop-up, shedding light of the 3D complexity of the whole structural framework (cf. 4.1.). In 3D, deformations are compartmentalized inside large-scale corridors bordered by N20° transfer zones, dividing laterally the thrust systems in several segments **(Fig. 12)**. The **Figure 13** proposes a temporal and spatial evolution of the Mauléon structural

template, synthetized in a conceptual "drawer system" model. We demonstrated that each N120° thrust segments is branching, from both sides, into N20° transfer zones, defining a drawer like geometry. Given that the whole Mauléon pop-up structure is edged by antithetic thrust systems, inside a corridor the same system is reproduced with antithetic thrusts superposing different drawers **(Fig. 13A)**. At the initiation of rift closure, due to the Iberian margin underthrusting, two drawers are upwards extruded, guided by antithetic thrusts which reactivating former normal faults. News antithetic thrusting appear, in a centripetal manner, as the shortening develops.

4.2.2. Scissor closure of the rift domain vs Labourd buttress impacting the evolution of the Mauléon basin drawer model

Two differing scenarios can be invoked to fit the current 3D Mauléon basin pop-up geometry, **Figures 13B and 13C** presenting respectively the scissor closure and the Labourd buttress scenarios.

In the scissor closure scenario, the shortening deformation propagates across the different corridors from East to West. The preliminary pop-up is circumscribed in the first corridor, resulting in the formation of two antithetic thrustings (**Fig. 13A and 13B** step T1, drawers a and a'). As inversion pursues, strain can no longer be entirely accommodated inside the preliminary pop-up and consequently migrates externally, leading to the underthrusting of two newly formed drawers (**Fig. 13A and 13B** step T2, drawers b and b'), the older ones being henceforth inactive (**Fig. 13A** step T2, drawers a and a'). The pop-up is thus tightening and slightly uplifted. At the same time, strain also migrates laterally in the second corridor, on two newly formed antithetic drawers (**Fig. 13B** step T2). In a more advanced time step, the same process of shortening, by stages, propagates westward in the third corridor and both the first and the second corridors are characterized by the underthrusting of two newly formed drawers (**Fig. 13A and 13B** step T3, drawers c and c'). Thus, the scissor closure scenario, drived by the plate kinematic motion, is responsible for the westward formation of the Mauléon basin pop-up.

In the Labourd buttress scenario, the shortening deformation propagates across the different corridors from West to East. The preliminary pop-up develops synchronously in the three corridors, with the underthrusting of two antithetic drawers in each corridor (**Fig. 13A and 13C** step T1, drawers a and a'). As inversion continues, the Labourd buttress inhibits strain propagation inside the neighboring third corridor. By contrast, in the second and in the first corridors, shortening can pursue, resulting in the development of two newly antithetic drawers in each corridor (**Fig. 13A and 13C** step T2, drawers b and b'). In last stage of compression, strain can no longer be accommodated in the second corridor while in the first one two newly drawers form (**Fig. 13A and 13C** step T2, drawers c and c'). Thus, the Labourd buttress scenario is responsible for the eastward formation of the Mauléon basin pop-up as it is inhibited to the west by the Labourd buttress.

Both the scissor closure and the Labourd buttress scenarios would lead to the same 3D current geometries, in other words: (1) an eastward tightened and uplifted pop-up, (2) heterogeneous shortening rates on both sides of transfer zones, but homogeneous inside a same corridor, (3) eastward increase, by stages, of both the shortening rates and the post-collisional Tmax of the Lakhoura thrust footwall in response to crust thickening and (4) the N-S gradual decrease, inside each corridor, of the deformation intensity from the core to the pop-up edges.

4.3. The non-cylindrical shape of the Pyrenean belt: result of inherited lithospheric segmentation

4.3.1. Pamplona and Barlanès inherited lithospheric transfer zones

Classically, the N20° Pamplona fault is not considered as a well-defined fault plane that can be observed at the outcrop scale, but rather as a broad lithospheric structure (Schoeffler, 1982; Rat et al., 1983; Richard, 1986; Razin, 1989; Claude, 1990). Indeed, the Pamplona transfer zone controlled the shift towards the southwest of the Early Cretaceous Pyrenean rift axis and has been recently interpreted as inherited from Permian time (Saspiturry et al., 2019b). As the Pamplona transfer zone, the Barlanès one plays a very

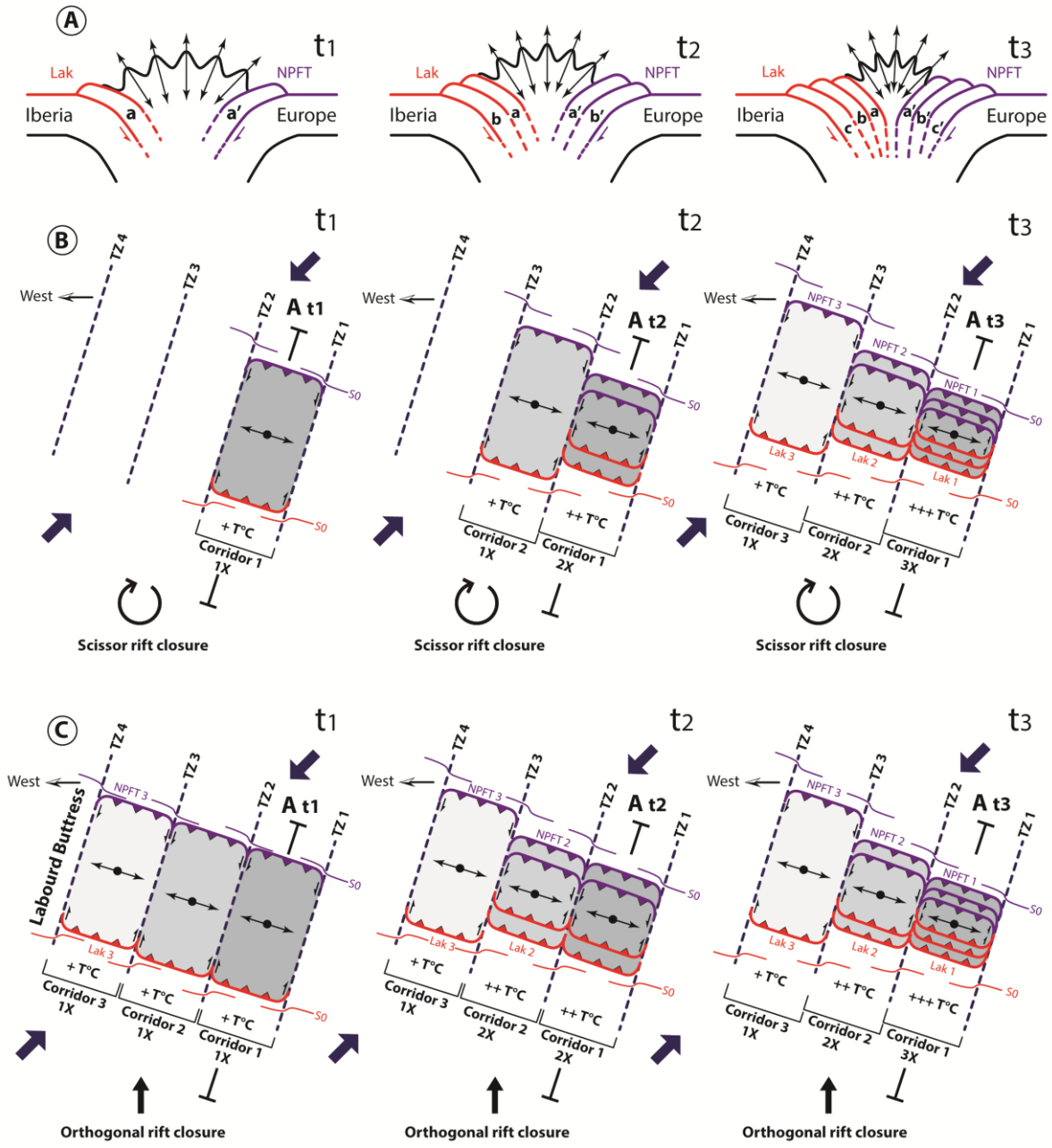


Fig. 13. (A) South-North cross-section showing the geometry of the Mauléon basin pop-up to the east of the Barlanès transfer zone through time; **(B)** Map view of drawer system model impacted by scissor rift closure; **(C)** Map view of drawer system model impacted by the Labourd buttress. The antithetic black arrows represent the sigma 1 direction; t1, t2, t3: time step; Lak: Lakhoura thrust system; NPFT: North Pyrenean Frontal thrust system; X: shortening rate; S0: strata plunge; T°C: Lakhoura thrust system footwall syn-collisional temperature; a-a', b-b', c-c' correspond respectively to active drawers during t1 time step, t2 time step and t3 time step; TZ1, TZ2, TZ3, TZ4 correspond respectively Ossau, Barlanès, Saison, Iholdy transfer zones; Lak 1, Lak 2, Lak 3 correspond respectively to the Lakhoura thrust segments 1, 2 and 3; NPFT 1, NPFT 2, NPFT 3 correspond respectively to the North Pyrenean Frontal thrust segments 1, 2 and 3.

substantial role during the Early Cretaceous hyperextension. It is responsible for the local denudation of the sub-continental mantle (Debroas et al., 2010; Canérot. 2017), currently evidenced by the presence of mantle clast in the synrift Urdach breccias (Roux, 1983; Fortané et al., 1986; Jammes et al., 2009; Debroas et al., 2010; Lagabrielle et al., 2010). It implies that the Barlanès transfer zone root at depth in the lithospheric mantle at the end of the Cretaceous hyperextension.

4.3.2. Tertiary structural discrepancies from both sides of the Barlanès lithospheric transfer zone

Two restored N20° balanced cross-sections separated laterally by 50 km have been proposed from both sides of the N20° Barlanès transfer zone (Teixell et al., 2016;

Saspiturry et al., 2019c). These restorations agree on the southward and northward thrusting of respectively the Iberian and European proximal rift margins and the propagation of the thin-skinned and thick-skinned structures outward of the pop-up. Nevertheless, the major discrepancy of the total shortening rates, documented in these sections shed light on the non-cylindrical shape of the Mauléon basin. Indeed, from these restorations, total shortening rates are estimated of respectively ~67 km to the west, i.e. 31% (Saspiturry et al., 2019c) and ~120 km to the east, i.e. 50% (Teixell et al., 2016). As well, they strongly differ from the compressive tectonic reactivation styles at the origin of the formation of the Mauléon basin pop-up.

To the west of the lithospheric Barlanès transfer zone, the last active extensional Lakhoura detachment system is reactivated as thrusting and accommodates the quasi-entire shortening of the Iberian rift margin (**Fig. 14A**; Saspiturry et al., 2019c). On the European margin, no major synrift structure was available for reactivation leading to the formation of thin-skinned nappe stack rooting at depth on the Lakhoura thrust. Synchronously, a blind in-sequence duplex-like crustal stack that propagates downward develop on the European basement. As compression continue, no major accommodation of the compressive strain was possible in the block of shallow mantle, exhumed during the Early Cretaceous hyperextension which thus acts as a major rigid buttress. This mode of rift inversion prevents the cold and strong mantle to be buried at depth.

To the east of the lithospheric Barlanès transfer zone, the middle continental crust is responsible for the compartimentalisation of the deformation between the upper and lower crust (**Fig. 14B**; Teixell et al., 2016). It implies the indentation of the European continental crust within the Iberian one, at the limit between the Iberian upper and lower crusts. The resulting "crocodile structure" is responsible for the burial of the previously exhumed sub-continental mantle under the Iberian crust and the quasi-complete closure of the former rift system. This mode of rift inversion attests of the current 30 km Moho depth under the basin **(Fig. 14)** and could be consistent with the absence of positive Bouguer anomaly to the east of the Barlanès transfer zone **(Fig. 1)**.

The significant discrepancy of the Tertiary reactivation style, global shortening rates and the shift from 10 km to 30 km of the Moho depth from both sides of the Barlanès transfer zone, attest for the impact of this latter at the lithospheric scale as well during the rifting phase as during the tertiary rift closure. The Pamplona and Barlanès lithospheric transfer zones currently edged the both border of the strong positive Bouguer anomaly localized under the Mauléon basin (Grandjean, 1992, 1994; Casas et al., 1997) interpreted as the presence of lithospheric mantle at ~ 10 km depth (Wang et al., 2016). Therefore, the preservation of this piece of rigid mantle is clearly favored by the occurrence of these two inherited major lithospheric transfer zones.

4.3.3. From crustal to lithospheric scale drawer system model

In the same way as we have identified at the crustal Mauléon scale drawer system (cf. 4.2.), the occurrence of these lithospheric transfer zones (i.e. Barlanès and Pamplona) supports the fact that the drawer system model could be applied at the lithospheric scale as well. It could explain the major discrepancy of the average shortening rates between western and eastern Pyrenees. Indeed, the restorations of balanced cross-sections across the Central and Eastern Pyrenees shows global shortening values ranging from 120 to 165 km (Roure et al., 1989; Muñoz, 1992; Vergés et al., 1995; Beaumont et al., 2000; Mouthereau et al., 2014; Grool et al., 2018; Teixell et al., 2018; Espurt et al., 2019), whereas the western Pyrenees shortening values range from 67 to 120 km (Teixell et al., 2016; Saspiturry et al., 2019c). These differences do not correspond to coherent spatial variabilities. They could be partly inherent to the initial authors' statements, i.e. notably the width of the exhumed sub-continental mantle domain. Nevertheless, this study evidenced that they are largely controlled by the inherited lithospheric scale segmentation of the Pyrenees, causing its non-cylindrical shape. The major discrepancy between the Western and Eastern Pyrenees implies the presence of at least another major lithospheric transfer

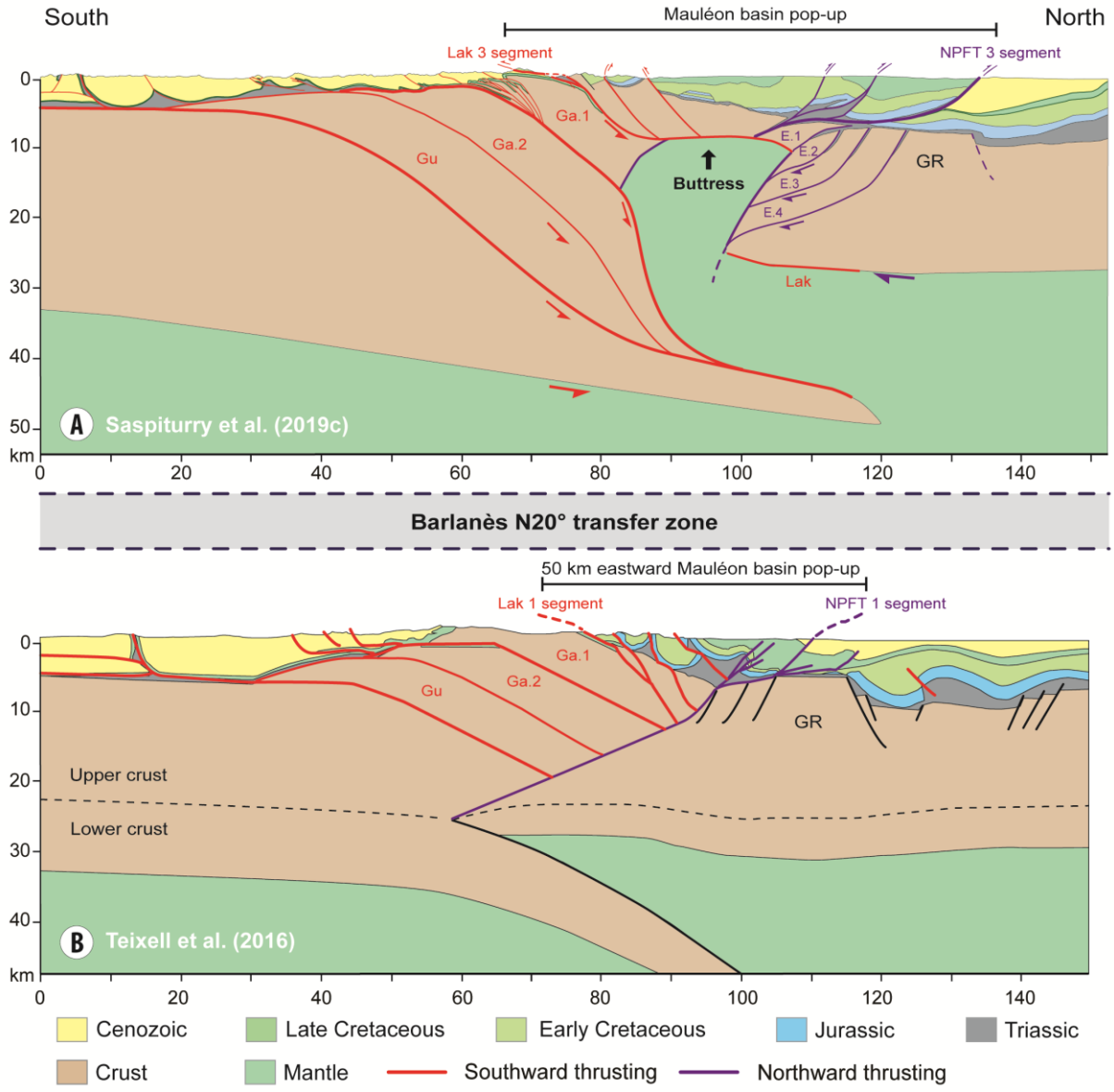


Fig. 14. Western Pyrenees N20° Crustal-scale balanced cross section, **(A)** to the west of the Barlanès transfer zone (Saspiturry et al., 2019c) and **(B)** to the east of the Barlanès transfer zone (Teixell et al., 2016). Thrust faults: Gu—Guarga; Ga.2—Gavarnie.2; Ga.1—Gavarnie.1; Lak—Lakhoura; SA—South Arbailles; NA—North Arbailles; St-P—Saint-Palais; Bel—Bellevue; St-S—Sainte-Suzanne. Structural units: E.1—European crustal unit 1; E.2—European crustal unit 2; E.3—European crustal unit 3; E.4—European crustal unit 4; GR—Grand Rieu. Location on figure. 1A.

zone responsible for the partitioning of the compressive strain at the scale of the Pyrenees. This structure could correspond to the Toulouse transfer zone, known to be lithospheric (Chevrot et al., 2015, 2018), and to be inherited from the Late Carboniferous to Permian time as well (Burg et al., 1994).

5. CONCLUSIONS

Seismic interpretation, RSMC thermometry, paleostress reconstruction and 3D implicit modeling bring out the presence of N20° crustal transfer zones in the Mauléon basin. The latter do not correspond to single fault planes but rather to strain accommodation zones between corridors inside which the shortening rates differ each others. Antithetic segmented thrust systems branching onto the transfer zones define an overall pattern presented as a drawer system model allowing the closure, by stages, of the former rift domain. This crustal deformation mode provided the current non-cylindrical shape of the inverted hyperextended Mauléon rift basin. In the same way, the drawer system model could be upscale to the lithosphere. This work highlights the importance to include such

major lithospheric transfer zones as data controlling future plate kinematic reconstructions to better reflect the non-cylindrical shape of the Pyrenean realm.

ACKNOWLEDGMENTS

This work is part of Saspiturry's Ph.D. research conducted as part of the OROGEN project, cofunded by Total S.A., BRGM, and CNRS. We thank OROGEN project managers Sylvain Calassou (Total), Emmanuel Masini (Total), Olivier Vidal (Centre National de Recherche Scientifique) and Isabelle Thinon (BRGM).

REFERENCES

Acocella, V., Faccenna, C., Funiciello, R., Rossetti, F., 1999. Sand-box modelling of basement-controlled transfer zones in extensional domains. Terra Nova 11, 149–156.

Acocella, V., Gudmundsson, A., Funiciello, R., 2000. Interaction and linkage of extension fractures and normal faults: examples from the rift zone of Iceland. J. Struct. Geol. 22, 1233–1246. https://doi.org/10.1016/S0191-8141(00)00031-6

Acocella, V., Morvillo, P., Funiciello, R., 2005. What controls relay ramps and transfer faults within rift zones? Insights from analogue models. J. Struct. Geol. 27, 397–408. https://doi.org/10.1016/j.jsg.2004.11.006

Angelier, J., 1985. Extension and rifting: the Zeit region, Gulf of Suez. J. Struct. Geol. 7, 605–612. https://doi.org/10.1016/0191-8141(85)90032-X

Aug, C., 2004, Modélisation géologique 3D et caractérisation des incertitudes par la méthode du champ de potentiel. 198. Doctoral thesis, E.N.S. des Mines de Paris, Paris.

Autin, J., Bellahsen, N., Leroy, S., Husson, L., Beslier, M.-O., d'Acremont, E., 2013. The role of structural inheritance in oblique rifting: Insights from analogue models and application to the Gulf of Aden. Tectonophysics 607, 51–64. https://doi.org/10.1016/j.tecto.2013.05.041

Basile, C., 2015. Transform continental margins — part 1: Concepts and models. Tectonophysics 661, 1–10. https://doi.org/10.1016/j.tecto.2015.08.034

Beaumont, C., Muñoz, J.A., Hamilton, J., Fullsack, P., 2000. Factors controlling the Alpine evolution of the central Pyrenees inferred from a comparison of observations and geodynamical models. J. Geophys. Res. 105, 8121–8145.

Behn, M.D., Lin, J., 2000. Segmentation in gravity and magnetic anomalies along the US East Coast passive margin: Implications for incipient structure of the oceanic lithosphere. J. Geophys. Res. Solid Earth 105, 25769–25790.

Bellahsen, N., Daniel, J.M., 2005. Fault reactivation control on normal fault growth: an experimental study. J. Struct. Geol. 27, 769–780.

Bellahsen, N., Leroy, S., Autin, J., Razin, P., d'Acremont, E., Sloan, H., Pik, R., Ahmed, A., Khanbari, K., 2013. Pre-existing oblique transfer zones and transfer/transform relationships in continental margins: New insights from the southeastern Gulf of Aden, Socotra Island, Yemen. Tectonophysics 607, 32–50. https://doi.org/10.1016/j.tecto.2013.07.036

Beyssac, O., Goffé, B., Chopin, C., Rouzaud, J.N., 2002a. Raman spectra of carbonaceous material in metasediments: a new geothermometer. J. Metamorph. Geol. 20, 859–871.

Beyssac, Olivier, Rouzaud, J.-N., Goffe, B., Brunet, F., Chopin, C., 2002b. Graphitization in a high-pressure, low-temperature metamorphic gradient: a Raman microspectroscopy and HRTEM study. Contrib. Mineral. Petrol. 143, 19–31.

Boillot, G., Beslier, M.O., Krawczyk, C.M., Rappin, D., Reston, T.J., 1995. The formation of passive margins: constraints from the crustal structure and segmentation of the deep Galicia margin, Spain. Geol. Soc. Lond. Spec. Publ. 90, 71–91.

Boissonnas, J., Le Pochat, G., Thibault, C., Bernatzk, M., 1974. Carte géologique de la France au 1/50000; feuille d'Iholdy, Orléans, France.

Bosworth, W., 1994. A model for the three-dimensional evolution of continental rift basins, north-east Africa. Geol. Rundsch. 83, 671–688.

Bosworth, W., 2015. Geological Evolution of the Red Sea: Historical Background, Review, and Synthesis. pp. 45–78.

Burg, J.-P., Van Den Driessche, J., Brun, J.-P., 1994. Syn- to post-thickening extension : mode and consequences. Comptes Rendus Académie Sci. Sér. 2 Sci. Terre Planètes 319, 1019–1032.

Calassou, S., Larroque, C., Malavieille, J., 1993. Transfer zones of deformation in thrust wedges: an experimental study. Tectonophysics 221, 325–344.

Canérot, J., 1989. Rifting éocrétacé et halocinèse sur la marge ibérique des Pyrénées Occidentales (France). Conséquences structurales. Bull. Cent. Rech. Explor.-Prod. Elf-Aquitaine 13, 87–99.

Canérot, J., 2008. Les Pyrénées: Histoire géologique. Atlantica.

Canérot, J., 2017. The pull apart-type Tardets-Mauléon Basin, a key to understand the formation of the Pyrenees. Bull. Société Géologique Fr. 188, 35. https://doi.org/10.1051/bsgf/2017198

Canérot, J., Hudec, M.R., Rockenbauch, K., 2005. Mesozoic diapirism in the Pyrenean orogen: Salt tectonics on a transform plate boundary. AAPG Bull. 89, 211–229. https://doi.org/10.1306/09170404007

Casas, A., Kearey, P., Rivero, L., Adam, C.R., 1997. Gravity anomaly map of the Pyrenean region and a comparison of the deep geological structure of the

western and eastern Pyrenees. Earth Planet. Sci. Lett. 150, 65–78.

Castéras, M., Canérot, J., Paris, J., Tisin, D., Azambre, M., Alimen, H., 1970. Carte géologique de la France au 1/50000; feuille d'Oloron Sainte Marie, Orléans, France.

Casteras, M., Gottis, M., Clin, M., Guignard, J.., Paris, J., Galharague, J., 1971. Carte géologique de la France au 1/ 50 000, feuille deTardets–Sorholus, Orléans, France.

Chevrot, S., Sylvander, M., Diaz, J., Ruiz, M., Paul, A., the PYROPE Working Group, 2015. The Pyrenean architecture as revealed by teleseismic P-to-S converted waves recorded along two dense transects. Geophys. J. Int. 200, 1094–1105. https://doi.org/10.1093/gji/ggu400

Chevrot, S., Sylvander, M., Diaz, J., Martin, R., Mouthereau, F., Manatschal, G., Masini, E., Calassou, S., Grimaud, F., Pauchet, H., Ruiz, M., 2018. The non-cylindrical crustal architecture of the Pyrenees. Sci. Rep. 8, 9591. https://doi.org/10.1038/s41598-018-27889-x

Chilès, J. P., et al., 2006, Modelling the geometry of geological units and its uncertainty in 3D from structural data: the potential-field method. In: C. Australasian Institute of Mining and Metallurgy, Victoria (Ed.) Orebody modelling and strategic mine planning - Uncertainty and risk management models. Spectrum Series, 329-336.

Chorowicz, J., 1989. Transfer and transform fault zones in continental rifts: examples in the Afro-Arabian Rift System. Implications of crust breaking. J. Afr. Earth Sci. Middle East 8, 203–214. https://doi.org/10.1016/S0899-5362(89)80025-9

Chorowicz, J., Sorlien, C., 1992. Oblique extensional tectonics in the Malawi Rift, Africa. Geol. Soc. Am. Bull. 104, 1015–1023.

Choukroune, P., 1976. Strain patterns in the Pyrenean chain. Philos. Trans. R. Soc. Lond. Math. Phys. Eng. Sci. 283, 271–280.

Choukroune, P., Mattauer, M., 1978. Tectonique des plaques et Pyrenees; sur le fonctionnement de la faille transformante nord-pyreneenne; comparaisons avec des modeles actuels. Bull. Société Géologique Fr. 7, 689–700.

Choukroune, P., ECORS Team, 1989. The ECORS Pyrenean deep seismic profile reflection data and the overall structure of an orogenic belt. Tectonics 8, 23–39.

Choukroune, P., Le Pichon, X., Seguret, M., Sibuet, J.-C., 1973a. Bay of Biscay and Pyrenees. Earth Planet. Sci. Lett. 18, 109–118.

Choukroune, P., Seguret, M., Galdeano, A., 1973b. Caracteristiques et evolution structurale des Pyrenees; un modèle de relations entre zone orogenique et mouvement des plaques. Bull. Société Géologique Fr. 7, 600–611.

Claude, D., 1990. Etude stratigraphique, sédimentologique et structurale des dépôts mésozoïques au nord du massif du Labourd: rôle de la faille de Pamplona (Pays Basque). Université de Bordeaux III.

Clerc, C., Lagabrielle, Y., Labaume, P., Ringenbach, J.-C., Vauchez, A., Nalpas, T., Bousquet, R., Ballard, J.-F., Lahfid, A., Fourcade, S., 2016. Basement – Cover decoupling and progressive exhumation of metamorphic sediments at hot rifted margin. Insights from the Northeastern Pyrenean analog. Tectonophysics 686, 82–97. https://doi.org/10.1016/j.tecto.2016.07.022

Cochran, J.R., Martinez, F., 1988. Evidence from the northern Red Sea on the transition from continental to oceanic rifting. Tectonophysics 153, 25–53.

Corti, G., van Wijk, J., Cloetingh, S., Morley, C.K., 2007. Tectonic inheritance and continental rift architecture: Numerical and analogue models of the East African Rift system. Tectonics 26, n/a-n/a. https://doi.org/10.1029/2006TC002086

d'Acremont, E., Leroy, S., Beslier, M.-O., Bellahsen, N., Fournier, M., Robin, C., Maia, M., Gente, P., 2005. Structure and evolution of the eastern Gulf of Aden conjugate margins from seismic reflection data. Geophys. J. Int. 160, 869–890. https://doi.org/10.1111/j.1365-246X.2005.02524.x

Daignières, M., Séguret, M., Specht, M., Team, E., 1994. The Arzacq-western Pyrenees ECORS deep seismic profile, in: Hydrocarbon and Petroleum Geology of France. Springer, pp. 199–208.

de Saint Blanquat, M., Bajolet, F., Grand'Homme, A., Proietti, A., Zanti, M., Boutin, A., Clerc, C., Lagabrielle, Y., Labaume, P., 2016. Cretaceous mantle exhumation in the central Pyrenees: New constraints from the peridotites in eastern Ariège (North Pyrenean zone, France). Comptes Rendus Geosci. 348, 268–278. https://doi.org/10.1016/j.crte.2015.12.003

Debroas, E.J., 1978. Evolution de la fosse du flysch ardoisier de l'Albien superieur au Senonien inferieur (zone interne metamorphique des Pyrenees navarro-languedociennes). Bull. Société Géologique Fr. 7, 639–648.

Debroas, E.-J., 1987. Modèle de bassin triangulaire à l'intersection de décrochements divergents pour le fossé albo-cénomanien de la Ballongue (zone nord-pyrénéenne, France). Bull. Société Géologique Fr. 3, 887–898. https://doi.org/10.2113/gssgfbull.III.5.887

Debroas, E.J., 1990. Le flysch noir albo-cenomanien temoin de la structuration albienne a senonienne de la Zone nord-pyreneenne en Bigorre (Hautes-Pyrenees, France). Bull. Soc. Geol. Fr. VI, 273–285. https://doi.org/10.2113/gssgfbull.VI.2.273

Debroas, E.J., Canérot, J., Bilotte, M., 2010. Les brèches d'Urdach, témoins de l'exhumation du manteau pyrénéen dans un escarpement de faille vraconnien-cénomanien inférieur (Zone nord-pyrénéenne, Pyrénées-Atlantiques, France). Géologie Fr. 2, 53–63.

Debroas, E.J., Souquet, P., 1976. Sédimentogenèse et position structurale des flyschs crétacés du versant nord des Pyrénées centrales. Bull Bur Rech Géol Min I 305–320.

Ducasse, L., Velasque, P.-C., 1988. Géotraverse dans la partie occidentale des Pyrénées, de l'avant-pays aquitain au bassin de l'Ebre: effet d'une inversion structurale sur l'édification d'une chaîne intracontinentale. Université Paul Cézanne (Aix-Marseille). Faculté des sciences et techniques de Saint-Jérôme.

Ducasse, L., Velasque, P.-C., Muller, J., 1986. Glissement de couverture et panneaux basculés dans la région des Arbailles (Pyrénées occidentales): Un modèle évolutif crétacé de la marge nord-ibérique à l'Est de la transformante de Pamplona. Comptes Rendus Académie Sci. Sér. 2 Mécanique Phys. Chim. Sci. Univers Sci. Terre 303, 1477–1482.

Espurt, N., Angrand, P., Teixell, A., Labaume, P., Ford, M., de Saint Blanquat, M., Chevrot, S., 2019. Crustal-scale balanced cross-section and restorations of the Central Pyrenean belt (Nestes-Cinca transect): Highlighting the structural control of Variscan belt and Permian-Mesozoic rift systems on mountain building. Tectonophysics 764, 25–45.

Etheridge, M.A., Branson, J.C., Stuart-Smith, P.G., 1987. The Bass, Gippsland and Otway basins, southeast Australia: a branched rift system formed by continental extension.

Fabriès, J., Lorand, J.-P., Bodinier, J.-L., Dupuy, C., 1991. Evolution of the Upper Mantle beneath the Pyrenees: Evidence from Orogenic Spinel Lherzolite Massifs. J. Petrol. Special_Volume, 55–76. https://doi.org/10.1093/petrology/Special_Volume.2.55

Fabriès, J., Lorand, J.-P., Bodinier, J.-L., 1998. Petrogenetic evolution of orogenic lherzolite massifs in the central and western Pyrenees. Tectonophysics 292, 145–167.

Ferrer, O., Roca, E., Benjumea, B., Muñoz, J.A., Ellouz, N., MARCONI Team, 2008. The deep seismic reflection MARCONI-3 profile: Role of extensional Mesozoic structure during the Pyrenean contractional deformation at the eastern part of the Bay of Biscay. Mar. Pet. Geol. 25, 714–730. https://doi.org/10.1016/j.marpetgeo.2008.06.002

Fortané, A., Duée, G., Lagabrielle, Y., Coutelle, A., 1986. Lherzolites and the western "Chaînons Béarnais" (French Pyrenees): Structural and paleogeographical pattern. Tectonophysics 129, 81–98. https://doi.org/10.1016/0040-1951(86)90247-7

Fossen, H., Rotevatn, A., 2016. Fault linkage and relay structures in extensional settings—A review. Earth-Sci. Rev. 154, 14–28. https://doi.org/10.1016/j.earscirev.2015.11.014

Fossen, H., Schultz, R.A., Rundhovde, E., Rotevatn, A., Buckley, S.J., 2010. Fault linkage and graben stepovers in the Canyonlands (Utah) and the North Sea Viking Graben, with implications for hydrocarbon migration and accumulation. AAPG Bull. 94, 597–613. https://doi.org/10.1306/10130909088

Gawthorpe, R.L., Hurst, J.M., 1993. Transfer zones in extensional basins: their structural style and influence on drainage development and stratigraphy. J. Geol. Soc. 150, 1137–1152. https://doi.org/10.1144/gsjgs.150.6.1137

Gibbs, A.D., 1984. Structural evolution of extensional basin margins. J. Geol. Soc. 141, 609–620.

Gibbs, A.D., 1990. Linked fault families in basin formation. J. Struct. Geol. 12, 795–803. https://doi.org/10.1016/0191-8141(90)90090-L

Gómez-Romeu, J., Masini, E., Tugend, J., Ducoux, M., Kusznir, N., 2019. Role of rift structural inheritance in orogeny highlighted by the Western Pyrenees case-study. Tectonophysics 766, 131–150. https://doi.org/10.1016/j.tecto.2019.05.022

Gong, Z., Langereis, C.G., Mullender, T.A.T., 2008. The rotation of Iberia during the Aptian and the opening of the Bay of Biscay. Earth Planet. Sci. Lett. 273, 80–93. https://doi.org/10.1016/j.epsl.2008.06.016

Grandjean, G., 1992. Mise en évidence des structures crustales dans une portion de chaîne et de leur relation avec les bassins sédimentaires. Application aux Pyrénées occidentales au travers du Projet ECORS Arzacq-Pyrénées. Université des Sciences et Techniques du Languedoc.

Grandjean, G., 1994. Etude des structures crustales dans une portion de chaîne et de leur relation avec les bassins sédimentaires. Application aux Pyrénées occidentales. Bull Cent Rech Explor Prod Elf Aquitaine 18, 391–420.

Grool, A.R., Ford, M., Vergés, J., Huismans, R.S., Christophoul, F., Dielforder, A., 2018. Insights into the crustal-scale dynamics of a doubly vergent orogen from a quantitative analysis of its forelands: A case study of the eastern Pyrenees. Tectonics 37, 450–476.

Heddebaut, C., 1967. Observations tectoniques sur le massif des Aldudes (Basses-Pyrénées). CR Som Soc Géol Fr. Fasc 7, 280–281.

Heddebaut, C., 1973. Etudes géologiques dans les massifs paléozoïques basques. Université des Sciences et Techniques de Lille.

Henry, J., Richert, J.-P., Ruhland, M., 1968. Les apports de l'analyse structurale à la connaissance des Pyrénées occidentales. Bull. Serv. Carte Géologique Alsace Lorraine 21, 135–136.

Henry, J., Zolnaï, G., Le Pochat, G., Mondeilh, C., 1987. Carte géologique de la France au 1/50 000: feuille d'Orthez, Orléans, France.

Jammes, S., Manatschal, G., Lavier, L., Masini, E., 2009. Tectono-sedimentary evolution related to extreme crustal thinning ahead of a propagating ocean: Example of the western Pyrenees. Tectonics 28. https://doi.org/10.1029/2008TC002406

Lagabrielle, Y., Bodinier, J.-L., 2008. Submarine reworking of exhumed sub-continental mantle rocks: field evidence from the Lherz peridotites, French Pyrenees: Cretaceous exhumation of pyrenean mantle. Terra Nova 20, 11–21. https://doi.org/10.1111/j.1365-3121.2007.00781.x

Lagabrielle, Y., Labaume, P., de Saint Blanquat, M., 2010. Mantle exhumation, crustal denudation, and gravity tectonics during Cretaceous rifting in the Pyrenean realm (SW Europe): Insights from the geological setting of the lherzolite bodies. Tectonics 29. https://doi.org/10.1029/2009TC002588

Lagabrielle, Y., Clerc, C., Vauchez, A., Lahfid, A., Labaume, P., Azambre, B., Fourcade, S., Dautria, J.-M., 2016. Very high geothermal gradient during mantle exhumation recorded in mylonitic marbles and carbonate breccias from a Mesozoic Pyrenean palaeomargin (Lherz area, North Pyrenean Zone, France). Comptes Rendus Geosci. 348, 290–300. https://doi.org/10.1016/j.crte.2015.11.004

Lajaunie, C., et al., 1997, Foliation fields and 3D cartography in geology; principles of a method based on potential interpolation. Mathematical Geology, 29, 571-584.

Lahfid, A., Beyssac, O., Deville, E., Negro, F., Chopin, C., Goffé, B., 2010. Evolution of the Raman spectrum of carbonaceous material in low-grade metasediments of the Glarus Alps (Switzerland). Terra Nova 22, 354–360.

Larrasoaña, J.C., Parés, J.M., Millán, H., del Valle, J., Pueyo, E.L., 2003. Paleomagnetic, structural, and stratigraphic constraints on transverse fault kinematics during basin inversion: The Pamplona Fault (Pyrenees, north Spain). Tectonics 22. https://doi.org/10.1029/2002TC001446

Le Pichon, X., Bonnin, J., Francheteau, J., Sibuet, J.C., 1971a. Une hypothèse d'évolution tectonique du Golfe de Gascogne. Hist. Struct. Golfe Gasc. 2, 11–44.

Le Pichon, X., Sibuet, J.-C., 1971b. Western extension of boundary between European and Iberian plates during the Pyrenean orogeny. Earth Planet. Sci. Lett. 12, 83–88. https://doi.org/10.1016/0012-821X(71)90058-6

Le Pochat, G., Bolthenhagen, C., Lenguin, M., Lorsignol, S., Thibault, C., 1976. Carte géologique de France au 1/50 000: Mauléon-licharre, Orléans, France.

Le Pochat, G., Heddebaut, C., Lenguin, M., Lorsignol, S., Souquet, P., Muller, J., Roger, P., 1978. Carte Géologique de France au 1/50 000: St Jean Pied de Port, Orléans, France.

Leroy, S., Razin, P., Autin, J., Bache, F., d'Acremont, E., Watremez, L., Robinet, J., Baurion, C., Denèle, Y., Bellahsen, N., Lucazeau, F., Rolandone, F., Rouzo, S., Kiel, J.S., Robin, C., Guillocheau, F., Tiberi, C., Basuyau, C., Beslier, M.-O., Ebinger, C., Stuart, G., Ahmed, A., Khanbari, K., Al Ganad, I., de Clarens, P., Unternehr, P., Al Toubi, K., Al Lazki, A., 2012. From rifting to oceanic spreading in the Gulf of Aden: a synthesis. Arab. J. Geosci. 5, 859–901. https://doi.org/10.1007/s12517-011-0475-4

Lister, G.S., Etheridge, M.A., Symonds, P.A., 1986. Detachment faulting and the evolution of passive continental margins. Geology 14, 246–250. https://doi.org/10.1130/0091-7613(1986)14<246:DFATEO>2.0.CO;2

Lucas, C., 1985. Le grès rouge du versant nord des Pyrénées: essai sur la géodynamique de dépôts continentaux du permien et du trias.

Masini, E., Manatschal, G., Tugend, J., Mohn, G., Flament, J.-M., 2014. The tectono-sedimentary evolution of a hyper-extended rift basin: the example of the Arzacq–Mauléon rift system (Western Pyrenees, SW France). Int. J. Earth Sci. 103, 1569–1596. https://doi.org/10.1007/s00531-014-1023-8

Masson, D.G., Miles, P.R., 1984. Mesozoic seafloor spreading between Iberia, Europe and North America. Mar. Geol. 56, 279–287. https://doi.org/10.1016/0025-3227(84)90019-7

McClay, K., Khalil, S., 1998. Extensional hard linkages, eastern Gulf of Suez, Egypt. Geology 26, 563–566.

Milani, E.J., Davison, I., 1988. Basement control and transfer tectonics in the Recôncavo-Tucano-Jatobá rift, Northeast Brazil. Tectonophysics 154, 41–70.

Mohriak, W.U., Leroy, S., 2013. Architecture of rifted continental margins and break-up evolution: insights from the South Atlantic, North Atlantic and Red Sea–Gulf of Aden conjugate margins. Geol. Soc. Lond. Spec. Publ. 369, 497–535.

Morley, C.K., Nelson, R.A., Patton, T.L., Munn, S.G., 1990. Transfer zones in the East African rift system and their relevance to hydrocarbon exploration in rifts (1). AAPG Bull. 74, 1234–1253.

Mortimer, E.J., Paton, D.A., Scholz, C.A., Strecker, M.R., 2016. Implications of structural inheritance in oblique rift zones for basin compartmentalization: Nkhata Basin, Malawi Rift (EARS). Mar. Pet. Geol. 72, 110–121. https://doi.org/10.1016/j.marpetgeo.2015.12.018

Moustafa, A.R., 1996. Internal structure and deformation of an accommodation zone in the northern part of the Suez rift. J. Struct. Geol. 18, 93–107. https://doi.org/10.1016/0191-8141(95)00078-R

Moustafa, A.R., 1997. Controls on the development and evolution of transfer zones: the influence of basement structure and sedimentary thickness in the Suez rift and Red Sea. J. Struct. Geol. 19, 755–768.

Mouthereau, F., Filleaudeau, P.-Y., Vacherat, A., Pik, R., Lacombe, O., Fellin, M.G., Castelltort, S., Christophoul, F., Masini, E., 2014. Placing limits to shortening evolution in the Pyrenees: Role of margin architecture and implications for the Iberia/Europe convergence. Tectonics 33, 2014TC003663. https://doi.org/10.1002/2014TC003663

Muller, J., Roger, P., 1977. L'Evolution structurale des Pyrénées (Domaine central et occidental) Le segment hercynien, la chaîne de fond alpine. Géologie Alp. 53, 149–191.

Muñoz, J.A., 1992. Evolution of a continental collision belt: ECORS-Pyrenees crustal balanced cross-section, in: McClay, K.R. (Ed.), Thrust Tectonics. Springer Netherlands, pp. 235–246. https://doi.org/10.1007/978-94-011-3066-0_21

Olivet, J.L., 1996. La cinématique de la plaque ibérique. Bull Cent Rech Explor Prod Elf Aquitaine 20, 131–195.

Pedreira, D., Pulgar, J.A., Gallart, J., Torné, M., 2007. Three-dimensional gravity and magnetic modeling of crustal indentation and wedging in the western Pyrenees-Cantabrian Mountains. J. Geophys. Res. 112. https://doi.org/10.1029/2007JB005021

Péron-Pinvidic, G., Manatschal, G., Masini, E., Sutra, E., Flament, J.M., Haupert, I., Unternehr, P., 2015. Unravelling the along-strike variability of the Angola–Gabon rifted margin: a mapping approach. Geol. Soc. Lond. Spec. Publ. 438, 49–76. https://doi.org/10.1144/SP438.1

Peybernès, B., 1978. Dans les Pyrenees la paleogeographie antecenomanienne infirme la theorie d'un coulissement senestre de plusieurs centaines de kilometres le long de la "faille nord-pyreneenne" des auteurs. Bull. Société Géologique Fr. S7-XX, 701–709. https://doi.org/10.2113/gssgfbull.S7-XX.5.701

Puigdefàbregas, C., Souquet, P., 1986. Tecto-sedimentary cycles and depositional sequences of the Mesozoic and Tertiary from the Pyrenees. Tectonophysics 129, 173–203.

Rat, P., Amiot, M., Feuillée, P., Floquet, M., Mathey, B., Pascal, A., Salomon, J., García Mondéjar, J., Pujalte, J., Lamolda, M., others, 1983. Vue sur le Cretacé basco-cantabrique et nord-ibérique. Une Marge Son Arriere-Pays Ses Environ. Sedimentaires Memoires Geol. Univ. Dijon 9, 191.

Razin, P., 1989. Evolution tecto-sédimentaire alpine des Pyrénées basques à l'ouest de la transformante de Pamplona, Province du Labourd. Bordeaux 3.

Reynolds, D.J., Rosendahl, B.R., 1984. Tectonic expressions of continental rifting. EOS Trans Am Geophys Union 65, 1055.

Richard, P., 1986. Structure et évolution alpine des massifs paléozoïques du Labourd (Pays Basque français). Éditions du Bureau de recherches géologiques et minières.

Richert, J.-P., 1967. Analyse structurale du pays basco-béarnais entre les Gaves de Mauléon et d'Oloron, Basses-Pyrénées (PhD Thesis).

Richert, J.-P., 1968. Analyse structurale de la zone charnière entre le Béarn et le Pays Basque. Bull. Serv. Carte Géologique Alsace Lorraine 21, 137–164.

Roca, E., Muñoz, J.A., Ferrer, O., Ellouz, N., 2011. The role of the Bay of Biscay Mesozoic extensional structure in the configuration of the Pyrenean orogen: Constraints from the MARCONI deep seismic reflection survey. Tectonics 30. https://doi.org/10.1029/2010TC002735

Rosenbaum, G., Lister, G.S., Duboz, C., 2002. Relative motions of Africa, Iberia and Europe during Alpine orogeny. Tectonophysics 359, 117–129. https://doi.org/10.1016/S0040-1951(02)00442-0

Roure, F., Choukroune, P., Berastegui, X., Munoz, J.A., Villien, A., Matheron, P., Bareyt, M., Seguret, M., Camara, P., Deramond, J., 1989. Ecors deep seismic data and balanced cross sections: Geometric constraints on the evolution of the Pyrenees. Tectonics 8, 41–50. https://doi.org/10.1029/TC008i001p00041

Roux, J.-C., 1983. Recherches stratigraphiques et sédimentologiques sur les flyschs crétacés pyrénéens au sud d'Oloron (Pyrénées Atlantiques). Université Paul Sabatier de Toulouse (Sciences).

Saspiturry, N., Razin, P., Baudin, T., Serrano, O., Issautier, B., Lasseur, E., Allanic, C., Thinon, I., Leleu, S., 2019a. Symmetry vs. asymmetry of a hyper-thinned rift: Example of the Mauléon Basin (Western Pyrenees, France). Mar. Pet. Geol. 104, 86–105. https://doi.org/10.1016/j.marpetgeo.2019.03.031

Saspiturry, N., Cochelin, B., Razin, P., Leleu, S., Lemirre, B., Bouscary, C., Issautier, B., Serrano, O., Lasseur, E., Baudin, T., Allanic, C., 2019b. Tectono-sedimentary evolution of a rift system controlled by Permian post-orogenic extension and metamorphic core complex formation (Bidarray Basin and Ursuya dome, Western Pyrenees). Tectonophysics 768, 228180. https://doi.org/10.1016/j.tecto.2019.228180

Saspiturry, N., Razin, P., Allanic, C., Issautier, B., Baudin, T., Lasseur, E., Serrano, O., Leleu, S., 2019c, submitted, Closure of a hyperextended system in an orogenic lithospheric pop-up, Western Pyrenees: The role of mantle buttressing and rift structural inheritance: Terra Nova.

Saspiturry, N., Lahfid, A., Baudin, T., Guillou-Frottier, L., Razin, P., Issautier, B., Le Bayon, B., Serrano, O., Lagabrielle, Y and Corre, B., 2019d, submitted, Paleogeothermal Gradients across an Inverted Hyperextended Rift System: Example of the Mauléon Fossil Rift (Western Pyrenees): Tectonics.

Schoeffler, J., 1965. Une hypothèse sur la tectogénèse de la chaîne pyrénéenne et de ses abords. Bull Soc Géol Fr 7, 917–920.

Schoeffler, J., 1982. Les transversales basco-landaises. Bull. Cent. Rech. ELF-Aquitaine 6, 257–263.

Sibuet, J.-C., Srivastava, S.P., Spakman, W., 2004. Pyrenean orogeny and plate kinematics. J. Geophys. Res. Solid Earth 109, B08104. https://doi.org/10.1029/2003JB002514

Souquet, P., Peybènes, B., Bilotte, M., Debroas, E.-J., 1977. La chaîne alpine des Pyrénées. Géologie Alp. 53, 193–216.

Souquet, P., Debroas, E.-J., Boirie, J.-M., Pons, P., Fixari, G., Roux, J.-C., Dol, J., Thieuloy, J.-P., Bonnemaison, M., Manivit, H., others, 1985. Le groupe du Flysch noir (albo-cénomanien) dans les Pyrénées. Bull Cent Rech Exlpo-Prod Elf-Aquitaine Pau 9, 183–252.

Teixell, A., 1993. Coupe géologique du massif d'Igountze: implications sur l'évolution structurale de la bordure sud de la zone nord-pyrénéenne occidentale. Comptes Rendus Académie Sci. Sér. 2 Mécanique Phys. Chim. Sci. Univers Sci. Terre 316, 1789–1796.

Teixell, A., Labaume, P., Lagabrielle, Y., 2016. The crustal evolution of the west-central Pyrenees revisited: Inferences from a new kinematic scenario. Comptes Rendus Geosci. 348, 257–267. https://doi.org/10.1016/j.crte.2015.10.010

Teixell, A., Labaume, P., Ayarza, P., Espurt, N., de Saint Blanquat, M., Lagabrielle, Y., 2018. Crustal structure and evolution of the Pyrenean-Cantabrian belt: A review and new interpretations from recent concepts and data. Tectonophysics 724, 146–170. https://doi.org/10.1016/j.tecto.2018.01.009

Thinon, I., 1999. Structure profonde de la marge Nord Gascogne et du Bassin armoricain. Université de Bretagne occidentale-Brest.

Thinon, I., Matias, L., RÉhault, J.P., Hirn, A., Fidalgo-GonzÁlez, L., Avedik, F., 2003. Deep structure of the Armorican Basin (Bay of Biscay): a review of Norgasis seismic reflection and refraction data. J. Geol. Soc. 160, 99–116. https://doi.org/10.1144/0016-764901-103

Vergés, J., Millán, H., Roca, E., Muñoz, J.A., Marzo, M., Cirés, J., Bezemer, T.D., Zoetemeijer, R., Cloetingh, S., 1995. Eastern Pyrenees and related foreland basins: pre-, syn- and post-collisional crustal-scale cross-sections. Mar. Pet. Geol., Integrated Basin Studies 12, 903–915. https://doi.org/10.1016/0264-8172(95)98854-X

Vielzeuf, D., 1984. Relations de phases dans le faciès granulite et implications géodynamiques: l'exemple des granulites des Pyrénées. Université Clermont-Ferrand II.

Wang, Y., Chevrot, S., Monteiller, V., Komatitsch, D., Mouthereau, F., Manatschal, G., Sylvander, M., Diaz, J., Ruiz, M., Grimaud, F., Benahmed, S., Pauchet, H., Martin, R., 2016. The deep roots of the western Pyrenees revealed by full waveform inversion of teleseismic P waves. Geology 44, 475–478. https://doi.org/10.1130/G37812.1

Wopenka, B., Pasteris, J.D., 1993. Structural characterization of kerogens to granulite-facies graphite: applicability of Raman microprobe spectroscopy. Am. Mineral. 78, 533–557.

Young, M.J., Gawthorpe, R.L., Hardy, S., 2001. Growth and linkage of a segmented normal fault zone; the Late Jurassic Murchison–Statfjord North Fault, northern North Sea. J. Struct. Geol. 23, 1933–1952. https://doi.org/10.1016/S0191-8141(01)00038-4

Yui, T.-F., Huang, E., Xu, J., 1996. Raman spectrum of carbonaceous material: a possible metamorphic grade indicator for low-grade metamorphic rocks. J. Metamorph. Geol. 14, 115–124.

Zolnai, G., 1975. Sur l'existence d'un réseau de failles de décrochement dans l'avant-pays nord des Pyrénées occidentales. Rev Géogr Phys Géol Dynam Fr 17, 219–238.

Zwaan, F., Schreurs, G., Adam, J., 2018. Effects of sedimentation on rift segment evolution and rift interaction in orthogonal and oblique extensional settings: Insights from analogue models analysed with 4D X-ray computed tomography and digital volume correlation techniques. Glob. Planet. Change 171, 110–133. https://doi.org/10.1016/j.gloplacha.2017.11.002

Chapitre 5

Evolution thermique Mésozoïque à Cénozoïque

Bref aperçu du chapitre 5 : Evolution thermique Mésozoïque à Cénozoïque

Le chapitre 5 présente l'évolution thermique en 3D d'un système de rift hyper-étiré de sa création à sa réactivation. Il correspond à un article soumis dans le journal *Tectonics* en juillet 2019. Ce chapitre est basé sur l'analyse de plus de 150 données de pics de température Raman (réalisée au BRGM par A. Lahfid). Ces données de spectroscopie Raman ont été recueillies au sein de puits d'exploration pétrolière et sur le terrain, le long des principaux domaines structuraux crétacés du bassin hyper-étiré de Mauléon. L'étude des données Raman a été couplée à une modélisation numérique reproduisant l'évolution thermique des Pyrénées nord occidentales depuis 120 Ma (réalisée au BRGM par L. Guillou-Frottier).

Chapitre 5.1

Paléo-gradients géothermiques au sein d'un système rift hyper-étiré réactivé : exemple du rift fossile de Mauléon (Pyrénées occidentales)

Chapitre 5.1. Paleogeothermal Gradients across an Inverted Hyperextended Rift System: Example of the Mauléon Fossil Rift (Western Pyrenees)

Sommaire

Résumé étendu p. 303
Abstract p. 307
1. Introduction p. 307
2. The Mauléon basin Rift Domains and Sedimentary Infill p. 308
3. The Cretaceous Pyrenean Metasomatic Event p. 309
3.1. High Temperature – Low Pressure Metamorphism p. 309
3.2. Alkaline Magmatism, Albitization, and Talc Mineralization p. 310
4. Methods p. 311
4.1. RSCM Thermometry p. 311
4.2. Calculation of Paleogeothermal Gradients p. 311
5. Results p. 312
5.1. Iberian Proximal Margin p. 312
5.2. Iberian Necking Zone p. 313
5.3. Hyperextended Domain p. 313
5.4. European Necking Zone p. 317
5.5. European Proximal Margin p. 318
5.6. Thermal Evolution of the Hyperextended Domain: Numerical Simulation p. 320
5.6.1. Numerical Approach p. 320
5.6.2. Heat Equation, Boundary Conditions, and Thermal Properties p. 322
5.6.3. Thermal Pulse p. 322
5.6.4. Thermal Evolution p. 325
6. Discussion p. 325
6.1. Age of RSCM Peak Temperature p. 325
6.2. Synrift Paleogeothermal Gradient p. 326
6.2.1. Proximal Margins p. 326
6.2.2. Necking Zones p. 326
6.2.3. Hyperextended Domain p. 327
6.3. Thermal Anomaly and Gravity Anomaly p. 327
6.4. The Mauléon basin Internal Metamorphic Zone p. 328
6.5. Role of Rift Inheritance on Postcollisional Thermal Imprint p. 328
7. Conclusion p. 330
Acknowledgments p. 330
References p. 330
Supporting information S1 p. 339
Supporting information S2 p. 341
Eléments supplémentaires p. 343

Résumé étendu

La phase d'hyperextension prenant place entre l'Albien et le Cénomanien est responsable du développement d'un gradient géothermique anormalement élevé typique des zones de rifting. L'étude présentée dans le chapitre 5 est basée sur plus de 150 pics de température Raman (RSCM) et permet d'évaluer la répartition en 3D de cette anomalie thermique et son devenir au cours de la phase d'inversion du bassin de Mauléon. Cette étude a été couplée à une modélisation numérique reproduisant l'évolution thermique des Pyrénées nord occidentales depuis 120 Ma. L'anomalie thermique présente dans le bassin de Mauléon est acquise au cours de la phase d'hyperextension crétacée et perdure à minima jusqu'au Campanien comme en témoigne les séries du Santonien supérieur qui sont affectées par des températures relativement basses mais qui s'alignent sur ce gradient synrift. La température maximale atteinte par les séries prérifts à synrifts est contrôlée à la fois par l'enfouissement (« burial », épaisseur sédimentaire) et par le flux thermique arrivant en base du domaine hyper-étiré.

Le puits Orthez-102, situé sur la marge proximale européenne, traverse un chevauchement majeur (chevauchement de Sainte-Suzanne). L'unité supérieure allochtone enregistre un paléo-gradient de 34°C/km. Ce gradient est similaire à celui d'un domaine continental classique caractérisé par un gradient géothermique de 30°C/km et un flux de chaleur de 80 mW/m^2. Cette unité allochtone atteint 240°C à sa base et est transportée vers le nord sur une unité autochtone qui est restée plus froide. En effet, les séries apto-albiennes de l'unité autochtone atteignent au maximum 120°C alors que les mêmes niveaux stratigraphiques de l'unité allochtone présentent une température oscillant entre 160°C et 200°C. Par conséquent, l'unité autochtone du puits Orthez-102 est ici interprétée comme appartenant à un domaine plus proximal de la marge européenne. Le paléo-gradient de la marge proximale ibérique, quant à lui, n'a pas pu être estimé. En effet, les pics de températures Raman mesurés dans les séries campano-maestrichtiennes du « footwall » du chevauchement de Lakhoura (marge proximale ibérique) sont supérieurs à ceux mesurés dans les formations albiennes du « hanging-wall » (zone de « necking » ibérique), bien que ce dernier soit positionné dans une domaine crétacé plus distal. Par conséquent, les températures mesurées dans le footwall du chevauchement de Lakhoura ne représentent pas les paléo-températures maximales atteintes pendant le rifting crétacé. Elles ont été acquises au cours de la compression pyrénéenne.

Le paléo-gradient de la zone de « necking » ibérique a été approché par l'intermédiaire du puits Hasparren-101 et des unités structurales de Mendibelza et des Arbailles. Le puits Hasparren-101 présente un enregistrement thermique relativement complexe. La partie basale de l'unité allochtone est caractérisée par une température constante de 280°C entre 2,8 km et 5,1 km de profondeur, tandis que la partie supérieure de cette unité enregistre un gradient élevé de l'ordre de 62°C/km. Cette température constante dans la partie inférieure et ce gradient relativement élevé au sommet peuvent être liés à la circulation de fluides et ou à l'individualisation, au sein du bassin, d'une cellule de convection ou du moins d'une arrivée de fluides profonds et chauds au niveau de la partie basale. Ce puits n'a donc pas pu être utilisé pour calibrer le paléo-gradient de la zone de « necking » ibérique. L'unité de Mendibelza présente, quant à elle, un paléo-gradient compris entre 39°C/km et 46°C/km. Au sein de l'unité des Arbailles, les pics de températures mesurés augmentent vers les séries stratigraphiques les plus jeunes : 180°C dans le Jurassique contre 230°C à 250°C dans l'Albien. Cette anomalie peut s'expliquer par le fait que les isothermes, subhorizontaux, scellent la structure en bloc basculée des Arbailles datant du Cénomanien moyen. Le puits de Les Cassières-2 recoupe une succession sédimentaire bien préservée et non perturbée par la déformation pyrénéenne. Ce puits fait donc office de référence pour calibrer le paléo-gradient de la zone de « necking » européenne. Ce dernier est ici estimé entre 37°C/km et 40°C/km. Le puits de Bellevue-1 également positionné le long de la zone de « necking » européenne, recoupe une structure complexe correspondant à la réactivation au cours du Tertiaire d'une ride diapirique albienne. Le paléo-gradient estimé au sein de ce puits oscille entre 38°C/km et 47°C/km. Les zones de « necking » ibérique et européenne présentent des paléo-gradients similaires et légèrement supérieurs à celui d'un domaine continental stable.

Le paléo-gradient du domaine hyper-étiré du bassin de Mauléon a été calibré à partir des puits de Chéraute-1, Uhart-Mixe-1 et Ainhice-1. Le puits Ainhice-1, situé à la transition avec la zone de « necking » ibérique, présente un paléo-gradient de 57°C/km. Le puits Uhart-Mixe-1, situé au cœur du domaine hyper-étiré, est exempt de déformation pyrénéenne majeure et présente un paléo-gradient de l'ordre de 60°C/km. Le puits Chéraute-1, localisé à proximité du diapir de Roquiague, est caractérisé par une augmentation du pic de température Raman de 240°C à 330°C sur 5 350m d'épaisseur, lui conférant un gradient thermique déformé de 21°C/km. Ce faible gradient s'explique par l'effet de proximité du diapir où la forte conductivité des évaporites tend à homogénéiser la température des roches encaissantes. Par conséquent, le gradient géothermique estimé dans ce puits n'est pas représentatif du domaine hyper-étiré. Seuls les paléo-gradients estimés dans les puits Uhart-Mixe-1 et Ainhice-1 permettent d'attribuer un paléo-gradient anormalement élevé au domaine hyper-étiré du bassin de Mauléon.

Les paléo-gradients géothermiques déterminés dans cette étude varient donc significativement en fonction des unités structurales échantillonnées. Ces variations apparaissent clairement le long d'un transect proximal-distal. En effet, le gradient augmente de manière centripète depuis les marges proximales jusqu'au domaine hyper-étiré : ~ 34°C/km sur la marge proximale européenne, ~ 37-47°C/km sur les deux « necking zones » et ~ 57-60°C/km dans le domaine hyper-étiré. La modélisation thermique suggère que les valeurs de flux de chaleur dans le manteau pourraient avoir atteint de 100 mW.m-2 avant l'inversion du bassin de Mauléon dans le domaine où le paléo-gradient géothermique atteint une valeur de l'ordre de 60°C/km. Cette valeur est en accord avec celles généralement admises dans des systèmes analogues de rift. L'augmentation du gradient géothermique en direction du centre du bassin influe sur le comportement rhéologique de la croûte avec une déformation essentiellement fragile sur bordures du système de rift et passant à une déformation ductile en son centre. Ce point précis est détaillé dans l'article de Yves Lagabrielle (Annexe X) et sera discuté dans le chapitre suivant.

Compte tenu du paléo-gradient géothermique évalué à 60°C/km dans le puits d'Uhart-Mixe-1, nous pouvons extrapoler la température atteinte à la base du domaine hyper-étiré du bassin de Mauléon dans la couverture prérift, celle-ci oscillant entre 500-600°C. Ces températures sont similaires à celles mesurées dans la Zone Interne Métamorphique (ZIM) des Pyrénées centrales et orientales ainsi que dans la Nappes des Marbres du bassin Basque-cantabre. Cependant, dans le cas du bassin de Mauléon, ces températures sont confinées entre les structures de transferts de direction N0-20° de Saint-Jean-Pied-de-Port et du Saison. En effet, vers l'est (chaînons béarnais) et vers l'ouest (domaine de Saint-Jean-de-Luz), les données publiées mettent en évidence que les températures à la base du bassin n'excédent pas 350°C. Les structures transverses de Saint-Jean-de-Pied-de Port et du Saison, héritées de la phase de rifting permienne, semblent conditionner et segmenter de manière significative la thermicité au cours du rifting crétacé.

Les résultats de cette étude mettent en évidence que le paléo-gradient géothermique anormalement élevé coïncide avec l'anomalie gravimétrique positive présente sous le bassin de Mauléon. Cette dernière a récemment été interprétée comme la présence à faible profondeur de manteau sous-continental (~ 10 km) exhumé au cours de la phase d'hyperextension crétacée soulignant le lien étroit entre l'anomalie thermique et cet épisode de rifting. Ce gradient élevé a perduré à minima jusqu'au Campanien, soulevant la question du processus responsable de la subsidence au cours du Crétacé supérieur, préalablement considérée comme une subsidence thermique postrift classique. En l'absence de mesure de T-max, dans la pile sédimentaire post-santonienne aucun gradient thermique n'a été établi dans la série postrift. Cependant, la modélisation thermique impose une diminution du gradient géothermique dès le début du raccourcissement alpin. En effet, sans diminution de gradient, la base du bassin atteindrait des températures bien supérieures à 650°C, ce qui n'a jamais été observé par ailleurs dans la ZIM.

La déformation compressive dans les Pyrénées occidentales a été moins intense que dans les Pyrénées centrales et orientales, les sédiments de base de bassin et leur substratum métamorphisé n'ayant jamais été exhumés. En effet, l'inversion par chevauchement du système de rift nord pyrénéen est connue pour avoir débuté à la fin du Santonien dans les Pyrénées orientales. Dans les Pyrénées

occidentales les premiers chevauchements apparaissent au cours de l'Eocène supérieur. Ce diachronisme de la déformation révèle un raccourcissement plus important dans les Pyrénées centrales et orientales puisque la ZIM qui constitue la base du bassin des « Flysch ardoisiers » est à actuellement à l'affleurement et est érodée depuis l'Eocène (Formation de Palassou). La base du bassin de Mauléon, quant à elle, reste aujourd'hui préservée sous 6km de sédiments.

Comme présenté dans la partie 4 du présent chapitre, la réactivation du bassin de Mauléon induit la formation d'un pop-up. Les isothermes précédemment hérités de la phase de rifting crétacée ont été déformés et plissés en son centre. Le long de la marge européenne, les observations recueillies dans cette étude montrent que les isothermes liés à cette phase de rifting ont été préservés et transportés passivement sur la marge proximale. Le long de la marge ibérique, le chevauchement de Lakhoura est marqué par une augmentation des pic de températures RSCM dans son « footwall » suggérant que ces températures ont été atteintes après le charriage de la nappe, ne permettant pas de conserver la thermicité héritée du rifting le long de la marge proximale ibérique. La différence de réponse thermique de part et d'autre du pop-up de Mauléon semble être liée au style de déformation au cours de l'inversion pyrénéenne. Contrairement à la marge européenne (Bellevue and Sainte Suzanne « thin-skin thrusts »), la marge ibérique est affectée par une déformation pyrénéenne de type « thick-skin » responsable de la formation de la Zone Axiale, dont le chevauchement de Lakhoura représente l'unité supérieure. Une fois épaissie, la croûte contiendra davantage de sources de chaleur radiogénique ce qui se traduira par une augmentation du gradient géothermique. Dans le cas du bassin de Mauléon, le réchauffement au cours du Tertiaire de la paléo-marge ibérique est dû au « sous » empilement des nappes de Lakhoura, de Gavarnie et de Guarga. Au contraire, le domaine hyper-étiré du bassin de Mauléon et sa marge européenne sont caractérisés par une décroissance du gradient géothermique depuis l'amorce de la compression pyrénéenne jusqu'à nos jours. Le gradient actuel mesuré dans les puits pétroliers est de 25.0 ± 2.7°C/km. Dans ce cas, le faible gradient géothermique est contrôlé par une moyenne à faible épaisseur de croûte continentale européenne (de 5 à 25 km autrement dit par lala présence d'un manteau sous-continental à faible profondeur.

Chapitre 5.1. Paleogeothermal Gradients across an Inverted Hyperextended Rift System: Example of the Mauléon Fossil Rift (Western Pyrenees)

Saspiturry, N., Lahfid, A., Baudin, T., Guillou-Frottier, L., Razin, P., Issautier, B., Le Bayon, B., Serrano, O., Lagabrielle, Y and Corre, B., **submitted**, Paleogeothermal Gradients across an Inverted Hyperextended Rift System: Example of the Mauléon Fossil Rift (Pyrenees): ***Tectonics***.

Abstract

Examples of fossil and present-day passive margins resulting from mantle exhumation at the ocean–continent transition appear to have developed under conditions of high mantle heat flow. The pattern of geothermal gradients along these hyperextended margins at the time of rifting is of interest for exploration of geothermal and petroleum resources, but is difficult to access. The fossil rift in the North Pyrenean Zone, which underwent high temperature–low pressure metamorphism and alkaline magmatism during Early Cretaceous hyperextension, was studied to explore the geothermal regime at the time of rifting. Data from a set of 155 samples from densely spaced outcrops and boreholes, analyzed using Raman spectroscopy of carbonaceous material, shed light on the distribution of geothermal gradients across the inverted hyperextended Mauléon rift basin during Albian and Cenomanian time, its period of active extension. The estimated paleogeothermal gradient is strongly related to the structural position along the Albian-Cenomanian rift, increasing along a proximal-distal margin transect from ~34°C/km in the European proximal margin to ~37–47°C/km in the two necking zones and 57–60°C/km in the hyperextended domain. This pattern of the paleogeothermal gradient induced a complex competition between brittle and ductile deformation during crustal extension. A numerical modeling approach reproducing the thermal evolution of the North Pyrenees since 120 Ma suggests that mantle heat flow values may have peaked up to 100 mW.m-2 during the rifting event. We demonstrate that the style of reactivation during subsequent convergence influences the thermal structure of the inverted rift system.

1 Introduction

The processes responsible for hyperextension of the continental crust have been widely studied in the present-day Atlantic conjugate margins based on interpretation of borehole data and petroleum seismic reflection profiles, for example in central Norway and East Greenland (Weigel et al., 1995; Kodaira et al., 1998; Reston, 2007; Mjelde et al., 2001, 2008; Peron-Pinvidic et al., 2012a, 2012b, 2013), in Iberia and Newfoundland (Boillot et al., 1987, 1989; Driscoll et al., 1995; Manatschal et al., 2001; Péron-Pinvidic et al., 2007; Péron-Pinvidic & Manatschal, 2009; Reston, 2009; Pérez-Gussinyé, 2013; Haupert et al., 2016), and in Angola and Brazil (Karner et al., 2003; Contrucci et al., 2004; Moulin et al., 2005, 2010; Karner & Gambôa, 2007; Aslanian et al., 2009; Unternehr et al., 2010; Aslanian & Moulin, 2013). These systems have been numerically modeled to reproduce the paleogeometry of the continental margins and the detachment faults responsible for crustal thinning (Huismans & Beaumont, 2003, 2008, 2011, 2014; Lavier & Manatschal, 2006; Brune et al., 2014, 2016; Bai et al., 2019). These studies have shown that the Atlantic passive margins are characterized by three domains that increase in continental crustal thickness toward the craton: the hyperextended rift domain (less than 10 km thick), the necking zone (10–25 km thick) and the proximal margin (~30 km thick) (e.g. Péron-Pinvidic et al., 2015). The paucity of in situ tectonic and stratigraphic data available from the Atlantic passive margins has led researchers to study fossil passive margins in the Alps to better constrain the tectonic, sedimentary, and structural evolution of these margin domains (Lemoine et al., 1987; Froitzheim & Manatschal, 1996; Manatschal & Nievergelt, 1997; Manatschal et al., 2000, 2006, 2011; Masini et al., 2011, 2013; Mohn et al., 2012; Beltrando et al., 2014; Decarlis et al., 2015). However, few studies describe the thermal aspects of such hyperextended systems (Clerc, 2012; Vacherat et al., 2014; Clerc et al., 2015; Corre, 2017; Hart et al., 2017).

Recent work on the fossil passive margin of the North Pyrenean Zone has established that outcrops of subcontinental mantle identified

there (Fabriès et al., 1991, 1998) result from hyperextension of the continental crust during the Albian-Cenomanian rifting stage (Lagabrielle & Bodinier, 2008; Jammes et al., 2009; Lagabrielle et al., 2010; Clerc et al., 2014; Clerc & Lagabrielle, 2014; Masini et al., 2014; Tugend et al., 2015; Corre et al., 2016; Teixell et al., 2016; Saspiturry et al., 2019). In contrast to the fossil margins in the Alps, where the hyperextended rift and oceanic domains were lost to Cretaceous subduction (Rubatto et al., 1998; Stampfli et al., 1998; Handy et al., 2010), the prerift to postrift sediments preserved in the inverted Pyrenean rift margins retain the imprint of the synrift thermal regime. The North Pyrenean Zone is a privileged place to trace the thermal imprint of hyperextension from the proximal rift margins to the hyperextended domain. The high-temperature, low-pressure metamorphism recorded on the North Pyrenean Zone rift system (Ravier, 1957; Albarède & Michard-Vitrac, 1978a, 1978b; Golberg et al., 1986; Montigny et al., 1986; Golberg & Maluski, 1988; Golberg & Leyreloup, 1990) is interpreted as the consequence of continental crustal thinning during Early Cretaceous time (Choukroune & Mattauer, 1978; Debroas, 1990; Vielzeuf & Kornprobst, 1984; Clerc et al., 2015).

The work reported in this paper, based on Raman spectroscopy of carbonaceous material (RSCM) on the prerift to postrift sediments of the Mauléon basin in the North Pyrenean Zone, integrates paleotemperature data from 102 borehole samples and 54 outcrop samples. All the major domains of the Mauléon rift system were sampled in order to (1) obtain RSCM peak temperatures on the precollisional sedimentary infill, (2) examine the paleogeothermal gradients related to hyperextension in the proximal margin, necking zone, and hyperextended domain of the rift, and (3) define the effect of rift inheritance on the postcollisional thermal regime.

2. The Mauléon basin Rift Domains and Sedimentary Infill

In the western Pyrenees, the North Pyrenean Zone corresponds to the inverted Mauléon basin (**Fig. 1**; Souquet et al., 1977; Ducasse & Vélasque, 1988). This basin is offset by the N20°E-trending Iholdy, Saison, and Barlanès transfer zones (**Fig. 1b**; Canérot, 2008, 2018a, 2018b; Debroas et al., 2010). These transfer zones are inherited from the Permian rifting stage (Saspiturry et al., 2019b). The Iberian proximal margin corresponds to the Axial Zone, consisting of a Paleozoic substratum overlain by a postrift Late Cretaceous carbonate platform (Souquet, 1967), and the Paleozoic « Massifs Basques » (Muller & Roger, 1977) represent its western prolongation **(Fig. 2)**.

The well-defined Iberian necking zone, currently thrusted over the Axial Zone along the Lakhoura thrust (Teixell, 1993, 1998), is represented by the Mendibelza and Arbailles units **(Fig. 2B)**. The Mendibelza unit is composed of deep-sea Albian (synrift) and Late Cretaceous (postrift) deposits overlying a Devonian to Permian substratum (**Fig. 2A**; Boirie, 1981). The Arbailles unit is a syncline in which Paleozoic to Late Triassic sediments are underlied by Jurassic (prerift) and Early Cretaceous (synrift) carbonates and marls (**Fig. 2**; Casteras et al., 1971; Lenoble, 1992).

The Saint-Palais domain, bounded by the North Arbailles and Saint-Palais reactivated Albian-Cenomanian detachments, corresponds to the Mauléon basin hyperextended domain (**Fig. 2B**; Saspiturry et al., 2019a). This domain is composed of (1) a Mesozoic carbonate cover displaced by gravity slides upon underlying evaporites of Triassic to Hettangian (earliest Jurassic) age (Bouquet, 1986; Ducasse et al., 1986; Lagabrielle et al., 2010; Corre et al., 2016), (2) Albian to early Cenomanian (synrift) marls and fine-grained turbidites of the Black Flysch group (Fixari, 1984; Souquet et al., 1985), and (3) Late Cretaceous turbidites derived from the North Aquitaine carbonate platform on the European (northern) margin (Razin, 1989; Claude, 1990).

The European necking zone and the European proximal margin are respectively represented by the Bellevue and Sainte-Suzanne units, separated by the Bellevue thrust **(Fig. 2B)**. Both are composed of a Jurassic to Albian carbonate platform and Late Cretaceous turbidites. The European margin is thrusted northward over the Arzacq basin on the Sainte-Suzanne thrust (**Fig. 2B**; Daignières et al., 1994; Teixell, 1998; Serrano et al., 2006).

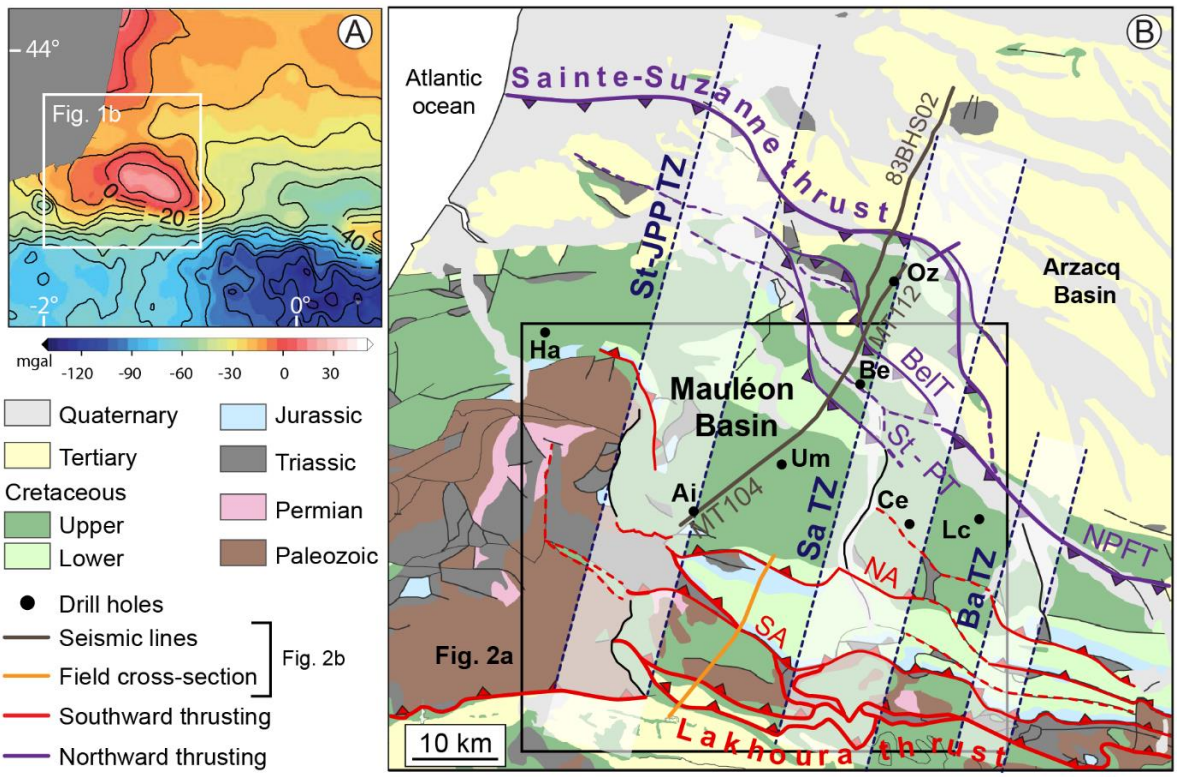


Fig. 1. (A) Gravity anomaly map of the Pyrenees showing a positive Bouguer anomaly at the same location as the Mauléon basin (modified from Chevrot et al., 2018). **(B)** Geologic map highlighting the current pop-up structure of the Mauléon basin. The basin is offset by three transfer zones: St-JPP TZ, Saint-Jean-Pied-de-Port transfer zone; Sa TZ, Saison transfer zone; Ba TZ, Barlanès transfer zone. Major thrusts include BelT, Bellevue thrust; NA, North Arbailles thrust; NPFT, North Pyrenean frontal thrust; SA, South Arbailles thrust; St-PT, Saint-Palais thrust. Teeth are on the upthrown side; dashed where inferred. Drill holes are Ai, Ainhice-1; Be, Bellevue-1; Ce, Chéraute-1; Ha, Hasparren-101; Lc, Les Cassières-2; Oz, Orthez-102; Um, Uhart-Mixe-1.

3. The Cretaceous Pyrenean Metasomatic Event

3.1. High Temperature–Low Pressure Metamorphism

Synrift Pyrenean metamorphism is localized within the Internal Metamorphic Zone, a narrow east-west-trending vertical zone of metamorphosed and strongly deformed rocks (Casteras, 1933; Mattauer, 1968; Choukroune, 1974). The high temperature–low pressure metamorphism is characterized by a typical assemblage of muscovite, phlogopite, tremolite, plagioclase, potassium feldspar, and scapolite (Albarède & Michard-Vitrac, 1978a; Montigny et al., 1986; Golberg & Maluski, 1988; Golberg & Leyreloup, 1990; Boulvais et al., 2006; Clerc et al., 2015). The mineral assemblages indicate a maximum temperature of 550–650°C and a maximum pressure of 3–4 kbar (Bernus-Maury, 1984; Golberg & Leyreloup, 1990; Vauchez et al., 2013). Previous authors have established that this metamorphic event, which affected deposits of Triassic to Late Cretaceous age, featured a very high geothermal gradient resulting from continental crustal thinning (Dauteuil & Ricou, 1989; Golberg & Leyreloup, 1990). This event is also associated with deep-sea synrift sediments of the Black Flysch group (Debroas, 1978, 1987, 1990) and outcropping subcontinental mantle (Debroas et al., 2010; Clerc et al., 2012).

Evidence for local denudation of the subcontinental mantle during the Early Cretaceous includes the presence of reworked clasts of mantle rock in the late Albian to Cenomanian synrift sediments (Roux, 1983; Duée et al., 1984; Fortané et al., 1986; Jammes et al., 2009; Debroas et al., 2010; Lagabrielle et al., 2010) and the association of a positive gravity anomaly with the Early Cretaceous North Pyrenean rift system (**Fig. 1A**; Gottis, 1972; Boillot et al., 1973; Grandjean, 1992, 1994; Daignières et al., 1994; Casas et al., 1997), interpreted as indicating the presence of subcontinental mantle at shallow depths (around 10 km) under the Mauléon basin

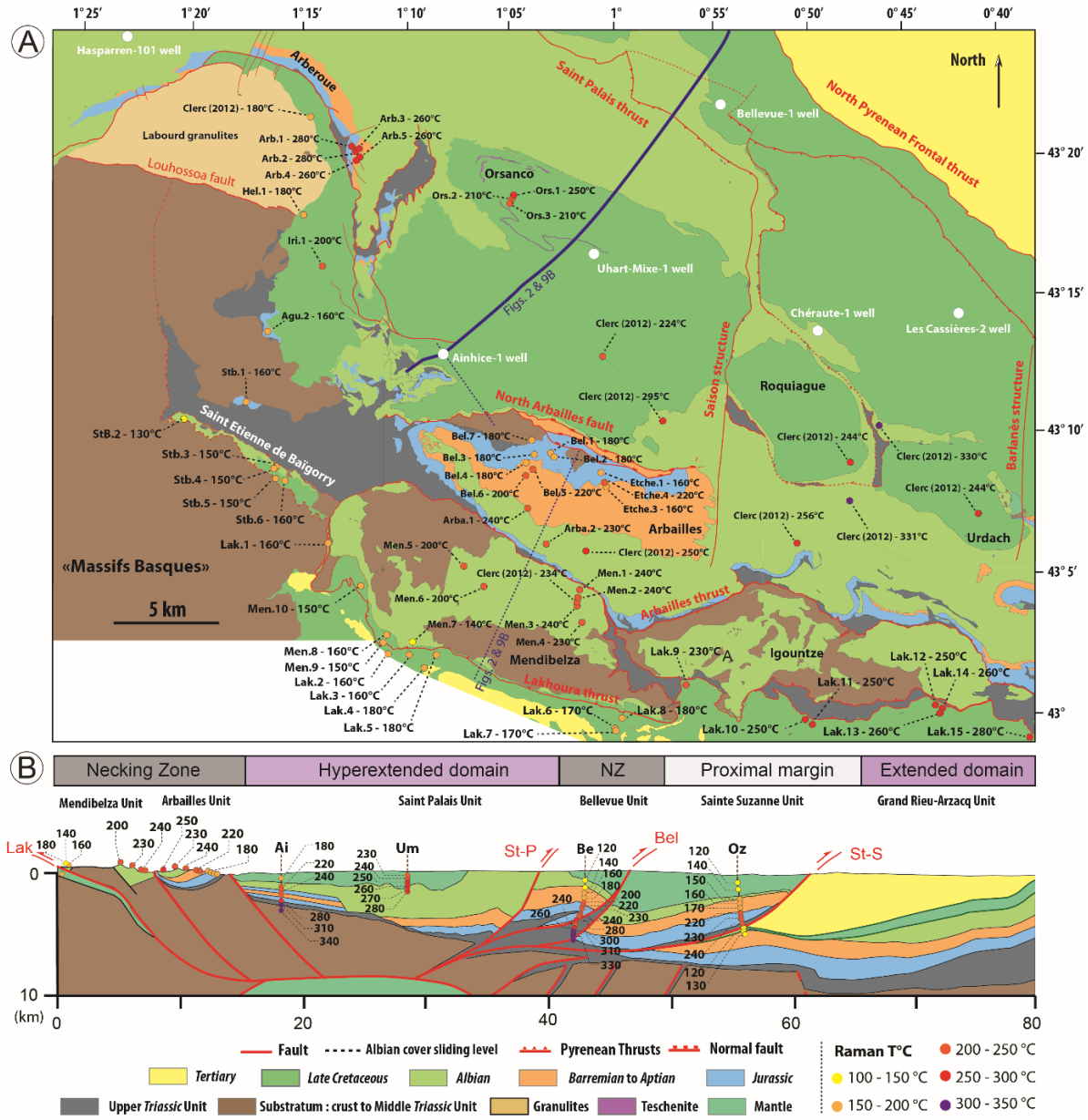


Fig. 2. (A) Geologic map of the Mauléon basin showing locations of field samples and boreholes. Colors of field samples indicate their RSCM peak temperature. **(B)** N-S composite cross section of the Mauléon basin and RSCM peak temperatures (Raman T°C) in outcrop and borehole samples. See Figure 1b for location. Major thrusts include Bel, Bellevue thrust; Lak, Lakhoura thrust; St-S, Sainte-Suzanne thrust; St-P, Saint-Palais thrust. Drill holes are Ai, Ainhice-1; Be, Bellevue-1; Oz, Orthez-102; Um, Uhart-Mixe-1; NZ, Neking Zone.

(**Fig. 2B**; Wang et al., 2016; Wang, 2017). Geochronological evidence indicates that spreading took place between 107 and 85 Ma (Albarède & Michard-Vitrac, 1978a; Golberg et al., 1986; Montigny et al., 1986; Golberg & Maluski, 1988; Thiébaut et al., 1992).

Recent studies based on RSCM have produced evidence that the Internal Metamorphic Zone reached temperatures ranging from 400–600°C in the central and eastern Pyrenees (Clerc, 2012; Clerc et al., 2015; Chelalou et al., 2016; Lagabrielle et al., 2016; Ducoux, 2017) to 200–630°C in the Nappes des Marbres at its western end (Lamare, 1936; Martínez-Torres, 1989; Mendia & Ibarguchi, 1991; Ducoux, 2017). Hydrothermal fluid circulation can account for the local thermal homogeneity in the Internal Metamorphic Zone, for instance in the North Pyrenean Boucheville basin, where the temperature range was 530–580°C (Boulvais, 2016).

3.2. Alkaline Magmatism, Albitization, and Talc Mineralization

The North Pyrenean Zone underwent widespread Mesozoic magmatic activity, attested by Cretaceous alkaline magmatism (Montigny et al., 1986; Rossy et al., 1992). The Cretaceous igneous rocks consist of alkaline basalt and trachyte, as well as intrusive teschenyte and syenite (Azambre & Rossy, 1976; Thiébaut et al., 1979; Azambre et al., 1992). The Cretaceous volcanism was predominantly submarine, characterized by pillow basalt and pyroclastic rocks. The position of these rocks within Cretaceous sedimentary deposits ensures reliable biostratigraphic ages for this magmatic event. They range in age from late Albian to Santonian in the western Pyrenees (Rat, 1959; Schoeffler et al., 1964; Casteras et al., 1970; Lamolda et al., 1983; Rat et al., 1983; Castañares et al., 1997; López-Horgue et al., 1999) and from late Albian to Turonian in the central Pyrenees (Dubois & Seguin, 1978; Debroas, 1990) and eastern Pyrenees (Montigny et al., 1986).

These biostratigraphically constrained ages are consistent with the radiometric dates available for the Cretaceous magmatic rocks, which range from 115 to 85 Ma (Golberg et al., 1986; Montigny et al., 1986; Henry et al., 1998). Some amphibolite, pyroxenite, and hornblende dikes in the North Pyrenean mantle rocks might be derived from alkaline magmatism (Bodinier et al., 1988, 2004). Radiometric ages of these rocks are similar to those of the alkaline magmatism: 116 ± 5 Ma (Verschure et al., 1967) and 101 ± 2.5 Ma (Golberg et al., 1986) in Lherz, 103 ± 2 Ma in Caussou (Albarède & Michard-Vitrac, 1978a), and 103 Ma in Urdach (Azambre & Monchoux, 1998).

The high temperature–low pressure metamorphism and alkaline magmatism affecting the North Pyrenean Zone were synchronous with the albitization of the Agly, Salvezine, Saint-Barthélémy, and Arize massifs in the North Pyrenean Zone (Boulvais et al., 2007; Poujol et al., 2010) and the formation of thick talc-bearing intervals (Moine et al., 1989), characterized by fluid temperatures ranging from 250°C to 550°C, during hydrothermal alteration that took place between 117 and 92 Ma (Schärer et al., 1999; Boulvais et al., 2006; Fallourd et al., 2014).

4. Methods

4.1. RSCM Thermometry

Raman measurements were performed at BRGM using a Renishaw inVia Reflex microspectrometer with a diode-pumped solid-state laser source excitation of 514.5 nm. The laser power reaching the sample surface, through the 100× objective (numerical aperture 0.90) of a Leica DM2500 microscope, did not exceed 0.1 mW. Before each measurement session, the microspectrometer was calibrated using the 520.5 cm^{-1} line of an internal silicon standard. After Rayleigh diffusion was eliminated by edge filters, the Raman signal was first dispersed using 1,800 lines/mm signal before analysis with a deep depletion CCD detector (1,024 × 256 pixels). Raman spectra were acquired from at least 10 particles to ensure consistent data. Renishaw Wire 4.1 was used for instrument calibration and Raman measurements.

The irreversible evolution of carbonaceous material with increasing temperature can be measured using Raman microspectroscopy (e.g., Wopenka & Pasteris, 1993; Yui et al., 1996). Consequently, a geothermometer based on RSCM has been calibrated, initially for the temperature range of 330–650°C (Beyssac et al., 2002), and subsequently extended to temperatures typical of diagenesis and low-grade metamorphism (Lahfid et al., 2010). In this study, all maximum temperatures determined by RSCM geothermometry (RSCM peak temperatures hereafter) were estimated qualitatively by comparing the obtained spectra to those of the Glarus area (Lahfid et al., 2010).

4.2. Calculation of Paleogeothermal Gradients

The geotherm, defined as the temperature profile versus depth, can be linear in the crust and the lithosphere if the medium is uniform and internal heat production is negligible. Where the crust is heterogeneous, however, contrasts in thermal conductivity may perturb the geotherm from linearity. In addition, radiogenic heat production in crustal rocks results in a curved geotherm in which the geothermal gradient decreases with depth. Advective processes of various scales can also disturb the thermal regime of the crust.

Diapirism, magmatism, and hydrothermal fluid circulation can significantly affect the geotherm over periods ranging from several tens of thousands to millions of years, and tectonic events such as collision and thrusting, rifting (crustal extension), and coeval erosion or sedimentation lead to transient evolution of crustal temperatures at longer time scales (e.g., Jaupart & Mareschal, 2011; Nábělek & Nábělek, 2014; Magri et al., 2015).

In this study, we estimated paleogeothermal gradients across the Cretaceous extended precursor of the Mauléon basin, using RSCM peak temperatures measured in transects of surface rocks and in cuttings from deep petroleum wells. Because the investigated depths do not exceed 6,000 m, the relatively fixed temperature conditions at the surface force the geotherm to remain nearly linear. Using RSCM peak temperatures to estimate paleogeothermal gradients is not an easy task because a rock may theoretically record several peak temperatures over the course of geologic time. However, simple thermal models (see section 5) show that for the Mauléon basin and its particular tectonic history, the maximum peak temperatures recorded during Cretaceous time were necessarily the highest ones since 120 Ma. Consequently, any inferred temperature-depth profiles deduced from RSCM peak temperatures represent paleogeotherms that were reached during the extensional event. On that basis we attempted to deconvolve the signal of the paleogeothermal gradient for each field section or well.

Of the seven boreholes used in this study, only the Ainhice-1 well was strictly vertical, thus the other six required adjustments for their deviations from vertical before evaluating their thermal gradients. The Chéraute-1 well had the largest deviation, amounting to 742 m at the bottom of the borehole. The other depth deviations were 313 m for Bellevue-1, 251 m for Les Cassières-2, 165 m for Hasparren-101, 88 m for Orthez-102, and 13 m for Uhart-Mixe-1. Linear regression lines drawn for all boreholes except the Chéraute-1 well were characterized by coefficient values of best fit (R^2) of 0.95 or greater, their slopes corresponding to the apparent thermal gradient. This gradient was then corrected for each borehole on the basis of the mean stratal plunge to yield the paleogeothermal gradient that existed before inversion of the Mauléon basin. When crustal deformation occurred prior to the time the RSCM peak temperature was reached, the paleogeothermal and apparent thermal gradients are the same.

We also had to consider the case where a segment of the paleogeotherm was vertical or nearly so. A homogeneous temperature profile over a substantial vertical depth may be caused by homogenization of temperatures due to hydrothermal convection (e.g., temperature profiles in geothermal systems; Guillou-Frottier et al., 2013), localized ascent or descent of hydrothermal fluids (e.g., upflow through permeable fault zones; Roche et al., 2018), or refraction effects due to bodies with high thermal conductivity, such as salt domes or evaporite layers (e.g., Mello et al., 1995; Magri et al., 2008; Guillou-Frottier et al., 2010). In this latter case, the geotherm is not truly vertical, but the temperature gradient can be decreased by a factor of 2 to 3. When temperature profiles describe such a decreased thermal gradient (DG), the paleogeothermal gradient cannot be evaluated, as was the case for the Hasparren-101 and Chéraute-1 wells.

5. Results

Representative RSCM peak temperature spectra are shown in **Figure 3**, for the field samples and for each of seven boreholes, and the resulting temperatures are listed in **Table 1** for the field samples and in **Table 2** for the borehole samples. Uncorrected and corrected borehole depths are reported as measured depth (MD) and true vertical depth (TVD), respectively, in **Table 2**. Columnar sections of the boreholes and field sites, annotated with these RSCM peak temperatures, are presented along a north-south transect in Figure 4 and an east-west transect in **Figure 5**. **Figure 6** presents the RSCM peak temperatures with respect to TVD. The linear regression lines drawn for the seven boreholes are characterized by R^2 values of 0.95 or greater, except in the case of the Chéraute-1 well.

5.1. Iberian Proximal Margin

Our paleogeothermal analysis of the Iberian proximal margin was calibrated from 15 outcrop samples of Santonian to Danian age (syncollisional) exposed beneath the Lakhoura

thrust in the Axial Zone just south of the Mendibelza unit **(Figs. 2 and 4)**. These samples yielded RSCM peak temperatures ranging from 160–180°C in the west to 280°C in the east **(Fig. 3A and Tab. 1)**. Because most of the samples were from the same stratigraphic level, it was not possible to estimate a paleogeothermal gradient for this structural unit. We tried to estimate RSCM peak temperatures in the Cenomanian to Santonian carbonate platform deposits (« Calcaires des Cañons » limestones), but the samples were too thoroughly recrystallized to yield reliable data.

5.2. Iberian Necking Zone

We calibrated RSCM peak temperatures in the Iberian necking zone from 33 outcrop samples from the Mendibelza, Arbailles, Saint-Etienne de Baïgorry, and Arberoue units **(Tab. 1)** and cuttings from the Hasparren-101 well **(Tab. 2)**. Ten samples were from Albian (synrift) to Santonian (postrift) deposits of the Mendibelza unit, for which a Mesozoic stratigraphic section 2,400 m thick has been reconstructed on the basis of new field observations and previously published data (**Fig. 4**; Boirie, 1981; Souquet et al., 1985; Saspiturry et al., 2019a). The 800-m section at the base of the Albian synrift sequence reached temperatures of 230–240°C, values that are consistent with those obtained by Clerc (2012). RSCM peak temperatures decreased upward from 230°C to 140–160°C in the late Albian siltstone and Santonian breccia **(Fig. 5)**. The temperature difference between the base and the top of the Mendibelza section defines a paleogeothermal gradient of 39–46°C/km. To the west, six samples from the Saint-Etienne-de-Baïgorry unit recorded the same range of RSCM peak temperatures (130–160°C) as samples from the top of the Mendibelza unit section **(Figs. 2 and 3A)**.

Twelve samples from the Arbailles unit represented Jurassic (prerift) to Albian (synrift) deposits **(Figs. 2 and 4)**. Surprisingly, the Jurassic to Barremian carbonate deposits, in the northern part, recorded a uniform RSCM peak temperature of 180°C whereas the younger Aptian and Albian carbonates and marls, in the southern part, recorded temperatures of 220–240°C **(Tab. 1)**. This range is close to the RSCM peak temperature range of 250°C and 256°C published by Clerc (2012). The anomalous temperature distribution in the Arbailles unit makes it difficult to make an estimate of the paleogeothermal gradient there.

The Hasparren-101 well penetrates two structural units separated by a major thrust at 5,400 m MD **(Fig. 5)**. The lower, autochthonous unit is made up of basement rocks and Permian red siltstone directly overlain by Turonian to Santonian carbonate turbidites. It yielded RSCM peak temperatures ranging from 220°C to 240°C **(Fig. 3B and Tab. 2)**. The tectonic contact between the two structural units is marked by a sharp paleotemperature gap of around 50°C. The upper, allochthonous unit is composed of a Late Triassic to Cenomanian sequence. The lower part of this unit yielded fairly uniform RSCM peak temperatures around 280°C between 2,800 and 5,400 m MD **(Fig. 5)**. However, Raman spectra of the two samples from 2,790 and 4,760 m were heterogeneous, yielding two different RSCM peak temperature values of 240°C and 280°C **(Fig. 5 and Tab. 2)**. The upper part of the upper unit yielded RSCM peak temperatures varying from 280°C at the base to 130°C at the top. The resulting linear regression line defines a 62°C/km deformed thermal gradient **(Fig. 6A)**. Because this unit is intensively tectonized and has variable stratal plunges, it was not possible to estimate a paleogeothermal gradient based on a mean plunge.

The Arberoue field section is paleogeographically in the same domain as the Hasparren-101 well. The Arberoue succession, composed of Late Jurassic to Aptian carbonates, yielded RSCM peak temperatures, ranging from 260°C to 280°C, that are similar to those obtained from the Hasparren-101 well in the same stratigraphic interval **(Figs 2, 3A, and 5 and Tab. 1)**.

5.3. Hyperextended Domain

Peak temperatures in the hyperextended domain of the Mauléon basin were determined from field samples and boreholes. The Orsanco section **(Figs. 2 and 5 and Tab. 1)**, the outcrop samples HEL-1, IRI-1 and AGU-2, the Ainhice-1, Chéraute-1, and Uhart-Mixe-1 wells represent the distal parts of the hyper-extended domain.

Table 1. *Description of outcrop samples; locations are in WGS84 coordinates*.

Sample	Latitude	Longitude	Age	Lithology	Raman temperature (°C)
Axial Zone: Iberian proximal margin					
LAK-1	43.102108	–1.219360	Late Santonian	Calcschist	160
LAK-2	43.036917	–1.177413	Danian	Calcschist	160
LAK-3	43.035055	–1.162842	Campanian	Calcschist	160
LAK-4	43.023748	–1.144220	Danian	Marl	180
LAK-5	43.034887	–1.135020	Campanian	Calcschist	180
LAK-6	42.991763	–0.986248	Campanian	Calcschist	170
LAK-7	42.991763	–0.986248	Campanian	Calcschist	170
LAK-8	42.998580	–0.985852	Campanian	Calcschist	180
LAK-9	43.018367	–0.937463	Campanian	Calcschist	230
LAK-10	42.999257	–0.838788	Campanian	Calcschist	250
LAK-11	42.994837	–0.834207	Campanian	Calcschist	250
LAK-12	43.005373	–0.731272	Campanian	Calcschist	250
LAK-13	43.002290	–0.725235	Campanian	Calcschist	260
LAK-14	43.003928	–0.724552	Campanian	Calcschist	260
LAK-15	42.996247	–0.684223	Campanian	Calcschist	280
Mendibelza unit: Iberian necking zone					
MEN-1	43.071898	–1.019520	Early Albian	Siltstone	240
MEN-2	43.069752	–1.021996	Early Albian	Siltstone	240
MEN-3	43.065726	–1.023290	Early Albian	Siltstone	240
MEN-4	43.053575	–1.017703	Early Albian	Siltstone	230
MEN-5	43.089358	–1.111091	Middle Albian	Siltstone	200
MEN-6	43.080316	–1.098856	Middle Albian	Siltstone	200
MEN-7	43.042209	–1.151609	Late Albian	Siltstone	140
MEN-8	43.040542	–1.172827	Santonian	Breccias	160
MEN-9	43.040623	–1.172787	Coniacian	Siltstone	150
MEN-10	43.069492	–1.194545	Santonian	Breccias	150
Saint-Etienne-de-Baïgorry unit: Iberian necking zone					
STB-1	43.181566	–1.284771	Early Jurassic	Limestone	160
STB-2	43.170830	–1.336082	Late Albian	Marls	130
STB-3	43.136767	–1.264075	Santonian	Calcschist	150
STB-4	43.141252	–1.261580	Santonian	Calcschist	150
STB-5	43.140792	–1.261903	Santonian	Calcschist	150
STB-6	43.137648	–1.257442	Santonian	Calcschist	160
Arbailles unit: Iberian necking zone					
BEL-1	43.151402	–1.042786	Early Jurassic	Marly limestone	180
BEL-2	43.152268	–1.045087	Middle Jurassic	Marly limestone	180
BEL-3	43.149475	–1.055378	Late Jurassic	Marly limestone	180
BEL-4	43.147340	–1.059262	Barremian	Marl	180
BEL-5	43.144710	–1.058376	Aptian	Marl	220
BEL-6	43.141317	–1.065354	Aptian	Limestone	200
BEL-7	43.157929	–1.053770	Early Jurassic	Marly limestone	180
ETCH-1	43.138797	–1.003380	Middle Jurassic	Marly limestone	160
ETCH-3	43.135267	–0.998984	Aptian	Limestone	160
ETCH-4	43.135725	–0.999518	Aptian	Limestone	220
ARBA-1	43.100010	–1.051226	Earliest Albian	Marl	240
ARBA-2	43.121969	–1.063731	Earliest Albian	Marl	230
Arberoue unit: Iberian necking zone					
ARB-1	43.332444	–1.200691	Late Jurassic	Marly limestone	280
ARB-2	43.331583	–1.199066	Late Jurassic	Marly limestone	280
ARB-3	43.331834	–1.198787	Barremian	Limestone	260
ARB-4	43.329313	–1.198841	Barremian	Limestone	260
ARB-5	43.327623	–1.197450	Aptian	Marl	260
Hyperextended domain					
ORS-1	43.300258	–1.075456	Turonian	Marl	250

ORS-2	43.301730	–1.074582	Turonian	Marl	210
ORS-3	43.302269	–1.074059	Turonian	Marl	210
IRI-1	43.257235	–1.232790	Santonian	Calcschist	200
AGU-2	43.222597	–1.271063	Late Jurassic	Limestone	160
HEL-1	43.293563	–1.240483	Santonian	Calcschist	180

Table 2. *Description of well samples*

Measured depth (m)	True vertical depth (m)	Age	Lithology	Raman temperature (°C)
Hasparren-101 well: Iberian necking zone				
210	210	Early Cenomanian	Marl	130
420	420	Early Cenomanian	Marl	140
550	550	Early Cenomanian	Marl	160
700	700	Early Cenomanian	Marl	170
860	860	Early Cenomanian	Marl	190
1,060	1,060	Early Cenomanian	Marl	200
1,298	1,298	Early Cenomanian	Marl	220
1,500	1,500	Early Cenomanian	Marl	230
1,740	1,740	Early Cenomanian	Marl	240
2,040	2,040	Early Cenomanian	Marl	250
2,290	2,290	Early Cenomanian	Marl	260
2,790	2,790	Early Cenomanian	Marl	240/280
3,120	3,120	Albian	Marl	280
3,260	3,260	Late Jurassic	Marl	300
3,410	3,410	Late Jurassic	Marl	280
3,680	3,680	Early Jurassic	Limestone	270
4,120	4,117	Early Jurassic	Clay	280
4,390	4,387	Late Triassic	Clay	280
4,760	4,757	Late Triassic	Clay	240/280
5,120	5,117	Late Triassic	Clay	280
5,550	5,543	Turonian	Calcschist	240
5,870	5,827	Turonian	Calcschist	220
6,050	5,960	Turonian	Calcschist	220
6,220	6,055	Permian	Clay	240
6,270	6,105	Permian	Clay	240
6,280	6,115	Paleozoic	Clay	230
Ainhice-1 well: hyperextended domain				
450	450	Middle Cenomanian	Calcschist	180
1,078	1,078	Late Jurassic	Marl	220
1,454	1,454	Early Jurassic	Marl	240
1,585	1,585	Early Jurassic	Limestone	240
1,652	1,652	Late Aptian	Limestone	240
1,878	1,878	Late Aptian	Limestone	240
2,555	2,555	Late Triassic	Clay	280
3,005	3,005	Late Triassic	Clay	310
3,504	3,504	Stephanian?	Limestone	340
Chéraute-1 well: hyperextended domain				
512	512	Cenomanian	Marl	240
1,010	1,005	Cenomanian	Marl	240
1,495	1,475	Senonian	Marl	270
2,032	1,982	Senonian	Marl	260
2,488	2,428	Senonian	Marl	270
3,014	2,924	Albian	Marl	260
3,495	3,375	Albian	Marl	290
3,995	3,841	Aptian	Marl	300
4,500	4,270	Aptian	Marl	300
4,974	4,644	Aptian	Marly limestone	330
5,507	5,002	Aptian	Marl	330

5,997	5,341	Late Jurassic	Marl	330
6,015	5,355	Late Jurassic	Marl	330
Uhart-Mixe-1 well: hyperextended domain				
500	500	Senonian	Marl	230
613	613	Senonian	Marl	230
902	896	Senonian	Marl	240
952	946	Senonian	Marl	250
952	948	Senonian	Marl	250
1,264	1,254	Senonian	Marl	260
1,508	1,496	Early Cenomanian	Marl	270
1,735	1,722	Early Cenomanian	Marl	280
1,777	1,764	Early Cenomanian	Marl	280
Bellevue-1 well: European necking zone				
560	560	Cenomanian	Marl	120
1,180	1,180	Albian	Marl	140
1,550	1,550	Aptian	Limestone	160
2,040	2,037	Aptian	Marl	180
2,570	2,565	Barremian	Siltstone	200
3,000	2,992	Late Jurassic	Limestone	220
3,500	3,470	Middle Jurassic	Marl	230
4,000	3,934	Middle Jurassic	Limestone	240
4,180	4,101	Late Jurassic	Marl	240
4,690	4,560	Barremian	Limestone	280
4,730	4,596	Barremian	Limestone	240
5,210	5,050	Late Triassic	Clay	260
5,780	5,480	Late Triassic	Clay	300
6,430	6,238	Late Triassic	Clay	310
6,710	6,470	Barremian	Limestone	330
6,890	6,591	Barremian	Limestone	330
Les Cassieres-2 well: European proximal margin				
535	535	Santonian	Marl	160
968	966	Santonian	Marl	200
1,492	1,488	Cenomanian	Marl	200
1,994	1,990	Cenomanian	Marl	200
2,510	2,505	Cenomanian	Marl	220
3,083	3,077	Aptian–Albian	Marl	240
3,580	3,560	Aptian–Albian	Marl	240
4,005	3,960	Aptian–Albian	Marl	270
4,523	4,443	Aptian–Albian	Marl	270
5,015	4,865	Aptian–Albian	Marl	300
Orthez-102 well: European proximal margin				
510	500	Senonian	Calcschist	120
1,140	1,127	Senonian	Calcschist	140
2,000	1,979	Albian	Limestone	150
2,600	2,577	Aptian	Limestone	160
2,770	2,747	Aptian	Limestone	170
3,350	3,325	Barremian	Marl	200
4,030	3,995	Late Jurassic	Marl	220
4,200	4,156	Early Jurassic	Marl	240
4,260	4,214	Early Jurassic	Limestone	230
4,360	4,310	Senonian	Marl	240
4,390	4,338	Aptian	Marl	240
4,470	4,416	Barremian	Marl	120
4,690	4,632	Senonian	Marl	120
4,830	4,769	Albian	Marl	120
4,910	4,846	Albian	Marl	120
5,010	4,943	Albian	Marl	120
5,120	4,953	Aptian	Limestone	130
5,481	5,399	Aptian	Limestone	130

The Ainhice-1 well reaches basement strata of Carboniferous (Stephanian) age at a depth of around 2,900 m MD **(Fig. 4)**. The Mesozoic cover is duplicated by basinward displacement on a décollement at 1,600 m MD that was active during early Albian time (**Fig. 4**; Saspiturry et al., 2019a). RSCM peak temperatures varied from 340°C at the base to 180°C at the top **(Figs 3C and 6B and Tab. 2)**. These values fit a linear regression line corresponding to a 52°C/km apparent thermal gradient and, after correcting for a mean stratal plunge of 25°, a paleogeothermal gradient of 57°C/km **(Fig. 6B)**. There is no significant variation in RSCM peak temperature across the décollement **(Fig. 6B)**.

The Chéraute-1 well penetrates a sequence of Jurassic to Late Cretaceous rocks **(Fig. 5)**. The upper part of the well displays an Albian-Cenomanian cover sequence that is duplicated in reverse order above approximately 1,500 m MD, a depth corresponding to the axis of a syncline with a Late Cretaceous core. The RSCM peak temperatures were more variable than in the other wells, ranging from 330°C to 290°C between 6,000 and 3,400 m MD **(Fig. 5 and Tab. 2)**. The folded Albian to Senonian sequence yielded RSCM peak temperatures of 240°C in the upper limb and 260–270°C in the lower limb of the syncline **(Figs 3D and 5)**. These RSCM peak temperatures define a deformed thermal gradient of 21°C/km, although the linear regression line falls short of significance with R^2 = 0.92 **(Fig. 6C)**. The complex fold structure makes it difficult to estimate a reliable paleogeothermal gradient for this well.

The Uhart-Mixe-1 well penetrates Cenomanian to Turonian turbidites **(Figs. 2 and 4)**. The RSCM peak temperatures vary from 280°C at the base to 230°C at the top **(Figs. 3E and 4 and Tab. 2)**. These values fit a linear regression line defining an apparent thermal gradient of 42°C/km and a paleogeothermal gradient of 60°C/km after taking into account a 45° mean stratal plunge **(Fig. 6D)**.

The Orsanco field section exposes the same paleogeographic domain as the Uhart-Mixe-1 well. Samples from that section yielded RSCM peak temperatures of 210–250°C, which are similar to those in the corresponding part of the Uhart-Mixe-1 well **(Fig. 2 and Tab. 1)**. Approximately 10 km west of the Orsanco section, outcrop samples HEL-1 and IRI-1, of Santonian age, yielded RSCM peak temperatures of 180°C and 200°C, respectively, and outcrop sample AGU-2 to their south, of Late Jurassic age, yielded a RSCM peak temperature of 160°C **(Fig. 2 and Tab. 1)**.

5.4. European Necking Zone

The paleotemperature of the European necking zone was derived from the Bellevue-1 and the Les Cassières-2 wells **(Figs. 2 and 4)**. The Bellevue-1 well penetrates a north-directed major thrust around 4,700 m MD that divides the drilled interval into a basal and an upper unit. The intensively deformed basal unit, made up of Late Triassic evaporites and Barremian-Aptian carbonate lenses, is characterized by RSCM peak temperatures ranging from 330°C at the base (6,900 m MD) to 240°C on the thrust plane **(Figs. 3F and 6E)**. Despite the intense deformation, the RSCM values of this unit fit a linear regression line defining an apparent thermal gradient of around 47°C/km **(Fig. 6E)**. The tectonic contact between the basal and upper units corresponds to a temperature gap of 40°C.

The upper unit is repeated in reverse across an anticline, with its axis at approximately 3,700 m MD, affecting Jurassic to Albian carbonates and marls. This complex structure has been interpreted as the result of Tertiary reactivation of an Albian diapiric ridge (Saspiturry et al., 2019a). The upper unit yielded RSCM peak temperatures progressing steadily from 280°C at the base to 120°C at the top **(Figs. 3F and 4 and Tab. 2)**. These temperatures fit a linear regression line defining an apparent thermal gradient of 38°C/km **(Fig. 6E)**.

RSCM peak temperatures in these two units define similar linear regression lines, meaning that the folded structure in the upper unit is clearly older than the thermal event that set the RSCM peak temperatures. In this case we cannot consider the structural data to restore the paleogeothermal gradient. However, the restored section **(Fig. 2B)** shows that the northward Bellevue thrust doesn't create major Pyrenean tilting at the site of the Bellevue-1 well. Consequently, the paleogeothermal

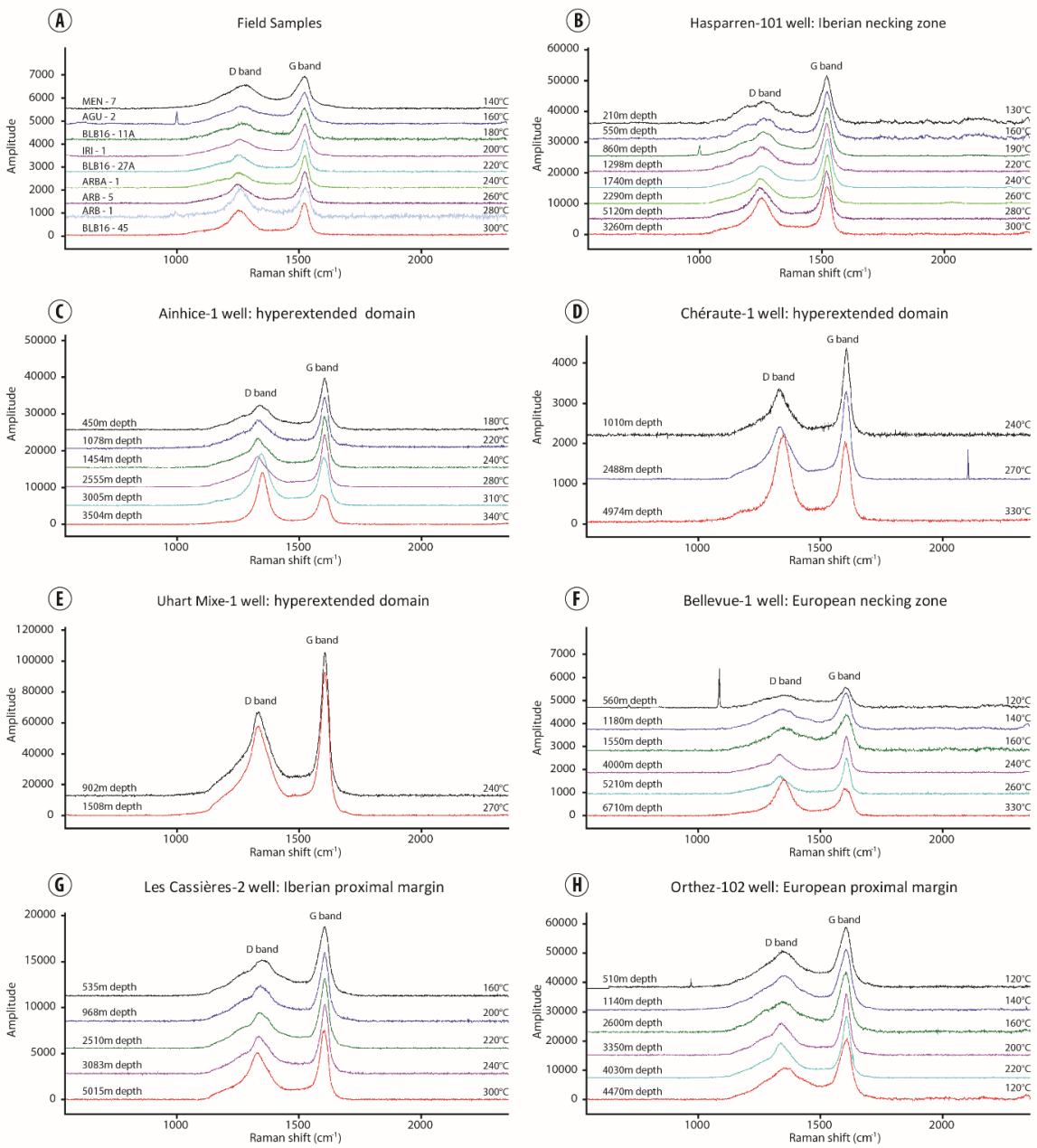


Fig. 3. Representative Raman spectra of carbonaceous materials showing temperature increases in **(A)** outcrops, **(B)** Hasparren-101 well, **(C)** Ainhice-1 well, **(D)** Chéraute-1 well, **(E)** Uhart-Mixe-1 well, **(F)** Bellevue-1 well, **(G)** Les Cassières-2 well, and **(H)** Orthez-102 well. Curves are offset for visibility.

gradient is the same as the apparent thermal gradients, i.e., 47°C/km in the basal unit and 38°C/km in the upper unit.

The Les Cassières-2 well penetrates a complete succession of Jurassic to Santonian sediments, unaffected by any Tertiary thrust **(Fig. 5)**. The Aptian sequence yielded a RSCM peak temperature of around 300°C whereas the Santonian turbidites had a peak temperature of 160°C **(Figs. 3G and 5 and Tab. 2)**. These data define an apparent thermal gradient of 30°C/km **(Fig. 6F)**. Taking into account a mean stratal plunge of 35-40°, the paleogeothermal gradient of this well is estimated at 37-40°C/km.

5.5. European Proximal Margin

The paleotemperature of the European proximal margin were defined using the Orthez-102 wells. The Orthez-102 well penetrates two structural units separated by the Sainte-Suzanne northward thrust at 4,400 m MD. The lower autochthonous unit, made up of Aptian to Late

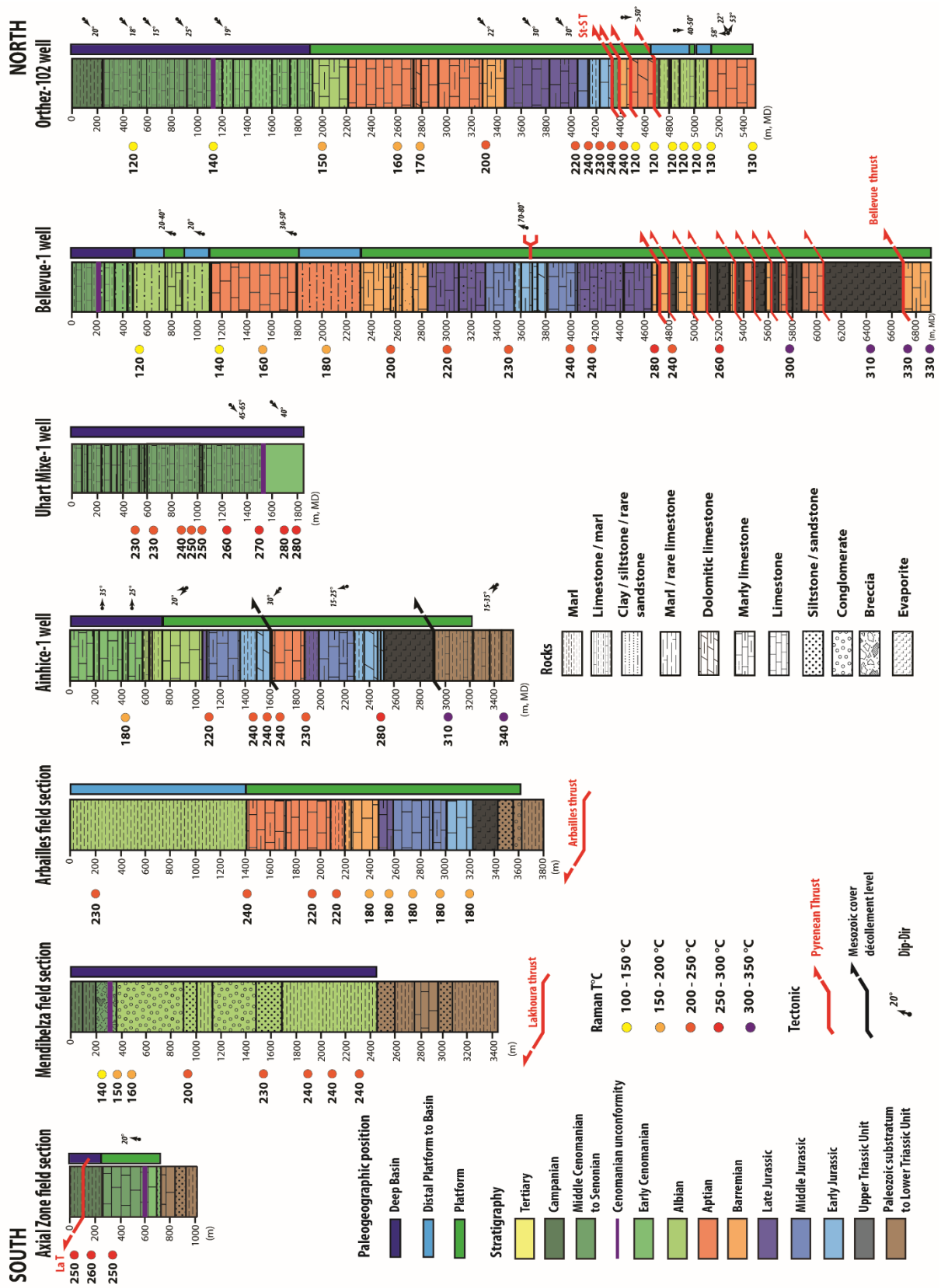


Fig. 4. Columnar sections along a north-south transect including RSCM peak temperatures (Raman T°C). The bars to the right of the columnar sections represent the paleogeographic position in the tectonic basin. MD, measured depth; St-ST, Sainte-Suzanne thrust.

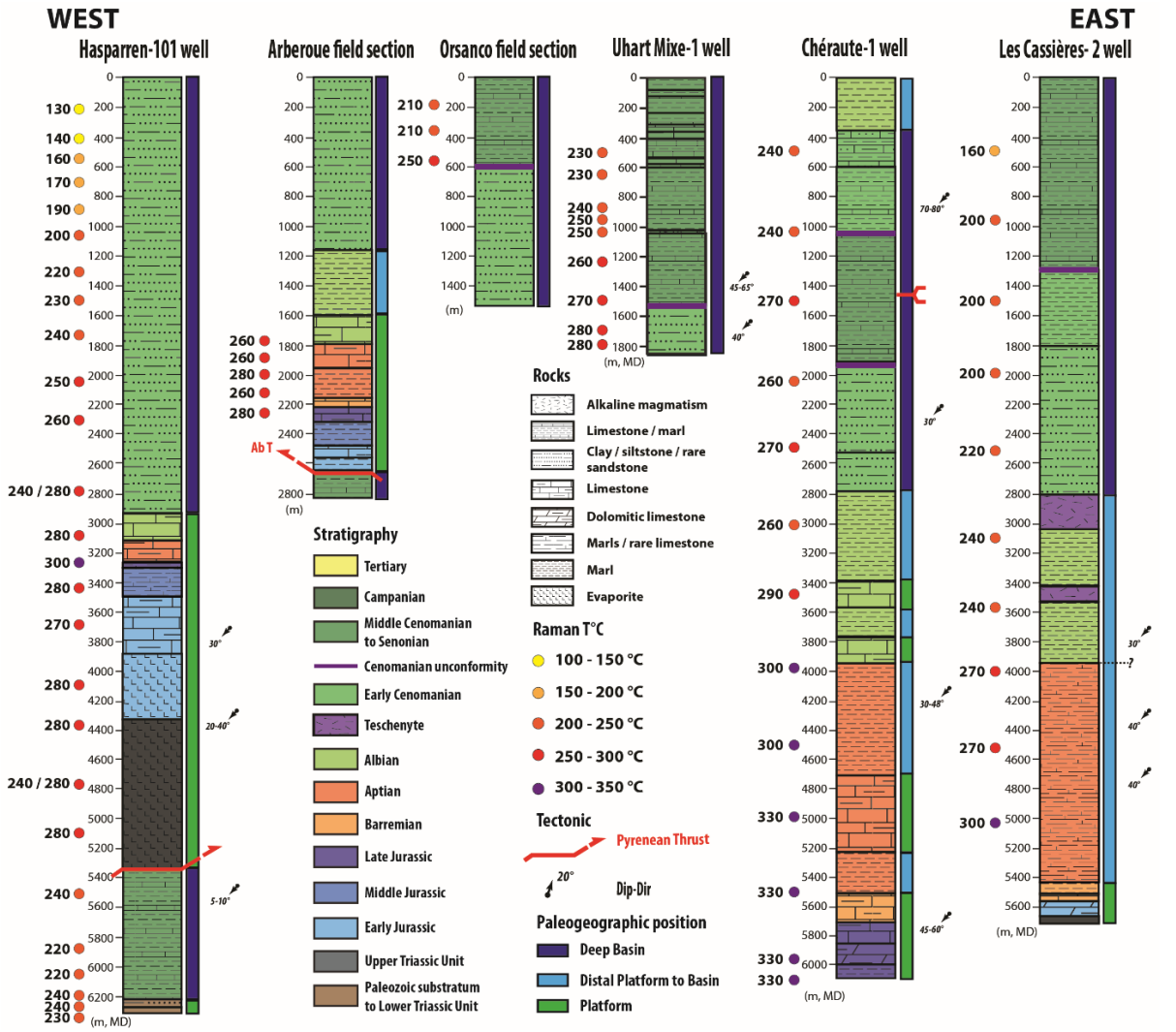


Fig. 5. Columnar sections along an east-west geologic transect including RSCM peak temperatures and paleogeographic positions.

Cretaceous limestone and marl, yielded RSCM peak temperatures of 120–130°C **(Fig. 4)**. The upper allochthonous unit is a complete sequence of Jurassic limestone to Senonian carbonate turbidites. The base and top of the upper unit yielded RSCM peak temperatures of 240°C and 120°C, respectively **(Figs. 3H and 4)**, for an apparent thermal gradient of 32°C/km. Taking into account a mean stratal plunge of 20°, the paleogeothermal gradient of this unit is estimated at 34°C/km.

5.6. Thermal Evolution of the Hyperextended Domain: Numerical Simulation

We derived a simplified model to constrain the thermal evolution of the Mauléon basin area since 120 Ma that was based on geological knowledge plus reasonable thermal properties and boundary conditions. The model calculates the thermal evolution of a crustal section undergoing four stages as shown in **Figure 7**: (1) an initial rifting stage (prerift to synrift) featuring increasing mantle heat flow from 120 to 80 Ma at the base of a thinning crust (initially 30 km thick), (2) sedimentation events from 120 to 80 Ma (synrift to postrift) and from 80 to 40 Ma (syncollisional) leading to a crust 21 km thick at 40 Ma, (3) postcollisional erosion from 40 to 15 Ma, ending with the present-day crustal thickness of 15 km, and (4) thermal relaxation from 15 Ma to the present.

5.6.1. Numerical Approach

Our model incorporates the thickness of the different crustal units, as well as the sedimentation and erosional rates, from this and previous studies (e.g., Vacherat et al., 2014; Saspiturry et al., 2019a and references therein).

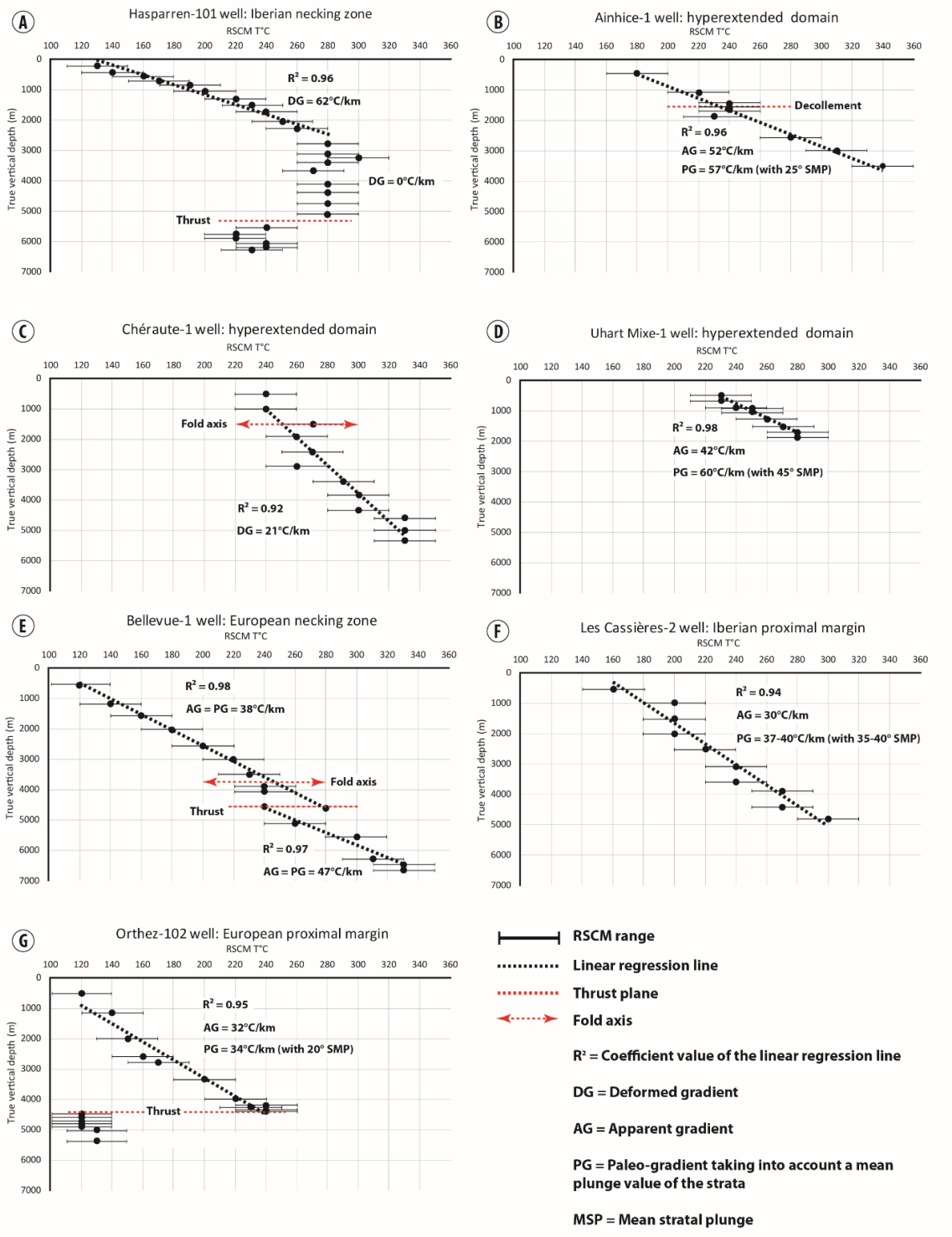


Fig. 6. RSCM peak temperatures at true vertical depths in **(A)** Hasparren-101 borehole, **(B)** Ainhice-1 borehole, **(C)** Chéraute-1 borehole, **(D)** Uhart-Mixe-1 borehole, **(E)** Bellevue-1 borehole, **(F)** Les Cassières-2 borehole, and **(G)** Orthez-102 borehole.

The main unknown variable is the mantle heat flow and its variation through time. However, we have the following two constraints: a maximum RSCM peak temperature of 600°C extrapolated at a depth of 10 km, and a present-day estimated temperature gradient of 25.0 ± 2.7°C/km (see **Supporting Information S1**). We assume that crustal extension is triggered or accompanied by a thermal pulse from the mantle. To reproduce this thermal pulse from 120 to 80 Ma, a gaussian-type horizontal profile is imposed at a depth of 30 km:

$$Q_m = Q_{m0} \times \exp(-x^2/\lambda^2), \quad (1)$$

where Q_m is the mantle heat flow, Q_{m0} is its maximum value at the model center (horizontal distance x = 0), and λ is a characteristic width of the thermal pulse (the half-width of the gaussian curve). We tested two values of λ, 25 km and 75 km. The maximum heat flow Q_{m0} is constrained such that 600°C is reached at 10 km depth at the end of the extension phase. After this heating phase, mantle heat flow decreases to a much lower value that is constrained by the present-day temperature gradient.

To simulate the thermal effects of the sedimentation and erosion events, we use the advective term of the heat equation (presented in the next section), assigning the rates of these events to the velocity term (e.g., Turcotte & Schubert, 2002).

The main objective of this simplified thermal model is to estimate at what date the maximum temperature was reached by a rock that underwent the series of tectonic events illustrated in **Figure 7**. The model may also help to constrain present-day mantle heat flow values beneath the basin.

5.6.2. Heat Equation, Boundary Conditions, and Thermal Properties

As illustrated in **Figure 7**, the top surface is considered fixed at z = 0. During the 120 million years (Myr) of thermal evolution, the underlying medium can move upward (during extension and erosion phases) or downward (during sedimentation). For a medium moving at velocity u (m/s), the heat equation is

$$\rho Cp \frac{\partial T}{\partial t} = \nabla(k \vec{\nabla} T) - \rho Cp \vec{u} \vec{\nabla} T, \quad (2)$$

where ρ is density (kg/m^3), Cp is heat capacity (J/kg K), ∇ and $\vec{\nabla}$ are the divergence and gradient operators, T is temperature (K), t is time (s), k is thermal conductivity (W/m K).

The chosen model box is 30 km thick, corresponding to the initial crustal thickness, and 80 km long for λ = 25 km and 160 km long for λ = 75 km. A fixed temperature condition (T = 10°C) is imposed at the surface of the model. Lateral boundaries are insulating, and the basal boundary condition corresponds to a varying mantle heat flow. A fixed heat flow of 30 mW/m^2 is imposed at time t = 0 (or t_0). A thermal pulse (equation 1) is imposed during the thinning phase (from t_0 to t_0+40 Myr), then the mantle heat flow decreases to a value that reproduces present-day surface temperature gradients **(Fig. 7)**.

Because the thermal properties of different lithologies would yield only slight variations in the temperature distribution, we chose to assign the crust and the mantle a uniform composition with a temperature-dependent thermal conductivity. Given the high temperatures to be computed, it is more relevant to account for thermal effects on thermal conductivity and diffusivity (e.g., Braun, 2009) than to account for 1–2 km of salt within a typical continental crust. The temperature-dependent law is given by (Clauser & Huenges, 1995)

$$k(T) = \frac{k(0)}{1.007 + T\left(0.0036 - \frac{0.0072}{k(0)}\right)}, \quad (3)$$

where k(0) approximates the room-temperature thermal conductivity, taken here as 2.5 W/m K. Changes in this value govern the mantle heat flow value needed to meet the 600°C constraint; for example, a k(0) value of 3.0 W/m K would require that the Q_{m0} value for λ = 25 km increases by 10%.

The heat capacity of the medium is 1,000 J/kg K, and its density is 3,000 kg/m^3. The heat production rate throughout the medium decreases exponentially according to

$$A(z) = A_0 \exp\left(-\frac{z}{D}\right), \quad (4)$$

where A_0 is 1.5 μW/m^3 and where the depth scale D is assumed at 13 km. These arbitrary although reasonable values allow the model to start with a thermally stable crustal regime with a basal temperature of 535°C and a surface heat flow of 48 mW/m^2.

5.6.3. Thermal Pulse

The mantle heat flow condition (equation 1) is applied at the bottom of the box,

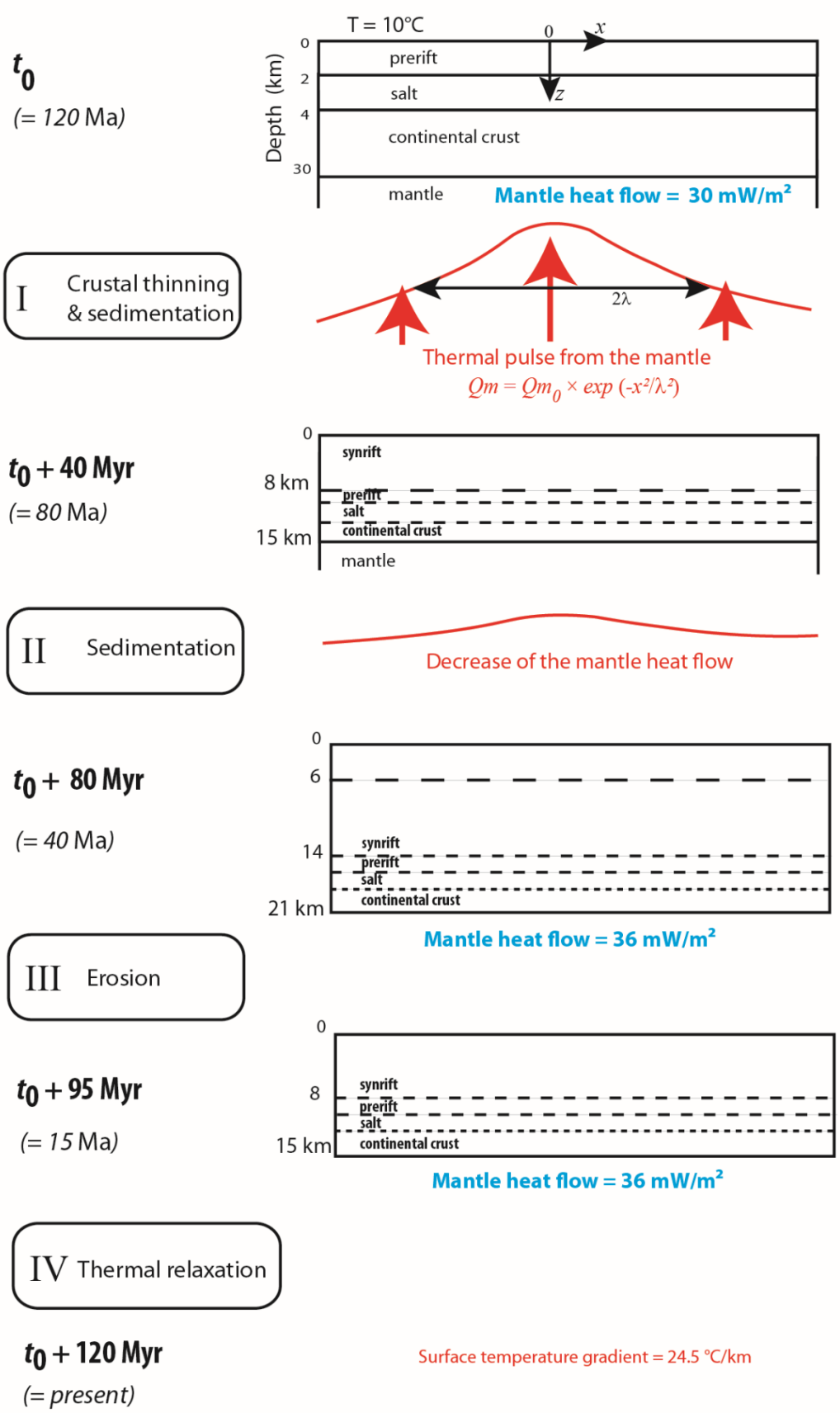


Fig. 7. Schematic diagram showing the four stages of thermal events since 120 Ma. Lithologies are shown but are not accounted for in thermal properties (see text). The final value of mantle heat flow (36 mW/m^2) accounts for present-day surface temperature gradients.

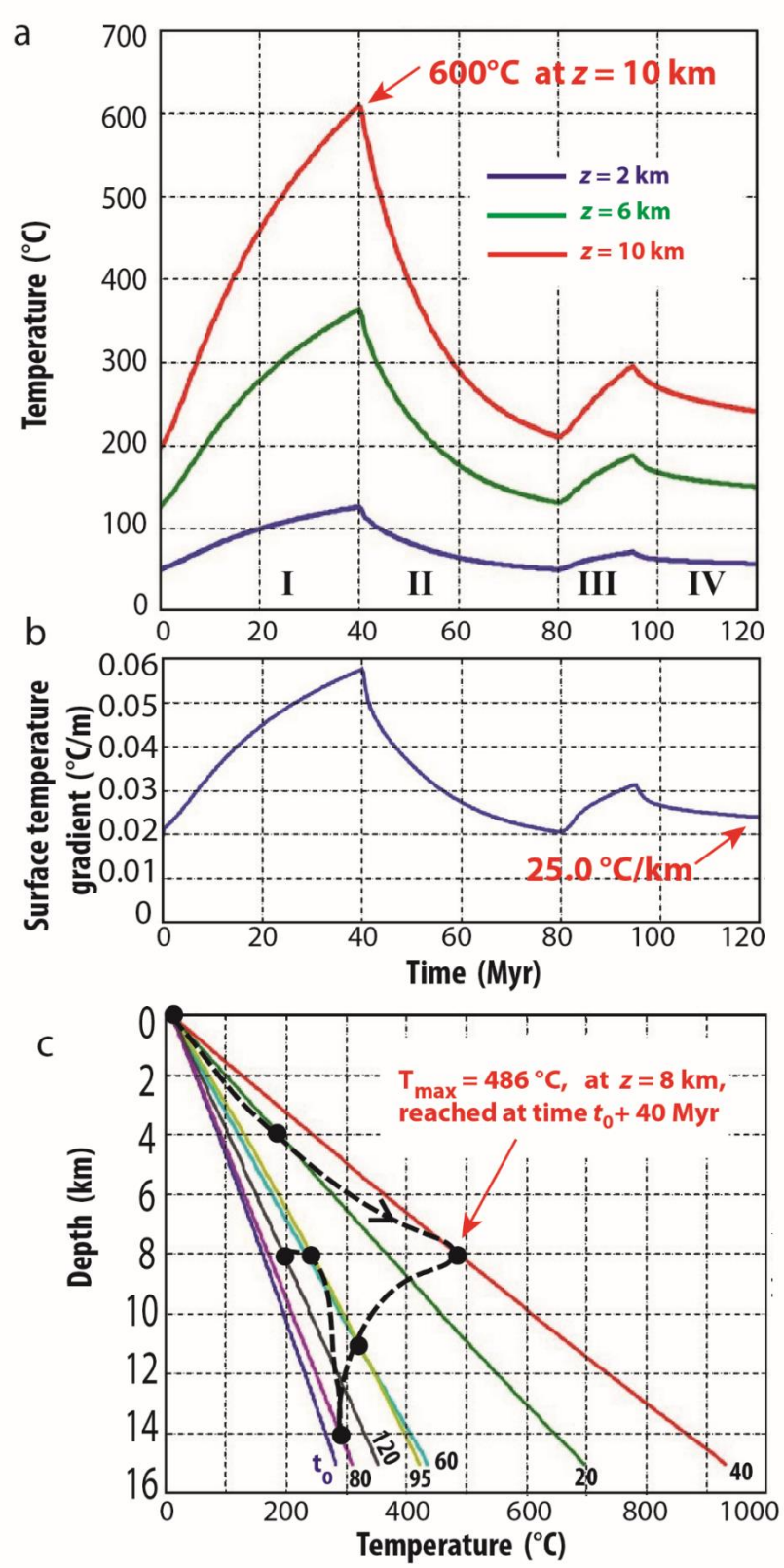


Fig. 8. Thermal evolution since 120 Ma showing **(A)** temperature at three fixed depths, **(B)** temperature gradient at the surface, and **(C)** temperature-pressure path (dashed black line) for a rock (black dot) initially at the surface. Colored lines indicate model geotherms at various times from t_0 to 120 Myr.

regardless of variations in the continental crust thickness, to avoid a spatially variable boundary condition. Hence, the thermal pulse imposed at a depth of 30 km is transferred to the moving base of the crust, as well as the advected heat component during the extension phase.

Different values for the maximum mantle heat flow (Q_{m0}) were tested in order to reach 600°C at a depth of 10 km. For the small-scale thermal pulse (λ = 25 km), Q_{m0} is 100 mW/m^2, and for the large-scale thermal anomaly (λ = 75 km), Q_{m0} is 71 mW/m^2. In both cases, the maximum heat flow at the base of the crust (at time t_0+40 Myr) ranges between 90 and 100 mW/m^2, and the surface heat flow (which includes the radioactive component) is 135–140 mW/m^2, a value consistent with surface heat flow values measured in continental rift zones (e.g., Jaupart & Mareschal, 2007; Lucazeau et al., 2010).

5.6.4. Thermal Evolution

Figure 8 shows the thermal regime of the crust from 120 Ma to present. Temperatures at three distinct depths **(Fig. 8A)** and evolution of surface temperature gradient **(Fig. 8B)** are shown. **Figure 8C** shows the evolution of temperature profiles together with the pressure-temperature-time path followed by a rock initially at the surface. The case shown in **Figure 8** corresponds to Q_{m0} = 100 mW/m^2, λ = 25 km, and $k(0)$ = 2.5 W/m K.

The model goes through four thermal stages: (I) the increased mantle heat flow at the base of the crust warms the entire crust while the coeval sedimentation and extension events have much smaller effects; (II) the crust cools due to the decrease of mantle heat flow and the effect of the sedimentation event; (III) temperatures increase due to the erosion event; and (IV) temperatures decrease toward equilibrium.

As shown in Figure 8c, the maximum temperature recorded by rock that initially (at t_0) was at the surface (486°C at 8 km depth) is reached at the end of the heating phase (t_0+40 Myr). The only way to reach higher temperatures would be to consider sustained high erosion rates that are not supported by field data.

6. Discussion

6.1. Age of RSCM Peak Temperature

In this study, we defined the thermal evolution of the Mauléon hyperextended rift based on RSCM peak temperatures from 155 outcrop and borehole samples that ranged from 120°C to 340°C. The youngest rocks affected by this thermal history in the core of the Mauléon basin are of late Santonian age, consequently the peak temperatures postdate the late Santonian. The timing of this temperature peak is consistent with geochronological data from elsewhere in the North Pyrenean Zone, which put the peak at 107 Ma and 85 Ma (Albarède & Michard-Vitrac, 1978b; Golberg et al., 1986; Golberg & Maluski, 1988; Montigny et al., 1986; Thiébaut et al., 1992). The timing of these RSCM peak temperatures suggests that erosion completely removed a thick Campanian to Miocene sedimentary succession. As shown by the geological cross-section **(Fig. 2B)**, the eroded sedimentary pile was no less than 5–6 km thick under the Sainte-Suzanne thrust. The thermal gradients from borehole data measured in this study correspond to well-constrained (R^2 > 0.95) paleogeothermal gradients in segments of the Mauléon basin. These data suggest that the temperature peaks were synchronous and define a paleogeothermal gradient at the same point in time, with different values depending on the well.

The younger age limit of this thermal peak is constrained by the onset of rift inversion and the resulting erosion. In the western Pyrenees, rift inversion started in middle Eocene time as recorded by the Lakhoura and Sainte-Suzanne thrusts (Labaume et al., 2016; Teixell, 1993, 1998). Indeed, the Sainte-Suzanne thrust plane is marked by a gap in RSCM peak temperature in the Orthez-102 well **(Figs. 4 and 6G)**, which suggests that the temperature peak predated the thrust. Consequently, the paleogeothermal gradients determined in this study probably date from the Paleocene to early Eocene. This is consistent with thermo-kinematic modeling showing that a high synrift thermal gradient lasted 30 Myr after the onset of convergence (~83 Ma) and thermal relaxation began during the collision at ~50 Ma (Vacherat et al., 2014). In fact, modeling combining topographic and buried loads with thermal subsidence shows that the western Pyrenean Aquitain foreland basin was created mainly by postrift thermal subsidence (Angrand et al., 2018).

Rift inversion is responsible for deformation of isotherms in the Mauléon basin core during the Pyrenean thrusting, as

highlighted by the Orthez-102 well and the wide range of RSCM peak temperatures (130–330°C) measured in surface outcrops. This deformation is the reason why the apparent thermal gradient had to be corrected from the mean stratal plunge to estimate the paleogeothermal gradient.

6.2. Synrift Paleogeothermal Gradient

The paleogeothermal gradients we obtained vary in the different structural units of the inverted hyperextended Mauléon basin. This variation is clearly evident along a proximal-distal margin transect: the paleogeothermal gradient increases basinward from ~34°C/km in the European proximal margin to ~37–47°C/km in the two necking zones to 57–60°C/km in the hyperextended domain **(Fig. 9)**.

6.2.1. Proximal Margins

The upper unit of the Orthez-102 well, in the European proximal margin, recorded a paleogeothermal gradient of 34°C/km. This gradient is consistent with the average geothermal gradient of ~30°C/km in continental domains and the average continental heat flow of 80 mW/m^2 (Jaupart & Mareschal, 2007). The isotherms in this borehole document northward transport of the warmer upper unit (240°C) over the cooler autochthonous unit (120°C). This latter RSCM peak temperature affects Aptian-Albian deposits of the authotonous unit whereas the same stratigraphic levels of the allochthonous unit recorded higher RSCM peak temperatures around 160–200°C. Consequently, we interpret the Orthez-102 autochthonous unit as representing a more proximal part of the European margin.

As mentioned in section 5.1, the paleogeothermal gradient could not be estimated for the Iberian proximal margin. The 15 outcrop samples collected on the footwall of the Lakhoura thrust recorded RSCM peak temperatures ranging from 160–180°C in the west to 280°C in the east. These temperatures are higher than those found in the Cenomanian to Santonian breccias of the Lakhoura thrust hanging wall (140–160°C). Consequently, the footwall peak temperatures must postdate the Lakhoura thrusting.

6.2.2. Necking Zones

The Iberian necking zone is represented by the Mendibelza and Arbailles field sections and the Hasparren-101 borehole. This domain had higher paleogeothermal gradients (e.g., 39–46°C/km in the Mendibelza unit) than normal stable crust (30°C/km). In the Arbailles field section, the RSCM peak temperature increases toward the younger stratigraphic levels, being 180°C in the Jurassic sequence and 230–250°C in the Albian synrift sequence. This increase could be interpreted as the result of early Cenomanian southward tilting of the Iberian necking zone (Saspiturry et al., 2019a) that occurred before peak temperatures were reached. To the northwest, the Hasparren-101 borehole presents a more complex thermal record. The thrust plane at 5,380 m depth is marked by an abrupt 40°C change in the RSCM peak temperature from 240°C in the footwall to 280°C in the hanging wall **(Fig. 5)**. In our interpretation, this thrust transported a basinal section over a more proximal one.

The lower part of the allochthonous unit displayed an adiabatic temperature gradient over a 2.5-km interval with a constant 280°C temperature, whereas the upper part yielded a 62°C/km deformed thermal gradient **(Fig. 6A)**. As mentioned in section 4.2, the homogeneous temperature was probably due to upward circulation of hot fluid from 5.1 to 2.8 km (hot upwelling), but it could also correspond to downward circulation of cold fluid from 2.8 to 5.1 km (cold downwelling). Such temperature profiles, in which an elevated temperature gradient at the surface overlies a zone of constant temperature over several hundreds to thousands of meters, are often seen in geothermal systems typified by hot upwelling (e.g., Muraoka et al., 2000; Guillou-Frottier et al., 2013). However, in this borehole we could not discriminate between hot upwelling and cold downwelling. Although the 62°C/km deformed thermal gradient was probably influenced by fluid transport, it is not necessarily higher than it would be with no fluid circulation. For example, in the case of a permeable medium where permeability is depth-dependent, the surface temperature gradient over a zone of cold downwelling may be lower than the purely conductive case (see **Supplementary Information S2**). It is thus

problematic to estimate a paleogeothermal gradient in the presence of a convective zone.

In the European necking zone, the paleogeothermal gradient was estimated using the Bellevue-1 borehole just north of the Saint-Palais thrust **(Fig. 2)**. The Bellevue-1 well intersects a complex structure corresponding to the Tertiary reactivation of an Albian diapiric ridge (Saspiturry et al., 2019a). The apparent thermal gradient shows, however, that the RSCM peak temperatures postdate the formation of this structure. Thus we considered the paleogeothermal gradient to be very close to the apparent gradients, or 38°C/km in the allochthonous unit and 47°C/km in the autochthonous unit **(Fig. 6E)**. These values are comparable to those obtained in the Iberian necking zone.

The Les Cassières-2 well, in the European necking zone, penetrates a well-preserved sedimentary succession undisturbed by major Pyrenean thrusting **(Fig. 2A)**. We consider it as a reference section for the European necking zone that defines a paleogeothermal gradient of ~37-40°C/km.

6.2.3. Hyperextended Domain

The paleothermal structure of the hyperextended domain was calibrated using the Chéraute-1, Uhart-Mixe-1, and Ainhice-1 boreholes **(Fig. 2)**. The Chéraute-1 borehole is just east of the Saison structure that accommodates the major Roquiague diapir (**Fig. 2A**; Canérot, 1988, 1989, 2008). We interpret the fold in this well as having been induced by the development of the Roquiague diapir during Senonian time **(Fig. 5)**. The well is characterized by a steady rise in RSCM peak temperatures from 240°C to 330°C across a sedimentary succession 5,350 m thick, defining a deformed thermal gradient of 21°C/km **(Fig. 6C and Tab. 2)**. Heat refraction by thermally conductive Late Triassic evaporites could be responsible for the homogenization of temperatures across the sedimentary basin infill near this structure. Consequently, the measured paleogeothermal gradient is incompatible with the gradients in the Uhart-Mixe-1 and Ainhice-1 wells. These two boreholes lie between the Saint-Jean-Pied-de-Port and Saison transfer zones (**Fig. 1**; Canérot, 2008). The Ainhice-1 well, located at the transition with the Iberian necking zone, yielded an unusually high paleogeothermal gradient of 57°C/km **(Fig. 6B)**. Because the paleogeothermal profile was not disturbed where a packet of strata ~400 m thick was duplicated above the décollement at 1,600 m, the peak temperatures there clearly postdate the displacement on the décollement. The Uhart-Mixe-1 well, in the heart of the hyperextended domain, is free of major Pyrenean deformation. It too yielded an abnormally high paleogeothermal gradient of 60°C/km **(Fig. 6D)**. The asymmetry in the paleogeothermal gradients across the basin may indicate a complex competition between brittle and ductile deformation along the Lakhoura detachment and within the sedimentary cover of the Mauléon basin.

For perspective, other estimated paleotemperature gradients in continental rifts range from 50 to 100°C/km in Antarctica (Berg et al., 1989), 80–100°C/km in Iceland (Bertani, 2017), and 110°C/km in the Soultz area in the Rhine graben (Genter et al., 2010). Our estimated paleogeothermal gradients for the Mauléon hyperextended domain are comparable to other recent estimates: Corre (2017) reported an estimate of 60–75°C/km based on RSCM data, and estimates of 80°C/km by Vacherat et al. (2014) and Hart et al. (2017) were based on detrital zircon fission-track data and (U-Th-Sm)/He thermochronology data, respectively.

6.3. Thermal Anomaly and Gravity Anomaly

The high paleogeothermal gradient we identified in the hyperextended domain coincides with the positive gravity anomaly associated with the Mauléon basin (**Fig. 1A**; Gottis, 1972; Boillot et al., 1973; Grandjean, 1992, 1994; Daignières et al., 1994; Casas et al., 1997), which has recently been interpreted as the presence of subcontinental mantle at around 10 km depth (**Fig. 2B**; Wang et al., 2016; Wang, 2017). This shallow subcontinental mantle has been interpreted as being locally exposed by denudation and as shedding detritus into the late Albian to early Cenomanian synrift deposits (Roux, 1983; Fortané et al., 1986; Jammes et al., 2009; Debroas et al., 2010; Lagabrielle et al., 2010) during the hyperextension of the continental crust (Masini et al., 2014; Teixell et al., 2016). This interpretation holds the Albian-Cenomanian hyperextension in the Mauléon

basin responsible for the high paleogeothermal gradient in the basin center. The inherited hyperextended structural template clearly controls the spatial distribution of the thermal gradient. This high gradient lasted at least until the Campanian to early Eocene, raising a question as to the process responsible for the Late Cretaceous subsidence. Indeed, the middle Cenomanian to late Santonian carbonate turbidites are considered part of a postrift sequence that covered the entire rift structure (Ducasse & Vélasque, 1988; Saspiturry et al., 2019a). However, because this study focused on the Late Triassic to Santonian deposits, we cannot address the timing of the postrift cooling.

6.4. The Mauléon basin Internal Metamorphic Zone

Considering the 60°C/km paleogeothermal gradient in the Uhart-Mixe-1 well **(Fig. 6D)**, we can extrapolate the temperature from the base of the well into the hyperextended domain in this sector of the Mauléon basin, between the Saint-Jean-Pied-de-Port and Saison transfer faults **(Fig. 1B)**, and estimate that the prerift cover reached a temperature of 500–600°C **(Fig. 9A)**. This temperature range is similar to those documented in the Internal Metamorphic Zone in the central and eastern Pyrenees (e.g., Bernus-Maury, 1984; Golberg & Leyreloup, 1990; Azambre et al., 1992; Clerc, 2012; Vauchez et al., 2013; Clerc et al., 2015; Chelalou et al., 2016) and the Nappes des Marbres in the Basque-Cantabrian basin (Lamare, 1936; Martinez-Torrez, 1989; Mendia & Ibarguchi, 1991; Ducoux, 2017). The Internal Metamorphic Zone has been interpreted as the inverted base of the North Pyrenean hyperextended rift domain (Clerc, 2012; Clerc & Lagabrielle, 2014; Clerc et al., 2015; Lagabrielle et al., 2016; Ducoux, 2017). Consequently, we can infer that marble corresponding to the Internal Metamorphic Zone marbles exists in this sector of the Mauléon basin. However, farther eastward the base of the basin does not exceed 350°C, as indicated by RSCM peak temperatures in the Chaînons Béarnais prerift cover (Corre, 2017) and Paleozoic basement (Asti et al., 2019). Contrary to the great east-west extent of the Internal Metamorphic Zone in the central and eastern Pyrenees, its extension in the Mauléon basin appears to be restricted to a very small area. Thus, we can deduce that the Internal Metamorphic Zone hyperextended basin was much wider than the hyperextended Mauléon system, raising a question about the way Cretaceous extension is distributed along the Pyrenean rift system.

6.5. Role of Rift Inheritance on Postcollisional Thermal Imprint

The Pyrenean deformation of the Mauléon basin was not intense **(Figs. 1B and 9B)**, and high-temperature marbles were not removed from the base of the Saint-Palais hyperextended domain. Indeed, rift inversion started during late Santonian to Campanian time to the east of the Mauléon basin (Choukroune & ECORS Team, 1989; Muñoz, 1992; Ford et al., 2016; Macchiavelli et al., 2017; Ternois et al., 2019) and in late Eocene time to the west (Teixell, 1993; Labaume et al., 2016). The compression should have resulted in a higher shortening rate in the central and eastern Pyrenees (Beaumont et al., 2000; Muñoz, 1992; Vergés et al., 1995; Mouthereau et al., 2014) than in the western Pyrenees (Teixell, 1996, 1998). Consequently, the central and eastern Pyrenees Internal Metamorphic Zone was uplifted and exposed during the Pyrenean compression whereas it is still buried in the Mauléon basin.

The compressive deformation of the Mauléon rift basin created a pop-up structure **(Fig. 9B)** as northward displacement on the Bellevue and Sainte-Suzanne thrusts affected the European margin and southward displacement on the Lakhoura thrust compressed the Iberian margin. The previously acquired postrift isotherms thus were folded and tilted inside this pop-up structure. On the European margin, our evidence demonstrates that the postrift isotherms were not erased by the Pyrenean thrusting, but instead were passively transported onto the proximal margin. On the Iberian margin, the Lakhoura thrust is marked by an increase of peak temperatures on its footwall, meaning that they were acquired after the thrusting. The different thermal responses on the opposite sides of the pop-up structure can be linked to their tectonic reactivation style. The Iberian margin was affected by Pyrenean thick-skin tectonics that

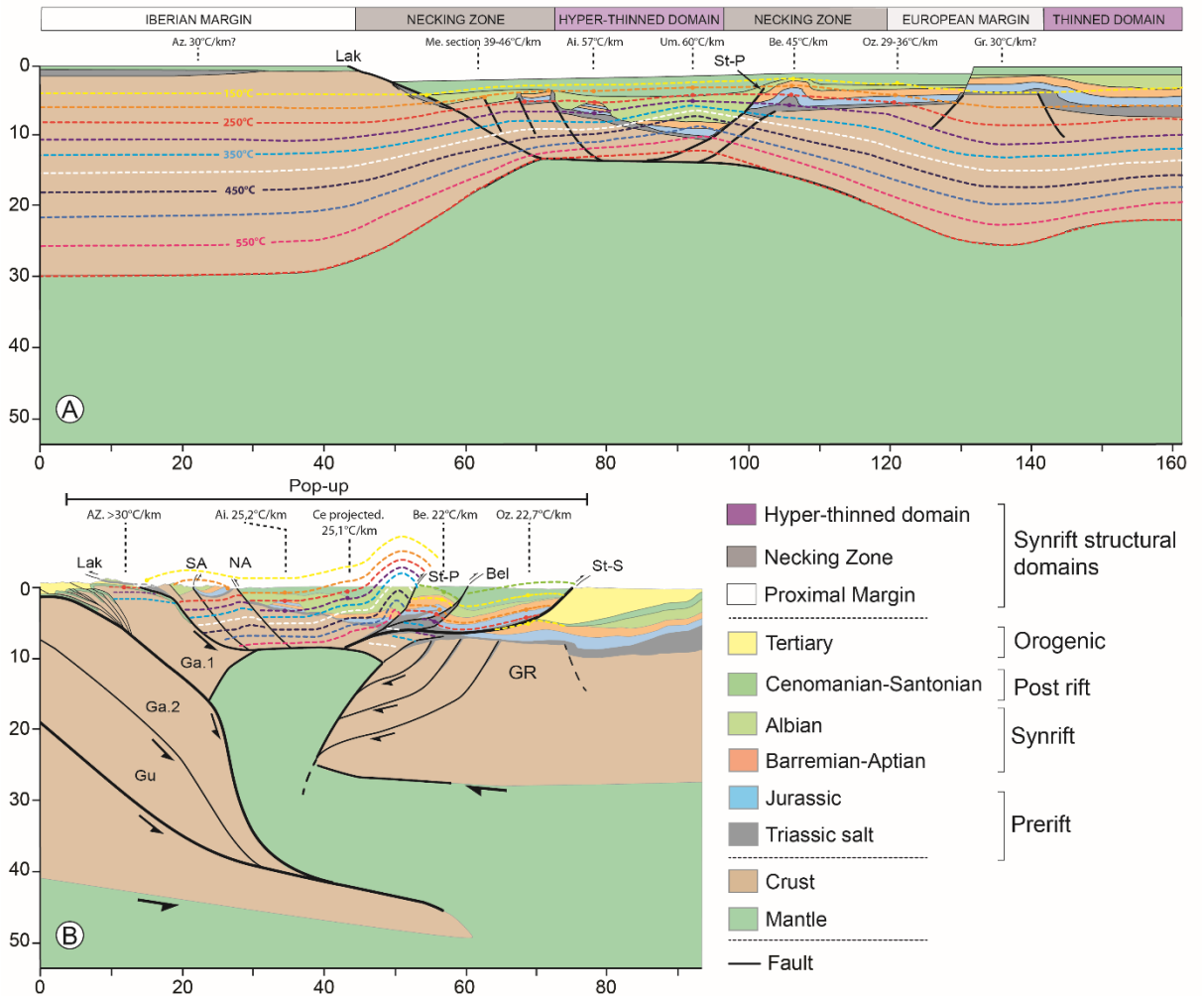


Fig. 9. (A) Late Cretaceous palinspastic restoration along a N-S cross section of the Mauléon basin, displaying the synrift paleogeothermal gradients for the different structural margin domains. The Mauléon rift is characterized by a basinward increase of the paleogeothermal gradient, which induced a complex competition between brittle vs. ductile deformation during early Cenomanian detachment on the Lakhoura fault (heavy black lines). Extension on the Saint-Palais detachment (dashed line) occurred during Albian time. Az, Axial Zone; Me, Mendibelza; Ai, Ainhice-1 borehole; Um, Uhart-Mixe-1 borehole; Be, Bellevue-1 borehole; Oz, Orthez-102 borehole; Gr, Grand Rieu. **(B)** Cross section through the modern Mauléon basin. Crustal section is modified from Saspiturry et al. (2019). The modern Mauléon basin is a pop-up structure whose southern edge reactivates the Lakhoura detachment, and the northern edge is a duplex crustal stack that laterally shortens the European basement. Thick-skin tectonics affecting the Iberian margin is responsible for postcollisional thermal heating, whereas the European margin is characterized by northward displacement of metamorphosed material and an unusually low postcollisional thermal gradient. Ce, Chéraute-1 borehole; Lak, Lakhoura thrust; St-P, Saint-Palais thrust; Bel, Bellevue thrust; St-S, Sainte-Suzanne thrust.

built up the 50-km-thick Axial Zone antiformal crustal stack, of which the Lakhoura thrust is the uppermost unit **(Fig. 9B)**. The Lakhoura thrust represents the reactivation of a crustal-scale detachment inherited from the hyperextension stage.

Thick-skin tectonics is known to lead to an increased thermal gradient (e.g., Jaupart & Provost, 1985; England & Thompson, 1986; Huerta et al., 1999). In our case, the increased thermal gradient is responsible for the postcollisional heating of the Iberian proximal margin. On the European margin and in the hyperextended domain of the Mauléon basin, a major decrease in the thermal gradient to the 25.0 ± 2.7°C/km gradients in modern boreholes (see **Supporting Information S1**) followed the onset of compression. In the Iberian margin, the northward motion of the Iberian slab under the Mauléon hyperextended domain greatly decreased the heat flow from the asthenosphere. The European margin, to the contrary, has never featured thick-skin tectonics, explaining the current Moho depth of ~27 km there **(Fig. 9B)**. Indeed, shortening of the European margin was accommodated by the Bellevue and Sainte-Suzanne thin-skin thrusts. The unusually low

thermal gradient there is directly controlled by the thinness of the European continental crust and the presence of nonradiogenic subcontinental mantle at shallow depths.

7. Conclusion

In this study, we estimated the 3D paleothermal structure of the Mauléon hyperextended rift, using RSCM peak temperatures obtained from 155 outcrop and borehole samples. The Mauléon basin recorded an abnormally high heat flow following Albian-Cenomanian hyperextension. The thermicity sealed the hyperextension structural scheme, and the prerift to postrift sedimentary infill was thus affected by a paleogeothermal gradient whose isotherms crosscut all older tectonic structures.

The paleogeothermal gradients estimated in this study probably reached their maximum during Paleocene to early Eocene time. They rise in magnitude from the proximal domains to the center of the Albian-Cenomanian rift, starting from ~34°C/km on the European proximal margin (typical of stable cratons), to ~37–47°C/km in the two necking zones, to 57–60°C/km in the hyperextended domain. The area of highest gradient corresponds with a positive gravity anomaly, interpreted as the presence at shallow depth (~10 km) of subcontinental mantle. Extrapolating the temperature at the base of the hyperextended domain, we infer that it reached 500–600°C in the segment of the basin between the Saint-Jean-Pied-de-Port and the Saison transfer faults. These temperatures are similar to those measured in marbles of the Internal Metamorphic Zone in the central and eastern Pyrenees. However, the east-west divisions of the Mauléon basin high temperature are very narrow compared to the Internal Metamorphic Zone of the central and eastern Pyrenees. This finding suggests that the Albian-Cenomanian Metamorphic Internal Zone hyperextended basin was much wider than in the western Pyrenees.

The pop-up structures on the northern and southern flanks of the Mauléon basin, formed during later compression across the rift, present differing postcollisional thermal responses. The European margin was affected by northward thrusting that transported the paleoisotherms across the proximal margin without heating the thrust footwalls. As a result, the precollisional maximum paleogeothermal gradients of both the hyperextended domain and the European margin were preserved. On the Iberian margin, the geothermal gradient increased as the footwall of the Lakhoura thrust underwent heating after the collision, which reset its precollisional paleogeothermal record. This gradient increase can be linked to thickening of the Iberian continental crust following the formation of the antiformal crustal stack in the Axial Zone. The northward motion of the Iberian slab beneath the Mauléon hyperextended domain is responsible for a steep decrease in the asthenospheric heat flow and explains the low postcollisional geothermal gradient (25.0 ± 2.7°C/km) in the Mauléon basin core and European margin. Unlike the Iberian margin, the European margin never underwent thick-skin tectonics and retained its current Moho depth of 25-27 km. Its low geothermal gradient is the consequence of a thin European continental crust and the presence at shallow depth of nonradiogenic subcontinental mantle.

Acknowledgments

This work is part of the Orogen geological research project cofunded by Total S.A., BRGM, and Institut national de sciences de l'Univers (INSU). We thank Orogen project managers Emmanuel Masini (Total), Olivier Vidal (CNRS), and Isabelle Thinon (BRGM).

References

Albarède, F., & Michard-Vitrac, A. (1978a). Age and Significance of the North Pyrenean Metamorphism. *Earth Planet. Sci. Lett*. 327–332.

Albarède, F., & Michard-Vitrac, A. (1978b). Datation du métamorphisme des terrains secondaires des Pyrenees par les méthodes 39 Ar-40 Ar et 87 Rb-87 Sr; ses relations avec les peridotites associées. *Bull. Société Géologique*, Fr. 7, 681–687.

Angrand, P., Ford, M., & Watts, A, B. (2018). Lateral variations in foreland flexure of a rifted continental margin: The Aquitaine basin (SW France). *Tectonics*. 37. https://doi.org/10.1002/2017TC004670

Aslanian, D., & Moulin, M. (2013). Palaeogeographic consequences of conservational models in the South Atlantic Ocean. *Geol. Soc. Lond. Spec. Publ*. 369, 75–90. https://doi.org/10.1144/SP369.5

Aslanian, D., Moulin, M., Olivet, J.-L., Unternehr, P., Matias, L., Bache, F., Rabineau, M., Nouzé, H., Klingelheofer, F., Contrucci, I., & Labails, C. (2009).

Brazilian and African passive margins of the Central Segment of the South Atlantic Ocean: Kinematic constraints. *Tectonophysics*, 468, 98–112. https://doi.org/10.1016/j.tecto.2008.12.016

Asti, R., Lagabrielle, Y., Fourcade, S., Corre, B., & Monié, P., (2019). How Do Continents Deform During Mantle Exhumation? Insights From the Northern Iberia Inverted Paleopassive Margin, Western Pyrenees (France). *Tectonics*, 28, 1666-1693. https://doi.org/10.1029/2018TC005428

Azambre, B., & Monchoux, P. (1998). Métagabbros amphiboliques et mise en place crustale des lherzolites des Pyrénées (France). *Comptes Rendus Académie Sci.-Ser. IIA-Earth Planet. Sci*. 327, 9–15.

Azambre, B., & Rossy, M. (1976). Le magmatisme alcalin d'âge crétacé, dans les Pyrénées occidentales et l'Arc basque; ses relations avec le métamorphisme et la tectonique. *Bull. Société Géologique Fr*. 7, 1725–1728.

Azambre, B., Rossy, M., & Albarède, F. (1992). Petrology of the alkaline magmatism from the Cretaceous North-Pyrenean rift zone (France and Spain). *Eur. J. Mineral*. 4, 813–834.

Bai, Y., Dong, D., Brune, S., Wu, S., & Wang, Z. (2019). Crustal stretching style variations in the northern margin of the South China Sea. *Tectonophysics* 751, 1–12. https://doi.org/10.1016/j.tecto.2018.12.012

Beaumont, C., Muñoz, J.A., Hamilton, J., & Fullsack, P. (2000). Factors controlling the Alpine evolution of the central Pyrenees inferred from a comparison of observations and geodynamical models. *J. Geophys. Res*. 105, 8121–8145.

Beltrando, M., Manatschal, G., Mohn, G., Dal Piaz, G.V., Brovarone, A.V., & Masini, E. (2014). Recognizing remnants of magma-poor rifted margins in high-pressure orogenic belts: The Alpine case study. *Earth-Sci. Rev*. 131, 88–115.

Berg, J. H., Moscati R. J., & Herz D. L. (1989). A petrologic geotherm from a continental rift in Antartica. *Earth Planet Sci. Lett*., 93, 98-108.

Bernus-Maury, C. (1984). Etude des paragéneses caractéristiques du métamorphisme mésozoïque dans la partie orientale des Pyrénées. (Doctoral dissertation). Pierre et Marie Curie, Paris.

Bertani, R. (2017). Perspectives for geothermal energy in Europe. World Scientific, 304 p.

Beyssac, O., Goffé, B., Chopin, C., & Rouzaud, J.N. (2002). Raman spectra of carbonaceous material in metasediments: a new geothermometer. *Journal of Metamorphic Geology*, 20, 859–871. http://dx.doi.org/10.1046/j.1525-1314.2002.00408.x.

Bodinier, J., Menzies, M.A., Shimizu, N., Frey, F.A., & McPherson, E. (2004). Silicate, hydrous and carbonate metasomatism at Lherz, France: contemporaneous derivatives of silicate melt–harzburgite reaction. *J. Petrol*, 45, 299–320.

Bodinier, J.L., Dupuy, C., & Dostal, J. (1988). Geochemistry and petrogenesis of Eastern Pyrenean peridotites. *Geochim. Cosmochim. Acta*, 52, 2893–2907.

Boillot, G., Capdevilla, R., Hennequin-Marchand, I., Lamboy, M., & Lepretre, J.P. (1973). La zone nord-pyrénéenne, ses prolongements sur la marge continentale nord-espagnole et sa signification structurale. *Comptes Rendus Acad. Sci. Paris*, 227, 2629–2632.

Boillot, G., Féraud, G., Recq, M., & Girardeau, J. (1989). Undercrusting by serpentinite beneath rifted margins: the example of the west Galicia margin (Spain). *Nature*, 341, 523–525.

Boillot, G., Recq, M., Winterer, E.L., Meyer, A.W., Applegate, J., Baltuck, M., Bergen, J.A., Comas, M.C., Davies, T.A., Dunham, K., & others. (1987). Tectonic denudation of the upper mantle along passive margins: a model based on drilling results (ODP leg 103, western Galicia margin, Spain). *Tectonophysics*, 132, 335–342.

Boirie, J.-M. (1981). Etude Sédimentologique des Poudingues de Mendibelza (Pyrénées Atlantiques). (Doctoral dissertation), Université Paul Sabatier de Toulouse (Sciences), Toulouse.

Boulvais, P. (2016). Fluid generation in the Boucheville basin as a consequence of the North Pyrenean metamorphism. *Comptes Rendus Géosciences*, 348, 301–311. https://doi.org/10.1016/j.crte.2015.06.013

Boulvais, P., de Parseval, P., D'Hulst, A., & Paris, P. (2006). Carbonate alteration associated with talc-chlorite mineralization in the eastern Pyrenees, with emphasis on the St. Barthelemy Massif. *Mineral. Petrol*, 88, 499–526. https://doi.org/10.1007/s00710-006-0124-x

Boulvais, P., Ruffet, G., Cornichet, J., & Mermet, M. (2007). Cretaceous albitization and dequartzification of Hercynian peraluminous granite in the Salvezines Massif (French Pyrénées). *Lithos*, 93, 89–106. https://doi.org/10.1016/j.lithos.2006.05.001

Bouquet, B. (1986). La bordure mésozoïque orientale du Massif du Labourd (Pyrénées occidentales) : Stratigraphie-Sédimentologie-Structure-Implications Géodynamiques: Pau, Université de Pau et des Pays de l'Adour, 219 p.

Braun, J. (2009). Hot blanket in Earth's deep crust. *Nature*, 458, 292-293.

Brune, S., Heine, C., Pérez-Gussinyé, M., & Sobolev, S.V. (2014). Rift migration explains continental margin asymmetry and crustal hyper-extension. *Nature Communication*, 5. https://doi.org/10.1038/ncomms5014

Brune, S., Williams, S.E., Butterworth, N.P., & Müller, R.D. (2016). Abrupt plate accelerations shape rifted continental margins. *Nature*, 536, 201–204. https://doi.org/10.1038/nature18319

Canérot, J. (1988). Manifestations de l'halocinèse dans les chaînons béarnais (zone Nord-Pyrénéenne) au Crétacé inférieur. *Comptes Rendus Académie Sci. Sér. 2 Mécanique Phys. Chim. Sci. Univers Sci. Terre*, 306, 1099–1102.

Canérot, J. (1989). Rifting éocrétacé et halocinèse sur la marge ibérique des Pyrénées Occidentales (France). Conséquences structurales. *Bull. Cent. Rech. Explor.-Prod. Elf-Aquitaine*, 13, 87–99.

Canérot, J. (2008). Les Pyrénées: Histoire géologique. Atlantica.

Canérot, J. (2018a). The pull apart-type Tardets-Mauléon basin, a key to understand the formation of the Pyrenees. *Bull. Soc. géol. Fr*, 188, 35.

Canérot, J. (2018b). Origine de la chaîne des Pyrénées : collision entre les plaques ibérique et européenne ou inversion d'un ancien rift intracontinental avorté ? *Bull. Soc. Hist. Nat. Toulouse*, 153, 95–110.

Casas, A., Kearey, P., Rivero, L., & Adam, C.R. (1997). Gravity anomaly map of the Pyrenean region and a comparison of the deep geological structure of the western and eastern Pyrenees. *Earth Planet. Sci. Lett*. 150, 65–78.

Castañares, L.M., Robles, S., & Vicente Bravo, J.C. (1997). Distribución estratigráfica de los episodios volcánicos submarinos del Albiense-Santoniense en la Cuenca Vasca (sector Gernika-Plentzia, Bizkaia).

Casteras, M. (1933). Recherches sur la structure du versant nord des Pyrénées centrales et orientales. Libraire Polytechnique, C. Béranger.

Casteras, M., Villanova, M., Godechot, J., Blanc, C., Labourguigne, J., Deloffre, R., Azambre, B., & Alimen, H. (1970). Carte géologique de la France au 1/50 000: feuille de Lourdes, Orléans, France.

Casteras, M., Gottis, M., Clin, M., Guignard, J.., Paris, J., & Galharague, J. (1971). Carte géologique de la France au 1/ 50 000, feuille de Tardets–Sorholus, Orléans, France.

Chelalou, R., Nalpas, T., Bousquet, R., Prevost, M., Lahfid, A., Poujol, M., Ringenbach, J.-C., & Ballard, J.-F. (2016). New sedimentological, structural and paleo-thermicity data in the Boucheville basin (eastern North Pyrenean Zone, France). *Comptes Rendus Géoscience*, 348, 312–321.

Chevrot, S., Sylvander, M., Diaz, J., Martin, R., Mouthereau, F., Manatschal, G., Masini, E., Calassou, S., Grimaud, F., Pauchet, H., & Ruiz, M. (2018). The non-cylindrical crustal architecture of the Pyrenees. *Scientific Report*, 8. https://doi.org/10.1038/s41598-018-27889-x

Choukroune, P. (1974). Structure et évolution tectonique de la zone nord-pyrénéenne: analyse de la déformation dans une portion de chaîne à schistosité sub-verticale.

Choukroune, P., & Mattauer, M. (1978). Tectonique des plaques et Pyrénées; sur le fonctionnement de la faille transformante nord-pyrénéenne; comparaisons avec des modèles actuels. *Bull. Société Géologique Fr*. 7, 689–700.

Choukroune, P. & ECORS Team. (1989). The ECORS Pyrenean deep seismic profile reflection data and the overall structure of an orogenic belt. *Tectonics* 8, 23–39.

Claude, D. (1990). Etude stratigraphique, sédimentologique et structurale des dépôts mésozoïques au nord du massif du Labourd: rôle de la faille de Pamplona (Pays Basque). (Doctoral dissertation), Université de Bordeaux III.

Clauser C., & Huenges E. (1995). Thermal conductivity of rocks and minerals. In: T.J. Ahrens, Ed., Rock physics and phase relations: a handbook of physical constants, vol 3. – AGU, Washington D.C., AGU Ref. Shelf, pp. 105-126.

Clerc, C. (2012). Evolution du domaine nord-pyrénéen au Crétacé: amincissement crustal extrême et thermicité élevée: un analogue pour les marges passives. (Doctoral dissertation), Paris 6.

Clerc, C., & Lagabrielle, Y. (2014). Thermal control on the modes of crustal thinning leading to mantle exhumation: Insights from the Cretaceous Pyrenean hot paleomargins. *Tectonics*, 33, 1340–1359. https://doi.org/10.1002/2013TC003471

Clerc, C., Lagabrielle, Y., Neumaier, M., Reynaud, J.-Y., & de Saint Blanquat, M. (2012). Exhumation of subcontinental mantle rocks: evidence from ultramafic-bearing clastic deposits nearby the Lherz peridotite body, French Pyrenees. *Bull. Société Géologique Fr*. 183, 443–459.

Clerc, C., Boulvais, P., Lagabrielle, Y., & de Saint Blanquat, M. (2014). Ophicalcites from the northern Pyrenean belt: a field, petrographic and stable isotope study. *Int. J. Earth Sci.* 103, 141–163. https://doi.org/10.1007/s00531-013-0927-z

Clerc, C., Lahfid, A., Monié, P., Lagabrielle, Y., Chopin, C., Poujol, M., Boulvais, P., Ringenbach, J.C., Masini, E., & de St Blanquat, M. (2015). High-temperature metamorphism during extreme thinning of the continental crust: a reappraisal of the North Pyrenean passive paleomargin. *Solid Earth*, 6, 643–668.

Contrucci, I., Matias, L., Moulin, M., Géli, L., Klingelhofer, F., Nouzé, H., Aslanian, D., Olivet, J.-L., Réhault, J.-P., & Sibuet, J.-C. (2004). Deep structure of the West African continental margin (Congo, Zaïre, Angola), between 5 S and 8 S, from reflection/refraction seismics and gravity data. *Geophys. J. Int*. 158, 529–553.

Corre, B. (2017). La bordure nord de la plaque ibérique à l'Albo-Cénomanien: architecture d'une marge passive de type ductile (Chaînons Béarnais, Pyrénées Occidentales), (Doctoral dissertation). Rennes 1.

Corre, B., Lagabrielle, Y., Labaume, P., Fourcade, S., Clerc, C., & Ballèvre, M. (2016). Deformation associated with mantle exhumation in a distal, hot passive margin environment: New constraints from the Saraillé Massif (Chaînons Béarnais, North-Pyrenean Zone). *Comptes Rendus Geosci*. 348, 279–289. https://doi.org/10.1016/j.crte.2015.11.007

Daignières, M., Séguret, M., Specht, M., & Team ECORS. (1994). The Arzacq-western Pyrenees ECORS deep seismic profile, in: Hydrocarbon and Petroleum Geology of France. Springer, 199–208.

Dauteuil, O., & Ricou, L.-E. (1989). Une circulation de fluides de haute-température à l'origine du métamorphisme crétacé nord-pyrénéen. *Geodin. Acta*, 3, 237–249. https://doi.org/10.1080/09853111.1989.11105190

Debroas, E.J. (1978). Evolution de la fosse du flysch ardoisier de l'Albien superieur au Senonien inferieur (zone interne metamorphique des Pyrenees navarro-languedociennes). *Bull. Société Géologique Fr*. 7, 639–648.

Debroas, E.-J. (1987). Modèle de bassin triangulaire à l'intersection de décrochements divergents pour le fossé albo-cénomanien de la Ballongue (zone nord-pyrénéenne,

France). *Bull. Société Géologique Fr*. 3, 887–898. https://doi.org/10.2113/gssgfbull.III.5.887

Debroas, E.J. (1990). Le flysch noir albo-cenomanien temoin de la structuration albienne a senonienne de la Zone nord-pyreneenne en Bigorre (Hautes-Pyrenees, France). *Bull. Soc. Geol. Fr.* 6, 273–285. https://doi.org/10.2113/gssgfbull.VI.2.273

Debroas, E.J., Canérot, J., & Bilotte, M. (2010). Les brèches d'Urdach, témoins de l'exhumation du manteau pyrénéen dans un escarpement de faille vraconnien-cénomanien inférieur (Zone nord-pyrénéenne, Pyrénées-Atlantiques, France). *Géologie de la France*. 2, 53–63.

Decarlis, A., Manatschal, G., Haupert, I., & Masini, E. (2015). The tectono-stratigraphic evolution of distal, hyper-extended magma-poor conjugate rifted margins: Examples from the Alpine Tethys and Newfoundland–Iberia. *Mar. Pet. Geol*. 68, 54–72. https://doi.org/10.1016/j.marpetgeo.2015.08.005

Driscoll, N.W., Hogg, J.R., Christie-Blick, N., & Karner, G.D. (1995). Extensional tectonics in the Jeanne d'Arc basin, offshore Newfoundland: implications for the timing of break-up between Grand Banks and Iberia. *Geol. Soc. Lond. Spec. Publ*. 90, 1–28. https://doi.org/10.1144/GSL.SP.1995.090.01.01

Dubois, P., & Seguin, J.C. (1978). Les flyschs cretace et eocene de la zone commingeoise et leur environnement. *Bull. Soc. Geol. Fr*. S7-XX, 657–671. https://doi.org/10.2113/gssgfbull.S7-XX.5.657

Ducasse, L., & Vélasque, P.-C. (1988). Géotraverse dans la partie occidentale des Pyrénées, de l'avant-pays aquitain au bassin de l'Ebre: effet d'une inversion structurale sur l'édification d'une chaîne intracontinentale. Université Paul Cézanne (Aix-Marseille). (Doctoral dissertation), Faculté des sciences et techniques de Saint-Jérôme.

Ducasse, L., Vélasque, P.-C., & Muller, J. (1986). Glissement de couverture et panneaux basculés dans la région des Arbailles (Pyrénées occidentales): Un modèle évolutif crétacé de la marge nord-ibérique à l'Est de la transformante de Pamplona. *Comptes Rendus Académie Sci. Sér. 2 Mécanique Phys. Chim. Sci. Univers Sci. Terre*, 303, 1477–1482.

Ducoux, M. (2017). Structure, thermicité et évolution géodynamique de la Zone Interne Métamorphique des Pyrénées. Institut des Sciences de la Terre d'Orléans (ISTO).

Duée, G., Lagabrielle, Y., Coutelle, A., & Fortané, A. (1984). Les lherzolites associées aux Chaînons Béarnais (Pyrénées Occidentales): Mise à l'affleurement anté-dogger et resédimentation albo-cénomanienne. *Comptes-Rendus Séances Académie Sci. Sér. 2 Mécanique-Phys. Chim. Sci. Univers Sci. Terre*, 299, 1205–1210.

England, P. C., & Thompson A. (1986). Some thermal and tectonic models for crustal melting in continental collision zones. In Coward, M.P. & A.C. Ries (eds), *Collision Tectonics, Geol. Spec. Pub*., 19, 83-94.

Fabriès, J., Lorand, J.-P., & Bodinier, J.-L. (1998). Petrogenetic evolution of orogenic lherzolite massifs in the central and western Pyrenees. *Tectonophysics*, 292, 145–167.

Fabriès, J., Lorand, J.-P., Bodinier, J.-L., & Dupuy, C. (1991). Evolution of the Upper Mantle beneath the Pyrenees: Evidence from Orogenic Spinel Lherzolite Massifs. *J. Petrol. Special_Volume*, 55–76. https://doi.org/10.1093/petrology/Special_Volume.2.55

Fallourd, S., Poujol, M., Boulvais, P., Paquette, J.-L., de Saint Blanquat, M., & Rémy, P. (2014). In situ LA-ICP-MS U–Pb titanite dating of Na–Ca metasomatism in orogenic belts: the North Pyrenean example. *Int. J. Earth Sci*. 103, 667–682. https://doi.org/10.1007/s00531-013-0978-1

Fixari, G. (1984). Stratigraphie, faciès et dynamique tecto-sédimentaire du flysch albien (flysch noir et poudingues de Mendibelza) dans la région de Mauléon-Tardets (Pyrénées Atlantiques). (Doctoral dissertation), Université Paul Sabatier de Toulouse (Sciences).

Ford, M., Hemmer, L., Vacherat, A., Gallagher, K., & Christophoul, F. (2016). Retro-wedge foreland basin evolution along the ECORS line, eastern Pyrenees, France. *J. Geol. Soc*. 173, 419–437.

Fortané, A., Duée, G., Lagabrielle, Y., & Coutelle, A. (1986). Lherzolites and the western "Chaînons Béarnais" (French Pyrenees): Structural and paleogeographical pattern. *Tectonophysics*, 129, 81–98. https://doi.org/10.1016/0040-1951(86)90247-7

Froitzheim, N., & Manatschal, G. (1996). Kinematics of Jurassic rifting, mantle exhumation, and passive-margin formation in the Austroalpine and Penninic nappes (eastern Switzerland). *Geol. Soc. Am. Bull*. 108, 1120–1133. https://doi.org/10.1130/0016-7606(1996)108<1120:KOJRME>2.3.CO;2

Genter, A., K. Evans, N. Cuenot, D. Frisch, & B. Sanjuan. (2010). Contribution of the exploration of deep crystalline fractured reservoir of Soultz to the knowledge of enhanced geothermal systems (EGS). *Comptes Rendus Geoscience*, 342, 502-516.

Golberg, J.-M., & Maluski, H. (1988). Données nouvelles et mise au point sur l'âge du métamorphisme pyrénéen. *Comptes Rendus Académie Sci. Sér. 2 Mécanique Phys. Chim. Sci. Univers Sci. Terre*, 306, 429–435.

Golberg, J.M., & Leyreloup, A.F. (1990). High temperature-low pressure Cretaceous metamorphism related to crustal thinning (Eastern North Pyrenean Zone, France). *Contrib. Mineral. Petrol*. 104, 194–207. https://doi.org/10.1007/BF00306443

Golberg, J.M., Maluski, H., & Leyreloup, A.F. (1986). Petrological and age relationship between emplacement of magmatic breccia, alkaline magmatism, and static metamorphism in the North Pyrenean Zone. *Tectonophysics*, 129, 275–290. https://doi.org/10.1016/0040-1951(86)90256-8

Gottis, M. (1972). Construction d'un modèle géodynamique pyrénéen. *Comptes Rendus Académie Sci*. 275, 2099.

Grandjean, G. (1992). Mise en évidence des structures crustales dans une portion de chaîne et de leur relation avec les bassins sédimentaires. Application aux Pyrénées occidentales au travers du Projet ECORS Arzacq-Pyrénées. (Doctoral dissertation), Université des Sciences et Techniques du Languedoc.

Grandjean, G. (1994). Etude des structures crustales dans une portion de chaîne et de leur relation avec les bassins sédimentaires. Application aux Pyrénées occidentales. *Bull Cent Rech Explor Prod Elf Aquitaine*, 18, 391–420.

Guillou-Frottier L., F. Lucazeau, C. Garibaldi, D. Bonté, & Coueffé R. (2010). Heat flow and deep temperatures in the Southeast basin of France: Implications for local rheological contrasts. *Bulletin de la Société Géologique de France*, 181, 6, 531-546. https://doi.org/10.2113/gssgfbull.181.6.531

Guillou-Frottier L., C. Carré, B. Bourgine, V. Bouchot, & Genter A. (2013). Structure of hydrothermal convection in the Upper Rhine Graben as inferred from corrected temperature data and basin-scale numerical models. *Journal of Volcanology and Geothermal Research*, 256, 29-49. https://doi.org/10.1016/j.jvolgeores.2013.02.008

Handy, M.R., M. Schmid, S., Bousquet, R., Kissling, E., & Bernoulli, D. (2010). Reconciling plate-tectonic reconstructions of Alpine Tethys with the geological–geophysical record of spreading and subduction in the Alps. *Earth-Sci. Rev*. 102, 121–158. https://doi.org/10.1016/j.earscirev.2010.06.002

Hart, N.R., Stockli, D.F., Lavier, L.L., & Hayman, N.W. (2017). Thermal evolution of a hyperextended rift basin, Mauléon basin, western Pyrenees: Thermal evolution of hyperextended rift. *Tectonics*. https://doi.org/10.1002/2016TC004365

Haupert, I., Manatschal, G., Decarlis, A., & Unternehr, P. (2016). Upper-plate magma-poor rifted margins: Stratigraphic architecture and structural evolution. *Mar. Pet. Geol*. 69, 241–261. https://doi.org/10.1016/j.marpetgeo.2015.10.020

Henry, P., Azambre, B., Montigny, R., Rossy, M., & Stevenson, R.K. (1998). Late mantle evolution of the Pyrenean sub-continental lithospheric mantle in the light of new 40Ar–39Ar and Sm–Nd ages on pyroxenites and peridotites (Pyrenees, France). *Tectonophysics*, 296, 103–123. https://doi.org/10.1016/S0040-1951(98)00139-5

Huerta A.D., L.H. Royde,, K.V. Hodges, 1999. The effects of accretion, erosion and radiogenic heat on the metamorphic evolution of collisional orogens. J. metamorphic Geol., 17, 349-366.

Huismans, R.S., & Beaumont, C. (2003). Symmetric and asymmetric lithospheric extension: Relative effects of frictional-plastic and viscous strain softening. *J. Geophys. Res. Solid Earth*, 108. https://doi.org/10.1029/2002JB002026

Huismans, R.S., & Beaumont, C. (2008). Complex rifted continental margins explained by dynamical models of depth-dependent lithospheric extension. *Geology*, 36, 163. https://doi.org/10.1130/G24231A.1

Huismans, R.S., & Beaumont, C. (2011). Depth-dependent extension, two-stage breakup and cratonic underplating at rifted margins. *Nature*, 473, 74–78. https://doi.org/10.1038/nature09988

Huismans, R.S., & Beaumont, C. (2014). Rifted continental margins: The case for depth-dependent extension. *Earth Planet. Sci. Lett*. 407, 148–162. https://doi.org/10.1016/j.epsl.2014.09.032

Jammes, S., Manatschal, G., Lavier, L., & Masini, E. (2009). Tectono-sedimentary evolution related to extreme crustal thinning ahead of a propagating ocean: Example of the western Pyrenees. *Tectonics*, 28. https://doi.org/10.1029/2008TC002406

Jaupart C., & Mareschal J.-C. (2007). Heat flow and thermal structure of the lithosphere. In: Watts, A.B. (Ed.), Crustal and Lithosphere Dynamics. Treatise on Geophysics, vol.6. Elsevier, New York, pp.217–251.

Jaupart C., & Mareschal J.-C. (2011). Heat generation and transport in the Earth. Cambridge University Press, 464p.

Jaupart C., & Provost, A. (1985). Heat focusing, granite genesis and inverted metamorphic gradients in continental collision zones. *Earth Planet. Sci. Lett*., 73, 385-397.

Karner, G.D., Driscoll, N.W., & Barker, D.H.N. (2003). Synrift regional subsidence across the West African continental margin: the role of lower plate ductile extension. *Geol. Soc. Lond. Spec. Publ*. 207, 105–129. https://doi.org/10.1144/GSL.SP.2003.207.6

Karner, G.D., & Gambôa, L. a. P. (2007). Timing and origin of the South Atlantic pre-salt sag basins and their capping evaporites. *Geol. Soc. Lond. Spec. Publ*. 285, 15–35. https://doi.org/10.1144/SP285.2

Kodaira, S., Mjelde, R., Gunnarsson, K., Shiobara, H., & Shimamura, H. (1998). Structure of the Jan Mayen microcontinent and implications for its evolution. *Geophys. J. Int*. 132, 383–400.

Labaume, P., Meresse, F., Jolivet, M., & Teixell, A. (2016). Exhumation sequence of the basement thrust units in the west-central Pyrenees. Constraints from apatite fission track analysis. *Geogaceta*, 60, 11–14.

Lagabrielle, Y., & Bodinier, J.-L. (2008). Submarine reworking of exhumed sub-continental mantle rocks: field evidence from the Lherz peridotites, French Pyrenees: Cretaceous exhumation of pyrenean mantle. *Terra Nova*, 20, 11–21. https://doi.org/10.1111/j.1365-3121.2007.00781.x

Lagabrielle, Y., Clerc, C., Vauchez, A., Lahfid, A., Labaume, P., Azambre, B., Fourcade, S., & Dautria, J.-M. (2016). Very high geothermal gradient during mantle exhumation recorded in mylonitic marbles and carbonate breccias from a Mesozoic Pyrenean palaeomargin (Lherz area, North Pyrenean Zone, France). *Comptes Rendus Geosci*. 348, 290–300. https://doi.org/10.1016/j.crte.2015.11.004

Lagabrielle, Y., Labaume, P., & de Saint Blanquat, M. (2010). Mantle exhumation, crustal denudation, and gravity tectonics during Cretaceous rifting in the Pyrenean realm (SW Europe): Insights from the geological setting of the lherzolite bodies. *Tectonics*, 29. https://doi.org/10.1029/2009TC002588

Lahfid, A., O. Beyssac, E. Deville, F. Negro, & Goffé B. (2010). Evolution of the Raman spectrum of carbonaceous material in low-grade metasediments of the Glarus Alps (Switzerland), *Terra Nova*, 22, 354–360.

Lamare, P. (1936). Recherches géologiques dans les Pyrénées basques d'Espagne. *Société géologique de France*.

Lamolda, M., Mathey, B., Rossy, M., & Sigal, J. (1983). La edad del volcanismo cretácico de Vizcaya y Guipuzcoa. Estud. Geológicos 39, 151–156.

Lavier, L.L., & Manatschal, G. (2006). A mechanism to thin the continental lithosphere at magma-poor margins. *Nature*, 440, 324–328. https://doi.org/10.1038/nature04608

Lemoine, M., Tricart, P., & Boillot, G. (1987). Ultramafic and gabbroic ocean floor of the Ligurian Tethys (Alps, Corsica, Apennines): In search of a genetic imodel. *Geology*, 15, 622–625. https://doi.org/10.1130/0091-7613(1987)15<622:UAGOFO>2.0.CO;2

Lenoble, J.-L. (1992). Les plates-formes carbonatées ouest-pyrénéennes du dogger à l'Albien, stratigraphie séquentielle et évolution géodynamique. (Doctoral dissertation), Université Paul Sabatier de Toulouse (Sciences).

López-Horgue, M.A., Owen, H.G., Rodríguez-Lázaro, J., Fernández-Mendiola, P.A., & García-Mondéjar, J. (1999). Late Albian–Early Cenomanian stratigraphic succession near Estella-Lizarra (Navarra, central northern Spain) and its regional and interregional correlation. *Cretac. Res*. 20, 369–402.

Lucazeau, F., S. Leroy, F. Rolandone, E. d'Acremont, L. Watremez, A. Bonneville, B. Goutorbe, & Düsünur D. (2010). Heat-flow and hydrothermal circulation at the ocean–continent transition of the eastern gulf of Aden . *Earth Planet. Sci. Lett*., 295, 554-570. https://doi.org/10.1016/j.epsl.2010.04.039

Macchiavelli, C., Vergés, J., Schettino, A., Fernàndez, M., Turco, E., Casciello, E., Torne, M., Pierantoni, P.P., & Tunini, L. (2017). A New Southern North Atlantic Isochron Map: Insights Into the Drift of the Iberian Plate Since the Late Cretaceous: Iberian Plate Kinematics Since 83.5 Ma. *J. Geophys. Res. Solid Earth*, 122, 9603–9626. https://doi.org/10.1002/2017JB014769

Magri, F., Littke, R., Rodon, S., Urai, J. L. (2008). Temperature fields, petroleum maturation and fluid flow in the vicinity of salt domes. - In: Littke, R., Bayer, U., Gajewski, D., Nelskamp, S. (Eds.), Dynamics of Complex Intracontinental basins: The Central European basin System, Springer, pp. 323—344.

Magri, F., Inbar N., Siebert C., Rosenthal E., Guttman J., & Möller P. (2015). Transient simulations of large-scale hydrogeological processes causing temperature and salinity anomalies in the Tiberias basin. *Journal of Hydrology*, 520, 342-355. Doi: 10.1016/j.jhydrol.2014.11.055

Manatschal, G., & Nievergelt, P. (1997). A continent-ocean transition recorded in the Err and Platta nappes (Eastern Switzerland). *Eclogae Geol. Helvetiae*, 90, 3–28.

Manatschal, G., Marquer, D., & Früh-Green, G.L. (2000). Channelized fluid flow and mass transfer along a rift-related detachment fault (Eastern Alps, southeast Switzerland). *Geol. Soc. Am. Bull*. 112, 21–33. https://doi.org/10.1130/0016-7606(2000)112<21:CFFAMT>2.0.CO;2

Manatschal, G., Froitzheim, N., Rubenach, M., & Turrin, B.D. (2001). The role of detachment faulting in the formation of an ocean-continent transition: insights from the Iberia Abyssal Plain. *Geol. Soc. Lond. Spec. Publ*. 187, 405–428. https://doi.org/10.1144/GSL.SP.2001.187.01.20

Manatschal, G., Engström, A., Desmurs, L., Schaltegger, U., Cosca, M., Müntener, O., & Bernoulli, D. (2006). What is the tectono-metamorphic evolution of continental break-up: The example of the Tasna Ocean–Continent Transition. *J. Struct. Geol*. 28, 1849–1869. https://doi.org/10.1016/j.jsg.2006.07.014

Manatschal, G., Sauter, D., Karpoff, A.M., Masini, E., Mohn, G., & Lagabrielle, Y. (2011). The Chenaillet Ophiolite in the French/Italian Alps: An ancient analogue for an Oceanic Core Complex? Lithos, Alpine Ophiolites and Modern AnaloguesContinental Rifting to Oceanic LithosphereAlpine Ophiolites and Modern Analogues 124, 169–184. https://doi.org/10.1016/j.lithos.2010.10.017

Martínez-Torres, L.M. (1989). El manto de los mármoles (Pirineo occidental): geología estructural y evolución geodinámica, (Doctoral dissertation), Universidad del País Vasco-Euskal Herriko Unibertsitatea.

Masini, E., Manatschal, G., Mohn, G., Ghienne, J.-F., & Lafont, F. (2011). The tectono-sedimentary evolution of a supra-detachment rift basin at a deep-water magma-poor rifted margin: the example of the Samedan basin preserved in the Err nappe in SE Switzerland: Tectono-sedimentary evolution of a supra-detachment rift basin. *basin Re*s. 23, 652–677. https://doi.org/10.1111/j.1365-2117.2011.00509.x

Masini, E., Manatschal, G., & Mohn, G. (2013). The Alpine Tethys rifted margins: Reconciling old and new ideas to understand the stratigraphic architecture of magma-poor rifted margins. *Sedimentology* 60, 174–196. https://doi.org/10.1111/sed.12017

Masini, E., Manatschal, G., Tugend, J., Mohn, G., & Flament, J.-M. (2014). The tectono-sedimentary evolution of a hyper-extended rift basin: the example of the Arzacq–Mauléon rift system (Western Pyrenees, SW France). *Int. J. Earth Sci*. 103, 1569–1596. https://doi.org/10.1007/s00531-014-1023-8

Mattauer, M. (1968). Les traits structuraux essentiels de la chaîne Pyrénéenne. *Rev. Géologie Dyn. Géographie Phys*. 10, 3–11.

Mello, U.T., Karner G.D., & Anderson R.N. (1995). Role of salt in restraining the maturation of subsalt source rocks. *Marine and Petroleum Geology*, 12, 7, 697-716. https://doi.org/10.1016/0264-8172(95)93596-V

Mendia, M.S., & Ibarguchi, J.I.G. (1991). High-grade metamorphic rocks and peridotites along the Leiza Fault (Western Pyrenees, Spain). *Geol. Rundsch*. 80, 93–107.

Mjelde, R., Digranes, P., Van Schaack, M., Shimamura, H., Shiobara, H., Kodaira, S., Naass, O., Sørenes, N., & Vågnes, E. (2001). Crustal structure of the outer Vøring Plateau, offshore Norway, from ocean bottom seismic and gravity data. *J. Geophys. Res. Solid Earth*, 106, 6769–6791. https://doi.org/10.1029/2000JB900415

Mjelde, R., Raum, T., Breivik, A.J., & Faleide, J.I. (2008). Crustal transect across the North Atlantic. *Mar. Geophys. Res*. 29, 73.

Mohn, G., Manatschal, G., Beltrando, M., Masini, E., & Kusznir, N. (2012). Necking of continental crust in magma-poor rifted margins: Evidence from the fossil

Alpine Tethys margins: Necking of continental crust. *Tectonics*, 31. https://doi.org/10.1029/2011TC002961

Moine, B., Fortune, J.P., Moreau, P., & Viguier, F. (1989). Comparative mineralogy, geochemistry, and conditions of formation of two metasomatic talc and chlorite deposits; Trimouns (Pyrenees, France) and Rabenwald (Eastern Alps, Austria). *Econ. Geol*. 84, 1398–1416.

Montigny, R., Azambre, B., Rossy, M., & Thuizat, R. (1986). K-Ar study of Cretaceous magmatism and metamorphism in the Pyrenees: Age and length of rotation of the Iberian Peninsula. Tectonophysics, The Geological Evolution of the Pyrenees 129, 257–273. https://doi.org/10.1016/0040-1951(86)90255-6

Moulin, M., Aslanian, D., Olivet, J.-L., Contrucci, I., Matias, L., Géli, L., Klingelhoefer, F., Nouzé, H., Réhault, J.-P., & Unternehr, P. (2005). Geological constraints on the evolution of the Angolan margin based on reflection and refraction seismic data (ZaïAngo project). *Geophys. J. Int*. 162, 793–810. https://doi.org/10.1111/j.1365-246X.2005.02668.x

Moulin, M., Aslanian, D., & Unternehr, P. (2010). A new starting point for the South and Equatorial Atlantic Ocean. *Earth-Sci. Rev*. 98, 1–37. https://doi.org/10.1016/j.earscirev.2009.08.001

Mouthereau, F., Filleaudeau, P.-Y., Vacherat, A., Pik, R., Lacombe, O., Fellin, M.G., Castelltort, S., Christophoul, F., & Masini, E. (2014). Placing limits to shortening evolution in the Pyrenees: Role of margin architecture and implications for the Iberia/Europe convergence. *Tectonics*, 33, 2014TC003663. https://doi.org/10.1002/2014TC003663

Muller, J., & Roger, P. (1977). L'Evolution structurale des Pyrénées (Domaine central et occidental) Le segment hercynien, la chaîne de fond alpine. Géologie Alp. 53, 149–191.

Muñoz, J.A. (1992). Evolution of a continental collision belt: ECORS-Pyrenees crustal balanced cross-section, in: McClay, K.R. (Ed.), Thrust Tectonics. Springer Netherlands, pp. 235–246. https://doi.org/10.1007/978-94-011-3066-0_21

Muraoka, H., Yasukawa K., & Kimbara K. (2000). Current state of development of deep geothermal resources in the world and implications to the future. Proceedings World Geothemal Congress, Kyushu-Tohoku, Japan, May 28 – June 10, pp. 1479-1484.

Nábělek, P.I., & Nábělek J.L. (2014). Thermal characteristics of the Main Himalaya Thrust and the Indian lower crust with implications for crustal rheology and partial melting in the Himalaya orogen. *Earth Planet. Sci. Lett*, 395, 116-123. https://doi.org/10.1016/j.epsl.2014.03.026

Pérez-Gussinyé, M. (2013). A tectonic model for hyperextension at magma-poor rifted margins: an example from the West Iberia–Newfoundland conjugate margins. *Geol. Soc. Lond. Spec. Publ*. 369, 403–427. https://doi.org/10.1144/SP369.19

Péron-Pinvidic, G., Manatschal, G., Minshull, T.A., & Sawyer, D.S. (2007). Tectonosedimentary evolution of the deep Iberia-Newfoundland margins: Evidence for a complex breakup history. *Tectonics*, 26, 1–19. https://doi.org/10.1029/2006TC001970

Péron-Pinvidic, G., & Manatschal, G. (2009). The final rifting evolution at deep magma-poor passive margins from Iberia-Newfoundland: a new point of view. *Int. J. Earth Sci*. 98, 1581–1597. https://doi.org/10.1007/s00531-008-0337-9

Péron-Pinvidic, G., Gernigon, L., Gaina, C., & Ball, P. (2012a). Insights from the Jan Mayen system in the Norwegian–Greenland sea—I. Mapping of a microcontinent. *Geophys. J. Int*. 191, 385–412. https://doi.org/10.1111/j.1365-246X.2012.05639.x

Péron-Pinvidic, G., Gernigon, L., Gaina, C., & Ball, P. (2012b). Insights from the Jan Mayen system in the Norwegian–Greenland Sea—II. Architecture of a microcontinent. *Geophys. J. Int*. 191, 413–435. https://doi.org/10.1111/j.1365-246X.2012.05623.x

Peron-Pinvidic, G., Manatschal, G., & Osmundsen, P.T. (2013). Structural comparison of archetypal Atlantic rifted margins: A review of observations and concepts. *Mar. Pet. Geol*. 43, 21–47. https://doi.org/10.1016/j.marpetgeo.2013.02.002

Péron-Pinvidic, G., Manatschal, G., Masini, E., Sutra, E., Flament, J.M., Haupert, I., & Unternehr, P. (2015). Unravelling the along-strike variability of the Angola–Gabon rifted margin: a mapping approach. *Geol. Soc. Lond. Spec. Publ*. 438, 49–76. https://doi.org/10.1144/SP438.1

Poujol, M., Boulvais, P., & Kosler, J. (2010). Regional-scale Cretaceous albitization in the Pyrenees: evidence from in situ U–Th–Pb dating of monazite, titanite and zircon. *J. Geol. Soc*. 167, 751–767. https://doi.org/10.1144/0016-76492009-144

Rat, P. (1959). Les pays crétacés: basco-cantabriques (Espagne). Presses universitaires de France.

Rat, P., Amiot, M., Feuillée, P., Floquet, M., Mathey, B., Pascal, A., Salomon, J., García Mondéjar, J., Pujalte, J., Lamolda, M., & others. (1983). Vue sur le Cretacé basco-cantabrique et nord-ibérique. Une Marge Son Arriere-Pays Ses Environ. Sedimentaires Memoires Geol. Univ. Dijon 9, 191.

Ravier, J. (1957). Le métamorphisme des terrains secondaires des Pyrénées. (Doctoral dissertation), Université, Faculté des Sciences.

Razin, P. (1989). Evolution tecto-sédimentaire alpine des Pyrénées basques à l'ouest de la transformante de Pamplona, Province du Labourd. (Doctoral dissertation), Bordeaux 3.

Reston, T. (2007). Extension discrepancy at North Atlantic non-volcanic rifted margins: Depth-dependent stretching or unrecognized faulting? *Geology*, 35, 367–370. https://doi.org/10.1130/G23213A.1

Reston, T.J. (2009). The structure, evolution and symmetry of the magma-poor rifted margins of the North and Central Atlantic: A synthesis. *Tectonophysics*, 468, 6–27. https://doi.org/10.1016/j.tecto.2008.09.002

Roche, V., Sternai P., Guillou-Frottier L., Menant A., Jolivet L., Bouchot V., & Gerya T. (2018). Emplacement of metamorphic core complexes and associated

geothermal systems controlled by slab dynamics. *Earth and Planetary Science Letters*, 498, 322-333. Doi: 10.1016/j.epsl.2018.06.043

Rossy, M., Azambre, B., & Albarède, F. (1992). REE and Sr/1bNd isotope geochemistry of the alkaline magmatism from the Cretaceous North Pyrenean Rift Zone (France-Spain). *Chem. Geol*. 97, 33–46. https://doi.org/10.1016/0009-2541(92)90134-Q

Roux, J.-C. (1983). Recherches stratigraphiques et sédimentologiques sur les flyschs crétacés pyrénéens au sud d'Oloron (Pyrénées Atlantiques). (Doctoral dissertation), Université Paul Sabatier de Toulouse (Sciences).

Rubatto, D., Gebauer, D., & Fanning, M. (1998). Jurassic formation and Eocene subduction of the Zermatt-Saas-Fee ophiolites: implications for the geodynamic evolution of the Central and Western Alps. *Contrib. Mineral. Petrol*. 132, 269–287. https://doi.org/10.1007/s004100050421

Saspiturry, N., Razin, P., Baudin, T., Serrano, O., Issautier, B., Lasseur, E., Allanic, C., Thinon, I., & Leleu, S. (2019a). Symmetry vs. asymmetry of a hyper-thinned rift: Example of the Mauléon basin (Western Pyrenees, France). *Mar. Pet. Geol*. 104, 86–105. https://doi.org/10.1016/j.marpetgeo.2019.03.031

Saspiturry, N., Cochelin, B., Razin, P., Leleu, S., Lemirre, B., Bouscary, B., Issautier, B., Serrano, O., Lasseur, E., Baudin, T., & Allanic, C. (2019b). Tectono-sedimentary evolution of a rift-system controlled by Permian post-orogenic extension and MCC formation (Bidarray basin and Ursuya dome, Western Pyrenees). *Tectonophysics*.

Schärer, De Parseval, Polvé, & De Saint Blanquat. (1999). Formation of the Trimouns talc-chlorite deposit (Pyrenees) from persistent hydrothermal activity between 112 and 97 Ma. *Terra Nova*, 11, 30–37. https://doi.org/10.1046/j.1365-3121.1999.00224.x

Schoeffler, J., Henry, J., & Villanova, M. (1964). État des travaux de cartographie géologique réalisés par la Société Nationale des Pétroles d'Aquitaine (SNPA) dans les Pyrénées occidentales. *CR Somm Soc Géol Fr*, 7, 241–246.

Serrano, O., Delmas, J., Hanot, F., Vially, R., Herbin, J.-P., Houel, P., & Tourlière, B. (2006). Le bassin d'Aquitaine: valorisation des données sismiques, cartographie structurale et potentiel pétrolier. Bureau de Recherche Géologique et minière.

Souquet, P. (1967). Le Crétacé supérieur Sud-Pyrénéen, en Catalogne, Aragon et Navarre. E. Privat.

Souquet, P., Peybènes, B., Bilotte, M., & Debroas, E.-J. (1977). La chaîne alpine des Pyrénées. Géologie Alp. 53, 193–216.

Souquet, P., Debroas, E.-J., Boirie, J.-M., Pons, P., Fixari, G., Roux, J.-C., Dol, J., Thieuloy, J.-P., Bonnemaison, M., Manivit, H., & others. (1985). Le groupe du Flysch noir (albo-cénomanien) dans les Pyrénées. *Bull Cent Rech Exlpo-Prod Elf-Aquitaine Pau*, 9, 183–252.

Stampfli, G.., Mosar, J., Marquer, D., Marchant, R., Baudin, T., & Borel, G. (1998). Subduction and obduction processes in the Swiss Alps. *Tectonophysics*, 296, 159–204. https://doi.org/10.1016/S0040-1951(98)00142-5

Teixell, A. (1993). Coupe géologique du massif d'Igountze: implications sur l'évolution structurale de la bordure sud de la zone nord-pyrénéenne occidentale. *Comptes Rendus Académie Sci. Sér. 2 Mécanique Phys. Chim. Sci. Univers Sci. Terre*, 316, 1789–1796.

Teixell, A. (1996). The Anso transect of the southern Pyrenees: basement and cover thrust geometries. *J. Geol. Soc*. 153, 301–310. https://doi.org/10.1144/gsjgs.153.2.0301

Teixell, A. (1998). Crustal structure and orogenic material budget in the west central Pyrenees. *Tectonics*, 17, 395–406. https://doi.org/10.1029/98TC00561

Teixell, A., Labaume, P., & Lagabrielle, Y. (2016). The crustal evolution of the west-central Pyrenees revisited: Inferences from a new kinematic scenario. Comptes *Rendus Geosci*. 348, 257–267. https://doi.org/10.1016/j.crte.2015.10.010

Ternois, S., Odlum, M., Ford, M., Pik, R., Stockli, D., Tibari, B., Vacherat, A., & Bernard, V. (2019). Thermochronological evidence of early orogenesis, eastern Pyrenees, France. *Tectonics*. https://doi.org/10.1029/2018TC005254

Thiébaut, J., Debeaux, M., Debroas, E.J., & Souquet, P. (1979). Découverte de roches d'affinités teschenitiques dans les marbres mésozoïques de Saint-Béat (Haute-Garonne). *CR Acad Sci Paris*, 288, 1695–1697.

Thiébaut, J., Durand-Wackenheim, C., Debeaux, M., & Souquet, P. (1992). Métamorphisme des évaporites triasiques du versant nord des Pyrénées centrales et Occidentales. *Bull. Société Hist. Nat. Toulouse*, 128, 77–84.

Tugend, J., Manatschal, G., & Kusznir, N.J. (2015). Spatial and temporal evolution of hyperextended rift systems: Implication for the nature, kinematics, and timing of the Iberian-European plate boundary. *Geology*, 43, 15–18. https://doi.org/10.1130/G36072.1

Turcotte, D.L., & Schubert, G. (2002). Geodynamics. Cambridge University Press, 2nd ed., 456p.

Unternehr, P., Peron-Pinvidic, G., Manatschal, G., & Sutra, E. (2010). Hyper-extended crust in the South Atlantic: in search of a model. *Pet. Geosci*. 16, 207–215. https://doi.org/10.1144/1354-079309-904

Vacherat, A., Mouthereau, F., Pik, R., Bernet, M., Gautheron, C., Masini, E., Le Pourhiet, L., Tibari, B., & Lahfid, A. (2014). Thermal imprint of rift-related processes in orogens as recorded in the Pyrenees. *Earth Planet. Sci. Lett*. 408, 296–306. https://doi.org/10.1016/j.epsl.2014.10.014

Vauchez, A., Clerc, C., Bestani, L., Lagabrielle, Y., Chauvet, A., Lahfid, A., & Mainprice, D. (2013). Preorogenic exhumation of the North Pyrenean Agly massif (Eastern Pyrenees-France). *Tectonics*, 32, 95–106. https://doi.org/10.1002/tect.20015

Vergés, J., Millán, H., Roca, E., Muñoz, J.A., Marzo, M., Cirés, J., Bezemer, T.D., Zoetemeijer, R., & Cloetingh, S. (1995). Eastern Pyrenees and related foreland basins: pre-, syn- and post-collisional crustal-scale cross-sections. *Mar. Pet. Geol*., Integrated basin Studies 12, 903–915. https://doi.org/10.1016/0264-8172(95)98854-X

Verschure, R.H., Hebeda, E.H., Boelrijk, N., Priem, H.N.A., & Ave Lallemant, H.G. (1967). K-Ar age of hornblende from a hornblendite vein in the Alpine-type ultramafic mass of the Etang de Lers (Ariege), French Pyrenees. *Leidse Geol. Meded*. 42, 59–59.

Vielzeuf, D., & Kornprobst, J. (1984). Crustal splitting and the emplacement of Pyrenean lherzolites and granulites. *Earth Planet. Sci. Lett*. 67, 87–96. https://doi.org/10.1016/0012-821X(84)90041-4

Wang, Y. (2017). High resolution imaging of lithospheric structures by full waveform inversion of short period teleseismic P waves. (Doctoral dissertation), Université Toulouse 3 Paul Sabatier (UT3 Paul Sabatier).

Wang, Y., Chevrot, S., Monteiller, V., Komatitsch, D., Mouthereau, F., Manatschal, G., Sylvander, M., Diaz, J., Ruiz, M., Grimaud, F., Benahmed, S., Pauchet, H., & Martin, R. (2016). The deep roots of the western Pyrenees revealed by full waveform inversion of teleseismic P waves. Geology 44, 475–478. https://doi.org/10.1130/G37812.1

Weigel, W., Flüh, E.R., Miller, H., Butzke, A., Dehghani, G.A., Gebhardt, V., Harder, I., Hepper, J., Jokat, W., & Kläschen, D. (1995). Investigations of the East Greenland continental margin between 70 and 72 N by deep seismic sounding and gravity studies. *Mar. Geophys. Res*. 17, 167–199.

Wopenka, B., & Pasteris, J.D. (1993). Structural characterization of kerogens to granulitefacies graphite: applicability of Raman microprobe spectroscopy. *American Mineralogist*, 78, 533–557.

Yui, T.F., Huang, E., & Xu, J. (1996). Raman spectrum of carbonaceous material: a possible metamorphic grade indicator for low-grademetamorphic rocks. *Journal of Metamorphic Geology*, 14, 115–124. http://dx.doi.org/10.1046/j.1525-1314.1996.05792.x.

Supporting Information S1: Estimating present-day temperature gradients in the Mauléon basin area from corrected bottom-hole temperature measurements

Abstract

This Supporting Information presents corrected bottom-hole temperature (BHT) data and the associated present-day temperature gradients. We used BHT information from the six petroleum boreholes that were used for estimates of RSCM peak temperatures.

Text

Present-day temperature gradients can be estimated from corrected bottom-hole temperature (BHT measurements. The six boreholes used in this study **(Table S1)** have been adjusted to yield true vertical depths (see text section 4.2). In addition, the measured BHT values had to be adjusted to remove transient perturbations due to mud circulation in the borehole shortly before the measurement. Because the available temporal information was insufficient for an analytical correction (see Goutorbe et al., 2007), we used the numerous temperature data from drillstem tests to devise a reference temperature profile in the area and thus define a correction profile for BHT data (see also Förster et al., 1997). The correction for BHT data below 2,000 m depth was

$$\Delta T = -25.076 + 0.0259z - 6\times10^{-6}\, z^2 + 4\times10^{-10}\, z^3. \quad (S1)$$

This correction was as great as 9.4°C at a depth of 3,000 m but decreased toward zero at greater depths. Although this correction method prevents underestimates of deep temperatures, the uncertainty of the corrected BHT data remains around ± 5–10°C, yielding temperature gradient estimates with a precision of 10–15% (Jaupart & Mareschal, 2007).

Figure S1 shows corrected BHT data for each borehole, with an imposed surface temperature of 12°C assumed as an additional data point. The dotted lines and linear relationships indicate the best-fitting temperature gradient together with the correlation coefficient (R^2). **Table S1** summarizes the obtained results. An average temperature gradient of 25.0 ± 2.7 °C/km is obtained.

References

Förster A., D.F. Merriam, J.C. Davis. (1997). Spatial analysis of temperature (BHT/DST) data and consequences for heat-flow determination in sedimentary basins. *Geologische Rundschau*, 86, 252-261. https://doi.org/10.1007/s005310050138

Goutorbe B., F. Lucazeau, A. Bonneville. (2007). Comparison of several BHT correction methods: a case study on an Australian data set. *Geophysical Journal International*, 170, 913-922. https://doi.org/10.1111/j.1365-246X.2007.03403.x

Jaupart C., J.-C. Mareschal. (2007). Heat flow and thermal structure of the lithosphere. In Treatise on Geophysics, G. Schubert (Ed.), Elsevier, pp. 217-251.

Table S1. Bottom-hole temperature data used in this study to estimate present-day temperature gradients for the six wells in the Mauléon basin.

Well name	Nb of BHT	Maximum depth (m)	Current temperature gradient (°C/km)	R^2
Les-Cassières-2	2	3635	29.9	0.992
Hasparren-101	7	6080	25.1	0.986
Bellevue-1	2	5197	22.0	0.993
Orthez-102	3	5389	22.7	0.997
Chéraute-1	7	5349	25.1	0.975
Ainhice-1	3	3449	25.2	0.986

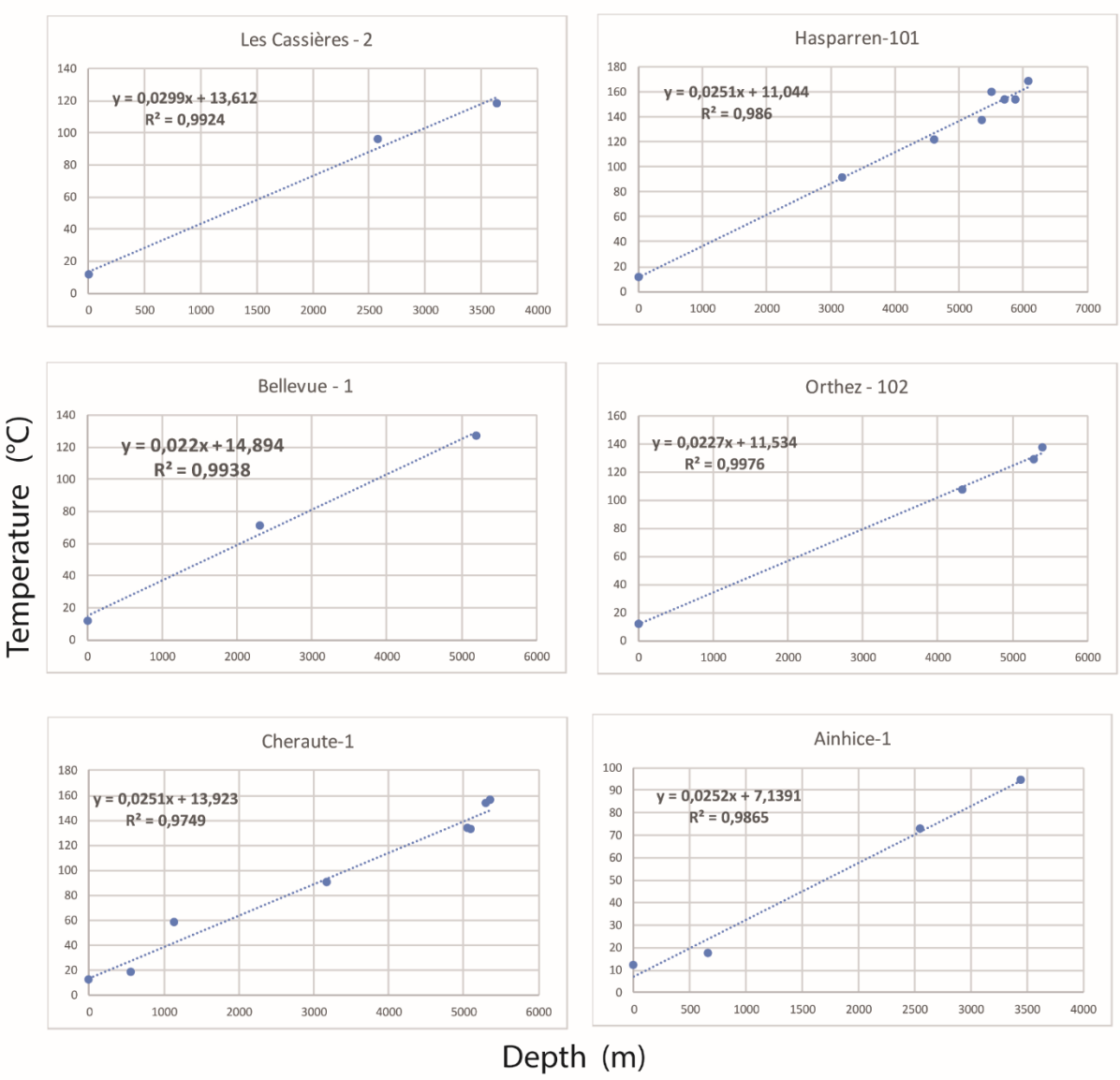


Fig. S1. BHT data used to estimate present-day temperature gradients for the six wells in the Mauléon basin area.

Supporting Information S2: Variations of temperature gradient within a convective medium

Abstract

This Supporting Information illustrates the variations of the surface temperature gradient due to fluid circulation (hydrothermal convection) within a permeable layer. It is based on simple numerical models initially published by Rabinowicz et al. (1998) and adapted by Garibaldi et al. (2010). We show that for a permeability decreasing with depth, cold downwellings are more efficient than hot upwellings, leading to temperature gradients that could be lower than the conductive temperature gradient.

Text

The RSCM peak temperatures recorded in the Hasparren-101 borehole were constant over a vertical distance greater than 2,000 m, which we interpreted as a convective signature. Either upwelling of hot fluid or downwelling of cold fluid could account for this finding. Consequently, the estimated apparent gradient of 62°C/km combines a conductive gradient in the upper 3,000 m and a convective gradient in the underlying 2,000 m.

However, convection of crustal fluids in permeable crust (hydrothermal convection) can produce various temperature patterns. Depending on the position where the temperature profile is determined, one could get either very high temperature gradients in the upper part of the profile or temperature gradients lower than the conductive gradient.

Figure S2 shows three numerical experiments of hydrothermal convection within a permeable layer 1.5 km thick (adapted from Rabinowicz et al., 1998; see also the benchmark of **Fig. 9A** in Garibaldi et al., 2010). Briefly, heat and fluid flow equations are coupled and boundary conditions are similar to those of Rabinowicz et al. (1998), who modeled hydrothermal convection in the oceanic crust. In the two first cases, permeability is constant through the medium (10^{-15} and 5×10^{-15} m²), and in the third case, permeability decreases exponentially with depth (parameter δ = 1 km). Three temperature profiles are shown for each experiment in the three bottom figures. Although most of the temperature gradients at the surface are close to (profiles C and F) or much greater than (profiles A, B, D, E, G, and H) the conductive temperature gradient (dashed green line), it appears that profile I has a low temperature gradient at the surface. Indeed, in the case of decreasing permeability with depth, downwelling is favored because the cold fluids are located where the medium is more permeable. Consequently, if the Hasparren-101 borehole, for example, were located above such a convective zone, the 62°C/km gradient determined in that well would underestimate the conductive gradient (see text section 6.2.2) It must be emphasized that cold zones in the third case outnumber hot zones, which are focused in narrow upwellings. Consequently, wells drilled in this setting are much more likely to intersect a low temperature gradient than a high one.

References

Garibaldi C., L. Guillou-Frottier, J.M. Lardeaux, D. Bonté, S. Lopez, V. Bouchot, P. Ledru. (2010). Thermal anomalies and geological structures in the Provence basin: Implications for hydrothermal circulations at depth. *Bull. Soc. Geol. Fr.*, 181, 4, 363-376. https://doi.org/10.2113/gssgfbull.181.4.363

Rabinowicz M., Boulègue J., Genthon P. (1998). Two- and three-dimen tional modeling of hydrothermal convection in the sedimented Middle Valley segment, Juan de Fuca Ridge. *J. Geophys. Res*,103. https://doi.org/10.1029/98JB01484

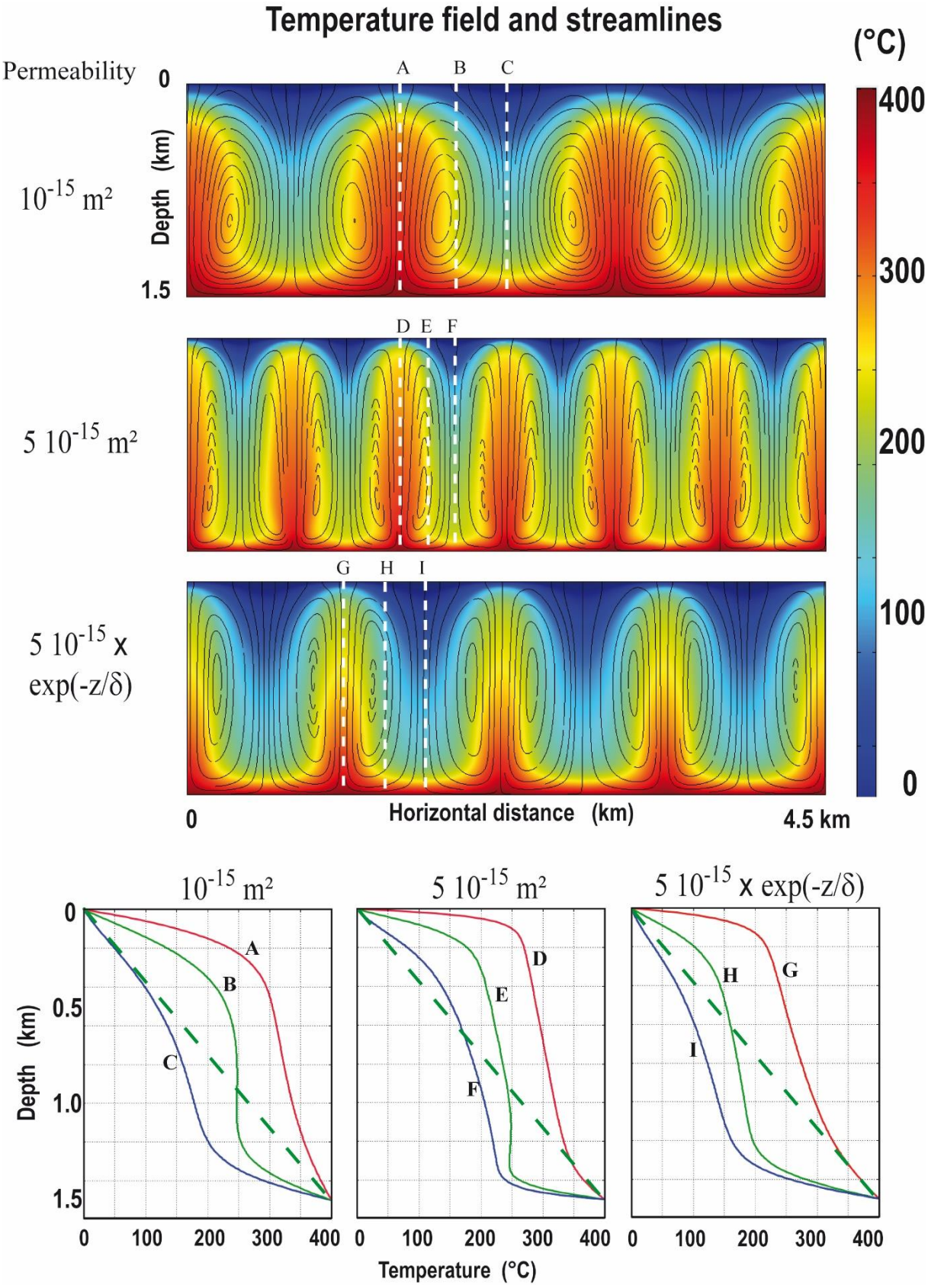
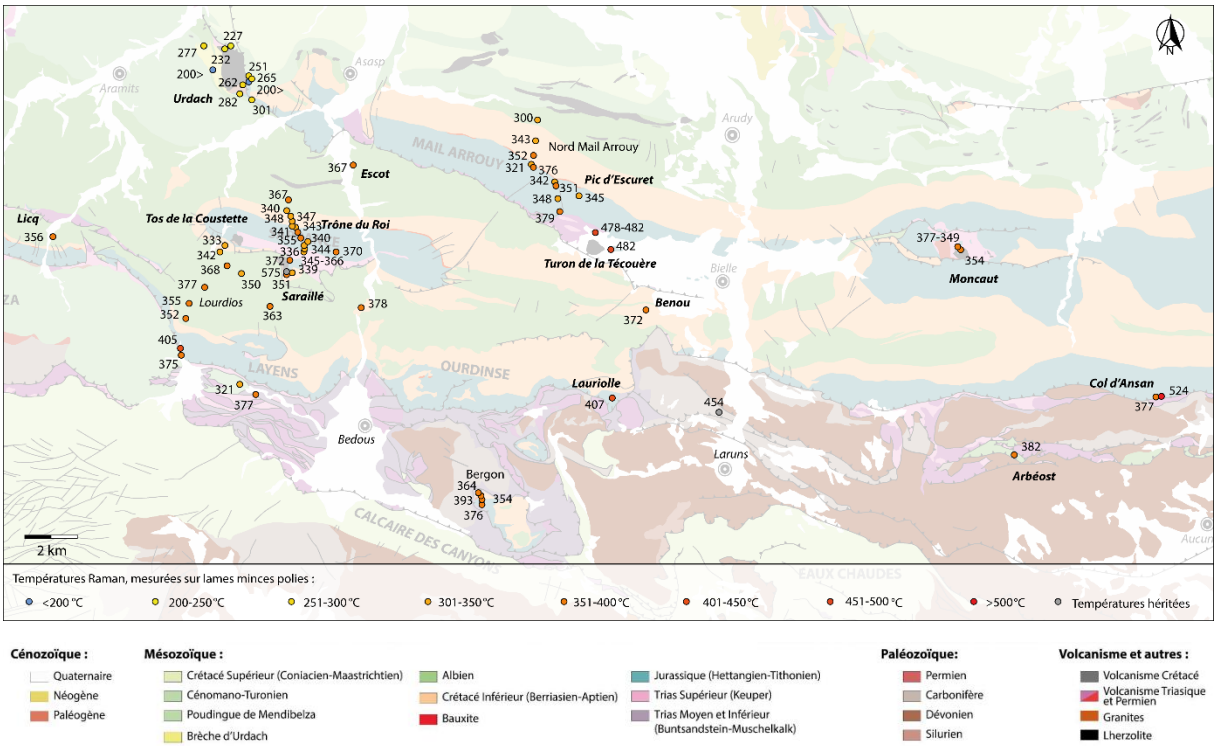


Fig. S2. Temperature fields (color) and streamlines (black contours) for three numerical experiments of hydrothermal convection (see details on numerical modeling in Rabinowicz et al., 1998 and Garibaldi et al., 2010). Three temperature profiles are extracted for each case and shown in the three bottom plots. Profile I, in a downwelling zone, shows a temperature gradient lower than the conductive temperature profile (green dashed line).

Eléments supplémentaires

A l'est du bassin de Mauléon, les températures maximales atteintes par la couverture mésozoïque sont largement inférieures à celles extrapolées à la base de l'unité de Saint-Palais. En effet, les températures de la couverture albienne du Massif d'Urdach et de la couverture aptienne à jurassique des Chaînons Béarnais n'excèdent pas les 300°C et 380°C (ES. 1). Pourtant, (1) le Massif d'Urdach est caractérisé par une dénudation totale du manteau sous-continental durant la phase d'hyperextension crétacée, comme en témoigne (i) son remaniement dans les brèches sédimentaires profondes d'Urdach datant de l'Albien terminal au Cénomanien inférieur et (ii) la présence d'ophicalcites ; (2) les Chaînons Béarnais sont caractérisés par une croûte continentale extrêmement fine à la fin de la phase de rifting albo-cénomanienne.

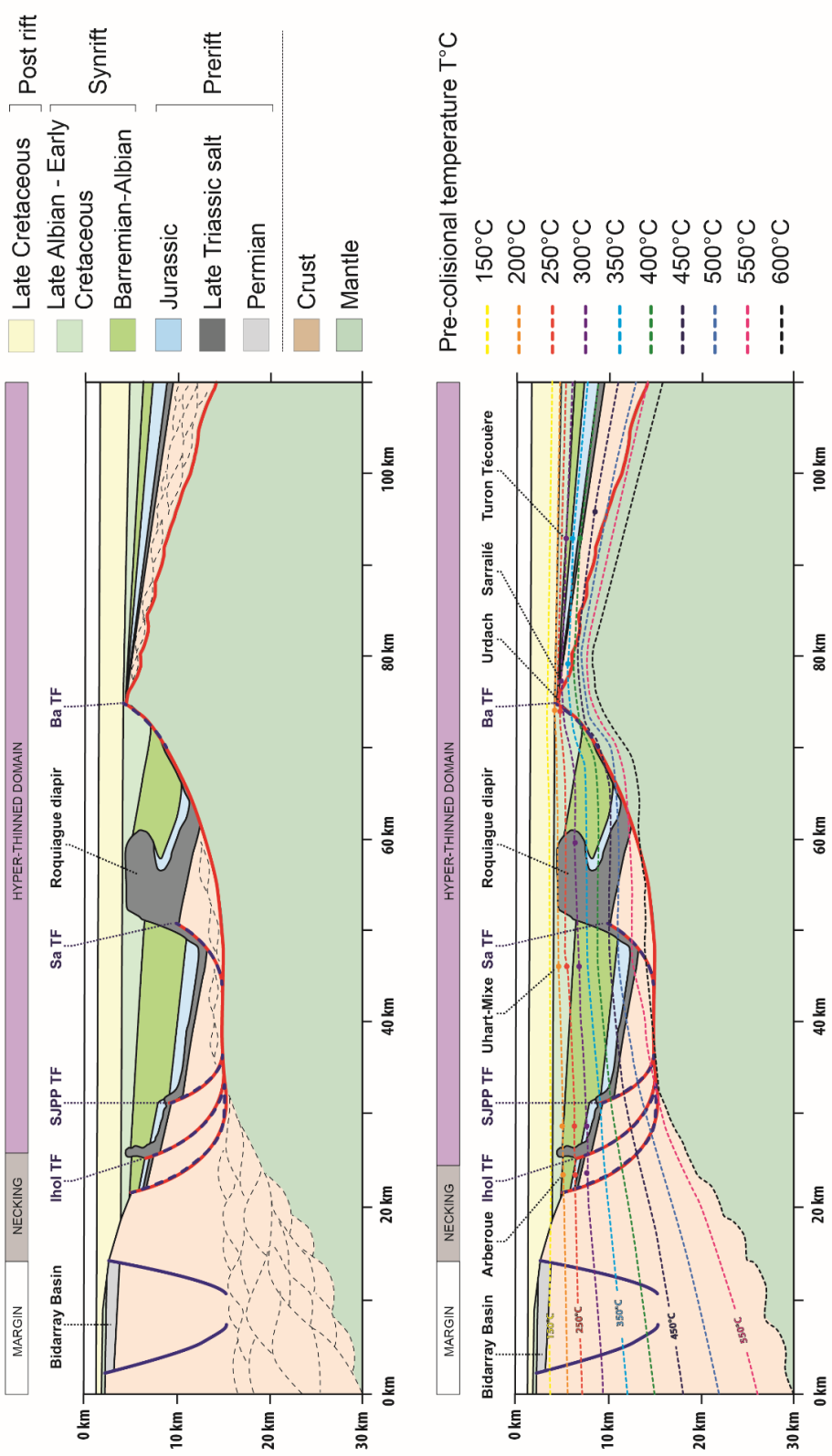


ES. 1. Carte de répartition des températures Raman (RSCM) estimées à travers les Chaînons Béarnais et leur bordure sud (Corre., 2016).

Le resserrement des isothermes en direction du Massif d'Urdach (ES. 2) souligne le fait que le gradient géothermique, au cours du rifting, devait être supérieur à celui estimé au centre de l'unité de Saint-Palais, à savoir 60°C/km. De fait, le gradient maximal atteint pendant le rifting crétacé ne coïncide pas avec le pic thermique maximal atteint par la base du domaine hyper-étiré. La pile sédimentaire au-dessus du Massif d'Urdach et des Chaînons Béarnais est bien moindre en comparaison à celle de l'unité de Saint-Palais (ES. 2). Comme démontré dans l'article précédent, le Tmax atteint par la base du bassin est essentiellement contrôlé par l'enfouissement des séries sédimentaires (« burial ») expliquant pourquoi ce domaine plus oriental n'est pas atteint des températures similaires à la Zone Interne Métamorphique des Pyrénées centrales et orientales.

Au cours de la phase de rifting il existe donc une compétition complexe entre gradient thermique et « burial » contrôlant la valeur de la température maximale atteinte par le domaine hyper-étiré. Dans le cas de Mauléon, nous avons démontré précédemment, que la structuration transverse N20°E, héritée du Permien, est responsable de la différence de taux de sédimentation au cours du Crétacé. Ceci induit un « burial » différentiel qui est directement rattachable à l'épaisseur de la pile sédimentaire. Au cours du rifting, la base de l'unité de Saint-Palais, atteignant 600°C va se déformer de manière plus ductile que la base des Massif d'Urdach et des Chaînons Béarnais. Suivant un transect, proximal / distal, l'augmentation, à la fois du gradient thermique et de l'épaisseur des séries

sédimentaires en direction du bassin est responsable du développement (1) d'une déformation essentiellement cassante le long de la marge proximale et de la zone de necking et d'une déformation à dominante ductile dans le domaine hyper-étiré.



ES. 2. Reconstitution schématique Ouest-Est du bassin de Mauléon, passant par le bassin Permien de Bidarray, l'unité de Saint-Palais, Urdach et les Chaînons béarnais.

Chapitre 6

Synthèse et Discussion

Bref aperçu du chapitre 6 : Synthèse et Discussion

Le chapitre 6.1 du présent manuscrit de thèse récapitule les principaux résultats présentés dans les chapitres précédents. Le chapitre 6.2 correspond à la discussion du manuscrit de thèse et est composé d'un article en préparation qui sera soumis dans le journal *Basin Research*. Cet article de review présente une synthèse de l'évolution tectono-sédimentaire des bassins mésozoïques à proximité de la limite de plaque entre l'Ibérie et l'Europe. Ce travail permet de classifier les bassins nommés « smooth-slope extensional basins » (Annexe. 1) suivant un ordre de maturité du système extensif, et de les comparer aux marges passives hyper-étirées de type atlantique.

Chapitre 6.1

Synthèse des principaux résultats

Chapitre 6.1. Synthèse des principaux résultats

Sommaire

1. Le Permien : un héritage structural, thermique et rhéologique complexe de la lithosphère des Pyrénées occidentales **p. 353**

2. Implications de l'héritage permien sur la phase d'hyperextension crétacée **p. 354**

3. Les bassins de Mauléon, Arzacq et Tartas : un point de départ pour définir un nouveau type de système de rift hyper-étiré **p. 354**

4. Rôle de l'héritage crétacé au cours de l'orogenèse alpine **p. 355**

5. Les zones de transferts N20° à l'origine de la non-cylindricité des Pyrénées **p. 356**

6. Rôle de l'héritage permien et crétacé sur l'évolution thermique du rift nord-pyrénéen depuis sa création jusqu'à son inversion **p. 357**

6.1. Thermicité pré-collisionnelle p. 357

6.2. Thermicité post-collisionnelle p. 358

Synthèse des Principaux résultats

1. Le Permien, un héritage structural, thermique et rhéologique complexe de la lithosphère des Pyrénées occidentales

La phase de rifting qui intervient au Permien après l'édification de la chaîne varisque, confère à la croûte continentale des Pyrénées occidentales une structure complexe avant l'extension mésozoïque. En effet, l'évolution conjointe du bassin permien de Bidarray et du dôme granulitique de l'Ursuya, localisés sur la bordure occidentale du bassin de Mauléon, reflète le passage de la convergence N-S reconnue dans la zone axiale (Denèle et al., 2007, 2009; Cochelin et al., 2017, 2018a, 2018b) de 310 à 290 Ma à une phase d'extension E-W prenant place entre 290 et 275 Ma **(Fig. 1)**. Ces résultats remettent en question les précédents travaux qui considèrent les granulites de l'Ursuya comme un élément de croûte inférieure ou moyenne exhumé le long d'un détachement crétacé (Jammes et al., 2009 ; Masini et al., 2014). Selon notre nouvelle interprétation, la croûte continentale de l'avant-pays de la chaîne varisque est restée chaude et partiellement fondue au cours de l'extension permienne, dans les Pyrénées occidentales. La déformation est alors partitionnée verticalement dans la croûte. La croûte inférieure se déforme de manière ductile et homogène par fluage longitudinal contrairement à la croûte supérieure qui est dominée par une déformation cassante responsable de la formation de failles normales de direction N20° qui contrôlent la création de bassins continentaux et, localement, de décrochements longitudinaux. Un tel style de déformation confère des caractéristiques thermique (gradient anormalement élevé), structurales (déformation cassante N20° localisée dans la croûte supérieure et croûte continentale amincie) et rhéologiques (granulites et migmatites exhumées en position de croûte supérieure) complexe à la lithosphère des Pyrénées occidentales.

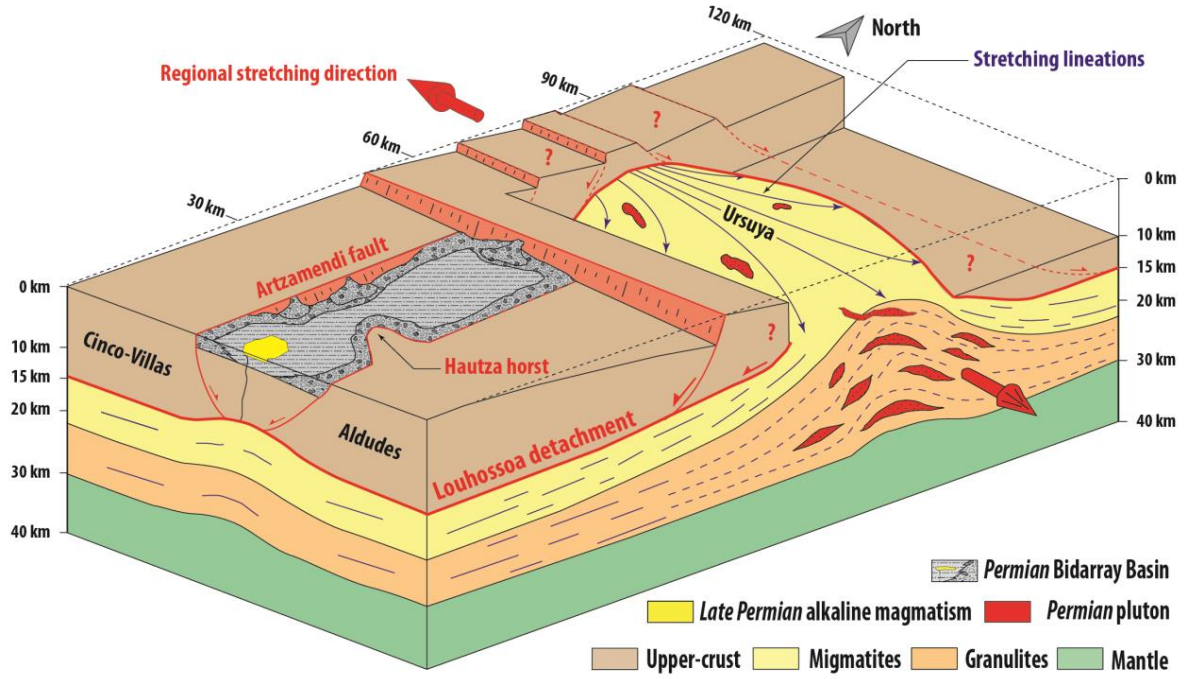


Fig. 1. Conceptual model of crustal thinning during Permian time. The N-S trending Bidarray Basin develops on the hanging wall of an « a-type » MCC, tectonically controlled by the Artzamendi normal fault and the Hautza horst. The Ursuya MCC is characterized by an E-W major stretching direction, as shown by the E-W top-to-the-east stretching lineation within the granulites. Near the Louhossoa detachment the stretching lineations take a top-to-the-south direction, showing a southward normal displacement along this major shear zone.

2. Implications de l'héritage permien sur la phase d'hyper-extension crétacée

Les hétérogénéités crustales de direction N20° telle que la « failles » de Pampelune, sont classiquement considérée comme des zones de transfert contrôlant la segmentation du rift crétacé. La zone de transfert de Pamplona, et, par extension, celles d'Iholdy, du Saison et du Barlanès sont interprétées ici comme héritées de la phase d'extension permienne. A l'échelle régionale, ces zones de transfert N20° sont réactivées au cours du rifting crétacé dans le bassin de Mauléon comme dans le bassin d'Aquitaine. Elles contrôlent notamment la localisation des structures diapiriques et des dépôcentres albo-cénomaniens. Plus localement, le bassin de Bidarray et le dôme de l'Ursuya sont préservés et alignés sur la zone de transfert N20° de Pamplona qui sépare deux branches du rift crétacé. Cette zone de transfert majeure est responsable du décalage vers le sud de l'axe du rifting mésozoïque entre le bassin de Mauléon et le bassin basco-cantabrique, lui conférant un caractère lithosphérique. La disposition actuelle des séries du Permo-Trias, et plus particulièrement la préservation du bassin de Bidarray dans la zone de transfert de Pamplona exclut tout mouvement décrochant sénestre de direction E-W au cours du mésozoïque entre les plaques ibérique et européenne dans cette zone des massifs basques. Ceci pose le problème de la reconstitution de la cinématique des plaques et des modalités d'ouverture des bassins crétacés nord-pyrénéens souvent interprétés comme résultant d'un décrochement senestre de grande ampleur entre l'Ibérie et l'Europe.

3. Les bassins de Mauléon, Arzacq et Tartas : un nouveau type de rift hyper-étiré

L'évolution tectono-sédimentaire des bassins de Mauléon, d'Arzacq et de Tartas au cours du Crétacé présente de nombreuses différences avec celle des marges passives de type atlantique. Contrairement aux marges atlantiques, ces bassins sont caractérisés par une série argilo-évaporitique du Trias supérieur, une épaisse série sédimentaire prerift à synrift et une géométrie du rift pouvant être qualifiée de pseudo-symétrique **(Fig. 2)**.

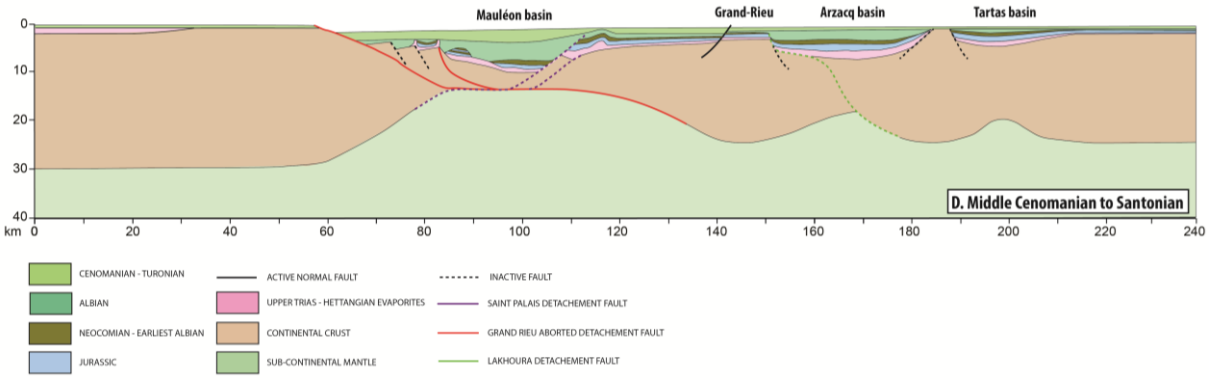


Fig. 2. North-south restored sections (no vertical exaggeration) showing the evolution of the Aquitaine Basin and North Pyrenean Zone, including the Arzacq and Tartas Basins. A half-graben developing in Late Triassic to Hettangian time accumulated a thick evaporite sequence, which in turn controlled the emplacement of the Arzacq and Tartas Basins in Berriasian-Barremian time. The two basins differentiated during the Albian, the Arzacq Basin acquiring an asymmetric cross section following gravity sliding of the sedimentary cover on the northern Grand Rieu flank and the Tartas Basin remaining a simple sag basin.

Selon le modèle d'évolution proposé, la déformation extensive est contrôlée par la présence de deux niveaux de découplage tectonique dès les premiers stades d'amincissement de la croûte continentale. La croûte moyenne permet un découplage de la déformation entre la croûte supérieure et la croûte inférieure, tandis que les évaporites du Trias découple la déformation entre la croûte supérieure et la couverture mésozoïque. L'amincissement ductile de la croûte inférieure, sans déformation cassante significative dans la croûte supérieure, engendre la formation d'un bassin rift symétrique de type sag. Au cours de cette étape, le profil de dépôt entre marge sud et nord est relativement symétrique et peu profond comme en témoigne le développement de plateformes carbonatées et l'absence de dépôt gravitaire. L'extension dans le bassin de Tartas semble avoir avorté à ce stade de déformation **(Fig. 2)**. L'extraction latérale de la croûte inférieure se poursuivant, les pentes sur les bordures du rift s'accusent provoquant localement un glissement de la couverture prerift

sur le niveau de décollement triasique. Contrairement à celui de Tartas, un glissement de la couverture s'est produit dans le bassin d'Arzacq mais ce dernier n'a pas subi une hyper-extension de la croûte continentale comme c'est le cas pour le bassin de Mauléon **(Fig. 2)**. Ce décollement entraine une dénudation des marges proximales du rift. Après cette dénudation de la crôute supérieure et la soustraction tectonique de la croûte inférieure, les marges proximales subissent une déformation fragile tandis que le futur domaine hyper-étiré enregistre un amincissement ductile de la croûte supérieure engendrant la formation d'un rift sensiblement symétrique. Au cours de cette phase ultime d'hyperextension, la subsidence au centre du bassin est accrue. Le profil de dépôt s'incline de manière significative. Les pentes sédimentaires deviennent plus abruptes et une importante sédimentation gravitaire se met en place.

4. Rôle de l'héritage crétacé au cours de l'orogenèse alpine

Dans les premiers stades d'inversion du bassin de Mauléon, la structure pseudo-symétrique du rift crétacé influence de manière significative la localisation de la contrainte compressive. Le bassin de Mauléon est inversé en une structure de type « pop-up » **(Fig. 3)**. Les deux bordures du « pop-up » accommodent la même quantité de raccourcissement bien qu'elles présentent des styles structuraux d'inversion différents.

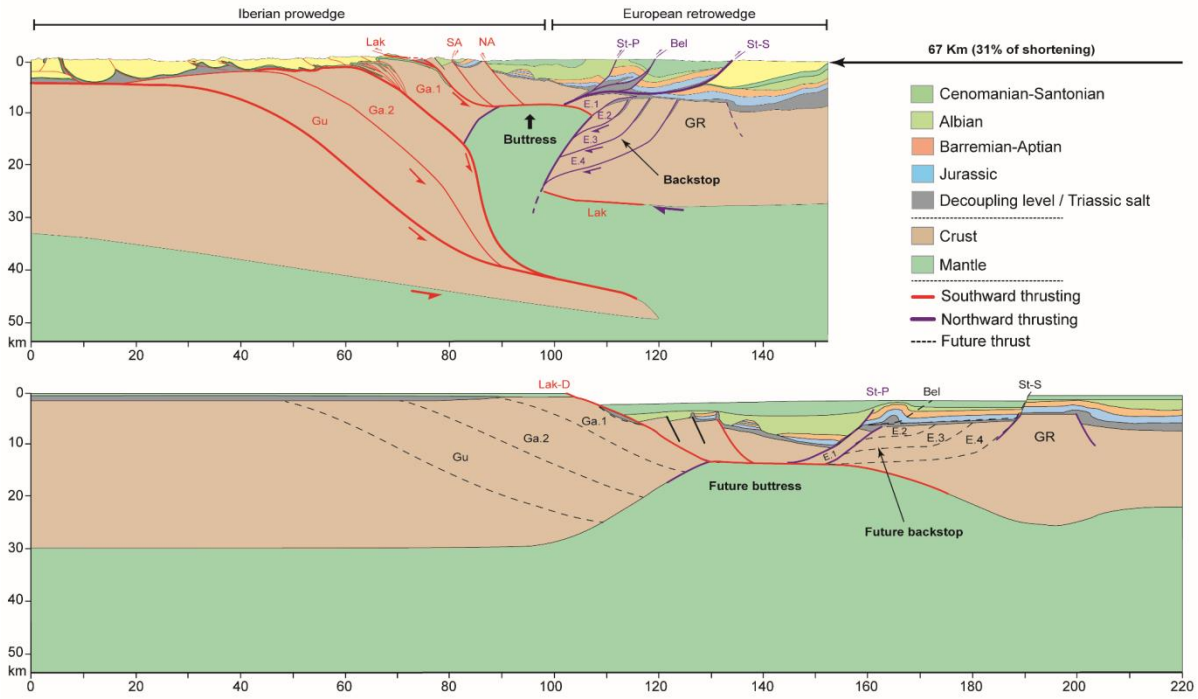


Fig. 3. Crustal-scale balanced cross section (top) and its palinspastic restoration to Santonian time (bottom). Thrust faults: SM—Sierras Marginalès; Gu—Guarga; Ga.2—Gavarnie.2; Ga.1—Gavarnie.1; Lak—Lakhoura; SA—South Arbailles; NA—North Arbailles; St-P—Saint-Palais; Bel—Bellevue; St-S—Sainte-Suzanne. Structural units: E.1—European crustal unit 1; E.2—European crustal unit 2; E.3—European crustal unit 3; E.4—European crustal unit 4; GR—Grand Rieu.

Au sud, le détachement cénomanien du Lakhoura est réactivé et favorise le sous-charriage d'une partie de la marge proximale ibérique (zone axiale) sous les unités de Mendibelza et Arbailles qui correspondent à la zone de « necking » ibérique **(Fig. 3)**. Au nord, la structure de Saint-Palais est réutilisée en chevauchement mais avec une quantité de déplacement limitée car il est recoupé par le chevauchement du Lakhoura. Au nord du chevauchement de St-Palais, les évaporites du Trias jouent le rôle de niveau de décollement sur lequel s'édifie un empilement de nappes de couverture impliquant les séries accumulées sur la marge nord du bassin. Cette tectonique de couverture est représentée par les chevauchements à vergence nord de Bellevue et de Saint-Suzanne qui rejoignent en profondeur vers le sud le chevauchement du Lakhoura. Dans le socle, sous le décollement du Trias supérieur, la zone de « necking » européenne relativement abrupte pourrait avoir joué le rôle de buttoir induisant le sous-charriage vers le sud de la marge proximale européenne. Il en résulterait la formation d'un

empilement aveugle de nappes de socle (unités E1-E4) **(Fig. 3)**. Dans le modèle proposé, cette accrétion basale d'unité de socle induit une verticalisation du contact entre la croûte continentale et le manteau européen. Une autre conséquence du sous charriage de la marge européenne pourrait être le recoupement du chevauchement de Lakhoura par les unités crustale E.1 à E.4, empêchant tout déplacement majeur sur sa portion la plus septentrionale.

Le sous-charriage vers le nord de la marge ibérique induit le développement du bassin d'avant-pays sud-pyrénéen qui est affecté d'une déformation synsédimentaire de type « thin-skin ». Dans le socle, les chevauchements de Gavarnie et de Guarga ont été successivement incorporés dans l'empilement de nappes crustales formant l'antiforme de la Zone Axiale **(Fig. 3)**. Ce processus a pu également aboutir à une verticalisation du contact croûte continentale - manteau sous la paléo-marge ibérique et ainsi accentuer la protubérance mantélique existante sous le rift crétacé nord-pyrénéen. Ce dôme rigide de manteau aurait joué le rôle de buttoir empêchant l'enfouissement du manteau sous-continental exhumé au cours du Crétacé.

5. Les zones de transferts N20° à l'origine de la non-cylindricité des Pyrénées

L'inversion alpine du bassin de Mauléon est influencée par les zones de transferts N20° interprétées ici comme héritées du Permien : zones de transfert d'Iholdy, du Saison et du Barlanès. Ces dernières ne se matérialisent par une zone diffuse d'accommodation de la déformation. Deux zones de transferts délimitent un corridor caractérisé par un taux de raccourcissement qui lui est propre. Le chevauchement du Lakhoura comme le chevauchement frontal nord-pyrénéen sont composés de plusieurs segments se branchant sur les zones de transferts N20° **(Fig. 4)**.

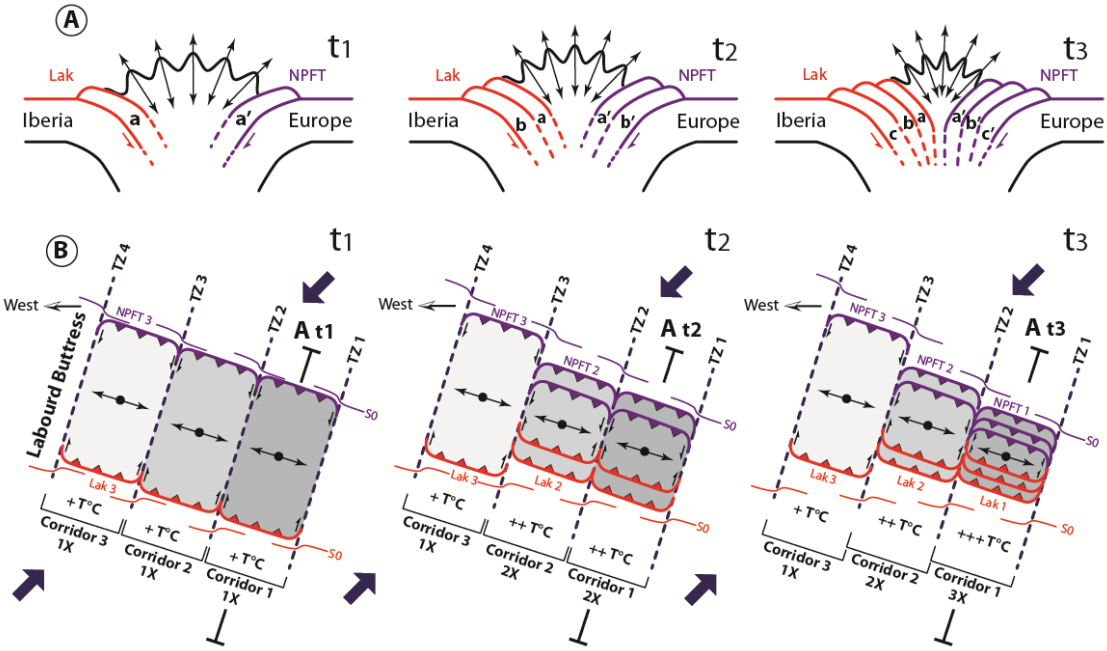


Fig. 4. (A) South-North cross-section showing the geometry of the Mauléon basin pop-up to the east of the Barlanès transfer zone through time; **(B)** Map view of drawer system model impacted by the Labourd buttress. The antithetic black arrows represent the sigma 1 direction; t1, t2, t3: time step; Lak: Lakhoura thrust system; NPFT: North Pyrenean Frontal thrust system; X: shortening rate; S0: strata plunge; T°C: Lakhoura thrust system footwall syn-collisional temperature; a-a', b-b', c-c' correspond respectively to active drawers during t1 time step, t2 time step and t3 time step; TZ1, TZ2, TZ3, TZ4 correspond respectively Ossau, Barlanès, Saison, Iholdy transfer zones; Lak 1, Lak 2, Lak 3 correspond respectively to the Lakhoura thrust segments 1, 2 and 3; NPFT 1, NPFT 2, NPFT 3 respectively the North Pyrenean Frontal thrust segments 1-3.

Cette structuration en « tiroirs » permet la déformation, par étapes, de l'ancien rift. A une échelle plus régionale, la zone de transfert de Pamplona pourrait jouer le rôle de buttoir engendrant le resserrage du pop-up de Mauléon en direction de l'est **(Fig. 4)**. Ce mode de déformation de la croûte continentale est responsable du caractère non cylindrique des structures tectoniques qui affectent le « pop-up » de Mauléon.

6. Rôle de l'héritage permien et crétacé sur l'évolution thermique du rift nord-pyrénéen depuis sa création jusqu'à son inversion

6.1. Thermicité pré-collisionnelle

La géométrie du rift crétacé semble contrôler de manière significative la répartition de la thermicité synrift. En effet, les valeurs de paléo-gradient géothermique synrift anormalement élevées se trouvent dans le domaine hyper-étiré du bassin de Mauléon. Ils augmentent de manière centripète et graduelle depuis les marges proximales jusqu'au domaine hyper-étiré : ~ 34°C/km sur la marge proximale européenne, ~ 37-47°C/km sur les deux « necking zones » et ~ 57-60°C/km dans le domaine hyper-étiré **(Fig. 5A)**.

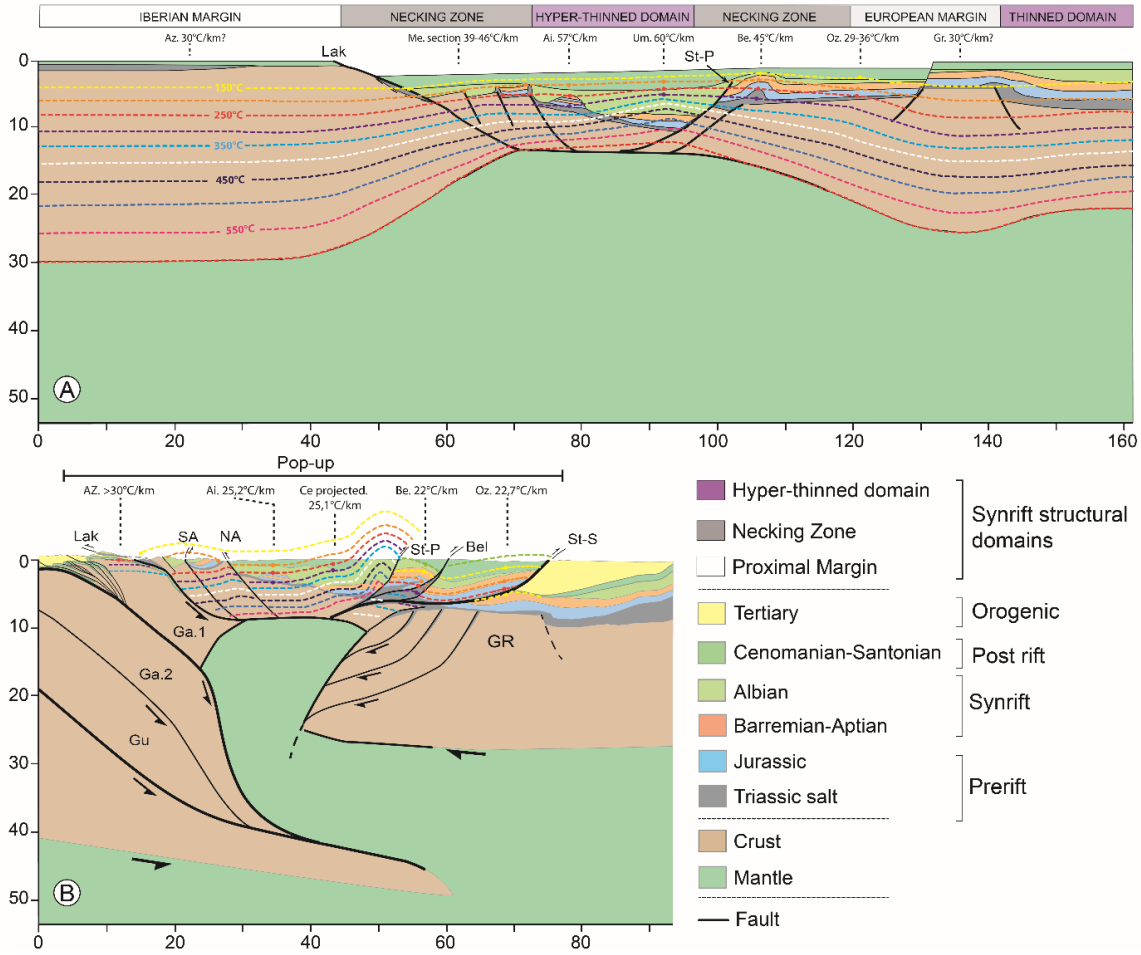


Fig 5. (A) Late Cretaceous palinspastic restoration along a N-S cross section of the Mauléon basin, displaying the synrift paleogeothermal gradients for the different structural margin domains. The Mauléon rift is characterized by a basinward increase of the paleogeothermal gradient, which induced a complex competition between brittle vs. ductile deformation during early Cenomanian detachment on the Lakhoura fault (heavy black lines). Extension on the Saint-Palais detachment (dashed line) occurred during Albian time. Az, Axial Zone; Me, Mendibelza; Ai, Ainhice-1 borehole; Um, Uhart-Mixe-1 borehole; Be, Bellevue-1 borehole; Oz, Orthez-102 borehole; Gr, Grand Rieu. **(B)** Cross section through the modern Mauléon basin. The modern Mauléon basin is a pop-up whose southern edge reactivates the Lakhoura detachment, and the northern edge is a duplex crustal stack that laterally shortens the European basement. Thick-skin tectonics affecting the Iberian margin is responsible for postcollisional thermal heating, whereas the European margin is characterized by northward displacement of metamorphosed material and an unusually low postcollisional thermal gradient. Ce, Chéraute-1 borehole; Lak, Lakhoura thrust; St-P, Saint-Palais thrust; Bel, Bellevue thrust; St-S, Sainte-Suzanne thrust.

La température maximale atteinte par les séries prérift à synrift paraît contrôlée à la fois par l'enfouissement (forte épaisseur de ces séries) et par le flux thermique arrivant en base du domaine hyper-étiré. La modélisation thermique suggère que les valeurs de flux de chaleur dans le manteau pourraient avoir atteint au maximum 100 mW/m^2 avant l'inversion tectonique du bassin de Mauléon. Compte tenu du paléo-gradient géothermique évalué à 60°C/km dans le puits d'Uhart-Mixe-1, la

température atteinte en base de couverture dans le domaine hyper-étiré du bassin de Mauléon a été extrapolée pour atteindre entre 500-600°C **(Fig. 5A)**. Cependant, ces températures sont confinées entre les zones de transfert N20° d'Iholdy et du Saison. Ce gradient élevé a perduré à minima jusqu'au Campanien, soulevant la question du processus responsable de la subsidence au cours du Crétacé supérieur, jusqu'ici considérée comme une subsidence thermique postrift classique.

6.2. Thermicité post-collisionnelle

Au cours de l'orogenèse alpine, les isothermes du Crétacé ont été déformés et plissés au sein du « pop-up » de Mauléon **(Fig. 5B)**. Le long de la marge européenne, les isothermes liés à la phase de rifting ont été préservés et transportés passivement sur la marge proximale. Sur la marge ibérique, une augmentation des pic de températures RSCM est enregistrée dans le « footwall » du chevauchement du Lakhoura ce qui suggère que ces températures ont été atteintes après le fonctionnement du chevauchement (thermicité post-collisionnelle) **(Fig. 5B)**.

La différence de réponse thermique entre les paléo-marges nord et sud du bassin de Mauléon est directement liée au style de déformation au cours de l'inversion pyrénéenne, lui-même conditionné par l'héritage structural crétacé **(Fig. 3)**. La marge ibérique est affectée par une déformation de type « thick-skin » responsable de l'édification de la zone axiale, dont le chevauchement du Lakhoura représente la structure la plus superficielle. L'augmentation du gradient géothermique est considérée comme lié à cet épaississement crustal qui fournit davantage de source de chaleur radiogénique. Dans le détail, les zones de transfert N20° influence également la réponse thermique post-collisionnelle le long du chevauchement de Lakhoura. En effet, le taux de raccourcissement augmente vers l'est à chaque fois qu'une zone de transfert N20° est franchie, induisant une augmentation du pic de température atteint pendant la compression pyrénéenne par le « footwall » du chevauchement **(Fig. 4)**.

Au contraire, le domaine hyper-étiré du bassin de Mauléon et sa marge européenne sont caractérisés par une décroissance du gradient géothermique depuis l'amorce de la compression pyrénéenne jusqu'à nos jours. Le gradient actuel mesuré dans les puits pétroliers est en effet de l'ordre de 25.0 ± 2.7°C/km. Dans ce domaine septentrional, le faible gradient géothermique peut être relié à l'épaisseur faible à moyenne de la croûte continentale (de 5 à 25 km), autrement dit à la présence du manteau sous-continental à faible profondeur hérité de la phase d'hyper-extension crétacée.

References

Cochelin, B., D. Chardon, Y. Denèle, C. Gumiaux, and B. Le Bayon, 2017, Vertical strain partitioning in hot Variscan crust: Syn-convergence escape of the Pyrenees in the Iberian-Armorican syntax: Bulletin de la Société Géologique de France, v. 188, no. 6, 39, doi:10.1051/bsgf/2017206

Cochelin, B., Lemirre, B., Denèle, Y., Blanquat, M. de S., Lahfid, A., Duchêne, S., 2018a, Structural inheritance in the central Pyrenees: the variscan to Alpine tectonometamorphic evolution of the axial zone. J. Geol. Soc., v. 175, 336–351, doi:10.1144/jgs2017-066.

Cochelin, B., Gumiaux, C., Chardon, D., Denèle, Y., Le Bayon, B., 2018b, Multi-scale strainfield analysis using geostatistics: Investigating the rheological behavior of the hot Variscan crust of the Pyrenees (Axial Zone). J. Struct. Geol., v. 116, 114–130, doi:10.1016/j.jsg.2018.07.024

Denèle, Y., Olivier, P., Gleizes, G., Barbey, P., 2007. The Hospitalet gneiss dome (Pyrenees) revisited: lateral flow during Variscan transpression in the middle crust, Terra Nova, v. 19, 445–453, doi:10.1111/j.1365-3121.2007.00770.x.

Denèle, Y., Olivier, P., Gleizes, G., Barbey, P., 2009. Decoupling between the middle and upper crust during transpression-related lateral flow: variscan evolution of the Aston gneiss dome (Pyrenees, France), Tectonophysics, v. 477, 244–261, doi:10.1016/j.tecto.2009.04.033.

Jammes, S., G. Manatschal, L. Lavier, and E. Masini, 2009, Tectono-sedimentary evolution related to extreme crustal thinning ahead of a propagating ocean: Example of the western Pyrenees: Tectonics, v. 28, no. 4, doi:10.1029/2008TC002406.

Masini, E., G. Manatschal, J. Tugend, G. Mohn, and J.-M. Flament, 2014, The tectono-sedimentary evolution of a hyper-extended rift basin: the example of the Arzacq–Mauléon rift system (Western Pyrenees, SW France): International Journal of Earth Sciences, v. 103, no. 6, p. 1569–1596, doi:10.1007/s00531-014-1023-8.

Chapitre 6.2. Discussion

Bassins extensifs à pente douce : comment l'enfouissement sédimentaire et le sel prérift contrôlent-ils le style d'amincissement de la croûte continentale durant l'hyperextension

Chapitre 6.2. Discussion: Smooth-slopes extensional basins: how sedimentary burial and prerift salt control deformation style during hyperextension

Sommaire

Résumé étendu p. 363

Abstract p. 365

1. Introduction p. 365

2. The Iberian-European plates Mesozoic basins p. 366

2.1. Aquitaine basin p. 366

2.1.1. Tartas sub-basin p. 366

2.1.2. Arzacq sub-basin p. 367

2.2. Camèros basin p. 367

2.3. Parentis Basin p. 369

2.4. Columbrets basin p. 370

2.5. The North Pyrenean Zone basins p. 372

2.5.1. Mauléon basin p. 373

2.5.2. Basque-Cantabrian basin p. 374

2.5.3. Internal Metamorphic Zone basins p. 375

3. Tectono-sedimentary evolution of a smooth-slope type extensional basin p. 375

3.1. Sag basin stage driven by prerift salt: dominant pure shear thinning p. 376

3.2. Gravity-driven gliding of the sedimentary cover during a transitional stage: onset of dominant simple shear thinning p. 376

3.3. Role of thermicity during hyperextended rifting stage p. 377

4. A comparison between Atlantic-type and smooth slope-type margins p. 378

5. Conclusion p. 381

Acknowledgements p. 381

References p. 381

Résumé étendu

L'étude tectono-sédimentaire des bassins mésozoïques de Mauléon, Arzacq et Tartas (développée dans le présent manuscrit de thèse, cf. chapitre. 3), couplé à un travail de synthèse bibliographique des bassins mésozoïques de Parentis, Basque-Cantabre, Camèros, Columbrets et la Zone Nord Pyrénéenne des Pyrénées centrales et orientales a mis en évidence les nombreuses différences avec les marges passives hyper-étirés de type atlantique.

Ces bassins arborent néanmoins des similitudes :

(1) Ils héritent d'une croûte continentale préalablement amincie (du Permien au Jurassique) qui subit une hyperextension entre le Jurassique supérieur et le Crétacé inférieur.

(2) Ils sont caractérisés par une importante épaisseur de séries prérift à synrift, un paléo-gradient géothermique et/ou un flux de chaleur mantellique synrift élevé responsable d'un métamorphisme HT/BP des sédiments en base de bassin.

(3) Leur domaine hyper-aminci coïncide généralement, dans certains secteurs peu raccourcis, avec une anomalie gravimétrique positive illustrant la présence du manteau sous-continental à faible profondeur.

(4) Dans le domaine hyper-étiré la croûte inférieure est très fine ou absente.

(5) La déformation extensive est partitionnée entre la croûte supérieure et la couverture prérift du fait de la présence d'un épais niveau évaporitique du Trias supérieur.

(6) Ils présentent une géométrie globalement pseudo-symétrique et sont affectés par le glissement gravitaire, en direction du bassin, de la couverture prerift le long du décollement matérialisé par le sel du Trias.

Ces bassins subissent une évolution extensive commune, polyphasée et synchrone de l'ouverture du domaine océanique du Golfe de Gascogne. Ils peuvent être classés en fonction du taux d'amincissement de la croûte continentale, suivant un ordre de maturité du système extensif, du moins aminci au plus aminci : (1) Tartas, (2) Arzacq, Columbrets et Camèros, (3) Parentis, (4) Basco-cantabric et Mauléon, (5) Bassin de la zone interne métamorphique des Pyrénées centrales et orientales. Ils ont récemment été définis comme des « smooth-slope type extensional basins » (Annexe 1), et diffèrent des marges passives hyper-étirées de type atlantiques par l'absence de bloc basculés et un amincissement à dominante ductile de la croûte continentale dans le domaine hyper-étiré.

Trois grandes phases d'amincissement ont pu être identifiées de manière à rendre compte de la complexité géométrique et de l'amincissement crustal de ces bassins de rift.

Dans les premiers stades d'amincissement de la croûte continentale, la déformation extensive est contrôlée par la présence de deux niveaux de découplage non connectés correspondant à la croûte moyenne et au sel du Trias supérieur. La croûte moyenne découple la déformation entre la croûte supérieure et inférieure, tandis que le sel découple la déformation entre la croûte supérieure et les séries sédimentaires mésozoïques. L'amincissement ductile de la croûte inférieure, sans déformation cassante significative dans la croûte supérieure, s'accompagne de la formation d'un bassin de rift symétrique de type sag. Au cours de cette étape, le profil de dépôt est relativement symétrique et peu profond comme en témoigne l'installation de plateforme carbonatée et l'absence de dépôt turbiditiques.

Au fur et à mesure que l'extraction latérale de la croûte inférieure (amincissement) se poursuit, les bordures du rift, à la surface de la croûte, s'inclinent en direction du bassin provoquant le glissement, sur la couche de sels triasiques, de la couverture prerift vers le centre du bassin. Des plis et des diapirs de sels vont accompagner le mouvement gravitaire. Le glissement de la couverture prérift engendre de fait la dénudation des marges proximales du système de rift.

Une fois que la couverture sédimentaire des marges proximales a complétement glissé, et que la croûte inférieure a été soustraite, le bassin change radicalement de système de dépôts sédimentaire. Au cours de cette ultime étape, le profil de dépôt s'incline de manière significative et le bassin enregistre le dépôt de série turbiditiques grossières qui s'affinent vers les marges. La déformation devient alors couplée à l'échelle de la croûte. Les marges proximales subissent une déformation fragile en surface tandis que le futur domaine hyper-étiré enregistre un amincissement ductile engendrant la formation d'un rift de profil pseudo-symétrique. Cette différence de style de déformation entre les marges et le domaine central est directement liée à l'augmentation de la température en base du bassin. Celle-ci est due à l'enfouissement de la croûte continentale du domaine hyper-étiré sous une série sédimentaire synrift dont l'épaisseur ne cesse de croitre, et à un flux thermique anormal au cœur du bassin transmis par le manteau. La sédimentation et l'héritage contrôle donc très clairement le style de déformation extensive le long de ce type de système hyper-étiré qui nécessitent à la fois un niveau de sel prérift et une importante épaisseur de séries sédimentaires synrifts pour se développer.

Chapitre 6.2. Smooth-slopes extensional basins: how sedimentary burial and prerift salt control deformation style during hyperextension

Saspiturry, N., Issautier, B., Razin, P., Baudin, T., Asti, R., Lagabrielle, Y., Duretz, T., Allanic, C., and Serrano, O., **in prep**, Smooth-slopes extensional basins: how sedimentary burial and prerift salt control deformation style during hyperextension: It will be submitted to ***Basin Research*** as a review article.

Abstract

This review documents the role of sedimentary burial and prerift salt layer in controlling the deformation style of the continental crust during hyperextension. During the Early Cretaceous, the Iberian-European plate boundary spans the development of rift basins, which undergo a complex polyphase thinning history. This extensional deformation is responsible for the development of smooth-slope type basins differing from the Atlantic-type margins by the absence of tilted block and dominant ductile thinning of the hyperextended domain. During the first steps of continental crust thinning, the deformation is controlled by two decoupling levels, the middle crust and the Late Triassic salt. The first one yields to a decoupled deformation between the lower and upper crust while the second one decouples the deformation between the upper crust and the prerift to synrift sedimentary cover. Basins' opening firstly results in the formation of a symmetric sag basin whose subsidence is accommodated by ductile thinning of the lower crust without significant brittle deformation of the upper crust and the sedimentary cover. As the lower crust is laterally extracted from the rift axis, the basement top is titled towards the basin inducing the basinward gliding of the sedimentary cover. Consequently, the sedimentary cover is removed from the proximal margins and the deformation becomes coupled at the entire upper crust-scale since lower crust has been completely subtracted below the basin center. At that time, the gliding plane is the emergent part of a detachment plane that root at depth on the continental crust. The proximal margins undergo brittle deformation while the hyperextended domain suffers from dominant ductile thinning resulting in the individualization of a pseudo-symmetric basin. This discrepancy in the extensional deformation style is directly linked to the basinward increase of paleo-thermal gradient (~60-100°C) and burial under important sedimentary thickness. In fact, the thick prerift sedimentary cover and the synrift sediments glided over prerift salt are stored in the hyperextended domain and favor a sharp temperature increase in a high-thermal gradient context. This process yields to the ductile thinning of the upper continental crust under high-temperature / low-pressure metamorphism (500-600°C). Thus, both prerift and synrift sedimentation clearly control the deformations style of smooth-slope type extensional basins whose genesis both requires a thick prerift salt level and a thick prerift to synrift sedimentary pile.

1. Introduction

Recent model and concepts on hyperextended continental margins have been defined on the basis of Atlantic-type margins, i.e. Angola/Brazil (Karner et al., 2003; Contrucci et al., 2004; Karner and Gambôa, 2007; Aslanian et al., 2009; Moulin et al., 2010; Unternehr et al., 2010; Aslanian and Moulin, 2013; Péron-Pinvidic et al., 2015), Iberia/Newfoundland (Boillot et al., 1980, 1995; Reston et al., 1995; Brun & Beslier., 1996; Whitmarsh et al., 2001; Manatschal et al., 2001, 2007; Reston, 2005, 2007; Péron-Pinvidic, 2006; Sibuet et al., 2007; Reston and Pérez-Gussinyé, 2007; Péron-Pinvidic et al., 2007; Péron-Pinvidic and Manatschal, 2009; Reston and McDermott, 2011; Mohn et al., 2015; Decarlis et al., 2015; Haupert et al., 2016), Norway/Greenland (Osmundsen et al., 2002; Osmundsen and Ebbing, 2008; Peron-Pinvidic et al., 2012a, 2012b; Osmundsen and Péron-Pinvidic, 2018), and Alps fossil analog (Lemoine et al., 1987; Froitzheim and Manatschal, 1996; Manatschal and Nievergelt, 1997; Manatschal et al., 2006, 2011; Masini et al., 2011, 2012, 2013; Beltrando et al., 2014; Mohn et al., 2014). All these works describe the mechanisms responsible for continental crust thinning and sub-continental mantle exhumation at the ocean-continent transition and they have shown that the hyperextended domain of these continental margins is characterized by (1) a very thin prerift to synrift sedimentary sequence, i.e. starved margins; (2) asymmetric margins; (3) coupled deformation

between basement and sedimentary cover resulting in the formation of extensional allochthons. Although Atlantic-type margins develop under conditions of high mantle heat flow as the product of asthenosphere upwelling and subsequent sub-continental mantle denudation (e.g. Huismans and Beaumont, 2003, 2008, 2011, 2014; Lavier and Manatschal, 2006; Brune et al., 2014, 2016). They do not undergo high temperature / low pressure metamorphism as the North-Pyrenean hyperextended rift system (Albarède and Michard-Vitrac, 1978a, 1978b; Golberg et al., 1986; Montigny et al., 1986; Golberg and Maluski, 1988; Golberg and Leyreloup, 1990; Thiébaut et al., 1992). On the contrary, the hyperextended domain of the North-Pyrenean rift basins is interpreted to stretch under high temperature conditions resulting in the formation of ductile boudins (Clerc et al., 2015a, 2015b; Corre et al., 2016; de Saint Blanquat et al., 2016; Teixell et al., 2016; Lagabrielle et al., 2016, 2019; Asti et al., 2019). Their major discrepancies with Atlantic type hyperextended margins are the lack of tilted crustal blocks and related stepping fault scarps in their central part, thus defining a dominant symmetrical smooth-slopes profile of the basement top (see Lagabrielle et al., 2019b for review, cf. Annexe. 1). Beside the North-Pyrenean rift basins, several rift basins develop in the Iberian-European plate boundary neighborhood: Tartas, Arzacq, Colombrets, Camèros, Maestrat and Parentis basins. They show a lot of common features and are time equivalent to the opening of the V-shaped Bay of Biscay margins (Montadert et al., 1979; Barbier et al., 1986; Thinon, 1999; Vergés and García-Senz, 2001; Thinon et al., 2003; Tugend et al., 2014). These basins developed at Late Jurassic/Early Cretaceous times and share identical pattern with the North-Pyrenean rift system as the: (1) small amount of brittle deformation affecting the upper crust (2) gravity-driven basinward gliding of the prerift sedimentary cover above a thick Late Triassic prerift salt unit (3) hyperthinned continental crust resulting from a synrift polyphase thinning history, (4) thick prerift to synrift sedimentary pile and (5) high temperature / low pressure synrift metamorphism. Based on a structural and sedimentological review of these basins, we shed light on the role of prerift salt décollement and the burial of the uppermost crust on the polyphase thinning of the continental crust. Finally, we compare the smooth-slope type basin to Atlantic type hyperextended systems.

2. The Iberian-European plates Mesozoic basins

2.1. Aquitaine basin

The Aquitaine basin starts to develop during the Late Permian in an extensional context related to the dislocation of Pangea (Burg et al., 1994). During the Triassic to Hettangian, extension leads to an aborted rift basin filled with clastic rocks, carbonates, and an evaporites sequence of ~1-2 km thick (Curnelle et al., 1982; Curnelle, 1983; Curnelle and Dubois, 1986). The Jurassic was a tectonically stable period marked by the development of a widespread carbonate platform (Peybernès, 1976). At the end of the Jurassic, the entire platform was confined, as suggested by the deposition of restricted dolomite and anhydrite facies (BRGM, 1974; Serrano et al., 2006). The Jurassic prerift carbonate platform was uplifted, weathered and partly eroded (Combes et al., 1998; James, 1998; Canérot et al., 1999), in response to asthenosphere upwelling preceding the Early Cretaceous rifting (Saspiturry et al., 2019a). In fact, the Early Cretaceous was a structurally active time in which the Aquitaine basin evolved into different sub-basins characterized by very rapid subsidence (up to 130 m/My, (Désaglaux and Brunet, 1990; Brunet, 1991), including the symmetric Arzacq and Tartas rift basins. The ~1-3 km thick Early Cretaceous synrift sedimentary sequence unconformably overlies the ~2-3 km thick prerift Triassic to Jurassic deposits (Serrano et al., 2006).

2.1.1. Tartas sub-basin

The Tartas basin is emplaced in the southern Aquitaine domain **(Fig. 1)**. It is bounded to the north by the Flexure Celtaquitaine (BRGM et al., 1974) which separates it from the North Aquitaine Platform, and to the south by the Audignon-Pécorade-Antin Maubourguet ridge. Tartas basin is a relative narrow (20 km) east-west elongated trough (Serrano et al., 2006). It lies on a slightly thinned continental crust (20-25 km in Wang et al., 2016). It undergoes symmetry opening

during the Berriasian with the development of widespread shallow facies, and this pattern pursues throughout the Early Cretaceous. Sediments range from marginal littoral (Berriasian to Barremian; e.g. Issautier et al., 2018, cf. chapter. 3.3), to build-up inner-platform type (Aptian, Albian; e.g. Delfaud, 1969; Arnaud-Vanneau et al., 1979; Bouroullec et al., 1979; Peybernès, 1979, 1982). Thus, during Berriasian to Albian time, the balance between carbonate production and creation of available space favors the aggradation of 2 500m thick shallow marine carbonate facies, witnessing a highly subsiding stage controlling a relative-flat depositional profile. The resulting paleogeography was smooth and uncontrolled by tectonic structures as no brittle deformation is visible within the basin. The high subsidence rate might result from lower crust ductile pure shear thinning engendering a symmetric synrift sag basin formation (**Fig. 2A**; Issautier et al., submitted, cf. chapter. 3.3). Furthermore, this regime is probably enhanced by the existence of a thick Rhaetian-Hettangian evaporites layer, favoring the mechanical decoupling between the prerift sediments and the basement. This salt blanket is believed to control the lack of brittle structures in the synrift succession, and might explain the continuous ductile regime during the Early Cretaceous (Issautier et al., submitted, cf. chapter. 3.3).

2.1.2. Arzacq sub-basin

The Arzacq basin is the southern prolongation of the Tartas basin **(Figs. 1 and 2B)**. Its dimensions and continental crust thickness are very similar to the Tartas basin. It is a 40 km wide and N110 elongated basin laying upon a 20 to 25 km thick continental crust, implying slight crustal-thinning (Wang et al., 2016). It is bounded to the North by the Audignon-Pécorade-Antin Maubourguet ridge (Mauriaud, 1987; Mediavilla, 1987; Serrano et al., 2006) and to the south by the North Pyrenean Frontal Thrust (Choukroune and ECORS Team, 1989; Daignières et al., 1994; Bourrouilh et al., 1995). Significant north-dipping normal faults emplaced on the southern flank of Grand Rieu Domain delimitates the southern Arzacq edge (e.g. Masini et al., 2014; Gómez-Romeu et al., 2019; Saspiturry et al., 2019a). A first major offset is recorded along this structure during the Early Mesozoic rifting stage (Triassic-Hettangian); accommodating high subsidence rate and thick anhydrite deposition (Curnelle, 1983). Synrift history is polyphase and characterized by two regimes: the first one is symmetric (Berriasian to the Aptian); and the second one is slightly asymmetric (Albian; Issautier et al., submitted). The first stage is identical to the Tartas basin and it is accommodated by ductile flow of the continental-crust. Again, no brittle structures affect the upper crust, probably because of a decoupled deformation resulting from the existence of the thick salt blanket (Canérot et al., 2005). Berriasian-Barremian paleogeography is dominated by shallow marginal carbonate facies in Berriasian to Barremian times (e.g. Bouroullec and Deloffre, 1970; Peybernès and Combes, 1994; Biteau et al., 2006; Biteau and Canérot, 2007). Differentiation occurs in Late Aptian time with the individualization of a marly trough bounded by carbonate reef and inner-platform deposits (Delfaud and Gautier, 1967; Delfaud and Villanova, 1967). The Albian marks a sudden change in both paleogeography and basin's geometry since depositional profile becomes asymmetric and controlled by salt tectonics on the northern Grand Rieu Ridge, and on the Audignon ridge. These halokinetic movements correspond respectively to cover-gliding of Grand-Rieu Domain sedimentary cover, and giant salt-diapir in Audignon (Mauriaud, 1987; Mediavilla, 1987; Issautier et al., 2018). The cover gliding on salt layer has to be considered here as the emergence of a detachment fault which follows the ductile thinning of the lower crust at the onset of the rifting stage (**Fig. 2B**; Issautier et al., submitted, cf. chapter. 3.3). Subsidence evolution of the Arzacq basin also shows that the latter developed under abnormally high thermal gradient that ended as soon as the beginning of the Pyrenean shortening (Angrand et al., 2018). The postrift stage is then marked by the Cenomanian shallow carbonate succession resting unconformably on the Albian deposits.

2.2. Camèros basin

The Cameros basin is located in the northwestern edge of the Iberian chain **(Fig. 1)**. This basin is a 80 km wide and 120 km long WNW-ESE synclinorium resulting from Early Cretaceous extension (Guimerà et al., 1995).

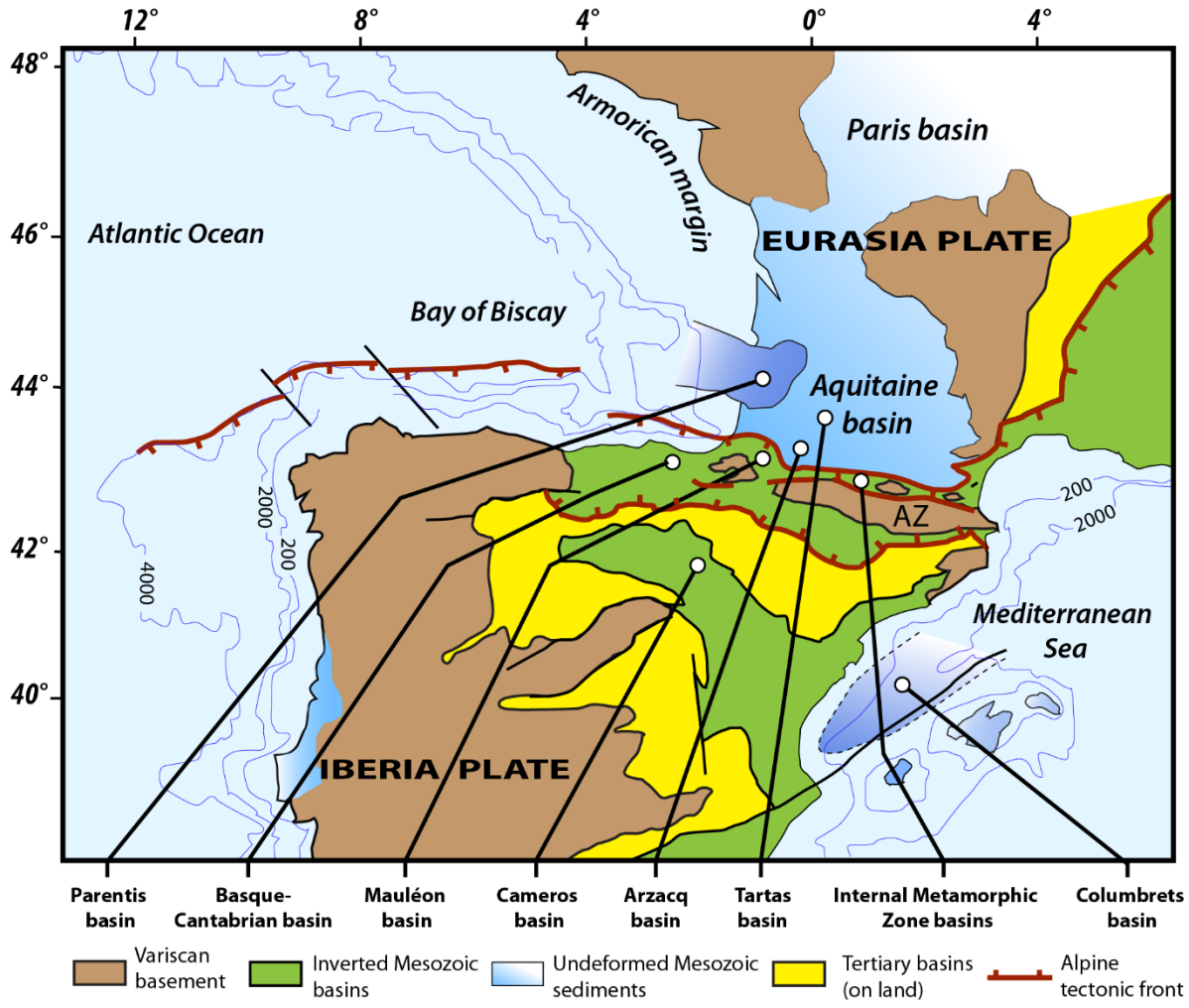


Fig. 1. Simplified structural map of the Cantabrian-Pyrenean orogenic system and adjoining Iberia showing (i) Eurasia deformed and undeformed domain and (ii) location of the studied basins (modified from Lagabrielle et al., submitted; Annexe. 1).

The Camèros basin is thrusted to the north and to the south onto the Ebro and Duero Cenozoic basins respectively. It underwent Permian to Triassic (Alvaro et al., 1979) and Late Jurassic to Early Cretaceous rifting stages (Platt, 1990; Mas et al., 1993; Casas-Sainz and Gil-Imaz, 1998; Salas et al., 2001). This second phase is highlighted by a tectonic subsidence passing to thermal subsidence (Omodeo Salè et al., 2014; Omodeo-Salé et al., 2017). The associated synrift sequence varies in thickness from 6.5 km to 8 km (Casas-Sainz and Gil-Imaz, 1998; Mas et al., 2011; Omodeo Salè et al., 2014; García-Lasanta et al., 2017).

The base of the Mesozoic sedimentary pile is characterized by the presence of a 500 m thick Late Triassic salt sequence (Casas Sainz, 1993; Casas-Sainz and Gil-Imaz, 1998). The prerift Jurassic sequence reaches 800 m thick and it is composed of shallow marine carbonate platform deposits, lying unconformably both over Paleozoic basement and Late Triassic evaporites (Valladares, 1980; Platt, 1990; Aurell and Meléndez, 1993; Aurell et al., 2003). The Late Jurassic to Barremian synrift sequence consists of nearly 3-6 km thick fluvial to lacustrine deposits and rare marine transgression layers (Guiraud and Séguret, 1985; Platt, 1990; Alonso and Mas, 1993; Mas et al., 1993, 2011; Quijada et al., 2010; Suárez González et al., 2010). The Late Barremian to Early Aptian depositional profile remains shallow and it is characterized by coastal-wetlands with both fresh-water and sea-water influences, grading laterally to alluvial and fluvio-lacustrine deposits (Platt, 1989, 1986). Consequently, during the rifting stage, the basin did not undergo a major deepening of the sedimentary profile. The Late Jurassic to Early Cretaceous synrift sequence thins gradually toward the basins' edges where it onlaps the

prerift Jurassic sequence **(Fig. 2C)**, suggesting a slight asymmetry of the basin with an apparent northward migration of the depocenter (Casas-Sainz and Gil-Imaz, 1998; Guimerà et al., 1995; Mas et al., 1993; Omodeo-Salè et al., 2014, 2017). The northward migration of the basin depocenter during the extension stage likely indicates a simple shear regime during the opening processes.

The Camèros basin is characterized by the (1) perfect continuity of the prerift Jurassic sequence, (2) absence of normal fault affecting both basement and cover and (3) lack of significant offset of the top basement (Casas-Sainz and Simón-Gómez, 1992; Casas Sainz, 1993; Casas-Sainz and Gil-Imaz, 1998; Casas et al., 2000, 2009; Omodeo Salè et al., 2014) **(Fig. 2C)**. These observations question the processes responsible for continental crust thinning during the Late Jurassic to Early Cretaceous.

The Camèros basin has therefore been interpreted as an extensional ramp syncline formed above a décollement in the Late Triassic evaporites, rooting at depth on a blind south-dipping extensional ramp or crustal detachment (Mas et al., 1993, 2011; Guimerà et al., 1995; Casas-Sainz and Gil-Imaz, 1998; Casas et al., 2009; García-Lasanta et al., 2017; Omodeo-Salé et al., 2017). This process induces the northward migration of the synrift depocenter and associated edgeward onlap on the synrift deposits, and the formation of synclinal-shape rift basin. The fault movement stretched the prerift Jurassic deposits, which remains however continuous (Casas et al. 2009). The Late Triassic evaporites layer played a major role in accommodating the extension because most of the shear strain is accommodated by this layer and both cover and basement remain well preserved. The resulting basinward gliding of the prerift cover induces some thickness reduction of the Late Triassic evaporates and diapirism (Casas Sainz, 1993; Casas-Sainz and Gil-Imaz, 1998; Rat et al., 2019).

The Camèros basin exhibits a low pressure / high temperature metamorphism affecting its deepest part (Guiraud and Séguret, 1985; Golberg et al., 1988; Rat et al., 2019). The rifting stage develops under a high thermal gradient estimated at around 70°C/km, assuming a sediment thickness of 8 km (Mata et al., 2001; Del Río et al., 2009). Towards the northern basin's edge, the paleothermal gradient decreases as the intensity of the low pressure / high temperature metamorphism, i.e. 41.5°C/km (Omodeo-Salé et al., 2017). This latter thermal gradient is consistent with the estimated value of thermal heat flow, i.e. around 60–65 mW/m^2 (Omodeo-Salé et al., 2017). However, peak temperature of the low-pressure and high temperature metamorphism is reached during the postrift stage (Golberg et al., 1988; Casquet et al., 1992; Casas-Sainz and Gil-Imaz, 1998; Mata et al., 2001).

2.3. Parentis Basin

The E-W elongated Parentis basin is localized between the Landes high (Ferrer et al., 2009) to the south and the Armorican arc to the north (Lefort and Agarwal, 1999) **(Fig. 1)**. It is a V-shape basin that opens westward to the eastern ending of the Bay of Biscay continental margins characterized by exhumed sub-continental mantle at the ocean-continent transition (Pinet et al., 1987; Bois and ECORS Scientific team, 1990; Bois and Gariel, 1994; Tugend et al., 2014). The basin is edged to the south by the north-dipping planar Ibis fault (Ferrer et al., 2008). As in the North-Pyrenean Zone, during Permian to Lower Triassic time, the continental crust of the future Parentis basin suffered several extensional deformations (Dardel and Rosset, 1971; Mathieu, 1986; Ferrer et al., 2009; Biteau et al., 2006). The latter led to the deposition of a 1-3 km thick sequence of Late Triassic to Early Jurassic evaporites (Curnelle, 1983; Ferrer et al., 2009). This basin is filled with a 10 km thick Jurassic to Early Cretaceous shallow carbonate platform and terrigenous synrift sequence that rest upon the thick prerift evaporites (Montadert and Winnock, 1971; Bourrouilh et al., 1995; Bois et al., 1997). It underwent tectonic subsidence during the Late Jurassic to Late Aptian synrift stage, followed by thermal subsidence during Albian to late Cretaceous postrift stage (Ferrer et al., 2008). The Cretaceous Parentis rift basin shows a profile with gentle-dipping margins' slopes that seem to be deprived from major normal fault scarps **(Fig. 2D)**. This basin is characterized by a hyperextended continental crust (Bois and ECORS Scientific team, 1990; Bois, 1992; Ferrer et al., 2008). The Moho depth below the Parentis basin is about 10 km and the lower continental crust seems to be absent or very thin in the hyperextended

domain, while the proximal margins are characterized by both upper and lower crust (Pinet et al., 1987; Marillier et al., 1988; Tomassimo and Marillier, 1997; Ruiz, 2007). Positive Bouguer gravity anomaly matches with the hyperextend domain of the Parentis rift basin (Pinet et al., 1987a) which results from the Late Jurassic to Early Cretaceous hyperextension stages affecting the Peri-Pyrenean realm (Jammes et al., 2009; Tugend et al., 2015).

The ECORS project evidenced the symmetrical syncline-shape of the Parentis basin and shed light on the little amount of normal faults in the stretched crust and proximal rift margins (Pinet et al., 1987b; Bois et al., 1997; Bois and Courtillot, 1988) **(Fig. 2D)**. During final hyperextensional stage, at Early Cretaceous time, the Parentis basin presents a slight asymmetric shape (Pinet et al., 1987a). More recently, the southern and northern margins of the rift have been several times interpreted as lower plate or upper plate in an asymmetric opening systems (Jammes et al., 2010a, 2010b, 2010c; Masini et al., 2014; Tugend et al., 2014). However, Pinet et al. (1987b) have evidenced that the lack of low angle normal faults and, most importantly, the location and the geometry of the thinned zone make it difficult to apply the simple shear model for the formation of the rifted Parentis basin. These authors proposed that the mantle uplift induces stretching and ductile flow in the lower crust and consequently a decoupling deformation between upper and lower crust. This explains the discrepancy between the slight superficial extension and the substantial thinning ratio greater than 6 at depth. This interpretation implies that the Parentis crust has been thinned under high temperature conditions to reach ductile strain regime as it is the case in the adjacent North Pyrenean Zone.

Jammes et al. (2010c) highlighted the major role of the thick prerift Late Triassic salt sequence in decoupling the deformation between the basement and the rest of the Mesozoic sedimentary cover. The southern margin seems to undergo first gravity-driven cover gliding and then synrift thin-skinned extensional faulting along the Late Triassic salt décollement plane (Tugend et al., 2014). Due to the physical properties of the salt, this process induces the development of synrift salt domes and weld diapirs affecting the Mesozoic sedimentary pile (Mathieu, 1986; Mediavilla, 1987 Ferrer et al., 2008). Moreover, Ferrer et al., 2012 have evidenced that salt structures are mainly localized on the basin edges, where the post Triassic sediments are the thinnest or absent, facilitating the formation of salt anticlines and diapirs **(Fig. 2D)**.

2.4. Columbrets basin

The Columbrets basin is the south-western part of the Valencia Trough between Spain and Balearic Islands **(Fig. 1)**. This ENE-WSW trending basin represents a mildly inverted Late Jurassic-Early Cretaceous hyperextended rift and thus exceptionally preserved (e.g. Etheve et al., 2018). The prerift and synrift successions are shaped in a large-scale synclinal with thinned borders, in relation with displacement along extensional detachment **(Fig. 2E)**. This domain underwent a polyphase rifting history since it spans three major rifting events. During Late Permian to Early Triassic, this domain is characterized by the development of distributed deformation inducing the formation of intracontinental rift basin filled by continental deposits (Arche and López-Gómez, 1996; Vargas et al., 2009). This rifting event is followed by a Late Triassic-Early Jurassic one related to the Alpine-Ligurian Tethys opening (Jiménez-Munt et al., 2010; Frizon de Lamotte et al., 2011; Schettino and Turco, 2011). The paroxysm of this rift event is characterized by the deposition of a thick layer of evaporites that will play a major décollement role in subsequent events (Ortí, 1974; Ortí et al., 2017). The Jurassic postrift sequence is mainly composed of shallow water limestones (e.g. Roca, 1996). It seems that the crust was partly thinned before the onset of the last, but principal Late Jurassic to Early Albian rifting stage (Salas et al., 2001; Nebot and Guimerà, 2016; Etheve, 2016; Etheve et al., 2018; Roma et al., 2018). The synrift successions are essentially made up of platform carbonate deposits that grade basinward into deep-water marls, giving way locally towards the basin's edges to fluvial to deltaic deposits (Etheve et al., 2018 and references therein). Carbonate platform limestones constitute the Middle Albian to Late Cretaceous postrift thermal subsidence record (Salas et al., 2001; Nebot and Guimerà, 2016; Etheve et al., 2018).

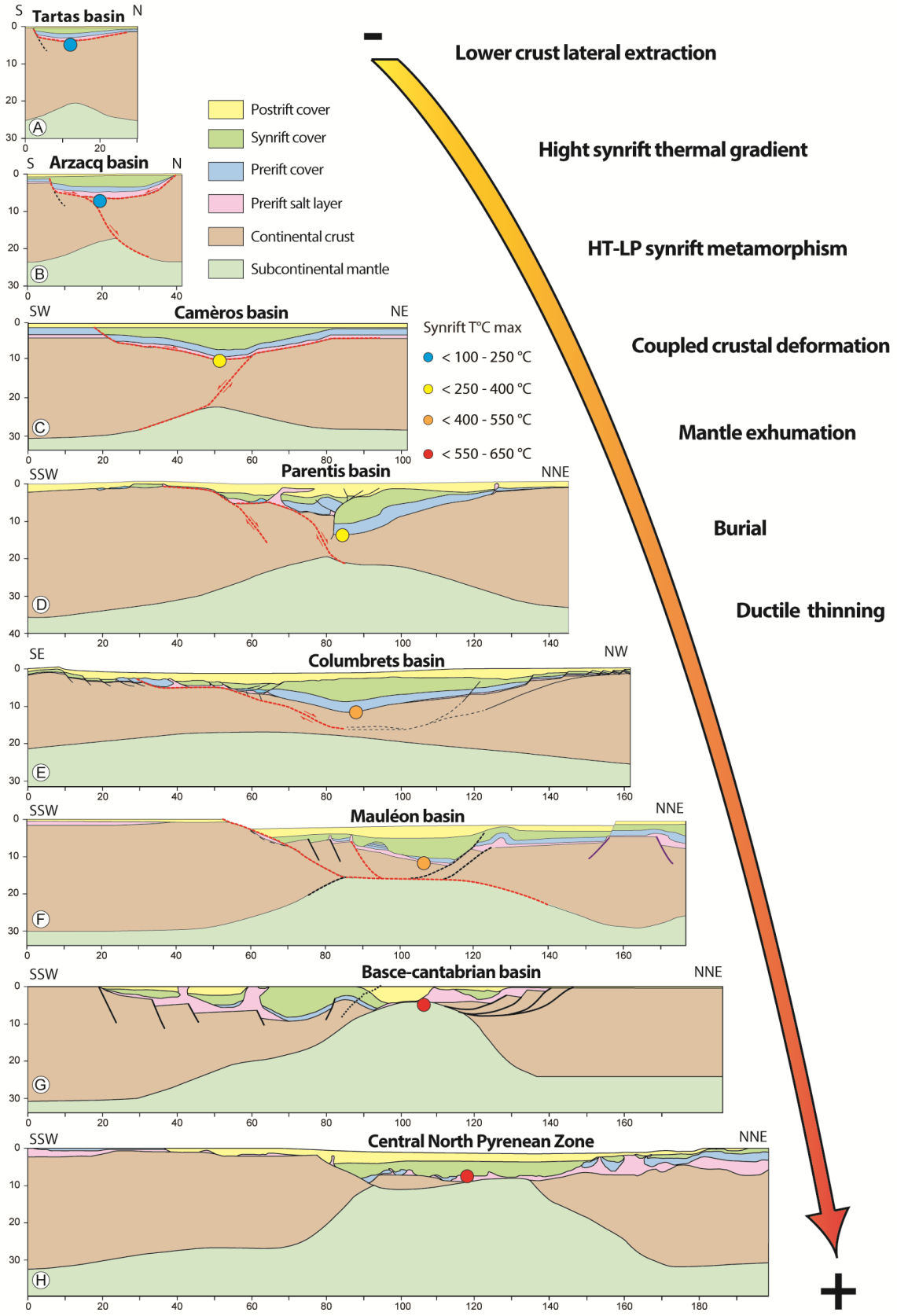


Fig. 2. Smooth-slope type basins classified following the continental crust amount of extension, **(A)** Tartas basin (Issautier et al., submitted, cf. chapter. 3.3); **(B)** Arzacq basin (Issautier et al., submitted, cf. chapter. 3.3); **(C)** Camèros basin (modified after Casas-Sainz and Gil-Imaz., 1998); **(D)** Parentis basin (Tugend et al., 2014); **(E)** Columbrets basin (Etheve et al., 2018); **(F)** Mauléon basin (Saspiturry et al., 2019a); **(G)** Basco-cantabric basin (Pedrera et al., 2017); **(H)** Central North Pyrenean Zone basins (Espurt et al., 2019); location in Figure 1.

The Late Jurassic to Early Albian rifting stage is responsible for the hyper thinning of the Columbrets basin's continental crust. It is evidenced by the Moho depth that reaches 25-30 km under the Columbrets basin margins and only 8-10 km under the trough center (Gallart et al., 1990; Banda and Santanach, 1992; Dañobeitia et al., 1992; Torné et al., 1996; Vidal et al., 1997; Ayala et al., 2003, 2015; Gomez-Ortiz et al., 2011; Etheve et al., 2018) **(Fig. 2E)**. The minimum thickness of the continental crust reaches 3.5 km on the hyperextended domain (Etheve et al., 2018). This latter is directly correlated with an abnormally high Bouguer gravity anomaly spreading between 60 and 80 mGal (Ayala et al., 2015). Both thinned continental crust and Bouguer anomaly match with the shallow lithosphere-asthenosphere boundary (i.e. 60 to 65 km depth) evidenced by geoid modeling and 3-D gravity highlighting extreme crustal thinning (Zeyen and Fernàndez, 1994; Ayala et al., 1996, 2003; Carballo et al., 2015).

The Columbrets basin has been interpreted as a salt-detached ramp-syncline basin (Roma et al., 2018). In fact, the eastern Columbrets basin edge shows an extensional detachment fault rooting at depth on the continental crust beneath the Columbrets hyperextended rift domain (Etheve et al., 2018). Toward the basin edge, this structure coincides with the Late Triassic salt décollement. It is responsible for the basinward gliding of the prerift sedimentary cover, causing halokinetic movements (thin-skinned extensional deformation and extensional raft; Etheve et al., 2018). Nevertheless, the detachment imaged by seismic reflection profiles alone cannot account for the extreme crustal thinning identified in the basin core (Etheve et al., 2018). In fact, the reflective lower crust becomes thinner towards the Columbrets trough axis where it appears to be either missing or to be reduced down to a l-2 km thick layer (Gallart et al., 1990, 1994; Dañobeitia et al., 1992; Torné et al., 1992; Sàbat et al., 1997; Vidal et al., 1997). These observations highlight the fact that the upper and lower crusts react differently to crustal stretching and thinning. Etheve et al. (2018) suggest that the lower crust suffered large-scale boudinage during Late Jurassic to Early Cretaceous hyperextension. Thus, the evolution of the Columbrets rift system is controlled by two main decoupling levels corresponding to the Late Triassic prerift evaporites, at shallow level, and to the middle crust at depth (Etheve et al., 2018).

The present-day surface heat flow density in the southwestern Valencia Trough is about 65 to 100 mW/m^2 according to seafloor measurements and oil well thermal data (e.g. Ayala et al., 2015; Carballo et al., 2015). It coincides with the area where the continental crust is the thinnest (Banda and Santanach, 1992; Fernandez et al., 1995; Ayala et al., 2015), demonstrating a stable high thermal regime inherited from the Late Jurassic-Cretaceous rifting despite the fact that the last rifting was Cenozoic in age.

2.5. The North Pyrenean Zone basins

The Pyrenees underwent Late-Hercynian extension (Permian-age) responsible for the development of continental deposits in endoreic extensional basins (Bixel and Lucas, 1983, 1987; Bixel, 1984). This post-orogeny equilibration goes together with exhumation of magmatic and granulitic rocks, all along the North Pyrenean Zone (Cochelin, 2016; Cochelin et al., 2017; de Saint Blanquat, 1993; Olivier et al., 2004; Saspiturry et al., 2019b). An immediate consequence of the Hercynian collapse stage is the major thinning of the previously hot lithosphere, defining an important inheritance before the Mesozoic stage. This latest Paleozoic thinning stage, as well as the Late Triassic regional extensional stage (ophitic intrusion) should not be neglected when trying to estimate the North Pyrenean Zone Cretaceous crustal-thinning. Recent works proposed that continental crust was already partly thinned before the onset of the Early Cretaceous hyperextension (Saspiturry et al., 2019c; Asti et al., 2019; Espurt et al., 2019). These authors show respectively that the restoration of the Iberian-European section across the Mauléon basin (western Pyrenees) and the Ballongue basin (central Pyrenees) even implies a very high MOHO position by the end of the Jurassic (around 20km depth).

The Triassic deposits of Western Pyrenees are typical of the German-type succession ending with thick evaporite and ophite complex (Curnelle, 1983; Lucas, 1985; Rossi et al., 2003). The salt unit plays a major role in the Pyrenees since it acts as a décollement layer at the base of the Mesozoic

sedimentary cover and strongly controls the Early Cretaceous hyperextensional stage deformation style (Canérot, 1989, 1988; Canérot and Lenoble, 1993; James and Canérot, 1999; Canérot et al., 2005; Jammes et al., 2010b; Lagabrielle et al., 2010; Duretz et al., 2019). Contrary to the previously described basins, Berriasian-Valanginian deposits are often lacking in the North Pyrenean Zone (Combes et al., 1998; James, 1998; Canérot, 2008) witnessing the emersion of the area. From Barremian to Aptian time, the Iberian and European margins of the North Pyrenean Zone basins were composed of carbonate platforms grading to distal marls toward the basin axis. Thus the North Pyrenean Zone hyperextended basins are characterized by thick sequence of: (1) Late Triassic to Early Jurassic prerift evaporites, i.e. 1-3 km (Curnelle., 1983), prerift Jurassic carbonate platform developing in a relatively stable tectonic context, i.e. 0.5-2 km (Delfaud and Henry, 1967; Lenoble, 1992; James, 1998), Barremian to Aptian synrift carbonates and marls, i.e. 0-1.6 km (Delfaud and Villanova, 1967, Arnaud-Vanneau et al., 1979), synrift Albian gravity deposits, i.e. 1-5 km, the Black Flysch or "Flysch Ardoisier" (Debroas, 1976, 1978, 1987, 1990; Boirie, 1981; Boirie and Souquet, 1982; Fixari, 1984; Roux, 1983; Souquet et al., 1985; Debroas et al., 2010) and postrift turbidites, i.e. 2-4 km (Casteras, 1971; Henry et al., 1987; Le Pochat et al., 1976; Razin., 1989).

2.5.1. Mauléon basin

The Mauléon basin located to the south of the Arzacq sub-basin **(Fig. 1)**, features a well-known strong positive gravity anomaly centered upon the basin axis (Gottis, 1972; Boillot et al., 1973). Firstly, interpreted as lower crustal material (Grandjean, 1994; Vacher and Souriau, 2001; Pedreira et al., 2007), the anomaly is currently attributed to the presence at shallow depth (~10 km) of sub-continental mantle (Casas et al., 1997; Jammes et al., 2010a). This last interpretation has been tightened by new acquisition of *Vp* seismic velocities, giving values of ~ 7.3 km/s (Wang et al., 2016; Chevrot et al., 2018). Above the mantle dome, the current thickness of the crust is estimated to roughly 5 km. Mantle exhumation is considered to have occurred during Cretaceous hyperextension and the Mauléon basin corresponds to a hyperextended rift (Lagabrielle and Bodinier, 2008; Jammes et al., 2009; Lagabrielle et al., 2010; Masini et al., 2014; Tugend et al., 2014; Corre et al., 2016; Teixell et al., 2016). Due to Eocene shortening, the Mauléon basin was inverted and it shows today a pop-up structure bordered to the north and south by conjugate thrusts (Saspiturry et al., 2019c).

The Mauléon basin, alike the other basins described previously, first develop as a symmetric synrift sag basin that subsided in response to lower crustal ductile thinning (Saspiturry et al., 2019a; Asti et al., 2019). From Albian to Early Cenomanian time, the structural style changed, with the acquisition of asymmetric basin's morphology and sedimentary facies distribution. Gravity-flow conglomerates accumulated at the foot of the Iberian margin slope (Boirie, 1981; Fixari, 1984; Souquet et al., 1985) are controlled by steep north-dipping normal faults (South Arbailles and North Arbailles faults; Saspiturry et al., 2019a). They were derived by fan deltas reworking freshly uplifted Paleozoic substratum. The restoration of the synrift geometries indicates that the Iberian substratum was tilted 30° toward the north in Albian time (Saspiturry et al., 2019a). It implies a thickening of synrift deposits to the north, toward the steep south-dipping Saint-Palais fault where they reach a maximum thickness of around 5 km **(Fig. 2F)**. This fault separated the marls basin (to the south) from the European proximal margin (to the north), where a carbonate platform developed (Saspiturry et al., 2019a). The gentle south-dipping European margin contrasts with the steep north-inclined Iberian one. Therefore, the Saint-Palais fault is an Albian to Early Cenomanian major normal fault responsible for the structural asymmetry of the basin margins. In this scheme, the steep north-dipping slope of the entire Iberian margin appears as a roll over structure in the hanging wall of the Saint Palais Fault. The roll over structure is also accommodated by north-dipping minor normal faults which propagated toward the south.

The mid-Cenomanian to Late Santonian is marked by a significant facies distribution reorganization. Shallow carbonate platforms developed on both the Iberian and European margins (Souquet, 1967; Alhamawi, 1992; Ternet et al., 2004; Serrano et al., 2006). The

European platform-basin transition coincided with the steep south-dipping South Grand Rieu fault. The Iberian carbonate platform graded northward to deep-sea calcareous breccias at the emplacement of the Lakhoura normal fault. This short platform-basin transition leads us to consider Lakhoura normal fault as the emergence of a significant northward detachment during mid-Cenomanian time. This detachment, responsible for a southward tilt of the Iberian basement cross-cuts the lower part of the older Saint-Palais structure rendering it inactive. Thus, the Early Cretaceous evolution of the Mauléon basin is defined, after an early development as a sag basin, by a succession of two antithetic diachronous extensional structures: (1) the south-verging Saint-Palais fault accommodating the thinning of the European margin, and (2) the north-verging Lakhoura detachment, cross-cutting Saint Palais fault **(Fig. 2E)**. Locally, the exhumed sub-continental mantle has been denuded and partly reworked into Early Cenomanian synrift deposits (Roux, 1983; Duée et al., 1984; Fortané et al., 1986; Jammes et al., 2009; Lagabrielle et al., 2010; Debroas et al., 2010; Teixell et al., 2016).

Hyperextension in the Mauléon basin developed under high paleogeothermal gradient as evidenced by Raman Spectroscopy of Carbon Materials (RSCM) peak temperatures reporting estimated synrift thermal gradient of 60-75°C/km (Corre, 2017; Saspiturry et al., 2019d, cf. chapter. 5), or by detrital zircon fission-track and (U-Th-Sm)/He thermochronology data, highlighting respectively a 80°C/km (Vacherat et al., 2014) and 80-100°C (Hart et al., 2017) synrift thermal gradient. Vitrinite reflectance values on the Mauléon basin argue also in favor of high temperature / low pressure synrift metamorphism (Lescoutre, 2019; Lescoutre et al., 2019). It should be noticed that peak temperature is reached in the lower part of the basin during the period of the postrift deposits (Vacherat et al., 2014; Saspiturry et al., 2019d), similarly to what is described in Camèros basin. Due to Pyrenean thrusting, a detached slice of mantle outcrop is visible in the eastern part of the basin (Urdach area). In this particular location, crustal material in contact with the Urdach lherzolites shows a ductile shearing suggesting a lateral extrusion of the middle crust from the basin axis outwards at temperatures between 450°C and 350°C (Asti et al., 2019) (Fig. 2F).

2.5.2. Basque-Cantabrian basin

The Basque-Cantabrian basin undergoes the same Mesozoic history than the north Pyrenean Zone rift basins although it develops to the south of the Pyrenean Axial Zone **(Fig. 1)**. The rift axis is characterized by a thick succession Upper Jurassic-Cretaceous sediments of around 8-10 km with interlayered Aptian to Santonian basic volcanic rocks (Azambre and Rossy, 1976; Rat et al., 1983; Rat, 1988; García Mondéjar et al., 1996; Castañares et al., 1997; Castañares and Robles, 2004) **(Fig. 2G)**. The Basque-Cantabrian basin displays an extremely thinned lithosphere in its western central part as evidenced by a positive Bouguer anomaly (Biscay Synclinorium, Pedreira et al., 2007), interpreted as the presence at shallow depth of lithospheric mantle (Pedrera et al., 2017). The Basque-Cantabrian basin continental crust was affected by hyperextension during the Early Cretaceous. Indeed, a peridotite outcrop, interpreted as a relic of the exhumed upper mantle during the Cretaceous hyperextension stage, is visible in the vicinity of the inverted Leiza major detachement fault (Mendia and Ibarguchi, 1991; DeFelipe et al., 2017; Ducoux, 2017; Ducoux et al., 2019). Hyperextension is also recorded by the development of Cretaceous high-temperature and low pressure metamorphism (Golberg and Leyreloup, 1990; Cuevas and Tubia, 1999). Mineral assemblages and RSCM on the Nappes des Marbres, that represent the inverted eastern Basque-Cantabrian hyperextended rift domain, is characterized by a prerift sedimentary cover reaching locally 500-600°C during hyperextension (Lamare, 1936; Martínez-Torres, 1989; Mendia and Ibarguchi, 1991; Ducoux et al., 2019) **(Fig. 2G)**. Interpretation of geophysical data shows that low-strength Triassic evaporites and mudstones favored the decoupling between basement and cover and induced, in the latter, the simultaneous formations of cover gliding, mini-basins, expulsion rollovers, and diapirs (Pedrera et al., 2017). Field observations and seismic interpretations evidenced that the Basque-Cantabrian basin is mainly characterized by an overall symmetric shape with brittle deformation on its edges and ductile deformation on its axis (DeFelipe et al., 2017;

Pedrera et al., 2017; Ducoux et al., 2019). The association of an exhumed mantle body, along the Leiza fault, with rift and postrift structural geometries suggests the activation of a major south-dipping ramp-flat-ramp extensional detachment arising during Valanginian to early Cenomanian times (Lagabrielle et al., 2019b).

2.5.3. Internal Metamorphic Zone basins

The central and eastern North Pyrenean Zone is bordered to the south by a narrow east-west-trending stretched zone of metamorphosed and strongly deformed rocks corresponding to the Internal Metamorphic Zone (Casteras, 1933; Mattauer, 1968; Choukroune, 1974), and it is characterized by the presence of numerous sub-continental mantle outcrops (Monchoux, 1970; Choukroune and Mattauer, 1978; Fabriès et al., 1991, 1998; Lagabrielle et al., 2010) **(Fig. 1)**. They result from hyperextension of the continental crust during the Early Cretaceous rifting stage (Lagabrielle and Bodinier, 2008; Lagabrielle et al., 2010; Clerc and Lagabrielle, 2014; Clerc et al., 2014, 2015; de Saint Blanquat et al., 2016; Teixell et al., 2018; Espurt et al., 2019). The same authors have shown that the whole continental crust of the North Pyrenean Zone underwent large-scale boudinage during the Early Cretaceous hyperextension and that the E-W trending rift basins present a relative symmetrical shape (Clerc et al., 2015; Lagabrielle et al., 2019). The existence of a thick prerift salt layer (Rhaetian-Hettangian) yielded to a basinward gliding of the detached prerift Jurassic cover during hyperextension (Lagabrielle et al., 2010; Clerc and Lagabrielle., 2014; Clerc et al., 2015; Duretz et al., 2019).

High-temperature / low-pressure metamorphism has been evidenced all along the North Pyrenean Zone (Ravier, 1957; Albarède and Michard-Vitrac, 1978a, 1978b; Golberg et al., 1988; Golberg and Maluski, 1988; Golberg and Leyreloup, 1990; Clerc et al., 2015). This metamorphism results from the Early Cretaceous continental crust thinning and associated thermal gradient increase (Choukroune and Mattauer, 1978; Vielzeuf and Kornprobst, 1984; Debroas, 1990; Clerc et al., 2015). RSCM peak temperatures show T-max reaching 400–600°C in the marbles of the IMZ, with some the highest temperatures recorded close to exhumed mantle outcrops (Clerc, 2012; Clerc et al., 2015; Boulvais, 2016; Lagabrielle et al., 2016; Chelalou et al., 2016; Ducoux, 2017) **(Fig. 2H)**. These values are consistent with those estimated from mineral assemblages giving Tmax of 550–650°C and pressure of 3–4 kbar (Bernus-Maury, 1984; Golberg and Leyreloup, 1990; Vauchez et al., 2013). Previous authors have established that this metamorphic event was linked to a very high synrift geothermal gradient (Dauteuil and Ricou, 1989; Golberg and Leyreloup, 1990; Clerc et al., 2015; Lagabrielle et al., 2016). Thus, the Jurassic to Early Cretaceous carbonate cover forming the Metamorphic Intern Zone corresponds to prerift to basal synrift sediments located in the deepest part of the basin **(Fig. 2H)**.

The WNW-ESE trending Lourdes and Saint-Gaudens positive Bouguer anomalies are localized beneath the maximum thickness of the Albian synrift turbiditic sequence (Casas et al., 1997). Espurt et al. (2019) interpret the Saint-Gaudens anomaly as an allochthonous mantle unit thrusted northward onto the European margin over the North Pyrenean Frontal Thrust. It corresponds to a allochthonous body of the sub-continental mantle, previously exhumed during Early Cretaceous time.

3. Tectono-sedimentary evolution of a smooth-slope type extensional basin

Through the comparison of all these basins, a lot of common patterns might be identified. They reflect similar processes, synchronous to the opening of the Bay of Biscay:

(1) These basins are characterized by a hyperextended continental crust fitting with the thick synrift depocenter showing an elevated synrift paleothermal gradient or mantle heat flow, responsible for a HT/LP metamorphism.

(2) They often coincide with positive Bouguer anomaly due to the mantle upwelling. Lower crust is very thin, and locally absent beneath the hyper-extended domain.

(3) The basins are affected by a strong partitioning of the extensional deformation between the Mesozoic cover and the upper continental crust due to the presence of a thick prerift salt décollement level. The first stage of

their evolution corresponds to sag geometry basins (stage 1 of rifting).

(4) They all present a relative symmetric shape, and record a basinward gliding of the prerift cover, marked by prerift cover rafts in the basin edges and a stretched but continuous cover on the hyper-extended domain. This event precedes the development of brittle rifting stage 2.

(5) Once cover gliding operated, deformation is no longer decoupled on the basin's edge and extensional detachment faults root at depth in the thinned crust and the top of the mantle. At the surface, they connect to the salt décollement level.

(6) All these basins are characterized by an inherited abnormally thin continental crust before the Late Jurassic to Early Cretaceous hyperextension **(Fig. 3A)**.

(7) In the most mature stage of their evolution, these basins are characterized by depocenters migration in response to progressive development of asymmetric structures controlling their late architecture.

All these basins share at least one common synrift thinning stage and can be classified following their continental crust amount of extension. Hence, these basins can be ranked from least mature to most mature as follows: (1) Tartas, (2) Arzacq, Columbrets and Camèros, (3) Parentis, (4) Basco-cantabric and Mauléon (5) Internal Metamorphic Zone basin of central and eastern Pyrenees **(Fig. 2)**. Three main stages of continental crust thinning can be inferred to describe the evolution of these smooth-slope type extensional basins **(Fig. 3B-D)**.

3.1. Sag basin stage driven by prerift salt: dominant pure shear thinning

First, the sag basin stage is driven by the lateral extrusion of the lower crust which causes a topographic depression at the surface of the upper crust **(Fig. 3B)**. During this stage, distributed ductile thinning of the lower crust induces a homogeneous subsidence partly balanced by the carbonate production. In fact, it results in the development of a relatively smooth sedimentary profile characterized by the deposition of a carbonate platform and marls in a central trough. At that time, the basin is symmetric and marked by edgeward onlap of the synrift deposits **(Fig. 3B)**. The Tartas basin, seems to represent the most immature smooth-slope type extensional basin presented in this review **(Fig. 2)**. Indeed, continental crust thinning did not evolve into brittle tectonic stage as the basin does not span the development of any active fault deformation affecting the upper continental crust. This stage has been described as a ductile pure shear thinning stage (Saspiturry et al., 2019a) since the crust is homogeneously and symmetrically thinned without major brittle deformation in the upper crust. In first stage of continental crust thinning, the upper crust might be affected by minor brittle deformation under the salt décollement level inducing the development of superficial diapirism affecting the prerift to synrift sedimentary cover **(Fig. 3B)**.

3.2. Gravity-driven gliding of the sedimentary cover during a transitional stage: onset of dominant simple shear thinning

As lower crust thinning and subsidence increases in the center of the basin, the extensional syncline geometry grows and pre- to synrift sequences get steeper **(Fig. 3B)**. After a certain amount of tilting, the prerift salt layer plays as décollement surface between the basement and the sedimentary cover. It induces a large-scale basinward cover gliding on a smooth substratum (Lagabrielle et al., 2019b, cf. Annexe. 1) forming a folded allochthonous lid resting on the future hyperextended rift domain **(Fig. 3C)**. In fact, gravity-driven cover gliding is controlled by (1) thickness variation of the sedimentary pile causing differential loading on the salt layer (Lundin, 1992; Liro and Coen, 1995; Rouby et al., 2002) and (2) basinward tilting of the proximal margin (Cobbold and Szatmari, 1991; Demercian et al., 1993; Gaullier et al., 1993; Fort et al., 2004a, 2004b). Due to the gravity gliding of its cover on the salt layer, the substratum of the proximal rift margin is denudated. As the prerift to early synrift sediments glide along the salt décollement, salt is expulsed in the tree dimensions towards the margin and the future hyper-extended rift domain. Thus the basinward cover gliding is responsible for the development of salt roll-over and diapirs affecting the synrift sediments as evidenced in the Columbrets basin (Etheve et al., 2018; **Fig.**

2E), the Mauléon basin (Canérot et al., 2005; **Fig. 2F**), the Arzacq basin (Issautier et al., submitted; **Fig. 2B**), the North Pyrenean Quillan basin (Clerc et al., 2016) and by numerical modeling (Duretz et al., 2019), resulting in the formation of syn-gliding wedge-shaped sedimentary geometries.

The Camèros, Arzacq, Columbrets and Parentis basins have suffered an onset of basinward sedimentary cover gliding **(Fig. 2)**. In fact, these basins become slightly asymmetric as evidenced by the only asymmetry of the basin depocenter. Due to progressive burial and continental crust thinning, the sedimentary cover of the basin center is affected by high-temperature and low-pressure metamorphism, as shown in the Camèros basin (Rat et al., 2019). However, in these basins, simple shear thinning has been aborted in the early stage of continental crust thinning as the mantle is not exhumed to the seafloor.

The seismic profiles in the Columbrets basin evidenced the development of a low-angle detachment fault developing in the continental crust, but the effects of the latter remain limited. The Parentis basin, on the other hand, has suffered a more advanced thinning history with a more pronounced simple shear thinning phase responsible of the hyper-thinning of the continental crust. Hence, this basin is more asymmetric than the Columbrets, Arzacq and Camèros ones. The Parentis basin is characterized by the development of two detachement faults that clearly controlled the local thickness of the synrift sedimentary pile (Jammes et al., 2010c; Tugend et al., 2014).

In the Mauleon basin, the increase of the northward dip of the slope is due to the roll over effect on the Iberian margin linked to the Saint Palais detachment. The resulting cover gliding is immediately followed by the deposition of deep basin gravity deposits reworking mainly the rafts of prerift sedimentary cover and the freshly denudated proximal margin basement (Saspiturry et al., in prep, cf. chapter; 3.2). This process marked the transition between dominant ductile pure shear thinning (sag basin stage, c.f. 3.1.) and simple shear thinning.

3.3. Role of thermicity during hyperextended rifting stage

Once the sedimentary cover of the proximal margins is removed and the lower crust has been laterally extracted, the deformation is coupled at the scale of the entire crust **(Fig. 3D)**. It results in the development of major brittle deformation on the basin edges and the formation of tilted basement blocks devoid of sedimentary cover, while the hyperextended domain undergoes dominant ductile thinning **(Fig. 3D)**. The hyperextend domain of the North Pyrenean basins are well known to suffered high temperature and low pressure metamorphism during hyperextension (Albarède and Michard-Vitrac, 1978a; Montigny et al., 1986; Golberg et al., 1986; Golberg and Maluski, 1988; Thiébaut et al., 1992). The peak temperature reached by the Jurassic to Albian sedimentary cover varies between 500°-600°C, as documented in the Internal Metamorphic Zone basins in the central and eastern Pyrenees (e.g., Bernus-Maury, 1984; Golberg & Leyreloup, 1990; Azambre et al., 1992; Clerc, 2012; Vauchez et al., 2013; Clerc et al., 2015; Chelalou et al., 2016), the Nappes des Marbres in the Basque-Cantabrian basin (Lamare, 1936; Martinez-Torrez, 1989; Mendia & Ibarguchi, 1991; Ducoux, 2017) and to a lesser extent in the Mauléon basin (Saspiturry et al., 2019d, cf. chapter. 5).

The Internal Metamorphic Zone and the Nappes des Marbres have been interpreted as the inverted base of the North Pyrenean hyperextended rift domain (Clerc, 2012; Clerc & Lagabrielle, 2014; Clerc et al., 2015; Lagabrielle et al., 2016; Ducoux, 2017). This metamorphism is the result of continental crust thinning that induces the development of an abnormally high geothermal gradient of around 60°-100°C/km (Vacherat et al., 2014; Corre. 2017; Hart et al., 2017; Saspiturry et al., 2019d, cf. chapter. 5). The maximum temperature reached by the sedimentary cover increases from the margins to the hyperextended domain as both the thermal gradient and the thickness of the sedimentary pile increases basinward (Saspiturry et al., 2019d, cf. chapter. 5). In fact, the basinward gliding of the prerift cover reactivated by a detachment is a major parameter controlling the peak temperature at the base of the hyperextended domain as it significantly contributes to the burial of this

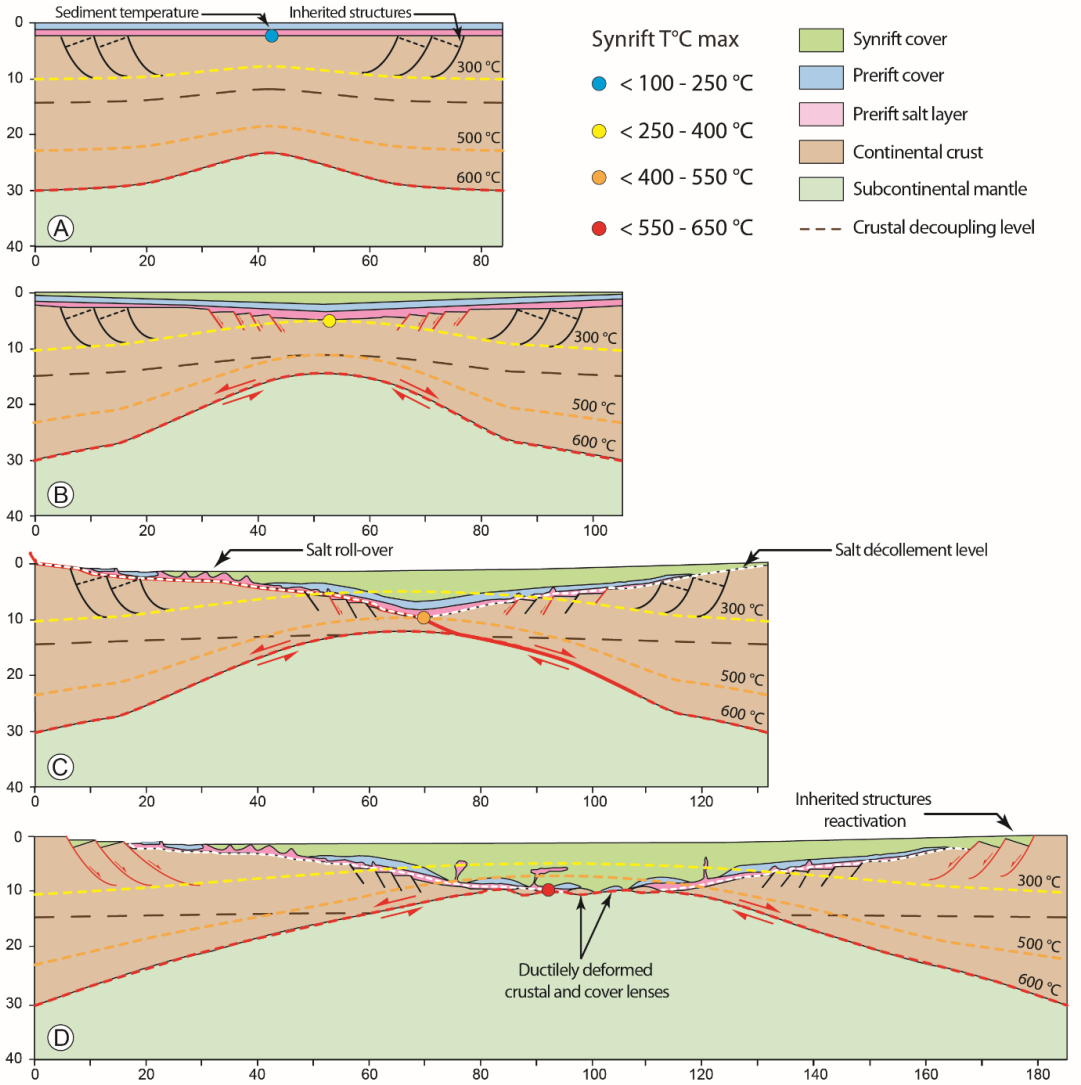


Fig. 3. Conceptual model of the evolutional stages of a smooth-slope type basins, **(A)** Inherited thin lithosphere; **(B)** Sag basin stage, formation of a symmetric basin characterized by a shallow sedimentary profile; **(C)** Transitional stage, basinward gliding of the prerift sedimentary cover along the prerift salt décollement potentially connected to a major detachement leading to an asymmetrical basin shape **(D)** Hyperextension stage, formation of a pseudo-symmetric basin characterized by dominant brittle deformation on the proximal margins and ductile deformation in the basin core.

latter **(Fig. 3D)**. Indeed, during the transitional gliding/detachment stage, 6-8 km thick of prerift to synrift sedimentary cover is stored in the center of the basin. The coupled effect of the thermal anomaly from the rising asthenosphere and the burial due to the thick prerift to synrift sedimentary pile prevents the development of crustal normal faults into the hyperextend domain. It leads, on the contrary, to a dominantly ductile thinning of both Paleozoic basement and glided prerift to very early synrift sedimentary pile on the hyperextended rift domain along a thick ductile shear zone. This process has induced the formation of boudins and lenses of continental crust at a large scale (Clerc and Lagabrielle, 2014; Clerc et al., 2015b; Corre et al., 2016; Asti et al., 2019; Duretz et al., 2019). These basins take then the shape of pseudo-symmetric hyperextended rift basins with margins affected by brittle normal faulting and the basin core dominated by ductile stretching.

4. A comparison between Atlantic-type and smooth slope-type margins

Atlantic-type margins as Iberia-Newfoundland (Boillot et al., 1987, 1989; Driscoll et al., 1995; Manatschal et al., 2001; Péron-Pinvidic et al., 2007; Péron-Pinvidic and Manatschal, 2009; Reston, 2009; Pérez-Gussinyé, 2013; Haupert et al., 2016) or the Alps fossil one (Beltrando et al., 2014; Decarlis et al., 2015; Froitzheim and Manatschal, 1996;

Lemoine et al., 1987; Manatschal et al., 2011, 2006; Manatschal and Nievergelt, 1997; Mohn et al., 2014) are characterized by (i) top-basement detachment faults accommodating crustal extension through tilted blocs of the basement and their prerift cover, (ii) by the individualization of continental extensional allochthons, made up of upper crust and prerift cover, tectonically lying over exhumed lower crust and / or serpentinized mantle, (iii) a wide domain of denudated sub-continental mantle at the ocean-continent transition and (iv) large scale serpentinisation of the exhumed mantle under sea-water temperature conditions **(Fig. 4A)**. Such template is possible because the only main shear zone accommodating the extensional deformation is located at the base of the upper crust and not in a prerift salt layer, which is lacking in the Atlantic margins case. These systems have been numerically modeled to reproduce the paleogeometry of the continental margins and the detachment faults responsible for crustal thinning (Huismans & Beaumont, 2003, 2008, 2011, 2014; Lavier & Manatschal, 2006; Brune et al., 2014, 2016). These studies have also evidenced that continental crust thinning develops under high mantle heat flow conditions due to asthenospheric mantle upwelling. In Atlantic-type margins, the hyperextended domain is characterized by a very thin or absent prerift to synrift sedimentary cover as these margins are starved (Masini et al., 2011, 2012; Péron-Pinvidic et al., 2015; Ribes et al., 2019) **(Fig. 4A)**. Although continental crust thinning occurs under high mantle heat flow (elevated thermal gradient), the continental crust thin under brittle conditions in the hyperextended domain due to the absence of burial of the continental crust under a thick prerift to synrift sedimentary cover **(Fig. 4A)**. Thus, the high thermicity of the system is neither recorded in the sedimentary system.

Contrary to Atlantic-type margins, paleogeographic reconstructions (Ziegler, 1982; Dercourt et al., 1986; Ortí et al., 2017; Soto et al., 2017), show that the distribution of Late Triassic evaporites and clays remarkably matches the distribution of the Pyrenean and peri-Pyrenean smooth-slope type extensional basins (cf. Annexe. 1). Numerical modeling shows that Triassic décollement level played a major role at the onset of continental rifting in the Pyrenean realm, as the deformation is decoupled between the Paleozoic basement and the Jurassic to Albian sedimentary cover (Duretz et al., 2019). This decoupled deformation induces the development of a symmetric synrift sag basin whose subsidence result from lower crust ductile thinning **(Fig. 4B)**. This geometry differs strongly from Atlantic-type margins that are characterized by the development, at the onset of the stretching phase, of symmetric rift whose continental crust is affected by pure shear thinning with distributed brittle deformation, resulting in the formation of tilted blocks in the upper crust (Whitmarsh et al., 2001; Manatschal, 2004; Lavier and Manatschal, 2006). Moreover, in smooth-slope type basins, the lower crust is not exhumed during the final hyperextension stage, contrarily to Atlantic type margins, as it has been laterally extracted in first rifting stage (sag basin). In fact, the only lower crust outcropping along the Cretaceous North Pyrenean Rift axis is quite old as it has already been exhumed during Permian time (de Saint-Blanquat, 1993; Olivier et al., 2004; Cochelin et al., 2018; Saspiturry et al., 2019b). Once the sedimentary cover is removed from smooth-slope type proximal margins and the lower crust has been laterally extracted (sag phase), the deformation becomes coupled at the scale of the entire crust and crustal detachments can then develop. Thus, coupled extensional deformation takes place later in the evolution of smooth slope-type systems than in Atlantic-type ones. Contrary to Atlantic-type margins, the hyperextended domain of the smooth slope basins deforms under ductile conditions and abnormal high thermicity due to (1) prerift salt décollement triggering mechanical decoupling and gliding of the prerift cover, (2) cover remaining preserved in the center of the basin while the lower crust is ductilely extracted and (3) burial of the continental crust over a thick prerift to synrift sedimentary cover. However, as in Atlantic-type margins, the proximal margins are finally affected by extensional brittle faulting as the crust presents a normal thermal gradient of ~30°C/km (cf. chapter. 5) and a thin or absent sedimentary cover **(Fig. 4B)**. Thus, along smooth slope type margins, the proximal margins undergo brittle deformation while the hyperextended domain suffered dominant ductile thinning due to a complex competition between salt, burial and synrift thermal gradient.

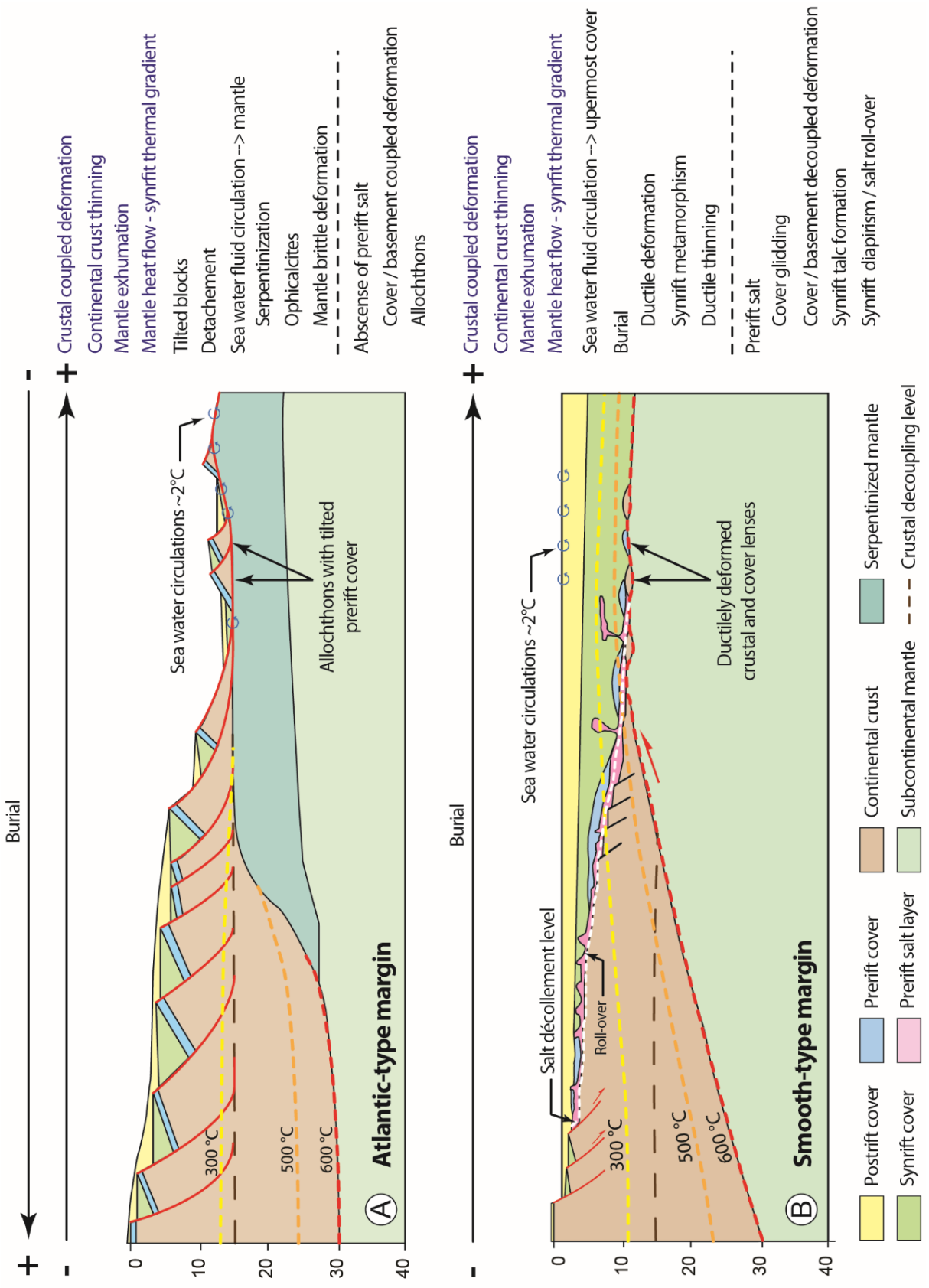


Fig. 4. (A) Atlantic-type margin geometry and characteristics (section modified from Péron-Pinvidic et al., 2015); **(B)** Smooth-slope type margin geometry and characteristics.

5. Conclusion

Three main stages of continental crust thinning can be inferred to describe the smooth-slope type basins evolution of the Iberian-Eurasian plates. During the first sag basin stage, continental crust thinning is dominantly controlled by pure shear mechanism and homogeneous ductile thinning of the lower crust due to the presence of two decoupling levels. Firstly, the middle crust allows to decouple the deformation between the upper and lower crust which is laterally extruding. Secondly, prerift Triassic salt décollement decouples deformation between the upper crust and the sedimentary cover. This thinning stage is responsible for the formation of a salt-controlled symmetric sag basin characterized by a smooth sedimentary slope. As crustal thinning continues, differential subsidence induces the basinward gliding of the sedimentary cover. This transitional stage marks the shift to a dominated simple shear regime responsible for the development of an asymmetric rift system. Once the sedimentary cover of the proximal margins is removed and the lower crust has been laterally extracted, the deformation is coupled at the scale of the entire crust and crustal detachment can occur. The proximal margins undergo brittle deformation while the hyperextended domain sufferes dominant ductile thinning. This discrepancy of the extensional deformation style is directly linked to the basinward increase of both thermal gradient and sedimentary thickness. In such a way, pre- and synrift sedimentation clearly controls the deformation style of smooth-slope type extensional basins, that primarily need a thick prerift salt level accommodating the extensional deformation and then allowing the storage of a thick prerift to synrift sedimentary pile in the internal part of the extensional system.

Acknowledgements

This work is part of Saspiturry's Ph.D. research conducted as part of the OROGEN project, cofunded by Total S.A., BRGM, and Institut national de sciences de l'Univers (INSU). We thank OROGEN project managers Sylvain Calassou (Total), Emmanuel Masini (Total), Olivier Vidal (Centre National de Recherche Scientifique) and Isabelle Thinon (BRGM).

References

Albarède, F., Michard-Vitrac, A., 1978. Datation du metamorphisme des terrains secondaires des Pyrenees par les methodes 39 Ar-40 Ar et 87 Rb-87 Sr; ses relations avec les peridotites associees. Bull. Société Géologique Fr. 7, 681–687.

Albarède, Francis, Michard-Vitrac, A., 1978. Age and Significance of the North Pyrenean Metamorphism. Earth Planet. Sci. Lett. 327–332.

Alhamawi, M., 1992. Sédimentologie, pétrographie sédimentaire et diagenèse des calcaires Crétacé supérieur de la marge ibérique, Vallées d'Ossau - Vallée d'Aspe, Haute Chaîne, Pyrénées Atlantiques. Université Bordeaux 1.

Alonso, A., Mas, J.R., 1993. Control tectónico e influencia del eustatismo en la sedimentación del Cretácico inferior de la cuenca de Los Cameros.

Alvaro, M., del Villar, R.C., Vegas, R., 1979. Un modelo de evolución geotectónica para la Cadena Celtibérica. Acta Geológica Hispánica 14, 172–177.

Angrand, P., Ford, M., Watts, A.B., 2018. Lateral Variations in Foreland Flexure of a Rifted Continental Margin: The Aquitaine Basin (SW France): Flexure of the Aquitaine Foreland Basin. Tectonics 37, 430–449. https://doi.org/10.1002/2017TC004670

Arche, A., López-Gómez, J., 1996. Origin of the Permian-Triassic Iberian Basin, central-eastern Spain. Tectonophysics 266, 443–464. https://doi.org/10.1016/S0040-1951(96)00202-8

Arnaud-Vanneau, A., Arnaud, H., Charollais, J., Conrad, M.-A., Cotillon, P., Ferry, S., Masse, J.-P., Peybernès, B., 1979. Paléogéographie des calcaires urgoniens du sud de la France. Géobios 3, 363–383.

Aslanian, D., Moulin, M., 2013. Palaeogeographic consequences of conservational models in the South Atlantic Ocean. Geol. Soc. Lond. Spec. Publ. 369, 75–90. https://doi.org/10.1144/SP369.5

Aslanian, D., Moulin, M., Olivet, J.-L., Unternehr, P., Matias, L., Bache, F., Rabineau, M., Nouzé, H., Klingelheofer, F., Contrucci, I., Labails, C., 2009. Brazilian and African passive margins of the Central Segment of the South Atlantic Ocean: Kinematic constraints. Tectonophysics 468, 98–112. https://doi.org/10.1016/j.tecto.2008.12.016

Asti, R., Lagabrielle, Y., Fourcade, S., Corre, B., Monié, P., 2019. How Do Continents Deform During Mantle Exhumation? Insights From the Northern Iberia Inverted Paleopassive Margin, Western Pyrenees (France). Tectonics 2018TC005428. https://doi.org/10.1029/2018TC005428

Aurell, M., Meléndez, A., 1993. Sedimentary evolution and sequence stratigraphy of the Upper Jurassic in the central Iberian Chain, northeast Spain. Spec. Publ. Int. Ass. Sediment.

Aurell, M., Robles, S., Bádenas, B., Rosales, I., Quesada, S., Meléndez, G., García-Ramos, J.., 2003. Transgressive–regressive cycles and Jurassic palaeogeography of northeast Iberia. Sediment. Geol.

162, 239–271. https://doi.org/10.1016/S0037-0738(03)00154-4

Ayala, C., Pous, J., Torné, M., 1996. The lithosphere-asthenosphere boundary of the Valencia Trough (western Mediterranean) deduced from 2D Geoid and Gravity Modelling. Geophys. Res. Lett. 23, 3131–3134. https://doi.org/10.1029/96GL03005

Ayala, C., Torne, M., Pous, J., 2003. The lithosphere–asthenosphere boundary in the western Mediterranean from 3D joint gravity and geoid modeling: tectonic implications. Earth Planet. Sci. Lett. 209, 275–290. https://doi.org/10.1016/S0012-821X(03)00093-1

Ayala, C., Torne, M., Roca, R., 2015. A review of the current knowledge of the crustal and lithospheric structure of the Valencia Trough Basin. Bol. Geológico Min. 126, 533–552.

Azambre, B., Rossy, M., 1976. Le magmatisme alcalin d'age cretace, dans les Pyrenees occidentales et l'Arc basque; ses relations avec le metamorphisme et la tectonique. Bull. Société Géologique Fr. 7, 1725–1728.

Banda, E., Santanach, P., 1992. The Valencia trough (western Mediterranean): An overview. Tectonophysics 208, 183–202. https://doi.org/10.1016/0040-1951(92)90344-6

Barbier, F., Duvergé, J., Le Pichon, X., 1986. Structure profonde de la marge Nord Gascogne. Implications sur le mécanisme de rifting et de formation de la marge continentale. Bull Cent Rech Explor Prod Elf Aquitaine 10, 105–121.

Beltrando, M., Manatschal, G., Mohn, G., Dal Piaz, G.V., Brovarone, A.V., Masini, E., 2014. Recognizing remnants of magma-poor rifted margins in high-pressure orogenic belts: The Alpine case study. Earth-Sci. Rev. 131, 88–115.

Bernus-Maury, C., 1984. Etude des paragéneses caractéristiques du métamorphisme mésozoïque dans la partie orientale des Pyrénées. Pierre et Marie Curie, Paris.

Biteau, J., Canérot, J., 2007. La Chaine des Pyrenees et ses avant-pays d'Aquitaine et de l'Ebre: caracteristiques structurales, evolution geodynamique et tectono-sedimentaire. Geol.-PARIS- 155, 16.

Biteau, J.-J., Le Marrec, A., Le Vot, M., Masset, J.-M., 2006. The Aquitaine Basin. Pet. Geosci. 12, 247–273.

Bixel, F., 1984. Le volcanisme stéphano-permien des Pyrénées. Université Paul Sabatier de Toulouse (Sciences).

Bixel, F., Lucas, C., 1987. Approche Géodynamique du Permien et du Trias des Pyrénées dans le cadre du sud-ouest européen. Cuad. Geol. Ibérica 11, 57–81.

Bixel, F., Lucas, C.L., 1983. Magmatisme, tectonique et sédimentation dans les fossés stéphano-permiens des Pyrénées occidentales. Rev. Géologie Dyn. Géographie Phys. 24, 329–342.

Boillot, G., Beslier, M.O., Krawczyk, C.M., Rappin, D., Reston, T.J., 1995. The formation of passive margins: constraints from the crustal structure and segmentation of the deep Galicia margin, Spain. Geol. Soc. Lond. Spec. Publ. 90, 71–91.

Boillot, G., Capdevilla, R., Hennequin-Marchand, I., Lamboy, M., Lepretre, J.P., 1973. La zone nord-pyrénéenne, ses prolongements sur la marge continentale nord-espagnole et sa signification structurale. Comptes Rendus Acad. Sci. Paris 227, 2629–2632.

Boillot, G., Féraud, G., Recq, M., Girardeau, J., 1989. Undercrusting by serpentinite beneath rifted margins: the example of the west Galicia margin (Spain). Nature 341, 523–525.

Boillot, G., Grimaud, S., Mauffret, A., Mougenot, D., Kornprobst, J., Mergoil-Daniel, J., Torrent, G., 1980. Ocean-continent boundary of the Iberian margin: a serpentinite diapir west of the Galicia Bank. Earth Planet. Sci. Lett. 48, 23–34.

Boillot, G., Recq, M., Winterer, E.L., Meyer, A.W., Applegate, J., Baltuck, M., Bergen, J.A., Comas, M.C., Davies, T.A., Dunham, K., others, 1987. Tectonic denudation of the upper mantle along passive margins: a model based on drilling results (ODP leg 103, western Galicia margin, Spain). Tectonophysics 132, 335–342.

Boirie, J.-M., 1981. Etude Sédimentologique des Poudingues de Mendibelza (Pyrénées Atlantiques). Université Paul Sabatier de Toulouse (Sciences), Toulouse.

Boirie, J.-M., Souquet, P., 1982. Les poudingues de Mendibelza: dépôts de cônes sous-marins du rift albien des Pyrénées. Bull. Cent. Rech. Explor.-Prod. Elf-Aquitaine 6, 405–435.

Bois, C., 1992. The evolution of the layered lower crust and the Moho through geological time in Western Europe: contribution of deep seismic reflection profiles. Terra Nova 4, 99–108.

Bois, C., Courtillot, V., 1988. Deep Seismic Profiling of the Crust and Evolution of the Lithosphere 69, 987–988.

Bois, C., ECORS Scientific team, 1990. Major geodynamic processes studied from the ECORS deep seismic profiles in France and adjacent areas. Tectonophysics 173, 397–410.

Bois, C., Gabriel, O., Lefort, J.-P., Rolet, J., Brunet, M.-F., Masse, P., Olivet, J.-L., 1997. Geologic contribution of the Bay of Biscay deep seismic survey: a summary of the main scientific results, a discussion of the open questions and suggestions for further investigation. Mém Soc Géol Fr. 193–309.

Bois, C., Gariel, O., 1994. Deep Seismic Investigation in the Parentis Basin (Southwestern France), in: Mascle, A. (Ed.), Hydrocarbon and Petroleum Geology of France. Springer Berlin Heidelberg, Berlin, Heidelberg, pp. 173–186. https://doi.org/10.1007/978-3-642-78849-9_13

Boulvais, P., 2016. Fluid generation in the Boucheville Basin as a consequence of the North Pyrenean metamorphism. Comptes Rendus Geosci. 348, 301–311. https://doi.org/10.1016/j.crte.2015.06.013

Bouroullec, J., Delfaud, J., Deloffre, R., 1979. Organisations sédimentaire et paléocologique de l'Aptien supérieur a faciès urgonien dans les Pyrénées occidentales et l'Aquitaine méridionale. Geobios 12, 25–43.

Bouroullec, J., Deloffre, R., 1970. Interprétation sédimentologique et paléogéographique par microfaciès du Crétacé inférieur basal d'Aquitaine Sud-Ouest. Bull. Cent. Rech. Pau-SNPA 4, 381–429.

Bourrouilh, R., Richert, J.-P., Zolnaï, G., 1995. The North Pyrenean Aquitaine Basin, France: Evolution and Hydrocarbons. AAPG Bull. 79, 831–853.

BRGM, Elf, Esso, & SNPA, 1974. Géologie du Bassin d'aquitaine. BRGM Editions, Paris.

Brune, S., Heine, C., Pérez-Gussinyé, M., Sobolev, S.V., 2014. Rift migration explains continental margin asymmetry and crustal hyper-extension. Nat. Commun. 5. https://doi.org/10.1038/ncomms5014

Brune, S., Williams, S.E., Butterworth, N.P., Müller, R.D., 2016. Abrupt plate accelerations shape rifted continental margins. Nature 536, 201–204. https://doi.org/10.1038/nature18319

Brunet, M.-F., 1991. Subsidence et géodynamique du Bassin d'Aquitaine. Relations avec l'ouverture de l'Atlantique.

Brun, J. P., Beslier M.O., 1996. Mantle exhumation at passive margin, Earth Planet. Sci. Lett., 142, 161– 173.

Burg, J.-P., Van Den Driessche, J., Brun, J.-P., 1994. Syn- to post-thickening extension : mode and consequences. Comptes Rendus Académie Sci. Sér. 2 Sci. Terre Planètes 319, 1019–1032.

Canérot, J., 2008. Les Pyrénées: Histoire géologique. Atlantica.

Canérot, J., 1989. Rifting éocrétacé et halocinèse sur la marge ibérique des Pyrénées Occidentales (France). Conséquences structurales. Bull. Cent. Rech. Explor.-Prod. Elf-Aquitaine 13, 87–99.

Canérot, J., 1988. Manifestations de l'halocinèse dans les chaînons béarnais (zone Nord-Pyrénéenne) au Crétacé inférieur. Comptes Rendus Académie Sci. Sér. 2 Mécanique Phys. Chim. Sci. Univers Sci. Terre 306, 1099–1102.

Canérot, J., Hudec, M.R., Rockenbauch, K., 2005. Mesozoic diapirism in the Pyrenean orogen: Salt tectonics on a transform plate boundary. AAPG Bull. 89, 211–229. https://doi.org/10.1306/09170404007

Canérot, J., Lenoble, J.-L., 1993. Diapirisme crétacé sur la marge ibérique des Pyrénées occidentales; exemple du pic de Lauriolle; comparaisons avec l'Aquitaine, les Pyrénées centrales et orientales. Bull. Société Géologique Fr. 164, 719–726.

Canérot, J., Majesté-Menjoulas, C., Ternet, Y., 1999. Le cadre stratigraphique et géodynamique des altérites et des bauxites sur la marge ibérique des Pyrénées occidentales (France). Comptes Rendus Académie Sci.-Ser. IIA-Earth Planet. Sci. 328, 451–456.

Carballo, A., Fernandez, M., Torne, M., Jiménez-Munt, I., Villaseñor, A., 2015. Thermal and petrophysical characterization of the lithospheric mantle along the northeastern Iberia geo-transect. Gondwana Res. 27, 1430–1445. https://doi.org/10.1016/j.gr.2013.12.012

Casas, A., Kearey, P., Rivero, L., Adam, C.R., 1997. Gravity anomaly map of the Pyrenean region and a comparison of the deep geological structure of the western and eastern Pyrenees. Earth Planet. Sci. Lett. 150, 65–78.

Casas, A.M., Cortés, A.L., Maestro, A., 2000. Intra-plate deformation and basin formation during the Tertiary at the Northern Iberian Plate: origin and evolution of the Almazán Basin. Tectonics 19, 258–289.

Casas, A.M., Villalaín, J.J., Soto, R., Gil-Imaz, A., del Río, P., Fernández, G., 2009. Multidisciplinary approach to an extensional syncline model for the Mesozoic Cameros Basin (N Spain). Tectonophysics 470, 3–20. https://doi.org/10.1016/j.tecto.2008.04.020

Casas Sainz, A.M., 1993. Oblique tectonic inversion and basement thrusting in the Cameros Massif (Northern Spain). Geodin. Acta 6, 202–216. https://doi.org/10.1080/09853111.1993.11105248

Casas-Sainz, A.M., Gil-Imaz, A., 1998. Extensional subsidence, contractional folding and thrust inversion of the eastern Cameros basin, northern Spain. Geol. Rundsch. 86, 802–818. https://doi.org/10.1007/s005310050178

Casas-Sainz, A.M., Simón-Gómez, J., 1992. Stress field and thrust kinematics: a model for the tectonic inversion of the cameros massif (Spain). J. Struct. Geol. 14, 521–530. https://doi.org/10.1016/0191-8141(92)90154-O

Casquet, C., Galindo, C., González-Casado, J.M., Alonso, A., Mas, R., Rodas, M., García, E., Barrenechea, J.F., 1992. El metamorfismo en la cuenca de los Cameros; geocronologia e implicaciones tectonicas. Geogaceta 11, 22–25.

Castañares, L.M., Robles, S., 2004. El vulcanismo del Albiense-Santoniense en la Cuenca Vasco-Cantábrica. Geol. Esp.

Castañares, L.M., Robles, S., Vicente Bravo, J.C., 1997. Distribución estratigráfica de los episodios volcánicos submarinos del Albiense-Santoniense en la Cuenca Vasca (sector Gernika-Plentzia, Bizkaia).

Casteras, M., 1971. Carte géologique de la France à 1/50 000: feuille de Tardets–Sorholus, Orléans, France.

Casteras, M., 1933. Recherches sur la structure du versant nord des Pyrénées centrales et orientales. Libraire Polytechnique, C. Béranger.

Chelalou, R., Nalpas, T., Bousquet, R., Prevost, M., Lahfid, A., Poujol, M., Ringenbach, J.-C., Ballard, J.-F., 2016. New sedimentological, structural and paleo-thermicity data in the Boucheville Basin (eastern North Pyrenean Zone, France). Comptes Rendus Géoscience 348, 312–321.

Choukroune, P., 1974. Structure et évolution tectonique de la zone nord-pyrénéenne: analyse de la déformation dans une portion de chaîne à schistosité sub-verticale.

Choukroune, P., ECORS Team, 1989. The ECORS Pyrenean deep seismic profile reflection data and the overall structure of an orogenic belt. Tectonics 8, 23–39.

Choukroune, P., Mattauer, M., 1978. Tectonique des plaques et Pyrenees; sur le fonctionnement de la faille transformante nord-pyreneenne; comparaisons avec des

modeles actuels. Bull. Société Géologique Fr. 7, 689–700.

Clerc, C., 2012. Evolution du domaine nord-pyrénéen au Crétacé: amincissement crustal extrême et thermicite élevée: un analogue pour les marges passives. Paris 6.

Clerc, C., Boulvais, P., Lagabrielle, Y., de Saint Blanquat, M., 2014. Ophicalcites from the northern Pyrenean belt: a field, petrographic and stable isotope study. Int. J. Earth Sci. 103, 141–163. https://doi.org/10.1007/s00531-013-0927-z

Clerc, C., Jolivet, L., Ringenbach, J.-C., 2015a. Ductile extensional shear zones in the lower crust of a passive margin. Earth Planet. Sci. Lett. 431, 1–7. https://doi.org/10.1016/j.epsl.2015.08.038

Clerc, C., Lagabrielle, Y., 2014. Thermal control on the modes of crustal thinning leading to mantle exhumation: Insights from the Cretaceous Pyrenean hot paleomargins. Tectonics 33, 1340–1359. https://doi.org/10.1002/2013TC003471

Clerc, C., Lagabrielle, Y., Labaume, P., Ringenbach, J.-C., Vauchez, A., Nalpas, T., Bousquet, R., Ballard, J.-F., Lahfid, A., Fourcade, S., 2016. Basement – Cover decoupling and progressive exhumation of metamorphic sediments at hot rifted margin. Insights from the Northeastern Pyrenean analog. Tectonophysics 686, 82–97. https://doi.org/10.1016/j.tecto.2016.07.022

Clerc, C., Lahfid, A., Monié, P., Lagabrielle, Y., Chopin, C., Poujol, M., Boulvais, P., Ringenbach, J.C., Masini, E., de St Blanquat, M., 2015b. High-temperature metamorphism during extreme thinning of the continental crust: a reappraisal of the North Pyrenean passive paleomargin. Solid Earth 6, 643–668.

Cobbold, P.R., Szatmari, P., 1991. Radial gravitational gliding on passive margins. Tectonophysics 188, 249–289.

Cochelin, B., 2016. Champ de déformation du socle paléozoïque des Pyrénées. Géosciences Environnement Toulouse (GET).

Cochelin, B., Chardon, D., Denèle, Y., Gumiaux, C., Le Bayon, B., 2017. Vertical strain partitioning in hot Variscan crust: Syn-convergence escape of the Pyrenees in the Iberian-Armorican syntax. Bull. Société Géologique Fr. 188, 39.

Combes, P.-J., Peybernès, B., Leyreloup, A.F., 1998. Altérites et bauxites, témoins des marges européenne et ibérique des Pyrénées occidentales au Jurassique supérieur—Crétacé inférieur, à l'ouest de la vallée d'Ossau (Pyrénées-Atlantiques, France). Comptes Rendus Académie Sci.-Ser. IIA-Earth Planet. Sci. 327, 271–278.

Contrucci, I., Matias, L., Moulin, M., Géli, L., Klingelhofer, F., Nouzé, H., Aslanian, D., Olivet, J.-L., Réhault, J.-P., Sibuet, J.-C., 2004. Deep structure of the West African continental margin (Congo, Zaïre, Angola), between 5 S and 8 S, from reflection/refraction seismics and gravity data. Geophys. J. Int. 158, 529–553.

Corre, B., 2017. La bordure nord de la plaque ibérique à l'Albo-Cénomanien: architecture d'une marge passive de type ductile (Chaînons Béarnais, Pyrénées Occidentales) (PhD Thesis). Rennes 1.

Corre, B., Lagabrielle, Y., Labaume, P., Fourcade, S., Clerc, C., Ballèvre, M., 2016. Deformation associated with mantle exhumation in a distal, hot passive margin environment: New constraints from the Saraillé Massif (Chaînons Béarnais, North-Pyrenean Zone). Comptes Rendus Geosci. 348, 279–289. https://doi.org/10.1016/j.crte.2015.11.007

Cuevas, J., Tubia, J.M., 1999. The discovery of scapolite marbles in the Biscay Synclinorium (Basque-Cantabrian basin, Western Pyrenees): geodynamic implications. Terra Nova 11, 259–265. https://doi.org/10.1046/j.1365-3121.1999.00255.x

Curnelle, R., 1983. Evolution structuro-sédimentaire du Trias et de l'Infra-Lias d'Aquitaine. Bull Cent Rech Explor Prod Elf-Aquitaine 7, 69–99.

Curnelle, R., Dubois, P., 1986. Evolution mesozoique des grands bassins sedimentaires francais; bassins de Paris, d'Aquitaine et du Sud-Est. Bull. Soc. Geol. Fr. II, 529–546. https://doi.org/10.2113/gssgfbull.II.4.529

Curnelle, R., Dubois, P., Seguin, J.C., Whitaker, D., Matthews, D.H., Roberts, D.G., Kent, P., Laughton, A.S., Kholief, M.M., 1982. The Mesozoic-Tertiary Evolution of the Aquitaine Basin [and Discussion]. Philos. Trans. R. Soc. Math. Phys. Eng. Sci. 305, 63–84. https://doi.org/10.1098/rsta.1982.0026

Daignières, M., Séguret, M., Specht, M., Team, E., 1994. The Arzacq-western Pyrenees ECORS deep seismic profile, in: Hydrocarbon and Petroleum Geology of France. Springer, pp. 199–208.

Dañobeitia, J.J., Arguedas, M., Gallart, J., Banda, E., Makris, J., 1992. Deep crustal configuration of the Valencia trough and its Iberian and Balearic borders from extensive refraction and wide-angle reflection seismic profiling. Tectonophysics 203, 37–55.

Dardel, R.A., Rosset, R., 1971. Histoire géologique et structurale du bassin de Parentis et de son prolongement en mer. Hist. Struct. Golfe Gasc. 2.

Dauteuil, O., Ricou, L.-E., 1989. Une circulation de fluides de haute-température à l'origine du métamorphisme crétacé nord-pyrénéen. Geodin. Acta 3, 237–249. https://doi.org/10.1080/09853111.1989.11105190

de Saint Blanquat, M., 1993. La faille normale ductile du massif du Saint Barthélémy. Evolution hercynienne des massifs nord-pyrénéens catazonaux considérée du point de vue de leur histoire thermique. Geodin. Acta 6, 59–77.

de Saint Blanquat, M., Bajolet, F., Grand'Homme, A., Proietti, A., Zanti, M., Boutin, A., Clerc, C., Lagabrielle, Y., Labaume, P., 2016. Cretaceous mantle exhumation in the central Pyrenees: New constraints from the peridotites in eastern Ariège (North Pyrenean zone, France). Comptes Rendus Geosci. 348, 268–278. https://doi.org/10.1016/j.crte.2015.12.003

Debroas, E.J., 1990. Le flysch noir albo-cenomanien temoin de la structuration albienne a senonienne de la Zone nord-pyreneenne en Bigorre (Hautes-Pyrenees, France). Bull. Soc. Geol. Fr. VI, 273–285. https://doi.org/10.2113/gssgfbull.VI.2.273

Debroas, E.J., Canérot, J., Bilotte, M., 2010. Les brèches d'Urdach, témoins de l'exhumation du manteau pyrénéen

dans un escarpement de faille vraconnien-cénomanien inférieur (Zone nord-pyrénéenne, Pyrénées-Atlantiques, France). Géologie Fr. 2, 53–63.

Decarlis, A., Manatschal, G., Haupert, I., Masini, E., 2015. The tectono-stratigraphic evolution of distal, hyper-extended magma-poor conjugate rifted margins: Examples from the Alpine Tethys and Newfoundland–Iberia. Mar. Pet. Geol. 68, 54–72. https://doi.org/10.1016/j.marpetgeo.2015.08.005

DeFelipe, I., Pedreira, D., Pulgar, J.A., Iriarte, E., Mendia, M., 2017. Mantle exhumation and metamorphism in the Basque-Cantabrian Basin (NSpain): Stable and clumped isotope analysis in carbonates and comparison with ophicalcites in the North-Pyrenean Zone (Urdach and Lherz). Geochem. Geophys. Geosystems 18, 631–652. https://doi.org/10.1002/2016GC006690

Del Río, P., Barbero, L., Mata, P., Fanning, C.M., 2009. Timing of diagenesis and very low-grade metamorphism in the eastern sector of the Sierra de Cameros (Iberian Range, Spain): a U-Pb SHRIMP study on monazite: U-Pb dating of diagenetic and low-grade monazite from the Iberian Range (Spain). Terra Nova 21, 438–445. https://doi.org/10.1111/j.1365-3121.2009.00900.x

Delfaud, J., 1969. Essai sur la géologie dynamique du domaine aquitano-pyrénéen durant le Jurassique et le Crétacé inférieur. Université de Bordeaux.

Delfaud, J., Gautier, J., 1967. Evolution des milieux de dépôts au passage Jurassique–Crétacé du forage de Lacq 104 (Aquitaine, France, Sud-Ouest). Bull. Cent. Rech. Pau-SNPA 1, 77–89.

Delfaud, J., Henry, J., 1967. Evolution des bassins jurassiques dans la zone nord-pyrénéenne occidentale. 64ème Congrès AFAS Bordx. 75–80.

Delfaud, J., Villanova, M., 1967. Evolution des bassins pendant le Crétacé inférieur dans les Pyrénees occidentales et la bordure de l'Aquitaine. 64ème Congrès AFAS Bordx. 87–92.

Demercian, S., Szatmari, P., Cobbold, P.R., 1993. Style and pattern of salt diapirs due to thin-skinned gravitational gliding, Campos and Santos basins, offshore Brazil. Tectonophysics 228, 393–433.

Dercourt, J., Zonenshain, L.P., Ricou, L.-E., Kazmin, V.G., Le Pichon, X., Knipper, A.L., Grandjacquet, C., Sbortshikov, I.M., Geyssant, J., Lepvrier, C., Pechersky, D.H., Boulin, J., Sibuet, J.-C., Savostin, L.A., Sorokhtin, O., Westphal, M., Bazhenov, M.L., Lauer, J.P., Biju-Duval, B., 1986. Geological evolution of the tethys belt from the atlantic to the pamirs since the LIAS. Tectonophysics 123, 241–315. https://doi.org/10.1016/0040-1951(86)90199-X

Deseglaux, P., Brunet, M.-F., 1990. Tectonic subsidence of the Aquitaine basin since Cretaceous times. Bull. Société Géologique Fr. 8, 295–306.

Driscoll, N.W., Hogg, J.R., Christie-Blick, N., Karner, G.D., 1995. Extensional tectonics in the Jeanne d'Arc Basin, offshore Newfoundland: implications for the timing of break-up between Grand Banks and Iberia. Geol. Soc. Lond. Spec. Publ. 90, 1–28. https://doi.org/10.1144/GSL.SP.1995.090.01.01

Ducoux, M., 2017. Structure, thermicité et évolution géodynamique de la Zone Interne Métamorphique des Pyrénées. Institut des Sciences de la Terre d'Orléans (ISTO).

Ducoux, M., Jolivet, L., Callot, J. -P., Aubourg, C., Masini, E., Lahfid, A., Homonnay, E., Cagnard, F., Gumiaux, C., Baudin, T., 2019. The Nappe des Marbres unit of the Basque-Cantabrian Basin: the tectono-thermal evolution of a fossil hyperextended rift basin. Tectonics 2018TC005348. https://doi.org/10.1029/2018TC005348

Duée, G., Lagabrielle, Y., Coutelle, A., Fortané, A., 1984. Les lherzolites associées aux Chaînons Béarnais (Pyrénées Occidentales): Mise à l'affleurement anté-dogger et resédimentation albo-cénomanienne. Comptes-Rendus Séances Académie Sci. Sér. 2 Mécanique-Phys. Chim. Sci. Univers Sci. Terre 299, 1205–1210.

Duretz, T., Asti, R., Lagabrielle, Y., Brun, J., Jourdon, A., Clerc, C., Corre, B., 2019. Numerical modelling of Cretaceous Pyrenean Rifting: The interaction between mantle exhumation and syn-rift salt tectonics. Basin Res. bre.12389. https://doi.org/10.1111/bre.12389

Espurt, N., Angrand, P., Teixell, A., Labaume, P., Ford, M., de Saint Blanquat, M., Chevrot, S., 2019. Crustal-scale balanced cross-section and restorations of the Central Pyrenean belt (Nestes-Cinca transect): Highlighting the structural control of Variscan belt and Permian-Mesozoic rift systems on mountain building. Tectonophysics 764, 25–45.

Etheve, N., 2016. Le bassin de Valence à la frontière des domaines ibérique et méditerranéen: Evolution tectonique et sédimentaire du Mésozoïque au Cénozoïque. Université de Cergy Pontoise.

Etheve, N., Mohn, G., Frizon de Lamotte, D., Roca, E., Tugend, J., Gómez-Romeu, J., 2018. Extreme Mesozoic Crustal Thinning in the Eastern Iberia Margin: The Example of the Columbrets Basin (Valencia Trough). Tectonics 37, 636–662.

Fabriès, J., Lorand, J.-P., Bodinier, J.-L., 1998. Petrogenetic evolution of orogenic lherzolite massifs in the central and western Pyrenees. Tectonophysics 292, 145–167.

Fabriès, J., Lorand, J.-P., Bodinier, J.-L., Dupuy, C., 1991. Evolution of the Upper Mantle beneath the Pyrenees: Evidence from Orogenic Spinel Lherzolite Massifs. J. Petrol. Special_Volume, 55–76. https://doi.org/10.1093/petrology/Special_Volume.2.55

Fernandez, M., Foucher, J.P., Jurado, M.J., 1995. Evidence for the multi-stage formation of the south-western Valencia Trough. Mar. Pet. Geol. 12, 101–109. https://doi.org/10.1016/0264-8172(95)90390-6

Ferrer, O., Jackson, M.P.A., Roca, E., Rubinat, M., 2012. Evolution of salt structures during extension and inversion of the Offshore Parentis Basin (Eastern Bay of Biscay). Geol. Soc. Lond. Spec. Publ. 363, 361–380. https://doi.org/10.1144/SP363.16

Ferrer, O., Roca, E., Benjumea, B., Muñoz, J.A., Ellouz, N., MARCONI Team, 2008. The deep seismic reflection MARCONI-3 profile: Role of extensional Mesozoic structure during the Pyrenean contractional deformation at the eastern part of the Bay of Biscay. Mar. Pet. Geol.

25, 714–730. https://doi.org/10.1016/j.marpetgeo.2008.06.002

Ferrer, O., Roca, E., Jackson, M.P.A., Muñoz, J.A., 2009. Effects of Pyrenean contraction on salt structures of the offshore Parentis Basin (Bay of Biscay). Trab. Geol. 29.

Fixari, G., 1984. Stratigraphie, faciès et dynamique tecto-sédimentaire du flysch albien (flysch noir et poudingues de mendibelza) dans la région de Mauléon-Tardets (Pyrénées Atlantiques). Université Paul Sabatier de Toulouse (Sciences).

Fort, X., Brun, J.P., Chauvel, F., 2004b. Contraction induced by block rotation above salt (Angolan margin). Mar. Pet. Geol. 21, 1281–1294.

Fort, X., Brun, J.-P., Chauvel, F., 2004a. Salt tectonics on the Angolan margin, synsedimentary deformation processes. AAPG Bull. 88, 1523–1544.

Fortané, A., Duée, G., Lagabrielle, Y., Coutelle, A., 1986. Lherzolites and the western "Chaînons Béarnais" (French Pyrenees): Structural and paleogeographical pattern. Tectonophysics 129, 81–98. https://doi.org/10.1016/0040-1951(86)90247-7

Frizon de Lamotte, D., Raulin, C., Mouchot, N., Wrobel-Daveau, J.-C., Blanpied, C., Ringenbach, J.-C., 2011. The southernmost margin of the Tethys realm during the Mesozoic and Cenozoic: Initial geometry and timing of the inversion processes: TETHYS SOUTHERNMOST MARGIN. Tectonics 30, n/a-n/a. https://doi.org/10.1029/2010TC002691

Froitzheim, N., Manatschal, G., 1996. Kinematics of Jurassic rifting, mantle exhumation, and passive-margin formation in the Austroalpine and Penninic nappes (eastern Switzerland). Geol. Soc. Am. Bull. 108, 1120–1133. https://doi.org/10.1130/0016-7606(1996)108<1120:KOJRME>2.3.CO;2

Gallart, J., Rojas, H., Diaz, J., Dañobeitia, J.J., 1990. Features of deep crustal structure and the onshore-offshore transition at the Iberian flank of the Valencia Trough (Western Mediterranean). J. Geodyn. 12, 233–252.

Gallart, J., Vidal, N., Danobeitia, J.., 1994. Lateral variations in the deep crustal structure at the Iberian margin of the Valencia trough imaged from seismic reflection methods. Tectonophysics 232, 59–75. https://doi.org/10.1016/0040-1951(94)90076-0

García Mondéjar, J., Agirrezabala, L., M., Aranburu, A., Fernandez-Mendiola, P., A., Gomèz-Pérèz, I., Lopez-Horgue, M., Rosales, I., 1996. Aptian—Albian tectonic pattern of the Basque—Cantabrian Basin (Northern Spain). Geol. J. 31, 13–45.

García-Lasanta, C., Casas-Sainz, A., Villalaín, J.J., Oliva-Urcia, B., Mochales, T., Speranza, F., 2017. Remagnetizations used to unravel large-scale fold kinematics: A case study in the Cameros Basin (Northern Spain): Unfolding in Basin Inversion. Tectonics 36, 714–729. https://doi.org/10.1002/2016TC004459

Gaullier, V., Brun, J.P., Gueīrin, G., Lecanu, H., 1993. Raft tectonics: the effects of residual topography below a salt deīcollement. Tectonophysics 228, 363–381.

Golberg, J.M., Guiraud, M., Maluski, H., Séguret, M., 1988. Caractères pétrologiques et âge du métamorphisme en contexte distensif du bassin sur décrochement de Soria (Crétacé inférieur, Nord Espagne). Comptes Rendus Académie Sci. Sér. 2 Mécanique Phys. Chim. Sci. Univers Sci. Terre 307, 521–527.

Golberg, J.M., Leyreloup, A.F., 1990. High temperature-low pressure Cretaceous metamorphism related to crustal thinning (Eastern North Pyrenean Zone, France). Contrib. Mineral. Petrol. 104, 194–207. https://doi.org/10.1007/BF00306443

Golberg, J.-M., Maluski, H., 1988. Données nouvelles et mise au point sur l'âge du métamorphisme pyrénéen. Comptes Rendus Académie Sci. Sér. 2 Mécanique Phys. Chim. Sci. Univers Sci. Terre 306, 429–435.

Golberg, J.M., Maluski, H., Leyreloup, A.F., 1986. Petrological and age relationship between emplacement of magmatic breccia, alkaline magmatism, and static metamorphism in the North Pyrenean Zone. Tectonophysics 129, 275–290. https://doi.org/10.1016/0040-1951(86)90256-8

Gomez-Ortiz, D., Agarwal, B.N.P., Tejero, R., Ruiz, J., 2011. Crustal structure from gravity signatures in the Iberian Peninsula. Geol. Soc. Am. Bull. 123, 1247–1257. https://doi.org/10.1130/B30224.1

Gómez-Romeu, J., Masini, E., Tugend, J., Ducoux, M., Kusznir, N., 2019. Role of rift structural inheritance in orogeny highlighted by the Western Pyrenees case-study. Tectonophysics 766, 131–150. https://doi.org/10.1016/j.tecto.2019.05.022

Gottis, M., 1972. Construction d'un modèle géodynamique pyrénéen. Comptes Rendus Académie Sci. 275, 2099.

Grandjean, G., 1994. Etude des structures crustales dans une portion de chaîne et de leur relation avec les bassins sédimentaires. Application aux Pyrénées occidentales. Bull Cent Rech Explor Prod Elf Aquitaine 18, 391–420.

Grandjean, G., 1992. Mise en évidence des structures crustales dans une portion de chaîne et de leur relation avec les bassins sédimentaires. Application aux Pyrénées occidentales au travers du Projet ECORS Arzacq-Pyrénées. Université des Sciences et Techniques du Languedoc.

Guimerà, J., Alonso, Á., Mas, J.R., 1995. Inversion of an extensional-ramp basin by a newly formed thrust: the Cameros basin (N. Spain). Geol. Soc. Lond. Spec. Publ. 88, 433–453. https://doi.org/10.1144/GSL.SP.1995.088.01.23

Guiraud, M., Séguret, M., 1985. A releasing solitary overstep model for the Late Jurassic-Early Cretaceous (Wealdian) Soria strike-slip basin (northern Spain). AAPG Bull.

Hart, N.R., Stockli, D.F., Lavier, L.L., Hayman, N.W., 2017. Thermal evolution of a hyperextended rift basin, Mauléon Basin, western Pyrenees: Thermal evolution of hyperextended rift. Tectonics. https://doi.org/10.1002/2016TC004365

Haupert, I., Manatschal, G., Decarlis, A., Unternehr, P., 2016. Upper-plate magma-poor rifted margins: Stratigraphic architecture and structural evolution. Mar.

Pet. Geol. 69, 241–261. https://doi.org/10.1016/j.marpetgeo.2015.10.020

Henry, J., Zolnaï, G., Le Pochat, G., Mondeilh, C., 1987. Carte géologique de la France au 1/50 000: feuille d'Orthez, Orléans, France.

Huismans, R.S., Beaumont, C., 2014. Rifted continental margins: The case for depth-dependent extension. Earth Planet. Sci. Lett. 407, 148–162. https://doi.org/10.1016/j.epsl.2014.09.032

Huismans, R.S., Beaumont, C., 2011. Depth-dependent extension, two-stage breakup and cratonic underplating at rifted margins. Nature 473, 74–78. https://doi.org/10.1038/nature09988

Huismans, R.S., Beaumont, C., 2008. Complex rifted continental margins explained by dynamical models of depth-dependent lithospheric extension. Geology 36, 163. https://doi.org/10.1130/G24231A.1

Huismans, R.S., Beaumont, C., 2003. Symmetric and asymmetric lithospheric extension: Relative effects of frictional-plastic and viscous strain softening. J. Geophys. Res. Solid Earth 108. https://doi.org/10.1029/2002JB002026

James, V., 1998. La plate-forme carbonatée ouest-pyrénéenne au jurassique moyen et supérieur stratigraphie séquentielle, stades d'évolution, relations avec la subsurface en aquitaine méridionale.

James, V., Canérot, J., 1999. Diapirisme et structuration post-triasique des Pyrénées occidentales et de l'Aquitaine méridionale (France). Eclogae Geol. Helvetiae 92, 63–72.

Jammes, S., Lavier, L., Manatschal, G., 2010b. Extreme crustal thinning in the Bay of Biscay and the Western Pyrenees: From observations to modeling. Geochem. Geophys. Geosystems 11. https://doi.org/10.1029/2010GC003218

Jammes, S., Manatschal, G., Lavier, L., 2010c. Interaction between prerift salt and detachment faulting in hyperextended rift systems: The example of the Parentis and Mauléon basins (Bay of Biscay and western Pyrenees). AAPG Bull. 94, 957–975. https://doi.org/10.1306/12090909116

Jammes, S., Manatschal, G., Lavier, L., Masini, E., 2009. Tectono-sedimentary evolution related to extreme crustal thinning ahead of a propagating ocean: Example of the western Pyrenees. Tectonics 28. https://doi.org/10.1029/2008TC002406

Jammes, S., Tiberi, C., Manatschal, G., 2010. 3D architecture of a complex transcurrent rift system: The example of the Bay of Biscay–Western Pyrenees. Tectonophysics 489, 210–226. https://doi.org/10.1016/j.tecto.2010.04.023

Jiménez-Munt, I., Fernàndez, M., Vergés, J., Afonso, J.C., Garcia-Castellanos, D., Fullea, J., 2010. Lithospheric structure of the Gorringe Bank: Insights into its origin and tectonic evolution: GORRINGE BANK STRUCTURE AND EVOLUTION. Tectonics 29, n/a-n/a. https://doi.org/10.1029/2009TC002458

Karner, G.D., Driscoll, N.W., Barker, D.H.N., 2003. Syn-rift regional subsidence across the West African continental margin: the role of lower plate ductile extension. Geol. Soc. Lond. Spec. Publ. 207, 105–129. https://doi.org/10.1144/GSL.SP.2003.207.6

Karner, G.D., Gambôa, L. a. P., 2007. Timing and origin of the South Atlantic pre-salt sag basins and their capping evaporites. Geol. Soc. Lond. Spec. Publ. 285, 15–35. https://doi.org/10.1144/SP285.2

Lagabrielle, Y., Asti, R., Fourcade, S., Corre, B., Poujol, M., Uzel, J., Labaume, P., Clerc, C., Lafay, R., Picazo, S., Maury, R., 2019. Mantle exhumation at magma-poor passive continental margins. Part I. 3D architecture and metasomatic evolution of a fossil exhumed mantle domain (Urdach lherzolite, north-western Pyrenees, France). BSGF - Earth Sci. Bull. 190, 8. https://doi.org/10.1051/bsgf/2019007

Lagabrielle, Y., Bodinier, J.-L., 2008. Submarine reworking of exhumed sub-continental mantle rocks: field evidence from the Lherz peridotites, French Pyrenees: Cretaceous exhumation of pyrenean mantle. Terra Nova 20, 11–21. https://doi.org/10.1111/j.1365-3121.2007.00781.x

Lagabrielle, Y., Clerc, C., Vauchez, A., Lahfid, A., Labaume, P., Azambre, B., Fourcade, S., Dautria, J.-M., 2016. Very high geothermal gradient during mantle exhumation recorded in mylonitic marbles and carbonate breccias from a Mesozoic Pyrenean palaeomargin (Lherz area, North Pyrenean Zone, France). Comptes Rendus Geosci. 348, 290–300. https://doi.org/10.1016/j.crte.2015.11.004

Lagabrielle, Y., Labaume, P., de Saint Blanquat, M., 2010. Mantle exhumation, crustal denudation, and gravity tectonics during Cretaceous rifting in the Pyrenean realm (SW Europe): Insights from the geological setting of the lherzolite bodies. Tectonics 29. https://doi.org/10.1029/2009TC002588

Lamare, P., 1936. Recherches géologiques dans les Pyrénées basques d'Espagne. Société géologique de France.

Lavier, L.L., Manatschal, G., 2006. A mechanism to thin the continental lithosphere at magma-poor margins. Nature 440, 324–328. https://doi.org/10.1038/nature04608

Le Pochat, G., Bolthenhagen, C., Lenguin, M., Lorsignol, S., Thibault, C., 1976. Carte géologique de France au 1/50 000: Mauléon-licharre, Orléans, France.

Lefort, J.-P., Agarwal, B.N.., 1999. Of what is the centre of the Ibero-Armorican arc composed? Tectonophysics 302, 71–81. https://doi.org/10.1016/S0040-1951(98)00275-3

Lemoine, M., Tricart, P., Boillot, G., 1987. Ultramafic and gabbroic ocean floor of the Ligurian Tethys (Alps, Corsica, Apennines): In search of a genetic imodel. Geology 15, 622–625. https://doi.org/10.1130/0091-7613(1987)15<622:UAGOFO>2.0.CO;2

Lenoble, J.-L., 1992. Les plates-formes carbonatées ouest-pyrénéennes du dogger à l'Albien, stratigraphie séquentielle et évolution géodynamique. Université Paul Sabatier de Toulouse (Sciences).

Lescoutre, R., 2019. Formation and reactivation of the Pyrenean-Cantabrian rift system : inheritance, segmentation and thermal evolution. Strasbourg.

Lescoutre, R., Tugend, J., Brune, S., Masini, E., Manatschal, G., 2019. Thermal Evolution of Asymmetric Hyperextended Magma-Poor Rift Systems: Results From Numerical Modeling and Pyrenean Field Observations. Geochem. Geophys. Geosystems 2019GC008600. https://doi.org/10.1029/2019GC008600

Liro, L.M., Coen, R., 1995. Salt deformation history and postsalt structural trends, offshore southern Gabon, West Africa.

Lucas, C., 1985. Le grès rouge du versant nord des Pyrénées: essai sur la géodynamique de dépôts continentaux du permien et du trias.

Lundin, E.R., 1992. Thin-skinned extensional tectonics on a salt detachment, northern Kwanza Basin, Angola. Mar. Pet. Geol. 9, 405–411.

Manatschal, G., 2004. New models for evolution of magma-poor rifted margins based on a review of data and concepts from West Iberia and the Alps. Int. J. Earth Sci. 93. https://doi.org/10.1007/s00531-004-0394-7

Manatschal, G., Engström, A., Desmurs, L., Schaltegger, U., Cosca, M., Müntener, O., Bernoulli, D., 2006. What is the tectono-metamorphic evolution of continental break-up: The example of the Tasna Ocean–Continent Transition. J. Struct. Geol. 28, 1849–1869. https://doi.org/10.1016/j.jsg.2006.07.014

Manatschal, G., Froitzheim, N., Rubenach, M., Turrin, B.D., 2001. The role of detachment faulting in the formation of an ocean-continent transition: insights from the Iberia Abyssal Plain. Geol. Soc. Lond. Spec. Publ. 187, 405–428. https://doi.org/10.1144/GSL.SP.2001.187.01.20

Manatschal, G., Müntener, O., Lavier, L.L., Minshull, T.A., Péron-Pinvidic, G., 2007. Observations from the Alpine Tethys and Iberia–Newfoundland margins pertinent to the interpretation of continental breakup. Geol. Soc. Lond. Spec. Publ. 282, 291–324. https://doi.org/10.1144/SP282.14

Manatschal, G., Nievergelt, P., 1997. A continent-ocean transition recorded in the Err and Platta nappes (Eastern Switzerland). Eclogae Geol. Helvetiae 90, 3–28.

Manatschal, G., Sauter, D., Karpoff, A.M., Masini, E., Mohn, G., Lagabrielle, Y., 2011. The Chenaillet Ophiolite in the French/Italian Alps: An ancient analogue for an Oceanic Core Complex? Lithos, Alpine Ophiolites and Modern AnaloguesContinental Rifting to Oceanic LithosphereAlpine Ophiolites and Modern Analogues 124, 169–184. https://doi.org/10.1016/j.lithos.2010.10.017

Marillier, F., Tomassino, A., Patriat, P., Pinet, B., 1988. Deep structure of the Aquitaine shelf: constraints from expanding spread profiles on the ECORS Bay of Biscay transect. Mar. Pet. Geol. 5, 65–74.

Martínez-Torres, L.M., 1989. El manto de los mármoles (Pirineo occidental): geología estructural y evolución geodinámica (PhD Thesis). Universidad del País Vasco-Euskal Herriko Unibertsitatea.

Mas, J.R., Alonso, A., Guimerà, J., 1993. Evolución tectonosedimentaria de una cuenca extensional intraplaca: la cuenca finijurásica–eocretácica de Los Cameros (La Rioja–Soria). Rev. Soc. Geológica Esp. 6, 129–144.

Mas, R., Benito, M.I., Arribas, J., Alonso, A., Arribas, M.E., Lohmann, K.C., González-Acebrón, L., Hernán, J., Quijada, E., Suárez, P., 2011. Evolution of an intra-plate rift basin: the latest Jurassic-early Cretaceous Cameros basin (Northwest Iberian ranges, North Spain). Geo-Guías 8, 117–154.

Masini, E., Manatschal, G., Mohn, G., Ghienne, J.-F., Lafont, F., 2011. The tectono-sedimentary evolution of a supra-detachment rift basin at a deep-water magma-poor rifted margin: the example of the Samedan Basin preserved in the Err nappe in SE Switzerland: Tectono-sedimentary evolution of a supra-detachment rift basin. Basin Res. 23, 652–677. https://doi.org/10.1111/j.1365-2117.2011.00509.x

Masini, E., Manatschal, G., Mohn, G., Unternehr, P., 2012. Anatomy and tectono-sedimentary evolution of a rift-related detachment system: The example of the Err detachment (central Alps, SE Switzerland). Geol. Soc. Am. Bull. 124, 1535–1551. https://doi.org/10.1130/B30557.1

Masini, E., Manatschal, G., Tugend, J., Mohn, G., Flament, J.-M., 2014. The tectono-sedimentary evolution of a hyper-extended rift basin: the example of the Arzacq–Mauléon rift system (Western Pyrenees, SW France). Int. J. Earth Sci. 103, 1569–1596. https://doi.org/10.1007/s00531-014-1023-8

Mata, M.P., Casas, A.M., Canals, A., Gil, A., Pocovi, A., 2001. Thermal history during Mesozoic extension and Tertiary uplift in the Cameros Basin, northern Spain. Basin Res. 13, 91–111.

Mathieu, C., 1986. Histoire géologique du sous-bassin de Parentis. Bull. Cent. Rech. Explor. Elf-Aquitaine 10, 22–47.

Mattauer, M., 1968. Les traits structuraux essentiels de la chaîne Pyrénéenne. Rev. Géologie Dyn. Géographie Phys. 10, 3–11.

Mauriaud, P., 1987. La tectonique salifère d'Aquitaine. Le bassin d'Aquitaine. Rev. Pétrole Tech. 335, 38–41.

Mediavilla, F., 1987. La tectonique salifère d'Aquitaine. Le Bassin de Parentis. Rev. Pétrole Tech. 335, 35–37.

Mendia, M.S., Ibarguchi, J.I.G., 1991. High-grade metamorphic rocks and peridotites along the Leiza Fault (Western Pyrenees, Spain). Geol. Rundsch. 80, 93–107.

Mohn, G., Karner, G.D., Manatschal, G., Johnson, C.A., 2015. Structural and stratigraphic evolution of the Iberia–Newfoundland hyper-extended rifted margin: a quantitative modelling approach. Geol. Soc. Lond. Spec. Publ. 413, 53–89. https://doi.org/10.1144/SP413.9

Mohn, G., Manatschal, G., Beltrando, M., Haupert, I., 2014. The role of rift-inherited hyper-extension in Alpine-type orogens. Terra Nova 26, 347–353. https://doi.org/10.1111/ter.12104

Monchoux, P., 1970. Les lherzolites pyrénéennes: contribution à l'étude de leur minéralogie, de leur genèse et de leurs transformations. Université Paul Sabatier de Toulouse (Sciences).

Montadert, L., de Charpal, O., Roberts, D., Guennoc, P., Sibuet, J.-C., 1979. Northeast Atlantic passive continental margins: Rifting and subsidence processes, in: Talwani, M., Hay, W., Ryan, W.B.F. (Eds.), Maurice Ewing Series. American Geophysical Union, Washington, D. C., pp. 154–186. https://doi.org/10.1029/ME003p0154

Montadert, L., Winnock, E., 1971. L'histoire structurale du Golf de Gascogne. Technip.

Montigny, R., Azambre, B., Rossy, M., Thuizat, R., 1986. K-Ar Study of cretaceous magmatism and metamorphism in the Pyrenees: Age and length of rotation of the Iberian Peninsula. Tectonophysics, The Geological Evolution of the Pyrenees 129, 257–273. https://doi.org/10.1016/0040-1951(86)90255-6

Moulin, M., Aslanian, D., Unternehr, P., 2010. A new starting point for the South and Equatorial Atlantic Ocean. Earth-Sci. Rev. 98, 1–37. https://doi.org/10.1016/j.earscirev.2009.08.001

Nebot, M., Guimerà, J.J., 2016. Structure of an inverted basin from subsurface and field data: the Late Jurassic-Early Cretaceous Maestrat Basin (Iberian Chain). Geol. Acta 14, 0155–177.

Olivier, P., Gleizes, G., Paquette, J.L., 2004. Gneiss domes and granite emplacement in an obliquely convergent regime: New interpretation of the Variscan Agly Massif (Eastern Pyrenees, France). Spec. Pap.-Geol. Soc. Am. 229–242.

Omodeo Salè, S., Guimerà, J., Mas, R., Arribas, J., 2014. Tectono-stratigraphic evolution of an inverted extensional basin: the Cameros Basin (north of Spain). Int. J. Earth Sci. 103, 1597–1620. https://doi.org/10.1007/s00531-014-1026-5

Omodeo-Salé, S., Salas, R., Guimerà, J., Ondrak, R., Mas, R., Arribas, J., Suárez-Ruiz, I., Martinez, L., 2017. Subsidence and thermal history of an inverted Late Jurassic-Early Cretaceous extensional basin (Cameros, North-central Spain) affected by very low- to low-grade metamorphism. Basin Res. 29, 156–174. https://doi.org/10.1111/bre.12142

Ortí, F., 1974. El Keuper del levante español. Estud. Geológicos 30, 7–46.

Ortí, F., Pérez-López, A., Salvany, J.M., 2017. Triassic evaporites of Iberia: Sedimentological and palaeogeographical implications for the western Neotethys evolution during the Middle Triassic–Earliest Jurassic. Palaeogeogr. Palaeoclimatol. Palaeoecol. 471, 157–180. https://doi.org/10.1016/j.palaeo.2017.01.025

Osmundsen, P.T., Ebbing, J., 2008. Styles of extension offshore mid-Norway and implications for mechanisms of crustal thinning at passive margins: STYLES OF EXTENSION OFFSHORE NORWAY. Tectonics 27, n/a-n/a. https://doi.org/10.1029/2007TC002242

Osmundsen, P.T., Péron-Pinvidic, G., 2018. Crustal-Scale Fault Interaction at Rifted Margins and the Formation of Domain-Bounding Breakaway Complexes: Insights From Offshore Norway. Tectonics 37, 935–964. https://doi.org/10.1002/2017TC004792

Osmundsen, P.T., Sommaruga, A., Skilbrei, J.R., Olesen, O., 2002. Deep structure of the Mid Norway rifted margin. Nor. J. Geol. Geol. Foren. 82.

Pedreira, D., Pulgar, J.A., Gallart, J., Torné, M., 2007. Three-dimensional gravity and magnetic modeling of crustal indentation and wedging in the western Pyrenees-Cantabrian Mountains. J. Geophys. Res. 112. https://doi.org/10.1029/2007JB005021

Pedrera, A., García-Senz, J., Ayala, C., Ruiz-Constán, A., Rodríguez-Fernández, L.R., Robador, A., González Menéndez, L., 2017. Reconstruction of the exhumed mantle across the North Iberian Margin by crustal-scale 3-D gravity inversion and geological cross section. Tectonics 36, 3155–3177.

Pérez-Gussinyé, M., 2013. A tectonic model for hyperextension at magma-poor rifted margins: an example from the West Iberia–Newfoundland conjugate margins. Geol. Soc. Lond. Spec. Publ. 369, 403–427. https://doi.org/10.1144/SP369.19

Peron-Pinvidic, G., 2006. Morphotectonique et architecture sédimentaire de la transition océan-continent de la marge ibérique. Strasbourg 1.

Peron-Pinvidic, G., Gernigon, L., Gaina, C., Ball, P., 2012a. Insights from the Jan Mayen system in the Norwegian–Greenland sea—I. Mapping of a microcontinent. Geophys. J. Int. 191, 385–412. https://doi.org/10.1111/j.1365-246X.2012.05639.x

Peron-Pinvidic, G., Gernigon, L., Gaina, C., Ball, P., 2012b. Insights from the Jan Mayen system in the Norwegian–Greenland Sea—II. Architecture of a microcontinent. Geophys. J. Int. 191, 413–435. https://doi.org/10.1111/j.1365-246X.2012.05623.x

Péron-Pinvidic, G., Manatschal, G., 2009. The final rifting evolution at deep magma-poor passive margins from Iberia-Newfoundland: a new point of view. Int. J. Earth Sci. 98, 1581–1597. https://doi.org/10.1007/s00531-008-0337-9

Péron-Pinvidic, G., Manatschal, G., Masini, E., Sutra, E., Flament, J.M., Haupert, I., Unternehr, P., 2015. Unravelling the along-strike variability of the Angola–Gabon rifted margin: a mapping approach. Geol. Soc. Lond. Spec. Publ. 438, 49–76. https://doi.org/10.1144/SP438.1

Péron-Pinvidic, G., Manatschal, G., Minshull, T.A., Sawyer, D.S., 2007. Tectonosedimentary evolution of the deep Iberia-Newfoundland margins: Evidence for a complex breakup history. Tectonics 26, 1–19. https://doi.org/10.1029/2006TC001970

Peybernès, B., 1982. Création puis évolution de la marge nord-ibérique des Pyrénées au Crétacé inférieur. Cuad. Geol. Ibérica 8, 987–1004.

Peybernès, B., 1979. L'Urgonien des Pyrénées, Essai de synthèse. Geobios 12, 79–87.

Peybernes, B., 1976. Le Jurassique et le Crétace inferieur des Pyrénées franco-espagnoles entre la Garonne et la Méditérranée. Toulouse.

Peybernès, B., Combes, P.-J., 1994. Stratigraphie séquentielle du Crétacé basal (intervalle Berriasien-Hauterivien) des Pyrénées centrales et orientales franco-espagnoles. Cretac. Res. 15, 535–546. https://doi.org/10.1006/cres.1994.1032

Pinet, B., Montadert, L., Curnelle, R., Cazes, M., Marillier, F., Rolet, J., Tomassino, A., Galdeano, A., Patriat, P., Brunet, M.F., 1987. Crustal thinning on the Aquitaine shelf, Bay of Biscay, from deep seismic data. Nature 325, 513.

Pinet, Bertrand, Montadert, L., ECORS Scientific Party, 1987. Deep seismic reflection and refraction profiling along the Aquitaine shelf (Bay of Biscay). Geophys. J. Int. 89, 305–312. https://doi.org/10.1111/j.1365-246X.1987.tb04423.x

Platt, N.H., 1990. Basin evolution and fault reactivation in the western Cameros Basin, Northern Spain. J. Geol. Soc. 147, 165–175. https://doi.org/10.1144/gsjgs.147.1.0165

Platt, N.H., 1989. Continental sedimentation in an evolving rift basin: the Lower Cretaceous of the western Cameros Basin (northern Spain). Sediment. Geol. 64, 91–109. https://doi.org/10.1016/0037-0738(89)90086-9

Platt, N.H., 1986. Sedimentology and Tectonics of the Western Cameros Basin, Province of Burgos, Northern Spain (PhD Thesis). University of Oxford.

Quijada, I.E., Suárez González, P., Isabel, B.M., Mas, J.R., Alonso, Á., 2010. Un ejemplo de llanura fluvio-deltaica influenciada por las mareas: el yacimiento de icnitas de Serrantes (Grupo Oncala, Berriasiense, Cuenca de Cameros, N. de España). Geogaceta 15–18.

Rat, J., Mouthereau, F., Brichau, S., Crémades, A., Bernet, M., Balvay, M., Ganne, J., Lahfid, A., Gautheron, C., 2019. Tectonothermal Evolution of the Cameros Basin: Implications for Tectonics of North Iberia. Tectonics 38, 440–469. https://doi.org/10.1029/2018TC005294

Rat, P., 1988. The Basque-Cantabrian Basin between the Iberian and European plates, some facts but still many problems. Rev Soc Geol Esp. 327–348.

Rat, P., Amiot, M., Feuillée, P., Floquet, M., Mathey, B., Pascal, A., Salomon, J., García Mondéjar, J., Pujalte, J., Lamolda, M., others, 1983. Vue sur le Cretacé basco-cantabrique et nord-ibérique. Une Marge Son Arriere-Pays Ses Environ. Sedimentaires Memoires Geol. Univ. Dijon 9, 191.

Ravier, J., 1957. Le métamorphisme des terrains secondaires des Pyrénées. Université, Faculté des Sciences.

Reston, T.J., 2009. The structure, evolution and symmetry of the magma-poor rifted margins of the North and Central Atlantic: A synthesis. Tectonophysics 468, 6–27. https://doi.org/10.1016/j.tecto.2008.09.002

Reston, T.J., 2007. The formation of non-volcanic rifted margins by the progressive extension of the lithosphere: the example of the West Iberian margin. Geol. Soc. Lond. Spec. Publ. 282, 77–110. https://doi.org/10.1144/SP282.5

Reston, T.J., 2005. Polyphase faulting during the development of the west Galicia rifted margin. Earth Planet. Sci. Lett. 237, 561–576. https://doi.org/10.1016/j.epsl.2005.06.019

Reston, T.J., Krawczyk, C.M., Hoffmann, H.-J., 1995. Detachment tectonics during Atlantic rifting: analysis and interpretation of the S reflection, the west Galicia margin. Geol. Soc. Lond. Spec. Publ. 90, 93–109. https://doi.org/10.1144/GSL.SP.1995.090.01.05

Reston, T.J., McDermott, K.G., 2011. Successive detachment faults and mantle unroofing at magma-poor rifted margins. Geology 39, 1071–1074. https://doi.org/10.1130/G32428.1

Reston, T.J., Pérez-Gussinyé, M., 2007. Lithospheric extension from rifting to continental breakup at magma-poor margins: rheology, serpentinisation and symmetry. Int. J. Earth Sci. 96, 1033–1046. https://doi.org/10.1007/s00531-006-0161-z

Ribes, C., Ghienne, J.-F., Manatschal, G., Decarlis, A., Karner, G.D., Figueredo, P.H., Johnson, C.A., 2019. Long-lived mega fault-scarps and related breccias at distal rifted margins: Insights from present-day and fossil analogues. J. Geol. Soc. jgs2018-181. https://doi.org/10.1144/jgs2018-181

Roca, E., 1996. La cubeta mesozoica de las Columbrets: aportaciones al conocimiento de la estructura del surco de Valencia. Geogaceta 20, 1711–1714.

Roma, M., Ferrer, O., Roca, E., Pla, O., Escosa, F.O., Butillé, M., 2018. Formation and inversion of salt-detached ramp-syncline basins. Results from analog modeling and application to the Columbrets Basin (Western Mediterranean). Tectonophysics 745, 214–228. https://doi.org/10.1016/j.tecto.2018.08.012

Rossi, P., Cocherie, A., Fanning, C.M., Ternet, Y., 2003. Datation U-Pb sur zircons des dolérites tholéiitiques pyrénéennes (ophites) à la limite Trias–Jurassique et relations avec les tufs volcaniques dits « infra-liasiques » nord-pyrénéens. Comptes Rendus Geosci. 335, 1071–1080. https://doi.org/10.1016/j.crte.2003.09.011

Rouby, D., Raillard, S., Guillocheau, F., Bouroullec, R., Nalpas, T., 2002. Kinematics of a growth fault/raft system on the West African margin using 3-D restoration. J. Struct. Geol. 24, 783–796.

Roux, J.-C., 1983. Recherches stratigraphiques et sédimentologiques sur les flyschs crétacés pyrénéens au sud d'Oloron (Pyrénées Atlantiques). Université Paul Sabatier de Toulouse (Sciences).

Ruiz, M., 2007. Caracterització estructural i sismotectònica de la litosfera en el domini Pirenaico-Cantàbric a partir de mètodes de sísmica activa i passiva. Universitat de Barcelona.

Sàbat, F., Roca, E., Muñoz, J.A., Vergès, J., Santanach, P., Masana, E., 1997. Role of extension and compression in the evolution of the eastern margin of Iberia: The ESCI-València trough seismic profile. Rev. Soc. Geológica Esp. 8, 431–448.

Salas, R., Guimerà, J., Mas, R., Martín-Closas, C., Meléndez, A., Alonso, A., 2001. Evolution of the Mesozoic central Iberian Rift System and its Cainozoic inversion (Iberian chain). Peri-Tethys Mem. 6, 145–185.

Saspiturry, N., Cochelin, B., Razin, P., Leleu, S., Lemirre, B., Bouscary, C., Issautier, B., Serrano, O., Lasseur, E., Baudin, T., Allanic, C., 2019a. Tectono-sedimentary evolution of a rift system controlled by Permian post-orogenic extension and metamorphic core complex formation (Bidarray Basin and Ursuya dome,

Western Pyrenees). Tectonophysics 768, 228180. https://doi.org/10.1016/j.tecto.2019.228180

Saspiturry, N., Razin, P., Baudin, T., Serrano, O., Issautier, B., Lasseur, E., Allanic, C., Thinon, I., Leleu, S., 2019b. Symmetry vs. asymmetry of a hyper-thinned rift: Example of the Mauléon Basin (Western Pyrenees, France). Mar. Pet. Geol. 104, 86–105. https://doi.org/10.1016/j.marpetgeo.2019.03.031

Schettino, A., Turco, E., 2011. Tectonic history of the western Tethys since the Late Triassic. Geol. Soc. Am. Bull. 123, 89–105. https://doi.org/10.1130/B30064.1

Serrano, O., Delmas, J., Hanot, F., Vially, R., Herbin, J.-P., Houel, P., Tourlière, B., 2006. Le bassin d'Aquitaine: valorisation des données sismiques, cartographie structurale et potentiel pétrolier. Bureau de Recherche Géologique et minière.

Sibuet, J.-C., Srivastava, S., Manatschal, G., 2007. Exhumed mantle-forming transitional crust in the Newfoundland-Iberia rift and associated magnetic anomalies. J. Geophys. Res. Solid Earth 112. https://doi.org/10.1029/2005JB003856

Soto, J.I., Flinch, F., Tari, G., 2017. Permo-Triassic Salt Provinces of Europe, North Africa and the Atlantic Margins: Tectonics and Hydrocarbon Potential, in: In Soto et Al., Eds, Permo-Triassic Salt Provinces of Europe, North Africa and the Atlantic Margins. Tectonics and Hydrocarbon Potential. Elsevier.

Souquet, P., 1967. Le Crétacé supérieur Sud-Pyrénéen, en Catalogne, Aragon et Navarre. E. Privat.

Souquet, P., Debroas, E.-J., Boirie, J.-M., Pons, P., Fixari, G., Roux, J.-C., Dol, J., Thieuloy, J.-P., Bonnemaison, M., Manivit, H., others, 1985. Le groupe du Flysch noir (albo-cénomanien) dans les Pyrénées. Bull Cent Rech Exlpo-Prod Elf-Aquitaine Pau 9, 183–252.

Suárez González, P., Quijada, I.E., Mas, J.R., Benito, M.I., 2010. Nuevas aportaciones sobre la influencia marina y la edad de los carbonatos de la Fm Leza en el sector de Préjano (SE de La Rioja). Cretácico Inferior, Cuenca de Cameros. Geogaceta 7–10.

Teixell, A., Labaume, P., Ayarza, P., Espurt, N., de Saint Blanquat, M., Lagabrielle, Y., 2018. Crustal structure and evolution of the Pyrenean-Cantabrian belt: A review and new interpretations from recent concepts and data. Tectonophysics 724, 146–170. https://doi.org/10.1016/j.tecto.2018.01.009

Teixell, A., Labaume, P., Lagabrielle, Y., 2016. The crustal evolution of the west-central Pyrenees revisited: Inferences from a new kinematic scenario. Comptes Rendus Geosci. 348, 257–267. https://doi.org/10.1016/j.crte.2015.10.010

Ternet, Y., Majesté-Menjoulas, C., Canérot, J., Baudin, T., Cocherie, A., Guerrot, C., Rossi, P., 2004. Carte géologique de la France au 1/50 000: Laruns-Somport, Orléans, France.

Thiébaut, J., Durand-Wackenheim, C., Debeaux, M., Souquet, P., 1992. Métamorphisme des évaporites triasiques du versant nord des Pyrénées centrales et Occidentales. Bull. Société Hist. Nat. Toulouse 128, 77–84.

Thinon, I., 1999. Structure profonde de la marge Nord Gascogne et du Bassin armoricain. Université de Bretagne occidentale-Brest.

Thinon, I., Matias, L., RÉhault, J.P., Hirn, A., Fidalgo-GonzÁlez, L., Avedik, F., 2003. Deep structure of the Armorican Basin (Bay of Biscay): a review of Norgasis seismic reflection and refraction data. J. Geol. Soc. 160, 99–116. https://doi.org/10.1144/0016-764901-103

Tomassimo, A., Marillier, F., 1997. Processing and interpretation in the tau-p domain of the ECORS Bay of Biscay expanding spread profiles. Mém. Société Géologique Fr. 171, 31–43.

Torné, M., Banda, E., Fernandez, M., 1996. The Valencia Trough: Geological and geophysical constraints on the basin formation model., in: In P. A. Ziegler, & F. Horvath (Eds.), Structure and Prospects of Alpine Basins and Forelands, Mem. Nat Hist. Mus. pp. 103–128.

Torné, M., Pascal, G., Buhl, P., Watts, A.B., Mauffret, A., 1992. Crustal and velocity structure of the Valencia trough (western Mediterranean), Part I. A combined refraction/ wide-angle reflection and near-vertical reflection study. Tectonophysics 203, 1–20. https://doi.org/10.1016/0040-1951(92)90212-O

Tugend, J., Manatschal, G., Kusznir, N.J., Masini, E., 2015. Characterizing and identifying structural domains at rifted continental margins: application to the Bay of Biscay margins and its Western Pyrenean fossil remnants. Geol. Soc. Lond. Spec. Publ. 413, 171–203. https://doi.org/10.1144/SP413.3

Tugend, J., Manatschal, G., Kusznir, N.J., Masini, E., Mohn, G., Thinon, I., 2014. Formation and deformation of hyperextended rift systems: Insights from rift domain mapping in the Bay of Biscay-Pyrenees. Tectonics 33, 1239–1276. https://doi.org/10.1002/2014TC003529

Unternehr, P., Peron-Pinvidic, G., Manatschal, G., Sutra, E., 2010. Hyper-extended crust in the South Atlantic: in search of a model. Pet. Geosci. 16, 207–215. https://doi.org/10.1144/1354-079309-904

Vacher, P., Souriau, A., 2001. A three-dimensional model of the Pyrenean deep structure based on gravity modelling, seismic images and petrological constraints. Geophys. J. Int. 145, 460–470. https://doi.org/10.1046/j.0956-540x.2001.01393.x

Vacherat, A., Mouthereau, F., Pik, R., Bernet, M., Gautheron, C., Masini, E., Le Pourhiet, L., Tibari, B., Lahfid, A., 2014. Thermal imprint of rift-related processes in orogens as recorded in the Pyrenees. Earth Planet. Sci. Lett. 408, 296–306. https://doi.org/10.1016/j.epsl.2014.10.014

Valladares, I., 1980. Evolucidn de facies en el Jurasico calcareo del sector sur-occidental de la provincia de Burgos. Stud. Geol. Salamanticensia 16, 37–57.

Vargas, H., Gaspar-Escribano, J.M., López-Gómez, J., Van Wees, J.-D., Cloetingh, S., de La Horra, R., Arche, A., 2009. A comparison of the Iberian and Ebro Basins during the Permian and Triassic, eastern Spain: A quantitative subsidence modelling approach. Tectonophysics 474, 160–183. https://doi.org/10.1016/j.tecto.2008.06.005

Vauchez, A., Clerc, C., Bestani, L., Lagabrielle, Y., Chauvet, A., Lahfid, A., Mainprice, D., 2013. Preorogenic exhumation of the North Pyrenean Agly massif (Eastern Pyrenees-France). Tectonics 32, 95–106. https://doi.org/10.1002/tect.20015

Vergés, J., García-Senz, J., 2001. Mesozoic evolution and Cenozoic inversion of the Pyrenean rift. Mém. Muséum Natl. Hist. Nat. 186, 187–212.

Vidal, N., Gallart, J., Dañobeitia, J.J., 1997. Contribution of the ESCI-Valencia Trough wide-angle data to a crustal transect in the NE Iberian margin. Rev. - Soc. Geológica Esp. 417–429.

Vielzeuf, D., Kornprobst, J., 1984. Crustal splitting and the emplacement of Pyrenean lherzolites and granulites. Earth Planet. Sci. Lett. 67, 87–96. https://doi.org/10.1016/0012-821X(84)90041-4

Wang, Y., Chevrot, S., Monteiller, V., Komatitsch, D., Mouthereau, F., Manatschal, G., Sylvander, M., Diaz, J., Ruiz, M., Grimaud, F., Benahmed, S., Pauchet, H., Martin, R., 2016. The deep roots of the western Pyrenees revealed by full waveform inversion of teleseismic P waves. Geology 44, 475–478. https://doi.org/10.1130/G37812.1

Whitmarsh, R.B., Manatschal, G., Minshull, T.A., 2001. Evolution of magma-poor continental margins from rifting to seafloor spreading. Nature 413, 150–154. https://doi.org/10.1038/35093085

Zeyen, H., Fernàndez, M., 1994. Integrated lithospheric modeling combining thermal, gravity, and local isostasy analysis: Application to the NE Spanish Geotransect. J. Geophys. Res. Solid Earth 99, 18089–18102. https://doi.org/10.1029/94JB00898

Ziegler, P.A., 1982. Triassic rifts and facies patterns in Western and Central Europe. Geol. Rundsch. 71, 747–772. https://doi.org/10.1007/BF01821101

Chapitre 7

Conclusion

Conclusion

Les Pyrénées occidentales, situées à la jonction entre le domaine océanique du Golfe de Gascogne et la chaîne alpine des Pyrénées abritent le bassin de Mauléon. Ce bassin est interprété depuis les années 1980, comme un système de rift crétacé (croûte amincie), réactivé au cours de la compression tertiaire (Puigdefàbregas and Souquet, 1986; Souquet, 1988; Ducasse and Vélasque, 1988 ; Daignières et al., 1994). Les récentes études réalisées au cours des dix dernières années (Jammes et al., 2009; Lagabrielle et al., 2010 ; Masini et al., 2014 ; Teixell et al., 2016), ont proposé que ce bassin correspondait à un rift hyper-étiré crétacé comparable aux marges passives actuelles, permettant d'appliquer les modèles et concepts d'amincissement de la croute continentale développés sur l'exemple des marges atlantiques et alpines (Whitmarsh et al., 2001; Manatschal et al., 2001, 2007; Lavier and Manatschal, 2006 ; Péron-Pinvidic et al., 2007).

En effet, cet analogue fossile semble présenter de nombreuses similitudes avec les marges passives hyper-étirées atlantiques actuelles et avec les marges fossiles alpines, à savoir :

(1) le développement de bassins de rifts relativement subsidents,

(2) l'exhumation et la dénudation de roches métamorphiques considérés comme de la crôute inférieure, comme le massif granulitique de l'Ursuya à la jonction entre le domaine d'amincissement ibérique (« necking zone ») et le domaine hyper-étiré,

(3) l'exhumation plus ou moins large du manteau sous-continental le long de failles de détachement lithosphériques, au cours du rifting, dont le paroxysme se traduit ici par sa dénudation et son remaniement dans le flysch synrift d'Urdach,

(4) la présence d'une importante anomalie gravimétrique positive interprétée comme la présence, à faible profondeur, de manteau sous-continental,

(5) le caractère asymétrique des marges du rift.

L'objectif de notre étude consiste à reconstituer l'évolution tectono-sédimentaire du bassin de Mauléon de manière à comprendre la structure pré-compressive de ce segment nord-pyrénéen et à déterminer l'impact de cette structure sur l'évolution thermique et l'inversion du bassin. Les précédents travaux (Jammes et al., 2009 ; Masini et al., 2014) suggèrent le développement dès l'Albien inférieur d'un système de detachements à vergence nord responsable de la dénudation de la croûte inférieure et du manteau sous-continental. L'analyse fine et détaillée de l'enregistrement sédimentaire de ce bassin révèle une histoire synrift plus complexe et polyphasée.

Le rifting crétacé est précédé par une phase d'émersion généralisée de la plateforme jurassique interprétée comme une phase de bombement prérift. Du Barrémien à l'Aptien, la subsidence est largement compensée par la production sédimentaire carbonatée conduisant à l'aggradation de plus de 1 500 m d'épaisseur de dépôts carbonatés peu profonds dans le centre du bassin. Durant cette période, le profil de dépôt reste globalement plat. Cette subsidence élevée ne semble pas s'accompagner d'une déformation cassante significative de la croûte supérieure (sauf si elle n'est pas transmise à la couverture du fait du découplage sur les évaporites) et résulterait par conséquent d'un amincissement ductile de la croûte inférieure engendrant la formation d'un bassin de rift symétrique de type « sag ». La croûte moyenne et la série argilo-évaporitique du Trias supérieur jouent un rôle prépondérant en permettant de découpler la déformation. A partir de l'Aptien terminal, l'extraction latérale de la croûte inférieure se poursuivant, le bassin s'approfondit et commence à devenir asymétrique avec une pente plus accusée sur la marge sud. Cette inclinaison apparaît responsable d'un glissement généralisé de la couverture prérift vers l'axe du bassin.

La nature des systèmes de dépôt synrift montre que le bassin acquiert une nette asymétrie entre l'Albien et le Cénomanien inférieur. Des dépôts turbiditiques silicoclastiques grossiers s'accumulent

sur la marge ibérique tandis que la marge européenne est le siège d'une sédimentation de plateforme et de pente carbonatée. Le fonctionnement de puissants systèmes gravitaires conglomératiques profonds remaniant des éléments de socle et très probablement alimentés par un système de fan-deltas aujourd'hui non préservés à l'affleurement, témoignent d'importants mouvements verticaux sur la marge nord-ibérique (Conglomérats de Mendibelza). Ces dépôts passent latéralement vers le NE à une série turbiditique gréseuse distale en direction de l'axe du bassin. Le substratum de la marge ibérique enregistre à ce stade un basculement de 15° à 30° vers le nord-est et la formation de failles normales syn-sédimentaires fortement inclinées / subverticales de direction N120°E. Ce basculement vers le nord-est est interprété comme lié à un « roll-over » induit par un détachement à vergence sud dont l'émergence se trouve au niveau de la Faille de Saint-Palais interprétée ici comme une paléo-faille albienne inversée. A la limite entre le Cénomanien inférieur et moyen, un nouveau système de faille de détachement, cette fois-ci à vergence nord, le détachement du Lakhoura, confère une géométrie finale d'apparence symétrique (ou « pseudo-symétrique ») au bassin.

Dans un second temps, une coupe équilibrée N-S d'échelle crustale recoupant l'ensemble de la chaîne des Pyrénées occidentales a été restaurée. Cette restauration suggère un taux de raccourcissement minimum de 67 km (31%) dans ce segment des Pyrénées. La structure « pseudo-symétrique » du système de rift paraît influencer de manière significative la localisation de la contrainte compressive. Le bassin de Mauléon est inversé pour former une structure de type « pop-up » dans laquelle les deux bordures présentent des styles de réactivation différents. Dans le modèle d'évolution proposé, le chevauchement du Lakhoura réactive le détachement cénomanien qui correspond à la dernière structure extensive du rift. Il est responsable du sous-charriage vers le nord d'une partie de la marge proximale ibérique. Au nord de la structure de Saint-Palais, le niveau de décollement triasique favorise l'édification d'un empilement de nappes de couverture (« thin-skin »). Dans le socle, la zone de « necking » abrupte européenne, délimité par le paléo-escarpement de Saint-Palais, joue le rôle de buttoir induisant le sous charriage de la marge proximale et formant un empilement de nappes crustales. Cette accrétion tectonique en base de croûte européenne induit une verticalisation du contact croûte / manteau (sous la paléo-marge européenne) et empêche tout déplacement majeur sur la portion septentrionale du chevauchement de Lakhoura. Vers le sud, la flexuration de la croûte ibérique entraine le développement du bassin d'avant pays sud pyrénéen. Dans le socle, les chevauchements de Gavarnie et de Guarga sont incorporés dans l'empilement de nappes crustales formant l'antiforme de la Zone Axiale. Ces chevauchements « thick-skin » ont conduit à la verticalisation du contact croûte continentale / manteau le long de l'Ibérie. Ce processus accentue la protubérance mantélique existante sous le rift antérieur. Ce buttoir mantélique, en étant soulevé tout au long de l'édification du système orogénique, a ainsi favorisé la préservation actuelle de ce rift hyper-étiré.

La restauration de cette coupe suggère également que les structures extensives crétacée à elles-seules ne suffisent pas à expliquer l'amincissement de la croûte continentale à la fin du rifting. L'étude du bassin permien de Bidarray et du dôme granulitique de l'Ursuya fournit d'important enseignements quant à la l'état de la lithosphère dans ce domaine avant le rifting crétacé. Elle conduit à remettre en question les précédant travaux considérant les granulites de l'Ursuya comme une portion de croûte inférieure exhumée et dénudée lors de la phase d'hyperextension crétacée (Jammes et al., 2009 ; Masini et al., 2014). La lithosphère continentale apparaît avoir été affecté pendant le Permien par une phase d'amincissement en cisaillement pur, induisant de manière synchrone : (1) le développement de failles normales conjuguées au sein de la croûte supérieure et (2) le fluage longitudinal de la croûte inférieure partiellement fondue. Cette première étape d'amincissement crustal est considérée comme responsable de l'initiation de l'exhumation des granulites au sein d'un dôme métamorphique. Dans un second temps, l'instabilité induite par la flottabilité de la croûte inférieure ductile engendre son fluage vertical en direction de la zone d'amincissement de la croûte supérieure, amorçant le développement d'un complexe à noyau métamorphique (« MCC »). L'exhumation des granulites dans la croûte supérieure est alors rendue possible par la localisation de la déformation dans le détachement de Louhossoa de direction N120°. Dans ce nouveau modèle, la formation du graben de Bidarray et du dôme de l'Ursuya s'inscrit dans le passage de la convergence N-S enregistrée dans la zone axiale pyrénéenne de 310 à 290 Ma (Denèle et al., 2007, 2009; Cochelin et al., 2017, 2018a, 2018b) à une

phase d'extension E-W prenant place entre 290 et 275 Ma. Cet épisode géodynamique permien confère donc des caractéristiques thermique (gradient élevé), structurale (déformation cassante localisée dans la croûte supérieure et croûte continentale amincie) et rhéologique (granulites en position de croûte supérieure) complexe à la lithosphère des Pyrénées occidentales avant le rifting crétacé.

Ces travaux montrent également que les discontinuités structurales N20°, connues pour jouer un rôle majeur durant le rifting crétacé, sont héritées du Permien. Le bassin de Bidarray et le dôme de l'Ursuya sont préservés et alignés dans la zone de transfert de Pamplona qui sépare deux branches du rift crétacé : le bassin de Mauléon et le bassin basco-cantabrique. Cette zone de transfert de direction N20° apparait ainsi comme une structure lithosphérique permienne réactivée lors du rifting crétacé. La préservation des dépôts permo-triasiques du bassin de Bidarray dans les massifs basques interdit tout décrochement sénestre E-W de grande ampleur entre les plaques ibérique et européenne dans ce domaine des massifs basques.

En parallèle, la réalisation d'un modèle 3D utilisant un algorithme de modélisation implicite implémenté dans le logiciel GeoModeller a soulevé de nombreuses questions, quant au rôle de ces zones de transfert qui semble être héritées du Permien sur la géométrie 3D du « pop-up » de Mauléon. Cette modélisation, qui s'appuie sur l'interprétation de lignes sismiques E-W, de données de thermométrie Raman et de mesure de mesures structurales sur le terrain, a permis d'interpréter le rôle de ces linéaments au cours de l'orogenèse alpine. Ces zones de transferts délimitent des corridors de déformation séparant des compartiments dont la quantité de raccourcissement diffère. Les systèmes de chevauchement bordant au sud et au nord le bassin de Mauléon sont composés de plusieurs segments. Ces segments de chevauchement antithétiques se branchent sur les zones de transferts N20° et définissent un système en « tiroirs » permettant la fermeture, par étapes, de l'ancien rift. Ce mode de déformation compressif est responsable du caractère non cylindrique des structures de la zone-pyrénéenne résultant de l'inversion alpine du bassin de Mauléon.

L'étude des paléotempératures Raman sur échantillons de surface et subsurface met en évidence que les paléo-gradients géothermiques anormalement élevés coïncident avec le domaine hyper-étiré du bassin de Mauléon. Ils augmentent de manière centripète et graduelle depuis les marges proximales (~ 34°C/km) jusqu'au domaine hyper-étiré (~ 57-60°C/km). Contrairement au modèle de thermicité récemment proposé qui considère de grandes similitudes avec les marges asymétriques alpines et atlantiques (Lescoutre et al., 2019), la thermicité synrift du bassin de Mauléon reflètent le caractère pseudo-symétrique de ce rift. La température maximale atteinte par les séries sédimentaires dans la partie la plus profonde du bassin résulte de l'enfouissement (~8 km) et du flux thermique mantélique estimé par modélisation thermique à 100 mW/m^2 pour un gradient de 60°C/km. Ce gradient élevé a perduré à minima jusqu'au Campanien, soulevant la question du processus responsable de la subsidence au cours du Crétacé supérieur, jusqu'ici considérée comme une subsidence thermique postrift classique.

Les isothermes issus de la phase de rifting ont été ensuite déformés et plissés lors de la compression alpine. Sur la marge européenne, les isothermes crétacés sont préservés et transportés passivement sur le domaine sud-aquitain. Par contre, la marge ibérique enregistre une thermicité post-collisionnelle. La différence de réponse thermique entre marge sud et nord découle du style de déformation au cours de l'inversion. La marge ibérique est affectée par une déformation de type « thick-skin », responsable de l'augmentation du gradient géothermique. Au contraire, le domaine hyper-étiré et la marge européenne enregistrent une décroissance du gradient géothermique depuis l'amorce de la compression, comme en témoigne le gradient actuel mesuré dans les puits ~ 25.0 ± 2.7°C/km. Ce faible gradient peut s'expliquer par une épaisseur faible à moyenne de la croûte continentale (de 5 à 25 km), autrement dit par la présence d'un manteau sous-continental à faible profondeur lié à l'hyperextension crétacée. En 3D, les zones de transfert N20° héritées du permien sont responsables d'une segmentation de la thermicité synrift dans le domaine hyper-étiré et des températures post-collisionnelle mesurée sous le chevauchement du Lakhoura.

La structure et l'évolution tectono-sédimentaire crétacée du bassin de Mauléon, mais aussi des bassins d'Arzacq et de Tartas situés dans le domaine aquitain ont été comparées à celles de plusieurs bassins mésozoïques situés à proximité de la limite entre la plaque européenne et le bloc ibérique, et décrits dans la bibliographie : bassin de Parentis (Pinet et al., 1987; Bois and Courtillot, 1988 ; Bois and ECORS Scientific team, 1990; Bois et al., 1997 ; Jammes et al., 2010 ; Tugend et al., 2014), bassin basco-cantabrique (DeFelipe et al., 2017; Pedrera et al., 2017; Ducoux et al., 2019), bassin de Camèros (Mas et al., 1993, 2011; Guimerà et al., 1995; Casas-Sainz and Gil-Imaz, 1998; Casas et al., 2009; García-Lasanta et al., 2017; Omodeo-Salé et al., 2017; Rat et al., 2019), bassin de Columbrets (Salas et al., 2001; Nebot and Guimerà, 2016; Etheve et al., 2018 ; Roma et al., 2018) et bassins nord pyrénéens des Pyrénées centrales et orientales (Lagabrielle and Bodinier, 2008; Lagabrielle et al., 2010; Clerc and Lagabrielle, 2014; Clerc et al., 2014; de Saint Blanquat et al., 2016; Espurt et al., 2019).

Ils présentent de nombreuses similitudes avec les bassins de Mauléon, Arzacq et Tartas :

(1) ils se forment entre le Jurassique supérieur et le Crétacé inférieur par un processus d'hyper-extension affectant une croûte continentale préalablement amincie entre le Permien et le Jurassique,

(2) ils sont caractérisés par une importante épaisseur de dépôts prérift à synrift, un paléo-gradient géothermique et/ou un flux de chaleur mantellique synrift élevé responsable d'un métamorphisme HT/BP dans la partie la plus profonde du bassin,

(3) leur domaine hyper-aminci coïncide généralement, dans certains secteurs peu raccourcis, avec une anomalie gravimétrique positive interprétée comme étant liée à la présence du manteau sous-continental à relative faible profondeur,

(4) dans le domaine hyper-étiré, la croûte inférieure est très fine ou absente,

(5) les structures extensives sont partitionnées entre le socle / la croûte supérieure et la couverture prérift du fait de la présence d'épaisses formations argilo-évaporitiques du Trias supérieur,

(6) ils se caractérisent par un important phénomène de glissement de couverture le long de ce niveau de décollement triasique,

(7) ils présentent une géométrie pseudo-symétrique.

Ces bassins subissent donc une évolution extensive commune, polyphasée et peuvent être classés en fonction du taux d'amincissement de la croûte continentale, du moins aminci au plus aminci : (1) bassin de Tartas, (2) bassins d'Arzacq, Columbrets et Camèros, (3) bassin de Parentis, (4) bassins basco-cantabrique et de Mauléon, (5) bassins nord-pyrénéens des Pyrénées centrales et orientales. Ils ont été récemment rassemblés sous le terme de « smooth-slope type extensional basins » (Lagabrielle et al., 2019 ; **Annexe 1**).

Dans le modèle proposé, trois grandes phases d'amincissement sont distinguées de manière à rendre compte de la complexité géométrique et de l'amincissement crustal de ce type de rift. Dans les premiers stades d'amincissement de la croûte continentale, la déformation extensive est contrôlée par la présence de deux niveaux de découplage/décollement non connectés correspondant à la croûte moyenne et aux évaporites du Trias supérieur. Le premier permet un découplage de la déformation entre la croûte supérieure et inférieure, tandis que le second permet le découplage de la déformation entre la croûte supérieure et les séries sédimentaires mésozoïques. L'amincissement ductile de la croûte inférieure, sans déformation cassante significative dans la croûte supérieure, s'accompagne de la formation d'un bassin de rift symétrique de type sag. Au cours de cette étape, le profil de dépôt entre les marges et l'axe du bassin est relativement symétrique et peu profond comme en témoigne le développement de plateformes carbonatées et l'absence de dépôt turbiditique. Au fur et à mesure de l'extraction latérale de la croûte inférieure (amincissement), les bordures du rift s'inclinent en direction du bassin provoquant le glissement de la couverture prerift. Des plis et des diapirs

accompagnent ce glissement de couverture. Ce décollement entraine une dénudation des marges proximales du rift. Après cette dénudation de la crôute supérieure et la soustraction tectonique de la croûte inférieure, les marges proximales subissent une déformation fragile tandis que le futur domaine hyper-étiré enregistre un amincissement ductile de la croûte supérieure engendrant la formation d'un rift sensiblement symétrique. Cette différence de style de déformation entre les marges et le domaine central est directement liée à l'augmentation de la température dans la partie axiale la plus profonde du bassin. Celle-ci est due à l'enfouissement de la croûte continentale du domaine hyper-étiré sous une série sédimentaire synrift épaisse, et à un flux thermique anormal au cœur du bassin. Au cours de cette phase ultime d'hyperextension, la subsidence au centre du bassin est accrue. Le profil de dépôt s'incline de manière significative. Les pentes sédimentaires deviennent plus abruptes et une importante sédimentation gravitaire se met en place dans le bassin profond. La sédimentation contrôle donc très clairement le style de déformation extensive le long de ce type de système hyper-étiré qui nécessitent à la fois un niveau de décollement évaporitique prérift et une importante épaisseur de séries sédimentaires synrifts pour se développer.

Les apparences étant parfois trompeuses, les bassins listés précédemment présentent de nombreuses différences avec les marges passives hyper-étirées de type atlantique. En effet, les reconstructions paléogéographiques mettent en évidence le lien étroit entre la distribution des évaporites du Trias et la répartition des « smooth-slope type extensional basins ». Ces derniers sont affectés par une déformation découplée, contrairement aux marges atlantiques qui se caractérisent par le développement de blocs basculés et d'allochtones au droit desquels la couverture prérift est solidaire du socle. De plus, les marges atlantiques et alpines sont caractérisées par une exhumation de la croûte inférieure dans le domaine hyper-étiré. Des études récentes (Denèle et al., 2007, 2009; Cochelin et al., 2017, 2018a, 2018b ; cf. chapitre. 2.2) tendent à montrer que l'exhumation des granulites pyrénéennes s'est produite entre le Carbonifère supérieur et le Permien, à l'instar des granulites de l'Ursuya. En effet, dans les « smooth-slope type extensional basins », la croûte inférieure est soustraite et amincie de manière ductile dès les prémices de l'extension. Bien que ces deux types de domaine hyper-étiré se développent sous des conditions de flux mantélique et de gradient thermique élevé, les systèmes alpins et atlantiques n'enregistrent pas de métamorphisme syn-extensif HT/BP significatif. Par opposition, les « smooth-slope type extensional basins » subissent une déformation ductile de la croûte continentale et de la pile sédimentaire dans le domaine hyper-étiré (métamorphisme HT/BP) tandis que les marges alpines et atlantiques, dépourvues de séries sédimentaires épaisse (« starved margins »), subissent une déformation cassante dans ce même domaine. Ces travaux de thèse mettent ainsi en évidence le contrôle de la sédimentation sur les processus d'extension qui régissent l'amincissement de la coûte continentale, et amènent, de fait, de nouvelles clés de lecture des rifts hyper-étirés.

References

Bois, C., Courtillot, V., 1988. Deep Seismic Profiling of the Crust and Evolution of the Lithosphere 69, 987–988.

Bois, C., ECORS Scientific team, 1990. Major geodynamic processes studied from the ECORS deep seismic profiles in France and adjacent areas. Tectonophysics 173, 397–410.

Bois, C., Gabriel, O., Lefort, J.-P., Rolet, J., Brunet, M.-F., Masse, P., Olivet, J.-L., 1997. Geologic contribution of the Bay of Biscay deep seismic survey: a summary of the main scientific results, a discussion of the open questions and suggestions for further investigation. Mém Soc Géol Fr. 193–309.

Casas, A.M., Villalaín, J.J., Soto, R., Gil-Imaz, A., del Río, P., Fernández, G., 2009. Multidisciplinary approach to an extensional syncline model for the Mesozoic Cameros Basin (N Spain). Tectonophysics 470, 3–20. https://doi.org/10.1016/j.tecto.2008.04.020

Casas-Sainz, A.M., Gil-Imaz, A., 1998. Extensional subsidence, contractional folding and thrust inversion of the eastern Cameros basin, northern Spain. Geol. Rundsch. 86, 802–818. https://doi.org/10.1007/s005310050178

Clerc, C., Boulvais, P., Lagabrielle, Y., de Saint Blanquat, M., 2014. Ophicalcites from the northern Pyrenean belt: a field, petrographic and stable isotope study. Int. J. Earth Sci. 103, 141–163. https://doi.org/10.1007/s00531-013-0927-z

Clerc, C., Lagabrielle, Y., 2014. Thermal control on the modes of crustal thinning leading to mantle exhumation: Insights from the Cretaceous Pyrenean hot paleomargins. Tectonics 33, 1340–1359. https://doi.org/10.1002/2013TC003471

Cochelin, B., D. Chardon, Y. Denèle, C. Gumiaux, and B. Le Bayon, 2017, Vertical strain partitioning in hot Variscan crust: Syn-convergence escape of the Pyrenees in the Iberian-Armorican syntax: Bulletin de la Société Géologique de France, v. 188, no. 6, 39, doi:10.1051/bsgf/2017206

Cochelin, B., Lemirre, B., Denèle, Y., Blanquat, M. de S., Lahfid, A., Duchêne, S., 2018a, Structural inheritance in the central Pyrenees: the variscan to Alpine tectonometamorphic evolution of the axial zone. J. Geol. Soc., v. 175, 336–351, doi:10.1144/jgs2017-066.

Cochelin, B., Gumiaux, C., Chardon, D., Denèle, Y., Le Bayon, B., 2018b, Multi-scale strainfield analysis using geostatistics: Investigating the rheological behavior of the hot Variscan crust of the Pyrenees (Axial Zone). J. Struct. Geol., v. 116, 114–130, doi:10.1016/j.jsg.2018.07.024

DeFelipe, I., Pedreira, D., Pulgar, J.A., Iriarte, E., Mendia, M., 2017. Mantle exhumation and metamorphism in the Basque-Cantabrian Basin (NSpain): Stable and clumped isotope analysis in carbonates and comparison with ophicalcites in the North-Pyrenean Zone (Urdach and Lherz). Geochem. Geophys. Geosystems 18, 631–652. https://doi.org/10.1002/2016GC006690

Denèle, Y., Olivier, P., Gleizes, G., Barbey, P., 2007. The Hospitalet gneiss dome (Pyrenees) revisited: lateral flow during Variscan transpression in the middle crust, Terra Nova, v. 19, 445–453, doi:10.1111/j.1365-3121.2007.00770.x.

Denèle, Y., Olivier, P., Gleizes, G., Barbey, P., 2009. Decoupling between the middle and upper crust during transpression-related lateral flow: variscan evolution of the Aston gneiss dome (Pyrenees, France), Tectonophysics, v. 477, 244–261, doi:10.1016/j.tecto.2009.04.033.

de Saint Blanquat, M., Bajolet, F., Grand'Homme, A., Proietti, A., Zanti, M., Boutin, A., Clerc, C., Lagabrielle, Y., Labaume, P., 2016. Cretaceous mantle exhumation in the central Pyrenees: New constraints from the peridotites in eastern Ariège (North Pyrenean zone, France). Comptes Rendus Geosci. 348, 268–278. https://doi.org/10.1016/j.crte.2015.12.003

Ducoux, M., Jolivet, L., Callot, J. -P., Aubourg, C., Masini, E., Lahfid, A., Homonnay, E., Cagnard, F., Gumiaux, C., Baudin, T., 2019. The Nappe des Marbres unit of the Basque-Cantabrian Basin: the tectono-thermal evolution of a fossil hyperextended rift basin. Tectonics 2018TC005348. https://doi.org/10.1029/2018TC005348

Espurt, N., Angrand, P., Teixell, A., Labaume, P., Ford, M., de Saint Blanquat, M., Chevrot, S., 2019. Crustal-scale balanced cross-section and restorations of the Central Pyrenean belt (Nestes-Cinca transect): Highlighting the structural control of Variscan belt and Permian-Mesozoic rift systems on mountain building. Tectonophysics 764, 25–45.

Etheve, N., Mohn, G., Frizon de Lamotte, D., Roca, E., Tugend, J., Gómez-Romeu, J., 2018. Extreme Mesozoic Crustal Thinning in the Eastern Iberia Margin: The Example of the Columbrets Basin (Valencia Trough). Tectonics 37, 636–662.

García-Lasanta, C., Casas-Sainz, A., Villalaín, J.J., Oliva-Urcia, B., Mochales, T., Speranza, F., 2017. Remagnetizations used to unravel large-scale fold kinematics: A case study in the Cameros Basin (Northern Spain): Unfolding in Basin Inversion. Tectonics 36, 714–729. https://doi.org/10.1002/2016TC004459

Guimerà, J., Alonso, Á., Mas, J.R., 1995. Inversion of an extensional-ramp basin by a newly formed thrust: the Cameros basin (N. Spain). Geol. Soc. Lond. Spec. Publ. 88, 433–453. https://doi.org/10.1144/GSL.SP.1995.088.01.23

Jammes, S., G. Manatschal, L. Lavier, and E. Masini, 2009, Tectono-sedimentary evolution related to extreme crustal thinning ahead of a propagating ocean: Example of the western Pyrenees: Tectonics, v. 28, no. 4, doi:10.1029/2008TC002406.

Jammes, S., Manatschal, G., Lavier, L., 2010. Interaction between prerift salt and detachment faulting in hyperextended rift systems: The example of the Parentis and Mauléon basins (Bay of Biscay and western Pyrenees). AAPG Bull. 94, 957–975. https://doi.org/10.1306/12090909116

Lagabrielle, Y., Bodinier, J.-L., 2008. Submarine reworking of exhumed sub-continental mantle rocks: field evidence from the Lherz peridotites, French Pyrenees: Cretaceous exhumation of pyrenean mantle. Terra Nova 20, 11–21. https://doi.org/10.1111/j.1365-3121.2007.00781.x

Lagabrielle, Y., Labaume, P., de Saint Blanquat, M., 2010. Mantle exhumation, crustal denudation, and gravity tectonics during Cretaceous rifting in the Pyrenean realm (SW Europe): Insights from the geological setting of the lherzolite bodies. Tectonics 29. https://doi.org/10.1029/2009TC002588

Lavier, L. L., and G. Manatschal, 2006, A mechanism to thin the continental lithosphere at magma-poor margins: Nature, v. 440, no. 7082, p. 324–328, doi:10.1038/nature04608.

Lescoutre, R., Tugend, J., Brune, S., Masini, E., Manatschal, G., 2019. Thermal Evolution of Asymmetric Hyperextended Magma-Poor Rift Systems: Results From Numerical Modeling and Pyrenean Field Observations. Geochem. Geophys. Geosystems 2019GC008600. https://doi.org/10.1029/2019GC008600

Manatschal, G., Froitzheim, N., Rubenach, M., Turrin, B.D., 2001. The role of detachment faulting in the formation of an ocean-continent transition: insights from the Iberia Abyssal Plain. Geol. Soc. Lond. Spec. Publ. 187, 405–428. https://doi.org/10.1144/GSL.SP.2001.187.01.20

Manatschal, G., Müntener, O., Lavier, L.L., Minshull, T.A., Péron-Pinvidic, G., 2007. Observations from the Alpine Tethys and Iberia–Newfoundland margins pertinent to the interpretation of continental breakup. Geol. Soc. Lond. Spec. Publ. 282, 291–324. https://doi.org/10.1144/SP282.14

Mas, J.R., Alonso, A., Guimerà, J., 1993. Evolución tectonosedimentaria de una cuenca extensional intraplaca: la cuenca finijurásica–eocretácica de Los Cameros (La Rioja–Soria). Rev. Soc. Geológica Esp. 6, 129–144.

Mas, R., Benito, M.I., Arribas, J., Alonso, A., Arribas, M.E., Lohmann, K.C., González-Acebrón, L., Hernán, J., Quijada, E., Suárez, P., 2011. Evolution of an intra-plate rift basin: the latest Jurassic-early Cretaceous Cameros basin (Northwest Iberian ranges, North Spain). Geo-Guías 8, 117–154.

Masini, E., G. Manatschal, J. Tugend, G. Mohn, and J.-M. Flament, 2014, The tectono-sedimentary evolution of a hyper-extended rift basin: the example of the Arzacq–Mauléon rift system (Western Pyrenees, SW France): International Journal of Earth Sciences, v. 103, no. 6, p. 1569–1596, doi:10.1007/s00531-014-1023-8.

Nebot, M., Guimerà, J.J., 2016. Structure of an inverted basin from subsurface and field data: the Late Jurassic-Early Cretaceous Maestrat Basin (Iberian Chain). Geol. Acta 14, 0155–177.

Omodeo-Salé, S., Salas, R., Guimerà, J., Ondrak, R., Mas, R., Arribas, J., Suárez-Ruiz, I., Martinez, L., 2017. Subsidence and thermal history of an inverted Late Jurassic-Early Cretaceous extensional basin (Cameros, North-central Spain) affected by very low- to low-grade metamorphism. Basin Res. 29, 156–174. https://doi.org/10.1111/bre.12142

Pedrera, A., García-Senz, J., Ayala, C., Ruiz-Constán, A., Rodríguez-Fernández, L.R., Robador, A., González Menéndez, L., 2017. Reconstruction of the exhumed mantle across the North Iberian Margin by crustal-scale 3-D gravity inversion and geological cross section. Tectonics 36, 3155–3177.

Péron-Pinvidic, G., G. Manatschal, T. A. Minshull, and D. S. Sawyer, 2007, Tectono-sedimentary evolution of the deep Iberia-Newfoundland margins: Evidence for a complex breakup history: Tectonics, v. 26, no. 2, p. 1–19, doi:10.1029/2006TC001970.

Pinet, Bertrand, Montadert, L., ECORS Scientific Party, 1987. Deep seismic reflection and refraction profiling along the Aquitaine shelf (Bay of Biscay). Geophys. J. Int. 89, 305–312. https://doi.org/10.1111/j.1365-246X.1987.tb04423.x

Rat, J., Mouthereau, F., Brichau, S., Crémades, A., Bernet, M., Balvay, M., Ganne, J., Lahfid, A., Gautheron, C., 2019. Tectonothermal Evolution of the Cameros Basin: Implications for Tectonics of North Iberia. Tectonics 38, 440–469. https://doi.org/10.1029/2018TC005294

Roma, M., Ferrer, O., Roca, E., Pla, O., Escosa, F.O., Butillé, M., 2018. Formation and inversion of salt-detached ramp-syncline basins. Results from analog modeling and application to the Columbrets Basin (Western Mediterranean). Tectonophysics 745, 214–228. https://doi.org/10.1016/j.tecto.2018.08.012

Salas, R., Guimerà, J., Mas, R., Martín-Closas, C., Meléndez, A., Alonso, A., 2001. Evolution of the Mesozoic central Iberian Rift System and its Cainozoic inversion (Iberian chain). Peri-Tethys Mem. 6, 145–185.

Teixell, A., P. Labaume, and Y. Lagabrielle, 2016, The crustal evolution of the west-central Pyrenees revisited: Inferences from a new kinematic scenario: Comptes Rendus Geoscience, v. 348, no. 3–4, p. 257–267, doi:10.1016/j.crte.2015.10.010.

Tugend, J., Manatschal, G., Kusznir, N.J., Masini, E., Mohn, G., Thinon, I., 2014. Formation and deformation of hyperextended rift systems: Insights from rift domain mapping in the Bay of Biscay-Pyrenees. Tectonics 33, 1239–1276. https://doi.org/10.1002/2014TC003529

Whitmarsh, R.B., Manatschal, G., Minshull, T.A., 2001. Evolution of magma-poor continental margins from rifting to seafloor spreading. Nature 413, 150–154. https://doi.org/10.1038/35093085

Annexe.1

A review of Cretaceous smooth-slopes-extensional basins along the Iberia-Eurasia plate boundary: how prerift salt controls the modes of continental rifting and mantle exhumation

Annexe 1. A review of Cretaceous smooth-slopes-extensional basins along the Iberia-Eurasia plate boundary: how prerift salt controls the modes of continental rifting and mantle exhumation

Sommaire

Abstract p. 407

1. Introduction p. 407

2. Symmetrical, smooth-slopes basins of the north Iberia margin: insights from the North Pyrenean Zone (NPZ) and the Basque-Cantabrian range p. 408

3. A review of smooth-slopes basins in the surroundings of the Pyrenees-Cantabrian Mountains p. 415

3.1. Parentis basin p. 415

3.2. South Bay of Biscay margin p. 415

3.3. North-eastern Iberia intra-crustal basins: Iberian Chain and Valencia trough p. 417

4. Evolution of smooth-slopes basins: some rheological considerations p. 417

4.1. Symmetrical smooth-slopes basins: simple or pure shear-dominated structures? p. 417

4.2. Smooth-slopes basins: crustal shear zones and lenticular fabrics at the mesoscale p. 419

4.3. Contrast between Iberian-Alpine and Pyrenean rifts: role of a basement-cover décollement p. 423

5. Discussion p. 424

5.1. Smooth-slopes basins formation, insights for the evolution of passive continental margins. p. 424

5.2. Comparison with thermo-mechanical models of crustal hyper-extension. p. 427

5.3. The prerift salt and clay décollement layer: a key factor for the evolution of smooth-slopes basins. Establishing a new link between Triassic paleogeography and rifting mechanisms. p. 428

5.4. Time-dependent rheology during the evolution of smooth-slopes basins p. 431

6. Conclusions p. 433

Acknowledgements p. 434

References p. 435

Annexe 1. A review of Cretaceous smooth-slopes-extensional basins along the Iberia-Eurasia plate boundary: how prerift salt controls the modes of continental rifting and mantle exhumation

Lagabrielle, Y., Asti, R., Duretz, T., Clerc, C., Fourcade, S., Teixell, A., Labaume, L., Corre, B., and Saspiturry, N., **accepted**, A review of Cretaceous smooth-slopes-extensional basins along the Iberia-Eurasia plate boundary: how prerift salt controls the modes of continental rifting and mantle exhumation: ***Earth Science Review***.

Abstract

This article points out for the first time a striking correlation between the paleogeography of Upper Triassic deposits and the mode of crustal stretching around and inside the Northern Iberia plate during the Cretaceous transtensional event. First, we propose a review of the architecture of the basins, which opened during the mid-Cretaceous times along the Iberia-Eurasia plate boundary. Similarly to the emblematic Parentis basin, these basins exhibit a peculiar synclinal-shaped profile and are devoid of prominent block faulting. The top of the basement is characterized by gentle slopes, which dip symmetrically towards the center of the basins. As revealed by recent comparisons with geologically-constrained rifting models established from the North Pyrenean Zone, this architecture results from the thinning of a heterogeneous continental crust under greenschist facies conditions. Basement deformations are thus dominantly ductile and are characterized by large-scale boudinage, hyper-thinning and subsequent lateral extraction. Bulk deformation of the upper and middle crust leads to the formation of anastomosed shear zones and the development of mylonitic fabric. Tectonic lenses consisting of crustal material remain welded on top of the exhuming mantle. The common character shared by all the prerift sequences of the studied basins is the presence of a thick low-strength Upper Triassic evaporites and clays layer belonging to the Keuper group (i.e. prerift salt and clay unit). In the studied basins, efficient décollement along the prerift salt and clay unit triggers mechanical decoupling and gliding of the prerift cover that remains in the center of the basin. Thus, during the early rifting phase, the basement undergoes thinning while the prerift cover remains preserved in the basin center. In response to hyper-thinning and horizontal extraction of the continental crust, hot mantle is exhumed beneath the pre- and synrift cover. Subsequent thermal exchange (i) promotes ductile deformation of the basement and (ii) induces the development of HT-LP metamorphic conditions in the prerift sediments and at the base of the synrift flysch units. This thermal event is well recorded in the axial portion of the Pyrenean realm (future North Pyrenean Zone) as well as in the prerift sediments of the Cameros basin (northern Spain). The architecture of the smooth-slopes type basins thus contrasts with the structure of Iberia-Newfoundland Atlantic margins which are characterized by (i) top-basement detachment faults accommodating crustal extension through rotation and translation of undeformed basement blocks, and (ii) the individualization of continental extensional allochthons tectonically emplaced over exhumed lower crust or mantle rocks. Finally, using recent paleogeographic reconstructions, we show that the distribution of the prerift salt and clay unit remarkably matches the distribution of the Pyrenean and peri-Pyrenean smooth-slopes type basins. This allows for the first time to propose a genetic link between the distribution of evaporite-bearing prerift sedimentary formations and the development of smooth-slopes basins.

1. Introduction

More than 30 years ago, important steps in our understanding of the mechanisms of continental rifting were achieved through the acquisition and interpretation of ECORS seismic reflection profiles (1983-1994) (Damotte et al., 1998) **(Fig. 1)**. New images of crustal and Moho geometries beneath stretched continental crust were obtained, shedding light on important discrepancies between structural patterns of rift systems. In particular, the ECORS profiles from the Rhine graben and the Parentis basin displayed contrasting images of the thinned upper lithosphere. In the first case, the upper crust appears clearly rifted and offset by stepping normal faults (Brun et al., 1991) whilst, despite slight tectonic inversion, the second case exhibits a smooth basement top, with gentle slopes dipping symmetrically towards the basin center (Bois et al., 1997). Because only few cases of Parentis-type

architecture were observed worldwide, little attention has been paid to this symmetrical, smooth-slopes type continental rifts, which apparently lacks major upper crustal faulting and block tilting. Rather, based on the emblematic case of the Iberia-Newfoundland conjugate margins, most of the current models of rift-related crustal thinning are characterized by tilted continental blocks and prominent detachment faulting **(Fig. 2)**. Such architecture indicates that the upper crustal levels behave under a dominant brittle mode in the proximal (or continentward) as well as in the distal (or oceanward) margin domains. In such models, shallow detachment faults accommodate upper crustal extension through the rotation and the translation of undeformed basement blocks. In the distal margin, these blocks, referred to as extensional allochthons, are covered by synrift and postrift sediments and may lie tectonically over exhumed units, including subcontinental mantle (Reston et al., 1995; Manatschal et al., 2001; Jammes et al., 2010c; Osmundsen and Péron-Pinvidic, 2018, and references therein).

Recent geological investigations in the northern units of the Pyrenean belt forming the North Pyrenean Zone (NPZ) as well as in the Basque-Cantabrian basin **(Fig. 1)** show that Parentis-type, smooth-slopes basins of mid-Cretaceous age were distributed along most of the boundary between the northern Iberia and southern Eurasia plates, thus introducing doubts regarding the ubiquitous character of Iberia-Newfoundland-type margins (Lagabrielle et al., 2010; Clerc and Lagabrielle, 2014; Teixell et al., 2016; 2018; Asti et al., 2019). In this article, we first list the main characteristics of these smooth-slopes basins, based on the analysis of detailed geological reconstructions from areas exposed all along the northern flank of the Pyrenean belt. We then review the distribution of such basins at the scale of the Iberia and Eurasia plates. We finally discuss some of the key-factors controlling the evolution of smooth-slopes basins and we evaluate how such information increases the understanding of the mechanisms of continental rifting and passive margin formation.

2. Symmetrical, smooth-slopes basins of the north Iberia margin: insights from the North Pyrenean Zone (NPZ) and the Basque-Cantabrian range

The Pyrenees and the Cantabrian mountain **(Fig. 1)** form a narrow, N110 trending fold-and-thrust belt resulting from the collision of the northern edge of the Iberia plate (north Iberia margin) with the southern edge of the Eurasia plate during the Late Cretaceous-Tertiary (Choukroune and ECORS team, 1989; Muñoz, 1992; Deramond et al., 1993; Roure and Choukroune, 1998; Teixell, 1998; Vergés and Garcia-Senz, 2001; Pedrera et al., 2017; Teixell et al., 2018). Convergence initiated ca. 83 Ma, following an almost 40 Ma long period of transtensional motion in relation with the counterclockwise rotation of Iberia relative to Eurasia, also leading to oceanic spreading in the Bay of Biscay between Chron M0 and A33o (ca. 125-83 Ma) (Le Pichon et al., 1971; Choukroune and Mattauer, 1978; Olivet, 1996; Sibuet et al., 2004). Convergence led to the partial or complete tectonic inversion of discontinuous Cretaceous rift basins opened along the Iberia-Eurasia plate boundary during the transtensional episode (Puigdefàbregas and Souquet, 1986; Debroas, 1990). Rotation was achieved just before the Albian according to paleomagnetic data collected inland (Gong et al., 2008). Earlier Triassic and Jurassic rifting events preceded the development of the Cretaceous rifts (Canérot, 2017, and references therein).

Along the northern flank of the Pyrenees, more than forty, up to km-sized exposures of subcontinental lherzolites are widespread within the Mesozoic prerift and synrift sediments forming the NPZ (Monchoux, 1970; Vielzeuf and Kornprobst, 1984; Fabriès et al., 1991, 1998). The NPZ is bounded by two major outward-verging thrusts, the North Pyrenean Fault (NPF)/Lakhoura thrust to the South and the North Pyrenean Frontal Thrust (NPFT) to the North. The NPF represents the tectonic boundary between the NPZ and the prominent axial zone of the belt (AZ) constituted of a stack of Paleozoic basement units (Choukroune, 1976a; 1976b; Choukroune et Mattauer, 1978).

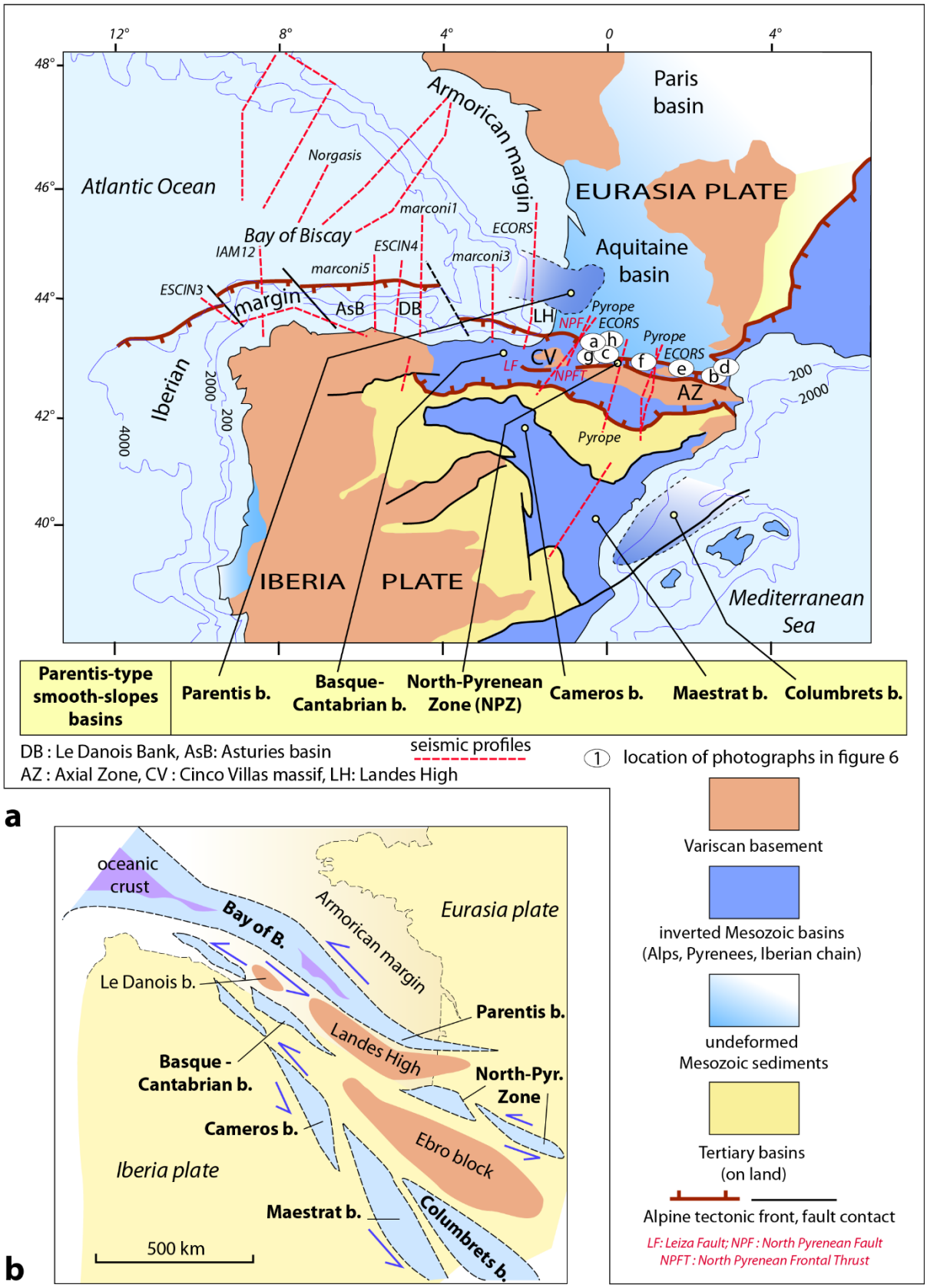


Fig. 1. Location of the studied basins and their paleogeographic position during the Cretaceous at the onset of the Iberia drift. **(A)** Simplified structural map of the Cantabrian-Pyrenean orogenic system and adjoining Iberia showing Eurasia deformed and undeformed domain (modified from Verges and Garcia-Senz, 2001 and Teixell et al., 2018). **(B)** Hypothetical reconstruction at the onset of the Iberia drift (modified after Tugend et al., 2014).

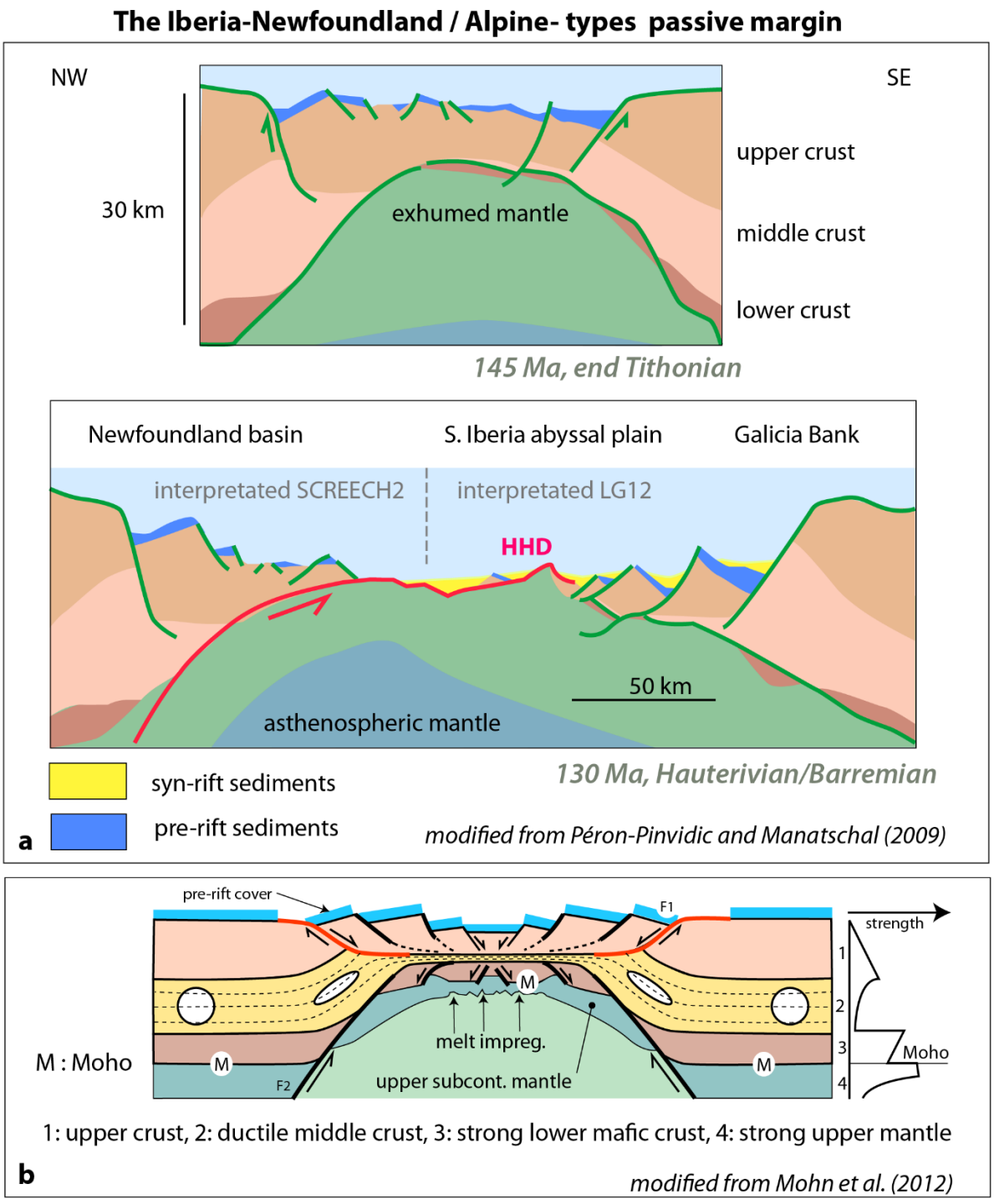


Fig 2. Structure and evolution of Iberia-Newfoundland-type and Alpine-type passive margins (modified from Péron-Pinvidic and Manatschal, 2009 and Mohn et al., 2012). **(A)** two sketches showing the main concepts linked to Iberia-Newfoundland-type margin evolution, namely: (i) strong final asymmetry with upper and lower plates separated by a single detachment fault (HHD, Hobby High detachment), (ii) emplacement of extensional allochthons as rigid crustal blocks over the exhumed mantle. **(B)** strain distribution and strain partitioning during lithospheric thinning at magma-poor rifted margin, with example from the fossil Alpine Tethys margin. In this model, the pre-rift cover remains welded on the tilted crustal blocks; the middle crust is thinned to zero and the upper crust and upper mantle are juxtaposed at the break up stage.

Based on field and geophysical evidence from the central and western NPZ, exhumation of sub-continental mantle is shown to have occurred coevally with extreme thinning of the continental crust in the Pyrenean realm during the mid-Cretaceous (Lagabrielle and Bodinier, 2008; Jammes et al., 2009; Masini et al., 2014). Therefore, mantle exhumation (locally followed

by peridotite exposure up to the floor of the Pyrenean basins) is now considered as a general mechanism accounting for the presence of ultramafic material within the NPZ. It is established that the well-known regional high temperature and low pressure (HT–LP) Pyrenean metamorphism (Ravier, 1957; Azambre & Rossy, 1976; Bernus-Maury, 1984) developed in the southern NPZ in relation with continental thinning during the major Cretaceous extensional event (Vielzeuf and Kornprobst, 1984; Dauteuil and Ricou, 1989; Golberg & Leyreloup 1990; Clerc et al., 2015b; 2016). Following the early ECORS profiles (Choukroune and ECORS team, 1989), additional information on the architecture of the paleo-margin of Northern Iberia in the Pyrenees is provided by recent interpretation of tomographic data acquired during the temporary PYROPE and IBERARRAY experiments across the Pyrenees (Chevrot et al., 2015; 2018; **Fig. 1**). Based on such data set, Wang et al. (2016) suggest the inversion of a northern Iberia margin characterized by a short necking domain and a large distal domain made of strongly attenuated crust (less than 10 km thick).

Various models of continental crust thinning and associated mantle exhumation have been proposed recently to account for geological constraints collected inside the metamorphic NPZ. In **Figure 3**, we present a selection of reconstructions extracted from recent literature, which highlights numerous similarities between recently published models of Cretaceous NPZ basins structure (Lagabrielle et al., 2010; Clerc and Lagabrielle, 2014; Masini et al., 2014; Tugend et al., 2014; 2015; Clerc et al., 2016; Teixell et al., 2016, 2018; Corre et al., 2016; Lagabrielle et al., 2016; DeFelipe et al., 2017; Pedrera et al., 2017; Espurt et al., 2019; Saspiturry et al., 2019; Asti et al., 2019; Ducoux et al., 2019). Most of these architecture models stress the role played by a major cover décollement layer during the Cretaceous crustal thinning. This weak layer corresponds to the Upper Triassic Keuper evaporites associated with clays, minor carbonates and doleritic MORB basalts (ophites). In the following, this décollement layer is referred to as the prerift salt and clay unit. Its maximum thickness in the Pyrenean realm probably reached up to 2.7 km, as deduced from field data in the southern Pyrenees coupled to well data in the Mauléon and Aquitaine basins and the Bay of Biscay region (James & Canérot, 1988; McClay et al., 2004; Biteau et al., 2006; Jammes et al., 2010a; 2010b; 2010c; Roca et al., 2011; Saura et al., 2016; Orti et al., 2017; Saspiturry et al., 2019). In the décollement layer now exposed in the metamorphic NPZ, Triassic clays were transformed into talc and chlorite-bearing rocks, and carbonates often suffered intense tectonic brecciation involving talc, tremolite and dolomite recrystallizations (Thiébault et al., 1992; Lagabrielle et al., 2019a, 2019b). Pre-rift to synrift salt diapirism is also frequently observed in the NPZ, the Aquitaine foreland basin and in the Southern Pyrenees (e.g. Canérot, 1988; 1989; Lenoble and Canérot, 1992; Canérot and Lenoble, 1989; 1993; James and Canérot, 1999; Canérot et al., 2005; Jammes et al., 2009; Jammes et al., 2010a; 2010b; Roca et al., 2011; Saura et al., 2016; Teixell et al., 2016).

As previously stated by Clerc and Lagabrielle, (2014), the main consequence of the presence of the prerift salt and clay unit along the north Iberia margin promoted mechanical decoupling between the prerift Mesozoic cover and the Paleozoic basement during cretaceous rifting. As a result, the prerift Mesozoic cover behaved as an allochthonous unit. It could remain in the center of the developing rift while the underlying basement and lithospheric mantle were accommodating stretching. Stretching amounts in the basement and the prerift cover remains difficult to accurately balance. This is mainly due to ductile deformation of both the prerift salt and clay unit and the Mesozoic carbonates in the center of the basin. It must be noted that in the external parts of the Pyrenean rift, the borders of the subsiding Cretaceous flysch basins remain at low temperature and display classical faulted and tilted blocks (e.g. half-grabens of Quillan basin, Camarade basin, Gensac-Bonrepos basin, western border of the Mauléon basin, edges of the Gran Rieu high and Lacq basin; Debroas, 1978; 1990; Biteau et al., 2006; Lagabrielle et al., 2010; Masini et al., 2014; Grool et al., 2018; Espurt et al., 2019).

To the west, the NPZ rift ends up against the Cinco Villas Paleozoic massif (CV in **Fig. 1**) and passes into the Basque-Cantabrian basin which developed along the current northern

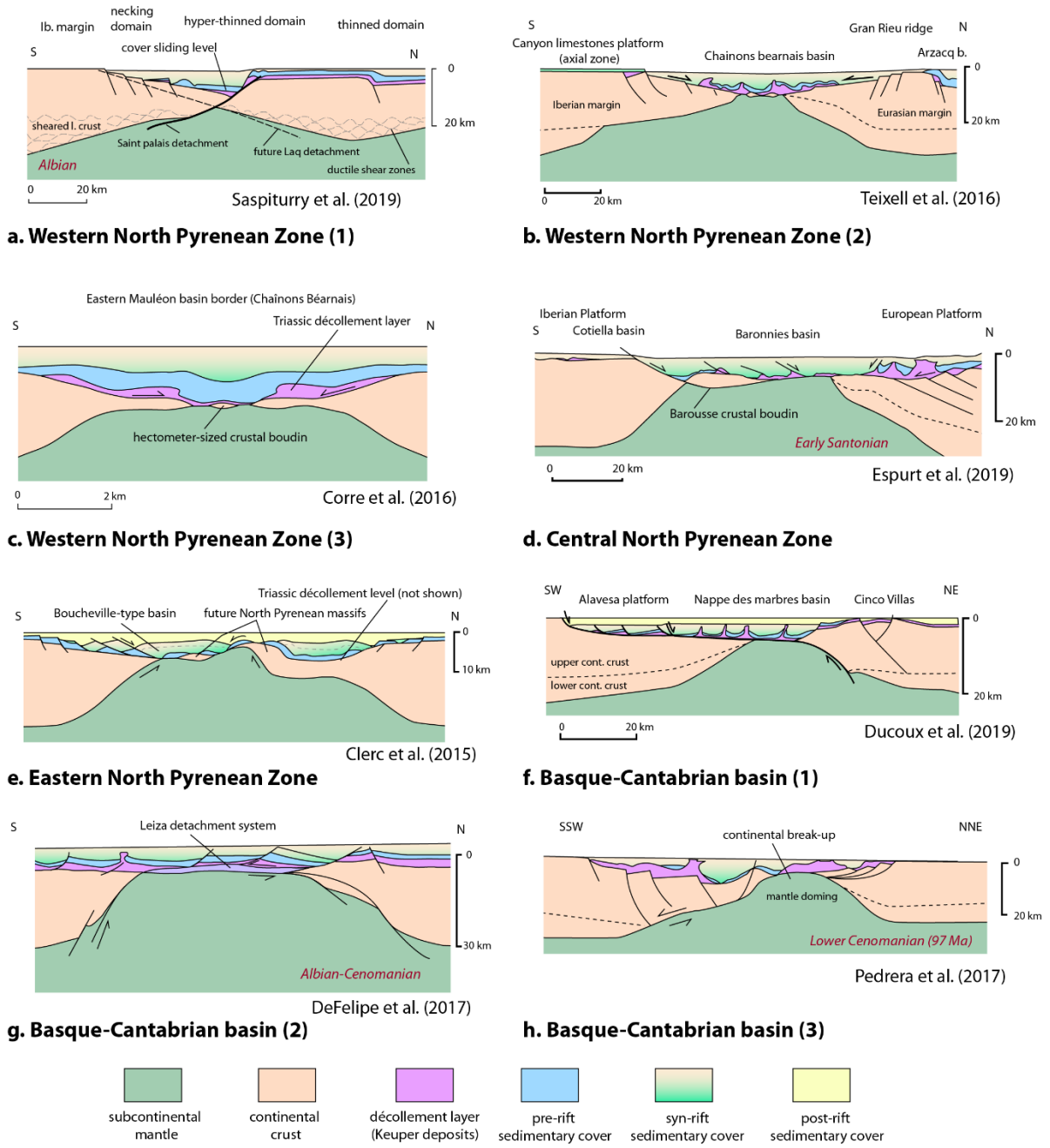


Fig. 3. A compilation of Cretaceous basins architecture from the Cantabrian-Pyrenean belt. Reconstructions from field and geophysical data collected by various authors in the Basque-Cantabrian basin **(A, B, C)** and in the North Pyrenean Zone (NPZ): Mauléon basin **(D)**, Chaînons Béarnais **(E, F)**, Baronnies basin **(G)** and Agly massif-Boucheville basin **(H)**.

Iberia Peninsula and terminated in turn at the Le Danois Bank (DB in **Fig. 1**). Upper Jurassic-Cretaceous sediments (12.5 km maximum thickness) with interlayered Aptian to Santonian basic volcanic rocks (Azambre and Rossy, 1976; Rat et al., 1983; Rat, 1988; Castañares et al., 2001; García-Mondéjar et al., 1996; 2004; Floquet, 2004) **(Figs. 3F to 3H)**. This basin was floored by an extremely thinned lithosphere in its central parts (Biscay Synclinorium and Nappes des Marbres) and was also affected by a Late Cretaceous thermal metamorphism (Golberg and Leyreloup, 1990; Cuevas and Tubía, 1999; Pedrera et al., 2017). A peridotite outcrop is exposed along the major Leiza fault (LF in **Fig. 1**), representing the hyperthinned central portion of the Basque-Cantabrian basin. This confirms that crustal thinning led to the exhumation of the upper mantle close to the basin floor (Mendia and Gil-Ibarguchi, 1991; DeFelipe et al., 2017). The basin architecture deduced from field investigations in the eastern part of the Basque-Cantabrian basin (the « Nappe des Marbres »

area) includes smooth-slopes margins with normal faults and tilted blocks restricted to the external domains (DeFelipe et al., 2017; Pedrera et al., 2017; Ducoux et al., 2019). These reconstructed geometries bear affinities with basin architectures deduced from geological observations in the NPZ **(Figs. 3F to 3H)**. Indeed, such architecture and the overall evolution deduced for this rift system imply gliding of the prerift sequence over its basement during crustal extension with ductile crustal thinning in its central part in a way similar to models proposed for the NPZ (e.g. Clerc and Lagabrielle, 2014; Corre et al., 2016; Teixell et al., 2016). The Leiza detachment system of DeFelipe et al. (2017) **(Fig. 3G)** coincides with the prerift salt and clay unit and promotes the allochthonous character of the overlying prerift units. The presence of a high-density body beneath the Basque-Cantabrian basin has been first interpreted as the result of intrusions of mafic magmatic rocks (Pedreira et al., 2007). Using lithospheric-scale gravity inversion, this anomaly was alternatively interpreted as a high-density mantle body emplaced at shallow level during the Cretaceous extensional event (Pedrera et al., 2017). Interpretation of geophysical data shows that low-strength prerift salt and clay unit favored decoupling of the cover and triggered the formation of diapirs, expulsion rollovers and mini-basins (Pedrera et al., 2017).

Hence, the presence of a thick prerift salt layer underlying the Mesozoic carbonates appears as an ubiquitous first-order parameter when reconstructing the evolution of the Cantabrian-Pyrenean range. Recent models of rift development at the northern Iberia margin show that Triassic lithology controls the three intrinsic characteristics of the Pyrenean rifting, which can be summarized as follows:

(1) Tectonic juxtaposition of exhumed peridotites and prerift sediments. This occurs when the lateral extraction of the thinned continental crust is completed. In response to plate separation, the stretched crust is removed horizontally from the center of the rift and decoupling of the prerift cover from its basement occurs along the prerift salt and clay décollement. As a consequence, a tectonic contact is established between the detached prerift sediments and the uplifted sub-continental mantle (Clerc and Lagabrielle, 2014) **(Fig. 3E)**. In some locations, due to subsequent removal of the prerift cover, mantle rocks may have been exposed at the seafloor as deduced around the Lherz, Urdach and Bestiac lherzolite bodies (Lagabrielle et al. 2010; 2016; de Saint Blanquat et al., 2016).

(2) Crustal stretching under dominantly ductile conditions. The geometry of the crustal units located in the distal domain of the rift margins does not correspond to that of extensional allochthons (succession of isolated, triangular-shaped and internally undeformed blocks) as described along the Iberia-Newfoundland conjugate margins and along the reconstructed alpine paleomargins (Manatschal, 2001; Manatschal et al., 2001; 2006; Péron-Pinvidic and Manatschal, 2009; Mohn et al., 2010; 2012; 2015) **(Fig. 2)**. In contrast, it appears as an assemblage of very thin lenses (10-50 m thickness) consisting of ductilely deformed pre-Mesozoic material, mainly originating from the middle crust. These lenses are separated by anastomozed shear zones, which formed in greenschist facies conditions at low pressure (e.g. Corre et al., 2016; Teixell et al., 2016; Asti et al., 2019; Espurt et al., 2019) **(Figs. 3B to 3D)**. Detailed study of crustal material welded on the Urdach lherzolites suggests that the middle crust was extracted laterally from the rift axis and that deformation occurred at temperatures ranging between 450°C and 350°C (Asti et al., 2019). Large strains in the greenschist facies affect ortho- and para-derived mylonites. They are testified by strongly elongate quartz ribbons with bulging recrystallization along with brittle fracturing of feldspar in cataclastic flows **(Figs. 4A & 4B)**. In general, high temperature is promoted by the presence of the overlying detached prerift cover, which mostly preserves its original thickness during the initial stages of rifting.

(3) Dominantly ductile deformation of the prerift and synrift sediments under HT-LP conditions. Throughout the rifting phase, the detached prerift cover remains in the center of the rift. At this location, the temperatures rises in reponse to the ascent of the underlying mantle. The local preservation of an overlying prerift cover and the deposition of synrift deposits contributes to the high temperatures recorded regionally. As a result, the detached prerift cover locally undergoes syn-

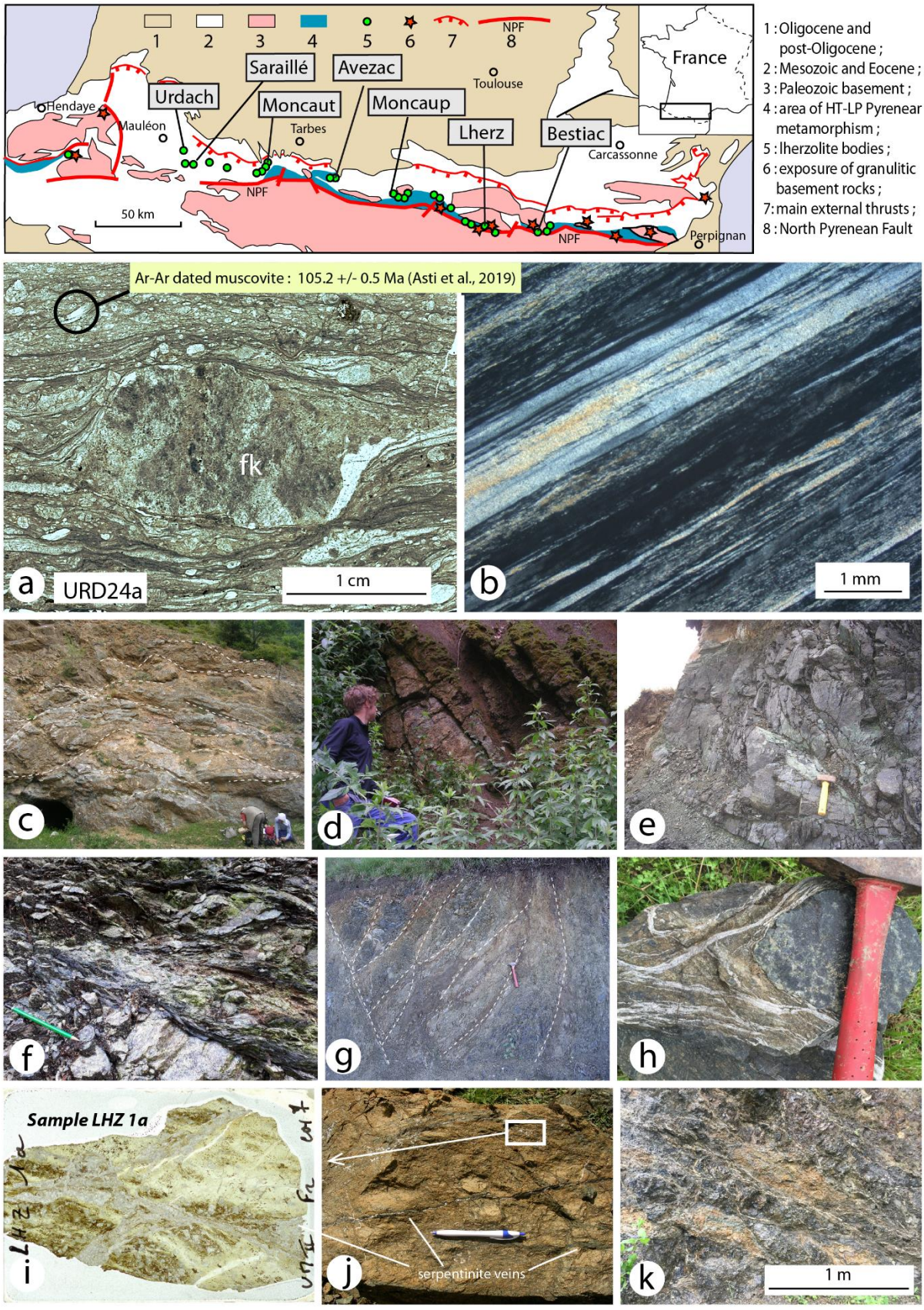


Fig. 4. The geological record of the Cretaceous extension in the Paleozoic basement and exhumed mantle of the North Pyrenean Zone (NPZ). The map shows the location of mantle bodies and crustal units illustrated in photographs a to k. **(A)** dated crustal mylonites associated with the Urdach lherzolites; thin section microphotograph (natural light) of the leucocratic gneissic mylonite exposed at Col d'Urdach and containing numerous micafishes (dated by Ar/Ar method at 105 Ma; after

Continued on the next page

Asti et al., 2019). **(B)** thin section of typical ultramylonite from lenses of Paleozoic material welded on the exhumed mantle rocks of the Saraillé lherzolite (Asti et al., 2019). **(C)** phacoidal fabric defined by anastomosed shear zones in the mantle body of Bestiac. This fabric is typical of the lenticular layer as defined by Lagabrielle et al. (2019a, 2019b). **(D)** phacoidal fabric in the lenticular layer of the lherzolite body of Moncaup. **(E)** phacoidal fabric in the lenticular layer of the lherzolite body of Saraillé (Lagabrielle et al., 2019b). **(F)** curved shear zones and elongated tectonic lenses in serpentinized lherzolites of the lenticular layer in the Moncaut peridotite body. **(G & H)** phacoidal fabric in the lenticular layer of the lherzolite body of Urdach: h shows pervasive carbonation (Lagabrielle et al., 2019a). **(I & J)** thin section and outcrop of anastomosed serpentinized shear bands in the lherzolites of Etang de Lers (Lherz). **(K)** anastomosed serpentinized shear bands in Avezac lherzolites.

metamorphic ductile thinning and boudinage during continental breakup **(Figs. 5A to 5D)**. Such mechanical behavior is outlined in all published rifting models (i.e. base of Nappe des Marbres basins, Leiza detachment system, base of Mauléon and Chaînons Béarnais basin infills, base of Baronnies and Boucheville basins infill: see references in **Fig. 3**). Progressive rifting triggers the upward propagation of the brittle-ductile transition which may reach synrift sediments deposited at the early stage of the basin opening (Clerc et al., 2016). Brittle deformation dominated by cataclastic brecciation overprints ductile shearing and flattening in the sedimentary units accompanying final exposure of mantle rocks to the seafloor, as proposed from studies in the Lherz area (Lagabrielle et al., 2016). The ductile-brittle transition is frequently observed at the mesoscopic and microscopic scale as sets of normal faults offsetting the extensional HT foliation **(Figs. 5E, 5F & 5H)**. Finally, at the scale of the entire rift, extensional deformation in the lower margin is accompanied by tectonic denudation of the cover in the upper margin (Lagabrielle et al., 2010; Teixell et al., 2016, 2018; Saspiturry et al., 2019).

To summarize, **Figure 6** presents the intrinsic characteristics of the Pyrenean rifting listed above, compiled along an idealized column of the NPZ lithologies with photographs illustrating the most relevant deformed levels exposed along the NPZ.

3. A review of smooth-slopes basins in the surroundings of the Pyrenees-Cantabrian Mountains

Seismic images of oceanic margins and intracontinental rifts in the proximity of the Pyrenees and Cantabrian ranges bear crucial information on the mode of crustal thinning along the northern Iberia margin and adjacent areas during the Cretaceous period.

3.1. Parentis basin

First interpretations of the Parentis ECORS profile point to a symmetrical, syncline-shaped basin, with only few normal faults in the stretched crust, even in the proximal domain (Pinet et al., 1987; Bois et al., 1997). Beneath the Parentis basin fill, the crust is less than 10 km thick and decreases westward from 7 km (along the ECORS Bay of Biscay profile, **Fig. 1**), to 6–5 km (along the MARCONI 3 profile, **Fig. 1**) (Tomassino and Marillier, 1997; Gallart et al., 2004; Ruiz, 2007). More recently, Jammes et al. (2010a), proposed that the southern Parentis basin represents a lower plate sag basin floored by a top-basement detachment system with an asymmetrical mode of opening. These authors emphasize the presence of a thick prerift salt layer in the area undergoing extreme crustal thinning, forcing sub- and suprasalt layers to deform differently. Whatever the processes of crustal thinning are favored, both older and recent models of Parentis basin evolution highlight three major features: (1) the occurrence of symmetrical smooth-slopes gently dipping basinward; (2) the presence of a crust thinning regularly towards the basin axis, without any observed steeply dipping faults, and (3) the presence of a thick prerift salt layer allowing décollement of the prerift cover from its basement (Jammes et al., 2010b, 2010c).

3.2. South Bay of Biscay margin

Both the northern and southern margins of the Bay of Biscay have been explored seismically. North-south transects of the Armorican margin (Norgasis profiles, **Fig. 1**: Thinon et al., 2003; Tugend et al., 2014) reveal a short necking domain that concentrates most of the crustal deformation. Crustal thickness decreases from 35 km at the shelf break to less than 10 km at the foot of the slope. Steep rise of mantle implies the disappearance of the lower crust beneath the slope. Based on results of gravity inversion combined with seismic interpretations, Tugend et al. (2014) map a

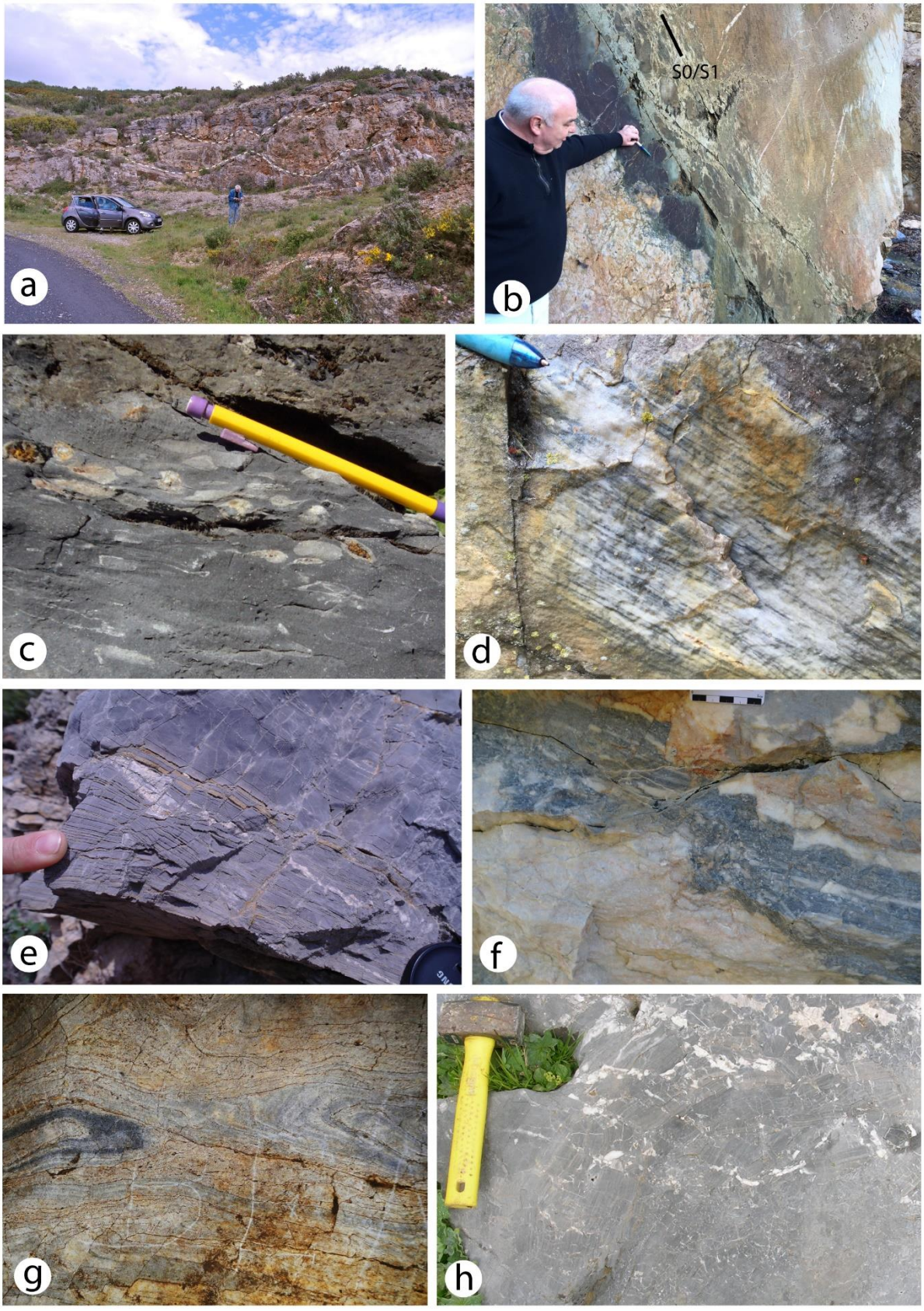


Fig. 5. The geological record of the Cretaceous extension in the pre-rift cover of the metamorphic North Pyrenean Zone (NPZ). Some field view of outcrops showing the layer perpendicular flattening and the S0/S1 syn-metamorphic foliation. **(A)** layer-parallel boudinage in the Calce quarry (Jurassic dolostones of the Agly massif cover, Eastern NPZ). **(B)** layer-parallel ductile stretching of the meta-laterite and carbonate breccia in the Benou quarry near Turon de la Tecouère lherzolite body (Chaînons Béarnais, Western NPZ). **(C)** flattened fossils in Jurassic meta-dolostones of the Saleix valley (Aulus basin,

Continued on the next page

Central NPZ). **(D)** extreme stretching of a rudist-rich Urgonian marbles at Sarrance (Chaînons Béarnais, Western NPZ) (see also Fig. 6C). **(E)** tight normal faults affecting the early S0/S1 syn-metamorphic foliation in pre-rift cover marbles of the Agly massif. These features characterize the ductile-brittle transition that occurred at the end of the rifting history. **(F)** same features as (e) but in marbles of the detached Lherz body cover (southern side). **(G)** recumbent folds associated with the early ductile foliation in marbles from the detached cover of the Pays de Sault Paleozoic basement (Eastern NPZ). **(H)** tectonic brecciation with calcite veining marking the ductile-brittle transition in the marbles of the Lherz body cover (western side).

continuous domain of exhumed mantle from the Armorican basin toward the hyperthinned Parentis basin where minimum crustal thickness occurs **(Fig. 7A)** (Pinet et al., 1987, Bois et al., 1996, Jammes et al., 2010a). According to Roca et al. (2011), the Bay of Biscay Abyssal Plain itself consists of a transitional zone formed by a thin (4–9 km) crust with riders of Mesozoic prerift and synrift sediments and continental crustal rocks that are extensionally detached over an exhumed sub-continental mantle with seismic velocities comprised between 7.2 and 8 km/s. In the distal domain, the Bay of Biscay Abyssal Plain bounds to the north the North Iberian margin, an extended continental margin with Cretaceous basins (e.g. the Asturian basin, up to 10 km thick, **Fig. 1**) and basement highs such as Le Danois Bank (Cadenas and Fernández Viejo, 2016; Teixell et al., 2018), where granulites have been dredged (Capdevila et al., 1980; Fügenschuh et al., 2003) **(Fig. 1)**.

3.3. North-eastern Iberia intra-crustal basins: Iberian Chain and Valencia trough

Helpful additional information regarding the thinning modes of the northern Iberia crust can be obtained from seismic images of the Cameros, Maestrat and Columbrets basins now partly inverted in the Iberian Chain **(Fig. 1)**. These basins result from the distributed extension of the northern Iberia plate synchronously with the opening of the Bay of Biscay-Pyrenees in the early and mid-Cretaceous (Verges and Garcia-Senz, 2001; Mas et al., 2011). They represent a well-developed Mesozoic rift sharing similarities with the North Atlantic margins (Salas and Casas, 1993; Salas et al., 2001). In their internal parts, reconstructed Iberian Chain basin geometries point to simple troughs exhibiting gentle slopes devoid of marked fault stepping, suggesting the absence of tilted blocks and a smooth basement top. The Moho generally shows an arched outline with a progressive shallowing toward the basin center where the crustal thickness is reduced to a few kilometers only (e.g. Guimerà et al., 1995; Casas-Sainz and Gil-Imaz, 1998; Omodeo et al., 2014). Triassic evaporites play an important role during the Albian rifting in the basins of northeast Iberia. This role was recently well illustrated by interpretation of seismic reflection profiles in the Valencia trough (Etheve et al., 2018) **(Fig. 7B)**. These profiles reveal the presence of a large Albian basin, the Columbrets basin **(Fig. 1)**, filled with up to 10 km thick Mesozoic sediments over a highly extended continental basement (locally only 3.5 km thick). The prerift and synrift successions form a large-scale syncline with thinned borders. Whole Basin deformation is interpreted to result from interaction between decoupling promoted by a prerift salt unit and dominantly ductile thinning of the basement (Etheve et al. 2018) leading to the development of an abnormally thin continental crust (Gallart et al., 1990; Dañobeitia et al., 1992; Ayala et al., 2015). In the Cameros basin **(Figs. 7C & 7D)**, the prerift cover is detached from the basement along the Keuper evaporites and is smeared all over the stretched domain. The synrift record does not document any major offset of the top basement (Casas-Sainz and Gil-Imaz, 1998; Casas-Sainz et al., 2000). In a similar fashion than in the NPZ, syn-thinning HT-LP metamorphism of the pre and synrift sediments is reported in the Cameros basin fill (Guiraud and Séguret, 1985; Goldberg et al., 1988; Rat et al., 2019).

4. Evolution of smooth-slopes basins: some rheological considerations

4.1. Symmetrical smooth-slopes basins: simple or pure shear-dominated structures?

A common characteristic of smooth-slopes basins is the lack of tilted crustal blocks and related stepping fault scarps in their central part, thus defining a dominant symmetrical smooth-slopes profile of basement tops **(Figs. 2 & 7)**. Based on field data from the NPZ, we have shown that stretching of the crustal basement occurs in a dominant ductile mode under greenschist facies conditions, since the central part of the basin remains overlain by a permanent cover of detached pre- and synrift sediments (Asti et al., 2019) and underlain by exhuming mantle.

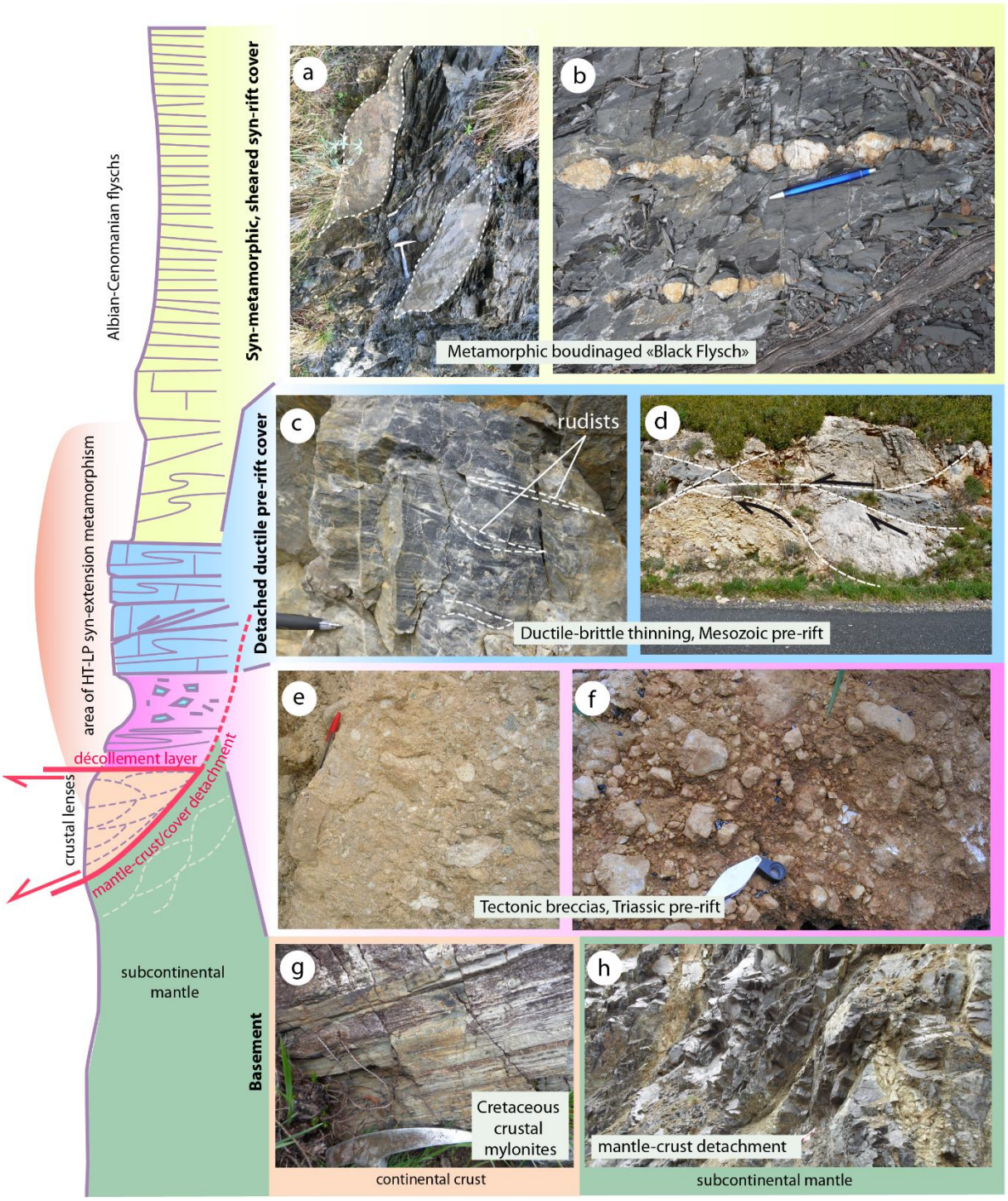


Fig. 6. A theoretical log of the lithological succession in the internal domain of the Cretaceous NPZ rift basins. The photographs illustrate the various rock-types forming the basin basement (crust and mantle) and the pre-rift and syn-rift series. **(A)** Chaînons Béarnais (Saraillé massif, western NPZ). **(B)** Boucheville basin (eastern NPZ). **(C)** Urgonian at Sarrance (western NPZ) (see also Fig. 5d). **(D)** Jurassic dolomites at Calce (eastern NPZ). **(E)** base of pre-rift series (Bestiac, eastern NPZ). **(F)** base of pre-rift series (Moncaup, central NPZ). **(G)** crustal lenses of Saraillé massif (western NPZ). **(H)** lenticular layer (Urdach mantle body, western NPZ).

The architecture of extended crustal systems depends on the geometrical and temporal associations between simple shear and pure shear regimes. Following the pioneer works of McKenzie (1978), Wernicke (1981, 1985), Lister and Davis (1989) and Lister et al. (1991), the symmetry and asymmetry of lithosphere stretching processes have been largely debated over the last 30 years (i.e. Buck et al., 1988; Allemand et al., 1989; Buck, 1991;

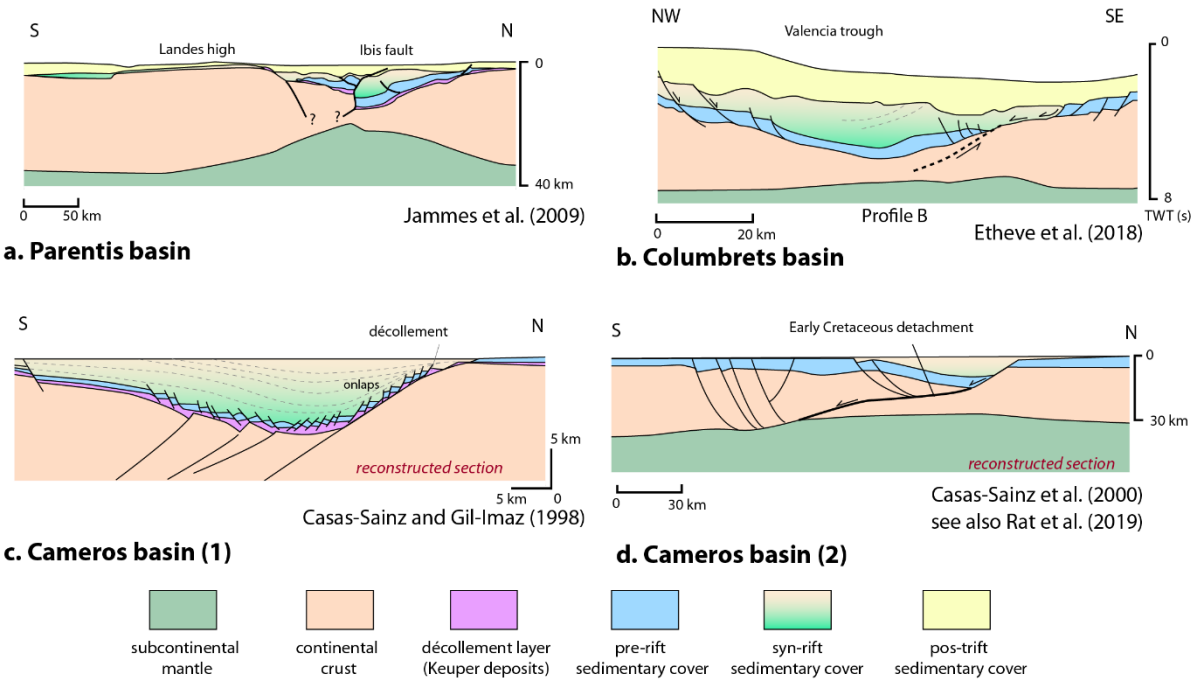


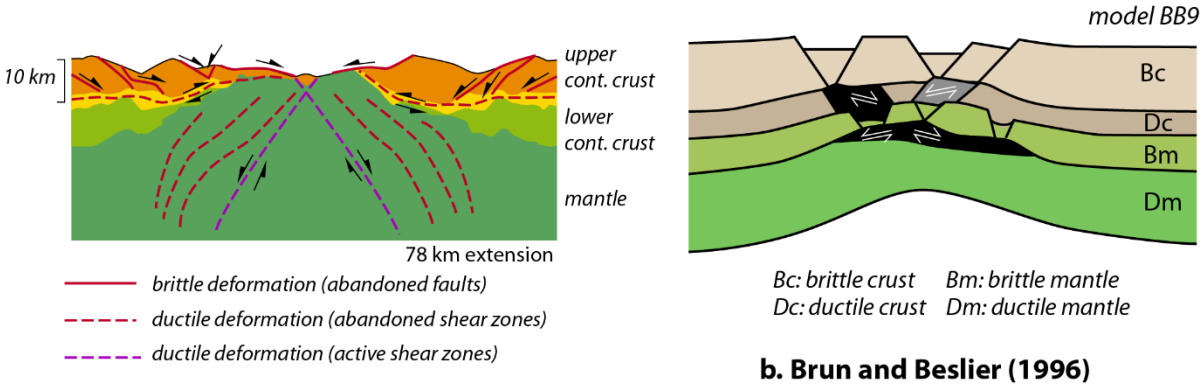
Fig. 7. Interpreted and reconstructed profiles of peri-Pyrenean Cretaceous basins architecture. **(A)** Parentis basin. **(B)** Columbrets basin. **(C & D)** Cameros basin. See location of basins in fig. 1.

Brun, 1999, Huismans and Beaumont, 2003). In the same way, the symmetrical character of the final architecture of passive margins following continental breakup has been discussed by many authors (i.e. Reston et al., 1995; Michon and Merle, 2003; Huismans and Beaumont, 2007; Reston and Perez-Gussinyé, 2007; Sutra et al., 2013; Brune et al., 2014). It follows that apparent architecture symmetry does not necessarily imply dominant pure shear thinning mechanisms but may result from asymmetrical tectonic processes involving large-scale discrete extensional shear zones (simple shear) as discussed by Brun and Beslier (1996) and Nagel and Buck (2004) **(Fig. 8)**.

In their four-layer laboratory model, Brun and Beslier (1996) combine simple and pure shear deformation in order to account for the exhumation of mantle rocks at ocean-continent boundaries **(Fig. 8B)**. Model layers are composed of sand and silicone putty, regarded as analogues of the brittle and ductile layers of both crust and mantle. The lower crust deforms ductilely whereas the upper mantle remains strong. The Brun and Beslier (1996) model shares characteristics with models derived from the geology of the Parentis and NPZ basins which involve homogeneous thinning of the crust during its lateral extraction from the rift axis (e.g. Corre et al., 2016; Teixell et al., 2016) **(Fig. 3)**. It does not favor the activation of a restricted number of crustal detachment faults. Therefore, necking of the whole lithosphere model appears nearly symmetrical (pure shear). However, asymmetrical structures (simple shear) develop internally, due to boudinage and/or faulting of brittle layers as deduced from field observations at the outcrop scale. The Brun and Beslier (1996) model also accounts for the symmetrical ductile deformation of the NPZ bulk crust as shown by Asti et al. (2019) and explains the occurrence of localized shear zones in the lithospheric mantle as described by Vissers et al. (1995) in the Pyrenean mantle.

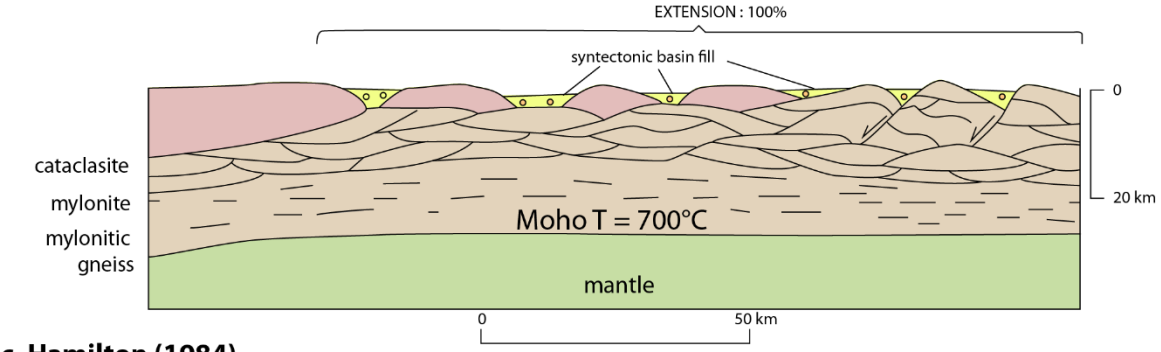
4.2. Smooth-slopes basins: crustal shear zones and lenticular fabrics at the mesoscale

Petrological studies of continental units exposed around the Urdach and Saraillé lherzolite bodies (western NPZ) provide information on the deformation mode associated with crustal thinning and mantle exhumation of northern Iberia (Corre et al., 2016; Asti et al., 2019). Reconstruction of sections across the NPZ Cretaceous basins by Clerc et al. (2015b), Teixell et al. (2016), Corre et al. (2016) and Asti et al. (2019) highlight the role of high-temperature ductile deformation of the basement induced by regional-scale, pure shear extension. It was shown that extension in the Paleozoic basement was achieved through

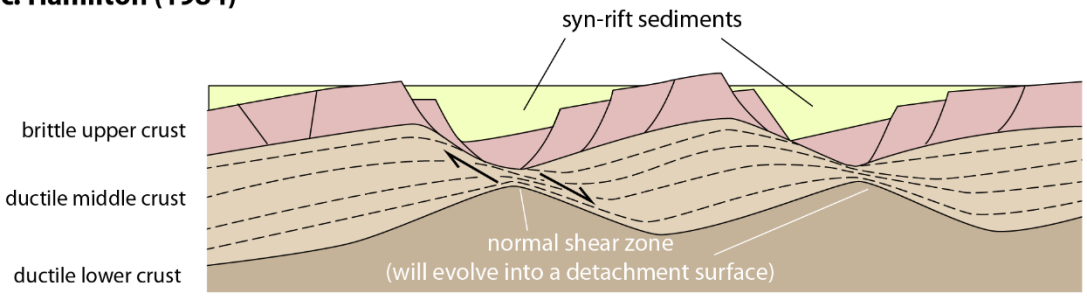


a. Nagel and Buck (2004)

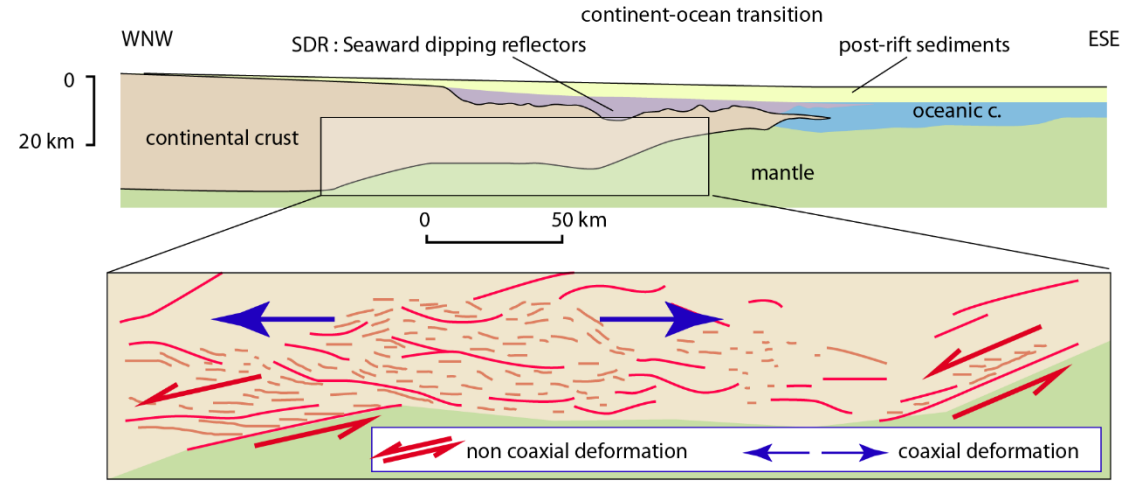
b. Brun and Beslier (1996)



c. Hamilton (1984)

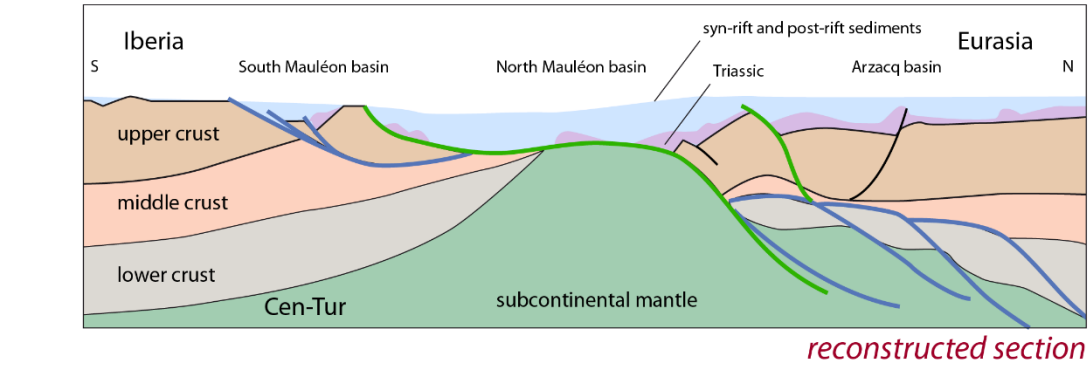


d. Gartrell (1997)

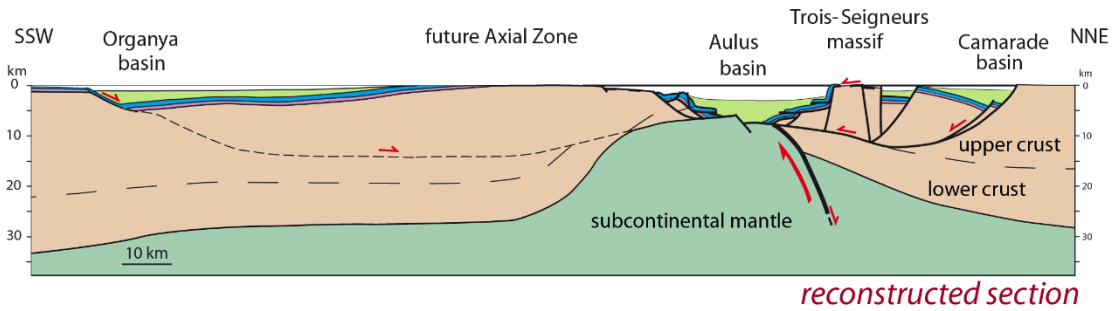


e. Clerc et al. (2018)

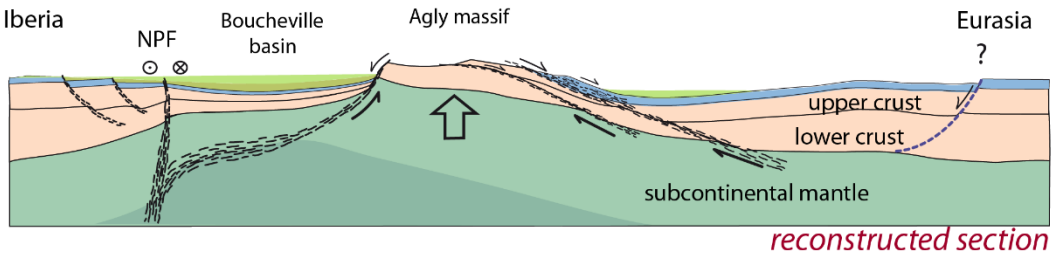
Fig. 8. A compilation of model results and conceptual representations of extended to hyper-extended continental crust. This compilation aims enhancing the main mechanical concepts involved in the processes of crustal extension and how they apply or not apply to the genesis and evolution of the smooth-slopes basins defined in this article (see text for discussion).



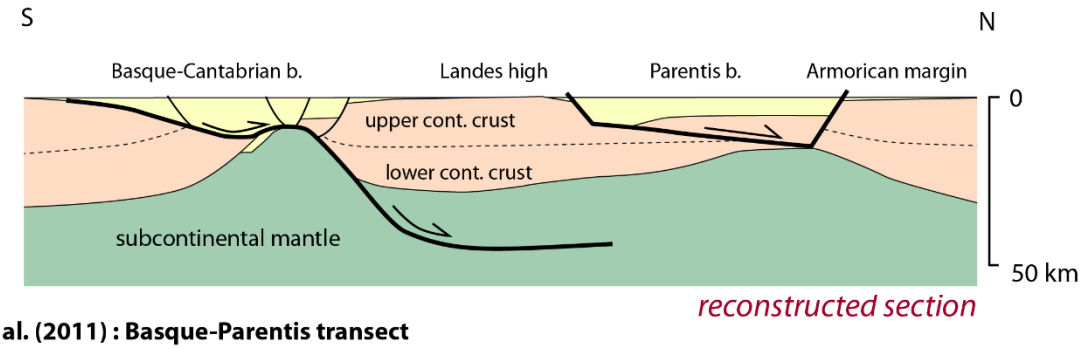
a. Masini et al. (2014): Mauléon basin



b. Lagabrielle et al. (2010): Central North Pyrenean Zone (Aulus basin, Etang de Lers)



c. Vauchez et al. (2013): Eastern North Pyrenean Zone (Boucheville basin)



d. Roca et al. (2011) : Basque-Parentis transect

Fig. 9. A compilation of reconstructed architecture of Pyrenean Cretaceous basins and a Basque-Parentis transect. All represented sections are based on the activation of a restricted number of detachment faults. As discussed in text, such representations do not match the newly defined smooth-slopes architecture that characterize the Pyrenean and peri-Pyrenean Cretaceous basins.

lenticular deformation and pervasive ductile flattening of the crust with anastomosed extensional mylonitic shear zones developing at temperatures of 350-450°C. Stretching led to the development of undulated shear contacts separating tectonic lenses of crustal rocks (phacoid-shaped) as described in **Figure 10**. At the final step of continental breakup, very thin continental crustal lenses (10-50 m thickness) remained welded to the exhumed mantle.

A similar lenticular mode of deformation derives from investigations in the Basin and Range province. Hamilton (1987) describes

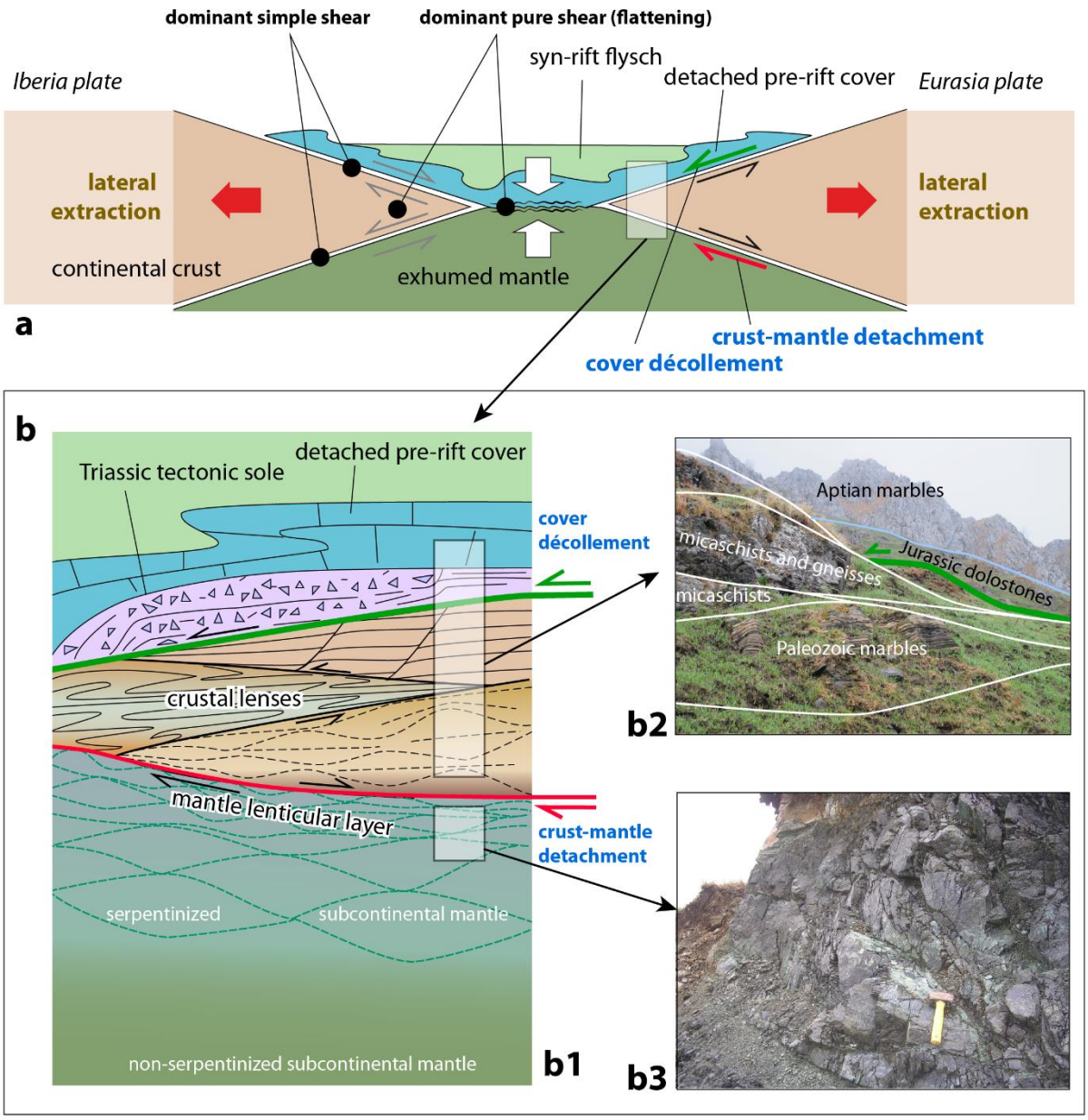


Fig. 10. Deformation regimes of the various units composing a typical smooth-slopes basin. **(A)** distribution of pure shear and simple shear regimes in a simplified smooth-slopes basin system. **(B)** Detail of the very distal part of the hyper-extended crust (area shown in a). **(B1)** simplified log showing the association of metric to hectometric crustal lenses separated from the mantle rocks by the crust-mantle detachment and from the detached pre-rift cover by the cover décollement (see definition in Lagabrielle et al., 2019a, 2019b). **(B2)** field view of crustal sheets from the base of the Saraillé massif (western NPZ). **(B3)** field view of anastomosed shear zones cutting through the serpentinized peridotite of the Saraillé body and forming the lenticular layer of the crust-mantle detachment (see also fig. 4c to k).

tectonic lenses of middle crustal rocks that normally lie at separate levels in the crust separated by undulating shear contacts **(Fig. 8C)**. This deformation mode allows the juxtaposition of different lithologies by uplifting deeper lenses during extensional deformation. In a different way, Gartrell (1997) propose a large-scale crustal boudinage involving successive necking regions where the ductile middle crust is extremely sheared **(Fig. 8D)**. The resulting architecture is a succession of tectonic lenses that may evolve toward a large-scale lenticular geometry as proposed by Espurt et al. (2019) for the evolution of the North Pyrenean massifs in the Central Pyrenees **(Fig. 3D)**.

In their recent detailed study of the tectonic and metamorphic evolution of the Urdach and Saraillé mantle bodies and associated units, Lagabrielle et al. (2019a; 2019b) describe two types of low-angle shear

zones that accommodated part of extension of the distal domain of the Iberia passive margin during the mid-Cretaceous **(Fig. 10A & 10B)**. The deepest shear zone is the crust-mantle detachment. It separates the ultramafic mantle rocks from strongly thinned basement Paleozoic rocks. It is composed of a basal 20-50 m thick lenticular layer of sheared serpentinites overlain by a 10 m thick damage zone. The lenticular layer consists of ultramafic symmetrical tectonic lenses (few meters long) separated by anastomosed serpentine-rich shear zones. The damage zone consists of an assemblage of centimeter-sized symmetrical lenses of a soft, talc-rich, sheared material, separated by conjugate shear zones. The shallowest shear zone is the basement-cover décollement. It corresponds to a tectonic boundary separating the base of detached prerift Mesozoic metasedimentary cover from either mantle lherzolites or continental basement rocks. It consists of a thick deformation zone (some meters to tens of meters) that was the locus of important metasomatic crystallizations involving notably fluids of Triassic origin (Corre et al., 2016). Detailed structural study of the basement and mantle rocks shows that it is not easy to discriminate between dominant pure shear and dominant simple shear processes at the outcrop and regional scales (Lagabrielle et al. 2019a; 2019b). Indeed, a major detachment fault zone (typically related to regional simple shear) may contain abundant symmetrical lenses suggesting locally dominant pure shear deformation.

Finally, in the studied smooth-slopes basins, dominant pure shear mechanisms concentrate into the strongly thinned continental tectonic lenses whereas simple shear mechanism occur along the main detachments. Pure shear deformation, causing the overall flattening of the synrift and prerift sedimentary pile, progressively develop into the basin center as represented in **Figure 10A**. Chronological constraints need to be integrated in this proposed temporal sequence in order to establish a possible succession from simple shear-dominated to pure shear-dominated deformation at the scale of the entire system.

4.3. Contrast between Iberian-Alpine and Pyrenean rifts: role of a basement-cover décollement

In contrast with the NPZ symmetrical model, recent models of margin evolution based on the Iberian or Alpine examples have put forward asymmetric architectures resulting from the development of few major detachment faults, and promoted the use of « lower-plate » and « upper-plate » terminology (Manatschal, 2004; Mohn et al., 2010, 2012, 2015; Sutra et al., 2013). Mohn et al. (2012) propose a model of three-layer continental crust where the brittle upper and lower crusts are strongly decoupled by a ductile middle crust **(Fig. 3B)**. Crustal thinning, accommodated through a so-called necking zone, is the result of the interplay between detachment faulting in the brittle layers and decoupling in the ductile quartzo-feldspatic mid-crustal levels along localized ductile décollements. The excision of ductile mid-crustal layers and the progressive embrittlement of the crust by coupling the lower and upper crusts enable major detachment faults to cut into the underlying mantle, exhuming it to the seafloor.

By studying the evolution of the western Betics, including the exhumation of the Ronda subcontinental mantle, Frasca et al. (2016) identify three successive steps: (i) ductile crust thinning and ascent of subcontinental mantle thanks to mid-crustal shear zone and crust-mantle shear zones acting synchronously; (ii) disappearance of the ductile crust bringing the upper crust in contact with the subcontinental mantle, (iii) complete exhumation of the mantle in the zone of localized stretching and high-angle normal faulting cutting through the Moho, with related block tilting. These steps do not fully apply to the Pyrenean case, notably because field and geophysical studies of the metamorphic NPZ never document the occurrence of brittle faulting across the Moho during the Cretaceous rifting.

Finally, based on these examples, we stress that both Alpine and Betic examples of reconstructed passive margins do not involve the activation of a prominent décollement at the base of the prerift cover. They rather promote evolutionary models with prerift sediments welded to the basement blocks, in contrast with the examples detailed in section 2 and 3. In

addition, both Alpine and Betic models refer to a progressive embrittlement of the thinning crust resulting in the complete elision of ductile crustal layers. Again, this contrasts with the NPZ examples where thin ductile crustal layers were extracted in the distal domain and remained welded to the exhumed mantle.

5. Discussion

5.1. Smooth-slopes basins formation, insights for the evolution of passive continental margins.

From the above section 4, we interpret that dominant pure shear deformation is responsible for the formation of the strongly stretched continental basement (anastomosed tectonic lenses) in the central region of smooth-slopes basins. In the following, we review examples of comparable uniform modes of ductile deformation in passive margins worldwide.

A lenticular mode of deformation devoid of any steep normal fault was proposed at the scale of an entire passive margin by Gernigon et al., (2014) to account for the symmetrical stretching of the continental crust during the formation of the Barents margin **(Fig. 11A)**. This lens-shaped lozenge geometry recalls the structures shown by Gartrell (1997) from laboratory models **(Fig. 8D)** and by Reston (1988) from lower crust reflection profiles. Lenticular fabric was also suggested for deep crustal units connected to tilted blocks through listric faults along the Norway margin (Osmundsen and Ebbing, 2008; **Fig. 11B**). These structures accommodate crustal thinning to only a few kilometer thicknesses through dominant ductile deformation. Symmetrical stretching, implying ductile thinning or boudinage of some crustal layers, can be compared to processes of depth-dependent stretching or thinning (DDS and DDT) envisioned by Reston and McDermott (2014) in order to account for extensional discrepancies at some passive margins.

Several distal domains of North Atlantic passive margins display geometries that suggest the presence of lens-shaped units of thinned to hyper-thinned continental crust detached along anastomosed shear zones and separated domains of exhumed mantle (e.g. Labrador and West Greenland margins; Chalmers and Pulvertaft, 2001; Reston and Perez-Gussinyé, 2007) **(Figs. 11C & 11D)**. These units do not resemble the extensional allochthons of the West Iberia-type margins **(Figs. 2 & 11E)** and show geometrical affinities with crustal boudins extracted during the Pyrenean extension in the center of the Cretaceous rift (e.g. the Baronnies and Agly crustal boudins; Espurt et al., 2019; Clerc et al., 2016) **(Fig. 3)**. Such large areas of hyper-thinned continental crust, composed of heterogeneous boudins, can be viewed as sheets representing considerable volumes of sheared and flattened continental material (thickness less than 10 km, width of 100 km and length of few 1000 km along the margin), formed through processes of uniform pure shear at a crustal scale. We infer that the modes of deformation exhibited by the Pyrenean crustal units welded to the exhumed mantle (although at a much smaller scale) can apply to the formation of these crustal sheets made up of greenschist facies mylonites. Similar crustal sheets underlying sag basins were modeled in recent numerical simulations of margin evolution (Brune et al., 2014; Huismans and Beaumont, 2011; 2014) as shown in **Figure 12A & 12B**. Crustal sheets are present along the Angola margin **(Fig. 12D)**, they may be present in the very distal domain of the Gulf of Lion margin where they may originate by extraction of lower crustal material (Jolivet et al., 2017) **(Fig. 11F)**. Similar long and thin sheets are typically imaged by Wang et al. (2016) at the base of the reconstructed Iberia margin of the Mauléon basin, and by Roca et al. (2011) in their reconstruction of the Iberia margin north of the Cantabrian coast **(Fig. 9D)**.

In their compilation of high-quality and deep penetration seismic profiles of several passive margins (Uruguay, Southern Namibia, Gabon, South China Sea and Barents Sea), Clerc et al. (2015a; 2018) suggest that the lower crust of some margins is weaker than assumed and accommodates a large part of extension by ductile shearing **(Fig. 8E)**. Boudinage appears as a recurrent deformation process accounting for the thinning of the continental crust at variable scales. This observation led authors to an unorthodox vision of some types of passive margins where: (i) the lower crust depicts heterogeneous ductile deformation patterns, (ii) boudinage and associated low-angle shear zones controls a large part of the deformation, and (iii) normal faults often dip toward the

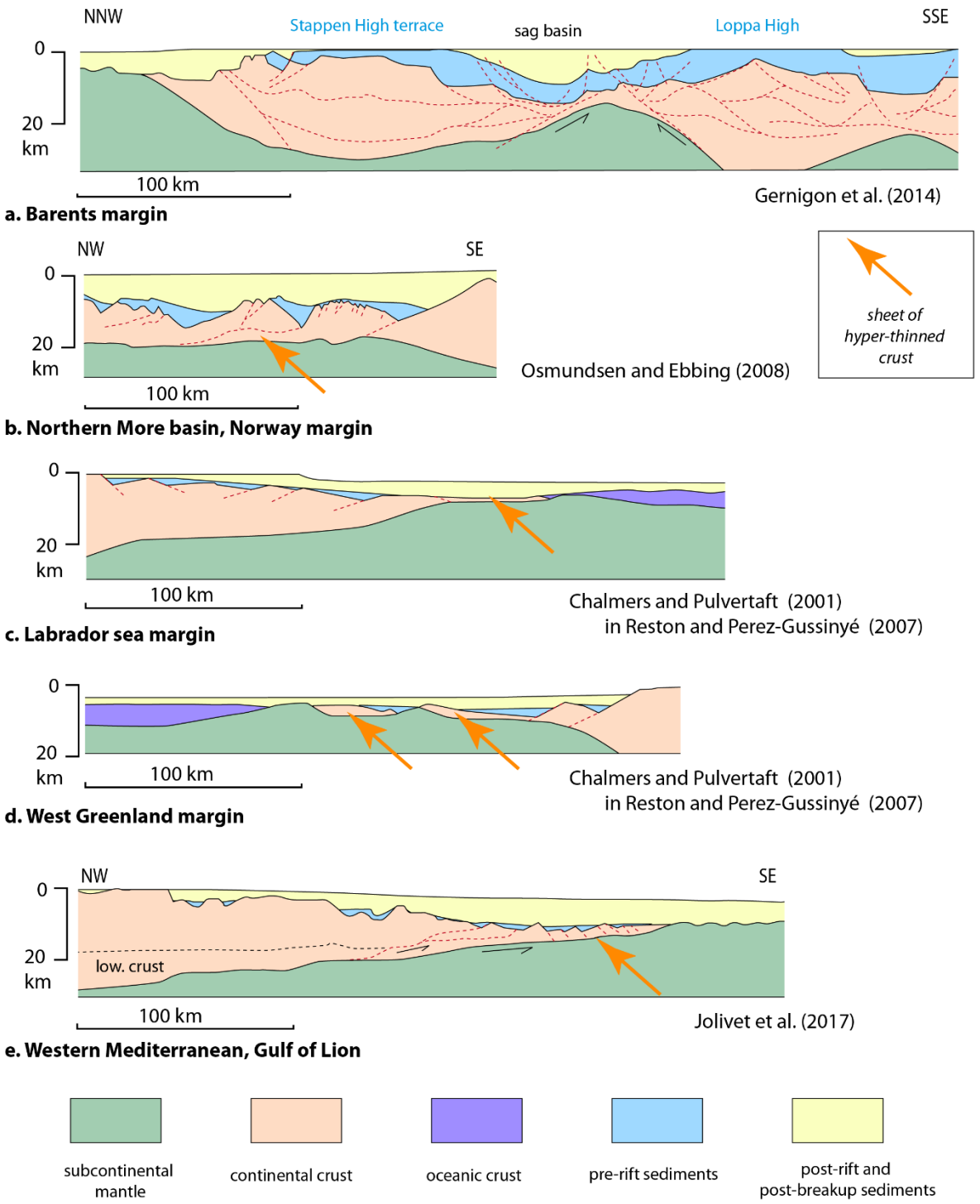


Fig. 11. A compilation of schematic architecture of selected Atlantic and Mediterranean passive margins. These margin profiles are selected because they offer architectures which contrast with the Iberia-Newfoundland-type margin (see fig. 2). In particular, they show large scale crustal boudinage and lenticulation that are consistent with a ductile regime of extensional deformation. Sheets of hyper thinned crustal material is indicated by the orange arrow (see comments in text). Note that scale is similar in all profiles.

continent. This study highlights a crustal behavior dominated by boudinage and lenticulation, implying interplay between ductile shear zones (boudin edges) and more competent crustal volumes (boudin cores). As discussed above in section 4.2, this deformation mode may apply to the thinned crustal levels located in the axis of the Cretaceous Pyrenean rifts (Teixell et al. 2016, 2018; Asti et al., 2019) **(Fig. 10)** and is supported by recent numerical models of lithospheric rifting incorporating macroscale anisotropy (Duretz et al., 2016).

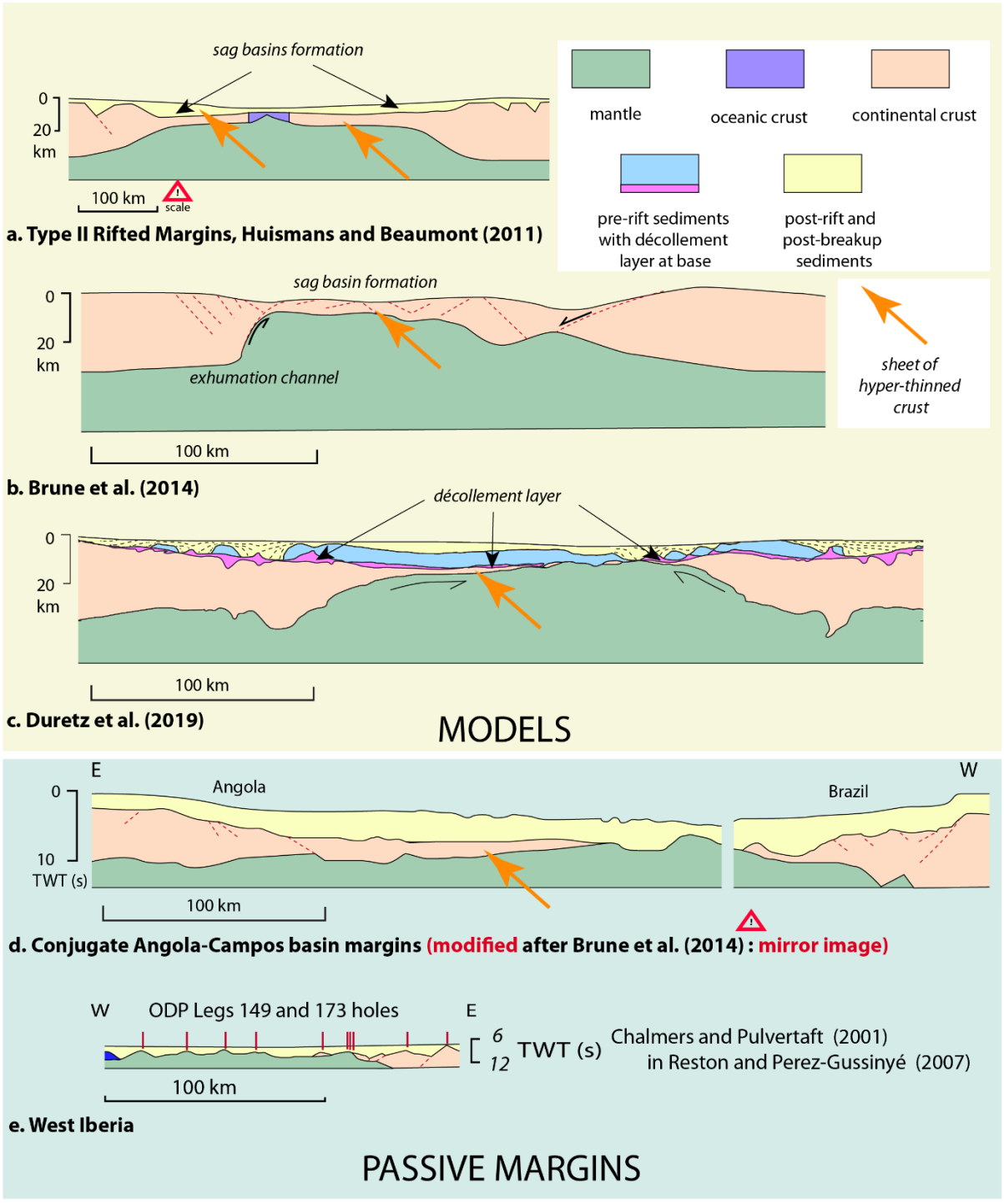


Fig. 12. Three numerical models of rift development compared to the Angola-Brazil and Iberia transects. All models highlight a mode of deformation that leads to the development of very thin and long sheets of crustal material also observed in the Angola-Campos transect but not in the Iberia transect. Such deformation necessarily implies a dominantly ductile behaviour of the crust consistent with processes acting in the central part of the smooth-slopes basins studied in this paper (see text for further comments).

In their interpretation of deep seismic profiles of the Gulf of Lion margin, Jolivet et al. (2015) point to an intense stretching of the distal margin and reveal a 80 km-wide ocean-continent transition zone that may consist of thin lower continental crust (the « Gulf of Lion metamorphic core complex ») and exhumed mantle **(Fig. 11E)**. These authors infer an overall hot geodynamic environment with a shallow lithosphere-asthenosphere boundary able to thermally weaken the upper mantle and the lower crust enough to make them flow

south-eastward. In this example, the lower crust bears an important role. Such process is not fully documented in the NPZ since evidence of lower crust exhumation during Cretaceous rifting has not yet been reliably reported. Moreover, in sections of **Figures 3A, E, F, H & 7**, the lower crust is considered as a high-strength layer that does not deform ductilely but rather tends to form large scale boudin which remain at depth during rifting.

5.2. Comparison with thermo-mechanical models of crustal hyper-extension.

The examples discussed above lead us to emphasize the abundance of lenticular fabrics at various scales reported from different studies in both the upper mantle and the crust. The formation of lenticular fabrics, necking and lateral extraction during continental rifting have been addressed in mechanical and thermo-mechanical numerical models (Duretz and Schmalholz, 2015; Duretz et al., 2016). These models emphasize the role of a pre-existing macroscopic mechanical anisotropy on the development of continental rifts. They illustrate the interplay between necking (boudinage) and lateral extraction of strong layers along weak décollements, thus defining a lenticular fabric and anastomosed shear zone networks at the regional scale as envisioned in the NPZ case.

Models of metamorphic core complexes (MCCs) formation generally involve a thick and hot continental crust (Brun and van den Driessche, 1994). This does not apply to the Pyrenean case but constructive inputs can be expected from a confrontation with the rheological parameters used for MCCs modeling. For instance, Tirel et al. (2008) use initial Moho temperatures of 800°C or higher, with crustal thicknesses of 45 km or greater. This contrast with the post-Variscan crust in the Pyrenees, whose thickness ranges between 30 and 20 km (Teixell et al., 2018, and references therein) with Moho temperature likely lower than 800°C. In the Tirel et al. (2008) experiment, exhumation process in metamorphic domes result in the progressive development of a detachment zone. Because both the lower crust and the mantle lithosphere have a low strength, no strain localization occurs in the mantle. As a result, the Moho remains flat. With Moho temperatures lower than 800°C, the sub-Moho mantle has higher strength, which can result in a Moho deflections and lithosphere-scale necking. Such conditions (relatively cold mantle and thin crust) may have prevailed in the Pyrenean region, explaining why the Pyrenean mantle reached the surface during rifting.

A former numerical model that applies to the formation of passive continental margins suggests that the crust may also be thinned by permanent pure shear both at the proximal and distal margin (Huismans and Beaumont, 2011) **(Fig. 12A)**. This scenario can be applied to the Pyrenean case where the ductile behavior of the middle crust is recognized (Asti et al., 2019). The model of Huismans and Beaumont (2011) produced symmetric margins associated with distal domain characterized by large sheets of thinned crustal material, as discussed above. The symmetrical outline is well imaged by current reconstructions of the Pyrenean basins from the North Pyrenean Zone and associated examples (Parentis, Cameros and Columbrets basins, **Figs. 1, 2 & 7**).

Brune et al. (2014) produced a model that emphasizes rift migration accomplished by sequential upper crustal faults and balanced through lower crustal flow **(Fig. 12B)**. The authors provided the concept of ‘exhumation channel’, which defines a region where the crust and the uppermost mantle are actively deformed and extremely thinned during their transfer from lower to shallower levels. This high strain volume is not formally a detachment fault and may be at the origin of the crustal lenses exhumed within the NPZ (Asti et al., 2019). As discussed in section 4.3, the resulting structure comprises sheets of drastically thinned crust forming the distal margin domain lying over a cooled and strengthened mantle. This mantle may become exposed at the rift axis depending on the extension rate. The final sketch derived from this model, a dome of strong mantle rimmed in its upper part by a thin layer of mylonitic crust, is a reliable image for the structure resulting from the Pyrenean rifting and associated basins at a lithospheric scale.

Jammes et al. (2015) and Jammes and Lavier (2016), introduced compositional complexities in the lithosphere by using an explicit bimineralic assemblage which results in the development of anastomosing shear zone. In their models, the deformation appears localized

in the middle/lower crust and the upper lithospheric mantle and leads to the preservation of almost undeformed lenses of material surrounded by localized shear zones concentrating most of the deformation. Such a lenticular final geometry is also evocative of the one observed in the North Pyrenean Zone as discussed in detail by Asti et al. (2019) and illustrated in **Fig. 10**.

To unravel the dynamic evolution of the Cretaceous Pyrenean rift, Duretz et al. (2019) carried out a set of thermo-mechanical numerical models of lithosphere-scale extension based on the available geological constraints listed above in section 2. The models were used to explore the role of a km-thick basement-cover décollement layer at the base of the prerift sediments. These numerical experiments highlight the first order role of the décollement layer that can alone explain collectively: (i) salt tectonics deformation style and cover décollement, (ii) high temperature metamorphism of the prerift cover, and (iii) widespread ductile deformation of the basement. In the axis of the synclinal-shaped basin (« sag » basin in the margin literature), extreme pure shear leads to the development of a very thin basement layer, overlain by slightly thinned prerift and synrift sediments and underlain by exhuming mantle. These models are in good agreement with the current knowledge of the architecture of the Cretaceous Pyrenean basins as exemplified by reconstructions of **Figures. 2 & 7**, as well as with the presence of large sheets of hyper thinned crustal material (crustal sheets) in the distal part of numerous magma-poor passive margins.

5.3. The prerift salt and clay décollement layer: a key factor for the evolution of smooth-slopes basins. Establishing a new link between Triassic paleogeography and rifting mechanisms.

As reported in section 2 and 3, the common character shared between all prerift sequences of the aforementioned smooth-slopes basins is the presence of the thick prerift salt and clay unit of the Keuper group. All related geological and geophysical studies highlight the importance of this décollement layer. Indeed, it triggers mechanical decoupling and gliding of the prerift cover that remains in the center of the basin while parts of the crust are boudinaged and laterally extracted from the rift axis. In response to hyper-thinning and horizontal extraction of the basement, hot mantle material approaches the detached prerift cover. As a consequence, HT-LP metamorphism developed in the prerift sediments and at the base of the synrift flysch levels as recorded in the NPZ and in the synrift sediments of the Cameros basin. The presence of abundant alkaline volcanic products in the Cantabrian basin and in the NPZ also argues for partial melting of the exhuming mantle. Subsequent deposition of blanketing synrift sediments allows for maintaining high temperatures in the underlying units with major consequences on the deformation style of the prerift sediments and basement. Temperature increase in the center NPZ basins progressively led to the rise of the brittle/ductile transition avoiding the development of prominent crustal normal faults and leading to the dominantly ductile thinning of the Paleozoic basement and parts of the prerift and synrift sediments (Clerc and Lagabrielle, 2014; Clerc et al., 2015b; Asti et al., 2019; Duretz et al., 2019). We may now question the paleogeographic distribution of the Keuper group sediments at the Europa-Iberia scale and evaluate the possibility of a genetic link between the occurrence of a thick prerift décollement and the style of rifting.

Several extensional systems interacted in the Iberia platform during the Triassic, resulting in the creation of intraplate basins or troughs including the Valencian, Basque-Cantabrian, and Pyrenean basins **(Figs. 1 & 13)**. The sedimentary infill of these platform basins continued throughout the Mesozoic. Seismic, well and field data from the Bay of Biscay region, the Pyrenees and the Aquitanian Basin, suggest initial thickness of Upper Triassic formations ranging from 1000 to 2700 m (James and Canérot, 1999; Biteau et al., 2006; Jammes et al., 2010a; Roca et al., 2011; Rowan, 2014; Lopez-Mir et al., 2014; Saura et al., 2016; Soto et al., 2017; Zamora et al., 2017; López-Gómez et al., 2019). In outcrop, the salt-rich layers generally consist of shales and evaporites including dominant gypsum and minor halite and anhydrite **(Figs. 13 & 14)**. Paleogeographic reconstructions are available for the Triassic period at the scale of the Iberia-western Europa region (Dercourt et al., 1986; 1993; Ziegler, 1988; Ortí et al., 2017; Soto et

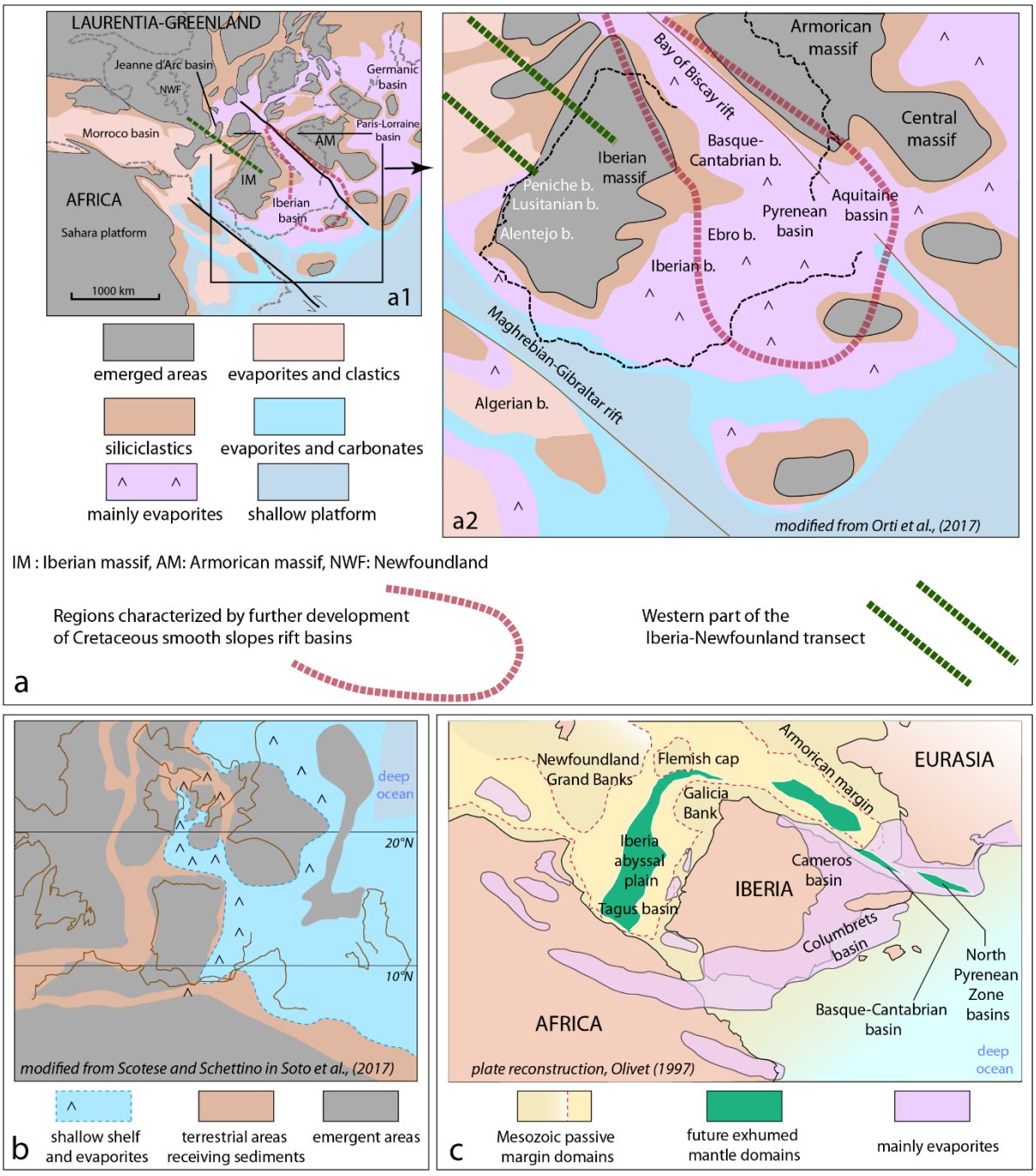


Fig. 13. Paleogeography of Triassic deposits and Cretaceous rifting around the Iberia plate. **(A)** paleogeographic maps for the Triassic period (modified from Orti et al., 2017) and location of some further Cretaceous rifted regions. Note that by contrast to the area where Cretaceous smooth-slopes basins will open, the area corresponding to the future Iberia-Newfoundland conjugate margins are devoid of thick evaporitic series. **(B)** paleogeographic maps for the Ladinian and Carnian (Middle-early Late Triassic times, 242-227 Ma) modified after Scotese and Schettino (2017). **(C)** paleogeography of Upper Triassic deposits prepared after a compilation of unpublished data by D. Frizon de Lamotte (pers. com.) superimposed on a plate reconstruction by Olivet (1996).

al., 2017). This paleogeography is confirmed by a compilation of data collected independently by D. Frizon de Lamotte **(Fig. 13C)**. Evaporites are well developed along the eastern edge of Iberia (Tethys side) and in the rifts located along the NPZ, the Basque-Cantabrian basin, the Bay of Biscay basin, the Asturian-Cantabrian Mountains and the southern part of the Armorican margin. At the location of the future North Atlantic rift system, evaporites are restricted to the Peniche, Lusitanian, Alentejo and Algarve basins along the southern half of the Portugal margin. They are lacking along the northern half of the Iberia Atlantic margin.

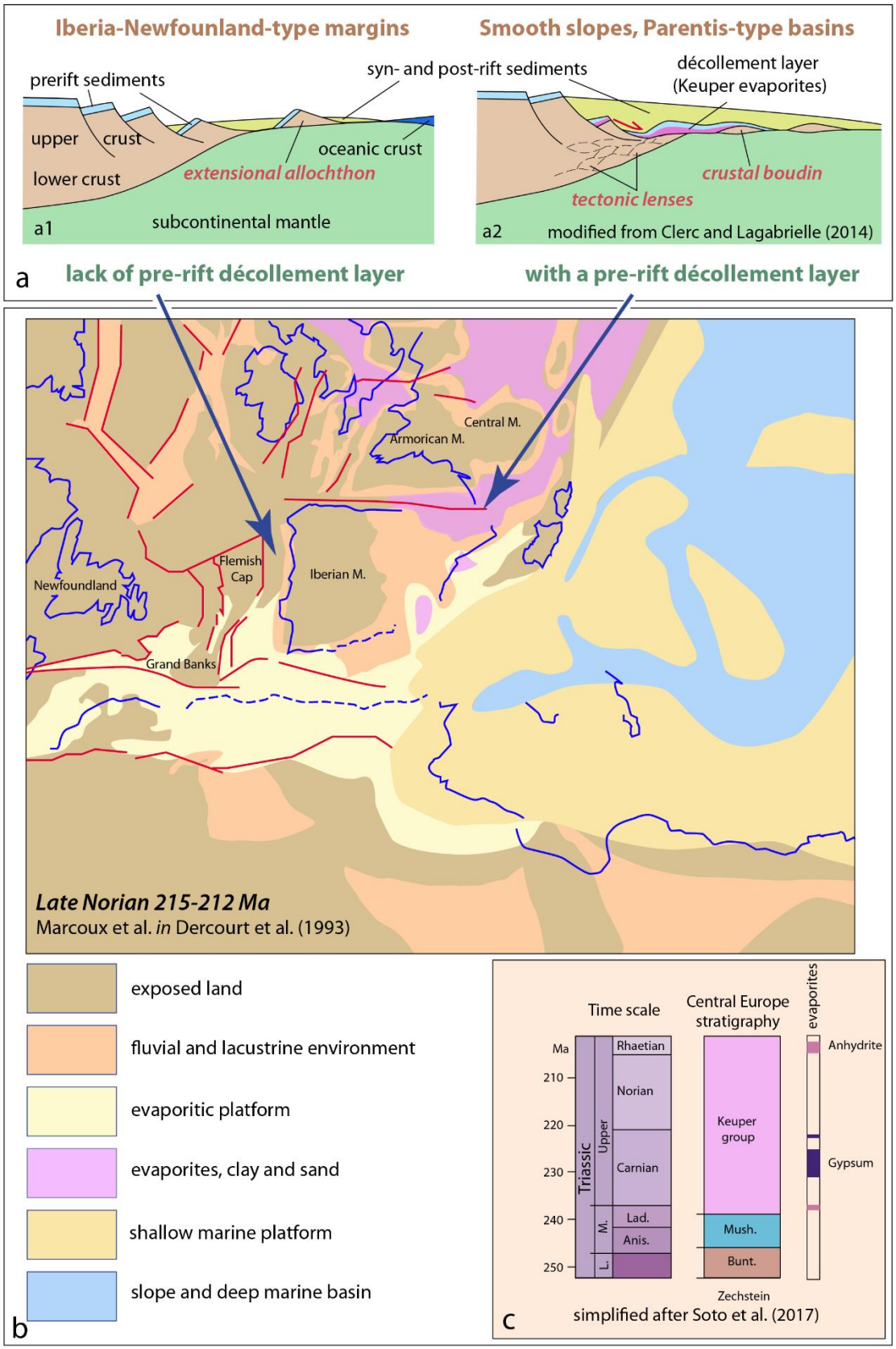


Fig. 14. Correlation between the paleogeography of Triassic deposits and the mode of rifting around the Iberia plate. **(A)** cartoons (a1 and a2) illustrating the contrasted rifting modes between the Iberia-Newfounland-type and the Parentis-type margins (modified from Clerc and Lagabrielle, 2014). **(B)** paleogeography of Triassic (Late Norian) deposits according to Marcoux et al. in the Dercourt et al. (1993) map atlas. As paleogeographic maps in fig. 13, this reconstruction points to the lack of thick evaporites deposits in the future Iberia-Newfoundland rifting domain (see text for discussion).

Along the conjugate North-American margin, evaporites are known only at the base of the Jeanne-d'Arc basin and are of restricted extent compared to the Keuper group exposed in Central Europe **(Figs. 13B & 13C)**.

Finally, along the western half of the Iberia-Newfoundland transect, the presence of a potential evaporitic formation is not reported. As outlined by **Figures 13 & 14**, this paleogeography matches the distribution of the two opposite types of basins discussed in this article (smooth-slopes type vs. Iberia-Newfoundland type). Thus, we suggest a link between the presence of a prerift salt layer and the style of rifting. Indeed, prerift salt and clay décollement allows for the preservation of a 5-6 km thick allochthonous prerift cover and overlying synrift sediments in the central part of the rift system. The exhumation of hot mantle and the presence of a thick sedimentary pile lead to abnormally high temperature in the thinning basement. It thus favors HT-LP metamorphism of the sedimentary cover and associated ductile deformation of the prerift cover and the underlying basement.

The lack of a major décollement level at the base of the prerift sequence may explain why prerift sediments remained welded and coupled to the basement on the top of tilted blocks in the Iberia-Newfoundland-type margins **(Figs. 3A & 3B)**. Indeed, in the Iberia as well as in Alpine margin-types, only synrift sediments are deposited over exhumed lower crustal levels and subcontinental mantle (Péron-Pinvidic et al., 2007; Péron-Pinvidic and Manatschal, 2009; Mohn et al., 2012), which contrasts with the evolution of the smooth-slopes type basins. Here, we focus on the influence of surficial Earth features, such as sedimentary formations, on deep-seated processes such as the evolution of lithospheric rifting. We are well aware that lithospheric and crustal heterogeneities acquired during superimposed geological cycles probably control at a first order the location and modalities of rifting processes. Structural inheritances are thus largely considered in the history of continental breakup during passive margins formation (i.e., Andersen et al., 2012; Chenin et al., 2014; Asti et al., 2019) as well during the formation of the Pyrenean rift (Munoz, 1992; 2002; Clerc and Lagabrielle, 2014; Teixell et al., 2018; Asti et al., 2019). Recently, Fernández-Lozano et al. (2019) conclude that differences in the nature of the lithosphere as a result of the Cantabrian orocline formation may be also responsible for the distribution and shape of the Cretaceous extensional basins north of the Iberia margin.

Based on examples clustering along the Iberia-Eurasia plate boundaries, we emphasize the major role played by the Upper Triassic evaporitic layer during extensional processes. In the reported smooth-slopes basin examples, cover gliding occurred on a prerift salt and clay layer, which with cases involving syn- to postrift salt tectonics. The latter cases have been largely documented by studies of passive margins displaying thick postrift salt formations such as the Angola margin where the post-salt sedimentary units have glided gravitationally after margin formation (e.g. Jammes et al., 2010c; Brun and Fort, 2011; Rowan, 2014 and references therein). To summarize, the specificities emphasized in this review are two-fold: (i) peri-Pyrenean salt is prerift and allows for the conservation of the prerift cover over the high-strain axial rift. Crustal faulting has not disrupted the continuity of the prerift salt and clay unit. This décollement promoted the detachment of prerift sequences, which were then preserved in the distal part of the margins. (ii) Consequently, the exhumation of hot mantle underneath thick overlying sedimentary cover promoted the occurrence of high temperature deformation and metamorphism. Dominant ductile deformation of the basement deformation prevented the development of fault–related scarps and led to formation of smooth-slopes basin edges.

5.4. Time-dependent rheology during the evolution of smooth-slopes basins

From the statements above (sections 2, 3, 4), we stress that the models of NPZ Pyrenean Cretaceous rifting differ significantly from the classical models of passive margin formation based on the Iberia-Newfoundland margins example involving a dominantly brittle crust with tilted fault blocks **(Fig. 3A)** (Péron-Pinvidic and Manatschal, 2009; Sutra et al., 2013; Osmundsen and Péron-Pinvidic, 2018, and references therein). In the models based on the geology of the NPZ (e.g. models of Clerc et al., 2016; Teixell et al., 2016; Espurt et al., 2019), the external borders of the subsiding

Cretaceous flysch basins remain at low temperature and display classical faulted and tilted blocks (e.g. half-grabens of Quillan basin, Camarade basin, Gensac-Bonrepos basin, western border of the Mauléon basin, Arbailles basin, edges of the Gran Rieu high and Lacq basin). This constrast with the internal regions of the rift system (corresponding to the future metamorphic NPZ), where basement thinning occurred in a dominant-ductile fashion as temperature conditions reached 350°C to 450°C beneath the detached prerift cover and the synrift flysch.

The peculiar evolution of the NPZ basins is depicted on **Figure 15** based on an original model by Clerc et al., (2016). This model is strictly conceptual and was designed to account for geological constraints gathered from various sites along the NPZ. The conceptual model includes subcontinental mantle, continental basement, a first decollement level in Triassic evaporites and a cover of prerift carbonates and synrift flysch. Corresponding lithologies are illustrated and briefly described in the NPZ lithostratigraphical column of **Figure 5**.

In order to better assess the time-dependent rheological changes that necessarily affect each geological layer involved during this three steps evolution, we provide synthetic rheological profiles and geotherms for selected parts of the basin: in the external portion representing the initial prerift model **(Fig. 15A)** and in the center of the basin for the following two steps **(Figs. 15B & C)**. The data used to construct these profiles are derived from the reference model of Duretz et al. (2019).

The three steps of this conceptual evolutionary model can be described as follows:

(1) At an early rifting stage **(Fig. 15A)** moderate extension leads to crustal thinning accommodated through normal faults in the upper crust. The rheological profile consists of a 15 km thick, cold and brittle upper crust (T < 300°C) overlying a 15 km thick ductile lower crust with Moho temperature around 550°C. The uppermost mantle is a strong 15 km thick layer. In the inner part of the system, normal faults may change downward to ductile shear zones dipping toward the external side thus delineating a small central horst. The prerift salt and clay unit acts as a décollement layer that allows the prerift carbonates to remain in developing basins on both sides of the central horst while the synrift flysch is deposited. Sliding of prerift carbonates towards distal domain leads to tectonic denudation of the margins where carbonates remnants form isolated rafts.

(2) At the mid-rifting stage **(Fig. 15B)**, dominantly ductile basement thinning occurs in response to stretching and heating due to mantle rise. Due to blanketing effect under the synrift sediments, HT prerift carbonates undergo syn-metamorphic ductile deformation. The rheological profile in the center of the basin underlines the prerift salt and clay unit and a newly formed weak zone corresponding to the thinned crust which deforms at temperatures between 300°C and 500°C. The lower crust has been extracted laterally and temperature increases from 400°C (step 1) to 1000°C at only 20 km depth in the strong lithospheric mantle.

(3) At the final rifting stage **(Fig. 15C)**, extreme thinning and boudinage of the crust leads to local denudation of exhumed mantle, which is locally emplaced in tectonic contact with the pre- or synrift sediments, occasionally associated with salt diapirism. The crust in the center of the basin has been split into few lenses that move independently. The crust at both edges of the proximal domain is laterally extracted from the basin axis (Clerc and Lagabrielle, 2014). The prerift salt and clay décollement layer undergoes thickness variations (e.g. diapirism) and is the locus of fluid-assisted tectonic brecciation with metasomatic dissolution and crystallization as observed in the Urdach and Saraillé massifs in the western NPZ (Lagabrielle et al., 2019a; 2019b). HT marbles of the prerift cover progressively accommodate a large part of the deformation at the base of the basin, involving calcite creep and recrystallization, pinch-and-swell, drag folding and low angle normal shear bands. In turn, the lower levels of the synrift flysch sequence are progressively affected by HT metamorphism and ductile deformation induces the development of bedding-parallel foliation and pinch-and-swell structures. Continuous extension of the basin floor leads also to the progressive exhumation of the metamorphic prerift sediments, originating from below the synrift cover (see complete description of this process in Clerc et al., 2016).

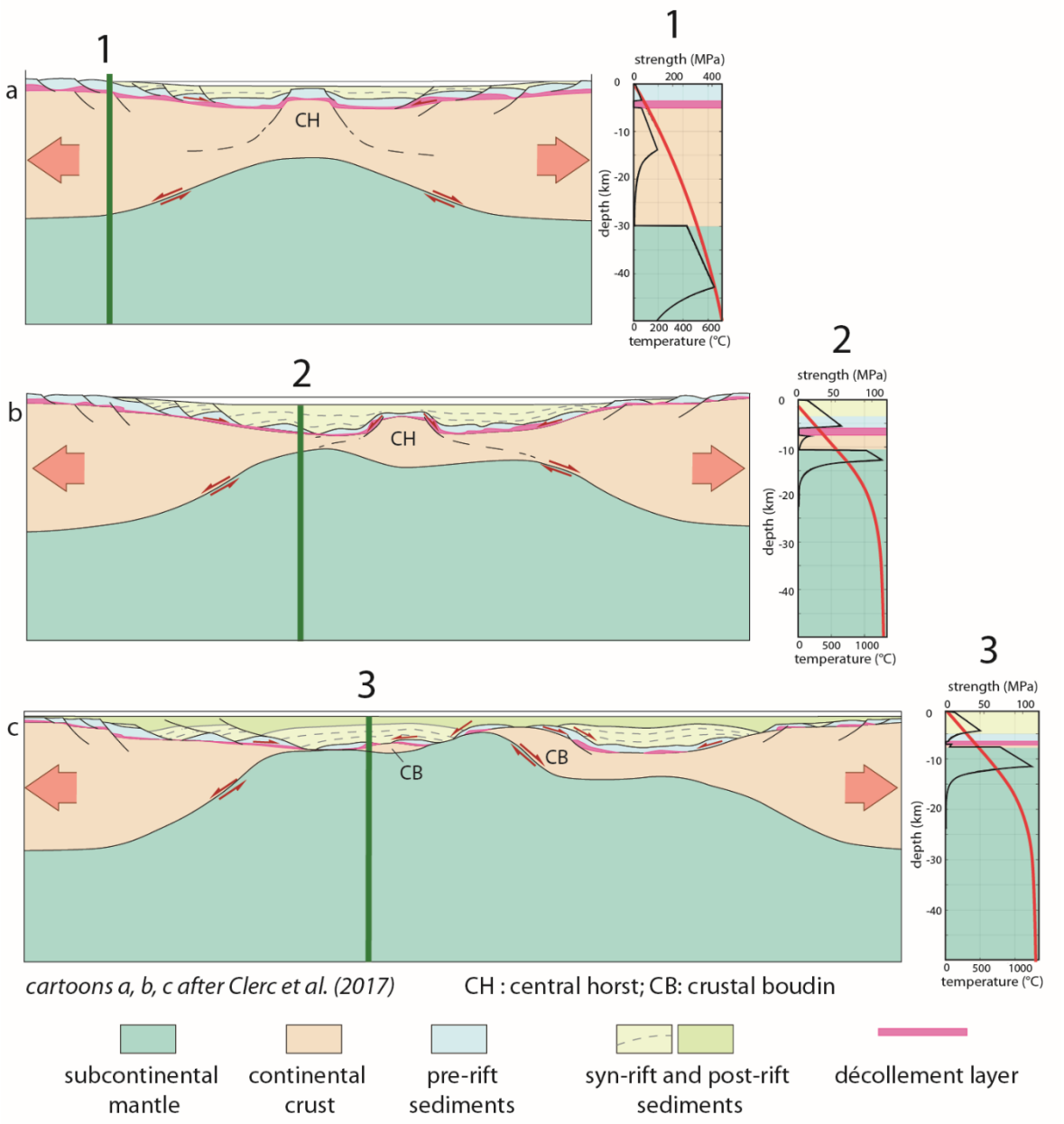


Fig. 15. Time-dependent rheological evolution of the Pyrenean rifting based on geological constraints from the North Pyrenean Zone and numerical results from a thermo-mechanical numerical modeling. Sketches depicting the geological evolution are extracted from the Clerc et al. (2016) model. Rheological profiles are derived from the Duretz et al., (2019) model. They are placed at critical locations (1, 2 and 3) of the rift in order to emphasize the drastic changes in the mechanical behavior during its evolution from limited crustal extension to local mantle exhumation (see detailed description in text).

In the thinnest crustal portion, the rheological profile bears similarities with that of step 2. The crustal thickness has now reduced to less than one km and the brittle/ductile transition has moved upward. The prerift cover, prerift salt and clay décollement as well as the thinned basement thus deform under dominant ductile deformation.

6. Conclusions

This review highlights the affinities between the architecture of the smooth-slopes extensional basins that opened during mid-Cretaceous times around the Iberia-Eurasia plate boundary, now variously inverted in the Pyrenean orogeny (Parentis, Basque-Cantabrian, NPZ and Cameros to Columbrets basins). Taking the Parentis basin profile as a reference and using geological reconstructions of NPZ rift architecture, we elaborate the concept of smooth-slopes type basins shown in **Figure 16**. The dominant features of this conceptual model are a dominant symmetrical profile and the absence of prominent normal

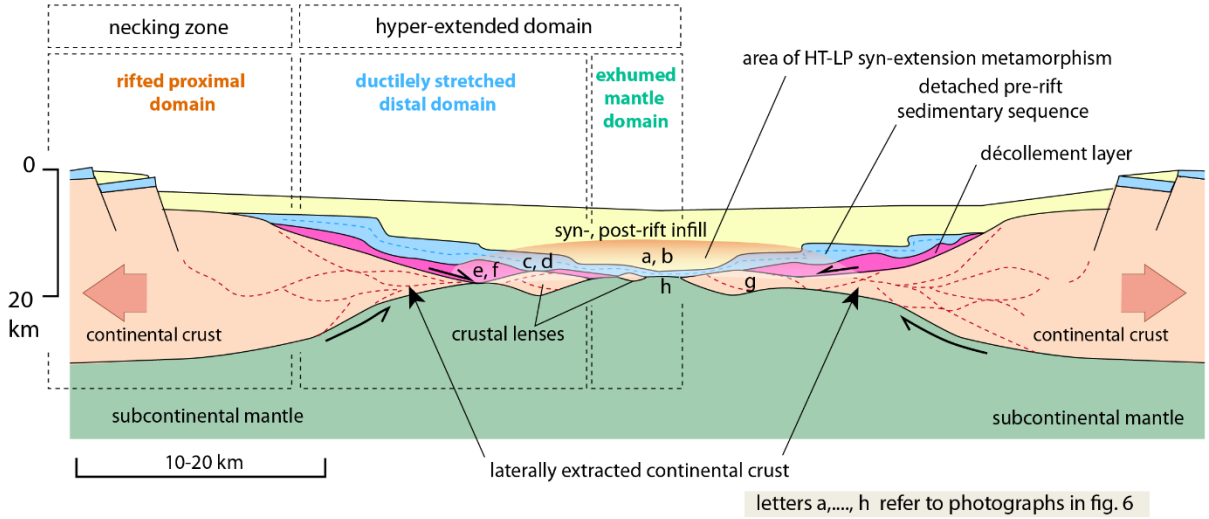


Fig. 16. A theoretical structural model for the Cantabrian, Pyrenean and Iberian symmetrical smooth-slopes basins based on the features and concepts discussed in this article (see comments in the Conclusion section).

faults and large-scale tilted crustal blocks in center of the basin. Smooth-slopes type basins involve the activation of décollements (e.g. basin-cover décollement) that promotes sedimentary cover gliding and lateral extraction of basement units. Basement and cover thinning occurs in a high temperature regime and thus lead to the widespread development of ductile deformation structures as well as metamorphism. The morphology of the margins of smooth-slopes basins is rather symmetrical and thus drastically contrasts with that of Iberia-Newfoundland type margins.

The common character between all prerift sequences of the study smooth-slopes basins is the presence of the thick low-strength Late Triassic evaporitic layer (Keuper facies). As established by geological studies in the NPZ, efficient décollement along this prerift salt and clay unit triggers mechanical decoupling and gliding of the prerift cover that remains in the center of the basin as the crust is laterally extracted. Subsequent deposition of synrift sediments allows for the preservation of the initial thermal anomaly with a major consequence on the deformation regime in the prerift sediments and crustal basement. The ubiquitous character of the ductilely deformed marbles in the metamorphic NPZ relates to a dominant-ductile deformation regime in the prerift cover during the Cretaceous extension. In these smooth-slopes basins, the ductilely stretched crust behaves homogeneously at the regional scale and extensional allochthons are not recognized. A lenticular mode of homogeneous deformation is thus defined implying interplay between hectometer-sized lenses of ductile crustal material separated by anastomosed shear zones.

Both laboratory and thermo-mechanical numerical models reproduce remarkably the mode of deformation deduced from geophysical and geological constraints compiled in this study. It appears that the occurrence of a prerift salt and clay unit and the activation of synrift salt tectonics is a key factor that affects the overall rifting style. This is in contrast with Atlantic margins where salt is either synrift or postrift. For the first time, we evidence a strong link between the occurrence of a sedimentary layer covering the future rifted region (here Keuper salt and clays deposits) and the style of rifting. Décollement along the prerift salt and clays units finally favors the formation of smooth-slopes type basins. This new mode of crustal deformation might not be restricted to the Pyrenean region, but may apply to other margins that host thick prerift décollement series. This rifting mode may indeed have affected distal portions of continental margins that are devoid of tilted blocks and extensional allochthons and where large volumes of extremely thinned continental crust are present.

Acknowledgements

This work is the result of a 10 years field and laboratory research conducted in the Pyrenean range with funding from various programs and institutions. We benefited of

grants from the French ANR Pyramid program, the Bureau de Recherche Géologique et Minière (BRGM), Référentiel Géologique de la France (RGF) program and the Total/INSU/BRGM OROGEN program with contributions from the CNRS, from Géosciences Montpellier and Rennes research units and Spanish MINECO-MINCIU research units. We thank Thierry Baudin (BRGM) and Sylvain Calassou (Total) for program management and encouraging discussions. We also thank Th. Nalpas, B. Azambre, P. Boulvais, M. Poujol, and many others for stimulating exchanges that helped improve our ideas. We are indebted to one anonymous referee, to Maria Laura Balestrieri and to Gabriel Gutiérrez-Alonso for their useful comments and remarks on a first version of this manuscript. We also benefited of comments by Editor Carlo Doglioni who is acknowledged here.

References

Allemand, P., Brun J.-P., Davy P., and Van Den Driessche J., 1989. Symétrie et asymétrie des rifts et mécanismes d'amincissement de la lithosphère, Bull. Soc. Géol. Fr., 5, 445–451.

Andersen, T.B., Corfu, F., Labrousse, L., and Osmundsen, P.T., 2012. Evidence for hyperextension along the pre-Caledonian margin of Baltica. *Journal of the Geological Society, London,* 169; 601-612. doi: 10.1144/0016-76492012-011

Asti, R., Lagabrielle, Y., Fourcade, S., Corre, B., Monié, P., 2019. How do continents deform during mantle exhumation? Insights from the northern Iberia inverted paleopassive margin, western Pyrenees (France). Tectonics, 38, 1666–1693. https://doi.org/10.1029/2018TC005428

Ayala, C., Torne, M., Roca, R., 2015. A review of the current knowledge of the crustal and lithospheric structure of the Valencia Trough Basin. Bol. Geológico Min. 126, 533–552.

Azambre, B., Rossy, M., 1976. Le magmatisme alcalin d'age cretace, dans les Pyrenees occidentales et l'Arc basque; ses relations avec le metamorphisme et la tectonique. Bull. Société Géologique Fr. 7, 1725–1728.

Bernus-Maury, C., 1984. Etude des paragéneses caractéristiques du métamorphisme mésozoïque dans la partie orientale des Pyrénées. Thèse, Pierre et Marie Curie, Paris.

Biteau, J.-J., Le Marrec, A., Le Vot, M., Masset, J.-M., 2006. The Aquitaine Basin. Pet. Geosci. 12, 247–273.

Bois, C., Gabriel, O., Lefort, J.-P., Rolet, J., Brunet, M.-F., Masse, P., Olivet, J.-L., 1997. Geologic contribution of the Bay of Biscay deep seismic survey: a summary of the main scientific results, a discussion of the open questions and suggestions for further investigation. Mém Soc Géol Fr. 193–309.

Brun, J. P., 1999. Narrow rifts versus wide rifts: Inferences for the mechanics of rifting from laboratory experiments, Philos. Trans. R. Soc. London, Ser. A, 357, 695–712.

Brun, J. P., Beslier M.O., 1996. Mantle exhumation at passive margin, Earth Planet. Sci. Lett., 142, 161– 173.

Brun, J.-P., and van den Driessche, J., 1994. Extensional gneiss domes and detachment fault systems; structure and kinematics. Bull. Société Géologique Fr. 165, 519–530.

Brun, J.P., Wenzel, F. and ECORS-DEKORP team, 1991. Crustal structure of the southern Rhine Graben from ECORS-DEKORP seismic reflection data, Geology, 19, 758-762. DOI: 10.1130/0091-7613(1991)019<0758:CSSOTS>2.3.CO

Brun, J.-P., Fort, X., 2011. Salt tectonics at passive margins: Geology versus models. Mar. Pet. Geol. 28, 1123–1145. https://doi.org/10.1016/j.marpetgeo.2011.03.004

Brune, S., Heine, C., Pérez-Gussinyé, M., Sobolev, S.V., 2014. Rift migration explains continental margin asymmetry and crustal hyper-extension. Nat. Commun. 5. https://doi.org/10.1038/ncomms5014

Buck, W. R., 1991. Modes of continental lithospheric extension, J. Geophys. Res., 96, 20,161–20,178.

Buck, W. R., F. Martinez, M. S. Steckler, and J. R. Cochran, 1988. Thermal consequences of lithospheric extension: Pure and simple, Tectonics, 7, 213 – 234.

Cadenas, P., Fernández-Viejo, G., 2017. The Asturian Basin within the North Iberian margin (Bay of Biscay): seismic characterisation of its geometry and its Mesozoic and Cenozoic cover. Basin Res. 29, 521–541. https://doi.org/10.1111/bre.12187

Canérot, J., 1988. Manifestations de l'halocinèse dans les Chaînons Béarnais (Zone Nord-Pyrénéenne) au Crétacé inférieur. Comptes Rendus de l'Académie des Sciences de Paris 306, 1099-1102.

Canérot, J., 1989. Rifting éocrétacé et halocinèse sur la marge ibérique des Pyrénées Occidentales (France). Conséquences structurales. Bull. Cent. Rech. Explor.-Prod. Elf-Aquitaine 13, 87–99.

Canérot, J., 2017. The pull apart-type Tardets-Mauléon Basin, a key to understand the formation of the Pyrenees. Bull. Société Géologique Fr. 188, 35. https://doi.org/10.1051/bsgf/2017198

Canérot, J., Hudec, M.R., Rockenbauch, K., 2005. Mesozoic diapirism in the Pyrenean orogen: Salt tectonics on a transform plate boundary. AAPG Bull. 89, 211–229. https://doi.org/10.1306/09170404007

Canérot, J., Lenoble, J.-L., 1989. Le diapir du Lichançumendy (Pyrénées-Atlantiques), nouvel élément de la marge ibérique des Pyrénées occidentales. Comptes Rendus Académie Sci. Sér. 2 Mécanique Phys. Chim. Sci. Univers Sci. Terre 308, 1467–1472.

Canérot, J., Lenoble, J.-L., 1993. Diapirisme crétacé sur la marge ibérique des Pyrénées occidentales; exemple du pic de Lauriolle; comparaisons avec l'Aquitaine, les

Pyrénées centrales et orientales. Bull. Société Géologique Fr. 164, 719–726.

Capdevila, R., Boillot, G., Lepvrier, C., Malod, J.-A., Mascle, G., 1980. Les formations cristallines du Banc Le Danois (marge nord ibérique). Comptes Rendus Académie des Sciences de Paris 291, 317–320.

Casas-Sainz, A.M., Gil-Imaz, A., 1998. Extensional subsidence, contractional folding and thrust inversion of the eastern Cameros basin, northern Spain. Geol Rundsch 86(4):802–818

Castanares, L.M., Robles, S., Gimeno, D. and Vicente Bravo, J.C., 2001. The Submarine Volcanic System of the Errigoiti Formation (Albian-Santonian of the Basque-Cantabrian Basin, Northern Spain): Stratigraphic Framework, Facies, and Sequences. Journ. Sedim. Research. 71 , 2, 318-333.

Chalmers, J.A. and Pulvertaft, T.C.R., 2001. Development of the continental margins of the Labrador Sea: a review. In Wilson, R.C.CL, Whitmarsh, R.B., Taylor, B., and Froitzheim, N., 2001. Non-Volcanic Rifting of Continental Margins: A Comparison of Evidence from Land and Sea. Geol. Soc. London Spec. Pub., 187, 77-105.

Chenin, P., Manatschal, G., Lavier, L., and Erratt, D., 2015. Assessing the impact of orogenic inheritance on the architecture, timing and magmatic budget of the North Atlantic rift system: a mapping approach. Journal of the Geological Society, London, doi:10.1144/jgs2014-139

Chevrot, S., Sylvander, M., Díaz, J., Ruiz, M., Paul, A., PYROPE Working Group, 2015. The Pyrenean architecture as revealed by teleseismic P-to-S converted waves recorded along two dense transects. Geophysical Journal International 200, 1094-1105.

Chevrot, S., Sylvander, M., Diaz, J., Martin, R., Mouthereau, F., Manatschal, G., Masini, E., Calassou, S., Grimaud, F., Pauchet, H., Ruiz, M., 2018. The non-cylindrical crustal architecture of the Pyrenees. Sci. Rep. 8. https://doi.org/10.1038/s41598-018-27889-x

Choukroune, P., 1976a. Strain patterns in the Pyrenean chain: Philosophical Transactions of the Royal Society of London A: Mathematical, Physical and Engineering Sciences, v. 283, no. 1312, p. 271–280.

Choukroune, P., 1976b. Structure et évolution tectonique de la zone nord pyrénéenne, Mem. Soc. Geol. Fr., 127, 1-116.

Choukroune, P., ECORS Team, 1989. The ECORS Pyrenean deep seismic profile reflection data and the overall structure of an orogenic belt. Tectonics 8, 23–39.

Choukroune, P., Mattauer, M., 1978. Tectonique des plaques et Pyrénées; sur le fonctionnement de la faille transformante nord-pyrénéenne; comparaisons avec des modèles actuels. Bull. Société Géologique Fr. 7, 689–700.

Clerc, C., and Lagabrielle, Y., 2014. Thermal control on the modes of crustal thinning leading to mantle exhumation: Insights from the Cretaceous Pyrenean hot paleomargins. Tectonics 33, 1340–1359. https://doi.org/10.1002/2013TC003471

Clerc, C., Jolivet, L., Ringenbach, J.-C., 2015a. Ductile extensional shear zones in the lower crust of a passive margin. Earth Planet. Sci. Lett. 431, 1–7. https://doi.org/10.1016/j.epsl.2015.08.038

Clerc, C., Lahfid, A., Monié, P., Lagabrielle, Y., Chopin, C., Poujol, M., Boulvais, P., Ringenbach, J.C., Masini, E., de St Blanquat, M., 2015b. High-temperature metamorphism during extreme thinning of the continental crust: a reappraisal of the North Pyrenean passive paleomargin. Solid Earth 6, 643–668.

Clerc, C., Lagabrielle, Y., Labaume, P., Ringenbach, J.-C., Vauchez, A., Nalpas, T., Bousquet, R., Ballard, J.-F., Lahfid, A., Fourcade, S., 2016. Basement – Cover decoupling and progressive exhumation of metamorphic sediments at hot rifted margin. Insights from the Northeastern Pyrenean analog. Tectonophysics 686, 82–97. https://doi.org/10.1016/j.tecto.2016.07.022

Clerc, C., Ringenbach, J.-C., Jolivet, L., Ballard, J.-F., 2018. Rifted margins: Ductile deformation, boudinage, continentward-dipping normal faults and the role of the weak lower crust. Gondwana Res. 53, 20–40. https://doi.org/10.1016/j.gr.2017.04.030

Corre, B., Lagabrielle, Y., Labaume, P., Fourcade, S., Clerc, C., Ballèvre, M., 2016. Deformation associated with mantle exhumation in a distal, hot passive margin environment: New constraints from the Saraillé Massif (Chaînons Béarnais, North-Pyrenean Zone). Comptes Rendus Geosci. 348, 279–289. https://doi.org/10.1016/j.crte.2015.11.007

Cuevas, J., Tubia, J.M., 1999. The discovery of scapolite marbles in the Biscay Synclinorium (Basque-Cantabrian basin, Western Pyrenees): geodynamic implications. Terra Nova 11, 259–265. https://doi.org/10.1046/j.1365-3121.1999.00255.x

Damotte, B., 1998. The ECORS Pyrenean Deep Seismic Surveys, 1985–1994, Mémoires de la Société géologique de France, 173, 104 p., 8 pl.

Dañobeitia, J.J., Arguedas, M., Gallart, J., Banda, E., Makris, J., 1992. Deep crustal configuration of the Valencia trough and its Iberian and Balearic borders from extensive refraction and wide-angle reflection seismic profiling. Tectonophysics 203, 37–55.

Dauteuil, O., and Ricou, L.-E., 1989. Une circulation de fluides de haute-température à l'origine du métamorphisme crétacé nord-pyrénéen. Geodin. Acta 3, 237–249. doi :10.1080/09853111.1989.11105190

de Saint Blanquat, M., Bajolet, F., Grand'Homme, A., Proietti, A., Zanti, M., Boutin, A., Clerc, C., Lagabrielle, Y., Labaume, P., 2016. Cretaceous mantle exhumation in the central Pyrenees: New constraints from the peridotites in eastern Ariège (North Pyrenean zone, France). Comptes Rendus Geosci. 348, 268–278. https://doi.org/10.1016/j.crte.2015.12.003

Debroas E.-J., 1978. Evolution de la fosse du flysch ardoisier de l'Albien supérieur au Sénonien inférieur (zone interne métamorphique des Pyrénées navarro-languedociennes), Bull. Soc. Géol. Fr. (7), XX, p. 639-648.

Debroas, E.J., 1990. Le flysch noir albo-cénomanien témoin de la structuration albienne à sénonienne de la

Zone nord-pyrénéenne en Bigorre (Hautes-Pyrénées, France). Bull. Soc. Geol. Fr. VI, 273–285. https://doi.org/10.2113/gssgfbull.VI.2.273

DeFelipe, I., Pedreira, D., Pulgar, J.A., Iriarte, E., Mendia, M., 2017. Mantle exhumation and metamorphism in the Basque-Cantabrian Basin (N Spain): Stable and clumped isotope analysis in carbonates and comparison with ophicalcites in the North-Pyrenean Zone (Urdach and Lherz). Geochem. Geophys. Geosystems 18, 631–652. https://doi.org/10.1002/2016GC006690

Deramond, J., Souquet, P., Fondecave-Wallez, M.-J., Specht, M., 1993. Relationships between thrust tectonics and sequence stratigraphy surfaces in foredeeps: model and examples from the Pyrenees (Cretaceous-Eocene, France, Spain). Geol. Soc. Lond. Spec. Publ. 71, 193–219.

Dercourt, J., Ricou, L. E., Vrielynck, B., 1993. Atlas Tethys Palaeoenvironmental maps Atlas and Explanatory Notes, Gauthier Villars Ed. diffusion CGMW Paris, 307 p., 14 maps

Dercourt, J., Zonenshain, L.P., Ricou, L.E. et al., 1986. Geological evolution of the Tethys belt from the Atlantic to the Pamirs since the Lias. Tectonophysics, 123, 1, 241-315.

Ducoux, M., Jolivet, L., Cagnard, F., Gumiaux, C., Baudin, T., Masini, E., Callot, J.P., Aubourg, C., Lahfid, A., Homonnay, E., 2019. The Nappe des Marbres unit of the Basque-Cantabrian basin: the tectono-thermal evolution of a fossil hyperextended rift basin. Tectonics in press doi: 10.1029/2018TC005348.

Duretz, T., Schmalholz, S.M., 2015. From symmetric necking to localized asymmetric shearing: the role of mechanical layering. Geology, 43, 8, 711-714.

Duretz, T., Petri, B., Mohn, G., Schmalholz, S.M., Schenker, F.L., Müntener, O., 2016. The importance of structural softening for the evolution and architecture of passive margins. Sci. Rep. 6, 38704. https://doi.org/10.1038/srep38704

Duretz,T., Asti, R., Lagabrielle, Y., Brun, J.P., Jourdon, A., Clerc, C., Corre, B., 2019. Numerical modelling of synrift salt tectonics during Cretaceous Pyrenean Rifting. Basin Research, in press.

Espurt, N., Angrand, P., Teixell, A., Labaume, P., Ford, M., de Saint Blanquat, M, and Chevrot, S., 2019. Crustal-scale balanced cross-section and restaurations of the Central Pyrenean belt (Nest- Cinca transect): superimposed orogenesis and Pyrenean rift system evolution. Tectonophysics, (to be completed)

Ethève, N., Mohn, G., Frizon de Lamotte, D., Roca, E., Tugend, J., Gómez-Romeu, J., 2018. Extreme Mesozoic Crustal Thinning in the Eastern Iberia Margin: The Example of the Columbrets Basin (Valencia Trough). Tectonics 37, 636–662.

Fabriès, J., Lorand, J.-P., Bodinier, J.-L., Dupuy, C., 1991. Evolution of the Upper Mantle beneath the Pyrenees: Evidence from Orogenic Spinel Lherzolite Massifs. J. Petrol. Special_Volume, 55–76. https://doi.org/10.1093/petrology/Special_Volume.2.55

Fabriès, J., Lorand, J.-P., Bodinier, J.-L., 1998. Petrogenetic evolution of orogenic lherzolite massifs in the central and western Pyrenees. Tectonophysics 292, 145–167.

Fernández-Lozano, J., Gutierrez-Alonso, G., Willingshofer, E., Sokoutis, D., de Vicente, G. and Cloething, S., 2019. Shaping of intraplate mountain patterns: The Cantabrian orocline legacy in Alpine Iberia. GSA, Lithosphere, https://doi.org/10.1130/L1079.1

Floquet, M., 1992. Outcrop sequence stratigraphy in a ramp setting: the Late Cretaceous Early Palaeogene deposits of the Castilian Ramp (Spain), Field Trip Guide Book in conjunction with the international symposium Sequence Stratigraphy of Mesozoic- Cenozoic European Basins: CNRS, Institut Français du Pétrole, Dijon. 130 p.

Frasca, G., Gueydan, F., Brun, J.-P., Monié, P., 2016. Deformation mechanisms in a continental rift up to mantle exhumation. Field evidence from the western Betics, Spain. Mar. Pet. Geol. 76, 310–328. https://doi.org/10.1016/j.marpetgeo.2016.04.020

Fügenschuh, B., Froitzheim, N., Capdevila, R., & Boillot, G. (2003). Offshore granulites from the Bay of Biscay margins: Fission tracks constrain a Proterozoic to Tertiary thermal history. Terra Nova, 15, 337–342, doi:10.1046/j.1365-3121.2003.00502.x.

Gallart, J., Rojas, H., Diaz, J., Dañobeitia, J.J., 1990. Features of deep crustal structure and the onshore-offshore transition at the Iberian flank of the Valencia Trough (Western Mediterranean). J. Geodyn. 12, 233–252.

García-Mondéjar J, Agirrezabala LM, Aranburu A, Fernández-Mendiola PA, Gómez-Pérez I, López-Horgue M, Rosales I., 1996. Aptian–Albian tectonic pattern of the Basque–Cantabrian Basin (Northern Spain). Geol J 31(1):13–45

García-Mondéjar J, Fernàndez-Mendiola PA, Agirrezabala LM, Aranburu A, López-Horgue MA, Iriarte E, Martinez de Rituerto S., 2004. Extensón del Aptiense-Albiense en la Cuenca Vasco-Cantábrica. SGEIGME, Madrid. Geological Society, London, Special Publications, 282, 111-138, 1 January, https://doi.org/10.1144/SP282.6

Gartrell, A.P., 1997. Evolution of rift basins and low-angle detachments in multilayer analog models. Geology 25, 615–618. doi:10.1130/0091 7613(1997)025<0615:EORBAL>2.3.CO;2

Gernigon, L., Brönner, M., Roberts, D., Olesen, O., Nasuti, A., Yamasaki, T., 2014. Crustal and basin evolution of the southwestern Barents Sea: From Caledonian orogeny to continental breakup: Evolution of the Barents Sea. Tectonics 33, 347–373. https://doi.org/10.1002/2013TC003439

Golberg, J.-M., Guiraud, M., Maluski, H., Séguret, M., 1988. Caractères pétrologiques et âge du métamorphisme en contexte distensif du bassin sur décrochement de Soria (Crétacé inférieur, Nord Espagne). Comptes Rendus de l'Académie des Sciences Paris, Série 11,307, 521-527.

Golberg, J.M., Leyreloup, A.F., 1990. High temperature-low pressure Cretaceous metamorphism related to crustal thinning (Eastern North Pyrenean Zone, France). Contrib.

Mineral. Petrol. 104, 194–207. https://doi.org/10.1007/BF00306443

Gong, Z., Langereis, C.G., Mullender, T.A.T., 2008. The rotation of Iberia during the Aptian and the opening of the Bay of Biscay. Earth Planet. Sci. Lett. 273, 80–93. https://doi.org/10.1016/j.epsl.2008.06.016

Grool, A. R., Ford, M., Vergés, J., Huismans, R. S., Christophoul, F., & Dielforder, A. (2018). Insights into the crustal-scale dynamics of a doubly vergent orogen from a quantitative analysis of its forelands: A case study of the Eastern Pyrenees. Tectonics, 37. https://doi.org/10.1002/2017TC004731

Guimerà, J., Alonso, Á., Mas, J.R., 1995. Inversion of an extensional-ramp basin by a newly formed thrust: the Cameros basin (N. Spain).). in: Basin Inversion (J.G. Buchanan, P.G. Buchanan, Eds). Geological Society, Special Publication, 88, 433-453. https://doi.org/10.1144/GSL.SP.1995.088.01.23

Guiraud, M., Séguret, M., 1985. A releasing solitary overstep model for the late Jurassic–early Cretaceous (Wealdian) Soria strike-slip basin (Northern Spain). In: Biddle KT, Christie-Blick N (eds) Strike slip deformation, basin formation and sedimentation, vol 37., SEPM Special Publication Society of Economic Paleontologists and Mineralogists, Tulsa, pp 159–175.

Hamilton, W., 1987. Crustal extension in the Basin and Range Province, southwestern United States. Geol. Soc. Lond. Spec. Publ. 28, 155–176. https://doi.org/10.1144/GSL.SP.1987.028.01.12

Huismans, R. S., Beaumont, C., 2003. Symmetric and asymmetric lithospheric extension: Relative effects of frictional-plastic and viscous strain softening, Journal of Geophysical Research 108 (B10)

Huismans, R. S., Beaumont, C., 2007. Roles of lithospheric strain softening and heterogeneity in determining the geometry of rifts and continental margins, Geological Society, London, Special Publications, 282, 111-138.

Huismans, R.S., Beaumont, C., 2011. Depth-dependent extension, two-stage breakup and cratonic underplating at rifted margins. Nature 473, 74–78. https://doi.org/10.1038/nature09988

Huismans, R.S., Beaumont, C., 2014. Rifted continental margins: The case for depth-dependent extension. Earth Planet. Sci. Lett. 407, 148–162. doi:10.1016/j.epsl.2014.09.032

James, V., Canérot, J., 1988. Diapirisme et structuration post-triasique des Pyrénées occidentales et de l'Aquitaine méridionale (France). Eclogae Geol. Helveticae 92, 63–72.

Jammes, S., Lavier, L., Manatschal, G., 2010a. Extreme crustal thinning in the Bay of Biscay and the Western Pyrenees: From observations to modeling. Geochem. Geophys. Geosystems 11. https://doi.org/10.1029/2010GC003218

Jammes, S., Tiberi, C., Manatschal, G., 2010b. 3D architecture of a complex transcurrent rift system: The example of the Bay of Biscay–Western Pyrenees. Tectonophysics 489, 210–226. https://doi.org/10.1016/j.tecto.2010.04.023

Jammes, S., Manatschal, G., Lavier, L., 2010c. Interaction between prerift salt and detachment faulting in hyperextended rift systems: The example of the Parentis and Mauléon basins (Bay of Biscay and western Pyrenees). AAPG Bull. 94, 957–975. https://doi.org/10.1306/12090909116

Jammes, S., Lavier, L.L., Reber, J.E., 2015. Localization and delocalization of deformation in a bimineralic material. J. Geophys. Res. Solid Earth 120, 3649–3663. https://doi.org/10.1002/2015JB011890

Jammes, S., Lavier, L.L., 2016. The effect of bimineralic composition on extensional processes at lithospheric scale. Geochem. Geophys. Geosystems 17, 3375–3392. https://doi.org/10.1002/2016GC006399

Jammes, S., Manatschal, G., Lavier, L., Masini, E., 2009. Tectono-sedimentary evolution related to extreme crustal thinning ahead of a propagating ocean: Example of the western Pyrenees. Tectonics 28. https://doi.org/10.1029/2008TC002406

Jolivet, L., Gorini, C., Smit, J., Leroy, S., 2015. Continental breakup and the dynamics of rifting in back-arc basins: The Gulf of Lion margin: Backarc rift and lower crust extraction. Tectonics 34, 662–679. https://doi.org/10.1002/2014TC003570

Lagabrielle, Y., Bodinier, J.-L., 2008. Submarine reworking of exhumed sub-continental mantle rocks: field evidence from the Lherz peridotites, French Pyrenees: Cretaceous exhumation of pyrenean mantle. Terra Nova 20, 11–21. https://doi.org/10.1111/j.1365-3121.2007.00781.x

Lagabrielle, Y., Labaume, P., de Saint Blanquat, M., 2010. Mantle exhumation, crustal denudation, and gravity tectonics during Cretaceous rifting in the Pyrenean realm (SW Europe): Insights from the geological setting of the lherzolite bodies. Tectonics 29. https://doi.org/10.1029/2009TC002588

Lagabrielle, Y., Clerc, C., Vauchez, A., Lahfid, A., Labaume, P., Azambre, B., Fourcade, S., Dautria, J.-M., 2016. Very high geothermal gradient during mantle exhumation recorded in mylonitic marbles and carbonate breccias from a Mesozoic Pyrenean palaeomargin (Lherz area, North Pyrenean Zone, France). Comptes Rendus Geosci. 348, 290–300. https://doi.org/10.1016/j.crte.2015.11.004

Lagabrielle Y, Asti R, Fourcade S, Corre B, Poujol M, Uzel J, Labaume P, Clerc C, Lafay R, Picazo S, Maury R. 2019. Mantle exhumation at magma-poor passive continental margins. Part I. 3D architecture and metasomatic evolution of a fossil exhumed mantle domain (Urdach lherzolite, north-western Pyrenees, France), BSGF - Earth Sciences Bulletin 190: 8. https://doi.org/10.1051/bsgf/2019007

Lagabrielle, Y., Asti, R., Fourcade, S., Corre, B., Uzel, J., Labaume, P., Clerc, C., Lafay, R., Picazo, S., 2019b. The mechanisms of mantle exhumation at magma-poor passive continental margins. Part II. Insights from high-displacement, low-angle faults preserved in a fossil distal margin domain (Saraillé lherzolites, north-western Pyrenees, France). BSGF Earth Science Bull., in press.

Le Pichon, X., Bonnin, J., Francheteau, J., Sibuet, J.C., 1971. Une hypothèse d'évolution tectonique du Golfe de Gascogne. Hist. Struct. Golfe Gasc. 2, 11–44.

Lenoble, J.-L., Canérot, J., 1992. La lame extrusive de Pont Suzon (Zone Nord-Pyrénéenne en Vallée d'Aspe): reprise pyrénéenne d'une ride diapirique transverse d'âge crétacé. Comptes Rendus Académie Sci. Sér. 2 Mécanique Phys. Chim. Sci. Univers Sci. Terre 314, 387–391.

Lister, G.S. and Davis, G.A. 1989. The origin of metamorphic core complexes and detachment faults formed during Tertiary continental extension in the northern Colorado River region, U.S.A. Journal of Structural Geology, Vol. 11, No. 112, pp. 65 to 94,

Lister, G.S., Etheridge, M.A., Symonds, P.A., 1991. Detachment models for the formation of passive continental margins. Tectonics 10, 1038–1064.

Lopez-Gomez, J., Martin-Gonzalez, F., Heredia, N., and co-authors, 2019. New lithostratigraphy for the Cantabrian Mountains: A common tectono-stratigraphic evolution for the onset of the Alpine cycle in the W Pyrenean realm,N Spain. Earth Science Reviews, 188, 249-271. https://doi.org/10.1016/j.earscirev.2018.11.008

Lopez-Mir, B., Muñoz, J.A., García Senz, J., 2014. Restoration of basins driven by extension and salt tectonics: Example from the Cotiella Basin in the central Pyrenees. J. Struct. Geol. 69, Part A, 147–162. https://doi.org/10.1016/j.jsg.2014.09.022

Manatschal, G., 2004. New models for evolution of magma-poor rifted margins based on a review of data and concepts from West Iberia and the Alps. Int. J. Earth Sci. 93. https://doi.org/10.1007/s00531-004-0394-7

Manatschal, G., Froitzheim, N., Rubenach, M., Turrin, B.D., 2001. The role of detachment faulting in the formation of an ocean-continent transition: insights from the Iberia Abyssal Plain. Geol. Soc. Lond. Spec. Publ. 187, 405–428. https://doi.org/10.1144/GSL.SP.2001.187.01.20

Manatschal, G., Engström, A., Desmurs, L., Schaltegger, U., Cosca, M., Müntener, O., Bernoulli, D., 2006. What is the tectono-metamorphic evolution of continental break-up: The example of the Tasna Ocean–Continent Transition. J. Struct. Geol. 28, 1849–1869. https://doi.org/10.1016/j.jsg.2006.07.014

Mas. R., Benito MI, Arribas J, Alonso A, Arribas ME, González-Acebrón L, Hernán J, Quijada E, Suárez-González P, Omodeo Salè S (2011) Evolution of an intra-plate rift basin: the Latest Jurassic-Early Cretaceous Cameros Basin (Northwest Iberian Ranges, North Spain). In: Post-Meeting field trips 28th IAS Meeting, vol Geoguías 8. Zaragoza (Spain)

Masini, E., Manatschal, G., Tugend, J., Mohn, G., Flament, J.-M., 2014. The tectono-sedimentary evolution of a hyper-extended rift basin: the example of the Arzacq–Mauléon rift system (Western Pyrenees, SW France). Int. J. Earth Sci. 103, 1569–1596. https://doi.org/10.1007/s00531-014-1023-8

McClay, K., Muñoz, J.-A., García-Senz, J., 2004. Extensional salt tectonics in a contractional orogen: A newly identified tectonic event in the Spanish Pyrenees. Geology 32, 737–740. https://doi.org/10.1130/G20565.1

McKenzie, D., 1978. Some remarks on the development of sedimentary basins. Earth Planet. Sci. Lett. 40, 25–32. https://doi.org/10.1016/0012-821X(78)90071-7

Mendia, M., and Gil Ibarguchi, J. I. 1991. High-grade metamorphic rocks and peridotites along the Leiza Fault (Western Pyrenees, Spain), Geologische Rundschau 80/1.

Michon, L. and Merle, O. 2003. Mode of lithospheric extension: Conceptual models from analogue modeling. Tectonics, 22 (4), pp.1028. https://10.1029/2002TC001435

Mohn, G., Karner, G.D., Manatschal, G., Johnson, C.A., 2015. Structural and stratigraphic evolution of the Iberia–Newfoundland hyper-extended rifted margin: a quantitative modelling approach. Geol. Soc. Lond. Spec. Publ. 413, 53–89. https://doi.org/10.1144/SP413.9

Mohn, G., Manatschal, G., Beltrando, M., Masini, E., Kusznir, N., 2012. Necking of continental crust in magma-poor rifted margins: Evidence from the fossil Alpine Tethys margins: Necking of continental crust. Tectonics 31, n/a-n/a. https://doi.org/10.1029/2011TC002961

Mohn, G., Manatschal, G., Müntener, O., Beltrando, M., Masini, E., 2010. Unravelling the interaction between tectonic and sedimentary processes during lithospheric thinning in the Alpine Tethys margins. Int. J. Earth Sci. 99, 75–101. https://doi.org/10.1007/s00531-010-0566-6

Monchoux, P., 1970. Les lherzolites pyrénéennes: contribution à l'étude de leur minéralogie, de leur genèse et de leurs transformations. Université Paul Sabatier de Toulouse (Sciences).

Muñoz, J.A., 1992. Evolution of a continental collision belt: ECORS-Pyrenees crustal balanced cross-section, in: Thrust Tectonics. Springer, pp. 235–246.

Muñoz, J.A., 2002. The Pyrenees. In: Gibbons, W., Moreno, T., (Eds.), The Geology of Spain, Geological Society, London, UK, pp. 370–385.

Nagel, T. J. and Buck, W. R., 2004. Symmetric alternative to asymmetric rifting models. Geology, 32, 11. pp 937-940 Doi 10.1130/G20785.1

Olivet, J.L., 1996. La cinématique de la plaque ibérique. Bull Cent Rech Explor Prod Elf Aquitaine 20, 131–195.

Omodeo Salè, S., Guimerà, J., Mas, R., & Arribas, J. (2014). Tectono-stratigraphic evolution of an inverted extensional basin: The Cameros Basin (north of Spain). International Journal of Earth Sciences, 103(6), 1597–1620. https://doi.org/10.1007/s00531-014-1026-5

Ortí, F., Pérez-López, A., Salvany, J.M., 2017. Triassic evaporites of Iberia: Sedimentological and palaeogeographical implications for the western Neotethys evolution during the Middle Triassic–Earliest Jurassic. Palaeogeogr. Palaeoclimatol. Palaeoecol. 471, 157–180. https://doi.org/10.1016/j.palaeo.2017.01.025

Osmundsen, P.T., Ebbing, J., 2008. Styles of extension offshore mid-Norway and implications for mechanisms of crustal thinning at passive margins: STYLES OF

EXTENSION OFFSHORE NORWAY. Tectonics 27, n/a-n/a. https://doi.org/10.1029/2007TC002242

Osmundsen, P.T., Péron-Pinvidic, G., 2018. Crustal-Scale Fault Interaction at Rifted Margins and the Formation of Domain-Bounding Breakaway Complexes: Insights From Offshore Norway. Tectonics 37, 935–964. https://doi.org/10.1002/2017TC004792

Pedreira, D., Pulgar, J.A., Gallart, J., and Torné, M., 2007, Three-dimensional gravity and magnetic modeling of crustal indentation and wedging in the western Pyrenees–Cantabrian Mountains: Journal of Geophysical Research–Solid Earth, v. 112, no. B12, B12405, https:// doi.org/10.1029/2007JB005021.

Pedrera, A., García-Senz, J., Ayala, C., Ruiz-Constán, A., Rodríguez-Fernández, L. R., Robador, A., & González Menéndez, L. (2017). Reconstruction of the exhumed mantle across the North Iberian Margin by crustal-scale 3-D gravity inversion and geological cross section. Tectonics, 36. https://doi.org/10.1002/ 2017TC004716

Péron-Pinvidic, G., Manatschal, G., Minshull, T.A., Sawyer, D.S., 2007. Tectonosedimentary evolution of the deep Iberia-Newfoundland margins: Evidence for a complex breakup history. Tectonics 26, 1–19. https://doi.org/10.1029/2006TC001970

Péron-Pinvidic, G., Manatschal, G., 2009. The final rifting evolution at deep magma-poor passive margins from Iberia-Newfoundland: a new point of view. Int. J. Earth Sci. 98, 1581–1597. https://doi.org/10.1007/s00531-008-0337-9

Pinet, B., Montadert, L., ECORS Scientific Party, 1987. Deep seismic reflection and refraction profiling along the Aquitaine shelf (Bay of Biscay). Geophys. J. Int. 89, 305–312. https://doi.org/10.1111/j.1365-246X.1987.tb04423.x

Puigdefàbregas, C., Souquet, P., 1986. Tecto-sedimentary cycles and depositional sequences of the Mesozoic and Tertiary from the Pyrenees. Tectonophysics 129, 173–203.

Rat, P., 1988. The Basque–Cantabrian basin between the Iberian and European plates: some facts but still many problems. Rev Soc Geol Esp 1(3–4):327–348

Rat, P., Amiot, M., Feuillée, P., Floquet, M., Mathey, B., Pascal, A., Salomon, J., García Mondéjar, J., Pujalte, J., Lamolda, M., et al., 1983. Vue sur le Cretacé basco-cantabrique et nord-ibérique. Une marge, son arrière-pays, ses environ. sédimentaires. Mémoires Géol. Univ. Dijon 9, 191.

Rat, J., Mouthereau, F., Brichau, S., Crémades, A., Bernet, M., Balvay, M., Ganne, J., Lahfid, A., Gautheron, C., 2019. Tectonothermal Evolution of the Cameros Basin: Implications for Tectonics of North Iberia. Tectonics 38, 440–469. https://doi.org/10.1029/2018TC005294

Ravier, J., 1959. Le métamorphisme des terrains secondaires des Pyrénées. Mémoires de la Société Géologique de France, N° 86, 250 p., 19 flg., 9 pl. phot.

Reston, T., McDermott, K., 2014. An assessment of the cause of the 'extension discrepancy' with reference to the west Galicia margin. Basin Res. 26, 135–153. https://doi.org/10.1111/bre.12042

Reston, T.J., 1988. Evidence for shear zones in the lower crust offshore Britain. Tectonics 7, 929–945. https://doi.org/10.1029/TC007i005p00929

Reston, T.J., Krawczyk, C.M., Hoffmann, H.-J., 1995. Detachment tectonics during Atlantic rifting: analysis and interpretation of the S reflection, the west Galicia margin. Geol. Soc. Lond. Spec. Publ. 90, 93–109. https://doi.org/10.1144/GSL.SP.1995.090.01.05

Reston, T.J., Pérez-Gussinyé, M., 2007. Lithospheric extension from rifting to continental breakup at magma-poor margins: rheology, serpentinisation and symmetry. Int. J. Earth Sci. 96, 1033–1046. https://doi.org/10.1007/s00531-006-0161-z

Roca, E., Muñoz, J.A., Ferrer, O., Ellouz, N., 2011. The role of the Bay of Biscay Mesozoic extensional structure in the configuration of the Pyrenean orogen: Constraints from the MARCONI deep seismic reflection survey. Tectonics 30. https://doi.org/10.1029/2010TC002735

Roma, M., Ferrer, O., Roca, E., Pla, O., Escosa, F., Butillé, M., 2018. Formation and inversion of salt-detached ramp-syncline basins. Results from analog modeling and application to the Columbrets Basin (Western Mediterranean), Tectonophysics 10.1016/j.tecto.2018.08.012

Roure, F., Choukroune, P., 1998. Contribution of the ECORS seismic data to the Pyrenean geology: Crustal architecture and geodynamic evolution of the Pyrenees. Mém. Société Géologique Fr. 173, 37–52.

Rowan, M.G., 2014. Passive-margin salt basins: hyperextension, evaporite deposition, and salt tectonics. Basin Res. 26, 154–182. https://doi.org/10.1111/bre.12043

Ruiz, M., 2007. Caracterització estructural i sismotectònica de la litosfera en el Domini Pirenaico-Cantàbric a partir de mètodes de sísmica activa i passiva, Ph.D. thesis, Univ. of Barcelona, Barcelona, Spain.

Salas, R., Casas, A., 1993. Mesozoic extensional tectonics, stratigraphy and crustal evolution during the Alpine cycle of the eastern Iberian basin. Tectonophysics 228, 33–55. https://doi.org/10.1016/0040-1951(93)90213-4

Salas, R., Guimerà, J., Mas, R., Martín-Closas, C., Meléndez, A., Alonso, Á., 2001. Evolution of the Mesozoic Central Iberian Rift System and its Cainozoic inversion (Iberian chain). In: Ziegler PA, Cavazza W, Robertson AHF, Crasquin-Soleau S (eds), Peri-Tethys Memoir 6: Peri-Tethyan Rift/Wrench Basins and Passive Margins, vol 186. Mémoires du Museum National d'Histoire Naturelle, Paris, pp 145–186

Saspiturry, N., Razin, P., Baudin, T., Serrano, O., Issautier, B., Lasseur, E., Allanic, C., Thinon, I., Leleu, S., 2019. Symmetry vs. asymmetry of a hyper-thinned rift: Example of the Mauléon Basin (Western Pyrenees, France). Mar. Pet. Geol. 104, 86–105. https://doi.org/10.1016/j.marpetgeo.2019.03.031

Saura, E., Ardèvol i Oró, L., Teixell, A., Vergés, J., 2016. Rising and falling diapirs, shifting depocenters, and flap overturning in the Cretaceous Sopeira and Sant Gervàs subbasins (Ribagorça Basin, southern Pyrenees):

Southern Pyrenees Cretaceous Diapirism. Tectonics 35, 638–662. https://doi.org/10.1002/2015TC004001

Scotese, C.R. and Schettino, A., 2017. Late Permian-Early Jurassic paleogeography of Western Tethys and the world. In Soto et al., eds, Permo-Triassic salt provinces of Europe, North Africa and the Atlantic margins. Tectonics and Hydrocarbon potential. Elsevier, pp. 57-91.

Sibuet, J.-C., Srivastava, S.P., Spakman, W., 2004. Pyrenean orogeny and plate kinematics. J. Geophys. Res. Solid Earth 109, B08104. https://doi.org/10.1029/2003JB002514

Soto, J.I, Flinch, J.F. and Tari, G., 2017. Permo-Triassic salt provinces of Europe, North Africa and the Atlantic margins: A synthesis. In Soto et al., eds, Permo-Triassic salt provinces of Europe, North Africa and the Atlantic margins. Tectonics and Hydrocarbon potential. Elsevier, pp. 3-41.

Sutra, E., Manatschal, G., Mohn, G., Unternehr, P., 2013. Quantification and restoration of extensional deformation along the Western Iberia and Newfoundland rifted margins. Geoch. Geoph. Geosys. 14 (8), 2575e2597.

Teixell, A., 1998. Crustal structure and orogenic material budget in the west central Pyrenees. Tectonics 17, 395–406. https://doi.org/10.1029/98TC00561

Teixell, A., Labaume, P., Lagabrielle, Y., 2016. The crustal evolution of the west-central Pyrenees revisited: Inferences from a new kinematic scenario. Comptes Rendus Geosci. 348, 257–267. https://doi.org/10.1016/j.crte.2015.10.010

Teixell, A., Labaume, P., Ayarza, P., Espurt, N., de Saint Blanquat, M., Lagabrielle, Y., 2018. Crustal structure and evolution of the Pyrenean-Cantabrian belt: A review and new interpretations from recent concepts and data. Tectonophysics 724, 146–170. https://doi.org/10.1016/j.tecto.2018.01.009

Thiébault J., Durand-Wackenheim C., Debeaux M. and Souquet P., 1992. Métamorphisme des évaporites triasiques du versant nord des Pyrénées centrales et occidentales. Bull. Soc. Hist. Nat. Toulouse. 128, 77-84.

Thinon, I., Matias, L., RÉhault, J.P., Hirn, A., Fidalgo-GonzÁlez, L., Avedik, F., 2003. Deep structure of the Armorican Basin (Bay of Biscay): a review of Norgasis seismic reflection and refraction data. J. Geol. Soc. 160, 99–116. https://doi.org/10.1144/0016-764901-103

Tirel, C., Brun, J.-P. and Burov, E., 2008. Dynamics and structural development of metamorphic core complexes. Journal of Geophysical Research, 113(B4): B04403.

Tomassimo, A., Marillier, F., 1997. Processing and interpretation in the tau-p domain of the ECORS Bay of Biscay expanding spread profiles. Mém. Société Géologique Fr. 171, 31–43.

Tugend, J., Manatschal, G. and Kusznir, N.J., 2015. Spatial and temporal evolution of hyperextended rift systems: Implication for the nature, kinematics, and timing of the Iberian-European plate boundary, Geology, 43(1), 15–18, doi:10.1130/G36072.1.

Tugend, J., Manatschal, G., Kusznir, N.J., Masini, E., Mohn, G., Thinon, I., 2014. Formation and deformation of hyperextended rift systems: Insights from rift domain mapping in the Bay of Biscay-Pyrenees. Tectonics 33, 1239–1276. https://doi.org/10.1002/2014TC003529

Vergés, J., García-Senz, J., 2001. Mesozoic evolution and Cainozoic inversion of the Pyrenean rift. Mém. Muséum Natl. Hist. Nat. 186, 187–212.

Vielzeuf, D., Kornprobst, J., 1984. Crustal splitting and the emplacement of Pyrenean lherzolites and granulites. Earth Planet. Sci. Lett. 67, 87–96. https://doi.org/10.1016/0012-821X(84)90041-4

Vissers, R.L.M., Drury, M.R., Newman, J. and Fliervoet, T.F., 1997. Mylonitic deformation in upper mantle peridotites of the North Pyrenean Zone (France) : implications for strength and strain localization in the lithosphere. Tectonophysics, 279, 303-325.

Wang, Y., Chevrot, S., Monteiller, V., Komatitsch, D., Mouthereau, F., Manatschal, G., Sylvander, M., Diaz, J., Ruiz, M., Grimaud, F., Benahmed, S., Pauchet, H., Martin, R., 2016. The deep roots of the western Pyrenees revealed by full waveform inversion of teleseismic P waves. Geology 44, 475–478. https://doi.org/10.1130/G37812.1

Wernicke, B., 1981. Low-angle normal faults in the Basin and Range Province: nappe tectonics in an extending orogen. Nature 291, 645–648. https://doi.org/10.1038/291645a0

Wernicke, B., 1985. Uniform-sense normal simple shear of the continental lithosphere. Can. J. Earth Sci. 22, 108–125. https://doi.org/10.1139/e85-009

Ziegler, 1988. Evolution of Arctic-North Atlantic and western Tethys. Tulsa. AAPG Memoir, 43, 198 pp.

Zamora, G., Fleming, M., Gallastegui, J., 2017. Salt Tectonics Within the Offshore Asturian Basin: North Iberian Margin, in Soto, J.I, Flinch, J.F. and Tari, G., 2017. Permo-Triassic salt provinces of Europe, North Africa and the Atlantic margins: A synthesis. In Soto et al., eds, Permo-Triassic salt provinces of Europe, North Africa and the Atlantic margins. Tectonics and Hydrocarbon potential. Elsevier, pp. 353-367.

Nicolas Saspiturry

Evolution sédimentaire, structurale et thermique d'un rift hyper-aminci : de l'héritage post-hercynien à l'inversion alpine

Exemple du bassin de Mauléon (Pyrénées)

Résume

Localisé dans les Pyrénées occidentales, l'étude du bassin de Mauléon, permet d'appréhender l'évolution tectono-sédimentaire et thermique d'un rift hyper-aminci de son héritage pré-extensif à son inversion (cycle complet de Wilson). L'épisode permien reflète le passage de la convergence N-S enregistrée dans la Zone Axiale (310 à 290 Ma) à une phase d'extension E-W (290 et 275 Ma), conférant un héritage thermique, structural et rhéologique complexe à la lithosphère des Pyrénées occidentales. La préservation des traits paléogéographiques permo-triasiques rend impossible la réalisation d'un mouvement décrochant sénestre E-W au Mésozoïque entre l'Ibérie et l'Europe, dans cette partie des Pyrénées, questionnant les modalités d'ouverture des bassins nord-pyrénéens au Crétacé. Au cours de l'orogenèse alpine, le bassin hyper-étiré de Mauléon est inversé. La réactivation des structures crétacées conduit à la formation d'un pop-up lithosphérique dont les bordures présentent des styles de réactivation différents, localisé (Ibérie) vs distribué (Europe). La protubérance mantélique héritée de la phase de rifting crétacée empêche l'inversion complète du rift en jouant le rôle de buttoir. En 3D, les systèmes de chevauchement sont composés de plusieurs segments délimités par les zones de transferts N20° héritées du Permien conférant un caractère non-cylindrique au structures orogéniques pyrénéennes. L'héritage permien et crétacé contrôle à la fois l'évolution thermique synrift et post-collisionnelle du bassin de Mauléon. Les paléo-gradients géothermiques synrifts augmentent de manière graduelle des marges (~ 34°C/km) vers le bassin (~ 60°C/km). La température maximale est alors contrôlée par l'enfouissement et le flux thermique mantélique (100 mW.m-2). La différence de réponse thermique observées sur les bordures du bassin de Mauléon est liée au style de déformation compressive : diminution du gradient dans le domaine hyper-étiré et la marge européenne ~ 25.0 ± 2.7°C/km vs augmentation du gradient sur la marge ibérique < 30°C/km). L'étude tectono-sédimentaire des bassins mésozoïques adjacents d'Arzacq et de Tartas, couplée à un travail de synthèse sur les bassins péri-ibériques souligne les nombreuses différences existant entre ces bassins et ceux des marges hyper-étirées atlantiques. L'évolution de ces « bassins extensifs à pente douce » comprend trois grands stades de déformation : (1) un amincissement ductile de la croûte inférieure, sans déformation cassante significative dans la croûte supérieure, formant un rift symétrique (sag) ; (2) un glissement de la couverture prerift sur les évaporites du Trias; (3) une phase d'hyper-extension avec déformation fragile des marges proximales et amincissement ductile du domaine distal hyper-étiré (métamorphisme HT/BP).

Mots clés : (1) Pyrénées ; (2) bassin de Mauléon ; (3) Géodynamique (4) Héritage post-hercynien ; (5) Hyper-extension crétacée ; (6) Inversion alpine ; (7) Zones de transfert ; (8) Métamorphisme HT/BP ; (9) Evolution thermique.